Journal of Robotics

Trends and Developments in Robotics Systems Based on Nanomaterials

Lead Guest Editor: Shahid Hussain
Guest Editors: Liyang Lin and Iqbal Ahmad

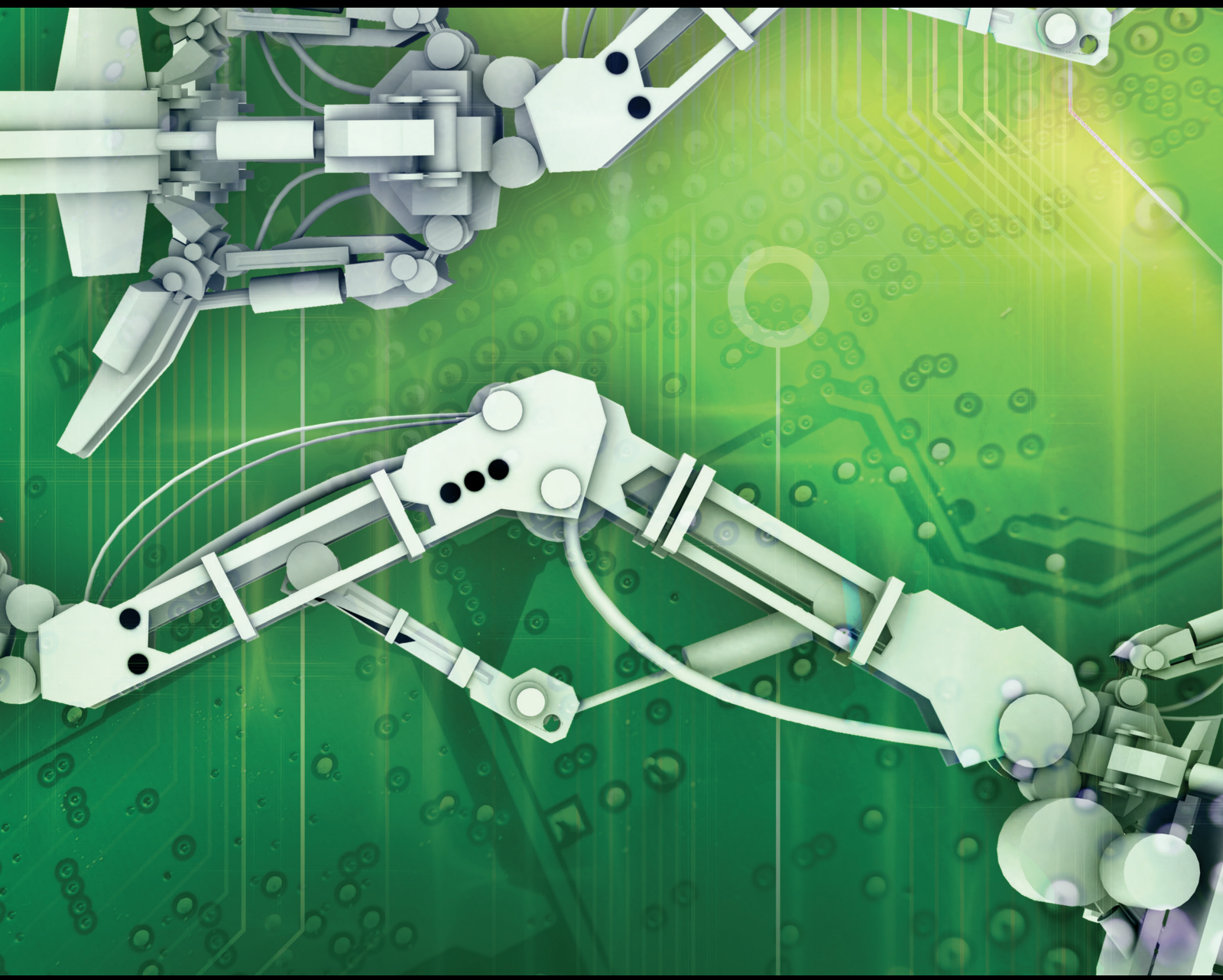

Trends and Developments in Robotics Systems Based on Nanomaterials

Journal of Robotics

Trends and Developments in Robotics Systems Based on Nanomaterials

Lead Guest Editor: Shahid Hussain
Guest Editors: Liyang Lin and Iqbal Ahmad

Copyright © 2024 Hindawi Limited. All rights reserved.

This is a special issue published in “Journal of Robotics.” All articles are open access articles distributed under the Creative Commons Attribution License, which permits unrestricted use, distribution, and reproduction in any medium, provided the original work is properly cited.

Chief Editor

Yangmin Li, Hong Kong

Academic Editors

Jean Baratgin, France
Constantin Florin Caruntu, Romania
Raffaele Di Gregorio, Italy
Bingxiao Ding, China
L. Fortuna, Italy
Farrokh Janabi-Sharifi, Canada
Li-Hong Juang, China
Changsheng Li, China
Giovanni Muscato, Italy
Shahram Payandeh, Canada
Oscar Reinoso, Spain
Ruthber Rodriguez Serrezuela, Colombia
Afaque Manzoor Soomro, Pakistan
Ramadoni Syahputra, Indonesia
Weitian Wang, USA
Yaoyao Wang, China
Keigo Watanabe, Japan
Shuofei Yang, China
Simon X. Yang, Canada
Xianfeng Yuan, China
Ting Zhang, China
Ting Zou, Canada

Contents

Retracted: Intelligent Control System Design of Ring Light via IOT Mobile Robot
Journal of Robotics
Retraction (1 page), Article ID 9898409, Volume 2024 (2024)

Retracted: Application and Analysis of Remote Sensing Image Processing Technology in Robotic Power Inspection
Journal of Robotics
Retraction (1 page), Article ID 9896301, Volume 2024 (2024)

Retracted: Security Risk and Preventive Measures of Multimedia Database System under Remote Control of Network Robot
Journal of Robotics
Retraction (1 page), Article ID 9893014, Volume 2024 (2024)

Retracted: Industrial Robot Assembly Line Design Using Machine Vision
Journal of Robotics
Retraction (1 page), Article ID 9891767, Volume 2024 (2024)

Retracted: Simulation Design of a Live Working Manipulator for Patrol Inspection in Power Grid
Journal of Robotics
Retraction (1 page), Article ID 9876760, Volume 2024 (2024)

Retracted: Integrated Urban Design Methodology of "Planning-Construction-Management" and Intelligent Management and Control Based on Teaching Reproduction Robot
Journal of Robotics
Retraction (1 page), Article ID 9876240, Volume 2024 (2024)

Retracted: Application of Intelligent Robot Palletizer Technology in the Optimization of High-Speed Train Operation and Simulation Verification
Journal of Robotics
Retraction (1 page), Article ID 9868549, Volume 2024 (2024)

Retracted: Optimization of Intelligent Distribution of Distribution Network in the Presence of Distributed Sources
Journal of Robotics
Retraction (1 page), Article ID 9863834, Volume 2024 (2024)

Retracted: Discovery and Discrimination of Bridge Engineering Safety Issues by BIM Virtual Scene Combined with Robotic Mapping
Journal of Robotics
Retraction (1 page), Article ID 9863534, Volume 2024 (2024)

Retracted: Safety Monitoring System and Method for Unmanned Operation of Unmanned Aerial Vehicle Distribution Network Based on Learning Control Robot Technology
Journal of Robotics
Retraction (1 page), Article ID 9848450, Volume 2024 (2024)

Retracted: Optimization Design of Mountain and Water Landscape of Traditional Mountain Village Based on New Robot Visual Technology
Journal of Robotics
Retraction (1 page), Article ID 9843025, Volume 2024 (2024)

Retracted: On the Performance and Efficiency of Surface Air Cooler Working under High Temperature and High Humidity Condition
Journal of Robotics
Retraction (1 page), Article ID 9837908, Volume 2024 (2024)

Retracted: Attitude Analysis and Evaluation of Camera Based on Planar Double Joint Robot
Journal of Robotics
Retraction (1 page), Article ID 9831614, Volume 2024 (2024)

Retracted: Transmission Line Condition Monitoring Method Based on Binocular Vision and Edge Computing for Line Changing Robot
Journal of Robotics
Retraction (1 page), Article ID 9830829, Volume 2024 (2024)

Retracted: Optimization Path and Design of Intelligent Logistics Management System Based on ROS Robot
Journal of Robotics
Retraction (1 page), Article ID 9830590, Volume 2024 (2024)

Retracted: Design and Simulation Analysis of a Flexible Clamping and Conveying Device of a Green Leafy Vegetable Cutting and Bundling Integrated Machine
Journal of Robotics
Retraction (1 page), Article ID 9819583, Volume 2024 (2024)

Retracted: Reinforcement Learning-Based Continuous Action Space Path Planning Method for Mobile Robots
Journal of Robotics
Retraction (1 page), Article ID 9819037, Volume 2024 (2024)

Retracted: Application of Multimedia Quality Evaluation Relying on Intelligent Robot Numerical Control Technology in New Energy Power Generation System
Journal of Robotics
Retraction (1 page), Article ID 9817514, Volume 2024 (2024)

Retracted: Application of Intelligent Signal Reflection in the Communication Model of an Electronic Controller
Journal of Robotics
Retraction (1 page), Article ID 9809817, Volume 2024 (2024)

Contents

Retracted: Application of Microcontroller-Based Multipath Servos in Industrial Robot Control Systems
Journal of Robotics
Retraction (1 page), Article ID 9797639, Volume 2024 (2024)

Retracted: Application of Image Processing Variation Model Based on Network Control Robot Image Transmission and Processing System in Multimedia Enhancement Technology
Journal of Robotics
Retraction (1 page), Article ID 9795848, Volume 2024 (2024)

Retracted: Collaboration and Management of Heterogeneous Robotic Systems for Road Network Construction, Management, and Maintenance under the Vision of "BIM + GIS" Technology
Journal of Robotics
Retraction (1 page), Article ID 9792362, Volume 2024 (2024)

Retracted: Design and Application of Electromechanical Control System Based on Computer Fault Tolerance Technology
Journal of Robotics
Retraction (1 page), Article ID 9785472, Volume 2024 (2024)

Retracted: Parameter-Tunable RBF Neural Network Control Facing Dual-Joint Manipulators
Journal of Robotics
Retraction (1 page), Article ID 9767914, Volume 2024 (2024)

Retracted: Analysis and Evaluation of Ecological Environment Monitoring Based on PIE Remote Sensing Image Processing Software
Journal of Robotics
Retraction (1 page), Article ID 9874013, Volume 2023 (2023)

Retracted: The Application of Multimedia Visualization Platform in Business Management from the Perspective of Supply Chain Management
Journal of Robotics
Retraction (1 page), Article ID 9852312, Volume 2023 (2023)

Retracted: Online Control Method of Small- and Medium-Sized Electromechanical Equipment Based on Deep Neural Network
Journal of Robotics
Retraction (1 page), Article ID 9827679, Volume 2023 (2023)

Retracted: Machinery Changes and Challenges of Architecture and Landscape Design in the Virtual Reality Perspective
Journal of Robotics
Retraction (1 page), Article ID 9824265, Volume 2023 (2023)

Retracted: Application of 5G Mobile Communication Technology Integrating Robot Controller Communication Method in Communication Engineering
Journal of Robotics
Retraction (1 page), Article ID 9780273, Volume 2023 (2023)

Retracted: Designing and Manufacturing of Industrial Robots with Dual-Angle Sensors Taking into Account Vibration Signal Fusion
Journal of Robotics
Retraction (1 page), Article ID 9768015, Volume 2023 (2023)

Retracted: Multiscale Motion Detection and Recognition Combining Still Images and Video Sequences
Journal of Robotics
Retraction (1 page), Article ID 9896453, Volume 2023 (2023)

Retracted: Appearance Design Method of Ceramic Art Based on VR Visualization Technology
Journal of Robotics
Retraction (1 page), Article ID 9872574, Volume 2023 (2023)

Retracted: Evaluation of the Students' Learning Status in the Foreign Language Classroom Based on Machine Vision
Journal of Robotics
Retraction (1 page), Article ID 9857401, Volume 2023 (2023)

Retracted: Deep Learning BP Neural Network Guided Evaluation of Students' Innovation and Entrepreneurship Education
Journal of Robotics
Retraction (1 page), Article ID 9845964, Volume 2023 (2023)

Retracted: A Russian Continuous Speech Recognition System Based on the DTW Algorithm under Artificial Intelligence
Journal of Robotics
Retraction (1 page), Article ID 9832350, Volume 2023 (2023)

Retracted: The Evaluation of Visual Clarity and Comfort of Light Environment in Multimedia Classroom
Journal of Robotics
Retraction (1 page), Article ID 9807401, Volume 2023 (2023)

Retracted: Discussion on Redundant Processing Algorithm of Association Rules Based on Hypergraph in Data Mining
Journal of Robotics
Retraction (1 page), Article ID 9789505, Volume 2023 (2023)

Retracted: Recognition and Modeling of Crisis Propagation Patterns Combined with Robot Simulation of Social Networks
Journal of Robotics
Retraction (1 page), Article ID 9768653, Volume 2023 (2023)

Contents

Retracted: Feature Extraction and Analysis Method of Trombone Timbre Based on CNN Model
Journal of Robotics
Retraction (1 page), Article ID 9768081, Volume 2023 (2023)

[Retracted] Application of Intelligent Robot Palletizer Technology in the Optimization of High-Speed Train Operation and Simulation Verification
Xiaoling Zhang
Research Article (10 pages), Article ID 2656636, Volume 2023 (2023)

[Retracted] Attitude Analysis and Evaluation of Camera Based on Planar Double Joint Robot
Zhi Xu, Xin Wang, Chun Chen, and Jiahai Zhang
Research Article (7 pages), Article ID 8143828, Volume 2023 (2023)

[Retracted] Optimization Design of Mountain and Water Landscape of Traditional Mountain Village Based on New Robot Visual Technology
Xinxin Jia, Ruixin Liu, and Zhi Qiao
Research Article (10 pages), Article ID 4155090, Volume 2023 (2023)

[Retracted] Security Risk and Preventive Measures of Multimedia Database System under Remote Control of Network Robot
Wenyan Deng and Pengfei Yan
Research Article (8 pages), Article ID 9276208, Volume 2023 (2023)

[Retracted] Designing and Manufacturing of Industrial Robots with Dual-Angle Sensors Taking into Account Vibration Signal Fusion
Jinshun Yan and Haiqing Cheng
Research Article (11 pages), Article ID 1855226, Volume 2023 (2023)

[Retracted] Discovery and Discrimination of Bridge Engineering Safety Issues by BIM Virtual Scene Combined with Robotic Mapping
Guilin Gong, Shaowu Zeng, Jingjing Gao, Qingliang Zhang, and Xinli Wang
Research Article (12 pages), Article ID 3028505, Volume 2023 (2023)

[Retracted] Intelligent Control System Design of Ring Light via IOT Mobile Robot
Xianzhi Kang and Yue Teng
Research Article (13 pages), Article ID 4303194, Volume 2023 (2023)

[Retracted] Machinery Changes and Challenges of Architecture and Landscape Design in the Virtual Reality Perspective
He Jin and Nan Zhang
Research Article (9 pages), Article ID 1430551, Volume 2023 (2023)

[Retracted] Application and Analysis of Remote Sensing Image Processing Technology in Robotic Power Inspection
Jie Chen, Hemeng Yang, and Rui Xu
Research Article (11 pages), Article ID 9943372, Volume 2023 (2023)

[Retracted] Collaboration and Management of Heterogeneous Robotic Systems for Road Network Construction, Management, and Maintenance under the Vision of "BIM + GIS" Technology
Zhizhong Liu, Weishen Yan, Jianguo Kou, and Zhida Li
Research Article (8 pages), Article ID 8259912, Volume 2023 (2023)

[Retracted] Application of Multimedia Quality Evaluation Relying on Intelligent Robot Numerical Control Technology in New Energy Power Generation System
Ruijuan Sun and Xiaoyuan Dang
Research Article (11 pages), Article ID 7480917, Volume 2023 (2023)

[Retracted] Application of 5G Mobile Communication Technology Integrating Robot Controller Communication Method in Communication Engineering
Yu Chen
Research Article (9 pages), Article ID 1857590, Volume 2023 (2023)

[Retracted] Application of Microcontroller-Based Multipath Servos in Industrial Robot Control Systems
Ruiming Hu
Research Article (11 pages), Article ID 7235120, Volume 2023 (2023)

[Retracted] Industrial Robot Assembly Line Design Using Machine Vision
Xiang Xie
Research Article (13 pages), Article ID 4409033, Volume 2023 (2023)

[Retracted] Transmission Line Condition Monitoring Method Based on Binocular Vision and Edge Computing for Line Changing Robot
Zheng Lu, Jiazhen Duan, Xiaoqiang Chen, and Yang Chen
Research Article (10 pages), Article ID 7747194, Volume 2023 (2023)

[Retracted] Optimization Path and Design of Intelligent Logistics Management System Based on ROS Robot
Ruijie Wu
Research Article (9 pages), Article ID 9505155, Volume 2023 (2023)

[Retracted] Reinforcement Learning-Based Continuous Action Space Path Planning Method for Mobile Robots
Weimin Zhang and Guoyong Wang
Research Article (9 pages), Article ID 9069283, Volume 2022 (2022)

[Retracted] Design and Simulation Analysis of a Flexible Clamping and Conveying Device of a Green Leafy Vegetable Cutting and Bundling Integrated Machine
Zhiquan Wang, Tianxing Yang, and Wei Wei
Research Article (9 pages), Article ID 4729480, Volume 2022 (2022)

Contents

[Retracted] Deep Learning BP Neural Network Guided Evaluation of Students' Innovation and Entrepreneurship Education
Jingyi Yi and Xiao Cui
Research Article (10 pages), Article ID 2425069, Volume 2022 (2022)

[Retracted] Application of Intelligent Signal Reflection in the Communication Model of an Electronic Controller
Lan Lan
Research Article (9 pages), Article ID 8031024, Volume 2022 (2022)

[Retracted] Integrated Urban Design Methodology of "Planning-Construction-Management" and Intelligent Management and Control Based on Teaching Reproduction Robot
Haipeng Wang
Research Article (9 pages), Article ID 4669792, Volume 2022 (2022)

[Retracted] Safety Monitoring System and Method for Unmanned Operation of Unmanned Aerial Vehicle Distribution Network Based on Learning Control Robot Technology
Boyan Jia, Yihu Jiang, Tianxiang Ma, Xin Duan, Dan Li, Jingran Jia, and Xiaoyu Li
Research Article (10 pages), Article ID 8559153, Volume 2022 (2022)

[Retracted] Recognition and Modeling of Crisis Propagation Patterns Combined with Robot Simulation of Social Networks
Yafei Wang
Research Article (12 pages), Article ID 3454396, Volume 2022 (2022)

[Retracted] Appearance Design Method of Ceramic Art Based on VR Visualization Technology
Hui Li
Research Article (11 pages), Article ID 7664404, Volume 2022 (2022)

[Retracted] Online Control Method of Small- and Medium-Sized Electromechanical Equipment Based on Deep Neural Network
Mengmeng Yang, Sanxing Deng, and Zhizheng Zhao
Research Article (10 pages), Article ID 1607694, Volume 2022 (2022)

[Retracted] Design and Application of Electromechanical Control System Based on Computer Fault Tolerance Technology
Rui Wei
Research Article (10 pages), Article ID 7716900, Volume 2022 (2022)

[Retracted] Analysis and Evaluation of Ecological Environment Monitoring Based on PIE Remote Sensing Image Processing Software
Xiaofeng Wang and Zhengran Wang
Research Article (12 pages), Article ID 1716756, Volume 2022 (2022)

[Retracted] Application of Image Processing Variation Model Based on Network Control Robot Image Transmission and Processing System in Multimedia Enhancement Technology
Yanmin Wu and Jinli Qi
Research Article (10 pages), Article ID 6991983, Volume 2022 (2022)

[Retracted] The Evaluation of Visual Clarity and Comfort of Light Environment in Multimedia Classroom
Yu Dong, Minshen Xi, and Minghua Hu
Research Article (12 pages), Article ID 4917352, Volume 2022 (2022)

[Retracted] On the Performance and Efficiency of Surface Air Cooler Working under High Temperature and High Humidity Condition
Juan Yang, Jing Yu, Shijing Wang, and Weidong Yan
Research Article (11 pages), Article ID 8656289, Volume 2022 (2022)

[Retracted] Evaluation of the Students' Learning Status in the Foreign Language Classroom Based on Machine Vision
Lin Yao and Qiongfang Qin
Research Article (12 pages), Article ID 6432133, Volume 2022 (2022)

[Retracted] Optimization of Intelligent Distribution of Distribution Network in the Presence of Distributed Sources
Youle Song, Ding Nie, and Litao Fan
Research Article (11 pages), Article ID 7063913, Volume 2022 (2022)

[Retracted] Feature Extraction and Analysis Method of Trombone Timbre Based on CNN Model
Yanjun Wang
Research Article (12 pages), Article ID 9460208, Volume 2022 (2022)

[Retracted] A Russian Continuous Speech Recognition System Based on the DTW Algorithm under Artificial Intelligence
Chunping Yu and Xin Wang
Research Article (11 pages), Article ID 5777472, Volume 2022 (2022)

[Retracted] The Application of Multimedia Visualization Platform in Business Management from the Perspective of Supply Chain Management
Nuan Wang
Research Article (10 pages), Article ID 1271691, Volume 2022 (2022)

[Retracted] Discussion on Redundant Processing Algorithm of Association Rules Based on Hypergraph in Data Mining
Jintan Zhu
Research Article (9 pages), Article ID 1007464, Volume 2022 (2022)

Contents

[Retracted] Simulation Design of a Live Working Manipulator for Patrol Inspection in Power Grid
Tao Xie, Zhengyu Li, Yongyun Zhang, Bin Yuan, and Xiao Liu
Research Article (8 pages), Article ID 7318090, Volume 2022 (2022)

[Retracted] Parameter-Tunable RBF Neural Network Control Facing Dual-Joint Manipulators
Weiying Xu
Research Article (10 pages), Article ID 4231117, Volume 2022 (2022)

[Retracted] Multiscale Motion Detection and Recognition Combining Still Images and Video Sequences
Zhuo Chen
Research Article (12 pages), Article ID 7682559, Volume 2022 (2022)

Hindawi
Journal of Robotics
Volume 2024, Article ID 9898409, 1 page
https://doi.org/10.1155/2024/9898409

Retraction

Retracted: Intelligent Control System Design of Ring Light via IOT Mobile Robot

Journal of Robotics

Received 23 January 2024; Accepted 23 January 2024; Published 24 January 2024

Copyright © 2024 Journal of Robotics. This is an open access article distributed under the Creative Commons Attribution License, which permits unrestricted use, distribution, and reproduction in any medium, provided the original work is properly cited.

This article has been retracted by Hindawi following an investigation undertaken by the publisher [1]. This investigation has uncovered evidence of one or more of the following indicators of systematic manipulation of the publication process:

(1) Discrepancies in scope
(2) Discrepancies in the description of the research reported
(3) Discrepancies between the availability of data and the research described
(4) Inappropriate citations
(5) Incoherent, meaningless and/or irrelevant content included in the article
(6) Manipulated or compromised peer review

The presence of these indicators undermines our confidence in the integrity of the article's content and we cannot, therefore, vouch for its reliability. Please note that this notice is intended solely to alert readers that the content of this article is unreliable. We have not investigated whether authors were aware of or involved in the systematic manipulation of the publication process.

Wiley and Hindawi regrets that the usual quality checks did not identify these issues before publication and have since put additional measures in place to safeguard research integrity.

We wish to credit our own Research Integrity and Research Publishing teams and anonymous and named external researchers and research integrity experts for contributing to this investigation.

The corresponding author, as the representative of all authors, has been given the opportunity to register their agreement or disagreement to this retraction. We have kept a record of any response received.

References

[1] X. Kang and Y. Teng, "Intelligent Control System Design of Ring Light via IOT Mobile Robot," *Journal of Robotics*, vol. 2023, Article ID 4303194, 13 pages, 2023.

Hindawi
Journal of Robotics
Volume 2024, Article ID 9896301, 1 page
https://doi.org/10.1155/2024/9896301

Retraction

Retracted: Application and Analysis of Remote Sensing Image Processing Technology in Robotic Power Inspection

Journal of Robotics

Received 23 January 2024; Accepted 23 January 2024; Published 24 January 2024

Copyright © 2024 Journal of Robotics. This is an open access article distributed under the Creative Commons Attribution License, which permits unrestricted use, distribution, and reproduction in any medium, provided the original work is properly cited.

This article has been retracted by Hindawi following an investigation undertaken by the publisher [1]. This investigation has uncovered evidence of one or more of the following indicators of systematic manipulation of the publication process:

(1) Discrepancies in scope
(2) Discrepancies in the description of the research reported
(3) Discrepancies between the availability of data and the research described
(4) Inappropriate citations
(5) Incoherent, meaningless and/or irrelevant content included in the article
(6) Manipulated or compromised peer review

The presence of these indicators undermines our confidence in the integrity of the article's content and we cannot, therefore, vouch for its reliability. Please note that this notice is intended solely to alert readers that the content of this article is unreliable. We have not investigated whether authors were aware of or involved in the systematic manipulation of the publication process.

Wiley and Hindawi regrets that the usual quality checks did not identify these issues before publication and have since put additional measures in place to safeguard research integrity.

We wish to credit our own Research Integrity and Research Publishing teams and anonymous and named external researchers and research integrity experts for contributing to this investigation.

The corresponding author, as the representative of all authors, has been given the opportunity to register their agreement or disagreement to this retraction. We have kept a record of any response received.

References

[1] J. Chen, H. Yang, and R. Xu, "Application and Analysis of Remote Sensing Image Processing Technology in Robotic Power Inspection," *Journal of Robotics*, vol. 2023, Article ID 9943372, 11 pages, 2023.

Hindawi
Journal of Robotics
Volume 2024, Article ID 9893014, 1 page
https://doi.org/10.1155/2024/9893014

Retraction

Retracted: Security Risk and Preventive Measures of Multimedia Database System under Remote Control of Network Robot

Journal of Robotics

Received 23 January 2024; Accepted 23 January 2024; Published 24 January 2024

Copyright © 2024 Journal of Robotics. This is an open access article distributed under the Creative Commons Attribution License, which permits unrestricted use, distribution, and reproduction in any medium, provided the original work is properly cited.

This article has been retracted by Hindawi following an investigation undertaken by the publisher [1]. This investigation has uncovered evidence of one or more of the following indicators of systematic manipulation of the publication process:

(1) Discrepancies in scope
(2) Discrepancies in the description of the research reported
(3) Discrepancies between the availability of data and the research described
(4) Inappropriate citations
(5) Incoherent, meaningless and/or irrelevant content included in the article
(6) Manipulated or compromised peer review

The presence of these indicators undermines our confidence in the integrity of the article's content and we cannot, therefore, vouch for its reliability. Please note that this notice is intended solely to alert readers that the content of this article is unreliable. We have not investigated whether authors were aware of or involved in the systematic manipulation of the publication process.

Wiley and Hindawi regrets that the usual quality checks did not identify these issues before publication and have since put additional measures in place to safeguard research integrity.

We wish to credit our own Research Integrity and Research Publishing teams and anonymous and named external researchers and research integrity experts for contributing to this investigation.

The corresponding author, as the representative of all authors, has been given the opportunity to register their agreement or disagreement to this retraction. We have kept a record of any response received.

References

[1] W. Deng and P. Yan, "Security Risk and Preventive Measures of Multimedia Database System under Remote Control of Network Robot," *Journal of Robotics*, vol. 2023, Article ID 9276208, 8 pages, 2023.

Hindawi
Journal of Robotics
Volume 2024, Article ID 9891767, 1 page
https://doi.org/10.1155/2024/9891767

Retraction

Retracted: Industrial Robot Assembly Line Design Using Machine Vision

Journal of Robotics

Received 23 January 2024; Accepted 23 January 2024; Published 24 January 2024

Copyright © 2024 Journal of Robotics. This is an open access article distributed under the Creative Commons Attribution License, which permits unrestricted use, distribution, and reproduction in any medium, provided the original work is properly cited.

This article has been retracted by Hindawi following an investigation undertaken by the publisher [1]. This investigation has uncovered evidence of one or more of the following indicators of systematic manipulation of the publication process:

(1) Discrepancies in scope
(2) Discrepancies in the description of the research reported
(3) Discrepancies between the availability of data and the research described
(4) Inappropriate citations
(5) Incoherent, meaningless and/or irrelevant content included in the article
(6) Manipulated or compromised peer review

The presence of these indicators undermines our confidence in the integrity of the article's content and we cannot, therefore, vouch for its reliability. Please note that this notice is intended solely to alert readers that the content of this article is unreliable. We have not investigated whether authors were aware of or involved in the systematic manipulation of the publication process.

Wiley and Hindawi regrets that the usual quality checks did not identify these issues before publication and have since put additional measures in place to safeguard research integrity.

We wish to credit our own Research Integrity and Research Publishing teams and anonymous and named external researchers and research integrity experts for contributing to this investigation.

The corresponding author, as the representative of all authors, has been given the opportunity to register their agreement or disagreement to this retraction. We have kept a record of any response received.

References

[1] X. Xie, "Industrial Robot Assembly Line Design Using Machine Vision," *Journal of Robotics*, vol. 2023, Article ID 4409033, 13 pages, 2023.

Hindawi
Journal of Robotics
Volume 2024, Article ID 9876760, 1 page
https://doi.org/10.1155/2024/9876760

Retraction

Retracted: Simulation Design of a Live Working Manipulator for Patrol Inspection in Power Grid

Journal of Robotics

Received 23 January 2024; Accepted 23 January 2024; Published 24 January 2024

Copyright © 2024 Journal of Robotics. This is an open access article distributed under the Creative Commons Attribution License, which permits unrestricted use, distribution, and reproduction in any medium, provided the original work is properly cited.

This article has been retracted by Hindawi following an investigation undertaken by the publisher [1]. This investigation has uncovered evidence of one or more of the following indicators of systematic manipulation of the publication process:

(1) Discrepancies in scope
(2) Discrepancies in the description of the research reported
(3) Discrepancies between the availability of data and the research described
(4) Inappropriate citations
(5) Incoherent, meaningless and/or irrelevant content included in the article
(6) Manipulated or compromised peer review

The presence of these indicators undermines our confidence in the integrity of the article's content and we cannot, therefore, vouch for its reliability. Please note that this notice is intended solely to alert readers that the content of this article is unreliable. We have not investigated whether authors were aware of or involved in the systematic manipulation of the publication process.

Wiley and Hindawi regrets that the usual quality checks did not identify these issues before publication and have since put additional measures in place to safeguard research integrity.

We wish to credit our own Research Integrity and Research Publishing teams and anonymous and named external researchers and research integrity experts for contributing to this investigation.

The corresponding author, as the representative of all authors, has been given the opportunity to register their agreement or disagreement to this retraction. We have kept a record of any response received.

References

[1] T. Xie, Z. Li, Y. Zhang, B. Yuan, and X. Liu, "Simulation Design of a Live Working Manipulator for Patrol Inspection in Power Grid," *Journal of Robotics*, vol. 2022, Article ID 7318090, 8 pages, 2022.

Hindawi
Journal of Robotics
Volume 2024, Article ID 9876240, 1 page
https://doi.org/10.1155/2024/9876240

Retraction

Retracted: Integrated Urban Design Methodology of "Planning-Construction-Management" and Intelligent Management and Control Based on Teaching Reproduction Robot

Journal of Robotics

Received 23 January 2024; Accepted 23 January 2024; Published 24 January 2024

Copyright © 2024 Journal of Robotics. This is an open access article distributed under the Creative Commons Attribution License, which permits unrestricted use, distribution, and reproduction in any medium, provided the original work is properly cited.

This article has been retracted by Hindawi following an investigation undertaken by the publisher [1]. This investigation has uncovered evidence of one or more of the following indicators of systematic manipulation of the publication process:

(1) Discrepancies in scope
(2) Discrepancies in the description of the research reported
(3) Discrepancies between the availability of data and the research described
(4) Inappropriate citations
(5) Incoherent, meaningless and/or irrelevant content included in the article
(6) Manipulated or compromised peer review

The presence of these indicators undermines our confidence in the integrity of the article's content and we cannot, therefore, vouch for its reliability. Please note that this notice is intended solely to alert readers that the content of this article is unreliable. We have not investigated whether authors were aware of or involved in the systematic manipulation of the publication process.

Wiley and Hindawi regrets that the usual quality checks did not identify these issues before publication and have since put additional measures in place to safeguard research integrity.

We wish to credit our own Research Integrity and Research Publishing teams and anonymous and named external researchers and research integrity experts for contributing to this investigation.

The corresponding author, as the representative of all authors, has been given the opportunity to register their agreement or disagreement to this retraction. We have kept a record of any response received.

References

[1] H. Wang, "Integrated Urban Design Methodology of "Planning-Construction-Management" and Intelligent Management and Control Based on Teaching Reproduction Robot," *Journal of Robotics*, vol. 2022, Article ID 4669792, 9 pages, 2022.

Hindawi
Journal of Robotics
Volume 2024, Article ID 9868549, 1 page
https://doi.org/10.1155/2024/9868549

Retraction

Retracted: Application of Intelligent Robot Palletizer Technology in the Optimization of High-Speed Train Operation and Simulation Verification

Journal of Robotics

Received 23 January 2024; Accepted 23 January 2024; Published 24 January 2024

Copyright © 2024 Journal of Robotics. This is an open access article distributed under the Creative Commons Attribution License, which permits unrestricted use, distribution, and reproduction in any medium, provided the original work is properly cited.

This article has been retracted by Hindawi following an investigation undertaken by the publisher [1]. This investigation has uncovered evidence of one or more of the following indicators of systematic manipulation of the publication process:

(1) Discrepancies in scope
(2) Discrepancies in the description of the research reported
(3) Discrepancies between the availability of data and the research described
(4) Inappropriate citations
(5) Incoherent, meaningless and/or irrelevant content included in the article
(6) Manipulated or compromised peer review

The presence of these indicators undermines our confidence in the integrity of the article's content and we cannot, therefore, vouch for its reliability. Please note that this notice is intended solely to alert readers that the content of this article is unreliable. We have not investigated whether authors were aware of or involved in the systematic manipulation of the publication process.

Wiley and Hindawi regrets that the usual quality checks did not identify these issues before publication and have since put additional measures in place to safeguard research integrity.

We wish to credit our own Research Integrity and Research Publishing teams and anonymous and named external researchers and research integrity experts for contributing to this investigation.

The corresponding author, as the representative of all authors, has been given the opportunity to register their agreement or disagreement to this retraction. We have kept a record of any response received.

References

[1] X. Zhang, "Application of Intelligent Robot Palletizer Technology in the Optimization of High-Speed Train Operation and Simulation Verification," *Journal of Robotics*, vol. 2023, Article ID 2656636, 10 pages, 2023.

Hindawi
Journal of Robotics
Volume 2024, Article ID 9863834, 1 page
https://doi.org/10.1155/2024/9863834

Retraction

Retracted: Optimization of Intelligent Distribution of Distribution Network in the Presence of Distributed Sources

Journal of Robotics

Received 23 January 2024; Accepted 23 January 2024; Published 24 January 2024

Copyright © 2024 Journal of Robotics. This is an open access article distributed under the Creative Commons Attribution License, which permits unrestricted use, distribution, and reproduction in any medium, provided the original work is properly cited.

This article has been retracted by Hindawi following an investigation undertaken by the publisher [1]. This investigation has uncovered evidence of one or more of the following indicators of systematic manipulation of the publication process:

(1) Discrepancies in scope
(2) Discrepancies in the description of the research reported
(3) Discrepancies between the availability of data and the research described
(4) Inappropriate citations
(5) Incoherent, meaningless and/or irrelevant content included in the article
(6) Manipulated or compromised peer review

The presence of these indicators undermines our confidence in the integrity of the article's content and we cannot, therefore, vouch for its reliability. Please note that this notice is intended solely to alert readers that the content of this article is unreliable. We have not investigated whether authors were aware of or involved in the systematic manipulation of the publication process.

Wiley and Hindawi regrets that the usual quality checks did not identify these issues before publication and have since put additional measures in place to safeguard research integrity.

We wish to credit our own Research Integrity and Research Publishing teams and anonymous and named external researchers and research integrity experts for contributing to this investigation.

The corresponding author, as the representative of all authors, has been given the opportunity to register their agreement or disagreement to this retraction. We have kept a record of any response received.

References

[1] Y. Song, D. Nie, and L. Fan, "Optimization of Intelligent Distribution of Distribution Network in the Presence of Distributed Sources," *Journal of Robotics*, vol. 2022, Article ID 7063913, 11 pages, 2022.

Hindawi
Journal of Robotics
Volume 2024, Article ID 9863534, 1 page
https://doi.org/10.1155/2024/9863534

Retraction

Retracted: Discovery and Discrimination of Bridge Engineering Safety Issues by BIM Virtual Scene Combined with Robotic Mapping

Journal of Robotics

Received 23 January 2024; Accepted 23 January 2024; Published 24 January 2024

Copyright © 2024 Journal of Robotics. This is an open access article distributed under the Creative Commons Attribution License, which permits unrestricted use, distribution, and reproduction in any medium, provided the original work is properly cited.

This article has been retracted by Hindawi following an investigation undertaken by the publisher [1]. This investigation has uncovered evidence of one or more of the following indicators of systematic manipulation of the publication process:

(1) Discrepancies in scope
(2) Discrepancies in the description of the research reported
(3) Discrepancies between the availability of data and the research described
(4) Inappropriate citations
(5) Incoherent, meaningless and/or irrelevant content included in the article
(6) Manipulated or compromised peer review

The presence of these indicators undermines our confidence in the integrity of the article's content and we cannot, therefore, vouch for its reliability. Please note that this notice is intended solely to alert readers that the content of this article is unreliable. We have not investigated whether authors were aware of or involved in the systematic manipulation of the publication process.

Wiley and Hindawi regrets that the usual quality checks did not identify these issues before publication and have since put additional measures in place to safeguard research integrity.

We wish to credit our own Research Integrity and Research Publishing teams and anonymous and named external researchers and research integrity experts for contributing to this investigation.

The corresponding author, as the representative of all authors, has been given the opportunity to register their agreement or disagreement to this retraction. We have kept a record of any response received.

References

[1] G. Gong, S. Zeng, J. Gao, Q. Zhang, and X. Wang, "Discovery and Discrimination of Bridge Engineering Safety Issues by BIM Virtual Scene Combined with Robotic Mapping," *Journal of Robotics*, vol. 2023, Article ID 3028505, 12 pages, 2023.

Hindawi
Journal of Robotics
Volume 2024, Article ID 9848450, 1 page
https://doi.org/10.1155/2024/9848450

Retraction

Retracted: Safety Monitoring System and Method for Unmanned Operation of Unmanned Aerial Vehicle Distribution Network Based on Learning Control Robot Technology

Journal of Robotics

Received 23 January 2024; Accepted 23 January 2024; Published 24 January 2024

Copyright © 2024 Journal of Robotics. This is an open access article distributed under the Creative Commons Attribution License, which permits unrestricted use, distribution, and reproduction in any medium, provided the original work is properly cited.

This article has been retracted by Hindawi following an investigation undertaken by the publisher [1]. This investigation has uncovered evidence of one or more of the following indicators of systematic manipulation of the publication process:

(1) Discrepancies in scope
(2) Discrepancies in the description of the research reported
(3) Discrepancies between the availability of data and the research described
(4) Inappropriate citations
(5) Incoherent, meaningless and/or irrelevant content included in the article
(6) Manipulated or compromised peer review

The presence of these indicators undermines our confidence in the integrity of the article's content and we cannot, therefore, vouch for its reliability. Please note that this notice is intended solely to alert readers that the content of this article is unreliable. We have not investigated whether authors were aware of or involved in the systematic manipulation of the publication process.

Wiley and Hindawi regrets that the usual quality checks did not identify these issues before publication and have since put additional measures in place to safeguard research integrity.

We wish to credit our own Research Integrity and Research Publishing teams and anonymous and named external researchers and research integrity experts for contributing to this investigation.

The corresponding author, as the representative of all authors, has been given the opportunity to register their agreement or disagreement to this retraction. We have kept a record of any response received.

References

[1] B. Jia, Y. Jiang, T. Ma et al., "Safety Monitoring System and Method for Unmanned Operation of Unmanned Aerial Vehicle Distribution Network Based on Learning Control Robot Technology," *Journal of Robotics*, vol. 2022, Article ID 8559153, 10 pages, 2022.

Hindawi
Journal of Robotics
Volume 2024, Article ID 9843025, 1 page
https://doi.org/10.1155/2024/9843025

Retraction

Retracted: Optimization Design of Mountain and Water Landscape of Traditional Mountain Village Based on New Robot Visual Technology

Journal of Robotics

Received 23 January 2024; Accepted 23 January 2024; Published 24 January 2024

Copyright © 2024 Journal of Robotics. This is an open access article distributed under the Creative Commons Attribution License, which permits unrestricted use, distribution, and reproduction in any medium, provided the original work is properly cited.

This article has been retracted by Hindawi following an investigation undertaken by the publisher [1]. This investigation has uncovered evidence of one or more of the following indicators of systematic manipulation of the publication process:

(1) Discrepancies in scope
(2) Discrepancies in the description of the research reported
(3) Discrepancies between the availability of data and the research described
(4) Inappropriate citations
(5) Incoherent, meaningless and/or irrelevant content included in the article
(6) Manipulated or compromised peer review

The presence of these indicators undermines our confidence in the integrity of the article's content and we cannot, therefore, vouch for its reliability. Please note that this notice is intended solely to alert readers that the content of this article is unreliable. We have not investigated whether authors were aware of or involved in the systematic manipulation of the publication process.

Wiley and Hindawi regrets that the usual quality checks did not identify these issues before publication and have since put additional measures in place to safeguard research integrity.

We wish to credit our own Research Integrity and Research Publishing teams and anonymous and named external researchers and research integrity experts for contributing to this investigation.

The corresponding author, as the representative of all authors, has been given the opportunity to register their agreement or disagreement to this retraction. We have kept a record of any response received.

References

[1] X. Jia, R. Liu, and Z. Qiao, "Optimization Design of Mountain and Water Landscape of Traditional Mountain Village Based on New Robot Visual Technology," *Journal of Robotics*, vol. 2023, Article ID 4155090, 10 pages, 2023.

Hindawi
Journal of Robotics
Volume 2024, Article ID 9837908, 1 page
https://doi.org/10.1155/2024/9837908

Retraction

Retracted: On the Performance and Efficiency of Surface Air Cooler Working under High Temperature and High Humidity Condition

Journal of Robotics

Received 23 January 2024; Accepted 23 January 2024; Published 24 January 2024

Copyright © 2024 Journal of Robotics. This is an open access article distributed under the Creative Commons Attribution License, which permits unrestricted use, distribution, and reproduction in any medium, provided the original work is properly cited.

This article has been retracted by Hindawi following an investigation undertaken by the publisher [1]. This investigation has uncovered evidence of one or more of the following indicators of systematic manipulation of the publication process:

(1) Discrepancies in scope
(2) Discrepancies in the description of the research reported
(3) Discrepancies between the availability of data and the research described
(4) Inappropriate citations
(5) Incoherent, meaningless and/or irrelevant content included in the article
(6) Manipulated or compromised peer review

The presence of these indicators undermines our confidence in the integrity of the article's content and we cannot, therefore, vouch for its reliability. Please note that this notice is intended solely to alert readers that the content of this article is unreliable. We have not investigated whether authors were aware of or involved in the systematic manipulation of the publication process.

Wiley and Hindawi regrets that the usual quality checks did not identify these issues before publication and have since put additional measures in place to safeguard research integrity.

We wish to credit our own Research Integrity and Research Publishing teams and anonymous and named external researchers and research integrity experts for contributing to this investigation.

The corresponding author, as the representative of all authors, has been given the opportunity to register their agreement or disagreement to this retraction. We have kept a record of any response received.

References

[1] J. Yang, J. Yu, S. Wang, and W. Yan, "On the Performance and Efficiency of Surface Air Cooler Working under High Temperature and High Humidity Condition," *Journal of Robotics*, vol. 2022, Article ID 8656289, 11 pages, 2022.

Hindawi
Journal of Robotics
Volume 2024, Article ID 9831614, 1 page
https://doi.org/10.1155/2024/9831614

Retraction

Retracted: Attitude Analysis and Evaluation of Camera Based on Planar Double Joint Robot

Journal of Robotics

Received 23 January 2024; Accepted 23 January 2024; Published 24 January 2024

Copyright © 2024 Journal of Robotics. This is an open access article distributed under the Creative Commons Attribution License, which permits unrestricted use, distribution, and reproduction in any medium, provided the original work is properly cited.

This article has been retracted by Hindawi following an investigation undertaken by the publisher [1]. This investigation has uncovered evidence of one or more of the following indicators of systematic manipulation of the publication process:

(1) Discrepancies in scope
(2) Discrepancies in the description of the research reported
(3) Discrepancies between the availability of data and the research described
(4) Inappropriate citations
(5) Incoherent, meaningless and/or irrelevant content included in the article
(6) Manipulated or compromised peer review

The presence of these indicators undermines our confidence in the integrity of the article's content and we cannot, therefore, vouch for its reliability. Please note that this notice is intended solely to alert readers that the content of this article is unreliable. We have not investigated whether authors were aware of or involved in the systematic manipulation of the publication process.

Wiley and Hindawi regrets that the usual quality checks did not identify these issues before publication and have since put additional measures in place to safeguard research integrity.

We wish to credit our own Research Integrity and Research Publishing teams and anonymous and named external researchers and research integrity experts for contributing to this investigation.

The corresponding author, as the representative of all authors, has been given the opportunity to register their agreement or disagreement to this retraction. We have kept a record of any response received.

References

[1] Z. Xu, X. Wang, C. Chen, and J. Zhang, "Attitude Analysis and Evaluation of Camera Based on Planar Double Joint Robot," *Journal of Robotics*, vol. 2023, Article ID 8143828, 7 pages, 2023.

Hindawi
Journal of Robotics
Volume 2024, Article ID 9830829, 1 page
https://doi.org/10.1155/2024/9830829

Retraction

Retracted: Transmission Line Condition Monitoring Method Based on Binocular Vision and Edge Computing for Line Changing Robot

Journal of Robotics

Received 23 January 2024; Accepted 23 January 2024; Published 24 January 2024

Copyright © 2024 Journal of Robotics. This is an open access article distributed under the Creative Commons Attribution License, which permits unrestricted use, distribution, and reproduction in any medium, provided the original work is properly cited.

This article has been retracted by Hindawi following an investigation undertaken by the publisher [1]. This investigation has uncovered evidence of one or more of the following indicators of systematic manipulation of the publication process:

(1) Discrepancies in scope
(2) Discrepancies in the description of the research reported
(3) Discrepancies between the availability of data and the research described
(4) Inappropriate citations
(5) Incoherent, meaningless and/or irrelevant content included in the article
(6) Manipulated or compromised peer review

The presence of these indicators undermines our confidence in the integrity of the article's content and we cannot, therefore, vouch for its reliability. Please note that this notice is intended solely to alert readers that the content of this article is unreliable. We have not investigated whether authors were aware of or involved in the systematic manipulation of the publication process.

Wiley and Hindawi regrets that the usual quality checks did not identify these issues before publication and have since put additional measures in place to safeguard research integrity.

We wish to credit our own Research Integrity and Research Publishing teams and anonymous and named external researchers and research integrity experts for contributing to this investigation.

The corresponding author, as the representative of all authors, has been given the opportunity to register their agreement or disagreement to this retraction. We have kept a record of any response received.

References

[1] Z. Lu, J. Duan, X. Chen, and Y. Chen, "Transmission Line Condition Monitoring Method Based on Binocular Vision and Edge Computing for Line Changing Robot," *Journal of Robotics*, vol. 2023, Article ID 7747194, 10 pages, 2023.

Hindawi
Journal of Robotics
Volume 2024, Article ID 9830590, 1 page
https://doi.org/10.1155/2024/9830590

Retraction

Retracted: Optimization Path and Design of Intelligent Logistics Management System Based on ROS Robot

Journal of Robotics

Received 23 January 2024; Accepted 23 January 2024; Published 24 January 2024

Copyright © 2024 Journal of Robotics. This is an open access article distributed under the Creative Commons Attribution License, which permits unrestricted use, distribution, and reproduction in any medium, provided the original work is properly cited.

This article has been retracted by Hindawi following an investigation undertaken by the publisher [1]. This investigation has uncovered evidence of one or more of the following indicators of systematic manipulation of the publication process:

(1) Discrepancies in scope
(2) Discrepancies in the description of the research reported
(3) Discrepancies between the availability of data and the research described
(4) Inappropriate citations
(5) Incoherent, meaningless and/or irrelevant content included in the article
(6) Manipulated or compromised peer review

The presence of these indicators undermines our confidence in the integrity of the article's content and we cannot, therefore, vouch for its reliability. Please note that this notice is intended solely to alert readers that the content of this article is unreliable. We have not investigated whether authors were aware of or involved in the systematic manipulation of the publication process.

Wiley and Hindawi regrets that the usual quality checks did not identify these issues before publication and have since put additional measures in place to safeguard research integrity.

We wish to credit our own Research Integrity and Research Publishing teams and anonymous and named external researchers and research integrity experts for contributing to this investigation.

The corresponding author, as the representative of all authors, has been given the opportunity to register their agreement or disagreement to this retraction. We have kept a record of any response received.

References

[1] R. Wu, "Optimization Path and Design of Intelligent Logistics Management System Based on ROS Robot," *Journal of Robotics*, vol. 2023, Article ID 9505155, 9 pages, 2023.

Hindawi
Journal of Robotics
Volume 2024, Article ID 9819583, 1 page
https://doi.org/10.1155/2024/9819583

Retraction

Retracted: Design and Simulation Analysis of a Flexible Clamping and Conveying Device of a Green Leafy Vegetable Cutting and Bundling Integrated Machine

Journal of Robotics

Received 23 January 2024; Accepted 23 January 2024; Published 24 January 2024

Copyright © 2024 Journal of Robotics. This is an open access article distributed under the Creative Commons Attribution License, which permits unrestricted use, distribution, and reproduction in any medium, provided the original work is properly cited.

This article has been retracted by Hindawi following an investigation undertaken by the publisher [1]. This investigation has uncovered evidence of one or more of the following indicators of systematic manipulation of the publication process:

(1) Discrepancies in scope
(2) Discrepancies in the description of the research reported
(3) Discrepancies between the availability of data and the research described
(4) Inappropriate citations
(5) Incoherent, meaningless and/or irrelevant content included in the article
(6) Manipulated or compromised peer review

The presence of these indicators undermines our confidence in the integrity of the article's content and we cannot, therefore, vouch for its reliability. Please note that this notice is intended solely to alert readers that the content of this article is unreliable. We have not investigated whether authors were aware of or involved in the systematic manipulation of the publication process.

Wiley and Hindawi regrets that the usual quality checks did not identify these issues before publication and have since put additional measures in place to safeguard research integrity.

We wish to credit our own Research Integrity and Research Publishing teams and anonymous and named external researchers and research integrity experts for contributing to this investigation.

The corresponding author, as the representative of all authors, has been given the opportunity to register their agreement or disagreement to this retraction. We have kept a record of any response received.

References

[1] Z. Wang, T. Yang, and W. Wei, "Design and Simulation Analysis of a Flexible Clamping and Conveying Device of a Green Leafy Vegetable Cutting and Bundling Integrated Machine," *Journal of Robotics*, vol. 2022, Article ID 4729480, 9 pages, 2022.

Hindawi
Journal of Robotics
Volume 2024, Article ID 9819037, 1 page
https://doi.org/10.1155/2024/9819037

Retraction

Retracted: Reinforcement Learning-Based Continuous Action Space Path Planning Method for Mobile Robots

Journal of Robotics

Received 23 January 2024; Accepted 23 January 2024; Published 24 January 2024

Copyright © 2024 Journal of Robotics. This is an open access article distributed under the Creative Commons Attribution License, which permits unrestricted use, distribution, and reproduction in any medium, provided the original work is properly cited.

This article has been retracted by Hindawi following an investigation undertaken by the publisher [1]. This investigation has uncovered evidence of one or more of the following indicators of systematic manipulation of the publication process:

(1) Discrepancies in scope
(2) Discrepancies in the description of the research reported
(3) Discrepancies between the availability of data and the research described
(4) Inappropriate citations
(5) Incoherent, meaningless and/or irrelevant content included in the article
(6) Manipulated or compromised peer review

The presence of these indicators undermines our confidence in the integrity of the article's content and we cannot, therefore, vouch for its reliability. Please note that this notice is intended solely to alert readers that the content of this article is unreliable. We have not investigated whether authors were aware of or involved in the systematic manipulation of the publication process.

Wiley and Hindawi regrets that the usual quality checks did not identify these issues before publication and have since put additional measures in place to safeguard research integrity.

We wish to credit our own Research Integrity and Research Publishing teams and anonymous and named external researchers and research integrity experts for contributing to this investigation.

The corresponding author, as the representative of all authors, has been given the opportunity to register their agreement or disagreement to this retraction. We have kept a record of any response received.

References

[1] W. Zhang and G. Wang, "Reinforcement Learning-Based Continuous Action Space Path Planning Method for Mobile Robots," *Journal of Robotics*, vol. 2022, Article ID 9069283, 9 pages, 2022.

Hindawi
Journal of Robotics
Volume 2024, Article ID 9817514, 1 page
https://doi.org/10.1155/2024/9817514

Retraction

Retracted: Application of Multimedia Quality Evaluation Relying on Intelligent Robot Numerical Control Technology in New Energy Power Generation System

Journal of Robotics

Received 23 January 2024; Accepted 23 January 2024; Published 24 January 2024

Copyright © 2024 Journal of Robotics. This is an open access article distributed under the Creative Commons Attribution License, which permits unrestricted use, distribution, and reproduction in any medium, provided the original work is properly cited.

This article has been retracted by Hindawi following an investigation undertaken by the publisher [1]. This investigation has uncovered evidence of one or more of the following indicators of systematic manipulation of the publication process:

(1) Discrepancies in scope
(2) Discrepancies in the description of the research reported
(3) Discrepancies between the availability of data and the research described
(4) Inappropriate citations
(5) Incoherent, meaningless and/or irrelevant content included in the article
(6) Manipulated or compromised peer review

The presence of these indicators undermines our confidence in the integrity of the article's content and we cannot, therefore, vouch for its reliability. Please note that this notice is intended solely to alert readers that the content of this article is unreliable. We have not investigated whether authors were aware of or involved in the systematic manipulation of the publication process.

Wiley and Hindawi regrets that the usual quality checks did not identify these issues before publication and have since put additional measures in place to safeguard research integrity.

We wish to credit our own Research Integrity and Research Publishing teams and anonymous and named external researchers and research integrity experts for contributing to this investigation.

The corresponding author, as the representative of all authors, has been given the opportunity to register their agreement or disagreement to this retraction. We have kept a record of any response received.

References

[1] R. Sun and X. Dang, "Application of Multimedia Quality Evaluation Relying on Intelligent Robot Numerical Control Technology in New Energy Power Generation System," *Journal of Robotics*, vol. 2023, Article ID 7480917, 11 pages, 2023.

Hindawi
Journal of Robotics
Volume 2024, Article ID 9809817, 1 page
https://doi.org/10.1155/2024/9809817

Retraction

Retracted: Application of Intelligent Signal Reflection in the Communication Model of an Electronic Controller

Journal of Robotics

Received 23 January 2024; Accepted 23 January 2024; Published 24 January 2024

Copyright © 2024 Journal of Robotics. This is an open access article distributed under the Creative Commons Attribution License, which permits unrestricted use, distribution, and reproduction in any medium, provided the original work is properly cited.

This article has been retracted by Hindawi following an investigation undertaken by the publisher [1]. This investigation has uncovered evidence of one or more of the following indicators of systematic manipulation of the publication process:

(1) Discrepancies in scope
(2) Discrepancies in the description of the research reported
(3) Discrepancies between the availability of data and the research described
(4) Inappropriate citations
(5) Incoherent, meaningless and/or irrelevant content included in the article
(6) Manipulated or compromised peer review

The presence of these indicators undermines our confidence in the integrity of the article's content and we cannot, therefore, vouch for its reliability. Please note that this notice is intended solely to alert readers that the content of this article is unreliable. We have not investigated whether authors were aware of or involved in the systematic manipulation of the publication process.

Wiley and Hindawi regrets that the usual quality checks did not identify these issues before publication and have since put additional measures in place to safeguard research integrity.

We wish to credit our own Research Integrity and Research Publishing teams and anonymous and named external researchers and research integrity experts for contributing to this investigation.

The corresponding author, as the representative of all authors, has been given the opportunity to register their agreement or disagreement to this retraction. We have kept a record of any response received.

References

[1] L. Lan, "Application of Intelligent Signal Reflection in the Communication Model of an Electronic Controller," *Journal of Robotics*, vol. 2022, Article ID 8031024, 9 pages, 2022.

Hindawi
Journal of Robotics
Volume 2024, Article ID 9797639, 1 page
https://doi.org/10.1155/2024/9797639

Retraction

Retracted: Application of Microcontroller-Based Multipath Servos in Industrial Robot Control Systems

Journal of Robotics

Received 23 January 2024; Accepted 23 January 2024; Published 24 January 2024

Copyright © 2024 Journal of Robotics. This is an open access article distributed under the Creative Commons Attribution License, which permits unrestricted use, distribution, and reproduction in any medium, provided the original work is properly cited.

This article has been retracted by Hindawi following an investigation undertaken by the publisher [1]. This investigation has uncovered evidence of one or more of the following indicators of systematic manipulation of the publication process:

(1) Discrepancies in scope
(2) Discrepancies in the description of the research reported
(3) Discrepancies between the availability of data and the research described
(4) Inappropriate citations
(5) Incoherent, meaningless and/or irrelevant content included in the article
(6) Manipulated or compromised peer review

The presence of these indicators undermines our confidence in the integrity of the article's content and we cannot, therefore, vouch for its reliability. Please note that this notice is intended solely to alert readers that the content of this article is unreliable. We have not investigated whether authors were aware of or involved in the systematic manipulation of the publication process.

Wiley and Hindawi regrets that the usual quality checks did not identify these issues before publication and have since put additional measures in place to safeguard research integrity.

We wish to credit our own Research Integrity and Research Publishing teams and anonymous and named external researchers and research integrity experts for contributing to this investigation.

The corresponding author, as the representative of all authors, has been given the opportunity to register their agreement or disagreement to this retraction. We have kept a record of any response received.

References

[1] R. Hu, "Application of Microcontroller-Based Multipath Servos in Industrial Robot Control Systems," *Journal of Robotics*, vol. 2023, Article ID 7235120, 11 pages, 2023.

Hindawi
Journal of Robotics
Volume 2024, Article ID 9795848, 1 page
https://doi.org/10.1155/2024/9795848

Retraction

Retracted: Application of Image Processing Variation Model Based on Network Control Robot Image Transmission and Processing System in Multimedia Enhancement Technology

Journal of Robotics

Received 23 January 2024; Accepted 23 January 2024; Published 24 January 2024

Copyright © 2024 Journal of Robotics. This is an open access article distributed under the Creative Commons Attribution License, which permits unrestricted use, distribution, and reproduction in any medium, provided the original work is properly cited.

This article has been retracted by Hindawi following an investigation undertaken by the publisher [1]. This investigation has uncovered evidence of one or more of the following indicators of systematic manipulation of the publication process:

(1) Discrepancies in scope
(2) Discrepancies in the description of the research reported
(3) Discrepancies between the availability of data and the research described
(4) Inappropriate citations
(5) Incoherent, meaningless and/or irrelevant content included in the article
(6) Manipulated or compromised peer review

The presence of these indicators undermines our confidence in the integrity of the article's content and we cannot, therefore, vouch for its reliability. Please note that this notice is intended solely to alert readers that the content of this article is unreliable. We have not investigated whether authors were aware of or involved in the systematic manipulation of the publication process.

Wiley and Hindawi regrets that the usual quality checks did not identify these issues before publication and have since put additional measures in place to safeguard research integrity.

We wish to credit our own Research Integrity and Research Publishing teams and anonymous and named external researchers and research integrity experts for contributing to this investigation.

The corresponding author, as the representative of all authors, has been given the opportunity to register their agreement or disagreement to this retraction. We have kept a record of any response received.

References

[1] Y. Wu and J. Qi, "Application of Image Processing Variation Model Based on Network Control Robot Image Transmission and Processing System in Multimedia Enhancement Technology," *Journal of Robotics*, vol. 2022, Article ID 6991983, 10 pages, 2022.

Hindawi
Journal of Robotics
Volume 2024, Article ID 9792362, 1 page
https://doi.org/10.1155/2024/9792362

Retraction

Retracted: Collaboration and Management of Heterogeneous Robotic Systems for Road Network Construction, Management, and Maintenance under the Vision of "BIM + GIS" Technology

Journal of Robotics

Received 23 January 2024; Accepted 23 January 2024; Published 24 January 2024

Copyright © 2024 Journal of Robotics. This is an open access article distributed under the Creative Commons Attribution License, which permits unrestricted use, distribution, and reproduction in any medium, provided the original work is properly cited.

This article has been retracted by Hindawi following an investigation undertaken by the publisher [1]. This investigation has uncovered evidence of one or more of the following indicators of systematic manipulation of the publication process:

(1) Discrepancies in scope
(2) Discrepancies in the description of the research reported
(3) Discrepancies between the availability of data and the research described
(4) Inappropriate citations
(5) Incoherent, meaningless and/or irrelevant content included in the article
(6) Manipulated or compromised peer review

The presence of these indicators undermines our confidence in the integrity of the article's content and we cannot, therefore, vouch for its reliability. Please note that this notice is intended solely to alert readers that the content of this article is unreliable. We have not investigated whether authors were aware of or involved in the systematic manipulation of the publication process.

Wiley and Hindawi regrets that the usual quality checks did not identify these issues before publication and have since put additional measures in place to safeguard research integrity.

We wish to credit our own Research Integrity and Research Publishing teams and anonymous and named external researchers and research integrity experts for contributing to this investigation.

The corresponding author, as the representative of all authors, has been given the opportunity to register their agreement or disagreement to this retraction. We have kept a record of any response received.

References

[1] Z. Liu, W. Yan, J. Kou, and Z. Li, "Collaboration and Management of Heterogeneous Robotic Systems for Road Network Construction, Management, and Maintenance under the Vision of "BIM + GIS" Technology," *Journal of Robotics*, vol. 2023, Article ID 8259912, 8 pages, 2023.

Hindawi
Journal of Robotics
Volume 2024, Article ID 9785472, 1 page
https://doi.org/10.1155/2024/9785472

Retraction

Retracted: Design and Application of Electromechanical Control System Based on Computer Fault Tolerance Technology

Journal of Robotics

Received 23 January 2024; Accepted 23 January 2024; Published 24 January 2024

Copyright © 2024 Journal of Robotics. This is an open access article distributed under the Creative Commons Attribution License, which permits unrestricted use, distribution, and reproduction in any medium, provided the original work is properly cited.

This article has been retracted by Hindawi following an investigation undertaken by the publisher [1]. This investigation has uncovered evidence of one or more of the following indicators of systematic manipulation of the publication process:

(1) Discrepancies in scope
(2) Discrepancies in the description of the research reported
(3) Discrepancies between the availability of data and the research described
(4) Inappropriate citations
(5) Incoherent, meaningless and/or irrelevant content included in the article
(6) Manipulated or compromised peer review

The presence of these indicators undermines our confidence in the integrity of the article's content and we cannot, therefore, vouch for its reliability. Please note that this notice is intended solely to alert readers that the content of this article is unreliable. We have not investigated whether authors were aware of or involved in the systematic manipulation of the publication process.

Wiley and Hindawi regrets that the usual quality checks did not identify these issues before publication and have since put additional measures in place to safeguard research integrity.

We wish to credit our own Research Integrity and Research Publishing teams and anonymous and named external researchers and research integrity experts for contributing to this investigation.

The corresponding author, as the representative of all authors, has been given the opportunity to register their agreement or disagreement to this retraction. We have kept a record of any response received.

References

[1] R. Wei, "Design and Application of Electromechanical Control System Based on Computer Fault Tolerance Technology," *Journal of Robotics*, vol. 2022, Article ID 7716900, 10 pages, 2022.

Hindawi
Journal of Robotics
Volume 2024, Article ID 9767914, 1 page
https://doi.org/10.1155/2024/9767914

Retraction

Retracted: Parameter-Tunable RBF Neural Network Control Facing Dual-Joint Manipulators

Journal of Robotics

Received 23 January 2024; Accepted 23 January 2024; Published 24 January 2024

Copyright © 2024 Journal of Robotics. This is an open access article distributed under the Creative Commons Attribution License, which permits unrestricted use, distribution, and reproduction in any medium, provided the original work is properly cited.

This article has been retracted by Hindawi following an investigation undertaken by the publisher [1]. This investigation has uncovered evidence of one or more of the following indicators of systematic manipulation of the publication process:

(1) Discrepancies in scope
(2) Discrepancies in the description of the research reported
(3) Discrepancies between the availability of data and the research described
(4) Inappropriate citations
(5) Incoherent, meaningless and/or irrelevant content included in the article
(6) Manipulated or compromised peer review

The presence of these indicators undermines our confidence in the integrity of the article's content and we cannot, therefore, vouch for its reliability. Please note that this notice is intended solely to alert readers that the content of this article is unreliable. We have not investigated whether authors were aware of or involved in the systematic manipulation of the publication process.

Wiley and Hindawi regrets that the usual quality checks did not identify these issues before publication and have since put additional measures in place to safeguard research integrity.

We wish to credit our own Research Integrity and Research Publishing teams and anonymous and named external researchers and research integrity experts for contributing to this investigation.

The corresponding author, as the representative of all authors, has been given the opportunity to register their agreement or disagreement to this retraction. We have kept a record of any response received.

References

[1] W. Xu, "Parameter-Tunable RBF Neural Network Control Facing Dual-Joint Manipulators," *Journal of Robotics*, vol. 2022, Article ID 4231117, 10 pages, 2022.

Hindawi
Journal of Robotics
Volume 2023, Article ID 9874013, 1 page
https://doi.org/10.1155/2023/9874013

Retraction

Retracted: Analysis and Evaluation of Ecological Environment Monitoring Based on PIE Remote Sensing Image Processing Software

Journal of Robotics

Received 19 December 2023; Accepted 19 December 2023; Published 20 December 2023

Copyright © 2023 Journal of Robotics. This is an open access article distributed under the Creative Commons Attribution License, which permits unrestricted use, distribution, and reproduction in any medium, provided the original work is properly cited.

This article has been retracted by Hindawi following an investigation undertaken by the publisher [1]. This investigation has uncovered evidence of one or more of the following indicators of systematic manipulation of the publication process:

(1) Discrepancies in scope
(2) Discrepancies in the description of the research reported
(3) Discrepancies between the availability of data and the research described
(4) Inappropriate citations
(5) Incoherent, meaningless and/or irrelevant content included in the article
(6) Manipulated or compromised peer review

The presence of these indicators undermines our confidence in the integrity of the article's content and we cannot, therefore, vouch for its reliability. Please note that this notice is intended solely to alert readers that the content of this article is unreliable. We have not investigated whether authors were aware of or involved in the systematic manipulation of the publication process.

Wiley and Hindawi regrets that the usual quality checks did not identify these issues before publication and have since put additional measures in place to safeguard research integrity.

We wish to credit our own Research Integrity and Research Publishing teams and anonymous and named external researchers and research integrity experts for contributing to this investigation.

The corresponding author, as the representative of all authors, has been given the opportunity to register their agreement or disagreement to this retraction. We have kept a record of any response received.

References

[1] X. Wang and Z. Wang, "Analysis and Evaluation of Ecological Environment Monitoring Based on PIE Remote Sensing Image Processing Software," *Journal of Robotics*, vol. 2022, Article ID 1716756, 12 pages, 2022.

Hindawi
Journal of Robotics
Volume 2023, Article ID 9852312, 1 page
https://doi.org/10.1155/2023/9852312

Retraction

Retracted: The Application of Multimedia Visualization Platform in Business Management from the Perspective of Supply Chain Management

Journal of Robotics

Received 19 December 2023; Accepted 19 December 2023; Published 20 December 2023

Copyright © 2023 Journal of Robotics. This is an open access article distributed under the Creative Commons Attribution License, which permits unrestricted use, distribution, and reproduction in any medium, provided the original work is properly cited.

This article has been retracted by Hindawi following an investigation undertaken by the publisher [1]. This investigation has uncovered evidence of one or more of the following indicators of systematic manipulation of the publication process:

(1) Discrepancies in scope
(2) Discrepancies in the description of the research reported
(3) Discrepancies between the availability of data and the research described
(4) Inappropriate citations
(5) Incoherent, meaningless and/or irrelevant content included in the article
(6) Manipulated or compromised peer review

The presence of these indicators undermines our confidence in the integrity of the article's content and we cannot, therefore, vouch for its reliability. Please note that this notice is intended solely to alert readers that the content of this article is unreliable. We have not investigated whether authors were aware of or involved in the systematic manipulation of the publication process.

Wiley and Hindawi regrets that the usual quality checks did not identify these issues before publication and have since put additional measures in place to safeguard research integrity.

We wish to credit our own Research Integrity and Research Publishing teams and anonymous and named external researchers and research integrity experts for contributing to this investigation.

The corresponding author, as the representative of all authors, has been given the opportunity to register their agreement or disagreement to this retraction. We have kept a record of any response received.

References

[1] N. Wang, "The Application of Multimedia Visualization Platform in Business Management from the Perspective of Supply Chain Management," *Journal of Robotics*, vol. 2022, Article ID 1271691, 10 pages, 2022.

Hindawi
Journal of Robotics
Volume 2023, Article ID 9827679, 1 page
https://doi.org/10.1155/2023/9827679

Retraction

Retracted: Online Control Method of Small- and Medium-Sized Electromechanical Equipment Based on Deep Neural Network

Journal of Robotics

Received 19 December 2023; Accepted 19 December 2023; Published 20 December 2023

Copyright © 2023 Journal of Robotics. This is an open access article distributed under the Creative Commons Attribution License, which permits unrestricted use, distribution, and reproduction in any medium, provided the original work is properly cited.

This article has been retracted by Hindawi following an investigation undertaken by the publisher [1]. This investigation has uncovered evidence of one or more of the following indicators of systematic manipulation of the publication process:

(1) Discrepancies in scope
(2) Discrepancies in the description of the research reported
(3) Discrepancies between the availability of data and the research described
(4) Inappropriate citations
(5) Incoherent, meaningless and/or irrelevant content included in the article
(6) Manipulated or compromised peer review

The presence of these indicators undermines our confidence in the integrity of the article's content and we cannot, therefore, vouch for its reliability. Please note that this notice is intended solely to alert readers that the content of this article is unreliable. We have not investigated whether authors were aware of or involved in the systematic manipulation of the publication process.

Wiley and Hindawi regrets that the usual quality checks did not identify these issues before publication and have since put additional measures in place to safeguard research integrity.

We wish to credit our own Research Integrity and Research Publishing teams and anonymous and named external researchers and research integrity experts for contributing to this investigation.

The corresponding author, as the representative of all authors, has been given the opportunity to register their agreement or disagreement to this retraction. We have kept a record of any response received.

References

[1] M. Yang, S. Deng, and Z. Zhao, "Online Control Method of Small- and Medium-Sized Electromechanical Equipment Based on Deep Neural Network," *Journal of Robotics*, vol. 2022, Article ID 1607694, 10 pages, 2022.

Hindawi
Journal of Robotics
Volume 2023, Article ID 9824265, 1 page
https://doi.org/10.1155/2023/9824265

Retraction

Retracted: Machinery Changes and Challenges of Architecture and Landscape Design in the Virtual Reality Perspective

Journal of Robotics

Received 19 December 2023; Accepted 19 December 2023; Published 20 December 2023

Copyright © 2023 Journal of Robotics. This is an open access article distributed under the Creative Commons Attribution License, which permits unrestricted use, distribution, and reproduction in any medium, provided the original work is properly cited.

This article has been retracted by Hindawi following an investigation undertaken by the publisher [1]. This investigation has uncovered evidence of one or more of the following indicators of systematic manipulation of the publication process:

(1) Discrepancies in scope
(2) Discrepancies in the description of the research reported
(3) Discrepancies between the availability of data and the research described
(4) Inappropriate citations
(5) Incoherent, meaningless and/or irrelevant content included in the article
(6) Manipulated or compromised peer review

The presence of these indicators undermines our confidence in the integrity of the article's content and we cannot, therefore, vouch for its reliability. Please note that this notice is intended solely to alert readers that the content of this article is unreliable. We have not investigated whether authors were aware of or involved in the systematic manipulation of the publication process.

Wiley and Hindawi regrets that the usual quality checks did not identify these issues before publication and have since put additional measures in place to safeguard research integrity.

We wish to credit our own Research Integrity and Research Publishing teams and anonymous and named external researchers and research integrity experts for contributing to this investigation.

The corresponding author, as the representative of all authors, has been given the opportunity to register their agreement or disagreement to this retraction. We have kept a record of any response received.

References

[1] H. Jin and N. Zhang, "Machinery Changes and Challenges of Architecture and Landscape Design in the Virtual Reality Perspective," *Journal of Robotics*, vol. 2023, Article ID 1430551, 9 pages, 2023.

Hindawi
Journal of Robotics
Volume 2023, Article ID 9780273, 1 page
https://doi.org/10.1155/2023/9780273

Retraction

Retracted: Application of 5G Mobile Communication Technology Integrating Robot Controller Communication Method in Communication Engineering

Journal of Robotics

Received 19 December 2023; Accepted 19 December 2023; Published 20 December 2023

Copyright © 2023 Journal of Robotics. This is an open access article distributed under the Creative Commons Attribution License, which permits unrestricted use, distribution, and reproduction in any medium, provided the original work is properly cited.

This article has been retracted by Hindawi following an investigation undertaken by the publisher [1]. This investigation has uncovered evidence of one or more of the following indicators of systematic manipulation of the publication process:

(1) Discrepancies in scope
(2) Discrepancies in the description of the research reported
(3) Discrepancies between the availability of data and the research described
(4) Inappropriate citations
(5) Incoherent, meaningless and/or irrelevant content included in the article
(6) Manipulated or compromised peer review

The presence of these indicators undermines our confidence in the integrity of the article's content and we cannot, therefore, vouch for its reliability. Please note that this notice is intended solely to alert readers that the content of this article is unreliable. We have not investigated whether authors were aware of or involved in the systematic manipulation of the publication process.

Wiley and Hindawi regrets that the usual quality checks did not identify these issues before publication and have since put additional measures in place to safeguard research integrity.

We wish to credit our own Research Integrity and Research Publishing teams and anonymous and named external researchers and research integrity experts for contributing to this investigation.

The corresponding author, as the representative of all authors, has been given the opportunity to register their agreement or disagreement to this retraction. We have kept a record of any response received.

References

[1] Y. Chen, "Application of 5G Mobile Communication Technology Integrating Robot Controller Communication Method in Communication Engineering," *Journal of Robotics*, vol. 2023, Article ID 1857590, 9 pages, 2023.

Hindawi
Journal of Robotics
Volume 2023, Article ID 9768015, 1 page
https://doi.org/10.1155/2023/9768015

Retraction

Retracted: Designing and Manufacturing of Industrial Robots with Dual-Angle Sensors Taking into Account Vibration Signal Fusion

Journal of Robotics

Received 19 December 2023; Accepted 19 December 2023; Published 20 December 2023

Copyright © 2023 Journal of Robotics. This is an open access article distributed under the Creative Commons Attribution License, which permits unrestricted use, distribution, and reproduction in any medium, provided the original work is properly cited.

This article has been retracted by Hindawi following an investigation undertaken by the publisher [1]. This investigation has uncovered evidence of one or more of the following indicators of systematic manipulation of the publication process:

(1) Discrepancies in scope
(2) Discrepancies in the description of the research reported
(3) Discrepancies between the availability of data and the research described
(4) Inappropriate citations
(5) Incoherent, meaningless and/or irrelevant content included in the article
(6) Manipulated or compromised peer review

The presence of these indicators undermines our confidence in the integrity of the article's content and we cannot, therefore, vouch for its reliability. Please note that this notice is intended solely to alert readers that the content of this article is unreliable. We have not investigated whether authors were aware of or involved in the systematic manipulation of the publication process.

Wiley and Hindawi regrets that the usual quality checks did not identify these issues before publication and have since put additional measures in place to safeguard research integrity.

We wish to credit our own Research Integrity and Research Publishing teams and anonymous and named external researchers and research integrity experts for contributing to this investigation.

The corresponding author, as the representative of all authors, has been given the opportunity to register their agreement or disagreement to this retraction. We have kept a record of any response received.

References

[1] J. Yan and H. Cheng, "Designing and Manufacturing of Industrial Robots with Dual-Angle Sensors Taking into Account Vibration Signal Fusion," *Journal of Robotics*, vol. 2023, Article ID 1855226, 11 pages, 2023.

Hindawi
Journal of Robotics
Volume 2023, Article ID 9896453, 1 page
https://doi.org/10.1155/2023/9896453

Retraction

Retracted: Multiscale Motion Detection and Recognition Combining Still Images and Video Sequences

Journal of Robotics

Received 8 August 2023; Accepted 8 August 2023; Published 9 August 2023

Copyright © 2023 Journal of Robotics. This is an open access article distributed under the Creative Commons Attribution License, which permits unrestricted use, distribution, and reproduction in any medium, provided the original work is properly cited.

This article has been retracted by Hindawi following an investigation undertaken by the publisher [1]. This investigation has uncovered evidence of one or more of the following indicators of systematic manipulation of the publication process:

(1) Discrepancies in scope
(2) Discrepancies in the description of the research reported
(3) Discrepancies between the availability of data and the research described
(4) Inappropriate citations
(5) Incoherent, meaningless and/or irrelevant content included in the article
(6) Peer-review manipulation

The presence of these indicators undermines our confidence in the integrity of the article's content and we cannot, therefore, vouch for its reliability. Please note that this notice is intended solely to alert readers that the content of this article is unreliable. We have not investigated whether authors were aware of or involved in the systematic manipulation of the publication process.

Wiley and Hindawi regrets that the usual quality checks did not identify these issues before publication and have since put additional measures in place to safeguard research integrity.

We wish to credit our own Research Integrity and Research Publishing teams and anonymous and named external researchers and research integrity experts for contributing to this investigation.

The corresponding author, as the representative of all authors, has been given the opportunity to register their agreement or disagreement to this retraction. We have kept a record of any response received.

References

[1] Z. Chen, "Multiscale Motion Detection and Recognition Combining Still Images and Video Sequences," *Journal of Robotics*, vol. 2022, Article ID 7682559, 12 pages, 2022.

Hindawi
Journal of Robotics
Volume 2023, Article ID 9872574, 1 page
https://doi.org/10.1155/2023/9872574

Retraction

Retracted: Appearance Design Method of Ceramic Art Based on VR Visualization Technology

Journal of Robotics

Received 8 August 2023; Accepted 8 August 2023; Published 9 August 2023

Copyright © 2023 Journal of Robotics. This is an open access article distributed under the Creative Commons Attribution License, which permits unrestricted use, distribution, and reproduction in any medium, provided the original work is properly cited.

This article has been retracted by Hindawi following an investigation undertaken by the publisher [1]. This investigation has uncovered evidence of one or more of the following indicators of systematic manipulation of the publication process:

(1) Discrepancies in scope
(2) Discrepancies in the description of the research reported
(3) Discrepancies between the availability of data and the research described
(4) Inappropriate citations
(5) Incoherent, meaningless and/or irrelevant content included in the article
(6) Peer-review manipulation

The presence of these indicators undermines our confidence in the integrity of the article's content and we cannot, therefore, vouch for its reliability. Please note that this notice is intended solely to alert readers that the content of this article is unreliable. We have not investigated whether authors were aware of or involved in the systematic manipulation of the publication process.

Wiley and Hindawi regrets that the usual quality checks did not identify these issues before publication and have since put additional measures in place to safeguard research integrity.

We wish to credit our own Research Integrity and Research Publishing teams and anonymous and named external researchers and research integrity experts for contributing to this investigation.

The corresponding author, as the representative of all authors, has been given the opportunity to register their agreement or disagreement to this retraction. We have kept a record of any response received.

References

[1] H. Li, "Appearance Design Method of Ceramic Art Based on VR Visualization Technology," *Journal of Robotics*, vol. 2022, Article ID 7664404, 11 pages, 2022.

Hindawi
Journal of Robotics
Volume 2023, Article ID 9857401, 1 page
https://doi.org/10.1155/2023/9857401

Retraction

Retracted: Evaluation of the Students' Learning Status in the Foreign Language Classroom Based on Machine Vision

Journal of Robotics

Received 8 August 2023; Accepted 8 August 2023; Published 9 August 2023

Copyright © 2023 Journal of Robotics. This is an open access article distributed under the Creative Commons Attribution License, which permits unrestricted use, distribution, and reproduction in any medium, provided the original work is properly cited.

This article has been retracted by Hindawi following an investigation undertaken by the publisher [1]. This investigation has uncovered evidence of one or more of the following indicators of systematic manipulation of the publication process:

(1) Discrepancies in scope
(2) Discrepancies in the description of the research reported
(3) Discrepancies between the availability of data and the research described
(4) Inappropriate citations
(5) Incoherent, meaningless and/or irrelevant content included in the article
(6) Peer-review manipulation

The presence of these indicators undermines our confidence in the integrity of the article's content and we cannot, therefore, vouch for its reliability. Please note that this notice is intended solely to alert readers that the content of this article is unreliable. We have not investigated whether authors were aware of or involved in the systematic manipulation of the publication process.

In addition, our investigation has also shown that one or more of the following human-subject reporting requirements has not been met in this article: ethical approval by an Institutional Review Board (IRB) committee or equivalent, patient/participant consent to participate, and/or agreement to publish patient/participant details (where relevant).

Wiley and Hindawi regrets that the usual quality checks did not identify these issues before publication and have since put additional measures in place to safeguard research integrity.

We wish to credit our own Research Integrity and Research Publishing teams and anonymous and named external researchers and research integrity experts for contributing to this investigation.

The corresponding author, as the representative of all authors, has been given the opportunity to register their agreement or disagreement to this retraction. We have kept a record of any response received.

References

[1] L. Yao and Q. Qin, "Evaluation of the Students' Learning Status in the Foreign Language Classroom Based on Machine Vision," *Journal of Robotics*, vol. 2022, Article ID 6432133, 12 pages, 2022.

Hindawi
Journal of Robotics
Volume 2023, Article ID 9845964, 1 page
https://doi.org/10.1155/2023/9845964

Retraction

Retracted: Deep Learning BP Neural Network Guided Evaluation of Students' Innovation and Entrepreneurship Education

Journal of Robotics

Received 8 August 2023; Accepted 8 August 2023; Published 9 August 2023

Copyright © 2023 Journal of Robotics. This is an open access article distributed under the Creative Commons Attribution License, which permits unrestricted use, distribution, and reproduction in any medium, provided the original work is properly cited.

This article has been retracted by Hindawi following an investigation undertaken by the publisher [1]. This investigation has uncovered evidence of one or more of the following indicators of systematic manipulation of the publication process:

(1) Discrepancies in scope
(2) Discrepancies in the description of the research reported
(3) Discrepancies between the availability of data and the research described
(4) Inappropriate citations
(5) Incoherent, meaningless and/or irrelevant content included in the article
(6) Peer-review manipulation

The presence of these indicators undermines our confidence in the integrity of the article's content and we cannot, therefore, vouch for its reliability. Please note that this notice is intended solely to alert readers that the content of this article is unreliable. We have not investigated whether authors were aware of or involved in the systematic manipulation of the publication process.

In addition, our investigation has also shown that one or more of the following human-subject reporting requirements has not been met in this article: ethical approval by an Institutional Review Board (IRB) committee or equivalent, patient/participant consent to participate, and/or agreement to publish patient/participant details (where relevant).

Wiley and Hindawi regrets that the usual quality checks did not identify these issues before publication and have since put additional measures in place to safeguard research integrity.

We wish to credit our own Research Integrity and Research Publishing teams and anonymous and named external researchers and research integrity experts for contributing to this investigation.

The corresponding author, as the representative of all authors, has been given the opportunity to register their agreement or disagreement to this retraction. We have kept a record of any response received.

References

[1] J. Yi and X. Cui, "Deep Learning BP Neural Network Guided Evaluation of Students' Innovation and Entrepreneurship Education," *Journal of Robotics*, vol. 2022, Article ID 2425069, 10 pages, 2022.

Hindawi
Journal of Robotics
Volume 2023, Article ID 9832350, 1 page
https://doi.org/10.1155/2023/9832350

Retraction

Retracted: A Russian Continuous Speech Recognition System Based on the DTW Algorithm under Artificial Intelligence

Journal of Robotics

Received 8 August 2023; Accepted 8 August 2023; Published 9 August 2023

Copyright © 2023 Journal of Robotics. This is an open access article distributed under the Creative Commons Attribution License, which permits unrestricted use, distribution, and reproduction in any medium, provided the original work is properly cited.

This article has been retracted by Hindawi following an investigation undertaken by the publisher [1]. This investigation has uncovered evidence of one or more of the following indicators of systematic manipulation of the publication process:

(1) Discrepancies in scope
(2) Discrepancies in the description of the research reported
(3) Discrepancies between the availability of data and the research described
(4) Inappropriate citations
(5) Incoherent, meaningless and/or irrelevant content included in the article
(6) Peer-review manipulation

The presence of these indicators undermines our confidence in the integrity of the article's content and we cannot, therefore, vouch for its reliability. Please note that this notice is intended solely to alert readers that the content of this article is unreliable. We have not investigated whether authors were aware of or involved in the systematic manipulation of the publication process.

Wiley and Hindawi regrets that the usual quality checks did not identify these issues before publication and have since put additional measures in place to safeguard research integrity.

We wish to credit our own Research Integrity and Research Publishing teams and anonymous and named external researchers and research integrity experts for contributing to this investigation.

The corresponding author, as the representative of all authors, has been given the opportunity to register their agreement or disagreement to this retraction. We have kept a record of any response received.

References

[1] C. Yu and X. Wang, "A Russian Continuous Speech Recognition System Based on the DTW Algorithm under Artificial Intelligence," *Journal of Robotics*, vol. 2022, Article ID 5777472, 11 pages, 2022.

Hindawi
Journal of Robotics
Volume 2023, Article ID 9807401, 1 page
https://doi.org/10.1155/2023/9807401

Retraction

Retracted: The Evaluation of Visual Clarity and Comfort of Light Environment in Multimedia Classroom

Journal of Robotics

Received 8 August 2023; Accepted 8 August 2023; Published 9 August 2023

Copyright © 2023 Journal of Robotics. This is an open access article distributed under the Creative Commons Attribution License, which permits unrestricted use, distribution, and reproduction in any medium, provided the original work is properly cited.

This article has been retracted by Hindawi following an investigation undertaken by the publisher [1]. This investigation has uncovered evidence of one or more of the following indicators of systematic manipulation of the publication process:

(1) Discrepancies in scope
(2) Discrepancies in the description of the research reported
(3) Discrepancies between the availability of data and the research described
(4) Inappropriate citations
(5) Incoherent, meaningless and/or irrelevant content included in the article
(6) Peer-review manipulation

The presence of these indicators undermines our confidence in the integrity of the article's content and we cannot, therefore, vouch for its reliability. Please note that this notice is intended solely to alert readers that the content of this article is unreliable. We have not investigated whether authors were aware of or involved in the systematic manipulation of the publication process.

In addition, our investigation has also shown that one or more of the following human-subject reporting requirements has not been met in this article: ethical approval by an Institutional Review Board (IRB) committee or equivalent, patient/participant consent to participate, and/or agreement to publish patient/participant details (where relevant).

Wiley and Hindawi regrets that the usual quality checks did not identify these issues before publication and have since put additional measures in place to safeguard research integrity.

We wish to credit our own Research Integrity and Research Publishing teams and anonymous and named external researchers and research integrity experts for contributing to this investigation.

The corresponding author, as the representative of all authors, has been given the opportunity to register their agreement or disagreement to this retraction. We have kept a record of any response received.

References

[1] Y. Dong, M. Xi, and M. Hu, "The Evaluation of Visual Clarity and Comfort of Light Environment in Multimedia Classroom," *Journal of Robotics*, vol. 2022, Article ID 4917352, 12 pages, 2022.

Hindawi
Journal of Robotics
Volume 2023, Article ID 9789505, 1 page
https://doi.org/10.1155/2023/9789505

Retraction

Retracted: Discussion on Redundant Processing Algorithm of Association Rules Based on Hypergraph in Data Mining

Journal of Robotics

Received 8 August 2023; Accepted 8 August 2023; Published 9 August 2023

Copyright © 2023 Journal of Robotics. This is an open access article distributed under the Creative Commons Attribution License, which permits unrestricted use, distribution, and reproduction in any medium, provided the original work is properly cited.

This article has been retracted by Hindawi following an investigation undertaken by the publisher [1]. This investigation has uncovered evidence of one or more of the following indicators of systematic manipulation of the publication process:

(1) Discrepancies in scope
(2) Discrepancies in the description of the research reported
(3) Discrepancies between the availability of data and the research described
(4) Inappropriate citations
(5) Incoherent, meaningless and/or irrelevant content included in the article
(6) Peer-review manipulation

The presence of these indicators undermines our confidence in the integrity of the article's content and we cannot, therefore, vouch for its reliability. Please note that this notice is intended solely to alert readers that the content of this article is unreliable. We have not investigated whether authors were aware of or involved in the systematic manipulation of the publication process.

Wiley and Hindawi regrets that the usual quality checks did not identify these issues before publication and have since put additional measures in place to safeguard research integrity.

We wish to credit our own Research Integrity and Research Publishing teams and anonymous and named external researchers and research integrity experts for contributing to this investigation.

The corresponding author, as the representative of all authors, has been given the opportunity to register their agreement or disagreement to this retraction. We have kept a record of any response received.

References

[1] J. Zhu, "Discussion on Redundant Processing Algorithm of Association Rules Based on Hypergraph in Data Mining," *Journal of Robotics*, vol. 2022, Article ID 1007464, 9 pages, 2022.

Hindawi
Journal of Robotics
Volume 2023, Article ID 9768653, 1 page
https://doi.org/10.1155/2023/9768653

Retraction

Retracted: Recognition and Modeling of Crisis Propagation Patterns Combined with Robot Simulation of Social Networks

Journal of Robotics

Received 8 August 2023; Accepted 8 August 2023; Published 9 August 2023

Copyright © 2023 Journal of Robotics. This is an open access article distributed under the Creative Commons Attribution License, which permits unrestricted use, distribution, and reproduction in any medium, provided the original work is properly cited.

This article has been retracted by Hindawi following an investigation undertaken by the publisher [1]. This investigation has uncovered evidence of one or more of the following indicators of systematic manipulation of the publication process:

(1) Discrepancies in scope
(2) Discrepancies in the description of the research reported
(3) Discrepancies between the availability of data and the research described
(4) Inappropriate citations
(5) Incoherent, meaningless and/or irrelevant content included in the article
(6) Peer-review manipulation

The presence of these indicators undermines our confidence in the integrity of the article's content and we cannot, therefore, vouch for its reliability. Please note that this notice is intended solely to alert readers that the content of this article is unreliable. We have not investigated whether authors were aware of or involved in the systematic manipulation of the publication process.

Wiley and Hindawi regrets that the usual quality checks did not identify these issues before publication and have since put additional measures in place to safeguard research integrity.

We wish to credit our own Research Integrity and Research Publishing teams and anonymous and named external researchers and research integrity experts for contributing to this investigation.

The corresponding author, as the representative of all authors, has been given the opportunity to register their agreement or disagreement to this retraction. We have kept a record of any response received.

References

[1] Y. Wang, "Recognition and Modeling of Crisis Propagation Patterns Combined with Robot Simulation of Social Networks," *Journal of Robotics*, vol. 2022, Article ID 3454396, 12 pages, 2022.

Hindawi
Journal of Robotics
Volume 2023, Article ID 9768081, 1 page
https://doi.org/10.1155/2023/9768081

Retraction

Retracted: Feature Extraction and Analysis Method of Trombone Timbre Based on CNN Model

Journal of Robotics

Received 8 August 2023; Accepted 8 August 2023; Published 9 August 2023

Copyright © 2023 Journal of Robotics. This is an open access article distributed under the Creative Commons Attribution License, which permits unrestricted use, distribution, and reproduction in any medium, provided the original work is properly cited.

This article has been retracted by Hindawi following an investigation undertaken by the publisher [1]. This investigation has uncovered evidence of one or more of the following indicators of systematic manipulation of the publication process:

(1) Discrepancies in scope
(2) Discrepancies in the description of the research reported
(3) Discrepancies between the availability of data and the research described
(4) Inappropriate citations
(5) Incoherent, meaningless and/or irrelevant content included in the article
(6) Peer-review manipulation

The presence of these indicators undermines our confidence in the integrity of the article's content and we cannot, therefore, vouch for its reliability. Please note that this notice is intended solely to alert readers that the content of this article is unreliable. We have not investigated whether authors were aware of or involved in the systematic manipulation of the publication process.

Wiley and Hindawi regrets that the usual quality checks did not identify these issues before publication and have since put additional measures in place to safeguard research integrity.

We wish to credit our own Research Integrity and Research Publishing teams and anonymous and named external researchers and research integrity experts for contributing to this investigation.

The corresponding author, as the representative of all authors, has been given the opportunity to register their agreement or disagreement to this retraction. We have kept a record of any response received.

References

[1] Y. Wang, "Feature Extraction and Analysis Method of Trombone Timbre Based on CNN Model," *Journal of Robotics*, vol. 2022, Article ID 9460208, 12 pages, 2022.

Hindawi
Journal of Robotics
Volume 2024, Article ID 9868549, 1 page
https://doi.org/10.1155/2024/9868549

Retraction

Retracted: Application of Intelligent Robot Palletizer Technology in the Optimization of High-Speed Train Operation and Simulation Verification

Journal of Robotics

Received 23 January 2024; Accepted 23 January 2024; Published 24 January 2024

Copyright © 2024 Journal of Robotics. This is an open access article distributed under the Creative Commons Attribution License, which permits unrestricted use, distribution, and reproduction in any medium, provided the original work is properly cited.

This article has been retracted by Hindawi following an investigation undertaken by the publisher [1]. This investigation has uncovered evidence of one or more of the following indicators of systematic manipulation of the publication process:

(1) Discrepancies in scope
(2) Discrepancies in the description of the research reported
(3) Discrepancies between the availability of data and the research described
(4) Inappropriate citations
(5) Incoherent, meaningless and/or irrelevant content included in the article
(6) Manipulated or compromised peer review

The presence of these indicators undermines our confidence in the integrity of the article's content and we cannot, therefore, vouch for its reliability. Please note that this notice is intended solely to alert readers that the content of this article is unreliable. We have not investigated whether authors were aware of or involved in the systematic manipulation of the publication process.

Wiley and Hindawi regrets that the usual quality checks did not identify these issues before publication and have since put additional measures in place to safeguard research integrity.

We wish to credit our own Research Integrity and Research Publishing teams and anonymous and named external researchers and research integrity experts for contributing to this investigation.

The corresponding author, as the representative of all authors, has been given the opportunity to register their agreement or disagreement to this retraction. We have kept a record of any response received.

References

[1] X. Zhang, "Application of Intelligent Robot Palletizer Technology in the Optimization of High-Speed Train Operation and Simulation Verification," *Journal of Robotics*, vol. 2023, Article ID 2656636, 10 pages, 2023.

Hindawi
Journal of Robotics
Volume 2023, Article ID 2656636, 10 pages
https://doi.org/10.1155/2023/2656636

RETRACTED

Research Article

Application of Intelligent Robot Palletizer Technology in the Optimization of High-Speed Train Operation and Simulation Verification

Xiaoling Zhang

Henan Rail Transit Intelligent Safety Engineering Technology Research Center, Zhengzhou, Henan 451460, China

Correspondence should be addressed to Xiaoling Zhang; 10359@zzrvtc.edu.cn

Received 4 November 2022; Revised 6 April 2023; Accepted 27 April 2023; Published 31 May 2023

Academic Editor: Iqbal Ahmad

Copyright © 2023 Xiaoling Zhang. This is an open access article distributed under the Creative Commons Attribution License, which permits unrestricted use, distribution, and reproduction in any medium, provided the original work is properly cited.

With the continuous development of society and economy, energy consumption and exhaust emissions of high-speed trains have also gained more and more attention from the industry. Hence, optimizing the operation of high-speed trains is of pivotal significance to achieve optimization as required. On the basis of the intelligent robot palletizer technology, a spatial construction method and intelligent robot palletizer capable of operating through the dispatching of high-speed trains are put forward in this paper on the basis of the situation of high-speed trains assigned. The method of changing the arrival time of the trains and the order of departure are adopted to control the operation of the high-speed trains in an efficient and intelligent manner. With regard to the intervals of departure time, the overtaking of trains and other issues, a three-dimensional spatial travel route is established and used for processing. The intelligent robot palletizer is used to implement the dispatching of trains in the aspect of height. Subsequently, the minimum value method and secure network technology are used to verify that the technology of the intelligent robot palletizer is mature and reliable. Finally, a practical case analysis is carried out in this paper on some sections of the Harbin–Dalian high-speed railway to verify the accuracy and effectiveness of the method proposed in this paper. Through the comparative analysis with other methods, the advantages of the algorithm put forward in this paper can be observed.

1. Introduction

As society and economy continue to develop, high-speed trains are no longer a luxury but a common commodity that is available to millions of households. With this comes the issue of security, and it is vital to ensure the safety of drivers, which is the first priority in the operation of high-speed trains. Thus, from the perspective of the manufacturers, reducing the car body weight of high-speed trains can achieve the effect of energy conservation and emission reduction on the one hand; on the other hand, with the reduction of car body weight, the corresponding inertia will also be smaller. In recent years, as the studies on the operational optimization of high-speed trains have intensified and become more in-depth, the application of operationally optimized materials, lighter structures, and other measures are adopted to lower the mass of the car body on the premise of ensuring that the structural properties of the car body remain unchanged. Both stiffness and modal indicators for the car body operation are optimized [1–4]. At the same time, the optimization of the car body operation does not mean that it has to be achieved at the cost of reduced security settings. On the one hand, high-strength steel, aluminum-magnesium alloy, and other related materials can be applied for the analysis and application in the optimization of the car body operation. On the other hand, on the premise of the existing materials and technologies, efforts are made to reduce the mass of each component as much as possible and finally achieve the goal of optimizing the vehicle mechanism operation [5, 6]. However, in the application of structure operation optimization in the high-speed trains, it is necessary to ensure that the demand of security in the event of car body collision can be met. Operation optimization of the car body is a multiparameter, complex optimization

proposition that requires constant and comprehensive testing of the body performance of trains. Efforts made to make modifications or mitigation based solely on the experiences often result in other effects that fail to meet and guaranty the demand for the performance as desired. Therefore, it is necessary to analyze the quantitative function of the structural performance of the car body so as to achieve the capacity to mitigate the car body issues and optimize the operation after multiple tests and simulation. When the actual train operation plan deviates from the planned train operation in some aspects, it can directly disrupt the overall order of train operation. In this case, the train dispatcher should adjust the train operation plan quickly so that the operation of trains can comply with the original plan as soon as possible and therefore reduce the deviation between the actual train operation plan and the planned train operation to a certain extent. In general, the deviation is measured by data such as throughput, accuracy, and so on, which is also the target for the control and adjustment in the dispatching of trains [7–9].

For the purpose of raising the comprehensive evaluation capability of all high-speed trains in the aspect of operation optimization, it is necessary to extract the features of the starting and ending points of high-speed train operation. Thus, a comprehensive evaluation method for all high-speed trains is put forward on the basis of machine image vision processing. In combination with the extraction of features related to edge contours and the detection method for determining the diagonal points, a comprehensive evaluation is carried out on the operating status of high-speed trains. The process of acquiring the operating state is verified for high-speed trains in the aspect of the edge contours in the images of the operating state acquired by the robot. At the same time, a distributed reconstructed model for the operational status information of high-speed trains is constructed by visualizing and integrating the operational status of high-speed trains based on the method of reconstructing the information on the boundary area. Through sorting out the corresponding business flow of high-speed trains during the operation, the relevant quality indicators for high-speed train are analyzed and the system is established and tested accordingly [10, 11]. On the basis of the operational state for action analysis, the LSTM model is adopted to carry out indicator screening, and the corresponding simulation experiments are performed to build a regression model, with the purpose to develop an appropriate operation plan corresponding to the quality of high-speed trains, thereby providing the corresponding decision-making basis as a reference and the support for the scientific operation of high-speed trains. For the purpose of acquiring an effective fusion of image information on the operating status of high-speed trains, a comprehensive evaluation of the routine operating status of high-speed trains can be implemented on the basis of the final results of image fusion. A linear integer programming method of the combination type is applied to create a model for the effective control of the train movement form. In this way, the ultimate goal to minimize delays and maximize the durability of the train operation can be accomplished in accordance with the plan. In addition, a heuristic algorithm is used to identify and resolve conflicts of the functions from a certain perspective. The strategy applied is to adjust trains that are late as soon as possible before station disruptions even occur, and a relatively mixed integer programming model is developed with the purpose to reduce the value of the total weighted train delays and the number of canceled trains as much as possible and to impose the constraints continuously by ensuring a certain interval of time, station capacity, and so on. A relatively rough serial model is developed for the control of train traffic, and an algorithm with more simplified operational control is put forward accordingly. However, two relatively significant problems have not yet been solved: no specific and operational adaptation strategies have been put forward, and the computational process is highly complicated in general [12, 13].

In this paper, an effective solution method for construction at the spatial level is put forward, which mainly transforms the timing problem into three spatial regions with different dimensions. For the purpose of further increasing the speed of convergence and improving the effectiveness of the algorithm, a series of heuristic coefficients, expectation type coefficients, and dynamic control methods required for the pheromone generation evaporation coefficients of the data are explored.

2. Train Dispatching Model Based on the Intelligent Robot Palletizer Technology

The structure of the train dispatching based on the technology of the intelligent robot palletizer is illustrated in Figure 1 as the following [14]. In this paper, a four-degree-of-freedom intelligent robot palletizer is used, which is mainly composed of a robot base, a waist, and large and small arms, in which the robot arms can perform actions at four degrees of rotation.

With regard to the operation of high-speed train operation, it can be divided into two steps. The first step is to carry out comprehensive research and judgment of the stiffness and modal performance of high-speed trains so as to ensure the quality of the high-speed trains on the premise of achieving the optimization goals without reducing the performance. In the optimization, the replacement of car body materials is taken into consideration, which is adjusted and optimized in accordance with the production cost of car body parts and the technical level of the modern processes. For passengers and drivers, the practical simulation of driving and riding simulation is carried out, and the operation results before and after the optimization of the simulation design are compared. If the difference of the simulation results exceeds the set threshold, the security performance requirements in case of collision are not met; on the other hand, if the difference of the simulation results is within the set threshold, the security performance requirements are met [15, 16]. The process is performed until the optimization process of high-speed train operation optimization is finally accomplished.

The so-called quantitative calculation of function approximation is carried out on the basis of statistical and

RETRACTED

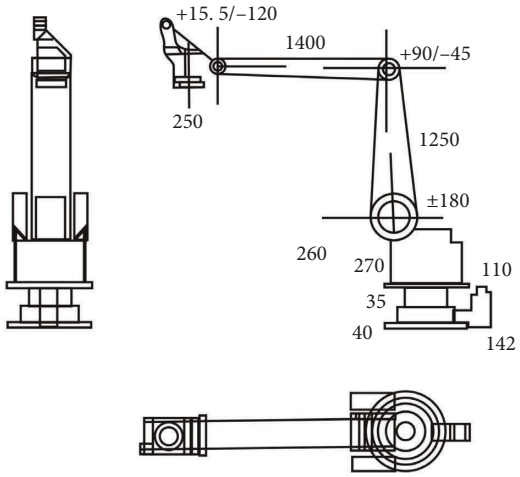

Figure 1: Structure diagram of robot palletizer.

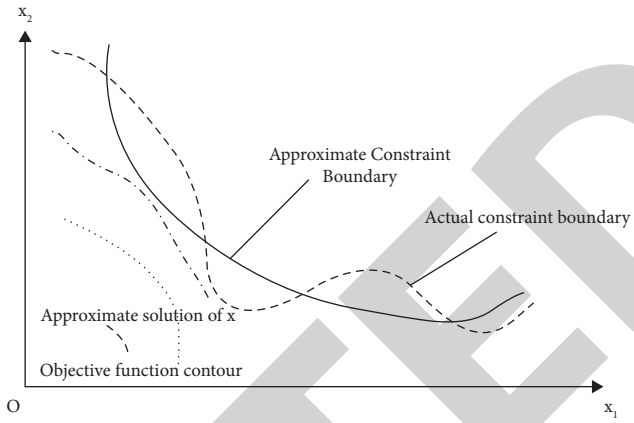

Figure 2: Difference in the actual/approximate constraint boundaries.

numerical calculations to implement the fitting of the function across all samples on the basis of a limited number of discrete samples, that is, the process of predicting the unknown part through establishing a function expression by using the existing sample points. Taking the number of samples and function simulation into comprehensive consideration, the minimization deviation sum of squares function is selected in this paper for parameter optimization, and the details are shown in equation (1) as follows:

$$\min \sum_{k=1}^{n} \left[\widehat{y}\left(X^{(k)}\right) - y\left(X^{(k)}\right)\right]^2. \tag{1}$$

In the abovementioned equation, the number of experiments is denoted by n, X stands for the vector of variables, y stands for the actual parameter response value, and $\min f(x)$ stands for the predicted value.

As far as the constraint function is concerned, comprehensive consideration is made in this paper to improve the accuracy of the proposed model by increasing the sample points, and the specific constraint boundary is shown in Figure 2 as follows.

For the purpose of further ensuring that the predicted value of the response function is closer to the actual value, the predicted value of the sample space needs to be distributed on the safe side of the constraint boundary as much as possible, and the details are shown in equation (2) as follows:

$$\widehat{g}(X) - g(X) \geq 0. \tag{2}$$

On the basis of equation (2) mentioned above, the corresponding constraint function is added for the optimization of the model, that is, the global approximation is carried out while ensuring the validity of the approximation boundary at the same time. The details are shown in equation (3) as follows:

$$\begin{aligned} &\min \sum_{k=1}^{n} \left[\widehat{g}\left(X^{(k)}\right) - g\left(X^{(k)}\right)\right]^2, \\ &s.t.\ \widehat{g}\left(X^{(k)}\right) - g\left(X^{(k)}\right) \geq 0. \end{aligned} \tag{3}$$

For the purpose of analyzing the starting point and the end point features of the routine operation status of high-speed trains in the operation status model, it is necessary to construct a model for acquiring the information related to the routine operation status of high-speed trains in the operation status model. In the process of acquiring the relevant operation status, the images of the routine operation status of high-speed trains obtained by the robot are verified in the edge contour. At the same time, a fusion analysis method is further used to verify the pixel points related to the routine operation sequence of high-speed trains in the operating state model on the basis of data samples with a higher dimension. The image processing model is applied to create profiles for the routine operation of high-speed trains in the operating model, and a three-dimensional geometric model of the distribution of the routine operating state of the high-speed train in the operating state model is established [17, 18]. Finally, the sequence of associated instantaneous feature distributions thus acquired is calculated according to the equation as follows:

$$Dif\left(C_1, C_2\right) = \min k(x, y). \tag{4}$$

In the abovementioned equation, the letter x and letter y stand for the sampling features of the high-speed train in the operating state mode based on the routine operating state information model, respectively, and the letter k stands for the specific value of the similar neighboring points. The mapping relationship formula for the display circuit is used to implement the relevant operating state of the high-speed train. In addition, the specific method for identifying the relevant edge profile is combined to analyze the main features of the routine operating state of high-speed trains in the operating state mode, and a specific model for the integration of the distribution of the fused features in the operation of the high-speed trains is obtained on this basis.

Through the identification of the relational data on the mapping equation between the low-dimensional space and the high-dimensional space and the computation on the basis of the variational approach provided by the Eulerian

REJECTED

Lagrangian equation, an image acquisition model dedicated to the routine operational state of the high-speed train operation can be established as follows [19]:

$$\frac{\partial \varphi}{\partial t} = \varphi Dif(C_1, C_2) + \delta(z)\left(\nabla^2 \varphi - \operatorname{div}\left(\frac{\nabla \varphi}{|\nabla \varphi|}\right)\right). \quad (5)$$

In equation (5) mentioned above, the symbol φ is used as a chunking function Heaviside to indicate the routine operating state of the high-speed trains in the operating state mode with regard to the pixel sequence distribution, and the function equation $\delta(z) = (d/dz)H(z)$ is used to indicate the grayscale value of the pixels. Thus, the relevant analysis can be carried out on the basis of the results of data acquisition at the starting point and the ending point of smashing in the volleyball sports.

In this model, a method related to visual fusion is adopted to convert the routine operating state of the high-speed trains in the operating state model into a specific stereo model of human motion for each frame. It is assumed that the specific geometric feature vector of the routine operating state of w high-speed trains in the operating state as a whole is denoted by the symbol e, which is further used to reconstruct the distribution of feature points associated with the contours, and thereby calculating the markers for the dynamic features related to the routine operating state of all the high-speed trains in the operating state. The expression formula for the specific operation of the entropy function feature $d_{mn}^{ij}(x, y)$ of the image block in a window with a size of s^2 in the area can be obtained as follows:

$$d_{mn}^{ij}(x, y) = \begin{cases} \dfrac{\sum_{k=-s}^{+s} \left|\theta_m^{ij}(x+k, y+k) - \theta_n^{ij}(x+k, y+k)\right|}{g(x, y)(\partial \varphi / \partial t)}, & m \neq n. \\ 0, \quad m = n, \end{cases} \quad (6)$$

In equation (6) mentioned above, the letter m and letter n are used as the number of image numbers that mark the routine operating state of the high-speed trains in the operating state; the letter i and letter j stand for the relevant sequences, which are used as the specific pixel codes to indicate the routine operating state θ of the high-speed trains in the operating state.

3. Application of the Intelligent Robot Palletizer Technology in the Optimization Process of High-Speed Train Operation

The visualization of spatial information can be restored to a certain extent. Subsequently, the analysis method of the profile angle for the routine operation status of the high-speed train operation status mode is further explored so as to raise the level of high-speed train skills and tactics, which has gained great attention at the same time. Both the starting point and the ending point in the analysis of the routine operating status of high-speed trains are on the basis of combining the analysis of spatial variation features and the method of three-dimensional reconstruction, as well as the visualization of the data on the routine operating status of high-speed trains [20, 21]. In accordance with the traditional mode, the beginning and the end of the routine operation of high-speed trains are analyzed based on the method of instantaneous attention extraction. The method of extracting Harris features and the method of identifying the edge contours are used to record the routine running state of the high-speed trains as a game image. In addition, the structure of the object can be adjusted to verify the angular distribution of the image points in conjunction with the relevant images of the motion environment. At the same time, the recognition of information and the capacity to synthesize the information subsequently can be improved. However, the routine operation analysis method for the high-speed train operation status mode is relatively poorly adapted to the departure and destination points as compared to the conventional mode. As the passenger lines for the operation of trains at a high speed are set up in parallel, it is possible to ensure that in most normal operating situations and the majority of emergencies, the trains with upper and lower connections can run independently of each other. In general, only in very rare cases when a line is blocked and vice versa, the flow of traffic will limit the connection up and down to some extent. Thus, the double line can be divided into two separate lines on this basis (Figure 3).

In accordance with the specific schematic diagram provided in Figure 3 mentioned above, the algorithm programming in this paper has improved the line model to a certain extent with regard to the data mode related to high-speed railroad transmission. For example, the distance between the stations and the restricted distance are equally processed to facilitate the subsequent algorithmic search. To some extent, there is no significant difference between the distance of stations and the limit interval distance unless there are otherwise restrictions.

In this paper, the exact arrival and departure time of the traveling train at the train platform is mapped to the information of the flight path data in the three-dimensional space through the relevant method of mapping. As a typical arrangement in the analysis process, the structure diagram of certain dispatching decomposition taking the departure pattern of the high-speed runway into comprehensive consideration is obtained, and the specific train departure mode is shown in Figure 4 as follows.

Through the rapid establishment of a high-speed solution dispatching in the three-dimensional space with search

RETRACTED

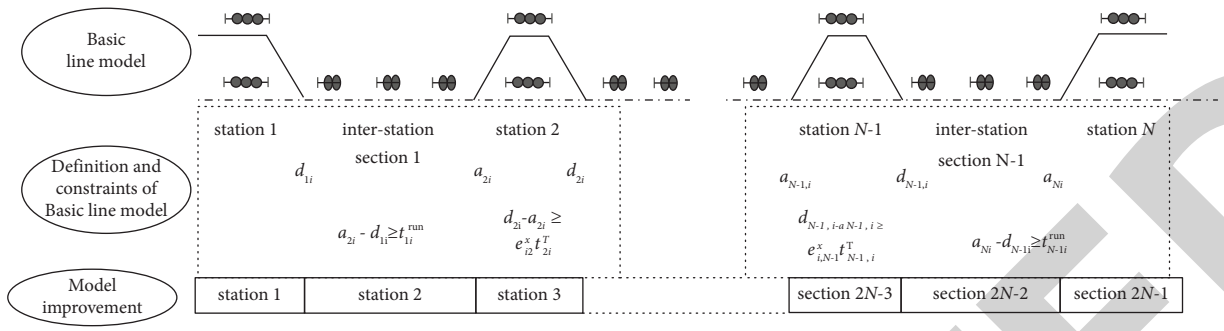

Figure 3: High-speed rail dispatch line model.

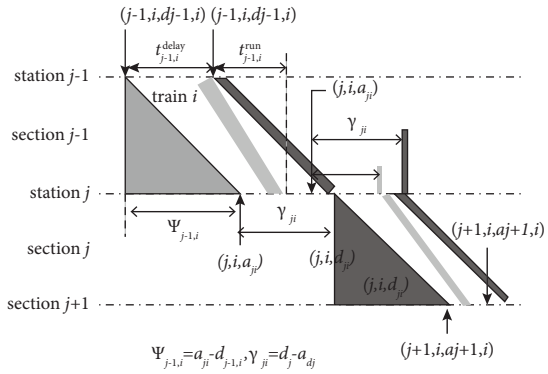

Figure 4: Construction of the solution space based on the high-speed rail dispatching model.

area and route path points, the problem generated in the high-speed solution dispatching can be converted into route path points to optimize a series of issues in route search. As the high-speed track for planning is a relatively limited optimization dispatching problem, the different coordinate points on the map space are not a part of a feasible solution, but rather a feasible route path point on the map thus created.

Firstly, the specific occurrence time of train i at the station $j-1$ is identified, and the time t is contained in the interval $[1, 1440]$. Subsequently, through the application of certain constraints and the model information that has been acquired so far, the relevant set of generation with feasible path points is carried out for train i that has been late before it finally arrives at station j. The details are shown as follows [22]:

$$a_{ji}^{a} = \left\{ (j,i,t) \middle| t \in \left[a_{ji}^{-}, a_{ji}^{+} \right] \right\}. \tag{7}$$

In the abovementioned set, the earliest time when train i departs from the beginning and when train i arrives late at station j is indicated by the symbol a_{ji}^{-}, and during the operation, the minimum running time is identified by the interval $j-1$ as follows:

$$a_{ji}^{-} = \max \left\{ d_{j-1,i} + t_{j-1,i}^{\text{run}}, \max_{k \in pre(i)} \left(a_{jk} + I_{kij}^{a} \right) \right\}. \tag{8}$$

The set $pre(i) \subset T$ stands for the sequence of train cars in front of train i when it arrives at station j. The interval limit between the time when train i and train k arrive at station j, respectively, is denoted by the symbol I_{kij}^{a}. With regard to a_{ji}^{+}, that is, the latest time for train i to arrive at station j, it can be specifically defined by the following operation:

$$a_{ji}^{+} = d_{j-1,i} + \varphi_{j-1,i}. \tag{9}$$

At this point, train i is already running late. Hence, it has to rush so as to maintain the original schedule. As a result, the subsequent operation time of the train usually have to be shorter than the original schedule $\varphi_{j-1,i}$ for the purpose of continuously adjusting the time and thus getting to the station at the right time. In some cases that are relatively more complicated, the upper limit of the arrival time can be extended even further, and the details are illustrated in Figure 5 as follows.

The set of grayscale feature edge pixels in the routine operating status screen of the high-speed trains is taken as the set a, and the segmentation method is combined with the feature function to detect the specific features at the starting point of the routine running operation of the high-speed trains in the operating state to some extent, so that an output value $S = \left\{ S_1, S_2, \cdots, S_{N_A} \right\}$ can be acquired after effective fusion of the relevant data [23]. Finally, the expression formula is obtained after the detection as follows:

$$p_{i,j}(A) = \begin{cases} \dfrac{w_{i,j} S}{w_i E_m^{ij}}, & \text{if } i \neq j \text{ and } e_{i,j} \in A, \\ 0, & if\ i \neq j \text{ and } e_{i,j} \notin A, \\ 1 - \dfrac{\sum_{j, e_{i,j} \in A} w_{i,j} S}{w_i E_m^{ij}}, & \text{if } i = j. \end{cases} \tag{10}$$

In the operation state of the motion scene as a whole, the dynamic features of the specific image for the routine operation state of the high-speed trains in the operation state are denoted by the symbol g. Thus, the distribution level of the feature intensity can comply with the requirement of $G_{\min} \sim G_{\max}$. Then, the final fusion parameters for the routine operation state of the high-speed trains in the operation state can be obtained as follows:

RETRACTED

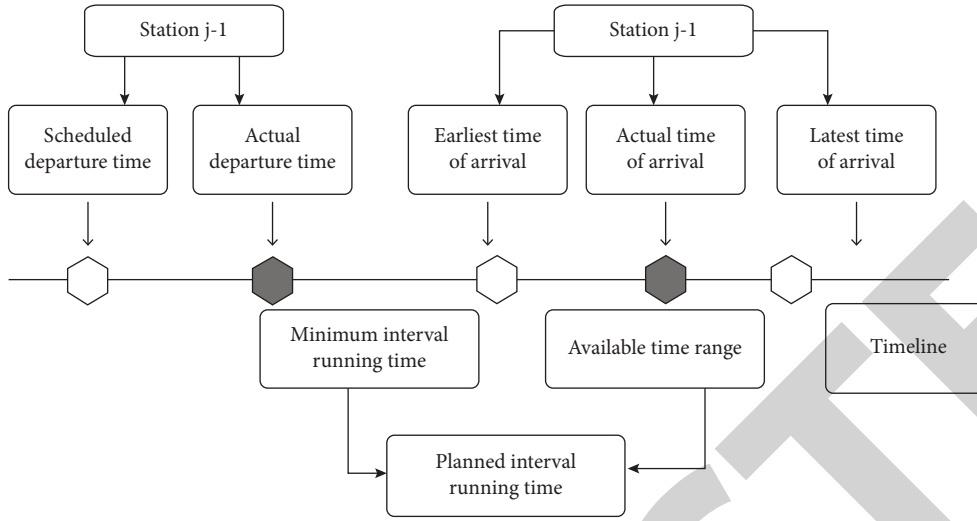

Figure 5: Determination of the range for the feasible train operating time.

$$w(i,j) = \frac{1}{Z(i)} \exp\left(-\frac{f(x,y)}{C(i)^2}\right). \tag{11}$$

In equation (11) mentioned above, the function $Z(i)$ stands for the region specific to the template matching value matched to the feature function within the chunked region, which corresponds to the subregion, and the output value g corresponding to the multimodule function can be obtained as follows:

$$g = G_{\min} + (G_{\min} - G_{\max})C(i)(G). \tag{12}$$

On the basis of the matching information within the chunked area combined, the extracted starting and ending feature points $S(k)$ related to the routine operating state can be obtained according to the following equation:

$$S(k) = \varphi \cdot S(k-1) + g(k). \tag{13}$$

Through the extensive forensic analysis performed above, we can construct the model for the routine operating status of high-speed trains in operation. At the same time, the method of information fusion in subspace can be combined to implement effective fusion of data related to the routine operating status of high-speed trains in operation. The results from the fusion of various data can be combined to extract the starting and ending features for the routine operating status of high-speed trains.

4. Simulation and Analysis of the Results

In this paper, a relatively typical downstream section is selected from the Harbin–Dalian high-speed railway for the experimental verification in the relevant operating scene. This section is generally quite busy in the aspect of train movement, and once the train arrives late, the influence of delay can easily result in a state of expanded impact, leading to a series of delays for subsequent trains. Hence, it can be observed that these parts of the interval segments are highly demanding for the presence of dispatchers. In the majority of practical cases, it is very difficult to make full use of the extra time by manual adjustment of the schedule. Therefore, with regard to this issue on the interval section, the improved algorithm proposed in this paper is more suitable for inspecting the effectiveness and carrying out the related optimization of the train group based on the dispatching algorithm [24, 25].

The operating scenes in the selected cases are composed of 8 different stations, and the experimental simulations are carried out with several trains operating at a high speed on the rail between 20:00 and 22:30. Table 1 below shows the configuration of the specific simulation scenarios, including the minimum station time, the interstation interval, and the minimum operating time within the interstation section for each station.

For the purpose of verifying the effectiveness of the proposed intelligent robot palletizer technology for high-speed train dispatching in an efficient manner, it is assumed in this paper that the train G399 has been late for 15 minutes on the northern highway of Shenyang. As the original train departure time is not excessively late, it will not lead to significant traffic disruption. The following strategy for the adaptation of the train carried out automatically is only applicable to optimal adjustment of the train operation, which can result in a series of delays and late arrival of several subsequent trains D27, D23, G8023, and so on. The results of the specific feasible operational adjustments acquired based on the algorithm are shown in Figure 6 as the follows.

In the operation diagram measured in Figure 6 mentioned above, the red dotted line stands for the original planned route of the initial delayed train, the blue fixed line stands for the actual route of the related affected train, and the other black fixed lines stand for the actual routes of the other trains. Figure 7 below shows the actual delays of each affected train.

Taking into account the advantages of the robot palletizer with intelligence as proposed in this paper, some relevant comparisons with the least dichotomous technique

RETRACTED

Table 1: Configuration table for the parameters of the simulation scenarios.

Station ID	Minimum station operating time	Interstation interval	Minimum interval operating time
Shenyang North Highway Yard	1	—	—
Liouwangtun Line Station	1	1	9
West Tieling Station	1	2	4
West Kaiyuan Station	1	3	8
West Changtu Station	1	4	5
East Siping Station	1	5	10
South Gongzhuling Station	1	6	9
West Changchun Station	1	7	11

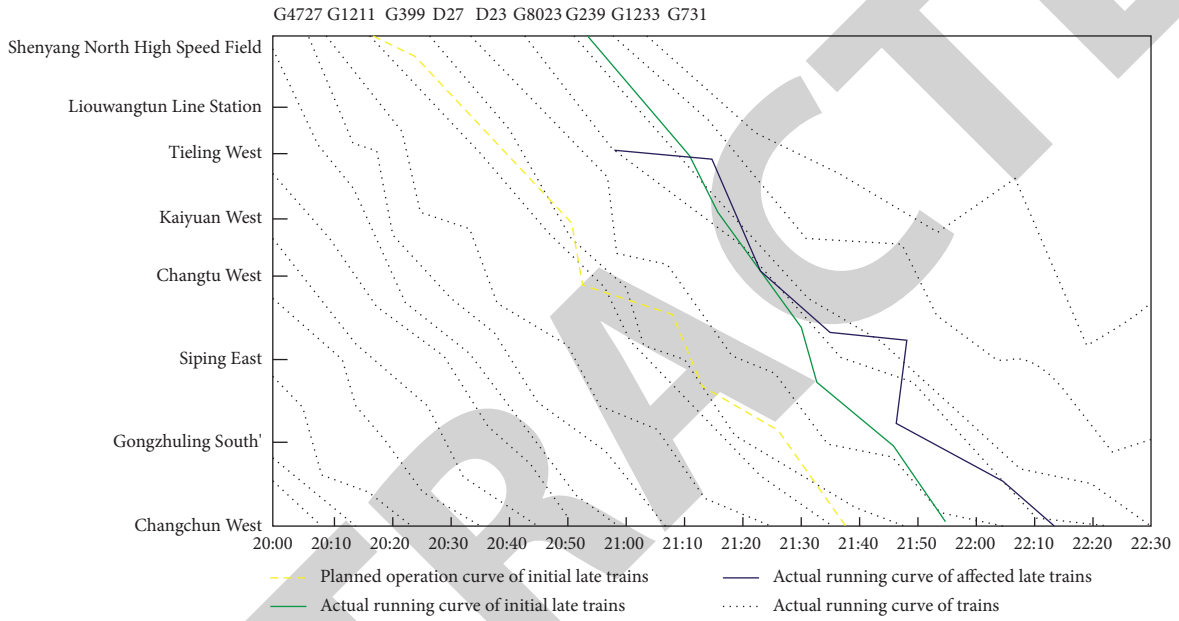

Figure 6: Actual running map of the train (scenario 1).

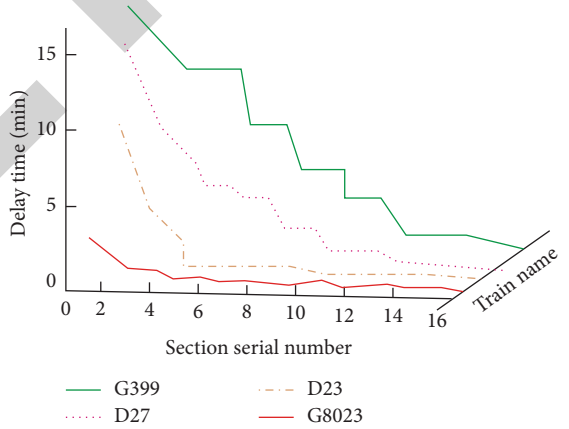

Figure 7: Statistics on the delay time of the affected trains (scenario 1).

(basic ACO) and the neural network technology (maximum and minimum ACO) of the robot palletizer with intelligence are carried out [26]. Since the robot palletizer with intelligence is equipped with two sets of $\alpha - \beta$ parameters in general, the comprehensive statistical analysis of the combination of parameters similar to $\alpha - \beta$ can be defined as the following: the relevant combination of parameters 1: α is equal to 1.3 and β is equal to 1.8; the other relevant combination of parameters 2: α is equal to 1.1 and β is equal to 1.54. The other parameter values are kept essentially

RETRACTED

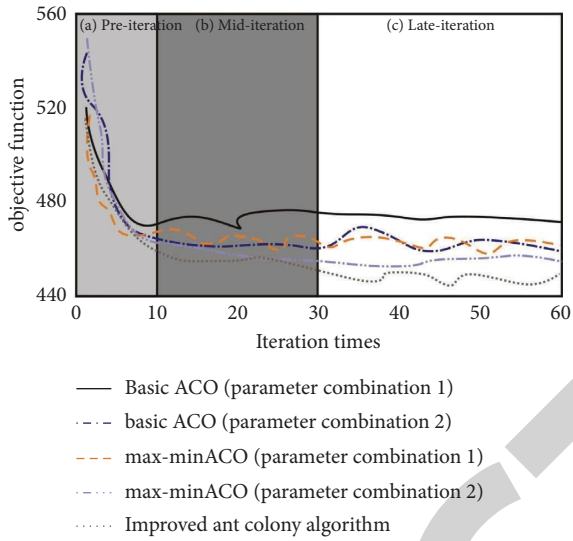

Figure 8: Comparison of the simulation results based on various algorithms.

Table 2: Comparison of the extraction time/s.

Number of experiments	Methods put forward in this paper	Method in the literature [2]	Method in the literature [3]
100	20.13	55.62	60.95
200	22.14	62.73	62.34
300	21.32	63.94	69.32
400	20.22	69.58	70.89

constant so that the two sets of parameters can correspond to the minimum dichotomy technique and the neural network technique, respectively. Each algorithm is run continuously for about 30 times to obtain the relatively average results of comparative convergence. The final results are shown in Figure 8 as the following, in which some of the results obtained after the comparison indicate that the improved algorithm can obtain relatively better convergence results with a higher efficiency in search.

For the purpose of providing further verification of the effectiveness of the method put forward in this paper, the running states of high-speed trains in operation are compared and analyzed in more details based on the method proposed in this paper, the method established in the literature [2], and the method proposed in the literature [3]. The detailed results are presented in Table 2 as follows.

In accordance with the analysis results reported in Table 2 mentioned above, it can be observed that the evaluation time for the routine operating status of high-speed trains in operation is gradually increased based on the three different methods as the number of iterations of data information increases. In addition, the evaluation time of the routine operating status of high-speed trains in operation is relatively stable and relatively shorter by using the method put forward in this paper than the extraction time by using the traditional methods.

5. Conclusions

For the purpose of ensuring the reliability and security of high-speed trains without changing the original route of the trains, attention has been paid to the high standard of responsiveness in the passage of trains with regard to the continuous progress in the optimization of trains. The power of high-speed trains and the environment friendly features are enhanced by minimizing the mass of high-speed trains through reasonable and feasible design methods. The intelligent robot palletizer technology is used to carry out the optimization of the high-speed train operation in the event of collision. On the premise that the stiffness, modal, and other basic requirements are met, quantitative function analysis is carried out on the car body of the trains to optimize the body structure quality, reduce the thickness of the relevant parts, and achieve the demand for the optimization of the body mechanism operation. Through rectifying and optimizing the delayed trains based on the intelligent robot

RETRACTED

palletizer, the operation of the delayed trains can be improved. In this way, the delay time can be calculated to develop the optimal rectification plan. Through the experiment, it is verified that the conversion and self-adjustment based on the theory that time is closely connected to space can improve the dispatching performance of the trains in an effective manner and realize the optimal deployment in the operation of trains.

Data Availability

The data used to support the findings of this study are included within the article.

Conflicts of Interest

The authors declare that they have no conflicts of interest.

Acknowledgments

This research study was sponsored by the following projects—project one: Technical Service of the State Railway Administration Commission, contract no. (2019) 19 and project two: Action Plan for Innovation and Development of Higher Vocational Colleges in Henan Province-JiaoGao, project no. (2017) 895.

References

[1] R. Yang, Z. Xia, B. Xu, Y. Liu, L. Zeng, and Z. Chen, "Study on vibration response of surrounding environment caused by high-speed train operation," *IOP Conference Series: Earth and Environmental Science*, vol. 719, no. 4, Article ID 42041, 42112 pages, 2021.

[2] Y. U. Cuiying, J. Xiang, S. Lin, C. Yuan, and H. Yang, "Influence of double-block ballastless track seam on high-speed train operation safety and maintenance standard research," *Journal of Railway Science and Engineering*, vol. 30, no. 9, Article ID 25902, 25915 pages, 2019.

[3] M. Zhang and X. Zhu, "Optimization study of jinghu high-speed railway train operation diagram. Journal of Physics," *Conference Series*, vol. 10, no. 6, Article ID 15503, 15512 pages, 2019.

[4] B. Alejandro, R. Higinio, S. H. Enrique, and C. Cristina, "Methodology for the integration of a high-speed train in maintenance 4.0," *Journal of Computational Design and Engineering*, vol. 13, no. 9, pp. 22–31, 2021.

[5] J. Zheng, J. Zhang, E. Bjrnson, Z. Li, and B. Ai, "Cell-free massive mimo-ofdm for high-speed train communications," *Maintenance and Reliability*, vol. 62, no. 10, pp. 6436–6447, 2022.

[6] B. Ning, H. Dong, S. Gao, T. Tang, and W. Zheng, "Distributed cooperative control of multiple high-speed trains under a moving block system by nonlinear mapping-based feedback," *Science China*, vol. 30, no. 1, pp. 2–25, 2018.

[7] J. Liu, Z. Jiang, and H. Zhou, "Integrated operation and maintenance optimization for high-speed train fleets considering passenger flow," *Eksploatacja i Niezawodność – Maintenance and Reliability*, vol. 24, no. 2, pp. 297–305, 2022.

[8] J. Liu, J. M. Lee, E. Strock et al., "Technology applications: use of digital health technology to enable drug development," *JCO Clinical Cancer Informatics*, vol. 2, no. 9, pp. 1–12, 2018.

[9] L. Wang, B. Ai, Y. Niu, X. Chen, and P. Hui, "Energy-efficient power control of train-ground mmwave communication for high speed trains," *IEEE Transactions on Vehicular Technology*, vol. 68, no. 8, pp. 7704–7714, 2019.

[10] M. Y. Zhang and H. Xiao, "The influence of strong cross wind and track irregularity coupling on high-speed train operation safety," *Railway Standard Design*, vol. 211, no. 20, pp. 171–184, 2018.

[11] S. Duan and S. Dai, "Application of discrete firefly algorithm in high-speed train operation adjustment," *Computer Engineering and Applications*, vol. 40, no. 8, pp. 892–896, 2018.

[12] X. J. Chen, Y. L. Wang, X. Long, H. R. Liao, and H. E. You-Quan, "High speed train operation condition monitoring and fault diagnosis," *Value Engineering*, vol. 9, no. 1, pp. 657–666, 2018.

[13] H. Zhou, Y. Zhou, Y. Liu, and Q. Tang, "Research on high-speed train load spectrum and bridge load effect spectrum," *IOP Conference Series: Earth and Environmental Science*, vol. 719, no. 3, Article ID 32095, 122707 pages, 2021.

[14] S. Xu, C. Chen, Z. Lin, X. Zhang, J. Dai, and L. Liu, "Review and prospect of maintenance technology for traction system of high-speed train," *Transportation Safety and Environment*, vol. 3, no. 3, pp. 236–252, 2021.

[15] Y. Rui and R. Mou, "Research on simulation model of high-speed railway train operation plan inspection," *Application Research of Computers*, vol. 9, no. 1, pp. 657–666, 2018.

[16] X. Z. Zhou, Q. Zhang, T. Wang, P. F. Song, Z. Cao, and P. Department, "An application research on high-speed railway train operation intelligent adjustment algorithm," *Railway Transport and Economy*, vol. 18, no. 2, pp. 97–102, 2018.

[17] M. A. Xiu-Fei and B. H. Wang, "Research on virtual simulation experimental teaching of high speed railway train operation control system," *Modern Computer*, vol. 26, no. 36, Article ID 36732, 36753 pages, 2018.

[18] Z. Wang, Y. Song, Z. Yin, R. Wang, and W. Zhang, "Random response analysis of axle-box bearing of a high-speed train excited by crosswinds and track irregularities," *IEEE Transactions on Vehicular Technology*, vol. 66, no. 11, Article ID 10607, 10617 pages, 2019.

[19] D. T. Wang, F. R. Wang, and K. Huang, "A simulation model for tracking operation of high-speed railway train group based on cellular automata," *Railway Standard Design*, vol. 7, no. 5, pp. 252–268, 2018.

[20] Q. Yu and Z. Hou, "Adaptive fuzzy iterative learning control for high-speed trains with both randomly varying operation lengths and system constraints," *IEEE Transactions on Fuzzy Systems*, A Publication of the IEEE Neural Networks Council, vol. 759, no. 2, , pp. 143-144, 2021.

[21] L. I. Kun-Yang, H. H. Chen, J. S. Guo, and Q. Y. Wang, "Research on automatic train operation algorithm for high-speed trains based on sliding mode active disturbance rejection control," *Modern Computer*, vol. 121, no. 1, pp. 107–115, 2019.

[22] L. I. Yu and Y. I. Tiehang, "Analysis on operation adaptability of traction motor cooling fan for high speed train on kunxiang line," *Railway Locomotive and Motor Car*, vol. 30, no. 9, Article ID 25902, 25915 pages, 2019.

[23] C. H. Shao, L. Miao-Miao, C. C. Zou, and N. I. Shao-Quan, "A design on beijing-shanghai high-speed railway train stop schedule based on cyclic train timetable," *Railway Transport and Economy*, vol. 10, no. 6, Article ID 15503, 15512 pages, 2018.

RETRACTED

Hindawi
Journal of Robotics
Volume 2024, Article ID 9831614, 1 page
https://doi.org/10.1155/2024/9831614

Retraction

Retracted: Attitude Analysis and Evaluation of Camera Based on Planar Double Joint Robot

Journal of Robotics

Received 23 January 2024; Accepted 23 January 2024; Published 24 January 2024

Copyright © 2024 Journal of Robotics. This is an open access article distributed under the Creative Commons Attribution License, which permits unrestricted use, distribution, and reproduction in any medium, provided the original work is properly cited.

This article has been retracted by Hindawi following an investigation undertaken by the publisher [1]. This investigation has uncovered evidence of one or more of the following indicators of systematic manipulation of the publication process:

(1) Discrepancies in scope
(2) Discrepancies in the description of the research reported
(3) Discrepancies between the availability of data and the research described
(4) Inappropriate citations
(5) Incoherent, meaningless and/or irrelevant content included in the article
(6) Manipulated or compromised peer review

The presence of these indicators undermines our confidence in the integrity of the article's content and we cannot, therefore, vouch for its reliability. Please note that this notice is intended solely to alert readers that the content of this article is unreliable. We have not investigated whether authors were aware of or involved in the systematic manipulation of the publication process.

Wiley and Hindawi regrets that the usual quality checks did not identify these issues before publication and have since put additional measures in place to safeguard research integrity.

We wish to credit our own Research Integrity and Research Publishing teams and anonymous and named external researchers and research integrity experts for contributing to this investigation.

The corresponding author, as the representative of all authors, has been given the opportunity to register their agreement or disagreement to this retraction. We have kept a record of any response received.

References

[1] Z. Xu, X. Wang, C. Chen, and J. Zhang, "Attitude Analysis and Evaluation of Camera Based on Planar Double Joint Robot," *Journal of Robotics*, vol. 2023, Article ID 8143828, 7 pages, 2023.

Hindawi
Journal of Robotics
Volume 2023, Article ID 8143828, 7 pages
https://doi.org/10.1155/2023/8143828

RETRACTED

Research Article

Attitude Analysis and Evaluation of Camera Based on Planar Double Joint Robot

Zhi Xu, Xin Wang, Chun Chen, and Jiahai Zhang

School of Mechanical and Electrical Engineering, Sanjiang University, Nanjing 210012, Jiangsu, China

Correspondence should be addressed to Xin Wang; 001582@sju.edu.cn

Received 24 October 2022; Revised 11 April 2023; Accepted 6 May 2023; Published 30 May 2023

Academic Editor: Iqbal Ahmad

Copyright © 2023 Zhi Xu et al. This is an open access article distributed under the Creative Commons Attribution License, which permits unrestricted use, distribution, and reproduction in any medium, provided the original work is properly cited.

Planar double-jointed robot is a kind of widely used robot. In the past decades, with the development of science and technology, planar double-jointed robot has a great breakthrough in many aspects, especially in the actual camera and attitude analysis. In recent years, pun-section manipulator has made great progress in technology, but its kinematic characteristics and the human body's ability to move have a great gap. So, in the moving plane, we need to study how to improve its camera ability to find a more stable and effective camera mode, and to a certain extent, to meet its requirements in complex working conditions. Simulating the pose of two joints, we seek a more stable and effective camera mode to improve its moving speed, expand its moving space, and lay a solid foundation for its application. Planar double-jointed robot is the most representative one at present. It includes machinery, material, electronics, computer, sensor, drive, intelligent control, artificial intelligence, and so on. Because it is closer to the human body, more suitable for people's work and work, so it does not need to change its environment, so it is regarded as having a high affinity for people's machinery. Its characteristic is that it has the good adaptability and the flexibility, but the double joint camera's support discontinuity enables it to be able to adapt each kind of complex situation well. It can not only climb the stairs but also in the messy ground smooth through and also in the inconvenient passage through. The aim of this paper is to analyze the unique advantages and irreplaceable characteristics of the planar double-jointed robot based on the bionic and mechanical research results. This paper analyzes the mechanical technology by means of literature review and actual data analysis. The experimental results show that the biggest difference between the two articulated robots and other robots is that they have two human-like joint motions.

1. Introduction

Since the 1980s, double-joint robot has become one of the most popular topics in the world. It has been paid much attention by researchers and engineers, and has great development potential in theory and practice. In recent years, there are more and more tasks of double joints, such as operations in dangerous places, rescue, improve the efficiency of operations, and expand the range of people's activities. America's defence advanced research (DARPA) is preparing the DARPA challenge (DRC). The purpose is to develop a kind of robot that can replace human in emergency rescue work, especially in rough terrain conditions, robot movement performance, and operation ability will be stronger than human. This can better meet the needs of people in the future environment and enhance the responsiveness and mobility of human and natural reactions. DRC is considered to have the highest level of robotics competition in the world. It is the most advanced technology in the world. Many types of robots, such as SCHAFT in Japan, Atlas in the United States, and HUBO in Korea, are representative. They made remarkable achievements in this project and made everyone realize that this kind of robot has a huge development space in the future [1–4].

1.1. Stable Camera Principle for Planar Two-Joint Robots. At present, most of the stabilization camera is based on the ZMP stability criterion. ZMP refers to a small circle point on the contact surface of the foot and the ground, and the transverse component of the equivalent moment of the center of the circle is 0 at this position. The stability criterion of ZMP is widely used due to its high efficiency. For example, Japan's famous ASIMO, HRP, Zhejiang University's

WUKONGL8, Beijing Institute of Technology's HRP, National University of Defense Technology's pioneer robot, and so on. However, the existing research results show that the stability criterion of ZMP is too harsh for two articulated cameras, which will cause some adverse effects on their motion performance. But in reality, higher mobility capabilities are required. Planar camera robot is a kind of mechanical device based on motion camera. The device has no feet and no support area. Based on feet, it contacts with the earth in a straight line or a point to achieve dynamic stability.

The motion control of planar camera robots has been continuously developed and developed for several years, and many new control techniques and methods have been developed. At present, the methods based on passive camera, decomposition control, virtual model, and multidegree of freedom control based on mixed zero dynamics are two mature control methods.

The camera pose proposed by McGeer et al. at Cornell was developed from the unpowered camera technique. Originally, passive photography refers to automatic photography propelled by gravity without any power. A passive camera system gives full play to its dynamic performance, no external energy or input only a small amount of energy to achieve the camera. Obviously, the energy use of this car is very good, and it is very consistent with people's walking habits. However, the assignment of a special mechanical structure with physical properties is a prerequisite for its stability in passive photography. In order to expand the diversity of its application, reduce the dependence on its mechanical parameters, and the sensitivity to the initial value of the system, a lot of optimization and improvement have been carried out. For example, passive control and potential energy shaping based on the connection mode and vibration reduction mode. The abovementioned research provides a strong impetus for the development of motion control technology for passive photography. In order to make the robot based on passive camera better meet the requirements of users in more complex works, it can better meet the requirements of users.

1.2. Robot Camera Pose Analysis and Evaluation System. In the 1980s, Raibert et al. proposed a simple and efficient motion control strategy. The key of the proposed method is to divide the robot action control into three quantities, which are torso, torso, and forward rate. It is a method close to decoupling, and through the steady state control of the three variables, the motion state of the system can be kept unchanged. In general, the robot jumps and jumps are achieved by the thrust at the joint, while the robot is controlled by the torque at the joint and hip, and the robot adjusts its action according to the angle of each landing. Once all three energies are controlled, then the robot can move smoothly [5].

Pratt et al. built a set of virtual devices in a virtual environment that can follow the desired control object to achieve its motion. Because a virtual device will finally apply a force or a moment on a passive object, in the end, the force or moment are all obtained from the corresponding articulated moments equally. In planar camera foot robots, lateral elastic shock absorbers, elastic shock absorbers, constant applied forces, and torques are commonly used. This method has the characteristics of a simple structure, is easy to grasp, is easy to implement, and does not need to use the cumbersome dynamic modeling technology so as to realize the dynamic simulation of the system. The control quantities are processed in a closed manner to ensure the stability of the system. From the application examples of virtual modeling, whether it is Spring Flamingo or MIT Cheetah, they all use the connection between the outside world and the controlled component, thus realizing the control of virtual control.

Based on the study of hybrid zero dynamics, Grizzle et al. presented a new hybrid zero dynamics algorithm. Compared with the real-time online plan tracking of conventional ZMP, mixed zero is a trajectory tracking method based on time invariance. The schedule of the control quantity does not change over time, but it is just a variable of a state, which is essentially a virtual limit [6]. This method uses the virtual limit of a plane camera device to plan a specific action and then uses the dynamic mode of the system to control so that the system has certain convergence to a certain extent.

2. Research Content

2.1. Camera Position Adjustment for Planar Two-Joint Robots. In addition, Hurst used a simple antipendulum spring model to realize the camera and running of ATRIAS. In view of the activity characteristics of human joint parts, Hurst et al. analyzed the reaction on the ground according to the physiological characteristics of human and animal, as well as in various situations, so as to determine the amount of human movement. This method gives full play to the active control characteristics of the elastic inverted pendulum and then adjusts the transmission device to achieve the ideal action form. Until now, Hurst et al. have continued with this approach and have achieved very good results. When photographing, the contact with the surface is a discontinuous collection of point groups. But each foot is in a dynamic continuous motion. When the feet switch, the system collides with the floor and puts the whole system in a jumping state.

Camera is one of the most basic robots, and it is also an important topic in robot technology. The dynamics of two articulated robots with planar camera motion has also received much attention. This paper introduces a control scheme of planar camera based on planar two-joint and makes motion plan and control for it so as to control the motion of each part in the process of camera [7, 8]. Then, according to the motion state and the change of the motion state, the motion parameters are used to adjust the motion trajectory so as to obtain the motion trajectory of the motion trajectory. Finally, the stationary planar imaging of the two articulated robots is completed on the experimental platform [9].

The camera strategy is a prerequisite for the realization of dynamic camera, and its action limits are given as the basis for its design. In this paper, a video strategy is proposed and

RETRACTED

the camera is used to describe the camera situation. The controller uses the camera as the top control system and realizes the control rate of multiple robots in each stage in the bottom layer. The transition of the camera state directly affects the conversion of various control rates and the operation of the control system.

The method of "feedforward + feedback" is used to control the balance of the human body. First, the motion status of the human body is obtained by an aerial gyroscope, and the corresponding feedback control is carried out. Second, the disturbance of the human body in the camera is analyzed, and a simplified mathematical model is used to predict the disturbance so as to obtain a forward compensation. In the joint part of the movement plan, the system state is used as the calculation parameters to achieve the movement plan required by the camera. For the dynamic characteristics of hardware, the kinematic control is carried out to converge the action of the joint position.

2.2. General Analysis of Robot Position for Planar Camera. Under planar camera, the camera rate is a key factor to realize the camera action of a two-arm robot. The optimal estimation of the motion velocity is obtained by fusing the information of the aeronautical runner and the joint coding so as to obtain the real-time data of the motion trajectory. Based on the motion trajectory in the current motion state, the motion speed of the motion is achieved by adjusting the tread position.

The simplified modeling of the two articulated robots in the 2D camera is five four-drive. These include trunk, right joint, right joint, and double joint. Its body is composed of a simple pillar connected by two hips and two large joints. The left and right feet are symmetrical, and the large and small joints of each foot are simply knee-connected. The end of the subsection can be regarded as a puncta foot in contact with the surface. The two hips and two knees are a single

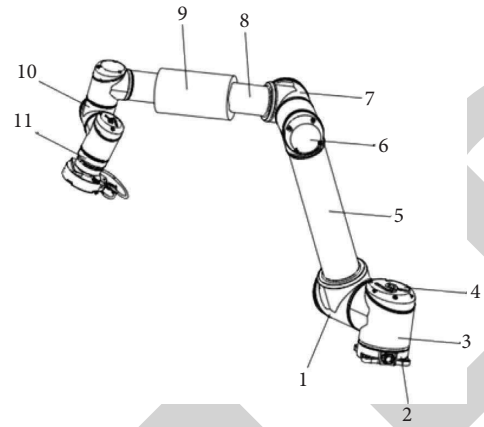

Figure 1: Camera generic pose for a planar two-joint robot.

actuator. The last simple pattern of the five four-wheel transmissions is as follows (in Figure 1).

The camera mode of the planar camera robot is carried out with one foot and two joints. One joint supports the body and one foot swings forward. The two-joint support phase is when the two feet are balanced on the ground. For the camera action of the planar camera, generally from the theory point of view, two joints will appear in a split second so as to realize the conversion between the two joints. The transition between the single-joint and the two-foot support phases is initiated by swinging and supporting joint part movements. The transition from a foot support phase to a foot support phase at the point where the swing joint touches the ground is an interchange of the swing foot and the support foot. If the swing foot moves from the ground to the air, it is a different story. So, the planar camera is a cyclic movement that combines two states. On this basis, a simple mathematical model of two swinging roots is established, whose static equations are as follows [10]:

$$\begin{aligned} \tau_k &= -\hat{m}_s g[-l_s \sin\ (\theta_b + \theta_k + \theta_h) + y_{cs} \cos\ (\theta_b + \theta_k + \theta_h)], \\ \tau_h - \tau_k &= \hat{m}_s g l_h \sin\ (\theta_b + \theta_h) + \hat{m}_h g l_h \sin\ (\theta_b + \theta_h) - \hat{m}_h g y_{ch} \cos\ (\theta_b + \theta_h). \end{aligned} \tag{1}$$

For equations (2) and (3), we define the parameter direction, the input vector, and the output direction to the basis.

$\alpha = [\hat{m}_s, \hat{m}_s y_{cs}]^T \lambda u = [g l_s \sin\ (\theta_b + \theta_h + \theta_k), -g \cos\ (\theta_b + \theta_h + \theta_k)] y = \tau_k$. Then, the abovementioned equation is simplified as follows:

$$u\alpha = y. \tag{2}$$

Considering the measurement error and noise in the experiment, a noise term is added to the abovementioned equation, denoted by the noise error difference, and written in discrete form:

$$y(k) = u(k)\alpha + e(k). \tag{3}$$

Different output data pairs can be obtained when the swing joint is in different configurations, and the estimation obtained according to the secondary observation results is, let be the system output of the chess type calculation, and let be the residual between the observation output and the model calculation, then the following relationship is obtained:

$$\varepsilon(k) = y(k) - y_m(k). \tag{4}$$

Combining the abovementioned system equations, the following equation can be obtained:

$$\varepsilon(k) = u(k)(a - \tilde{a}) + e(k). \tag{5}$$

RETRACTED

For the input and output data of the secondary measurement, we let

$$Y = \begin{bmatrix} y(1) \\ \vdots \\ y(n) \end{bmatrix}, U = \begin{bmatrix} u(1) \\ \vdots \\ u(n) \end{bmatrix}, e = \begin{bmatrix} e(1) \\ \vdots \\ e(k) \end{bmatrix}, \varepsilon = \begin{bmatrix} \varepsilon(1) \\ \vdots \\ \varepsilon(n) \end{bmatrix}. \quad (6)$$

Then, the system equation and residual equation are as follows:

$$\begin{cases} Y = U\alpha + e, \\ \varepsilon = Y - U\widetilde{\alpha} = U(\alpha - \widetilde{\alpha}) + e. \end{cases} \quad (7)$$

The least squares parameters are estimated as in

$$J = \varepsilon^T \varepsilon. \quad (8)$$

When the minimum value is obtained, the value is the least squares estimate of the parameter $\widetilde{\alpha}$. When enough data are collected and most of the data are uncorrelated, the full rank of the matrix can be guaranteed, and the least square estimate of the parameters has a unique solution. The result is as follows:

$$\widetilde{\alpha} = \left(U^T U\right)^{-1} U^T Y. \quad (9)$$

By finding the simple model parameters and, similarly, by finding the least squares parameters, estimates are obtained. The off-line least square method is used to identify the sum of the static parameters of each connecting mechanism. According to the parameters, the dynamic and static analysis in dynamic control can be realized so as to adjust the machine position as shown in Figure 2.

In daily walking, there will be no flight state, but if it is at the beginning of the system operation, or in some specific circumstances, there will be such a change. Therefore, during the whole process, the reliability of the process must be fully explained and guaranteed. In addition, the left and right feet can act as support feet and sway at the same time, so the whole camera has six forms. In the two joint support phases and in the flight phase, the position of the single joint is subsequently adjusted according to the sway of the previous single joint support phase and the sway of the support joint and the support joint, as shown in Figure 3.

In the different point positions mentioned previously, the condition of 1 is that the left foot is a supporting joint part and the condition of 2 is the support phase of two joints in the condition of I, that is, the support phase of two joints, one is a flight phase in a situation and one is a situation in a situation. 4 is a support phase of one joint, 5 is a support phase of two joints in four conditions, one is a support phase of two joints, one is a support phase of four conditions, and one is a support phase of four conditions. In this image, the black arrow represents a normal camera, and in general, at the beginning of the system, the state will be from 3 to I, or from 6 to 4, and then between states 1, 2, 4, and 5; according to the direction indicated by the arrow, the movement will be made periodically [11]. For example, after the transfer from phase 3 to phase I, in phase I, the right foot is stepped forward, the front swing touches the ground, and then the

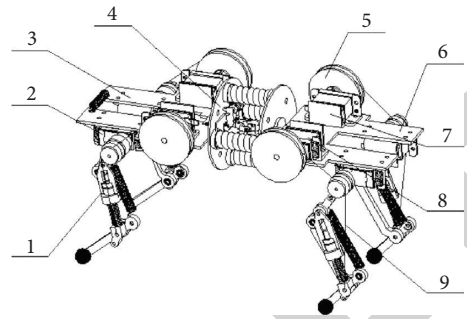

Figure 2: Camera pose transformation for a two-joint robot.

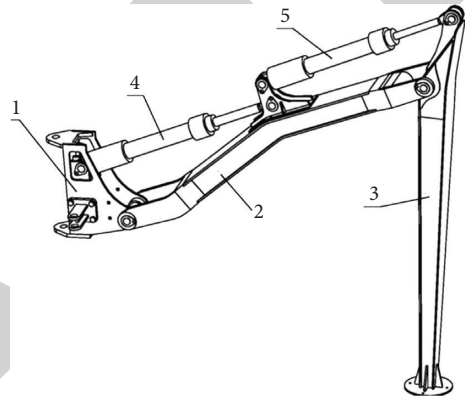

Figure 3: Single joint camera pose for a two-joint robot.

second phase is reached. In the second condition, the left foot leaves the ground and enters the fourth position. In the fourth case, the left foot was moved forward and the forward swing point of the body reached 5. Step 5 involves the right foot off the ground at 1. At this point, the system is back to level 1 and the two-joint robot has already taken one camera. From the cyclic transition of the states described previously, it can be seen that in the cycle of one camera, the mobile robot will move forward twice. If the system is working, the camera will repeat from 1 to 2, 4, 5, 1, and so on. In the event of an anomaly, the camera can switch to the third or sixth. This phenomenon is when the robots of both joints are detached from the floor at the same time. At this point, the camera will determine the abnormality and perform abnormal operation.

According to the abovementioned camera, in a planar camera, the two main motion phases are a joint and the support phase of a joint. So, the camera scheme of the planar camera can be regarded as a mobile strategy of the robot based on two joint support stages.

2.3. Camera Pose Analysis of Two-Joint Robots in Different Planes. In the support phase of a joint, the connection between the joint part and the floor is supported. When the foot sliding is not considered, it can be regarded as a non-transmission rotation assist limit, and at this time, the robot is a planar camera system. When filming, we used a simple method of supporting the joint length unchanged, that is, in

RETRACTED

the single-joint support stage, by controlling the angle of the knee supporting the joint. The joint support joint is connected by the hip and the body, where the hip joint is to maintain the stability of the body posture. At the same time, the swinging joint should not interfere with the floor and take a long distance forward to prepare for entering the joint support stage.

When both feet touch the ground during the support phase, the system is not a flat camera. In the support phase of the two joints, the center of gravity of the system is overloaded and the swing joint part of the support joint is exchanged, and then the swing joint part is retracted from the ground so that the whole system is in a single support phase. In a movement cycle, the length of the support phase of the two joints lasting in a cycle is small. Its primary job is also to realize the transformation of the support sway in order to maximize the introduction of the whole system to the next support stage.

The abovementioned several camera strategies can be summarized as follows: maintain the stability of the body posture while filming, the length of the support joint is unchanged, and the foot balls of the swing joints move according to the predetermined plan, and we ensure that the floor is not disturbed when swinging. In other words,

$$\begin{aligned} \theta_b &= 0, \\ l_{sp} &= l_0, \\ x_s &= f_1(x_h), \\ y_s &= f_2(x_h). \end{aligned} \tag{10}$$

In this paper, we present four programming equations for the system. When the controller makes the state of the system converge to the above plan, the robot converges to the designed gait. The analysis can be obtained, the motion plan is given, and the motion plan is given. Planning on the arc trajectory, that is,

$$\sqrt{x_h^2 + y_h^2} = l_0. \tag{11}$$

The massage joints are used to adjust the joint length, and the joints and knees of the swing foot are used for activities. However, there are five degrees of freedom in this system, while there are only four planning equations in the camera method, so the system still has one degree of freedom [12]. We take it as a condition of freedom under the abovementioned restrictions. As the movement of the system is determined, the state movement of the system as a whole is also determined. All other system states are arbitrary with the step size control. Depending on the camera strategy, it is easy to obtain

$$\begin{aligned} \theta_b &= 0, \\ y_h &= \sqrt{l_0^2 - x_h^2}, \\ x_s &= f_1(x_h), \\ y_s &= f_2(x_h). \end{aligned} \tag{12}$$

Therefore, in the case of stable degrees of freedom, other motions of the system are relatively stable; that is to say, the overall motion of the motion is stable. In a plane shooting process, there is no direct control of any position. It is affected by the starting conditions of the camera cycle, the action control of the camera, and other factors. In the process of photographing a two-arm robot, the difference method for time is characterized by its photographed gait. This is a difference from regular static photography, and it is also a major operation in planar photography.

3. Result Analysis

3.1. The Balance of the Camera Poses of the Robot and the Motion Control and Planning of the Joint Position. In the process of robot joint movement, maintaining the stability of human posture is the key to ensure its movement ability and application ability. The movement of the joint parts is the basic premise of the continuous camera of the robot, which not only supports the torso and upper arm but also allows the swaying joint parts to advance to ensure continuous camera shooting. The stability of the joint position is also a very critical issue in the continuous camera process of a two-joint robot. During the movement of the robot, these two problems cannot be avoided. The quality of its control has a great impact on the performance of the whole robot.

$$\tau_{fb} + m_b g C_b \sin\theta_b = J_b \ddot{\theta}_b. \tag{13}$$

It can be seen from the abovementioned formula that the dynamic equation of the body link is a nonlinear differential equation. Therefore, the feedback linearization method is used to design the controller. The opposite deformation can be obtained as follows:

$$\ddot{\theta}_b = \frac{1}{J_b}\left(\tau_{fb} + m_b g C_b \sin\ \theta_b\right). \tag{14}$$

Suppose the system formula is as follows:

$$v = \frac{1}{J_b}\left(\tau_{Ab} + m_b g C_b \sin\ \theta_b\right). \tag{15}$$

Thus, the abovementioned nonlinear differential equation becomes a double integral system, namely,

$$\ddot{\theta}_b = v. \tag{16}$$

Let the control target of the body posture be and the deviation between the control target and the actual state be $\theta_d e$. When it converges to 0, $e\theta_b = \theta_d$. That is, the body pose converges to the target pose. For the second-order differential equation, the poles are configured to converge as follows:

$$\ddot{e} + a\dot{e} + be = 0. \tag{17}$$

Appropriately chosen values of the poles can be configured such that the convergence to 0 follows the desired rate a, bee. For equation, it can be obtained as follows:

$$\ddot{\theta}_d + a\left(\dot{\theta}_d - \dot{\theta}_b\right) + b\left(\theta_d - \theta_b\right) = v. \tag{18}$$

RETRACTED

Putting in equation, we can obtain

$$\tau_{fb} = J_b\left(\ddot{\theta}_d + a\left(\dot{\theta}_d - \dot{\theta}_b\right) + b\left(\theta_d - \theta_b\right)\right) - m_b g C_b \sin\theta_b. \tag{19}$$

In the process of dynamic walking, the target attitude of attitude control will be set as follows:

$$\ddot{\theta}_d = \dot{\theta}_d = \theta_d = 0. \tag{20}$$

In a real system, the controller design requires to obtain the parameters of that system. On this basis, the parameter identification technique is introduced to obtain the parameters of this system. The relevant information of nodes and the existing parameters are obtained through experiments so that the physical parameters of the system to be measured can be identified. After getting the physical indexes of the human body, the posture and joint movements of the human body can be controlled. Using the idea of combining feedforward and feedback, the feedback control rate of the human motion system is designed and a simple modeling method is used to correct the disturbance. Combined with the action plan of the joint parts, based on the attitude of the system, the combination of the robot action and the forward movement of the robot are realized. According to the dynamic characteristics of the joystick on the test bench, combined with the motion trajectory control of the joint parts, the system simulation is carried out [13]. The relevant parameters are summarized in Table 1 as follows.

As shown in Table 1 previously, in planar photography, the balance of posture is a key issue that affects the stability of the whole system, while the deviation of posture will inevitably cause the divergence of the camera. On the test platform, the gyro system connected to the human body can realize the attitude information of the human body, and according to the measurement results, a feedback controller for human posture equalization is designed. In addition, in the process of power photography, the motion of the human body encounters a lot of interference, such as in the case of a joint, the shaking joint will interfere with the connection of the body, the inertial influence of the camera, and some random interference. This makes it possible to control the attitude equilibrium of the aircraft in a sense. Model prediction is an effective way to deal with complex system disturbance. For some disturbances, if the mathematic model of the disturbance can be established in the system, the dynamic prediction and calculation can be carried out, and the compensation of the disturbance is introduced into the feedback controller of the system so that the interference to the system can be eliminated well. To this end, the pose equalization control of the system is carried out in the way of "feedback + feedforward." By using the feedback of the gyro sensor, some disturbances of the human motion in the human motion are realized, thus providing an effective compensation for the disturbances in the motion. Through the fusion of feedforward and feedback inputs, the posture equilibrium of the human body is realized.

Table 1: Camera parameters for planar two-joint robots.

Quality parameters (kg)	m_s	0.519
	m_h	1.684
	m_b	3.5
Size parameters (m)	l_s	0.355
	l_h	0.342
	l_b	0.612

3.2. Combinatorial Optimization of Planar Camera and Two-Joint Robot. When the planar camera robot moves, the human motion chain will produce a variety of disturbances, such as swing foot torque, inertial torque, and others. In reality, due to real time, time uncertainty, uncertainty, and other reasons, the motion state in reality cannot meet the requirements well. On this basis, the control method is studied and optimized. Especially for the abovementioned disturbance problem, it is necessary to give the corresponding control strategy to ensure that the better control results can be obtained when the disturbance occurs in the system. For a disturbance with certain nature, if it has certain modeling ability, this method can be used to predict the disturbance. Based on the forecast results, the corresponding correction is carried out, which can effectively eliminate the negative impact brought by the disturbance. In this paper, a feedforward control system based on disturbance model prediction is proposed.

In the single-foot support stage, the swinging feet will swing forward and prepare for the starting line of the next stage. So, during the single-foot support phase, the trunk connection is also disturbed by the swaying joint part. Using the dynamic parameters, the torque of the rocker arm connecting to the human body is compensated in real time. However, in reality, it is difficult to measure the dynamic acceleration of the link in real time. In the test bed described in this paper, the calculated velocity and acceleration must go through the first difference method and the second difference method because the sensors at the joint sites only contain the position encoders of each joint. However, this method will produce a lot of noise, especially the obtained acceleration signal. If a low-pass filter is used for filtering, it will cause a large delay to the interference of the system, and the delay to the acceleration will cause an error between the dynamic simulation and the real interference. In some cases, the feedforward source with delay and offset cannot improve the posture balance of the human body but will reduce the efficiency of its control. For the interference of the oscillating support, the static torque method is proposed, which is an important factor of the interference at low speed.

The abovementioned controller is briefly analyzed, where the former term is the positive relationship between the loading rate and the input, the latter term is the feedback of elastic compression, and the last term is the feedback of the speed deviation, which is the active vibration reduction. The second and three parameters are the effective vibration reduction of the control system. The fourth part is the feedback of positioning error, and the fifth part is the static compensation phase. The test shows that, in the test, the weight of the pendulum joint is mainly concentrated on the

RETRACTED

Hindawi
Journal of Robotics
Volume 2024, Article ID 9843025, 1 page
https://doi.org/10.1155/2024/9843025

Retraction

Retracted: Optimization Design of Mountain and Water Landscape of Traditional Mountain Village Based on New Robot Visual Technology

Journal of Robotics

Received 23 January 2024; Accepted 23 January 2024; Published 24 January 2024

Copyright © 2024 Journal of Robotics. This is an open access article distributed under the Creative Commons Attribution License, which permits unrestricted use, distribution, and reproduction in any medium, provided the original work is properly cited.

This article has been retracted by Hindawi following an investigation undertaken by the publisher [1]. This investigation has uncovered evidence of one or more of the following indicators of systematic manipulation of the publication process:

(1) Discrepancies in scope
(2) Discrepancies in the description of the research reported
(3) Discrepancies between the availability of data and the research described
(4) Inappropriate citations
(5) Incoherent, meaningless and/or irrelevant content included in the article
(6) Manipulated or compromised peer review

The presence of these indicators undermines our confidence in the integrity of the article's content and we cannot, therefore, vouch for its reliability. Please note that this notice is intended solely to alert readers that the content of this article is unreliable. We have not investigated whether authors were aware of or involved in the systematic manipulation of the publication process.

Wiley and Hindawi regrets that the usual quality checks did not identify these issues before publication and have since put additional measures in place to safeguard research integrity.

We wish to credit our own Research Integrity and Research Publishing teams and anonymous and named external researchers and research integrity experts for contributing to this investigation.

The corresponding author, as the representative of all authors, has been given the opportunity to register their agreement or disagreement to this retraction. We have kept a record of any response received.

References

[1] X. Jia, R. Liu, and Z. Qiao, "Optimization Design of Mountain and Water Landscape of Traditional Mountain Village Based on New Robot Visual Technology," *Journal of Robotics*, vol. 2023, Article ID 4155090, 10 pages, 2023.

Hindawi
Journal of Robotics
Volume 2023, Article ID 4155090, 10 pages
https://doi.org/10.1155/2023/4155090

RETRACTED

Research Article

Optimization Design of Mountain and Water Landscape of Traditional Mountain Village Based on New Robot Visual Technology

Xinxin Jia,[1] Ruixin Liu,[2] and Zhi Qiao [3]

[1]*Xi'an University of Architecture and Technology Huaqing College, Xi'an, Shaanxi 710043, China*
[2]*Xi'an University of Architecture and Technology, Xi'an, Shaanxi 710055, China*
[3]*Xi'an University of Technology, Xi'an, Shaanxi, China*

Correspondence should be addressed to Zhi Qiao; qiaozhi001@xaut.edu.cn

Received 26 October 2022; Revised 5 December 2022; Accepted 1 April 2023; Published 17 May 2023

Academic Editor: Shahid Hussain

Copyright © 2023 Xinxin Jia et al. This is an open access article distributed under the Creative Commons Attribution License, which permits unrestricted use, distribution, and reproduction in any medium, provided the original work is properly cited.

The reasonable application of the random sampling consistent algorithm can be used to eliminate the theoretically possible error points and then complete the initial aiming pairing. The interior points obtained after this algorithm are used to estimate the relative adjacent poses of the new robot in the operation of the least squares method, so as to make certain improvements to the ICP (iterative closest point) algorithm, making it useful for accurate aiming pairing. Finally, by using the optimization method of G20, the posture of the new mobile robot relative to the adjacent position is optimized to a certain extent. In order to reasonably plan and design the landscape of mountain villages, this paper proposes the corresponding solution by analyzing the multidimensional value and landscape design data of traditional mountain villages, which not only needs to adapt to modern economic development but also needs to live in harmony with the natural ecological environment. Taking a village as a case for analysis, the village houses, roads, services, greening, ecology, and other aspects were reconstructed, and then, the detailed landscape design of the multimedia multidimensional resource village was analyzed and implemented.

1. Introduction

China has a large proportion of the rural population. In order to realize the goal of building a well-off society in an all-round way, we must first deal with various problems in rural areas. In recent years, many municipal governments have responded to the call of the state and carried out reforms and transformations in the countryside [1, 2]. Of course, some cities have urbanized rural areas without reasonable measures, just demolishing old buildings and building new ones, forming high-rise buildings everywhere, large-scale renovations, and losing the original rural scene of rural characteristics. There are pressures of cultural scenic spots in many regions, and the rural scene with rural characteristics in the past has gradually disappeared. From another point of view, because only the pursuit of rural economic construction, due to insufficient utilization of rural resources, this directly leads to the destruction of the natural ecological environment in rural areas to a certain extent. For example, the area of land used for farming in rural areas is decreasing, and the area of natural spots is gradually being artificially reduced. Excessive use of chemical fertilizers, hormones, pesticides, and herbicides has also caused great damage to the entire ecological environment in rural areas. In addition, the rapid processing of more rural enterprises and companies has also brought serious and irreversible pollution and damage to the entire ecosystem of the rural environment [3, 4].

In the process of economic development in recent years, the simultaneous opening of the new mobile robot's positioning system and the reconstruction and mapping of the robot map have become a hot spot in the field of robotics research, which is worthy of attention [5, 6]. In the past, many scientists in China and other countries have done a lot of constructive research on the visual technology of new mobile robots but found that a lot of valuable shape and geometry information was lost in the research of visual technology instead. The village landscape corresponding to the traditional village as a type of cultural heritage has gradually formed a complex of material landscape and immaterial landscape with the continuous development of the village involved, which is of profound cultural heritage and historical value. China is a country with a variety of terrain such as plains, islands, and mountains. The village landscape is affected by a number of factors such as regional culture, topography, and social economy of the villages. Thus, the external form and internal value of various villages can be different. The geographical landscape in which the village is located has prominent features. Compared with other forms of traditional villages, the regional traditional villages with their topographic features have more evident characteristics of mountainous landscape. Thus, the evaluation of their value in multiple dimensions is a multiangle and multiobjective assessment process. At present, domestic researchers and scholars mainly focus on ecological adaptability, village space study, and evaluation of traditional mountain villages, concentrating in the analysis of traditional village value assessment and landscape formation studies. Traditional villages have specific regional characteristics and historical and cultural heritage. Many mountain traditional villages with remarkable regional culture and unique architectural appearance have been gradually formed in the course of continuous development. Hence, there are relatively a large number of samples available for research, which can be used to study the value assessment and spatial optimization of the landscape formed by mountain traditional villages and lay a sound foundation for further development [7, 8]. The value of traditional villages is not only demonstrated in the fact that traditional production patterns are still present in mountainous traditional villages but also reflected in the case where some villagers still retain their traditional agricultural activities. The traditional folk culture is highly preserved as a regional activity, and there are relatively many types of intangible cultural heritage. In the process of continuous development and enhancement of traditional cultural values, it has endowed the development of tourism connection projects with better tourism prospects and can also contribute to the continuous improvement of tourism reception facilities.

In view of some of the problems mentioned above, as for how to solve these problems more targeted, this paper proposes a method for the visual technology level of new mobile robots in more traditional mountain village landscapes. Facing the problems of large matching error and low efficiency in point cloud aiming, a correlation aiming strategy for layered point cloud is proposed. In addition, the relevant matching algorithm for volume fusion is introduced again. The method puts forward in this paper can be used to optimize the position and posture of the new robot, and the practicality of the method can also be effectively verified by the results of the experimental analysis.

2. The Overall Plan and Suggestions on Improving the Design of Mountain Landscapes

2.1. Visual Technology under the New Robot. In this paper, the design of the new robot is optimized by applying the vision technology to the landscape of mountain traditional villages, and the system architecture constructed at the level of vision technology is shown in Figure 1 as the following. In accordance with the diagram of the system framework depicted in Figure 1, it can be observed that the system designed in this paper can be divided into the following three parts: feature point detection, image correlation matching, and Kinect expression and point cloud generation so as to achieve the purpose of position and pose optimization through conducting the operation of alignment [9].

In this paper, the attribute features of feature points are detected and analyzed in combination of three algorithms (Harris, SIFT, and SURF). At the same time, for the purpose of conducting comprehensive consideration and analysis to ensure that better algorithm robustness and stability can be obtained in the detection results of the system, the traditional algorithm is applied in this paper while at the same time, the SURF algorithm is effectively combined for its rotational attribute characteristics and dimensional changes. The feature values of this algorithm are acquired mainly by using the method of eigenpoint extraction. The eigenpoints are mainly divided into the detection eigenpoints and the attribute eigenpoints, focusing on the function direction selection and the description process of their feature values. The feature values are determined based on the presence of consistency as a way to demonstrate that it can be calculated by using the Euclidean distance calculation method. If the corresponding set of feature points in the image is denoted by letter x and letter y in turn, the expression based on the Euclidean distance operation can be obtained as follows:

$$D(X,Y) = \|X - Y\| = \sqrt{\sum_{i=1}^{d} (X_i - Y_i)^w}. \quad (1)$$

It can be known from the above expression that the similarity of the corresponding distance feature points will be very high, provided that the value of the distance calculated based on Euclidean theorem becomes smaller. During the matching process of all data in this paper, if the maximum adjacency vector related matching algorithm is applied, that is, the attributes of the neighboring feature points and the attribute feature points are calculated for their respective Euclidean distances, $D1$ is used to denote the Euclidean distance corresponding to the nearest feature point, and $D2$ is used to denote the Euclidean distance of

RETRACTED

the second closest neighboring node, and if $D_1 \le \alpha D_2$ (in which α is set to the closest ratio $\alpha = 0.60$), then the two attribute feature points can be regarded as the same and matched correspondingly; otherwise, this point can be ignored.

For the purpose of acquiring the color and depth of the image obtained with the Kinect algorithm, its internal parameters can be optimized to avoid the drift that may occur between the depth camera and the infrared image. Subsequently, the Kinect algorithm is improved. In this paper, the method proposed in the literature [10] is optimized and improved, and the Kinect algorithm is put forward and applied in the process of acquiring the depth values of the image, which allows to obtain the values for the 3D coordinates corresponding to the image. In this way, the corresponding 3D color point cloud data can be generated. By using the function (x_d, x_y) to denote the pixel points of the random image being set, the coordinate points of the image are projected to the 3D spatial points $P(x, y, z)$, and the depth image pixel points can be obtained accordingly. The corresponding coordinates are expressed in the equation as follows:

$$\begin{aligned} x &= \frac{(x_d - c_{xd}) \times depth(x_d, y_d)}{f_{xd}}, \\ y &= \frac{(x_d - c_{yd}) \times depth(x_d, y_d)}{f_{yd}}, \\ z &= depth(x_d, y_d). \end{aligned} \tag{2}$$

It can be known from the above expressions that f_{xd} and f_{yd} can be calculated in combination with the calibration value of coordinates by using c_{xd} and c_{xd} to stand for the depth values at the pixel point of the image, and two symbols denote the coordinates of the image center point, f_{xd} and f_{xd}, to stand for the focal length of the camera.

The new robot visual recognition variable is represented by a ternary array $(r_1, r_2, r_3) r_1 < r_2 < r_3$ composed of zeroed numbers, and its subordinate function is

$$\mu(x) = \begin{cases} \dfrac{x - r_1}{r_2 - r_1}, \text{if } r_1 \le x \le r_2 \\ \dfrac{x - r_3}{r_2 - r_3}, \text{if } r_2 \le x \le r_3. \\ 0, \text{others} \end{cases} \tag{3}$$

The new robot visual recognition is set to $\alpha = (a_1, a_2, a_3)$, $\beta = (b_1, b_2, b_3)$, according to the expansion principle of the addition and power of the new robot visual recognition number

$$\begin{aligned} \mu_{\overline{\alpha}+\overline{\beta}}(z) &= \sup\left\{\min\left\{\mu_{\overline{\alpha}}(x), \mu_{\overline{\beta}}(y)\right\} z = x + y\right\} \\ &= \begin{cases} \dfrac{z - (a_1 + b_1)}{(a_2 + b_2) - (a_1 + b_1)}, a_1 + b_1 \le z \le a_2 + b_2 \\ \dfrac{z - (a_3 + b_3)}{(a_2 + b_2) - (a_3 + b_3)}, a_2 + b_2 \le z \le a_3 + b_3 \\ 0, \text{others} \end{cases}. \end{aligned} \tag{4}$$

That is, the new robot visual recognition, and then

$$\overline{\alpha} + \overline{\beta} = (a_1 + b_1, a_2 + b_2, a_3 + b_3). \tag{5}$$

From $\mu_{\lambda\overline{\alpha}}(z) = \sup\{\mu_{\overline{\alpha}}(x) | z = \lambda x\}$
It can be obtained

$$\lambda\overline{\alpha} = \begin{cases} (\lambda a_1, \lambda a_2, \lambda a_3), \lambda \ge 0 \\ (\lambda a_4, \lambda a_3, \lambda a_2), \lambda < 0 \end{cases}. \tag{6}$$

Let $\overline{\alpha}_i = (a_{i1}, a_{i2}, a_{i3})$, $i = 1, 2, \cdots, m$ is a new type of robot visual recognition, and the resulting non-negative linear combination of $\overline{\alpha}_i$ and the new type of robot visual recognition planning

$$\sum_{i=1}^{m} \lambda_i \overline{\alpha}_i, \lambda_i \ge 0. \tag{7}$$

It is still a type of new robot visual recognition, and

$$\sum_{i=1}^{m} \lambda_i \overline{\alpha}_i = \left(\sum_{i=1}^{m} \lambda_i a_{i1}, \sum_{i=1}^{m} \lambda_i a_{i3} \right). \tag{8}$$

At present, the recognition of new robots in terms of vision technology is still realized through random programming, and the constraints also include data of random parameters, which may provide a certain probability that the constraints are related. In the context of visual recognition of novel robots, the understanding of chance is defined as a limited possible behavior. New robots have planning constraints on recognition technology. The new robot with strong randomness provides a powerful tool for solving the optimization problem of random parameters and new type robot identification parameters at the level of visual recognition technology and the control scheme of new robot visual recognition technology.

In this paper, the new robot performs a certain rough matching of attribute feature points at the visual technology level; therefore, the common areas of the two sets of point sets can be roughly overlapped, so that the corresponding matching can be done for the next step more accurately. Subject to constraints in the process of planning, the new

RETRACTED

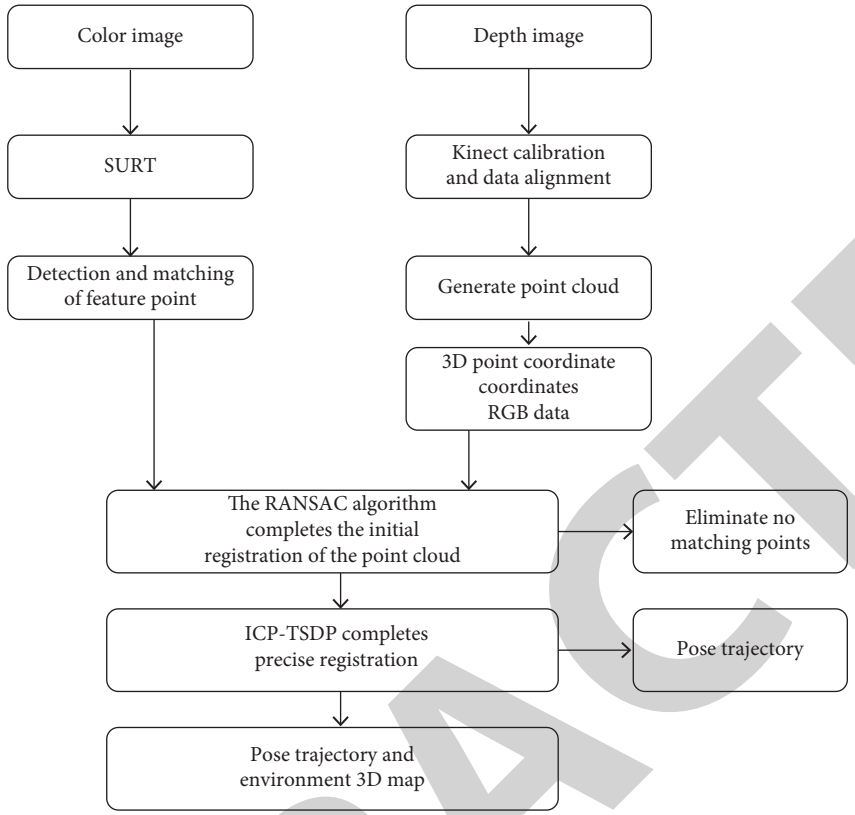

Figure 1: Framework diagram of the vision technology system for mobile robot.

robot vision technology is of relatively flexible randomness. The control method based on the new robot vision technology can be used to obtain the random parameters effectively and provide a valid solution path for the optimization of robot parameters.

The new robot vision control technology applied in this paper has a certain roughness in the process of processing attribute feature points, which can ensure that a state of overlap will be achieved in the corresponding common region between the two sets of point sets as a means to obtain more accurate preconditions. The method adopted in this paper can be used to set the error values that may occur in the range and match them to the internal and external points under the conditions of the experiments set in this paper. Among them, the value for the threshold can be set to 3.00, and if the error obtained is greater than d, then it indicates that this point (outlier point) should be discarded. During the course of the experiments, the least squares approximation is also invoked to obtain the variation of the camera position in real time [11]. By using the algorithm proposed in this paper, all interior points are calculated. Subsequently, the nearest neighboring positions and poses of the new robot can be assessed effectively based on the least squares method. The equation for the transformation relationship between the positions P_j at time i and time j is $P_j = P_i T_i^j$, in which the camera is denoted by T_i^j, which stands for the value of the rigid transformation matrix.

$$T_i^j = \begin{bmatrix} R_{3\times3} & t_{3\times1} \\ 0 & 1 \end{bmatrix}. \tag{9}$$

In accordance with the above expression, the rotation matrix can be denoted by the symbol $R_{3\times3}$; $t_{3\times1}$ stands for the translation translation matrix. With regard to the simultaneous localization of the new mobile robot and the mapping construction of the map, the translation matrix of all the time data to the start time can be acquired according to the following equation:

$$T_0^k = T_0^1 * T_1^2 \cdots T_{k-1}^k. \tag{10}$$

Through the features demonstrated in this paper, the most straightforward point-to-cut derivation method is adopted. In addition, a more comprehensive computational numerical method is used in the experimental part of the paper; at the same time, the application of the Euclidean algorithm can reduce the generated noise to a great extent, which has exerted the effect of sound elimination and improved the success rate of the initial values.

In the traditional calculation method, there is always a defect: if the point cloud of two frames is integrated, redundant points can be generated at the fused point cloud. Hence, a calculation method that allows the volume space to be fused as a background before being converted is adopted in this paper to address this situation. The purpose of this calculation method is to present the cubic data in three

RETRACTED

dimensions by creating a way that can convert the cubes to spatial pixels with the specific resolution values. The specific conduct of each point to the cut plane is documented in detail in a timely manner. The point cloud fusion map is shown in Figure 2 as the following. The positive and negative values stand for the distance to meet the tangent, and a point of the surface is denoted by a zero point. The values are processed in sequence, and the new values are generated and calculated according to the equations (8) and (9). The different values generated for each frame are collected and fused, and finally, the point generated by the surface can represent the zero pixel of the spatial volume.

2.2. The Overall Plan for the Design of the Relatively Traditional Village Landscape in the Mountains

2.2.1. Taking the Basic Functions of Mountain Village Landscapes as the Basis for Zoning Planning. Regarding the various functions of the mountain village landscape, the whole village can be divided into five areas, namely the leisure area for reception, the Yinhe Street commercial area for business, the central area for rural community services, and the residential tourism area, and a resort area for residential tourism and an ecosphere for green ecological protection.

Leisure area for reception: the location is around the reservoir to the east of the mountain village and could be programmed to function as a water recreation area and a reception for premium leaders. All the leisure and entertainment methods mainly include a water playground on the sandy shoal, a small pier on the lakeside that can be used for boating, a fishing area along the lake, and facilities such as manpower, wind power, and water vehicles on the south bank of the lake. On both sides of the lake, there are also room for nourishing the heart, gate tower, Goddess Pavilion, and various buildings to provide a higher level of reception. There is also a garden on the south bank of the lake, where all kinds of flowers are grown for viewing, and a small folk playground can also be used for some small entertainment.

Yinhe Street commercial area for business: a stone pedestrian street with residential shops on both sides is set along the riverside of the village, and three small distribution places are opened along the road for festivals and local activities, reflecting some local ethnic characteristics. The custom of going to the market exists locally, transforming the front of the road house into a commercial store, and the residents live in the residential building at the back. The buildings on both sides of the road in the entire building complex are different in height and are scattered in a well-arranged manner. Entering and exiting is also a kind of fun and has different characteristics.

Central area for rural community service: this central area is mainly in the north of the room where the village committee lives. Six groups of dwellings and scattered earthen houses were demolished and later formed a large courtyard unique to the village. This location becomes the new dedicated activity center for the rural community according to the function. The main activities of the whole community include projects that provide life services, such as village committees, community activities, and centers specially designed to receive tourists or visitors, marriage agencies, maternal and child health centers, science and technology, culture and education, youth activity centers, and senior citizens activity center.

Resort areas for residential tourism: the function of this location is as a residence service for tourists or visitors.

Ecosphere for the protection of green ecology: the mountains surrounding the picturesque village come together. They are an untouchable environmental backdrop and a source of water for the mountain village. This paper strengthens the greening and decoration of this environment by planning to make it have a certain ornamental value. Nanliangzi and Dongshantou are dedicated areas for mountaineering activities that tourists can expect, climb, and arrive at. In addition, the hills surrounding this location are planted with seasonal fruit trees and greenhouse plants, which visitors can also experience.

2.2.2. Some Plans for the Current Building of the Residence. The structure of the current residential buildings can basically maintain the spatial structure left over from the original village in the piedmont. On the basis of harmony with the surrounding natural environment, some old residential buildings have been correspondingly protected and better transformed in this spatial structure. Most of the remaining walls of the residential buildings have been modified to some extent, and some have been demolished and rebuilt. The reconstructed overall architectural shape highlights the unique characteristics of the ancient residential style of Laiwu Mountain Village. According to its function, some floors are changed to two-story structure to accommodate more tourists and provide them with accommodation services. There is also a small part of the platform built according to its unique terrain, in the form of three layers. The houses inhabited by the villagers are largely the same as before, only a part of which has been renovated, and the residential standards of the new buildings have been improved. Based on the needs of tourism activities, the corresponding folk daily necessities are configured in the regional environment, which fundamentally reflects the characteristics of folk customs. The south wall of the residential house should be properly lowered in order to promote the ventilation of the house and provide a better view. Figure 3 shows the reconstructed three-story residential structure.

2.2.3. Planning and Protection of Green Environment. In order to optimize the existing plants and water systems more effectively, fully excavate the context structure in the existing natural landscape in terms of planning and protection, an overall greening system is designed that combines points, lines, and planes to form a unique green structure. This greening structure is implemented around the three main bodies of "greening circle of ecological environment—greening lines on roads—greening points in residents' courtyards." The ecological environment green circle protects the original ecological tree species and wild flowers

RETRACTED

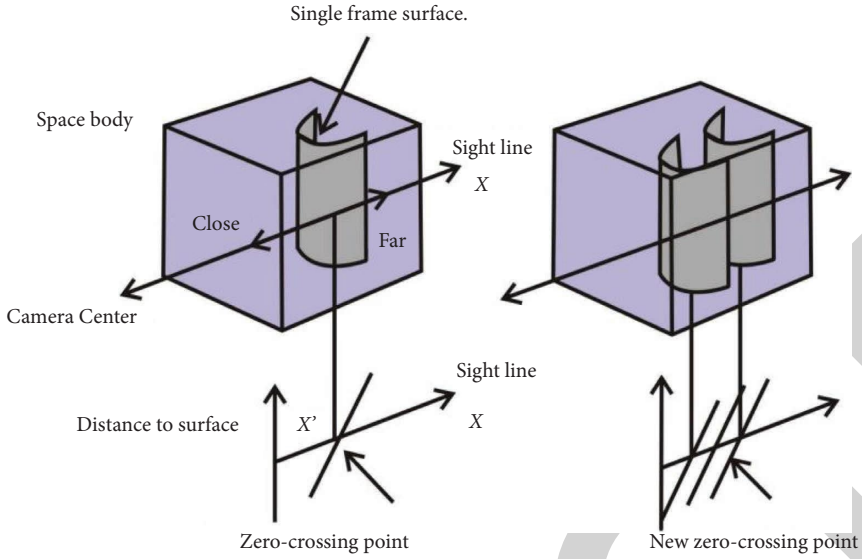

Figure 2: Point cloud fusion results based on volume space.

in the mountains around the village to a certain extent and further improves the greening degree on this basis, thus forming a combination of fruit trees, economic trees, and characteristic ornamental trees. In addition to planting trees in the garden, the greening of the residential area also focuses on vertical greening in terms of earth walls and walls. At the same time, according to the topographic structure and spatial layout of the mountain, some suitable trees are appropriately planted on both sides of the road and on both sides of the river. The ecological green circle outside the village and the small green space in the village form a green corridor that intersects with each other. The dotted lines are connected to each other to maintain the continuity of the green area in space. After planning the above points, it is necessary to prohibit the passage of large vehicles in the village, and private cars are scattered in and around the village, so as to prevent noise and air pollution and maintain a very good ecological environment. Figure 4 is a view of the village landscape after green planning for reference.

2.3. Suggestions on Improving the Design of Mountain Landscapes

2.3.1. Effectively Improve the Unique Design System of Mountain Landscape. Continue to strengthen publicity efforts to raise awareness of village names and awareness of environmental protection: the most critical point in the design of mountain landscapes is to raise the awareness of local people to consciously protect the local mountains. First, take protection as the theme of propaganda, and formulate a very eye-catching and easy-to-understand propaganda slogan, thus emphasizing the importance of red landscape in design and its meaning to people themselves. Second, it is necessary to choose a publicity method that is closer to the masses, so as to strengthen the publicity and protection of the red landscape, and to publicize the value and significance of protecting the mountains from the

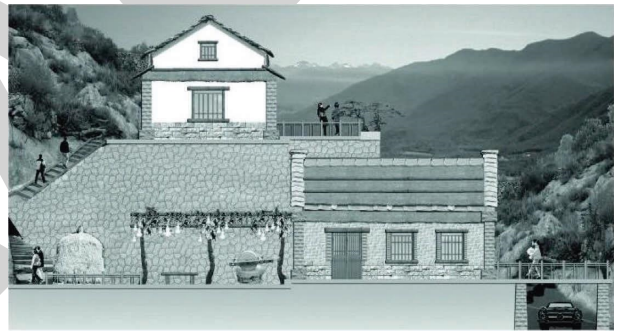

Figure 3: Side elevation view of the fake three-story residential house after renovation.

spiritual, economic, and social levels. Finally, it is also possible to publicize the relevant responsibilities of protecting mountains from the legal level, thereby creating a general atmosphere of protection for mountains.

The main landscape design and completion of the mountain area: many of the existing mountain ranges have been damaged to a great extent due to the development of the age and different degrees of natural disasters. If this paper wants to develop the mountain reasonably and effectively and try to convert the benefits brought by multimedia into economic benefits, it is necessary to realize the relevant maintenance of multimedia benefits. For example, the multimedia prototype is repaired, so as to improve the unique value system of multimedia. On the other hand, local authorities must also pay attention to the unique social and economic value of mountainous areas, continuously increase investment in the design of major mountain landscapes, and even set up special protection funds to repair some damaged areas, to protect the existing valuable cultural heritage and ensure sustainable development. In addition, local governments must also change their thinking on protection, decentralize the development rights of some

RETRACTED

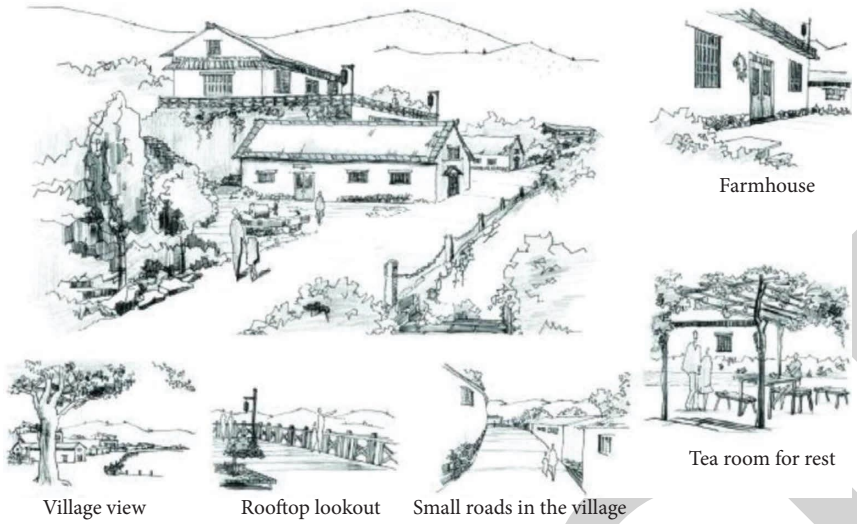

Figure 4: The local landscape rendering of the village.

picturesque places, and attract foreign investment. Only by attracting social capital can we protect and develop local mountainous areas under the guise of more social forces [12, 13].

Arouse the public's environmental awareness and attach importance to environmental protection in the development process: during the development of the whole mountain area, local authorities should also pay attention to protecting the ecological environment through multimedia, and the environment around multimedia should also pay more attention. It is strictly forbidden to arbitrarily destroy the green ecological environment around the local mountains. During the entire development process, the prototype and characteristics should be maintained as much as possible, and the excessive commercial development of the mountainous area should be fundamentally avoided. At the same time, strengthen the strong maintenance of local public security and social order, prevent or eliminate the bad influence brought by some bad cultures, and protect the original ecology unique to the place and the simple characteristics of the villagers as much as possible.

2.3.2. Effective Analysis of Mountain Landscape Design Process Data. Effectively develop local mountain products based on the benefits brought by the advantages of multimedia: in addition to the effective development of the mountainous area, the area also enriches the multimedia of various tourism types such as ecological environment, natural customs, folk culture, and red culture. When developing the mountainous environment, it is also necessary to strengthen the mutual integration and penetration with the local ecological environment, natural customs, folk culture, red culture, and other types of tourism multimedia and constantly integrate the advantages of multimedia, so as to promote cooperation and development between scenic spots and scenic spots, between scenic spots and travel agencies, and between travel agencies and travel agencies, so as to jointly develop relevant tourist routes and launch mountain products that meet local characteristics. In the actual development process, the emphasis is placed on the advantages of the combination of red and black and the combination of red and green, that is, to make reasonable use of the unique national charm of the black-clothed Zhuang people and then launch a very distinctive tourist route of "travelling through the old revolutionary bases and looking for the black-clothed people." Using multimedia functions, such as ecological environment, green and low carbon, and adventure exploration, is to promote the popularization of mountain characteristics and jointly launch tourist routes such as "red city adventure journey" with local environmental characteristics.

Unique identification of product characteristics to create a characteristic brand exclusive to the place of origin: the development of the brand can also serve as an important foundation for the survival and development of tourism products. If you want to expand the influence and attraction brought by the municipal mountain area, you must constantly highlight its own characteristics, so as to build local brands. First, you can combine the characteristics related to the mountain and at the same time use the "wind and thunder, the red flag between the two rivers" to determine the most important image position of the mountain, that is, focus on the region and emphasize the status of "left and right rivers and mountains." Second, through the use of the development of multiple tourism multimedia such as ecological environment, folk characteristics, natural customs, red culture, combined with the mountains, a secondary image positioning featuring "Blessed Land in the Red City, with thousands of postures" is constructed to emphasize the unique beneficial result brought about by red travel. Third, this article will utilize the influence of the uprising on Comrade Deng Xiaoping to establish a third-level image positioning with the slogan "The second birth city of Deng Xiaoping old area" and use the great Deng Xiaoping to enhance the brand value of the mountain itself.

RETRACTED

Segment the current market and continuously expand the source of customers: taking into account the unique characteristics of tourism multimedia and the current composition of various types of tourists, the tourism market can be roughly divided into mountainous areas and can be divided into more detailed divisions to expand the supply of tourism resources. From the perspective of geographical distribution, tourists from mountainous areas are mainly tourists from Guangxi, which can gradually develop Guizhou, Hunan, Yunnan, Pearl River Delta, Vietnam, and other regions—the source of tourists from these surrounding cities, and finally supplement other domestic cities and quickly enter the national market. From the perspective of tourism purposes, this paper can also develop a series of political groups, such as patriotism education, integrity education, and socialist core values research, and these aspects of learning can be used as a source of tourists, or through cooperation with other tourism multimedia to attract tourists. According to the type of tourists, in the current relatively stable tourism resource groups such as government institutions, higher education institutions, primary and secondary schools, military forces, enterprises, this paper can increase the development of individual tour groups targeting tourism. At the same time, the city will benefit from the opening of the "mountain special train," and the organization of the tourism fleet advertising activities and the development of tourism festivals continue to expand the relevant channels for publicity and continue to strengthen the publicity of tourism, so as to further develop more tourist sources market [14, 15].

2.3.3. Continuously Optimize the Industrial Structure of the Current Tourism Area, So as to Comprehensively Improve the Development Quality of the Mountains. Widespread promotion of mountain culture: in today's society, the main operation status of each mountain tourist attraction is still independent operation, which is not conducive to the promotion of the entire mountain landscape tourism. In response to this, this paper proposes that it is necessary to break the situation that each region is independent and divide the existing mountainous areas in the region according to different themes to form connecting routes to become a tourist area. It is even more necessary to radiate and popularize the entire mountainous area in the form of a cone, fundamentally improve the utilization rate of the entire mountainous area, and strive to convert the existing advantages of multimedia into economic advantages, and do our best to save the investment cost required in tourism construction. To a certain degree of adjustment to the industrial chain structure of this tourist mountain area, in order to improve the development quality of the whole mountain area, internal and external cooperation is strengthen in various places, so as to present a win-win situation for several parties: What the city needs to do now is to seize all possible development opportunities in the entire mountainous area of Guangxi, so as to strengthen the effective cooperation between various regions and Nanning, Chongzuo, Longzhou, Hechuan, and by complementing the respective multimedia advantages and disadvantages of the regions, sharing their respective network marketing platforms, we can jointly carry out effective and reasonable publicity to the mountainous areas, so as to build a very high-quality image and create a brand with certain competitiveness and to expand the market scope of existing land in mountainous areas. On the other hand, this article will take advantage of a high-quality geographical location such as the junction of Yunnan, Guizhou, and Guangxi, get rid of the restrictions brought by geographical location, search for more opportunities for cooperation with surrounding provinces, and establish a cooperative relationship between partners in the mountains, and jointly promote the further development of the mountains.

3. Analysis of Examples and Results

The traditional mountain village landscape is selected, and the network electronic map is used as the technical support. In addition, a total of 200 cases of modern mountain traditional village landscapes that won the professional award constitute a statistical sample. Taking the formation mechanism of landscape ornamental as the classification benchmark: among the 100 landscape samples, there are 17 active mountain traditional village landscapes which occupy the 17% of the total. The mountain traditional village landscapes loaded for the first time accounted for 6% of the total. There were 78 cases of active and passive secondary load ornamental landscape, accounting for 78% of the total.

The pattern prototype of the spatial interface of multimedia multidimensional control comes from the pyramid, the main visual information is concentrated on the eye line, and the visual focus presents a stable triangular composition. 200 examples of samples are counted based on the visual-dominant spatial interface classification as shown in Figure 5. Among them, the mountain traditional village landscape with multimedia multidimensional dominant spatial interface accounts for 85%, accounting for an absolute proportion. In this way, having a clear ornamental subject is often a means of landscape design for mountain villages.

The entire landscape is effectively controlled by a very clear and definite axis, which not only functions as a visual channel but is also the most important tourist route. Because the existing tourist routes and decks within the line of sight have certain restrictions on the viewing of tourists to a certain extent, the main body of its decoration is mostly beyond the ordinary buildings, and it is also the most prominent sign and visual focus in the entire landscape environment. This paper can use the corridor characteristics of the line of sight and the visual-dominant space interface caused by the symbolic decorative subject, so as to show a relatively stable structure similar to the pyramid, which will have a strong impact on the visual and psychological levels, and it conveys the beauty of nature at the landscape level. The design method in this way is usually applied to watch the rural landscapes visited by celebrities, the rural landscapes where important historical events have happened, etc. These landscapes often take a single view as the viewing center.

RETRACTED

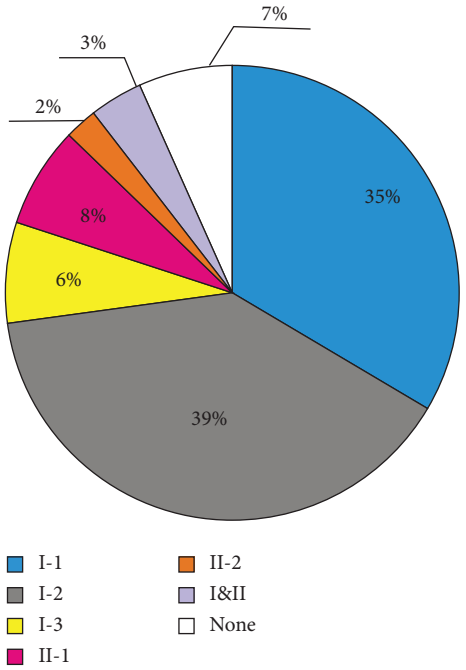

Figure 5: Proportion of various visual-dominant spatial interfaces in the statistical sample.

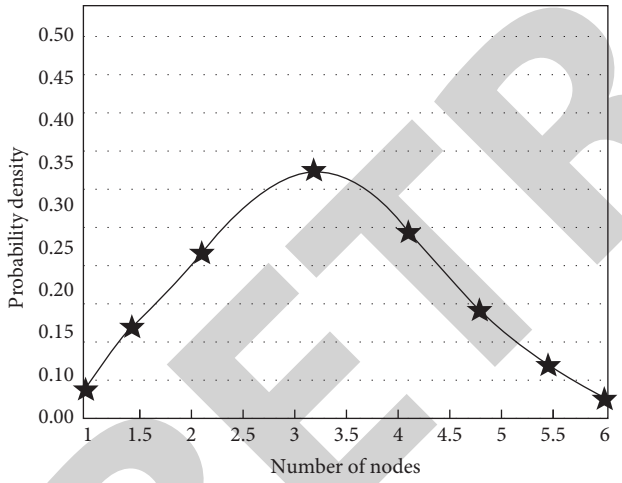

Figure 6: Probability density distribution of the number of nodes.

In the statistical sample, there are 55 examples of both landscape corridors and multimedia multidimensional leading space interfaces. Twenty-six examples were randomly selected to form a secondary statistical sample. Extract the data of each visual factor, and make statistics from the following aspects through numerical value. The proportional relationship between the number of landscape nodes and each axis is calculated, and the ornamental subject is located at the position of the axis. Quantitative relationship analysis of axes and plan planes is shown in the following section (Figures 6–8).

From this, the following conclusions are drawn: (1) the number of landscape nodes presents a normal distribution, and the distribution characteristics show that there are more in the middle and less on both sides. The average number of

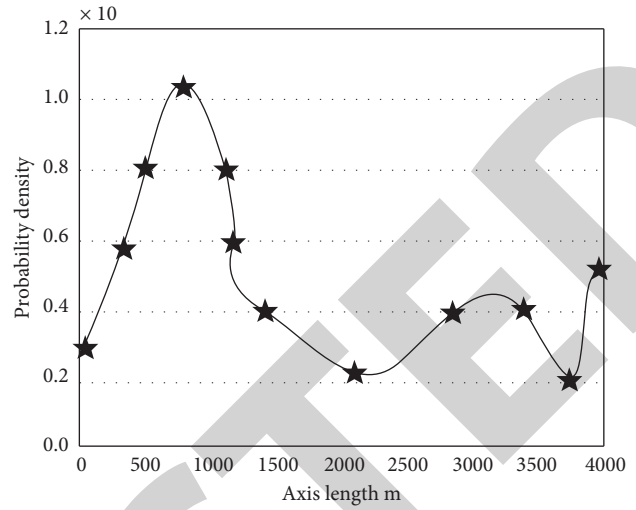

Figure 7: Probability density distribution diagram of axis length.

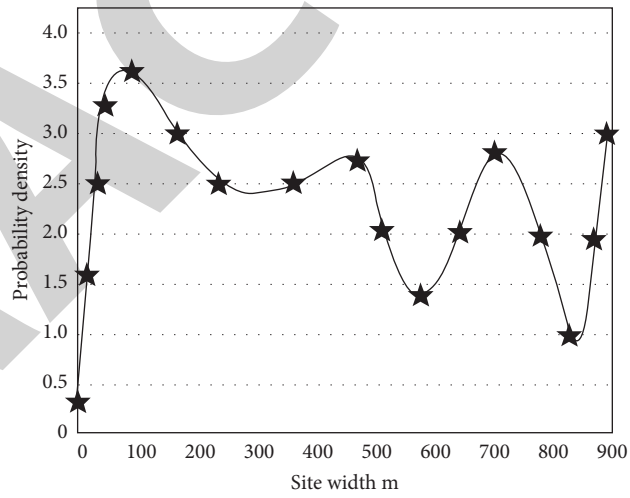

Figure 8: Probability density distribution map of site width.

nodes is about 3; (2) the distribution characteristics of the two peaks in the axial length, one is close to 700 meters, the other is close to 3300 meters, the first peak distribution is more; (3) the width of the site is centrally controlled within the range of about 400 m. This is especially evident in the dataset at a range of 200 meters, the same as the city square, which is almost identical in scale.

4. Conclusion

Aiming at the problems existing in the point cloud aiming process of the new mobile robot in the visual recognition technology, such as large matching errors and low recognition efficiency, this paper proposes a more traditional optimization method for mountain village landscapes. Aiming at some problems in the process of splicing and combining point clouds, a matching algorithm based on the fusion of volume and space is proposed. In the generation of 3D map, a multiframe fusion method based on volume space is proposed to reduce the redundant problem of points. After several experiments for effective verification, the final results

RETRACTED

Hindawi
Journal of Robotics
Volume 2024, Article ID 9893014, 1 page
https://doi.org/10.1155/2024/9893014

Retraction

Retracted: Security Risk and Preventive Measures of Multimedia Database System under Remote Control of Network Robot

Journal of Robotics

Received 23 January 2024; Accepted 23 January 2024; Published 24 January 2024

Copyright © 2024 Journal of Robotics. This is an open access article distributed under the Creative Commons Attribution License, which permits unrestricted use, distribution, and reproduction in any medium, provided the original work is properly cited.

This article has been retracted by Hindawi following an investigation undertaken by the publisher [1]. This investigation has uncovered evidence of one or more of the following indicators of systematic manipulation of the publication process:

(1) Discrepancies in scope
(2) Discrepancies in the description of the research reported
(3) Discrepancies between the availability of data and the research described
(4) Inappropriate citations
(5) Incoherent, meaningless and/or irrelevant content included in the article
(6) Manipulated or compromised peer review

The presence of these indicators undermines our confidence in the integrity of the article's content and we cannot, therefore, vouch for its reliability. Please note that this notice is intended solely to alert readers that the content of this article is unreliable. We have not investigated whether authors were aware of or involved in the systematic manipulation of the publication process.

Wiley and Hindawi regrets that the usual quality checks did not identify these issues before publication and have since put additional measures in place to safeguard research integrity.

We wish to credit our own Research Integrity and Research Publishing teams and anonymous and named external researchers and research integrity experts for contributing to this investigation.

The corresponding author, as the representative of all authors, has been given the opportunity to register their agreement or disagreement to this retraction. We have kept a record of any response received.

References

[1] W. Deng and P. Yan, "Security Risk and Preventive Measures of Multimedia Database System under Remote Control of Network Robot," *Journal of Robotics*, vol. 2023, Article ID 9276208, 8 pages, 2023.

Hindawi
Journal of Robotics
Volume 2023, Article ID 9276208, 8 pages
https://doi.org/10.1155/2023/9276208

RETRACTED

Research Article

Security Risk and Preventive Measures of Multimedia Database System under Remote Control of Network Robot

Wenyan Deng[1] **and Pengfei Yan**[2]

[1]*Information Technology Department, Shanxi Professional College of Finance, Taiyuan, China*
[2]*Qinhuangdao Vocational and Technical College, Qinhuangdao, Hebei 066000, China*

Correspondence should be addressed to Pengfei Yan; ypftrybytry@163.com

Received 4 November 2022; Revised 1 February 2023; Accepted 29 April 2023; Published 17 May 2023

Academic Editor: Shahid Hussain

Copyright © 2023 Wenyan Deng and Pengfei Yan. This is an open access article distributed under the Creative Commons Attribution License, which permits unrestricted use, distribution, and reproduction in any medium, provided the original work is properly cited.

The rapid development of network technology makes the world enter a new era, but it also brings a variety of severe information security problems, which makes the network security more and more important. Based on the existing literature and information, this paper expounds the current situation of database information system security. In view of the security risks of the media database information, this paper proposes to use the remote control system of the network robot, through sorting out the organizational structure characteristics and technology of multimedia data, establish the security defense system, and try to manage the multimedia data security. This system takes the mobile robot as the control object and adds the vision and ultrasonic transducer for the robot, so that it can carry on the semi-autonomous movement under the control of human. In addition, the host PC is used as the main control terminal to send instructions to the remote robot and receive the feedback data information. The simulation results show that the robot remote control system has good security, can ensure the establishment of database security defense technology system, and has the characteristics of convenient operation, easy to expand, and strong mobility. From the research point of view of this paper, the combination of robotics and multimedia information security is booming and will become a new application prospect.

1. Introduction

With the continuous development of computer system technology and database technology, the current society has gradually become a "data society," producing all kinds of data, and the same is true for multimedia data [1–3]. The database is the main part of the computer system. It provides convenient information storage function for our users. However, when using the database, it has the characteristics of resource sharing, so there are certain security problems. If you are not careful, the data security of our users will be threatened, resulting in unpredictable losses. Therefore, we must ensure the security of the computer database. In the process of multimedia data storage or transmission, it is very necessary to store, manage, and search multimedia data in a timely and efficient manner. In order to meet the needs of the development of social informatization, we must pay attention to the research and improvement of the current multimedia database, develop new technologies, and continuously improve its use effect [4–6]. The development of robotic remote control technology began in the early 1960s. With the continuous expansion of people's cognition of the natural world and the application of robots, some harsh working environments cannot be avoided, such as exploration in volcanoes, sea exploration, space exploration, patrol, reconnaissance, and monitoring of military bases, and biological, chemical, and nuclear test site operations. High-risk environments bring great harm to the personal safety and mental health of workers and sometimes even endanger their lives. Therefore, many robots working in such harsh environments have changed their on-site control methods from the previous on-site control to wireless remote control [7, 8]. In China, the remote monitoring system of heterogeneous monitoring platforms developed by the

Institute of Automation of Shenyang Branch of the Chinese Academy of Sciences, the shared control system of space robots developed by Harbin Institute of Technology, the remote monitoring system based on the Internet developed by Beijing University of Aeronautics and Astronautics, etc. are prime examples of robotic remote monitoring systems [9–11]. The current models of remote monitoring systems are mostly based on a single point-to-point network control. When the robot is in a complex environment or when multiple robots are required to cooperate, this control method cannot cope with it. The control method based on wireless local area network can easily extend a single robot into a robot group and let it balance its movements while ensuring real time and stability of data transmission.

Multimedia information data have the characteristics of many types, large data scale, and complicated transmission. Therefore, when storing, searching, and managing, it must have a comprehensive design and ensure its data security. Faced with such requirements, this paper, according to the network robot remote control system, organizes the important characteristics of database security, integrates the structure management of multimedia information, and carries out mutual blending to establish a preventive system for information security, aiming at discussing the security management of multimedia database.

2. Network Robot Remote Control System

In the specific use of the database, data backup should be based on effective security principles. If there is a problem with the database due to some reason, the relevant data content can be restored in the case of data backup, so as to ensure the accuracy and comprehensiveness of the data. With the application of this method, problems such as data changes and malicious attacks during database operation can be avoided. A complete set of hardware equipment diagram is shown in Figure 1.

The upper host computer communicates wirelessly with the lower computer based on the wireless connector. In order to ensure the signal quality between the two production workshops and achieve remote wireless control of the robot, a router is added between the two production workshops, which can increase the strength of the signal, prolonging the signal transmission time. The onboard computer uses the EPIA-P700 serial Pico-system motherboard, which has many extended interfaces, small size, and low power. The use of the embedded system motherboard saves development time and increases the stability of the system. Imaging devices and ultrasonic sensors have been added to this motherboard to improve the functionality of every aspect of the mobile robot.

The overall robot system can be divided into wireless communication module, body controller module, motor control unit and main program, sensor, and image collection module. The configuration diagram of each module is shown in Figure 2.

According to the framework of the mobile robot control system in Figure 2, the body operation controller of the robot, as a key part of the control system, that is, the brain of

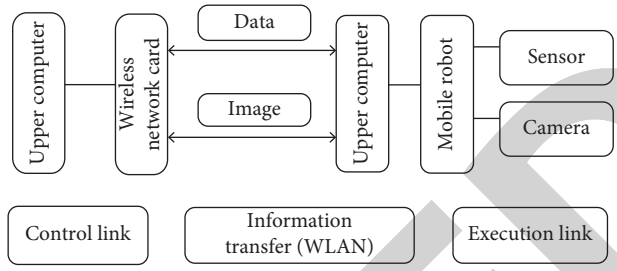

Figure 1: System hardware structure diagram.

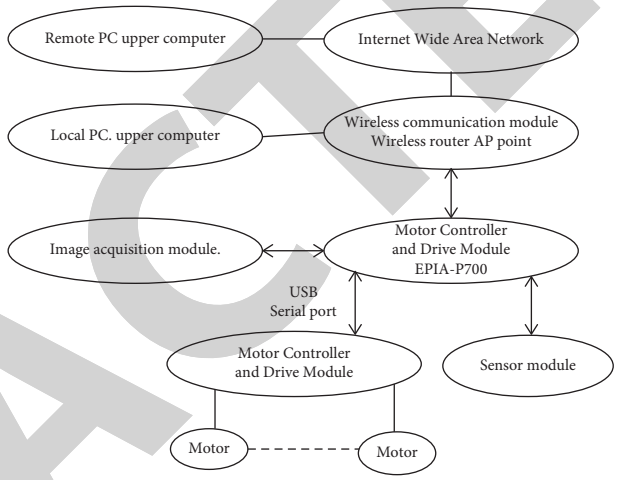

Figure 2: Frame diagram of mobile robot control system.

the robot, not only needs to use the wireless module to communicate with the host computer but also executes according to the received information instructions and sends the received information and instructions to the controller of the next level according to its own port to realize the control of the motor. In addition, the function module for receiving image information can transmit data information to the host computer, so that the main control terminal can know the environment where the mobile robot is located at all times.

The advantage of using templated distributed control is that each control template of each layer of the control system is basically independent of each other. When a problem occurs, it is easy to find out where the error occurred. At the same time, it also simplifies the shift of the system. Any template can be shifted to other systems, as long as the underlying function corresponding to the new system is changed. The vehicle-mounted PC uses a small control board and forms a wireless LAN environment based on a WNIC, a router, and its upper-level control PC [12, 13].

Because the remote control of the robot is mainly based on the received data information, the wireless communication module carried by the host computer PC and the robot itself mainly uses the socket communication method, combined with different transmission data information instructions. Sockets can be divided into connection-facing data flow sockets and connectionless data flow sockets. The

RETRACTED

system uses connection-oriented data streaming sockets in this paper, as shown in Figure 3.

When using face-to-face streaming socket communication, the server side should be turned on first; otherwise, an error will occur when the client connects. The communication steps are shown in Figure 3. The vehicle-mounted controller is used as the communication server. After turn-on, first use socket () to set up a socket, then call bind () to combine the socket with the local network IP, and then use listen () to make the socket ready for listening. Ask for the length of the queue, and then use accept () to receive the connection from the PC client. The remote PC can use connect () to establish a connection with the server after turning on the setup socket. As long as the connection is established, the ddc of the frame and the remote PC can transmit and receive information according to the wireless network based on the sub-functions send () and recv () identified by the system.

After the fuselage ddc receives the instructions sent by the remote host computer (the detailed walking path or pace), it will be saved. When the data information is received, close the socket, forward it to the next motor ddc, the motor ddc interprets and executes it, and the body ddc transmits it to the motor ddc. The data transmission steps are shown in Figure 4.

Before the serial communication between the fuselage computer and the motor computer is turned on, the serial port should be set first. Here, we use the underlying function library of the motor computer [14, 15].

Suppose that the input of the Qth sample is P_n and the output of the Qth sample is P_{n-1}.

$$I_{qj} = \sum_{i=1}^{n} w_{ij} \times x_{qi} - \theta_j. \tag{1}$$

The ith neuron in the hidden layer and the weight value are P_{back}. At the same time, P_n is the threshold.

The output value of the jth neuron is shown in the following formula:

$$Q_{qj} = f\left(I_{qj}\right) = \tan sig\left(I_{qj}\right) = \frac{2}{1 + e^{-2I_{qj}}} - 1. \tag{2}$$

The input value of the jth neuron is shown in the following formula:

$$I_q = \sum_{j=1}^{h} w_j \times Q_{qj} - \theta. \tag{3}$$

The output value of the qth neuron is shown in the following formula:

$$Q_q = f\left(I_q\right) = \tan sig\left(I_q\right) = \frac{2}{1 + e^{-2I_q}} - 1. \tag{4}$$

3. Analysis of Security Prevention Technology of Multimedia Information Database

3.1. The Main Characteristics of Database Security. According to the important characteristics of database security, its characteristics include many aspects such as security, comprehensiveness, concurrent control, and fault recovery. The important features of database security are described in detail. The details are as follows [16, 17].

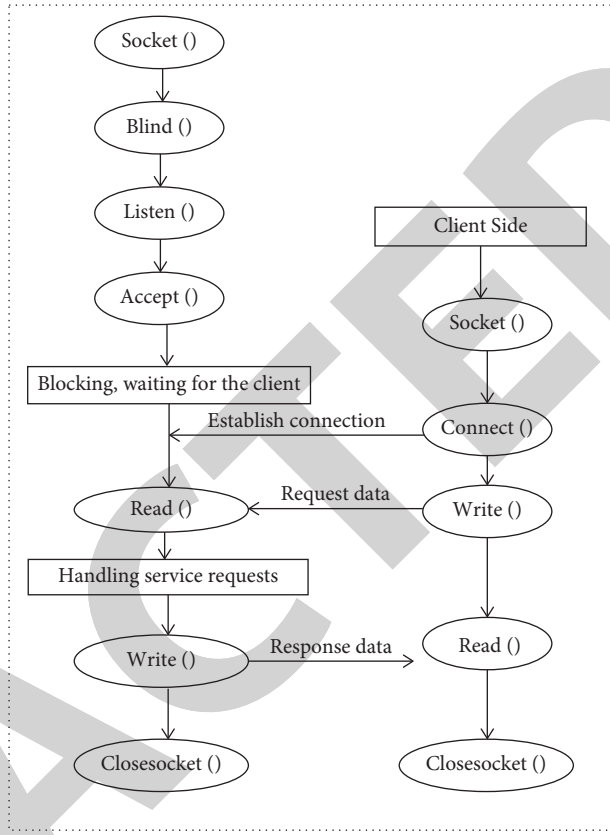

Figure 3: Flow socket programming flowchart.

Security. In order to better ensure the security of database information, the important data should be managed separately and separated from other data during management, so as to better ensure the security of the data and prevent the loss of important data. In addition, attention should be paid to standard access, timely control of access, and access through relevant requirements to ensure the security of the database in each link. In addition, all kinds of information stored in the database should be encrypted, and audit-related work should be done to ensure the security of the information.

The data collection interface is the main component in the application of the multimedia information database. It completes the data exchange between the production process control system and the real-time database system. The industrial communication gateway based on the embedded configuration has the advantages of high reliability, small size, light weight, easy to carry and maintain, easy to extend, and sufficient functions. The main service software of the embedded computing platform can run on the desktop. Because the data are complete and easy to forward, they can be used at ease. At the same time, the platform can access different types of protocols and convert them into standard protocols (such as OPC methods) to connect with other systems. Therefore, the data collection gateway is used in the field data collection system and the real-time database server to realize data collection.

RETRACTED

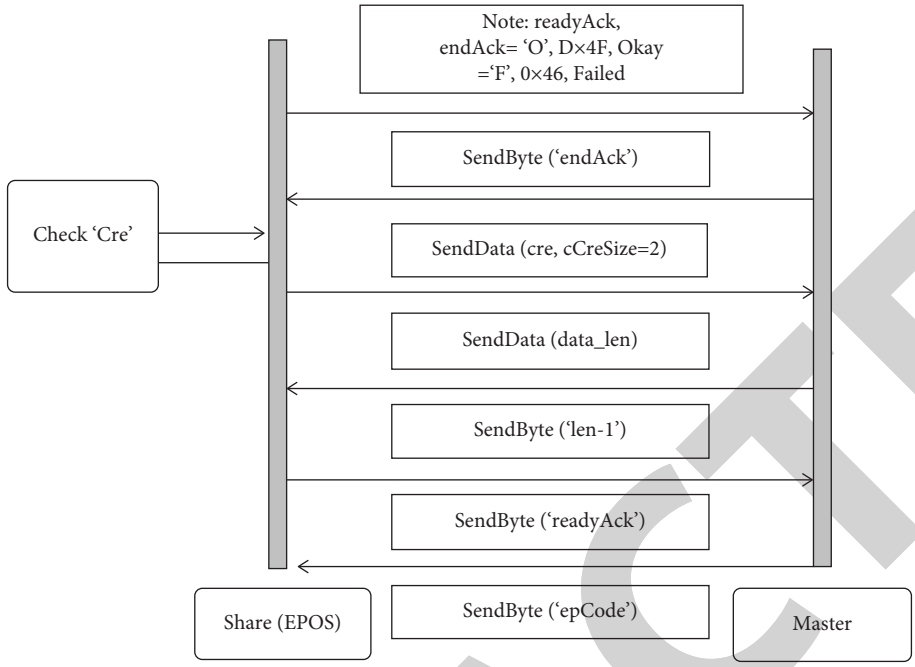

Figure 4: Flowchart of data transmission of robot control system.

Comprehensiveness. Comprehensiveness mainly includes many contents such as data accuracy, validity, and compatibility, and these contents cannot be lost. If lost, the integrity of the data will be affected.

Concurrency Control. In a database, each data resource is used not only for a single purpose but also for multiple users. Users who use resources together can also operate the database, that is, multiple users manipulate data. Although this method has certain convenience, it also has many disadvantages. When carrying out the same operation, if users access the relevant data together, it is easy to cause errors and pose a serious threat to the security of the data. In this case, concurrency control is very necessary. Fourthly, in terms of the function of fault recovery, it is beneficial to ensure data security. In addition, the database can self-correct and recover the correct information, so that the fault in the first time can be efficiently handled, which plays a great role in ensuring data security.

The purpose of database management is to efficiently implement unified management and security inspection of the information transmitted by the network database, which needs to ensure the correct logic of the data, and in addition, the transmitted data information needs to be implemented according to the actual use needs. There are many ways of user identification and identification, and user identification and identification are often used together in a system in multiple forms. While ensuring database security to a certain extent, it is significantly more expensive during operation.

The most prominent expression in the system is the communication and interaction between the object and the subject. Under normal circumstances, users determine the access of subjects and objects at the level of data deletion and modification, which shows many advantages such as comprehensiveness, practicability, and confidentiality of data information. Furthermore, access manipulation is also a major part of establishing resource access handling. Access control can best show that its essential purpose is to carry out forced control, especially in the face of special circumstances, and this method of forced control should be implemented. Mandatory access manipulation is quite different when compared to this approach. Its security attributes are often aggregated at the subject and object level, but this security attribute cannot be changed by the database user. At this time, the access rights are limited to administrators for management and distribution. No matter which of the two methods mentioned above is used, the security of the database can be ensured. Therefore, the above two methods can be used to achieve the goal of ensuring the security of the database.

The main process of auditing database information is to provide information managers with a set of data that can be used for analysis and then perform security audits on this set of information, so that all unsafe information can be found in time. Such a method is very convenient and is conducive to improving the work progress of managers and carrying out management work efficiently [18–20]. If the auditing function is turned off in data management, it is easy to increase the probability of data loss, which will have a negative impact on the development and improvement of the enterprise. It is necessary to pay attention to the work of security audit, in order to ensure the security and comprehensiveness of information.

3.2. Organization and Management Technology of Multimedia Information. For multimedia, different from other data management, the data type of multimedia information is

RETRACTED

complex and the amount of data is large, such as video, audio, and image. There are obvious differences in each type of multimedia data, and they cannot be stored or retrieved directly according to a rule or method [18, 19].

For the corresponding data management and storage of the existing relational database, its essence is to carry out a meaning mapping to the unformatted data through a fixed file. The relational database does not need to consider unformatted data and only stores the corresponding index files. Users can access the indexes in the database and directly find the location of the multimedia files. This ensures the efficiency of data retrieval. The storage of multimedia information data can ensure the safety and effectiveness of the data.

The database operating system is used to connect with the data information function module of the operating platform, so as to realize the real-time management of the asymmetric speech data information. The method adopted in this paper is to assume that the data information of a specific row and column appears in the relationship between the two. As an asymmetric structure, these row and column data can be stored in a specific folder, and the name of the folder is stored in the corresponding location [20]. This method can be used not only to make the DBMS regardless of the storage configuration of the unformatted data but also to complete the management of DBMS unstructured information. It only manages the use of unstructured information, that is, file names, but not unstructured data. Therefore, under this method, the DBMS lacks the common control and recovery of unstructured data, and this can only be completed by using the OS system and application programs. In addition, this method needs to include OS file I/O in the disposal, resulting in a relatively low progress. But it can easily expand the database management platform that does not support unstructured data and indirectly "manage" unstructured data. The biggest advantage is that it can make good use of the advantages of the OS platform to complete the file sharing of unstructured information data. It is very important to store only this data name in the database to reduce the unnecessary storage of unformatted information, so most of the unstructured data are relatively large.

In addition, the formatted data of multimedia information and unformatted data can be encapsulated together to form a complete closed loop. Since unformatted multimedia information occupies a major part and the data volume is large, more data storage space needs to be set.

Unformatted data can be divided into index parts or data sources according to the attributes of the data, and the data space can be matched and set according to the attributes. If it is the data index part, the space does not need to be set too large; if it is the data source, you need to consider the size of the data volume.

In addition to the original relational data model, there is also an object-oriented data model. In terms of supporting multimedia information data, the object-oriented data model can well perform data aggregation, realize and handle complex objects such as multimedia information, and support the definition and operation of abstract data types of multimedia information data; it can further reduce the redundancy of multimedia information data, improve the retrieval and management efficiency of multimedia information data, optimize the query process, and directly conduct relevant retrieval and query of multimedia information through the index.

4. Application Analysis of Multimedia Information Security Protection System

4.1. Process Description. For the construction of the multimedia information security protection system, the specific process can be described as follows [21, 22].

The ciphertext C is

$$C = ECB(DCA(K)). \tag{5}$$

After receiving C, B obtains the key K through the encryption algorithm:

$$ECA(DCB(C)) = ECA(DCB(ECB(DCA(K)))) = ECA(DCA(K)) = K. \tag{6}$$

In this way, B is sure that the key K is sent from A, and the text content is obtained through the key K (P) of the encryption algorithm.

4.2. System Security Analysis. Now based on the network robot remote control system, fingerprint identification and hash function are added to construct a new encryption system [23, 24]. The architecture is shown in Figure 5.

For the multimedia information security protection system, the process is that A first calculates the multimedia information through a quantitative function, encrypts it with an encryption algorithm, then performs identity authentication after signing, and then passes the signature together with the multimedia information to B. During the whole process, if someone wants to pass the message directly without authentication, it will be displayed as unsuccessful.

RETRACTED

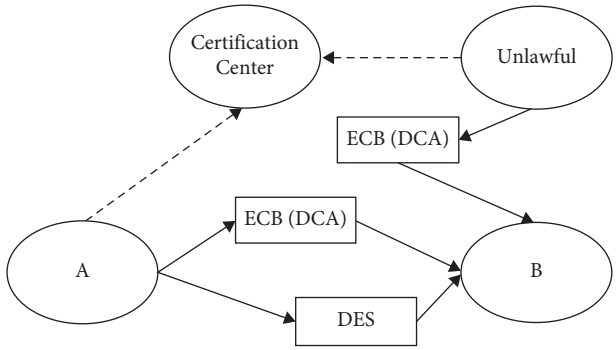

Figure 5: Security analysis flowchart.

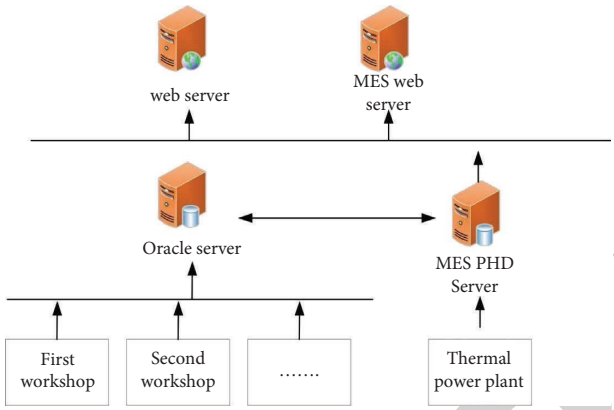

Figure 6: Real-time database system network topology.

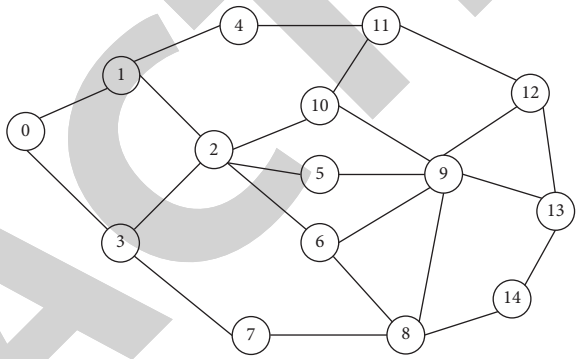

Figure 7: Open multimedia information transmission node diagram.

If B wants to directly modify the data passed by A, it cannot be modified without A's secret key.

For simple data in transmission, no protocol is used to constrain it, but for some advanced data, format conversion must be implemented first, which must be implemented in the corresponding service level, and finally the purpose of encapsulation is completed (Figure 6).

For the validity detection of encrypted multimedia information retrieval, transmission, and management, in the environment of simulation experiment, 20 multimedia information data are selected and corresponding data samples are set [25, 26]. After a certain transmission rule is implemented, the specific multimedia information data transmission node is shown in Figure 7, and the probability of its transmission crossing is set to 0.95.

From the analysis of the data results, it can be seen that when the multimedia information data are transmitted, due to the large amount of data, the effect of transmission control may have a certain weakness, and the information required by the user is not directly placed in the corresponding transmission channel. However, the network robot remote control system proposed in this paper uses the desired control method to encrypt, so that users can obtain safe and effective multimedia information data through reasonable

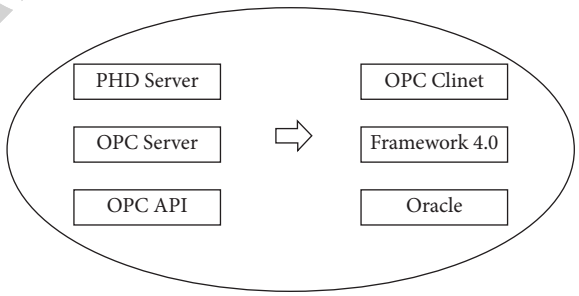

Figure 8: Principle of PHD external data output.

transmission and effectively realize the data control of multimedia information transmission (Figure 8).

From the result analysis in Figure 9, it shows that the circle represents the packet loss that occurs when the remote control system of the network robot is not used. It can be seen intuitively from the results that the multimedia information data security of the network robot remote control system is higher, and the packet loss rate remains below 7%. The results show that the network robot remote control system proposed in this paper has obvious multimedia security prevention technology, which ensures the safe and effective storage, management, and transmission of multimedia information data.

RETRACTED

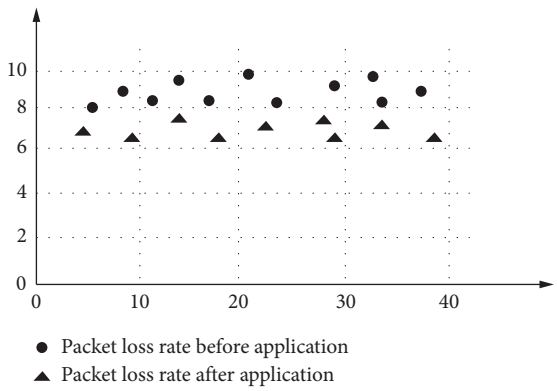

Figure 9: Relative packet loss rate in the state of information network congestion.

5. Conclusion

With the continuous development of social economy, multimedia data show a growing momentum, thus causing the problem of data security. For this demand, this paper relies on the network robot remote platform control system and establishes a security defense system by sorting out the organization and management characteristics and technologies of multimedia information. The application of the remote control platform of the displacement robot through the wireless local area network allows the robot to leave the dependence on the upper control PC terminal in the region. During the work of the robot, the remote operator can continuously observe their working status and adjust their working conditions due to the working environment. The robot can control and deal with changes or emergencies in time, which greatly improves the flexibility of the mobile robot. This scheme uses a small embedded motherboard, which increases the speed of the robot's self-processing of data, improves the ability to recognize the environment, tries to implement multimedia data security management, and uses simulation experiments to verify the calculation method. The simulation experiment results show that the robot remote control system has high effectiveness and can support the establishment of the security protection system of multimedia information big data.

Data Availability

The data used to support the findings of this study are included within the article.

Conflicts of Interest

The authors declare that they have no conflicts of interest.

References

[1] M. Toapanta, E. Mafla, and J. Orizaga, "Conceptual model for identity management to mitigate the database security of the registry civil of Ecuador," *Materials Today Proceedings*, vol. 5, no. 1, pp. 636–641, 2018.

[2] G. D. Dalvi, S. D. Wakde, and P. V. Kale, "Database security using multi-shares visual cryptography," *IOSR Journal of Electronics and Communication Engineering*, vol. 14, no. 2, pp. 37–43, 2019.

[3] H. Tufail, K. Zafar, and A. R. Baig, "Relational database security using digital watermarking and evolutionary techniques[J]," *Computational Intelligence*, vol. 7, no. 3, pp. 42–60, 2019.

[4] W. A. Yasnoff, "Breach risk magnitude: a quantitative measure of database security," *AMIA Symposium*, vol. 2016, no. 4, pp. 1258–1263, 2016.

[5] F. Thams, A. Venzke, R. Eriksson, and S. Chatzivasilleiadis, "Efficient database generation for data-driven security assessment of power systems," *IEEE Transactions on Power Systems*, vol. 5, no. 6, pp. 1–10, 2019.

[6] S. Malhotra, M. N. Doja, and B. Alam, "Cloud Database Management System security challenges and solutions: an analysis[J]," *Csi Transactions on Ict*, vol. 3, no. 4, pp. 1–9, 2016.

[7] X. Tao, Y. Liu, and F. Zhao, "Graph database-based network security situation awareness data storage method[J]," *EURASIP Journal on Wireless Communications and Networking*, vol. 18, no. 1, pp. 56–63, 2018.

[8] W. El-Hajj, G. Ben Brahim, H. Hajj, H. Safa, and R. Adaimy, "Security-by-construction in web applications development via database annotations," *Computers & Security*, vol. 59, no. 3, pp. 151–165, 2016.

[9] C. Tan and X. Lu, "Research on user security authentication method of eco-environmental monitoring database," *Arabian Journal of Geosciences*, vol. 14, no. 11, pp. 1–11, 2021.

[10] S. Vavilis, A. Egner, M. Petkovic, and N. Zannone, "An anomaly analysis framework for database systems," *Computers & Security*, vol. 53, no. 9, pp. 156–173, 2015.

[11] J. D. Domingo-Ferrer, Sánchez, and J. Soria-Comas, "Database anonymization: privacy models, data utility, and microaggregation-based inter-model connections," *Synthesis Lectures on Information Security, Privacy, and Trust*, vol. 8, no. 1, pp. 1–136, 2016.

[12] Jeong-hyeon and J C. Kim, "A recovery method for deleted records in the ESE Database," *Journal of the Korea Institute of Information Security & Cryptology*, vol. 25, no. 5, pp. 1143–1151, 2015.

[13] R. Xu, K. Morozov, Y. Yang, J. Zhou, and T. Takagi, "Efficient outsourcing of secure k -nearest neighbour query over encrypted database," *Computers & Security*, vol. 69, no. 8, pp. 65–83, 2017.

[14] S. M. Darwish, "Machine learning approach to detect intruders in database based on hexplet data structure," *Journal of Electrical Systems and Information Technology*, vol. 3, no. 2, pp. 261–269, 2016.

[15] H. I. Kim, A. A. Hossain, and J. W. Chang, "A spatial transformation scheme supporting data privacy and query integrity for security of outsourced databases: t," *Security and Communication Networks*, vol. 7, no. 10, pp. 1498–1509, 2014.

[16] M. Y. AlYousef and N. T. Abdelmajeed, "Dynamically detecting security threats and updating a signature-based intrusion detection system's database," *Procedia Computer Science*, vol. 159, no. 5, pp. 1507–1516, 2019.

[17] O. M. Pereira, D. D. Regateiro, and R. L. Aguiar, "Secure, dynamic and distributed access control stack for database applications," *International Journal of Software Engineering and Knowledge Engineering*, vol. 25, pp. 1703–1708, 2015.

[18] G. Mohamed, Y. Attila, and H. Bechir, "Location privacy preservation in database-driven wireless cognitive networks through encrypted probabilistic data structures," *IEEE*

RETRACTED

Hindawi
Journal of Robotics
Volume 2023, Article ID 9768015, 1 page
https://doi.org/10.1155/2023/9768015

Retraction

Retracted: Designing and Manufacturing of Industrial Robots with Dual-Angle Sensors Taking into Account Vibration Signal Fusion

Journal of Robotics

Received 19 December 2023; Accepted 19 December 2023; Published 20 December 2023

Copyright © 2023 Journal of Robotics. This is an open access article distributed under the Creative Commons Attribution License, which permits unrestricted use, distribution, and reproduction in any medium, provided the original work is properly cited.

This article has been retracted by Hindawi following an investigation undertaken by the publisher [1]. This investigation has uncovered evidence of one or more of the following indicators of systematic manipulation of the publication process:

(1) Discrepancies in scope
(2) Discrepancies in the description of the research reported
(3) Discrepancies between the availability of data and the research described
(4) Inappropriate citations
(5) Incoherent, meaningless and/or irrelevant content included in the article
(6) Manipulated or compromised peer review

The presence of these indicators undermines our confidence in the integrity of the article's content and we cannot, therefore, vouch for its reliability. Please note that this notice is intended solely to alert readers that the content of this article is unreliable. We have not investigated whether authors were aware of or involved in the systematic manipulation of the publication process.

Wiley and Hindawi regrets that the usual quality checks did not identify these issues before publication and have since put additional measures in place to safeguard research integrity.

We wish to credit our own Research Integrity and Research Publishing teams and anonymous and named external researchers and research integrity experts for contributing to this investigation.

The corresponding author, as the representative of all authors, has been given the opportunity to register their agreement or disagreement to this retraction. We have kept a record of any response received.

References

[1] J. Yan and H. Cheng, "Designing and Manufacturing of Industrial Robots with Dual-Angle Sensors Taking into Account Vibration Signal Fusion," *Journal of Robotics*, vol. 2023, Article ID 1855226, 11 pages, 2023.

Hindawi
Journal of Robotics
Volume 2023, Article ID 1855226, 11 pages
https://doi.org/10.1155/2023/1855226

RETRACTED

Research Article

Designing and Manufacturing of Industrial Robots with Dual-Angle Sensors Taking into Account Vibration Signal Fusion

Jinshun Yan[1] **and Haiqing Cheng**[2]

[1]*Department of Mining Engineering, Lyuliang University, Lyuliang, 033001, China*
[2]*China Railway Hohhot Bureau Group Co. Ltd., Hohhot, Nei Monggol 010000, China*

Correspondence should be addressed to Jinshun Yan; 20131065@llu.edu.cn

Received 4 September 2022; Revised 17 October 2022; Accepted 24 November 2022; Published 4 May 2023

Academic Editor: Iqbal Ahmad

Copyright © 2023 Jinshun Yan and Haiqing Cheng. This is an open access article distributed under the Creative Commons Attribution License, which permits unrestricted use, distribution, and reproduction in any medium, provided the original work is properly cited.

Industrial robots are an important way to realize the development of industrial industry intelligence and automation, an important driving force to accelerate the construction of Industry 4.0, and an important basic force to improve the professional level of industrial industry. The development of industrial robot technology has enhanced the requirements of its detection quality and the demand for data comprehensiveness. Most of the previous robots obtain the corresponding data through a single sensor system, which has a large error and a high limitation of the range of data obtained. The detection method of industrial robots has the problems of high cost and high professionalism. Therefore, this paper constructs a dual-angle sensor industrial robot detection system based on the fusion of multisource vibration signals and achieves the fusion of multisensor signals through Kalman filtering to provide reliable analysis data for the dual-angle sensor detection system. The experimental results show that Kalman filtering can effectively remove noise while preserving the original vibration signal characteristics and structure and improve the reliability and validity of the vibration signal. In addition, the dual-angle sensor detection system can realize the position detection of industrial robots according to the command standard and obtain the corresponding residual and standard values through system data analysis. The overall optimization of the system algorithm enhances the accuracy and reliability of the measurement.

1. Introduction

The application of modern intelligent technology has driven the development of Industry 4.0, raising the demand for industrial specialization and intelligence. At the same time, industrial robots have become an important direction for the future development of industrial industry as labor costs increase and the population ages. The in-depth research of intelligent technology has provided the technical guarantee for the intelligence of industrial robots and expanded the performance and usage of industrial robots, enabling them to develop from completing basic and simple task instructions to completing assembly lines according to industrial needs [1]. The application of a large number of intelligent industrial robots can effectively liberate labor and promote productivity improvement. In addition, with the enhancement of industrial robot technology, the classification of robots is becoming more specialized and refined, and the requirements for their performance testing are also increasing [2]. For example, intelligent robots applied in high-risk industries not only need to be able to adapt to special terrain and complex environments, etc., but also need to be able to achieve a high degree of accuracy in positioning. In the past, industrial robots used a single vibration signal source, which was not able to obtain comprehensive and accurate data from the surrounding environment and feedback on the robot's operating status due to the limitation of space and time conditions when positioning the robot [3]. The multisource vibration signals of industrial robots, i.e., the multidimensional spatial data information of the environment obtained by multisensors, provide a reliable data basis for the robot to identify the environment, transmit data, capture and extract dynamic features, etc. [4]. The key aspect of multisensor applications

in industrial robots is the fusion of different sensor data information, i.e., the multisource vibration signals are processed in a uniform manner and are able to describe the observed target jointly according to the corresponding rules [5]. Therefore, vibration signal fusion technology has a great impact on the development of industrial automation and robot intelligence and is an important element of research.

The application of intelligent sensors to the detection field of industrial robots is a new field of robot detection technology research at present. It faces many key technical problems, which can be summarized in two aspects. On the one hand, it is the practicality of sensor systems. The research focus is on the modeling, planning, and fusion technology of multi intelligent sensor systems and the control strategy of group behavior. This includes the following items: multiagent group architecture, mutual communication and negotiation mechanism, perception principle, and learning method. The other is a stable and reliable multi intelligent sensor fusion algorithm 7, which involves the capture, recognition, extraction, analysis, and evaluation of static and dynamic features of multisensor data, especially in the case of nonlinear, nonstationary, non-normal distribution, and multisensor system fusion algorithm. In addition, it also includes the noise interference of the external environment on the system, the accuracy evaluation of the multisensor system, the principle of data communication, the error compensation mechanism, and the calibration performance evaluation. Therefore, it is of great significance to study the fusion technology of multiple intelligent sensors to improve the level of industrial automation in China. With the expansion of industrial robots' applications, their detection problems are gradually highlighted. Some common detection methods currently have high costs, difficult operation, technical condition restrictions, and large error variations, and many robots applied in special working environments are relatively difficult to detect, which require the safety and reliability of their detection to be considered in robot design. The application of intelligent sensors in industrial robots has expanded the development direction for their detection field, and the fusion of vibration signals has become an important part of the key technologies to be solved for their application. Therefore, this paper designs a dual-angle sensor industrial robot performance detection system and introduces Kalman filtering in the detection module to achieve vibration signal fusion, reduce the original data noise, improve the accuracy of data analysis, and conduct the corresponding performance analysis through experiments. The vibration signal fusion technology reduces the residual vibration at the end of motion and the vibration caused by high-frequency torque in the process of motion by optimizing the acceleration waveform. The optimized velocity waveform and acceleration waveform are obtained from the optimized acceleration waveform and boundary conditions. The optimal joint torque is obtained. The vibration reduction effect of inverse dynamics is simulated by the modal analysis method.

2. Status of Vibration Signal Fusion Technology and Industrial Robot Research

The research and application of industrial robotics is an important element to promote the development of industrial automation and intelligence, and the in-depth research of sensor technology provides strong data and information basis for robot development. In the past, robots obtained information by means of a monolithic sensor measurement system, and the verification index of the robot performance was relatively monolithic, with relatively low data comprehensiveness, which was not conducive to the analysis of robot systems and the detection and diagnosis of their performance [6]. Cruz Miguel et al. pointed out that single-source vibration signals not only have noise signal interference but also may generate more redundant information due to system reasons, which add burden to the system transmission data, and at the same time, the single system data transmission path is largely affected by external influences, and the data accuracy and authenticity are relatively low [7]. Based on this, Fu et al. proposed to achieve multidirectional diversified access to the corresponding environmental data through different sensor systems, but their existence of multiple sensor systems with different time standards and a certain amount of repetition in the data transmitted by each independent sensor system increases the energy consumption of the whole robot system [8]. Multisource vibration signal fusion, i.e., multisensor information fusion, can achieve a uniform representation of the data information obtained from different sensors through comprehensive technical processing, and the redundant data transmitted by different sensors can complement each other to improve the comprehensiveness and integrity of the overall system information. Among them, the estimation algorithm is one of the common and widely used methods, which includes the weighted average method and the Kalman filter. Wei et al. proposed to combine multivariate statistics and the artificial intelligence algorithm to achieve the fusion of multisource vibration signals. They propose to combine multivariate statistical methods and fusion accuracy to derive the optimal assignment of weighted averaging [9]. Other scholars have reconstructed for vibration signal combustion information combined with multichannel vibration acceleration signal, and the signal with high correlation of combustion information is obtained in a new way, while the fusion of its vibration acceleration signal is achieved by weighting coefficients [10]. With the development of artificial intelligence technology, the application of the Kalman filter has been gradually expanded, and Li et al. have used the extended Kalman filter method to achieve the fusion of position and acceleration signals in vibration sensors to achieve the prediction of dynamic displacement of the infrastructure [11]. Other scholars have incorporated Kalman filtering in intelligent vehicle location systems to reduce the risk probability of failure in vehicle health maintenance systems through the fusion of fuzzy sensor data [12].

RETRACTED

The artificial intelligence technology method is to extract the feature information of multisource vibration signals through neural networks and obtain the best vibration signal fusion processing results after model training, whose advantage is that neural networks have good autonomous learning ability and self-organization ability and can process and store large-scale data effectively [13]. Its disadvantage is that it requires model training of a large amount of data to be able to reduce the error rate of data fusion, the stability of data fusion is low, and the generalization ability needs to be improved. Li et al. introduced convolutional neural networks for multisensor data fusion in rotating machinery fault identification and achieved optimization of neural networks through bottleneck layers, which can be effective in improving the richness of information obtained by the sensors [14]. Zhang et al. introduced dynamic integrated convolutional neural networks in fault diagnosis, which constructed a multilevel wavelet coefficient matrix based on wavelet packets for the description of nonsmooth vibration signals, and the fusion of its dynamic ensemble layer and multilevel wavelet packets enhanced the effectiveness of diagnosis [15]. In addition to neural networks, Ikuta et al. introduced the fuzzy theory into the field of signal processing and combined it with other algorithms to achieve the fusion of vibration signals and enhance their effectiveness and accuracy [16]. Other scholars have combined multisensor technology and fuzzy information fusion algorithms to improve the accuracy and reliability of chemical enterprise safety assessment systems in the analysis of chemical enterprise accidents and related casualty probabilities [17]. Other scholars have combined the fuzzy theory and neural networks to build a system that can extract signal features according to the principle of adaptive fuzzy control and establish a system for diagnosing energy dissipation information of mechanical equipment faults [18].

In addition to the fault diagnosis of industrial machinery and robots, intelligent sensor technology is widely used in the field of industrial robot inspection. With the improvement of industrial robot technology and the expansion of its uses, Bai et al. have proposed higher and more comprehensive performance testing standards and a performance evaluation model incorporating neural networks [19]. It has also been proposed for wheeled robots to build a ground classification system based on convolutional neural networks, combining feature-level and decision-level data fusion [20]. Thus, it can be seen that sensor technology has an important role in promoting future research in industrial robotics, and multisensor data fusion is a key aspect and technology for its development.

3. Construction of the Kalman Filter-Based Measurement Module for Industrial Robots with Dual-Angle Sensors

3.1. Multivibration Signal Fusion Technology. The design of industrial robots involves various disciplines and technologies such as computers, mechanical electronics, and artificial intelligence. They often need to have good mobility and stability and cooperate with each other through multiple joints in the range of motion to complete the command tasks, and this process requires data information obtained through different types of sensors as the basis for analysis and decision making. The information obtained from single-source vibration signals is redundant and limited by the environmental space and sensor location, which cannot meet the environmental information needs of industrial robots. In addition, multisource vibration signal fusion can reasonably and effectively utilize the redundant information in various sensors, redistribute the redundant information from the perspective of the system as a whole, supplement the uncertainty in the information obtained by other sensors, and improve the accuracy and integrity of the information of the whole system. Multisource vibration signal fusion is also beneficial to optimize the system structure of industrial robots, avoiding the corresponding costs due to the increase of individual sensor systems.

Artificial intelligence technology is widely used in industrial robot design, which can improve the intelligence level of robots and achieve the goal of industrial intelligence and automation. One of the common methods of multisource vibration signal fusion in artificial intelligence is Kalman filtering, which can predict the data afterwards based on the data obtained from the vibration sensors at the moment, and it can also effectively reduce the impact of noise in multisource vibration signal data. The Kalman filter can be understood as a way to perceive a noisy world. When we want to locate the robot, it depends on two conditions. We know how the robot moves from one moment to the next because we command it to move in a certain way. This is called state transition (that is, how a robot moves from one state to another), and we can use various sensors such as cameras, lidars, or echo detectors to measure the robot's environment. The problem is that both types of information are affected by noise. We cannot accurately know the accuracy of the robot's transition from one state to the next because the executive parts are not perfect. And we cannot measure the distance between objects with infinite precision. This is where the Kalman filter comes into play.

Different types of sensors collect and transmit data according to different time series; so, industrial robots need to synchronize the time-stamped relationship of multisource vibration signals and transform the coordinate systems of different sensors into a unified world coordinate system, as shown in Figure 1.

Let the state at time t be denoted as $M(t)$ and its filtered value be denoted as $\widehat{M}(t/t)$, then the prediction of the next state is shown in the following equation:

$$\widehat{M}\left(\frac{t+1}{t}\right) = \alpha(t)\widehat{M}\left(\frac{t}{t}\right) + \beta(t)U(t), \tag{1}$$

where $t+1$ indicates the next moment, the state description is $\widehat{M}(t+1/t)$, the system parameters are described as $\alpha(t), \beta(t)$, and the state control quantity is noted as $U(t)$.

Let the covariance matrix at time t be denoted as (t/t), whose prediction matrix is shown in the following equation:

RETRACTED

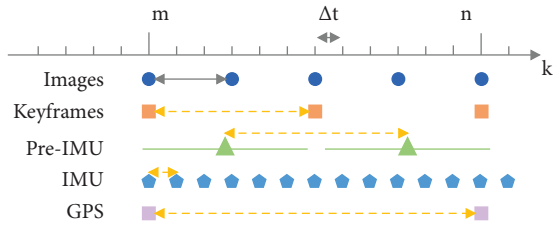

Figure 1: Time-stamped relational synchronization condition of multisource vibration signals.

$$P\left(\frac{t+1}{t}\right) = \alpha(t)P\left(\frac{t}{t}\right)\alpha^T(t) + Q(t), \tag{2}$$

where $\alpha^T(t)$ represents the transpose matrix of $\alpha(t)$.

The predicted values of the measurements are calculated as shown in the following equation:

$$\widehat{S}\left(\frac{t+1}{t}\right) = H(t+1)\widehat{M}\left(\frac{t+1}{t}\right). \tag{3}$$

The new information covariance matrix is described as shown in the following equation:

$$X(t+1) = H(t+1)P\left(\frac{t+1}{t}\right)H^T(t+1) + R(t+1). \tag{4}$$

The gain matrix is represented as shown in the following equation:

$$Kg(t+1) = P\left(\frac{t+1}{t}\right)H^T(t+1)X^{-1}(t+1). \tag{5}$$

The state filter values are calculated as shown in the following equation:

$$\widehat{M}\left(\frac{t+1}{t+1}\right) = \widehat{M}\left(\frac{t+1}{t}\right) + Kg(t+1)\left[S(t+1) - \widehat{S}\left(\frac{t+1}{t}\right)\right]. \tag{6}$$

The filtering covariance matrix is described as shown in the following equation:

$$P\left(\frac{t+1}{t+1}\right) = P\left(\frac{t+1}{t}\right) - Kg(t+1)S(t+1)Kg^T(t+1). \tag{7}$$

3.2. Dual-Angle Sensor-Based Measurement System for Industrial Robots. In order to improve the operability of the industrial robot measurement, this paper selects a dual-angle sensor measurement system consisting of two sensors and a microprocessor module, one of which has a detection function and the other a calibration function, and each of which contains a three-axis gyroscope and accelerometer and a digital motion processor, both of which maintain a cooperative communication state with the microprocessor module. The measurement system is embedded in the industrial robot in a simple way, and its corresponding position needs to be adjusted and determined as a basis for adjusting and optimizing the circuit layout to enhance its safety and stability. Before carrying out the detection group to initialize the operation of the two sensors, that is, the calibration results determined according to the dynamic and static characteristics of the response, we also need to detect the two parts of the sensor and the composition of the system accuracy and the corresponding requirements for comparison through continuous adjustment and threshold information feedback to achieve the results and industrial robot position command data comparison analysis. The microprocessor module is responsible for the control of the operating state of the system, data communication, and the corresponding processing of the received real-time data. At present, based on multisensor signal fusion, data registration is mainly used to realize mutual estimation of state and parameters. State information fusion is suitable for target tracking, while feature information fusion is suitable for combined classification, which is mainly based on traditional pattern recognition technology to achieve classification fusion. Feature-level fusion can automatically extract information sources with representative features from the original data, integrate them, and retain important information, so as to provide data support for later decisions. This mode has low requirements for communication broadband.

The system works on the principle that the two sensors take the angular velocity data of each axis obtained by gyroscope and accelerometer and derive the corresponding position analog signal according to the difference method; then, the data are transformed by the data motion processor and the industrial robot attitude data are derived according to the calibration sensor. The data are then transferred to the microprocessor module for the next step of data processing and analysis. In order to improve the accuracy and reliability of the data analysis results, Kalman filtering is used in the microprocessor module to remove noise from the raw data transmitted by the sensors. Based on the existing input and output laws, the system adjusts the data acquisition frequency in the form of iterative approximation to obtain the optimal value in the characteristic threshold, maintain the input and output correspondence, and avoid the distortion problem. The dynamic response characteristics obtained in this process will be smoothened by error compensation to reduce the errors generated by the system due to installation operations, gyroscope angle integration accumulation, and other problems, so as to obtain better static response characteristics.

The key of initialization lies in the calibration of detection sensor and calibration sensor. The calibration results are divided into static characteristic response and dynamic characteristic response. The dual-angle sensor measurement system is composed of STM32 microprocessor module and two MPU6050 modules. The system is simple in structure, easy to install, and realize. Fix the sensor MPU6050 for detection at the center point (TCP) of the industrial robot tool with screws. Ensure that the MPU6050 does not vibrate significantly during the high-speed movement of the robot. The other MPU6050- and STM32-embedded modules are fixed close to the zero point of the robot base coordinate system, and this sensor is used as the reference, that is, the sensor for calibration. In the accuracy analysis, the system needs to analyze the accuracy, sensitivity, stability, and other

RETRACTED

changes in state and amplitude, according to the response situation to select the response compensation factor so that it meets the corresponding requirements. After the accuracy meets the standard is the correction of zero point drift, that is, according to the principle of the minimum error, the distance between the predicted value and the target point of the system is driven to the minimum through the adjustment of the static and dynamic characteristics weights. A flowchart of the Kalman filter-based measurement system for industrial robots with dual-angle sensors is shown in Figure 2.

The original data of the system are filtered by low-pass filter to remove noise interference, especially white noise generated by mechanical vibration. Observe the law of input and output, and adopt the iterative approximation method to adjust the sampling frequency and optimize the characteristic threshold. The method of multiple iterations is used for error compensation, referring to Dr. Zhang Xiaoping's MDH kinematic error model. Optimize the compensation coefficient, reduce the process error of system installation and drift error accumulated by gyro angular velocity integral, and obtain good static response characteristics. Continue error compensation. It is required to redistribute the weight, modify the weight proportion of static and dynamic characteristics, and refer to the principle of the least square method. According to the principle of the minimum error, adjust the zero position to make the estimated value approach the sample point. If the standard is met, the final result will be the output; otherwise, the second step will be returned, starting from adjusting the characteristic threshold, and the dynamic characteristic response will be repeated until the standard is met. Let the commanded and actual measured positions of the industrial robot be described as $Z(x_i, y_i, z_i, \alpha_i, \beta_i, \lambda_i)$ and $(x_i, y_i, z_i, \alpha_i, \beta_i, \lambda_i)$, respectively, and the deviation results between the actual measured and estimated values can be analyzed by the position residuals; the settlement process of which is shown in the following equation:

$$R = \sqrt{\left(\sum_{i=1}^{N} x_{M,i} - x_{Z,i}\right)^2 + \left(y_{M,i} - y_{Z,i}\right)^2 + \left(z_{M,i} - z_{Z,i}\right)^2}. \tag{8}$$

The dynamical observations of the entire system that have been calibrated, after removing the noise disturbances, show a nonlinear relationship between the measured values, and the minimum value of the total squared error between the actual and commanded values is determined by combining regression analysis and the least squares theory. The results of the next stage of calibration are then estimated by the minimum distance between the input data points and the straight line.

Let the point A_1, A_2, A_3, A_4, A_5 be the position point in the determined working range, and the industrial robot moves according to the number of point sequences. Let the attitude O, P, Q denote the direction of the corresponding industrial robot's working surface, and its corresponding commanded position is (x_l, y_l, z_l), and the accuracy is calculated according to equations (9) and (10).

$$W_i = \sqrt{(\overline{x} - x_l)^2 + (\overline{y} - y_l)^2 + (\overline{z} - z_l)^2}, \tag{9}$$

$$\begin{cases} \overline{x} = \dfrac{1}{N}\displaystyle\sum_{i=1}^{N} x_i, \\ \overline{y} = \dfrac{1}{N}\displaystyle\sum_{i=1}^{N} y_i, \\ \overline{z} = \dfrac{1}{N}\displaystyle\sum_{i=1}^{N} z_i. \end{cases} \tag{10}$$

The attitude command is $(\alpha_l, \beta_l, \lambda_l)$, and its accuracy is calculated as shown in (11) and (12).

$$\begin{cases} T_\alpha = (\overline{\alpha} - \alpha_l), \\ T_\beta = \left(\overline{\beta} - \beta_l\right), \\ T_\lambda = \left(\overline{\lambda} - \lambda_l\right), \end{cases} \tag{11}$$

$$\begin{cases} \overline{\alpha} = \dfrac{1}{N}\displaystyle\sum_{i=1}^{N} \alpha_i, \\ \overline{\beta} = \dfrac{1}{N}\displaystyle\sum_{i=1}^{N} \beta_i, \\ \overline{\lambda} = \dfrac{1}{N}\displaystyle\sum_{i=1}^{N} \lambda_i. \end{cases} \tag{12}$$

The corresponding positional repeatability can be calculated according to equations (13)–(16).

$$R_d = \overline{d} + 3S_d, \tag{13}$$

$$\overline{d} = \frac{1}{N-1}\sum_{i=1}^{N} d_i, \tag{14}$$

$$d_i = \sqrt{(x_i - \overline{x})^2 + (y_i - \overline{y})^2 + (z_i - \overline{z})^2}, \tag{15}$$

$$S_d = \sqrt{\frac{1}{N-1}\sum_{i=1}^{N} \left(d_i - \overline{d}\right)^2}. \tag{16}$$

The attitude repeatability can be calculated according to the following equation:

RETRACTED

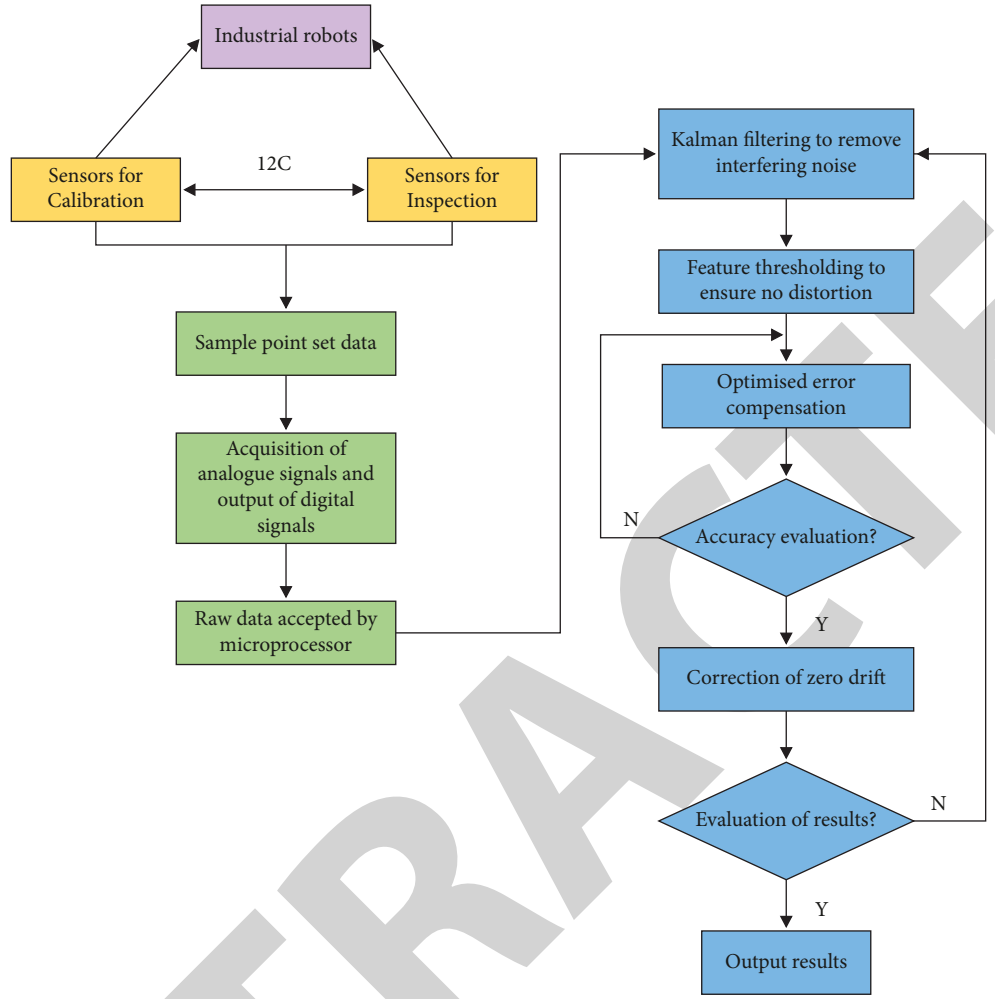

Figure 2: Flowchart of the Kalman filter-based dual-angle sensor industrial robot measurement system.

$$\begin{cases} R_\alpha = \pm 3S_\alpha = \pm 3\sqrt{\dfrac{1}{N-1}\sum_{i=1}^{N}(\alpha_i - \overline{\alpha})^2}, \\ R_\beta = \pm 3S_\beta = \pm 3\sqrt{\dfrac{1}{N-1}\sum_{i=1}^{N}(\beta_i - \overline{\beta})^2}, \\ R_\lambda = \pm 3S_\lambda = \pm 3\sqrt{\dfrac{1}{N-1}\sum_{i=1}^{N}(\lambda_i - \overline{\lambda})^2}. \end{cases} \quad (17)$$

The root mean square is able to provide a measure of the degree of dispersion of a group of points with discrete characteristics, and it reflects the degree of offset between the measured and commanded values of the robot, which is calculated as shown in the following equation:

$$\mathrm{RMS} = \sqrt{\frac{1}{N}\sum_{i=1}^{N}\left(x_{M,i} - x_{Z,i}\right)^2}. \quad (18)$$

The standard deviation can reflect the relationship between the sample data with your own and the mean self-test, which is calculated as shown in (19) and (20).

$$B_{StdDev} = \sqrt{\frac{1}{N}\sum_{i=1}^{N}(x_i - \delta)^2}, \quad (19)$$

$$\delta = \frac{1}{N}\sum_{i=1}^{N} x_i. \quad (20)$$

RETRACTED

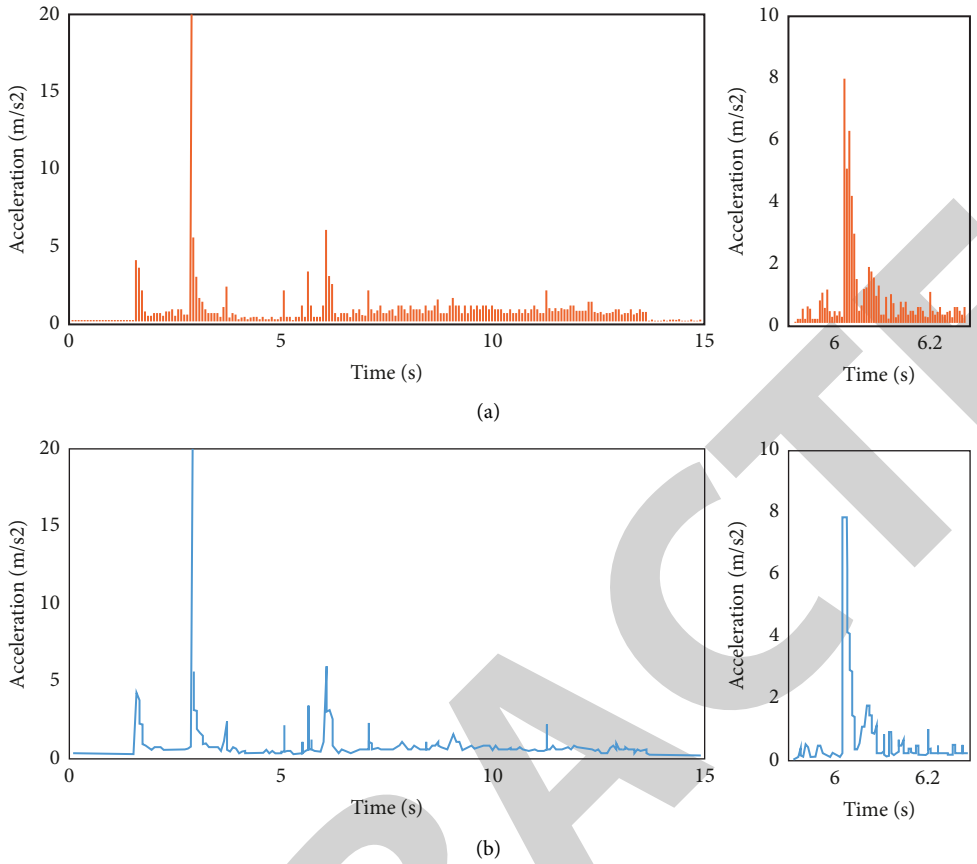

Figure 3: Original signal and filtered effect of multisource vibration signal of industrial robot. (a) Raw data. (b) Filtered data.

4. Experimental Results of the Kalman Filter-Based Measurement Model for Industrial Robots with Dual-Angle Sensors

The Kalman filter algorithm implementation steps are as follows: first measurement. The filter receives the pose and velocity of the robot in the coordinates from the radar or laser radar as the initial measurement and next the inverse initialization, state, and covariance matrix. The filter will initialize the position of the robot based on the first measurement. The filter receives a new sensor measurement after the time period. The predicted position and the measured position are combined to give an updated position. The Kalman filter will assign different weights to the predicted position or the measured position according to the uncertainty of each value. The filter will then receive a new sensor measurement. The algorithm then performs another prediction and updates the step. In the actual detection system, the working environment of the sensor is complex and harsh, the amplitude of the output electrical signal is small, and there is a certain distance between the sensor and the circuit. The noise generated by the cable resistance that needs to transmit signals, the internal resistance of the sensor, and the amplifier circuit will affect the amplifier circuit and its normal operation. Therefore, targeted measures must be taken to improve the anti-interference ability of the sensor circuit. Remote transmission of analog quantity shall be avoided as far as possible when selecting sensors and designing equipment interfaces, and digital communication interfaces can be selected. This kind of communication interface has a long transmission distance and less interference and can be extended by adding relay. Before conducting experiments on industrial robots with dual-angle sensors, the raw data need to be filtered. The raw and filtered signals of the multisource vibration signal of the industrial robot are shown in Figure 3. The results show that there are many noise signals in the local part of the original vibration signal of the robot, and the overall signal waveform has many small-amplitude peaks. After filtering, the overall signal is smoother, and the small-amplitude peaks in the local signal effectively reduce the interference noise, especially the white noise. At the same time, the filtering process maintains the waveform structure of the original vibration signal as much as possible, avoiding its distortion problem and ensuring the authenticity and validity of the multisource vibration signal.

The industrial robots involved in the experiments are six-axis robots with handling functions, and the appropriate joint motion range, corresponding speed limit, working space, and center position are set according to the experimental requirements to ensure that the handling robots can bypass the singularities to the maximum extent. Thirty points were randomly selected from the sample data set for calibration and none of the selected points had singularities.

RETRACTED

The actual and average values of the position residuals and attitude residuals of the robot after reaching the calibration points through various postures are shown in Figures 4 and 5, respectively. The results in Figure 4 shows that the residual values of each random position point of the handling robot are identical, but the overall fluctuation is within a certain range, and there are individual sample data points whose position residual values fluctuate more compared with others. However, the average of the residual values of all sample data points in the experiment is very low, less than 0.1 mm, and the overall fluctuation condition also gradually stabilizes. This indicates that although there is a certain error between the actual data and the command data of the handling robot, the degree of closeness between them is high, the fluctuation is small, the error is small, and the reliability and validity of the calibration results are high.

The results of the analysis of the actual and mean values of the robot's posture residuals are shown in Figure 5. The results show that most of the actual measured residuals of the robot fluctuate in the range of 0.00018°–0.00065°, and there are a few sample data points where the actual measured residuals are too high or too low. The mean values of the posture residuals of the sample data points in the experiment are very small, i.e., they reflect that the actual results of the robot posture and the calibration results are highly accurate, relatively stable, and in good agreement with the command data.

In the process of signal acquisition and transmission, it is bound to be interfered by the surrounding environment and internal noise; so, we need to process the signal correctly to eliminate the influence of interference and try to obtain the required signal, which requires filtering the received signal. Filtering is the process of extracting signals from noisy observation data. Kalman introduced the concept of state space into the theory of random estimation and regarded the signal as the output of a linear system excited by white noise. This input-output relationship is described by state equation. Because the signal information used is the time domain, it can estimate not only the one-dimensional stationary random process but also the multidimensional, nonstationary random process. This overcomes various limitations encountered in the design of Wiener filtering in the frequency domain and has a wide range of applications.

As shown in Figure 6, the measured results of the position of the handling robot are in the A_1 points, the number of cycles of the process of approaching each position in each experimental direction is 20, and some of the measured data results are shown in the figure.

The calculated results of the robot's posture at A_1 are shown in Figure 7. The combination of the results with Figure 6 shows that the accuracy of the robot's posture in different directions is high, and the effective mean value of the dispersion of the point group is small, which indicates that the actual measured value and the commanded value are

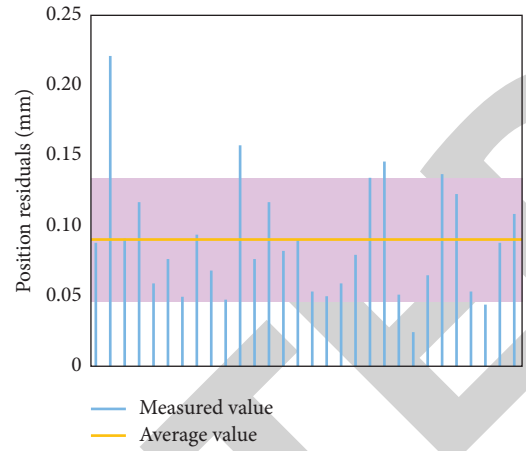

Figure 4: Actual and mean value analysis results of the position residuals of the handling robot.

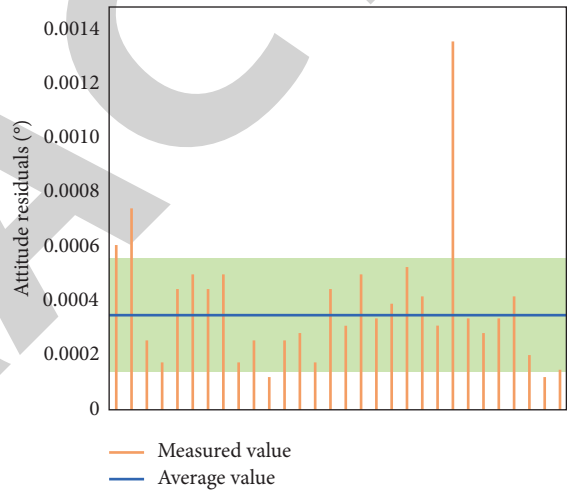

Figure 5: Actual and mean value analysis results of the pose residuals of the handling robot.

in good agreement and the position of the measured point is basically in the range close to the commanded point. The smaller average value of the standard deviation value reflects the higher concentration of the distribution of the actual data measurement points in space, and the high degree of fit with the mean value, and the high stability of the system.

In summary, the Kalman filter-based dual-angle sensor industrial robot measurement model can effectively fuse the multisource vibration signal and reduce the noise interference in the signal, providing a more accurate data information basis for subsequent analysis while maintaining its authenticity and reliability. The dual-angle sensor system in the model can improve the performance of the system algorithm, increase the validity and accuracy of the measurement data, and has good efficiency and practicality.

RETRACTED

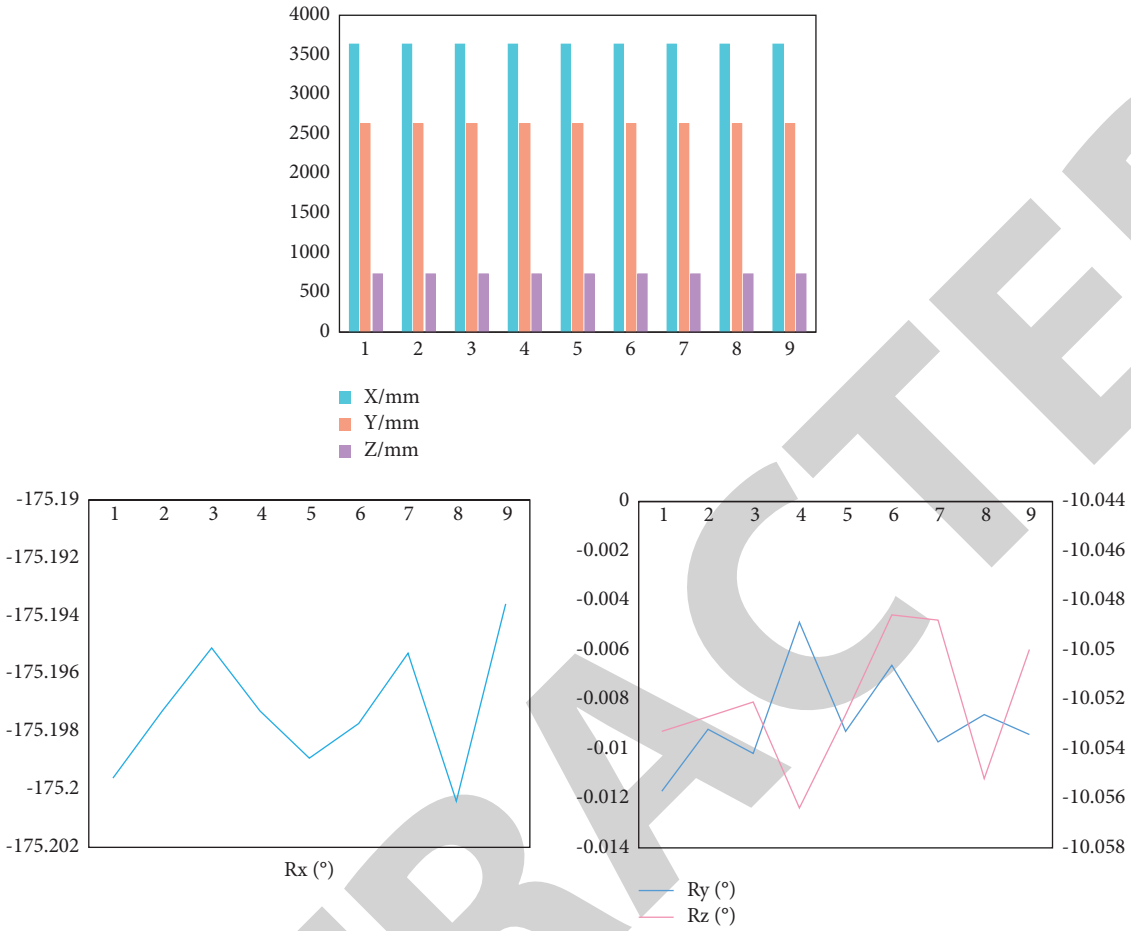

Figure 6: Position measurement results of the handling robot in A_1 points.

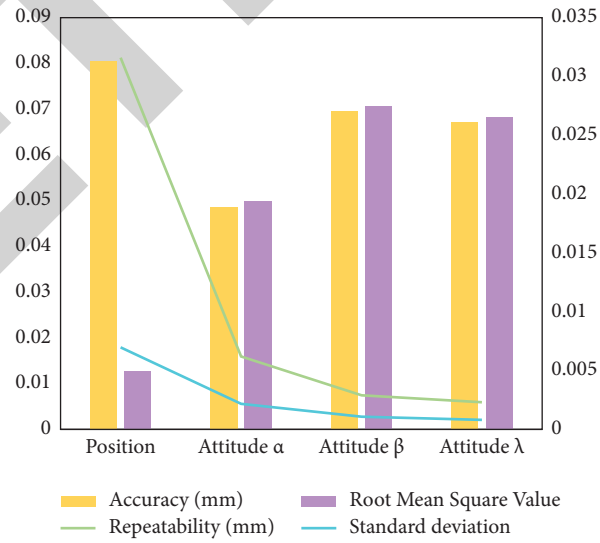

Figure 7: Calculated results of the position pose of the handling robot at A_1.

5. Conclusion

The advent of Industry 4.0 era has promoted the optimization process of industrial structure and opened a new period of high-quality development of industrial industry, and the traditional industrial model to improve automation, intelligence, and specialization standards has become the inevitable development direction. Industrial robots can not only liberate part of the labor force and improve production efficiency but also enhance the degree of intelligence and

RETRACTED

automation of industrial industries. In addition, the working environment of some industrial industries is complex, and it is difficult to obtain corresponding spatial information data artificially. Obtaining data through individual sensors will be restricted by time and space, and the accuracy of single-source vibration signals is relatively low. Industrial robots are able to obtain multidirectional spatial information through multiple sensors, providing a more reliable data base for robot measurement and analysis. Therefore, this paper introduces the Kalman filter algorithm to achieve the fusion of multisource vibration signals in the industrial robot design and builds a measurement system based on dual-angle sensors in the industrial robot detection module. The experimental results show that the data information obtained by the handling robot through multiple sensors can effectively reduce the noise signal interference and improve the accuracy and validity of the original signal after Kalman filtering processing, while maintaining its basic signal characteristics and structure. In addition, the dual-angle sensor-based industrial robot measurement system can detect the corresponding robot position data according to any command and standard and obtain the corresponding data analysis results through the system calculation. The results show that the system can reduce the error rate of the industrial robot, enhance its reliability, improve the system algorithm, and show good practicality and efficiency. However, the design of the industrial robot in this paper needs further improvement, its measurement of itself is still inadequate, and there is a gap between the complexity of the experimental environment and the actual environment, which needs further verification of its performance in the actual environment.

Data Availability

The data used to support the findings of this study are included within the article.

Conflicts of Interest

The authors declare that they have no conflicts of interest.

Acknowledgments

This work was supported by the National Natural Science Foundation of China (Grant no. 52165035) and the Postgraduate Research and Innovation Funding Project of Inner Mongolia Autonomous Region of China (Grant no. BZ2020037).

References

[1] Z. Zheng, X. W. Dai, and Z. W. Gao, "Pick-and-place robot sensor fault detection based on unknown input observer," *Control Engineering*, vol. 27, no. 12, pp. 2063–2069, 2020.

[2] R. Liu, F. Wang, B. Yang, and S. J. Qin, "Multiscale kernel based residual convolutional neural network for motor fault diagnosis under nonstationary conditions," *IEEE Transactions on Industrial Informatics*, vol. 16, no. 6, pp. 3797–3806, 2020.

[3] R. N. A. Algburi and H. Gao, "Health assessment and fault detection system for an industrial robot using the rotary encoder signal," *Energies*, vol. 12, no. 14, p. 2816, 2019.

[4] H. Kolvenbach, C. Bartschi, L. Wellhausen, R. Grandia, and M. Hutter, "Haptic inspection of planetary soils with legged robots," *IEEE Robotics and Automation Letters*, vol. 4, no. 2, pp. 1626–1632, 2019.

[5] V. Bijalwan, V. B. Semwal, and T. K. Mandal, "Fusion of multi-sensor-based biomechanical gait analysis using vision and wearable sensor," *IEEE Sensors Journal*, vol. 21, no. 13, pp. 14213–14220, 2021.

[6] G. Li, S. Liu, L. Wang, and R. Zhu, "Skin-inspired quadruple tactile sensors integrated on a robot hand enable object recognition," *Science Robotics*, vol. 5, no. 49, Article ID eabc8134, 2020.

[7] E. E. Cruz-Miguel, J. R. García-Martínez, J. Rodríguez-Reséndiz, and R. V. Carrillo-Serrano, "A new methodology for a retrofitted self-tuned controller with open-source fpga," *Sensors*, vol. 20, no. 21, p. 6155, 2020.

[8] Y. Fu, X. Chen, Y. Liu, C. Son, and Y. Yang, "Multi-source information fusion fault diagnosis for gearboxes based on SDP and VGG," *Applied Sciences*, vol. 12, no. 13, p. 6323, 2022.

[9] J. Wei, F. Zhang, J. Lu, X. Yang, and Y. Yan, "Fault diagnosis method for machinery based on multi-source conflict information fusion," *Measurement Science and Technology*, vol. 33, no. 11, Article ID 115007, 2022.

[10] A. Aria, E. Lopez Droguett, S. Azarm, and M. Modarres, "Estimating damage size and remaining useful life in degraded structures using deep learning-based multi-source data fusion," *Structural Health Monitoring*, vol. 19, no. 5, pp. 1542–1559, 2020.

[11] C. I. Li, G. D. Chen, T. Y. Sung, and H. F. Tsai, "Novel adaptive Kalman filter with fuzzy neural network for trajectory estimation system," *International Journal of Fuzzy Systems*, vol. 21, no. 6, pp. 1649–1660, 2019.

[12] X. Liu, Z. Ren, H. Lyu, Z. Jiang, P. Ren, and B. Chen, "Linear and nonlinear regression-based maximum correntropy extended Kalman filtering," *IEEE transactions on systems, man, and cybernetics: Systems*, vol. 51, no. 5, pp. 3093–3102, 2021.

[13] M. Ma, C. Sun, X. Chen, X. Zhang, and R. Yan, "A deep coupled network for health state assessment of cutting tools based on fusion of multisensory signals," *IEEE Transactions on Industrial Informatics*, vol. 15, no. 12, pp. 6415–6424, 2019.

[14] Z. Li, J. Li, Y. Wang, and K. Wang, "A deep learning approach for anomaly detection based on SAE and LSTM in mechanical equipment," *The International Journal of Advanced Manufacturing Technology*, vol. 103, no. 1–4, pp. 499–510, 2019.

[15] X. Zhang, Z. Zhao, Z. Wang, and X. Wang, "Fault detection and identification method for quadcopter based on airframe vibration signals," *Sensors*, vol. 21, no. 2, p. 581, 2021.

[16] A. Ikuta, H. Orimoto, and K. Hasegawa, "A noise suppression method for speech signal by jointly using bayesian estimation and fuzzy theory," *Journal of Software Engineering and Applications*, vol. 14, no. 12, pp. 631–645, 2021.

[17] M. I. Tariq, S. Ahmed, N. A. Memon et al., "Prioritization of information security controls through fuzzy AHP for cloud computing networks and wireless sensor networks," *Sensors*, vol. 20, no. 5, p. 1310, 2020.

RETRACTED

Hindawi
Journal of Robotics
Volume 2024, Article ID 9863534, 1 page
https://doi.org/10.1155/2024/9863534

Retraction

Retracted: Discovery and Discrimination of Bridge Engineering Safety Issues by BIM Virtual Scene Combined with Robotic Mapping

Journal of Robotics

Received 23 January 2024; Accepted 23 January 2024; Published 24 January 2024

Copyright © 2024 Journal of Robotics. This is an open access article distributed under the Creative Commons Attribution License, which permits unrestricted use, distribution, and reproduction in any medium, provided the original work is properly cited.

This article has been retracted by Hindawi following an investigation undertaken by the publisher [1]. This investigation has uncovered evidence of one or more of the following indicators of systematic manipulation of the publication process:

(1) Discrepancies in scope
(2) Discrepancies in the description of the research reported
(3) Discrepancies between the availability of data and the research described
(4) Inappropriate citations
(5) Incoherent, meaningless and/or irrelevant content included in the article
(6) Manipulated or compromised peer review

The presence of these indicators undermines our confidence in the integrity of the article's content and we cannot, therefore, vouch for its reliability. Please note that this notice is intended solely to alert readers that the content of this article is unreliable. We have not investigated whether authors were aware of or involved in the systematic manipulation of the publication process.

Wiley and Hindawi regrets that the usual quality checks did not identify these issues before publication and have since put additional measures in place to safeguard research integrity.

We wish to credit our own Research Integrity and Research Publishing teams and anonymous and named external researchers and research integrity experts for contributing to this investigation.

The corresponding author, as the representative of all authors, has been given the opportunity to register their agreement or disagreement to this retraction. We have kept a record of any response received.

References

[1] G. Gong, S. Zeng, J. Gao, Q. Zhang, and X. Wang, "Discovery and Discrimination of Bridge Engineering Safety Issues by BIM Virtual Scene Combined with Robotic Mapping," *Journal of Robotics*, vol. 2023, Article ID 3028505, 12 pages, 2023.

Hindawi
Journal of Robotics
Volume 2023, Article ID 3028505, 12 pages
https://doi.org/10.1155/2023/3028505

RETRACTED

Research Article

Discovery and Discrimination of Bridge Engineering Safety Issues by BIM Virtual Scene Combined with Robotic Mapping

Guilin Gong,[1] Shaowu Zeng,[1] Jingjing Gao,[1] Qingliang Zhang,[2] and Xinli Wang[1]

[1]*Shaanxi Railway Institute, Weinan, Shaanxi 714099, China*
[2]*China Railway Jian'an Engineering Design Institute Co., Ltd., Shijiazhuang, Hebei 050043, China*

Correspondence should be addressed to Shaowu Zeng; zyyxgjd2002@163.com

Received 1 November 2022; Revised 12 December 2022; Accepted 5 April 2023; Published 22 April 2023

Academic Editor: Shahid Hussain

Copyright © 2023 Guilin Gong et al. This is an open access article distributed under the Creative Commons Attribution License, which permits unrestricted use, distribution, and reproduction in any medium, provided the original work is properly cited.

All along, safety accidents in the field of bridge construction have continued to arise, costing society's development financial and material resources and taking away people's personal safety, turning into an urgent need for safety managers in the field to solve the subject research. Researchers look forward to continued innovative exploration to find new ways of working safely and using them in the construction industry. On this basis, BIM virtual scenes are introduced to create a universal scene specification dataset in the field of bridge construction and a dataset of unsafe potential hazard characteristics in the field of bridge construction. Nanobots are artificial intelligence systems built to simulate biological nanomachine constructions in life activities and important biological events in life processes. In this paper, BIM virtual scenarios incorporating intelligent nanomaterial robot mapping technology are migrated to bridge engineering safety management. According to the collected construction scene images and BIM (building information model) virtual scenes, build the construction scene dataset, use intelligent robots to obtain construction scenes, and load them into the trained construction on-the-spot neural network modeling to complete the bridge construction scene identification safety discrimination to select more comprehensive and more stringent management solutions as safety management personnel management methods on-the-spot.

1. Introduction

In recent years, with the implementation of construction projects as an important component of the bridge span, bridge pile height, and bridge bearing capacity needs have also been rising, and the construction of bridges with engineering precision and high efficiency has also been subject to more regulations. So we want to reasonably carry out all aspects of bridge engineering under the new standards and the new mandatory requirements to further strengthen the bridge engineering mapping work, enhance the bridge mapping work on a variety of resource integrations, and actively explore and improve the various aspects of professional technology. Mapping work can effectively promote the establishment of road bridges and improve the overall quality of bridge engineering [1]. Figure 1 shows the discovery and discrimination of safety problems at the construction site.

Nanorobotics is an emerging technology in robotics engineering. The development of nanorobots belongs to the category of molecular nanotechnology, which designs and manufactures "functional molecular devices" that can operate in nanospace based on biological principles at the molecular level. As a prototype, nanorobot technology has been applied to bridge mapping technology, early design and planning stage mapping, middle and late engineering construction stage mapping, and late operation and management stage mapping. This method can effectively ensure the overall quality and accuracy of bridge projects, but in practice, bridge mapping cannot be reasonably carried out due to the influence of various factors. Therefore, in bridge construction, the world's leading surveying and mapping technology and mechanical equipment should be actively introduced, for example, through the introduction of nanorobotic surveying and mapping technology, integrate road and bridge construction rules, reasonable mapping

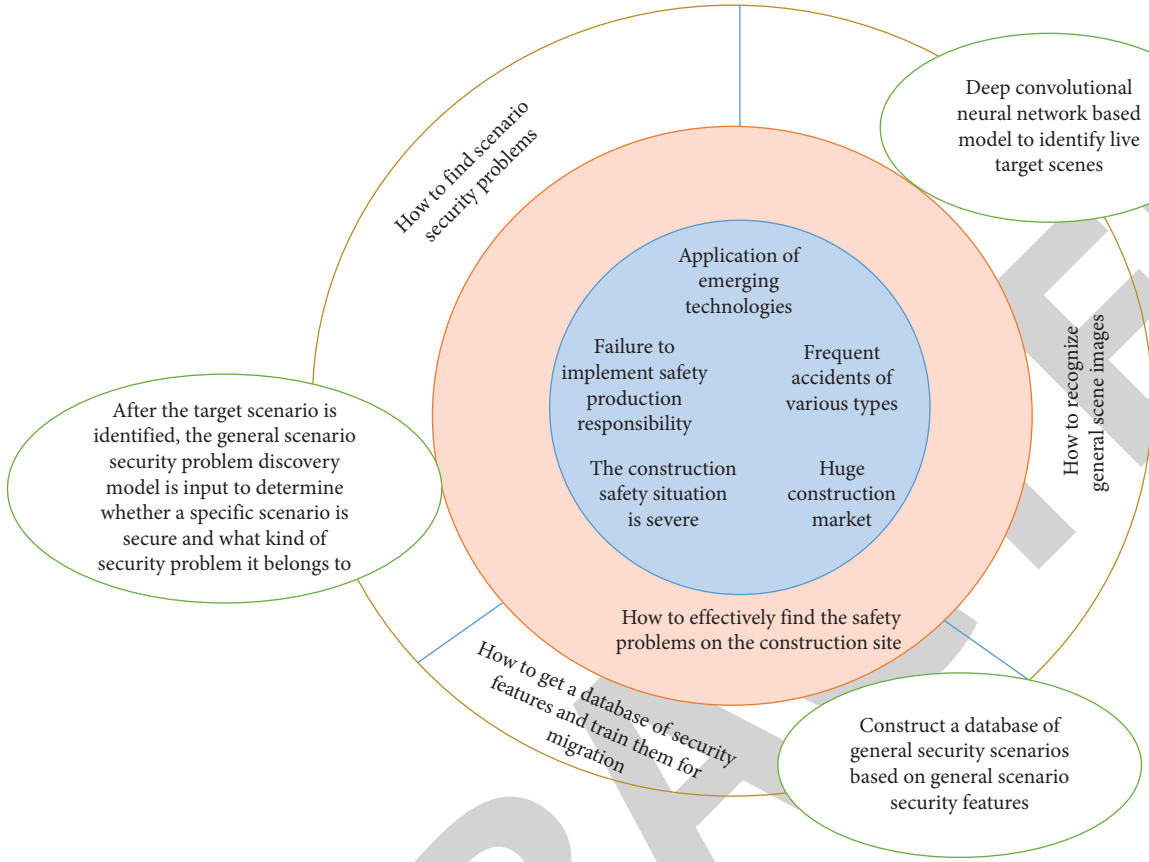

Figure 1: For the construction site safety problem detection and discrimination.

work, and the basis for the construction of high-quality, high-level bridge projects.

"BIM," that is "building information modeling," is Chinese for "building information model." BIM is used for engineering construction. BIM is a 3D digital technology used for the whole life cycle of a project building. In all life cycles, it applies public data types to establish and collect all information about the building and develop a solid model of information integration based on the information as a network resource for project decision-making and information interoperability. The BIM entity model overcomes the problem of sharing information in multiple technical work types and dimensions throughout the project construction life cycle, yet there are also problems [2].

In other words, the lack of three-dimensionality and modernity prevents bidders or lay staff from visualizing, systematically cognizing, and understanding the design intent of the architects. Applying only 3D images and animation may lead to "not getting the results." Robotic remote sensing technology is slowly replacing traditional surveying and mapping technology in the engineering measurement process. The use of robotic remote sensing technology can not only greatly accelerate the progress of engineering measurement but also realize the premise of information collection and processing upgrades and quickly and easily obtain the most accurate information, analysis, and storage. Thus, the application of robotic remote sensing technology must be analyzed.

2. Theory and Method

2.1. Research on the Application of BIM + VR Technology in Architectural Planning and Design

2.1.1. BIM Platform. 3D model data information model according to Revit, BIM platform is shown in Figure 2 below. The platform is used to build a platform based on the cooperation and sharing of the model database, with architectural wood templates as the project model [3]. The platform contains: (1) parametric modeling of 3D information model; (2) visualization of data to see and dynamic interaction (3) project progress and process simulation; (4) 3D rendering of 3D model design effects and other services. Excellent adaptation with Unity3D of Revit VR module, Unity3D is applicable to FBX file format exported from Revit, which can realize unhindered connection between BIM 3D model and VR scene and ensure the integrity of model grain to the maximum.

2.1.2. VR Simulation Platform. Figure 3 shows the application of VR simulation platform, "VR" in Chinese means "virtual reality." It is a technology that creates interactive 3D animation effects in the virtual background and environment with the help of electronic computer technology, so that participants can interact with the experience in virtual reality instantly. Participants are able to explore the exterior interior spaces inside the virtual-like architectural modeling

RETRACTED

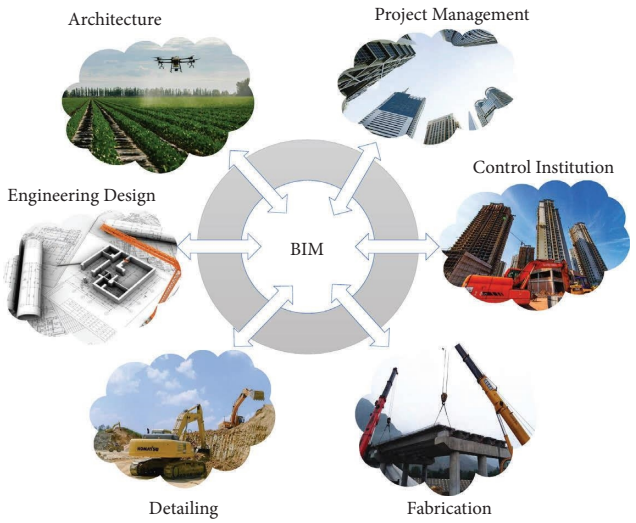

Figure 2: BIM platform.

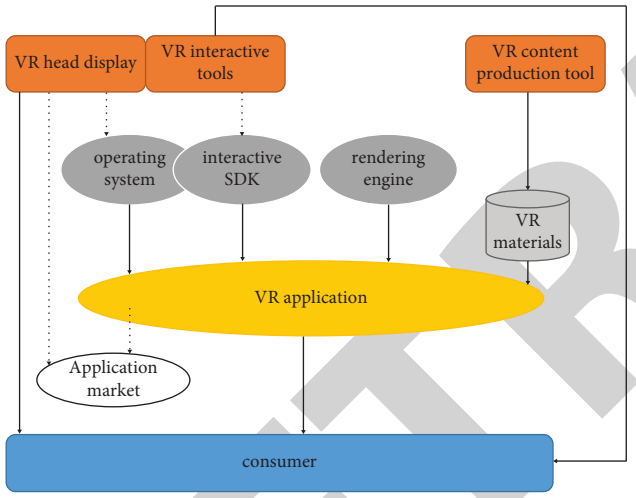

Figure 3: Application of VR simulation platform.

by assembling VR hardware configurations [4]. After the release of Cardboard at the GoogleI/o exchange in 2014, VR is rapidly coming into the lives of the general public, and its hardware and software are moving toward the lighter side. In the architectural planning industry, the introduction of virtual reality technology has built a highway bridge between design teams and bidders.

The pairing of BIM VR and BIM VR completes a mutually beneficial win-win situation. As opposed to interior designers, rendering BIM solid models with VR animation reduces redundant workload and enhances the coordination of BIM design. For consumers and owners, VR technology can be more realistic to feel the effect of architectural planning and design with and the cost of communication between workers in the field. In addition, the application of BIM VR technology can be effective resource integration, resource application efficiency, beneficial to the rapid development of the engineering and construction industry [5].

2.2. Measuring Robots

2.2.1. Introduction to Robotic Surveying and Mapping Technology. Figure 4 shows the most basic performance parameters of the surveying and mapping UAV. The measurement intelligent robot is an intelligent electronic device that can replace people to automatically search, identify, track and get accurate perspective, spacing, coordinates, and images. Its use of hazard sensors and other related sensors can also accurately identify the overall target in geomorphological surveys and quickly carry out specific analysis. It can realize intelligent practical operations such as automatic control, fully automatic photographing of geomorphological information content, and data acquisition, and can well replace manual control.

At this stage, there are three main types of nano-type surveying intelligent robots [6]. (1) Active triangulation or polar coordinate method is chosen to measure the geomorphology. In other words, the corresponding mark is set on the object to be measured and the reflection prism is applied to carry out the measurement. (2) Active triangulation method is selected, in which the structured light is used as the viewpoint, consisting of the generator in the sensor, software and hardware warp, and the viewpoint rendezvous method is used to clarify the precise coordinates. (3) Single overall target measurement is the main feature of the old revolutionary object, using digital image processing to carry out automatic retrieval, find the precise marker point, and use the principle of indoor spatial rendezvous to get the three-dimensional coordinates.

The measurement nano-type intelligent robot carries out automatic retrieval using the rotation of the telescope of the motor look-alike section and the measurement using the look-alike prism. The important principle of measurement is that the instrumentation shoots a laser data signal to the destination part, which is reflected by the prism and accepted by the sensor in the instrumentation [7]. Subsequently, the position of the reflected light is measured and the adjusted special data information is obtained. Later, the motor is turned on and the measuring intelligent robot is pointed at the prism to clearly aim at the target.

2.2.2. Application of Measurement Robot in Topographic Measurement and Mapping Automation. Nanorobotics is envisioned as the application of biological principles to discover new phenomena and develop programmable molecular robots at the nanoscale. Synthetic biology has redesigned cell signaling and gene regulatory networks, resulting in another way of nanorobotics. For practical topographic survey work, nanorobots can be used. On the actual topographic survey work, GPS, software and hardware measuring instruments and equipment cannot be executed uniformly because of environmental elements, mainly because of the harsh environment such as mountainous areas causing GPS data signals to be blocked out and GPS receivers not working properly in. At this stage, the application of measurement robots can solve this problem. A new measurement system software will automatically collect

RETRACTED

Model	DJI M600
Wheelbase	1133 mm
Size	1668*1518*759 (mm)
Weight	9.6 Kg
Takeoff weight	15.1 Kg
Endurance	No load: 40 min Load: 5.5 Kg; 18 min
Operating time	4.4 Kg Load: 18 min
Maximum speed	18 m/s (No wind)

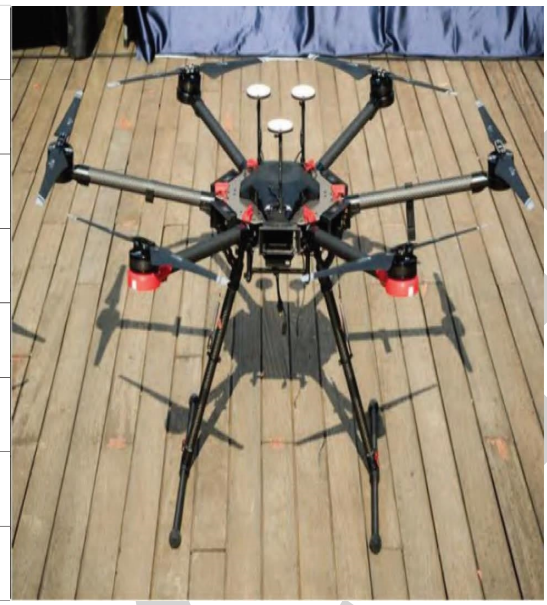

Figure 4: Basic technical parameters of the mapping UAV.

the information of measurement points in the record [8]. When the comprehensive measurement cell phone software collects data about the depth of the landscape, the measurement robot will also automatically obtain the coordinate system matching this, and reasonably combine these two data to get accurate and complete three-dimensional coordinate data, so as to efficiently carry out the topographic measurement, thus improving the efficiency and quality of the construction of road surfaces and other related construction.

2.2.3. Specific Steps and Considerations for the Application of Nano-Type Measuring Measurement Robots. Nano-type measuring robot application specific steps: (1) Make complete advance preparation before measuring, introduce the datum into the measuring area, pick the best installation worker position, assemble the reflection prism on the measuring instrument equipment so that the reflection prism is located at the top of the measuring machine; it may block the prism and the measurement data collection terminal occurs. (2) Carry out the actual measurement practical operation in accordance with the basic principles of integration, connect the detector, GPS system, electronic computer, open the measurement cell phone software, set the main parameters of the measurement instruments and equipment, and ensure the normal operation of all measurement instruments and equipment. (3) Set RTK, open the relevant measurement cell phone software, pick new requirements in the menu bar, set the relevant measurement station, overall target and reflection prism pointing, turn on the locking power switch, enter the geomorphology menu bar, set the starting point and detection time spacing [9].

In addition, in the geomorphology measurement and fully automatic mapping engineering session, the communication base station worker has to pay high attention to the detector so that the measurement cell phone software score is consistent with the measurement robot score. In this process, may suffer from the influence of external factors, and then please record down the number. When the interference is too strong, it is necessary to finish the measurement first and wait for the influence to clear before carrying out the geomorphological measurement.

2.3. According to the Accident Modern Logic Site Safety Management Problem Characteristics Identification. In order to be able to scientific research control and effective prevention of building construction accidents, from the accident detection system, to the construction of aerial falls, object strikes, lifting injuries, collapse, and other typical accidents as an example, from the essence of the accident generator unsafe and behavior objects unsafe situation, the key factors of its text subtext, semantic network, and other text retrieval manipulation accidents can effectively prevent the vast majority of accidents. Tables 1–4 show the characteristics of the four unsafe scenarios. On the premise of the above scientific research, this section clarifies the main theme of the whole text, identifies the characteristics under typical unsafe scenarios on the spot, and completes the database of accident prevention.

On this basis the unsafe features of the four scenarios are summarized, and the unsafe features of the scenario cause only a part of the unsafe elements of the accident.

2.4. Generalized Scene Image Recognition Technique for Building Construction Based on Convolutional Neural Networks

2.4.1. Structural Characteristics of Convolutional Neural Networks. In general, convolutional kernels have different sizes, and the subspace of convolutional kernels is slightly smaller [10]. According to the multidimensional

RETRACTED

Table 1: Features of unsafe scene of fall.

Category	Failure factors	Core key factors	Scenario problem characteristics
People	A1 work in violation of regulations A2 no protective measures A3 safety education in form A4 defective site management A5 weak safety awareness A6 construction without license A7 inadequate supervision A8 blind command, organization construction	AB1 work in violation of regulations AB2 no protective measures AB3 management is not in place AB4 not hanging safety belt AB5 safety awareness is weak	F1 no safety belt F2 no protective measures F3 no edge protection F4 material damage F5 violation of regulations F6 management is not in place F7 weak safety consciousness
Object	B1 not hanging safety belt B2 wire rope breakage B3 destabilization B4 no protection near the edge B5 no horizontal protection net B6 unqualified scaffolding material B7 no shelter at the hole B8 overload of unloading platform		

convolutional kernel, the features are acquired by certain step level or vertical smooth movement. Small filters of different sizes prevent simplistic acquisition of features, and then bias terms can be imported to extract cognitive content from partial features. In addition, discrete system features are introduced into the convolutional network according to the activation function, and finally a two-dimensional feature map is derived. The pattern of fold stacking is shown in formulas (1) and (2).

$$Cj^1 = \sum_{i \in M_{ij}} Xi^1 * Kij^1 + bj^1, \tag{1}$$

$$Xj^{i+1} = Yj^i = f\left(Cj^1\right), \tag{2}$$

Cj^1 indicates the result obtained from the computation of the convolution layer, l is the number of superimposed layers, and j is the feature plane indicating the first Ith feature of the first layer. It indicates that the feature plane of the fully connected layer of the Ith feature plane and the jth feature plane connected by the first layer is the bias term. The convolution and output are measured, and the $l+1$th layer keying features are obtained based on the activation function solution plane, i.e., the feature plane. In order to be able to excite the words this function, the discrete system function is introduced into the neural network that measure the output neuron's entry data, transform the output conclusion, restrict the categorization category, and provoke the common neurons [11]. There are Sigmoid functions, hyperbolic tangent functions, calibrated linear enterprises, etc. The activation function used in this chapter is ReLU, which is calculated as shown in formula (3) below:

$$f(x) = \max(0, x). \tag{3}$$

The domain of definition is $(-\infty, +\infty)$ and the domain of value is R. The image of the function is shown in Figure 5.

The following convolution operation is illustrated in Figure 6, where an image matrix of dimension $5 * 5$ is used with a $3 * 3$ convolution kernel, and the step size is set to 1 [12].

The size of the output feature map after the convolution calculation is shown in formula (4).

$$w' = \frac{w + 2p - k}{\text{stride}} + 1. \tag{4}$$

where w represents the size of the input image matrix, k is the convolutional kernel size, stride is the convolutional kernel sliding step, and p is the number of complementary zero layers, which serves to complement the presence of image matrix filters that cannot be fully extracted.

2.4.2. Fully Connected Layer. The principle of fully connected layer is to obtain all the information from the previous layer and process it together, usually at the end of the network. In the fully connected layer, all two-dimensional features are stitched together into one-dimensional features for better classification by the classifier, which is called "fully connected." Figure 7 shows the schematic diagram of the fully connected layer. Formulas (5) for the fully connected layer shows

$$X^l = f\left(w^l x^{l-1} + b^l\right). \tag{5}$$

2.4.3. Convolutional and Neural System Network Boosting. Dropout techniques are applied to convolutional neural networks. In the forward phase of network training, the activation value of a certain neuron is restricted to participate in the training with a certain probability p, which reduces the dependence of the model on certain local features and enhances the generalization ability of the model [13]. The main principle of this method is to prevent the nodes in the hidden layer of the network from participating

RETRACTED

RETRACTED

Table 2: Object striking unsafe scene characteristics.

Category	Failure factors	Core key factors	Scenario problem characteristics
People	C1 blind operation, improper standing C2 violation of work rules C3 not wearing helmet F1: not wearing helmet C4 entering the dangerous area of the city C5 poor safety awareness C6 confusion in site management C7 blind command and organization of construction	CD1 working in violation of rules and regulations CD2 poor safety awareness CD3 falling from height CD4 equipment overturning CD5 dangerous area CD6 safety helmet	F1 not wearing helmet F2 improper standing F3 equipment overturning F4 falling objects from height F5 legal operation F6 poor safety awareness
Object	D1 falling from height D2 equipment overturning D3: equipment failure		

Table 3: Lifting injury unsafe scenario features.

Category	Failure factors	Core key factors	Scenario problem characteristics
People	E1 illegal operation E2 failure to maintain a safe distance E3 no license to work E4 chaotic site management	EF1 illegal operation EF2 crane	F1 improper standing F2 soft foundation F3 rope missing strands F4 illegal operation
Object	F1 crane F2 hook F3 loose foundation F4 wire rope missing strands	EF3 inappropriate standing position EF4 hook EF5 soft foundation	F5 falling hook

Table 4: Unsafe scenario characteristics of collapse accidents.

Category	Failure factors	Core key factors	Scenario problem characteristics
People	G1 illegal operation G2 management G3 blind command G4 unqualified construction	GH1 illegal operation GH2 no support, support	F1 no support F2 blind slope release F3 uneven soil quality F4 wall lost support
Object	H1 blind slope release H2 no pit support H3 uneven soil quality H4 loss of wall support	GH3 uneven soil quality GH4 pit	F5 illegal operation

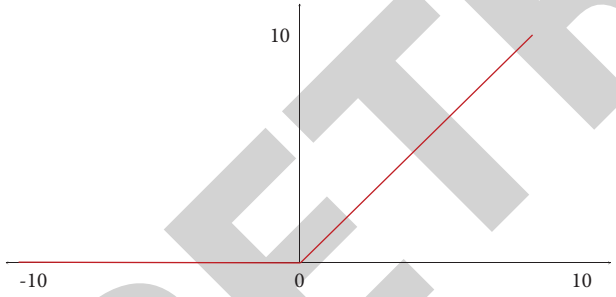

Figure 5: ReLU function graph line.

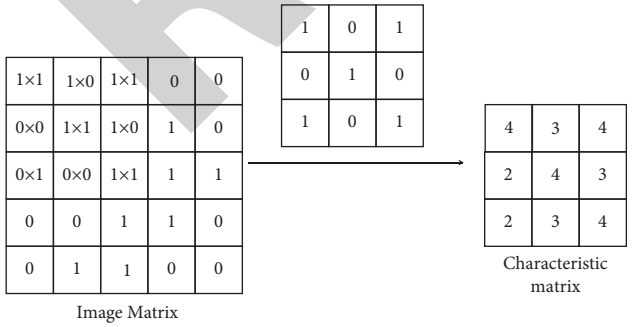

Figure 6: Convolutional operation diagram.

in the computation by randomly limiting their weights during the network training. The variation of the network formula with Dropout is as follows:

The network operation without Dropout is shown in formulas (6) and (7). Network operations with Dropout are shown in formulas (8)–(11).

Network computing without Dropout

$$z_i^{l+1} = w_i^{l+1} yl + b_i^{l+1}, \tag{6}$$

$$y_i^{l+1} = f\left(z_i^{l+1}\right). \tag{7}$$

Network computing with Dropout

$$r_j^{l} \sim \text{Bernoulli}(p), \tag{8}$$

$$\tilde{y} = r^{(l)} * y^{(l)}, \tag{9}$$

$$z_i^{(l+1)} = w_i^{(l+1)} yl + b_i^{l+1}, \tag{10}$$

$$y_i^{(l+1)} = f\left(z_i^{(l+1)}\right). \tag{11}$$

The Bernoulli function generates a random limit of 0 and engages the work if it is 1.

RETRACTED

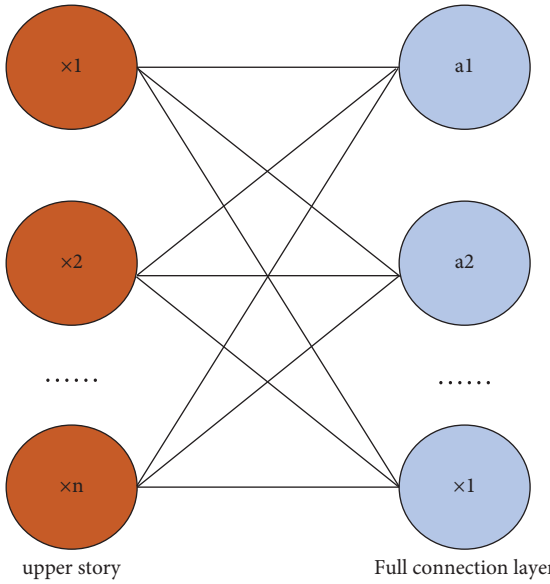

Figure 7: Schematic diagram of the fully connected layer.

3. Specific Description of the Use of Surveying and Mapping Technology in the Application of Bridge Engineering Project Measurement Measures

3.1. Active Marketing to Promote the Application of New Technologies. At this stage, numerous new surveying and mapping technologies can be employed in the bridge engineering project measurement industry. However, it is essential to actively and proactively market these innovations to encourage their widespread adoption. For example, automation technology is used to implement the actual operation of measurement. The service supports the appearance and performance assessment and is used to conduct performance tests of bridge structures through a series of mechanical tests. Control systems such as surveillance cameras and laser sensors are used to take pictures of the bottom edge and surface, obtain image data, create a physical model of the bridge, and obtain bridge configuration information based on measurements to support bridge operation and management [14]. In addition, the application of intelligent robotic tilt photography technology was explored on some measurement work in the predesign of bridge construction projects, and assisted in organizing the relevant measurement and mapping work in the same time combined with 3S technology for efficient measurement and mapping.

The idea of nanorobotics is to apply biological principles on the nanoscale to discover new phenomena and develop programmable molecular robots. Synthetic biology redesigned cell signaling and gene regulation networks to develop "in vivo" or "wet" biocomputers or cellular robots, resulting in an alternative approach to nanorobotics, which is now used in measurement In the future, nanorobots will be used for measurement. Thus, it is necessary to attach great importance to professional and technical personnel, grasp the measurement technology used as well as the technicality of surveying and mapping, and carry out bridge engineering project measurement control development design and implementation. Bridge measurement work should be strictly enforced in the preparation of professional and technical personnel standards and standardized organization of the external environment in the work, to collect the necessary data information for the next step in the work and implementation of professional data information to ensure the quality of bridge projects and operational safety.

3.2. Carry Out Data Information Quality Testing. Although the various surveying and mapping technologies commonly used in bridge surveying work are in a state of continuous improvement, there are still difficulties in the practical application because of the limitations of various conditions. Therefore, in order to ensure the available use value of mapping effectiveness, we must pay attention to the quality inspection of data information, ensure the quality of the acquired data, provide data information for bridge construction engineering design, engineering construction management, and operation manipulation, achieve a variety of business needs, and complete the bridge project measurement its value function. Bridge infrastructure construction is large and complex, the project construction period is easy to produce unfavorable conditions, measurement precision is reduced, and even deviations can occur. Thus, it is necessary to do a good job of measuring and monitoring operations in the construction of the project, and strictly control the quality of operation and bridge safety [15]. The operator is supposed to standardize the use of surveying and mapping data information and implement various control measures.

3.3. Bridge Operation and Management Link in the Mapping Work

3.3.1. Measurement and Inspection of Bridge Structure. In the bridge construction process, in order to further strengthen supervision and management, we need to ensure the overall quality of the construction of the bridge project. At first, it is advisable to carry out a reasonable test analysis of the road bridge structure, including the coordinate points of the bridge structure, bridge pile deviation, bracket deviation, centerline deviation, etc. The corresponding regulatory work should be carried out according to the test results [16, 17]. However, in the specific measurement and testing of bridges, most of the supervisors choose the traditional measurement method, and the relevant measuring machines and equipment, such as RTK, commonly used in the traditional type of measurement method are easily restricted by various natural environmental conditions around. As a result, the information obtained with it has certain deviations, which will further jeopardize the final measurement and inspection results. The fusion of the BIM virtual environment and nanoscale robotic mapping system software can also set fixed, immobile measurement points during the bridge construction process. That way, bridge

RETRACTED

construction and measurement within a certain range are done on this basis, reasonably ensuring the accuracy and precision of bridge measurement. At the same time, using the mobile measurement station to collect and sample the information of the overall structure of the bridge, the information collected is transmitted and processed in real time, which enhances the measurement efficiency of the bridge.

3.3.2. Deformation Measurement and Monitoring of Bridges. Through the long-term use and damage of bridges, certain deformation may occur, which seriously endangers the safety and stability of bridges. Thus, it is of important practical significance to improve its deformation measurement and detection [18]. According to the efficient measurement and inspection technology means, the deficiencies are found early and then solved scientifically and reasonably to ensure the bridge safety and reliability reasonably. In the bridge deformation monitoring link, the close combination of BIM virtual environment and robot mapping system software can effectively improve the bridge deformation monitoring efficiency and precision. At the same time, the work efficiency efficiently shortens the time of bridge deformation measurement and enhances the bridge safety and reliability.

3.4. Construction Site Identification and Safety Hazard Detection System Software Design. In recent years, with the implementation of construction projects, as an integral part of bridges, the demand for bridge span, relative height of bridge piles, and bridge bearing capacity has continued, and there are more regulations on the construction precision and erection efficiency of bridge projects. So we want to reasonably carry out all aspects of the bridge project under new standards and the new mandatory requirements to further strengthen the bridge project mapping work, enhance the bridge mapping work on a variety of resource integration, and actively explore and improve the various aspects of professional technology, which can effectively give full play to mapping in bridge construction to promote the role of the bridge project and enhance the overall quality of the bridge project [19].

In this paper, BIM technicality is combined with robotics to collect needed data and use data enhancement technicality to expand the data sample set. Finally, the test set of network model exercise is created and the system software for safe construction problem discovery is given. The first step of the system software design principle is to identify the overall target scenario, and the second step is to distinguish whether the overall target scenario is a safety hazard problem, so that site safety managers can make a more comprehensive analysis and manage the method site safety protection situation [20].

3.4.1. Overall Target Scenario Collection Link. Nanoscale intelligent robots periodically take pictures of construction sites, repair, and slice the collected images, and select images that have discriminatory value and safety status discrimination significance as a basis for leaders to carry out safety work judgments.

3.4.2. System Software Product Testing. Show that the overall target scenario test set with reference to the overall target scenario identification sample version; implementation of the identification entity model; export; target identification entity model export data to be identified as a sample version of the security hazard detection model test sample version of the scenario to be identified; export the results of the implementation of the security hazard detection model.

3.4.3. Early Warning Information and Decision-Making Stage. The system software generates detection results, providing early warning information about the on-site situation to management staff. This enables them to determine whether it is necessary to implement security risk improvement measures at the site.

In Figure 8, for the operation process of the safety construction problem discovery system software, the system software, according to the visited target scenario, identifies the target scenario according to the general engineering project scenario identification entity model enabled in the previous section of the exercise and filters the identified images. For security hazards found in the entity model of unidentified data samples, we can directly complete the entity model identification. According to the inspection of an image, the fusion of building construction safety problem discovery involves an entity model, the identification of 4 categories of classification incident site, so that the system software could distinguish the effect of the scene as "safe" or "unsafe;" the conclusion was "unsafe."

3.5. Establish and Improve the Integrated Bridge Survey Management System. The use of bridge surveying and mapping technology in China can be divided into three stages: early design and planning, middle and late construction, and late operation and management. This method can effectively ensure the overall quality and precision of the bridge project, but because of a variety of conditions restricting bridge mapping cannot be reasonably carried out. Therefore, in the road and bridge construction, it is necessary to actively introduce the world's leading-edge surveying and mapping technology and equipment, integration of the construction of the bridge specific conditions, reasonable surveying and mapping work, and the basic construction of high quality and high level of bridge engineering.

Along with the rapid development of China's science and technology, more and more high-tech technology is widely used in our own daily work lives. Accordingly, bridge engineering, according to the application of high-tech technology, including the establishment of a complete bridge accurate measurement design program integration management system, can effectively promote the structural stability and safety coefficient of bridge engineering [21]. The first use of intelligent robotic aerial photogrammetry

RETRACTED

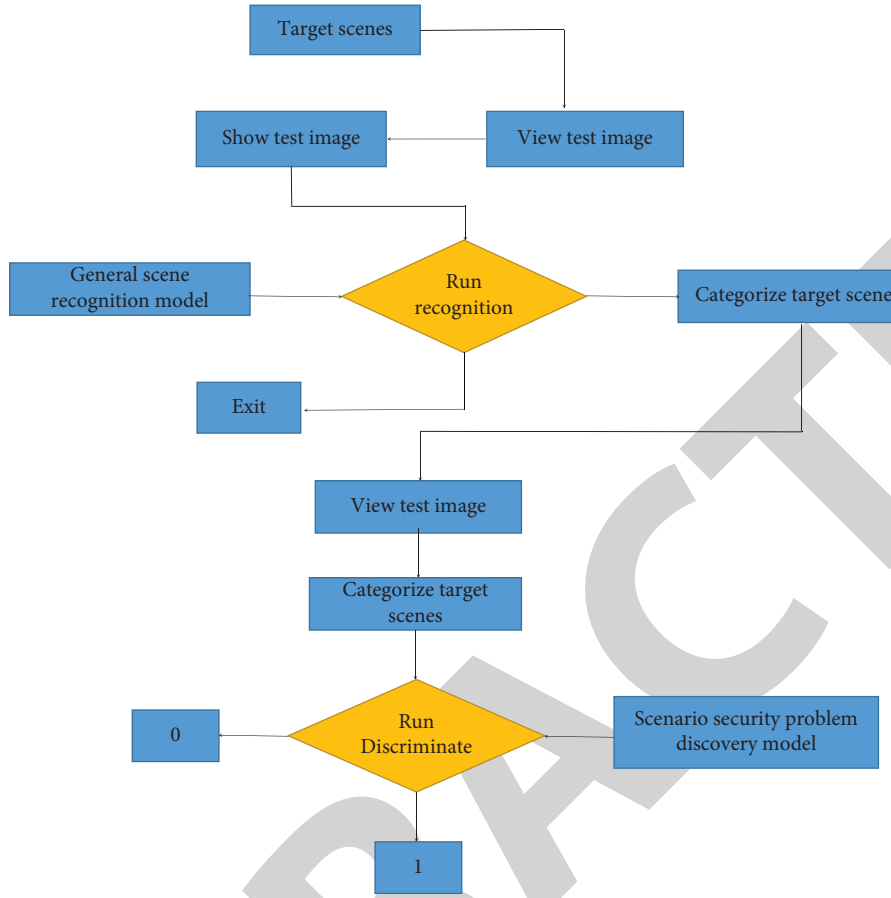

Figure 8: Construction site safety problem discovery system process.

technology was to take pictures around the bridge and upload the captured data images to computer software for backup purposes. In the following, the positioning information of the nanoscale intelligent robot application was recorded using GPS positioning technology. A complete map of the bridge project was produced by fusing the data images obtained from the earlier photographs and using digital photographic nanoscale measurement technology. In addition, when measuring along the road and bridge, we were able to use remote sensing technology technique to collect the geological structure and water engineering around the bridge in all directions, further reducing the cost and high efficiency of accurate measurement. Then, all the collected data will be keyed into the computer software after a reasonable statistical analysis for road and bridge engineering design planning, engineering construction management, and development management decisions to give the necessary information and data. The establishment and perfection of an integrated bridge engineering survey management system can grasp bridge engineering design planning in general and reasonably ensure the quality of bridge engineering.

4. Conclusion

In a word, the BIM virtual environment and nanoscale robotic mapping technology play an important role in surveying and mapping construction. The application of intelligent nanoscale robotic remote sensing technology has created a new era for mapping engineering projects and has endless potential for future development in the construction engineering measurement industry. BIM being closely based on three-dimensional digital technology, the BIM design model not only contains the new project entity line but also includes the functional characteristics data. In addition to the content of three-dimensional graphic information, the entity model also contains a lot of data information content, such as the type of material on the building and the entity model, the relevant data of the building materials, and their spatial relationship with the docking fasteners. This kind of data is suitable for simulating the behavior of individuals in this world of reality. It completes the efficient collection of mapping data and high efficiency of mapping, reduces the cost of mapping fees, and ensures the precision of mapping. In practice, applications can lead to early detection of difficult problems, survey area problems, further improve the security of mapping, reduce the need for precise measurement when conditions are not good, the environment is poor resulting in accidents and risks, and allow the middle and later phases of construction projects to use accurate data.

Along with the current state of Chinese society, the level of economic and technological strength of the rapid development and the surveying and mapping technology of bridges have also become more advanced. A variety of new

RETRACTED

surveying and mapping technologies in road and bridge engineering construction and the extensive use of accurate measurement methods and construction technology in China's bridges have contributed to this subversive change. In addition, along with the rapid development of surveying and mapping technology, the scope of surveying and mapping is not only limited to bridge design and engineering construction but also includes the initial design of the bridge, the middle and later engineering construction, and later management aspects. The application of new surveying and mapping technology can effectively enhance the precision and efficiency of bridge surveying and mapping, which can better ensure the overall quality of the bridge project. Therefore, as the relevant personnel of road and bridge surveying and mapping, they should be deeply aware of the need for efficient use of surveying and mapping technology in bridge engineering. Integrate the specific natural environment of bridge engineering, select the most ideal precise measurement and mapping technology, accurately and systematically reflect the real situation of bridge engineering, and further promote the rapid development of the capital construction level of bridge engineering in China.

Data Availability

The labeled dataset used to support the findings of this study are available from the corresponding author upon request.

Conflicts of Interest

The authors declare that there are no conflicts of interest.

Acknowledgments

This study was supported by the Shaanxi Provincial Department of Education in the 2020 General Special Scientific Research Plan Project, Application of BIM Technology in Large Span Arch Bridge, 20JK0580; 2017 Annual Science and Technology Plan Project of Weinan City, Shaanxi Province, linear control research of main arch rib assembly construction of concrete raised steel tube basket arch bridge, 2017JCYJ-3-6; and China Railway 20th Bureau in 2021, BIM House Building Forward Design Software Development Research, YF2112QT24B.

References

[1] Y. Wang, "Research on the application of simulation technology based on "BIM+VR" in architectural design," *Journal of Huangshan College*, vol. 24, no. 3, pp. 59–61, 2022.

[2] R. Yang, "Application of "BIM+VR" technology in highway engineering: the example of fushan county excelsior river special bridge," *Shanxi Transportation Science and Technology*, no. 3, pp. 69–71+79, 2021.

[3] G. Song, "Research on mobile measurement robot technology for blasting quality evaluation of excavation workface," *Coal Engineering*, vol. 54, no. 4, pp. 182–186, 2022.

[4] G. Zhang and Z. Gai, "Basic development of measurement robot and its data processing research," *Mapping and Spatial Geographic Information*, vol. 45, no. 6, pp. 223–225+228, 2022.

[5] T. Nie, "Analysis of the application of new surveying and mapping technology in engineering measurement," *Real Estate World*, vol. 108, no. 14, pp. 82–84, 2022.

[6] J. Pan, "Analysis of the application of new technologies of measurement and mapping in bridge engineering measurement," *Enterprise science and technology and development*, vol. 481, no. 11, pp. 105–107, 2021.

[7] S. Yao, "Analysis of the application of new technologies based on surveying and mapping in construction engineering measurement," *China Equipment Engineering*, vol. 500, no. 12, pp. 191–193, 2022.

[8] F. Z. Wang, H. C. Sui, W. D. Kong, and H. Zhong, "Application of BIM+ VR technology in immersed tunnel construction//IOP conference series: earth and environmental science," *IOP Conference Series: Earth and Environmental Science*, vol. 798, no. 1, Article ID 012019, 2021.

[9] F. Han and Y. Liu, "Indoor intelligent decoration system based on BIM+ VR technology[C]//IOP conference series: earth and environmental science," *IOP Conference Series: Earth and Environmental Science*, vol. 783, no. 1, Article ID 012121, 2021.

[10] T. Mo, F. Wu, Y. Zhang, and M. Wang, *Application of BIM Technology in Zhuhai Port Project of Hong Kong-Zhuhai-Macao Bridge//ICCREM 2019: Innovative Construction Project Management and Construction Industrialization*, American Society of Civil Engineers, Reston, VA, USA, 2019.

[11] A. Girardet and C. Boton, "A parametric BIM approach to foster bridge project design and analysis," *Automation in Construction*, vol. 126, Article ID 103679, 2021.

[12] J. Zhang, C. Zhao, H. Li, H. Huijser, and M. Skitmore, "Exploring an interdisciplinary BIM-based joint capstone course in highway engineering," *Journal of Civil Engineering Education*, vol. 146, no. 3, Article ID 05020004, 2020.

[13] V. Dayan, N. Chileshe, and R. Hassanli, "A scoping review of information-modeling development in bridge management systems," *Journal of Construction Engineering and Management*, vol. 148, no. 9, Article ID 03122006, 2022.

[14] A. Gupta, S. Soni, N. Chauhan, M. Khanuja, and U. Jain, "Nanobots-based advancement in targeted drug delivery and imaging: an update," *Journal of Controlled Release*, vol. 349, pp. 97–108, 2022.

[15] Y. C. Lin, Y. T. Hsu, and H. T. Hu, "BIM model management for BIM-based facility management in buildings," *Advances in Civil Engineering*, vol. 2022, Article ID 1901201, 13 pages, 2022.

[16] M. A. Rahhal Al Orabi, "A framework of selecting building flooring finishing materials by using building information modeling (BIM)," *Advances in Civil Engineering*, vol. 2022, Article ID 8556714, 22 pages, 2022.

[17] Z. Yu, Z. Qiu, H. Li, J. Xue, W. Hu, and C. Wang, "Design and calibration of torque measurement system of comprehensive performance test instrument of industrial robot reducer," *Computational Intelligence and Neuroscience*, vol. 2022, Article ID 8155818, 18 pages, 2022.

[18] T. Wang, K. Fang, W. Wei, J. Tian, Y. Pan, and J. Li, "Microcontroller unit chip temperature fingerprint informed machine learning for IIoT intrusion detection," *IEEE Transactions on Industrial Informatics*, vol. 19, no. 2, pp. 2219–2227, 2023.

[19] M. Mathesh, E. Bhattarai, and W. R. Yang, "2D active nanobots based on soft nanoarchitectonics powered by an ultralow fuel concentration," *Angewandte Chemie*, vol. 134, no. 7, 2022.

RETRACTED

Hindawi
Journal of Robotics
Volume 2024, Article ID 9898409, 1 page
https://doi.org/10.1155/2024/9898409

Retraction

Retracted: Intelligent Control System Design of Ring Light via IOT Mobile Robot

Journal of Robotics

Received 23 January 2024; Accepted 23 January 2024; Published 24 January 2024

Copyright © 2024 Journal of Robotics. This is an open access article distributed under the Creative Commons Attribution License, which permits unrestricted use, distribution, and reproduction in any medium, provided the original work is properly cited.

This article has been retracted by Hindawi following an investigation undertaken by the publisher [1]. This investigation has uncovered evidence of one or more of the following indicators of systematic manipulation of the publication process:

(1) Discrepancies in scope
(2) Discrepancies in the description of the research reported
(3) Discrepancies between the availability of data and the research described
(4) Inappropriate citations
(5) Incoherent, meaningless and/or irrelevant content included in the article
(6) Manipulated or compromised peer review

The presence of these indicators undermines our confidence in the integrity of the article's content and we cannot, therefore, vouch for its reliability. Please note that this notice is intended solely to alert readers that the content of this article is unreliable. We have not investigated whether authors were aware of or involved in the systematic manipulation of the publication process.

Wiley and Hindawi regrets that the usual quality checks did not identify these issues before publication and have since put additional measures in place to safeguard research integrity.

We wish to credit our own Research Integrity and Research Publishing teams and anonymous and named external researchers and research integrity experts for contributing to this investigation.

The corresponding author, as the representative of all authors, has been given the opportunity to register their agreement or disagreement to this retraction. We have kept a record of any response received.

References

[1] X. Kang and Y. Teng, "Intelligent Control System Design of Ring Light via IOT Mobile Robot," *Journal of Robotics*, vol. 2023, Article ID 4303194, 13 pages, 2023.

Hindawi
Journal of Robotics
Volume 2023, Article ID 4303194, 13 pages
https://doi.org/10.1155/2023/4303194

RETRACTED

Research Article

Intelligent Control System Design of Ring Light via IOT Mobile Robot

Xianzhi Kang and Yue Teng

School of Electronic and Electrical Engineering, Cangzhou Jiaotong College, Huanghua 061199, HeBei, China

Correspondence should be addressed to Yue Teng; tengyue@czjtu.edu.cn

Received 28 October 2022; Revised 30 November 2022; Accepted 30 March 2023; Published 21 April 2023

Academic Editor: Shahid Hussain

Copyright © 2023 Xianzhi Kang and Yue Teng. This is an open access article distributed under the Creative Commons Attribution License, which permits unrestricted use, distribution, and reproduction in any medium, provided the original work is properly cited.

In the Internet of Things (IoT) era, the combination of mobile robots and IoT technology has realized the complementary advantages of the IoT and robots, which has brought new challenges and opportunities for the development and application of the IoT and mobile robots. In this study, a mobile robot positioning system based on the wireless positioning technology of the IoT is first designed, and an adaptive federated filtering algorithm based on the confidence of the sensor measurement data is given, and the data fusion processing is carried out for the positioning system to achieve the accurate positioning of the mobile robot. Then, we embed the intelligent control system of the ring lamp and propose an adaptive fuzzy PI double closed loop equalization control strategy, which can automatically identify the number of interlaced parallel and ensure its equalization effect. The experimental results show that the equalization strategy designed in this study has a good equalization effect in the loop interleaving parallel topology, strong adaptive parameter adjustment ability, good robustness, and anti-interference.

1. Introduction

With the acceleration of urbanization and infrastructure construction in China, the market demand for lighting products is gradually expanding. Traditional lighting equipment has high energy consumption and is limited by its technical bottleneck, which is not intelligent enough in the control method, which not only causes the waste of nonrenewable energy use but also increases the investment of human and material resources [1]. Figure 1 shows a ring light used at home, which can be used to generate electricity by using solar energy. In recent years, due to the increasing awareness of energy conservation and environmental protection in China, the installation of ring lights in the industry has been growing, with about 735,000 ring lights installed in China in 2010, reaching 4,972,000 in 2018, which shows the rapid development of ring lights and indicates that the research on ring lights has good application prospects.

Mobile robots are intelligent robots that combine environmental information perception, autonomous task planning, intelligent task control and execution, and other capabilities that are highly autonomous in planning, organizing, and adapting and can operate in complex environments, greatly expanding the application areas of robots [2–4]. Mobile robots are also more and more widely used, because they have a high degree of autonomy, can complete many tasks that are difficult for human beings to complete in dangerous or other restrictive environments, and have gradually penetrated into all areas of human social life. To some extent, autonomy is similar to the concept of human autonomy. This concept emphasizes that "moral subjects can actively use their abilities in pursuit of goals." This concept emphasizes that in the process of pursuing goals, artificial systems or moral subjects can make choices. Therefore, the moral subject should at least have a mechanism to make decisions and display goals. If it is ideal, it is better to have display mechanisms indicating other goal states (such as desire and motivatio) and nongoal states (such as task display).

IoT is a kind of intelligent network to realize the interconnection of all things, which connects all objects to the Internet through information sensing devices such as radio

Figure 1: Ring lamp.

frequency identification and can realize intelligent identification, provide real-time online management, and service functions that are safe and controllable and even personalized and complete the integration of "management, control, and management" of "all things" [5]." The main feature of IoT is to obtain various information of the physical world by means of radio frequency identification and sensors, to transmit and interact with information by combining with networks such as Internet and mobile communication networks, and to analyze and process information by using an intelligent computing technology, so as to improve the perception ability of the material world and realize intelligent decision-making and control [6]. The emergence of IoT has broken the barrier between the physical world and the information world, successfully integrating reinforced concrete, machines, and the Internet into a new whole and better serving human production and life. Therefore, IoT is also called a new wave of technology in the world of information and has become a hotspot for research and development and a technological high point in the new round of information technology [7]. The IoT positioning technology is an important technology of IoT, which refers to the technology of obtaining the location of objects through various sensors in the IoT [8]. Throughout the application field of IoT, positioning technology is widely used in logistics and transportation, manufacturing, transportation, mining, and healthcare. Many information collected through IoT sensing system will be difficult to play its proper value without the corresponding location information identification [9]. Therefore, how to use positioning technology to obtain location information more accurately and comprehensively has become an important research topic in the era of IoT.

In this study, we combine the IoT with robot technology and embed the intelligent control system of a ring lamp to achieve intelligent control. The main contributions of this study are in two aspects. First of all, we designed the mobile robot positioning system in the Internet of Things environment, including the specific design of the UWB wireless positioning module and scanning and matching module, and realized the mobile robot positioning. Second, we designed an adaptive fuzzy PI double closed loop current equalization strategy and constructed an interleaved bidirectional DC/DC simulation circuit using Matlab/Simulink to test its current equalization effect.

2. Related Work

2.1. Ring Light System Based on IOT Technology. Based on the importance of intelligent monitoring of street lamps and the problem that ring lamps cannot be maintained in time in actual operation, the Internet of Things technology is applied to the ring lamp measurement and control system to achieve remote management and control of the street lamp system [10–12]. Based on the development status of the Internet of Things industry in China, this study puts forward a conclusion that the value of the Internet of Things industry needs to be further explored [13]. Based on the detailed study of IEEE802.15.4 communication standard and ZigBee protocol stack, this study proposes a remote street lamp monitoring scheme based on the ZigBee wireless communication technology, analyzes the advantages and disadvantages of LoRa technology, and studies its application in intelligent street lamps. Three key technologies of intelligent urban street lamp remote control system are studied, and the feasibility of "4G + LoRa" communication scheme for a single lamp remote control is analyzed. The above literature shows that the application prospect of IoT technology in the ring light system is very good, but research on the solar ring light system with IoT technology at home and abroad is still in the stage of exploration and attempt, and there is no good balance between cost and practicality.

2.2. Robot Positioning Technology. Accurate positioning of the mobile robot is the key to ensure that it can perform the navigation task correctly. The mobile robot uses internal sensors and external sensors to obtain information about the distribution of obstacles in the environment, the shape of the obstacles, and the position of the mobile robot itself. At present, the positioning methods commonly used for mobile robots are divided into three categories: absolute positioning, relative positioning, and combined positioning methods.

(1) Relative positioning or trajectory projection determines the position of the mobile robot in the environment by calculating the accumulated value of the body state of the mobile robot in real time. Relative positioning mainly uses internal sensors, such as optical encoder, odometer, and inertial guidance system (gyroscope and accelerometer) [14]. A localization algorithm based on a known map environment with a known initial robot posture is proposed in. This algorithm can locate mobile robots in a known environment. Chen et al. proposed a trajectory projection algorithm based on inertial sensors to achieve robot positioning in the 3D environment [15].

RETRACTED

(2) Absolute positioning mainly calculates the position of the mobile robot by calculating the position information of objects in the environment that can be recognized by the mobile robot [16]. The sensors used for absolute positioning include active beacons, global positioning system (GPS), and special landmarks. A GPS based mobile robot positioning system is proposed to realize the large range positioning of mobile robots [17]. A location method based on real-time location and mapping (SLAM) is proposed to solve the problem of high precision location of mobile robots. Absolute positioning has the advantages of high precision and small error [18, 19].

(3) Due to the advantages and disadvantages of both relative positioning and absolute positioning methods, there are various literatures about the combination of several positioning methods to achieve the reliability and accuracy of positioning in recent years. For example, in [20], a mobile robot positioning method based on Hough transform was proposed, which estimated the robot's attitude distribution in the global map by establishing the Hough energy spectrum function of the global map. Reference [21] proposed a relative positioning method for mobile robots based on the fuzzy data fusion method, which combines ultrasonic sensor and laser radar information. The location coordinates of indoor mobile targets are estimated by building the ZigBee wireless network indoor positioning system [22, 23]. Fuzzy logic is used to process the information of multiple ultrasonic sensors carried by mobile robots to achieve positioning. A mobile robot positioning system based on distance sensor, manual landmark, and triangulation is designed and proved through physical experiments [24, 25].

Although the above algorithms have made some achievements in the localization of mobile robots, sensor errors, different map scenes and map noises, and dynamic and highly occluded environments will bring uncertainty and seriously affect the localization accuracy. Therefore, how to ensure the accuracy and robustness of the attitude tracking algorithm in different dynamic and complex environments is still a challenge for mobile robots.

3. Methodology

3.1. IoT-Based Mobile Robot Positioning System Design. In order to effectively control the mobile robot, the position, angle, speed, and angular velocity information of the mobile robot as well as the basic information of the surrounding environment are the data information that needs to be acquired. In order to obtain these necessary information, a multisensor positioning system is designed to collect and process the data information. The designed positioning system is shown in Figure 2, where the UWB BSi is the anchor node (base station) of the ultrawideband (UWB) positioning module, and the UWB Tag is the mobile node,

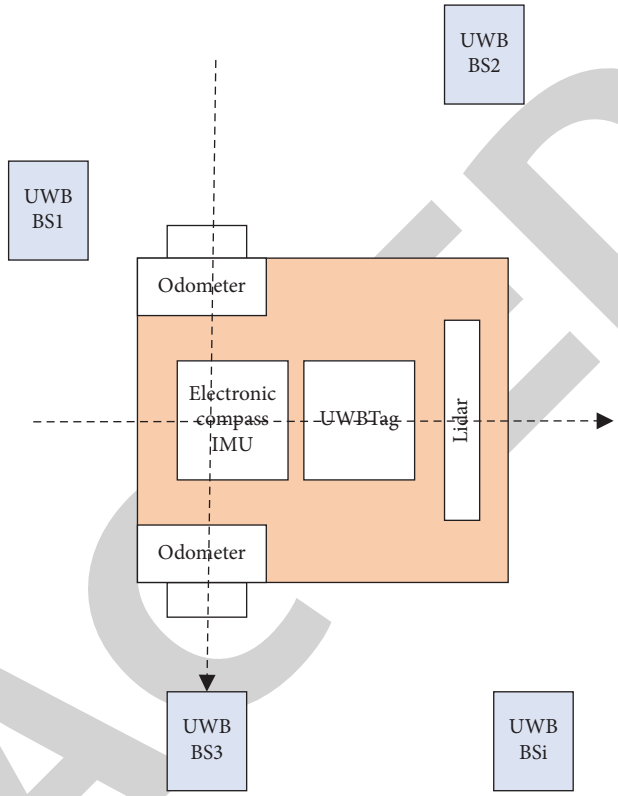

Figure 2: Schematic diagram of the mobile robot positioning system.

i.e., the target to be positioned. From the figure, we can see the main sensors installed in the mobile robot, including position sensor, velocity sensor, and scanner, to obtain the global position information, angle information, velocity information, and environment information of the mobile robot, respectively. The position sensor is a UWB wireless positioning sensor, which is mainly used to measure the position information of the mobile robot. The velocity sensor includes odometer and inertial measurement unit (IMU), which are mainly responsible for collecting linear and angular velocities of the mobile robot. The electronic compass is responsible for collecting the heading angle data of the mobile robot, and the LIDAR is used for scanning and positioning by scanning. The following is a specific design analysis of several sensor systems.

UWB positioning is a high-precision wireless positioning technology, which can achieve decimeter or even centimeter level positioning accuracy under ideal conditions. The hardware principle of the UWB positioning system is shown in Figure 3. The whole positioning system includes anchor node BSi, target to be located, and other communication equipment. The UWB transmitter module is responsible for receiving and sending UWB signals for positioning, and the WiFi module is responsible for interacting the collected distance data with other nodes and targets to be located. A single DW1000 chip communicates with the WiFi module through the USB interface. The targets to be located include the UWB transmitter module, ZigBee communication module, and controller. The controller is

RETRACTED

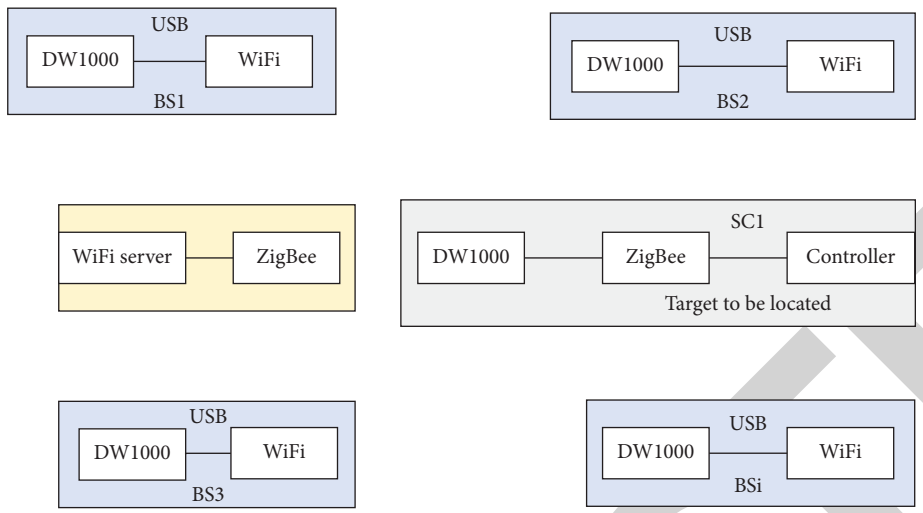

Figure 3: Schematic diagram of the UWB positioning system.

used to further process these distance measurements and obtain the final location value by solving the corresponding location algorithm. ZigBee module and controller communicate with each other through an SCI serial port. In order to facilitate the expansion of the positioning node and improve the real-time performance of the positioning system, the communication system here uses a WiFi positioning system. The WiFi node acts as a server, responsible for aggregating the distance information measured by each UWB anchor node, communicating with the ZigBee module through the SCI serial port, and finally sending it to the controller of the target to be located. For this positioning system, we choose the time of arrival (TOA) based UWB positioning method, which is a ranging based positioning method, as shown in Figure 3. The positioning system shall include at least one tag node to be located.

The time synchronization of each positioning node has a very important impact on the accuracy of TOA positioning, so the TOA positioning method requires time synchronization of nodes. The common time synchronization method is hardware synchronization, but the hardware synchronization method is difficult to wire, and the requirement and cost are high, so a software synchronization method based on wireless communication is designed for the designed UWB positioning system. Unlike the unidirectional synchronization method of hardware synchronization, the software synchronization method is a bidirectional clock synchronization method, and its basic principle is shown in Figure 4.

In the designed positioning system, when the UWB transmitter module is successfully networked, the UWB signal is firstly sent by the target Tag to be located, which is broadcasted and contains the time synchronization information (SYNC_MSG). In addition to UWB wireless localization, a scan-matching-based localization method is also designed in this study, and the applied sensor is radar. The range and scanning frequency of the URG-40LX-UG01 laser scanner enable it to obtain a sufficient number of laser data points in most indoor environments and scan a large amount of environmental features in a short period of time to ensure the subsequent scan matching and other positioning algorithms. The implementation of after obtaining the scanned point data of the environment by LIDAR, this study uses the iterative closest method (ICP) to locate the mobile robot. The time complexity of the entire ICP algorithm is directly related to the number of data points to be matched between the two sets. The number of data points scanned by the URG-04LX laser scanner in the study is 668, and the ICP alignment of the two data point sets before and after the sensor motion using the original data points will consume a lot of time, which is not conducive to the real-time implementation of the subsequent localization algorithm. The IoT experimental environment of the mobile robot in the study is indoor, which is relatively structured and the contours of many objects (e.g., walls, doors, windows, tables, and chairs) can be described by line segments. When LIDAR scans these objects, the measured data point sets reflect distinct line segment features. In an indoor environment, a frame of LiDAR data can usually be divided into several line segment features. If a number of features (e.g., line segment endpoints and midpoints) on the line segment are used instead of all data points on the line segment for the ICP alignment, this will greatly reduce the number of data points for Tem and Ref, and thus improve the real-time performance of the ICP algorithm, as shown in Figure 5. Based on the above analysis, the study proposes the line segment feature-based ICP algorithm to replace the basic ICP algorithm for scan matching solution. The flow of the line segment feature-based ICP algorithm is shown in Figure 6. Compared with the traditional ICP algorithm, the line segment matching-based ICP method mainly has an additional step of line segment feature extraction.

3.2. Dual Closed-Loop Flow Control Strategy Based on Adaptive Fuzzy PI Technique. Fuzzy control is based on the process of people's self-experience in dealing with complex problems. If the accumulated practical experience of human beings can be summarized and processed and described in the appropriate language, it can be summarized

RETRACTED

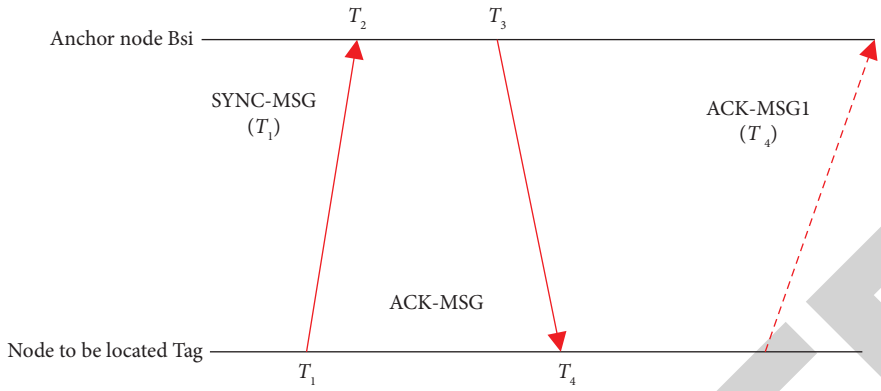

Figure 4: Software time synchronization principle.

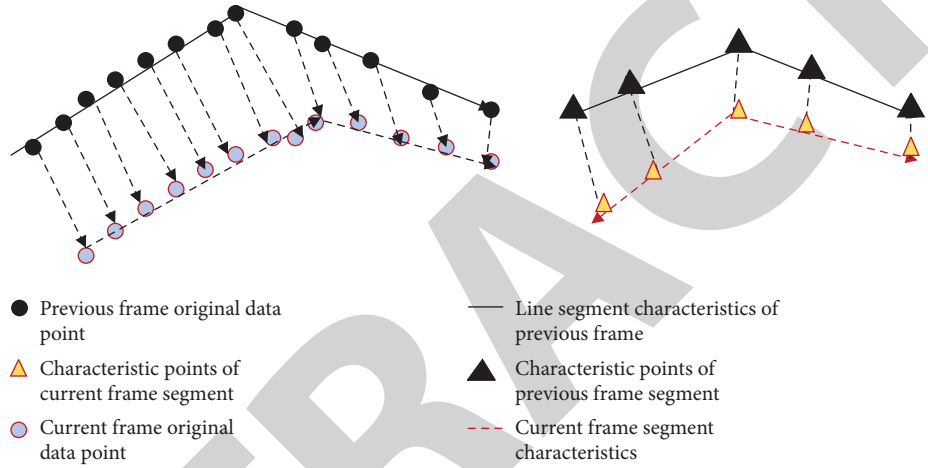

Figure 5: Schematic diagram of ICP based on line segment characteristics.

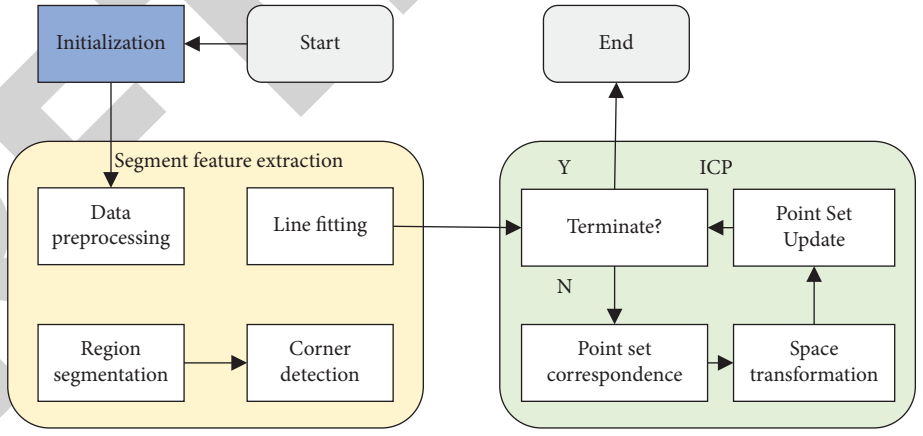

Figure 6: ICP algorithm flow based on line segment features.

as a fuzzy control method, and if combined with the concept of fuzzy mathematics, it can form a fuzzy control theory. If the voltage external loop current independent internal loop PI control is used, although the stability is good, the dynamic regulation ability is poor because the actual system is mostly nonlinear, and it is difficult to calculate more accurate PI parameters, thus the control effect cannot be guaranteed. On the contrary, fuzzy control can better adapt to the changes of nonlinear systems, but has the problem of poor steady-state performance. If the two algorithms are combined, the control effect will be more satisfactory, so this study proposes an adaptive fuzzy PI-based double closed-loop control equalization strategy, i.e., adding fuzzy control to the voltage outer-loop current independent inner-loop PI control. Then, the fuzzy controller can output the correction value of the regulation

RETRACTED

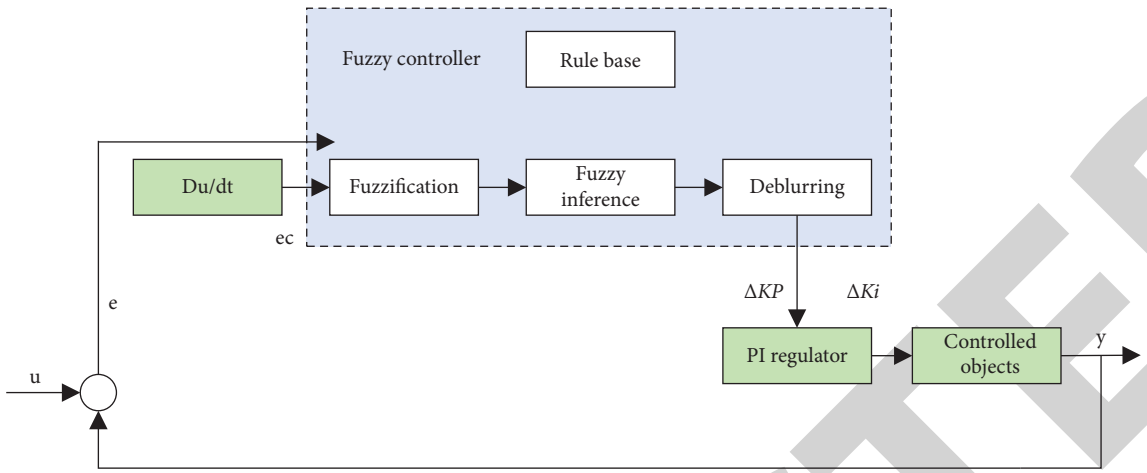

Figure 7: Structure of adaptive fuzzy PI control.

coefficient according to the real-time system deviation and input to the PI regulator to achieve the purpose of PI parameter adaption.

As shown in Figure 7, the adaptive fuzzy PI control structure is mainly divided into two parts: the fuzzy controller and PI regulator. The results are then defuzzified to obtain ΔKp and ΔKi, which are input to the PI regulator and superimposed with the Kp and Ki set in the PI regulator. When the actual situation of the control system changes, the PI parameters can be adaptively adjusted by fuzzy inference. Adaptive fuzzy control is mainly applied to the outer voltage loop and multiple inner current loops in the dual-loop control of an interleaved parallel bidirectional DC/DC converter. The voltage outer-loop fuzzy controller and current inner-loop fuzzy controller have the same control rules except that the corresponding input and output variables are different, so the two fuzzy PI controllers have similar structures. Based on the fact that a fuzzy control system is composed of input and output variables, fuzzification, rule base, fuzzy inference, and defuzzification, the adaptive fuzzy PI controller design will be carried out from the following parts [26, 27].

Figure 8 shows the input and output diagram of the fuzzy control of the voltage loop and current loop. For the design of the fuzzy controller of the voltage loop, the input is the voltage error value Ve and its change rate is Vec at the output end of the converter, and the output is ΔKp-V, and ΔKi-V is used as the correction parameter input of the voltage loop PI regulator to obtain the total current reference value Iref of the current loop fuzzy PI controller. The input of the current loop fuzzy controller is the inductor current error value Ie and the conversion rate Iec, and the corresponding output is input to the current loop PI regulator ΔKp-i and ΔKi-i, and the output is duty cycle D. The effect of the fuzzy PI control depends on the reasonable formulation of fuzzy control rules. In order to better achieve the effect of uniform flow control, the control rules of voltage loop and current loop are the same. The following is an example of voltage loop. The fuzzy control rules are as follows: (1) when |Vec| is relatively large, regardless of the Vec value, it means that the voltage difference is large, and kp and ki should be significantly increased to ensure the system response speed. (2) When the deviation Ve and the rate of change Vec are moderately large, Kp and Ki can be increased to reduce the overshoot of the system response and ensure a certain system responsiveness. (3) When the deviation is small, the output voltage will soon reach the reference value, so Kp and Ki should be significantly reduced. According to the above rules, ΔKp and ΔKi's fuzzy control rules are shown in Tables 1 and 2.

According to Table 2, it can be entered in the fuzzy rule editor in the form of If ⋯ then. The common defuzzification methods are centroid, MOM, and bisector, and the maximum affiliation method is chosen in this study.

4. Experiments

4.1. Experimental Analysis of Robot Positioning. The results of the positioning experiments are shown in Figure 9. It can be seen from the figure that the positioning accuracy of the UWB is significantly improved after time synchronization compared with the positioning of the UWB without time synchronization, and the accuracy can reach ±0.15 m, which can basically meet the positioning requirements of the mobile robot.

In order to compare the superiority of the applied UWB localization methods, the experiment was also conducted without NLOS identification and processing, and the results of the two experiments are shown in Figure 10. The results of the two experiments are shown in Figure 10. It can be seen from the figure that without NLOS identification and processing, the UWB localization results show large localization errors and large randomness of the data, while with NLOS identification and localization by the WLS algorithm, the localization results are better than those without NLOS identification and processing, although they are worse than those without NLOS identification and processing.

Scan matching localization verification of the experimental data collection site for the line segment feature-based ICP was located in a corner of the laboratory, and a total of two sets of experimental data were collected. In order to highlight the higher execution efficiency of the line segment

RETRACTED

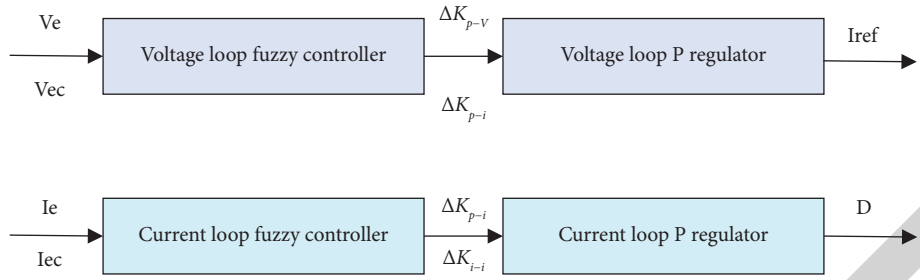

Figure 8: Input and output diagram of a voltage loop and current loop fuzzy control.

Table 1: Fuzzy rules of ΔKp.

Ve	Vec						
	NB	NM	NS	ZE	PS	PM	PB
NB	PB	PB	PB	PB	PB	PB	PB
NM	PB	PB	PM	PM	ZE	NS	NS
NS	PB	PM	PM	PS	NS	NM	NB
ZE	NB	NM	ZE	ZE	ZE	NM	NB
PS	NB	NM	NS	PS	PM	PM	PB
PM	NS	NS	PS	PM	PM	PB	PB
PB	PB	PB	PB	PB	PB	PB	PB

Table 2: Fuzzy rules of ΔKi.

Ve	Vec						
	NB	NM	NS	ZE	PS	PM	PB
NB	PB	PB	PB	PB	PB	PB	PB
NM	PB	PB	PM	PM	NS	NM	NB
NS	PB	PM	PM	PS	NS	NM	NB
ZE	NB	NB	ZE	ZE	ZE	NB	NB
PS	NB	NB	NM	PS	PM	PM	PB
PM	NB	NM	NS	PM	PM	PB	PB
PB	PB	PB	PB	PB	PB	PB	PB

based ICP algorithm, the experiments are compared with the normal ICP algorithm. In the first set of experiments, the actual heading deflection angle is −11°, and the actual x-direction and y-direction displacements are 0.15 m and 0.20 m, respectively. In the second experiment, the actual heading deflection angle was 18°, and the actual x-direction and y-direction displacements were −0.15 m and −0.15 m, respectively. In this section, we evaluate the performance of the 1DSP-IE using MATLAB R2015b software and a computer with an Intel(R) Core(TM) i5-6200 CPU @ 2.30 GHz and 8 GB of RAM. The experimental results of the two groups are shown in Figures 11 and 12, and the comparative data of the experimental results are shown in Table 3. From the experimental results, it can be seen that the time required to solve the ICP algorithm based on line segment characteristics is greatly reduced compared with the common ICP algorithm, and the accuracy does not deteriorate significantly, which verifies the effectiveness and superiority of the algorithm.

The LIDAR was installed on the mobile robot, and the mobile robot was set to move in a rectangle with a length and width of 3.6 m × 3.0 m . The positioning results of the ICP algorithm based on line segment features are shown in Figure 13, which shows that the positioning accuracy is good and can meet the general positioning requirements of the mobile robot.

4.2. Control System Analysis of Ring Light Circuit. For the 2–4 way staggered parallel bidirectional DC/DC simulation model, the input 24 V and output 12 V are set uniformly, the inductor and capacitor parameters are kept the same, and a resistor of 0.2 Ω is added in series in one of the circuits. It is convenient to simulate the equalization effect of the 2–4 channels interleaved parallel model under the inconsistent parameters. (1) Simulation analysis of the two-way staggered parallel bidirectional DC/DC model.

As can be seen from Figure 14, the value of each inductor current is equal to half of the output current, after the BUCK step-down, despite the inconsistency of the resistor parameters, the output voltage is still 12 V, and the effect of equalizing the current of each circuit is still maintained. Figure 15 shows the effect of phase shifting and equalization of inductor current, it can be clearly seen that the phase difference between the two inductor currents is 180°, and the waveform is more stable.

RETRACTED

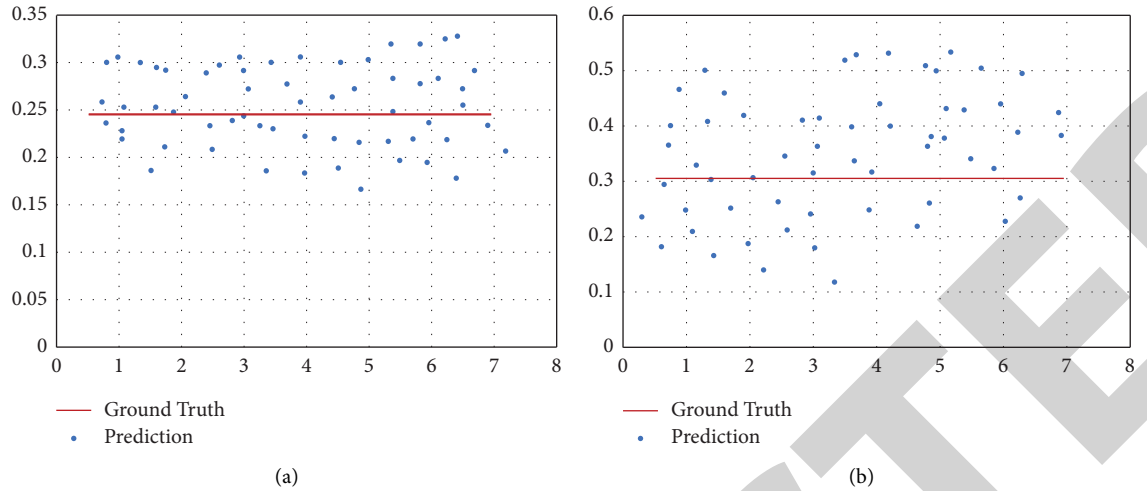

Figure 9: UWB positioning results (no NLOS). (a) Performing time synchronization. (b) Without performing time synchronization.

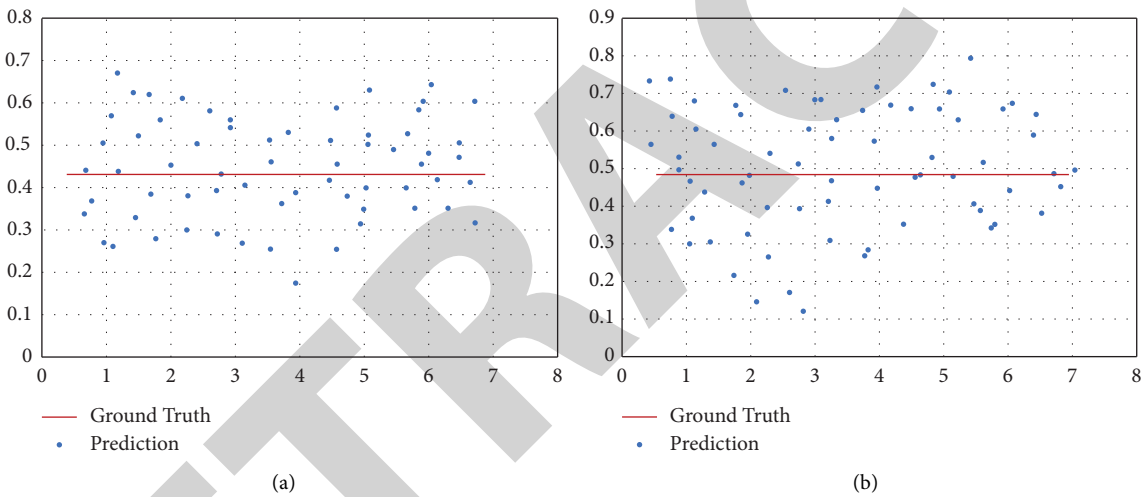

Figure 10: UWB positioning results in the presence of NLOS. (a) Performing NLOS. (B) Without performing NLOS.

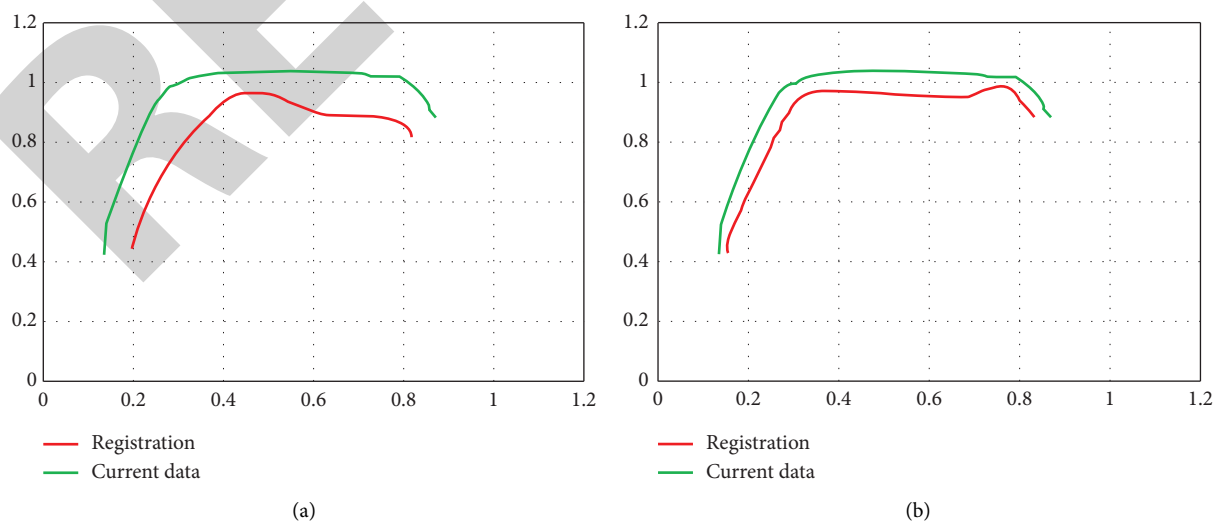

Figure 11: ICP experimental results based on line segment features (group I). (a) Common ICP methods. (b) Line based ICP methods.

RETRACTED

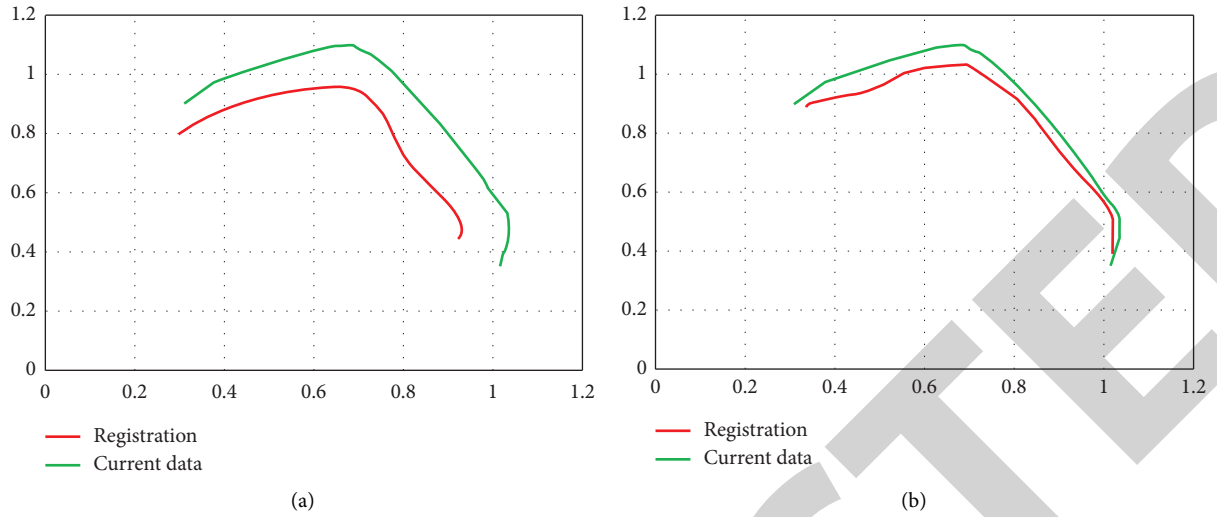

Figure 12: ICP experimental results based on line segment characteristics (the second group). (a) Common ICP methods. (b) Line based ICP methods.

Table 3: ICP experimental results based on line segment characteristics.

Group	Algorithm	Yaw angle (degrees)	Displacement in x-direction (m)	Y-direction displacement (m)	Tem data points	Ref data points	Alterations	Execution time (seconds)
1	ICP	−0.63	0.1504	0.1765	682	660	29	2.4776
	ICP based on line segment features	−0.30	0.1478	0.1799	33	30	7	0.0243
2	ICP	21.29	−0.1296	0.1514	621	663	36	2.4402
	ICP based on line segment features	21.08	−0.1309	0.1641	51	42	19	0.0753

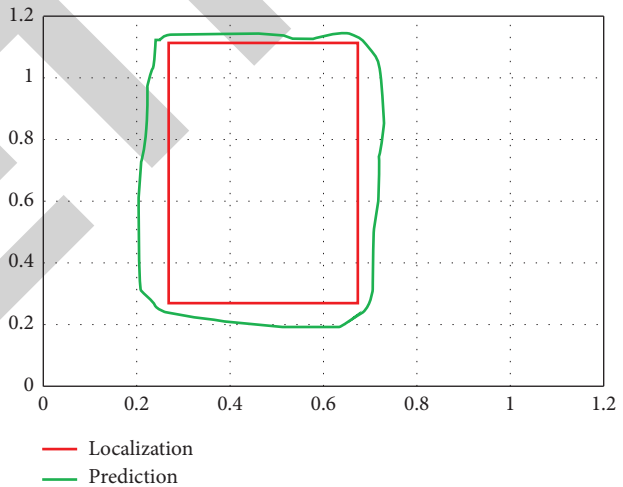

Figure 13: ICP indoor positioning experiment results based on line segment characteristics when moving along a rectangular route.

Then, we simulate and analyze the three-way interleaved parallel bidirectional DC/DC model.

As can be seen from Figures 16 and 17, the waveforms of each inductor current and output voltage current in the three-way staggered parallel bidirectional DC/DC are relatively stable, and the value of each inductor current is equal to 1/3 of the output current Io, and each inductor current maintains the equalization effect under the inconsistent parameters. The simulation results of the above 2–4 interleaved parallel bidirectional DC/DC show that the adaptive fuzzy PI double closed loop current equalization control strategy designed in this study can achieve the purpose of current equalization under the inconsistent parameters, and the output value of the system remains stable, and the current ripple of each channel

RETRACTED

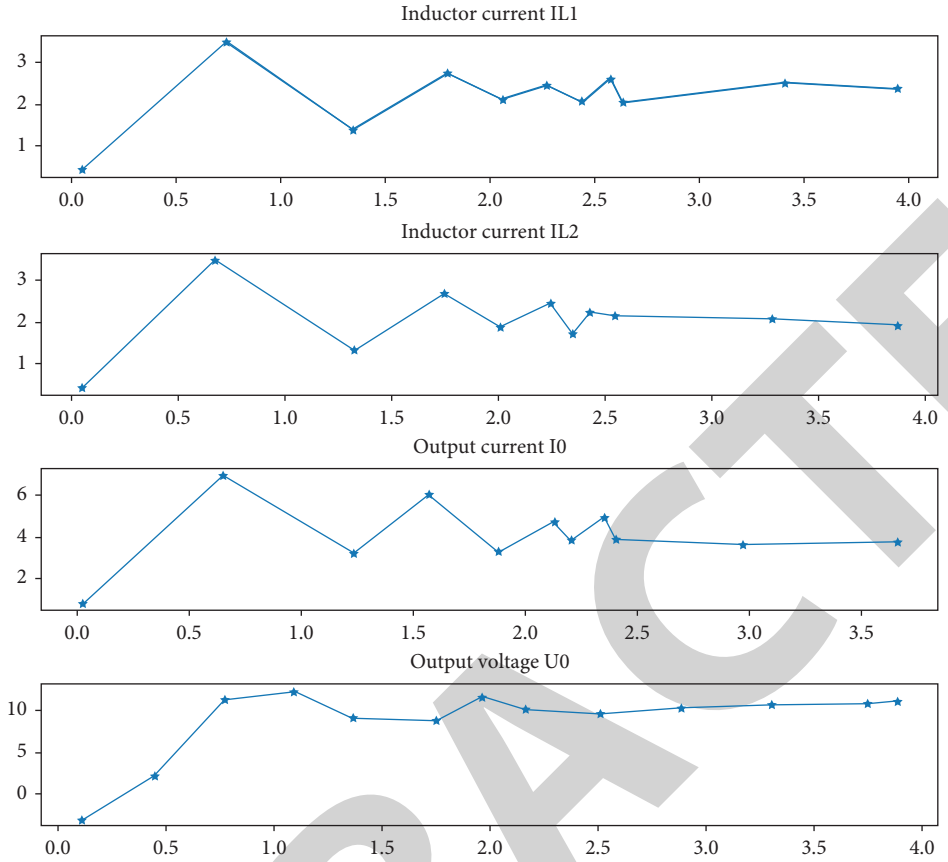

Figure 14: Simulation diagram of inductive current and output voltage current of each circuit.

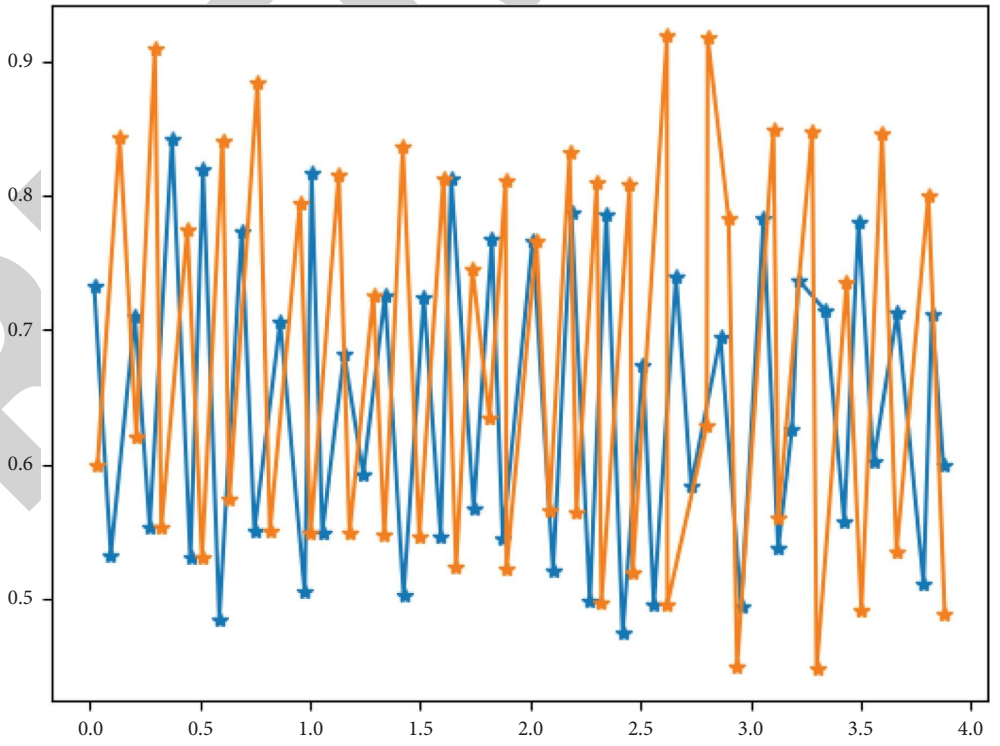

Figure 15: Effect diagram of phase shifting current sharing of inductance current under inconsistent parameters.

RETRACTED

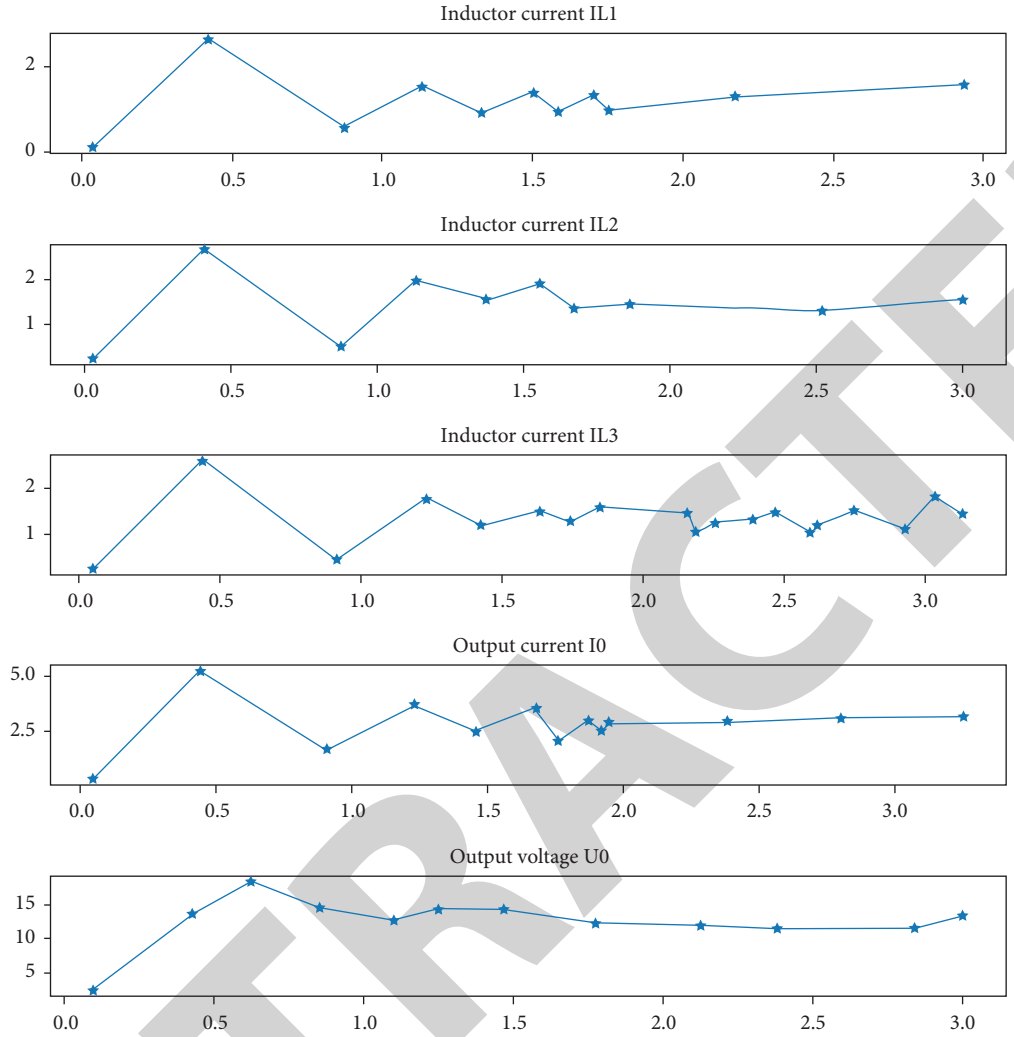

Figure 16: Simulation diagram of inductive current and output voltage current of each circuit.

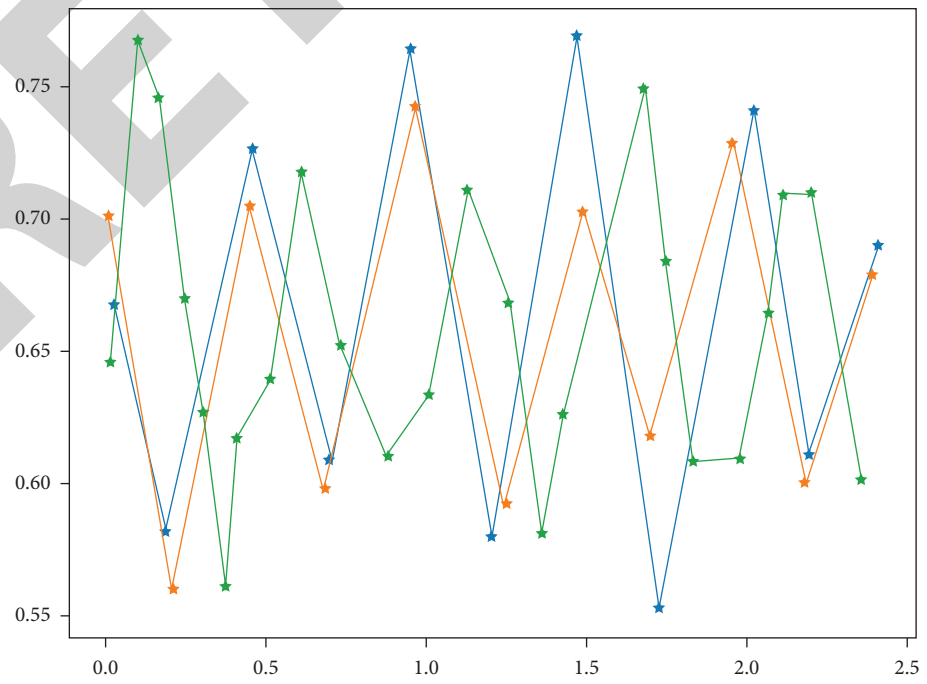

Figure 17: Inductor and output voltage current waveforms.

RETRACTED

cancels each other in the phase shift control, which helps to reduce the ripple size of the total output current.

5. Conclusion

In this study, we propose the idea of combining the IoT mobile robot with the ring light intelligent control system, mainly to solve the positioning problem and the hair problem of the intelligent control circuit. We designed an autonomous positioning system for mobile robots in the IoT environment based on UWB wireless sensors and inertial sensors carried by mobile robots. We have realized high precision and high reliability positioning of mobile robot. The simulation results show that the system maintains equilibrium, the system output is stable, and the ripple is low when the parameters are inconsistent.

Data Availability

The experimental data used to support the findings of this study are available from the corresponding author upon request.

Conflicts of Interest

The authors declare that they have no conflicts of interest regarding this work.

Acknowledgments

This study was supported by Cangzhou Science and Technology Plan Project, project no. 213109003, project Name: Research and Design of Bohai Sea Environmental Monitoring System Based on Internet of Things Technology.

References

[1] C. M. D. Junior, S. P. Da Silva, R. V. Da Nobrega et al., "A new approach for mobile robot localization based on an online IoT system," *Future Generation Computer Systems*, vol. 100, pp. 859–881, 2019.

[2] M. Vanitha, M. Selvalakshmi, and R. Selvarasu, "Monitoring and controlling of mobile robot via internet through raspberry Pi board," in *Proceedings of the 2016 Second International Conference on Science Technology Engineering and Management (ICONSTEM)*, pp. 462–466, Chennai, India, March 2016.

[3] P. S. N. Suryavamsi and A. Arockia Selvakumar, "IoT controlled mobile robot for home security and surveillance," in *Proceedings of the International Conference on Intelligent Data Communication Technologies and Internet of Things*, pp. 431–438, Coimbatore, India, August, 2018.

[4] B. Li, A. Zhou, C. Yang, and S. Zheng, "The design and realization of fruit harvesting robot based on IOT," in *Proceedings of the 2016 International Conference on Computer Engineering*, pp. 158–161, Cairo, Egypt, September, 2016.

[5] Y. C. Jeon, H. Choi, K. C. Yoon, and G. G. Kim, "IoT based vision and remote control a compact mobile robot system," *Journal of Korea Multimedia Society*, vol. 24, no. 2, pp. 267–273, 2021.

[6] S. Wang, H. Zhao, and X. Hao, "Design of an intelligent housekeeping robot based on IOT," in *Proceedings of the 2015 International Conference on Intelligent Informatics and Biomedical Sciences (ICIIBMS)*, pp. 197–200, Okinawa, Japan, November, 2015.

[7] J. A. Kim and J. Jeong, "Smart warehouse management system utilizing IoT-based autonomous mobile robot for SME manufacturing factory," *The Journal of the Institute of Internet, Broadcasting and Communication*, vol. 18, no. 5, pp. 237–244, 2018.

[8] A. D. Salman and M. A. Abdelaziz, "Mobile robot monitoring system based on IoT," *Journal of Xi'an University of Architecture and Technology*, vol. 12, no. 3, pp. 5438–5447, 2020.

[9] M. Kumari, A. Kumar, and R. Singhal, "Design and analysis of IoT-based intelligent robot for real-time monitoring and control," in *Proceedings of the 2020 International Conference on Power Electronics & IoT Applications in Renewable Energy and its Control (PARC)*, pp. 549–552, Uttar Pradesh, India, February, 2020.

[10] Y. Cao, Z. Xu, F. Li, W. Zhong, K. Huo, and K. Ramani, "V. ra an in-situ visual authoring system for robot-iot task planning with augmented reality," in *Proceedings of the 2019 on Designing Interactive Systems Conference*, pp. 1059–1070, California, CA, USA, June, 2019.

[11] M. Kanwar and L. Agilandeeswari, "IOT based fire Figurehting robot," in *Proceedings of the 2018 7th International Conference on Reliability, Infocom Technologies and Optimization (Trends and Future Directions) (ICRITO)*, pp. 718–723, Noida, India, August, 2018.

[12] C. Qiu, F. Wu, Q. Shi, C. Lee, and M. R. Yuce, "Sensors and control interface methods based on triboelectric nanogenerator in IoT applications," *IEEE Access*, vol. 7, pp. 92745–92757, 2019.

[13] X. Xie, X. Pan, W. Zhang, and J. An, "A context hierarchical integrated network for medical image segmentation," *Computers & Electrical Engineering*, vol. 101, Article ID 108029, 2022.

[14] T. M. N. U. Akhund, M. A. B. Siddik, M. R. Hossain, M. M. Rahman, N. T. Newaz, and M. Saifuzzaman, "IoT Waiter Bot: a low cost IoT based multi functioned robot for restaurants," in *Proceedings of the 2020 8th International Conference on Reliability, Infocom Technologies and Optimization (Trends and Future Directions) (ICRITO)*, pp. 1174–1178, Noida, India, June, 2020.

[15] X. Q. Li, X. Ding, Y. Zhang, Z. P. Sun, and H. W. Zhao, "IoT family robot based on Raspberry Pi," in *Proceedings of the 2016 International Conference on Information System and Artificial Intelligence (ISAI)*, pp. 622–625, Hong Kong, China, June, 2016.

[16] R. Kazala, A. Taneva, M. Petrov, and S. Penkov, "Wireless network for mobile robot applications," *IFAC-PapersOnLine*, vol. 48, no. 24, pp. 231–236, 2015.

[17] X. Xie, X. Pan, F. Shao, W. Zhang, and J. An, "Mci-net: multiscale context integrated network for liver ct image segmentation," *Computers & Electrical Engineering*, vol. 101, Article ID 108085, 2022.

[18] X. Wang and P. Liu, "A new full chaos coupled mapping lattice and its application in privacy image encryption," *IEEE Transactions on Circuits and Systems I: Regular Papers*, vol. 69, no. 3, pp. 1291–1301, 2022.

[19] S. Bhutada, L. S. Tejasri, and R. Tejaswini, "IoT based mobile robot for smoke detection," *International Research Journal of Engineering and Technology (IRJET)*, vol. 5, no. 4, pp. 1381–1383, 2018.

[20] X. Xie, W. Zhang, H. Wang et al., "Dynamic adaptive residual network for liver CT image segmentation," *Computers & Electrical Engineering*, vol. 91, Article ID 107024, 2021.

RETRACTED

Hindawi
Journal of Robotics
Volume 2023, Article ID 9824265, 1 page
https://doi.org/10.1155/2023/9824265

Retraction

Retracted: Machinery Changes and Challenges of Architecture and Landscape Design in the Virtual Reality Perspective

Journal of Robotics

Received 19 December 2023; Accepted 19 December 2023; Published 20 December 2023

Copyright © 2023 Journal of Robotics. This is an open access article distributed under the Creative Commons Attribution License, which permits unrestricted use, distribution, and reproduction in any medium, provided the original work is properly cited.

This article has been retracted by Hindawi following an investigation undertaken by the publisher [1]. This investigation has uncovered evidence of one or more of the following indicators of systematic manipulation of the publication process:

(1) Discrepancies in scope
(2) Discrepancies in the description of the research reported
(3) Discrepancies between the availability of data and the research described
(4) Inappropriate citations
(5) Incoherent, meaningless and/or irrelevant content included in the article
(6) Manipulated or compromised peer review

The presence of these indicators undermines our confidence in the integrity of the article's content and we cannot, therefore, vouch for its reliability. Please note that this notice is intended solely to alert readers that the content of this article is unreliable. We have not investigated whether authors were aware of or involved in the systematic manipulation of the publication process.

Wiley and Hindawi regrets that the usual quality checks did not identify these issues before publication and have since put additional measures in place to safeguard research integrity.

We wish to credit our own Research Integrity and Research Publishing teams and anonymous and named external researchers and research integrity experts for contributing to this investigation.

The corresponding author, as the representative of all authors, has been given the opportunity to register their agreement or disagreement to this retraction. We have kept a record of any response received.

References

[1] H. Jin and N. Zhang, "Machinery Changes and Challenges of Architecture and Landscape Design in the Virtual Reality Perspective," *Journal of Robotics*, vol. 2023, Article ID 1430551, 9 pages, 2023.

Hindawi
Journal of Robotics
Volume 2023, Article ID 1430551, 9 pages
https://doi.org/10.1155/2023/1430551

RETRACTED

Research Article

Machinery Changes and Challenges of Architecture and Landscape Design in the Virtual Reality Perspective

He Jin and Nan Zhang

Institute of Architecture and Civil Engineering, Kunming University, Kunming, Yunnan 650214, China

Correspondence should be addressed to Nan Zhang; zn@kmu.edu.cn

Received 16 August 2022; Revised 27 October 2022; Accepted 27 March 2023; Published 17 April 2023

Academic Editor: Shahid Hussain

Copyright © 2023 He Jin and Nan Zhang. This is an open access article distributed under the Creative Commons Attribution License, which permits unrestricted use, distribution, and reproduction in any medium, provided the original work is properly cited.

With the in-depth study of architectural planning in China, more and more designers and developers are aware of the superiority of the use of technological robots to improve the speed and quality of construction, weakening past experience and based on real-world research through modern technology. However, the application of this method in the predesign work is not mature. To be specific, designers may lack expertise due to the overly detailed division of labor. In addition, the developer's blind pursuit of profitability leads to inaccurate market positioning and forecasting. At the same time, the lack of effective communication between designers and developers, architects and owners makes the predesign work ineffective and does not provide reasonable and accurate guidance for the building design. Therefore, the predesign work requires the designer to analyze and select the site reasonably. In addition, it is necessary to conduct in-depth research on the target customers. At the same time, it is necessary to accurately position and predict the dynamic market, and then to have a thorough understanding of the norms and regulations. As a result, the predesign work enables the design to be analyzed in the context of the actual situation. Then, according to the data and information from various aspects, effective planning and argumentation are carried out, and corresponding decisions are made to provide guidance for the design. Overall, predesign is a process of rational planning of the design process. In fact, in the process of landscape design innovation, it is necessary to fully consider the requirements of the intelligent era. Therefore, multimedia and advanced robotics can continuously enhance the interaction and experience of urban landscape to make it integrate into the intelligent system of the future city. In other words, multimedia technology can enhance the new image of the city in an intelligent, digital, and humanized interactive experience. Especially in the landscape design process, the advent of computers has enabled landscape designers to use relevant design software to design their own works, thus giving them unlimited design possibilities. Virtual reality technology, as a form of computer technology, provides designers with a new creative experience in the design phase of a landscape project. To be specific, this technology allows designers to freely grasp the design space and scientifically compare the differences between design options to make the design more reasonable and complete. Therefore, this paper analyzes the differences in the general environment and concepts of 3D software virtual reality technology, starting from the characteristics of the application of 3D technology as an entry point. At the same time, this study uses the similarities and differences in technology to discover the vital role of using virtual reality technology to reconstruct the space and the impact of robots on modern architecture.

1. Introduction

Landscape is a very broad concept that first began in geography. To be specific, landscape is a general term for a surface phenomenon or type of unit, such as urban landscape, grassland landscape, and forest landscape, and has the meaning of landscape, scenery, or view [1]. As a result, a discipline such as landscape design is closely related to its concept. In a nutshell, the profession is used to address the environmental modification actions taken by humans to adapt to various natural living conditions [2]. The development of landscape design has also gone through a long historical process [3]. During this time, the clarity and scientific nature of the concept has evolved with the times and has been

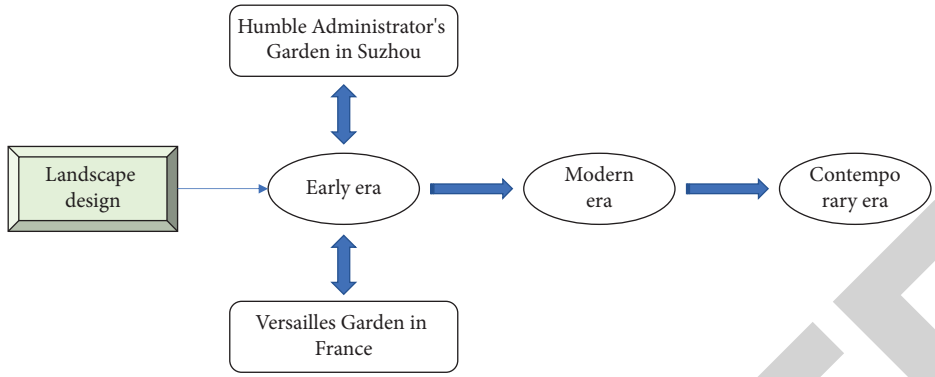

Figure 1: Development of landscape design.

constantly supplemented and improved. As shown in Figure 1, the history of landscape design is divided into early, modern, and contemporary. The most representative of early Chinese and Western landscape design are the Versailles Garden in France as well as the Humble Administrator's Garden in Suzhou during the Ming Dynasty in China. In other words, both the Western emphasis on the orderliness of layout and the pursuit of rigorous geometric composition style, as well as the landscape mood of the Chinese classical gardens, reflect the values of early landscape designers [4]. Modern landscape design and its development, in addition to the change of form, also include a huge change in design thinking and traditional concepts [5]. Furthermore, modern landscape design and its development are fundamentally due to the advent of industrialization, which led to a double impact on nature and human mind and body [6]. As such, it is a spatial planning that originates from nature and is designed to meet the needs of people. Modern landscape architects consider landscape design to be a comprehensive discipline. As a result, the discipline is primarily oriented toward the construction of outdoor environments [7]. It combines art, science, culture, and engineering and is a highly applied professional discipline. In fact, the main research direction of the discipline is to design the environment for human outdoor living.

With the development of human society, landscape has long ceased to be the task of landscape architects in today's social life, especially for today's diversified market economy [8]. In this context, the diversified economy requires the involvement of a number of other stakeholders. In fact, this includes relevant government departments, developers, investors, as well as the general audience [9]. As a result, today's landscape design needs to meet conditions that are no longer as homogeneous as before, considering the diversity of its audience. In the new world economic and environmental conditions, new design tools are being applied to landscape planning [10]. To be specific, it is possible to navigate through the various contradictions and interests, making the design form visible. Then, the design process becomes reversible and the design approach becomes multifunctional: digital technology [11]. In the age of technology, the use of more technological robotics for landscape analysis and multidimensional landscape design is the trend in landscape design.

Architectural design preplanning is a clear design basis based on scientific and practical research, analysis, discussion, and experimentation on the basis of the master plan [12]. As a result, architectural design preplanning is not only the first stage of a building project design but also an important guide and component of the project quality at the later stage of the project, as well as the series of impacts and benefits that will be formed after the project is completed [13]. As illustrated in Figure 2, with the development of the times, architectural design has evolved from the traditional study of proportional division, morphological composition, and spatial distribution to a systematic study of the impact of architecture on human life, social development, ecological environment, economic development, as well as other elements [14]. This requires the designer to no longer create a single artistic creation but to consider all aspects of the design process comprehensively. Therefore, preplanning of architectural design becomes particularly important [15]. In fact, it is quite important for the designer to strengthen the coordination within the design team and to conduct a comprehensive study of the predesign planning together with the investment and construction departments [16]. Furthermore, this will allow for balanced economic, social, and ecological benefits of the project and avoid inconsistencies in the design and construction process as well as after the project is completed. In the preconstruction phase, the results of different studies of architectural design planning determine the outcome of different building projects [17]. As a result, it has a distinctive individual character on the way the building is used, the environmental impact, the economic development, and even the cultural formation of the building area. In short, designers should give full play to their personal subjectivity in the preliminary stage of architectural design and conduct in-depth research on the actual state of the architectural project [18]. In addition, after a thorough and multifaceted analysis of the research results, the results are determined on the basis of building science using modern computer science simulation and modeling. Also, the results are then cross-referenced with other disciplines to arrive at design conclusions. This ensures that the design is logically rigorous, theoretically complete, and objectively sound, and that the project will proceed smoothly [19].

RETRACTED

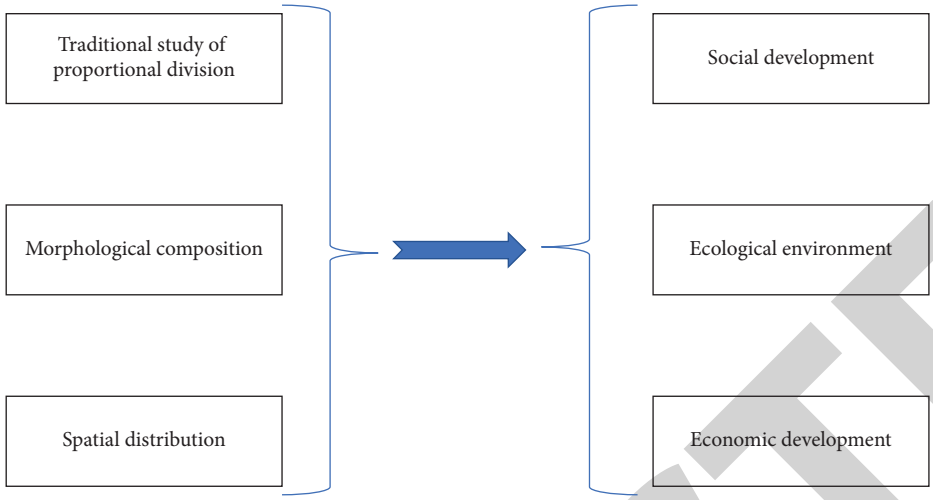

Figure 2: Change of architectural design.

In recent years, with the advent of digital intelligence, a new technological revolution has provided people with tools and methods to understand and transform the world. In the context of the invention and development of Internet of Things technology, advanced multimedia technology has gradually replaced traditional media, which is also an inevitable trend of social development. The rise of multimedia technology has provided unlimited creative power and space for architecture and landscape design. As a matter of fact, art is the source of ideas for landscape design, and designers can obtain diversified design intentions and design inspirations from various art forms. Among them, multimedia technology can present a different art form from traditional media art. Therefore, it can be seen that multimedia technology plays a huge role in promoting innovation for landscape innovative design.

Virtual reality technology is a system that uses robotic systems to simulate and create digital information, virtual world. Specifically, it incorporates robots graphics, computer simulation, artificial intelligence, human-computer interface, multimedia, network technology, and other technologies [20]. Through various high-performance computer hardware and software and advanced virtual reality input and output devices, this technology can bring a virtualized information environment to users. To date, virtual reality technology has been widely used in the military, education, architecture, civil engineering, and entertainment industries. In the architectural design process, graphics and images are also gaining importance and can play a very important role in communication between clients, designers, various engineering technicians, and users [21]. The introduction of virtual reality technology can successfully solve the problems of abstraction and professionalism of traditional two-dimensional drawings, as well as the unfamiliarity of clients with drawings and the increasing difficulties of communication between designers and clients [22]. In short, the robots' architectural design based on virtual reality technology is a process of planning the space again in the virtual space and modifying the information in the virtualized digital information. In addition, it can be improved in layers directly during the design process, thus making the design more and more perfect [23]. Virtual reality technology is now increasingly used in architectural design. For example, the multispatial presentation of building information models, the remote design, demonstration as well as circulation of building plans via the Internet, the simulation of disaster prevention techniques for buildings, and the simulation of the feasibility of restoring historical buildings. As a result, many people realize that the combination of virtual reality technology and architectural design will be an advanced research in the field of architectural design in the future [24]. The ability to invest in more robots and large machines is a prerequisite for an architectural design. Advanced machinery and equipment can be a better representation of the design and can provide more ideas for the design.

The changes that digital technology has brought to design are revolutionary. It is no less significant than the industrial revolution, the invention of movable type and the telephone. In some respects, digital technology has gone far beyond the changes listed above [25]. In fact, the current changes brought about by digitalization are only the beginning of the information revolution [26]. In the future, this technology will continue to have a radical effect on social, political, and cultural communication worldwide. As such, it has enormous potential to be exploited [27]. The pioneering of this technology has given designers previously unimagined priorities. To be specific, advanced scientific technologies have allowed them to eliminate the need for complicated processes, redundant tools, and repetitive creative techniques [28]. This has greatly enhanced the enthusiasm of designers. For instance, the digital model as well as the digital building is shown in Figure 3. It would be difficult to complete such a building without large mechanical equipment.

Virtual reality technology is a combination of multimedia, computers, artificial intelligence, and so on a variety of recent high-tech disciplines. Virtual reality technology

RETRACTED

Figure 3: Digital model and digital building.

constructs a form of image interaction for users that can reflect changes in physical objects and virtual three-dimensional space in real time [29]. Therefore, this technology has a variety of sensory experience and can have a very realistic feeling, so that the experience can directly and quickly understand and experience the role of virtual objects changing in the environment, as if in a real world, so that people can have a sense of immersion in the experience [30]. This paper presents a study on the application of virtual reality technology in the predesign stage of architecture, based on the ideas of design planning, predesign stage of architecture, predesign stage of architecture and operation, and the possibility of virtual reality technology to solve the abovementioned problems. In the predesign phase, any design activity requires the cooperation of designers and people from other fields. The real-time and interactive nature of virtual reality technology in the predesign stage can effectively integrate designers with marketing, management, as well as the operations while the design is being transformed from a concept to a finished product.

2. Virtual Reality Technology

2.1. Composition of Virtual Reality Technology. Virtual reality is a comprehensive technology that integrates computer graphics, sensor technology, interaction technology, and network technology. The most basic requirement for virtual reality technology is to be able to realize real-time interaction with users. As a result, a basic virtual reality system mainly consists of a computer, input and output devices, application software, and database, as shown in Figure 4.

The computer is the host of the virtual reality world and is the core of the whole virtual world. As a result, the computer is mainly responsible for the generation of the virtual reality world and the processing of information about the user's interaction with the virtual world. Depending on the complexity of the virtual world, the performance requirements of the computer vary. When generating complex and large-scale scenes, the amount of computation required is enormous, which requires a high level of computing performance.

Furthermore, input and output devices are the medium of interaction between the computer and the user. The input device is the interface through which the user sends commands to the virtual world. As a result, its function is to accept commands from the user and convert the user's actions into information data for input into the computer. Depending on the requirements and purposes of use, input devices include not only the mouse and keyboard but also spatial tracking locators, data gloves, and data suits (Figure 5).

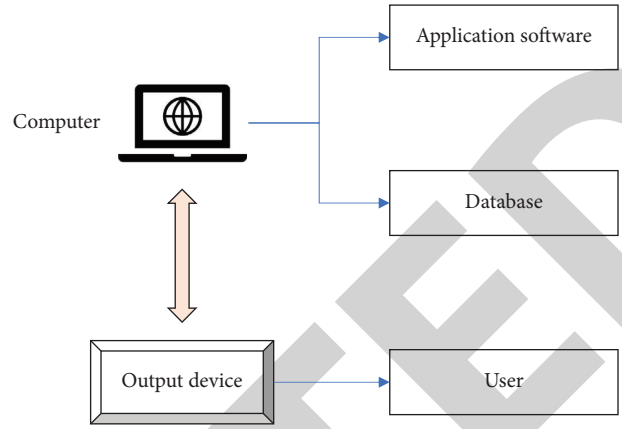

Figure 4: Composition of virtual reality technology.

A database is a repository of all relevant information in the virtual world, such as geometric and physical models of the virtual reality environment and captured user actions. In a virtual reality world scenario, a large amount of information needs to be stored for use, and this requires a database to manage this information. The software application in the virtual reality system is the key to the realization of the virtual environment. It is specifically responsible for the creation of models in virtual scenes, for ensuring the fluidity of direct interaction between people and the virtual environment, and for the synthesis of sound and spatial orientation.

2.2. System Architecture of the Virtual Environment. A virtual reality environment is an environment that exists inside a computer and requires special equipment to experience it, generated by a computer through the construction of geometric and physical models. In order to be called a virtual reality environment, it must have the ability to interact with the user in real time and the user must have absolute autonomy. The structural composition of the virtual environment is presented in Figure 6.

Virtual reality is a discipline where technology and art merge. In order to realize the value of virtual reality technology, it must be supported by hardware technology and equipment for immersion and interaction. Without the support of related equipment, the value of virtual reality technology cannot be realized. As a collection of multiple technologies, virtual reality requires the use of multiple devices, including computers, stereo displays, user sensory trackers, human motion trackers, feedback devices, and voice input/output devices. Interactivity is the most fundamental and important function of a virtual reality system. In order to achieve human-computer interaction, special human-computer interaction interfaces and devices must be used. It enables both the user to send information to the computer and the computer to send real-time information back to the user. The internal magnetic field transmitter of a low-frequency magnetic field sensing device generates a low-frequency magnetic field. The transmitter is composed of three orthogonal antennas and there is also an orthogonal

RETRACTED

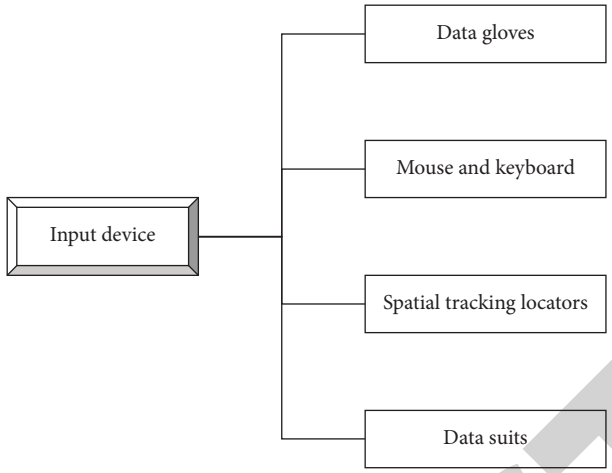

Figure 5: Various input devices.

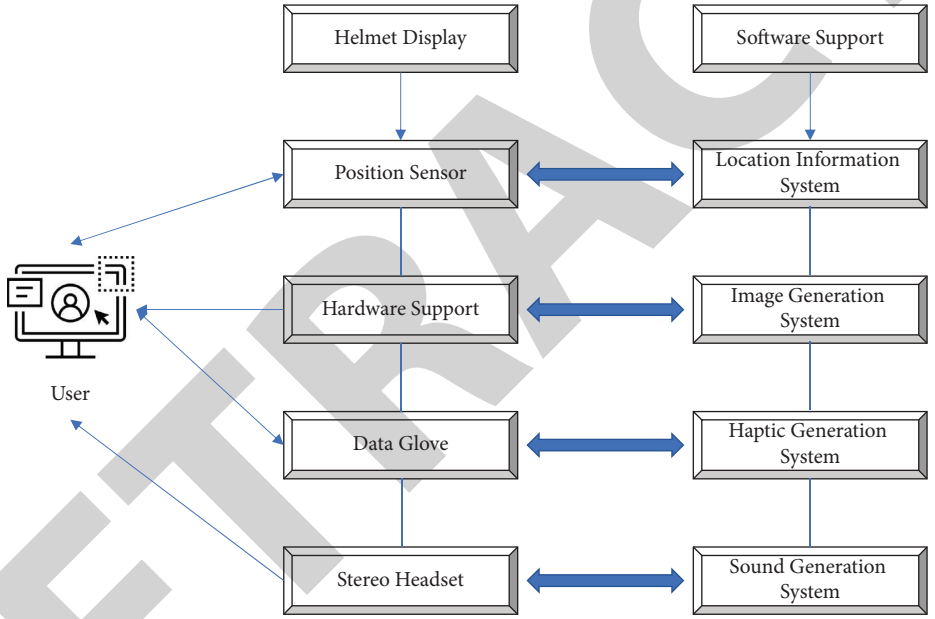

Figure 6: Structural composition of the virtual environment.

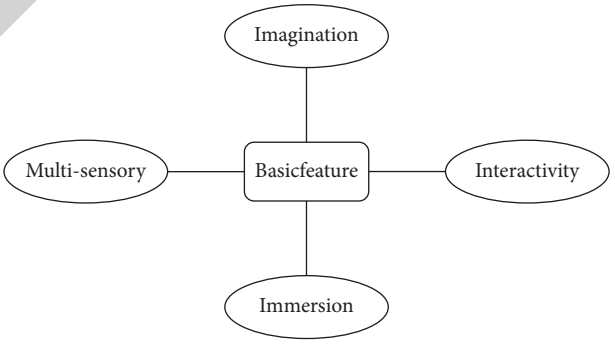

Figure 7: Basic features of virtual reality.

antenna in the receiver. The receiver is placed on top of the moving object under test, and based on the magnetic field obtained by the receiver, the location and relative direction of the moving object can be determined and the relevant data information can be transmitted to the computer device by means of a communication device. Thus, the computer

RETRACTED

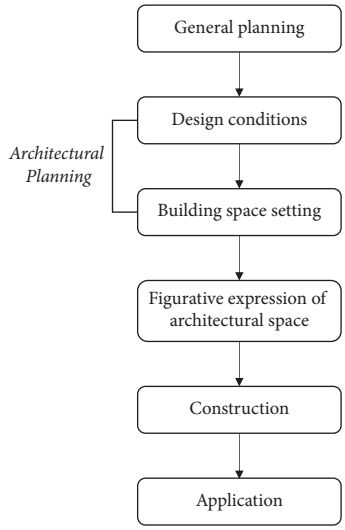

Figure 8: Diagram of the building project process.

equipment can monitor the area and the target direction of the moving object in this way.

2.3. Basic Feature of Virtual Reality Technology. Figure 7 shows the basic features of virtual reality. Interactivity is the main characteristic of virtual reality technology. Instead of passively watching and listening, users can control and even create things in the virtual world. At the same time, users can interact with other users and change the content of the virtual world through their own thinking and actions. In addition, with the help of computer hardware and software, such as head-mounted stereo displays, digital gloves, or digital suits, the user is fully immersed in the virtual simulation environment constructed by the computer. This can give the user a sense of immersive reality. In fact, the user's senses and perceptions are similar to those in the real world. As a result, it is quite difficult to distinguish between the feelings of a person immersed in a virtual environment as well as those in the real world.

People immersed in the virtual world can rely on their own perception and cognitive ability to obtain information in a comprehensive manner. In addition, people can use their own initiative to broaden their cognitive scope. Therefore, they can not only reproduce what already exists in the virtual world, but also use their own imagination to construct things that do not exist in the real world and seek new concepts and ideas. In addition, multisensory means that in addition to the visual and auditory experiences that virtual reality technology can provide, it can also provide tactile, olfactory, and force experiences, and even more so, it can provide taste experiences. It is envisioned that virtual reality technology could allow humans to experience all the effects of the experience. However, due to the lack of science and technology development, at this stage, virtual reality technology can only provide the public with a few basic sensory experiences, such as visual, auditory, and tactile senses, and its perceptual scope and accuracy are not comparable to the real world.

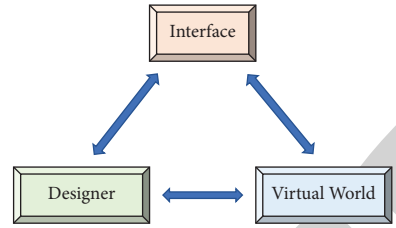

Figure 9: Digital landscape design generation process.

3. Architecture and Landscape Design

3.1. Architectural Planning. From the perspective of building science, a scientific and systematic building process should include building planning, through building design, mechanical equipment, construction, delivery of the building, and postuse feedback. Figure 8 shows a diagram of the building project process. Among these processes, the last three steps are usually familiar. As for the first two, in the domestic construction market, there is a significant portion of the public who cannot distinguish between the two and often confuse architectural planning with architectural design. The reason for this is that at present in China's construction industry, the preconstruction work is not systematic and complete, resulting in unclear and imperfect work in the interval from the project to the design of the construction project. Usually, the design of a building is guided by the design task book. If the design task book is not strictly controlled by the preliminary architectural planning, then the building designed by such task book will not achieve the expected design effect and will not bring the social and economic benefits of the building itself. At the same time, the later use of the building will not meet the needs of the target customers. From the point of view of effectiveness, architectural planning is classified as a discipline of architectural value management. A great plan not only guides the design effectively and accurately, but also has a great impact on the overall effect of the building.

3.2. Digital Landscape. Digital design and machine-based construction have brought new forms and structures never before seen in the history of human civilisation. At the same time, it has provided mankind with new design theories and technical tools. The use of digital technology has provided landscape architects with a richer creative space. In addition, digital technology offers more diverse possibilities for the implementation of landscape solutions. In other words, the development of this technology has greatly increased the efficiency of the implementation of landscape planning. The introduction of nanomaterial robotics in landscape planning allows for a more efficient, faster, comprehensive, and in-depth collection of information and data about the site than traditional methods. In the digital age, all robotic devices using nanomaterials will produce a data trail. This allows for purposeful and informed site planning. In fact, nanomaterial robots will be a powerful technical support for contemporary landscape design.

RETRACTED

Today, the computer is integrated into the approach to landscape installation design as both, a tool and a medium. As the medium of landscape design has evolved from handwriting to drawing paper to computers, the advancement of robots of nanomaterials has also brought about a revolution in design methods, moving through stages of development from low to high. This logic is usually simulated by digital tools. The third stage is the closest to the real state of existence of the landscape. The formal self-logic is usually expressed as a self-organising system. Self-organising systems are a complex class of systems that are typically used in open environments and can change in response to changing external and internal environments. The system dynamically adapts itself to better meet design purposes by interactively transforming data about its own components. With the development of digital technology, more and more computer systems are becoming self-organising. At the same time, related research systems are becoming very active and are receiving a lot of attention from academia and industry. The digital landscape design generation process is illustrated in Figure 9.

Virtual reality is a digital technology that generates a virtual simulation of a three-dimensional world through computer simulation, thus enabling the user to feel an immersive experience. This technology is widely used in all areas of design, providing an experimental environment that provides a realistic representation and emphasis of the real world. Compared to traditional design, experimental results are more realistic and experiential. In recent years, nanomaterials for robots virtual reality technology has been increasingly used in the field of landscape design. The impact of this technology on the development of landscape design is undoubtedly huge, as it provides an immersive experience and display of design solutions, which can effectively eliminate research errors and data mistakes in the design in a timely manner and improve the accuracy of academic research.

3.3. Virtual Scene Design. Design concept is usually the core point of concern for designers in the design process. Conceptualization is a language of thought, and even the most precise computer presentation cannot be conceptually clever, or the concept cannot be generated. However, the use of virtual reality technology can indirectly help designers to generate design concepts. The image display capability of virtual reality technology is by far the most realistic visual representation in terms of image presentation capabilities. Its most important feature is its interactivity. The designer can intuitively create a rough model of the building block directly in the virtual project site by controlling the joystick and analyzing the building massing and other information.

In the early stages of design, concept generation is always vague and uncertain. After all, many factors can influence the designer's concept generation. Once the designer enters the virtual site based on the project site state of affairs data, he or she can roam around the real site space in full view and analyze the site information as it emerges. At this time, the designer's mind is active and stimulated by a large amount of information to generate relevant branches of the design concept. Through the operation of the virtual site, these conceptual branches are transformed into computerized information and stored for later integration. The real-time, interactive nature of virtual reality technology makes it possible for designers to accurately grasp design ideas and store fleeting design concepts in a timely manner, as well as provide screening for subsequent architectural design concept generation to optimize design solutions.

3.4. Application of Advanced Machinery. Under the trend of mechanisation, landscape design innovation must be a combination of technology, networking, digital technology, and function and form. As such, mechanised technologies can transform landscape design from a traditional single visual appreciation function to a human-computer interaction experience. In other words, nanomaterials for robotics can contribute to the functional diversity, intelligence, and humanization of urban landscapes. At the same time, robotics can also enhance the artistic and scientific aspects of landscape design, and to a certain extent, the value of digital media art.

In addition, the innovative integration of nanomaterial robotics and urban landscape design plays a role in driving urban economic development and vigorously spreading urban culture, while at the same time playing a role in the protection of the urban ecological environment. Traditional urban landscape design generally uses stone, wood, metal, or composite materials, which can lead to the consumption of environmental resources. The intervention of nanomaterial robotics has diversified the material options for urban landscape design. Specifically, digital technologies such as digital lighting, laser projection, and energy-saving induction are applied to urban landscape design. These sustainable energy sources reduce the burden of environmental resource consumption to a certain extent and play a role in the protection of the urban ecology.

4. Conclusion

In the modern design industry, the use of virtual reality technology is becoming more and more widespread. However, the application of virtual architectural landscape roaming with interactivity is a new field with a very broad development prospect. Successful research on this topic will enable viewers to view projects remotely through a web-based platform, improving the chances of successful project negotiations and increasing the efficiency of use, while also reducing communication costs for designers and related personnel. In addition, the application of interactive virtual landscape technology is also very extensive, such as the tourism industry, architectural planning, and landscape teaching practice, have a broad development space. In this paper, the impact of virtual reality technology on landscape design is studied in detail, and the production of interactive virtual landscape scenery systems is studied in depth by combining the two. In addition, this study summarises the methods and approaches to improve the quality and

RETRACTED

efficiency of landscape design using existing virtual reality technology machines and advanced mechanisation technologies.

Due to the continuous advancement of modern technology, virtual reality and advanced mechanisation technologies are bound to make huge leaps in the coming years. The proliferation of virtual reality software in recent years is a proof of this. Many researchers have now introduced interactive virtual roaming technology and robotics with nanomaterials into the design field, which will gradually become the new technology of the future in everyday work.

Data Availability

The labeled data set used to support the findings of this study is available from the corresponding author upon request.

Conflicts of Interest

The authors declare that there are no conflicts of interest.

Acknowledgments

This work was supported by the Institute of Architecture and Civil Engineering, Kunming University.

References

[1] M. Liu and S. Nijhuis, "Mapping landscape spaces: methods for understanding spatial-visual characteristics in landscape design," *Environmental Impact Assessment Review*, vol. 82, Article ID 106376, 2020.

[2] Z. Li, Y. Cheng, and Y. Yuan, "Research on the application of virtual reality technology in landscape design teaching," *Educational Sciences: Theory and Practice*, vol. 18, no. 5, 2018.

[3] E. G. O'Neill and C. T. Maravelias, "Towards integrated landscape design and biofuel supply chain optimization," *Current Opinion in Chemical Engineering*, vol. 31, Article ID 100666, 2021.

[4] W. Yang, Y. Lin, and C. Q. Li, "Effects of landscape design on urban microclimate and thermal comfort in tropical climate," *Advances in Meteorology*, vol. 2018, Article ID 2809649, 13 pages, 2018.

[5] P. R. Urech, M. A. Dissegna, C. Girot, and A. Grêt-Regamey, "Point cloud modeling as a bridge between landscape design and planning," *Landscape and Urban Planning*, vol. 203, Article ID 103903, 2020.

[6] K. Cao, J. Xiao, and Y. Wu, "Simulation and formation mechanisms of urban landscape design based on discrete dynamic models driven by big data," *Discrete Dynamics in Nature and Society*, vol. 2022, Article ID 1012900, 9 pages, 2022.

[7] E. M. Alpak, D. G. Özkan, and T. Düzenli, "Systems approach in landscape design: a studio work," *International Journal of Technology and Design Education*, vol. 28, no. 2, pp. 593–611, 2018.

[8] S. Lavorel, K. Grigulis, D. R. Richards, T. R. Etherington, R. M. Law, and A. Herzig, "Templates for multifunctional landscape design," *Landscape Ecology*, vol. 37, no. 3, pp. 913–934, 2022.

[9] P. Shan and W. Sun, "Research on 3D urban landscape design and evaluation based on geographic information system," *Environmental Earth Sciences*, vol. 80, no. 17, pp. 597.1–597.15, 2021.

[10] W. Jiang and Y. Zhang, "Application of 3D visualization in landscape design teaching," *International Journal of Emerging Technologies in Learning*, vol. 14, no. 6, p. 53, 2019.

[11] P. Shan and W. Sun, "Research on landscape design system based on 3D virtual reality and image processing technology," *Ecological Informatics*, vol. 63, Article ID 101287, 2021.

[12] Y. Liu, Y. Ban, and W. Yang, "Microstructural engineering and architectural design of metal–organic framework membranes," *Advanced Materials*, vol. 29, no. 31, Article ID 1606949, 2017.

[13] B. Cheng, J. Huang, K. Lu et al., "BIM-enabled life cycle assessment of concrete formwork waste reduction through prefabrication," *Sustainable Energy Technologies and Assessments*, vol. 53, Article ID 102449, 2022.

[14] S. Li, L. Liu, and C. Peng, "A review of performance-oriented architectural design and optimization in the context of sustainability: dividends and challenges," *Sustainability*, vol. 12, no. 4, p. 1427, 2020.

[15] U. Emmanuel, E. D. Osondu, and K. C. Kalu, "Architectural design strategies for infection prevention and control (IPC) in health-care facilities: towards curbing the spread of Covid-19," *Journal of environmental health science and engineering*, vol. 18, no. 2, pp. 1699–1707, 2020.

[16] S. Ceylan, P. Şahin, S. Seçmen, M. E. Somer, and K. H. Süher, "An evaluation of online architectural design studios during COVID-19 outbreak," *Archnet-IJAR: International Journal of Architectural Research*, vol. 15, no. 1, pp. 203–218, 2020.

[17] A. M. Soliman, "Appropriate teaching and learning strategies for the architectural design process in pedagogic design studios," *Frontiers of architectural research*, vol. 6, no. 2, pp. 204–217, 2017.

[18] Y. Tulubas Gokuc and D. Arditi, "Adoption of BIM in architectural design firms," *Architectural Science Review*, vol. 60, no. 6, pp. 483–492, 2017.

[19] B. Cheng, J. Huang, Z. Guo, J. Li, and H. Chen, "Towards sustainable construction through better construction and demolition waste management practices: a SWOT analysis of Suzhou, China," *International Journal of Construction Management*, vol. 2022, Article ID 2081406, 11 pages, 2022.

[20] P. Wang, P. Wu, J. Wang, H. L. Chi, and X. Wang, "A critical review of the use of virtual reality in construction engineering education and training," *International Journal of Environmental Research and Public Health*, vol. 15, no. 6, p. 1204, 2018.

[21] B. Cheng, K. Lu, J. Li, H. Chen, X. Luo, and M. Shafique, "Comprehensive assessment of embodied environmental impacts of buildings using normalized environmental impact factors," *Journal of Cleaner Production*, vol. 334, Article ID 130083, 2022.

[22] J. F. Hartless, S. K. Ayer, J. S. London, and W. Wu, "Comparison of building design assessment behaviors of novices in augmented-and virtual-reality environments," *Journal of Architectural Engineering*, vol. 26, no. 2, 2020.

[23] Y. Zhang, H. Liu, S. C. Kang, and M. Al-Hussein, "Virtual reality applications for the built environment: research trends and opportunities," *Automation in Construction*, vol. 118, Article ID 103311, 2020.

[24] R. Zaker and E. Coloma, "Virtual reality-integrated workflow in BIM-enabled projects collaboration and design review: a case study," *Visualization in Engineering*, vol. 6, no. 1, pp. 4–15, 2018.

RETRACTED

Hindawi
Journal of Robotics
Volume 2024, Article ID 9896301, 1 page
https://doi.org/10.1155/2024/9896301

Retraction

Retracted: Application and Analysis of Remote Sensing Image Processing Technology in Robotic Power Inspection

Journal of Robotics

Received 23 January 2024; Accepted 23 January 2024; Published 24 January 2024

Copyright © 2024 Journal of Robotics. This is an open access article distributed under the Creative Commons Attribution License, which permits unrestricted use, distribution, and reproduction in any medium, provided the original work is properly cited.

This article has been retracted by Hindawi following an investigation undertaken by the publisher [1]. This investigation has uncovered evidence of one or more of the following indicators of systematic manipulation of the publication process:

(1) Discrepancies in scope
(2) Discrepancies in the description of the research reported
(3) Discrepancies between the availability of data and the research described
(4) Inappropriate citations
(5) Incoherent, meaningless and/or irrelevant content included in the article
(6) Manipulated or compromised peer review

The presence of these indicators undermines our confidence in the integrity of the article's content and we cannot, therefore, vouch for its reliability. Please note that this notice is intended solely to alert readers that the content of this article is unreliable. We have not investigated whether authors were aware of or involved in the systematic manipulation of the publication process.

Wiley and Hindawi regrets that the usual quality checks did not identify these issues before publication and have since put additional measures in place to safeguard research integrity.

We wish to credit our own Research Integrity and Research Publishing teams and anonymous and named external researchers and research integrity experts for contributing to this investigation.

The corresponding author, as the representative of all authors, has been given the opportunity to register their agreement or disagreement to this retraction. We have kept a record of any response received.

References

[1] J. Chen, H. Yang, and R. Xu, "Application and Analysis of Remote Sensing Image Processing Technology in Robotic Power Inspection," *Journal of Robotics*, vol. 2023, Article ID 9943372, 11 pages, 2023.

Hindawi
Journal of Robotics
Volume 2023, Article ID 9943372, 11 pages
https://doi.org/10.1155/2023/9943372

RETRACTED

Research Article

Application and Analysis of Remote Sensing Image Processing Technology in Robotic Power Inspection

Jie Chen,[1] Hemeng Yang ,[2,3] and Rui Xu[2,3]

[1]*State Grid Fujian Zhangzhou Electric Power Company, Zhangzhou, Fujian 363000, China*
[2]*China Academy of Space Technology, Beijing 100081, China*
[3]*Tianjin Zhongwei Aerospace Data System Technology Co Ltd, Tianjin 300301, China*

Correspondence should be addressed to Hemeng Yang; remotesensing@spacezw.com

Received 1 November 2022; Revised 9 December 2022; Accepted 27 March 2023; Published 15 April 2023

Academic Editor: Shahid Hussain

Copyright © 2023 Jie Chen et al. This is an open access article distributed under the Creative Commons Attribution License, which permits unrestricted use, distribution, and reproduction in any medium, provided the original work is properly cited.

Along with the increase of electricity consumption in society, it means that the quality of power inspection gives higher requirements. The traditional manual inspection method is difficult to ensure the stability of checking quality. Without the popularization of manned distribution stations and smart grid methods, replacing manual inspection with electric power inspection robots can improve the inspection quality and inspection efficiency to a certain extent. Along with theimage processing process which is widely used in the robot system, visual impact is not only an effective way for us to obtain information but also the key reflection of the robot system intelligence. Unmanned aircraft as an extremely important robot has long been widely used in all walks of life. Power inspection is the most common use of unmanned aircraft robot inspection. However, due to extreme criteria such as bad weather, relative motion, and shaking of imaging equipment, inspection images are obtained ambiguously. The quality of the inspection image is related to the timely understanding, analysis, and judgment of the power engineering quality inspection database. In the paper, the unmanned aircraft power inspection robot as a scientific research foothold, according to explore the key technology of anti-internet technology to clear the image ambiguity, proposed a complete disambiguation optimization calculation method. The image denoising optimization calculation method based on the directional characteristics of time-frequency analysis and edge maintenance is selected to carry out the finding of the image, which reasonably solves the image resolution bottleneck problem of GIS in unmanned aircraft robot line inspection. Meanwhile, with the emergence of nanorobots in the 21st century, the application and analysis of remote sensing image processing technology in the field of robotic power inspection in this paper will also bring new vitality and vigor to the research of nanopower inspection robots and solve the problem of unclear images existing in nanorobots.

1. Introduction

The production and manipulation of nanorobots has been realized with the integration of robotics and information technology applications and the development of nanomaterials and technologies in manufacturing, measurement, sensors, and control systems as well as the birth of new methods [1].

The power inspection robot is a medium for the comprehensive application of power electronics, electromagnetic compatibility, image recognition, security, multisensor data fusion, big data communication, and navigation technologies in the field of substation inspection, which can discover substation equipment defects and faults in real time and at the same time can call the database for state prediction, which reduces the task of power inspection work and guarantees safe and reliable operation of the power system. In the work of electric power system, robots already have significant advantages in visual processing, distance measurement, data recording and storage, output transmission, etc., and can replace manual work with their own technical characteristics, and using robots to replace manual power inspection work can overcome the defects of manual inspection.

Drones are widely used in the daily life of the general public, and civilian-type drones are highly preferred by

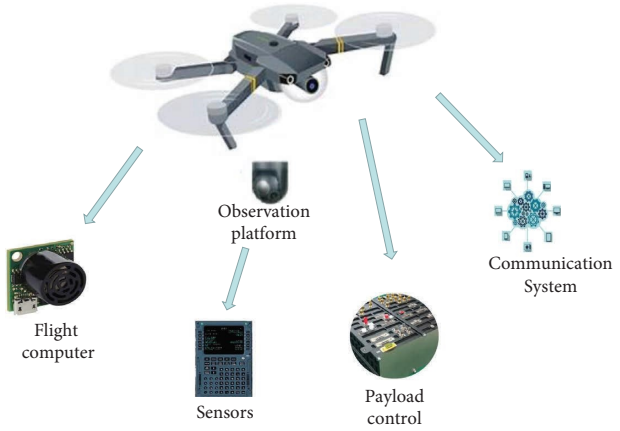

Figure 1: Structural composition of UAV remote sensing system.

young people today. UAVs are drones that can be controlled and flown by wireless remote control or by their own systems. Related industries include communication technology and information processing technology.

In the development of drones, the technicality of image processing is also important, because it can effectively distinguish the working state of the cable line. Robot system software as a contemporary high-end equipment manufacturing in the high-end equipment manufacturing is a product of the era of cross-fertilization of disciplines, with high-tech flow, high efficiency, and high socio-economic benefits of the characteristics. Drones are also the most critical kind of electric power inspection robots. Although Unmanned Aerial Vehicle (UAV) power equipment inspection technology significantly conserves both human and material resources, several pressing issues persist in its development and application process that warrant further investigation. Firstly, in the context of UAV power inspection image processing, the mobile application platform exhibits a considerable tilt angle, which is both large and irregular. This results in adjacent image navigation direction overlaps that are insufficient, with an average value of less than 20%. Moreover, the inconsistent gray values of adjacent images are detrimental to image alignment, compromising the accuracy of subsequent image processing. Secondly, the curved flight trajectory of UAVs leads to minimal horizontal overlap between adjacent images, which hinders the precise arrangement and acquisition of nodes. This issue significantly impacts the accuracy of aerial triangulation, necessitating the development of novel solutions to address these challenges in order to fully harness the potential of UAV power equipment inspection technology.. Once again, the number of images is large, the amount of data is large, and the image frames are small, and the work of piecing together the solution behind is intensive [2].

2. Theory and Methodology

2.1. Robotic Remote Sensing Technology—Take "UAV as an Example". In nanotechnology iterative upgrade in practice, intelligent robots face numerous tests, and the use of UAV aerial remote sensing for power patrol is the main filler of manned aerospace remote sensing [3]. The so-called UAV remote sensing technology refers to the combination of UAV GIS and remote sensing technology, using L-band cameras, scanners, radar detection, and other facilities, and its communication, precise measurement, and positioning technology will automatically and rapidly obtain low-altitude flight high-resolution remote sensing image data, which is an effective complement to space remote sensing and manned aerial remote sensing technology, in agriculture, forestry, land resources survey, and military. It is widely used in agriculture, forestry, land resource survey, military reconnaissance, and environmental protection.

UAV remote sensing technology can closely combine communication satellite and manned high-definition aerial photography to produce a vertical three-dimensional environmental protection monitoring service platform. The basic UAV remote sensing technology system software is mainly composed of carrier-based aircraft observation service platform, navigation electronic computer, remote sensing technology sensor, gravity gradient control board, and communication system, in which the remote sensor is shown in Figure 1, including digital cameras, scanners, radar, and other sensors.

The advantages of using UAVs for aerial remote sensing include their ability to provide fast response time, easy and reliable control, efficient data acquisition, and low cost of application [4].

2.2. Remote Sensing Image Processing Technology. Remote sensing image processing technology is the digital image processing technology that uses remote sensing technology to obtain information. The self-contained nanotechnology electronic circuit can load and process analog and digital signals and communicate with other intelligent robots external control systems. Remote sensing technology obtains information in a complicated way and must be mapping engineering and other technical ways. First of all, the earth is a sphere and must indicate the results of mapping in a plane. Because of the difference between 3D and 2D, it is possible to carry out calibration of remote sensing images directly on 2D space. The loss of the prototype of the mountains and the change of the meridian into an irregular curve map are completely unusable [5]. Thus, an efficient solution technique is important.

2.2.1. Components of Remote Sensing Image Processing Technology

(1) Indoor Spatial Resolution and Mapping Percentage. In the map production process, resolution and scale are the most important settings. On the other hand, the resolution manipulation is critically limited to the map size. Under the same specification, the larger the cut rate, the greater the precision; on the other hand, the scale of operation is also limited by the small size. Thus, when making a large HD map, the minimum specification is generally set to ensure the integrity of the scale. From the 2 specifics can learn that the limit immediately determines the level of resolution.

RETRACTED

(2) Popper Resolution. The resolution of Popper is critically endangered by wavelength and signal frequency, and wavelength and resolution are inversely proportional. As the wavelength increases, there is an inverse relationship with resolution, resulting in diminished image quality. This phenomenon may subsequently influence the accuracy of analytical outcomes derived from the data. Typically, a shorter wavelength is preferable, as it often correlates with enhanced performance in various applications. However, there are also wavelengths restricted by the living environment. Short and medium wavelengths are difficult to obtain remote sensing technology conclusions. In order to ensure the resolution, the transmission frequency of the frequency band must have the relative density resolution.

(3) Time and Phase Difference Resolution. Remote sensing technology image processing process is applied, using the special time-length information content obtained according to the GIS and the way and method to obtain accurate images. But the image is not fixed, especially in the environment. Therefore, there are differences in the temporal resolution of the remote sensing technology conclusions in different time frames. In order to ensure the effectiveness of remote sensing technology in unique applications, it is necessary to obtain periodic transformations through long-term surveys.

2.3. Introduction of Electric Power Inspection Robots

2.3.1. Types of Power Inspection Robots. Nanorobots as a kind of functional special tool different from the past have shown strong power in all walks of life [6]. Power inspection robots as a key kind of robots, according to the basic elements and integration into the place, can be divided into in-room inspection robots, outdoor inspection robots, tunnel construction inspection robots, and unmanned aircraft inspection robots. It is divided into crawler, wheel test, and crawler based on the posture type.

(1) Electric tunnel construction track inspection robot is used for electric tunnel construction environment, such as comprehensive electric underground corridor. Electric power tunnel construction necessitates the assembly of a stationary, fixed track system. A patrol robot traverses this track, inspecting areas designated for the installation of fixed, immobile tracks.

(2) Outdoor crawler patrol robot for outdoor environment, such as outdoor column power switch and substation transformer area, has no requirement for the road environment, according to the navigation and positioning system to carry out inspections in the set area.

(3) Unmanned aerial inspection robots, designed for high-voltage transmission lines and other elevated environments, employ navigation and positioning systems within designated channel areas to conduct safety inspections effectively and accurately.

2.3.2. UAV Robot Power Inspection. Along with the development of intelligent robotics, robots with very different roles play an increasingly important role in human daily life and industrialized production, becoming the right-hand man. The application range of robotic technology extends from the depths of the ocean floor to terrestrial environments and into the vast expanse of outer space, facilitating human exploration of an increasingly expansive realm. Among them, the application of robots in power inspection is also becoming more and more extensive.

Traditional power inspection relies on human resources, and in order to ensure the normal operation of the supply and distribution system, regular inspection and maintenance of the Koran voltage power system such as tower poles, power lines, and composite insulators in power lines are carried out according to the on-site survey of power workers. On the other hand, in remote mountainous areas, inspectors can use binoculars to view and check the distant areas or climb to the tower base in mountainous areas to carry out inspections which is restricted by the accumulated experience of people of all shapes and sizes and the extreme terrain of remote areas. This type of inspection is not efficient, and labor efficiency, low safety factor, and some visually blind areas cannot be inspected [7]. The occurrence of drone inspection technology can well prevent the dangers and shortcomings of manual inspection. Contemporary drone reconnaissance is a new type of reconnaissance technicality that combines drones closely with infrared thermal imager, remote sensing technology, surveillance camera machines, and equipment to carry out reconnaissance daily tasks in certain scenes which is widely used in all walks of life.

At this stage, the power inspection industry is the most common use of drones in the industry. In contrast to manual power inspection methods, drone technology offers superior capabilities, such as vertical descent at any given moment and a high degree of precision in navigation. These features enable the execution of inspections at any time and location along the designated route. Furthermore, the drone's perspective can be adjusted as needed to ensure a comprehensive examination of the power inspection route, adhering to established guidelines. The drone has intelligent control technology, which can remotely control and adjust the aircraft flight height, target, and course according to the inspection regulations, with high fault tolerance.

2.4. Image Denoising Algorithm. During the utilization of Unmanned Aerial Vehicle (UAV) robots for power inspection processes, including power station monitoring, line imagery, and image transmission, the presence of signal interference may introduce Gaussian noise into the captured images. This phenomenon not only disrupts the UAV's normal flight but also significantly impacts the imaging quality of the inspected circuitry.

2.4.1. Noise Source and Model. Noise is one of the key factors in controlling image resolution. There are three key sources of image noise. First, the Gaussian function noise caused by

RETRACTED

arbitrary thermal motion of electrons during the operation of the component is generally indicated by the zero-mean, Gaussian function white noise with stable compressive strength scattering. Second, the optical lens photoelectric conversion link by the influence of light Poisson noise is particularly weak, often indicated by a Poisson density distribution of random variables [8]. Third, the particle noise generated in the optical induction in the image is generally indicated by Gaussian function noise. Gaussian function noise is the most common and important noise with a probability density function of

$$p(z) = \frac{1}{\sqrt{2\pi}\sigma} \exp\left[\frac{-(z-\mu)^2}{2\sigma^2}\right], \quad (1)$$

where z indicates the gray level and relative standard deviation of the sharpness of the image. When z follows the above equation throughout, 70% of the values fall in the range $[(\mu - \sigma), (\mu + \sigma)]$, 95% fall in the range $[(\mu—2\sigma), (\mu + 2\sigma)]$, and 99.7% fall in the range $[(\mu - 3\sigma), (\mu + 3\sigma)]$.

2.4.2. Basic Principle of Wavelet Transform Denoising. Wavelet transform is a new way of transform analysis. It inherits and cultivates the concept of localization of short-time Fourier transform and at the same time solves the defect that the window size does not follow the change of frequency. It is an ideal tool for analyzing and processing the signal-duration-frequency by providing a "duration-frequency" dialog box with frequency. The wavelet optimization algorithm can decompose the complex filtering process into many simple processes, each of which is reversible. The wavelet transform maintains the concept of excellent localization of short-time Fourier transform, while solving the defect that the window size does not follow the frequency change, bringing the time-frequency dialog box with frequency change. The subband signal obtained by the decomposition has multiresolution, dual-frequency, and multidirectional characteristics, called optical microscopy [9]. The main advantages are low entropy, multiresolution, selective substrate picking coordination capability.

(1) Continuous Wavelet Transform. Let $\psi(t)$ be a square can accumulate function formula function whose Fourier transform has $\omega = 0$ at $\psi(0) = 0$, i.e., $\int_{-\infty}^{\infty} \psi(t)dt = 0$, then $\psi(t)$ is said to be the fundamental wavelet or mother wavelet [10]. The mother function formula is deflated to become:

$$\psi_{a,b}(t) = \frac{1}{\sqrt{|a|}} \psi\left(\frac{t-b}{a}\right), a, b \in R, a \neq 0, \quad (2)$$

in which $\psi_{a,b}(t)$ is referred to as the wavelet function formula. Here, the average error or total width of the wavelet function represented by the independent variable a is called the scale factor, and the spacing of the independent variable b moving in the t-axis is called the translation factor. The energy of the mother wavelet $\psi(t)$ is concentrated at the

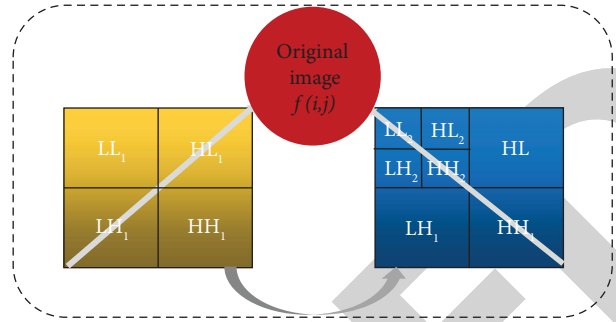

Figure 2: Wavelet decomposition schematic.

starting point, and the kinetic energy of the wavelet function $\psi_{a,b}(t)$ is concentrated at point b.

The formula for the continuous wavelet transformation of the arbitrary function is shown as follows:

$$W_f(a,b) = \langle f, \psi_{a,b} \rangle = \frac{1}{\sqrt{|a|}} \int f(t) \psi * \left(\frac{t-b}{a}\right) dt, \quad (3)$$

in which $\psi * (t)$ is expressed as the complex conjugate point of $\psi(t)$.

When the wavelets are orthogonal, the reconstructed formula according to the wavelet inverse transform is

$$f(t) = \frac{1}{C_\psi} \int_{-\infty}^{\infty} \int_{-\infty}^{\infty} \frac{1}{a^2} W_f(a,b) \psi\left(\frac{t-b}{a}\right) dadb. \quad (4)$$

(2) Discrete Wavelet Transformation. In the majority of computer implementations, discrete wavelet transforms are employed. The primary parameters, including the scaling factor and the translation factor, are derived from the discrete wavelet transform process.

Generally, we use the method of continuous wavelet conversion parameter discretization formula for $a = 2^{-j}$ and move the main parameters for $b = k2^{-j}$, where $k, j \in Z$. The formula for wavelet conversion $\psi_{j,k}(t)$ is shown as follows:

$$\psi_{j,k}(t) = 2^{j/2} \psi\left(\frac{t - k2^{-j}}{2^{-j}}\right) = 2^{j/2} \psi\left(2^{-j}t - k\right). \quad (5)$$

Discrete wavelet transformation index is shown as follows:

$$C_{j,k} = \langle f, \psi_{j,k} \rangle = \int_{-\infty}^{\infty} f(t) \psi_{j,k}(t) dt. \quad (6)$$

The reconstructed formula is shown as follows:

$$f(t) = C \sum_{-\infty}^{\infty} \sum_{-\infty}^{\infty} C_{j,k} \psi_{j,k}(t). \quad (7)$$

C is a constant that is not associated with the data signal. The power precision of the signal can be reconstructed according to picking the best j and k.

After discrete quadrature and wavelet transformations, as shown in Figure 2, each image is decomposed into four subimages. The top left is originally a smooth analog of the image, called the low frequency LL subimage, and the rest of

RETRACTED

the image is originally a small detail of the image, with high frequency information content. The lower left has small details of vertical edges with high frequency LH subimages, the upper right has small details of level edges with high frequency HL subimages, and the lower right has small details of diagonal edges with high frequency HH subimages. We have 3N high frequency bands and 1 low frequency band for different types of (3N-1) body height images when we carry out nth-order wavelet dissolution for 2D images. Due to uneven sunlight, dust, and other relatively complex natural environment, the UAV power inspection robot vision recognition system to extract images, there is a certain amount of noise. Employing wavelet optimization algorithms for rapid denoising can conserve computational memory, thereby enhancing the overall performance of inspection robots' visual navigation systems.

2.5. Defuzzification Loss Function. Due to the weather and instability of the airframe and other reasons, the UAV power inspection recognition images have the problem of blurring. And with the wide application of remote sensing image processing technology in the field of nanorobot research, the research related to blurred image recovery has become increasingly mature. This study takes the deblurring loss function as the starting point to solve the blurring problem of robotic power inspection images.

2.5.1. Content Loss Function. The content missing function is a computational function formula used to measure the difference between the estimated value of the model $f(x)$ and the middle of the true value y. This is the nonnegative real-valued function formula, which is generally indicated by $L(Y, f(x))$. The lower the loss function is, the better the robustness of the model is. Content loss is used to accurately measure the content similarity between the generated instance image and the actual instance image [11]. The concept of image content is very general and contains multisensor fusion, pixel content, image construction, and gradient orientation. In this paper, the constraints on the generated images are carried out in terms of both pixel content and image spatial features to ensure the consistency in content between the generated reconstructed images and the real clear images, which is the core of the remote sensing image processing technique in this paper and provides a solution to the image blurring problem in robotic power inspection.

(1) Pixel Deviation Constraint. Among the loss functions constrained according to pixel deviation, $L1$ loss and $L2$ loss are commonly used. $L1$ depletion and $L2$ loss are also known as mean relative error (MAE) and root mean square error (MSE). They are able to measure the mean value of the distance $L1$-$L2$ of the corresponding pixel points between the generated sample plate image and the actual sample plate image.

In the image super-resolution reconstruction and blur removal approach, $L2$ loss of key is used as content loss. The image quality is reconstructed based on the $L2$ spacing between the pixel values of the two images reduced to the minimum. However, because of the $L2$ spacing self-design problem, the reconstructed image becomes smoother, and blurring in the image details is inevitable. In the paper, LI damage is selected as the pixel deviation constraint of the model. The calculation formula is shown as follows:

$$L_{\text{pix}} = \frac{1}{WH} \sum_{x=1}^{W} \sum_{y=1}^{H} \left| I_s - G_{\theta_G}(I_B)_{x,y} \right|, \tag{8}$$

in this context, W and H represent the dimensions and overall width of the sample image, respectively. Here, this is also the generated image that is specific to the image. Depending on the bounded LI spacing, the consistency of the generated image with the actual image's middle pixel content can be ensured.

(2) Spatial Feature Tubing. With the rapid development of science and technology, the generation, fabrication, and development of nanomaterials in the UAV robotic power inspection technology gradually formed a good possibility; however, robotic power inspection technology faces with the problem of unclear images of the inspection system, and pixel-level deviation ensures the similarity of the content of two images clarity but ignores the cognitive differences between the images [12]. Therefore, by acquiring the feature maps of each convolutional layer keyed to the image in the special network model, the $L2$ spacing between the feature maps of the formed image and the real image is improved according to limiting the high-frequency information content of the formed image and leaving more image key points. However, the network model of the convolutional layer must be available to measure the feature cognitive damage of the image [13]. Here, the VGG Internet is used as an example, and the flow of the measurement procedure is shown in Algorithm 1.

The equation of the geospatial elements governing the relationship in the entity model is shown as follows:

$$L_{\text{feat}} = \frac{1}{W_{i,j} H_{i,j}} \sum_{x=1}^{W_{i,j}} \sum_{y=1}^{H_{i,j}} \left(\phi_{i,j}(I_S)_{x,y} - \phi_{i,j}\left(G_{\theta_G}(I_B)\right)_{x,y} \right)^2. \tag{9}$$

In the given context, the terms refer to the subspaces of feature images prior to the jth convolutional layer and subsequent to the Ith max-pooling layer within the VGG19 network architecture, respectively. The calculation steps of the specific feature-aware deficit are shown in Figure 3. The perceptual damage of the formed image in the convolutional layer Conv3_2 and the feature map of the actual image are measured on the figure using the VGG19 Internet as an example.

3. Solution Measures

3.1. Image Denoising Optimization Algorithm Based on Wavelet Transform Directional Characteristics and Edge Maintenance

3.1.1. Directional Characteristics of Wavelet Transform. After wavelet transform dissolution, the low frequency component of the image is very similar to the original image,

RETRACTED

Input: Generate sample Im_1 and real sample Im_2
(1) Initialize the trained VGG network based on the sample images
(2) Feature extraction of input sample images using VGG
(3) For $m = 1, 2, \ldots, n$ do
(4) Calculate the $L2$ distance of the corresponding feature map of the image to be measured
(5) For $m = 1, 2, \ldots, n$ do
(6) End
Output: Perceptual loss of the two images

Algorithm 1: Perceived Loss Calculation Process.

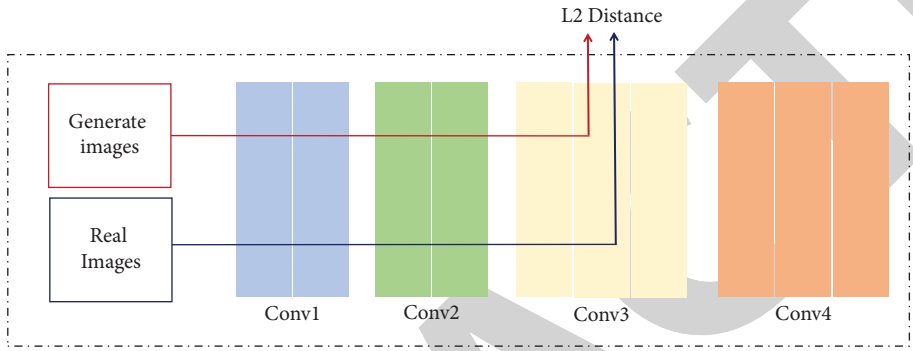

Figure 3: Feature perception loss calculation.

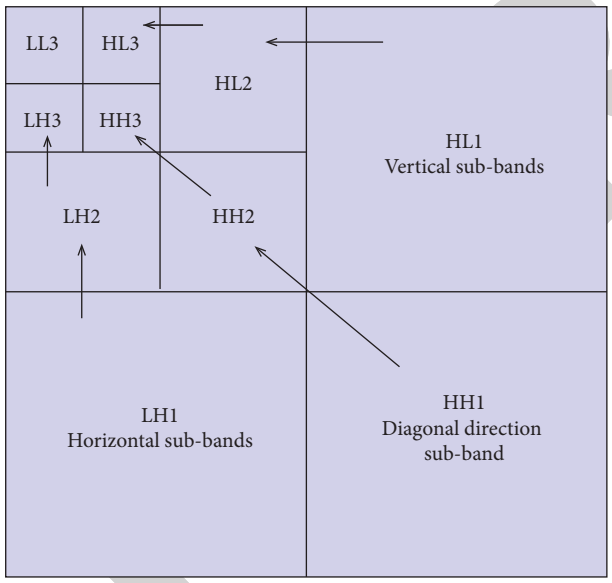

Figure 4: Wavelet decomposition high frequency subband directional characteristics.

but the high frequency component converges the important kinetic energy of the original image and exhibits the characteristics of the original image transformation such as edges [14]. In addition, most of the noise is also present in this component; thus, there is a great need to remove the high frequency component noise. As shown in Figure 4, the triple wavelet transform construction diagram shows the low frequency components of the original image, and HL1, HL2, and the three dissolved scales of the original image in the vertical direction of the edges and details. As well, LH, LH2, HH2, and HH each indicate the data in the horizontal and diagonal directions.

3.1.2. Algorithm Flow. Drive technology is one of the important components of the scholarly study of microstructure intelligent robots. Different types of drive forms not only have a great impact on the speed and form of motion of micro and nanorobots and limit the application scenarios of micro and nanorobots [15]. The process of robotic power inspection applications involves the drive technology of the controller, and this paper uses wavelet conversion directional characteristics and edge-maintained image denoising algorithms to design unique algorithmic processes for the development of nanorobot drive technology. The steps are summarized in Figure 5.

(1) We perform wavelet dissolution on images with Gaussian white noise primaries.
(2) We perform filtering of the high frequency orientation subgraph to remove noise based on the SVD decomposition of the orientation characteristics and reconstruct the number of singular values determined by the response equation of the elasticity coefficient of the highest value frequency stability. On the other hand, the edges of each subgraph are obtained using the azimuthal edge checking algorithm.

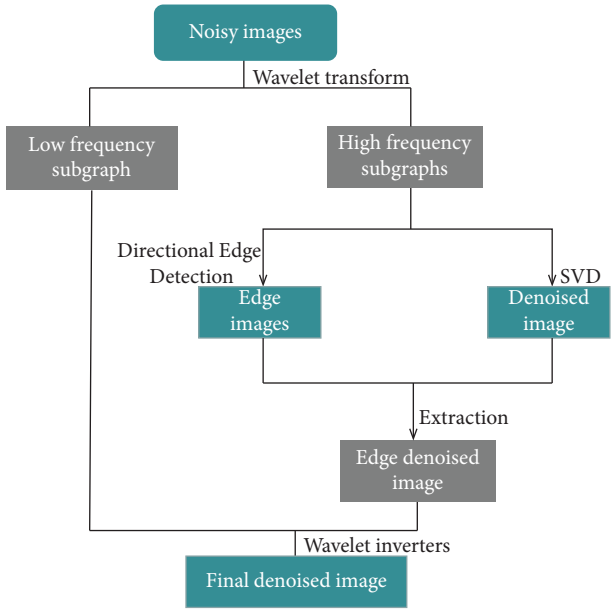

Figure 5: Image denoising algorithm flow.

3.2. Optimization Algorithm for Power Generation Cast Power Safety Inspection Deambiguation According to RRDB

3.2.1. The Imaging Stage Model of Intelligent Robot Power Safety Inspection—Taking UAV as an Example. Intelligent monitoring robot development has the characteristics of manipulation and operation mode dexterity and will not be affected by temperature factors. In unmanned or unmanned distribution stations, substations repeatedly implement inspection daily tasks. Unmanned Aerial Vehicle (UAV) technology facilitates power safety inspections by acquiring imagery of power infrastructure, enabling technicians to perform routine examinations and analyses of electrical circuits more efficiently. From the perspective of electro-optical imaging, a process of UAV reconnaissance image acquisition is to reconnoitre the target radiation source keyed to the load module output electro-optical stage. However, the full imaging process includes not only electro-optical imaging but also the main parameters used to specify the imaging quality with a daily task model corresponding to the daily task of the specific loop system [16]. The full process of UAV robotic power inspection imaging can be understood as a reconnaissance imaging stage model consisting of imaging model, main parameter model, and daily task model. The small details of the model are shown in Figure 6.

(1) Inspection task model: According to the specific inspection system daily task requirements, the relevant evaluation index system is applied to clarify the daily task evaluation index system. Before oil and gas well inspection, the planned task should be developed, including inspection line, inspection task, and main parameter setting.

(2) Main parameter model: The main parameter model is created according to the gimbal attitude shift, the main parameters of the surveillance camera image, geomorphology, pathways, and other environmental elements in the mission planning. It brings an important guarantee for the successful completion of the UAV inspection.

In the above UAV reconnaissance image linking model, the sensing device transmits the visible light band of the photographed image. However, the entire transmission process suffers from the inherent characteristics of the machine and equipment and the influence generated by electromagnetic interference, which also generates inevitable random noise, and the quality of the collected inspection images will be reduced. In addition, the UAV in the navigation link, the shaking of the gimbal, attitude shift, and relativity calibration transport will cause the image bias position, resulting in circular system image motion blur. Thus, there are more than 2 causes of UAV reconnaissance image recession: random noise and motion blur caused by poor fitness movement during imaging.

3.2.2. Construction of Power Patrol Dataset. Drones and nanorobots can cause blurred recognition images during power inspections due to weather, vibration, and other reasons. The image defuzzification daily task is used to perform defuzzification on a dataset in order to train and test the model's defuzzification level. A common blurred clearing dataset is a pair of images that must be "blurred-dynamically blurred". In paired datasets, the blurred and clear images should be one-to-one in terms of content and structure. Obtaining the appropriate "blurred-clear" image pairs is not a simple daily task.

The basic principles of image degradation were used to simulate the motion blur generated by the unmanned aircraft during the process of image development, resulting in an electronic reconnaissance blurred image. The motion blur process is generally a linear degradation process, and the degraded entity model can be defined as follows:

$$g(x, y) = \oint(x, y) * h(x, y) + n(x, y), \tag{10}$$

in which $h(x, y)$ is the space of degradation function indicates that the convolution sum is degraded blurred image and clear image. In the specific image process, the effect of random noise is inevitable.

The change in direction and speed of the UAV robot after implementing the electric power engineering inspection task depends on the direction and level of the motion blur [17]. The point spread function formulation has two extremely important main parameters: the fuzzy direction and the fuzzy scale. The direction of blurring needs to be indicated by the angle between the direction of motion and the horizontal direction, and the blurring limit can control the level of the degraded image. Different types of blurring main parameters can mix different directions and levels of motion blurred images. Thus, in this paper, the point spread function formula is used to create a "blurred-clear" image pair for the robotic power inspection. Then, to

RETRACTED

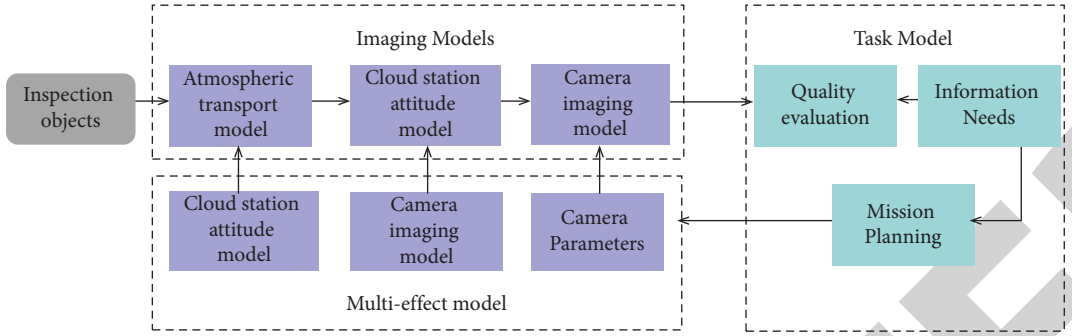

Figure 6: UAV inspection imaging link model.

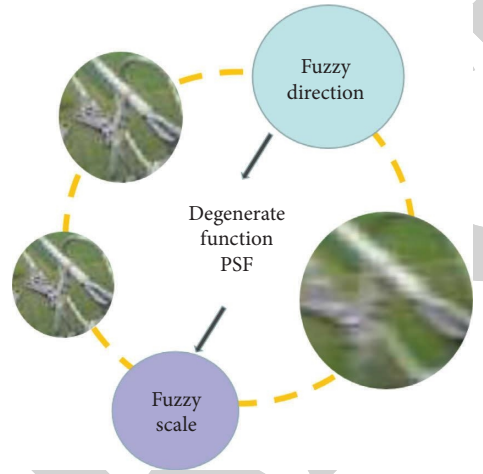

Figure 7: Motion blur patrol image synthesis.

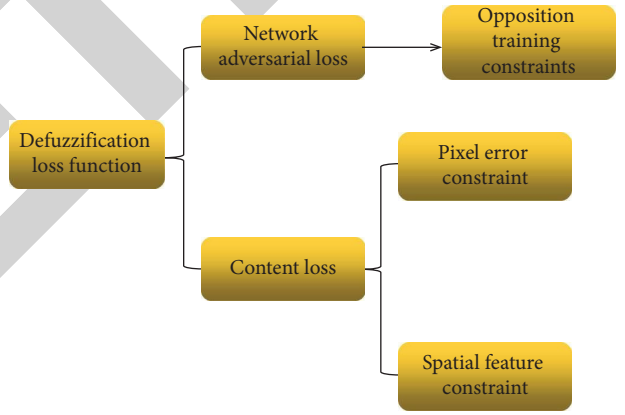

Figure 8: Overall design of the deblurring model.

ensure the diversity of the generated fuzzy inspection image samples, different types of fuzzy main parameters are set. Eventually, the prepared processed circulatory system image is keyed in, and the blurred unclear degradation solution is carried out using the degradation function formula PSF to generate the motion blurred system image corresponding to the clear circulatory system image. The full process of generation is shown in Figure 7.

3.2.3. Overall Scheme Design of Fuzzy Loss Function Formulation. The output language of the fuzzy controller expresses the independent variables selected as easy as possible, and taking into account the specific situation of intelligent robot walking and obstacle avoidance, the range sensor and direction sensor are selected to be able to better integrate into the whole process of robot obstacle avoidance. The collected information content of external factors is made

RETRACTED

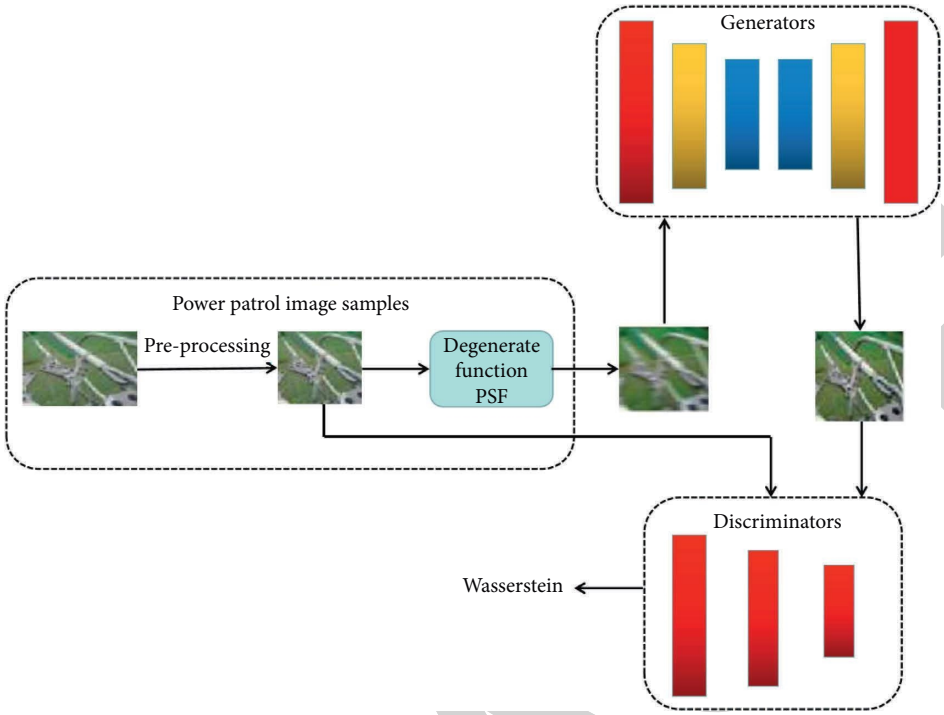

Figure 9: Overall process of deblurring power inspection image.

as the key to the fuzzy controller, the damage of the fuzzy controller is made as the robot target control, and the core of fuzzy controller is the establishment of fuzzy loss function [18].

The loss function formulation of the fuzzy unclear model contains two categories of Internet adversarial loss and content loss. Confrontation loss practices the maker and classification algorithm confrontation according to a very small notion of gaming [19]. Specific content loss means that the produced image information is managed to form a high-quality deblurred image based on the clarity deviation and spatial characteristics of the image. The integrated design of the ambiguity removal model is shown in Figure 8.

The coefficients of the three loss functions are computed, representing the loss functions of the ambiguity model discussed in the text. The expressions for these functions are as follows:

$$L = L_{\text{adv}} + \lambda_1 L_{\text{pix}} + \lambda_2 L_{\text{feat}} \tag{11}$$

3.3. Electricity Inspection Image Deblurring Process. For the image blurring problem in the power inspection of the UAV robot, the fuzzy entity model of the power generation grid-connected power inspection according to the RRDB network unit is developed, and the repair and reconstruction of the blurred inspection image are completed. The blurred processing of the switching power check image is shown in Figure 9.

A process of power inspection wild blur simulation can be summarized as follows: the first use of image recession model to simulate the blurred inspection images is generated during the robot inspection, and then, the "blurred and clear" power inspection image pairs are each keyed into the generator and classification algorithm in the entity model. Under the practice of the generator and classification algorithm, the generator maintains the image formation level and finally forms a replica image that is highly consistent with the clear power electronic reconnaissance image sample. The whole process is completed with a UAV representing the actual operation of robotic power inspection image deblurring [20]. At present, the development of nanomaterial robots in industries such as natural environment exploration, cosmic exploration, and power inspection is still in the preliminary stage, and the above-mentioned deblurring process to solve the image blurring problem can recommend its further commercialization.

4. Conclusion

At the present stage, the panoramic image imaging technology based on image stitching within the UAV panoramic image remote sensing technology system has many problems such as relatively slow development speed, poor practicality, difficulty in obtaining dynamic and complete panoramic images, large amount of image data obtained, and complicated stitching optimization algorithm. According to the exploration of the UAV remote sensing

RETRACTED

technology instant panoramic imaging technology and remote sensing technology, image processing process, for this subject research, has practicality, wide line of sight, strong manipulation, low cost, and relatively loose operating standards, and good image visual quality of remote sensing images can also establish the technical strength of the current stage of UAV robotic power inspection and promote the full effectiveness of the UAV monitoring system.

The key in the paper explores the UAV instant panoramic image GIS as well as the image processing process. The test results show that the denoising optimization algorithm proposed in the paper is useful to preserve small details of Kor-voltage towers, power lines, and Kor-voltage hardware configurations, giving effective application for safety risk evaluation in the electric power industry. In the future, the use of remote sensing technology image processing process in robotic power inspection will become more and more critical. The visual recognition system of nanocomposite robots has the advantages of noncontact, relatively high dexterity, rich content, and visualization of figurative data, which also gives higher technical performance to the software of high precision visual effect sensor system, and it is believed that the remote sensing image processing technology will also be applied to the manufacturing and research of nanocomposite robots in the future [21].

Data Availability

The labeled data used to support the findings of this study are available from the corresponding author upon request.

Conflicts of Interest

The authors declare that there are no conflicts of interest.

Acknowledgments

This work was supported by the Science and Technology Project of State Grid Fujian Electric Power Company (Research on Risk Prediction Technology of Transmission Channel Tree Obstacle based on UAV LiDAR, No. 52135020000N).

References

[1] A. Benouhiba, L. Wurtz, J. Rauch, J. Agnus, K. Rabenorosoa, and C. Clévy, "Nanorobotic structures with embedded actuation via ion induced folding," *Advanced Materials*, vol. 33, no. 45, Article ID 2103371, 2021.

[2] W. Wang, X. Yu, B. Fang et al., "Cross-modality LGE-CMR segmentation using image-to-image translation based data augmentation," *IEEE/ACM Transactions on Computational Biology and Bioinformatics*, vol. 1, 2022.

[3] A. B. Alhassan, X. Zhang, H. Shen, H. Xu, K. Hamza, and G. Masengo, "Precise motion control of a power line inspection robot using hybrid time delay and state feedback control," *Frontiers in Robotics and AI*, vol. 9, Article ID 746991, 2022.

[4] D. Salley, G. Keenan, J. Grizou, A. Sharma, S. Martín, and L. Cronin, "A nanomaterials discovery robot for the Darwinian evolution of shape programmable gold nanoparticles," *Nature Communications*, vol. 11, no. 1, p. 2771, 2020.

[5] A. Tiwari, S. K. Sharma, A. Dixit, and V. Mishra, "UAV remote sensing for campus monitoring: a comparative evaluation of nearest neighbor and rule-based classification," *Journal of the Indian Society of Remote Sensing*, vol. 49, no. 3, pp. 527–539, 2020.

[6] S. Ghaffarian, J. Valente, M. van der Voort, and B. Tekinerdogan, "Effect of attention mechanism in deep learning-based remote sensing image processing: a systematic literature review," *Remote Sensing*, vol. 13, no. 15, p. 2965, 2021.

[7] N. Guan and P. Zhang, "Active compliance control system for intelligent inspection robot in power room," *Journal of Control Science and Engineering*, vol. 2022, Article ID 7829082, 7 pages, 2022.

[8] T. Wang, K. Fang, W. Wei, J. Tian, Y. Pan, and J. Li, "Microcontroller unit chip temperature fingerprint informed machine learning for IIoT intrusion detection," *IEEE Transactions on Industrial Informatics*, vol. 19, no. 2, pp. 2219–2227, 2023.

[9] D. Dhongade and M. Patil, "EEG based brain computer interfacing for hand assistant system using wavelet transform," *ITM Web of Conferences*, vol. 32, p. 03035, 2020.

[10] H. Rao, S. Wang, X. Hu et al., "A self-supervised gait encoding approach with locality-awareness for 3D skeleton based person Re-identification," *IEEE Transactions on Pattern Analysis and Machine Intelligence*, vol. 1, 2021.

[11] S. Kesornprom, P. Cholamjiak, and C. Park, "New proximal type algorithms for convex minimization and its application to image deblurring," *Computational and Applied Mathematics*, vol. 41, no. 7, p. 333, 2022.

[12] G. Rigatos, N. Zervos, P. Siano, M. Abbaszadeh, J. Pomares, and P. Wira, "A nonlinear optimal control approach for underactuated power-line inspection robots," *Robotica*, vol. 40, no. 6, pp. 1979–2009, 2022.

[13] W. Xiong, S. Yang, Z. Zhang, L. Chen, and S. Huang, "Research on image recognition of power inspection robot based on improved YOLOv3 model," *Journal of Physics: Conference Series*, vol. 1486, no. 4, Article ID 042034, 2020.

[14] D. K. Alves, R. L. A. Ribeiro, L. F. D. Q. Silveira, and T. O. A. Rocha, "Real-timewavelet-based adaptive algorithm for low inertia AC microgrids power measurements," *International Journal of Electrical Power & Energy Systems*, vol. 140, Article ID 108043, 2022.

[15] T. Wang, B. Lu, W. Wang, W. Wei, X. Yuan, and J. Li, "Reinforcement learning-based optimization for mobile edge computing scheduling game," *IEEE Transactions on Emerging Topics in Computational Intelligence*, vol. 7, no. 1, pp. 55–64, 2023.

[16] C. Wang, Z. Li, Y. Kang, and Y. Li, "Applying SLAM algorithm based on nonlinear optimized monocular vision and IMU in the positioning method of power inspection robot in complex environment," *Mathematical Problems in Engineering*, vol. 2022, Article ID 3378163, 14 pages, 2022.

[17] T. Wang, J. Li, W. Wei, W. Wang, and K. Fang, "Deep-learning-based weak electromagnetic intrusion detection method for zero touch networks on industrial IoT," *IEEE Network*, vol. 36, no. 6, pp. 236–242, 2022.

[18] Y. Kim, J. K. Chae, J. H. Lee, E. Choi, Y. K. Lee, and J. Song, "Free manipulation system for nanorobot cluster based on complicated multi-coil electromagnetic actuator," *Scientific Reports*, vol. 11, no. 1, p. 19756, 2021.

RETRACTED

Hindawi
Journal of Robotics
Volume 2024, Article ID 9792362, 1 page
https://doi.org/10.1155/2024/9792362

Retraction

Retracted: Collaboration and Management of Heterogeneous Robotic Systems for Road Network Construction, Management, and Maintenance under the Vision of "BIM + GIS" Technology

Journal of Robotics

Received 23 January 2024; Accepted 23 January 2024; Published 24 January 2024

Copyright © 2024 Journal of Robotics. This is an open access article distributed under the Creative Commons Attribution License, which permits unrestricted use, distribution, and reproduction in any medium, provided the original work is properly cited.

This article has been retracted by Hindawi following an investigation undertaken by the publisher [1]. This investigation has uncovered evidence of one or more of the following indicators of systematic manipulation of the publication process:

(1) Discrepancies in scope
(2) Discrepancies in the description of the research reported
(3) Discrepancies between the availability of data and the research described
(4) Inappropriate citations
(5) Incoherent, meaningless and/or irrelevant content included in the article
(6) Manipulated or compromised peer review

The presence of these indicators undermines our confidence in the integrity of the article's content and we cannot, therefore, vouch for its reliability. Please note that this notice is intended solely to alert readers that the content of this article is unreliable. We have not investigated whether authors were aware of or involved in the systematic manipulation of the publication process.

Wiley and Hindawi regrets that the usual quality checks did not identify these issues before publication and have since put additional measures in place to safeguard research integrity.

We wish to credit our own Research Integrity and Research Publishing teams and anonymous and named external researchers and research integrity experts for contributing to this investigation.

The corresponding author, as the representative of all authors, has been given the opportunity to register their agreement or disagreement to this retraction. We have kept a record of any response received.

References

[1] Z. Liu, W. Yan, J. Kou, and Z. Li, "Collaboration and Management of Heterogeneous Robotic Systems for Road Network Construction, Management, and Maintenance under the Vision of "BIM + GIS" Technology," *Journal of Robotics*, vol. 2023, Article ID 8259912, 8 pages, 2023.

Hindawi
Journal of Robotics
Volume 2023, Article ID 8259912, 8 pages
https://doi.org/10.1155/2023/8259912

RETRACTED

Research Article

Collaboration and Management of Heterogeneous Robotic Systems for Road Network Construction, Management, and Maintenance under the Vision of "BIM + GIS" Technology

Zhizhong Liu, Weishen Yan, Jianguo Kou, and Zhida Li

Hebei Expressway Yanchong Management Center, Zhangjiakou 075400, Hebei, China

Correspondence should be addressed to Zhizhong Liu; 15211020408@stu.cpu.edu.cn

Received 4 October 2022; Revised 21 December 2022; Accepted 27 March 2023; Published 12 April 2023

Academic Editor: Shahid Hussain

Copyright © 2023 Zhizhong Liu et al. This is an open access article distributed under the Creative Commons Attribution License, which permits unrestricted use, distribution, and reproduction in any medium, provided the original work is properly cited.

In modern society, intelligent spatial analysis services have been playing an important role in building smart cities. Especially, people's spatial information needs have changed with the technological progress of times, from traditional two-dimensional appearance to three-dimensional interior. In this case, the construction of street networks is a key part of spatial information analysis research. Establishing an integrated indoor-outdoor street network data model with accurate information and complete attributes can provide strong technical support for indoor-outdoor navigation, emergency evacuation, and other application services. However, most of the current studies on internal and external road networks are independent of each other. This means that indoor road networks are mainly based on floor plans, which contain little information and do not represent the spatial relationships between floors. Indoor and outdoor links often suffer from poor connectivity and data loss. Heterogeneous robotics is a high degree of integration of intelligent control and platform control technologies. In a sense, it is a technology platform for connecting heterogeneous robotic populations. By developing effective collaboration and control strategies, tasks can be performed with the highest success rate and the lowest risk while respecting spatial and temporal constraints. As a result, the study of the coordination and management of heterogeneous robotic systems for road network construction, management, and maintenance is a topic of a great theoretical value and significance. Therefore, this paper proposes an intelligent road network construction method that incorporates BIM and GIS technologies. This study uses the building information model to enrich the information of indoor building components and combines the strong spatial analysis capability of outdoor areas with GIS road network technology to build an indoor road network and design a connection scheme for indoor and outdoor areas. After that, the construction of an integrated indoor-outdoor street network is completed, and the interaction between indoor as well as outdoor spatial data is very smooth.

1. Introduction

With the development of urbanization, information, and automation technologies and the rapid spread of the Internet, people's movements are becoming more complex and diverse [1]. Under such circumstances, spatial information technology becomes increasingly necessary. However, as urban population continues to grow, building density is also increasing [2]. At the same time, the configuration of urban space and road networks is becoming more and more complex. Outdoor navigation technologies are also becoming more and more complex. Nevertheless, research on spatial data analysis has been slow due to the complex spatial structure of buildings, high accuracy requirements, and the major technical bottlenecks of traditional indoor positioning technologies [3]. As urbanization progresses, people are also increasingly moving indoors. Consequently, GPS positioning technology, which is widely used outdoors, is no longer applicable to geographic environments with complex spatial structures and high requirements for positioning accuracy [4]. As a result, for applications that affect human life and safety, such as pedestrian navigation and emergency evacuation, there is an urgent need for spatial data that can support precise geometric locations and clear hierarchical

relationships in complex indoor and outdoor environments. In short, the development of road networks will play an important role in the overall urban life cycle and the use of geospatial data [5].

In the rapidly developing information age of the Internet, outdoor navigation is widely used in people's lives. For example, location-based services of Gaode Map and Baidu Map are ubiquitous. However, indoor navigation technologies are relatively lagging behind compared to outdoor navigation applications [6]. As a result, research on indoor navigation technologies is becoming increasingly essential. As a matter of fact, indoor navigation systems are different from outdoor navigation systems to some extent. In particular, the technology of outdoor navigation systems cannot be directly applied to indoor navigation systems because geographic signals are sensitive to buildings [7]. After all, people now spend most of their day indoors. Actually, this means that there is a growing demand for location-based services inside buildings. Indoor navigation enables people to know exactly where they are indoors and get to their indoor destinations quickly. At the same time, this makes people's lives easier. In short, using indoor navigation to establish spatial relationships between people and objects can make people's lives more comfortable [8]. Indoor navigation systems need more research in many aspects than outdoor navigation systems. As illustrated in Figure 1, the main research directions in this field focus on positioning methods, positioning accuracy, and building road network models, as well as road network representation.

In fact, the needs about road network construction are included in the idea of a smart city. To be specific, a smart city is a beautiful vision. It is a solution that integrates multiple ICT and IoT in a secure way [9]. As a result, in order to understand what is happening in a city and how to improve the quality of life of its inhabitants, smart city applications require a large amount of data, both static and dynamic, contemporary and historical, geometric and semantic, and microscopic and macroscopic [10]. Collecting, managing, and applying these data often require the use of technologies such as building information modeling (BIM) and geographic information systems (GISs). In particular, BIM technologies can be used to create, manage, and share data across the vertical facility lifecycle [11]. GIS technologies can be applied to store, manage, and analyze descriptions of the urban environment. As a result, the combined application of BIM and GIS is quite essential for smart city applications that require facility and urban environment data. In other words, while GIS has a long history of application and BIM has been developed for more than a decade, their combined application begins a new direction that is still in the early stages of exploration [12].

With the continuous development of GIS technology, GIS can integrate spatial information and spatial analysis into different applications. For pedestrian navigation and emergency response, indoor and outdoor route planning is quite crucial [13]. As a result, such route planning requires detailed indoor information. This information is often obtained from industry floor plans for architectural design, engineering, and construction services [14]. Currently, most of the outdoor navigation systems that people come across for route planning and navigation are two-dimensional. In other words, planning and navigation information needed for these electronic maps can be obtained from existing spatial datasets. However, for indoor navigation, since indoor is a three-dimensional space, the indoor road network model in indoor navigation should also be a three-dimensional model [15]. Therefore, route planning should be carried out on a three-dimensional basis. However, there is no mature unified standard for the construction of indoor road network models. At the same time, BIM technology, as an emerging technology in the field of architecture, engineering, and construction, is widely used in the whole life cycle of buildings [16]. In addition, BIM is regarded as an ideal source of spatial information because it contains rich geometric and semantic information on building components [17]. In summary, the study of 3D road network model technology for indoor navigation with a data-rich building information model and GIS integration is of great significance for the indoor navigation industry based on location services.

Along with the technological development of computers, artificial intelligence, and robotics, robotics, one of the greatest creations of mankind, has developed rapidly in just a few decades. Today, the scope of robotic applications has expanded to include all aspects of human life. Figure 2 illustrates the applications of robotics in various fields such as healthcare, services, and entertainment.

In real-life situations, many single robots are unable to complete tasks due to the variability of living conditions and the complexity of tasks [18]. Especially in dynamic environments with complex tasks and special situations, it is quite necessary to consider multiple robots or a mix of different types of robots working together [19]. As tasks become more difficult, the quest for efficiency increases. In other words, a single robot is no longer sufficient to meet many requirements. As a result, there is a growing interest in the development of multiple robots. To be specific, there is a desire to coordinate different types of robots or robots with other tools to accomplish many tasks that cannot be performed by a single robot [20]. In the past, research on multirobot systems has focused more on homogeneous robotic systems. Heterogeneous robotic systems, on the other hand, often have widely varying dynamics and kinematics due to different functions and shapes, loads, and motion capabilities of individual robots [21]. As a result, when these individuals work together, there are redundancy and coupling effects, which are challenging.

There are two main types of robots, namely, aerial drones and ground mobile robots [22]. Table 1 lists the relevant characteristics of unmanned aircraft and mobile robots. Table 1 shows that, on the one hand, both unmanned aircraft and mobile robots have their own limitations. In fact, this can reduce the efficiency of their tasks to some extent. On the other hand, unmanned aircraft and mobile robots are very complementary [23]. In fact, the complementarity between unmanned aircraft and mobile robots can be seen in several ways. To start with, sensors located on drones are often

RETRACTED

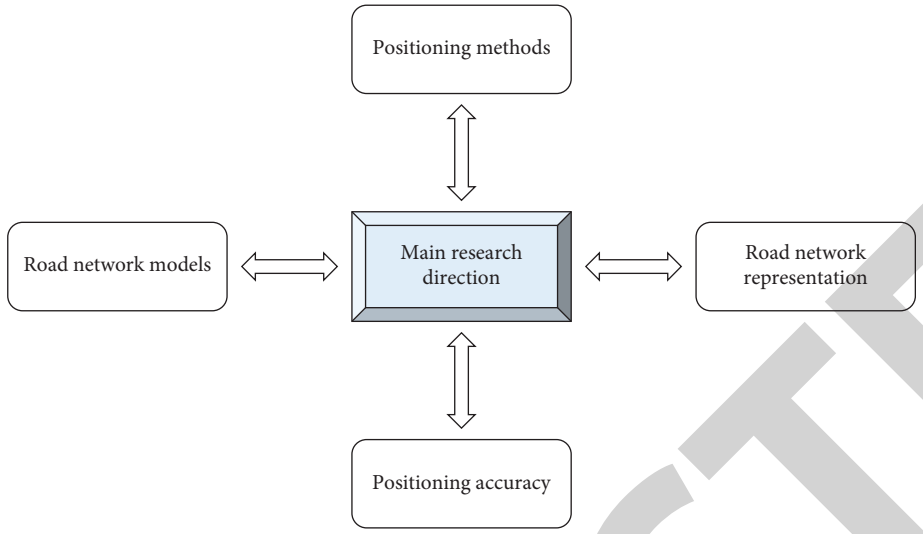

Figure 1: Main research directions in indoor navigation systems.

Figure 2: Applications of robotics in various fields.

limited by flight speed and altitude when capturing ground features [24]. As a result, mobile robots can be deployed to precisely locate ground targets. Furthermore, the communication links between unmanned aerial vehicles are less likely to be blocked by obstacles due to the altitude advantage. Consequently, mobile robots at different locations can be indirectly connected with the support of unmanned aerial vehicles used as communication relays. Finally, unmanned aerial vehicles are often limited by short-range navigation due to load energy constraints, while mobile robots have a larger payload capacity [25].

Existing studies on path planning for heterogeneous robotic systems often do not consider the motion range of ground mobile robots [26]. In real environments, roads are intricate and complex. As a result, the ground vehicle should move in the road. In addition, there are some studies that consider the limitation of the motion range of ground mobile robots and restrict the motion of ground robots to the road network. However, the ground robot following the given path may not necessarily get the best path to complete the task, nor is it guaranteed to get the shortest time to complete the task, which results in energy waste.

In fact, traditional indoor data collection is time consuming. After all, there are many technical difficulties in automatically extracting interior information from complex buildings. At the same time, this information is influenced by the type of input data. As a result, interior building properties are often incomplete. BIM technology has the potential to become the indoor road network data with its advantages of including data information of the whole building life cycle and 3D visualization [27]. As a database of the whole building information, the introduction of BIM technology and building spatial topological relationship analysis in the indoor path planning study is both an effective way to improve the accuracy of indoor road networks and a useful extension of the application area of BIM models. BIM and GIS each have their own common data standards. In other words, their geometric modeling, semantic networks, and logical relationships are significantly different [28]. As a result, more and more research is focused on the integration of building-scale and city-scale spatial information for different applications, especially those requiring indoor and outdoor information. At the same time, the integration of BIM and GIS will become a key task in smart city applications. To this end, this paper proposes a BIM-based indoor network model and the integration with outdoor GIS models.

Table 1: Relevant characteristics of unmanned aircraft and mobile robots.

Categories	Advantage	Disadvantage
Unmanned aircraft	Fast speed	Low load
Mobile robot	High load	Slow speed

RETRACTED

2. Overview of Related Technologies

2.1. BIM Technology. Building information modeling (BIM) is the digital transmission of information about the entire life cycle of a building in the form of a three-dimensional digital building information model, which includes information about the building at all stages of its life cycle, from design, construction, and completion to operation and maintenance. BIM is a three-dimensional digital building information model that contains information about the building at all stages of its life cycle, from design, construction, and completion to operation and maintenance. As a result, it can be used as a lifecycle solution to integrate building information through digital technology and be used for the design, construction, operation, and maintenance of buildings. In other words, BIM technology can integrate all building information into one 3D model database.

As a carrier of information exchange among various units in the construction process and an important part of the construction big data, the building information model expresses the information about urban buildings comprehensively. As a result, BIM technology plays an important role in the application of big data in smart cities. At the same time, BIM can be converted into 2D or 3D forms by using engineering application software. Consequently, its rich data forms increase the cross-use of data. In addition, with the popularity of the mobile Internet and smart phones, people can view building data information in real time on their cell phones. In other words, this has significantly improved the ease of information interaction. For example, Figure 3 shows the building information model of a building and the construction attributes.

In practical application, in order to make BIM support the storage and interaction of information about the whole construction project, researchers build BIM servers as the carrier of information. Then, they can complete the storage of BIM data by interacting with the server through the client. As shown in Figure 4, the information interaction mode can be divided into the C/S architecture and B/S architecture according to the different forms of interaction between the client and the server. At present, commonly used BIM servers are the C/S architecture. In other words, when people use BIM applications, they need to download the corresponding BIM application client to their computers, and then, they can perform BIM modeling and information maintenance after installation. In addition, there are also some differences in the operation methods of different clients. As a matter of fact, users usually need to go through training before they can operate the application, and the B/S architecture has a clearer separation between data processing and result appearance than the C/S architecture. In short, with the development of mobile communication technology and mobile application technology, especially the maturity and popularity of mobile browsers, the advantages of the B/S architecture's flexibility are becoming more and more obvious.

In recent years, with the development of 3D web rendering technologies, there are 3D web-side rendering technologies such as HTML5 and WebGL. These technologies can be effectively applied to 3D graphics rendering on the website. Although most of the research studies focus on the application of WebGL technology, these research studies also provide reference for the combination of BIM technology and WebGL technology. In addition, although the existing rendering technologies can improve the efficiency of model loading to some extent, the speed of model loading and rendering is very low. However, model loading and rendering speed is largely affected by the volume of the building information model itself. Therefore, according to the specific purpose of the model, the BIM data should be processed redundantly, and some unnecessary model information should be removed through light weighting. In fact, the process of BIM light weighting mainly includes the analysis of the BIM model information organization structure and BIM model data format conversion. After that, through the reorganization of the BIM data structure and format conversion, we achieve the purpose of simplifying the building information model. In this study, the road network model BIM data preprocessing process is illustrated in Figure 5.

2.2. GIS and Road Network Model. A road network model is a network model that maps the spatial and attribute information about roads and relationships between them and can manage and reprocess the data in the model. In fact, the early studies of road network models were oriented towards the geometry of lanes and the representation of traffic information. In other words, road network data were commonly used for route analysis. With the rapid development of computer technology, the information accuracy of road network models has been continuously improved. As a result, the road network model has been able to meet the transformation of complex terrain in outdoor environments in terms of spatial capability and focus on the construction of topological logic relationships between road networks. For the study of outdoor road network models, the centerline of streets is usually extracted as edges and formed into a network and road intersections are extracted as nodes, and then, information is given in the nodes and edges.

In contrast to navigation in an outdoor network, navigation in an indoor environment is not efficient for route planning because there is no clear road network to navigate. In fact, pedestrians and vehicles can navigate in outdoor networks. However, in indoor environments, it is also necessary to predefine the road network for indoor navigation so that the algorithms for outdoor route planning can be applied to indoor route planning. This requires a navigation network with indoor access conditions and then proposes a corresponding data organization method for the map model of the indoor navigation network. After all, the indoor map model is the basis for the implementation of indoor location services. In fact, one of the goals of building an indoor map model is to abstract the indoor navigation network for indoor positioning and navigation as well as for route planning. Therefore, the indoor road network model is the basis for indoor location services such as navigation and route planning, which directly affect the effectiveness of indoor navigation and route planning. As the current research and application of indoor positioning technology

RETRACTED

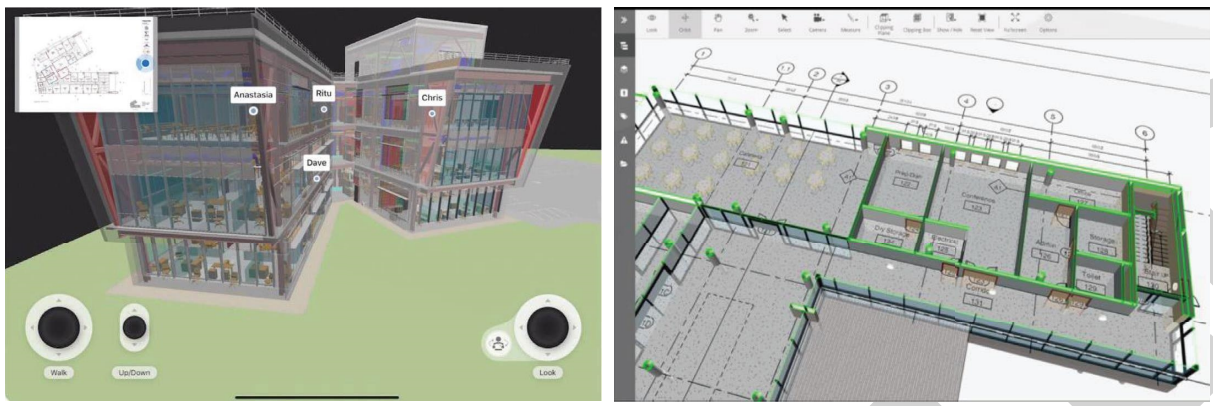

Figure 3: Building information model of a building and the construction attributes.

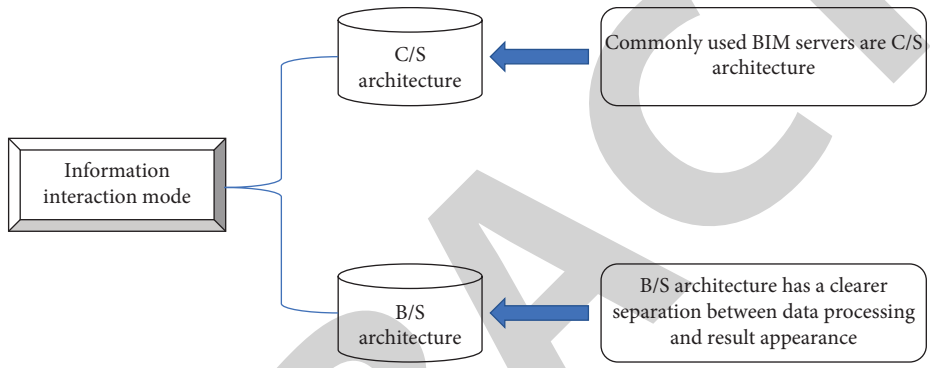

Figure 4: Architectures of information interaction mode.

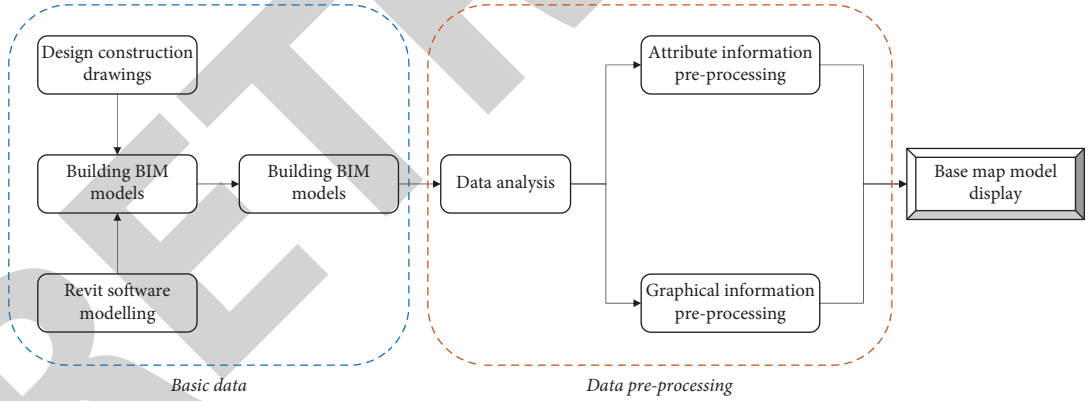

Figure 5: Road network model BIM data preprocessing process.

continue to mature, the research on the construction method of indoor road network models becomes particularly important. This is of great importance to promote the development of indoor navigation technology. In summary, the interior space of the building is divided, as shown in Figure 6.

3. Heterogeneous Robotic System for Road Networks

3.1. Road Network Model. When designing, designers often use a series of grids to fill in interior spaces. In fact, this is a method of interior space segmentation, which can be further defined as a grid model. Each grid represents a subspace of the interior space in the road network model. Thus, the topological relationships in the interior space can be expressed by the connections between adjacent grids. As a matter of fact, there are two types of cellular grids: regular and irregular. The regular grid is usually a square, hexagonal, or spatial cube. The information accuracy of the regular grid model is closely related to the grid size. In other words, the finer the grid is divided, the higher the accuracy of the model. The processing of a large amount of grid data is very demanding on the computer equipment. When applied to

RETRACTED

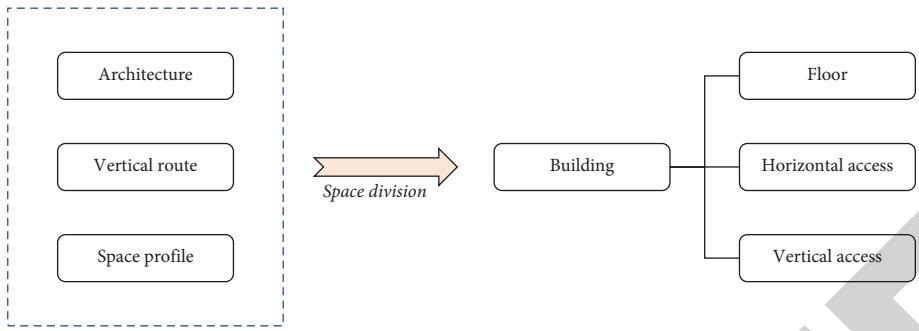

Figure 6: Interior space of the building.

a real system, it will generate a large memory load and affect the operation efficiency of the overall spatial service system. Figure 7 illustrates a partitioning diagram of an irregular triangular mesh. To be specific, it could form a road network model by extracting the center points of triangles and the midpoints of neighboring edges between triangles.

In fact, graph-based models have a greater advantage in describing the relational information and structure of interior spaces. More specifically, the diagram model is able to represent complex spatial structures with simple logical relationships. At the same time, the graph model also supports hierarchical classification of building entity information in interior spaces. As a result, the graph-based node and edge model has much room for development in terms of geometric information complementation, model semantic network construction, and model extraction efficiency. In summary, the structure of nodes and edges should be used as the basis for the construction of road network models for path planning and further research on road network construction.

3.2. Heterogeneous Robotic System. As one of the most popular branches of robotics, mobile robotics is a hot and difficult area of research. As a result, the scope of research includes navigation and localization, multisensor information fusion, path planning, multirobot coordination, and robot vision. Path planning, as one of the most important aspects of robotics, is a classical yet challenging area of research. In fact, for some specific tasks, mobile robots often need to make further decisions about their motion behavior based on the corresponding environmental characteristics. For example, pipeline inspection, robotic mine clearance, and high-voltage line work all require the robot to generate its own flow or path according to the actual working environment in order to prepare for the next task. These are essentially path planning problems for mobile robots.

Heterogeneous robotic systems are often connected together in some ways when performing a task and can move separately and independently when certain conditions are met. In fact, the diverse distribution of task points and the obstacles in the environment are the main factors that affect the motion decisions of a robotic system. Therefore, the establishment of a safe and effective model is the key and difficult part of path planning for heterogeneous robotic

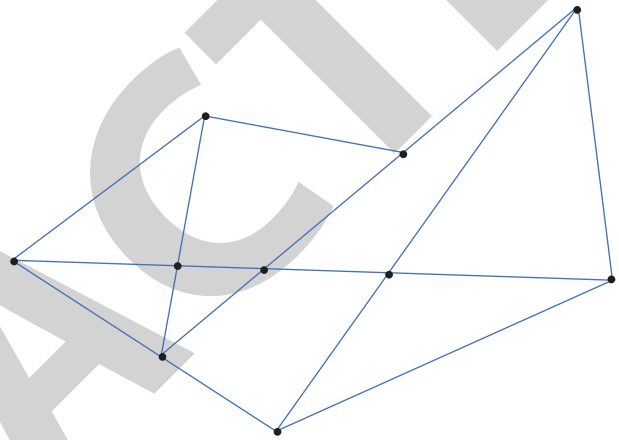

Figure 7: Partitioning diagram of an irregular triangular mesh.

systems. An understanding of architectural requirements is essential for the research and design of new generic control systems for heterogeneous mobile robots. Currently, there are two requirements for the study of generic control system architectures. The first requirement is standardization, i.e., the need for a unified, standard control strategy technology that can be applied to different controllers. In addition, the second requirement is openness, i.e., the need for a middleware module that is scalable and can run in a variety of heterogeneous computing environments. The commonality between these two requirements is the urgent need for an approach to improve the general serviceability of mobile robotic software modules. This approach can greatly improve the openness, scalability, and reusability of intelligent robotic architectures.

4. Conclusion

In recent years, the concept of a smart city has gradually gained popularity. In this context, intelligent information services have been greatly popularized by the rapid development of communication technology. Especially in spatial location information analysis, although the traditional outdoor traffic network can bring great convenience to people's travel, it is slightly insufficient in dealing with complex indoor space. Especially in intelligent spatial services such as indoor and outdoor navigation or emergency evacuation, complete and accurate integrated indoor and

RETRACTED

outdoor information data are needed to support. The construction of integrated indoor-outdoor road networks is the key to solving these problems. In this paper, we propose to integrate the BIM model and GIS data to build an indoor-outdoor integrated road network to achieve a seamless connection between indoor and outdoor road networks and finally to realize the application in the web-based route planning system, in response to the problems of simple indoor data structure, poor information completeness, and poor indoor-outdoor communication in the current indoor-outdoor road network research.

In terms of theoretical research, this paper investigates the current research on indoor and outdoor road networks at home and abroad and summarizes the basic needs and outstanding problems of indoor and outdoor road networks. For the difficult indoor space in road network construction, we focus on the analysis of indoor space characteristics and choose the diagram-based model as the indoor road network model according to indoor characteristics. Then, this study introduces the BIM model as an indoor data source and analyzes the advantages of BIM in indoor information representation. In the indoor-outdoor integration part, this paper proposes to build an integrated road network model that integrates BIM model data and GIS outdoor road network data. Based on the current research on the integrated application of BIM and GIS, this study further investigates the feasibility of the indoor-outdoor road network integrating BIM and GIS and illustrates the advantages and significance of the integrated indoor-outdoor road network integrating BIM and GIS. In the future, related research can be performed in the following aspects. In terms of the loading speed and rendering efficiency of the indoor road network map model, the loading time of the indoor road network map model obtained through experiments is long, which affects the user's use effect, and the loading method of the model needs to be further improved.

Data Availability

The labeled dataset used to support the findings of this study is available from the corresponding author upon request.

Conflicts of Interest

The authors declare that there are no conflicts of interest.

Acknowledgments

This work was supported by the Hebei Expressway Yanchong Management Center.

References

[1] H. B. Ticha, N. Absi, D. Feillet, and A. Quilliot, "Empirical analysis for the VRPTW with a multigraph representation for the road network," *Computers & Operations Research*, vol. 88, pp. 103–116, 2017.

[2] H. Ben Ticha, N. Absi, D. Feillet, and A. Quilliot, "Vehicle routing problems with road-network information: state of the art," *Networks*, vol. 72, no. 3, pp. 393–406, 2018.

[3] T. Chen, S. Wu, J. Yang, G. Cong, and G. Li, "Modeling of emergency supply scheduling problem based on reliability and its solution algorithm under variable road network after sudden-onset disasters," *Complexity*, vol. 2020, Article ID 7501891, 2020.

[4] A. Miatto, H. Schandl, D. Wiedenhofer, F. Krausmann, and H. Tanikawa, "Modeling material flows and stocks of the road network in the United States 1905–2015," *Resources, Conservation and Recycling*, vol. 127, pp. 168–178, 2017.

[5] G. Shi, J. Shan, L. Ding, P. Ye, Y. Li, and N. Jiang, "Urban road network expansion and its driving variables: a case study of Nanjing City," *International Journal of Environmental Research and Public Health*, vol. 16, no. 13, p. 2318, 2019.

[6] W. C. Simões, G. S. Machado, A. Sales, M. M. de Lucena, N. Jazdi, and V. F. de Lucena, "A review of technologies and techniques for indoor navigation systems for the visually impaired," *Sensors*, vol. 20, no. 14, p. 3935, 2020.

[7] D. Plikynas, A. Žvironas, A. Budrionis, and M. Gudauskis, "Indoor navigation systems for visually impaired persons: mapping the features of existing technologies to user needs," *Sensors*, vol. 20, no. 3, p. 636, 2020.

[8] R. N. Kandalan and K. Namuduri, "Techniques for constructing indoor navigation systems for the visually impaired: a review," *IEEE Transactions on Human-Machine Systems*, vol. 50, no. 6, pp. 492–506, 2020.

[9] L. W. Chen and J. X. Liu, "Time-efficient indoor navigation and evacuation with fastest path planning based on Internet of Things technologies," *IEEE Transactions on Systems, Man, and Cybernetics: Systems*, vol. 51, no. 5, pp. 3125–3135, 2021.

[10] A. Meliones and D. Sampson, "Blind MuseumTourer: a system for self-guided tours in museums and blind indoor navigation," *Technologies*, vol. 6, no. 1, p. 4, 2018.

[11] B. Cheng, K. Lu, J. Li, H. Chen, X. Luo, and M. Shafique, "Comprehensive assessment of embodied environmental impacts of buildings using normalized environmental impact factors," *Journal of Cleaner Production*, vol. 334, Article ID 130083, 2022.

[12] W. Jeamwatthanachai, M. Wald, and G. Wills, "Indoor navigation by blind people: behaviors and challenges in unfamiliar spaces and buildings," *British Journal of Visual Impairment*, vol. 37, no. 2, pp. 140–153, 2019.

[13] N. A. Giudice, B. A. Guenther, T. M. Kaplan, S. M. Anderson, R. J. Knuesel, and J. F. Cioffi, "Use of an indoor navigation system by sighted and blind travelers: performance similarities across visual status and age," *ACM Transactions on Accessible Computing*, vol. 13, no. 3, pp. 1–27, 2020.

[14] W. Sakpere, M. Adeyeye-Oshin, and N. B. Mlitwa, "A state-of-the-art survey of indoor positioning and navigation systems and technologies," *South African Computer Journal*, vol. 29, no. 3, pp. 145–197, 2017.

[15] M. Sattarian, J. Rezazadeh, R. Farahbakhsh, and A. Bagheri, "Indoor navigation systems based on data mining techniques in internet of things: a survey," *Wireless Networks*, vol. 25, no. 3, pp. 1385–1402, 2019.

[16] D. Liu, S. Guo, Y. Yang, Y. Shi, and M. Chen, "Geomagnetism-based indoor navigation by offloading strategy in NB-IoT," *IEEE Internet of Things Journal*, vol. 6, no. 3, pp. 4074–4084, 2019.

[17] C. Schuldt, H. Shoushtari, N. Hellweg, and H. Sternberg, "L5in: overview of an indoor navigation pilot project," *Remote Sensing*, vol. 13, no. 4, p. 624, 2021.

[18] Y. Rizk, M. Awad, and E. W. Tunstel, "Cooperative heterogeneous multi-robot systems: a survey," *ACM Computing Surveys*, vol. 52, no. 2, pp. 1–31, 2019.

RETRACTED

Hindawi
Journal of Robotics
Volume 2024, Article ID 9817514, 1 page
https://doi.org/10.1155/2024/9817514

Retraction

Retracted: Application of Multimedia Quality Evaluation Relying on Intelligent Robot Numerical Control Technology in New Energy Power Generation System

Journal of Robotics

Received 23 January 2024; Accepted 23 January 2024; Published 24 January 2024

Copyright © 2024 Journal of Robotics. This is an open access article distributed under the Creative Commons Attribution License, which permits unrestricted use, distribution, and reproduction in any medium, provided the original work is properly cited.

This article has been retracted by Hindawi following an investigation undertaken by the publisher [1]. This investigation has uncovered evidence of one or more of the following indicators of systematic manipulation of the publication process:

(1) Discrepancies in scope
(2) Discrepancies in the description of the research reported
(3) Discrepancies between the availability of data and the research described
(4) Inappropriate citations
(5) Incoherent, meaningless and/or irrelevant content included in the article
(6) Manipulated or compromised peer review

The presence of these indicators undermines our confidence in the integrity of the article's content and we cannot, therefore, vouch for its reliability. Please note that this notice is intended solely to alert readers that the content of this article is unreliable. We have not investigated whether authors were aware of or involved in the systematic manipulation of the publication process.

Wiley and Hindawi regrets that the usual quality checks did not identify these issues before publication and have since put additional measures in place to safeguard research integrity.

We wish to credit our own Research Integrity and Research Publishing teams and anonymous and named external researchers and research integrity experts for contributing to this investigation.

The corresponding author, as the representative of all authors, has been given the opportunity to register their agreement or disagreement to this retraction. We have kept a record of any response received.

References

[1] R. Sun and X. Dang, "Application of Multimedia Quality Evaluation Relying on Intelligent Robot Numerical Control Technology in New Energy Power Generation System," *Journal of Robotics*, vol. 2023, Article ID 7480917, 11 pages, 2023.

Hindawi
Journal of Robotics
Volume 2023, Article ID 7480917, 11 pages
https://doi.org/10.1155/2023/7480917

RETRACTED

Research Article

Application of Multimedia Quality Evaluation Relying on Intelligent Robot Numerical Control Technology in New Energy Power Generation System

Ruijuan Sun[1] **and Xiaoyuan Dang**[2]

[1]*College of Engineering, Shanxi Agricultural University, Shanxi 030800, Jinzhong, China*
[2]*College of Mobile Telecommunications, Chongqing University of Posts and Telecommunications, Chongqing 401520, China*

Correspondence should be addressed to Ruijuan Sun; 160409133@stu.cuz.edu.cn

Received 23 September 2022; Revised 2 November 2022; Accepted 23 March 2023; Published 8 April 2023

Academic Editor: Shahid Hussain

Copyright © 2023 Ruijuan Sun and Xiaoyuan Dang. This is an open access article distributed under the Creative Commons Attribution License, which permits unrestricted use, distribution, and reproduction in any medium, provided the original work is properly cited.

New energy (NE) power generation technology has become an important means to solve the problems of global energy demand and environmental governance due to its sustainability and cleanliness. However, restricted by climate and other factors, the instability of its power generation capacity has a serious impact on the voltage multimedia quality evaluation of small microgrids, which even causes damage to important equipment. This paper proposed a multimedia quality evaluation method in the new energy power generation system relying on intelligent robot numerical control technology. According to the state characteristics of different units, the expanded representation models of conventional units, wind turbines, and photovoltaic units were established, respectively. Based on intelligent robot numerical control technology, a multimedia quality monitoring model of the new energy power generation system in random production simulation was established. The planned outage condition of the unit, which was ignored by the current stochastic simulation method, has been fully considered to ensure the rationality of the simulation of intelligent robot numerical control technology. The intelligent robot numerical control technology was used to explore the expected production power change of the unit and to improve the calculation speed and accuracy. In this paper, an appropriate wind and solar power generation model was constructed based on the output characteristics of wind and solar. Secondly, the influence of random faults between units on the subsequent loading rate was studied through probability calculation. The start-stop factors of conventional units were comprehensively analyzed. Then, the expected value of unit start-stop times was obtained. The average relative error of the expected value of the power shortage of the new energy electricity generation system (EGS) was 2.45%, and the error was lower than 2.98%. In the intelligent robot numerical control technology in this paper, the planned outage condition of the unit was considered, which showed the correctness and superiority of the multimedia quality evaluation of the proposed model.

1. Introduction

Since the completion of the construction of the power system in the late 19th century, with the advancement of technology, the voltage level, installed capacity, and geographical scope have been continuously increased. However, the links supporting the power system are still composed of electromagnetic conversion devices such as rotating devices and stationary devices. The working state is stable, and the characteristics are single. Energy is a necessary material guarantee for the development of human civilization and society. It is also an indispensable source of power for modern industrial progress. Centralized power generation, interconnected power grids, and long transmission distances highlight the shortcomings of transmission power systems, such as the inability to change dispatch strategies in time and the inability to flexibly respond to load changes. Based on the abovementioned reasons, the development of new energy power generation technology research and the optimal design of various types of power systems that combine new

energy power generation with user-side needs are important in China's power grid. Under suitable weather conditions, the new energy power generation system can greatly improve the continuity and stability of the system power supply, which makes the entire power supply system more reliable. In this paper, the intelligent robot numerical control technology is applied to the new energy power generation system, which is more conducive to realizing the real-time monitoring of the new energy power generation system and improving the multimedia quality in the new energy power generation system.

When the new energy generator system is in a steady state, the intersection of static characteristics of generator group frequency determines the frequency of the system. Bao et al. put forward the idea of adapting power output to power demand [1]. Onuka et al. proposed a virtual inertial control system to reduce power system frequency fluctuations caused by renewable energy (RE) output fluctuations [2]. Jaiganesh et al. argued that the appropriate choice of renewable energy could greatly reduce the demand for fossil fuels, thereby increasing the sustainability of the electricity supply [3]. Guichi et al. developed an optimal control technique for hybrid power generation systems [4]. Meddad et al. explored the properties of piezoelectric patches using thermoelectric generators [5]. However, their proposed new energy generator system is not very stable. In this paper, intelligent robot numerical control technology was introduced to evaluate the bulk quality of multimedia phase change materials in new energy power generation systems.

The intelligent robot numerical control technology power generation microgrid has an "elasticity" effect in the face of electric energy fluctuation, which realizes the ability to suppress voltage fluctuation and power mismatch. Watanabe et al. compared the corresponding power outputs of these turbines. This dataset showed 23% annual mean wind speed and less turbulent intensity at offshore locations, resulting in a doubling of annual power generation [6]. Vereide et al. investigated the effects of surge storage tanks on governor stability, power control, and hydraulic transients in hydropower plants [7]. Roy and Rengarajan believed that distributed energy systems were gaining popularity recently because they could generate electricity with the lowest operating cost [8]. Rahmani-Andebili applied the concept of stochastic model predictive control to a problem for the first time to have a dynamic and adaptive future in optimization problems. Uncertainty and variability in renewable energy were addressed [9]. Magdy et al. believed that the interconnection between the digital and analog parts was usually achieved through sampling and control equipment [10]. However, their proposed intelligent robot numerical control technology has not been applied in practice.

In the new energy power system represented by photovoltaic power stations and wind farms, it is necessary to conduct a detailed simulation of the output of photovoltaic power stations and wind farms in order to calculate the relative economics and reliability. In this way, the combination of conventional units is reasonably arranged to meet the needs of actual dispatching so as to make full use of renewable solar and wind energy and reduce environmental pollution and power generation costs. Reasonable evaluation indicators are established. The peak-shaving problem brought by the grid connection of new energy to conventional units and the impact on the low-carbon benefit of the system are evaluated. On the one hand, the integration of new energy into the grid greatly reduces the carbon emissions of the system. On the other hand, it is inevitable that the conventional units are frequently started and stopped due to their own randomness. Excessive start-stop operation of conventional units increases additional coal consumption and reduces the low-carbon benefit of the system. When the load is 25% of the rated load (6 s), the output current of the load terminal is 0.66 A. The method in this paper reduces CO_2 emissions by about 60,000 t.

2. Application of the Multimedia Quality Evaluation Method

2.1. Application of Intelligent Robot Numerical Control Technology in the New Energy Power Generation System. In the traditional electricity generation system, the transient characteristics of electromagnetic conversion devices such as synchronous motors in the time scale corresponding to the primary frequency modulation determine the electromagnetic transient process of the electricity generation system. The core content of electricity generation system transient analysis and electricity generation system steady-state analysis of the traditional electricity generation system is formed. In the whole process of the electricity generation system being gradually assimilated by the amount of power electronic equipment, transient characteristics of the ubiquitous power electronic equipment and the traditional electromagnetic conversion equipment are obviously different. The transient component current quickly saturates the transformer core. The secondary current of the transformer is distorted, which may cause the protection to fail or reduce the reliability and accuracy of the relay protection. When the equipment is disturbed and a transient event occurs, the power electronic equipment needs to rely on the corresponding control and protection circuit to ensure the safety of the equipment. During stable operation, the power flow in the electricity generation system becomes a bidirectional flow (the steady-state distribution of voltage (each node) and power (active power, reactive power) (each branch)) due to the power electronic equipment, which is very different from the transmission route of energy from the power generation end to the consumer end of the traditional electricity generation system. Therefore, the controlled transient characteristics of power electronic equipment and the steady-state characteristics of bidirectional energy flow have changed the traditional operation mode of the EGS in which the direction of the power flow is fixed and the transient characteristics are stable. It affects the security and stability of the traditional operating state of the EGS [11]. The typical structure of the NE hybrid EGS is shown in Figure 1.

At present, the main way to develop and apply new energy is still distributed or lumped grid-connected power generation (it refers to the connection between the

RETRACTED

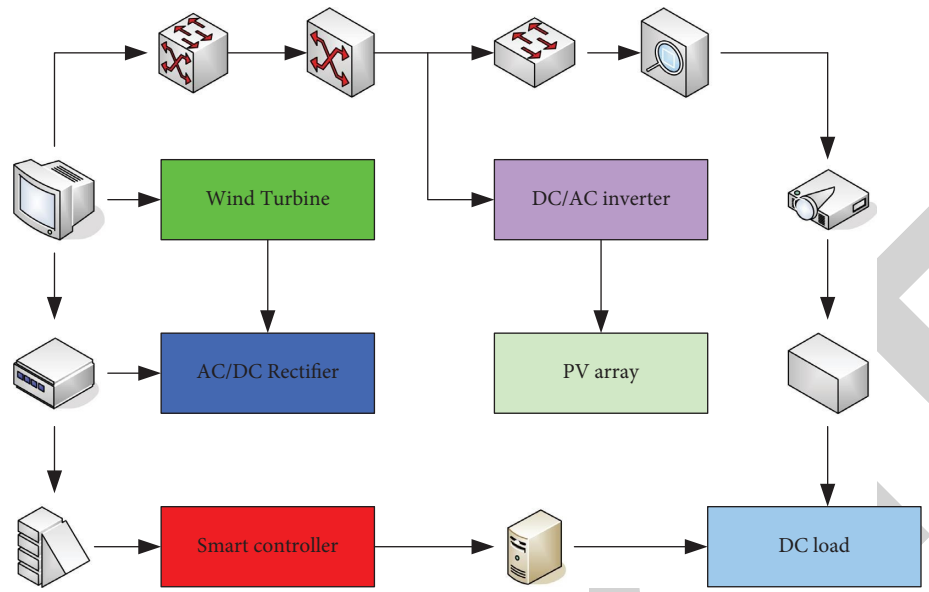

Figure 1: Typical structure of NE hybrid EGS.

transmission line of the generator set and the transmission network). However, a large amount of renewable energy is distributed in remote areas. The construction sites of wind farms and photovoltaic power stations are relatively remote, which are mostly scattered in remote areas. It needs to be transmitted to the remote user side through the power grid to complete the consumption and use of electric energy. In order to transmit the generated electric energy, the equivalent grid impedance (the obstruction of current flow in circuits with resistance, inductance, and capacitance) formed by the transformers in the transmission and distribution network and the distribution parameters that cannot be ignored in the long-distance transmission line may cause the failure of the damping strategy of the grid-connected inverter itself. Thus, the resonance between the grid-connected power generation system and the grid is induced. Such grids are also called weak grids [12]. Due to the existence of grid impedance, the grid becomes weak. At the same time, the grid impedance value is not stable. On the other hand, a large number of grid-connected inverters integrated into the power grid, as the interface device between the new energy and the power grid, are coupled with each other to form a complex high-order nonlinear time-varying system. This is very easy to form a coupled resonance (which can transmit relatively large power, reaching the kW level, and is sensitive to distance. The increase of distance seriously affects the transmission efficiency) with the grid impedance, thereby causing the power system to become unstable. The existence of weak grid impedance and grid-connected power generation system constitute harmonic interaction, which further exacerbates the resonance. It may cause harmonic amplification at the grid connection point, resulting in overvoltage, overcurrent, and other undesirable situations, resulting in power quality problems. It even causes the grid-connected inverter to disconnect from the grid due to faults and endangers the safe and stable operation of the power system.

Considering that the voltage source should be stable without load and the ideal voltage source with load, the stability of the system can only consider the function on the right, which is defined as $H(s)$ [13].

$$H(s) = \frac{Z_s(s)}{1 + Z_l(s)}. \tag{1}$$

Impedance adapters (which adjust the wavelength of the transmission line by changing the impedance) require virtual impedance at high frequencies. Therefore, its filter must have a wide passband for middle and high frequencies. However, at the same time, it must have a sufficient suppression effect on high-frequency switching ripple. The filter of the impedance adapter needs to be designed according to the following two principles. One is to meet the requirements of the cutoff frequency, which ensures that the impedance adapter can have virtual resistance characteristics in the high frequency band. At the same time, higher frequency switching harmonics do not leak. Second, the dynamic response is required to be fast enough, which can quickly track the present harmonic level of the grid-connected access point, as well as a stable virtual resistance (it can be set arbitrarily, and its temperature characteristics can also be set). The relationship between output and input voltage can be expressed as follows [14]:

$$G_{LC}(s) = \frac{1}{L_1 C s^2}. \tag{2}$$

The empirical formula for the output power of photovoltaic panels is as follows:

$$Cs = \sigma E. \tag{3}$$

In the formula, Cs represents the output power of the photovoltaic cell [15].

The unpredictability of light intensity with climate determines that photovoltaic output is also random. However, different from the regular characteristics of wind speed

RETRACTED

distribution, the light has the characteristics of "nocturnal and diurnal." Sunlight is generally only possible during the day. The light intensity is at its maximum at noon. The light intensity is weak in the early morning and evening, and there is no sunlight at night. The one-day change of visible light intensity is more consistent with the one-day change of load.

Therefore, unlike the randomness of wind power output, which has antipeak-shaving characteristics, the grid-connected photovoltaic power generation has a relatively stable output. Conventional energy units do not reduce the economics of their own operation by absorbing the volatility of photovoltaic output. It can be seen that the environmental friendliness of photovoltaic power generation is more prominent. For the photovoltaic power generation system, the randomness of its output comes from the randomness of the weather on the one hand and the failure of its own components on the other hand. In the modeling of photovoltaic power generation output, the influence of photovoltaic array and inverter faults is mainly considered. The series-parallel combination of photovoltaic components is as follows. A photovoltaic array consists of n strings of photovoltaic cells in parallel. The working states of each string of photovoltaic cells are independent of each other and are connected to an inverter in parallel without any influence. As long as the inverter works normally, the derating capacity (when the system is in a derating operation state, the transmission capacity of the system is reduced due to equipment or other nonscheduling reasons) of the system depends on the working state of the n-series photovoltaic panel group. Then, assuming that the failure rate of each string of photovoltaic cells is P_1 and the failure rate of the inverter is P_2, the rate of the i-th derating operating state of the photovoltaic inverter group is as follows [16, 17]:

$$P_{S,i} = C_n^i P_1 (1 - P_2). \tag{4}$$

The basic requirement for the design of an independent new energy hybrid power generation system is to meet the power load in the area covered by the power generation system and the needs of reliable operation of the power generation system. The capacity and operation control strategy of each component of the system is determined. Wind power generation and photovoltaic array output can meet the requirements of most electricity loads, which minimizes the number of diesel generator starts, that is, to calculate the total photovoltaic cell capacity, wind turbine power, and battery capacity required for the hybrid power generation system to work reliably throughout the year. At the same time, attention should also be paid to the relationship between the coordination system reliability and its economy. It is necessary to minimize the power generation cost of the hybrid system while meeting the maximum reliability [18].

2.2. Multimedia Quality Evaluation Platform Relying on Intelligent Robot Numerical Control Technology. The configuration of rotating reserve capacity can ensure the reliability of system operation. However, the size of the spare capacity is the key to choosing between two contradictory indicators of system economy and reliability. Therefore, the configuration of the size of the reserve capacity can be combined with the operation risk analysis theory and the forecast error of wind power generation. A set of backup risk theory strategies considering the influence of wind power forecast errors on system operation reliability are formulated. Its multimedia quality evaluation is as follows [19]:

When the predicted power value of wind power is lower than the actual value of wind power, it means that wind power is underestimated, which results in those wind power resources that cannot be fully absorbed. At this time, it is necessary to increase the negative spinning reserve of the system on the basis of the original planned negative spinning reserve [20]. Negative spinning reserves are added to the model to underestimate costs.

The purpose of introducing robots is to improve efficiency, so the bottleneck process can be considered first. Generally, the process with a longer processing time is the bottleneck process. The use of robots can reduce auxiliary time, thereby shortening the production cycle of the entire power generation process. The robot itself is a kind of automation equipment, and the equipment integrated with it should also have an automatic working mode. It is equipped with automatic fixtures and can provide feedback working status signals to the outside world so that the best performance of the two can be exerted. After the robot model is determined, the parameters such as the allowed maximum speed and maximum acceleration of each axis have been determined. The running time in a single cycle mainly depends on the posture and movement distance of the robot end. The evaluation of the movement distance in the operation space refers to the minimum sum of the distances moved by the end of the robot in a single cycle. In practical applications, the end of the robot can choose a variety of moving methods between the target points of the operation. The actual moving distance is difficult to determine. According to the principle of "the shortest line segment between two points," this indicator is replaced by the sum of the Euclidean distances between the target points visited by the robot in turn. Its mathematical expression is as follows [21, 22]:

$$\min D = \sum_{i,j=1}^{m} D_{ij}. \tag{5}$$

Based on the evaluation function with the smallest movement distance in the joint space, its mathematical expression is as follows:

$$\min F = \sum_{i=1,j=i+1}^{m-1} \sum_{k=1}^{n} \left[q_{ik} - q_{jk} \right]. \tag{6}$$

In the formula, m is the number of equipment (that is, job target points) that the robot needs to access in one cycle.

Based on the layout evaluation function with the shortest robot movement time in the cycle, its mathematical expression is as follows [23]:

$$\min T = \sum_{i,j=1}^{m} b_{ij} + b_{d0} d_0. \tag{7}$$

The high-energy load has the characteristics of interruptible, transferable, continuous adjustment, rapid

RETRACTED

adjustment, and group switching. It has the advantages of large power load capacity, strong adjustment ability, and good peak shaving and valley filling. According to the electricity consumption rules of different users, the electricity consumption time of various users is arranged and organized reasonably and in a planned way. The high energy load is used to make up for the insufficiency of conventional power sources in regulating the fluctuation of large-scale wind and solar farms. The adjustment range can reach 30%–100% of the production load capacity. It is the best choice to change the wind power consumption level with suppressed wind power output fluctuation to realize the adjustment of the output fluctuation of the wind and solar power plant group through the coordinated optimization of the high load energy load and the conventional power supply. When evaluating the multimedia quality in the NE power generation system, the mathematical model of the adjustable load is as follows [24]:

$$P_{Ld_i}^{t} = P_{Ld_i}^{t-1} - x_i^t. \tag{8}$$

At present, with the vigorous development of energy storage technology, especially the increasingly mature energy storage technologies such as batteries, compressed air, and pumped storage, more and more energy storage systems have been applied in power systems with new energy characteristics. Through the charging and discharging characteristics of the energy storage system itself, the system fluctuations caused by new energy power generation can be suppressed. However, the energy storage system itself is relatively expensive. If the location and capacity configuration are unreasonable, it would not only cause waste of resources but also increase the unnecessary investment of the system. The specific objective function of multimedia quality evaluation in the new energy power generation system is as follows:

$$\begin{aligned} \min f_1 &= \sum_{i=1}^{6} b_i \cdot \cos t_i, \\ \min f_2 &= \sum_{k=1}^{n} V_k^{\text{spec}} / V_k^{\max}. \end{aligned} \tag{9}$$

In the formula, n is the total number of system nodes. The first objective function needs to consider the total cost of running. The system voltage fluctuates wildly as the output of the wind farm changes. Therefore, the node voltage of the new energy power generation system is improved by using the second objective function.

The multimedia quality evaluation platform relying on intelligent robot numerical control technology is shown in Figure 2. The interaction of the robot with the lathe is more complicated because the robot itself is located inside the lathe and has many moving parts. The interior space of the lathe is also irregular. It is very complicated and even difficult to perform interference detection directly on each geometry that constitutes a new energy power generation equipment. New energy power generation equipment with complex shapes is usually surrounded by a simple enclosure. If the simple bounding volume is detached, the device must be detached. To realize the multimedia status monitoring and control of the new energy power generation system, the signal lines are directly drawn from both ends of the indicator lights or buttons of the operation panel. It is transferred to the input and output terminals of the system controller through the intermediate relay (which are often used to transmit signals and control multiple circuits simultaneously and can also be used to directly control small-capacity motors or other electrical actuators). Using this method, the input and output of the system controller and the indicator lights or buttons of the operation panel are activated, which forms a "parallel" form of multimedia quality feedback and control for the new energy power generation system.

With the continuous improvement and upgrading of the CNC system, drive device, and main structure, the production efficiency (feed speed, machining accuracy, and so on) of CNC machine tools continues to be improved. However, the operating processes connected to it, such as workpiece loading and unloading and logistics transportation, have not grown at a matching rate. Robots and CNC machine tools are integrated into flexible manufacturing cells/systems, which can play advantages of accurate robot movements, sustainable work, and precise repeatability. This removes the constraints on the overall productivity improvement of the CNC machine work cell. The introduction of robots in the production workshop generally follows the following steps:

(1) *Feasibility Analysis*. On the basis of on-site investigation of the production workshop and reference to similar cases, the technical feasibility and advancement are analyzed. From the perspective of capital input and output, the possibility and rationality of introducing robot numerical control technology are considered. Combined with the site environment, the feasibility of project implementation is considered.

(2) *Detailed Design and Production Line Planning of Robotic Work Cells*. It includes new energy power generation system planning, layout design, auxiliary equipment selection, control system design, engineering construction plan, and so on.

(3) *Physical Construction and Trial Operation*. According to the design scheme, the installation and debugging of hardware and software are completed and the trial operation is started. In response to the problems that have arisen, they are improved. Multimedia quality assessments are carried out, and managers and operators are trained.

3. Multimedia Quality Evaluation Results

New energy power generation has many advantages, but it also has its own unique constraints. Wind and solar energy are taken directly from nature. Therefore, new energy is greatly affected by natural factors such as season and climate, which makes it more uncertain than conventional power generation. The uncertainty of photovoltaic power

RETRACTED

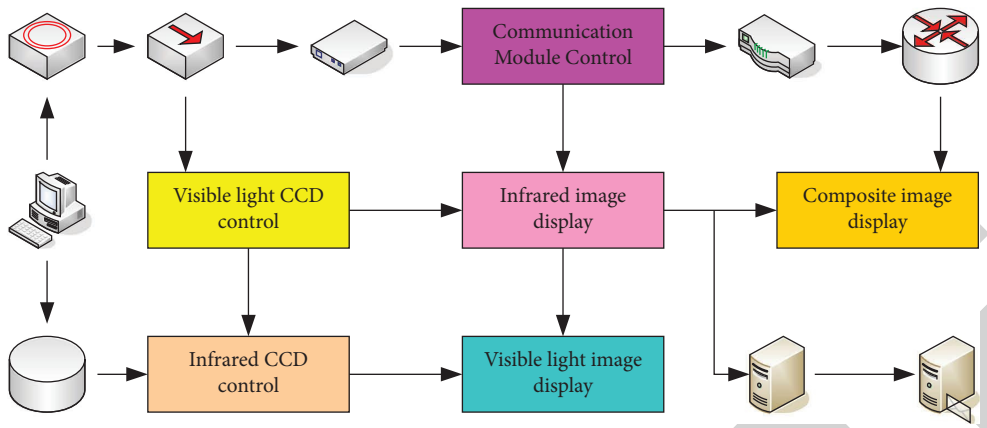

Figure 2: Multimedia quality evaluation platform relying on intelligent robot numerical control technology.

generation is mainly manifested in the randomness of the light intensity and the ambiguity of the components of the photovoltaic system. The integration of NE into the grid is bound to change the output mode of traditional energy power generation, which makes the power generation output more random and uncontrollable. It has become an important restrictive factor affecting the safe, stable, economical, and efficient operation of new energy power generation systems.

The relative errors of the generating units GE1, GE2, and GE3 are about 0%, 0.83%, and 2.45%, respectively. In the multimedia quality evaluation, the average relative error of the expected value of the power shortage of the NE EGS is 2.45% and the errors are all within 2.98%. The effects of different methods on power generation are shown in Table 1.

To illustrate the effectiveness of the intelligent robot numerical control technology in this paper and evaluate the effect of new energy grid connection on the power system, the simulation results of each scenario are shown in Table 2 (Scenario 1: new energy units are directly added to the system to cooperate with the original units. Scenario 2: new energy units of equal capacity based on intelligent robot numerical control technology are used to replace conventional units. Scenario 3: new energy units are simply added to the original system). By comparing the simulation results of scenario 1 and scenario 3, it is found that scenario 3 simply adds new energy to the original system. Its wind power generation is 128177 MW, and photovoltaic power generation is 31631 MW. This shows that although the output power of wind turbines and photovoltaic generators is intermittent and fluctuating, there is still a considerable confidence capacity. At the same time, the reliability indicators of the system in scenario 3, that is, the probability of insufficient power and the expected value of insufficient power, are both lower than those in scenario 1. This shows that the new energy unit directly added to the system can cooperate with the original unit to participate in the load balance, which effectively improves the reliability level of the multimedia new energy system. However, the new energy injection changes the energy structure of the system. The randomness and uncontrollability of its output power greatly affect the economy of some conventional thermal power generating units. Direct connection of NE to the grid makes a significant contribution to the system load balance and reliability. However, this is premised on sacrificing the economy of the operation of conventional thermal power generating units. Therefore, the integration of new energy into the grid needs to balance the interests of traditional energy units. The formulation of effective incentive measures and management mechanisms can not only ensure the economy of traditional energy but also actively consume new energy, thus greatly improving the efficiency of energy conservation and emission reduction of the power system.

Comparing the simulation results of scenario 1 and scenario 2, it is found that scenario 2 replaces conventional units with new energy units of equal capacity based on intelligent robot numerical control technology. Its wind power generation capacity is 128,001 MW, and photovoltaic power generation capacity is 31,522 MW. The total power generation of new energy replacing conventional units is 159,523 (the sum of the two) MW. According to statistics, the load of the NE electricity generation system based on intelligent robot numerical control technology is 1300731 MW in one month. The new energy power generation system based on intelligent robot numerical control technology has contributed nearly 12.3% of the power generation instead of conventional units. This further shows that the development of new energy power generation has practical significance to replace the consumption of fossil fuels. However, comparing the reliability indicators of the systems in scenario 1 and scenario 3, it is found that the probability of insufficient power and the expected value of insufficient power in scenario 3 have nearly tripled. This shows that the great influence of climate cannot guarantee full power generation at every moment.

Comparing the simulation results of scenario 2 and scenario 3, it is found that the wind power generation and photovoltaic power generation of scenario 2 are slightly smaller than those of scenario 3. This is because, under the policy of encouraging the full purchase of clean energy, the general situation is to give priority to the dispatch of clean energy power generation. However, since scenario 2 is directly connected to the new energy unit based on intelligent robot numerical control technology on the basis of the

RETRACTED

Table 1: Effects of different methods on power generation.

Different units	Relying on intelligent robotic control technology (kW·h)	Traditional methods (kW·h)	Insufficient battery relative error (%)
GE1	780	780	2.2
GE2	476	480	2.6
GE3	99.5	102	2.55

Table 2: Simulation results for each scenario.

Scenes	Wind power generation volume (MW)	Photovoltaic power generation (MW)	Probability of loss of load (%)	Expected loss of electricity (MW)	Unit capacity start and stop frequency
Scene 1	0	0	0.091	70.003	10.072
Scene 2	128001	31522	0.048	40.221	12.893
Scene 3	128177	31631	0.272	210.464	12.166

original system, that is, there are 2 more conventional units compared to scenario 3. Therefore, the choice of the grid-connected form of new energy generating units is crucial to the system peak regulation, the rationality of dispatching of conventional units, and the multimedia quality evaluation of new energy consumption.

Comparing the start-stop frequency indicators per unit capacity of scenarios 1, 2, and 3, it is found that the start-stop frequency per unit capacity of the system is greater than the random production simulation results of the new energy power generation system without the use of intelligent robot numerical control technology, whether it is simply adding wind turbines and photovoltaic generators or replacing conventional units with new energy units. The increase in the start-stop frequency index of unit capacity indicates that more peak-shaving units are needed to balance the intermittent and fluctuating output of new energy units. On the one hand, the frequent start and stop of these thermal power units can easily damage the equipment. On the other hand, excessive start-stop operation also consumes additional fossil fuel, which has a certain positive impact on the low-carbon benefit of the system. Therefore, the integration of NE into the grid greatly affects the economics of conventional units. The grid-connected power of new energy cannot be increased without limit. It is necessary to balance the relevant interests, in order to mobilize the enthusiasm of the relevant stakeholders to consume new energy, to maximize the environmental benefits and economic benefits.

Comparing the simulation results, it is found that the total fuel cost and the total environmental cost of the system are reduced in scenarios 2 and 3 with the NE power generation system based on the intelligent robot numerical control technology compared with scenario 1 without the NE power generation system based on the intelligent robot numerical control technology. At the same time, the CO_2 emission of the system is reduced by about 60,000 tons. This shows that new energy sources such as wind farms and photovoltaic farms can effectively reduce the carbon emissions of the power system, thereby reducing the fuel cost of the system. It also improves environmental benefits and low-carbon benefits, which is of great significance to the realization of low-carbon electricity in the system. However, on the other hand, it also shows that the power generation of conventional thermal power is replaced. The economic benefits of thermal power plants are being challenged. Scenario 3 increases the power shortage cost of the system when the new energy unit replaces the thermal power of the same capacity. Therefore, new energy has a certain confidence capacity. For conventional units with higher reliability than the same capacity, the reliability index of the NE electricity generation system with intelligent robot numerical control technology needs to be known before determining the penetration rate and grid connection scale of new energy. The economic indicators of different scenarios and the CO_2 emissions of the system are shown in Figure 3.

Conventional units participate in peak shaving more frequently, which consumes higher costs. It cannot be ignored in the economic evaluation of power supply with new energy. Therefore, how to include both conventional indicators and comprehensive analysis of new energy grid-connected benefits in the power system production simulation results, as well as low-carbon benefit indicators that reflect the dynamic start and stop of new energy units that rely on robotic numerical control technology, is crucial. Figure 4 shows the change in the expected power production of conventional units before and after simply adding a new energy power generation system. The grid-connected wind farms and photovoltaic farms have different capacities to replace units at different load positions. For example, for the units that undertake the base load, the power output is basically unchanged; that is, new energy cannot replace the power generation of such units, such as the No. 3 and No. 9 base-load units. The output change of the waist-loaded unit is also relatively small. The reduction ratio is about 9% to 23%, such as the No. 8 and No. 6 waist-loaded units. The replacement rate of peak load units is the largest. For example, the replacement ratio of No. 1 and No. 5 units is over 74%. This reduces the peak-shaving capacity of the system and is not conducive to system peak shaving. This is why, units under peak load generally require good peak-shaving

RETRACTED

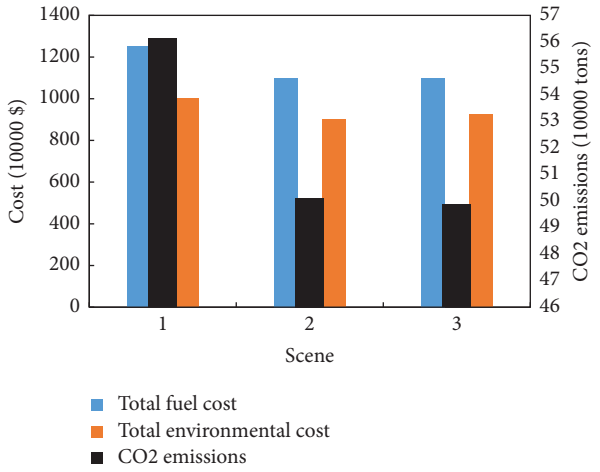

Figure 3: Economic metrics and system CO_2 emissions for different scenarios.

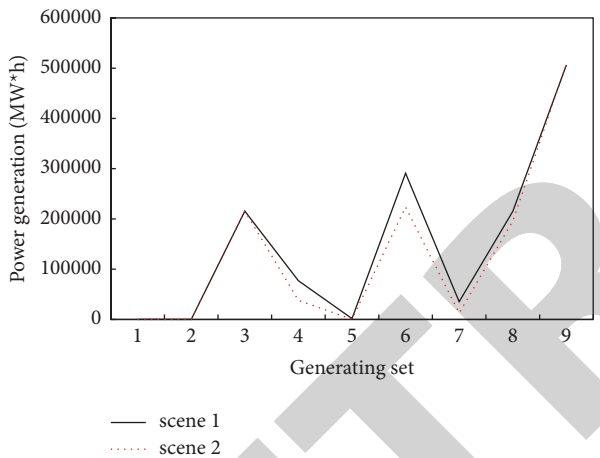

Figure 4: Changes in the expected electricity production of conventional units before and after simply adding a new energy power generation system.

performance, which can quickly start and stop, or transfer to hot standby. On the other hand, this also means that due to coping with the volatility and intermittency of NE, peak-load units spend more on start-stop operations.

With the continuous increase of the scale of NE power generation and the capacity of a single unit, the randomness and uncertainty of its own output also have a positive impact on the operation of the power system. The uncontrollable output of new energy sources affected by the environment and climate makes them not have the good dispatchability of conventional units. The output characteristics of different NE are different, which requires the selection of different distribution models as the multimedia quality evaluation and estimation scheme. The error of the predicted output of different distribution models is also different. This is obviously complicated by the use of forced outage rates to characterize random failure states for conventional units. Taking wind farms as an example, the wind turbine output should also consider the correlation of different wind farms when necessary, which is sometimes affected by wind direction and wake effects. The photovoltaic power generation needs to consider the component failure rate of the photovoltaic array. Therefore, it is particularly important to fully consider the natural environmental factors and distribution characteristics that affect new energy and to construct a new energy source that conforms to its respective output characteristics.

Due to the differences in the spatial locations of wind farms 1, 2, and 3, their respective outputs are affected by the wake effect of wind energy, the geographical dispersion effect of wind farms, and different climates, which lead to different output fluctuations of the three wind farms. However, with the increase of the coverage area and the number of wind farm groups, the irrelevance of the spatial position makes the output of each subwind farm also show irrelevant characteristics. Therefore, to a certain extent, the fluctuations of each subwind farm in the wind farm group cancel each other out, which shows the complementary characteristics of the wind farm group. It can alleviate the influence of wind power output fluctuation and intermittent so as to achieve the effect of reducing the total output fluctuation of the wind farm group. The output fluctuation of the wind farm is shown in Figure 5.

The simulation model of the solar photovoltaic power generation system based on the intelligent robot numerical control technology is built on the MATLAB (matrix and laboratory) simulation platform. Simulation experiments of 3000 W photovoltaic cells are carried out in the afternoon session. The light intensity of solar photovoltaic cells has dropped from 1000 W/m^2 to 500 W/m^2. The weather changes from noon to afternoon in autumn are simulated. Figure 6 shows the output voltage waveform of 3 solar cell arrays in series (3000 W). When the light intensity decreases, the solar output voltage also decreases. The output voltage waveform of the solar cell array is easily affected by environmental factors, which may easily lead to the defect that the power supply to the load is unstable. Therefore, it is necessary to establish an energy storage system that uses a bidirectional converter to control charge and discharge. Energy conversion of the energy storage system is realized through the robot numerical control technology of controlling the nonlinear bidirectional converter. The bidirectional flow of energy is completed, thereby realizing the instantaneous power balance and voltage stability control of the clean energy power generation system.

Figure 7 shows the output current and voltage waveforms when the load is 25% of the rated load. When the load is 25% of the rated load (6 s), the output current of the load terminal is 0.66 A and the output voltage is 99.34 V. Eventually, a steady state can be achieved, which satisfies the multimedia quality design requirements.

The reliability indicators under different system basic configurations are shown in Figure 8. The reliability of adding energy storage to power generation systems with different new energy sources is higher than that of not installing energy storage. Under the same installed capacity, the reliability of light/diesel/storage system is higher than that of wind/light/diesel/storage and wind/diesel/storage

RETRACTED

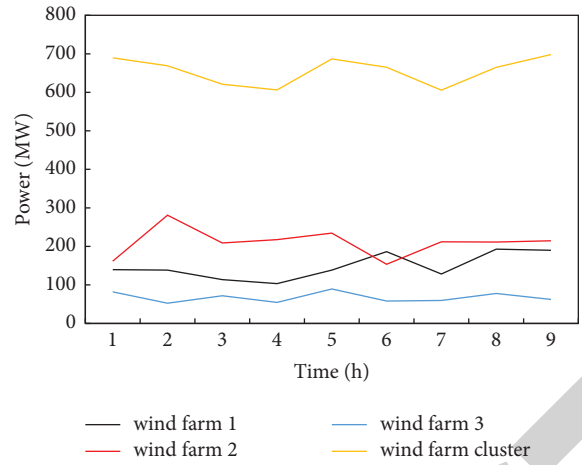

Figure 5: Output fluctuations of wind farms.

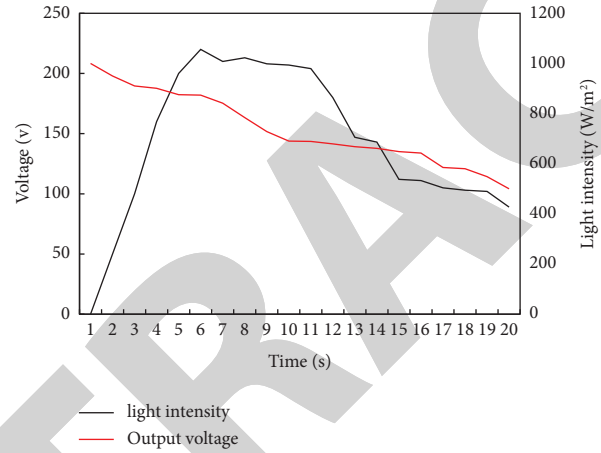

Figure 6: Output voltage waveform of 3 solar cell arrays in series (3000 W).

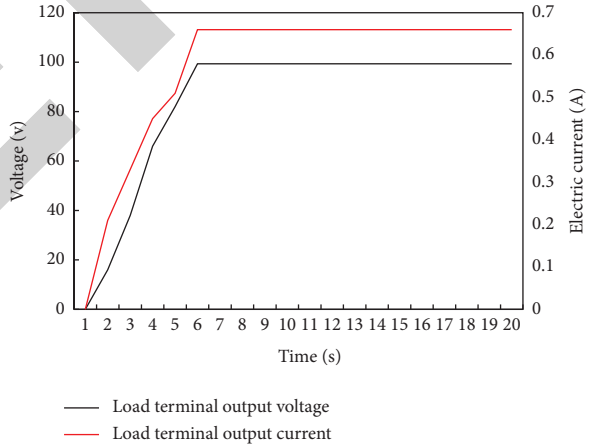

Figure 7: Output current and voltage waveforms at 25% of the rated load.

system. This is due to the uncertainty and randomness of wind speed, which makes the reliability of the system with wind power generation lower than that without a wind power generation system. In the wind power generation system, the reliability of the wind/light/diesel/storage power generation system is higher than that of the wind/diesel/storage power generation system. Therefore, the reliability of the wind/light/diesel/storage system with photovoltaic power generation is higher than that of the wind/diesel/storage power generation system without photovoltaic power generation. However, in the absence of light at night, diesel engines are basically used to generate electricity. The

RETRACTED

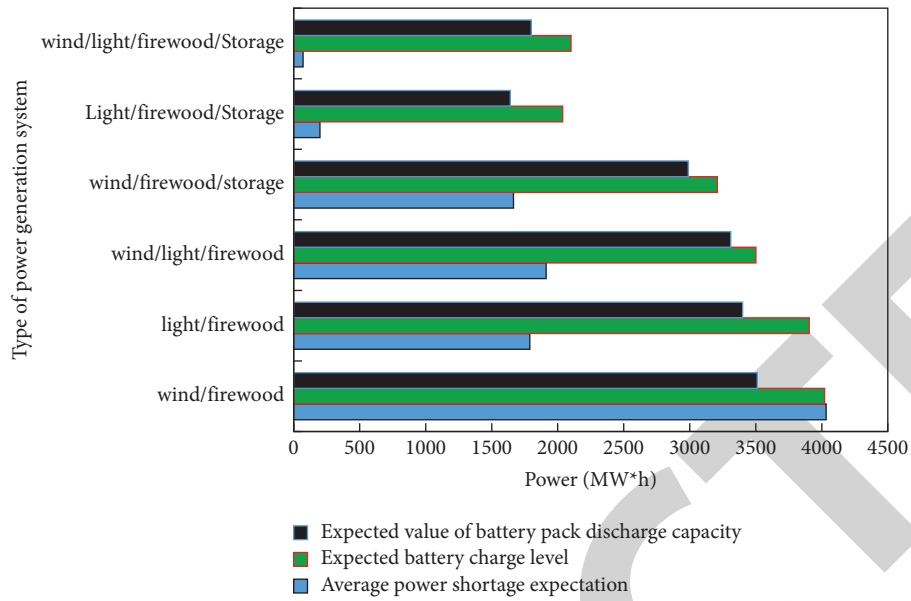

Figure 8: Reliability metrics for different system basic configurations.

consumption of diesel oil is more, and the cost is higher. Therefore, it is not used as a research object. Considering the complementary factors between economy and environmental protection and photovoltaic and wind power generation, the reliability of wind/solar/diesel/storage system is the best.

The development of NE and the reduction of excessive use of fossil energy have become urgent problems for countries to solve. Especially in recent years, global warming and more environmental pollution problems have restricted the healthy development of human beings. The vigorous development of RE is a very important part in developing a low-carbon economy, alleviating energy supply pressure, implementing energy development strategies of various countries, and improving the living environment of human beings. In the new energy power system represented by photovoltaic power stations and wind farms, output simulation is required in order to calculate the relative economics and reliability. In this way, the combination of conventional units is rationally arranged and the actual dispatching needs are met, thereby making more full use of renewable solar and wind energy, which reduces environmental pollution and power generation costs. The influence of the random characteristics of NE sources on the thermal power units of the system should also be considered. By establishing reasonable evaluation indicators, the peak-shaving problem brought by the grid connection of NE to conventional units and the impact on the low-carbon benefit of the system are evaluated.

4. Conclusion

With its sustainability and cleanliness, new energy power generation technology has become an important means to solve the problems of global energy demand and environmental governance. Among them, wind power generation projects and photovoltaic power generation projects have been vigorously promoted all over the world. In view of the lack of assessment of the impact of the new energy grid connection on the power system, this paper evaluated the multimedia quality and low-carbon benefit indicators of the new energy power system from both positive and negative aspects. On the one hand, the NE power generation system relying on intelligent robot numerical control technology has greatly reduced the carbon emissions of the system. On the other hand, the excessive start-stop operation of conventional units has increased the extra coal consumption to reduce the low-carbon benefit of the NE power generation system, which has improved the quality of multimedia evaluation in the environment of the NE power generation system. For large power grids, due to its large structure and high energy capacity, it has a certain ability to regulate voltage fluctuations, which has strong integration for a new energy power generation system with an appropriate proportion. However, in the microgrid, its simple structure and small energy capacity make it to not have good self-regulation ability. When a large number of new energy systems are incorporated into it, it would cause serious voltage fluctuations in the microdot grid system. The large voltage quality fluctuations in the microgrid may also hinder the normal operation of important equipment on the load side, which may seriously cause failure. With the development of multimedia new energy, factors such as climate have caused instability and intermittent problems in power output. In future works, it is necessary to consider the factors that bring trouble to the efficient utilization of new energy power, including some problems that are difficult to predict, difficult to control, difficult to schedule, and system fluctuations.

Data Availability

The data used to support the findings of this study are available from the corresponding author upon request.

RETRACTED

Hindawi
Journal of Robotics
Volume 2023, Article ID 9780273, 1 page
https://doi.org/10.1155/2023/9780273

Retraction

Retracted: Application of 5G Mobile Communication Technology Integrating Robot Controller Communication Method in Communication Engineering

Journal of Robotics

Received 19 December 2023; Accepted 19 December 2023; Published 20 December 2023

Copyright © 2023 Journal of Robotics. This is an open access article distributed under the Creative Commons Attribution License, which permits unrestricted use, distribution, and reproduction in any medium, provided the original work is properly cited.

This article has been retracted by Hindawi following an investigation undertaken by the publisher [1]. This investigation has uncovered evidence of one or more of the following indicators of systematic manipulation of the publication process:

(1) Discrepancies in scope
(2) Discrepancies in the description of the research reported
(3) Discrepancies between the availability of data and the research described
(4) Inappropriate citations
(5) Incoherent, meaningless and/or irrelevant content included in the article
(6) Manipulated or compromised peer review

The presence of these indicators undermines our confidence in the integrity of the article's content and we cannot, therefore, vouch for its reliability. Please note that this notice is intended solely to alert readers that the content of this article is unreliable. We have not investigated whether authors were aware of or involved in the systematic manipulation of the publication process.

Wiley and Hindawi regrets that the usual quality checks did not identify these issues before publication and have since put additional measures in place to safeguard research integrity.

We wish to credit our own Research Integrity and Research Publishing teams and anonymous and named external researchers and research integrity experts for contributing to this investigation.

The corresponding author, as the representative of all authors, has been given the opportunity to register their agreement or disagreement to this retraction. We have kept a record of any response received.

References

[1] Y. Chen, "Application of 5G Mobile Communication Technology Integrating Robot Controller Communication Method in Communication Engineering," *Journal of Robotics*, vol. 2023, Article ID 1857590, 9 pages, 2023.

Hindawi
Journal of Robotics
Volume 2023, Article ID 1857590, 9 pages
https://doi.org/10.1155/2023/1857590

RETRACTED

Research Article

Application of 5G Mobile Communication Technology Integrating Robot Controller Communication Method in Communication Engineering

Yu Chen

Office of Academic Affairs, Chongqing Industry Polytechnic College, Chongqing, China

Correspondence should be addressed to Yu Chen; chenyu2@cqipc.edu.cn

Received 6 September 2022; Revised 19 October 2022; Accepted 28 March 2023; Published 8 April 2023

Academic Editor: Iqbal Ahmad

Copyright © 2023 Yu Chen. This is an open access article distributed under the Creative Commons Attribution License, which permits unrestricted use, distribution, and reproduction in any medium, provided the original work is properly cited.

Following the ongoing advancement of the communication industry, data traffic and information have achieved rapid growth. As the core technology of contemporary mobile communication, 5G technology can not only meet the transportation needs of massive data traffic but also be expanded to various industries, expanding the development field of intelligent communication and realizing further improvement of production efficiency. At present, 5G mobile communication technology is widely used in communication engineering, providing effective technical support for engineering construction and operation. However, while the progress of the times brings innovation and refinement in mobile communication technology, it also increases the complexity of market development, in this context, the practical application of 5G technology in communication engineering is limited, which limits the development of both. In order to solve this dilemma, this paper integrated the communication method of the robot controller, and based on the analysis of the characteristics and application status of mobile communication technology, the application of 5G technology in communication engineering was deeply studied. In order to prove the effect of the robot controller communication method, in this paper, simulation experiments were carried out to analyze the application effect of 5G in communication engineering from three aspects of throughput rate, energy efficiency, and signal suppression effect and to compare it with traditional communication methods. The results of the signal suppression experiment showed that the average peak value of the signal under the traditional communication method was 18.134 dB, and the average peak value of the signal under the method in this paper was 11.296 dB, which showed that the 5G technology integrating the communication method of the robot controller is more practical in communication engineering.

1. Introduction

In the information age, the development of mobile communication technology is becoming more and more mature, which not only improves the efficiency of social production and life but also enriches the material and spiritual life of the masses. With the widespread popularization of 5G technology, the mobile communication industry is gradually developing towards high quality. As an improvement and upgrade of 4G technology, 5G technology can realize the rapid transmission of information data flow in communication engineering, improve the construction level of communication projects, and provide effective guarantee for the subsequent development of intelligent network communication. However, due to the uncertainty of development and the complex market environment and structure, the practical application of 5G technology in communication engineering is not ideal, and there are still many problems in both. Therefore, it is necessary to strengthen the application value of 5G mobile communication technology in communication engineering and improve the development adaptability and matching degree of the two. The communication method of the robot controller plays an extremely critical auxiliary role in the processing of the target task. As a communication mechanism between independent machine systems, it is also of great significance to the realization of the control target. At present, with the in-depth development of robot technology and wireless

communication, the communication method of robot controller has achieved good application results and has made achievements in satellite navigation, geological survey, and other professional fields. It can improve the stability of communication and is of great significance for promoting the application and development of 5G technology in communication engineering.

In recent years, 5G mobile communication technology has been widely used in communication engineering, and many scholars have carried out research on it. Bhattacharjee proposed a 5G mobile communication authentication technology system based on artificial intelligence and applied it in communication engineering to solve the corresponding uncertainty problem [1]. Hussain and Audah proposed hard-decision decoding for orthogonal frequency division multiplexing systems to improve the data reliability of 5G mobile communication technology on multipath fading channels in communication engineering [2]. Gharsallah et al. proposed a new optimized vertical handover method to improve the service quality of 5G mobile communication technology and realize seamless vertical handover in communication engineering [3]. Abbas et al. believed that 5G network can achieve extremely low latency and high-speed data transmission and introduced its application and latest development in communication engineering [4]. In order to enhance the manageability and resilience of future 5G in communication engineering, an end-to-end hybrid satellite-terrestrial network was proposed by Zhang et al. [5]. Mowla et al. proposed an energy-efficient communication model for 5G heterogeneous networks to minimize power consumption while satisfying user quality of service requirements in communication engineering [6]. It can be seen that the application of 5G mobile communication technology in communication engineering is relatively mature, but most studies have explored it at the theoretical level. In order to pay attention to its practicality and improve its application value, the robot controller communication method is a more intelligent choice.

As one of the core parts of the robot, the communication method of the robot controller is of great significance. Pandey et al. used the augmented reality controller to innovate the communication method of the robot controller and realized the better remote interaction effect of the mobile communication technology in the communication engineering [7]. Nguyen et al. described a communication method of robot controller based on quadratic curve path tracking and applied it in mobile communication system, improving communication engineering [8]. The robot controller communication method has achieved good application results in many fields, but the research on the combination with the mobile communication technology is rare. In order to facilitate the further progress of communication engineering, the application research of 5G technology integrating the communication method of robot controller in communication engineering is urgent.

In this paper, combined with the communication method of the robot controller, the application of 5G technology in communication engineering was studied, and the application simulation test was carried out. The throughput rate, energy efficiency, and signal suppression effect of 5G technology in communication engineering applications were compared with those of traditional communication methods. The experimental results showed that in the throughput rate test, the throughput rates of the initial node and the final node under the communication method of the robot controller reached 480 bits and 2911 bits, respectively, which had good data transmission capability. In the energy efficiency test, the range of network health value was 387–453, which had high stability and work efficiency. In the signal suppression test, the overall average value of signal peaks under the traditional communication method reached 18.134 dB, while the overall average value of signal peaks under the robot controller communication method was only 11.296 dB. It can be seen from the experimental data that the 5G technology integrating the communication method of the robot controller has strong application feasibility in communication engineering.

2. Application of 5G Mobile Communication Technology in Communication Engineering

2.1. Overview of 5G Mobile Communication Technology. 5G mobile communication technology refers to a new generation of new technology system after 4G mobile communication technology. As an improvement and upgrade of 4G technology, it provides more convenient and fast mobile communication services for human society. Its basic structure is shown in Figure 1. With the development of communication engineering construction, 5G technology has gradually entered the field of vision of the public. Many countries or organizations with relatively mature mobile communication industries, including China, have successively started the research and deployment of 5G mobile communication technology.

In comparison with 4G technology, 5G technology greatly improves the speed of data delivery and resource utilization by virtue of its unique advantages such as high capacity, high stability, low latency, and wide coverage, which have greatly improved the efficiency and convenience of production and life. Its parameter standard is shown in Table 1.

As can be seen from Table 1, 5G technology has strict high standards compared with previous mobile communication technologies in terms of technical performance. Its standard frequency spectrum is mainly in the middle and high frequency bands, which can provide users with a better experience, promote the continuous progress of communication engineering, and bring it more development space. However, with the improvement of parameter standards, its transmission loss is constantly increased, and the coverage cost is increasingly high, so it must be supported by a number of core technologies [9]. At present, the key technologies in 5G mobile communication recognized by the industry include filtered-orthogonal frequency division multiplexing (F-OFDM), software-defined wireless network technology, massive multiple-input multiple-output (massive MIMO), ultra-dense cellular, and device to device (D2D), as shown in Figure 2.

RETRACTED

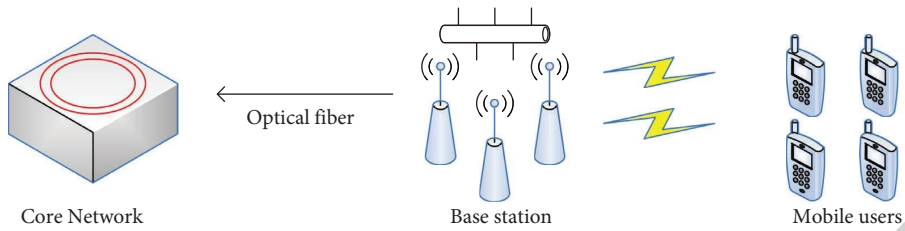

Figure 1: 5G mobile communication technology basic structure.

Table 1: 5G mobile communication technical parameters.

Sequence	Item	Specification
1	Standard spectrum	3.3–39 GHz
2	Communication frequency band	3.3–3.6 GHz and 4.8–5.0 GHz
3	Wavelength	mmWave
4	Transfer method	1–10 mm
5	Supported access rate	10 GP/s

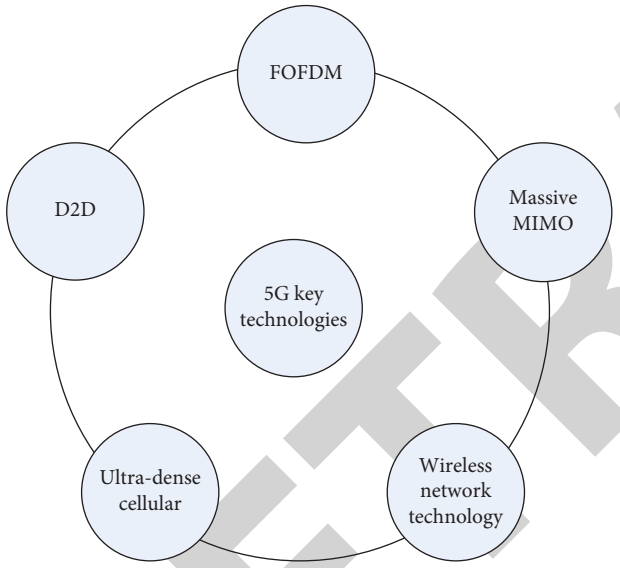

Figure 2: Key technologies in 5G.

Under the support of these key technologies, 5G technology not only includes various advantages of 4G technology but also is able to fulfill market developments and the new demands of different users, such as performance demands such as transmission speed and flexibility, as well as service demands including smart home and medical care, which bring different experiences to different users, as shown in Figure 3.

2.2. Application of 5G Mobile Communication Technology in Communication Engineering. Since the mid-1980s, the communication industry has ushered in its own rapid development in the market, and communication engineering has become the construction focus of major operators [10]. With the continuous fierce competition in the telecommunications industry, the cost and risk of communication engineering construction are increasing, and the requirements for the practicability and value of communication engineering construction are also getting higher and higher.

As one of the most popular mobile communication technologies at present, 5G has been widely used in a large number of communication projects, greatly improving the work efficiency and benefits of the project. While improving the quality of communication engineering construction, it makes its operation more intelligent and its functions more flexible. This paper summarizes its application value in communication engineering into the following 4 points.

2.2.1. Network Capacity. At present, the network construction of the communication project adopts a star network structure, and users communicate with each other through the base station and the network to enjoy network services. However, the distribution range and user capacity of each base station are limited, and due to the influence of the network structure, the amount of access and the amount of output are often in an unbalanced state. 5G mobile communication technology can bring extremely convenient user experience to communication engineering (ultra-high access rate, ultra-low latency, ultra-high reliability, etc.), realize direct connection between users, and expand network capacity. In this way, different degrees of data access requirements are met, and cost reduction is achieved on the basis of ensuring data transmission efficiency.

2.2.2. Level of Intelligence. Intelligence is the foundation of communication engineering construction, and 5G mobile communication technology can comprehensively improve the intelligent construction level of communication engineering, for example, to achieve a new level of improvement and promotion in perception and decision making, according to different construction conditions and needs, such as geographical location, user preferences, terminal status and network context, and other characteristics, so that targeted perception and decision making can be carried out and a solution with a high degree of matching can be designed, thereby enabling data-driven feature deployment, resource configuration, and automation.

RETRACTED

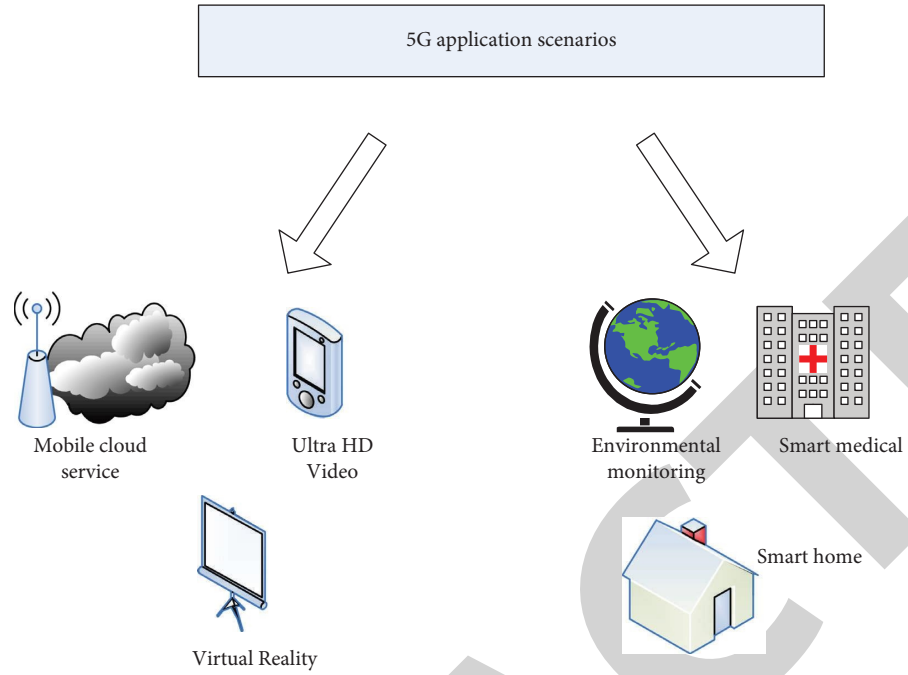

Figure 3: 5G technology application scenarios.

2.2.3. Functional Services. Communication engineering penetrates into all aspects of people's life, study, and work, and its functions and services play an important role in people's daily life. 5G technology supports diversified and rich Internet services and can provide people with more personalized functions and services. In the engineering access network, 5G can realize a variety of network access functions in the form of direct access, including ad hoc network, lightweight, easy deployment, and easy maintenance. Based on the evolution grouping of the engineering core network, it can also simplify and reorganize the functions of the network, which makes the control and forwarding capabilities of the network more flexible and effective.

2.2.4. Network Environment. 5G mobile communication supports the application development of new network ecological industry and vertical industry with a more open technical space. It provides a flexible service deployment environment for third parties through open network functions, enabling good interaction between communication engineering and third-party applications. The 5G network can meet the individual needs of communication engineering entities, create conditions for enterprises' business activities and network service innovation, and thus enhance the ecological value of the network environment.

2.3. Method of Robot Controller Communication. From the analysis of the characteristics of 5G technology and its application in communication engineering in this paper, it can be seen that 5G mobile communication technology plays a crucial role in the construction of communication engineering. However, in the actual application process, the existing 5G technology system still has many serious problems, such as excessive signal peaks appearing in communication engineering construction which can increase the pressure of data transmission invisibly, resulting in poor transmission effect, or the high-performance level of 5G mobile communication technology leading to excessive energy consumption of communication engineering and uniformity of resource allocation in daily operation [11]. These problems make communication engineering unable to adapt to the market development requirements and seriously affect its follow-up development. For this reason, this paper improves the problems generated by combining the communication method of the robot controller.

Robot controller communication is an important branch of robotics development in recent years. Its main working principle is to use the robot to perceive the surrounding environment information and to exchange and integrate information with the controller in real time [12]. The technical method is based on a wireless network. On the one hand, operations can be performed to improve work efficiency, and on the other hand, redundant information can be used to ensure the stability of the system. Robot controller communication has the following 4 characteristics.

2.3.1. Randomness. During the communication process, it is usually unpredictable which node the robot target node can establish a connection with or when the connection can be established [13].

RETRACTED

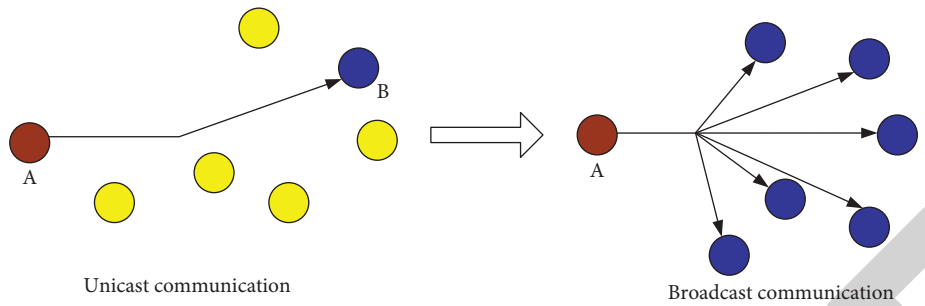

Figure 4: Robot controller communication method.

2.3.2. Discontinuity. The communication constructed by two independent machine systems cannot maintain a long-term state but can only be maintained for a short period of time. After the communication target is completed, the controller can automatically interrupt the communication [14].

2.3.3. Locality. In order to effectively ensure the operation of the communication mechanism in the follow-up work, it is necessary to reduce a certain amount of energy consumption. Therefore, the communication of the robot controller is only established locally in a single robot system.

2.3.4. Dynamicality. The network topology structure constructed by the communication system changes dynamically.

There are two main communication methods for the robot controller: unicast communication and broadcast communication, as shown in Figure 4.

As can be seen from Figure 4, unicast communication requires the establishment of a separate data channel between robots, and data packets sent from one node A can only be sent to one node B. If other nodes can also receive A's information, A must continuously generate multiple identical messages to send, which can cause a waste of computing resources and a large delay for a single robot. However, the broadcast communication is a "one-to-all" communication mode. Node A can send the data packet to all nodes within the communication range without choosing a special path, and other nodes only need to monitor whether there is information coming [15]. The cost of this design method is very low and is well adapted to the communication requirements of 5G technology in communication engineering applications. Therefore, this paper uses broadcast communication to conduct research on the implementation of 5G in communication engineering.

In order to facilitate the analysis, the number of time slots included in the transmission process of each frame of the communication engineering data channel is set to N. These time slots are synchronized by the robot controller. Labels can be set in advance, and the time slots are selected through the label extraction to ensure randomness [16]. Assuming that n is the preset number of tags, the selection of the time slot requires the tags to be extracted in the time frame with a probability order of $1/N$. After selection, the target communication data are sent by the time slot. The probability that k tags in a time slot simultaneously send target communication data can be calculated as follows:

$$P(k) = \binom{n}{k}\left(\frac{1}{N}\right)^{k}\left(1-\frac{1}{N}\right)^{n-k}. \tag{1}$$

The number of tags that can be successfully identified in a frame is as follows:

$$N \cdot P(1) = N \cdot \binom{n}{1}\left(\frac{1}{N}\right)^{1}\left(1-\frac{1}{N}\right)^{n-1}. \tag{2}$$

The throughput rate of the communication engineering system is defined as follows:

$$T(n,N) = \frac{N_t}{L_f} = P(1). \tag{3}$$

Among them, N_t is the number of labels identified in a frame. L_f is the frame length of the current frame. $T(n,N)$ is related to n,N. When the throughput rate T of the communication engineering system is the highest, $\partial P(1)/\partial n = 0$, and the solution is as follows:

$$n = \frac{1}{\ln N/N-1} = \frac{1}{\ln(1+1/N-1)}. \tag{4}$$

When the number of tags is approximately equal to the frame length, the throughput rate of the communication engineering system reaches the maximum.

If the distribution function of the number of tags has been obtained, the average value of the random variable of the throughput rate of 5G technology in communication engineering can be calculated as follows:

$$E(S) = \sum_{n=0}^{n_{\max}} T(n,N)P(n). \tag{5}$$

Once the distribution function of the number of tags is determined, information exchange can be carried out through the communication components under the controller to select the appropriate time frame length to maximize the average value of the random variable of the throughput rate. At this point, it is assumed that the number of tags around the communication component of the robot controller in a given time range approximately obeys a Poisson distribution:

$$P(n=k) = \frac{\lambda^{k}}{k!}e^{-\lambda}. \tag{6}$$

RETRACTED

The data information to be acquired includes the number of time slots in different states (collision, success, and vacancy) of the current time frame, and the robot controller can complete the effective prediction of the number of tags based on the number of time slots in different states [17, 18]. Taking the number of time slots obtained in the latest frame as an example, it can be calculated according to the following formula:

$$P(n|I) = \frac{P(I \cap n)}{P(I)} = \frac{P(I \cap n)P(n)}{P(I)}. \quad (7)$$

In the same frame, $P(I)$ is usually regarded as a constant, which can be normalized and eliminated in the actual calculation of the average value of random variables.

According to the probability distribution function of the number of updated tags and the number of tags that have been successfully identified, the length of the next frame can be adjusted. If there are S tags in the t-th frame that are completely recognized by 5G mobile communication technology, then in the state without any new changes, the distribution function of the $t + 1$-th frame can be obtained according to the following formula:

$$P_{t+1}(n - S) = P_t(n|I). \quad (8)$$

The average value of random variables of the number of labels in $t + 1$ frames is calculated according to the distribution function, as shown in the following formula:

$$E_{t+1}(n) = \frac{\sum_{n_{\min}}^{n_{\max}} (n - S)P_{t+1}(n - S)}{\sum_{n_{\min}}^{n_{\max}} P_{t+1}(n - S)}. \quad (9)$$

When the communication component of the robot controller tries to identify the label, there is a certain rule in the number of labels in the previous frame, the current frame, and the next frame [19, 20]. The 5G mobile communication technology under the traditional communication method often ignores this law, which only performs the subsequent operation of the communication project according to the information identified in the latest frame, while the robot controller communication method can record the law between the number of tags inside the system. In the follow-up operation, this law can be extracted for prediction and guidance, so as to minimize the power consumption of communication engineering and improve its usability.

2.4. Application Simulation of 5G Mobile Communication Technology in Communication Engineering. In order to prove the practicability of 5G technology under the communication method of robot controller in communication engineering, this paper used the MATLAB platform to conduct simulation experiments and tested the throughput rate, energy efficiency, and signal suppression effect of 5G in communication engineering application simulation. In order to directly reflect the effect of the method, the application effect of 5G technology in communication engineering under the traditional communication method was compared. The experimental scene design conditions are shown in Table 2.

Table 2: Experimental scenario design conditions.

Sequence	Item	Specification
1	Maximum number of nodes	100
2	Regional area	100 m ∗ 120 m
3	Base station location	(50, 100)
4	Node communication radius	20 m

2.4.1. Test of Throughput. The throughput rate of 5G technology in communication engineering refers to the maximum amount of data that the engineering equipment interface can accept and transmit without any communication abnormality. As a limit index, the throughput rate has an extremely important reference role in judging the construction effect of communication projects. By setting different numbers of nodes (50, 60, 70, 80, 90, and 100), this paper investigated the throughput of 5G technology in communication engineering under two methods. The results are shown in Figure 5.

Generally speaking, the larger the number of nodes, the greater the tuning probability of the network, and the throughput rate can also increase, which can be seen from the test results of the two methods in Figure 5. However, from the perspective of the overall test results and the degree of change, the throughput test results of the 5G technology integrating the communication method of the robot controller in the communication engineering had more obvious advantages. In Figure 5(a), the throughput rate of the initial node reached 480 bits per second, and as the number of nodes continued to increase, the throughput rate also increased. When the number of nodes was 100, the throughput rate reached a maximum of 2911 bits per second, indicating that the 5G mobile communication technology under the communication method in this paper can make full use of the network environment, effectively transmit data traffic, and provide good support for the normal operation of communication projects. In the test results of the traditional communication method in Figure 5(b), in the initial stage when the number of nodes was 50 and 60, the throughput rates were slightly higher than the test results under the communication method in this paper, which were 491 bits and 627 bits, respectively. However, when the number of nodes reached 70, its advantages no longer appeared, and the subsequent throughput results were far from the method in this paper. This might be related to the network environment, and the increase in the number of nodes led to a complex network environment. The 5G mobile communication technology under the traditional communication method cannot filter the interference factors in it well, which affected the normal transmission of communication engineering data and affected the throughput results. From this aspect, the throughput performance of our method was indeed impressive.

RETRACTED

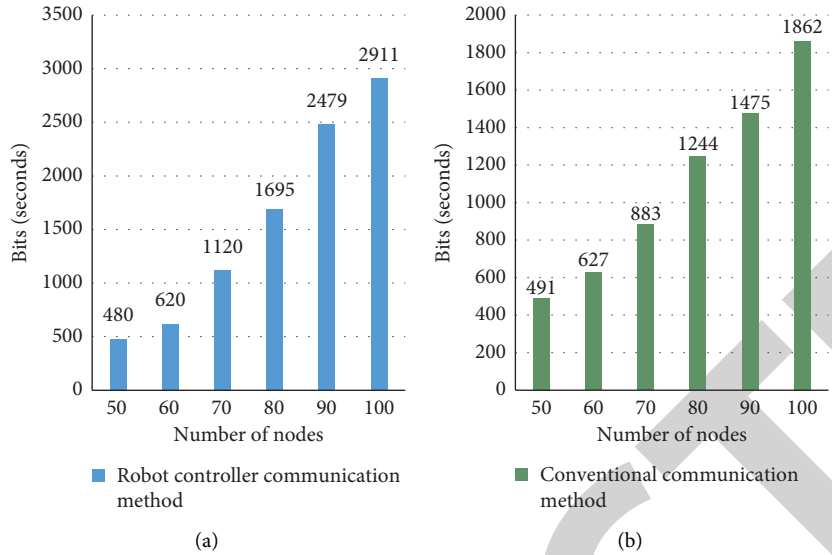

Figure 5: Test results of throughput. (a) The results of this communication method. (b) The results of the traditional communication method.

2.4.2. Test of Energy Efficiency. The energy efficiency test mainly examines the energy resource utilization efficiency of 5G technology in communication engineering. At present, the construction of market communication engineering has been carried out in a comprehensive manner. Under the environment of imbalance between supply and demand, the utilization of communication engineering resources is extremely critical. The energy efficiency test conditions in this paper are shown in Table 3, and the test results are shown in Figure 6.

From the energy efficiency test results in Figure 6, the energy resource utilization efficiency of the 5G mobile communication technology under this method in communication engineering was significantly higher than that of the traditional communication method. In Figure 6(a), the fluctuation range of the results of the robot controller communication method under 50 rounds of simulation tests was relatively small and was basically maintained within the range of 387–453. However, under the traditional communication method in Figure 6(b), the test result range fluctuated greatly, and the network life was short, with the range of 297–379. The highest point of life value was lower than the lowest point of this method. From the perspective of network life time, the 5G mobile communication technology integrating the communication method in this paper prolonged the life of the communication engineering network, and its energy efficiency was high. The communication method of the robot controller could simultaneously take into account the energy and density of the communication engineering network nodes in the subsequent operation and manage and optimize them in real time, reducing unnecessary energy consumption of 5G mobile communication technology to achieve better energy efficiency and resource allocation in engineering construction, which is where traditional communication methods are difficult to break through.

Table 3: Test conditions of energy efficiency.

Sequence	Item	Specification
1	Raw energy of the node	2 J
2	Length of packet	6 kbit
3	Energy parameter	60 nJ/bit
4	Error level	120 nJ/bit/square meter
5	Rounds of simulation	50

2.4.3. Effect of Signal Suppression. Signal suppression refers to the effect of 5G on the suppression of high signal peaks of transmitted data in the actual operation of communication projects. Different number of carriers, which were 4, 16, 64, 256, and 1024, respectively, were set in the experiment in this paper. Under different conditions, the signal peak suppression effect of 5G in communication engineering was observed. The results are shown in Figure 7.

In the data transmission of communication engineering, abnormal signal peaks are easily generated. Excessive signal peaks can cause more significant spread spectrum interference and signal distortion inside the system, which can not only increase the operational complexity of communication engineering but also affect its work efficiency. Therefore, it is necessary for mobile communication technology to suppress it. From the results in Figure 7, although the signal peaks all showed a rising trend with the increase of the number of carriers, the signal suppression effects of the two methods were different. In Figure 7(a), the signal peaks under different carrier numbers were 4.11 dB, 6.79 dB, 9.32 dB, 14.44 dB, and 21.82 dB, respectively, and the overall average value was 11.296 dB. In Figure 7(b), the signal peaks under different carrier numbers were 6.03 dB, 12.77 dB, 18.32 dB, 23.74 dB, and 29.81 dB, respectively, and the overall average value reached 18.134 dB. From these data, it can be seen that the

RETRACTED

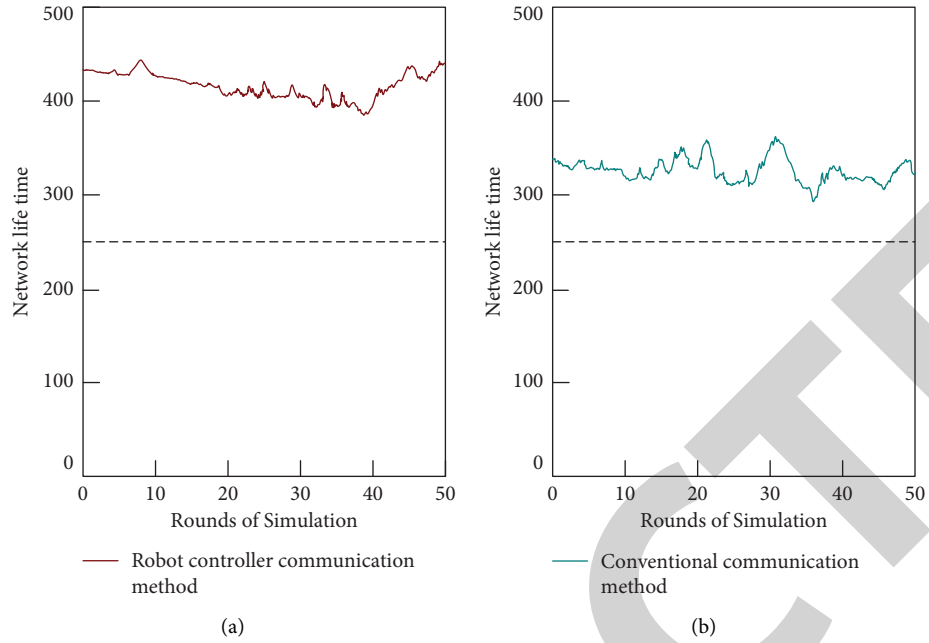

Figure 6: Test results of energy efficiency. (a) The results of the communication method in this paper. (b) The results of the conventional communication method.

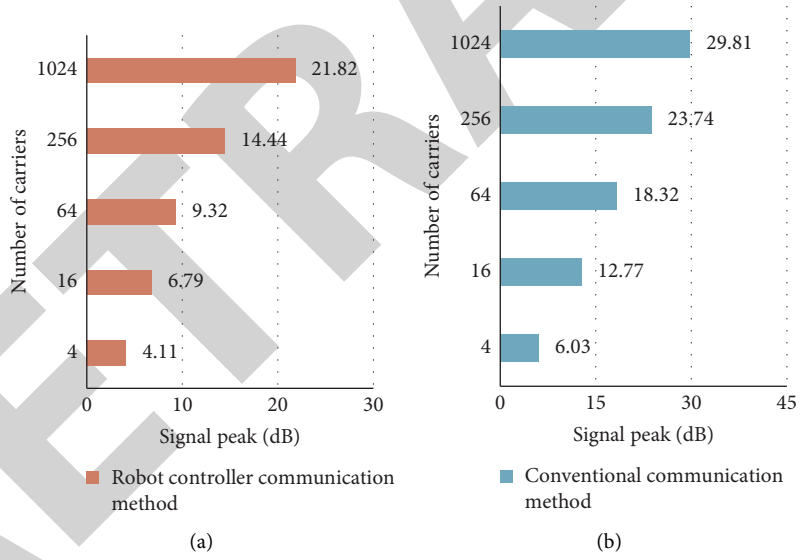

Figure 7: Test effect of signal suppression. (a) The results of the communication method in this paper. (b) The results of the conventional communication method.

5G technology that integrates the communication method of the robot controller can reduce the impact of signal peaks on communication engineering within a reasonable range. Even under more extreme peak conditions, the communication system can be guaranteed to operate stably and achieve good gain. Although the traditional communication method has a certain inhibitory effect on the signal peak, it has many limitations. Especially in the dynamic frequency switching, the weakened peak is very likely to be regenerated.

3. Conclusion

With the changing application scenarios and business requirements, the market has higher and higher requirements for the application value of 5G technology in communication engineering. Giving full play to the advantages of 5G technology, accelerating communication efficiency, and strengthening the construction of communication projects are the key directions of current development. In this paper,

RETRACTED

Hindawi
Journal of Robotics
Volume 2024, Article ID 9797639, 1 page
https://doi.org/10.1155/2024/9797639

Retraction

Retracted: Application of Microcontroller-Based Multipath Servos in Industrial Robot Control Systems

Journal of Robotics

Received 23 January 2024; Accepted 23 January 2024; Published 24 January 2024

Copyright © 2024 Journal of Robotics. This is an open access article distributed under the Creative Commons Attribution License, which permits unrestricted use, distribution, and reproduction in any medium, provided the original work is properly cited.

This article has been retracted by Hindawi following an investigation undertaken by the publisher [1]. This investigation has uncovered evidence of one or more of the following indicators of systematic manipulation of the publication process:

(1) Discrepancies in scope
(2) Discrepancies in the description of the research reported
(3) Discrepancies between the availability of data and the research described
(4) Inappropriate citations
(5) Incoherent, meaningless and/or irrelevant content included in the article
(6) Manipulated or compromised peer review

The presence of these indicators undermines our confidence in the integrity of the article's content and we cannot, therefore, vouch for its reliability. Please note that this notice is intended solely to alert readers that the content of this article is unreliable. We have not investigated whether authors were aware of or involved in the systematic manipulation of the publication process.

Wiley and Hindawi regrets that the usual quality checks did not identify these issues before publication and have since put additional measures in place to safeguard research integrity.

We wish to credit our own Research Integrity and Research Publishing teams and anonymous and named external researchers and research integrity experts for contributing to this investigation.

The corresponding author, as the representative of all authors, has been given the opportunity to register their agreement or disagreement to this retraction. We have kept a record of any response received.

References

[1] R. Hu, "Application of Microcontroller-Based Multipath Servos in Industrial Robot Control Systems," *Journal of Robotics*, vol. 2023, Article ID 7235120, 11 pages, 2023.

Hindawi
Journal of Robotics
Volume 2023, Article ID 7235120, 11 pages
https://doi.org/10.1155/2023/7235120

RETRACTED

Research Article

Application of Microcontroller-Based Multipath Servos in Industrial Robot Control Systems

Ruiming Hu

Hebi Institute of Engineering and Technology, Henan Polytechnic University, Hebi, Henan 458030, China

Correspondence should be addressed to Ruiming Hu; 20208065@hbzy.edu.cn

Received 1 November 2022; Revised 2 December 2022; Accepted 17 March 2023; Published 31 March 2023

Academic Editor: Shahid Hussain

Copyright © 2023 Ruiming Hu. This is an open access article distributed under the Creative Commons Attribution License, which permits unrestricted use, distribution, and reproduction in any medium, provided the original work is properly cited.

In recent years, nanotechnology has continued to develop, especially the use of nanomaterials in various fields. Microcontroller is the most typical embedded system at this stage. With the development of science and technology, microcontroller has been widely used in people's production life. A simple and practical multiservo controller can be built by using microcontroller and LED control chip PCA9685, which can realize at least 16 channels of servo control. In this paper, the control program of multichannel actuator is designed in detail, and the speed regulation of multichannel actuator is studied, which is applied to the industrial robot system driven by actuator. Nanomaterials, as new materials with various unique properties, have great application prospects, and this paper investigates the extension of nanomaterials in the field of robotic systems.

1. Introduction

1.1. Servo. Servos are control systems with constantly changing angles and are often used as position servo drives capable of holding angles. They have many advantages and are often used in a wide variety of civil electromechanical systems.

In microcontroller-based systems, the simplest way to control rudder motion is to generate PWM waves and vary the duty cycle using the microcontroller's internal timing source. Using a single microcontroller to generate multiple rudder control signals is a cost-effective and versatile method currently used to accurately, reliably, and consistently control multiple rudders in a reasonable and compact design. A typical rudder motion control is achieved by generating 20 ms PWM pulses and varying the duty cycle [1].

Simple rudder control can be achieved using the PWM control principle by simply connecting the control line of the rudder to one of the control pins of the microcontroller. However, articulated and multilegged robots need to control multiple servos simultaneously, i.e., multiple PWM signals must be controlled by a single multiplexed servo controller.

The internal structure of the servo is shown in Figure 1, including DC motor, reducer, potentiometer comparator, and control circuit. The DC motor is driven at high speed and through the reducer at low speed and high torque.

1.2. Microcontroller Overview. Microcontrollers are very small and complex microcomputers with data processing capabilities, integrated using very large-scale integrated circuit technology to enable high speed processing of data and information [2]. Microcontrollers are mainly used to interconnect components through a bus, each with different characteristics and playing different roles.

Microcontrollers are used in industrial automation because of the large number of I/O lines, very rich instructions, and very powerful logic operation performance.

1.3. Current Status of Robot System Development. Industrial robots are important automation equipment for modern manufacturing and have a very wide range of applications in many fields. Regarding the history of industrial robots, the first industrial robot was developed in the United States in 1962. Robotics is an important part of the high-tech field. The development of industrial robots in China is promising and dynamic, but there are still many difficulties and shortcomings to fully meet the needs of

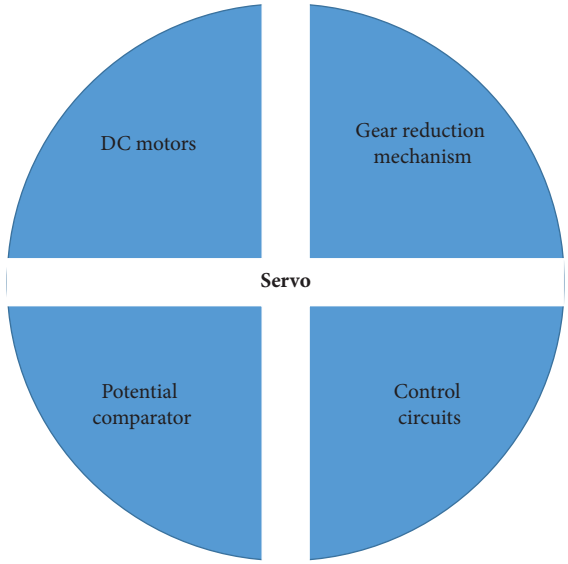

Figure 1: The internal structure of the servo.

industrial production and life. The traditional industrial robots often appear in front of people with the image of cold steel, and this image has been solidified, but this is only the traditional industrial robots, and the flexible robots currently under development are different from this, changing people's view of robots in terms of adaptability, safety, and interactivity [3]. Figure 2 shows a general industrial robot system.

1.4. Development of Nanotechnology. Nanotechnology is an integrated field of science and technology that studies the properties and interactions of materials at the nanoscale (generally considered to be less than 100 nm) and the exploitation of these properties. Nanobiosensor is a fusion of nanotechnology and biosensor, and its research includes several important disciplines, including biotechnology, information technology, nanoscience, and interface science. It also combines the application of various advanced detection technologies such as light, sound, electricity, and color. In recent years, nanobiosensors have attracted more attention than ever before due to the active development of nanoscience and interface science. Their development is remarkable and applications are widespread [4].

Nanomaterials are materials with nanoscale structures and molecular sizes of 1–100 nm, which are invisible at the macroscopic level. Nanomaterials themselves possess many unique properties such as small size, surface, and quantum effects. For example, inorganic antimicrobial agents can be incorporated into materials by nanodispersion and modification techniques to create nanobacterial materials and the small size effect of nanomaterials can be used to create infrared photodetectors and infrared cloaking technologies [5].

Another active area of research in the biomedical field is "nanorobotics." The development of nanorobots is related to the field of molecular bionics and involves the development of prototypes for the design and fabrication of "functional molecular devices" that operates in the nanoscale space based on biological principles at the molecular level.

2. Technology Principle

2.1. Servo Control Principle. The composition of the rudder is relatively simple. The power provided by the DC motor is attenuated by a reduction gear, and the torque is transmitted outward through the output axis. The rudder control process is shown in Figure 3. The servo contains a reference circuit that generates a reference signal with a period of 20 ms and a width of 1.5 ms. The actuator control signal is a pulse width modulated PWM signal of 0.5 to 2.5 ms, which corresponds to a steering angle of 0° to 180°[6]. If the control pulse signal does not change, the actuator can remain at a certain angle without moving. The three wires of the servo are connected to a multiservo controller, which can drive multiple servos in coordinated motion by multiservo control.

Here is an example of the PCA9685 chip, which is a controller chip designed to control LED backlighting [7]. The brightness of the PCA9685 chip can be changed according to the need and modified program output. Its main features are as follows

(1) The chip has a wide operating voltage range within which it can be adjusted arbitrarily, and each output can be configured for an open-drain operation at 25 mA or a pull-pull operation at 10 mA.

(2) The output frequency can be synchronized between several different devices by adjusting the internal 25 MHz oscillator. The output frequency range of the chip is 40~1000 Hz.

(3) The chip uses the I^2C bus to read or write new programs to the chip. The PCA9685 chip has four programmable I^2C bus addresses, which can be addressed simultaneously in these four bus addresses, which greatly improve the efficiency of

RETRACTED

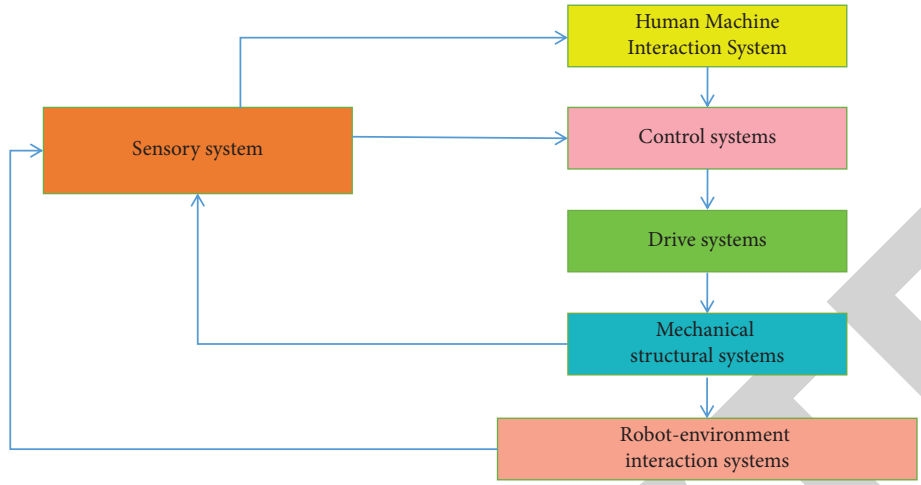

Figure 2: Industrial robot system composition.

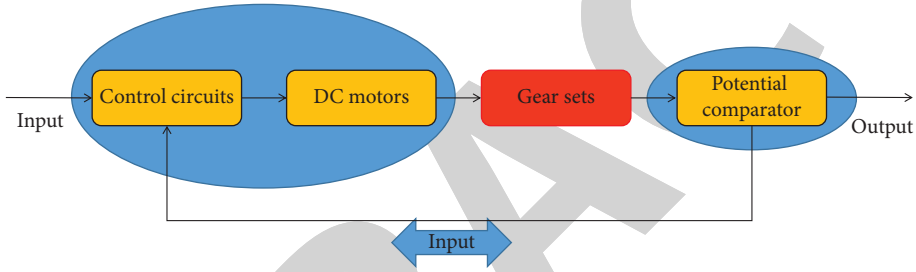

Figure 3: Servo control principle.

reading and writing. Up to six pieces of hardware can be connected to the I^2C. The PCA9685 chip is generally connected through these six pins.

(4) The chip can independently output a high number of pulses, which makes the implementation of multiplexed servos provide the necessary conditions.

(5) The chip form factor in the TSSOP28 package commonly used for the PCA9685 chip is shown in Figure 4.

Some pin definitions about the chip are shown in Table 1.

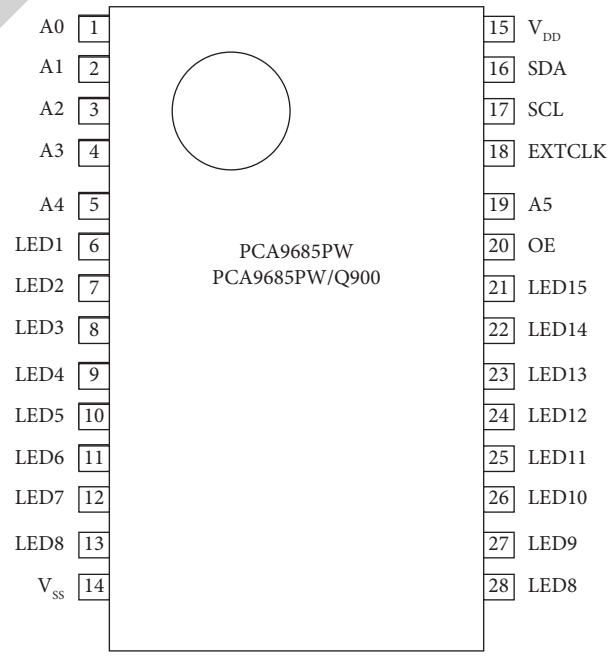

Figure 4: Chip form factor of PCA9685 chip.

2.2. Nanobots. The emergence of nanorobots has provided new ideas for the innovation and development of modern biomedicine, with the ability to enter the human body in a minimally invasive manner, which is not possible with any conventional medical technology. However, despite the advances made in medical nanorobotics over the past decade, the immature technical requirements of the field such as the actuation and cluster control of microrobots limit the widespread use of these tools in clinical settings, and the simultaneous actuation of a certain number of nanorobots often requires cumbersome procedures and advanced instrumentation.

Fabrication, actuation, and degradation are fundamental to the application of nanorobots. At the nanoscale, the motion of a microrobot is influenced by both low Reynolds number and Brownian motion, and its motion must take into account environmental effects; so designing a nanorobot is primarily about enabling it to produce continuous motion and requiring it to have sufficient power to overcome the resistance of its environment. For example, microrobots

RETRACTED

Table 1: Partial pin definition of PCA9685 chip.

Symbols	Pins		Type	Description
	TSSOP28	HVQFN28		
A0	1	26	I	Enter address 0
...	...	...	...	...
A4	5	28	I	Enter address 4
LED0	6	3	O	LED driver 0
...	...	...	...	...
LED15	22	19	O	LED driver 15
V_{SS}	14	11	Power supply	Supply land
OE	23	20	I	Active low output enable
A5	24	21	I	Enter address 5
EXTCLK	25	22	I	External clock input
SCL	26	23	I	Serial clock line
SDA	27	24	I/O	Serial data line
V_{DD}	28	25	Power supply	Supply voltage

can be made from catalytic materials and propelled into directional motion by using a catalytic reaction in H_2O_2 to create bubbles; microrobots with a spiral structure can be given magnetism, and a magnetic field can be used to cause the spiral to rotate itself, which in turn propels it into linear motion; for nanorobots with an asymmetric structure, ultrasound can be applied to create a pressure gradient to propel them into motion. Different types of micro-nanorobots have different manufacturing methods and drive methods, and the nontoxic degradation of the nanorobots is important for the safety of living organisms.

2.3. Industrial Robot Control System. Industrial robots, which represent modern technology, are used in many production sites. Industrial robots also have a certain degree of danger, and the slightest carelessness can cause irreparable damage, which means that the control system of industrial robots is very demanding. The study of robot control systems is to prevent all kinds of losses and injuries, and of course, advanced control systems are also a manifestation of strong technical power [8].

Today, robots are mainly used for repetitive labor in industrial production. Generally, repetitive simple labor that is more injurious or polluting has been replaced by robots for manual labor, and a structure of five joints is generally considered sufficient. The schematic structure of this type of robot body is shown in Figure 5.

As can be seen in the figure, the composition of a universal robot is not complex, and the movement of multiple joints is all that is needed to fully control the actions of that robot. For example, the wrist joint determines the posture of the wrist. Therefore, centralized or hybrid control, as in the past, is difficult, and in the latest research, distributed control systems are promising and less technically difficult to implement. In this paper, the system control scheme, the hardware architecture, and the software architecture are described separately.

2.3.1. Overview of the Robot Control System. Distributed control system (DCS-Distributed ControlSystem) is an advanced control technology that was rapidly developed in the 1970s. Due to the various disadvantages of traditional control systems and the advantages of distributed control systems, most modern robot control systems now use distributed control structures. The development of distributed control systems has evolved with times, which means that the structure of industrial robots is diversified [9].

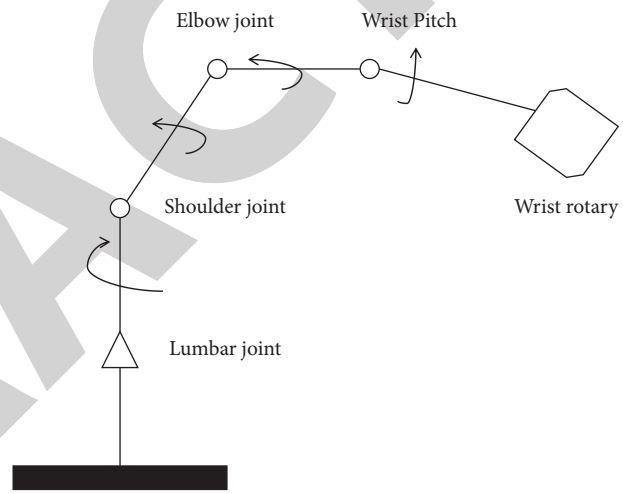

Figure 5: General-purpose robot structure.

While the general-purpose industrial robot in the above example is a three-joint structure, an industrial robot using the now common distributed control system is a five-joint multijoint structure. This structure uses a distributed control system consisting of a central unit and five contactors. It consists of an upper and lower structure with an upper unit and a lower unit. The upper unit (master) uses an industrial PC to manage the entire system, perform human-machine interaction, coordinate conversion, and route interpolation calculations, coordination between slaves, and fault detection. The role of the lower unit (slave) is to provide feedback to the signals from the host machine, specifically in the form of control of the five joints, by which the motion of the robot is changed. The entire control system is shown in Figure 6.

RETRACTED

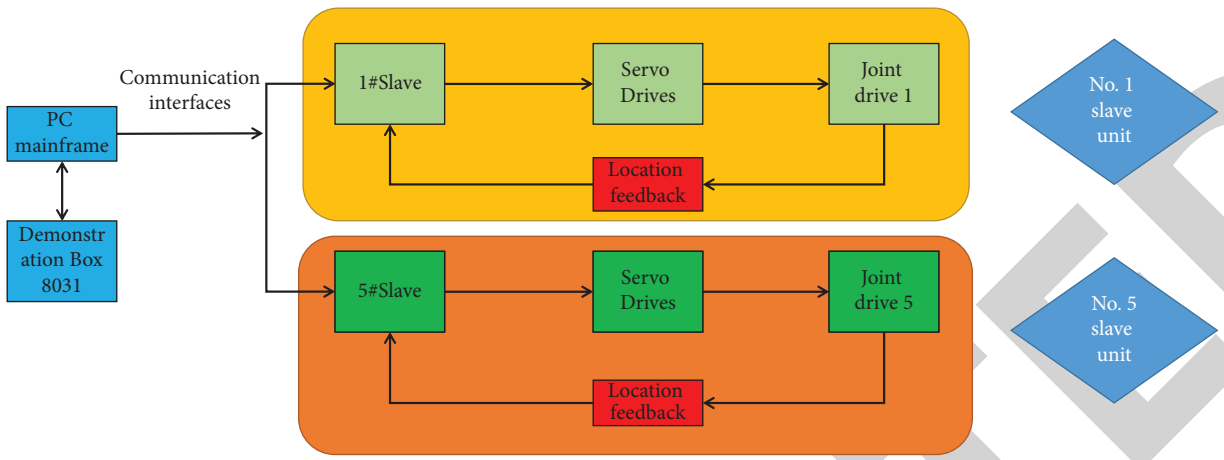

Figure 6: Distributed control system.

Based on the above five-joint robot theory, the control system has been developed for many years, and various component modules have become quite popular and cheap, so the development difficulty is low. In the control system, not only the weak electrical system but also the strong electrical system is needed to cooperate with it. Here, the five-joint motor unit is part of the strong electrical system, and the strong electrical control line is also essential. In terms of structure, the combination of strong and weak control systems makes the structure quite compact, especially when changing the design of the robot body. Thus, the control system is highly flexible and versatile [10].

During operation, the control system controls peripheral devices, coordinates their movement with the robot, and receives signals from sensors inside the robot. The peripheral devices are managed by the host computer, and information interaction between the major units within the control system does not go through the host computer, but uses serial communication interaction. Full-duplex asynchronous serial ports are used to communicate between the main control unit and them. All I/Os of the controller and sensors inside the robot of peripheral devices are isolated by optical coupling [11].

2.3.2. Joint Servo. Unlike the more complex unit model of the control system, in the basic structure, the joints have a motor composition, which is simpler. The principle of the motor is shown in Figure 7. The position signals from the coding channels A and B of the coding board are converted into signals that can be recognized by the next unit after a series of processing and feedback on the action of the motor. 8031 compares the position with the position given by the host in a 2-byte operation to form a position deviation. This control quantity is converted into an analog signal by a 12-bit D/A converter, converted to level, amplified, and then sent to the joint servo unit as control power to close the joint motor position. To make the counter work more accurately, the method generally used is to synchronize the counter latch with the timing of the 8031 via clock pulses. The slave must also smooth the given position and smooth the moving joints according to the robot's needs [12].

2.3.3. Master-Slave Communication Method. There are various ways of information interaction between master and slave machines, but their fundamentals are all one principle. After a long time of development, the communication technology between the master and slave machines has become very mature. Technically speaking, it is a single-chip communication method using serial communication in this system to solve the information exchange between multiple CPUs. Common single-chip communication methods are parallel port and serial communication. Based on the characteristics of the transmission signal, serial communication is generally used because of its simple structure and can be used for long-distance communication [13]. Although parallel communication has the advantage of fast communication speed, it is not practical and is very unsuitable for master-slave communication applications. Asynchronous serial communication is used in industrial robot controllers because many microcontroller chips have built-infull-duplex asynchronous serial ports that can send and receive data simultaneously. This allows the use of serial communication directly between a master processor and several slave 8031 communication processors.

2.4. Nanomaterial Preparation Methods. Nanomaterials are formed in three dimensions by transforming ordinary materials into microparticles using multidisciplinary knowledge of chemistry, physics, and biology. The following five methods are commonly used to prepare nanomaterials [14]:

(1) *Hydrothermal Method.* Nanomaterials need to be prepared under high temperatures and pressure. Under high temperature and pressure conditions, raw materials are hydrolyzed into nanomaterials through chemical reactions. Many nanomaterials are reactive, and high temperatures and pressure provide

RETRACTED

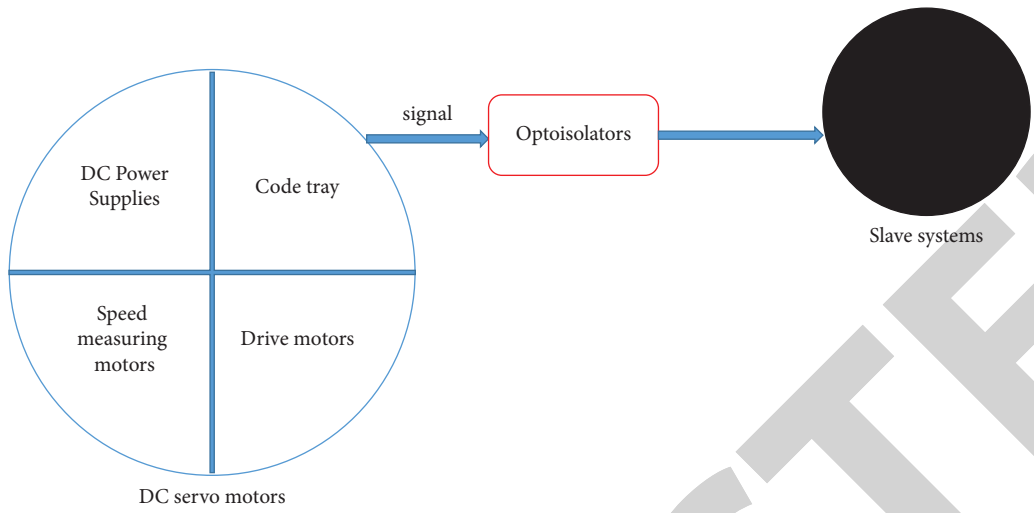

Figure 7: Motor principle.

suitable conditions for the preparation of nanomaterials.

(2) *Precipitation Method*. The precipitation method is a form of nanomaterial preparation that uses chemical conclusions. Generally, precipitation involves chemical changes, and solution reactions are extremely good chemical reactions that are usually carried out in solution when using this method of preparation. After ensuring that the reaction is complete, it needs to be precipitated and dried to obtain the desired nanomaterial. Nanomaterials prepared by the precipitation method usually have high purity.

(3) *Gas-Phase Reaction Method*. The gas-phase reaction method is also very efficient in preparing nanomaterials by reacting with gaseous metal compounds using a chemical reaction. Because the contact area of the gaseous material is maximized, this method is energy efficient and environmentally friendly compared to other methods.

(4) *Evaporation Coalescence Method*. The evaporation coalescence method is also a common method for preparing nanomaterials, which involves the decomposition of nanoparticles by heating and evaporation, separation into single molecular and atomic structures under high-temperature conditions, and rearrangement of the decomposed atoms and molecules by scientific means and formulas. Unlike the hydrothermal method, this method does not require a high-pressure environment. The advantage of nanomaterials produced by the evaporation-drying and solidification method lies in their small diameter, which far exceeds the requirements of general nanomaterials and their wide range of applications.

(5) *Spray Method*. Unlike the chemical reaction of the precipitation method, this method does not involve a material change in the raw material and is based on physical changes that do not require complex experiments and only require atomization of the solution by various physical means. Nanomaterials prepared in this way can generally reach submicron standards and produce uniformly dispersed fine particles. Table 2 summarizes the characteristics of the five methods.

2.5. Overview of Microcontroller Principles and Application Design. No matter what the system is, it is used by people, so it is necessary to go to the community first to research the needs of the system and other aspects. Therefore, the design of a microcontroller application system is also inseparable from the first step of research to clarify the feasibility characteristics of the software and hardware. As part of the feasibility study, it is necessary to collect information about the research on the system from all over the world to study and use the successful and advanced experiences, advantages, and disadvantages. Disadvantages need to be analyzed, and if there is no similar experience, detailed study and research on the design and development environment of the microcomputer system are needed. The final design is still up to the people themselves, but in the design process, the stability of the structure must be considered, the cost also needs to be accounted for, and a combination of all aspects also needs to be tried to improve the compatibility of the system, so that the designed system is excellent. Ensure the efficiency of the software and hardware designs [15].

2.5.1. Software Design of the Microcontroller. In the design process of the microcontroller software system, it is required that after the circuit design is finalized, the hardware design and software design must be considered comprehensively to clarify the software design issues and ensure that the design meets the functional requirements of the system.

The generality of the microcontroller software is very important. The purpose of the design process should be clear and modified according to the actual situation in the field.

RETRACTED

RETRACTED

Table 2: Five preparation methods of nanomaterials.

Preparation method	Main process	Features
Evaporation coalescence method	Decomposition of raw materials and rearrangement of the atoms and molecules	Small diameter of nanomaterials
Sedimentation method	Solution state mixed precipitation, prepared after drying	Higher purity of nanomaterials
Spray method	Atomizing raw material solution to break up nanomaterials	Uniform material distribution and fine grain
Hydrothermal method	Hydrolysis of raw materials under high temperature and pressure	Guaranteed balance
Gas-phase reaction method	Synthesis of ultrafine particles through chemical experiments	Low energy consumption, low cost, and high efficiency

The design tasks should be changed under the following different requirements:

(1) After understanding the needs of the microcontroller, the first thing to consider is how to use the software rationally. It is necessary to understand the functions of the software, the need for a deep analysis of the software architecture. When necessary, the software can be decomposed so that the software design is seen from an independent perspective.

(2) In order to improve the efficiency of the software design, it is necessary to create a proper flow chart of the program. After this step, it is very clear to observe the improvement of efficiency, which is very beneficial for the software design of the microcontroller.

(3) The mathematical software design model accurately describes the mathematical relationships between various input and output variables in order to provide improved software design performance based on the general system requirements of the software. In microcontroller application system software, RAM is a very important component. 8031's on-chip RAM has fewer cells but an extremely large number of reserved bytes, so it is a great challenge to apply the cells and bytes resources in a reasonable way, so the allocation must give full play to their respective advantages. Second, when the 8 cells of RAM are working registers, R0 and R1 have certain pointer functions, some of which are very large and cannot be applied elsewhere. Third, the 16 bytes of 2OH–2FH also have a straightforward function and can be used to store various flag bits, store logic variables, store status variables, and so on by means of bit addressing. Once the RAM resource allocation design is completed, it should be easy to read and use in the programming session. A detailed resource allocation table should be created. The resource allocation design for this RAM is shown in Figure 8.

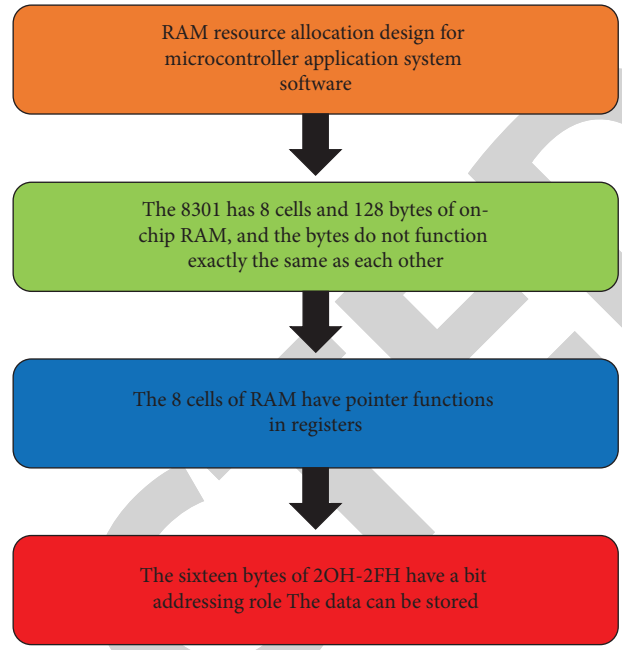

Figure 8: Design of RAM resource allocation.

2.5.2. Hardware Design of the Microcontroller. The hardware design of the microcontroller-based system mainly includes the design of system extensions and functional modules. Since microcontrollers are very application-oriented and require different hardware modules for different requirements, a detailed consideration of requirements in terms of hardware expansion is needed. After considering the requirements, it is also necessary to focus on the human-computer interaction aspect. For example, after the microcontroller has finished running the required program, it is necessary to display the results in front of the subject, for which the hardware module is necessary. The design of the system hardware should focus on the development of a general layout plan and a detailed and thorough technical justification. At the same time, the key circuit components should be studied in detail and in depth, tested, and analyzed before the design begins, and the results obtained should be verified as satisfactory by designing several indicators. If the requirements of the design are not met, i.e., if it does not pass the test, then such a design is substandard and must be improved upon to ensure that the entire analog circuit design is verified.

3. Application of Multipath Servo in Industrial Robot Control System

3.1. PCA9685-Based Design. By reviewing the manual, we can understand the characteristics of the PCA9685 chip [16]. There are many reasons for choosing this chip in this paper, including its low power consumption, fast response, and more pins and thus more functions, but the main thing is the output capability of the PCA9685 chip. We can learn that the chip can independently output multiple PWM waves and can be adjusted. By adjusting the 16 PWM pulses from the chip to match the PWM pulses required for steering control and changing the duty cycle as needed, multiple steering control can be achieved. The system uses the widely used STC microcontroller as the main controller and the PCA9685 chip as the PWM signal generator to establish multiplexed servo control.

3.1.1. Hardware Circuit Design. The PCA9685 chip has a relatively good design with many pins and comes with more functions, so many functions can still be implemented without adding peripheral devices. Here, the six address pins of the chip are used to determine the address at high and low levels. This system uses a PCA9685 with all address pins connected low as the chip address [17].

In the manual, you can learn that the PCA9685 uses the I^2C bus communication method.

RETRACTED

3.1.2. Software Design. The PCA9685 is designed to output PWM waveforms through several basic steps, which are the same in most devices that output PWM, but the exact details vary. The following is an overview of the basic steps to output a PWM waveform [18]:

(1) Determination of Chip Access Address. The chip access format of the PCA9685 is shown in Figure 9. The upper bits are fixed to 1, the lower bits are read/write mode selection, and bits 2 through 7 are determined by the external level of the chip. In this system, all six pins of the hardware address are connected to a low level, so the chip read/write commands are determined. In the PCA9685 chip, the role of each register is determined by setting different parameters; after that, it is very convenient to implement the required function because we only need to write control words to the set registers. The operating mode and communication registers of the chip are not the same under different addresses. The PWM output is also changed by controlling the registers.

(2) Control Mode Selection. The PCA9685 has two operating modes, and for reasons of ease of use, operating mode 1 is used, and the corresponding register address can be queried to be 00h. The chip is designed to be used in the following ways. The specific C program code is as follows: write8 (PCA9685_MODE1, 0×0), where write8 ( ) is the I^2C write function; PCA9685_MODE1 is the mode 1 register address [19].

(3) PWM Wavelength Setting. It is very important to control the action period of the servo; too fast or too slow will lead to different degrees of consequences. After the study, it was decided that the PWM period required for the control of the servo is set to 20 ms [20]. At the same time, the frequency of the PWM wave is set to 50 Hz, and the value of the frequency setting is calculated by the following formula:

$$\text{prescale_value} = \text{round}\left(\frac{\text{osc}_{\text{clock}}}{4096 * \text{upda te}_{\text{rate}}}\right) - 1. \quad (1)$$

Formula (1) outputs frequency calculation.

The set value is calculated to be 121 when a PWM frequency of 50 Hz is required to be the output. The chip's operating frequency can be changed by loading a value into the frequency setting register. Please note that the frequency can only be changed when the PCA9685 chip is in the sleep mode. Set the frequency by formula (2).

$$\text{unsigned char pulse} = 121. \quad (2)$$

Formula (2) calculates the frequency setting.

(4) Pulse Width Adjustment. From the control principle of the servo, to make the servo rotate, it is necessary to change its control parameters, as mentioned above that the rotation of the servo is achieved by adjusting the pulse width of the PWM wave output by the microcontroller. Each output port of the PCA9685 has a 12-bit counter that can count from 0 to 4095 with a count interval of 1/4096 PWM cycles. The output ports rely on two on/off control registers, LED_ON and LED_OFF. By writing the count values to the corresponding registers, the on/off times of the ports and the corresponding pulse widths can be obtained, thus controlling the output waveform [21]. The servo can generally rotate half a week, which corresponds to a PWM waveform with a positive pulse width of 0.5 to 2.5 ms, and then the relationship between the servo rotation angle θ and the pulse width ω is calculated by the following formula:

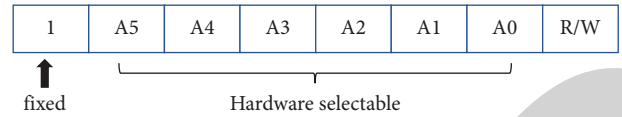

Figure 9: PCA9685 chip access format.

$$\omega = 0.5 + \frac{2}{180}\theta. \quad (3)$$

Formula (3) calculates the rotation angle and pulse width relationship.

The PCA9685 operates at 20 ms cycles with each count interval of 20/4096, and the corresponding count value is calculated by the following formula:

$$\text{Count} = \text{Round}\left(\frac{4096}{20}w\right) - 1. \quad (4)$$

Formula (4) is used for counting interval calculation.

Regarding the correspondence between the pulse width of the servo and the axis position in the software, it is listed in Table 3.

The response time of each stage of the servo movement according to the points in Table 3 was tested under both no load and nominal load, and the results are shown in Table 4.

3.2. Servo Smooth Drive. Let a certain way servo travel S be set from (initial axis position P0) 45° to (desired axis position P1) 90°. This amount of travel is subdivided into intermediate positions, each of which has a drive signal [22]. Subdividing the travel S into N intermediate positions, the response time required from the 45° position to the first position and each subsequent position is: T_{m0}, T_{m1}, T_{m2}, ...T_{mN}, setting the response time relationship as in formulas (5) and (6).

$$T_{m_0} = T_{m1} = T_{m2} = \ldots = T_{mN}. \quad (5)$$

Formula (5) calculates response time relationship.

$$T_{m0} + T_{m1} + T_{m2} + \ldots + T_{mN} = T_{\text{sum}}. \quad (6)$$

Formula (6) is used for actual movement time calculation.

T_{sum} is the actual time of motion, while the mean angular velocity ω is calculated with the following formula:

$$\overline{\omega} = \frac{S}{T_{m0} + T_{m1} + T_{m2} + \ldots + T_{mN}} = \frac{S}{T_{\text{sum}}}. \quad (7)$$

Formula (7) is used to calculate average angular velocity.

RETRACTED

Table 3: Correspondence between pulse width and axis position.

Pulse width (ms)	0.5	1	1.5	2	2.5
Axis position	0°	45°	90°	135°	180°

Table 4: Response for no load and nominal load.

Response time (ms)	Phase (°)			
	0~45	45~90	90~135	135~180
No-load response	140	140	140	140
Nominal response	140	140	140	140

For this example of 45° stroke, set $N \geq 6$, $T_{m0} = T_{m1} = T_{m2} = \ldots = T_{mN} = 20$ ms; the advantages of this method are as follows: (1) the average angular velocity is lower; stability can be guaranteed; (2) motion controllability increases the motion process of controllable features position more; motion smoothness is improved.

3.3. Nanobot Drives. Nanorobots can move both individually and in clusters. Their actuation methods largely influence their speed, ease of control, and biocompatibility, which in turn affects their application in biological systems. The main driving methods for nanorobots are chemically driven by local chemical and biochemical energy, physically driven by external fields (e.g., light, ultrasound, or magnetic fields), and biologically driven by microorganisms or cells.

External field drive is mainly used here. Most externally field-driven nanorobots do not require fuel and are, therefore, biocompatible and sustainable, mainly using light, ultrasonic, or magnetic field drives. They are more flexible in terms of controlled movement than chemically-driven nanorobots. Magnetic field-driven nanorobots can also be driven without any added fuel or harm to the human body. Magnetic field drive is based on the use of magnetic materials to build nanorobots that respond to external magnetic fields. The external magnetic fields are classified as rotating, gradient, oscillating, etc. For example, remote controllability and precise motion of three-dimensional magnetic tubular robots can be achieved by external magnetic fields, and these tubular robots have good capabilities in the capture, targeted delivery, and release of silica particles.

4. Conclusion

This paper focuses on the application of multiplexed servos in industrial robot systems, introducing the principles of nanomaterials, multiplexed servos, and industrial robot control systems. Based on the PCA9685 chip, a multiplexed servo control system can be established with a single machine as the core controller to realize the group control function of more than 16 servos. The principle of the servo and the software and hardware for designing the servo are highlighted to achieve smooth and stable drive control. The multi-way servo has a coherent and smooth motion with reduced jitter characteristics. Because its control is not affected by the timing fluctuations of the microcontroller, it has quite good accuracy and antiinterference performance, and experiments show that it is quite versatile.

Data Availability

The labeled data set used to support the findings of this study is available from the corresponding author upon request.

Conflicts of Interest

The author declares that there are no conflicts of interest.

Acknowledgments

This study was funded by the Research and Practice Project of Higher Education Teaching Reform in Henan Province-key project, the research and practice of the integration path of "post course competition certificate" of industrial robot major under the perspective of modern apprenticeship, 2021SJGLX676.

References

[1] W. Wang, X. Yu, B. Fang et al., "Cross-modality LGE-CMR segmentation using image-to-image translation based data augmentation," *IEEE/ACM Transactions on Computational Biology and Bioinformatics*, vol. 1, 2022.

[2] W. Shao, Z. You, L. Liang et al., "A multi-modal gait analysis-based detection system of the risk of depression," *IEEE Journal of Biomedical and Health Informatics (JBHI)*, vol. 26, no. 10, pp. 4859–4868, 2022.

[3] H. Rao, S. Wang, X. Hu et al., "A self-supervised gait encoding approach with locality-awareness for 3D skeleton based person Re-identification," *IEEE Transactions on Pattern Analysis and Machine Intelligence*, vol. 44, no. 10, pp. 6649–6666, 2022.

[4] T. Wang, K. Fang, W. Wei, J. Tian, Y. Pan, and J. Li, "Microcontroller unit chip temperature fingerprint informed machine learning for IIoT intrusion detection," *IEEE Transactions on Industrial Informatics*, vol. 19, no. 2, pp. 2219–2227, 2023.

[5] T. Wang, B. Lu, W. Wang, W. Wei, X. Yuan, and J. Li, "Reinforcement learning-based optimization for mobile edge computing scheduling game," *IEEE Transactions on Emerging Topics in Computational Intelligence*, vol. 7, no. 1, pp. 55–64, 2023.

[6] E. Emad, O. Alaa, M. Hossam, M. Ashraf, and M. A. Shamseldin, "Design and implementation of a low-costmicrocontroller-based an industrial delta robot," *WSEAS Transactions on Computers*, vol. 20, pp. 289–300, 2021.

[7] Z. Zhong, Y. Ding, S. Wu, and Y. Guo, "Design of RS422 bus-basedmulti-servo network controller[J]," *Journal of Kunming Metallurgical High School*, vol. 37, no. 3, pp. 71–77, 2021.

[8] X. Chen, C. Zhang, and L. Zhu, "Design of a six-degree-of-freedom robotic arm control system based on micro-controller," *Journal of Tongling College*, vol. 20, no. 2, pp. 106–109, 2021.

[9] W. Li, Y. Liu, S. Ge, and D. Liao, "Research of mechanical resonance analysis and suppression control method of the servo drive system," *Shock and Vibration*, vol. 2021, Article ID 5627734, 15 pages, 2021.

[10] R. Rodríguez-Ponce and F. G. Mota-Muñoz, "Microcontroller-based direct torque control servodrive,"

RETRACTED

Hindawi
Journal of Robotics
Volume 2024, Article ID 9891767, 1 page
https://doi.org/10.1155/2024/9891767

Retraction

Retracted: Industrial Robot Assembly Line Design Using Machine Vision

Journal of Robotics

Received 23 January 2024; Accepted 23 January 2024; Published 24 January 2024

Copyright © 2024 Journal of Robotics. This is an open access article distributed under the Creative Commons Attribution License, which permits unrestricted use, distribution, and reproduction in any medium, provided the original work is properly cited.

This article has been retracted by Hindawi following an investigation undertaken by the publisher [1]. This investigation has uncovered evidence of one or more of the following indicators of systematic manipulation of the publication process:

(1) Discrepancies in scope
(2) Discrepancies in the description of the research reported
(3) Discrepancies between the availability of data and the research described
(4) Inappropriate citations
(5) Incoherent, meaningless and/or irrelevant content included in the article
(6) Manipulated or compromised peer review

The presence of these indicators undermines our confidence in the integrity of the article's content and we cannot, therefore, vouch for its reliability. Please note that this notice is intended solely to alert readers that the content of this article is unreliable. We have not investigated whether authors were aware of or involved in the systematic manipulation of the publication process.

Wiley and Hindawi regrets that the usual quality checks did not identify these issues before publication and have since put additional measures in place to safeguard research integrity.

We wish to credit our own Research Integrity and Research Publishing teams and anonymous and named external researchers and research integrity experts for contributing to this investigation.

The corresponding author, as the representative of all authors, has been given the opportunity to register their agreement or disagreement to this retraction. We have kept a record of any response received.

References

[1] X. Xie, "Industrial Robot Assembly Line Design Using Machine Vision," *Journal of Robotics*, vol. 2023, Article ID 4409033, 13 pages, 2023.

Hindawi
Journal of Robotics
Volume 2023, Article ID 4409033, 13 pages
https://doi.org/10.1155/2023/4409033

Research Article

Industrial Robot Assembly Line Design Using Machine Vision

Xiang Xie

Chongqing Creation Vocational College, Yongchuan 402160, China

Correspondence should be addressed to Xiang Xie; xiexiang202207@126.com

Received 30 September 2022; Revised 20 December 2022; Accepted 22 March 2023; Published 30 March 2023

Academic Editor: Shahid Hussain

Copyright © 2023 Xiang Xie. This is an open access article distributed under the Creative Commons Attribution License, which permits unrestricted use, distribution, and reproduction in any medium, provided the original work is properly cited.

In order to further improve the functional requirements and performance indicators of the industrial robot assembly system and more accurately realize the measurement and recognition of the target position of the assembly line by the vision system, this article constructs a robot assembly line system based on obstacle detection and robot arm obstacle path planning based on machine vision technology and further improves the intelligence and accuracy of the assembly line system through the design and optimization of the system software module. Through the experimental verification of the positioning error based on the eye-to-hand binocular vision system and eye-in-hand monocular vision system, the system proposed in this article meets the design accuracy requirements of less than 0.1 mm in x/*y* direction and less than 1 mm in depth direction and verifies the feasibility and high accuracy of the system.

RETRACTED

1. Introduction

The development of science and technology has not only impacted the traditional manufacturing industry but also provided strong technical support for the production innovation and upgrading of the traditional manufacturing industry. The traditional manufacturing industry gradually began to transform and upgrade towards a more intelligent production line. At this stage, because the production and assembly of reducer requires relatively high precision and most of them need to be assembled manually, the work efficiency is low. The intervention of industrial robots can greatly improve the production efficiency of the assembly line, minimize the investment of traditional labor, and further improve the labor efficiency of the assembly line and the comprehensive economic benefits of the enterprise. The industrial robot assembly line is mainly through the combination of industrial robots, machine vision, and automatic assembly equipment to jointly complete the processes of mass product storage, transportation, detection and assembly, which further improves the efficiency of traditional production and manufacturing. Based on this, this article discusses and designs a higher precision assembly line system from the direction of improving and perfecting the functional requirements and performance indicators of the industrial robot assembly system [1, 2].

2. Literature Review

Taking the assembly process of automobile gearbox as the research goal, this article studies the key technologies that need to be solved in the automatic assembly line and provides a theoretical reference for the actual gearbox assembly work. According to the requirements of the main engine factory and the purpose of adapting to the batch production of single variety and realizing the replacement of machines, an industrial robot air filter assembly line has been developed and designed by the passenger car assembly production line of the No. 2 air filter manufacturing plant. This production line is the key equipment for the production of the passenger car air filter. A company has developed a fully automatic assembly line of automobile interior door handles based on industrial robots. This assembly line can reduce labor costs by 90%, increase production efficiency to the original 400%, and reduce the monthly average failure rate to less than 1%. It provides a feasible reference scheme for the upgrading and transformation of manufacturing methods in the same industry [3]. Talaat et al. pointed out the necessity of industrial robots in wind turbine blade assembly and the enlightenment to the establishment of wind turbine blade automatic assembly production line by analyzing the problems existing in the existing wind turbine blade

assembly and combining the application of industrial robots in automobile assembly and aircraft assembly [4]. However, these production lines are not intelligent enough and still need manual intervention. They have not really realized fully automated production. With the development of science and technology, the birth of more efficient fully automated production lines is called for. Kumar et al. deeply studied the kinematics and trajectory interpolation of palletizer, discussed the application of the scattered node interpolation algorithm in robot trajectory planning, and used this algorithm to interpolate the robot path trajectory to make the robot motion trajectory smoother. Through the simulation and comparison of joint space trajectory planning of the industrial robot through cubic polynomial interpolation and quintic polynomial interpolation, the advantages and disadvantages of the two trajectory planning methods are obtained, which has good reference significance for the trajectory planning of the robot [5]. Zhang et al. proposed a smooth curve transition algorithm for continuous trajectory planning of industrial robot operation space to improve the motion speed of industrial robots during continuous trajectory transition. Under the condition of ensuring the accuracy of continuous trajectory transition, the algorithm tries to improve the speed of the transition area, reduce the transition time, and make the calculation process as simple as possible, so as to be used for online planning and improve the versatility of the algorithm [6].

3. Target Workpiece Recognition Based on the BP Neural Network

3.1. Artificial Neural Network. The artificial neural network is composed of a large number of artificial neurons. Each input x_j in the artificial neuron has a weight w_{ij} related to it. In the processing area, the sum of the input and its corresponding weight values are calculated to calculate the unique output. The mapping relationship between the output y and the weight sum is called the transfer function of neurons. This process can be expressed by the following formula:

$$y = f\left(\sum_j w_{ij}x_j + b\right), \tag{1}$$

where f represents the type of the transfer function used by the neuron in the neural network.

3.2. BP Neural Network Structure Algorithm. The basic idea of using the BP learning algorithm to train the feedforward network is as follows: First, calculate the actual output value of the input characteristics in the training sample after passing through the feedforward network through a forward process. Then, compare the output value with the expected value to get the error signal and then adjust the connection strength between each neuron from back to front according to the error signal. Repeat the forward process calculation again to reduce the error and then compare the new output value with the expected value to obtain a new error signal smaller than the original. Then, according to the small error signal, the connection strength between neurons in each neural network layer is adjusted from back to front. This forward process and backward process are carried out repeatedly until the error meets the requirements. In order to determine all the connection weights of the network, these weight parameters are generally learned through the training sample set [7, 8]. A training set containing n samples can be expressed as

$$X = \{x_n, t_n\}_{n=1}^{N}, \tag{2}$$

where x_n represents the n_i dimensional input characteristics corresponding to the sample and t_n is the n_0 dimensional category output variable.

The define loss function is as follows:

$$l(\Theta; x_n, t_n). \tag{3}$$

To calculate the loss value of a specific set of model parameters on a sample, where Θ is a parameter set, representing all connection weights, namely,

$$\Theta = \left\{W_{ij}^{l}, b_j^{l}\right\}, \tag{4}$$

where W_{ij}^{l} refers to the weight connecting the j^{th} node of the layer l and the i^{th} node of layer $l+1$ and b_j^{l} refers to the offset term of the i^{th} node of the layer $l+1$. In order to obtain the optimal connection weight, the following optimization problems need to be solved:

$$\widehat{\Theta} = \underset{\Theta}{\operatorname{argmin}} \frac{1}{N}\sum_{n=1}^{N} l(\Theta; x_n, t_n). \tag{5}$$

The goal of this optimization problem is to obtain specific parameter values to minimize the total loss of the loss function on the training set. If the square sum error is taken as the optimization objective, the loss function $l(\Theta; x_n, t_n)$ can be expressed as

$$l(\Theta; x_n, t_n) = \frac{1}{2}\left\|t_n - y_n\right\|^2, \tag{6}$$

where y_n represents the output function value obtained when the input of the feedforward network is x_n. Accordingly, the target loss function on the whole training set can be expressed as

$$L\Theta = \frac{1}{2}\sum_{n=1}^{N} l(\Theta; x_n, t_n). \tag{7}$$

The gradient direction of the objective function relative to parameter Θ is

$$\Delta L\Theta = \frac{\partial L\Theta}{\partial \Theta} = \frac{1}{N}\sum_{n=1}^{N}\left(h_\Theta(x_n) - t_n\right)\frac{\partial h_\Theta(x_n)}{\partial \Theta}. \tag{8}$$

Assuming that the initial value of parameter Θ is Θ_0, the parameter Θ is continuously modified according to the gradient descent method.

$$\Theta_{k+1} = \Theta_k + \Delta\Theta_k = \Theta_k - \eta\Delta L(\Theta_k), \tag{9}$$

RETRACTED

where

$$\Delta\Theta_k = -\eta\Delta L(\Theta_k). \tag{10}$$

The above formula represents the update amount of the k^{th} iteration parameters and $\eta \in (0,1)$ is the learning rate.

Assuming that the nonlinear function used by the computing nodes in the network is the sigmoid function, in order to facilitate the later derivation of the back-propagation algorithm, the total input of the i^{th} node of the l^{th} layer of the feedforward network is recorded as z_i^l and its output is recorded as a_i^l. For the hidden layer of the network, there are

$$\begin{cases} a_i^l = \sigma\left(z_i^l\right) = \dfrac{1}{1+\exp\left(-z_i^l\right)}, \\ z_i^{l-1} = \displaystyle\sum_{j=1} W_{ij}^{l-1} a_i^{l-1} + b_i^{l-1}. \end{cases} \tag{11}$$

Assuming that the error of the current network is $E = L(\Theta)$, for the connection weight ΔW_{ij}^l and offset Δb_i^l, the update amount in an update process is, respectively,

$$\begin{cases} \Delta W_{ij}^{n_l} = \dfrac{\partial E}{\partial W_{ij}^{n_l}}, \\ \Delta b_i^j = \dfrac{\partial E}{\partial b_i^j}. \end{cases} \tag{12}$$

The back-propagation process starts from the last layer, continuously applies the chain derivation rule, calculates ΔW_{ij}^l and offset Δb_i^l layer by layer from back to front, and then updates the parameters of each layer. For the output layer, the update amount of the connection offset $\Delta b_i^{n_l-1}$ is

$$\Delta b_i^{n_l-1} = \frac{\partial E}{\partial a_i^{n_l}} \frac{\partial a_i^{n_l}}{\partial z_i^{n_l}} \frac{\partial z_i^{n_l}}{\partial b_i^{n_{l-1}}} = -\left(t_i - a_i^{n_l}\right)\sigma'\left(z_i^{n_l}\right). \tag{13}$$

The update amount of its connection weight $\Delta W_{ij}^{n_l-1}$ is

$$\Delta W_{ij}^{n_l-1} = \frac{\partial E}{\partial z_i^{n_l}} \frac{\partial z_i^{n_l}}{\partial W_{ij}^{n_l-1}} = \Delta b_i^{n_l-1} a_i^{n_l-1}. \tag{14}$$

For the hidden layer, its connection offset $\Delta b_i^{(l-1)}$ is updated as

$$\Delta b_i^{(l-1)} = \sum_{j=1}^{s_{l+1}} \frac{\partial E}{\partial z_j^{l+1}} \frac{\partial z_j^{l+1}}{\partial a_i^l} \frac{\partial a_i^l}{\partial z_i^l} \frac{\partial z_i^l}{\partial W_{ij}^{l-1}} = \Delta b_i^{l+1} a_i^{l-1}. \tag{15}$$

3.3. Target Recognition Process Based on the BP Neural Network. Continuous training of the neural network with a large number of data samples is the premise of using the BP neural network to recognize different targets. The samples include the training input and expected output. The training input data is often some feature quantity of the image, and the expected output can be set as the code corresponding to the image. In the process of training neural network with samples, there are many interference information in the image, which increases the difficulty of network training. Therefore, this article adopts the strategy based on moment invariants to filter out the interference items. The method based on moment invariants combines the moment invariants in the target image and the code of the sorting target in the image to form a training sample, which can change the target image into a set of moment invariants containing 7 numbers. This strategy can simplify the training sample, filter out the interference information, greatly improve the training efficiency, and improve the recognition accuracy at the same time. In order to filter the interference information to the greatest extent, it is also necessary to binarize the target image and make necessary preparations for extracting moment invariant features [9, 10].

In this article, the BP neural network is used to recognize the workpiece, and samples based on moment invariants are used to train the network. The realization process of the recognition algorithm is as follows:

3.3.1. Obtain Target Image Information. Obtain the image of each angle of the object to be recognized.

3.3.2. Image Preprocessing. Graying and binarization form images suitable for moment invariants.

3.3.3. Find Invariant Moment. Highly concentrated image features are used as the basis for image recognition.

3.3.4. Generate Training Samples and Recognition Samples of the Neural Network. After preprocessing the target image taken from multiple angles, the invariant moment of each image is obtained, and the formed vector is combined with the target code to form a training sample. Each image can get a training sample. If the target code in the training sample is removed, the remaining moment invariant sequence can be used as the sample to be identified.

3.3.5. Establish Neural Network. In this article, the BP neural network with the single hidden layer structure is used to recognize the workpiece. Its structure is shown in Figure 1. The transfer functions of 20 neurons in its hidden layer are *s* functions. Since there are three kinds of workpieces to be identified, the output layer is set to three neurons and the transfer function is linear [11].

3.3.6. Training Neural Network. In order to make the training algorithm have the local convergence of the Gauss–Newton method and the global characteristics of the gradient descent method, the Levenberg–Marquardt algorithm with stable performance is used in this article.

3.3.7. Identify the Target. The weight value of the neural network trained by a large number of moment invariant feature samples tends to be stable. When the moment

RETRACTED

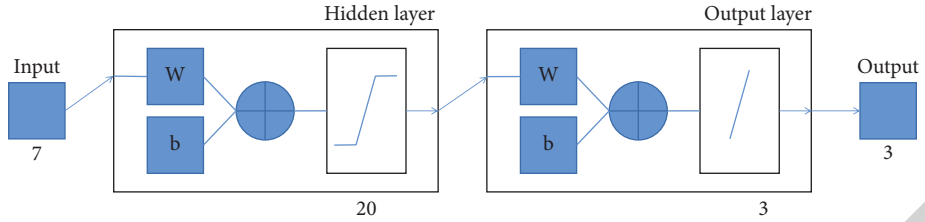

Figure 1: Single hidden layer BP neural network structure.

invariant of the image to be recognized is given, the neural network gives the recognition result through mapping.

3.4. Target Workpiece Recognition Experiment. Take 400 pictures of each workpiece from different angles, each picture can extract a set of moment features, and combined with the workpiece label as a group of training samples, a total of 1200 groups of training samples are obtained to train the neural network. In the identification part, 33 pictures of each workpiece were collected, and a total of 99 groups of moment invariants were used as test samples. Through the above training samples, the weights of neurons in the neural network are determined, and the learning of the whole neural network is completed [12]. Then, take the moment invariant feature of the image to be recognized as the recognition data, and the recognition results obtained through the classification of the neural network are drawn as follows. The recognition results of the classifier based on the BP neural network are shown in Table 1.

The total number of recognition errors and the corresponding classification error rate of the 10 weak classifiers constituting the strong classifier are shown in Table 2, and the number of recognition errors and the corresponding error rate of the strong classifier are shown in Table 3.

Comparing and analyzing the data in Tables 2 and 3, it can be found that the classification error rate of strong classifiers is lower than the average classification error rate of 10 weak classifiers, which shows that the recognition effect of multiple neural networks through weighted voting is better than that of a single neural network [13, 14]. The reason why the recognition effect of strong classifier is better is that strong classifier can adjust the weight according to the training situation of each network, constantly weaken useless features, and finally make the overall recognition rate higher.

Comparison of the accuracy of strong and weak classifiers in identifying workpieces is shown in Table 4.

Through a large number of experiments, it can be found that the classifier based on the BP neural network has a high recognition rate in identifying the mechanical workpiece in this article. However, if the angle of shooting the target workpiece pattern is special, it will have a great impact on the recognition effect of the weak classifier. Compared with the strong classifier based on the AdaBoost algorithm, it is more reliable in both the accuracy of recognition and the anti-interference degree of recognition.

Table 1: Statistics of recognition results of a single weak classifier.

Error type	Small bolt	Large bolt	Nut	Total error	Error rate (%)
Error statistics	3	3	1	7	7.07

Table 2: Statistics of recognition results of multiple weak classifiers.

Weak classifier	1	2	3	4	5	6	7	8	9	10	Total error	Overall classification error rate of weak classifier (%)
Number of errors	6	9	7	8	7	6	9	7	5	9	73	7.37

Table 3: Statistics of strong classifier recognition results.

Error type	Small bolt	Large bolt	Nut	Total error	Error rate (%)
Error statistics	2	1	1	4	4.04

Table 4: Comparison of recognition effects between strong and weak classifiers.

Classification method	Weak classifier based on the BP neural network (%)	Strong classifier based on the AdaBoost algorithm (%)
Accuracy rate	91.93	94.82

4. Software Design and Implementation of the Robot Vision Assembly Line System

4.1. Software Design Scheme of the Robot Visual Assembly System

4.1.1. Software Requirements Analysis. Robot vision assembly system software is an important part of the system. Its purpose is to realize the integration of the vision system and robot control system [15]. This article adopts the upper computer software and the lower control software to form the software control scheme. The functional block diagram of the system software is shown in Figure 2.

4.1.2. Overall Software Architecture. The software design of this article includes the design of upper computer software and lower control software. The main functions of the upper

RETRACTED

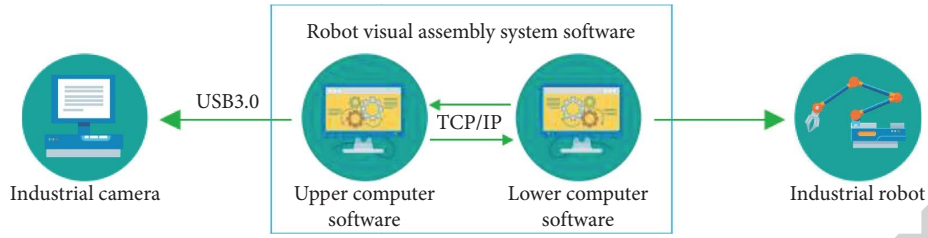

Figure 2: System software function block diagram.

computer software include camera image acquisition, visual processing, obstacle visual detection, and data communication. As an important part of the system software, the lower control software mainly realizes the motion control of the manipulator according to the application request of the upper software, so as to achieve the final assembly execution operation. According to the module division, the upper computer software mainly includes the server side of the visual processing module and the data communication module. The lower control software mainly includes the robot motion control module and the client of the data communication module. The overall architecture of the system software is shown in Figure 3.

After the upper software obtains the parameter information of targets and obstacles in the working environment through the visual processing module, it sends the coordinate point information to the lower software through the data communication module through the path planning. After receiving the information, the lower software converts the coordinate point information into position variables and realizes the control of the manipulator through the motion control program.

4.2. Software Modular Design and Implementation

4.2.1. Visual Processing Module. In this article, the eye-to-hand binocular vision system combined with the eye-in-hand monocular vision system is used to locate the target workpiece. Therefore, the whole system shares three cameras. When collecting images, it should be noted that the two cameras fixed on the bracket should be synchronized [16, 17]. For the camera fixed at the end of the manipulator, image acquisition is carried out by calling OpenCV library functions in the visual studio 2010 development environment. The two cameras fixed on the bracket are mercury series cameras developed by Daheng imaging. The way of image acquisition is more troublesome. Because the camera comes with a sealed SDK, when opening and closing the camera, you need to call the SDK of the camera through OpenCV. The overall workflow of the camera is shown in Figure 4.

The main purpose of the software design of the visual positioning function is to package the visual positioning algorithm studied in Chapter 3 with MFC through software development. In this article, the internal and external parameters of the camera are calibrated through the MATLAB camera calibration toolbox. Combined with these parameters, the software design of the visual positioning function is realized through C++ programming and calling the OpenCV computer vision library function. According to the visual localization algorithm studied in the third chapter, the visual localization software design of this article mainly includes the software design of the eye-to-hand binocular vision system and eye-in-hand monocular vision system [18].

4.2.2. Data Communication Module. The data communication module mainly realizes the communication between the upper computer software and the lower control software. The system adopts the TCP/IP network communication protocol to realize the data transmission between the upper computer and the robot controller. The robot controller is used as the client, and the assembly system software is used as the server. The data transmission is carried out by the sending socket. Figure 5 shows the TCP/IP protocol communication flowchart.

4.2.3. Manipulator Motion Control Module. As an important part of the whole system software, the software development of the manipulator motion control module is the final execution part of the whole assembly process. The traditional industrial robot assembly mode realizes the motion control of the manipulator through teaching programming, that is, the robot teaching device programming is used to record the motion trajectory of the manipulator and reproduce these trajectories repeatedly. This article uses visual guidance to realize the motion control of the manipulator, mainly through the lower computer to receive the coordinate information of the upper computer to control the movement of the manipulator and perform the assembly task.

After the vision system recognizes and detects the target workpiece and obstacles in the working environment and obtains their positions, it plans a path without obstacle collision through the obstacle avoidance path planning algorithm. These paths are composed of multiple smaller straight-line motion tracks. According to the step length set by the artificial potential field method, the size of each straight-line segment can be controlled. It will be sent to the manipulator in the form of coordinate point information and stored in the string variable of the manipulator. Therefore, it is necessary to convert these coordinate point information into the motion trajectory of the manipulator through the lower level program. The design flowchart of the manipulator motion control program is shown in Figure 6.

RETRACTED

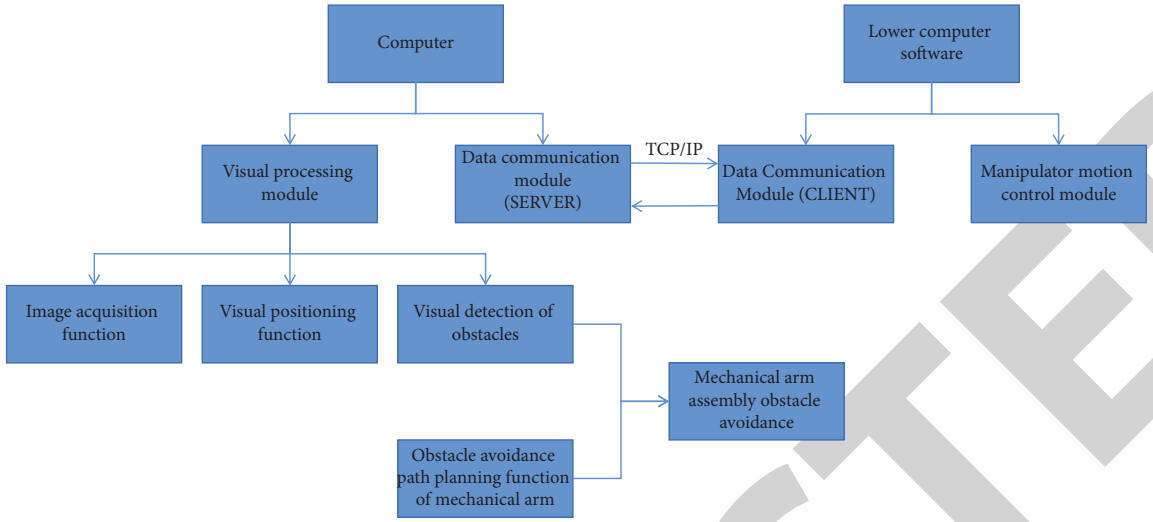

Figure 3: Software architecture of the robot visual assembly system.

4.2.4. Industrial Robot Assembly Program

(1) Trajectory Planning. To complete the tasks of handling and assembly, we must first plan the motion of the robot, that is, action planning and trajectory planning. (1) *Action planning.* According to the design, the robot needs to carry out three subtasks: handling, assembly, and disassembly. The robot handling task refers to the robot carrying the workpieces 1–4 at the position G1 on the workpiece assembly line to the assembly area of the assembly line and recycles the pallet. The robot assembly task refers to that the robot transports the workpiece 1 of the finished product warehouse and the workpiece 2–4 of the spare parts warehouse of the assembly line to the assembly area, respectively, carries out assembly after secondary positioning, and transports the finished products to the finished product warehouse. The task of robot disassembly refers to that the robot carries the finished products in the finished product warehouse to the assembly area, disassembles them after secondary positioning, and places them at four positions in the assembly area [19]. (2) *Trajectory planning.* Trajectory planning is to decompose each action into the motion trajectory of the robot TCP. Considering the robot posture and the interference between the robot and surrounding equipment, each action needs to have one or more points to form a motion trajectory. The trajectory planning of the robot handling task is shown in Figure 7.

(2) Procedure Flow. The whole workflow of the robot handling program includes "grabbing or sucking the workpiece and pallet," "placing the workpiece and pallet," and "returning to the safety point," as shown in Figure 8, the whole workflow of the robot assembly and disassembly program.

5. System Experiment and Analysis

5.1. Experiment and Analysis of Visual Positioning Error Measurement. The accuracy of the robot visual assembly system is mainly determined by the accuracy of visual positioning and the accuracy of repeated positioning of industrial robots. The Gugao GRB-4016 industrial robot used in this system has a repeated positioning accuracy of 0.03 mm, which is high in positioning accuracy, and can meet most industrial assembly needs. For the accuracy of visual positioning, this article designs an experiment of visual positioning error measurement. In this article, a 9-point calibration block is used to measure the visual positioning error by measuring the distance between the centers of two adjacent circles and calculating the relative position between the centers.

First, use a nine-point calibration block with a height of 50 mm and place it in the field of view. Click the "multipoint measurement" button of the upper software to calculate the position of each circle center under the camera coordinate system. By calculating the difference of the coordinate positions of the adjacent two circle centers, the distance between the adjacent two circle centers can be calculated. There are 9 points on each calibration block, and 12 groups can be measured. The average value of them is the first group of data. Then, change the position of the calibration block within the field of view, measure in the upper left area, upper right area, lower left area, and lower right area within the field of view, respectively, and obtain four groups of data. Replace the nine-point calibration block with a depth of 35 mm, and the measurement method is similar to the above. The measurement errors obtained from the experiment are shown in Tables 5 and 6.

In the binocular vision measurement system, the positioning error in the x/y direction is proportional to the measurement distance and the error in the depth direction is proportional to the square of the measurement distance. Therefore, with the increase of the measurement distance, the error in the depth direction is more difficult to control than the error in the x/y direction. According to the experimental data analysis of the positioning error of the eye-to-hand binocular vision system, the error in the X direction is 0.220 mm, the error in the Y direction is 0.199 mm, and the error in the depth direction is 0.630 mm, which conforms to

RETRACTED

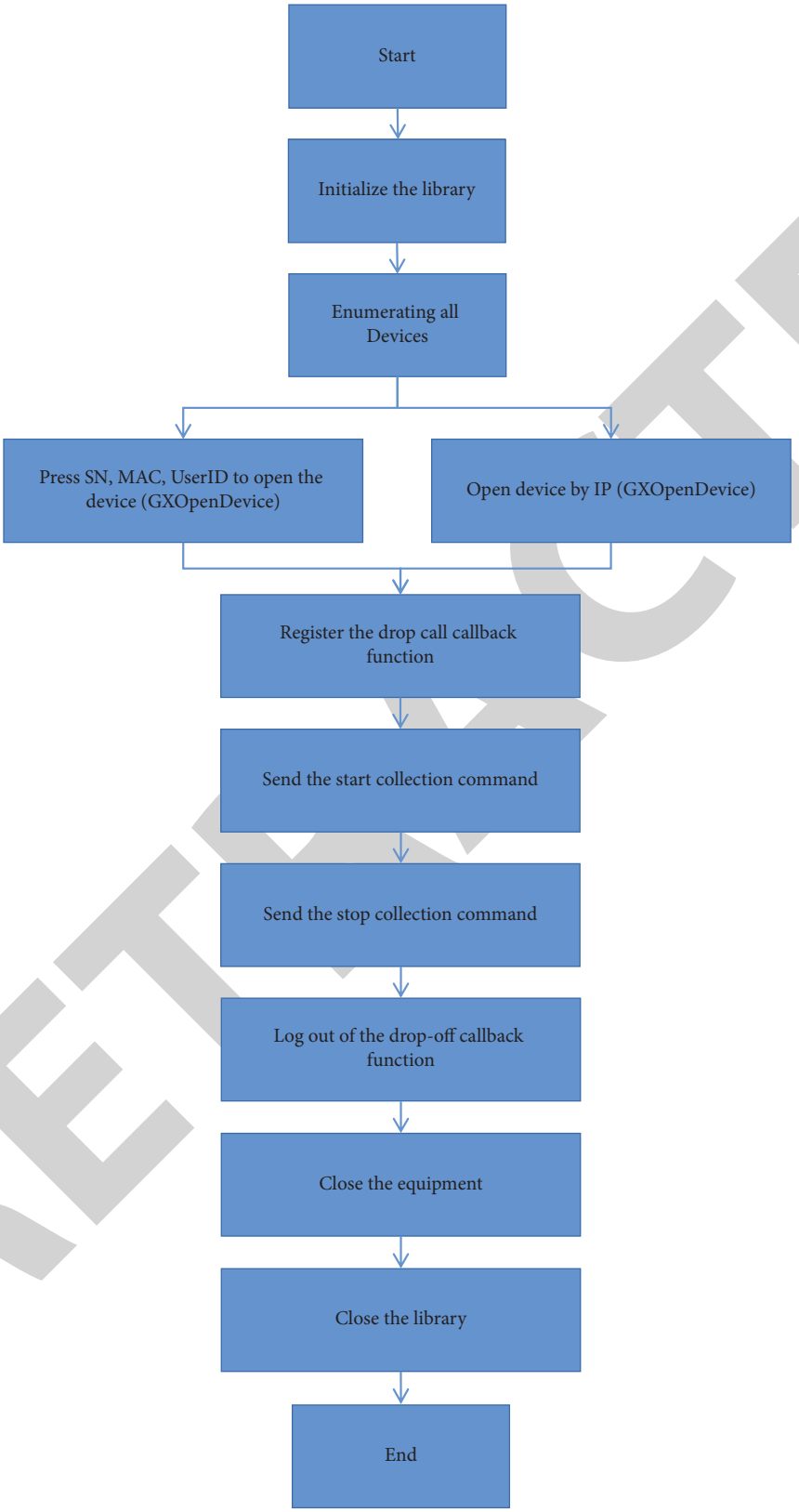

Figure 4: Overall workflow of mercury camera.

RETRACTED

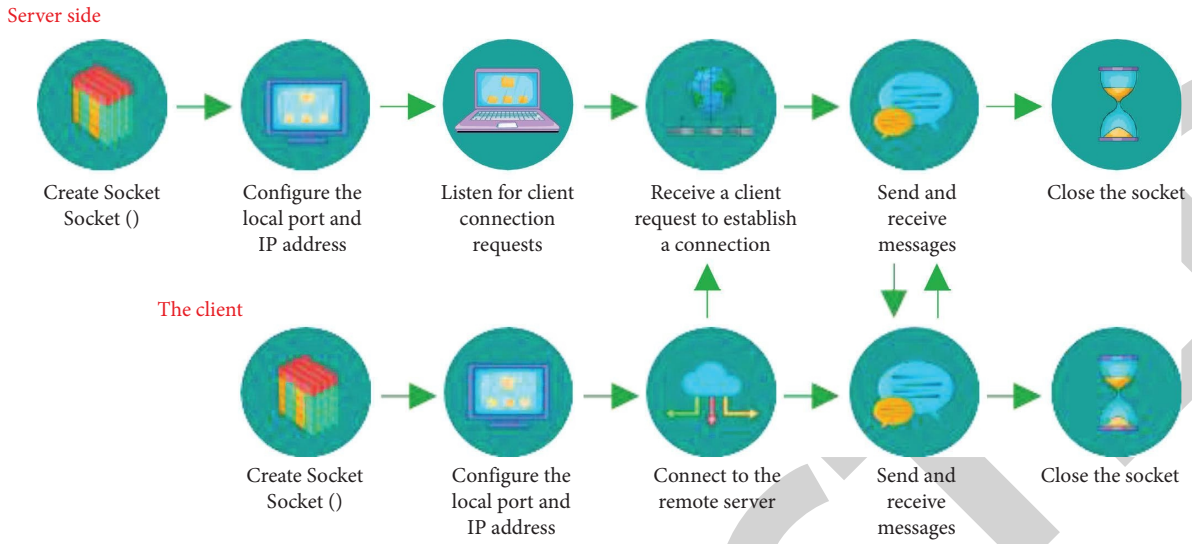

Figure 5: TCP/IP communication protocol flowchart.

the characteristics of the binocular vision system measurement error. Due to the high accuracy requirements of the x/y direction of this system, in order to solve the problem that the accuracy of the eye-to-hand binocular vision system in the x/y direction cannot meet the requirements due to the long measurement distance, this article introduces the eye-in-hand monocular vision system to accurately locate the two-dimensional information of the target. According to the analysis of its experimental error data, the positioning error in the X direction is 0.033 mm and the positioning error in the Y direction is 0.045 mm.

Based on the above analysis, by introducing the eye-in-hand monocular vision system, the visual positioning accuracy in the x/y direction is greatly improved, which verifies the feasibility of the visual-positioning method based on the combination of the eye-to-hand and eye-in-hand system.

5.2. Experiment and Analysis of Overall Accuracy Measurement of the System

5.2.1. Simulation after Trajectory Optimization. On the premise that the maximum speed of the robot is constant, a five-order s-curve optimization method with time and impact as optimization indexes is proposed. The variable parameters are introduced into the optimization of impact force, which greatly shortens the acceleration time of the robot while ensuring the minimum impact force. In order to verify the effectiveness of the optimized fifth-order s-curve method, the traditional fifth-order s-curve and the optimized fifth-order s-curve are compared and analyzed, and the two curves are simulated and compared by MATLAB simulation software, so as to verify the effectiveness of the optimized curve. The simulation curves of displacement, velocity, and acceleration of the two curves are shown in Figures 9(a)–9(c).

As can be seen from the curves in Figure 9, compared with the traditional five-order s-curve, the acceleration time of the optimized five-order s-curve for robot trajectory planning is reduced from 0.65 s to 0.54 s and the maximum acceleration is increased from 3.5 m/s^2 to 4.7 m/s^2. The acceleration time is shortened, and the motion efficiency of the robot is also improved. Therefore, the acceleration curve of the robot is smoother, greatly improving the stability of operation.

5.2.2. Overall Accuracy Measurement Results. In order to verify the overall accuracy of the robot visual assembly system, this article takes the shaft hole assembly experiment as an example. As shown in Figure 10, the axial calibration workpiece and hole calibration workpiece used in the experiment are shown. The radius of the hole calibration workpiece is 0.1 mm larger than that of the axial calibration workpiece. Therefore, as long as the positioning error is greater than 0.1 mm, the assembly cannot be successful.

First, start the six degree of freedom industrial robot, open the robot control cabinet, and check whether the servo driver of each axis starts normally. If it is normal, control the rotation of each axis through the robot teaching pendant, check whether there is any abnormality in the rotation of each axis, start the upper software of the robot visual assembly system, set the port number, wait for the robot controller to establish a connection with it, open the left and right cameras fixed on the bracket and the cameras at the end of the robot arm, and check whether the three cameras can collect images normally. After the connection is established, place the workpiece randomly on the assembly console and ensure that it is within the field of vision. The upper software controls the camera to collect the image of the workpiece and obtains the position information through the visual positioning algorithm, which is sent to the industrial robot for assembly after coordinate conversion. First, after rough positioning by the eye-to-hand binocular vision system, the robot controls the camera at the end of the manipulator to move to 15 cm above the target workpiece and triggers the camera at the end of the manipulator to take photos for secondary positioning. After secondary positioning, adjust the position of the end of the manipulator, and finally

RETRACTED

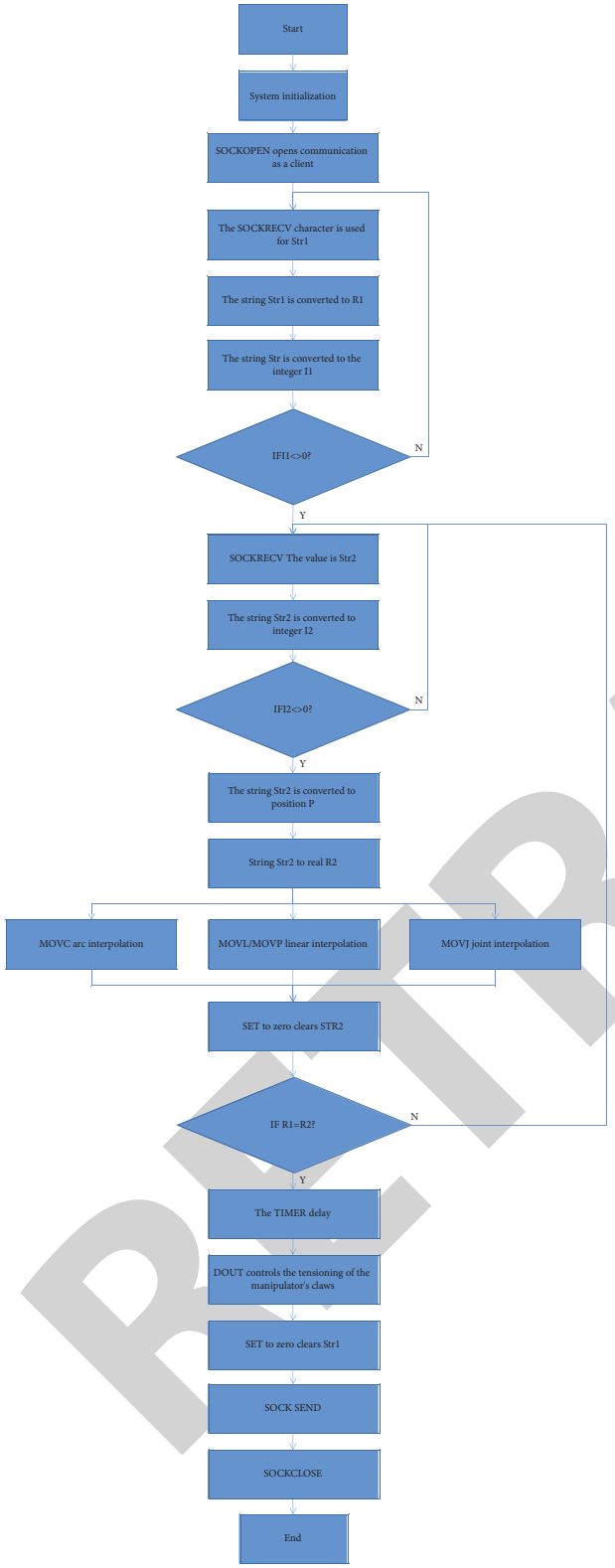

Figure 6: Software design flow of the manipulator motion control module.

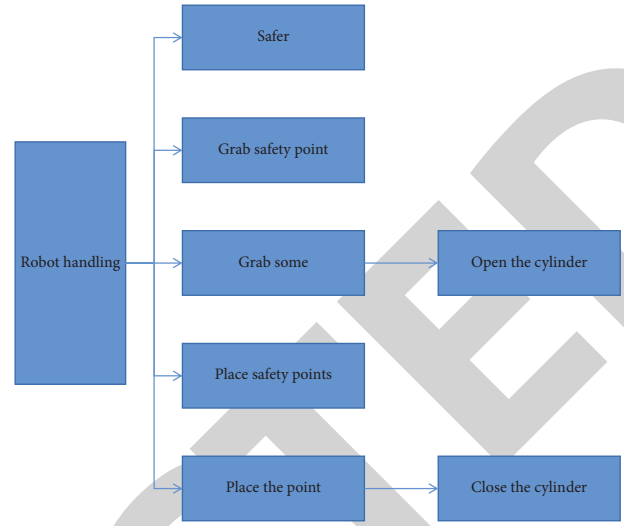

Figure 7: Trajectory planning.

control the assembly system for assembly operation. After assembly, the robot returns to the waiting area.

Through the analysis of the results of 10 visual guided assembly experiments at different positions and heights, the overall accuracy of the system is less than 0.1 mm in the X and Y directions and less than 1 mm in the depth direction. Through the experimental verification of the obstacle avoidance function in the assembly process of the manipulator and according to the analysis of the experimental results, it is verified that the assembly system developed in this study can autonomously avoid the obstacles encountered in the movement process when performing tasks, and the motion trajectory of the end of the manipulator is relatively smooth, there is no significant angle change, ensuring the safety in the assembly process of the manipulator [20].

This chapter mainly focuses on the experimental verification and analysis of the system function. Aiming at the accuracy measurement of the assembly system, this article first carried out the experiment of visual-positioning error measurement and measured the positioning error of the eye-to-hand binocular vision system and eye-in-hand monocular vision system through the experiment. Then, through the overall accuracy measurement experiment of the system, it is verified that the system meets the accuracy requirements of less than 0.1 mm in the x/y direction and less than 1 mm in the depth direction. Finally, the obstacle avoidance function of the manipulator in the assembly process is verified by experiments. The results show that the manipulator can successfully avoid obstacles with regular and irregular shapes in the assembly process. Through the experimental verification and analysis of the robot visual assembly system, it shows that the assembly system developed in this article has the characteristics of intelligence and high precision.

RETRACTED

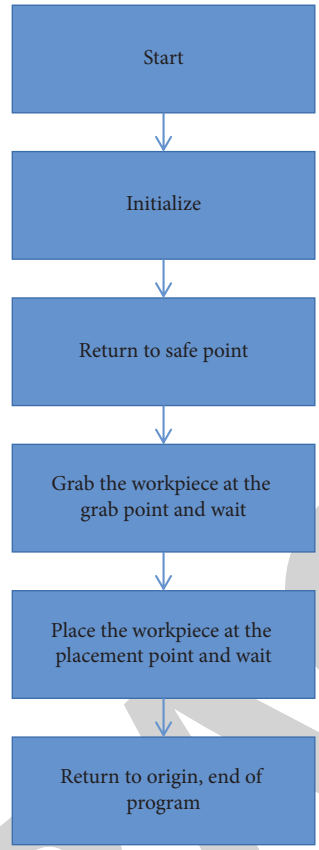

Figure 8: Procedure flowchart.

Table 5: Experimental data of the eye-to-hand binocular vision system positioning error.

Number	1	2	3	4	5	6	7	8	Average values
$\triangle x$ (mm)	0.202	0.192	0.352	0.215	0.162	0.265	0.135	0.238	0.220
$\triangle y$ (mm)	0.315	0.163	0.138	0.136	0.222	0.217	0.230	0.170	0.199
$\triangle z$ (mm)	0.713	0.825	0.695	0.912	0.835	0.652	0.325	0.625	0.630

Table 6: Experimental data of the eye-in-hand monocular vision system positioning error.

Number	1	2	3	4	5	6	7	8	Average values
$\triangle x$ (mm)	0.017	0.040	0.022	0.072	0.069	0.017	0.014	0.026	0.033
$\triangle y$ (mm)	0.034	0.008	0.050	0.070	0.081	0.009	0.009	0.092	0.045

RETRACTED

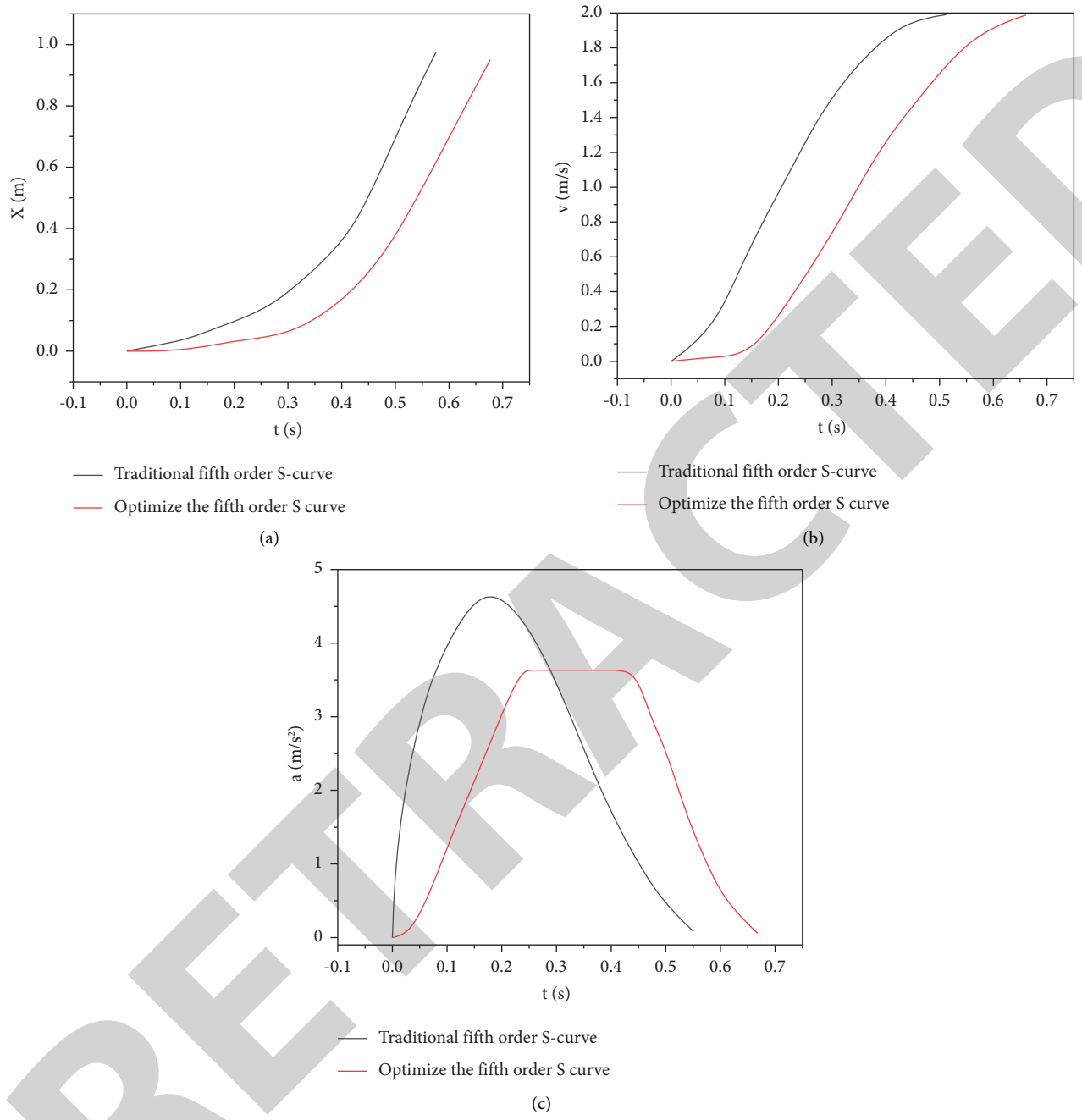

Figure 9: Simulation curves of different algorithms: (a) displacement curve, (b) velocity curve, and (c) acceleration curve.

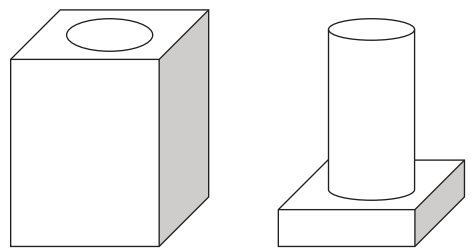

Figure 10: Experimental workpiece.

RETRACTED

6. Conclusion

This article takes the industrial robot assembly technology based on machine vision as the research object, mainly studies the visual measurement technology and the robot arm obstacle avoidance technology in the assembly process, and shows the theoretical research results by developing the robot visual assembly system. The system can be flexibly applied in complex and changeable working environment, which greatly improves the practical application range of the industrial robot assembly technology.

(1) According to the analysis of the system function and performance index requirements, the visual-positioning method combining the eye-to-hand and eye-in-hand system is used to measure the position of the target. By studying camera calibration technology, robot hand eye calibration technology, and image feature extraction technology, the accurate positioning of the target workpiece is achieved.

(2) The obstacle avoidance problem of the manipulator in the assembly process is studied. Firstly, the obstacle circle is used.

The cylindrical minimum bounding box models various irregular obstacles and realizes the visual location of obstacles through the minimum bounding circle algorithm. Combined with the obtained obstacle information and target workpiece information, the artificial potential field method is used to realize the obstacle avoidance path planning of the manipulator.

(3) The feasibility of the visual-positioning method used in this system is verified by setting up and completing the visual positioning error measurement experiment and the overall accuracy measurement experiment of the system. The obstacle avoidance function of the system is verified by the obstacle avoidance function verification experiment of the manipulator.

The system adopts the visual-positioning method combining the eye-to-hand and eye-in-hand system to improve the positioning accuracy in the X and Y directions of the system, and the depth information is measured by eye-to-hand binocular vision system. Through the experimental verification of the positioning error based on the eye-to-hand binocular vision system and eye-in-hand monocular vision system, the system proposed in this article meets the design accuracy requirements of less than 0.1 mm in the x/y direction and less than 1 mm in the depth direction. Considering that the currently developed binocular vision system is not accurate enough in measuring the target depth information, the next step will be to study the methods to improve the measurement accuracy of the depth direction.

Data Availability

The labeled data set used to support the findings of this study is available from the corresponding author upon request.

Conflicts of Interest

The author declares that there are no conflicts of interest.

Acknowledgments

This work was supported by the Chongqing Higher Education Teaching Reform Research Project (no. 192095).

References

[1] J. Zhou and J. Yu, "Chisel edge wear measurement of high-speed steel twist drills based on machine vision," *Computers in Industry*, vol. 128, no. 5–8, Article ID 103436, 2021.

[2] B. Lza, C. Jian, A. Zy, Y. A. Hao, A. Mc, and B. Xy, "Research on precision automatic tool setting technology for kdp crystal surface damage mitigation based on machine vision," *Journal of Manufacturing Processes*, vol. 64, no. 2, pp. 750–757, 2021.

[3] X. Lin, X. Wang, and L. Li, "Intelligent detection of edge inconsistency for mechanical workpiece by machine vision with deep learning and variable geometry model," *Applied Intelligence*, vol. 50, no. 7, pp. 2105–2119, 2020.

[4] M. Talaat, I. Arafa, and H. Metwally, "Advanced automation system for charging electric vehicles based on machine vision and finite element method," *IET Electric Power Applications*, vol. 14, no. 13, pp. 2616–2623, 2020.

[5] R. Kumar, O. Patil, K. Nath S, K. S. Sangwan, and R. Kumar, "A machine vision-based cyber-physical production system for energy efficiency and enhanced teaching-learning using a learning factory," *Procedia CIRP*, vol. 98, no. 9, pp. 424–429, 2021.

[6] Y. Zhang, H. G. Soon, D. Ye, J. Y. H. Fuh, and K. Zhu, "Powder-bed fusion process monitoring by machine vision with hybrid convolutional neural networks," *IEEE Transactions on Industrial Informatics*, vol. 16, no. 9, pp. 5769–5779, 2020.

[7] Y. Guo, L. Chai, S. E. Aggrey, A. Oladeinde, J. Johnson, and G. Zock, "A machine vision-based method for monitoring broiler chicken floor distribution," *Sensors*, vol. 20, no. 11, pp. 3179–3183, 2020.

[8] Z. Liu, Y. He, C. Wang, and R. Song, "Analysis of the influence of foggy weather environment on the detection effect of machine vision obstacles," *Sensors*, vol. 20, no. 2, pp. 349–352, 2020.

[9] C. Li, Y. Huang, H. Li, and X. Zhang, "A weak supervision machine vision detection method based on artificial defect simulation," *Knowledge-Based Systems*, vol. 208, no. 4, Article ID 106466, 2020.

[10] T. Zhang, X. Hu, J. Xiao, and G. Zhang, "A machine learning method for vision-based unmanned aerial vehicle systems to understand unknown environments," *Sensors*, vol. 20, no. 11, pp. 3245–3250, 2020.

[11] A. M. Karimi, J. S. Fada, N. A. Parrilla et al., "Generalized and mechanistic pv module performance prediction from computer vision and machine learning on electroluminescence images," *IEEE Journal of Photovoltaics*, vol. 10, no. 3, pp. 878–887, 2020.

[12] Z. Jiang, M. Huang, X. Tang, and Y. Guo, "A new calibration method for joint-dependent geometric errors of industrial robot based on multiple identification spaces," *Robotics and Computer-Integrated Manufacturing*, vol. 71, no. 1, pp. 102175–102182, 2021.

RETRACTED

Hindawi
Journal of Robotics
Volume 2024, Article ID 9830829, 1 page
https://doi.org/10.1155/2024/9830829

Retraction

Retracted: Transmission Line Condition Monitoring Method Based on Binocular Vision and Edge Computing for Line Changing Robot

Journal of Robotics

Received 23 January 2024; Accepted 23 January 2024; Published 24 January 2024

Copyright © 2024 Journal of Robotics. This is an open access article distributed under the Creative Commons Attribution License, which permits unrestricted use, distribution, and reproduction in any medium, provided the original work is properly cited.

This article has been retracted by Hindawi following an investigation undertaken by the publisher [1]. This investigation has uncovered evidence of one or more of the following indicators of systematic manipulation of the publication process:

(1) Discrepancies in scope
(2) Discrepancies in the description of the research reported
(3) Discrepancies between the availability of data and the research described
(4) Inappropriate citations
(5) Incoherent, meaningless and/or irrelevant content included in the article
(6) Manipulated or compromised peer review

The presence of these indicators undermines our confidence in the integrity of the article's content and we cannot, therefore, vouch for its reliability. Please note that this notice is intended solely to alert readers that the content of this article is unreliable. We have not investigated whether authors were aware of or involved in the systematic manipulation of the publication process.

Wiley and Hindawi regrets that the usual quality checks did not identify these issues before publication and have since put additional measures in place to safeguard research integrity.

We wish to credit our own Research Integrity and Research Publishing teams and anonymous and named external researchers and research integrity experts for contributing to this investigation.

The corresponding author, as the representative of all authors, has been given the opportunity to register their agreement or disagreement to this retraction. We have kept a record of any response received.

References

[1] Z. Lu, J. Duan, X. Chen, and Y. Chen, "Transmission Line Condition Monitoring Method Based on Binocular Vision and Edge Computing for Line Changing Robot," *Journal of Robotics*, vol. 2023, Article ID 7747194, 10 pages, 2023.

Hindawi
Journal of Robotics
Volume 2023, Article ID 7747194, 10 pages
https://doi.org/10.1155/2023/7747194

RETRACTED

Research Article

Transmission Line Condition Monitoring Method Based on Binocular Vision and Edge Computing for Line Changing Robot

Zheng Lu,[1] **Jiazhen Duan**,[2] **Xiaoqiang Chen**,[3] **and Yang Chen**[4]

[1]*Changzhou Jinling Electric Power Industrial Co., Ltd., State Grid Changzhou Power Supply Company, Changzhou, Jiangsu 213000, China*
[2]*Transmission and Distribution Engineering Company, State Grid Changzhou Power Supply Company, Changzhou, Jiangsu 213000, China*
[3]*State Grid Changzhou Power Supply Company, Changzhou, Jiangsu 213000, China*
[4]*School of Microelectronics and Control Engineering, Changzhou University, Changzhou, Jiangsu 213164, China*

Correspondence should be addressed to Yang Chen; chenyang.heu@gmail.com

Received 19 August 2022; Revised 15 September 2022; Accepted 16 September 2022; Published 27 February 2023

Academic Editor: Shahid Hussain

Copyright © 2023 Zheng Lu et al. This is an open access article distributed under the Creative Commons Attribution License, which permits unrestricted use, distribution, and reproduction in any medium, provided the original work is properly cited.

Efficient and accurate state detection of transmission cables is an important means to ensure reliable transmission. Aiming to realize fast and efficient transmission cable state analysis with the help of a binocular vision tool on a loop dismantling robot, this paper proposes a transmission cable state recognition method combining motion control and image segmentation technology. In this method, the fuzzy *PID* control method is adopted to ensure that the wire removal robot can realize high-precision and rapid response control and effectively improve the collection quality of the cable image sample set. Meanwhile, aiming to achieve faster and more efficient data acquisition and state analysis, the state analysis model is sunk to the edge side, and the cable state detection and recognition model is constructed based on the fast RCNN model at the edge of the network to realize the in-depth extraction of feature information, enhance the transmission cable state recognition effect of the state detection model, and improve the response analysis speed of the model. The simulation results show that the accuracy of the proposed method is 97.54%, and its calculation time is 1.034 s, which can effectively realize the analysis and research of transmission cable state under complex working conditions.

1. Introduction

After the high-voltage transmission line has been exposed to the outside and has been infringed by the external environment, such as rainstorms and lightning, for a long time, it is very prone to conductor strand breakage, insulator contamination, hardware damage, bolt loosening, and other phenomena. If it is not found and maintained in time, it will threaten the transmission stability of the transmission line, cause regional power failures, and bring huge economic losses [1–3].

Aiming to ensure the stable operation of the power system and reduce the labor intensity of line maintenance operators, cable condition monitoring has become the focus of the electrical field in recent years [4].

At present, there are three common inspection methods [5, 6]. The first is the manual visual inspection method. The inspectors can accurately judge the line status by observing at a close distance on the site, but the staff needs to walk in the mountainous area. The inspection frequency is relatively low and the work intensity is high. The second is the manned helicopter aerial survey method, which can realize more efficient cable state identification, but it has the disadvantages of high cost and dangerous flight in mountainous areas. The third way is Unmanned Aerial Vehicle (UAV) patrol inspection, but it has high requirements for the weather, so it is difficult to control a UAV in the case of strong wind [7].

Compared with traditional inspection methods, the line-changing robot that can climb the power line can climb the

power line with a camera and infrared equipment at a certain speed, cross various obstacles on the power line and inspect the power line and various fittings on it, which has the characteristics of lower inspection cost and higher inspection efficiency [8, 9].

Because the line-changing robot can complete tasks that cannot be completed manually and has high precision and efficiency, its great value has attracted numerous scientific research institutions to use it as the main research object [10]. It can improve the shortcomings of the original inspection method, reduce the maintenance cost of the transmission line, and complete the line inspection at a high frequency, greatly improving the performance of the power system [11].

In recent years, artificial intelligence technology and machine learning technology have been developed by leaps and bounds, which provides a new solution for intelligent line inspection of line-changing robots [12, 13]. The image data file is obtained through the sensor of the image acquisition terminal, and the feature extraction and learning of the sample data information are realized based on the multi-layer network model, so as to realize the condition monitoring and analysis of the transmission cable according to the training model [14–16]. At present, some scholars have carried out an analysis of the cable state based on a deep network model. Reference [17] Based on convolutional neural networks, feature extraction and accurate identification of high-voltage transmission lines are carried out to judge the abnormal state of high-voltage lines. Reference [18] takes the mask region convolutional neural network (RCNN) model as the basic network to realize the identification, judgment, and analysis of foreign matters in transmission cables. Reference [19] adopts the combination of a fast smooth tracking algorithm and a deep learning network to realize the identification and analysis of transmission equipment based on a UAV terminal. Reference [20] adopts content-based image retrieval technology to build a monitoring system for transmission lines so as to provide reliable support for high-voltage transmission. However, we should also see that, due to the limitations of the working environment of the transmission cable and the complex motion environment of the robot, aiming to ensure the collection of high-quality cable state sample data sets, there is an urgent need for reliable and stable control methods to provide a reliable guarantee for the motion of the robot [21]. At the same time, for the state analysis model, accurate and complete information feature extraction is the key support to improving the intelligent line inspection of robot cables [22].

Efficient and fast transmission line state analysis is an important guarantee for long-distance transmission. From the point of view of robot motion stability and image analysis optimization, we propose a method for monitoring and analyzing the status of power transmission lines based on motion control technology and a deep network model. The innovations of this method are as follows:

(1) To provide stable mobile support for cable state acquisition and image analysis, firstly, the fuzzy *PID* control method is used to realize the motion trajectory control of the line removal and replacement robot, and the weighted average method is used to solve the fuzzy process to further support the smooth and accurate control of the motion mechanism and provide a reliable motion guarantee for the robot;

(2) In order to realize more rapid and accurate cable image analysis, image analysis and recognition models are built based on the fast RCNN model to strengthen the depth acquisition ability of information features, optimize the model loss function, further reduce the recognition error of model training and testing, and extract the information features of the collected images in depth.

2. Motion Control of the Line-Changing Robot Based on Binocular Vision

A high-quality image sample set is an important prerequisite for efficient analysis of the cable state recognition network model. Aiming to ensure that the robot can stably collect the actual transmission line image, we optimize the robot motion control method to ensure its stable and controllable motion. Figure 1 is a schematic diagram of the motion working scene of the wire removal robot.

Even if the overhead cables in mountainous areas are tightened, it is difficult to achieve the goal of being parallel to the ground. When the robot travels on an inclined cable, its stress is shown in Figure 2.

It is not difficult to analyze that if (1) holds, the robot can be stable on the cable without slipping.

$$f = g_x. \tag{1}$$

Here, f is the comprehensive force provided by the wire hanging mechanism, g_x is the component of gravity g, and the size of g_x depends on the inclination of the cable. In order to make the robot travel in the arrow direction of f on the cable, the comprehensive force is provided by the wire hanging mechanism $f > g_x$.

2.1. Determination of the Target Coordinate System. In this paper, the binocular camera is applied to the line patrol robot, and the target coordinates in the three-dimensional coordinate system of the camera are uniformly transformed into the coordinates in the robot's coordinate system, that is, the coordinate transformation relationship of the line patrol robot should be found through hand-eye calibration.

If the coordinate point of the identified target in the manipulator world coordinate system is (x_1, y_1, z_1), the corresponding coordinate in the camera coordinate system is (x_2, y_2, z_2). The two can coincide through rotation and translation. The transformation relationship expression is as follows:

$$\begin{bmatrix} x_1 \\ y_1 \\ z_1 \end{bmatrix} = R \begin{bmatrix} x_2 \\ y_2 \\ z_2 \end{bmatrix} + T, \tag{2}$$

where R is the orthogonal identity matrix and belongs to the rotation matrix of the coordinate system, T is the column vector, which belongs to the translation matrix of the coordinate system.

RETRACTED

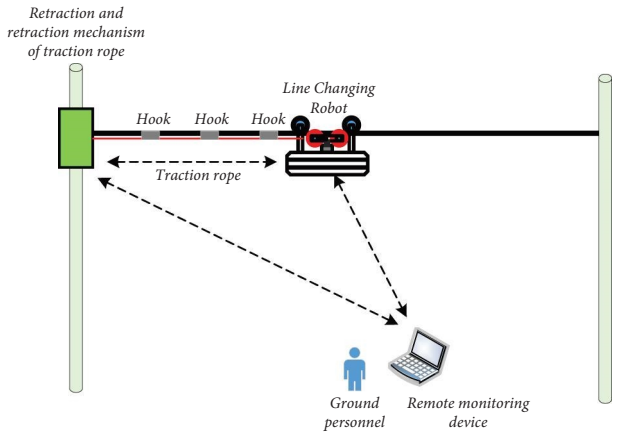

Figure 1: Working scene diagram of the intelligent robot system for disassembly and replacement line.

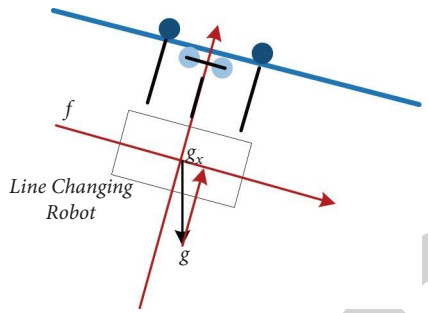

Figure 2: Force analysis of the wire dismantling robot.

The rotation of the coordinate system is divided into three steps; that is, the rotation angles around the x axis, y axis, and z axis are θ, σ, and ω, respectively. Then the rotation amount of each time is described as follows:

$$R_x = \begin{bmatrix} 1 & 0 & 0 \\ 0 & \cos\theta & -\sin\theta \\ 0 & \sin\theta & \cos\theta \end{bmatrix},$$

$$R_y = \begin{bmatrix} \cos\sigma & 0 & \sin\sigma \\ 0 & 1 & 0 \\ -\sin\sigma & 0 & 1 \end{bmatrix}, \quad (3)$$

$$R_z = \begin{bmatrix} \cos\omega & -\sin\omega & 0 \\ \sin\omega & \cos\omega & 0 \\ 0 & 0 & 1 \end{bmatrix}.$$

Among them, there is $R = R_x R_y R_z$. In addition, the translation matrix T indicates that the translation distances on the x axis, y axis, and z axis of the coordinate system are a,b, and c, respectively. The expression is described as

$$T = \begin{bmatrix} a \\ b \\ c \end{bmatrix}. \quad (4)$$

Since the relative position between the binocular camera and the line patrol robot always keeps one point, only the unknown parameters R and T need to be solved to find the changing relationship between the point in the camera coordinate system and the coordinate system of the line patrol robot.

2.2. Fuzzy PID Control. The motion mechanism of the line patrol robot is affected by factors such as motor load change, connector clearance, mechanism wear, and external interference. Its motion mechanism parameters may change at any time, and the whole system has a certain time variability [23, 24].

In the motion mechanism of the line inspection robot, the whole system is nonlinear and unpredictable. The key to fuzzy *PID* is to dynamically change the three important parameters of the *PID* process in the control process by combining the fuzzy algorithm to make the control more accurate and stable.

The traditional *PID* control method is difficult to achieve the expected control effect, and the conventional *PID* needs to establish an accurate mathematical model to set the parameters of the motion mechanism, which is quite complex and not practical. Therefore, we use the fuzzy *PID* control method to control the robot to meet the needs of different degrees of error for *PID* parameter self-adjustment so as to improve the accuracy and dynamic response of the control system.

The principle of fuzzy *PID* control is shown in Figure 3. The deviation and deviation change rate between the expected motion and the actual motion of the motion mechanism are taken as the inputs of the fuzzy controller. The fuzzy controller fuzzies the input signal and then defuzzifies the fuzzy reasoning and reasoning results to obtain the adjustment values ΔG_p, ΔG_i, and ΔG_d of the three *PID* parameters.

Considering the response ability and robustness of the system, the paper formulates the establishment of following fuzzy control rules:

(1) When the deviation s is large, increase G_p to increase the adjustment force, reduce G_d and remove G_i;

(2) when the deviation s and deviation change rate Δs are large, appropriately reduce the G_i value, and select the medium equivalent of G_p and G_d;

(3) if the deviation s is very small, the G_d selection is medium. If Δs is also small, the G_d can be larger. If Δs is larger, G_d is smaller;

(4) when the deviation s increases, if s is large, increase G_p, reduce G_i and select the medium equivalent of G_d. If s is small, G_p is selected as the medium equivalent, increasing G_i and reducing G_d;

(5) when the deviation s decreases, if G_p is large, G_p should select the medium equivalent, increase G_i and reduce G_d. If s is small, reduce G_p and G_i, and select the medium equivalent of G_d.

RETRACTED

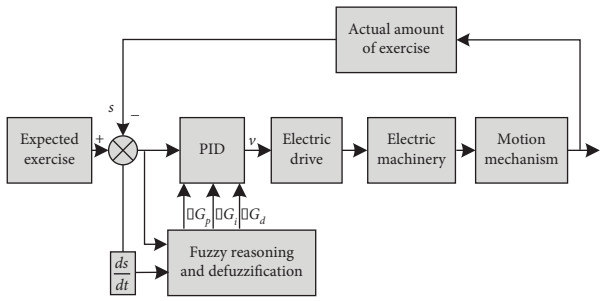

Figure 3: Fuzzy *PID* control block diagram of line changing robot.

The fuzzy universe of three parameter variables of *PID* controller is set as $\{-2.5, -1.5, -0.5, 0, 0.5, 1.5, 2.5\}$, and $\{NB, NM, NS, ZE, PS, PM, PB\}$ is used to represent the subset of input and output. The corresponding language values are defined as: negative large, negative medium, negative small, zero, positive small, positive medium, and positive large.

Output the fuzzy quantity corresponding to the current deviation and deviation change rate, get the parameter correction item after defuzzification, and adjust the parameter variable of *PID* controller.

$$\begin{cases} G_p = G_{p0} + \Delta G_p, \\ G_i = G_{i0} + \Delta G_i, \\ G_d = G_{d0} + \Delta G_d, \end{cases} \tag{5}$$

where G_{p0}, G_{i0}, and G_{d0} represent the initial values of the three parameters of the *PID* controller; ΔG_p, ΔG_i, and ΔG_d are the adjustment values of corresponding parameters.

In the process of operation, according to the detection position deviation s and deviation rate Δs, 3 parameters of the *PID* controller are adjusted in real time, and then the motor speed is controlled by the adjusted parameters in formula (5).

$$v(j) = G_p s(j) + G_i T \sum_{l=0}^{j} s(j) + G_d \frac{s(j) - s(j-1)}{T}, \tag{6}$$

where j is the sampling sequence number, T is the sampling time, and $s(j)$ is the motion deviation at the current time, G_p, G_i, and G_d are model parameters of the *PID* controller.

Among them,

$$\begin{aligned} s(j) &= e - v, \\ \Delta s(j) &= s(j) - s(j-1). \end{aligned} \tag{7}$$

2.3. Defuzzification. The fuzzy output is obtained by fuzzy reasoning, while the speed control actuator can only recognize the clear output. Therefore, the controller must defuzzify the fuzzy quantity and convert it into an accurate quantity. Defuzzification is the inverse process of fuzzification. The weighted average method is a widely used defuzzification method in fuzzy control systems, namely,

$$Q = \frac{\sum_{i=1} r_i q_i}{\sum_{i=1} q_i}, \tag{8}$$

where q_i is the ith membership value of the output fuzzy set, which can also be called weighting coefficient; r_i is the weight of the ith membership function of the output fuzzy set.

In the actual processing, the above calculations are carried out offline, and the control decision table is made and stored in the edge computing equipment. In the control process, the look-up table method is used to read the data, which reduces the online calculation time and improves the real-time performance of the system.

3. Transmission Line State Analysis Based on Deep Learning

Edge computing mode has the advantages of data perception and efficient decision analysis. Therefore, we introduce the edge calculation model into the analysis of transmission cables, which can realize the condition monitoring and analysis of transmission cables at the edge of the network so as to ensure the reliable and stable power supply state of the transmission network.

3.1. Edge Computing. The transmission line has complex and diverse characteristics, and its data also has the characteristics of being high-dimensional and massive. The traditional analysis and decision-making method using a single computing center is difficult to meet the needs for efficient and fast processing.

With the rapid development of edge computing technology in recent years, small edge servers are distributed near the equipment and processes in each edge server, which can effectively improve the efficiency of power inspection and facilitate the rapid and accurate identification of faults [25].

We sink the transmission line state analysis model to the edge of the network and build an image analysis model near the data source to realize the situation awareness and state recognition of the transmission line.

As shown in Figure 4, the edge computing device mainly includes a partition model acquisition unit, management unit, calculation unit, and calculation result transmission unit. The main purpose of the partition information acquisition unit is to obtain the corresponding model weight file and the corresponding transmission destination information. The snap-in is used to manage the number of devices connected and communicating. The computing unit detects and analyzes various states of the cable by constructing an identification model. The calculation result transmission unit feeds back the predicted result to the upper center.

3.2. Improved Faster-RCNN Model. In the process of patrol inspection, the line changing robot is far away from the photographed target object, and the size of spacer, vibration damper, and insulator defects on the line is small, which makes them account for a small proportion of the picture, resulting in poor model recognition effect. Therefore, the Faster-RCNN model is optimized.

RETRACTED

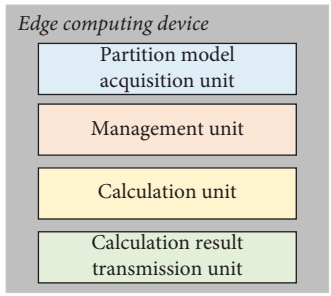

Figure 4: Edge computing device.

Firstly, by deepening the convolution layers of the feature extraction part, deeper feature information can be extracted. The second is the improvement of the model structure. Finally, by increasing the size, the number of candidate areas is increased so that the network can screen out the line components in the patrol picture as much as possible.

The shallow features and deep features of the feature extraction part in the model are respectively downsampled and upsampled to the same size, and then the feature map is spliced, so that the size of the feature map is enlarged and the dimension of the feature map is increased, which can prevent the loss of small features and strengthen other feature information at the same time.

Then the dimension is reduced by the convolution of the newly added layer $2 * 2$ to realize the adjustment of the number of channels and the fusion of features. Figure 5 shows the overall framework of the improved target detection model.

At present, the common way to expand the size of the feature map in deep learning is up-sampling and deconvolution as the inverse process of convolution [26]. However, the deconvolution process needs to train the parameters first, which is too complex. Therefore, we adopt the bilinear interpolation algorithm, which can retain the deep feature information obtained by the fifth convolution module when processing the image on the basis of enlarging the size of the feature image.

Using the four real pixel values in the original image, one pixel value in the target image can be determined, which is the double line interpolation algorithm. The transition to the new image is more natural, and the expected result is more perfect. For example, if the original image of $d * d * d$ is enlarged to the target image of $u * u * u$, the target image needs to be filled with pixel values from the original image.

If its coordinates are $(x + j, y + k, z + l)$ (where x, y, and z are integer parts of floating-point coordinates, and j, k, and l are decimal parts of floating-point coordinates), the value of this pixel can be determined by the value of the surrounding pixels corresponding to the coordinates (x, y, z), $(x + 1, y, z)$, $(x + 1, y + 1, z)$, $(x + 1, y, z + 1)$, $(x + 1, y + 1, z + 1)$, $(x, y + 1, z)$, $(x, y + 1, z + 1)$, and $(x, y, z + 1)$ in the original image.

In the feature extraction part, the feature map of the Conv. 3 layer is extracted through a down-sampling operation, the feature map of the Conv. 4 layer is directly

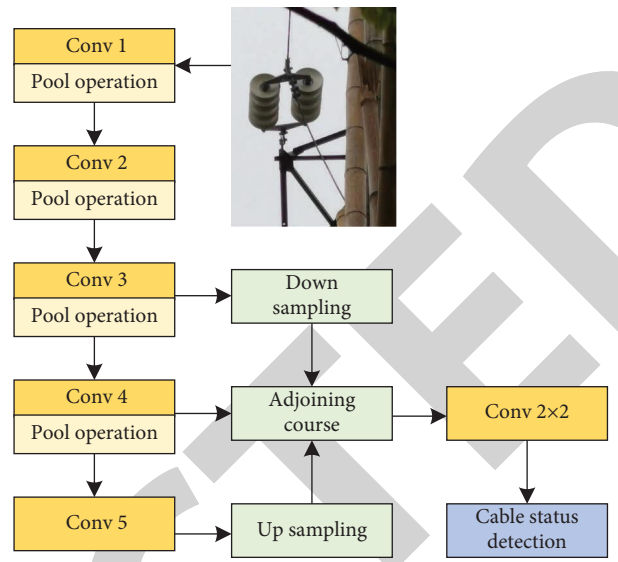

Figure 5: Frame diagram of the improved Faster-RCNN line part detection model.

extracted, and the feature map output by the Conv. 5 layer is upsampled. The bilinear interpolation algorithm can retain the deep features learned by the Conv. layer, enlarge the size of the feature map and highlight the feature information.

Before the feature maps of different convolution layers are sent to the connection layer, the feature orders of magnitude of different layers will be inconsistent. If they are directly stacked, the behavior of large-scale data drowning decimal data may occur, resulting in chaotic expression of feature information and poor fusion effect. Aiming to avoid this situation, local response normalization (LRN) is performed on the feature maps extracted from different layers, so that the features extracted from each layer can be fused into the same order of magnitude.

It appears on AlexNet for the first time. LRN is used to make the larger value in the data larger, which can highlight the effective information and suppress the interference information. In general, the LRN layer is to divide the input value $\alpha^i_{x,y,z}$ by a number to achieve the purpose of normalization. Normalize the local area so as to unify the dimensions, highlight the data with larger values, and suppress the data with smaller values. The formula is

$$\beta^i_{x,y,z} = \frac{\alpha^i_{x,y,z}}{\left(\varepsilon + a\sum\left(\alpha^i_{x,y,z}\right)^2\right)^b}. \tag{9}$$

Here, $\alpha^i_{x,y,z}$ is the input value and i is the position of the channel, representing the value of the updated channel. x, y, and z represent the location of the pixel to be updated. ε, a, and b are user-defined parameters. Select $\varepsilon = 3$, $a = 1.5 \times 10^{-3}$, and $b = 0.85$ here.

Aiming to adapt to the size of the corresponding parts of the transmission line and make the model more sensitive to the target, this paper adds two smaller sizes (16^2, 32^2, in pixels) on the basis of the traditional model, and adds two

RETRACTED

proportions of 1: 6 and 6: 1 as the aspect ratio. At this time, 30 candidate boxes can be generated at each position on the feature map.

3.3. Loss Function. The training of a line state detection network model is essentially a function optimization problem. Aiming to improve the accuracy of the recognition model and minimize the error, it is necessary to construct a loss function and optimize the model with the help of derivatives.

The loss function is divided into two parts, one of which is the confidence loss and the other is the positional loss. The two parts are combined as the total loss function.

$$\text{loss}_{\text{total}}(\,) = \frac{1}{N}\left(\text{loss}_{\text{conf}}(p,r) + \mu\text{loss}_{\text{loc}}(p,d,e)\right), \tag{10}$$

where N is the number of positive samples. If $N = 0$, set the loss function value to 0. $\text{loss}_{\text{conf}}(p,r)$ is the confidence loss function. $\text{loss}_{\text{loc}}(p,d,e)$ is the position loss function. μ is the weight coefficient, $\mu = 1$, p, d, and e are xyz coordinates of the coordinate system, respectively.

The position loss function $\text{loss}_{\text{loc}}(p,d,e)$ in the algorithm, the specific calculation process is

$$\begin{aligned}\text{loss}_{\text{loc}}(p,d,e) &= \sum p_{ij}^{k}\text{smooth}_{L1}\left(d_i - \hat{e}_j\right),\\ \text{smooth}_{L1} &= \begin{cases} 0.5p^2, & |p| < 1,\\ |p| - 0.5, & \text{other},\end{cases}\end{aligned} \tag{11}$$

where p_{ij}^{k} is the category matching parameter. When $p_{ij}^{k} = 1$, it means that the i a priori box matches the j ground truth, and the category of ground truth is k. $\hat{e}_j$ is the parameter after encoding the ground truth and a priori box. d_i represents the predicted offset value, which will be updated iteratively in the loss function.

The classification confidence $\text{loss}_{\text{conf}}(p,r)$ adopts the cross entropy loss function, and the calculation formula is

$$\text{loss}_{\text{conf}}(p,r) = -\sum p_{ij}^{k}\log(r_i) - \sum\log(r_{i0}), \tag{12}$$

where r_{i0} represents the probability value of the prediction frame with the background and correct classification, and r_i is the probability value calculated by SoftMax function.

4. Experimental Analysis

The training of deep networks requires a high operating environment. The computer hardware configuration of the experimental simulation is Intel core i5-10400 and NVIDIA GeForce UTX 3080ti. The network model is trained and tested using the Keras open-source library with TensorFlow as the back end.

The embedded platform of the model adopts the NVIDIA Jetson TX2. We put the transmission line condition monitoring model trained on the server on Jetson TX2. The hardware and configuration of Jetson TX2 are shown in Table 1.

Table 1: Hardware and configuration parameters.

Item	Parameter
GPU	Pascal 256 CUDA cores
CPU	Denver 2, ARM A57 complex
Display	DSI, DP
Memory	8 GB 128 bit LPDDR4
Storage	32 GB

4.1. Experimental Data Preprocessing. The dataset used in this paper is the relevant images of high-voltage transmission lines collected from power-related channels and network power-related data, including garbage on high-voltage transmission lines, broken strands of high-voltage transmission lines, loose strands of high-voltage transmission lines and other types of photos.

We take a series of data enhancement measures such as rotating, flipping, color adjustment, scaling, and so on. Rotate the image and enhance the data as shown in Figure 6(a). The image is randomly cropped or zeroed to the specified size, as shown in Figure 6(b). Further, the original lightness, saturation, and hue of the image are randomly adjusted by using the color space *HSV*. *V* stands for lightness. The higher the value, the brighter the color; *S* represents saturation. The larger the value, the more saturated the color is; *H* represents hue, and the value range is 0°~360°.

After data enhancement processing, we get a total of 16305 image photos, of which 13044 images are used as the training sample data set and 3261 images are used as the training test dataset.

4.2. Model Performance Analysis. First, we use the loss function as the evaluation index to optimize the feasibility of the model, in which the comparison model is the traditional CNN network model and the RCNN network model. The change in loss value of training sample set analysis by different network models is shown in Figure 7.

As shown in Figure 7, the $\text{loss}_{\text{total}}$ values of all models decreased rapidly after the training began. Among them, the $\text{loss}_{\text{total}}$ value of the proposed model converges rapidly at the beginning of training, and the increase in the number of iterations makes the $\text{loss}_{\text{total}}$ value gradually tend to 0. After 20 iterations, the loss function of the model decreases to within 0.01, the curve fluctuation is small and tends to be gentle, and the transmission line identification model converges effectively.

However, the calculation and analysis process of the RCNN model and CNN model is relatively slow. After 40 rounds of iterative calculation, the model converges effectively, and the loss function $\text{loss}_{\text{total}}$ remains around 0.25.

Meanwhile, we analyze the recognition efficiency of the above model. Table 2 shows the identification of some identified items.

As shown in Table 2, the method proposed in this paper has obvious advantages over the comparative model and can realize cable condition monitoring in different states to deal with the complex transmission line inspection environment.

RETRACTED

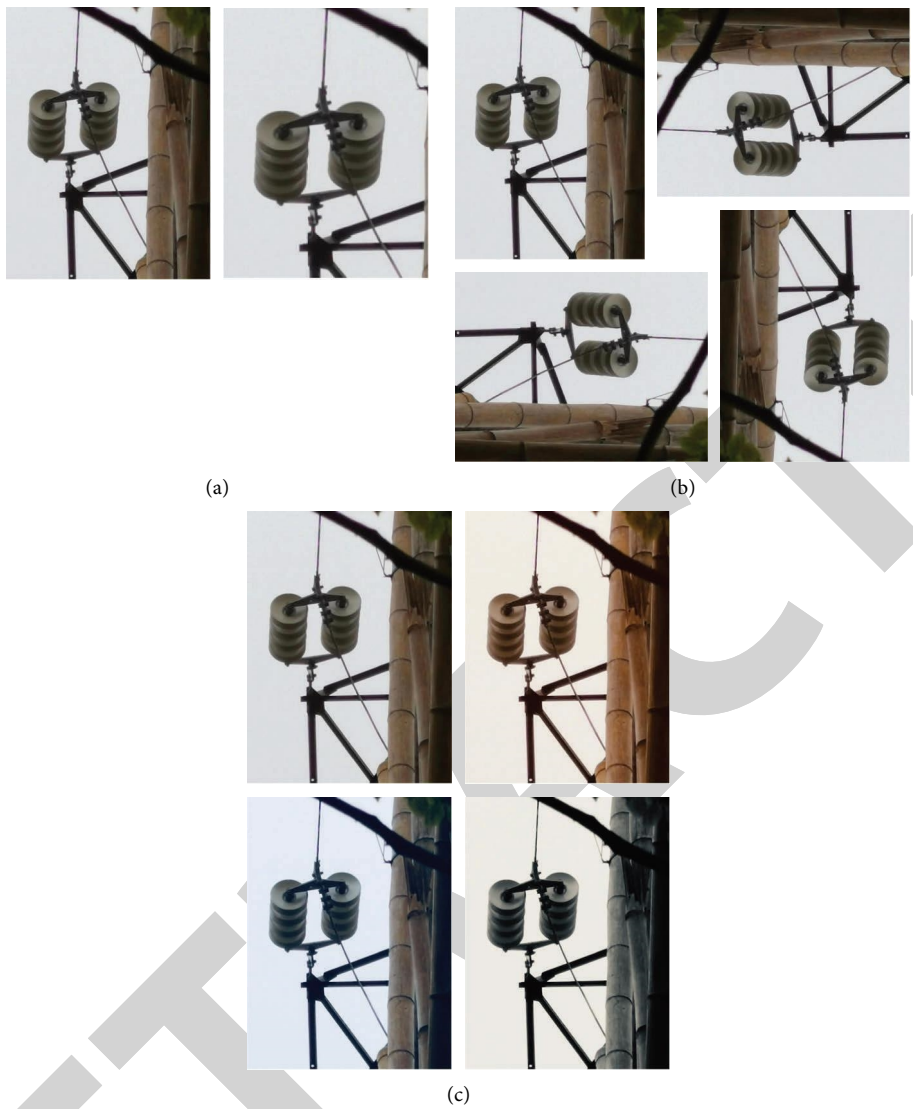

Figure 6: Transmission line image preprocessing. (a) Auto clipping. (b) Image rotation. (c) HSV treatment.

The detection accuracy of the proposed method for the normal state of the line is as high as 96.56%, which is 2.97% higher than that of the CNN model. However, the accuracy of the proposed method for the insulator damage is low, at 93.92%, but it is still 1.99% higher than that of the RCNN model.

4.3. Simulation Analysis

4.3.1. Evaluation Index. In this paper, p*recision*Precision, r*ecall*Recall, and a*ccuracy*Accuracy are selected as performance evaluation indexes.

In addition, the number of images correctly identifying the status of the line and cable is recorded as TP, the number of images identifying the correct sample as the wrong sample is recorded as FP, the number of images incorrectly identifying the status of the cable is recorded as TN, and the number of images identifying the wrong sample as the correct sample is recorded as FN.

The calculation formula of each performance index is

$$\begin{aligned} \text{Precision} &= \frac{TP}{TP + FP}, \\ \text{Recall} &= \frac{TP}{TP + FN}, \\ \text{Accuracy} &= \frac{TP + TN}{TP + FN + FP + TN}. \end{aligned} \tag{13}$$

At the same time, we fuse and optimize the index Precision and index Recall, and propose to use the average accuracy index AP instead of it to achieve more reliable performance analysis.

RETRACTED

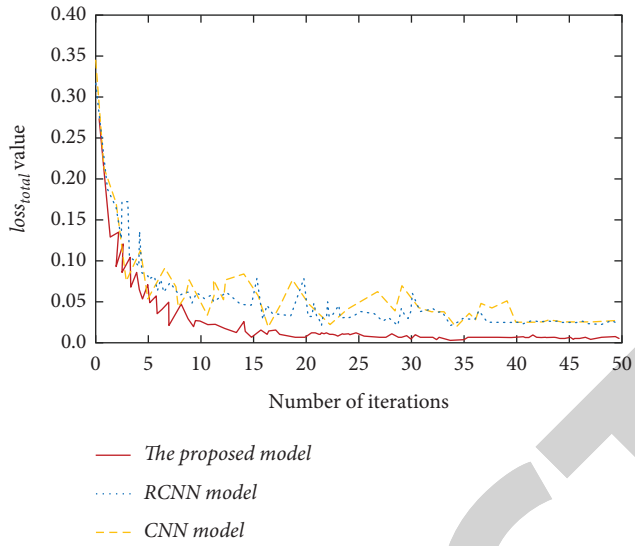

Figure 7: Variation of loss function $loss_{total}$.

Table 2: Identification results of different models.

Item	The proposed method (%)	CNN model (%)	RCNN model (%)
Normal state	96.56	93.59	94.19
Cable damage	95.48	94.36	94.00
Insulator damage	93.92	92.34	91.93
Line foreign matter	94.11	93.11	93.59

The calculation formula of *AP* index is

$$AP = \int_0^1 \text{Precision d Recall}. \quad (14)$$

4.3.2. Identification and Analysis of Line Status. Through the comparative analysis of reference [17] and reference [19], this paper enables the verification of the optimality of the proposed model. All the samples are preanalyzed in the same environment.

The analysis results of the same dataset by different methods are shown in Figure 8.

As shown in Figure 8, the transmission line state analysis method proposed in this paper has obvious state diagnosis advantages over the comparison method. The accuracy of the proposed method is 97.54%, and that of Reference [17] and Reference [19] is 95.61% and 94.91%, respectively. At the same time, the average accuracy is 98.01%, which is 2.93% and 3.87% higher than the Reference [17] and reference [19], respectively.

The reason is that the proposed method optimizes the structure of the depth network model, which can accurately obtain and analyze the feature information of the deep image. Meanwhile, the loss function of the line state recognition model is reconstructed so that the network model can achieve better antinoise characteristics. On the contrary, Reference [17] and Reference [19] lack consideration of multilayer feature fusion, and there may be a problem of insufficient acquisition of deep features.

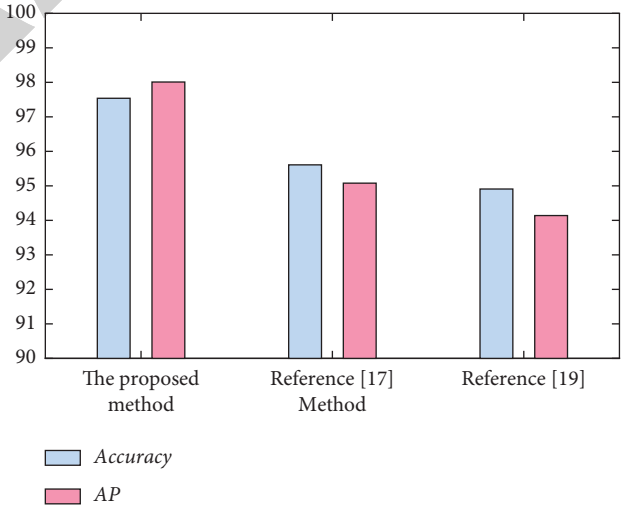

Figure 8: Image analysis performance of different analysis methods.

In addition, we should also note that the high precision and accuracy of the recognition method we proposed also benefits from the stable and controllable motion support of the line patrol robot provided by the fuzzy *PID* control method.

Furthermore, we analyze the operation efficiency of the cable state analysis method. The calculation efficiency of different methods is shown in Table 3.

RETRACTED

Table 3: Calculation efficiency of each method.

Methods	Time (s)
The proposed method	1.034
Reference [17]	2.189
Reference [19]	2.292

Because we sink the state analysis model into the edge computing device, the cable state analysis method we proposed is faster than the comparison method. In Table 3, the calculation time of our method is 1.034 s, which is nearly twice as long as that in reference [19].

5. Conclusion

Aiming to realize high-precision and fast transmission cable condition analysis, we propose a cable condition monitoring and analysis method integrating motion control and image analysis technology. In this method, fuzzy PID technology is introduced to realize the smooth and accurate motion control of the line-changing robot and improve the quality of collecting transmission cable images. At the same time, the CNN model and loss function are optimized at the edge to ensure that the state analysis model has the advantages of small error and high speed so as to realize the efficient identification of the state of transmission lines. The simulation results show that the accuracy of the proposed method is 97.54% in 1.034 s, which can realize the high-efficiency transmission cable state analysis under complex conditions.

Although the analysis method we proposed has a good effect on cable state recognition, it should also be noted that the parameter settings in the model are fixed values and are not adaptive. Future research methods will discuss the adaptive optimization of model parameters to further improve the efficiency of network model analysis.

Data Availability

The data used to support the findings of this study are available from the corresponding author upon request.

Conflicts of Interest

The authors declare that they have no conflicts of interest.

Acknowledgments

This work was supported by the State Grid Jiangsu Electric Power Co., Ltd. (incubate project: Research on the Intelligent Cable Method-Based Robot Used for Power Line Removing and Changing under grant JF2021022).

References

[1] L. Yang, J. Fan, Y. Liu, E. Li, J. Peng, and Z. Liang, "A review on state-of-the-art power line inspection techniques," *IEEE Transactions on Instrumentation and Measurement*, vol. 69, no. 12, pp. 9350–9365, 2020.

[2] H. G. Liang, C. Zuo, and W. M. Wei, "Detection and evaluation method of transmission line defects based on deep learning," *IEEE Access*, vol. 8, no. 1, pp. 38448–38458, 2020.

[3] X. Y. Zheng, R. Jia, Aisikaer, L. Gong, G. Zhang, and J. Dang, "Component identification and defect detection in transmission lines based on deep learning," *Journal of Intelligent and Fuzzy Systems*, vol. 40, no. 2, pp. 3147–3158, 2021.

[4] P. Y. Zhang, Z. Zhang, Y. P. Hao, Z. Zhou, B. Luo, and T. Wang, "Multi-scale feature enhanced domain adaptive object detection for power transmission line inspection," *IEEE Access*, vol. 8, no. 1, Article ID 182105, 2020.

[5] J. Zhao, K. Zhang, Z. H. Wang et al., "Limited sliding network: fine-grained target detection on electrical infrastructure for power transmission line surveillance," *International Journal of Circuit Theory and Applications*, vol. 49, no. 4, pp. 1212–1224, 2021.

[6] H. Jiang, X. J. Qiu, J. Chen, X. Liu, X. Miao, and S. Zhuang, "Insulator fault detection in aerial images based on ensemble learning with multi-level perception," *IEEE Access*, vol. 7, no. 1, pp. 61797–61810, 2019.

[7] D. S. Zhang, J. Wang, R. J. Han, and A. Tian, "A three-step synthetic extraction algorithm for transmission lines," *Proceedings of the Institution of Mechanical Engineers, Part C: Journal of Mechanical Engineering Science*, vol. 233, no. 17, pp. 6218–6228, 2019.

[8] L. Cheng and G. P. Wu, "Obstacles detection and depth estimation from monocular vision for inspection robot of high voltage transmission line," *Cluster Computing*, vol. 22, no. S2, pp. 2611–2627, 2019.

[9] W. R. Bai, X. Zhang, X. Q. Zhu et al., "E-FCNN based electric power inspection image enhancement," *Electric power*, vol. 54, no. 5, pp. 179–185, 2021.

[10] H. T. Wang, B. W. Yan, Z. H. Pu et al., "Optimal design and stress analysis of the transmission line changing robot along the ground line," *Journal of Engineering-Joe*, vol. 16, no. 1, pp. 3088–3091, 2019.

[11] A. T. Zengin, G. Erdemir, T. C. Akinci, and S. Seker, "Measurement of power line sagging using sensor data of a power line inspection robot," *IEEE Access*, vol. 8, no. 1, pp. 99198–99204, 2020.

[12] X. H. Yan, Z. G. Zhao, and Y. Q. Liu, "Real-time on-site inspection system for power transmission based on heterogeneous computing," *Journal of High Speed Networks*, vol. 27, no. 3, pp. 215–224, 2021.

[13] J. Y. Liu, G. P. Wu, F. Fan, and Y. Li, "A robot hybrid hierarchical network for sensing environmental variables of a smart Grid," *Sensors*, vol. 20, no. 19, pp. 5521–5525, 2020.

[14] J. Zhang, J. Y. Wang, and S. H. Zhang, "An ultra-lightweight and ultra-fast abnormal target identification network for transmission line," *IEEE Sensors Journal*, vol. 21, no. 20, pp. 23325–23334, 2021.

[15] Y. P. Guo, Z. J. Pang, J. Du, F. Jiang, and Q. Hu, "An improved AlexNet for power edge transmission line anomaly detection," *IEEE Access*, vol. 8, pp. 97830–97838, 2020.

[16] J. C. Chen, Y. C. Yu, Z. Chen et al., "An improved method for defect identification of transmission lines based on YOLOv3 [J]," *Southern Power System Technology*, vol. 15, no. 1, pp. 114–120, 2021.

[17] Y. H. Luo, X. Yu, and D. S. Yang, "A new recognition algorithm for high-voltage lines based on improved LSD and convolutional neural networks," *IET Image Processing*, vol. 15, no. 1, pp. 260–268, 2020.

[18] W. X. Chen, Y. N. Li, and C. Li, "A visual detection method for foreign objects in power lines based on mask R-CNN," *International Journal of Ambient Computing and Intelligence*, vol. 11, no. 1, pp. 34–47, 2020.

RETRACTED

Hindawi
Journal of Robotics
Volume 2024, Article ID 9830590, 1 page
https://doi.org/10.1155/2024/9830590

Retraction

Retracted: Optimization Path and Design of Intelligent Logistics Management System Based on ROS Robot

Journal of Robotics

Received 23 January 2024; Accepted 23 January 2024; Published 24 January 2024

Copyright © 2024 Journal of Robotics. This is an open access article distributed under the Creative Commons Attribution License, which permits unrestricted use, distribution, and reproduction in any medium, provided the original work is properly cited.

This article has been retracted by Hindawi following an investigation undertaken by the publisher [1]. This investigation has uncovered evidence of one or more of the following indicators of systematic manipulation of the publication process:

(1) Discrepancies in scope
(2) Discrepancies in the description of the research reported
(3) Discrepancies between the availability of data and the research described
(4) Inappropriate citations
(5) Incoherent, meaningless and/or irrelevant content included in the article
(6) Manipulated or compromised peer review

The presence of these indicators undermines our confidence in the integrity of the article's content and we cannot, therefore, vouch for its reliability. Please note that this notice is intended solely to alert readers that the content of this article is unreliable. We have not investigated whether authors were aware of or involved in the systematic manipulation of the publication process.

Wiley and Hindawi regrets that the usual quality checks did not identify these issues before publication and have since put additional measures in place to safeguard research integrity.

We wish to credit our own Research Integrity and Research Publishing teams and anonymous and named external researchers and research integrity experts for contributing to this investigation.

The corresponding author, as the representative of all authors, has been given the opportunity to register their agreement or disagreement to this retraction. We have kept a record of any response received.

References

[1] R. Wu, "Optimization Path and Design of Intelligent Logistics Management System Based on ROS Robot," *Journal of Robotics*, vol. 2023, Article ID 9505155, 9 pages, 2023.

Hindawi
Journal of Robotics
Volume 2023, Article ID 9505155, 9 pages
https://doi.org/10.1155/2023/9505155

RETRACTED

Research Article

Optimization Path and Design of Intelligent Logistics Management System Based on ROS Robot

Ruijie Wu

Henan Vocational College of Information and Statistics, Zhengzhou, Henan 450008, China

Correspondence should be addressed to Ruijie Wu; ruijie@st.btbu.edu.cn

Received 6 September 2022; Revised 13 October 2022; Accepted 24 November 2022; Published 7 February 2023

Academic Editor: Shahid Hussain

Copyright © 2023 Ruijie Wu. This is an open access article distributed under the Creative Commons Attribution License, which permits unrestricted use, distribution, and reproduction in any medium, provided the original work is properly cited.

With the rapid development of the Internet of Things (IoT), the logistics and transportation industry is booming. At the same time, with the advancement of AI technology, intelligent logistics is also gradually emerging, and the purpose of intelligent logistics is to use different types of automatic guided transport machines to replace people to handle and move products. At the same time, with the help of big data, cloud computing, artificial intelligence, sensor technology, and other technologies, we can achieve logistics automation. However, the current logistics robot creation platforms are diverse, which makes intelligent logistics robots diverse in variety and wide in application and also makes the creation and use of robots more challenging. Robot Operating System (ROS) is an open-source software platform that supports programming in multiple languages and has excellent adaptability. In addition, most of the currently used path planning focuses on a single target point, which is insufficient to support the current needs of multitasking in intelligent logistics. Therefore, this paper aimed to design an intelligent logistics management system based on ROS robot and proposed to use the A-star algorithm to calculate the shortest path of the robot so as to achieve the optimal path. In the simulation experiment, 20 ROS robots were selected and divided into two groups. In the logistics warehouse of different transportation nodes, 20 ROS robots were set up to transport goods of different weights in the experiment, and the transportation data were collected at last. The final simulation results have shown that the power consumption and response delay performance of the ROS robot are good, and the logistics transportation speed is significantly improved. In addition, compared with the traditional transportation method, the daily transportation weight of each robot is up to 310.1% and the monthly profit is up to 171%, which shows that the intelligent logistics management system designed in this paper is more efficient in logistics and transportation and can bring more profits.

1. Introduction

With the popularity of IoT and the rise of intelligent logistics, the logistics industry's dependence on industrial robots has increased. Because industrial robots are compact and adaptable to the environment, they can complete various activities better than humans, such as working in highly polluted, hot, or cold environments. The ROS platform makes the development and testing of robots significantly more efficient, supports multiple programming languages, and includes a wide range of functional packages. It is an open-source operating system, and all source codes will be open to the public for free use by users. Therefore, the use of ROS is beneficial for people to continue their research and learning. In addition, ROS can be used to realize the modular architecture of logistics robots on a single platform, realize the sharing of open-source components, facilitate multilanguage programming, and shorten the development cycle of robots. If the scientific research of ROS intelligent logistics transportation robot is used, researchers can improve the efficiency of cross-platform communication and development. In addition, path planning is the benchmark for determining the amount of robot intelligence, which is crucial for robot positioning and navigation. Therefore, the research on the related technologies of the intelligent logistics robot path optimization platform is very important for the field of intelligent logistics management.

Regarding logistics management, some scholars have carried out related research on it. In order to calculate the efficiency of logistics management, Liu Y used case analysis

and bibliographic analysis methods and used GIS spatial analysis technology to analyze the management efficiency of logistics under the 5G Internet of Things, but he lacked the understanding of management methods [1]. On a strategic level, Marzantowicz identified areas in which logistics management has changed due to the use of smart technologies. He also established the assumption that modern supply chain management is superior to classical logistics management methods based on intelligent logistics, but it lacks the design of logistics supply chain network [2]. Levans understood from a time perspective that logistics and managers were racing to transform their operations into a seamless digital supply chain network, but with less practical application of their network [3]. However, Yuen et al. used the IoT outbound logistics knowledge management system to monitor environmentally sensitive products and predict the quality of goods, but lacked the description of its application effect [4]. Therefore, Yang et al. introduced the workflow and application effects of the intelligent logistics supply chain management system in the management of medical consumables [5]. However, although the above research has obtained some theoretical results, the effect in practical application is not ideal, and it cannot significantly improve the efficiency of logistics management.

In order to effectively improve the efficiency of logistics management, some scholars have proposed the use of ROS robots to achieve intelligent logistics management and improve management efficiency. Petac studied the characteristics and uses of ROS, providing a complete set of tools and basic architecture, allowing developers to launch applications with higher abstraction, but the architecture cannot be controlled in real time [6]. Delgado et al. proposed a real-time control architecture for controlling service robots and non-real-time ROS packages; however, this architecture cannot integrate management [7]. Rovida et al. have researched and developed an autonomous task execution framework and a knowledge integration framework in ROS to provide support and reference for key ROS components, but the architecture lacked the necessary monitoring layer [8]. Hu et al. proposed a ROS-based runtime verification method called a multilayer robot monitor to monitor whether the operation of a robot swarm violates a given temporal property [9]. Although these methods have promoted the development and application of ROS robots to a certain extent, their application in intelligent logistics management is not mature enough, so it needs to be further improved and applied.

In order to further improve and use the application of ROS robot in logistics management, this paper adopted the A-star algorithm to optimize the transportation path of ROS robot. It designed an intelligent logistics management system and then simulated the system from various aspects through two sets of experiments. The test results have shown that in the first set of experiments, the transport path length of the ROS robot is between 16 m and 37.9 m, and the single transport time is between 7.8 min and 18.9 min. The average power consumption of the robot is about 3.6 kW, the average response delay is about 132 ms, the average transport weight of each robot is about 22.64 tons, and the transport speed is increased by 27.7% to 85.1%. In the second set of experiments, the transport path length of the ROS robot is between 22.8 m and 44.6 m, and the single transport time is between 13.2 min and 37.7 min. The maximum power consumption of the robot is 3.18 kW to 6.23 kW, the response delay of the robot is 152 ms to 297 ms, the transportation weight is above 33.52 tons, and the logistics transportation speed is increased by 11.7% to 24.4%. Overall, the intelligent logistics management system designed in this paper can effectively improve logistics speed and bring greater benefits.

2. Design of Intelligent Logistics Management System

2.1. Logistics Management System. Intelligent logistics can effectively reduce logistics costs and solve the problem of excessive logistics costs. As one of the key equipments in the intelligent logistics system, the robot plays an increasingly important role in the logistics business [10]. In order to realize a fully automated logistics mode, smart logistics combines a variety of cutting-edge sensors and information reading devices to automatically collect external information. It optimizes changes through information fusion and selects optimal operating parameters. In order to improve the scientificity and efficiency of logistics management, the system selects the best distribution route, product flow direction, and warehousing equipment through professional geographic data analysis functions [11, 12]. The implementation of transportation management mode mainly solves the problem of distribution mode, supply, and demand balance. The main goal of the distribution model is to reduce inventory and transportation costs while maintaining the effectiveness of product flow and the quality of service. To this end, the logistics management system should be considered from many aspects, and the hierarchical design and management should be carried out [13]. The logistics management system should also fully consider factors such as robot capacity, commodity demand, and the distance between the logistics center and the customer so as to maximize the reduction of commodity distribution costs or shorten the transportation path so as to minimize the cost of logistics companies.

In the logistics management system framework designed in this paper as shown in Figure 1, it includes the execution layer, the transport layer, and the management layer. The execution layer is mainly composed of multiple ROS robots and industrial computers. It is the main layer for logistics cargo transportation and the source of data. The transmission layer is to transmit the data in the logistics and collect it to the management and control layer, and the management and control layer analyzes and processes the transmitted data to make corresponding decisions.

In the intelligent logistics management system designed in this paper, RFID technology is used to identify and label the pallets, cargo spaces, and shelves to form a data carrier, which is convenient for reading or writing related item data information, and at the same time, it is transmitted to the computer for processing. The ROS robot is used as a handling tool, and the label is used as a positioning label for multiple vehicles as well as a data carrier [14, 15]. At the

RETRACTED

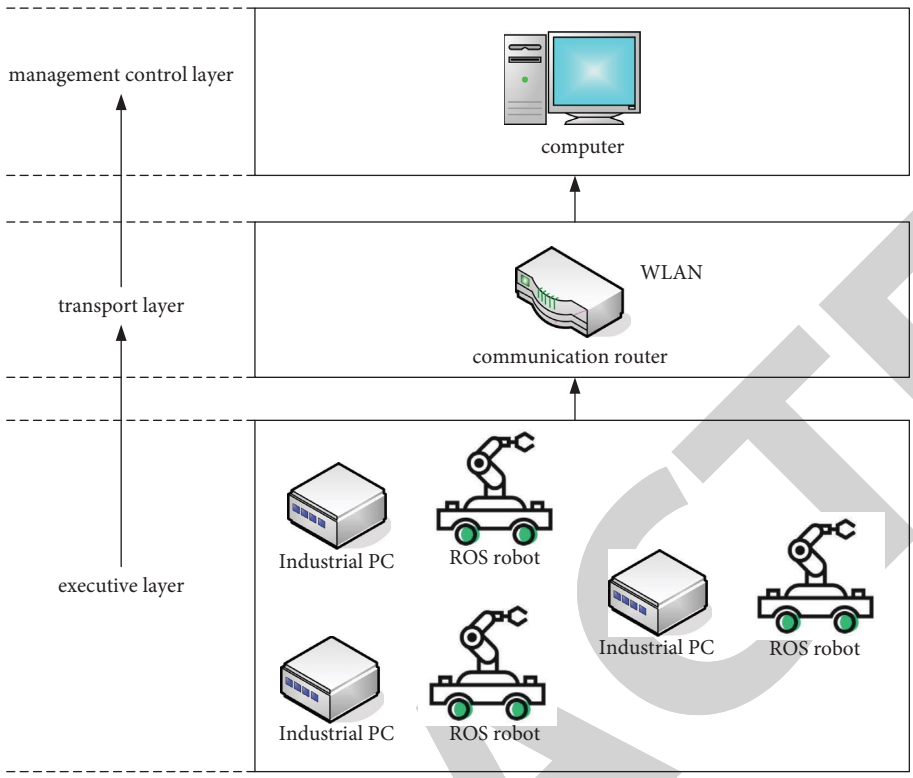

Figure 1: Framework of intelligent logistics management system.

same time, the system performs robot management, route management, monitoring management, and task management on the established user management system by digitizing the warehouse environment. Handling multiple transport robots in the warehouse would reduce the labor required by the company and improve the efficiency of the logistics system, the speed and precision of logistics transportation, and the competitiveness of the enterprise [16, 17].

2.2. ROS Robot. Intelligent logistics transportation robots have developed into a key component in this field, which is essential for processing procedures in production, express delivery, e-commerce, and other economic sectors. Intelligent logistics and transportation robots prioritize autonomous navigation, and path planning is an important part of autonomous navigation [18, 19]. The structure of the ROS robot system used in this paper is shown in Figure 2. The system mainly includes a controller, an encoder, a motor, and a deceleration mechanism. The ROS robot carries out logistics transportation under the command of the controller, and the controller completes the control of the machine motor under multiple industrial encoders and acoustic wave devices, and the motor will perform deceleration operations under the action of the DC deceleration mechanism. The encoder can realize coordinate conversion by calculating the mileage of the robot and then transmitting it to the computer for processing.

In addition, some problems may be encountered in the operation of ROS robots. For example, path planning does not take into account different operating environments. This method often fails to consider enough aspects, the overall situation and the situation encountered in actual operation, resulting in accidents, including collisions and traffic congestion during operation, of which these problems can be largely solved by using online scheduling. Among them, the collision mainly includes the opposite collision: when the two vehicles are driving in the opposite direction, no conflict resolution method is adopted, and the two vehicles have traffic jams and collisions. Chasing collision: the rear car is faster than the front car, the rear car will chase and overtake the front car, and if there is no solution, the rear car will collide with the front car. Node collision: there are overlapping sections in the path planning of two vehicles, and the running time is the same, which will cause node conflict. When the current resource is competed by two vehicles at the same time, resource conflict will occur. Online scheduling considers many factors. After many approaches are developed, online scheduling can provide an effective solution; therefore, the whole system will operate more safely and consistently. Considering the problem of traffic conflicts in operations and avoiding frequent occurrences in the future, online scheduling is a method that needs to be used in intelligent logistics management systems [20, 21].

However, different scheduling theories emphasize different perspectives. Shortest driving route scheduling states that while the overall driving path is kept as short as possible across all activities, the shortest path must be planned for each job. Nonetheless, it may result in higher shipping costs and longer overall shipping times. Minimum travel time scheduling states that all activities must take the least amount of time to complete, which usually includes actual

RETRACTED

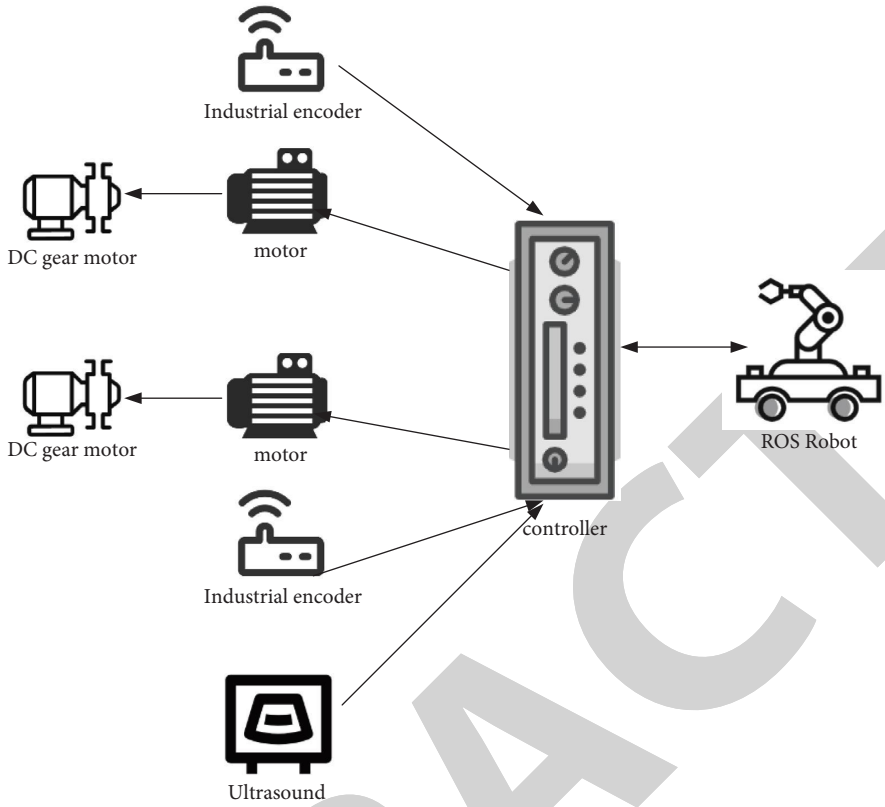

Figure 2: The structure of the ROS robot system.

route travel time and waiting time for conflicts or emergencies. The optimal allocation scheduling is that the allocation of each warehouse location should be different to ensure the effective use of resources and prevent resource waste [22, 23]; otherwise, the remaining quantity may sit idle, wasting resources and driving up logistics costs. On the contrary, if the number is too small, the job wait time will be too long. It will reduce the overall efficiency of the system, resulting in poor performance of the logistics system. In order to determine if the amount of logistics warehouse space is optimal, it is therefore important to check the task level and utilization of this warehouse area in most cases. Of course, the goal of logistics management is to reduce overall costs without reducing overall efficiency. According to the concept of least cost, logistics systems always prefer the cheapest option. The shortest total travel path, shortest total travel time, and ideal volume are all used to reduce system cost and increase productivity, maximizing benefits [24, 25].

2.3. A-Star Algorithm. At present, there are few path optimizations for multiobjective points in the research of path optimization, and most of the available path planning algorithms only consider one starting point and one destination point, such as the ant colony algorithm, particle swarm algorithm, and classification algorithm. However, as industrial production lines become more complex and diverse, the study of multiobjective point path optimization will become more important. The A-star method has received a lot of attention and has a wide range of applications because it has a simple procedure and is easy to implement [26]. Therefore, this study adopts the A-star method to optimize the robot's transportation path.

The A-star algorithm is an efficient shortest path search method. This paper uses this algorithm to optimize the path of the designed intelligent logistics system so as to reduce the logistics transportation time of ROS robots and improve the efficiency of logistics management. The path optimization method of the algorithm can be expressed by the path estimation function:

$$f(n) = k(n) + v(n). \tag{1}$$

Among them, $k(n)$ represents the actual estimated value from the starting point to the node n where the robot is located and $v(n)$ is the best estimated value from n to the target node.

When the A-star algorithm finds the shortest path, it often uses a variety of distances for calculation. Assuming that the coordinates of the logistics transportation target position of the ROS robot are (x, y) and the current position is (u, v), then when using the Chebyshev distance calculation, $v(n)$ is

$$v(n) = \max(|x - u|, |y - v|). \tag{2}$$

The maximum absolute value of the difference between two location coordinates is called the Chebyshev distance, which is a unit of measure in a vector space, a measure derived from the uniform norm, and a hyperconvex measure.

RETRACTED

When calculated using Euclidean distance, it is

$$v(n) = (\sqrt{x-u} + \sqrt{y-v})^2. \quad (3)$$

When using the Manhattan distance, it is

$$v(n) = |x-u| + |y-v|. \quad (4)$$

Since repeated paths should not appear at the same time in path planning, resulting in transportation conflicts, each node can be visited at most once at the same time. Assuming that the length of the ROS robot transportation path is represented by D, then

$$D_r = \sum_{i=1}^{n}\sum_{j=1}^{n} L_{ij}X_{ij}. \quad (5)$$

Among them, i and j represent two nodes, L is the distance between the two nodes, and r represents the target path, and

$$X_{ij} = \begin{cases} 0, \text{when any other robot visits the node,} \\ 1. \end{cases} \quad (6)$$

In addition, in order to prevent conflicts at the same time, it is assumed that the time difference between two ROS robots about to pass through the same node is t', and the minimum distance for two ROS robots to collide is s', so that the robots do not conflict, and they need to meet the following:

$$T = t' < \frac{s'}{v}. \quad (7)$$

Among them, v represents the current travel speed of the ROS robot.

When T does not satisfy the above formula, T is set to 0, and then the robot passing through the node stops moving forward, so as to avoid conflicts.

3. Results of Simulation Test of Logistics Management System

3.1. Simulation Design and Related Data of Logistics Management System. The logistics management system includes not only ROS robots but also various sensors, computer systems, and databases. This part of the tools and equipment used in the experiments is shown in Table 1.

Then, this paper divides 20 ROS robots of the same model into two groups for simulation experiments by simulating a square logistics storage warehouse with a length of 40 meters and a width of 40 meters, including the test of the robot's transportation path, transportation weight, and performance, as well as the calculation of profit. The parameter settings of each group of experiments are shown in Table 2. The weight of the first group of goods is 10 kg, including 40 logistics warehouses, and the weight of the second group of goods is 20 kg, with only 20 nodes.

Transport route comparison: in order to optimize the transportation path, which will shorten the transportation time of the robot and improve the transportation efficiency,

Table 1: Related equipment for simulation experiments.

Code	Device name	Types
E1	Development platform	ROS
E2	Transportation robot	VGA
E3	Computer CPU	Intel core i7
E4	Computing system	Win 10

Table 2: Simulation experiment parameter settings.

Groups	1st group	2nd group
Number of ROS robots	10	10
Goods weight	10 kg	20 kg
Number of transport nodes	40	20

this paper summarizes the single average transportation path length and transportation time of each ROS robot. The test results are shown in Figure 3.

Figure 3(a) shows that in the first set of experiments, the transport path length of the ROS robot is between 16 m and 37.9 m, and the single transport time is between 7.8 min and 18.9 min. The overall average path length is about 26.5 m, the average single transportation time is 14.4 min, and the path optimization effect is relatively good. As shown in Figure 3(b), the transport path length and time of the ROS robot increased in the second set of experiments. Among them, the path of the No. 3 robot is the longest, 44.6 m, and the path of the No. 9 robot is the shortest, 22.8 m; the fastest single transportation time is 13.2 min, and the slowest average transportation time is 37.7 min. The overall average path length is about 34 m, and the average single transit time is 23.9 min. Compared with the first set of experiments, the average transport path length increased by about 7.5 m, and the single transport time was increased by 9.5 min. The reason is that the number of transport nodes is reduced, the robot has fewer routes to choose from, the waiting time increases, the weight of the transported goods increases, and the speed and action delay of the transport also increase, but the average path length path is less than 40 m, indicating that the optimization effect is good.

ROS robot performance: in order to use the robot for logistics management more stably and safely, it is necessary to analyze the performance of the ROS transport robot. Therefore, this paper conducts a statistical analysis from the response delay and power consumption of the robot, and the results are shown in Figure 4.

In Figure 4(a), the power consumption of robot no. 8 is relatively lower, which is 2.72 kW; the power consumption of robot no. 4 is higher, which is 4.47 kW; robot no. 3 has a shorter response delay of 96 ms; robot no. 5 has the longest delay of 179 ms. The average power consumption of these robots is about 3.6 kW, and the average response delay is about 132 ms. In Figure 4(b), the maximum power consumption of the robot is 6.23 kW, and the minimum is 3.18 kW. The response delay of the robot is up to 297 ms and the shortest is 152 ms. The robots of the second group of experiments have increased power consumption and delay, which are related to the weight of the transported goods of the second group of robots mentioned earlier. The weight of

RETRACTED

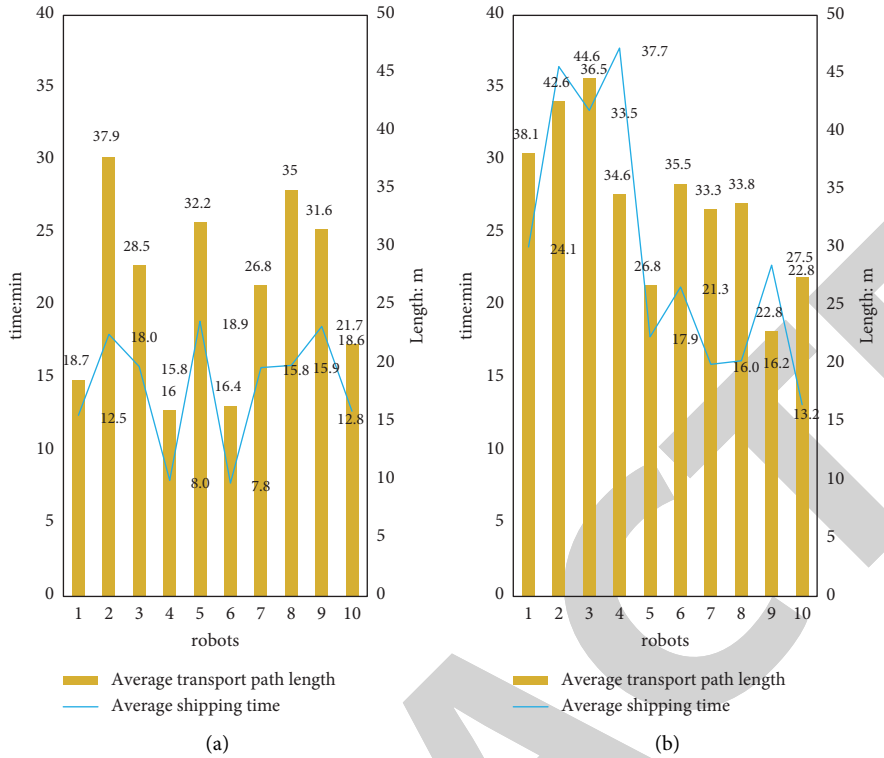

Figure 3: Transport path comparison. (a) The first set of experiments. (b) The second set of experiments.

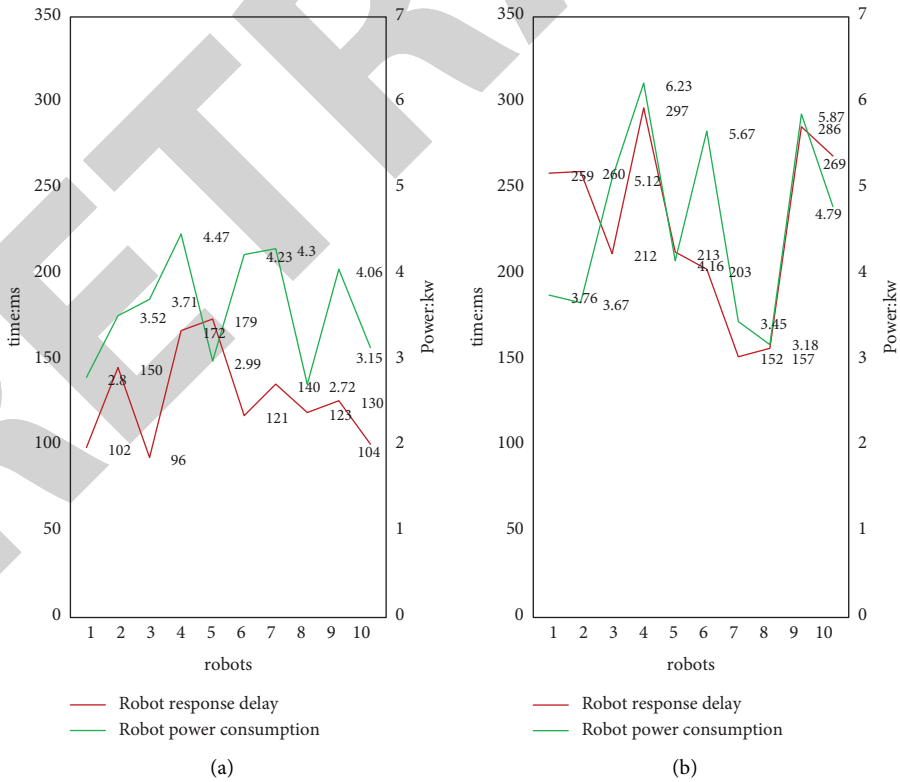

Figure 4: ROS robot performance. (a) The first set of experiments. (b) The second set of experiments.

RETRACTED

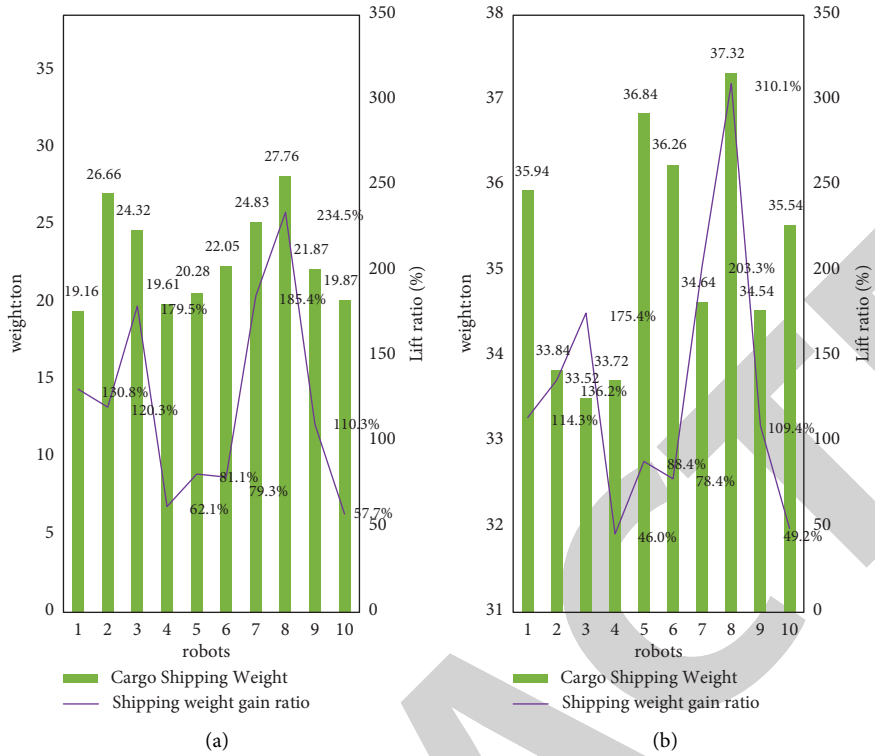

Figure 5: Changes in logistics transportation volume. (a) The first set of experiments. (b) The second set of experiments.

the robot in the first group of experiments is only 10 kg, while the weight of the second group is 20 kg. Therefore, the power consumption and delay of the second group of robots are increased. However, the robot performance of both groups was stable and in good condition.

Changes in the volume of logistics and transportation: changes in the quantity or weight of cargo transported can more intuitively reflect the gains brought by robotic transport. This paper summarizes the daily cargo transport weight and the transport weight lift ratio of the two groups of experiments, and the results are shown in Figure 5.

In Figure 5(a), the daily weight of goods transported by the robot ranges from 19.16 tons to 27.76 tons, and the overall average transport weight is about 22.64 tons. Compared with traditional transportation methods, the daily transportation weight of robots increased from 57.7% to 234.5%. In Figure 5(b), the No. 3 robot with the least transport capacity reaches 33.52 tons, and the No. 8 robot with the largest transport capacity reaches 37.32 tons. The daily transport weight of the robots in this group of experiments has increased from 46% to 310.1%. This shows that the use of ROS robots for transportation can significantly increase the daily logistics transportation weight.

Logistics management effect: in this paper, the purpose of using ROS robot to design an intelligent logistics management system is to improve logistics speed and company profits. Therefore, in the end, this paper compares the two groups of experiments with traditional transportation methods and obtains the ratio of the improvement of the transportation speed of goods to the company's profit. The results are shown in Figure 6.

Figure 6(a) shows that, compared with the traditional transportation method, the daily transportation speed of the first group of ROS robots has increased by at least 27.7%, the largest by 85.1%, and the monthly profit has increased by the smallest by 39% and the largest by 171%, among which the improvement of No. 8 robot is the most obvious. After investigation, it was found that the response delay of No. 8 robot is low, and the daily cargo transportation weight is relatively large, which may be the reason for its large improvement. As can be seen from Figure 6(b), in the second set of experiments, the logistics transportation speed increased the minimum by 11.7% and the maximum by 24.4% and the monthly profit increased the minimum by 32.2% and the maximum by 75.7%. Among them, the profit of the No. 10 robot has increased the most. From the above, it can be seen that the single transportation time of the No. 10 robot is the shortest, which may be the reason for its greater profit increase. In general, the logistics speed and monthly profit both increase in direct proportion, which shows that the ROS robot logistics transportation management system designed in this paper can effectively improve the logistics management effect.

Although this experiment tests the intelligent logistics management system designed in this paper from the aspects of transportation path, robot performance, transportation volume change, and profit improvement, this shows that the system has a good logistics management effect. However, there are still many deficiencies in this paper, and the research on the algorithm of path optimization is not deep enough. In addition, the introduction of ROS robot is not detailed enough. The test method of the experiment may need to be further improved.

RETRACTED

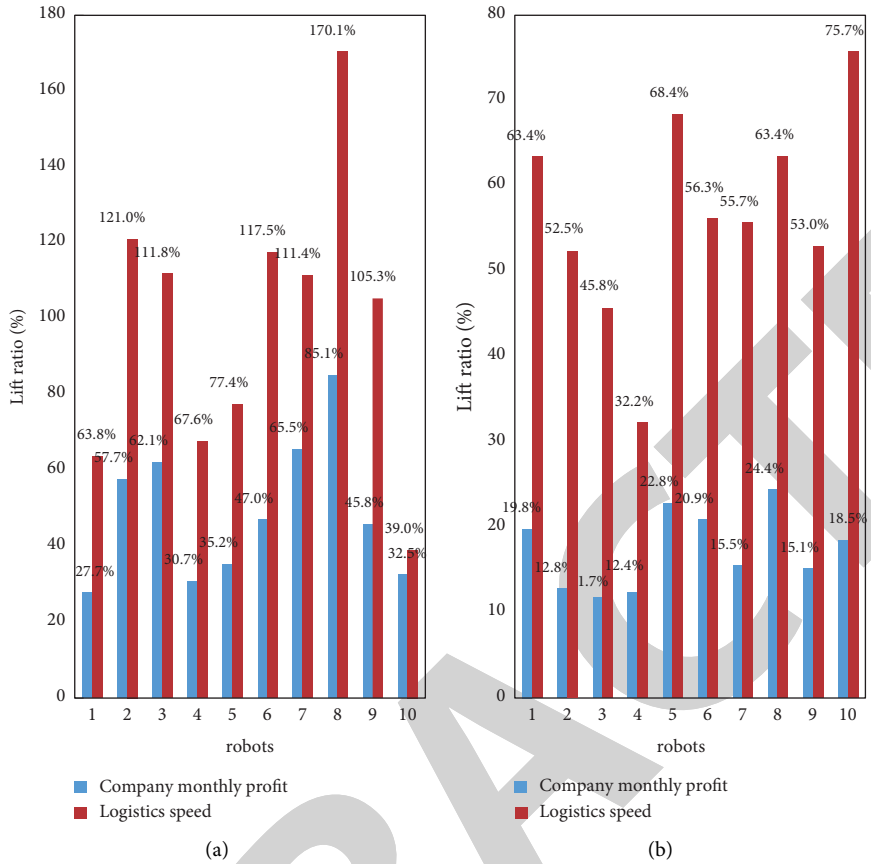

Figure 6: Changes in logistics management efficiency. (a) The first set of experiments. (b) The second set of experiments.

4. Conclusion

With the rapid development of e-commerce and IoT, customers' expectations for timeliness and transparency in logistics continue to increase, and the demand for the social and economic transformation of logistics management continues to grow. Therefore, the existing logistics management methods and technologies have been unable to keep up with the pace of times. Most of the domestic small- and medium-sized logistics enterprises currently lack the resources and professional knowledge required to meet the actual needs of logistics informatization, which has caused some obstacles to the standardization of domestic logistics management informatization. Combined with the characteristics of ROS robot, this paper designed and tested an intelligent logistics management system with an optimized path. It first started from the concept of intelligent logistics management and understood that the logistics management system should be considered from many aspects, and the hierarchical design and management should be carried out. Therefore, this paper designed a logistics management system from the execution layer, the transmission layer, and the control layer and introduced the structure and composition of the ROS robot used in this paper. Secondly, this paper describes the A-star algorithm for path optimization, and through simulation experiments, it is concluded that the path optimization effect of this paper is good and the performance of the ROS robot is stable, which can effectively increase the amount of transported goods, improve logistics speed, and increase profits. However, there are some deficiencies in this paper. For example, the research on the A-star algorithm is not deep enough, and the simulation experiments need to be divided into multiple groups and compared many times to draw more reliable conclusions. Therefore, this paper still needs to be further improved.

Data Availability

The data used to support the findings of this study are available from the corresponding author upon request.

Conflicts of Interest

The author declares that there are no conflicts of interest.

Acknowledgments

This research study was sponsored by Henan Higher Education Teaching Reform Research and Practice Project. The project number is 2021SJGLX704. The author would like to thank the project for supporting this article.

RETRACTED

Hindawi
Journal of Robotics
Volume 2024, Article ID 9819037, 1 page
https://doi.org/10.1155/2024/9819037

Retraction

Retracted: Reinforcement Learning-Based Continuous Action Space Path Planning Method for Mobile Robots

Journal of Robotics

Received 23 January 2024; Accepted 23 January 2024; Published 24 January 2024

Copyright © 2024 Journal of Robotics. This is an open access article distributed under the Creative Commons Attribution License, which permits unrestricted use, distribution, and reproduction in any medium, provided the original work is properly cited.

This article has been retracted by Hindawi following an investigation undertaken by the publisher [1]. This investigation has uncovered evidence of one or more of the following indicators of systematic manipulation of the publication process:

(1) Discrepancies in scope
(2) Discrepancies in the description of the research reported
(3) Discrepancies between the availability of data and the research described
(4) Inappropriate citations
(5) Incoherent, meaningless and/or irrelevant content included in the article
(6) Manipulated or compromised peer review

The presence of these indicators undermines our confidence in the integrity of the article's content and we cannot, therefore, vouch for its reliability. Please note that this notice is intended solely to alert readers that the content of this article is unreliable. We have not investigated whether authors were aware of or involved in the systematic manipulation of the publication process.

Wiley and Hindawi regrets that the usual quality checks did not identify these issues before publication and have since put additional measures in place to safeguard research integrity.

We wish to credit our own Research Integrity and Research Publishing teams and anonymous and named external researchers and research integrity experts for contributing to this investigation.

The corresponding author, as the representative of all authors, has been given the opportunity to register their agreement or disagreement to this retraction. We have kept a record of any response received.

References

[1] W. Zhang and G. Wang, "Reinforcement Learning-Based Continuous Action Space Path Planning Method for Mobile Robots," *Journal of Robotics*, vol. 2022, Article ID 9069283, 9 pages, 2022.

Hindawi
Journal of Robotics
Volume 2022, Article ID 9069283, 9 pages
https://doi.org/10.1155/2022/9069283

RETRACTED

Research Article

Reinforcement Learning-Based Continuous Action Space Path Planning Method for Mobile Robots

Weimin Zhang[1] **and Guoyong Wang**[2]

[1]*School of Electrical Engineering and Automation, Luoyang Institute of Science and Technology, Luoyang 471023, Henan, China*
[2]*School of Computer and Information Engineering, Luoyang Institute of Science and Technology, Luoyang 471023, Henan, China*

Correspondence should be addressed to Weimin Zhang; zwm@lit.edu.cn and Guoyong Wang; wgy@lit.edu.cn

Received 21 September 2022; Revised 30 September 2022; Accepted 5 October 2022; Published 15 October 2022

Academic Editor: Shahid Hussain

Copyright © 2022 Weimin Zhang and Guoyong Wang. This is an open access article distributed under the Creative Commons Attribution License, which permits unrestricted use, distribution, and reproduction in any medium, provided the original work is properly cited.

A reinforcement learning-based continuous action space path planning method for mobile robots is proposed in this article. First, the kinematic model of the mobile robot is analyzed, and on this basis, the optimal state space is constructed according to the minimum depth of the field value in the depth image to characterize the distance between the robot and the obstacle. Then, by setting the reward function of the mobile robot based on the artificial potential field method, the information of the robot's distance from obstacles is continuous, and a new reinforcement learning training process is proposed. Finally, by introducing a DDPG algorithm, the path planning of a mobile robot in an unknown environment is described as a Markov decision process, and the optimal planning of the mobile robot's continuous action space path is realized with a high success rate. The results show that compared with other three comparison methods, the final success rates of the proposed method are the highest, which are 97.2%, 99.1%, 98.4%, and 98.6%, respectively.

1. Introduction

The mobile robot can sense the environment information and its own state information through the sensor, so as to realize the autonomous movement in the obstacle environment and complete some operations [1–3]. A mobile robot plays an important role in various fields of life and can replace people to complete some special work [4, 5]. However, with the expansion of mobile robot application scenarios, its working environment is becoming quite complex. In order to achieve better adaptability to the environment, the autonomous learning ability of robots needs to be improved [6–8].

In order to successfully complete various tasks, mobile robots must avoid colliding with obstacles in the environment and complete the navigation from one point to another. The goal of mobile robot path planning is to find a collision-free optimal path from the starting position to the target position in the environment. Path planning can be divided into global path planning and local path planning according to the amount of environmental prior information. Global path planning means that environment information is all known relative to the mobile robot. The mobile robot models the environment and then finds an optimal path. The obstacle information in global path planning is known and fixed, so it belongs to static path planning and is also called offline planning. Local path planning requires mobile robots to obtain information from the environment constantly through sensors and real-time path planning. Therefore, local path planning belongs to dynamic planning and is also called online planning [9–11]. At present, research on navigation strategies using deep reinforcement learning has attracted considerable attention. Reinforcement learning technology can learn appropriate strategies from the state of the environment. In the process of interaction between the agent and the external environment, the agent obtains the surrounding environmental information through repeated trial-and-error learning, so as to continuously optimize the agent's

strategy [12, 13]. Applying reinforcement learning to mobile robot path planning does not need to build maps. Through deep reinforcement learning networks, mature navigation strategies are trained so that mobile robots can navigate in unknown environments [14].

The traditional spatial path planning method of mobile robots is discontinuous and has a low success rate. A continuous action spatial path planning method for mobile robots based on reinforcement learning is proposed. Compared with the traditional service robot route recommendation method, the innovations of the proposed method are as follows:

(1) The artificial potential field is introduced to make the target point and obstacle produce attraction and repulsion force to the mobile robot, respectively, and the control performance of the robot is improved under the superposition of the two forces.

(2) By introducing the DDPG algorithm, the ability of the algorithm to deal with higher dimensional observation space and the stability of the algorithm are improved.

The remainder of this paper is arranged as follows: The second section is related work, introducing several representative research results. The third section introduces the path-planning algorithm based on DDPG. In section 4, experiments are designed to verify the performance of the proposed model. The fifth section is the conclusion.

2. Related Research Studies

At present, some scholars have conducted in-depth research on the path planning of mobile robots and achieved some results. The authors in [15] constructed a global planner for finding the shortest safe path by combining the evolutionary algorithm, mutated cuckoo optimization algorithm, and genetic algorithm. On this basis, a mobile robot navigation system for path optimization is constructed based on a sensor source, map format, and basic controller. However, when the number of nodes is too large, the algorithm will consume a lot of time and memory, resulting in low efficiency. In [16], aiming at the mutual restriction between the execution speed and path quality of mobile robots, a new path planning strategy was proposed by ignoring all static obstacles outside the robot and the destination, focusing on the processing of key areas around obstacles and target points to improve the execution speed, and finding a linear shortcut between any two points in the path to improve the path quality. However, this method cannot achieve good results in a dynamic environment. The authors in [17] proposed a centralized decoupling algorithm for solving the multirobot path-planning problem in grid graphs, which can be set automatically as needed. On the one hand, a group of robots can be moved from their initial positions to the target positions; on the other hand, they can adapt to the target configuration adjustment through continuous replanning. However, this method cannot effectively avoid the local optimization in path planning. The authors in [18] proposed a trajectory-planning algorithm for parallel parking mobile robots based on polynomial parameterization and genetic algorithm optimization by defining a new law of motion to avoid obstacles on the road without interruption and guide the vehicle from the initial posture close to the parking space to the final posture in the parking space in a stable way. However, this method will still produce a large amount of calculation when the map accuracy is large.

In [19], the authors designed an adaptive firefly algorithm for mobile robot path planning by optimizing the adaptive parameters of the firefly algorithm to solve the problem that the traditional firefly algorithm is easy to fall into the local optimal solution. However, this method does not fundamentally improve the success rate and path optimization performance of the path optimization algorithm. The authors in [20] aimed at the problem that the traditional graph neural network depends on the message aggregation mechanism and is not conducive to the priority processing of important information. Based on a mechanism similar to a key query, the relative importance of features in messages received from various adjacent robots is determined and the path optimization of autonomous mobile robots is realized. However, this method will incur a large time cost in the process of judging the relative importance of messages, making the convergence speed of the algorithm slow. The authors in [21] constructed global path planning and local path planning strategies based on the hybrid artificial fish swarm algorithm. By developing the scoring function, the time of local path planning is shortened. On this basis, an obstacle avoidance and real-time navigation algorithm for the multirobot cooperative path is proposed. However, this method will produce a lot of computation and cannot be used for real-time path planning.

3. Path Planning Based on DDPG Deep Reinforcement Learning

3.1. Kinematic Model of Mobile Robots. In the process of studying the kinematic model of mobile robots, the Pioneer3 mobile robot is taken as a research object, and its model is shown in Figure 1.

As shown in Figure 1, the Pioneer3 mobile robot is composed of the rear driving wheel and the front steering wheel, in which the rear wheel is the driving wheel, the speed is v, and the front wheel is the steering wheel. The position of the mobile robot is represented by a three-dimensional state vector $P(x, y, \alpha)$. (x, y) represents the midpoint of the robot's rear axle. The midpoint of the rear axis is used as a reference point to represent the position coordinates of the robot. α represents the included angle between the robot-fixed coordinate system and the spatial-fixed coordinate system, that is, the direction angle of the robot. β represents the steering angle of the robot, which is the angle of the steering wheel. The wheelbase of the driving wheel and steering wheel is Z_1.

The kinematic model of the Pioneer3 mobile robot is shown in the following formula:

$$\begin{bmatrix} \dot{x} \\ \dot{y} \\ \dot{\alpha} \end{bmatrix} = \begin{bmatrix} \cos\alpha & 0 \\ \sin\alpha & 0 \\ 0 & 1 \end{bmatrix} \begin{bmatrix} v \\ \dfrac{v\tan\beta}{Z_1} \end{bmatrix}. \tag{1}$$

RETRACTED

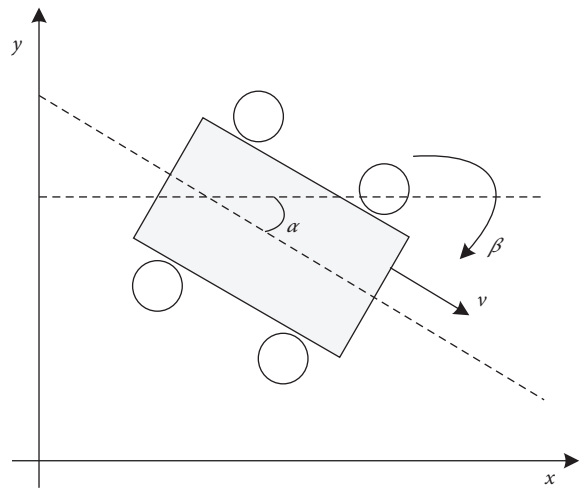

Figure 1: Basic structure of the Pioneer3 mobile robot.

3.2. Construction of the Optimized State Space. Traditionally, reinforcement learning is generally used in mobile robot path planning. Although unsupervised autonomous learning can be realized, there is also an inevitable problem; that is, it is highly dependent on training set information, and the learning process is very long. In addition, the solution to the problem is often not achieved overnight, but through the transition sequence of multiple state actions to reach the target state to obtain the final delayed return. In this way, the robot must repeatedly access these state-action transition sequences in order to find the optimal state-action transition sequence [22]. Therefore, reinforcement learning can converge to the optimal solution only when it runs to a certain extent. In the field of large and complex real problems, especially in the field of multirobots, the learning speed of reinforcement learning is very slow and learning efficiency is very low [23]. There will be problems such as "dimension disaster" and "state space combination explosion."

On the premise of ensuring the training results, how to greatly accelerate the efficiency of learning and the speed of reinforcement learning and training and expand reinforcement learning to larger and more complex applications has always been a hot spot in the field of reinforcement learning. Especially, in today's atmosphere, where most studies emphasize the performance of online, real-time adaptability to quickly adapt to the changes in the environment, the improvement of learning efficiency of reinforcement learning has increasingly become the research focus of researchers [24].

At the beginning of learning, the robot is very strange to the unknown environment and does not establish a stable state space. It must make actions randomly to obtain the reward value of different actions in each state, so as to slowly establish the understanding of the environment. For the motion decision-making of the robot, at the beginning of training, the robot collects the real-time depth image information in the environment as a real-time state, randomly gives the line speed and angular speed to move, calculates the reward value of this movement, collects the depth image information after the movement, and repeats this process until enough states and the probability distribution of the reward values of the corresponding actions are collected, Finally, training is completed when the reward values converges to a certain value.

In the process of repeated trial-and-error learning, the state when the robot moves to a place far away from the obstacle can be called the state not required for obstacle avoidance. Due to the random action selection, it is often in the collection state without obstacles for a long time so that the constructed state space contains a large number of states not required for obstacle avoidance, as shown in Figure 2.

What we hope is that the robot can move a large number of random near the obstacle and collect the current state to construct the state space, so as to obtain the obstacle avoidance ability when encountering the obstacle. Therefore, in the process of training, it is hoped that the robot can establish a state space for obstacle avoidance motion. In order to improve the efficiency of subsequent training, in the construction process of the initial state space, the distance between the robot and the obstacle is characterized according to the minimum depth of the field value in the depth image. Combined with robot kinematics, the motion of the robot is constrained and its training process is guided. A new reinforcement learning training process for path planning is proposed.

3.3. Algorithm Design

3.3.1. DDPG Algorithm Design. The path planning of the mobile robot in an unknown environment can be described as a Markov decision process. The process of the mobile robot interacting with the environment in offline time can be described as a decision sequence shown in the following formula:

$$\{S_0, A_0, R_1, S_1, A_1, R_2, \ldots, S_{T-1}, A_{T-1}, R_t, S_t, A_t\}. \quad (2)$$

In formula (2), S_t represents the state of the robot at the moment t, A_t represents the action of the robot at the moment t, and R_t represents the reward value obtained by the robot at the moment $t-1$. The mobile robot maximizes the total reward by finding an optimal action strategy. The total reward is defined as follows:

$$G_t = R_{t+1} + \gamma R_{t+2} + \cdots = \sum_{\tau=0}^{+\infty} \gamma^{\tau} R_{t+\tau+1}. \quad (3)$$

In formula (3), λ represents the discount factor, which is used to calculate the cumulative reward.

The strategy π represents the mapping from the state to action probability distribution, which is generally the probability distribution of the state. The output of the deterministic policy gradient algorithm is a specific action. The definition of the deterministic strategy π is shown in formula:

$$a = \pi(s, \theta). \quad (4)$$

RETRACTED

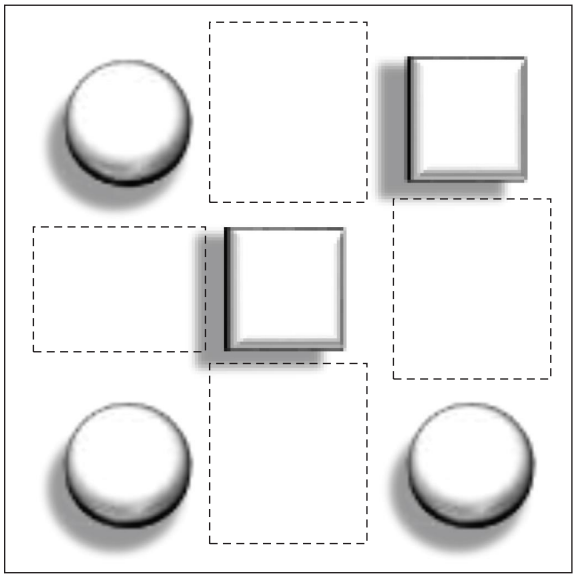

Figure 2: Collection status of areas not required for obstacle avoidance.

In formula (4), θ represents the parameters of the deterministic strategy, and the purpose of its update is to find an appropriate parameter θ to optimize the strategy π.

In the DDPG algorithm, the parameter θ is updated by the following formula:

$$\theta \leftarrow \theta + \beta \gamma^t \nabla_\theta \pi(S_t, \theta) [\nabla_a q(S_t, a, \eta)]_{a=\pi(S_t,\theta)}. \quad (5)$$

In formula (5), η represents the parameters of the value function. η can be updated by the following formula:

$$\eta \leftarrow \eta + \alpha [y - q_\pi(S_t, A_t; \eta)] \nabla_\eta q_\pi(S_t, A_t; \eta). \quad (6)$$

Compared with the DPG algorithm, the DDPG algorithm uses the experience replay and target network technology, which can deal with higher dimensional observation space and improve the stability of the algorithm. The flow of the algorithm is as follows:

(1) We initialize the policy network $\pi(S, \theta)$, value network $q(s, a)$, and parameters θ and η. Then, we initialize the target policy network $\pi'(s)$, target value network $q'(s, a)$, and parameters $\theta' \leftarrow \theta$ and $\eta' \leftarrow \eta$. We also initialize the target network learning rate σ. The batch size of each learning sample is N, and the experience pool size is R.

(2) We select the action $a_t = \pi(s_t)$ in the state S_t.

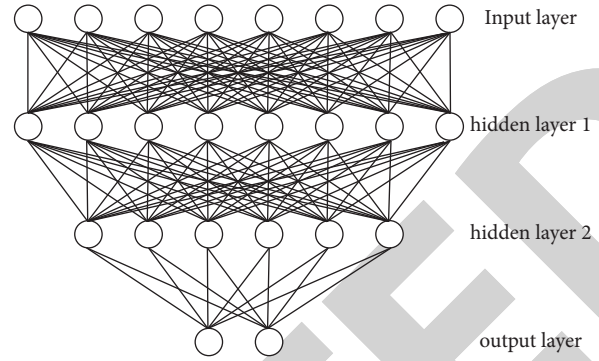

Figure 3: The basic structure of the path-planning strategy neural network.

(3) We perform actions to get rewards r_{t+1} and S_{t+1} from the environment.

(4) We save $\{S_T, a_t, r_{t+1}, S_{t+1}\}$ to the experience pool.

(5) When the samples in the experience pool meet the conditions for starting training, P samples are randomly selected from the experience pool, $\{(S_t, a_t, r_{t+1}, S_{t+1})\}_{i=1}^{N}$.

(6) We update the policy network and value network:

$$y_i = r_{i+1} + \gamma q(s_{i+1}, \pi(s_{i+1}, \theta'), \eta'), \quad (7)$$

$$\eta \leftarrow \eta + \alpha \frac{1}{N} \sum_i [y_i - q(s_i, a_i, \eta)] \nabla_\eta q(s_i, a_i, \eta), \quad (8)$$

$$\theta \leftarrow \theta + \beta \frac{1}{N} \sum_i \nabla_\theta \pi(h_i, \theta) [\nabla_a q(h_i, a, \eta)]_{a=\pi(h_i,\theta)}. \quad (9)$$

(7) We update the target network at regular intervals:

$$\eta' \leftarrow \varepsilon \eta + (1 - \varepsilon) \eta', \quad (10)$$

$$\theta' \leftarrow \varepsilon \theta_c + (1 - \varepsilon) \theta'. \quad (11)$$

3.3.2. Design of the Reward and Punishment Function and State Space. In order to simplify the model of path planning, it is assumed that the robot moves at a fixed speed; that is, the robot has a fixed moving distance in each time step. Therefore, the steering angle β of the robot is taken as an action space, and the dimension is 1. In the training of deep reinforcement learning, the purpose of the robot is to avoid obstacles and move to the target point at the same time. The state space of the robot is defined as follows:

RETRACTED

$$Z = \begin{cases} \dfrac{(x, y)}{\rho}, \\ \dfrac{\delta}{2\pi}, \\ \dfrac{D_{\min,o}}{\rho}, \\ \dfrac{\left[\left(x - x_{\min,o}\right), \left(y - y_{\min,o}\right)\right]}{\rho}, \\ \dfrac{D_{\min,g}}{\rho}, \\ \dfrac{\left[\left(x - x_{\min,g}\right), \left(y - y_{\min,g}\right)\right]}{\rho}. \end{cases} \tag{12}$$

In formula (12), (x, y) represent the position of the robot in the current map, δ represents the orientation of the robot in the current map, ρ represents the standardization coefficient, $D_{\min,o}$ represents the distance between the robot and the nearest obstacle, $D_{\min,g}$ represents the distance between the robot and the nearest target point, $(x - x_{\min,o})$, $(y - y_{\min,o})$ represent the distance information between the robot and the nearest obstacle, and $(x - x_{\min,g})$, $(y - y_{\min,g})$ represent the distance information between the robot and the nearest target. In actual motion, the distance between the robot and obstacles in the environment can be obtained by using sensors.

In the process of reinforcement learning, the quality of the reward function affects the effect of reinforcement learning. According to the basic framework of reinforcement learning, the agent evaluates the action through the feedback of the environment and selects the action that can obtain the maximum reward after learning. Therefore, the reasonable design of the reward function plays a vital role in reinforcement learning. Usually, the distance information between the robot and the target point is processed as the reward value; that is, the closer the robot is to the end point, the greater the reward it will get in each step of movement. However, this method of setting the reward function does not consider the changes between the robot and obstacle. A negative reward value is given only when the robot hits the obstacle, and the information of the robot's distance from the obstacle is not continuous. In view of the problems of setting the reward function in the abovementioned way, an artificial potential field method is proposed to set the reward function.

The artificial potential field method is a virtual force method. In the artificial potential field, the target end point will attract the mobile robot, while the obstacle will repel the robot. The superposition of these two forces is the control force of the mobile robot's motion process. Under the action of the control force, the mobile robot plans a path to the end point. Among them, the attractive force of the robot near the end point will become larger. If the robot approaches an obstacle, the repulsion force will become greater. In the classical artificial potential field, the attractive field function is shown in the following formula:

$$L_1(x) = \frac{1}{2}\kappa_1 d\left(x, x_g\right). \tag{13}$$

In formula (8), $\kappa_1 > 0$ represents the coefficient constant of the attractive field and $d(x, x_g)$ represents the distance of the robot from the target point. At the target point, the attractive potential energy L_1 is the smallest. The attractive function can be obtained by calculating the negative derivative of formula (8), as shown in the following formula:

$$F_1(x) = -\nabla L_2(x) = -\kappa_2 d\left(x, x_g\right). \tag{14}$$

The formula of the repulsion field function is shown in the following formula:

$$L_2(x) = \begin{cases} \dfrac{1}{2}\kappa_2\left(\dfrac{1}{d\left(x, x_{g0}\right)} - \dfrac{1}{d_{\max}}\right), & d\left(x, x_{g0}\right) \le d_{\max}, \\ 0, & d\left(x, x_{g0}\right) > d_{\max}. \end{cases} \tag{15}$$

In formula (15), $\kappa_2 > 0$ represents the coefficient constant of the repulsion field, $d(x, x_{g0})$ represents the straight-line distance of the robot from the target point, and $d_{\max}$ represents the maximum influence range of the obstacle. When $d(x, x_{g0}) > d_{\max}$, the robot is not affected by obstacles. The repulsive potential energy at obstacles has the maximum value. The repulsion function can be obtained by calculating the negative derivative of formula (10), as shown in the following formula:

$$F_2(x) = \begin{cases} \left(\dfrac{1}{d\left(x, x_{g0}\right)} - \dfrac{1}{d_{\max}}\right)\dfrac{\kappa_2 \partial d\left(x, x_{g0}\right)}{d^2\left(x, x_{g0}\right)\partial x}, & d\left(x, x_{g0}\right) \le d_{\max}, \\ 0, & d\left(x, x_{g0}\right) > d_{\max}. \end{cases} \tag{16}$$

The resultant potential field $L(x)$ and resultant force $F(x)$ received by the mobile robot during movement are shown in the following formula:

$$\begin{cases} L(x) = L_1(x) + L_2(x), \\ F(x) = F_1(x) + F_2(x). \end{cases} \tag{17}$$

When the robot has not reached the target or touched an obstacle, according to the idea of the artificial potential field, the reward value includes two parts: (1) the negative reward value of the distance information between the robot and the nearest obstacle and (2) the positive reward value of the distance information between the robot and the target point.

RETRACTED

Table 1: Neural network-related parameter settings.

Parameters	Value	Meaning
Network learning rate	0.001	Network learning speed
Reward discount rate	0.92	Future rewards at the current value
Soft update parameters	0.01	Update parameters of the strategy network and target network
Steps per round	250	Maximum number of exploration steps per round
Total number of rounds	20000	Maximum number of rounds
Experience pool capacity	60000	Experience storage limit
Batch size	32	Update network training batch size

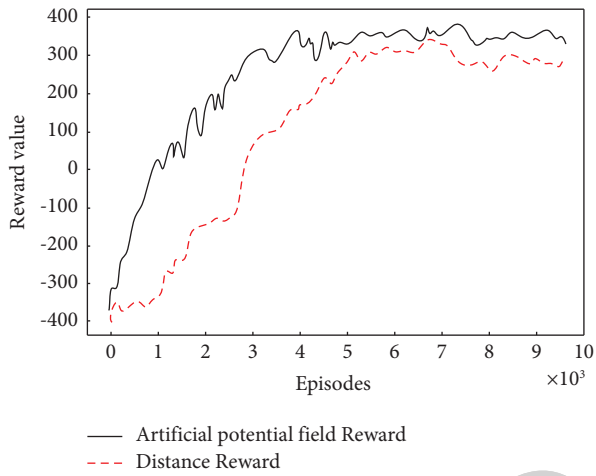

Figure 4: Total reward value per episode.

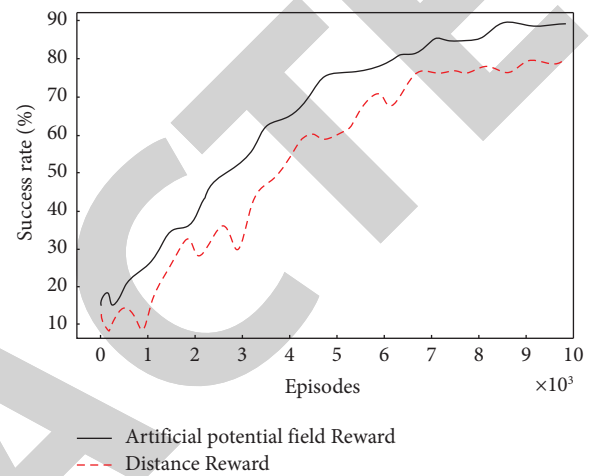

Figure 5: Change trend of the overall success rate.

The sum of the two reward values is taken as the final reward value obtained after the robot performs each action, as shown in the following formula:

$$C = C_1 + C_2 = \frac{1}{2^{d_{g/\kappa}}} - \frac{1}{2^{d_{o/\kappa}}}. \tag{18}$$

In formula (18), $d_{g/\kappa}$ represents the distance between the robot and the target point and $d_{o/\kappa}$ represents the distance between the robot and the obstacle.

The reward function of the robot action is obtained as shown in the following formula:

$$R = \begin{cases} 200, \\ \dfrac{1}{2^{d_{g/\kappa}}} - \dfrac{1}{2^{d_{o/\kappa}}}, \\ -200. \end{cases} \tag{19}$$

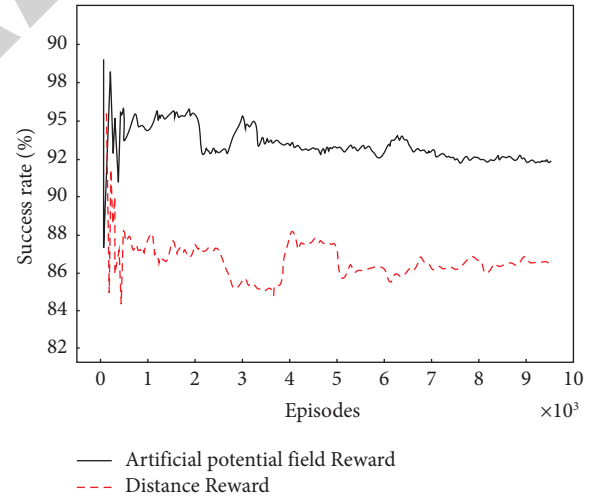

Figure 6: Change trend of the final success rate of training.

3.3.3. Neural Network Design. The designed path-planning strategy neural network is composed of four layers of the neural network, and its network structure is shown in Figure 3.

In Figure 3, the input layer is the current state of the mobile robot, the output layer is the linear velocity and angular velocity of the mobile robot, and there are two hidden layers in the middle. The input layer contains 12 neurons, and hidden layer 1 contains 250 neurons. The connection mode between the input layer and hidden layer 1 is full connection, and the ReLU nonlinear activation function is adopted. The input of hidden layer 2 contains 250 neurons. Hidden layer 1 and hidden layer 2 are fully connected, and the ReLU activation function is used. The output layer contains two neurons. Hidden layer 2 and the output layer are also fully connected, using the sigmoid activation function. The value network adopts a similar network structure. The main difference from the strategy network is that the input layer includes two parts: one is the current

RETRACTED

Table 2: The total length of paths planned by different algorithms in different situations.

Method	Situation 1 (m)	Situation 2 (m)	Situation 3 (m)	Situation 4 (m)
Proposed method	2.8	4.6	5.9	8.3
Reference. [15]	3.7	5.5	7.2	9.5
Reference. [18]	3.2	4.9	6.5	8.8
Reference. [19]	3.5	5.1	6.6	9.2

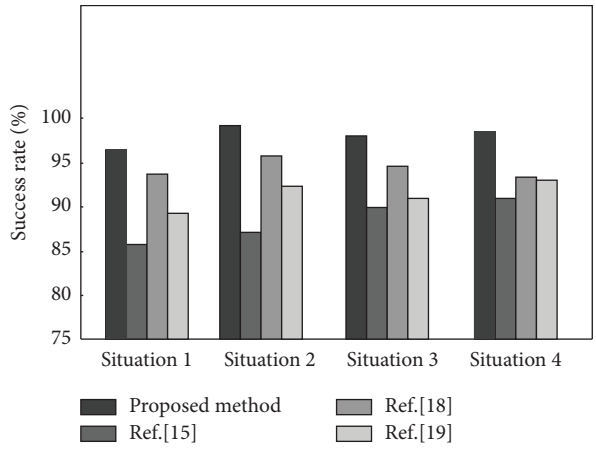

Figure 7: The success rate of path planning of different methods in different situations.

state of the robot and the other is the current action value of the robot. The output layer contains 1 neuron.

4. Experiment and Analysis

4.1. Experimental Environment. All the experiments in this chapter are implemented on the Windows7 professional 64 bit system and Python3.6. The simulation environment is designed by using pyglet, a multimedia framework under Python. A shape map with a pixel size of 1000 * 1000 is created. The pixel coordinates of four inner corners in the map are (300, 300), (700, 300), (300, 700), and (700, 700), respectively. The size of the robot in the environment is 100-pixel long and 50-pixel wide. The front end of the robot has five sensors to detect the distance, which can obtain the distance from the environmental boundary in all directions. The initial pose of the robot is $(500, 250, -\pi/2)$, and the speed is $v = 50$. The purpose of path planning is to enable the mobile robot to return to the initial position from the initial pose. The mobile robot cannot turn around in the environment under set speed conditions, so the mobile robot will complete the path planning around the map.

The pose of the robot can be solved by the following formula , and t is the sampling time.

$$\begin{cases} x_{P+1} = x_P + t \cdot v \cdot \cos \alpha_P, \\ \alpha_{P+1} = \alpha_P + t \cdot v \cdot \dfrac{\tan \beta_P}{Z_1}, \\ y_{P+1} = y_P + t \cdot v \cdot \sin \alpha_P. \end{cases} \tag{20}$$

After building the neural network and environment, we set the relevant parameters of the neural network according to Table 1.

4.2. Simulation Analysis. In this paper, deep reinforcement learning is trained based on the reward function built by the artificial potential field method and by using the distance information of the mobile robot from the target point. During the training process, the change trend of the total reward value, the change trend of the overall success rate, and the final success rate of training are shown in Figures 4–6, respectively.

It can be seen from Figures 4–6 that the reward function based on the artificial potential field method used in this paper converges more rapidly than the method that only takes the information of the distance from the target point of the mobile robot as the reward function. In addition, under the same training times, its success rate is also higher, and it has better goal orientation and obstacle avoidance ability.

The following is a comparative analysis of the proposed method and the mobile robot path-planning method proposed in [15], [18], and [19] under the same conditions for four different situations. The total length of mobile robot paths planned by different algorithms in different situations is shown in Table 2. The success rate of the proposed method in four different situations compared with the other three methods is shown in Figure 7.

It can be seen from Table 2 that in four different situations, compared with the other three comparison methods, the total lengths of the final planned path of the proposed method are both the shortest, which are 2.8 m, 4.6 m, 5.9 m, and 8.3 m, respectively. Compared with the other three methods, the maximum increased values are 0.9 m, 0.9 m, 1.3 m, and 1.2 m, respectively, and the minimum increased values are 0.4 m, 0.3 m, 0.6 m, and 0.5 m, respectively. This is because the method proposed in this paper uses the artificial potential field method to set the reward function, collects the information of the robot from the continuous obstacle, improves the performance of the path planning of the algorithm, and obtains the optimal path with a shorter path length.

As can be seen from Figure 7, in four different situations, compared with the other three comparison methods, the final success rates of the proposed method are the highest, which are 97.2%, 99.1%, 98.4%, and 98.6%, respectively. Compared with other comparison methods, it has been improved to a certain extent. The results show that the learning efficiency and training speed can be improved by combining the kinematic constraint motion of the robot and guiding its training process to establish the optimal state

RETRACTED

space for obstacle avoidance motion. The proposed algorithm can describe the path planning of the mobile robot in the unknown environment as a Markov decision-making process by introducing the DDPG algorithm. The stability of the algorithm and the success rate of path planning are greatly improved by using experience replay and target network technology.

5. Conclusion

Aiming at the problems of poor continuity and low success rate of the mobile robot spatial path-planning method, a continuous action spatial path-planning method of the mobile robot based on reinforcement learning is proposed. Through simulation experiments, the proposed method is compared with the other three methods. The basic ideas are as follows: ① Through the analysis of the kinematic model of the mobile robot, the optimal state space is constructed. ② The reward function of the mobile robot is set based on the artificial potential field method, and the information of the robot's distance from the obstacle is continuous. ③ By introducing the deep deterministic policy gradient (DDPG) algorithm, the success rate of mobile robot path planning is improved. By introducing the depth deterministic strategy, the gradient algorithm can use experience replay and target network technology to deal with higher dimensional observation space and improve the stability of the algorithm and the success rate of path planning.

This paper studies the path planning of mobile robots in static and dynamic environments only for one robot. Although there is research on the dynamic environment, the situation of multiple robots is different from the dynamic environment, so independent training and knowledge sharing need to be considered. In addition, there is a problem of cooperation among multiple robots, and there will be some new problems to be further solved.

Data Availability

The data used to support the findings of this study are included within the article.

Conflicts of Interest

The authors declare that there are no conflicts of interest regarding the publication of this paper.

Acknowledgments

This work was supported by the Key Scientific Research Projects of Colleges and Universities in Henan Province (No.20A520029, No.21B520012).

References

[1] J. R. Bourne, E. R. Pardyjak, and K. K. Leang, "Coordinated bayesian-based bioinspired plume source term estimation and source seeking for mobile robots," *IEEE Transactions on Robotics*, vol. 35, no. 4, pp. 967–986, 2019.

[2] C. Jiang, S. Sun, and J. Liu, *Global Path Planning of Mobile Robot Based on Improved JPS+ algorithm [C]*, Chinese Automation Congress (CAC), Shanghai, China, 2020.

[3] J. Guo, C. Li, and S. Guo, "A novel step optimal path planning algorithm for the spherical mobile robot based on fuzzy control," *IEEE Access*, vol. 8, no. 12, pp. 1394–1405, 2020.

[4] W. Chi, Z. Ding, J. Wang, G. Chen, and L. Sun, "A generalized voronoi diagram-based efficient heuristic path planning method for RRTs in mobile robots," *IEEE Transactions on Industrial Electronics*, vol. 69, no. 5, pp. 4926–4937, 2022.

[5] K. R. Jensen-Nau, T. Hermans, and K. K. Leang, "Near-optimal area-coverage path planning of energy-constrained aerial robots with application in autonomous environmental monitoring," *IEEE Transactions on Automation Science and Engineering*, vol. 18, no. 3, pp. 1453–1468, 2021.

[6] C. Tatino, N. Pappas, and D. Yuan, "Multi-robot association-path planning in millimeter-wave industrial scenarios," *IEEE Networking Letters*, vol. 2, no. 4, pp. 190–194, 2020.

[7] N. S. Monteiro, V. M. Gonçalves, and C. A. Maia, "Motion planning of mobile robots in indoor topological environments using partially observable Markov decision process," *IEEE Latin America Transactions*, vol. 19, no. 8, pp. 1315–1324, 2021.

[8] Q. Lu, D. Zhang, W. Ye, J. Fan, S. Liu, and C. Y. Su, "Targeting posture control with dynamic obstacle avoidance of constrained uncertain wheeled mobile robots including unknown skidding and slipping," *IEEE Transactions on Systems, Man, and Cybernetics: Systems*, vol. 51, no. 11, pp. 6650–6659, 2021.

[9] Z. Jian, S. Zhang, S. Chen, Z. Nan, and N. Zheng, "A global-local coupling two-stage path planning method for mobile robots," *IEEE Robotics and Automation Letters*, vol. 6, no. 3, pp. 5349–5356, 2021.

[10] F. Ugalde Pereira, P. Medeiros de Assis Brasil, M. A. De Souza Leite Cuadros, A. R. Cukla, P. Drews Junior, and D. F. Tello Gamarra, "Analysis of local trajectory planners for mobile robot with robot operating system," *IEEE Latin America Transactions*, vol. 20, no. 1, pp. 92–99, 2022.

[11] R. Zhou and L. Hui, "Path planning of mobile robot based on improved dynamic programming algorithm," *Computer Engineering and Application*, vol. 56, no. 21, pp. 20–24, 2020.

[12] X. Y. Zhong, J. Tian, H. S. Hu, and X. Peng, "Hybrid path planning based on safe a algorithm and adaptive window approach for mobile robot in large-scale dynamic environment," *Journal of Intelligent and Robotic Systems*, vol. 99, no. 1, pp. 65–77, 2020.

[13] B. Wang, Z. Liu, Q. Li, and A. Prorok, "Mobile robot path planning in dynamic environments through globally guided reinforcement learning," *IEEE Robotics and Automation Letters*, vol. 5, no. 4, pp. 6932–6939, 2020.

[14] S. K. Angappamudaliar Palanisamy, D. Selvaraj, and S. B. K. Ramasamy, "Hybrid multi-objective optimization approach intended for mobile robot path planning model," *Journal of Intelligent and Fuzzy Systems*, vol. 42, no. 3, pp. 2681–2693, 2022.

[15] M. Alireza, D. Vincent, and W. Tony, "Experimental study of path planning problem using EMCOA for a holonomic mobile robot," *Journal of Systems Engineering and Electronics*, vol. 32, no. 6, pp. 1450–1462, 2021.

[16] R. Fareh, M. Baziyad, T. Rabie, and M. Bettayeb, "Enhancing path quality of real-time path planning algorithms for mobile robots: a sequential linear paths approach," *IEEE Access*, vol. 8, no. 3, pp. 167090–167104, 2020.

[17] S. D. Han and J. Yu, "DDM: fast near-optimal multi-robot path planning using diversified-path and optimal sub-

RETRACTED

Hindawi
Journal of Robotics
Volume 2024, Article ID 9819583, 1 page
https://doi.org/10.1155/2024/9819583

Retraction

Retracted: Design and Simulation Analysis of a Flexible Clamping and Conveying Device of a Green Leafy Vegetable Cutting and Bundling Integrated Machine

Journal of Robotics

Received 23 January 2024; Accepted 23 January 2024; Published 24 January 2024

Copyright © 2024 Journal of Robotics. This is an open access article distributed under the Creative Commons Attribution License, which permits unrestricted use, distribution, and reproduction in any medium, provided the original work is properly cited.

This article has been retracted by Hindawi following an investigation undertaken by the publisher [1]. This investigation has uncovered evidence of one or more of the following indicators of systematic manipulation of the publication process:

(1) Discrepancies in scope
(2) Discrepancies in the description of the research reported
(3) Discrepancies between the availability of data and the research described
(4) Inappropriate citations
(5) Incoherent, meaningless and/or irrelevant content included in the article
(6) Manipulated or compromised peer review

The presence of these indicators undermines our confidence in the integrity of the article's content and we cannot, therefore, vouch for its reliability. Please note that this notice is intended solely to alert readers that the content of this article is unreliable. We have not investigated whether authors were aware of or involved in the systematic manipulation of the publication process.

Wiley and Hindawi regrets that the usual quality checks did not identify these issues before publication and have since put additional measures in place to safeguard research integrity.

We wish to credit our own Research Integrity and Research Publishing teams and anonymous and named external researchers and research integrity experts for contributing to this investigation.

The corresponding author, as the representative of all authors, has been given the opportunity to register their agreement or disagreement to this retraction. We have kept a record of any response received.

References

[1] Z. Wang, T. Yang, and W. Wei, "Design and Simulation Analysis of a Flexible Clamping and Conveying Device of a Green Leafy Vegetable Cutting and Bundling Integrated Machine," *Journal of Robotics*, vol. 2022, Article ID 4729480, 9 pages, 2022.

Hindawi
Journal of Robotics
Volume 2022, Article ID 4729480, 9 pages
https://doi.org/10.1155/2022/4729480

RETRACTED

Research Article

Design and Simulation Analysis of a Flexible Clamping and Conveying Device of a Green Leafy Vegetable Cutting and Bundling Integrated Machine

Zhiquan Wang, Tianxing Yang, and Wei Wei

School of Bailie Mechanical Engineering, Lanzhou City University, Lanzhou, Gansu 730070, China

Correspondence should be addressed to Zhiquan Wang; wangzhiquan@lzcu.edu.cn

Received 28 July 2022; Revised 9 September 2022; Accepted 12 September 2022; Published 15 October 2022

Academic Editor: Shahid Hussain

Copyright © 2022 Zhiquan Wang et al. This is an open access article distributed under the Creative Commons Attribution License, which permits unrestricted use, distribution, and reproduction in any medium, provided the original work is properly cited.

In order to improve the harvesting production efficiency of green leafy vegetables, this paper designs and simulates the flexible clamping and conveying device of the green leafy vegetable cutting and bundling integrated machine. Through theoretical calculation and 3D modeling, the design optimization of key components is carried out in this paper. The cutter head of the guillotine cutting and throwing device is a wheel cutter type. The throwing blades are axially symmetrically distributed on the cutter head, and the movable blades are radially distributed at equal angles and are located in the middle of the two throwing blades. The electronic control system of the wrapping device uses a pressure sensor to cooperate with the baling device to realize automatic wrapping after baling. In addition, the drive chassis of the machine is a hydrostatic drive system, which is convenient for step-less speed change and automatic control within a certain range. Through the simulation study, it can be seen that the flexible clamping and conveying device of the green leafy vegetable cutting and bundling integrated machine proposed in this paper can meet the industrialization needs of green leafy vegetables.

1. Introduction

At present, the domestic method of bundling vegetables is mostly carried out manually, which has low work efficiency, high labor intensity, and high-cost consumption. In order to make up for the lack of single technology of traditional vegetable harvesters, a baling device is installed on the basis of traditional vegetable harvesters so that the whole machine can integrate the functions of harvesting and bundling. At the same time, according to the development trend of mechatronics technology, modern sensor detection technology, lithium battery management technology, and advanced mechanical design and manufacturing technology are used to innovate and optimize the structure of traditional vegetable harvesters.

With the continuous improvement of product functions of vegetable harvesters, consumers are no longer limited to traditional industrial design with their functionality as market-oriented products but increasingly pay attention to the actual user experience and visual experience of their products. This brings challenges to the design work of the harvester product. In other words, today's consumer demand structure has shifted from a functional focus to a spiritual focus. In view of this, the appearance design of the vegetable harvester is particularly important. The solution is to replace manual labor with more mechanized operations, so as to improve the production efficiency of the enterprise as much as possible and achieve the goal of liberating labor [1]. The product design of a vegetable harvester is complex and changeable work. In the whole process of product design, it is necessary to fully consider many influencing factors such as the requirements of users in the actual application scenario and the limitations of the environment used. Whether the product design of the vegetable harvester is successful or not requires us to test it in practical application scenarios. Therefore, in the design process of vegetable harvester series products, we need to analyze these relevant situations and methods, find the key points of the

design, and then carry out the design work to make it more reasonably suitable for its future practical application [2].

The concept of context first appeared in the field of social psychological science. It has different names and can be called context, background, etc. In the field of design, the concept of context is widely used. The practical point of view has made a rich substantive inquiry. In terms of considering multiple factors, theoretical analysis and experiments, literature [3] obtained second-order differential equations about blade weight, knife thickness, cutting speed, friction factor, straw section size, and other factors through theoretical analysis and derivation, and conducted cutting tests on vegetables using the designed cutting test bench to verify the accuracy of the equation analysis results, and obtained the influence of parameters in the equation on cutting power consumption. Literature [4] designed a lettuce harvester, which uses batteries to provide cutting and transportation power. The cutting device is a double action knife, which can perform reciprocating cutting. This model is characterized by the design and use of an electric push rod to achieve the movement of the cutting device and ensure the harvest height of different vegetables. Literature [5] has designed and completed a stubble cutting grassland harvester, which is self-propelled and can meet the needs of weeds. The problems pointed out in the paper have guiding significance for the design of harvesting machinery. Literature [6] has developed a vegetable harvesting, sowing and transplanting machine. Through parallel control of the hydraulic landing gear and the micro adjustment device, the position of the cutter and the collecting device can be adjusted to ensure that the stubble height of the leafy vegetables after cutting is consistent, so that the machine can harvest on the flat and ridge at the same time, and improve the versatility of mechanical harvesting. Literature [7] designed a vegetable sowing and harvesting combined machine. The machine adopts a walking operation and a chain cutter. The cutter is a sickle shaped machine. The cutting device is operated by turning wheels and combining gear and chain drive.

Literature [8] proposed the research and development of a small leafy vegetable harvester, mainly for golden cauliflower and bean sprouts. The use of a high-voltage battery drive mode can provide a continuous power supply, which can easily complete the planting, production, harvesting, and transportation of various vegetables, and can ensure that the machine can move or turn freely in the field. Although the tools used for the cultivation and harvesting of these kinds of crops have been able to improve the production efficiency by dozens of times, for the cultivation ground of agronomic plants with poor flatness, the mechanization height of the tools used for harvesting has not yet fully met the relevant national regulations [9]. The authors in [10] designed a small multifunctional machine suitable for harvesting water cabbage grown in South China. In this design, only theoretical calculations are involved, and a prototype has not been manufactured and verified in the field. The working efficiency of this machine is also worthy of consideration. Although some progress has been made in mechanization and harvesting technologies for vegetables and agricultural products, the pace of development has been slower. The main reason for this is that agricultural production and planting environments are differentiated. As far as the same green leafy vegetable is concerned, there are also large gaps in terms of land leveling and planting density under different regional planting environments [11]. Harvesting machines currently manufactured are not suitable for the adjustment of objective differences between the above two. According to relevant statistical results, there are as many as 30 kinds of green leafy vegetables grown. Different vegetable varieties utilize different harvesting techniques and requirements. For market demand, cilantro and spinach require rhizomes to be retained; Chinese cabbage requires rhizomes to be removed. Therefore, a vegetable harvester with high compatibility features has a long way to go in its design and manufacture [12]. In the process of mechanized picking of green leafy vegetables, if there are problems such as improper handling, it is easy to cause serious damage to the appearance of agricultural products, which will be further aggravated in the subsequent recovery, transportation, and sales process [13]. In the vegetable market, the sales appearance of vegetables has always been an important indicator that consumers are very concerned about. Any damage to the appearance will directly lead to a plummeting vegetable price, which has become a difficult point in the design of leafy green vegetable harvesting machinery [14].

The working process of the cutter and baler is to cut stalks and then bundle them. The bundles need to be laid out in an orderly manner. Therefore, the designed cutter and baler must meet many conditions. According to the harvesting experience, the following points can be summarized: (1) In order to adapt to the complexity of the terrain, the baler needs to have a good ability to walk on the ground; (2) the harvesting effect does not change due to the height of the stalk, allowing crops to have a difference in the height of the stalk; (3) for lodging stems, normal harvesting can be achieved without missing cuts [15]; (4) the harvesting effect does not change due to the maturity or yield of crops; (5) the knotted rope ends should be moderately tight and should be transported and sun-dried in bundles; (6) for different stem crops, specific agronomy should be considered [16]. According to the complex structure and design conditions of the cutter and baler, the operation overview of the existing cutter and baler is introduced: in the preprocessing device of the cutter and baler, after the stalks are separated by using the crop divider, the reel star wheel cooperates with the helper board. The stalks to be cut are sent to the cutting area. When the cutter cuts the stalks, the front-end processing device plays a supporting role. After cutting, the stalks are discharged to the baling mechanism through the conveyor belt on one side [17]. When bundling, due to the action of the pressing rod, the stalk is transported between the harvesting platform and the rope guide plate, and the clutch control rod prevents it from coming out. At this time, the baling needle makes a rotary motion and wraps the rope around the stalk, and the knotting nozzle ties the rope at the top of the baling needle to the other rope end on the rope pressing plate and is acted by the release rod to release the rope. When the bale is pushed out of the bale frame, the bale rope is cut off, and finally, the clutch is reset to complete one bale [18].

RETRACTED

This paper designs and simulates the flexible clamping and conveying device of the green leafy vegetable cutting and bundling integrated machine to improve the working efficiency of the green leafy vegetable cutting and bundling machine.

2. Structural Design

2.1. Working Principle. When the machine is working in the field, green leafy vegetables are supported by the grass-supporting device on the integrated header and then divided by using the grass-dividing fork. Then, green leafy vegetable straws are cut by using the saw disc and the conveying drum, and the cut green leafy vegetable straws are forcibly fed through the feeding mechanism of the header and transported to the material chopping and throwing device. After that, the green leafy vegetable straws are cut and thrown, and then, the crushed green leafy vegetable straws are thrown into the bin of the baling device through the throwing tube. Then, the crushed green leafy vegetable straws are fed into the baling chamber from the forage feeding mechanism below the silo in an orderly manner for baling operation. After the baling device bales broken straws into dense round bales, the hydraulic cylinder controls the opening of the bin door of the baling device to transport the round bales to the coating device for coating operation. The coating device starts to work under the control of the hydraulic system. With the cooperation of the wrapping rotating mechanism of the wrapping device and the rolling frame, round straw bales are evenly wrapped. When the round straw bales are wrapped, the unloading guide of the wrapping device is opened, and the round bale slides down to the ground along the unloading guide. Then, the unloading bale guide is recovered and restored to prepare for the next operation. Finally, the round straw bales can be stored and transported or packaged and directly ensiled on the field. The flowchart of the machine operation is shown in Figure 1.

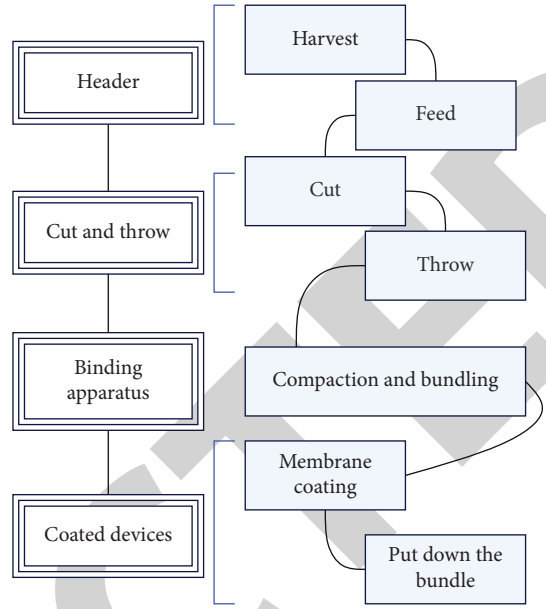

Figure 1: Flowchart of the whole machine operation.

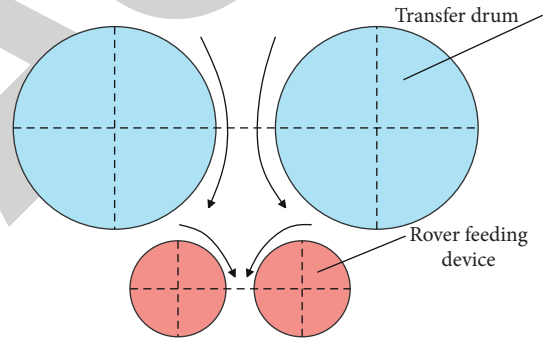

Figure 2: Schematic diagram of the transmission route.

2.2. Design of Key Components for Green Leafy Vegetable Harvesting. The integrated header suspension mechanism of the green leafy vegetable harvesting, baling, and wrapping machine adopts a four-bar linkage mechanism, and a four-bar linkage mechanism consisting of an upper connecting rod and two lower connecting rods is mounted on the chassis. Two lifting cylinders play a supporting role, which can control the header to rise and fall within a certain range (lifting range 0~715 mm). The four-bar linkage is equipped with a safety-locking device, which can be locked during transportation or maintenance under the header, which can protect the hydraulic system of the header and the personal safety of the driver. The main working mechanism of the header is two header-conveying rollers, and a saw disc is installed at the lower part of each conveying roller. When the green leafy vegetable harvester is working, green leafy vegetables are fed by using the weeding device. Then, it is divided into the conveying drum using the crop divider and the crop fork, green leafy vegetables are cut by using the saw disc, and the whole corn is transported to the rolling feeding device by using five-level shifting teeth I–V. It is forcibly fed from the rolling feeding device to the material cutting and throwing device. The material cutting and throwing device chops and throws green leafy vegetables, and the broken straw is guided by using the throwing cylinder and transported to the silo of the baling device. Figure 2 shows a schematic diagram of the transmission route of the conveying drum and the rolling feeding device of the green leafy vegetable harvester header.

The V-belt is selected for speed regulation, and the diameters of the driving pulley and the driven pulley (conveying roller pulley) are designed to be d_1 = 118mm and d_2 = 1090mm, respectively. n_1 and n_2 are the rotational speeds of the main and driven pulleys, respectively, and then, the speeds of the two pulleys are as follows:

$$v_1 = \frac{\pi d_1 n_1}{60 \times 1000},$$
$$v_2 = \frac{\pi d_2 n_2}{60 \times 1000}. \quad (1)$$

In the formula, v_1 is the peripheral speed of the driving pulley, m/s; v_2 is the peripheral speed of the driven pulley, m/s; d_1 is the diameter of the driving pulley, mm; d_2 is the

RETRACTED

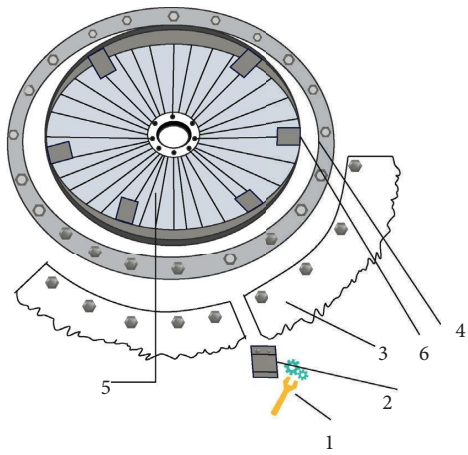

1. Fixed bolt 2. Cleaner 3. Blade 4. Blade fixed holder 5. Cone 6. Reinforcement plate

Figure 3: Exploded view of the saw disc.

diameter of the driven pulley, mm; n_1 is the rotational speed of the driving pulley, r/min; and n_2 is the rotational speed of the driven pulley, r/min.

Since the slip rate of the V-belt drive is very small, it can be ignored in the general calculation, and the transmission ratio of the belt drive is obtained as follows:

$$i_1 = \frac{n_1}{n_2} = \frac{d_2}{d_1}. \tag{2}$$

The rotational speed of the driven pulley is obtained by the following formula:

$$n_2 = \frac{n_1 d_1}{d_2}. \tag{3}$$

The speed n_2 of the driven pulley is calculated to be 1010r/min.

Then, the main reducer is used for deceleration, the double output shaft reducer is selected, and its transmission ratio i_2 is 2.5; then, the speed n_3 of the output shaft is as follows:

$$n_2 = \frac{n_3}{i_2}. \tag{4}$$

The rotational speed n_3 of the output shaft calculated by formula (4) is 2525r/min.

The saw disc of the integrated header is composed of fixing bolts, cleaners, blades, blade-fixing seats, cones, and reinforcing plates. The saw disc is installed under the conveying drum to neatly saw off the green leafy vegetables to be harvested. The blade inertia force of this cutting method is easy to balance, the vibration is small, and the structure is simple. Figure 3 shows an exploded view of the saw disc.

In order to ensure that the conveying roller can keep working normally, there are certain position requirements between the comb-tooth plate and the conveying roller. Figure 4 shows a schematic diagram of the positional relationship between the comb-tooth plate and the conveying roller.

During the vertical lift process, the crushed straw with mass m is thrown by using the throwing blade at the initial velocity of V_1. The throwing speed is V_2 (in order to make the broken straw leave the pipe neatly, there should be $2 \sim 3m/s$), so it takes $V_2 = 2 \sim 3m/s$. According to the law of conservation of energy, we can get

$$\frac{1}{2}mV_1^2 = mgH + \frac{1}{2}mV_2^2. \tag{5}$$

Considering the lost energy, we get

$$\frac{1}{2}mV_1^2 = mgH(1+\mu_1) + \frac{1}{2}mV_2^2. \tag{6}$$

In the formula, V_1 is the initial velocity of the shredded straw thrown, m/s; V_2 is the final speed at the exit, m/s; and μ_1 is the energy loss coefficient of friction loss with the pipe wall and the loss of materials colliding with each other and the resistance of the air in the pipe during the lifting process. It is often taken as $\mu_1 = 0.22$.

The initial speed at which the broken straw is thrown is as follows:

$$V_1 = \sqrt{2gH(1+\mu_1) + V_2^2}. \tag{7}$$

Combined with formula (7), considering the speed loss of the throwing blade on the cutter head when it hits the straw, the actual speed of the throwing blade during the vertical lift should be

$$V_{\text{Ò¶}} = (1+\mu_2)V_1 = (1+\mu_2)\sqrt{2gH(1+\mu_1) + V_2^2}. \tag{8}$$

In the formula, V_1 is the initial velocity of the shredded straw, m/s; V_{leaf} is the actual speed of the throwing blade, m/s; and μ_2 is the difference loss coefficient between the peripheral speed of the thrown blade and the initial speed V_1 of the broken straw (it is often taken as $\mu_2 = 0.55$).

According to formula (8), the rotational speed required to throw the blade is as follows:

$$n = \frac{30V_{leaf}}{\pi R} = \frac{30}{\pi R}(1+\mu_2)\sqrt{2gH(1+\mu_1) + V_2^2}. \tag{9}$$

In the formula, H is the lift height (height of the model), m; R is the inner diameter of the blade taken (the most unfavorable when throwing at this point), m.

Since the designed throwing device is not a vertical lift but has a certain inclination $\alpha = 73^\circ$, at this time, the initial velocity of throwing is no longer V_1, but we obtain the following equation:

$$V_1' = V_1 \sin\alpha. \tag{10}$$

Therefore, we get

$$V_1 = \frac{V_1'}{\sin\alpha}. \tag{11}$$

Combined with formula (8), the actual speed of the throwing blade is as follows:

RETRACTED

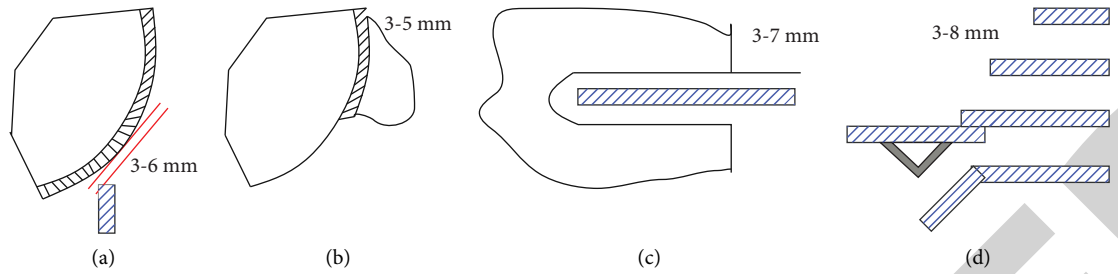

Figure 4: Schematic diagram of the positional relationship between the comb plate and the conveying roller: (a) clearance between the conveying roller and the vertical plate, (b) clearance between the delivery roller and the transverse comb plate, (c) space between the transport roller flange and the comb-tooth plate groove, and (d) clearance between the transport roller flange and the middle separator.

$$V_{leaf} = \frac{(1+\mu_2)}{\sin\alpha}\sqrt{2gH(1+\mu_1)+V_2^2}. \quad (12)$$

Combined with formula (9), the rotational speed of the throwing blade in the design model is obtained at least as follows:

$$n = \frac{30V_{leaf}}{\pi R} = \frac{30}{\pi R}\frac{(1+\mu_2)}{\sin\alpha}\sqrt{2gH(1+\mu_1)+V_2^2}. \quad (13)$$

According to formula (13), the rotational speed $n = 800r/\text{min}$ of the throwing blade of the guillotine cutting and throwing device is obtained; that is, it is determined that the rotational speed of the cutter head shall not be lower than $800r/\text{min}$.

The cutter head is the main working mechanism of the guillotine cutting and throwing device, and its structure is a wheel cutter type, which is composed of a cutter wheel, a fixed blade, and a cutter wheel box. The rolling feeding device squeezes corn stalks and feeds them to the entrance of the cutter wheel box forcibly. Under the support of the fixed blade installed at the entrance of the cutter wheel box, the straw is slid and cut into pieces by a high-speed rotating moving blade, and the cutting process is completed. The throwing piece is welded on the edge of the cutter wheel, which has achieved the purpose of throwing. This design method has the advantages of simple structure, convenient installation, and use and can meet the above requirements for cutting stalks of different lengths and consume less power. Figure 5 shows a schematic diagram of the structure of the material shredding and throwing device.

The gap between the movable and fixed blades of the guillotine-cutting and throwing device and the sharpness of the cutting edge directly affect the cutting quality of green leafy vegetable straws and the power consumption of the machine. In order to ensure the cutting quality of straws and reduce the loss of power, the gap between the movable and fixed knives is 0.5~1 mm.

Unbalanced masses in rotational motion cause inertial forces, which can be expressed as follows:

$$P_B = -\left(m + \frac{1}{2}M_L\right)r\omega^2. \quad (14)$$

In the formula, P_B is the inertial force caused by an unbalanced mass in rotary motion, N; m is the mass of the crank pin, g; M_L is the mass of the connecting rod (1/2 of M_L makes a rotary motion on the crank pin, and 1/2 makes a reciprocating motion on the cutter), g; r is the radius of gyration, mm; and ω is the rotational angular velocity, rad/s.

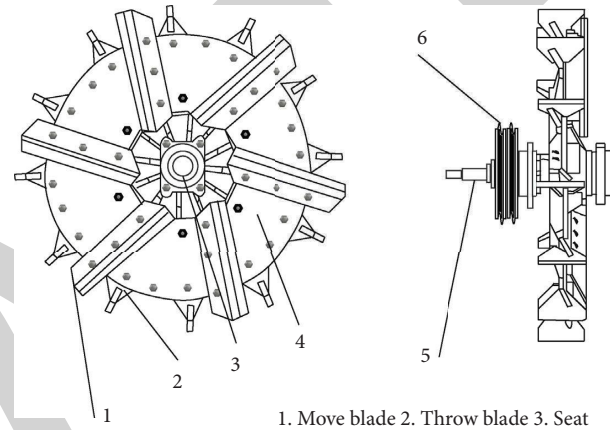

1. Move blade 2. Throw blade 3. Seat bearing 4. Knife plate 5. Main shaft 6. Pulley

Figure 5: Cutter assembly diagram.

In general, a balance weight mounted on the crank disc can balance all the rotational inertia force P_B and part of the reciprocating inertia force P_A (1/3 ~ 1/2) to determine the quality of the weight can be expressed as follows:

$$P_P = P_B + \frac{1}{2}P_{A\max} = \left(m + \frac{1}{2}M_L\right)r\omega^2 + \frac{1}{2}\left(M_H + \frac{1}{2}M_L\right)r\omega^2,$$

$$P_A = -\left(M_H + \frac{1}{2}M_L\right)r\omega^2\cos\omega t,$$

$$P_{A\max} = -\left(M_H + \frac{1}{2}M_L\right)r\omega^2. \quad (15)$$

In the formula, P_P is the weight of the counterweight, N; P_A is the inertial force caused by the unbalanced mass in reciprocating motion, N; $P_{A\max}$ is the maximum inertial force of part of the reciprocating motion, N; and M_H is the mass of the cutter, g.

After calculating the mass P_P of the counterweight, the weight of the counterweight and the radius of the counterweight can be calculated according to the following formula:

RETRACTED

$$P_P = m_P r_p \omega^2. \quad (16)$$

In the formula, m_P is the weight of the balance block, N; r_P is the radius of the balance block, mm.

If any one of m_P, r_P is selected, another parameter can be obtained. Here, the radius r_P = 8mm is taken to obtain the mass $m_p = 25g$ of the counterweight.

2.3. Design of the Main Components of the Baling Device. The baling device can perform fixed work and pulling work. During fixed operation, the baling device is placed on flat ground, and the frame is adjusted to make the baling device in a horizontal state. Then, the shredded straw is directly fed into the silo to complete the baling operation. During towing operation, the baler is placed on the chassis of the silage-integrated machine, and the power input shaft of the baling device is connected to the hydraulic motor of the integrated machine so that the control of the baling device can be completed in the cab. Figure 6 shows a flowchart of the operation of the baling device.

The control system of the coating device is composed of a pressure-sensing module, signal detection module, optocoupler, single chip AT90CAN64, drive module, control relay, A/D conversion, and display module.

The signal detection module is connected to the optocoupler, the optocoupler and the pressure- sensing module are connected to the single-chip microcomputer, the single-chip microcomputer is connected to the driving module and the A/D conversion module, and the driving module is connected to the control relay. The signal detection module collects the signal, and the signal is transmitted to single chip AT90CAN64 through the optocoupler, and the single chip processes the received signal. Then, the drive module sends a command signal to the control relay to respond, and the control relay controls the solenoid valve to change the start and stop of the oil circuit and the engine. The system uses the pressure sensor to cooperate with the baling device to achieve automatic wrapping after baling. Figure 7 shows a schematic diagram of the control system.

The film has extremely high elasticity, which can reach 70% of the tensile strength in the working state, and high elasticity can improve the wrapping degree of straw bales. Moreover, the purpose of saving the film can be achieved, and the film has good adhesion properties so that the wrapping effect cannot be affected by the external temperature.

The hydrostatic drive system of the drive chassis of the green leafy vegetable harvesting, baling, and wrapping machine is composed of the high-pressure closed quantitative motor, reduction mechanism, mechanical gearbox, walking front wheel, hydraulic oil pipe, fuel tank, radiator, high-pressure closed variable displacement plunger pump, and high-pressure plunger pump oil port. The hydrostatic drive has a series of advantages such as high stability, fast response speed, and good control performance, which facilitates the realization of the functions of continuously variable speed change and automatic control within a certain range. The schematic diagram of the hydrostatic drive system is shown in Figure 8.

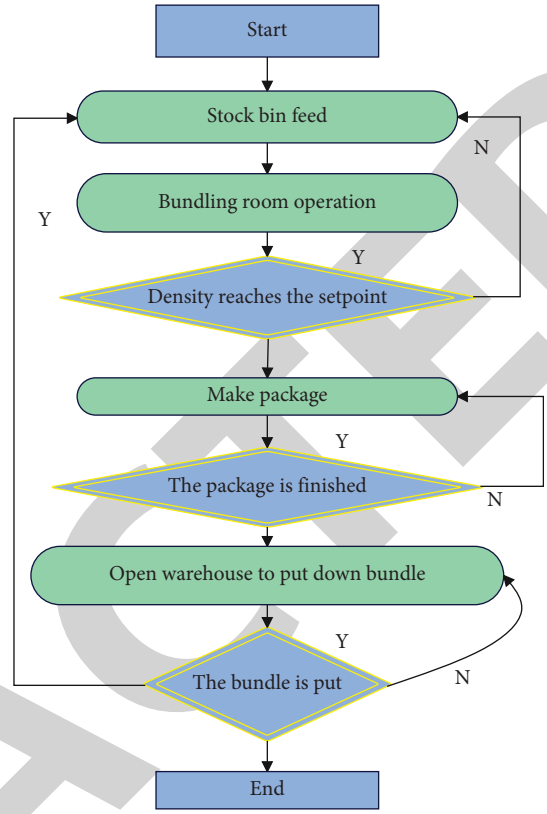

Figure 6: Operation flowchart of the baling device.

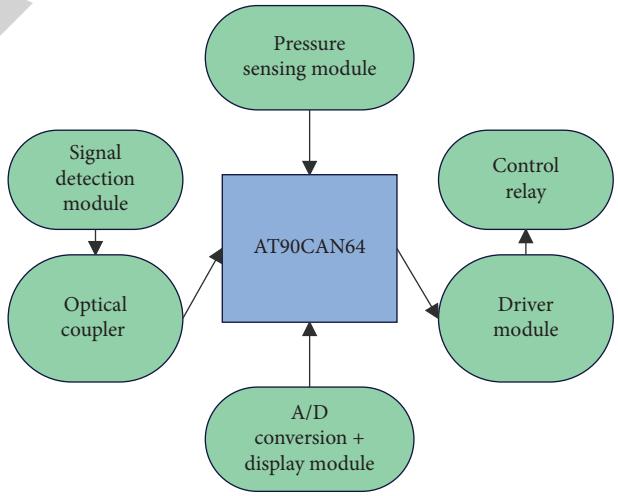

Figure 7: Schematic diagram of the control system of the coating device.

A hydraulic pump provides liquid with certain pressure and flow to the system and converts mechanical energy into pressure energy of liquid. Hydraulic pumps are divided into gear pumps, plunger pumps, vane pumps, and screw pumps according to the shape and movement mode of the main moving components and can be divided into variable pumps and quantitative pumps according to whether the flow can

RETRACTED

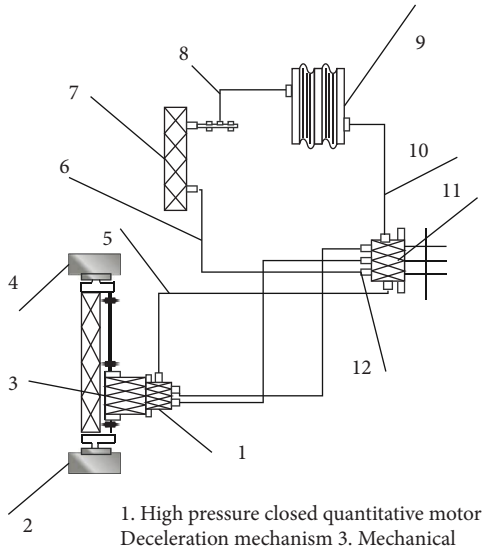

1. High pressure closed quantitative motor 2. Deceleration mechanism 3. Mechanical transmission 4. Walking front wheel 5. I hydraulic pipe 6. Hydraulic pipe 7. Tank 8. Hydraulic pipe 9. Radiator 10. IV hydraulic pipe 11. High pressure closed variable plunger pump 12. High pressure plunger pump port

Figure 8: Schematic diagram of the hydrostatic drive system of the drive chassis.

be adjusted. Moreover, a diesel engine with a rated speed of 3000 r/min was selected as the power source, and a dual-pump dual-motor drive scheme was adopted in consideration for economic needs.

The formula for calculating the maximum displacement of the hydraulic pump is as follows:

$$q_{p\max} \le \frac{q_{m\min} n_{\max} z}{0.95^2 n_{ph}}. \quad (17)$$

In the formula, $q_{p\max}$ is the maximum displacement of the hydraulic pump, cm^3/r; $q_{m\min}$ is the low displacement of the drive motor, cm^3/r; z is the number of drive motors; and n_{ph} is the engine speed, r/min.

Through calculation, we can get $q_{p\max} \ge 50.11 cm^3/r$, and finally, we choose a Linde Hydraulics HPV-02 series closed-circuit hydraulic pump with displacement $54.7 cm^3/r$.

The high-pressure closed-type quantitative motor, gearbox, and reduction mechanism can control the walking speed of the front wheel of the integrated machine in the field. The radiator is installed above the motor to dissipate heat and keep the machine running normally. The high-pressure closed variable displacement piston pump adjusts pressure, flow, and direction by controlling the pressure of the pilot oil, which reduces the control of the electrical proportion. Therefore, it has simple and convenient operability and safe and reliable usability.

The central electronic control and detection monitoring system of the whole machine mainly relies on the onboard monitoring device. It is mainly composed of five submodules, namely, the overall vehicle controller, the integrated instrument cluster module, the intelligent alarm system, the video processing system, and the working

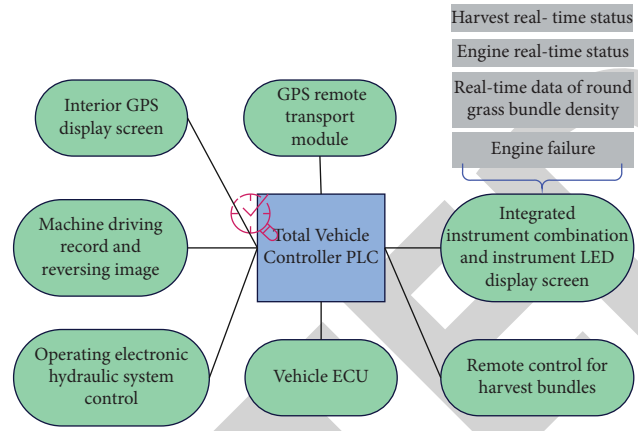

Figure 9: Architecture diagram of the central electronic control and detection and monitoring system of the whole machine.

electronic hydraulic control system module. The general controller of the whole vehicle monitors the working conditions of the key components of the whole machine at any time through the output terminal and displays the running data of the whole vehicle on the LCD screen. The architecture diagram of the central electronic control and detection and monitoring system of the whole machine is shown in Figure 9.

3. System Simulation

The driving force is set to 360 d*time, which means that the crank makes one revolution per second, and the feasibility of the model is verified. The simulation analysis time is set to 2 s, and the analysis step size is 200. By clicking the simulation button to get the animation verification, Figure 10(a) shows the change in the speed and acceleration of the baling needle. It can be seen that the baling needle rotates first before bundling, and then the speed changes suddenly, and the speed is zero at the instant of baling. The maximum change in the acceleration of the baling needle in the figure is about 3500 mm/s. Figure 10(b) shows the changes in angular velocity and angular acceleration of the baling needle. It can be seen that the variation of angular velocity is similar to the variation of velocity, and the variation range of angular acceleration is also relatively large, so the selection of materials and processing requirements are relatively high during physical manufacturing. Figure 10(c) shows the force change diagram of the baling needle, and the variation range is small. In conclusion, the virtual design size of the baling needle frame is reasonable and can be used as a reference for subsequent prototype processing.

Through the above simulation research, it can be seen that the flexible clamping and conveying device of the green leafy vegetable cutting and bundling integrated machine proposed in this paper can meet the industrialization needs of green leafy vegetables and can effectively improve the production efficiency in the harvesting of green leafy vegetables.

RETRACTED

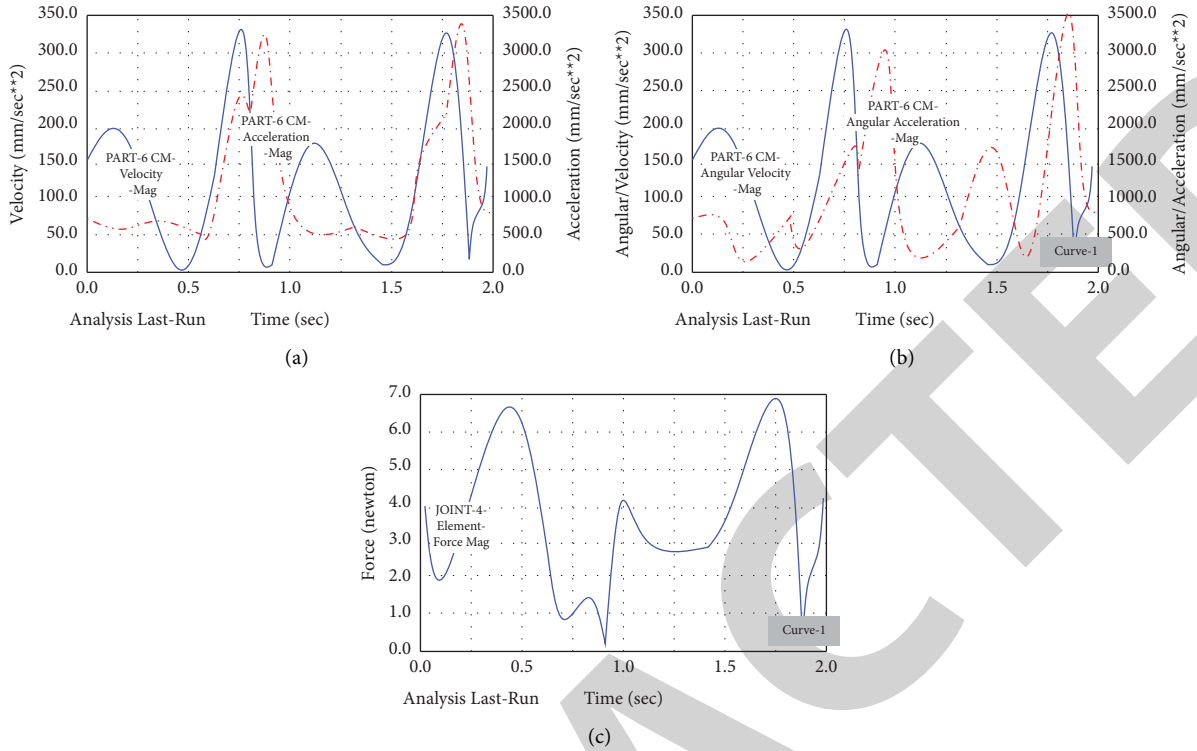

Figure 10: Simulation test: (a) the variation curve of baling needle speed and acceleration, (b) the variation curve of baling needle angular velocity and angular acceleration, and (c) the variation curve of baling needle stress.

4. Conclusion

With the adjustment of the rural industrial structure and the development of the vegetable industry, the growing area of vegetables continues to expand, and the scale and simplified management level of vegetable greenhouse bases are also increasing. However, there is no mature special vegetable harvester, and a large-scale harvester cannot meet the harvesting of small-area mountain vegetables. Moreover, the ecological characteristics of different types of vegetables are different, and traditional harvesters can only support harvesting technology and can only harvest one or similar crops. Its working mode is relatively simple, which limits the scope of use of the harvester. The bundling of vegetables after harvesting is the most labor-intensive link. This paper designs and simulates the flexible clamping and conveying device of the green leafy vegetable cutting and baling integrated machine, so as to improve the working efficiency of the green leafy vegetable cutting and binding integrated machine. Through the simulation study, it can be seen that the flexible clamping and conveying device of the green leafy vegetable cutting and bundling integrated machine proposed in this paper can meet the industrialization needs of green leafy vegetables.

Data Availability

The labeled dataset used to support the findings of this study is available from the corresponding author upon request.

Conflicts of Interest

The authors declare no conflicts of interest.

Acknowledgments

This work was supported by the Scientific Research Project of Colleges and Universities in Gansu Province, the Intelligent Harvesting and Binding Machine for Green Leafy Vegetables, 2021A-138.

References

[1] S. P. Singh, M. K. Singh, and U. Ekka, "Battery-assisted offset rotary cutter for leafy green spinach and coriander," *RASSA Journal of Science for Society*, vol. 2, no. 3, pp. 187–192, 2020.

[2] R. P. Singh, S. Tiwari, M. Singh, A. Singh, and A. K. Singh, "Important diseases of greenhouse crops and their integrated management: a review," *Journal of Entomology and Zoology Studies*, vol. 8, no. 1, pp. 962–970, 2020.

[3] S. Birrell, J. Hughes, J. Y. Cai, and F. Iida, "A field-tested robotic harvesting system for iceberg lettuce," *Journal of Field Robotics*, vol. 37, no. 2, pp. 225–245, 2020.

[4] S. M. Sam and C. Wahua, "Phytochemical and micro anatomical studies on leaf, stem and petiole of two species of Dioscorea (Dioscorea alata L. And Dioscorea bulbifera L.)," *Journal of Applied Sciences & Environmental Management*, vol. 26, no. 3, pp. 467–474, 1970.

[5] G. Martin, J. L. Durand, M. Duru et al., "Role of ley pastures in tomorrow's cropping systems. A review," *Agronomy for Sustainable Development*, vol. 40, no. 3, pp. 17–25, 2020.

RETRACTED

Hindawi
Journal of Robotics
Volume 2023, Article ID 9845964, 1 page
https://doi.org/10.1155/2023/9845964

Retraction

Retracted: Deep Learning BP Neural Network Guided Evaluation of Students' Innovation and Entrepreneurship Education

Journal of Robotics

Received 8 August 2023; Accepted 8 August 2023; Published 9 August 2023

Copyright © 2023 Journal of Robotics. This is an open access article distributed under the Creative Commons Attribution License, which permits unrestricted use, distribution, and reproduction in any medium, provided the original work is properly cited.

This article has been retracted by Hindawi following an investigation undertaken by the publisher [1]. This investigation has uncovered evidence of one or more of the following indicators of systematic manipulation of the publication process:

(1) Discrepancies in scope
(2) Discrepancies in the description of the research reported
(3) Discrepancies between the availability of data and the research described
(4) Inappropriate citations
(5) Incoherent, meaningless and/or irrelevant content included in the article
(6) Peer-review manipulation

The presence of these indicators undermines our confidence in the integrity of the article's content and we cannot, therefore, vouch for its reliability. Please note that this notice is intended solely to alert readers that the content of this article is unreliable. We have not investigated whether authors were aware of or involved in the systematic manipulation of the publication process.

In addition, our investigation has also shown that one or more of the following human-subject reporting requirements has not been met in this article: ethical approval by an Institutional Review Board (IRB) committee or equivalent, patient/participant consent to participate, and/or agreement to publish patient/participant details (where relevant).

Wiley and Hindawi regrets that the usual quality checks did not identify these issues before publication and have since put additional measures in place to safeguard research integrity.

We wish to credit our own Research Integrity and Research Publishing teams and anonymous and named external researchers and research integrity experts for contributing to this investigation.

The corresponding author, as the representative of all authors, has been given the opportunity to register their agreement or disagreement to this retraction. We have kept a record of any response received.

References

[1] J. Yi and X. Cui, "Deep Learning BP Neural Network Guided Evaluation of Students' Innovation and Entrepreneurship Education," *Journal of Robotics*, vol. 2022, Article ID 2425069, 10 pages, 2022.

Hindawi
Journal of Robotics
Volume 2022, Article ID 2425069, 10 pages
https://doi.org/10.1155/2022/2425069

RETRACTED

Research Article

Deep Learning BP Neural Network Guided Evaluation of Students' Innovation and Entrepreneurship Education

Jingyi Yi[1] **and Xiao Cui**[2]

[1]*Shaanxi College of Communications Technology, Xi'an 710018, China*
[2]*School of navigation, Northwest University of Technology, Xi'an 710072, China*

Correspondence should be addressed to Jingyi Yi; yjy19871007@163.com

Received 13 July 2022; Accepted 25 September 2022; Published 15 October 2022

Academic Editor: Shahid Hussain

Copyright © 2022 Jingyi Yi and Xiao Cui. This is an open access article distributed under the Creative Commons Attribution License, which permits unrestricted use, distribution, and reproduction in any medium, provided the original work is properly cited.

With the promotion and development of the "Internet+," the computer major has become a hot major in innovation and entrepreneurship education. It is more and more necessary to carry out the refined differences between majors. This is a training issue, but not an employment issue. It has become a major measure for the development of international education. The international vocational training system of "three combinations and five drives" has been established and implemented. In February 2020, the State Department of Higher Education issued the key work points of the Department of Higher Education of the Ministry of Education in 2020. The document makes it clear that it must be implemented in the whole process of talent training. BP neural net model will be a brand-new research and development idea. By constructing a scientific and reasonable training assessment index system, the efficiency of computer professional technology training can be improved. Taking the development of computer specialty as the main research objective, this paper firstly establishes the evaluation index system of computer specialty for the first time, then makes a scientific evaluation of computer specialty by using BP neural net model and then carries out an empirical study of innovative employment mode through the evaluation index system and makes an empirical quantitative analysis. It is expected to be an effective basis for the social policy research of developing computer specialties.

1. Introduction

Innovation and entrepreneurship education refers to a new type of traditional higher education that can grow into market economy actors with innovative jobs. It is the basic education related to the future of the country. In order to cultivate talents, it is closely linked with talent training. It has been widely valued by countries all over the world and has profoundly affected the innovation and development of higher education [1].

In recent years, with the development of BP neural net technology, the application of BP neural net is becoming more and more popular, and the core of artificial neural net is calculation. BP neural net is a kind of feedforward network trained by error backpropagation. Applied BP neural net to the field of innovation and entrepreneurship education is one of the current research hotspots.

Since the 1990s, driven by western countries and famous international institutions, it has attracted special attention [2]. Chinese government departments have listed the cultivation of IT talents as a major national strategy [3]. In 1991, at the Tokyo International Innovation and entrepreneurship education seminar, the Japanese government summarized "innovation and entrepreneurship education" as cultivating people with personal ideas, creative spirit, creative ability, and management skills. From 1998 to 1999, the British Ministry of Education launched two special projects [4]. The level of it is ahead of other countries. Its courses have been extended to American college classrooms for the first time [5].

Under the background of economic informatization and globalization, the integration of various fields will be the new trend of it [6]. In October 2010, the general office of the State Council issued several opinions on vigorously promoting the

innovation training of colleges and universities and the independent innovation management of our university students, which further pointed out the direction and significance of developing innovation and entrepreneurship in higher education [7]. The article points out that innovation and entrepreneurship training should be further improved as a national plan [8]. This is also an important factor in China's higher education system. In March 2018, Premier Li proposed 13 innovations and entrepreneurship in the government work report, which fully highlighted the importance of innovation and entrepreneurship to China's development and pushed it to a climax [9]. Emphasizing that it is a national plan, and talent training is related to the future of the country [10]. At present, many domestic colleges and universities have offered innovation and entrepreneurship courses, but few universities have set it up. Its courses account for relatively few undergraduate courses, and the participants only account for a small part of the students. Its courses have not formed a systematic curriculum system or a complete evaluation system.

To sum up, innovation and entrepreneurship education are of great significance to the country, especially for the cultivation of innovation [11]. There is no model of it and no evaluation system. Therefore, studying this system for computer majors is in line with education and the need for reform [12].

First, it has further broadened the theoretical field of information technology evaluation, brought new thinking to the evaluation of science and technology entrepreneurship education of computer science in China and promoted the construction and development of the discipline. This paper mainly points out the teaching improvement strategies of computer majors, enriches the modern information technology basic theory of Chinese higher education and the employment-oriented theory of college students and further expands the theory of Chinese higher education [13].

According to the theory of BP neural net, this paper studies the information of students majoring in computer science at Jiangxi Normal University gives opinions on the informatization construction of computer science in the University and has great practical significance for the construction of network informatization in the College of computer technology and application [14]. This can improve the employment rate and self-improvement ability of computer majors [15].

2. State of the Art

2.1. Research on the Distribution Structure of Innovation and Entrepreneurship Education. The goal of it is to cultivate all students into the most revolutionary generation with entrepreneurial qualities. This means a comprehensive reform of the system of talent training ideas, talent training foundations, courses, talent training methods, implementation courses, education quality, teaching resource allocation, and all teacher training links. The number of research papers on "College Students' Innovation and Entrepreneurship Education" generally tends to increase. By January 2020, the keywords "innovation and entrepreneurship education" and "innovation and entrepreneurship teaching evaluation" will be determined first, and then the keywords will be imported into the CNKI database to realize fuzzy queries [16]. 43990 journal papers have been searched, including all CSCD and CSSCI sources. There are a total of 2737 journal papers and 2347 doctoral and master's theses, including 212 doctoral theses and 2135 master's theses. In recent years, although the number of researches related to it has declined partially, the overall trend has been on the rise, especially after 2019, the number of published papers has increased significantly [17].

The central point of the display is colleges and universities and the entrepreneurship education of college students [18], as shown in Figure 1.

2.2. Research on Innovation and Entrepreneurship Education Methods and Models. Most researchers at home and abroad have introduced a more flexible, participatory, and practical teaching mode of innovation and entrepreneurship in universities [19]. Researchers at home and abroad have conducted extensive discussions on the theory and mode of innovation and entrepreneurship education [20]. Deng pointed out that it is very important to correctly grasp the objectives, process, and support system. Experts have made many achievements in setting up measurement indexes and measurement models for the market. They mainly use the AHP analysis method (hierarchical index analysis method), fuzzy comprehensive judgment method, Delphi analysis method, and index weighted average method to measure the importance of the index. Among them, the hierarchical index analysis method and the Delphi analysis method have become the methods recognized by many experts. Delphi analysis method, also known as expert communication analysis method, expert evaluation analysis method, and others, refers to consulting the prediction opinions of the members of the expert group through back-to-back communication. It corresponds to the brainstorming method, which is different from the above back-to-back investigation, which is to organize a meeting together, constantly put forward ideas and constantly questions and find a set of practical solutions through objective and continuous analysis.

2.3. Research on the Evaluation of Innovation and Entrepreneurship Education. In recent years, due to China's need for high-quality innovation and entrepreneurship talent training, the task of talent training in colleges and universities has become more and more important. Behind the upsurge of innovation and entrepreneurship training in China, it is particularly important to form a certain talent training evaluation mechanism. Research on information technology evaluation theory states that Liu Haibin used the AHP method to create the core evaluation index system. Ge Li introduced the CIPP method to assist the evaluation research in colleges and universities. As shown in Figure 2, in order to reduce the employment pressure, various departments have jointly formulated employment policy initiatives, which are characterized by departmental promotion and internal coordination [21].

RETRACTED

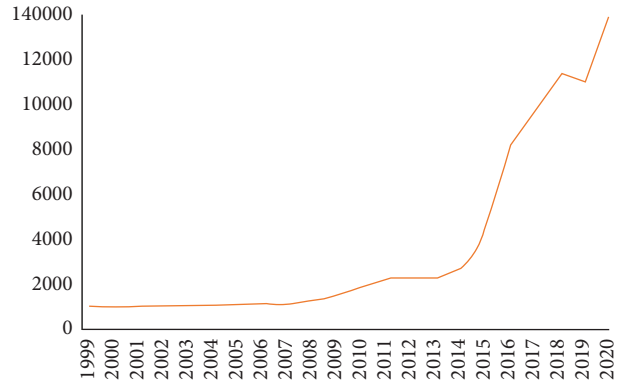

Figure 1: The overall trend of innovation and entrepreneurship education research.

From 2010 to now, it is in the second stage. The key is the preferential policies for job hunting issued by the competent social departments, which fundamentally alleviate the employment difficulties and stabilize society. In 2012, the state listed a large number of college projects as the second batch of national key university students' science and technology entrepreneurship training program pilots. From 2015 to 2016, it was also an important part of China's higher education system and was gradually promoted, as shown in Figure 3.

3. Methodology

3.1. Introduction to BP Neural Net. BP neural net is a concept proposed by physicists led by Rumelhart and McClelland in 1986. It is one of the most widely used neural net models. BP algorithm is a unique and charming program, while neural nets are challenging. For cutting-edge technology, the two are combined into a BP neural net. According to different principles and properties, neural nets can scientifically study complex phenomena and find the most reasonable countermeasures and methods. As shown in Figure 4.

3.2. The Main Steps of Applying BP Neural Net to Evaluation

3.2.1. BP Neural Net Structure. As the starting point of information input, the input vector plays a key role in information input. The expression method is as follows: and it can be assumed that $x0 = -1$; the hidden layer is the middle layer, which can directly control the change in the training efficiency of the neural net because the output vector is derived from the data. Therefore, it brings great training value. In the expression formula, the hypothesis y zero = - negative one can be directly added, which is of great value for the threshold change through the neurons in the output layer and also plays an important role in terminal training. The output vector of the output layer is $o = (o_1, o_2, \ldots\ldots, o_k, \ldots\ldots, o_t)^T$, and the hidden layer is an important process of transmission and change. The neural net has a great effect, and the matrix expression is $v = (v_1, v_2, \ldots\ldots, v_k, \ldots\ldots v_m)^T$ and because the output layer is the export port of the data, the generation between it and the hidden layer is of great significance to the BP neural net, so the matrix expression is $\omega = (\omega_1, \omega_2, \ldots\ldots, \omega_j, \ldots\ldots, \omega_l)^T$.

In the whole system, the mathematical connection between each part plays a role. First, the front part is also called the input layer, and the front-end part is used by ok and netk.

$$O_k = f(net_k), \quad k = 1, 2, \cdots, n,$$
$$net_k = \sum_{j=0}^{m} \omega_{ij} y_j, \quad k = 1, 2, \cdots, n. \tag{1}$$

The second is the middle part, also known as the hidden layer, which affects the middle part through yj and netj.

$$y_j = f\left(net_j\right), \quad j = 1, 2, \cdots, m, \tag{2}$$

$$net_j = \sum_{i=0}^{m} j v_{ij} x_i, \quad j = 1, 2, \cdots, m. \tag{3}$$

The unipolar sigmoid function is a category of functions, and the transfer function f(x) is applied to the neural net to play a role, and $f(x)$ can choose the unipolar sigmoid function.

$$f(x) = \frac{1}{1 + e^{-x}}. \tag{4}$$

Continuous functions generally have continuity and derivability. Then $f(x)$ has this property.

$$f'(x) = f(x)[1 - f(x)]. \tag{5}$$

Another category of function is the bipolar sigmoid function.

$$f(x) = \frac{1 - e^{-x}}{1 + e^{-x}}. \tag{6}$$

The final three-layer BP neural net is composed of the above parts.

BP coaching method is a process of introducing methods based on BP neural net and implementing coaching methods. The specific steps are shown in the figure.

Step 1: first determine the coefficient of the variable, which is a vector, and N is the number of samples.

$$\omega_{MI}(n) = \begin{bmatrix} \omega_{11}(n) & \omega_{12}(n) & \cdots & \omega_{1I}(n) \\ \omega_{21}(n) & \omega_{22}(n) & \cdots & \omega_{2I}(n) \\ \vdots & \vdots & \vdots & \vdots \\ \omega_{MI}(n) & \omega_{MI}(n) & \cdots & \omega_{MI}(n) \end{bmatrix}, \tag{7}$$

(7) The expression is the weight vector between the beginning part and the middle part I at the nth iteration.

RETRACTED

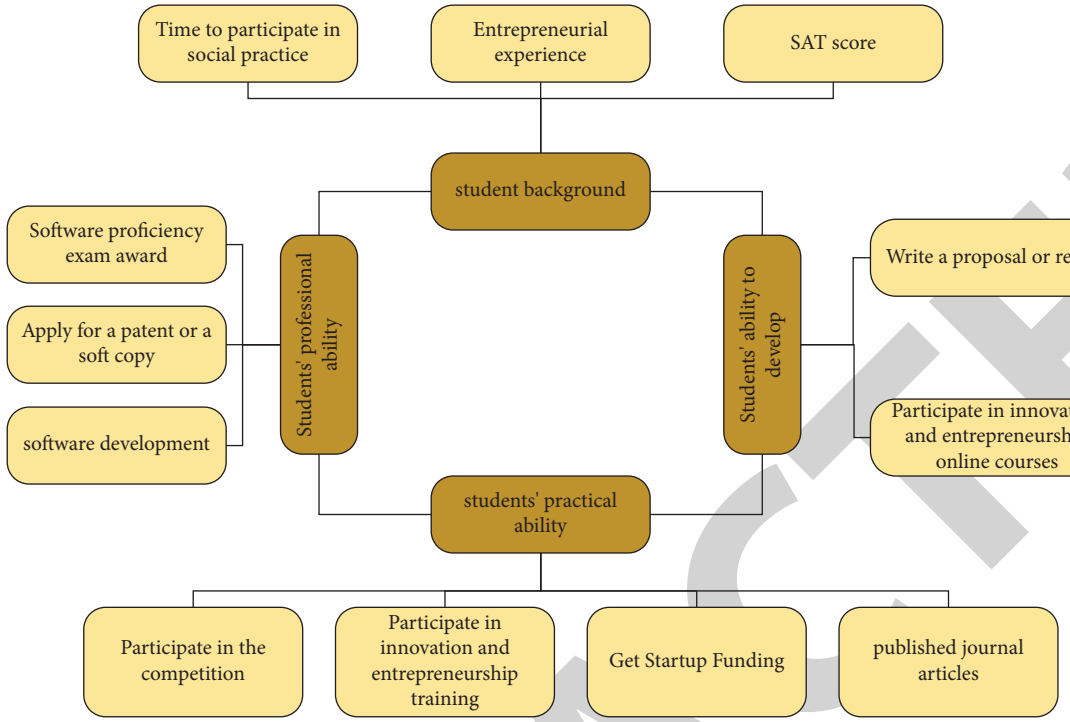

Figure 2: The main content of innovation and entrepreneurship education evaluation.

$$\omega_{MI}(n) = \begin{bmatrix} \omega_{11}(n) & \omega_{12}(n) & \cdots & \omega_{1J}(n) \\ \omega_{21}(n) & \omega_{22}(n) & \cdots & \omega_{2J}(n) \\ \vdots & \vdots & \vdots & \vdots \\ \omega_{I1}(n) & \omega_{I2}(n) & \cdots & \omega_{IJ}(n) \end{bmatrix}, \quad (8)$$

(8) is the weight vector between the middle part and the middle part J at the nth iteration.

$$\omega_{JP}(n) = \begin{bmatrix} \omega_{11}(n) & \omega_{12}(n) & \cdots & \omega_{1P}(n) \\ \omega_{21}(n) & \omega_{22}(n) & \cdots & \omega_{2P}(n) \\ \vdots & \vdots & \vdots & \vdots \\ \omega_{J1}(n) & \omega_{J2}(n) & \cdots & \omega_{JP}(n) \end{bmatrix}, \quad (9)$$

For the nth iteration, the weight vector is between the middle part J and the end part. After the output result is generated after n loop iterations, the actual output value is $y_k = [y_{k1}(n), y_{k2}(n), \cdots\cdots, y_{kn}(n)]$, $(k = 1, 2, 3, \cdots\cdots n)$, the expected output value is $d_k = [d_{k1}, d_{k2}, \ldots\ldots, d_{k3}]$, $(k = 1, 2, 3, \cdots\cdots, n)$.

Step 2: during the network initialization process, each $\omega_{MI}(n), \omega_{IJ}(n), \omega_{JP}(n)$ is assigned a nonzero random number and $n = 0$ at the same time.

Step 3: input the information about the sample XK. Since the sample information is the basic information of neural net training and is related to the network, $n = 0$.

Step 4: the weight of the middle part and the last part and the relationship between the output vectors.

$$v_p(np)\ p = 1, 2, \cdots, p. \quad (10)$$

Step 5: calculate the error E(n) according to dk and yk(n). Assuming that the set error is met, jump to the eighth step; assuming that the set error is not met, jump to the sixth step.

Step 6: firstly, all parameters and iteration times in BP neural net are counted, and then it is compared with $N+1$. If the former is equal to the latter, then the adjustment is in step 8. If the latter exceeds the former, the local gradient of neurons must be measured δ.

$$\delta_{\mathrm{pp}}(n) = y_p(n)\big(1 - y_p(n)\big)\big(d_p(n) - y_p(n)\big), \quad (11)$$

Step 7: inside the BP neural net, the weights between the front-end, middle, and end parts have a huge influence, so the premise is to calculate the weights, and then modify the weights according to the training error.

$$\begin{aligned} \Delta\omega_{jp}(n) &= \eta\delta_p^P(n)v_j^J(n), & j &= 1, 2, \ldots, J, \\ \omega_{jp}(n+1) &= \omega_{jp}(n) + \Delta\omega_{jp}(n), & p &= 1, 2, \ldots, P, \\ \Delta\omega_{ij}(n) &= \eta\delta_j^J(n)v_i^I(n), & i &= 1, 2, \ldots, I, \\ \omega_{ij}(n+1) &= \omega_{ij}(n) + \Delta\omega_{ij}(n), & j &= 1, 2, \ldots, J. \end{aligned} \quad (12)$$

Step 8: neural net training samples take time. Once the task is completed, please exit the training process directly. If not, adjust to step 3 above.

3.2.2. Improvement of BP Neural Net. BP neural nets are mature in both network theory and performance. Its performance varies with the difference in structure, but there are also disadvantages.

RETRACTED

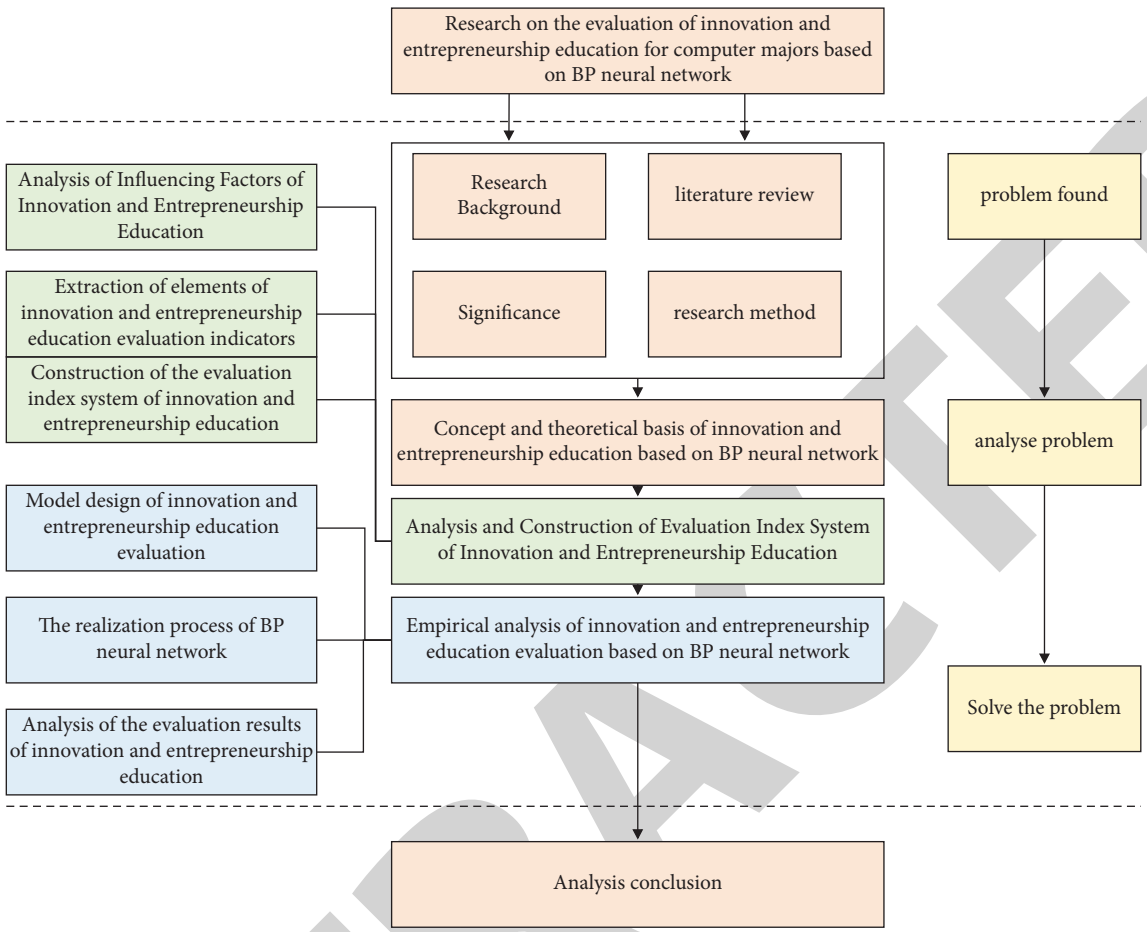

Figure 3: Technology roadmap.

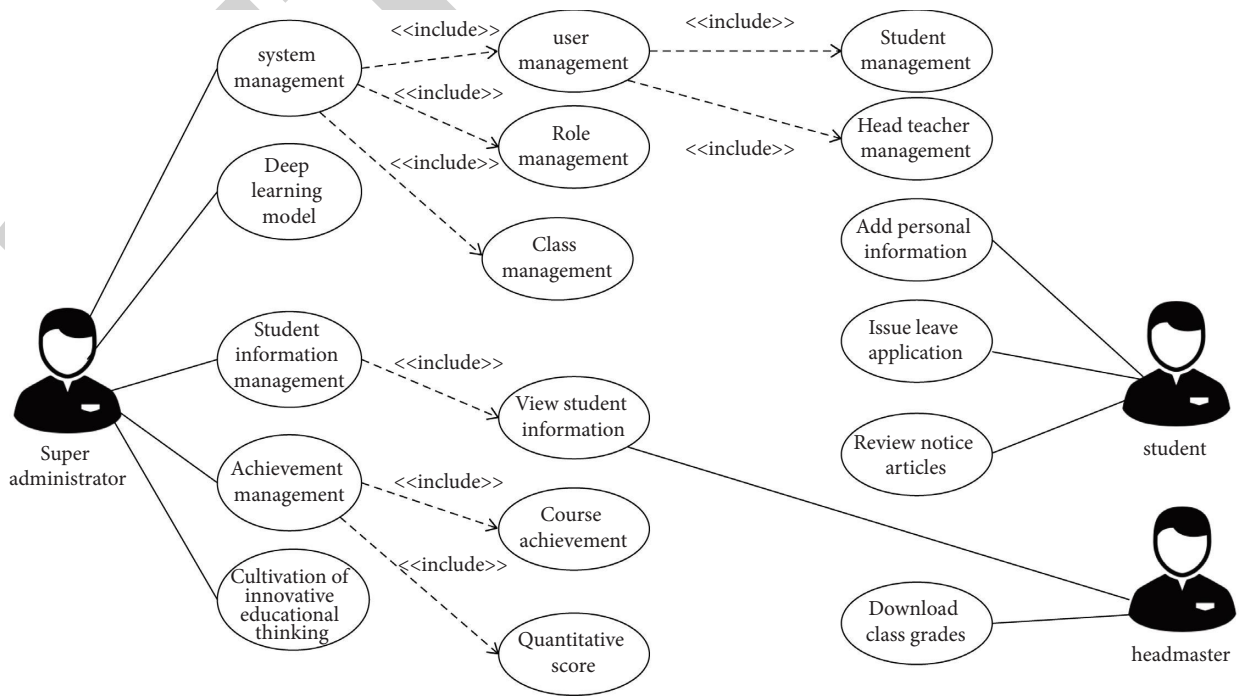

Figure 4: Construction of student innovation and entrepreneurship education based on the neural net.

(1) There is a contradiction between the local minimum and the global optimum, and it is difficult to obtain the global optimum.

(2) If the number of neural net training is large, the disadvantage is that the efficiency is low.

(3) Only on the basis of theoretical basis can we determine the scientific correctness of the estimation conclusion, especially the determination of the number of hidden layer nodes needs a theoretical basis.

(4) There is a conflict between mastering new data and forgetting old data, and neural nets often forget old data.

To address the shortcomings of neural nets, algorithms need to be tweaked and modified.

(1) The momentum term is increased. Learning rate η is related to the calculation of the BP neural net hypothesis η. If the value is too large, the network will accelerate convergence, but it will produce instability; and suppose η, if the value is too small, instability will be avoided, but the convergence rate is too slow. Therefore, the momentum term is introduced, where α is the momentum term.

$$\Delta\omega_{ij}(n) = \alpha\Delta\omega_{ij}(n-1) + \eta\delta_j(n)_v^i(n). \tag{13}$$

Considering (14) as a time series with t as a variable, t is from 0 to n, then

$$\Delta\omega(n) = \eta\sum_{t-0}^{n} a^{n-1}\delta_j(t)v_i(t). \tag{14}$$

(2) Adjust the learning rate. Assumed learning rate η, When the weight is changed, the overall error decreases, and with the change of the overall learning rate, the weight will also change in different amplitude, so that the value of the overall error changes. Therefore, it can be said that the overall learning rate has been adjusted.

(3) It is an excitation function of an odd number of dependent variables. The odd function is also a unique function. By taking the full odd function as the excitation function, the BP neural net algorithm can be accelerated. Among them, the hyperbolic tangent function is the most common odd function.

$$f(u) = a\ \tanh(bu) = \left[\frac{1-\exp(-bu)}{1+\exp(-bu)}\right] = \frac{2a}{1+\exp(-bu)} - a. \tag{15}$$

4. Result, Analysis, and Discussion

4.1. Reliability Analysis. By analyzing the number of hidden neurons and errors in the hidden layer of the BP neural net, as shown in Table 1, it is found that the more hidden layers, the less the training error, and the test error. When the number of hidden layers is 10, the test error reaches the minimum.

Table 1: Relationship between the number of neurons in the hidden layer and the error.

The number of hidden layers	Training error	Test error
3	1.2714	1.1282
4	0.8015	0.8244
5	0.6421	0.7299
6	0.5711	0.6713
7	0.5536	0.6910
8	0.4467	0.6588
9	0.3846	0.6474
10	0.2577	0.4532
11	0.1869	0.6655
12	0.1812	0.5994
13	0.1851	0.6880

Table 2: Reliability analysis of the questionnaire.

Attributes	α coefficient value
Student background	0.847
Students' professional ability	0.736
Students' practical ability	0.781
Students' ability to develop	0.701

The reliability value generally accepted by experts is 0.7. According to the conclusion of the reliability analysis, as shown in Table 2, the reliability value of all the questionnaires exceeds 0.7, the consistency of the questionnaires is high, and the corresponding reliability coefficient exists, indicating that the design of the questionnaire is reasonable and meets the corresponding conditions. Therefore, it can be found that the students' background, students' professional ability, practical ability, and development ability have certain reliability in the evaluation and analysis of the improved BP neural net.

4.2. Validity Analysis. This paper mainly uses SPSS software to analyze the validity. The data in Table 3 show that the load value and kmo value of each variable are equal to 0.5, the test results of their significance are equal to 0.01, and the interpretation rate of each variable is less than 60%.

4.3. Analysis of the Evaluation Results of Innovation and Entrepreneurship Education. Through the analysis of Table 4 and Figure 5, it can be seen that after the training of the improved BP neural net is completed, some test data corresponding evaluation value of innovation and entrepreneurship education for computer majors is obtained. The real value and the expected value of the network output are reasonably calculated. The real value and the expected value must be consistent without substantial change. Using BP neural net to detect and calculate the real value, it is proved that the real value is effective and the expected value is correct. The maximum relative error of both was 1.64%, which basically reached a reasonable level. After training, the real value of the neural net is as large as the expected value.

RETRACTED

Table 3: Validity analysis of the graduate questionnaire.

Attributes	Question number	Factor loading values	Degree of explanation of variables (%)	Kmo value	Bantltt significance test
Student background	3	0.775	71.65	0.724	0.000
	4	0.834			
	5	0.801			
	6	0.772			
	7	0.766			
Students' professional ability	8	0.781	74.02	0.766	0.000
	9	0.766			
	10	0.872			
	11	0.734			
	12	0.702			
	13	0.832			
Students' practical ability	14	0.858	72.68	0.736	0.000
	15	0.734			
	16	0.703			
	17	0.832			
	18	0.724			
	19	0.802			
	20	0.728			
	21	0.731			
Students' ability to develop	22	0.801	69.98	0.736	0.000
	23	0.712			

Table 4: Comparison of expected and real values.

No.	Expected value	Real value	Error (%)
1	95.0102	95.7107	−0.91
2	92.7401	93.2035	−0.07
3	80.0677	81.0092	−1.20
4	90.9584	90.2540	0.82
5	86.6052	85.6033	1017
6	93.6740	83.4056	0.32
7	87.0932	88.0102	−1.05
8	96.0741	97.5013	−1.46
9	75.6738	76.4081	−0.96
10	78.3495	79.6019	−1.59
11	82.9821	82.6709	0.37
12	96.7531	95.6802	1012
13	70.0724	71.2078	−1.59
14	73.1706	72.3419	1.15
15	78.0367	77.1071	1.21
16	76.3853	75.3097	1.43
17	70.1039	70.9325	−1.17
18	88.4359	89.5176	−1.21
19	85.7920	84.6251	1.38
20	83.0978	84.4624	−1.64

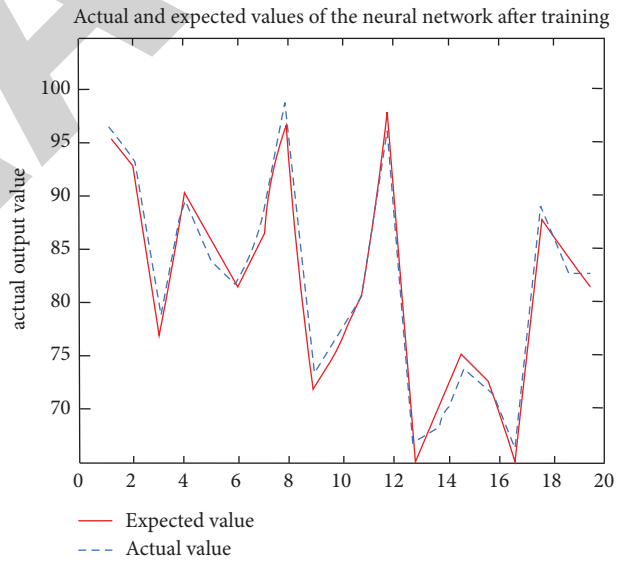

Figure 5: Comparison of the real value and the expected value predicted by the neural net.

There are only some fluctuations between the 9th, 10th, 15th, 16th, 19th, and 20th serial numbers, which are all within an understandable range.

Through the analysis of Table 4 and Figure 5, it can be found that the comparison result between the real value and the expected value is ideal. These evaluation results are equivalent to the results of 21 assessment standards for each grade, and different results are equivalent to their innovative employment skills. Therefore, the research conclusions are analyzed as follows

(1) Graduates with high scores in the evaluation have a solid foundation in the field of computer technology. That is to say, it is mainly reflected in the high-level qualification certificate, knowledge, and technology obtained from the qualification test of national import and export commodity quality inspection and certification personnel of computer science and software professional technology, and participation in national competitions and basic camping of centralized employment projects. The computer professional school is based on solid technical knowledge and the postgraduate training program that participated in the national competition. In the computer major, the most outstanding performance

RETRACTED

Table 5: Comparison results of different learning rates.

Study rate	0.010	0.003	0.04	0.05	0.06	0.03	0.06	0.08
Times of training	19	12	20	24	30	37	48	52
Error (e–001)	7.9002	4.0157	6.0043	10.0907	4.2743	10.0887	9.8691	11.235

of its discipline level is that it has obtained a high-level certificate in the application software ability test. But at the same time, according to the data, we collected the proportion of graduates who have obtained the advanced certificate in the national qualification examination for import and export commodity inspection and appraisal personnel of computer science and software professional technology that is very small, which means that the advanced certificate of application ability level test occupies a large part. According to the analysis results of big data collected by the university, the basic knowledge of computer science in the university is relatively solid.

(2) Some college graduates with basic test scores of more than 90 have participated in national competitions and concentrated entrepreneurship training camps. Students' participation in national competitions and entrepreneurship training camps plays a key role in cultivating their awareness of science and technology entrepreneurship. In particular, students who win the domestic competition can not only participate in the domestic competition but also participate in the centralized entrepreneurial training camp when they have a solid knowledge base. The development of concentrated entrepreneurship training camps and the acquisition of projects from entrepreneurship funds are also important manifestations of professional skills. From the comprehensive statistical analysis of the theoretical data and simulation experimental data collected in the college, it can be seen that the actual level of computer majors in Chinese universities needs to be further improved, as shown in Table 5.

(3) Most of the graduates with an assessment score of more than 80 have participated in community practice activities, have entrepreneurial experience, and improved students' innovation and entrepreneurship ability. The time spent in social practice and the entrepreneurial experience of the project have a positive impact on its innovation and entrepreneurial performance. Participating in community practice can help us understand the problems and deficiencies in our daily life and then draw our own views and solutions.

4.4. Countermeasures and Suggestions

4.4.1. Pay Attention to the Role of Competition-Oriented and Coordinate Multiple Participants. Pay attention to the international innovation and entrepreneurship competition and improve personal professional quality. The competition and the reality are interrelated, and the entries are applicable to reality. The key is to establish a scientific and reasonable practical teaching plan and talent training model so that colleges and universities can provide help for entrepreneurs.

4.4.2. Further Consolidated the Basic Knowledge of Computer Science and Highlighted the New Characteristics of Specialized and Integrated Development. Build a professional software development standard system and consolidate the foundation of computer professional software development. Aiming at the software development direction required by modern society and integrating talents of entrepreneurship and innovation, build a standard system for software development direction, and create an enterprise-oriented working environment and operation mode to complete teaching and management. This teaching mode achieves the organic integration of course teaching, experiment, and practical training and cultivates students who are seamlessly connected with society.

4.4.3. Science and Technology Development, Innovation and Entrepreneurship Training, And Strengthening Innovation Policy Guarantee. Select students with independent thinking skills and solid basic knowledge to become training organizations for innovation and entrepreneurship, especially in the field of innovation and entrepreneurship. Colleges and universities should try their best to organize subject innovation teachers and community members to carry out joint training between winter and summer vacation and conduct experimental innovation training in teams so as to learn from work and enhance their own innovation ability.

4.4.4. Enrich Diversified Innovation Practice and Carry Out Social Practice in Multiple Industries. Carry out various forms of entrepreneurial practice. On the one hand, with the help of the college students' network platform, they accumulated entrepreneurial knowledge. Small entrepreneurship projects with students as representatives, to become the agent of college students and enhance their interpersonal communication skills. As a teacher, I can understand the prospects, advantages, and disadvantages of education. At the same time, we can carry out diversified innovative practices with the help of the school platform. In addition, with the help of community resources, family enterprises can innovate together with partners. Family enterprises can carry out innovation practices through family relations and can also independently carry out innovation and

RETRACTED

entrepreneurship projects, carry out social practice in multiple industries and cultivate practical skills in multiple industries.

5. Conclusion

According to the difficulties faced by the innovation and entrepreneurship training mode and evaluation system, the innovation and entrepreneurship model is first established with the computer major undergraduate as the training objective. Through the evaluation and empirical results, professional knowledge and skills are found. Participation in national competitions and concentrated entrepreneurship training camps plays a key role in the innovation ability of computing machines. The higher the evaluation score, the more solid the foundation of a computer major. Some students with a score of over 90 in the assessment will have experience in participating in national competitions and strengthening entrepreneurship training camps. Then, it makes an empirical quantitative analysis of the training of innovative talents in computer majors. The results show that the BP neural net model can reasonably evaluate the innovation ability of college students and expand the application value and research fields of the BP neural net. However, this paper still has some shortcomings. The evaluation model of China's innovation and entrepreneurship education established in this paper still has more perfect development space. This paper expects to raise the correlation analysis to the theoretical level and carry out the evaluation research on each dimension in the later stage.

Data Availability

The labeled data set used to support the findings of this study is available from the corresponding author upon request.

Conflicts of Interest

The authors declare that they have no conflicts of interest.

References

[1] H. Eki, M. Zgenel, and E. Metlilo, "The effect of motivation of success of university students on personal-professional competence: mediation role of lifelong learning tendency," *International Journal of Evaluation and Research in Education*, vol. 9, no. 3, pp. 583–593, 2020.

[2] H. S. Jung and S. Park, "A study on the deep learning based prediction of production demand by using LSTM under the state of data sparsity," *IOP Conference Series: Materials Science and Engineering*, vol. 926, no. 1, Article ID 012031, 2020.

[3] C. Watson, N. Cooper, D. N. Palacio, M. Kevin, and P. Denys, "A systematic literature review on the use of deep learning in software engineering research," 2020, https://arxiv.org/abs/2009.06520.

[4] A. . Majid, "Evaluation on students' service design concepts using the principles of service innovation and design process," *Test Engineering and Management*, vol. 82, pp. 9638–9646, 2020.

[5] K. Lee, S. Yi, S. Hyun, and C. Kim, "Review on the recent welding research with application of CNN-based deep learning Part II: model evaluation and visualizations," *Journal of Welding and Joining*, vol. 39, no. 1, pp. 20–26, 2021.

[6] K. Aggarwal, S. K. Singh, and M. Chopra, "Deep learning in robotics for strengthening industry 4.0.: opportunities, challenges and future directions," *Robotics and AI for Cybersecurity and Critical Infrastructure in Smart Cities*, vol. 80, pp. 34311–34317, Springer, Berlin, Germany, 2022.

[7] E. Godaert, K. Aesaert, J. Voogt, and B. Johan van, "Assessment of Students' Digital Competences in Primary School: A Systematic review," *Education and Information Technologies*, vol. 27, pp. 1–59, 2022.

[8] I. Tomory, "Work-in-Progress: evaluation in Hungarian education: evaluation knowledge and reflections on engineering and technical teacher students," in *Proceedings of the International Conference on Interactive Collaborative Learning*, Dresden, Germany, 2022.

[9] M. López, B. A. Natalia, S. Sáenz, and J. Luis, "A service-learning experience applied in corporate identity design of newly created companies," in *Proceedings of the International Conference on Design, Simulation, Manufacturing: the Innovation Exchange*, Rome, Italy, 2022.

[10] B. Putra, R. Amirudin, and B. Marhaenanto, "The evaluation of deep learning using convolutional neural net (CNN) approach for identifying arabica and robusta coffee plants," *Journal of Biosystems Engineering*, vol. 47, pp. 118–129, 2022.

[11] M. Bohori, R. Rosiqoh, H. Hikmat, and R. Efendi, "Evaluation of physics learning on momentum and impulse topic of the senior high school students," *Journal of Physics: Conference Series*, vol. 1521, no. 2, Article ID 022050, 2020.

[12] M. Munawaroh and N. S. Setyani, "The effect of problem based learning (pbl) model on student learning motivation inproducts, creative and entrepreneurship subject in Eleventh Grade of SMK PGRI 1 Jombang," *Journal of Physics: Conference Series*, vol. 1464, Article ID 012021, 2020.

[13] Y. H. Jiang, W. B. Jiang, and H. L. Ni, "Research on cost-benefit evaluation model of social security project based on fuzzy entropy," *Advanced Hybrid Information Processing*, Springer, vol. 11, no. 3, , pp. 38–42, Berlin, Germany, 2022.

[14] J. Saremi, Z. Zarei-Behjani, and E. Vojoudi, "Evaluation of viability and cell attachment of human endometrial stem cells on electrospun silk scaffolds prepared under different degumming conditions and solvents," *Regenerative Engineering and Translational Medicine*, vol. 35, no. 4, pp. 95–97, 2022.

[15] J. Klamert-Schmid, S. Zangl, and M. Lackner, "The phenomenon of 'opportunity recognition' among engineering students," in *Proceedings of the International Conference on Interactive Collaborative Learning*, Hilton Park Vienna, Austria, 2022.

[16] J. A. Rising, C. Taylor, M. C. Ives, and R. E. T. Wardb, "Challenges and innovations in the economic evaluation of the risks of climate change," *Ecological Economics*, vol. 197, no. 3, pp. 119–127, 2022.

[17] M. Effendi, Zainuddin, and M. S. Ahmad, "The influence of the Kirkpatrick evaluation level on the quality of learning systems in UPBJJ-UT Ternate students: empirical study on open university," *International Journal of Research in Business and Social Science*, vol. 11, 2022.

[18] Y. Li, "Innovative strategies of primary school calligraphy education model under the background of big data," *Innovative Computing*, Springer, vol. 8, no. 1, , pp. 1–8, Berlin, Germany, 2022.

[19] A. Brown and M. Rich, "Researching student learning on business management degree courses: the problem of

RETRACTED

Hindawi
Journal of Robotics
Volume 2024, Article ID 9809817, 1 page
https://doi.org/10.1155/2024/9809817

Retraction

Retracted: Application of Intelligent Signal Reflection in the Communication Model of an Electronic Controller

Journal of Robotics

Received 23 January 2024; Accepted 23 January 2024; Published 24 January 2024

Copyright © 2024 Journal of Robotics. This is an open access article distributed under the Creative Commons Attribution License, which permits unrestricted use, distribution, and reproduction in any medium, provided the original work is properly cited.

This article has been retracted by Hindawi following an investigation undertaken by the publisher [1]. This investigation has uncovered evidence of one or more of the following indicators of systematic manipulation of the publication process:

(1) Discrepancies in scope
(2) Discrepancies in the description of the research reported
(3) Discrepancies between the availability of data and the research described
(4) Inappropriate citations
(5) Incoherent, meaningless and/or irrelevant content included in the article
(6) Manipulated or compromised peer review

The presence of these indicators undermines our confidence in the integrity of the article's content and we cannot, therefore, vouch for its reliability. Please note that this notice is intended solely to alert readers that the content of this article is unreliable. We have not investigated whether authors were aware of or involved in the systematic manipulation of the publication process.

Wiley and Hindawi regrets that the usual quality checks did not identify these issues before publication and have since put additional measures in place to safeguard research integrity.

We wish to credit our own Research Integrity and Research Publishing teams and anonymous and named external researchers and research integrity experts for contributing to this investigation.

The corresponding author, as the representative of all authors, has been given the opportunity to register their agreement or disagreement to this retraction. We have kept a record of any response received.

References

[1] L. Lan, "Application of Intelligent Signal Reflection in the Communication Model of an Electronic Controller," *Journal of Robotics*, vol. 2022, Article ID 8031024, 9 pages, 2022.

Hindawi
Journal of Robotics
Volume 2022, Article ID 8031024, 9 pages
https://doi.org/10.1155/2022/8031024

RETRACTED

Research Article

Application of Intelligent Signal Reflection in the Communication Model of an Electronic Controller

Lan Lan

Henan College of Transportation, Zhengzhou, Henan 450000, China

Correspondence should be addressed to Lan Lan; lanxin112@126.com

Received 25 August 2022; Revised 19 September 2022; Accepted 27 September 2022; Published 12 October 2022

Academic Editor: Shahid Hussain

Copyright © 2022 Lan Lan. This is an open access article distributed under the Creative Commons Attribution License, which permits unrestricted use, distribution, and reproduction in any medium, provided the original work is properly cited.

This paper analyses the automatic control effect of an electronic controller, combined with artificial intelligence technology in order to improve the automatic control of an electronic controller. In order to improve the automatic control effect of the electronic controller, a novel centralized intelligent reflective surface-assisted millimeter-wave computational imaging scheme based on pixel block division and block sparse signal recovery is proposed in this paper. Meanwhile, this paper proposes a fast block-sparse Bayesian learning algorithm. It combines the GAMP algorithm with machine learning, so it can achieve similar performance with much lower computational complexity than the traditional block sparse Bayesian learning algorithm. The simulation clustering study shows that the electronic controller automation system based on artificial intelligence technology proposed in this paper can effectively improve the control effect of the electronic controller.

1. Introduction

Since the beginning of the twenty-first century, electronic technology, especially microelectronics technology, has been changing with each passing day, and the performance requirements of automobiles are also becoming more stringent [1]. The rapid development of the automotive market has also driven the continuous advancement of body control systems. At present, the original distributed body control system is being eliminated from the market, and products are developing from the centralized body control system to the distributed body control system [2]. A body control system (BCM) refers to the automotive electrical system in which a controller is responsible for monitoring and controlling all electrical equipment in the vehicle body. Usually, the body control system is responsible for controlling the door and window lifts, electric rear view mirrors, air conditioning, central locking, and antitheft password systems. At the same time, the body control system can communicate with other controllers through various automobile buses [3]. The development trend of the future body control system is digital, intelligent, and networked. Connecting various electrical devices and control units through the bus can simplify the wiring harness layout of the whole vehicle, facilitate the expansion of future system functions, and reduce the weight of the vehicle wiring harness. At the same time, the diagnosable function is also conducive to the inspection and maintenance of the car. The driver can easily understand the working status of each system of the car through the display of the combination instrument before starting, so as to ensure the safety of the car [4]. The maintenance personnel can quickly determine the specific location of the fault by reading the fault information through the fault diagnosis instrument, which reduces the difficulty of troubleshooting and reduces the maintenance time [5]. At the same time, the car bus can realize information sharing and cooperative work between different electrical systems, laying the foundation for greater car intelligence in the future.

The centralized body control system means that multiple body electrical subsystems are controlled centrally through one controller. All switches and sensors are connected to the same controller. A certain logical relationship can occur between each body's electrical subsystem, and at the same time, through the bus connection, a certain logical relationship can occur between the body control system and the

power system and even the entertainment system, air conditioning system, and instrumentation system, such as the alarm of the air conditioning system. The main controller component of the centralized system is the body controller (BCM), which is the core of the centralized body control system [6]. The body controller can be further divided into a bus-type body controller and a non-bus-type body controller. The bus-type body control system can simultaneously function as a gateway. The aforementioned CBCU is a centralized body control system [7].

The centralized body control system greatly strengthens the control functions of humanization, comfort, and safety, and the fault diagnosis of the electric equipment of the whole vehicle is also simplified. Reasonable use, under the premise of the same technical requirements, can reduce the overall cost of the body control system [8]. Of course, there are downsides to centralized body control systems. Compared with the distributed system, the development of the body controller is more difficult, especially in terms of the software structure of the controller and the reliability of the system; since many electrical devices are controlled by one controller, when the configuration of the vehicle electrical system changes a lot, the centralized body control system tends to exist in many states, requiring a lot of repeated development and testing. Redundant development will result in a waste of resources, and the cost is not easy to control [9].

In terms of form, the distributed body control system is similar to the decentralized system in that each subsystem of the body electrical appliances is controlled by a separate controller, but there are great differences in essence. There is no relationship between the electrical appliances of the distributed body control system and the distributed body control system inherits the advantages of the centralized body control system in functional control. In addition to the logic control, it also communicates through the bus to realize the functional interaction of various areas and subsystems, such as body appliances, power systems, entertainment systems, and instrumentation systems [10]. In the distributed body control system, the communication of all control modules becomes very critical, and the realization of almost all control functions is inseparable from the existence of communication [11]. For example, in a centralized control system, all door lock motors are directly driven by the body controller, while in a distributed system, each door control module first obtains a lock and unlock signal through the bus, and then each door control module independently drives each door lock motor. When OEMs use the distributed body control system, they should define the basic bus protocol, all messages and their reasonable attributes (message sending method, period, signal meaning, etc.), network management methods, diagnosis according to the system functional requirements, protocol, etc. and formulate strict test specifications and complete the test software design to ensure that the communication effect of the bus meets the functional requirements [12].

With the rapid development of Internet services, network management has become more and more complex on the existing network architecture, and it is difficult for researchers to conduct new innovative experiments. In order to simplify network management and reduce the difficulty for researchers to conduct innovative experiments, a new network architecture of software defined networking (SDN) is proposed, which decouples the control plane and data plane of network devices [12], so that network administrators can easily manages network services flexibly and conveniently and, at the same time, cooperate with the OpenFlow protocol, making it easier for researchers to conduct innovative network experiments. The emergence of SDN quickly attracted the attention of a large number of enterprises, such as equipment manufacturers, telecom operators, and Internet companies. Compared with the existing network, SDN can improve the intelligent forwarding capability of the network edge, make the deployment and upgrade of network equipment more convenient, and improve the network's open capability [13]. As the middle layer of the SDN architecture, the SDN controller, on the one hand, opens network programming capabilities to the application layer through the northbound interface, so that the application layer does not need to care about specific details and has the ability to control network behavior; the underlying network equipment is managed and dispatched in a unified manner. It is a bridge connecting the infrastructure layer and the application layer and has an important position as a "network operating system" [14]. In recent years, with the development and maturity of SDN, many enterprises have begun to commercialize SDN deployment, and various open-source controllers have been developed one after another. However, there are still many deficiencies in the research work on the performance testing of SDN controllers in the industry. For example, the test content of the SDN controller performance test is not comprehensive enough; there are few open-source test tools, and most of the test tools can only simulate independent switches for testing but cannot form the topology between switches [15]. Most of the open source testing tools do not support testing controller clusters; therefore, it is difficult for the existing open-source test tools to make a comprehensive evaluation of the performance of the SDN controller, which is unfavorable for the further development of the SDN controller, and the SDN controller is the core component of the SDN architecture which hinder the development of SDN [16].

Any network is in constant change, and so is an SDN network. In the SDN network, when the network changes, for example, a new switch is turned on/off, the switch port is turned on/off, the switch needs to send a specific message to the SDN controller to notify the SDN controller that the network has changed, and the SDN control The response time of the SDN controller to such messages reflects the sensitivity of the SDN controller to network changes and determines whether the SDN controller can perceive network changes in a timely manner [17]. Four indicators are added to the test system to test the response time of the SDN controller to topology events. In an SDN network, since the SDN controller is the brain of the entire network, when the switch encounters a packet that cannot be

RETRACTED

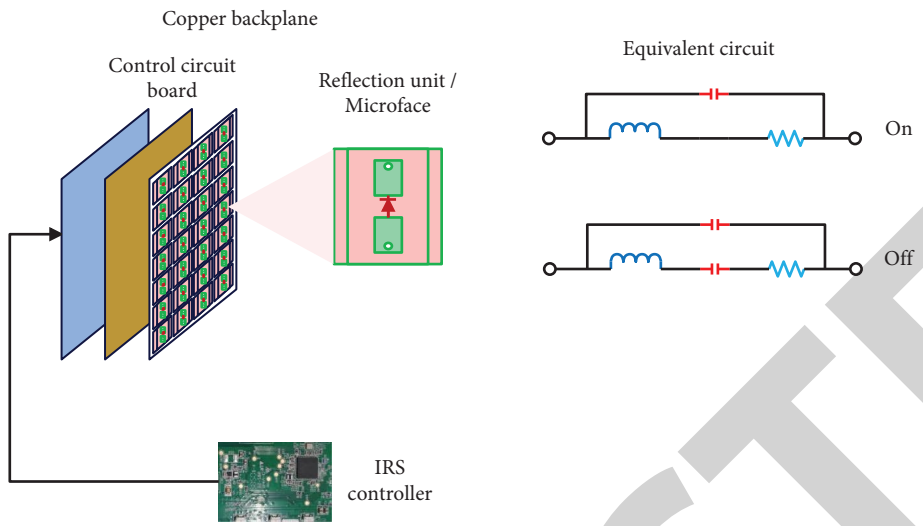

Figure 1: The hardware architecture of the smart reflector.

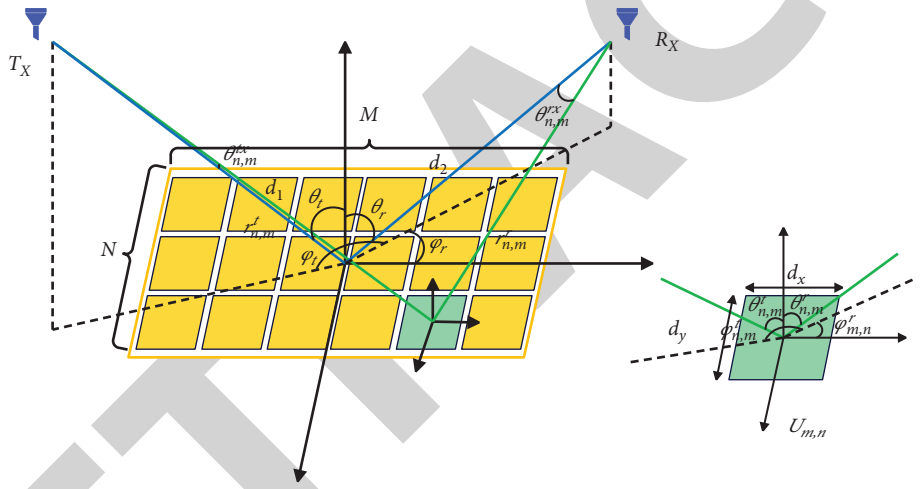

Figure 2: Physical model of the smart reflector.

processed, it will send a request to the SDN controller, and then the SDN controller decides how to process the packet. The processing speed of the SDN controller, that is, the response time, affects the transmission efficiency of data packets in the SDN network, which is of great significance [18]. The end-to-end path establishment time indicator is to test this capability of the SDN controller. The end-to-end path establishment time indicator not only tests the processing time of the SDN controller for a packet request but also tests the sum of the processing times of the SDN controller for each switch on a complete path, which is more suitable. realistic scene. Therefore, we chose the end-to-end path setup time metric as a metric for the SDN controller response time class.

This paper combines artificial intelligence technology to analyze the automatic control of the electronic controller and constructs an automatic control system for the electronic controller based on the artificial intelligence technology to promote the intelligent application effect of the electronic controller.

2. Communication Model of Electronic Controller Based on Intelligent Reflector

2.1. Smart Reflector. As shown in Figure 1, the typical architecture of the IRS consists of three layers and an intelligent controller. The physical model of the smart reflector when it reflects the signal is shown in Figure 2. The area of each microfacet on the IRS is $d_x \times d_y$, where d_x and d_y are the side lengths along the x-axis and y-axis, respectively, and their sizes are generally between $\lambda/10$ and $\lambda/2$. G is the gain of the microfacet, which is defined as

$$G = \frac{4\pi}{\int_{\phi=0}^{2\pi}\int_{\theta=0}^{\pi} F(\theta,\phi)\sin\theta \mathrm{d}\theta\mathrm{d}\phi}. \quad (1)$$

It is only related to the normalized power pattern $F(\theta,\phi)$ of the microfacet.

The power of the signal incident on a single microfacet $U_{n,m}$ can be expressed as

REJECTED

$$P_{n,m}^{in} = \frac{G_t P_t}{4\pi\left(r_{n,m}^t\right)^2} F^{tx}\left(\theta_{n,m}^{tx}, \phi_{n,m}^{tx}\right) F\left(\theta_{n,m}^t, \phi_{n,m}^t\right) d_x d_y. \quad (2)$$

The electric field of the incident signal to $U_{n,m}$ is

$$E_{n,m}^{in} = \sqrt{\frac{2Z_0 P_{n,m}^{in}}{d_x d_y}} e^{\left(-j2\pi r_{n,m}^t\right)/(\lambda)}. \quad (3)$$

Among them, Z_0 is the characteristic impedance of air, and $r_{n,m}^t$ can be written as

$$r_{n,m}^t = \sqrt{\left(x_t - \frac{2m-1}{2} d_x\right)^2 + \left(y_t - \frac{2n-1}{2} d_y\right)^2 + z_t^2}, \quad (4)$$

$$P_{n,m}^{in} \left|\Gamma_{n,m}^2\right| = P_{n,m}^{\text{reflect}}.$$

Among them, $P_{n,m}^{\text{reflect}}$ is the total power of the reflected signal of the microfacet $U_{n,m}$. The power of the reflected signal received by the receiver from $U_{n,m}$ can be expressed as

$$P_{n,m}^r = \frac{G P_{n,m}^{\text{reflect}}}{4\pi\left(r_{n,m}^r\right)^2} F\left(\theta_{n,m}^r, \phi_{n,m}^r\right) F^{rx}\left(\theta_{n,m}^{rx}, \phi_{n,m}^{rx}\right) A_r,$$

$$E_{n,m}^r = \sqrt{\frac{2Z_0 P_{n,m}^r}{A_r}} e^{-j\left(\left(2\pi r_{n,m}^t/\lambda\right) + \left(2\pi r_{n,m}^r/\lambda\right)\phi_{n,m}\right)},$$

$$= \sqrt{\frac{Z_0 P_t G_t G d_x d_y F_{n,m}^{\text{combine}}}{8\pi^2}} \frac{\Gamma_{n,m}}{r_{n,m}^t r_{n,m}^r} e^{\left(-j2\pi\left(r_{n,m}^t + r_{n,m}^r\right)\right)/\lambda}. \quad (5)$$

Among them, $F_{n,m}^{\text{combine}} = F^{tx}(\theta_{n,m}^{tx}, \phi_{n,m}^{tx}) F(\theta_{n,m}^t, \phi_{n,m}^t) F(\theta_{n,m}^r, \phi_{n,m}^r) F^{rx}(\theta_{n,m}^{rx}, \phi_{n,m}^{rx})$ represents the effect of the normalized power pattern on the received signal power. The total electric field of the received signal is the superposition of the electric fields reflected from all unit cells towards the receiver

$$E^r = \sum_{m=1-(M/2)}^{M/2} \sum_{n=1-(N/2)}^{N/2} E_{n,m^\circ}^r. \quad (6)$$

The received signal power of the receiver is

$$P_r = \frac{\left|E^r\right|^2}{2Z_0} A_r. \quad (7)$$

Among them, $A_r = (G_r \lambda^2)/(4\pi)$ is the aperture of the receive antenna. The received signal power is as follows

$$P_r = P_t \frac{G_t G_r G d_x d_y \lambda^2}{64\pi^3} \left| \sum_{m=1-(M/2)}^{M/2} \sum_{n=1-(N/2)}^{N/2} \frac{\sqrt{F_{n,m}^{\text{combine}} \Gamma_{n,m}}}{r_{n,m}^t r_{n,m}^r} e^{\left(-j2\pi\left(r_{n,m}^t + r_{n,m}^r\right)\right)/(\lambda)} \right|^2. \quad (8)$$

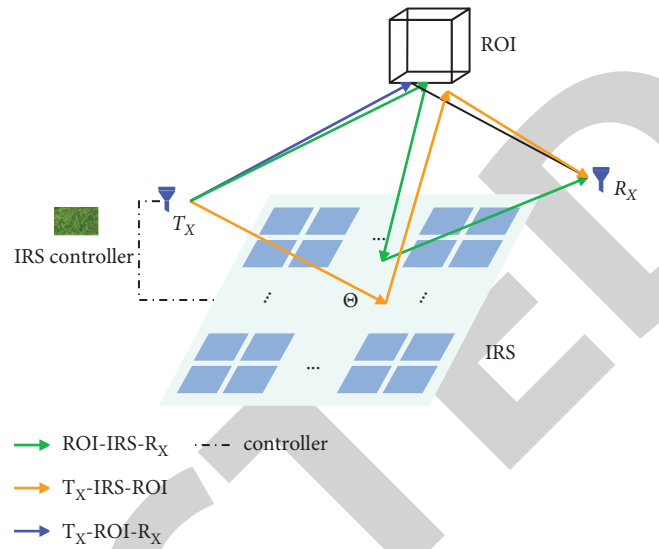

Figure 3: Imaging system model (centralized IRS mode).

2.2. System Model and Problem Description. The imaging system is shown in Figure 3. Both the transmitter (Tx) and receiver (Rx) are equipped with a single antenna for imaging and are connected to the control equipment through control lines, and the centralized IRS working mode is used here. The imaging system corresponding to the separate IRS working mode is shown in Figure 4. The IRS is connected to the control device through the IRS controller. That is, each microfacet is composed of $\overline{K}$ minimum unit faces, as shown in $\overline{K} = 4$ in Figure 4. The microfacet mentioned in the following refers to the microfacet after the combination. The three-dimensional imaging region to be detected and reconstructed in the imaging system model is called the region of imaging (ROI). The reflectance of all pixels in the ROI is represented by

$$x = \left[x_1, x_2, \ldots, x_N\right]^T \in \mathscr{C}^{N\times 1}, \quad (9)$$

we assume that the locations of T_x, R_x, IRS, and ROI are all known in advance.

It is assumed that the IRS consists of K microfacets:

$$\Theta = \text{diag}\left(\Theta_1, \ldots, \Theta_K\right) \in \mathscr{C}^{K\times K}. \quad (10)$$

Among them, $\Theta_k = \rho_k e^{j\theta_k}$ represents the reflection characteristic of the k-th microfacet of the IRS, and $\rho_k \in [0, 1]$ and $\theta_k \in [0, 2\pi]$ are diagonal matrices. If b_1 bits are used to represent the amplitude reflection coefficient, ρ

RETRACTED

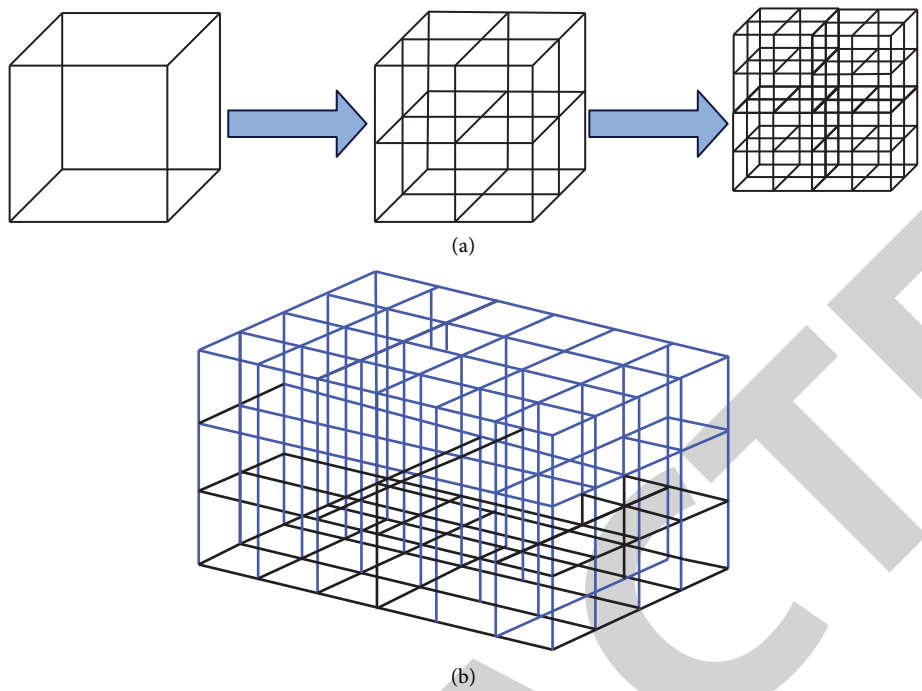

Figure 4: Pixel division method of target area. (a) Division method of the ROI. (b) An example of a target division.

has 2^{b_1} different values with uniform intervals, of which the maximum value is $\rho_{\max}$, the minimum value is $\rho_{\min}$, and the interval is $\Delta\rho = (\rho_{\max} - \rho_{\min})/(2^{b_1-1})$, that is, $\rho \in \{\rho_{\min}, \rho_{\min} + \Delta\rho, \ldots, \rho_{\max}\}$. If b_2 bits are used to represent the phase offset, then θ has 2^{b_2} different values with uniform intervals, of which the minimum value is 0 and the interval is $\Delta\theta = (2\pi)/(2^{b_2})$, that is, $\rho \in \{0, \Delta\theta, 2\Delta\theta, \ldots, (2^{b_2} - 1)\Delta\theta\}$. In the process of imaging, Θ does not always remain constant, but adjusts with time, so Θ is actually a hop function $\Theta(t)$ that changes with time.

It is assumed that all channels in the figure are constant parameter channels, that is, the influence of the channel on the signal is fixed or changes very slowly with time. Among them, the channels from Tx to ROI and IRS are $H_{TO} = [h_1^{TO}, \ldots, h_N^{TO}] \in \mathscr{C}^{1\times N}$ and $H_{TI} = [h_1^{TI}, \ldots, h_K^{TI}] \in \mathscr{C}^{1\times K}$, respectively. Among them, $h_n^{TO} = a_n^{TO} e^{i\phi_n^{TO}}$ represents the channel from Tx to the nth pixel of R0I, a_n^{TO} and ϕ_n^{TO} are the amplitude parameter and phase offset of this channel, respectively, $h_k^{TI} = a_k^{TI} e^{i\phi_k^{TI}}$ represents the channel from Tx to the k-th microfacet of IRS, and a_n^{TI} and ϕ_k^{TI} are the amplitude parameter and phase offset of the channel, respectively. The IRS and ROI to Rx channels are $H_{IR} = [h_1^{IR}, \ldots, h_K^{IR}] \in \mathscr{C}^{1\times K}$ and $H_{OR} = [h_1^{OR}, \ldots, h_N^{OR}] \in \mathscr{C}^{1\times N}$, respectively. Among them, $h_k^{IR} = a_k^{IR} e^{i\phi_k^{IR}}$ is the channel to which the k-th microfacet of the IRS to Rx, a_k^{IR}, and ϕ_k^{IR} are the amplitude characteristic and phase offset of this channel, respectively, $h_n^{OR} = a_n^{OR} e^{i\phi_n^{OR}}$ is the channel to which the nth pixel of the ROI to Rx, and a_n^{OR} and ϕ_n^{OR} are the amplitude characteristics and phase offset of this channel, respectively. The channel from IRS to ROI is the channel of H_{IO} = pixels, and $a_{k,n}^{IO}$ and $\phi_{k,n}^{IO}$ are the amplitude characteristics and phase offset of this channel, respectively. It is assumed that the channel from IRS to ROI and the channel from ROI to IRS are the same.

If it is assumed that the transmitted signal is (t), the received signal of the subchannel from Tx to the nth pixel of ROI and then to Rx is

$$y_n^{\mathrm{TOR}}(t) = a_n^{TO} e^{i\phi_n^{TO}} x_n a_n^{OR} e^{i\phi_n^{OR}} s(t) = x_n h_n^{\mathrm{TOR}} s(t). \tag{11}$$

Among them, $h_n^{TOR} = a_n^{TO} a_n^{OR} e^{i\phi_n^{TO}} e^{i\phi_n^{OR}}$ is the subchannel at $x_n = 1$. The received signal from the sub-channel Tx to the k-th microfacet of the IRS to the nth pixel of the ROI and finally to Rx is

$$\begin{aligned} y_{n,k}^{\mathrm{TIOR}}(t) &= a_k^{TI} e^{i\phi_k^{TI}} \rho_k e^{j\theta_k} a_{k,n}^{IO} e^{i\phi_{k,n}^{IO}} x_n a_n^{OR} e^{i\phi_n^{OR}} s(t) \\ &= x_n h_{n,k}^{\mathrm{TIOR}} s(t). \end{aligned} \tag{12}$$

Among them, $h_{n,k}^{\mathrm{TIOR}} = a_k^{TI} a_{k,n}^{IO} a_n^{OR} \rho_k e^{i(\phi_k^{TI} + \theta_k + \phi_{k,n}^{IO} + \phi_n^{OR})}$ is the subchannel at $x_n = 1$. The received signal from sub-channel Tx to the nth pixel of the ROI to the k-th microfacet of the IRS to Rx is

$$\begin{aligned} y_{n,k}^{\mathrm{TOIR}}(t) &= a_n^{TO} e^{i\phi_n^{TO}} a_{k,n}^{IO} e^{i\phi_{k,n}^{IO}} x_n \rho_k e^{j\theta_k} a_k^{IR} e^{i\phi_k^{IR}} s(t) \\ &= x_n h_{n,k}^{\mathrm{TOIR}} s(t). \end{aligned} \tag{13}$$

Among them, $h_{n,k}^{\mathrm{TOIR}} = a_n^{TO} e^{i\phi_n^{TO}} a_{k,n}^{IO} e^{i\phi_{k,n}^{IO}} \rho_k e^{j\theta_k} a_k^{IR} e^{i\phi_k^{IR}}$ is the subchannel at $x_n = 1$. The total received signal received by the final receiver is

RETRACTED

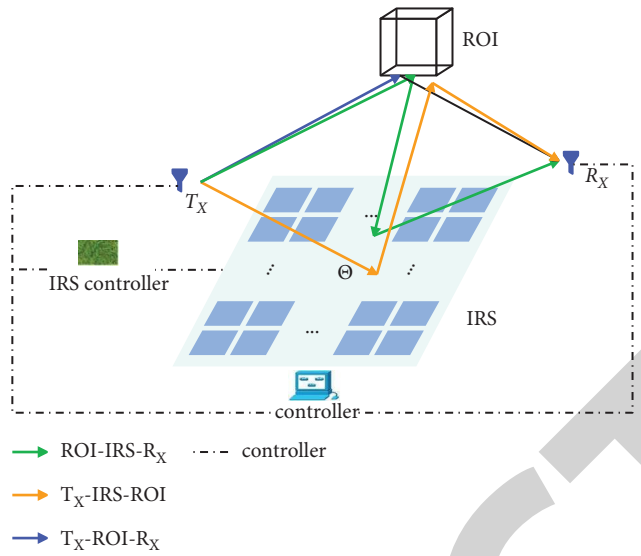

Figure 5: Schematic diagram of the use of centralized smart reflectors (separate IRS mode).

$$\begin{aligned} y(t) &= \sum_{n=1}^{N} y_n^{\mathrm{TOR}}(t) + \sum_{k=1}^{K}\sum_{n=1}^{N} y_{n,k}^{\mathrm{TIOR}}(t) + \sum_{k=1}^{K}\sum_{n=1}^{N} y_{n,k}^{\mathrm{TOIR}}(t) + w \\ &= \sum_{n=1}^{N} x_n h_n^{\mathrm{TOR}} s(t) + \sum_{k=1}^{K}\sum_{n=1}^{N} x_n h_{n,k}^{\mathrm{TIOR}} s(t) + \sum_{k=1}^{K}\sum_{n=1}^{N} x_n h_{n,k}^{\mathrm{TOIR}} s(t) \\ &\quad + w \\ &= \sum_{n=1}^{N} \left(h_n^{\mathrm{TOR}} + \sum_{k=1}^{K} h_{n,k}^{\mathrm{TIOR}} + \sum_{k=1}^{K} h_{n,k}^{\mathrm{TOIR}} \right) s(t) x_n + w \\ &= \sum_{n=1}^{N} \Phi_n(t) x_n + w. \end{aligned} \tag{14}$$

Among them, $\Phi_n(t) = (h_n^{\mathrm{TOR}} + \sum_{k=1}^{K} h_{n,k}^{\mathrm{TIOR}} + \sum_{k=1}^{K} h_{n,k}^{\mathrm{TOIR}})$ $s(t)$, $\mathbf{w}$ is additive white noise. If we assume that we use uniform sampling at the transmitter and receiver, the sampling frequency is f_s, and the duration of the transmitted signal is T, the number of sampling points is $M = Tf_S$. If uniform sampling is performed according to $t = [t_1, t_2, \ldots, t_M]^T$, we can get:

$$\begin{bmatrix} y(t_1) \\ \vdots \\ y(t_M) \end{bmatrix} = \begin{bmatrix} \Phi_1(t_1) \cdots \Phi_N(t_1) \\ \vdots \ddots \vdots \\ \Phi_1(t_M) \cdots \Phi_N(t_M) \end{bmatrix} \begin{bmatrix} x_1 \\ \vdots \\ x_N \end{bmatrix} + \mathbf{w}. \tag{15}$$

If we record $\mathbf{y} = \begin{bmatrix} y(t_1) \\ \vdots \\ y(t_M) \end{bmatrix}$, $\Phi = \begin{bmatrix} \Phi_1(t_1) \cdots \Phi_N(t_1) \\ \vdots \ddots \vdots \\ \Phi_1(t_M) \cdots \Phi_N(t_M) \end{bmatrix}$, we can get the relationship between the received signal sequence and the sequence composed of the reflection parameters of the pixels of ROI as follows

$$y = \Phi x + w, \tag{16}$$

The transmitted signal is a random frequency hopping signal, which consists of P time slots. First, the entire bandwidth B is divided into C_a subcarriers, and in each time slot, C is randomly selected as a signal carrier, and each carrier is subjected to random amplitude and phase modulation to form a transmitted signal. The transmitted signal of the p-th time slot is:

$$s_p(t) = \sum_{c=1}^{c} a_{c,p} e^{-j\omega_{c,p}t} e^{jb_{c,p}}, \ (p-1)\tau \le t \le p\tau. \tag{17}$$

Among them, $\omega_{c,p}, a_{c,p}$, and $b_{c,p}$ are the frequency, amplitude, and phase of the c-th carrier selected for this slot, respectively. Then, the final composition of the transmitted signal is

$$s(t) = \sum_{p=1}^{P} s_p(t) = \sum_{p=1}^{P}\sum_{c=1}^{c} a_{c,p} e^{-j\omega_{c,p}t} e^{jb_{c,p}}. \tag{18}$$

From the physical model of IRS, it can be known that the received signal power of the signal reaching the receiver or ROI after being reflected by the intelligent reflective surface is negatively correlated with the distance between the IRS and the position where the signal is sent/received. That is, the farther the IRS is from the location where the signal is sent/received, the smaller the received signal power will be. The performance is that in the received signal $y(t)$, the proportion of the two parts $\sum_{k=1}^{K}\sum_{n=1}^{N} y_{n,k}^{\mathrm{TIOR}}(t)$ and $\sum_{k=1}^{K}\sum_{n=1}^{N} y_{n,k}^{\mathrm{TIOR}}(t)$ passing through the IRS will decrease, and the part $\sum_{n=1}^{N} y_n^{\mathrm{TOR}}(t)$ that does not pass through the IRS will increase accordingly. Therefore, the different positions of the IRS will change the role of the IRS. Accordingly, we propose two different working modes of IRS: centralized/distributed IRS. We call the centralized IRS working mode when the distance between the IRS and the location where the signal is sent/received is close, and the distributed IRS working mode when the distance is farther. A schematic diagram of the use of centralized smart reflectors is shown in Figure 5.

RETRACTED

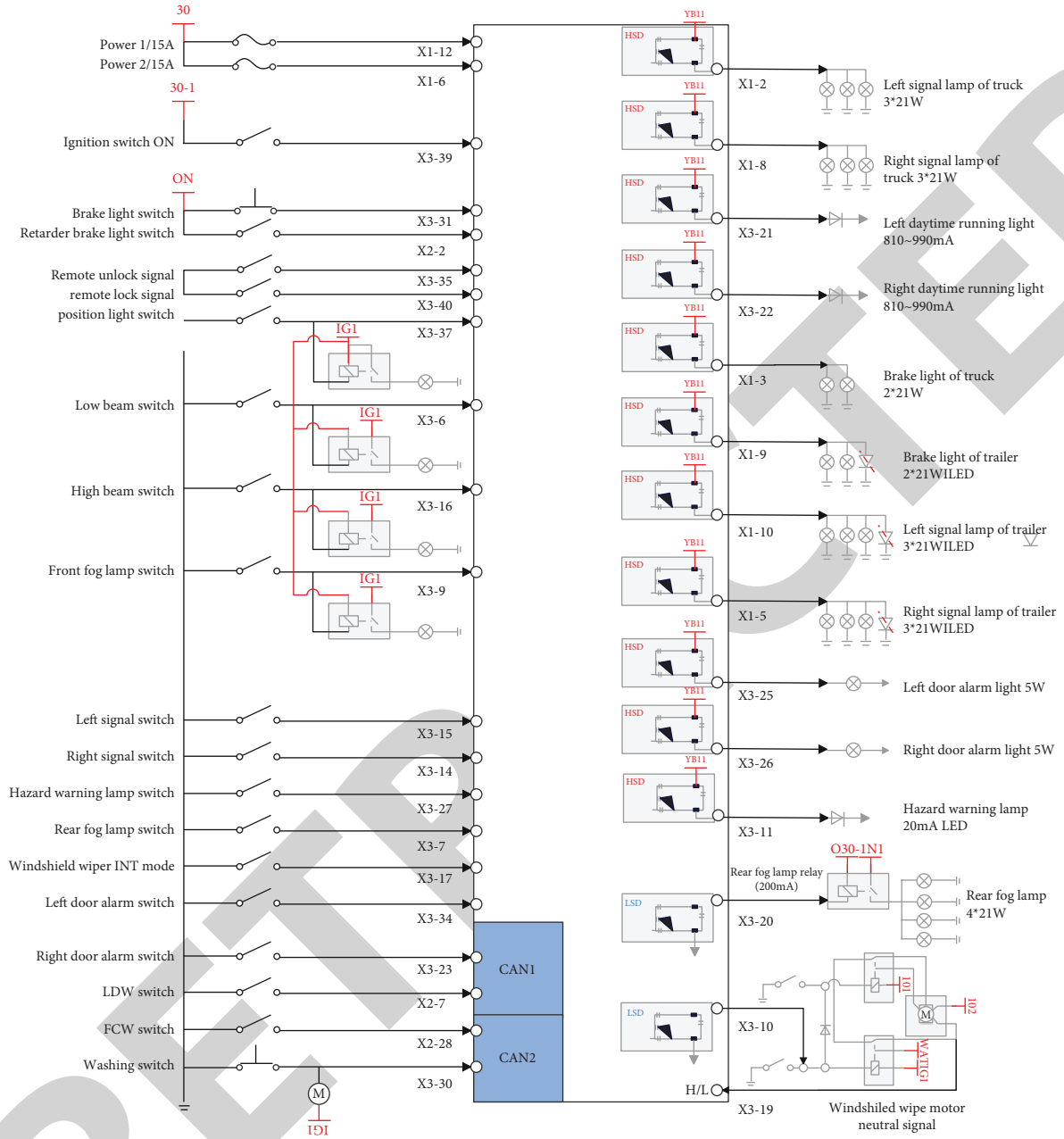

Figure 6: Schematic diagram of the body controller system.

3. Electronic Controller Automation Control System

According to the function of the body control system and the definition requirements of the peripheral input and output interfaces, the schematic diagram of the body control system is designed as shown in Figure 6.

The overall framework of the SDN controller performance test platform is designed as shown in Figure 7. As can be seen from the figure, the SDN controller performance test platform framework designed in this paper is divided into four modules, including the virtual switch module, service analysis module, test dispatch center module, and user interaction center module. The virtual switch module is mainly responsible for simulating the behavior of the switch, including establishing and maintaining the connection with the SDN controller, processing the topology request of the SDN controller, forming the corresponding topology according to the topology information configured by the user, sending and receiving test packets, etc.

The effect of the electronic controller automation system based on artificial intelligence technology proposed in this paper is verified, and the system performance is verified by cluster analysis, and the results shown in Figure 8 are obtained.

It can be seen from the above research that the electronic controller automation system based on artificial intelligence technology proposed in this paper can effectively improve the control effect of the electronic controller.

RETRACTED

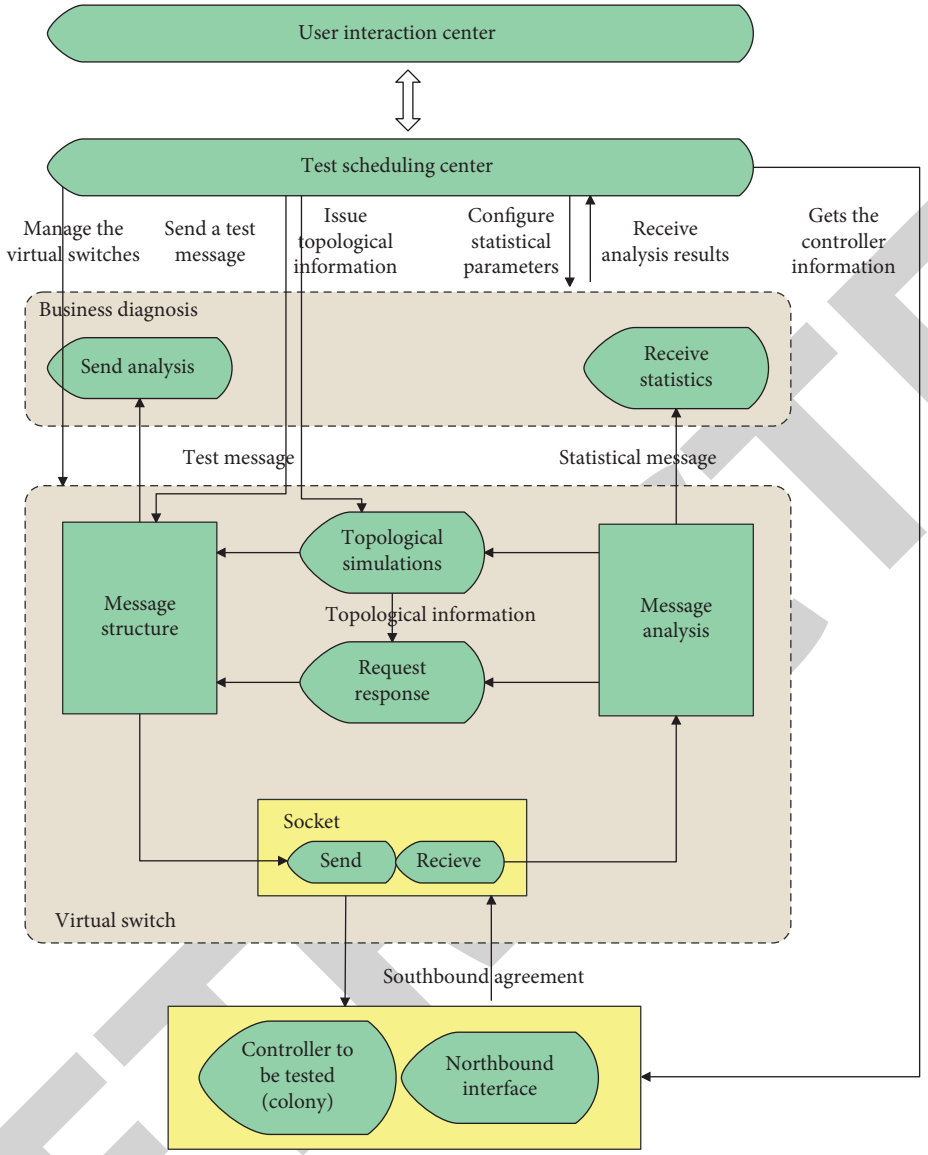

Figure 7: Frame diagram of the controller performance test platform.

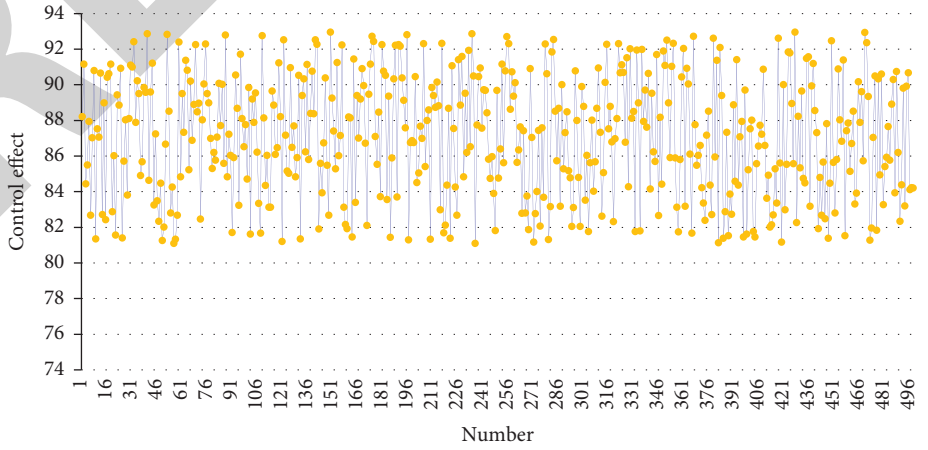

Figure 8: Verification of the effect of the electronic controller automation system based on artificial intelligence technology.

RETRACTED

Hindawi
Journal of Robotics
Volume 2024, Article ID 9876240, 1 page
https://doi.org/10.1155/2024/9876240

Retraction

Retracted: Integrated Urban Design Methodology of "Planning-Construction-Management" and Intelligent Management and Control Based on Teaching Reproduction Robot

Journal of Robotics

Received 23 January 2024; Accepted 23 January 2024; Published 24 January 2024

Copyright © 2024 Journal of Robotics. This is an open access article distributed under the Creative Commons Attribution License, which permits unrestricted use, distribution, and reproduction in any medium, provided the original work is properly cited.

This article has been retracted by Hindawi following an investigation undertaken by the publisher [1]. This investigation has uncovered evidence of one or more of the following indicators of systematic manipulation of the publication process:

(1) Discrepancies in scope
(2) Discrepancies in the description of the research reported
(3) Discrepancies between the availability of data and the research described
(4) Inappropriate citations
(5) Incoherent, meaningless and/or irrelevant content included in the article
(6) Manipulated or compromised peer review

The presence of these indicators undermines our confidence in the integrity of the article's content and we cannot, therefore, vouch for its reliability. Please note that this notice is intended solely to alert readers that the content of this article is unreliable. We have not investigated whether authors were aware of or involved in the systematic manipulation of the publication process.

Wiley and Hindawi regrets that the usual quality checks did not identify these issues before publication and have since put additional measures in place to safeguard research integrity.

We wish to credit our own Research Integrity and Research Publishing teams and anonymous and named external researchers and research integrity experts for contributing to this investigation.

The corresponding author, as the representative of all authors, has been given the opportunity to register their agreement or disagreement to this retraction. We have kept a record of any response received.

References

[1] H. Wang, "Integrated Urban Design Methodology of "Planning-Construction-Management" and Intelligent Management and Control Based on Teaching Reproduction Robot," *Journal of Robotics*, vol. 2022, Article ID 4669792, 9 pages, 2022.

Hindawi
Journal of Robotics
Volume 2022, Article ID 4669792, 9 pages
https://doi.org/10.1155/2022/4669792

RETRACTED

Research Article

Integrated Urban Design Methodology of "Planning-Construction-Management" and Intelligent Management and Control Based on Teaching Reproduction Robot

Haipeng Wang

School of Architecture, Southeast University, Nanjing, Jiangsu, China

Correspondence should be addressed to Haipeng Wang; dongnandaxue2022@163.com

Received 22 July 2022; Accepted 19 September 2022; Published 11 October 2022

Academic Editor: Shahid Hussain

Copyright © 2022 Haipeng Wang. This is an open access article distributed under the Creative Commons Attribution License, which permits unrestricted use, distribution, and reproduction in any medium, provided the original work is properly cited.

With regard to the problems in the integrated urban construction based on "planning-construction–management," the main issues that include the tight construction cycle, the high operation standards, the relatively extensive range of management data sources, the uneven information control, the relatively significant difficulty of management and control, and so on. In this paper, an integrated urban system of "planning-construction-management" based on the management level of the construction projects is established mainly through the application of the teaching reproduction robot (TRR), the engineering information, management and control procedures, and the system framework and performance. Among them, the management and control cover the design control, the quality supervision, the schedule control module, the safety control, the video monitoring, and the facility movement control. The digital technology is included to achieve an integrated management and control model for the engineering design, construction, and operation in its practical operational form. The introduction of the management and control described above has led to relatively good results for the project by operating on the road project with a public-private partnership (PPP) in the startup area of the Chengdu Tianfu International Airport New Town.

1. Introduction

With the rapid development of urban construction, breakthroughs have been made in traditional engineering construction management and control with new models and concepts, and the digital control model based on information technology has been adopted. In this way, the modern urban construction management and control can be more intelligent, humanized, and standardized; more planning and attention have been paid to the accuracy of details with regard to the concept of modern urban construction. Urban control and intelligent management and control are corresponding to each other, in which the intelligent management and control concern more about the cooperation and collaboration of multiple elements, which are also the requirements for effective urban construction and the completion of urban development. The intelligent management and control methods adopted in foreign countries in the early stages are adopted in the development of urban construction. For example, the United States introduced participatory planning in the 1960s, which is an act that primarily involves all the users of the spaces. The release of this act represented a move from a monolithic approach to a multifactorial approach in the urban construction [1, 2]. The smart city management and control in China are typically observed in the construction of Guangzhou city. However, it is not effective in the intelligent management and control of the project with regard to the waste incineration power plant and the form of integrated management and control. Hence, in the new model of intelligent management and control, more attention is paid to the estimation of the interests of stakeholders in the integrated "planning-construction-management" urban construction. At the same time, this act is reflected in the whole process of urban construction. In 2003, the Her Majesty's Treasury (HM Treasury) of the United Kingdom released three

processes required for the planning before construction, during construction, and after construction [3, 4]. As compared to its performance and results in foreign countries, China still focuses on the assessment of construction results and schemes, without taking the comparison between the various stakeholders in the urban construction process into consideration. The effective implementation of the integrated "planning-construction-management" urban construction management and control system has driven the rapid progress of the interactive network based on the Internet. The interactive network is still a rather effective way to develop educational information technology. At present, many colleges and universities have already carried out research on the urban construction methods and intelligent management and control in the interactive networks based on the Internet. Due to the packet loss, delay, and lag in the data transmission process of urban design and intelligent management and control, this situation has directly influenced the progress and quality of the integrated "planning-construction-management" urban construction. In addition, digital enhancement technology is applied in the process of planning, design, construction, and operation, except that their effects are all demonstrated in the current stages. The levels of the teaching reproduction robot and project information management and control are relatively low, and there is a lack of project management and control platforms, which can meet the requirements of intelligent management and control.

The integrated "planning-construction-management" urban design has gradually become popular among massive users. It is mainly implemented on the basis of the ratio of different green areas in the integrated "planning-construction-management" urban design. The integrated urban design based on "planning-construction-management" can not only provide a warm, comfortable, and environment-friendly living experience but also offer flexibility and economy. With the continuous advancement of science and technology, it is necessary to apply the teaching reproduction robot to the process of integrated urban "planning-construction-management." In this way, the relevant technology can be better used to implement integrated urban construction. At the same time, it is also of important significance for the measurement and control of the engineering cost of urban buildings [5–7]. It is a challenge to apply the mathematical model to the process of integrated urban design, and there are significant problems in the traditional design methods during the process of integrated "planning-construction-management" urban construction on a large scale. In combination with the urban construction process at present, domestic and foreign research scholars have applied the existing OpenGL software in the 3D virtual environment to assist and simulate the cost modeling and the construction project based on the data used in practice. However, there are two major defects in the two levels of communication and tool convenience because the memory required for the relevant technology is relatively large and the transmission efficiency fails to achieve the expected result. The analysis algorithm for the integrated urban design and intelligent management and control of "planning-construction-management" is put forward through an in-depth study of building construction in all aspects. Through the application of the teaching reproduction robot, the construction schedule of a building project is consolidated and numbered in a certain order by using an objective function from the perspectives of construction cycle, labor cost, material cost, and safety input, so as to achieve the purpose of saving the cost and reducing the design input of the project. With the advantages of integrated "planning-construction-management" urban design in the aspects of energy saving and environmental protection, production cost reduction, acceleration of construction speed, and so on, to fully comply with the standard of the principle "four savings and one environmental protection," it is necessary to carry out proper management and control of the construction quality during the integrated urban construction period. The management and control of construction quality has become a key issue in integrated urban construction [8–10]. Hence, in the integrated urban design process of "planning-construction-management," it is required to assess the construction quality of the system in all aspects accordingly. In the integrated "planning-construction-management" urban quality assessment model, the teaching reproduction robot should be combined to make full use of its technical advantages more effectively. At the same time, effective evaluation can be carried out in accordance with the urban design assessment index system established. In particular, the application of the teaching reproduction robot can facilitate the robust development of construction projects, and the simulation model established needs to be visualized in three dimensions.

With regard to the analysis of the teaching reproduction robot, through the integration of the Internet of Things (IoT), cloud data, and other big data technologies, on the basis of the practical demand of engineering, a municipal engineering planning-construction-management construction software based on the teaching reproduction robot has beendeveloped. It is a collection of the design control module, the quality supervision module, the progress development module, the safety control module, the monitoring video module, and the operation module for the comprehensive and detailed understanding of the situation in each stage of the project and the full presentation of all relevant data. The research and development of this software has offered strong support for urban construction and can accelerate the progress and improve the quality of urban construction.

2. Algorithm Related to the Teaching Reproduction Robot

The TRR software is designed for the management and control of urban projects in a general direction as well as for cases with more specific management and control. In general, the TRR technology is applied in relatively niche areas, mainly in the construction work, and it cannot operate on a larger scale. At the same time, it is not very effective in coping with the geographical environment [11, 12]. The teaching reproduction robot can make up for the

RETRACTED

insufficiency of processing in this relatively small aspect, and TRR plays a significant role in the GIS refinement of the construction model details. However, the teaching reproduction robot can enhance the integrity of information by understanding the surrounding geography and presenting the micro and macro information while, at the same time, it can also carry out consolidation, analysis, and processing on the basis of the spatial geographic information.

The reason is that the computation method of the teaching reproduction robot has reduced the computation time and improved the task efficiency as compared to the conventional computation methods. It is assumed that the function of each point in the teaching reproduction robot is an S-shaped function. At the same time, the input of the first node i in the teaching reproduction robot is net_i, the output is denoted as o_i, and the output of the k-th node in the output layer is $\widehat{y}_k$, then the input of the j-th node in the middle is shown in the following equations:

$$\text{net}_j = \sum_j w_{ji} o_i, \tag{1}$$

$$o_j = f\left(net_j\right), \tag{2}$$

$$\text{net}_k = \sum_j w_{kj} o_j, \tag{3}$$

$$\begin{aligned} \widehat{y}_k &= o_k \\ &= f\left(\text{net}_k\right). \end{aligned} \tag{4}$$

It is assumed that the deviation of the teaching reproduction robot $e_k = y_k - \widehat{y}_k$ is the difference between the expected value and the practical value. If there are i neurons in the output layer obtained through calculation, then the squared deviation for the true output and the expected outputs can be obtained as follows:

$$E = \frac{1}{2} \sum_{n=1}^{i} \left(y_k - \widehat{y}_k\right)^2. \tag{5}$$

The numerical calculation and the planning results of the teaching reproduction robot in the integrated planning-construction-management urban construction and the WiFi/geomagnetic coupling protection results are used to establish a thinking matrix, and the target output is the coordinates of the real location. The formula for the final results is shown in the equation as follows:

$$\begin{cases} \text{InputData} = \begin{bmatrix} x_{pi} \\ y_{pi} \\ x_{ci} \\ y_{ci} \end{bmatrix}, \quad i = 1, 2, \ldots, n, \\ \text{TargetData} = \begin{bmatrix} x_{ri} \\ y_{ri} \end{bmatrix}. \end{cases} \tag{6}$$

In the above equation, InputData stands for the input result; (x_{pi}, y_{pi}) and (x_{ci}, y_{ci}) are the coordinates of digital protection and development and the coordinates of WiFi/geomagnetic combination protection at the i-th point to be protected based on the integrated urban design of "planning-construction-management," respectively; TargetData stands for the target output sample, and (x_{ri}, y_{ri}) stands for the real location coordinates of the i-th point to be protected.

The digital calculation in the integrated "planning-construction-management" urban construction has become more and more sophisticated through the application of the teaching reproduction robot, which has played a more significant role in the performance of mutual calculation. In this paper, the calculation method and intelligent management and control of the design concept in the teaching reproduction robot are used [13, 14]. As the symbols and constraints in the model (1) lack clear meaning due to the presence of the technical parameter η for virtual reality (VR) and augmented reality (AR) and the random parameter ξ, the symbols in model (1) and the constraint conditions lack clear meaning. Thus, the equation can be obtained as follows:

$$\begin{cases} \max\limits_{x} \quad f(x, \xi, \eta), \\ \text{s.t.} \quad g_j(x, \xi, \eta) \le 0, \; j = 1, 2, \ldots, m. \end{cases} \tag{7}$$

In the above formula, x stands for the decision vector, ξ stands for the random vector parameter, η stands for the virtual reality and augmented reality technology vector parameter, $f(x, \xi, n)$ stands for the objective function, and $g_j(x, \xi, n)$ stands for the constraint function.

The stochastic data are summarized based on the computational theory of the teaching reproduction robot, and the constraint conditions are included in the teaching reproduction robot. The stochastic control of the teaching reproduction robot can be used to deal with the issues of stochastic parameters and technical parameters. The integrated technology of planning-construction-management is applied to the whole life cycle of construction projects. In this way, the information in each stage of the project can be shared and interoperated, while at the same time the big data related to the cloud computing and Internet of Things (IoT) can provide intelligent solutions. Among them, the contents include the fusion of heterogeneous data of the teaching reproduction robot from multiple sources; the integrated indoor and outdoor integration and positioning; the monitoring and early warning of engineering on all fronts; the data interaction; the data storage; the intelligent research and scheme development for engineering construction and management; and so on. The integrated system is used to carry out visualized management and control by using multidimensional information and data, and the processes are interconnected to complete the spatial management and control of the design, planning, and operation in municipal engineering, so as to implement the modernized integrated management and control of urban construction.

RETRACTED

3. Integrated Urban Design Method of "Planning-Construction-Management" and Intelligent Management and Control

In general, the design link in urban construction is a comparison between the urban design measures and the practical operation and maintenance issues, which usually indicates the comparison of the relationship between the "current situation" and the "urban design planning" as well as the evaluation of the results obtained from the specific control plan. The so-called "current situation" refers to the actual situation at the time the current urban design is estimated, while the "urban design plan" refers to the design solution for the urban construction in accordance with the governmental standards [15, 16]. At the same time, the "implementation results" mentioned in this paper refer to the results of the implementation of urban planning on the basis of the urban design, instead of the results of construction on the basis of the urban design deliverables. In this way, a series of information and suggestions for the improvement of the urban design scheme and the content of the results can be presented. There are a lot of factors influencing the price of the integrated "planning-construction-management" urban design projects, including the top design elements in the integrated "planning-construction-management" urban design projects and the skill level of the construction personnel in the integrated "planning-construction-management" urban design project. The top design elements of the integrated "planning-construction-management" urban design project and the skill level of the construction personnel in the integrated "planning-construction-management" urban design project are the human factors that can influence the price of the integrated "planning-construction-management" urban design projects. The changes in the project, the national policy control, and the natural factors are objective factors that can influence the price of the integrated "planning-construction-management" urban design project. Since there are many factors that can affect the price of the integrated "planning-building-management" urban design project, it is necessary to avoid the leakage of any element in the design process. During the process of price design and intelligent management and control, the overall price of the integrated "planning-construction-management" urban design project can be influenced, and the estimation accuracy will be reduced without obtaining the influencing factors through calculation. In the process of building construction, any increase in the number of floors and building area can affect the cost of the integrated "planning-construction-management" urban design project. In addition, any change in the supplies procured in the construction process and the change in the construction personnel expenses can affect the accuracy of the integrated "planning-construction-management" urban design and the intelligent management and control. Hence, during the process of the integrated "planning-construction-management" urban design project cost estimation and reasonable cost control, it is necessary to take the potential influencing factors into full consideration and include labor cost and material cost in the design of the project and in the estimation of the project cost so as to enhance the stability of the construction project more effectively. The cost estimation in the integrated "planning-construction-management" urban design project is set out in the intelligent management and control center. In general, the subjective factors, objective factors, and dynamic factors of the construction project cost are deemed as the input values for the system parameters, and it is necessary to ensure that the cost estimation and management and control of the integrated "planning-construction-management" urban design projects are more accurate in accordance with the requirements.

There are relatively few studies conducted by domestic researchers at present with regard to the concept of urban construction, and there are mainly two methodological approaches. One of the methodological approaches is the evaluation of the project being carried out, the criteria of the urban design, and the presentation of the implementation results; the other methodological approach is the comparison of the two values for the operation of the results and the results of implementation. In case that only one of these two methods is adopted, the practical urban design and construction is essentially a model of four parties, that is, designers, users, development operators, and controllers. The methods of evaluation and calculation at present focus on the comparison of the gaps between the results of the operation and the concept of the design [17, 18]. In this way, no attention is paid to the response of the controllers or the other users, and the studies on the stakeholders of the construction project can also be ignored. Hence, the urban design concept should be applied to the process of urban construction design while taking feedback from controllers and other participants into consideration to finally form the urban design plan through the "consolidation of the planning process-analysis of the urban design control elements and the fit of implementation-the evaluation of the control process-the evaluation by the users" (the details are shown in Figures 1 and 2).

The development process is consolidated in a chronological manner by comparing the results and feedback between the urban design schemes and the planning solutions. Through the comparison of the urban design management and control situation with the detailed urban standardized planning, the urban planning and design can be assessed for the timely accomplishment of the planning requirements. The implementation of the design requirements is compared on the basis of the urban design control elements and the results of the operation. The significance of urban design in the construction and operation of the city is used to select different elements at different levels through various tasks.

Through the top-level design framework of "three software, one support, and N applications," the main planning functions of the planning and construction management platform are shown in Figure 3. At the same time, it is further expanded based on the relevant engineering standards.

RETRACTED

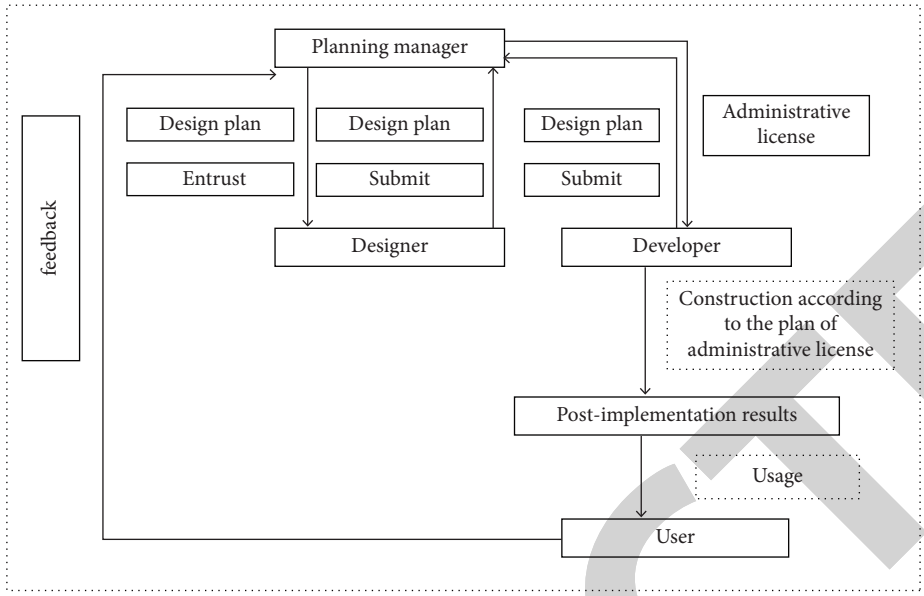

Figure 1: Schematic diagram of the relationship among urban design participants.

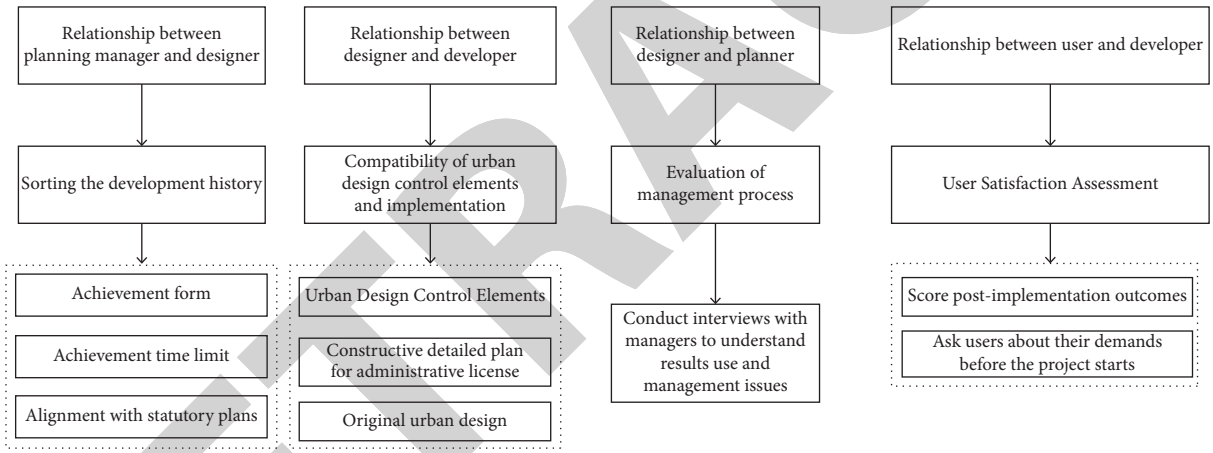

Figure 2: Schematic diagram of the urban design method.

In the platform for the analysis of the business information and the presentation of the application results as indicated in the above diagram, the information from the business management and control software is used to integrate the digital technology module of the municipal engineering, quality situation analysis chart, safety management and control chart, personnel allocation form, and image progress chart to present the total situation of the success case. The main modules include the design module, the construction control submodule, and the operation submodule. With regard to the lightweight digital technology, the design values, documents, schemes, and contents obtained through calculation in the standard and design are organized by planning in an organized manner. At the same time, model planning management and control, information design, progress control, and even information change control, are implemented accordingly. The details of the design planning diagram for the submodules are shown in Table 1.

3.1. Construction Submodule. Through the process and demand for the quality, schedule, safety, personnel, supplies, and other management and control concerns in the construction process and at the same time, the management and control of the visualized construction process are carried out by using the teaching reproduction robot. The planning of the construction submodule functions is shown in Table 2.

3.2. Operation and Maintenance Submodule. It mainly includes facility management and control, the emergency management and control, the video surveillance and analysis, and other functions. The planning of the business functions of the operation and maintenance submodule is shown in Table 3.

Through the platform of the data acquisition and the operation process, the APP related to the mobile items can be used to carry out the project development and operation at any time, so that the process can be understood and

RETRACTED

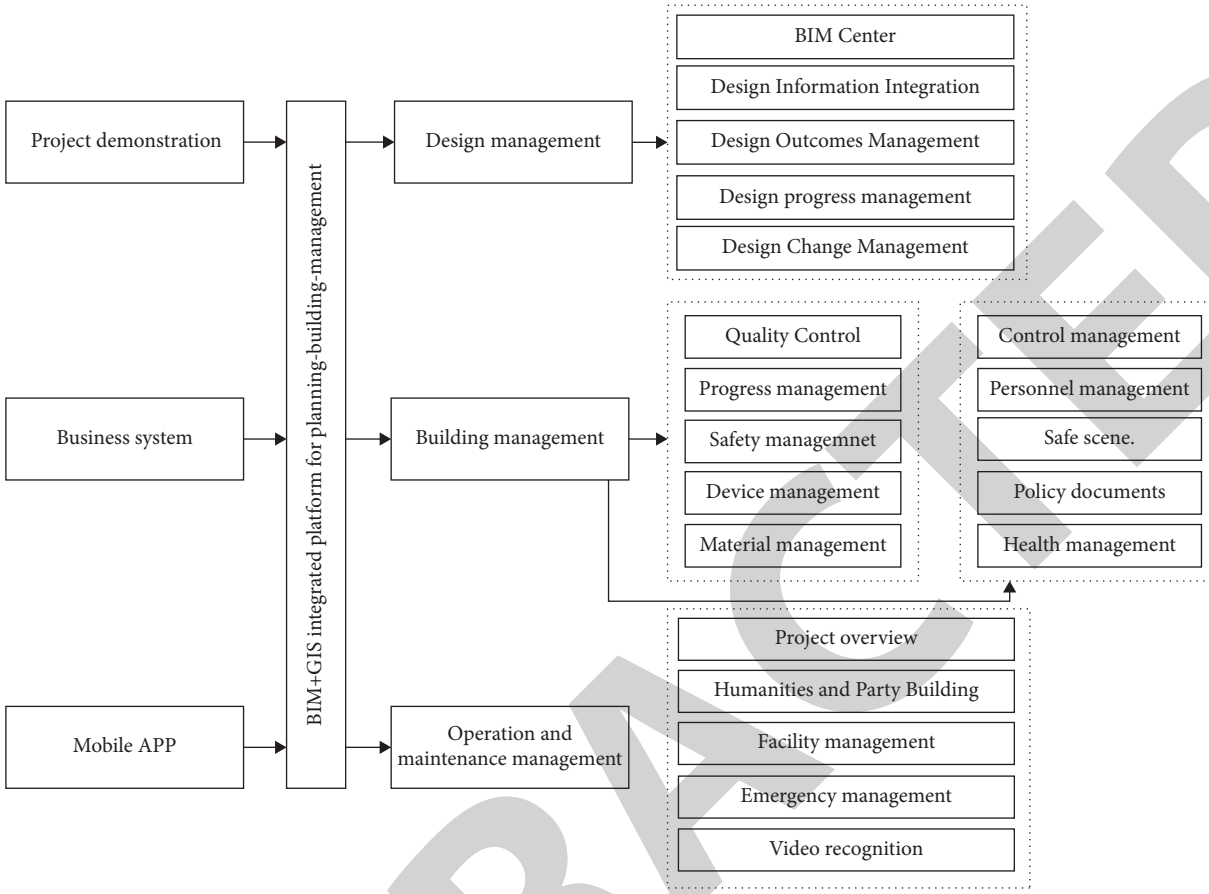

Figure 3: Planning of the platform functions.

Table 1: Planning of the design submodule functions.

Serial number	Business module	Business function
1	TRR center	(1) Scheme comparison and review (2) Browse, query, data conversion, and intergration
2	Design management and control	(1) Integration of the design information (2) Management and control of the design data

handled in a timely manner, which allows for more convenient and intelligent management and control of the project. The system is implemented through multiple levels of engineering design, operation, and management and control. The three levels of project control, task completion, and practical operation are integrated, and the submodule development and operation are used to develop a comprehensive interpretation of the system platform. The TRR modules can be used to combine the model and the engineering information while enabling visual management control in the reengineering system at the same time.

With the system of three inspections as the center, the quality control module uses the final inspection results to verify the process of the three inspections, and each process can be implemented via the cell phone APP on the mobile phone. In addition, the cell phone operation process of the three inspections and the operation process at the web terminal can also be mutually browsed on the platform.

4. Practical Cases and Analysis of the Results

The "planning-construction-management" integrated urban design approach and the intelligent management and control method designed in this paper are analyzed in a PPP project of urban road construction in a certain city. The construction period of this project in the city is three years, which can mainly be divided into 7 subprojects, involving 44 roads, 4 bridges made of steel, and 10 small bridges made of steel, with a total construction length of 46 km. However, the difficulty factor of the project design, construction requirements, supervision units, construction cycle, and maintenance control in the later stage is relatively high, which has put forward higher requirements for the construction quality and the project control level of the urban project engineering.

In the design process of the engineering submodules, the construction projects are named in a uniform manner

RETRACTED

Table 2: Planning of the construction submodule functions.

Serial number	Business module	Business function
1	Management and control of the schedule	(1) Display of the project progress image (2) Progress management and control associated with three quality inspections
2	Management and control of the quality	(1) Internal quality control system of the three inspections by the construction party (2) Construction quality supervision, inspection, and rectification (3) Quality inspection and control of the raw supplies
3	Management and control of the contract	(1) Contract information control and inquiry for various tender sections (2) Control and approval of contract payment and receipt information
4	Management and control of the safety	(1) Major safety risk source control of the project (2) Project safety supervision, inspection, and rectification
5	Management and control of the equipment	(1) All-round management and control of the entry and exit of supplies (2) Certification of operators for the operation of large construction machinery on-site and management and control of the maintenance records
6	Management and control of the personnel	(1) On-site personnel management and control (2) Real name system for labor services
7	Safety on-site	(1) Remote video monitoring (2) Safety education and training

Table 3: Planning of the operation and maintenance submodule functions.

Serial number	Business module	Business function
1	Management and control of the facility	(1) Management and control of the 3D visualization facility (2) Quick location of the facilities (3) Maintenance of the facility information (4) Training of the facility control personnel
2	Management and control of the emergency	(1) Drill of the emergency plan (2) Response to the emergencies
3	Video surveillance	(1) Monitoring area information query and display (2) Diagnostic information upload feedback

according to the TRR working standards for urban construction. In combination with seven subprojects of the project and a total of five design units, the model for urban roads, bridges, and pipe corridors is established by using a variety of design tools. The established model has effectively integrated more than 5,000 engineering design drawings related to the urban construction project and includes design drawings, design reports, change instructions, and other relevant documents related to the urban integrated construction. It can be mainly divided into the minimal control module that is in line with the accurate urban construction management and control. The construction projects for 24 roads and 2 bridges with steel structure landscape under construction are imported into the design platform to establish a basic database of urban integrated construction. This allows for the dynamic data update and the online data query of engineering construction, which can lay a sound foundation for the implementation of intelligent management and control of urban construction effectively.

The "planning-construction-management" integrated urban design approach and the intelligent management and control function module are implemented mainly based on the three inspections, where the mobile data collection system can be used to carry out the urban integrated design statistics and analysis in the business management and control module. Through the quality control of the urban integrated design, engineering project control data can be used to achieve management and control in real time. The application of the teaching reproduction robots can reduce the labor cost spent on the "planning-construction-management" and improve the level of intelligent management and control in an effective manner. The compliance rate in the three inspections of engineering projects can be significantly improved, and the processing efficiency of all engineering construction quality issues as well as the process of the three inspections can also be greatly enhanced. In this paper, an actual project is selected as a practical analysis case to explore and compare the integrated urban design method

RETRACTED

Table 4: Implementation situation of the urban design control elements.

Hierarchy	Level	Element	Implementation
Required urban design control elements	Plan layout	Natural elements	The river chute is retained, which is in line with the requirements of the urban design control
		Public space	Public space inside the plot is reserved in accordance with the urban design requirements. Public space is reserved at the TCL site in the form of elevated space, which has increased the total area of the public space and has a high level of compliance
		Urban traffic	The structure of the traffic road network is essentially in line with the urban design plan in the implementation process, and the construction progress of the road system is about 70% completed at present; the unfinished part is mainly located in the northeast area of the feeder roads in the city
	Building form	Location of the podium tower	990% of the plots comply with the urban design requirements; only the plots of tencent have a staggered building form that is beyond the control range of the podium tower
		Building corridor	About 9% of the sky corridors are inconsistent with the design scheme, which is mainly because the elevation of the building corridor is inconsistent with the urban design scheme
		Building interface	About 5% of the retail commercial interface in the building fails to meet the management and control requirements
	Underground space	Boundary of the underground space	Essentially conform to the urban design plan requirements
		Underground traffic	Essentially conform to the urban design plan requirements
Optional urban design control elements	—	Building overhang space	The width and location of the building overhang are adjusted for about 17% of the plots

with practical engineering construction. From the process of the engineering construction that has been completed, the implementation situation of the key elements in the "planning-construction-management" urban design can be obtained. The details are shown in Table 4.

In the practical process of the urban "planning-construction-management" integrated design, part of the construction is relatively difficult; in the design process of urban building corridors and the detailed planning scheme review and construction process, it is necessary to submit the solutions for the connection of modules with different ownership for approval in accordance with the relevant design scheme. At the same time, due to the uncertainty of the audit objectives, the integrated design process of urban "planning-construction-management" may include coordination between urban projects before and after construction, and the construction units often have problems in the coordination process, which can make the integrated urban construction process even more difficult. The key issue in the effective integrated design management and control of urban "planning-construction-management" is the separation of construction goals from the planning contents and the inability of urban construction planning departments to manage and control the crucial factors. For example, in accordance with the design concept of a low-carbon green lifestyle, design rationality and compliance, as well as many other standards, it is necessary to carry out design and management and control in accordance with energy saving, emission reduction, and other related standards in combination with the comprehensive coefficient of the urban design sites, the engineering construction of water permeability, and so on, effectively. In addition, the volume of the urban "planning-construction-management" integrated

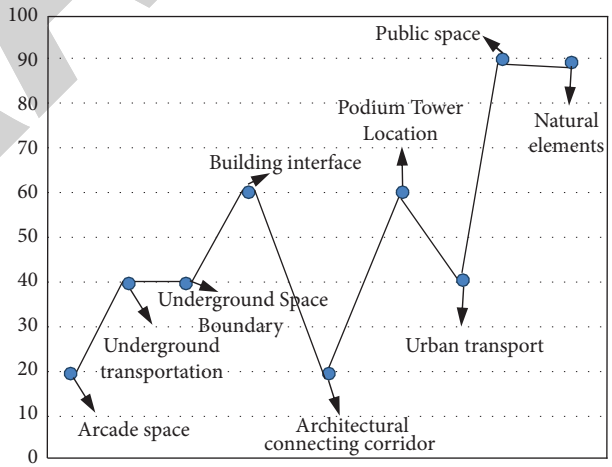

Figure 4: Evaluation score for the implementation.

design is relatively huge, and the lack of effective management control of the integrated urban design scheme can make it very difficult for designers to carry out design for the practical project in an effective manner. In this paper, the standard response to urban design is adopted. After the completion of the urban project, a study of the users was carried out, and the results suggest that about 80% of the users did not have good feedback with regard to the building corridors in the city. At the same time, it can also be observed that the use of the connecting corridors in the city is not sufficient. The main problem is that the corridors are outside the office buildings and fail to serve the purpose of facilitating connectivity when the office buildings are closed. On the other hand, about eighty percent of the users gave a

RETRACTED

Hindawi
Journal of Robotics
Volume 2024, Article ID 9848450, 1 page
https://doi.org/10.1155/2024/9848450

Retraction

Retracted: Safety Monitoring System and Method for Unmanned Operation of Unmanned Aerial Vehicle Distribution Network Based on Learning Control Robot Technology

Journal of Robotics

Received 23 January 2024; Accepted 23 January 2024; Published 24 January 2024

Copyright © 2024 Journal of Robotics. This is an open access article distributed under the Creative Commons Attribution License, which permits unrestricted use, distribution, and reproduction in any medium, provided the original work is properly cited.

This article has been retracted by Hindawi following an investigation undertaken by the publisher [1]. This investigation has uncovered evidence of one or more of the following indicators of systematic manipulation of the publication process:

(1) Discrepancies in scope
(2) Discrepancies in the description of the research reported
(3) Discrepancies between the availability of data and the research described
(4) Inappropriate citations
(5) Incoherent, meaningless and/or irrelevant content included in the article
(6) Manipulated or compromised peer review

The presence of these indicators undermines our confidence in the integrity of the article's content and we cannot, therefore, vouch for its reliability. Please note that this notice is intended solely to alert readers that the content of this article is unreliable. We have not investigated whether authors were aware of or involved in the systematic manipulation of the publication process.

Wiley and Hindawi regrets that the usual quality checks did not identify these issues before publication and have since put additional measures in place to safeguard research integrity.

We wish to credit our own Research Integrity and Research Publishing teams and anonymous and named external researchers and research integrity experts for contributing to this investigation.

The corresponding author, as the representative of all authors, has been given the opportunity to register their agreement or disagreement to this retraction. We have kept a record of any response received.

References

[1] B. Jia, Y. Jiang, T. Ma et al., "Safety Monitoring System and Method for Unmanned Operation of Unmanned Aerial Vehicle Distribution Network Based on Learning Control Robot Technology," *Journal of Robotics*, vol. 2022, Article ID 8559153, 10 pages, 2022.

Hindawi
Journal of Robotics
Volume 2022, Article ID 8559153, 10 pages
https://doi.org/10.1155/2022/8559153

RETRACTED

Research Article

Safety Monitoring System and Method for Unmanned Operation of Unmanned Aerial Vehicle Distribution Network Based on Learning Control Robot Technology

Boyan Jia,[1,2] **Yihu Jiang**,[1,2] **Tianxiang Ma**,[1,2] **Xin Duan**,[1,2] **Dan Li**,[1,2] **Jingran Jia**,[1,2] **and Xiaoyu Li**[1,2]

[1]*Electric Power Research Institute of State Grid Hebei Electric Power Supply Co., Ltd, Shijiazhuang, Hebei 050021, China*
[2]*State Grid Hebei Energy Technology Service Co., Ltd., Shijiazhuang, Hebei 050035, China*

Correspondence should be addressed to Boyan Jia; 2004010207@st.btbu.edu.cn

Received 24 August 2022; Revised 20 September 2022; Accepted 29 September 2022; Published 11 October 2022

Academic Editor: Shahid Hussain

Copyright © 2022 Boyan Jia et al. This is an open access article distributed under the Creative Commons Attribution License, which permits unrestricted use, distribution, and reproduction in any medium, provided the original work is properly cited.

The continuous expansion of the scale of power grid construction has led to the emergence and development of the uninterrupted operation of the unmanned aerial vehicle (UAV) distribution network. However, in the actual power production process, due to the limitations of operating conditions and environment, power safety accidents are inevitable. With the support of intelligent technology, the monitoring effect and application level of the safety monitoring system for the uninterrupted operation of the UAV distribution network have been improved. Unified planning and scheduling were carried out throughout the job implementation process. The efficiency of equipment safety management has been strengthened, which is of great practical significance to the safe production of electric power. Based on the analysis of the environmental characteristics and implementation difficulties of the unmanned aerial vehicle distribution network, this paper studied the safety monitoring system and method by combining the high intelligence and high-efficiency characteristics of the learning control robot technology. The designed unmanned aerial vehicle distribution network safety monitoring system and method were tested. In order to understand the effect of the system intuitively, this paper analyzed from three aspects: system sensitivity, anti-interference, and data acquisition and management. It also contrasted with traditional monitoring systems. The test data showed that the sensitivity test value of the traditional monitoring system in the R1 circuit with the lowest voltage intensity was 71.3%. In the R4 circuit with the strongest voltage intensity, the test value only reached 84.4%. The test values of the system in this paper in the two types of circuits were 85.6% and 93.3%, respectively. In the data acquisition and management test, the acquisition and management rates under the highest numerical information could reach more than 97%. It can be seen that it has strong feasibility in actual operation.

1. Introduction

With the improvement of the level of economic development and material living conditions, the market demand for power supply continues to expand. Power supply stability and safety have become the focus of attention of the public. As an important technical means to ensure the stable operation of power supply equipment and improve the power quality of users, the emergence of unmanned aerial vehicles (UAVs) has improved the reliability of uninterrupted operation of the distribution network, which is of great significance to the automation construction of the power grid. However, the main target of traditional UAV operations is high-voltage transmission lines, which generally exist in residential power areas. The environment where it is located is generally narrow, and there are many obstacles around it. The difficulty of signal acquisition and the lack of real-time and precision seriously affect the implementation of the operation. To this end, an effective safety monitoring system and method must be established. In today's highly developed science and technology, the learning and control robot technology is becoming increasingly intelligent and systematic, contributing to the development efficiency, as well as the efficiency of major industries. For example, it has

exerted its application value in medical, manufacturing, sports, astronomy, and other professional fields. It can continuously test the repetitive control tasks and correct the control quantity within a limited time range to achieve high-precision tracking of the target task. It plays an important role in establishing the safety monitoring system and method for the uninterrupted operation of the UAV distribution network.

The safety monitoring of the UAV distribution network without power outage has always been an important issue in power grid development. Sun proposed an adaptive unscented Kalman filter algorithm for the safety monitoring of the distribution network without power outages. It was proved by simulation experiments that it could reduce the influence of prediction errors on estimation accuracy [1]. Guoqiang proposed a network reconfiguration model based on the distribution system security domain. This model also achieved better power loss and safety monitoring compared to the load balancing model [2]. Zhuang proposed a wireless sensor network based on the Internet of Things technology for the safety monitoring of the UAV distribution network, which was used for insulation state perception [3]. Tao proposed a method for detecting the capacity of distributed photovoltaic power generation integrated into the distribution network based on the fusion of multiple data sources, which can realize real-time detection when the UAV distribution network is not powered off [4]. To reduce the occurrence of safety accidents, Zhang proposed a live installation tool for the uninterrupted operation of the UAV distribution network. Through different structures and sensor combinations, grid data monitoring could be achieved [5]. To effectively identify the electric shock current in the uninterrupted operation of the distribution network, Liu proposed a support vector machine method to classify and monitor it [6]. These monitoring systems and methods can identify and monitor the security risks of the power grid to a certain extent. However, as the scale of the uninterrupted operation of the distribution network expands, the complexity of its implementation environment continues to rise. The real-time performance and accuracy of safety monitoring systems and methods should also be improved. This is where learning-to-control robotics offers unique advantages.

The learning control robot technology has made great progress in recent years. It has important research and application value. To improve the acquisition of real samples, Cutler proposed an efficient learning-controlled robotics framework in a multi-simulator-available scenario for a target task [7]. Turan incorporated learning-controlled robotic technology into minimally invasive intestinal diagnosis and treatment, which enabled high-precision diagnosis [8]. Clever proposed a dynamic model based on learning-controlled robotics to create feasible and optimal motion primitives [9]. Lim computed mutual information by approximate computation of nonparametric methods. He also detected the network's largest number of objects by learning-controlled robotics [10]. Perico believed that programming based on learning-controlled robotics allowed complex tasks with input from different types of sensors and could adapt complex tasks to new environments and objects [11]. Kim proposed a learning-controlled robotic technology with a tactile sensing mechanism, which changed the limitations in performance and efficiency of robotic teleoperation [12]. It can be seen that the learning and control robot technology has exerted its value in many fields. However, its integration with power grid development has not been deeply explored. In order to promote the safe and effective operation of the distribution network without power failure, it is very important to study the safety monitoring system and method of the unmanned power distribution network operation based on the learning control robot technology.

In this paper, combined with the learning control robot technology, effective research was carried out on the safety monitoring system and method for the unmanned operation of the UAV distribution network. The system test data showed that the sensitivity test value of the system in the R1 circuit with the lowest voltage intensity was 85.6%. In the R4 circuit with the strongest voltage intensity, the test value reached 93.3%, which was highly sensitive. The traditional monitoring system was only 71.3% and 84.4% in the R1 and R4 circuits, respectively. In the anti-interference test, the noise frequency range of the system in this paper was reduced from $20\ dB\ \mu A \sim 60\ d\beta\ \mu A$ to $-40\ dB\ \mu A \sim 0\ d\beta\ \mu A$, which could shield a large amount of electromagnetic interference. In the data collection and management test, the collection rates under different numerical information were 99.2%, 98.6%, 98.2%, and 97.4%. The corresponding management rates were 98.7%, 98.3%, 97.8%, and 97.1%, respectively, which had good applicability.

2. Establishment of the Safety Monitoring System and Method

2.1. Overview of the Uninterrupted Operation of the UAV Distribution Network. The distribution network refers to the power network that receives electricity from the transmission system or regional power stations and then distributes it on-site or sequentially according to different voltage levels to users. It is located at the terminal of the power grid and is directly connected to the power system where each user is located. Its main function is to realize power distribution and ensure that every user can get a power supply [13]. The uninterrupted operation is to use the live operation method, which uses professional power equipment, such as insulation tools, arc suppression devices, and bypass equipment. A reasonable operation plan is adopted to reduce the scope of power outages as much as possible. In the state of a partial power outage or complete power outage, electric construction can be realized. Before the unmanned operation of the UAV distribution network is implemented, the safety monitoring system can detect the abnormality and fault of the power system in time, which can accurately locate the fault point in the power grid. Then, the purpose of eliminating hidden dangers of power safety and reducing power outages for users is achieved.

RETRACTED

However, the uninterrupted operation of the UAV distribution network is often hindered by line environment problems because the surrounding environment of most distribution lines is relatively complex. Overall, its operating environment has the following characteristics:

(1) Most of the distribution network lines are located in areas with complex terrain, dangerous terrain, inconvenient traffic, and insufficient signals. Many standardized work practices cannot be implemented effectively.

(2) The height of the tower structure is low, and the wiring structure is relatively simple.

(3) The operating life of distribution network lines is generally long, resulting in weak towers and poor load-bearing capacity.

(4) Part of the power equipment in the distribution network area is scattered. It is difficult to implement the operation without a power outage in the distribution network.

After a power accident, many places are affected by environmental problems. It is difficult for electrical equipment such as insulated bucket trucks to reach the operating point. It is necessary to use the operating lever method or use an insulating platform for operation. In addition, due to the existence of some hidden problems in the construction and maintenance process, the operation site equipment is complicated. At the same time, the large equipment required for the traditional bypass operation cannot be transported to the designated location for installation. This adds great difficulty to implementing the existing unmanned aerial vehicle distribution network without power outages.

Therefore, only by establishing a high-precision power monitoring system and mastering the operation status of the distribution network can it be adjusted in time to reduce the line loss caused by environmental factors, thereby improving the economic benefits of electricity [14]. However, the current power system generally has a large capacity. The unstable operation of the voltage makes the distribution structure more complicated. The traditional approach to safety monitoring systems is increasingly inapplicable. This changing trend has correspondingly increased the requirements for the accuracy and implementation of safety monitoring systems.

2.2. Learning Controlled Robotics. With the continuous progress of human cognitive ability and the development of science and technology, the learning and control robot technology plays an important role in modern human life and production [15]. It effectively combines deep learning, iterative learning control algorithms, and robotics. At present, in the field of robot control, the service-oriented learning control robot technology can improve the reusability and scalability of the control system [16]. The application of learning control robot technology to the safety monitoring system for the uninterrupted operation of the UAV distribution network can improve the development efficiency of the system and ensure its performance requirements. Through the continuous learning and correction of the technology itself, the data information generated during the iterative operation of the monitoring system is used. Constantly correcting its control behavior, the system finally achieves complete tracking of the reference signal set for the uninterrupted operation of the UAV distribution network after a limited number of iterations. Its technical principle is shown in Figure 1.

The optimization problem of the safety monitoring system is attributed to

$$\min_{u_k}\left\{e_k^2\right\}. \tag{1}$$

Among them, u_k is the control term and e_k is the error term. y_k is represented as an output item. Considering the single-input single-output form in the learning control robot technology, the dynamic monitoring of the unmanned operation of the UAV distribution network is described as a supervector form using this technology:

$$y_k = Gu_k + d_0. \tag{2}$$

Among them, the calculation basis of each parameter is shown in Table 1.

In order not to lose generality, $x_k(0) = 0$ is usually taken and $CB \neq 0$ is satisfied. The minimization of system monitoring errors should be considered when designing monitoring performance indicators to optimize the safety monitoring system. It is also necessary to make the changes of the control items not too drastic to ensure the stability of the control variables, which enables the system output to be monitored smoothly [17]. The problem can be optimized as

$$\min_{u_{k+1}} J_{k+1}(u_{k+1}) = e_{k+1}^2 + u_{k+1} - u_k^2. \tag{3}$$

Among them, the error constraint is

$$\mathrm{e}_{\mathrm{k+1}} = \mathrm{y_d} - \mathrm{Gu_{k+1}}. \tag{4}$$

By finding the optimal solution for control item u_{k+1} in the performance index formula, the optimized safety monitoring system controller can be expressed as

$$u_{k+1}^* = u_k + \mathrm{G}^T e_{k+1}. \tag{5}$$

In order to further improve the monitoring performance, the optimization problem can be expressed as

$$\min_{u_{k+1}} J_{k+1,N}(u_{k+1}) = \sum_{i=1}^{N} \lambda^{i-1}\left(e_{k+1}^2 + u_{k+i} - u_{k+i-1}^2\right). \tag{6}$$

By learning the theory of control robot technology, the optimal solution is given as

$$\begin{aligned} u_{k+1}^* &= u_k + G^T(I + \lambda Q_{N-1})e_{k+1}, \\ e_{k+1} &= \left[I + GG^T(I + \lambda Q_{N-1})\right]^{-1} e_k, \\ Q_N &= \left[I + GG^T(I + \lambda Q_{N-1})\right]^{-1}(I + \lambda Q_{N-1}). \end{aligned} \tag{7}$$

RETRACTED

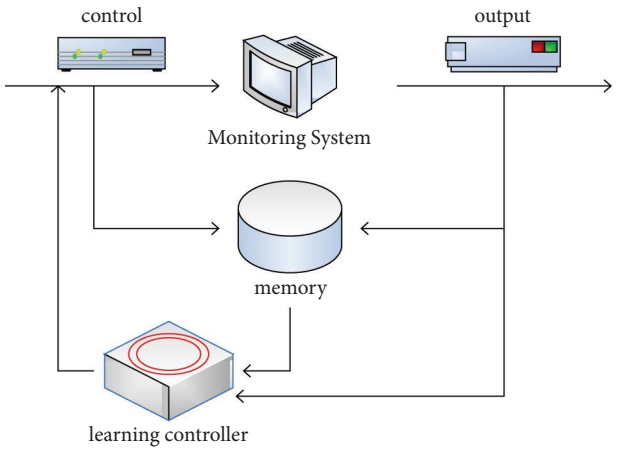

Figure 1: Principles of learning-controlled robotics.

Table 1: Calculation basis of each parameter.

Sequence	Parameter	Calculation basis
1	u_k	$[u_k(0), u_k(1), \cdots, u_k(T-1)]^T$
2	y_k	$[y_k(1), y_k(2), \cdots, y_k(T)]^T$
3	d_k	$[CA, CA^2, \cdots, CA^T]^T x_k(0)$
4	G	$\begin{bmatrix} CB & 0 & \cdots & 0 \\ CAB & CB & \cdots & 0 \\ \vdots & \vdots & \ddots & \vdots \\ CA^{T-1}B & CA^{T-2}B & \cdots & CB \end{bmatrix}$

Among them, N is the number of predicted items and I is the identity matrix. $\lambda > 0$ is the weight parameter.

In fact, in this process, the learning control robot technology can effectively increase the initial control input and improve signal reception. It can also improve the real-time performance of the monitoring system and improve the convergence speed of the system.

2.3. Establishment of the Safety Monitoring System and Method. Under the guidance of learning control robot technology, a new UAV distribution network safety monitoring system was established. It can reflect the actual situation in real time when the distribution network is not powered off. According to the actual voltage of the monitoring power equipment, the monitoring of various parameters is completed, and real judgment is made. Its system structure is shown in Figure 2.

In the functional module, the safety monitoring system based on the learning control robot technology can not only measure the insulation performance parameters of the live device in real time, but also analyze and process the obtained values. Its specific functions include the following:

(1) The changes in resistance and capacitive current in the operation of the distribution network are measured to analyze the damp condition of the internal insulating device and the aging state of the valve plate.

(2) The leakage current of the corresponding capacitive equipment and the specific condition of the dielectric loss are measured to determine the state of the internal equipment (such as moisture state and insulation aging degree) and whether there is damage.

(3) During the implementation of the operation, the condition of the flammable gas inside the insulating oil of the device is verified to monitor whether there are problems such as discharge caused by excessive temperature.

(4) The quality of the signal transmitted by the UAV is judged, which makes the transmitted signal not distorted. While not affected by other signals, it does not affect other surrounding signals.

The user organization structure is the basis for building the system's functions, which is related to the system's role, user authority, and user unit structure, among others. After the user's organizational structure is determined, the units, departments, and personnel involved in the entire system can be determined [18]. In other words, the basic scope of the construction of the system is delineated and formally determined. The user organization structure of this system is shown in Figure 3.

The safety monitoring of the uninterrupted operation of the UAV distribution network includes four links: power transmission, substation, distribution, and power consumption. There are many departments involved. In this paper, the system is divided into two major structures: the monitoring department and the electric power bureau. In Figure 3, there are four categories of user roles. The first category is the system administrator, who is responsible for the establishment and maintenance of the system organizational structure, the user's authority management, and the configuration of the system's basic data. The second category is safety monitoring personnel. The main responsibility of the safety monitoring personnel in the division of user roles is to perform system security monitoring and analyze the monitoring data. The third category is equipment managers. After the monitoring personnel makes an unqualified judgment on the monitoring content, the equipment manager needs to make corrections. The fourth category is the system query user. They are the managers of the general power supply department, the staff of various departments of the Electric Power Bureau, and some other authorized browsing users. When the authority is assigned, the staff of each department of the Electric Power Bureau or other authorized browsing users can only view or operate the security monitoring process of the department. The managers of the power supply department have the right to view or operate the monitoring data of the entire system. According to the management requirements of power safety monitoring standardization, its configuration requirements are shown in Figure 4.

The system database design is divided into four parts: standardized content of safety monitoring, basic data, monitoring process management table, and operation log.

RETRACTED

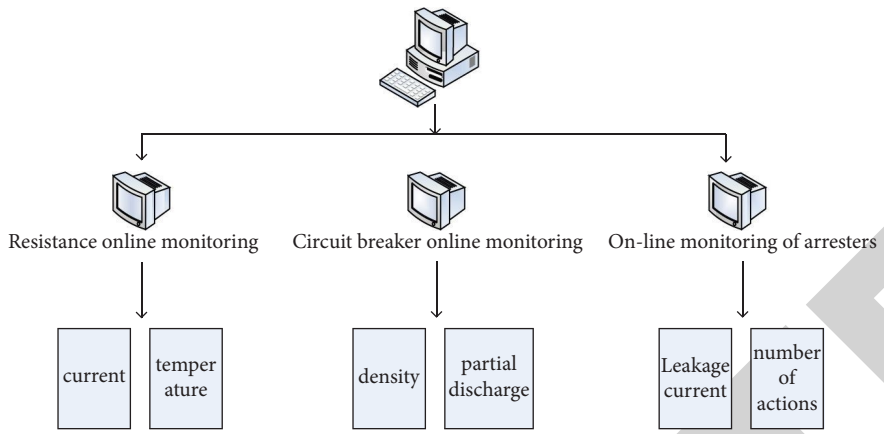

Figure 2: Safety monitoring system structure.

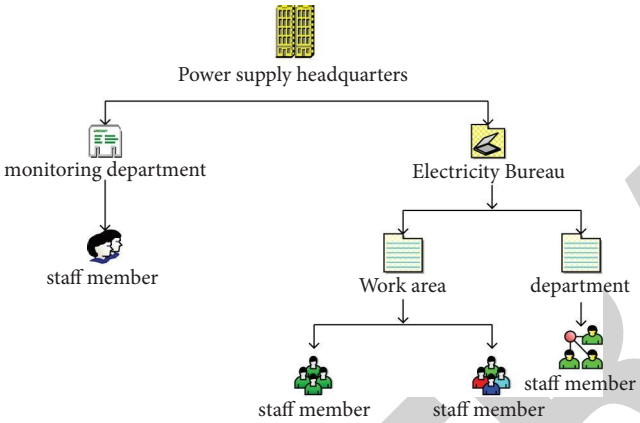

Figure 3: User organization structure.

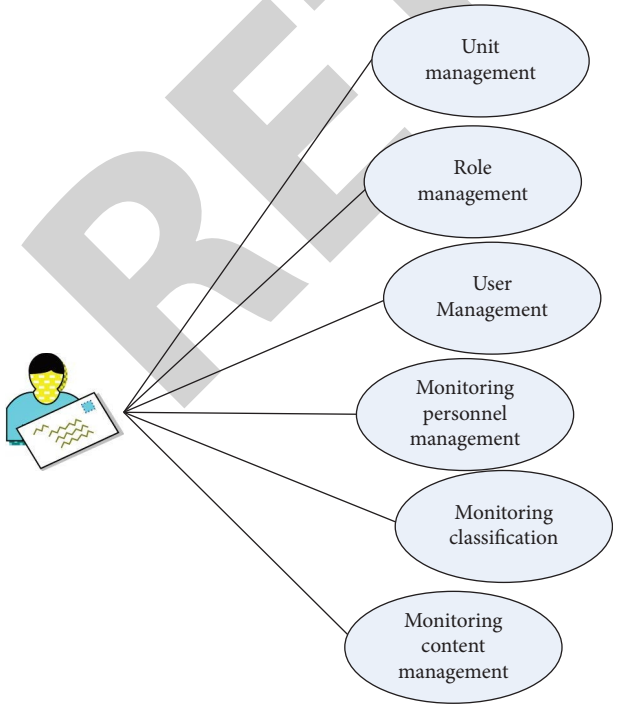

Figure 4: Configuration requirements for managers.

Among them, the safety monitoring standardization content includes the following: the standard directory structure is used to divide the safety monitoring standard content structure directory. The content of monitoring standardization is used to record the scope of standardized monitoring, monitoring basis, and monitoring focus, among others. The basic data includes the organizational structure of the departments involved in safety monitoring and supervision, monitoring personnel information, user information, and authority management. The monitoring process management table records the data of the whole process of safety monitoring, including the safety monitoring plan and its plan decomposition, distribution information, supervision and execution time, execution personnel, and execution results, which is based on the rectification process and results of the problems found in the monitoring process. The operation log is to improve the security of the system. Through system operation, relevant personnel can view the data recording log, such as user login time and data type records. The monitoring task and monitoring record data dictionary are shown in Tables 2 and 3.

The monitoring task is a task assignment table formulated according to the monitoring plan. The main user of this table records the task creation time and completion time. Among them, ID is the unique identification of the monitoring task to ensure the uniqueness of the task in the system [19]. The plan ID is to record the plan associated with this task, which can realize the tracking management of the monitoring plan through the plan ID.

The monitoring record data dictionary includes the creator, name, creation time, and other information. The table associated with it is the catalog classification table. Associated with it is the monitoring task, which can operate or understand the monitoring content through the data dictionary [20].

3. Test of Safety Monitoring System for Unmanned Operation

In order to verify the efficiency of the UAV distribution network uninterrupted operation safety monitoring system and method based on the learning-controlled robotics

RETRACTED

Table 2: Monitoring task data dictionary.

Field name	Field description	Type of data	Length
ID	Unique ID of the row	VARCHAR2 (50)	50
PLAN-ID	Plan number	VARCHAR2 (50)	50
CARD-ID	Supervision card number	VARCHAR2 (50)	50
USER-ID	Executor number	VARCHAR2 (50)	50
ORG-ID	Supervised unit number	VARCHAR2 (50)	50
LEADER-ID	Accompanying leader number	VARCHAR2 (50)	50
EXCUTEDATE	Executive supervision time	DATE	8
NOTE	Remark	VARCHAR2 (500)	500

Table 3: Monitoring record data dictionary.

Field name	Field description	Type of data	Length
ID	Unique ID of the row	VARCHAR2 (50)	50
USER-ID	Creator number	VARCHAR2 (50)	50
CLASSIFY-ID	Catalog number	VARCHAR2 (50)	50
NAME	Supervision card name	VARCHAR2 (50)	50
CREATEDATE	Creation time	DATE	8
NOTE	Other instructions	VARCHAR2 (500)	500

technology, it was tested from three aspects: system sensitivity, anti-interference, and data acquisition and management. The test results were compared with those of traditional safety monitoring systems to confirm their feasibility. The experimental environment of this paper is shown in Table 4.

3.1. Sensitivity Test. In the initial stage of uninterrupted operation of the UAV distribution network, the monitoring system needs to receive the signal from the voltage divider circuit (VDC). The operating environment was determined accordingly. If the numerical signal conditions specified by the operation were met, the operation could be performed. However, the voltage divider circuit in actual operation is often in an unstable state, which affects the reception of the monitoring system signal. In this paper, the sensitivity of the two types of systems was tested with four different voltage divider circuits. The voltage intensity from low to high was divided into R1, R2, R3, and R4. The results are shown in Figure 5.

Generally speaking, the lower the voltage of the voltage divider circuit, the lower the sensitivity of the system and the weaker the received signal, as shown in Figure 5. The sensitivity of the two monitoring systems increased with the voltage increase, but the test values were quite different. Figure 5(a) shows that the sensitivity test value of the system in this paper in the R1 circuit with the lowest voltage intensity was 85.6%. In the R4 circuit with the strongest voltage intensity, the test value reached 93.3%. The sensitivity of the system in this paper was high. With the support of the learning control robot technology, the system control quantity was stable. It enabled the system to ensure signal reception even in a weaker operating environment. In contrast, the traditional monitoring system in Figure 5(b) had the lowest sensitivity of 71.3% and the highest of only 84.4% in the four circuit tests. Under this condition, the strength of the signal received by the system varies. The authenticity and reference of its judgment were also weak, which affected the implementation of the uninterrupted operation of the UAV distribution network.

3.2. Anti-Interference Test. There are electronic circuits interconnecting various units in the equipment inside and outside the monitoring system. Due to the influence of system structure design, component selection, wiring, installation, and other processes, electromagnetic energy may be transmitted in the form of current between the equipment and unit lines along with wires (such as power supply wires, signal transmission lines, and common ground wires), resulting in interference and affecting monitoring results. In this paper, the anti-interference test of the system was carried out under the noise of different frequencies, as shown in Figure 6.

In the monitoring process, in the face of electromagnetic interference, the system needs to shield the noise well to realize real-time monitoring smoothly. Figure 6(a) shows that the preset standard based on the monitoring system in this paper did not meet the required noise filtering, which completed the diagnosis of electromagnetic interference well. Its noise frequency changed from high-frequency to low-frequency regions. Under the learning control robot technology, the noise superscalar collected by the system in the specified frequency range could be basically consistent with the actual measurement value of the interference measurement module. The antijamming performance of the monitoring system was used to analyze the time-frequency characteristics of the processing results. It has high accuracy, which can well assist the implementation of uninterrupted operation of the UAV distribution network. Figure 6(b) shows that the noise frequency of the traditional system before and after antijamming did not change significantly. The noise frequency was still mostly concentrated in the

RETRACTED

Table 4: Safety monitoring system test environment.

Attributes	Item	Specification
Hardware	CPU	Intel Xeon E5-4650 2.70 GHz
	RAM	4G
	Hard disk	300G SATA2 16M
	Network	Dual-port gigabit local area network
Software	Operating system	Windows 2019
	Middleware	Apache Tomcat 7.0.109
	Database	Oracle 11 g

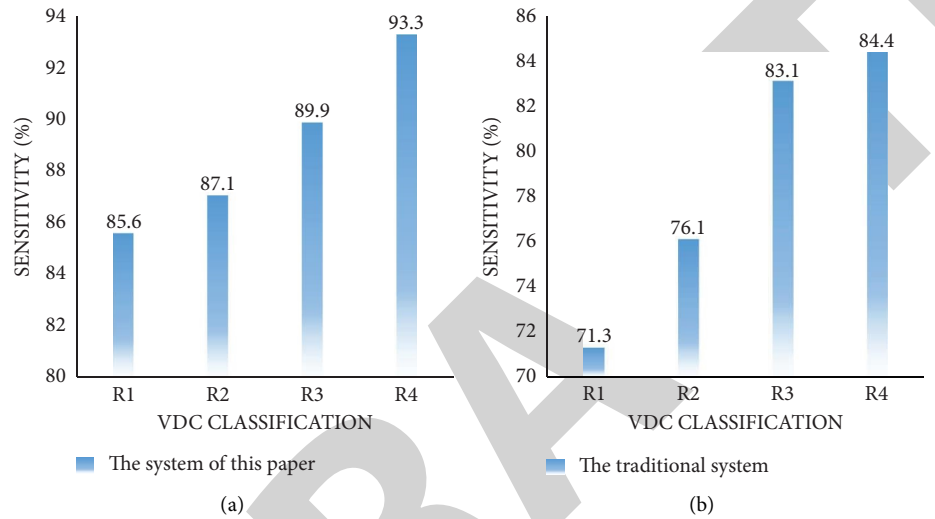

Figure 5: Sensitivity test results. (a) The monitoring system of this study. (b) The traditional monitoring system.

high-frequency region. In this state, electromagnetism causes continuous interference to the system, which not only affects the normal operation of the monitoring system, but also makes it unable to operate for a long time. A comparison of the two clearly shows that the interference measurement and suppression functions of the system in this paper are well designed, meeting the requirements of the operation indicators.

3.3. Data Collection and Management. The data collection and management of the monitoring system mainly focus on the data collection and management of the actual operating state of the electrical equipment. This is also an important indicator to measure the practicability of the monitoring system. In this paper, the data collection rate and management efficiency of the two types of systems were investigated under different amounts of numerical information (500, 1,000, 1,500, and 2,000), as shown in Figure 7.

In Figure 7, the two types of systems show different levels of collection rate and management rate under different numerical information. Generally speaking, the larger the numerical information, the lower the collection and management rates. However, Figure 7(a) shows that this trend had less impact. Under different numerical information, the acquisition rates were 99.2%, 98.6%, 98.2%, and 97.4%, respectively. The corresponding management rates were 98.7%, 98.3%, 97.8%, and 97.1%, respectively. Under the highest digit value of 2,000, the collection and management rates still reached more than 97%. It shows that the system can perform autonomous collection work. The system can display various information parameters of electrical equipment on the main wiring, which provides data support for the uninterrupted operation of the UAV distribution network. The learning control robot technology uses the actual situation value collected by the system to input and change the setting value. The status information query of the equipment and the specific data analysis, calculation, and diagnosis functions are completed, which brings great convenience to the actual operation of the system. Figure 7(b) shows that the acquisition rates of the traditional monitoring system under different numerical information are 89.2%, 82.1%, 79.5%, and 71.1%, respectively. The corresponding management rates are 83.4%, 78.5%, 74.3%, and 65.8%, respectively. Collection efficiency is easily affected by numerical information. The management efficiency also cannot match the collection efficiency, which brings great problems and challenges to subsequent information transmission.

RETRACTED

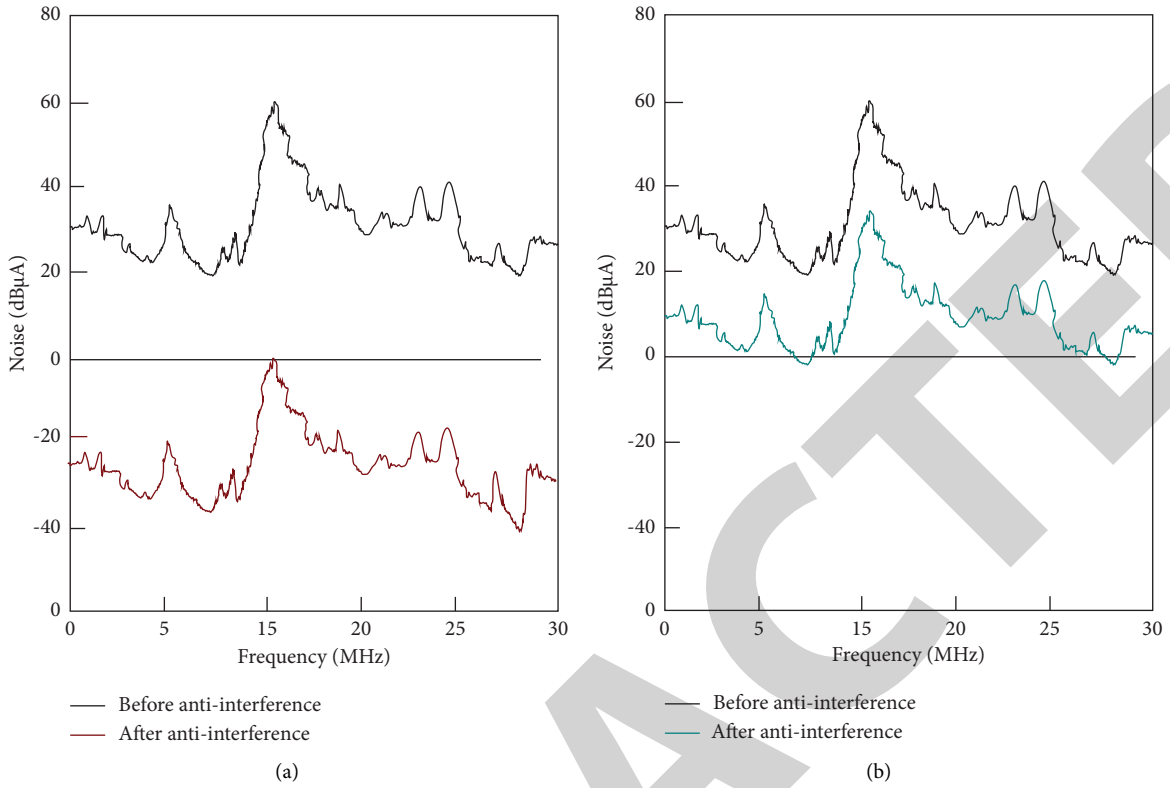

Figure 6: Immunity test results. (a) The monitoring system of this study. (b) A traditional monitoring system.

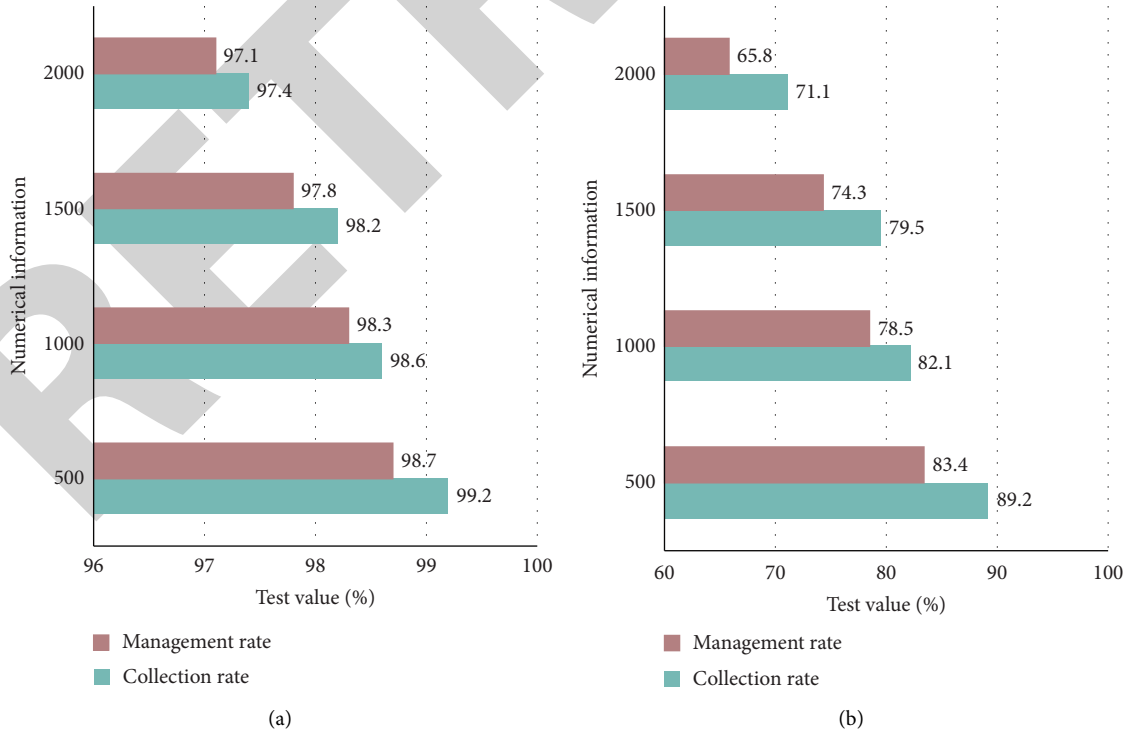

Figure 7: Data collection and management results. (a) The monitoring system of this study. (b) A traditional monitoring system.

RETRACTED

4. Conclusion

The most important thing in the implementation process of the uninterrupted operation of the UAV distribution network is to ensure safety. The monitoring system is a key part of ensuring the safe production of electricity, which plays a key supporting role in the reliable operation of the operation. In this paper, combined with the learning control robot technology, the safety monitoring system and method for unmanned operation of the UAV distribution network were studied. With the support of the technical theory, the sensitivity and anti-interference of the monitoring system have been improved so that the system could still ensure signal reception in the operating environment with weak voltage. The electromagnetic signal was effectively shielded, which provided a more reliable guarantee for the implementation of the operation. Since the research on the safety monitoring system and method for uninterrupted operation of UAV distribution network based on learning control robot technology is still in the exploratory stage, some problems need to be further solved in the operation process. This paper only studies the development of the safety monitoring system and method and does not think about the later operation and maintenance services of the system. Power grid construction covers a wide range. Therefore, the system's universality in this paper needs to be continuously verified. These questions are also the main directions of follow-up research. In future research, the reliability of the safety monitoring system and method for the uninterrupted operation of the UAV distribution network can be more effectively improved.

Data Availability

The data used to support the findings of this study are available from the corresponding author upon request.

Conflicts of Interest

The authors declare no conflicts of interest.

Acknowledgments

This research study was sponsored by Science and Technology Project of State Grid Corporation of China. The authors acknowledge the project "Research and Development of Intelligent Safety Monitoring System for Live Operations in Distribution Network Based on UAV AI Recognition" (project no. TSS2020-05) for supporting this article.

References

[1] J. Sun, M. Liu, and L. Deng, "State estimation of distribution network based on AUKF," *Power System Protection and Control*, vol. 46, no. 11, pp. 1–7, 2018.

[2] Z. U. Guoqiang, J. Xiao, and L. Zuo, "A reconfiguration model for distribution network based on security region," *Proceedings of the Csee*, vol. 37, no. 5, pp. 1401–1409, 2017.

[3] T. Zhuang, M. Ren, X. Gao, M. Dong, W. Huang, and C. Zhang, "Insulation condition monitoring in distribution power grid via IoT-based sensing network," *IEEE Transactions on Power Delivery*, vol. 34, no. 4, pp. 1706–1714, 2019.

[4] Q. Tao, D. Wang, and J. Ye, "Capacity analysis of distributed photovoltaic generation integrated into power grid considering energy storage configuration mode based on fusion of multiple data sources," *Gaodianya Jishu/High Voltage Engineering*, vol. 44, no. 4, pp. 1093–1098, 2018.

[5] J. Zhang, Y. Hu, S. Xu, T. Zhang, S. Ren, and M. Wang, "Design and analysis of terminal live installation tool for robot in distribution work," *Procedia Computer Science*, vol. 183, no. 1, pp. 412–417, 2021.

[6] Y. Liu, S. Du, and W. Sheng, "Classification and identification of electric shock current for safety operation in power distribution network," *IET Cyber-Physical Systems Theory & Applications*, vol. 5, no. 2, pp. 145–152, 2020.

[7] M. Cutler, T. J. Walsh, and J. P. How, "Real-World reinforcement learning via multifidelity simulators," *IEEE Transactions on Robotics*, vol. 31, no. 3, pp. 655–671, 2015.

[8] M. Turan, J. Shabbir, H. Araujo, E. Konukoglu, and M. Sitti, "A deep learning based fusion of RGB camera information and magnetic localization information for endoscopic capsule robots," *International Journal of Intelligent Robotics and Applications*, vol. 1, no. 4, pp. 442–450, 2017.

[9] D. Clever, M. Harant, K. Mombaur, M. Naveau, O. Stasse, and D. Endres, "COCoMoPL: a novel approach for humanoid walking generation combining optimal control, movement primitives and learning and its transfer to the real robot HRP-2," *IEEE Robotics and Automation Letters*, vol. 2, no. 2, pp. 977–984, 2017.

[10] J. Lim and H. J. Kim, "Mutual information–based tracking of multiple moving targets using networked robots," *Journal of Institute of Control, Robotics and Systems*, vol. 23, no. 3, pp. 165–171, 2017.

[11] C. A. V. Perico, J. De Schutter, and E. Aertbelien, "Combining imitation learning with constraint-based task specification and control," *IEEE Robotics and Automation Letters*, vol. 4, no. 2, pp. 1892–1899, 2019.

[12] J. I. Kim, D. W. Kim, M. Krebs, Y. S. Park, and Y. L. Park, "Force sensitive robotic end-effector using embedded fiber optics and deep learning characterization for dexterous remote manipulation," *IEEE Robotics and Automation Letters*, vol. 4, no. 4, pp. 3481–3488, 2019.

[13] S. Gao, J. Zhao, Y. Liu et al., "Research into power transformer health assessment technology based on uncertainty of information and deep architecture design," *Mathematical Problems in Engineering*, vol. 2021, Article ID 8831872, 12 pages, 2021.

[14] L. Wang, G. Wu, J. Wang, M. Jin, and Y. Song, "Numerical investigation of the core outlet temperature fluctuation for the lead-based reactor," *Annals of Nuclear Energy*, vol. 117, pp. 194–201, 2018.

[15] Y. W. Zhang and W. J. Zeng, "Mechanical Shim core operational strategy designed for CPR1000 nuclear power plant," *Nuclear Engineering and Design*, vol. 322, pp. 14–26, 2017.

[16] S. Eryilmaz and Y. Devrim, "Theoretical derivation of wind plant power distribution with the consideration of wind turbine reliability," *Reliability Engineering & System Safety*, vol. 185, pp. 192–197, 2019.

[17] A. M. Salman, Y. Li, and E. Bastidas-Arteaga, "Maintenance optimization for power distribution systems subjected to hurricane hazard, timber decay and climate change," *Reliability Engineering & System Safety*, vol. 168, no. dec, pp. 136–149, 2017.

RETRACTED

Hindawi
Journal of Robotics
Volume 2023, Article ID 9768653, 1 page
https://doi.org/10.1155/2023/9768653

Retraction

Retracted: Recognition and Modeling of Crisis Propagation Patterns Combined with Robot Simulation of Social Networks

Journal of Robotics

Received 8 August 2023; Accepted 8 August 2023; Published 9 August 2023

Copyright © 2023 Journal of Robotics. This is an open access article distributed under the Creative Commons Attribution License, which permits unrestricted use, distribution, and reproduction in any medium, provided the original work is properly cited.

This article has been retracted by Hindawi following an investigation undertaken by the publisher [1]. This investigation has uncovered evidence of one or more of the following indicators of systematic manipulation of the publication process:

(1) Discrepancies in scope
(2) Discrepancies in the description of the research reported
(3) Discrepancies between the availability of data and the research described
(4) Inappropriate citations
(5) Incoherent, meaningless and/or irrelevant content included in the article
(6) Peer-review manipulation

The presence of these indicators undermines our confidence in the integrity of the article's content and we cannot, therefore, vouch for its reliability. Please note that this notice is intended solely to alert readers that the content of this article is unreliable. We have not investigated whether authors were aware of or involved in the systematic manipulation of the publication process.

Wiley and Hindawi regrets that the usual quality checks did not identify these issues before publication and have since put additional measures in place to safeguard research integrity.

We wish to credit our own Research Integrity and Research Publishing teams and anonymous and named external researchers and research integrity experts for contributing to this investigation.

The corresponding author, as the representative of all authors, has been given the opportunity to register their agreement or disagreement to this retraction. We have kept a record of any response received.

References

[1] Y. Wang, "Recognition and Modeling of Crisis Propagation Patterns Combined with Robot Simulation of Social Networks," *Journal of Robotics*, vol. 2022, Article ID 3454396, 12 pages, 2022.

Hindawi
Journal of Robotics
Volume 2022, Article ID 3454396, 12 pages
https://doi.org/10.1155/2022/3454396

RETRACTED

Research Article

Recognition and Modeling of Crisis Propagation Patterns Combined with Robot Simulation of Social Networks

Yafei Wang

Department of Basic Education, Huanghe Jiaotong University, Jiaozuo 454000, China

Correspondence should be addressed to Yafei Wang; 2016090302@zjtu.edu.cn

Received 13 August 2022; Revised 1 September 2022; Accepted 24 September 2022; Published 11 October 2022

Academic Editor: Shahid Hussain

Copyright © 2022 Yafei Wang. This is an open access article distributed under the Creative Commons Attribution License, which permits unrestricted use, distribution, and reproduction in any medium, provided the original work is properly cited.

In order to improve the identification effect of a crisis propagation mode, this paper studies the crisis propagation mode of social networks and uses an intelligent method to identify the crisis propagation mode. Moreover, this paper analyzes and deduces the features of the modulated signal from the two aspects of spectrum and autocorrelation functions and extracts and simulates the features of signals of different modulation types. In addition, this paper verifies the proposed recognition method from two aspects through theoretical experiments and measured data and builds an intelligent model. Through the experimental research, it can be seen that the identification effect and the control effect of the crisis propagation model based on the social network proposed in this paper are relatively obvious.

1. Introduction

In the real world, the phenomenon of coevolving crisis communication between different crisis communication processes is common. It is also a huge challenge for scholars to model and analyze these complicated coevolving crisis communication processes and propose corresponding and feasible intervention strategies.

The security and privacy-hidden dangers in social networks have brought trouble to users, which has attracted the attention of researchers [1]. For example, on a social platform, when it comes to sensitive topics such as money transactions and privacy disclosure, users need to clearly judge the trustworthiness of the other user. For another example, when a mobile social network is applied to a location-based service, people pay particular attention to how private information such as location is known to surrounding users. That is, when a user displays or hides location information from other individual users or a specific group, an appropriate security level needs to be set [2]. Interactions in social networks sometimes occur between unfamiliar users, and on social platforms, sensitive interactions such as economics or privacy often occur, so trust plays an important role. It can be said that the normal operation of a social network depends on the level of trust among users, and the trust among users in a real social network is the basis of people's communication [3].

It is particularly important to study an appropriate trust relationship model to ensure the security of social networks. Specifically, users need to measure the degree of trust in other users to decide how to disclose and share personal privacy information and how to choose which users to interact with. However, the existing social network trust models still have certain drawbacks; for example, there is no clear description of the calculation rules of trustworthiness (quantitative representation of trust). A trust model based on semiring algebra theory is proposed [4], which can well describe credibility calculation rules and can express other trust models flexibly, so it becomes a very important trust model. Literature [5] proposed a trust path search algorithm and established a semiring trust model for privacy protection. However, the trust model still has some shortcomings, such as it does not define and describe the time-based dynamic change problem. One of the typical characteristics of the social network is its dynamic nature, for example, users are added and deleted at any time in social networks. In this way, the topology of the network changes at any time, causing changes in the links between nodes, and the user's

trust is propagated and calculated through the links between users so that the user's trust will also have dynamic variability [6]. Therefore, from an objective point of view, the trust model for calculating user credibility needs to reflect this dynamic nature, timely reflect changes in users' behavior, and improve adaptability.

Identifying key users in a network is an important research content for complex networks, including social networks. For example, in various social networks, it is often necessary to know which users are the most active and influential, in order to provide a useful basis for the content distribution of mobile social networks or to provide operators with guidance on marketing strategies [7]. In social network analysis, "centrality" is used to describe the importance of nodes in the network [8]. Establishing an accurate centrality measurement model is an important method to identify key users. Early network research did not consider the weight of links between users, but only whether users were connected. This will lose a lot of network information, resulting in inaccurate centrality measures. In recent years, researchers have found that in order to more accurately identify key users, it is necessary to integrate the weights into the links between users (such as link strength, intimacy, and credibility), and such a social network is called a weighted social network [9].

An important feature of social networks is that they consist of multiple communities. Then, the most important nodes in a social network should belong to different communities. The centrality measurement method of the above weighted network has certain defects because it cannot effectively identify the important nodes of each community in the social network [10]. Since weighted networks can be viewed as multigraphs mapped into unweighted networks, the classical centrality measures of weighted networks inherit their weaknesses in unweighted networks. Degree centrality is the simplest method that only considers localized structural information but does not consider the global structure of the network, including multicommunity features [11]. Then, the dominant nodes ranked based on degree centrality are likely not the most influential nodes in each community. The closeness and betweenness centrality of weighted networks is based on the shortest path algorithm with the limitation that nodes that are not on the shortest path between any two other nodes will have the same centrality value (i. e. 0) [12]. Then, when applied to large sparse networks, the effective centrality values for most nodes will not be available based on them. More importantly, they do not explicitly state the relationship between centrality and community structure. Based on EVC, the most influential nodes are clustered in a community in a weightless network, which also suffers from the same flaws in a weighted network [13].

The dissemination of information on the real network can affect all aspects of human society. In view of the fact that most of the current theoretical analysis methods of information dissemination on complex networks are based on nodes and the theoretical research based on network edges is still relatively lacking, a set of information dissemination analysis methods based on the dynamic state of edges has been developed [14]. Based on this, an indicator is proposed to measure the influence of potential connections in promoting information dissemination. This indicator can effectively screen out the optimal potential links that can promote information dissemination in the network. In addition, based on the analysis of the optimal latent edge, literature [15] proposed an information propagation intervention strategy based on the optimal latent edge. A set of theoretical analysis methods of information propagation based on the dynamic state of the connection edge is developed, and a propagation intervention strategy that combines the characteristics of the network structure in the network propagation dynamic system and the characteristics of propagation dynamics itself is proposed.

Compared with single information propagation, information-information coevolution propagation has a more complex evolution mechanism, and its corresponding theoretical research is still rare. It is very challenging to effectively intervene in information-information coevolution propagation dynamics on complex networks by combining the characteristics of network structure and propagation dynamics themselves [16]. Literature [17] proposed an index to quantitatively describe the influence of potential connections of the network in promoting information-information coevolution propagation, aiming at the symmetrical propagation of two types of information in the coevolution system. Literature [18] proposed an information-information coevolution propagation intervention strategy based on optimal latent connections. The strategy effectively combines the structural characteristics of the network in the coevolution propagation system and the characteristics of coevolution propagation dynamics itself and is better than the heuristic strategy that only relies on the network topology centrality in intervening information-information coevolution propagation on the network. In this paper, the information-information co-evolution propagation mechanism on complex networks is studied, and a coevolution propagation intervention strategy that effectively combines the characteristics of the network structure and propagation dynamics is proposed for the symmetrical propagation of two types of information in the coevolution system.

This paper studies the crisis communication mode of the social network, identifies the crisis communication mode through intelligent methods, and builds an intelligent model to promote the effective control of crisis communication.

2. Artificial Feature Parameter Extraction for Social Network Crisis Data Recognition

2.1. Signal Extraction. The theory of signal feature extraction from social network crisis data has been greatly complemented by decades of research. The earliest used feature parameters are the features obtained based on the instantaneous information of the signal. This feature is greatly disturbed by noise and has almost no classification effect on the signal under the condition of a low signal-to-noise ratio. The feature parameters used in this paper are divided into three categories, with a total of 11 kinds, and all feature vectors are shown in Figure 1.

RETRACTED

The time-domain waveform of a social network crisis data signal contains a lot of instantaneous information about the signal. By analyzing and calculating the waveform of the social network crisis data signal, the signal amplitude, frequency, phase, and other information can be obtained, which constitute the most basic features of the social network crisis data signal.

The signal used in the experiment is a complex signal, and the signal is modeled as an analytical signal $s(t)$ before the experiment:

$$s(t) = x(t) + jy(t). \tag{1}$$

The imaginary part in the analytical expression $s(t)$ is the Hilbert transform of the real signal $x(t)$. The Hilbert transform is different from the Fourier transform. The signal after the Fourier transform maintains positive and negative frequencies and carries redundant information. The Hilbert transform can eliminate redundant frequencies and reduce frequency band occupation. The analytical expression $s(t)$ of the signal is sampled at the sampling frequency f_s, and the sampled signal is expressed as follows:

$$s(i) = x(i) + jy(i) = A(i)e^{\phi(i)}. \tag{2}$$

Among them, $A(i)$ represents the instantaneous amplitude sequence of the signal, which is expressed as follows:

$$A(i) = \sqrt{\left(x^2(i) + y^2(i)\right)}. \tag{3}$$

The instantaneous phase in the experiment is denoted by the unfolded phase, and $\phi(i)$ represents the unfolded phase sequence of the signal. $\theta(i)$ is the instantaneous phase sequence, and according to the inverse trigonometric function, $\theta(i)$ can be expressed as follows:

$$\theta(i) = \begin{cases} \arctan\left[\dfrac{y(i)}{x(i)}\right], x(i) > 0, \\ \arctan\left[\dfrac{y(i)}{x(i)}\right] - \pi, x(i) < 0, y(i) \le 0, \\ \arctan\left[\dfrac{y(i)}{x(i)}\right] + \pi, x(i) < 0, y(i) > 0, \\ -\dfrac{\pi}{2}, x(i) = 0, y(i) \le 0, \\ \dfrac{\pi}{2}, x(i) = 0, y(i) > 0. \end{cases} \tag{4}$$

The value range of the folding phase $\theta(i)$ is between $(-\pi, \pi)$. The phase used in the experiment is the unfolded phase, and the unfolded phase $\phi(i)$ needs to be obtained from $\theta(i)$ through phase correction. The correction sequence $C(i), C(i)$ used in this process is as follows:

$$C(i) = \begin{cases} C(i-1) - 2\pi, \theta(i+1) - \theta(i) > \pi, \\ C(i-1) + 2\pi, \theta(i) - \theta(i+1) > \pi, \\ C(i-1), \text{others}. \end{cases} \tag{5}$$

According to the above definition, the first value $C(1)$ in the correction sequence cannot be given and the default $C(1)$ is 0. The unfolded instantaneous phase $\phi(i)$ is obtained by adding the folded phase sequence and the modified sequence:

$$\phi(i) = \theta(i) + C(i). \tag{6}$$

The frequency of the continuous signal is differential of the phase. In the sampled signal, the differential relationship is used instead of the differential relationship. The instantaneous frequency $f(i)$ can be defined as follows:

$$f(i) = \frac{1}{2\pi T_s}[\phi(i) - \phi(i-1)]. \tag{7}$$

Among them, T_s is the sampling period.

After obtaining the instantaneous amplitude, instantaneous phase, and instantaneous frequency of the social network crisis data signal, four instantaneous features based on the above three basic information are calculated according to statistical principles. They are the maximum spectral density $\gamma_{\max}$ of the amplitude based on the envelope amplitude, the standard deviation δ_{aa} of the absolute value of the amplitude that is more distinguishable in the high-order social network crisis data type, the standard deviation δ_{ap} of the absolute value of the amplitude, which is more distinguishable in the high-order social network crisis data type, the standard deviation of the absolute value of the phase based on the phase information, and the standard deviation δ_{af} of the absolute value of the frequency based on the frequency information.

The social network crisis data signals based on the amplitude social network crisis data are quite different in the instantaneous amplitude of the envelope, and the amplitude modulation signals of different social network crisis data parameters can be distinguished by using statistical features based on the instantaneous amplitude. This paper mainly uses two statistical features based on the instantaneous amplitude, which are the normalized amplitude maximum spectral density $\gamma_{\max}$ and the normalized amplitude absolute value standard deviation δ_{aa}.

2.1.1. Normalized Amplitude Maximum Spectral Density γ_{max}. $\gamma_{\max}$ is a feature that can distinguish the envelope fluctuation information. $\gamma_{\max}$ can sense small changes in the signal envelope, and the obvious envelope changes are the MASK signal and the MQAM signal. At the same time, the MFSK signal and the MPSK signal also produce subtle envelope changes when the phase is discontinuous. According to formula (3), the instantaneous amplitude sequence $A(i)$ of the social network crisis data signal is obtained, and the instantaneous amplitude average value m_a is calculated as follows:

RETRACTED

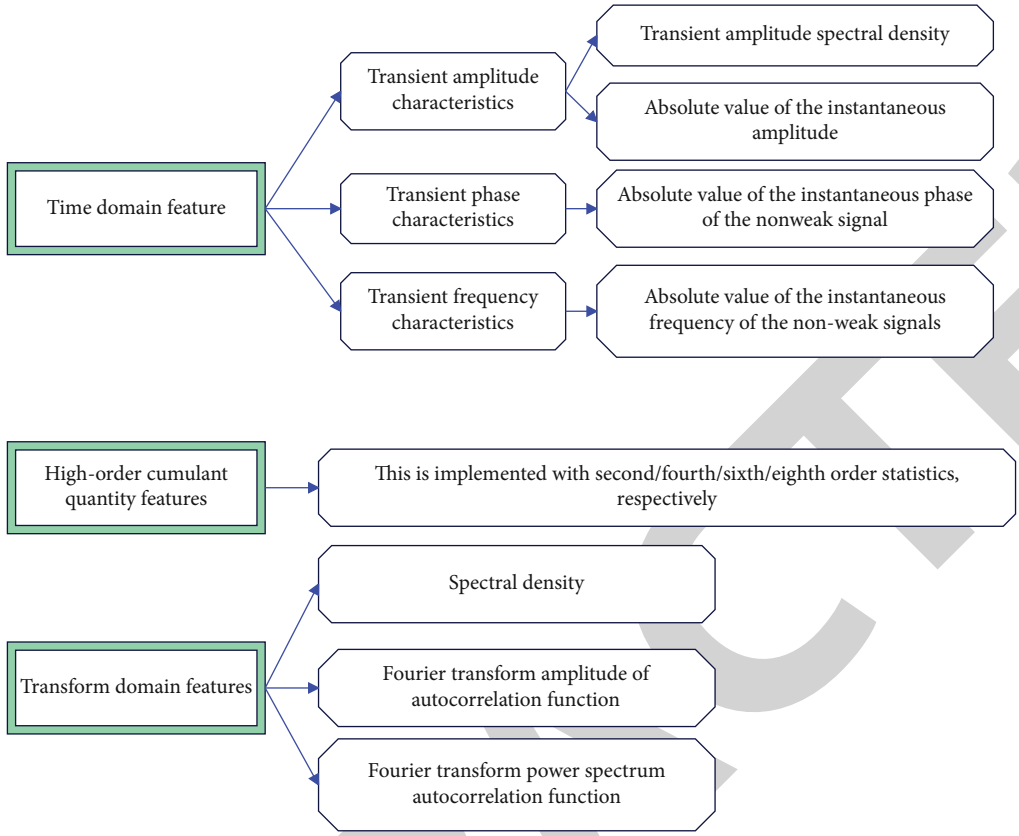

Figure 1: Feature parameters of social network crisis data recognition.

$$m_a = \frac{1}{N_s}\sum_{i=1}^{N} A(i). \tag{8}$$

Among them, N_s represents the number of sampling points, and the zero-center normalization of $A(i)$ is performed to obtain $A_{cn}(i)$:

$$A_n(i) = \frac{A(i)}{m_a}, \qquad A_{cn}(i) = A_n(i) - 1. \tag{9}$$

The normalized amplitude maximum spectral density $\gamma_{\max}$ of the signal is defined by $A_{cn}(i)$, which is as follows:

$$\gamma_{\max} = \frac{\max\left|\mathrm{FFT}\left[A_{cn}(i)\right]\right|^2}{N_s}. \tag{10}$$

Figure 2 shows the normalized magnitude maximum spectral density feature $\gamma_{\max}$ of 13 signal social network crisis data types as a function of the signal-to-noise ratio SNR. The $\gamma_{\max}$ feature is generated based on the instantaneous amplitude and has a good effect on distinguishing the MASK signals that have changes in amplitude during the social network crisis data process and can completely separate the 2ASK, 4ASK, and 8ASK signals from the rest of the signals. When the SNR > 10 dB, the feature $\gamma_{\max}$ can distinguish the 2PSK signal and the 8QAM signal at the same time, and the feature $\gamma_{\max}$ of the remaining signals is similar but different.

2.1.2. Normalized Amplitude Absolute Value Standard Deviation δ_{aa}. δ_{aa} is the feature used to describe the absolute amplitude information of the social network crisis data signal. By calculating the amplitude absolute value deviation of different amplitude modulation signals, δ_{aa} completes the classification of the signals with obvious changes in the absolute value of the envelope. δ_{aa} is particularly effective in identifying high-order signals, which can distinguish different signals such as MASK and MQAM.

$$\delta_{aa} = \sqrt{\frac{1}{N_s}\left(\sum_{i=1}^{N_s} A_{cn}^2(i)\right) - \left(\frac{1}{N_s}\sum_{i=1}^{N_s}\left|A_{cn(i)}\right|\right)^2}. \tag{11}$$

Figure 3 describes the distribution of the feature δ_{aa} of 13 social network crisis data signals under different signal-to-noise ratios, and δ_{aa} is used to characterize the absolute instantaneous amplitude information of the signal, which is clearly distinguished from high-order amplitude-modulated signals. When SNR > 6 dB, the feature δ_{aa} can successfully distinguish MASK signals. At the same time, the feature δ_{aa} is able to distinguish the MQAM signal under a high signal-to-noise ratio.

RETRACTED

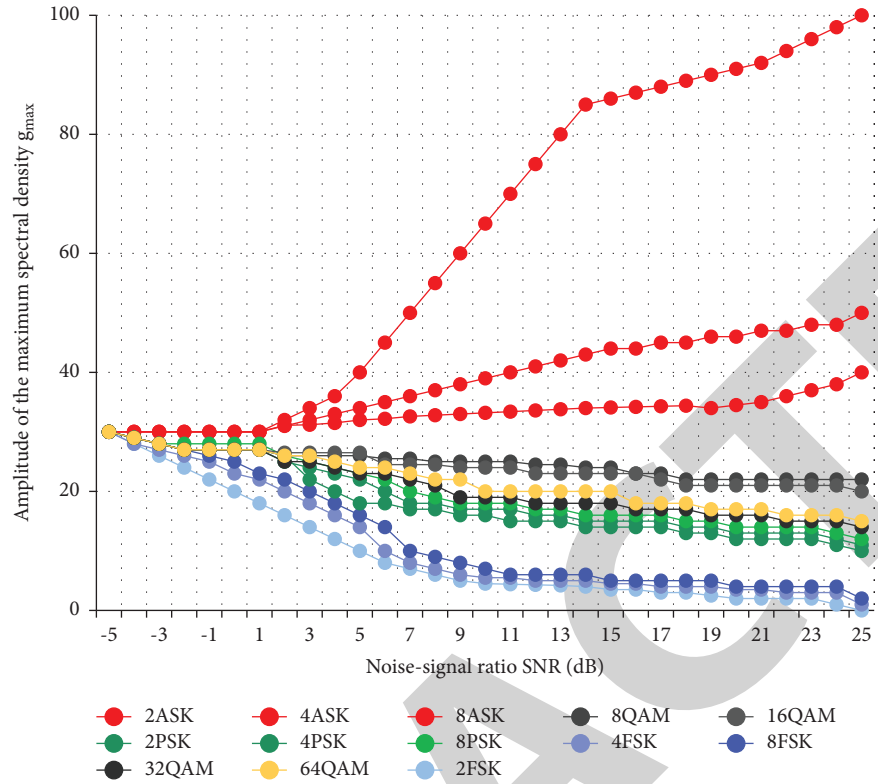

Figure 2: A variation curve of the feature γ_{max} with the signal-to-noise ratio under different social network crisis data methods.

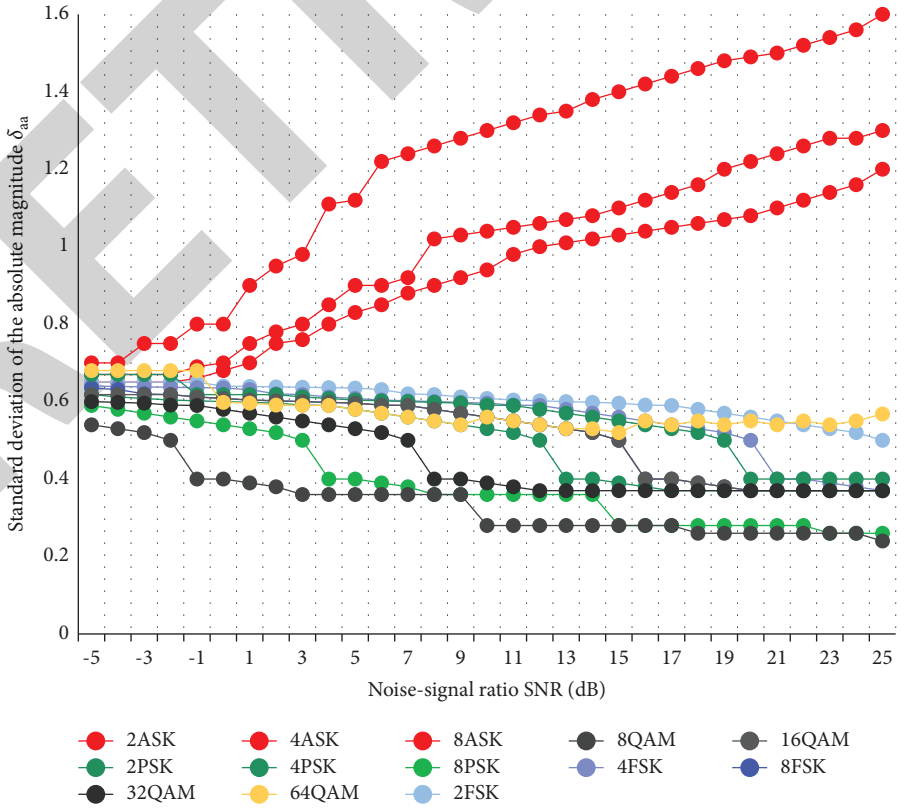

Figure 3: A variation curve of the feature δ_{aa} with the signal-to-noise ratio under different social network crisis data methods.

RETRACTED

The standard deviation δ_{ap} of the phase absolute value is a feature that characterizes the instantaneous phase absolute value of the social network crisis data signal. It is used to distinguish signals with large changes in absolute phase information and has a better effect on high-order MPSK signals. First, we perform zero centering on the phase information.

$$\phi_{NL}(i) = \phi(i) - \frac{2\pi f_c i}{f_s}. \tag{12}$$

In order to ensure the accuracy of the calculation results, the signal segment with strong energy is selected for detection, and the strong and weak signal judgment threshold a_t is set; the feature δ_{ap} is expressed as follows:

$$\delta_{ap} = \sqrt{\frac{1}{C}\left(\sum_{A_n(i) > a_t} \phi_{NL}^2(i)\right) - \left(\frac{1}{C}\sum_{A_n(i) > a_t} \left|\phi_{NL}(i)\right|\right)^2}. \tag{13}$$

f_c and f_s represent the carrier frequency and sampling frequency of the signal, respectively, and C represents the number of signal values that satisfy the nonweak signal decision threshold.

Figure 4 describes the distinction between different signals by δ_{ap}. In the case of SNR > 15 dB, the feature δ_{ap} can accurately distinguish the 2PSK signal and the 4PSK signal, but the 8PSK signal and the rest of the signals produce feature aliasing. Affected by noise, feature δ_{ap} is not highly discriminative to MPSK signals at the low SNR.

The standard deviation δ_{af} of the absolute value of frequency is used to represent the frequency information of social network crisis data signals, which is used to distinguish the social network crisis data signals that are different in the frequency dimension. First, the frequency information is processed to obtain the zero-center normalized frequency $f_N(i)$:

$$m_f = \frac{1}{N_s}\sum_{i=1}^{N_s} f(i) f_n(i) = f(i) - m_f f_N(i) = \frac{f_n(i)}{r_b}. \tag{14}$$

Among them, r_b is the signal rate, and δ_{af} is defined as follows:

$$\delta_{af} = \sqrt{\frac{1}{C}\left(\sum_{A_n > a_t} f_N^2(i)\right) - \left(\frac{1}{C}\sum_{A_n > a_t} \left|f_N(i)\right|\right)^2}. \tag{15}$$

Figure 5 shows the variation of the feature δ_{af} with the signal-to-noise ratio of different social network crisis data methods. It can be seen from the figure that the feature δ_{af} of the MFSK signal is obviously different from other social network crisis data methods, and the feature δ_{af} has a good distinguishing effect on the 2ASK signal when the SNR > 5 dB.

2.2. Higher Order Cumulant Feature Parameters. Another feature used in the study is based on HOC generation, the cumulant of Gaussian white noise is zero, and the high-order cumulant feature can reduce the interference of Gaussian white noise on the signal. Higher order cumulants are an important part of higher order statistical theory. Higher order statistical theory is aimed at statistics above the second order, and its main contents include higher order moments, higher order cumulants, and higher order spectra. The purpose of signal identification is achieved by calculating the cumulative amounts of different social network crisis data signals at various stages and using different settings of the cumulative amounts to distinguish the thresholds of social network crisis data signals. At present, the recognition algorithms based on HOC usually use second-order, fourth-order, and sixth-order cumulants, and cumulants higher than tenth-order are not often used due to the complexity of calculation. In the experiment, the features based on HOC are obtained by the composite use of the second-order, fourth-order, sixth-order, and eighth-order cumulants.

For a continuous random variable x, its probability density function is $f(x)$. The mathematical expectation of the function $g(x)$ is as follows:

$$E\{g(x)\}^{\text{def}} = \int_{-\infty}^{\infty} f(x) g(x) \mathrm{d}x. \tag{16}$$

In particular, when $g(x) = e^{j\omega x}$, there is

$$\phi(\omega)^{\text{def}} = E\left\{e^{i\omega x}\right\} = \int_{-\infty}^{\infty} f(x) e^{j\omega x} \mathrm{d}x. \tag{17}$$

$\phi(\omega)$ is called the first characteristic function. The k-order origin moment m_k and central moment μ_k of a random continuous variable x are defined as follows:

$$\begin{aligned} m_k^{\text{def}} &= E\left\{x^k\right\} = \int_{-\infty}^{\infty} x^k f(x) \mathrm{d}x, \\ \mu_k^{\text{def}} &= E\left\{(x-\eta)^k\right\} = \int_{-\infty}^{\infty} (x-\eta)^k f(x) \mathrm{d}x. \end{aligned} \tag{18}$$

Among them, $\eta = E\{x\}$ represents the first moment of the random variable x. Since the random variable x has zero mean, its k-order origin moment and central moment are equivalent. We set $\omega = 0$ and use the k-th derivative of the first eigenfunction to obtain the k-th moment of x:

$$m_k = E\left\{x^k\right\} = (-j)^k \frac{d^k \phi(\omega)}{d\omega^k}\Big|_{\omega=0} = (-j)^k \phi^{(k)}(0). \tag{19}$$

The k-th order moment of the random variable x is generated by the first characteristic function, and $\phi(\omega)$ is also called the moment generating function. The natural logarithm $\psi(\omega)$ of $\phi(\omega)$ is called the second characteristic function, denoted as follows:

$$\psi(\omega)^{\text{def}} = \ln \phi(\omega). \tag{20}$$

RETRACTED

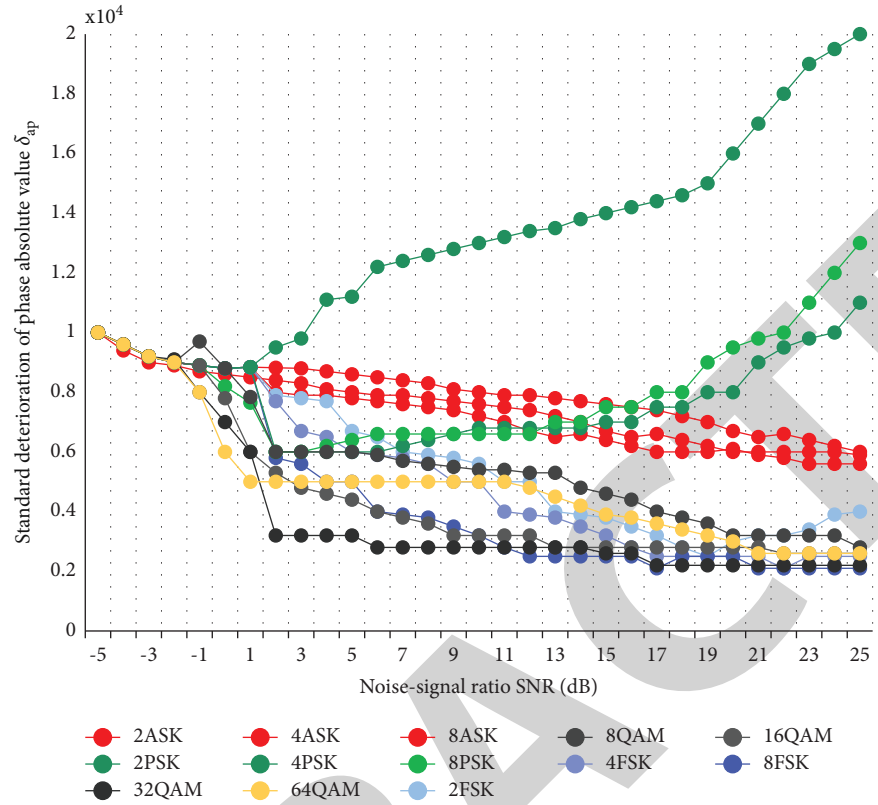

Figure 4: A variation curve of the feature δ_{ap} with the signal-to-noise ratio under different social network crisis data methods.

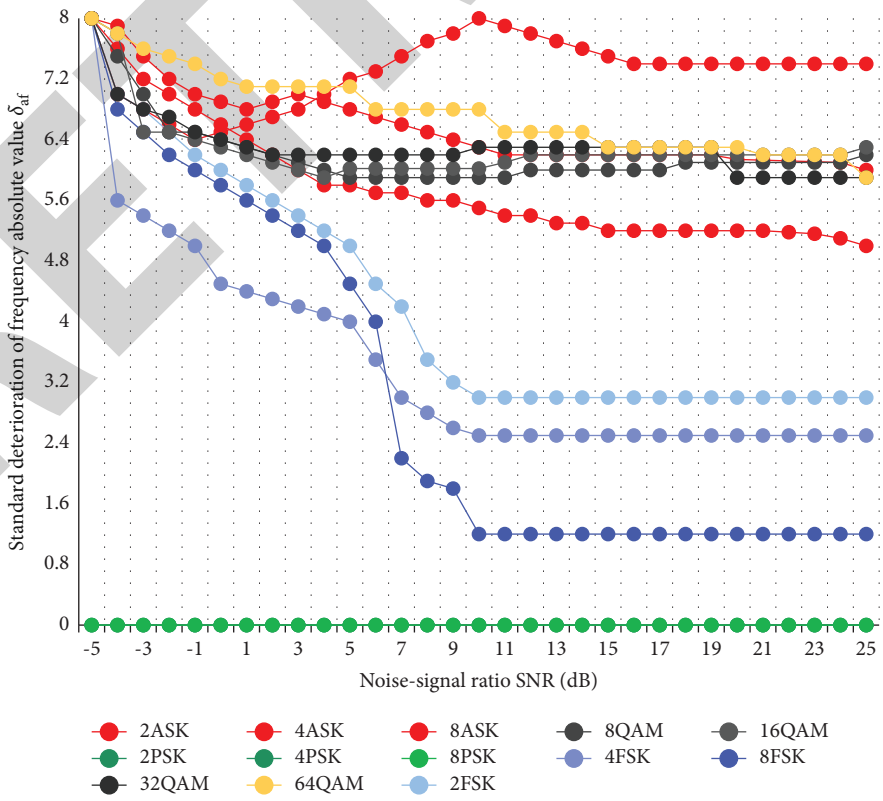

Figure 5: A variation curve of the feature δ_{af} with the signal-to-noise ratio under different social network crisis data methods.

RETRACTED

Similar to the definition of the k-order moment, the k-order cumulant of the random variable x can be defined as follows:

$$c_{kx} = (-j)^k \frac{d^k \ln \phi(\omega)}{d\omega^k}|_{\omega=0} = (-j)^k \psi^{(k)}(0). \tag{21}$$

The second characteristic function is also called the cumulant generating function.

The moment and cumulant are used to calculate the high-order cumulant feature. For the stationary continuous random signal $X(t)$, we set $X_1 = X(t), X_2 = X(t+\tau_1), \ldots\ldots, X_k = X(t+\tau_{k-1})$ and define the k-order cumulant of the random signal as follows:

$$C_{kx}(\tau_1, \tau_2, \ldots\ldots \tau_{k-1}) = \mathrm{Cum}\{X(t), X(t+\tau_1), \ldots\ldots, X(t+\tau_{k-1})\}. \tag{22}$$

Its k-order mixing moment can be expressed as follows:

$$M_{km} = E\left[X(t)^{k-m} X^*(t)^m\right]. \tag{23}$$

Among them, $X^*(t)$ represents the conjugation of $X(t)$. Higher order moments and cumulants have the following conversion relationship:

$$\mathrm{Cum}[X_1, X_2, \ldots\ldots, X_k] = \sum (-1)^{q-1}(q-1)! \prod_{p=1}^{q} E\left\{\prod_{i\in U_p} X_i\right\}. \tag{24}$$

The higher order cumulant of a zero-mean stationary complex random process $X(t)$ is expressed as follows:

The second-order cumulant is

$$\begin{aligned} C_{20} &= \mathrm{Cum}(X, X) = M_{20} = E[X(t)X(t)], \\ C_{21} &= \mathrm{Cum}(X, X^*) = M_{21} = E[X(t)X^*(t)]. \end{aligned} \tag{25}$$

The fourth-order cumulant is

$$\begin{aligned} C_{40} &= \mathrm{Cum}(X, X, X, X) = M_{40} - 3M_{20}^2, \\ C_{42} &= \mathrm{Cum}(X, X, X^*, X^*) = M_{42} - \left|M_{20}^2\right| - 2M_{21}^2. \end{aligned} \tag{26}$$

The sixth-order cumulant is

$$\begin{aligned} C_{60} &= \mathrm{Cum}(X, X, X, X, X, X) = M_{60} - 15M_{40}M_{20} + 30(M_{20})^3, \\ C_{63} &= \mathrm{Cum}(X, X, X, X^*, X^*, X^*) = M_{63} - 9M_{42}M_{21} - 6(C_{21})^2. \end{aligned} \tag{27}$$

The eighth-order cumulant is

$$\begin{aligned} C_{80} &= \mathrm{Cum}(X, X, X, X, X, X, X, X), \\ &= M_{80} - 28M_{60}M_{20} - 36M_{40}^2 + 420M_{40}M_{20}^2 - 630M_{40}^4. \end{aligned} \tag{28}$$

Usually, the complex signal of digital social network crisis data disturbed by noise is expressed as follows:

$$s(t) = x(t) + n(t) = \sum_k a_k \sqrt{E} p(t - kT_s) e^{j(2\pi f_c t + \theta_c)} + n(t). \tag{29}$$

Among them, $k = 1, 2, \ldots\ldots, N, N$ represents the length of the transmitted symbol sequence, a_k represents the symbol sequence, $p(t)$ is the baseband waveform, T_s is the symbol duration, E is the signal energy, and the noise $n(t)$ is zero-mean complex white Gaussian noise. The receiver preprocesses the signal to obtain $s(t)$ as follows:

$$s(t) = \sum_k a_k \sqrt{E} p(t - kT_s) e^{j\Delta\theta_c} + n(t). \tag{30}$$

According to the basic principle of the digital social network crisis data signal, a_k in various digital social network crisis data signals can be expressed as follows: the MASK signal is

$$a_k \in \{(2m - 1 - M)d, m = 1, 2, \ldots, M\}, d = \sqrt{\frac{3E}{(M^2 - 1)}}. \tag{31}$$

The MPSK signal is

$$a_k \in \left\{e^{i2\pi(m-1)/M}, m = 1, 2, \ldots, M\right\}. \tag{32}$$

The MFSK signal is

$$a_k = e^{i2\pi f_k t}. \tag{33}$$

Among them, $f_k \in \{(2m - 1 - M)\Delta f/2\pi, m = 1, 2, \ldots, M\}$.

The MQAM signal is

$$a_k = p_k + jq_k = \sqrt{p_k^2 + q_k^2} \times e^{j\phi_k}, \phi_k = \arctan\left(\frac{q_k}{p_k}\right). \tag{34}$$

Among them, $p_k, q_k \in \{(2m - 1 - \sqrt{M})d, m = 1, 2, \ldots, \sqrt{M}\}, d = \sqrt{3/[2(M-1)]}$.

The experiments use the second-, fourth-, sixth-, and eighth-order cumulants of digital social network crisis data signals to generate four high-order cumulant-based features $T1$, $T2$, $T3$, and $T4$, respectively.

$$\begin{aligned} T_1 &= \frac{|C_{40}|}{|C_{21}|^2}, \\ T_2 &= \frac{|C_{40}|}{|C_{42}|} + \frac{|C_{41}|}{|C_{42}|}, \\ T_3 &= \frac{|C_{63}|^2}{|C_{42}|^3}, \\ T_4 &= \frac{|C_{80}|}{|C_{21}|^2}. \end{aligned} \tag{35}$$

RETRACTED

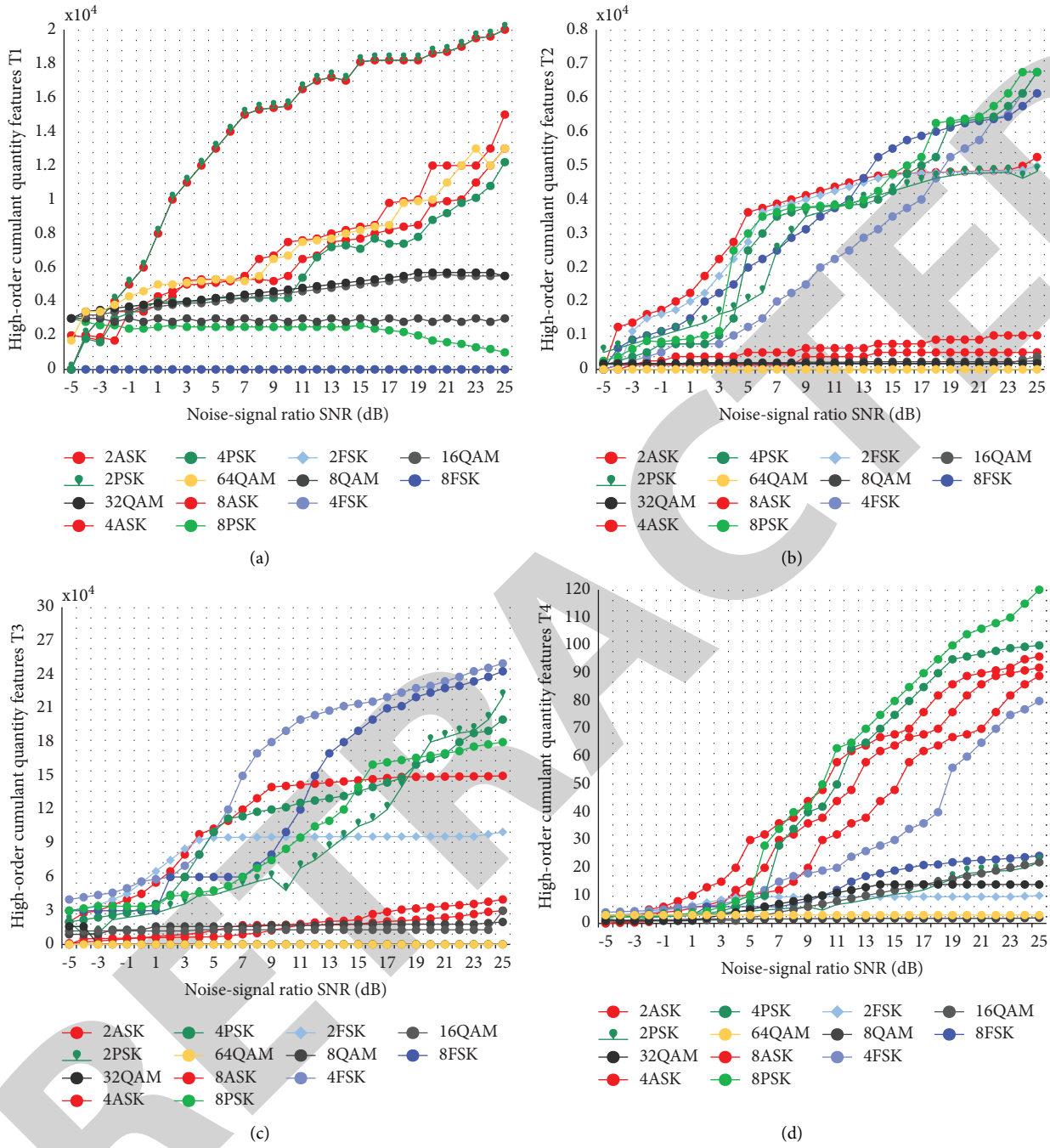

RETRACTED

Figure 6: A variation curve of the feature with the signal-to-noise ratio under different social network crisis. (a) A variation curve of the feature T_1 with the signal-to-noise ratio under different social network crisis data methods. (b) A variation curve of the feature T_2 with the signal-to-noise ratio under different social network crisis data methods. (c) A variation curve of the feature T_3 with the signal-to-noise ratio under different social network crisis data methods. (d) A variation curve of the feature T_4 with the signal-to-noise ratio under different social network crisis data methods.

The four high-order cumulant features T_1, T_2, T_3, T_4 of social network crisis data signals vary with the signal-to-noise ratio SNR as shown in Figure 6.

According to theory, the fourth-order cumulant |C40| of the MFSK signal is 0. Based on this characteristic, the MFSK signal can be distinguished from the rest of the social network crisis data signals. The feature T_1 can successfully separate two ASK signals of 4ASK and 8ASK and three kinds of QAM signals of 16QAM, 32QAM, and 64QAM under the condition of SNR > 5 dB. The feature T_2 can completely distinguish the MFSK signal, 2PSK signal, and 4ASK signal when SNR > 15 dB. The feature T_3 has a good identification effect on 2ASK, 2FSK, and 8FSK signals when SNR > −2 dB and can completely distinguish MPSK signals under the

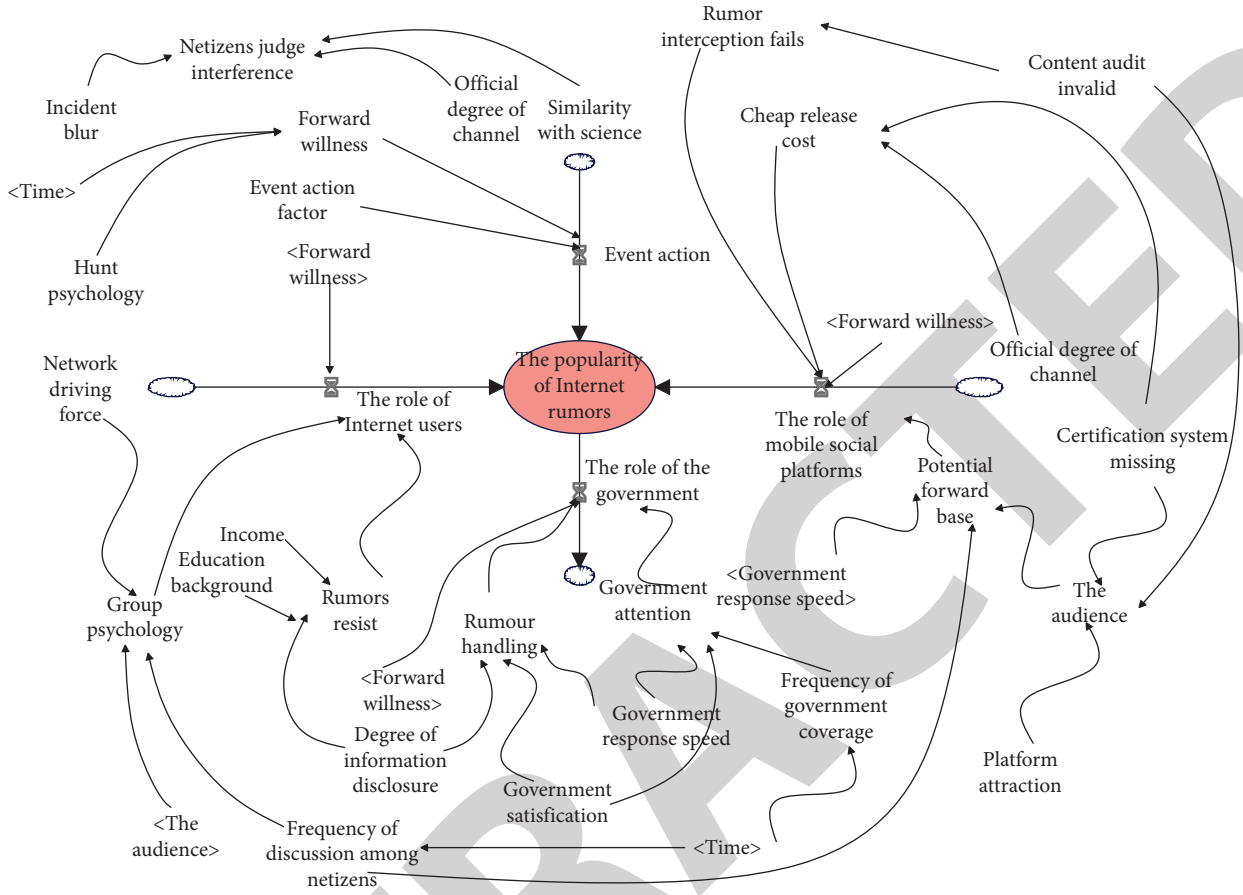

Figure 7: A flow diagram of the rumor-spreading system in the mobile social network.

condition of SNR > 15 dB, and it also has a good distinguishing effect on MFSK and MQAM signals. The feature T_4 has a good effect on distinguishing 13 kinds of social network crisis data signals participating in the experiment. When the SNR > 10 dB, the characteristics of each social network crisis data signal can be clearly separated, and the overall signal differentiation degree is high.

2.3. Transform Domain Feature Parameters. The normalized spectral density is a transform domain feature based on spectral analysis. The spectrum of the signal is P, the normalized spectral density is P_x, and the normalized spectral density statistic S_d obtained by statistical calculation is defined as follows:

$$P_x = \left| \frac{|P|}{E(|P|)} - 1 \right|,$$
$$S_d = \frac{\left| (1/N - 1) \cdot \sum_{n=1}^{N} \left(|P_x(n)| - \overline{P}_x \right)^2 - \overline{P}_x \right|}{\overline{P}_x^2}. \tag{36}$$

The normalized spectral density can effectively realize the distinction between the MASK signal and the MFSK signal. When SNR > 0 dB, the feature S_d can already distinguish MASK signals. In the case of SNR > 15 dB, S_d can accurately separate MASK and MFSK, i.e., two types of social network crisis data signals.

According to the description of the social network crisis data signal, the feature extraction is carried out using the analytical signal sequence $s(i)$ obtained by the social network crisis data signal after the Hilbert transform. The autocorrelation function of $s(i)$ is Fourier transformed, denoted as $A_1(i)$ and then normalized to $A_1(i)$ to obtain the normalized instantaneous amplitude after Fourier transformation, denoted as $A_2(i)$, and the feature A_{auto} is obtained by statistical calculation as follows:

$$A_1(i) = \text{FFT}\{E[s(i)s(i+\tau)]\},$$
$$A_2(i) = \frac{|A_1(i)|}{1/N \sum_{n=1}^{N} |A_1(i)|} - 1, \tag{37}$$
$$A_{\text{auto}} = \frac{D[A_2(i)]}{\{E[A_2(i)]\}^2},$$

When SNR > 3 dB, A_{auto} can distinguish the 2PSK signal and the 8QAM signal, and the discrimination degree of the 2FSK

RETRACTED

Table 1: The identification effect and the control effect of the crisis propagation mode based on the social network.

Number	Crisis identification	Crisis control	Number	Crisis identification	Crisis control
1	88.53	79.79	21	86.05	79.18
2	88.69	80.55	22	86.14	77.61
3	86.50	79.09	23	91.88	81.05
4	87.59	77.44	24	87.76	80.81
5	89.73	79.39	25	88.52	80.19
6	87.94	78.75	26	90.77	81.60
7	87.67	81.11	27	91.03	79.05
8	89.46	80.63	28	88.07	81.05
9	88.62	81.69	29	87.44	76.33
10	88.25	76.31	30	87.70	76.98
11	90.37	80.44	31	87.89	79.79
12	91.92	80.28	32	87.27	76.54
13	88.68	76.36	33	88.37	77.61
14	90.98	76.02	34	89.78	80.76
15	90.05	81.82	35	88.35	76.94
16	88.65	77.88	36	87.51	78.36
17	91.65	78.81	37	90.00	76.14
18	86.94	78.94	38	91.12	80.41
19	91.95	76.09	39	89.44	78.10
20	87.30	80.42	40	86.29	77.76

signal is also very high under the high signal-to-noise ratio, and at the same time, it can distinguish large categories of the MASK signal.

P_{auto} is a feature based on the power spectrum of the autocorrelation function. The Fourier transform is performed on the autocorrelation function of $s(i)$ to obtain the power spectrum $C_2(i)$, and then, the standard deviation coefficient is calculated to obtain P_{auto} as follows:

$$\begin{aligned} A_1(i) &= \text{FFT}\{E[s(i)s(i+\tau)]\}, \\ C_2(i) &= \left|A_1(i)\right|^2, \\ P_{\text{auto}} &= \frac{\sigma[C_2(i)]}{E[C_2(i)]} = \frac{\sqrt{D[C_2(i)]}}{E[C_2(i)]}. \end{aligned} \tag{38}$$

The feature P_{auto} has a high degree of discrimination for different signal categories, and the MASK signal and the MFSK signal clearly belong to different regions. The MASK signal can be effectively distinguished when the SNR ≤ 10 dB, and the 8FSK signal can be distinguished from the rest of the MFSK signal when the SNR ≥ 7 dB.

3. Identification Model of the Crisis Propagation Pattern Based on the Social Network

The system flow diagram refers to the model diagram representing the interaction form of each state variable and its flow rate variable and the interconnection between the feedback loops in the whole system. What must be identified in the system flow diagram are the flow level variable and the flow rate variable. The flow level variable refers to a variable with an accumulation effect, its value is the value of the original time plus the variable that occurs when the change occurs, and the flow level variable is changed from the original value to the current time value by the action of the flow rate variable. In addition, flow rate variables are variables that affect state variables that are constantly changing over time. Based on the determined system boundary problem and causal loop diagram analysis, the system flow diagram that affects the spread of online rumors on the mobile social platform is finally determined as shown in Figure 7.

Combined with the algorithm in the second part, the effect of the social network-based crisis propagation model proposed in this paper is verified and the identification effect and control effect of the crisis propagation model are counted, and the results shown in Table 1 are finally obtained.

From the above research, we can see that the crisis propagation model proposed based on the social network in this paper has an obvious effect of identification and control.

4. Conclusion

The research on the dynamics of crisis communication on complex networks has yielded abundant results. However, due to the complexity of network topology and the evolution mechanism of crisis communication in the network crisis communication system, there are still many drawbacks and difficulties in the study of crisis communication dynamics on complex networks. First, most of the current intervention strategies for network crisis communication only consider the topology of the network while ignoring the characteristic information of crisis communication dynamics itself. How to intervene network crisis communication dynamics based on the characteristics of the network structure and the characteristics of crisis communication dynamics itself needs further exploration by scholars. This paper studies the crisis communication mode of social networks, identifies the crisis communication mode through intelligent methods, and builds an intelligent model. Through experimental

RETRACTED

Hindawi
Journal of Robotics
Volume 2023, Article ID 9872574, 1 page
https://doi.org/10.1155/2023/9872574

Retraction

Retracted: Appearance Design Method of Ceramic Art Based on VR Visualization Technology

Journal of Robotics

Received 8 August 2023; Accepted 8 August 2023; Published 9 August 2023

Copyright © 2023 Journal of Robotics. This is an open access article distributed under the Creative Commons Attribution License, which permits unrestricted use, distribution, and reproduction in any medium, provided the original work is properly cited.

This article has been retracted by Hindawi following an investigation undertaken by the publisher [1]. This investigation has uncovered evidence of one or more of the following indicators of systematic manipulation of the publication process:

(1) Discrepancies in scope
(2) Discrepancies in the description of the research reported
(3) Discrepancies between the availability of data and the research described
(4) Inappropriate citations
(5) Incoherent, meaningless and/or irrelevant content included in the article
(6) Peer-review manipulation

The presence of these indicators undermines our confidence in the integrity of the article's content and we cannot, therefore, vouch for its reliability. Please note that this notice is intended solely to alert readers that the content of this article is unreliable. We have not investigated whether authors were aware of or involved in the systematic manipulation of the publication process.

Wiley and Hindawi regrets that the usual quality checks did not identify these issues before publication and have since put additional measures in place to safeguard research integrity.

We wish to credit our own Research Integrity and Research Publishing teams and anonymous and named external researchers and research integrity experts for contributing to this investigation.

The corresponding author, as the representative of all authors, has been given the opportunity to register their agreement or disagreement to this retraction. We have kept a record of any response received.

References

[1] H. Li, "Appearance Design Method of Ceramic Art Based on VR Visualization Technology," *Journal of Robotics*, vol. 2022, Article ID 7664404, 11 pages, 2022.

Hindawi
Journal of Robotics
Volume 2022, Article ID 7664404, 11 pages
https://doi.org/10.1155/2022/7664404

RETRACTED

Research Article

Appearance Design Method of Ceramic Art Based on VR Visualization Technology

Hui Li

College of Fine Arts, Anhui Normal University, Wuhu 241003, China

Correspondence should be addressed to Hui Li; zaozao@ahnu.edu.cn

Received 29 July 2022; Revised 31 August 2022; Accepted 6 September 2022; Published 10 October 2022

Academic Editor: Shahid Hussain

Copyright © 2022 Hui Li. This is an open access article distributed under the Creative Commons Attribution License, which permits unrestricted use, distribution, and reproduction in any medium, provided the original work is properly cited.

In order to improve the effect of ceramic art appearance design, this work studies the appearance design method of ceramic art combined with VR visualization technology and builds an intelligent model. According to the needs of the industrial site and the requirements of the lighting system, the area type of the lighting area is determined in this study, and the light of the virtual ceramic product is irradiated on the target detection plane through the refraction of the lens. Based on the Lambertian luminescence characteristics of the point light source virtual ceramic products and the uniform distribution of illuminance on the lighting surface, a mathematical model of the lighting system is established. Taking the realization of a rectangular lighting area with high uniformity as the main goal, the mathematical model is used to construct a system of partial differential equations of free-form surfaces, and the effect of the method in this study is verified by combining with the simulation research. The experimental research shows that the appearance design system of ceramic art based on VR visualization technology proposed in this study has a good effect and can effectively improve the interaction effect of appearance design of ceramic art.

1. Introduction

As a branch of artistic design, ceramic art creation is the material and spiritual result of production. It not only meets people's material needs but also meets people's spiritual needs. It is a perfect combination of aesthetic and practical functions. Art design is a highly comprehensive independent art discipline, mainly involving social, economic, cultural, technological, commercial, and other factors. Moreover, its aesthetic cognition and creative needs change with the changes of various factors such as these. Creative ability is one of the most important elements in art design, and it is the comprehensive performance of the designer's comprehensive quality, that is, expressive ability, perception ability, and imagination ability. Although the design of each major is different, the basic elements that make up the art are the same. The creation of ceramic art has roughly the same requirements for aesthetic cognition, metrical order, and rhythm. Therefore, it can be said that the creation of ceramic art integrates the two aspects of material creation and spiritual creation in the development of human society and is an indispensable product in social civilization.

Composition means that the visual elements in the two-dimensional space of the visual plane, according to the beautiful visual effects, use the principles of mechanics to rearrange and combine points, lines, and surfaces and create images based on rational and logical reasoning. The principle of orderly arrangement between shapes. Although it is not a study of the interior of an object, but a study of the manifestation of the external form of the object, it requires the shape to reflect the internal principle [1]. In modern design activities, the composition language is reflected in all fields of design and almost covers all kinds of design modeling methods. No design can be separated from a constitutive language. The composition language stimulates the designer's rich imagination and creativity and opens up different design ideas from the past [2]. On the basis of rational thinking, constitutive language has strong visual laws and artistic expression in the teaching theory of "Bauhaus." This theoretical system of composition has

influenced many countries such as the Netherlands, Switzerland, Hungary, the United States, and Japan [3]. Constructivism expresses the basic elements of modeling, and the condition required for its modeling is to abandon general forms and strip away those expressive qualities and subjective diagrams. This stripped shape becomes a conceptual form without characteristics. The recombined graph has all the attributes that make up the language [4]. According to the principle of composition, any form can be rearranged and combined. The forms that constitute objects mainly include natural forms and abstract forms. Therefore, the composition is divided into the natural form and the abstract form [5]. The composition of natural form is a form based on the natural form itself. This method of composition maintains the characteristics of the original form and reconstructs another image by breaking up, separating, ordering, and reconstructing the whole or part of the image [6]. The composition of abstract forms is based on abstract geometric images, that is, elements such as language points, lines, and surfaces are formed, and various arrangements and reorganization of geometric figures are carried out. The method is to use the geometric form as the constituent element and then make a regular combination and arrangement [7]. Modern pottery creation is a utensil and medium through which artists use clay as a material carrier to convey aesthetic emotions and realize individual spiritual value, while modeling is the physical gesture of pottery works created by various artistic means. The most important carrier of aesthetic taste is also the most intuitive visual element that works present to people. The characteristics of modern pottery modeling and the aesthetic performance effect presented are the embodiments of the artist's comprehensive ability. Different modeling structures produce different tension effects, resulting in different visual impacts and psychological feelings. Therefore, modeling has become the most critical factor for an artist to express tension [8].

Vision is most sensitive to color, and color is more perceptual than shape. The emotion aroused by color itself is an internal psychological tension, so under certain conditions, color is more tense than shape [9]. In modern pottery art, color always accompanies all stages of creation; from different clay materials, different metal glazes, to different firing forms, each stage produces different color changes, but color is very important in modern pottery art. It must be attached to a certain morphological space to express emotions, which requires artists to cooperate with the shape of the work according to the physical properties and emotional needs of color when creating, and skillfully use firing, a special link that is different from other art categories, to create color. The contrast changes between them thus trigger the tension performance, which can clearly show the characteristics of the work and the theme of the design, impress the viewer, and convey the information while giving people a sense of aesthetic enjoyment [10].

Ceramic modeling detail design includes two meanings of ceramic modeling design and detail design. The former is the design of the overall ceramic shape, including height, size, and proportion, and the ceramic shape design is considered from an overall perspective; the latter is some parts included in the overall ceramic shape, such as shoulders, mouths, feet, buttons, and abdomen. The design of the partial close-up [11]. Specifically, for the details of a ceramic utensil, such as the handle and the pot flow, which are reflected in the overall ceramic utensils, by better controlling the detail design, the entire utensil will be more aesthetically perfect, making it more perfect. The information on display is richer, making the appreciator more obsessed with him. Ceramic modeling is a basic form of independent existence of ceramics for daily use and furnishings. The generation and development of this form are closely related to human production and life activities [12]. In order to meet the needs of people's daily production and life and with the development and progress of society, the improvement of human living conditions and the improvement of ceramic shapes are also enriched and diversified. It is more in line with its function and aesthetic value. With its own unique form, ceramic modeling brings people the enjoyment of beauty and enriches people's spiritual and cultural life [13]. At the beginning of the creation, the main purpose of the shape of pottery was to meet the practicality. With the differentiation of social classes, the shape of some utensils was separated from the practical function and then transformed into ritual utensils and even developed into pure display. Up to now, ceramics of different shapes and functions have been created. With the demand for aesthetics, people have created various types and forms of ceramic shapes to enrich their lives. Therefore, ceramic modeling is not only the needs of human material life but also serves the spiritual and cultural life of human beings. Its production, development, enrichment, and innovation are inseparable from human life [14]. In contemporary times, ceramic modeling art is a category of art. With the introduction of modern art concepts, the boundary between the practical function and the display function of ceramic modeling is becoming more and more blurred, and even integrated, and more designers are designers. Or the emotional expression and emotional communication of ceramic artists for ceramic plastic arts [15]. Detail design can also be referred to as design detail. The design here is perceptual design, artistic creation, and detail design is perceptual artistic creation of small links. It includes artistic practice and artistic creation in people's daily life and is embodied in some designs that can serve people's production and life, such as architecture, plane, sculpture, industry, and other fields [16].

In order to improve the effect of appearance design of ceramic art, this work studies the method of appearance design of ceramic art combined with VR visualization technology and constructs an intelligent model to promote the development of appearance design of ceramic art technology.

2. VR Visualization Technology

2.1. Basic Concepts of Nonimaging Optics

2.1.1. Luminous Flux and Luminous Efficiency. The luminous flux represents the amount of light emitted from the LED light-emitting surface per unit time, and its unit is

RETRACTED

lumens (lm). Luminous flux is generally discussed with luminous efficiency. The unit of luminous efficiency is lumens/watt (lm/W), which represents the amount of light emitted by a unit of power LED in a unit of time. As a new type of high-efficiency light source, the luminous efficiency of LED is generally above 100 lm/W.

2.1.2. Luminous Intensity. Luminous intensity, also known as light intensity, refers to the average Poynting vector flowing through a point in the light field. In photometry, it refers to the size of the luminous flux $d\phi$ within a unit solid angle $d\omega$, the unit is candela, and its abbreviation is cd, which is represented by I.

$$I = \frac{d\phi}{d\omega}. \tag{1}$$

2.1.3. Illumination. Different from light intensity, in photometry, illuminance characterizes the luminous flux $d\phi$ received on a unit area dS, and the unit is Lux, which is represented by E in this study.

$$E_T = \frac{d\phi}{dS}. \tag{2}$$

2.1.4. Brightness. Brightness describes the reflective ability of an object in a lighting environment, representing the luminous intensity per unit projected area $dA \cos \theta$. Different from irradiance, brightness represents the reflection intensity of the illuminated object in the human eye, which is a concept describing the senses. When the human eye sees the illuminated object in a certain direction, the brightness is equal to the ratio of the light intensity of the object in this direction to the unit projected area of the object in this direction, usually expressed by L, and the unit is candela/square meter ($c\ d/m^2$).

$$L = \frac{d\phi}{d\omega dA \cos \theta}, \tag{3}$$

where dA represents the unit area, $d\omega$ represents the unit solid angle, and θ is the angle between the given direction and the normal direction of the unit area dA.

2.1.5. Radiation Intensity. The radiant intensity belongs to radiometry, and its meaning refers to the radiant flux E emitted by a point light source within a unit solid angle $d\omega$ in a transmission direction, and the unit is W/sr, which is expressed by I_e in this study:

$$I_e = \frac{d\phi}{d\omega}. \tag{4}$$

2.1.6. Irradiance and Irradiance Uniformity. Irradiance refers to the radiant flux received on a unit plane, and its unit is W/m^2, which is expressed by E_e in this study. On the other hand, the radiant output degree represents the radiant flux emitted to the hemispherical space per unit area dS in the unit time dt.

$$E_e = \frac{d\phi}{dS}. \tag{5}$$

Irradiance uniformity is an important evaluation index in the field of lighting design. Its meaning is the ratio of the average irradiance value E_{Ave} to the maximum irradiance value E_{Max} on the target lighting surface:

$$\overline{E} = \frac{E_{\text{Ave}}}{E_{\text{Max}}}. \tag{6}$$

2.1.7. Lighting Efficiency. Lighting efficiency is another important evaluation index in the field of lighting design. In this study, lighting efficiency refers to the ratio of the emitted luminous flux ϕ_r of the LED light source received by the target lighting surface to the total luminous flux ϕ_s emitted by the LED light source in the experimental results:

$$Q = \frac{\phi_r}{\phi_s}. \tag{7}$$

2.1.8. Bidirectional Reflection Distribution Function. The bidirectional reflection distribution function (BRDF) characterizes the reflection characteristics of an object surface reflecting light energy from any incident direction to any viewpoint direction. There is a proportional relationship between the irradiance value of the emitted light of the LED light source irradiating the discrete point of diffuse reflection and the radiation output E_e reflected from the point, and this proportional relationship is the reflectivity ρ. In this study, the BRDF function is introduced to describe the optical characteristics of the diffuse reflection surface, and the Lambertian model is used as the outgoing model of the diffuse reflection material. It is not difficult to obtain:

$$\begin{cases} \phi_e = \int d\phi_e = \int I_e d\omega = \int L_e dS \cos \theta d\omega = \int L_e dS \cos \theta \sin \theta d\theta d\varphi = \pi L_e S, \\ E_T = \dfrac{\phi_e}{S} = \rho E_e. \end{cases} \tag{8}$$

RETRACTED

Among them, ϕ_e represents the radiant flux, L_e represents the radiance, ω represents the solid angle, and ρ represents the reflectivity of the diffuse reflection material. It is not difficult to deduce the expression of BRDF from (8) as

$$\text{BRDF} = \frac{\rho}{\pi}. \tag{9}$$

2.2. Design Method of LED Secondary Optics. An LED is a solid-state semiconductor device that converts electrical energy directly into light energy. LED lights have many features, including low operating voltage, low power consumption, high luminous efficiency, and long life. In terms of energy saving, since the power consumption of LED is 20% of that of incandescent lamps and 50% of that of fluorescent energy-saving lamps, it can be seen that LED will become the main light source in the field of energy-saving lighting.

The free-form surface lighting design of the lens follows two basic laws: Snell's law and the law of conservation of energy. Snell's law specifies the deflection of light by the curved surface, which realizes the redistribution of light energy. The law of energy conservation defines the relationship between the incident light energy and the output light energy of the free-form surface lighting system and determines the energy transmission efficiency of the system.

Free-form surface design is generally carried out using three methods.

The first method is trial and error. Initially, the basic outline of the free-form surface is determined, and then, repeated changes of the value are used to perform multiple inspections and resolve errors to achieve the best results for the data it presents. This continuous process of change and observational analysis is carried out by computer programs. When designing free-form surfaces by this method, the mold that has been used as a real object is often used. Then, the free-form lens is automatically optimized by the Monte Carlo simulation method or differential evolution algorithm on the computer, or the improved design of the lens is directly performed by the nonimaging condenser. However, for the free-form surface directly represented by the spline curve, it is necessary to use the data of constantly changing nodes on the curve to optimize. In different classical free-form surface designs, the method of determining the initial point and then continuously modifying it is an efficient method that often achieves results. Since the design surface cannot be expressed by specific equations, it is impossible to manually correct the data to obtain a good optimization. Of course, it adds a lot of difficulties in the design and makes the optimization process more cumbersome and wastes a lot of time.

The second method is the analytical method of partial differential equations. That is, the free surface is designed by solving a set of partial differential equations. The establishment of this equation system is determined by the position of the light source point of the lighting fixture and the lighting surface. Its parameters are based on the normal vector and tangent vector on the free-form surface, so by means of the equation result obtained by the equation, the design value of the design surface can be directly obtained to achieve the ideal lighting result. This avoids the time wasted by the trial and error method and greatly improves the work efficiency of the designer.

The third method is simultaneous multiple surface, or SMS for short, which means that multiple optical surfaces can be designed simultaneously. The principle is actually similar to the second method, but it is aimed at the modeling calculation of the area surface.

First, it is necessary to establish a coordinate system including the light source, free-form surface, and illumination area, as shown in Figure 1.

The coordinate system is established with point $0, 0'$ as the coordinate origin, and if 0 is the center of the $C - \gamma$ ball, $0'(x_1, y_1, z_1)$ can be expressed as the following equations:

$$\begin{cases} x_1 = \rho(C, \gamma)\cos C \sin \gamma, \\ y_1 = \rho(C, \gamma)\sin C \sin \gamma, \\ z_1 = \rho(C, \gamma)\cos \gamma. \end{cases} \tag{10}$$

Then, the algebraic expression of the incident ray $00'$ can be expressed by the coordinates of the above formula $0'(x, y, z)$ as given in the following equation:

$$\overrightarrow{I} = xi + yj + zk. \tag{11}$$

Equation (12) is obtained by substituting equation (10) into equation (11), and by unitizing the incident ray $00'$,

$$\begin{aligned} \overrightarrow{I} = {} & i\rho(C, \gamma)\cos C \sin \gamma + j\rho(C, \gamma)\sin C \sin \gamma \\ & + k\rho(C, \gamma)\cos \gamma, \end{aligned} \tag{12}$$

$$\overrightarrow{I}' = i \cos C \sin \gamma + \sin C \sin \gamma + k \cos \gamma. \tag{13}$$

Taking $0'$ as the center of ball $\theta - \varphi$, $R(x_2, y_2, z_2)$ can be expressed as

$$\begin{cases} x_2 - x_1 = \rho(\theta, \varphi)\cos \theta \sin \varphi, \\ y_2 - y_1 = \rho(\theta, \varphi)\sin \theta \sin \varphi, \quad \theta\varepsilon[0, 2\pi]\varphi\varepsilon[0, \pi], \\ z_2 - z_1 = \rho(\theta, \varphi)co\varphi. \end{cases} \tag{14}$$

Then, the coordinate $O'(x, y, z)$ of the above formula can represent the refracted ray, and in the same way, the unit algebra of the outgoing ray $O'R$ can be expressed as

$$\overrightarrow{I}' = i \cos \theta \sin \varphi + j \sin \theta \sin \varphi + k \cos \varphi. \tag{15}$$

The following equation is derived from Snell's law.

$$\overrightarrow{N} = n_R \overrightarrow{R} - n_I \overrightarrow{I}'. \tag{16}$$

In the equation, n_R is the refractive index of the medium where the refracted light is located, and n_I is the refractive index of the medium where the incident light is located. Then, the normal vector on the free-form surface is

RETRACTED

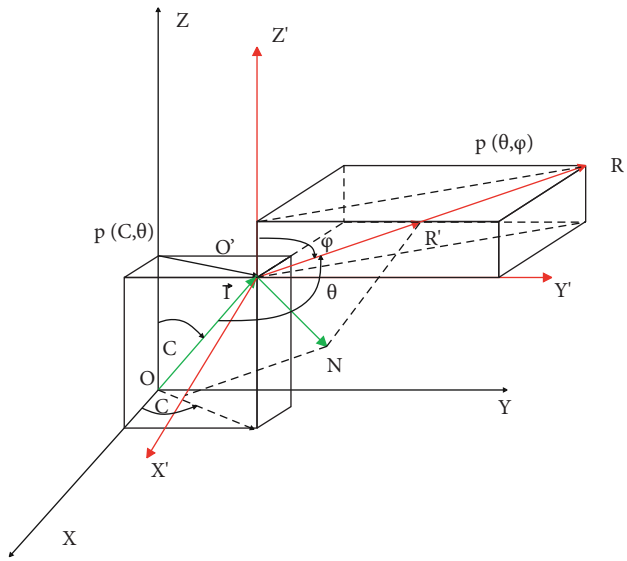

Figure 1: Light refraction path in a dual coordinate system.

$$\vec{N}\left(N_x, N_y, N_z\right) = \begin{cases} n_R \cos\theta \sin\varphi - n_I \cos C \sin\gamma, \\ n_R \sin\theta \sin\varphi - n_I \sin C \sin\gamma, \\ n \cos\varphi - n \cos\gamma. \end{cases} \tag{17}$$

Since $\vec{N}$ is a normal vector on the surface, the tangent vector $\vec{T}$ of the surface should be perpendicular to it, that is,

$$\vec{N} * \vec{T} = 0. \tag{18}$$

If it is assumed that there are any two points $A(x_a, y_a, z_a), B(x_b, y_b, z_b)$ on the free-form surface and the two points AB are close enough, the tangent vector $\vec{T}$ here can be expressed as

$$\vec{T} = (x_b - x_a)i + (y_b - y_a)j + (z_b - z_a)k. \tag{19}$$

The tangent vector can be expressed as

$$\begin{cases} (x_b - x_a) = \Delta\rho \times \dfrac{\partial x}{\partial \rho}, \\ (y_b - y_a) = \Delta\rho \times \dfrac{\partial y}{\partial \rho}, \\ (z_b - z_a) = \Delta\rho \times \dfrac{\partial z}{\partial \rho}. \end{cases} \tag{20}$$

Equation (20) is substituted into equation (19) to obtain

$$\vec{T} = \Delta\rho\left(\frac{\partial x}{\partial \rho} i + \frac{\partial y}{\partial \rho} j + \frac{\partial z}{\partial \rho} k\right). \tag{21}$$

By deriving, transforming, and substituting the partial differential of equation (10) into equation (21) and then substituting it into equation (18), the following partial differential equation of the correlation between the free-form surface and the light-emitting angle of the light source is obtained through simplification.

$$\frac{\partial \rho}{\partial C} = \frac{\rho \cdot n_R \sin\gamma \sin\varphi \sin(\theta - C)}{n_I - n_R(\sin\gamma \sin\varphi \cos(\theta - C) + \cos\gamma \cos\varphi)}, \tag{22}$$

$$\frac{\partial \rho}{\partial \gamma} = \frac{\rho \cdot (n_R \sin\gamma \sin\varphi - n_R \cos\gamma \sin\varphi \cos(\theta - C))}{n_R(\sin\gamma \sin\varphi \cos(\theta - C) + \cos\gamma \cos\varphi) - n_I}. \tag{23}$$

3. Appearance Design Virtual System of Ceramic Art

The specific process of 2D image modeling generation and evaluation is shown in Figure 2. In the design process, the ellipse Fourier coefficient data of the preliminary individual two-dimensional modeling plan completed by the designer is added to the data matrix of the overall modeling sample, and its principal component score is calculated. The data perturbation of the added individual scheme to the principal component data matrix of the overall modeling sample is very small and can be ignored. Therefore, the key principal component score of the individual scheme corresponding to each target image is substituted into the modeling image prediction model based on the key principal component, and the target image value of the scheme is obtained. Then, the target image values of the remaining plans are calculated in sequence, and the perceptual image evaluation of all the two-dimensional modeling plans is completed. After that, the optimal two-dimensional modeling scheme is determined with reference to the overall design objectives. If the optimal solution still does not meet the overall design objectives, after comparing the differences, determine the optimization direction of the optimal solution. In the process of clarifying the optimization direction, it is judged whether there is a consistent correlation between the key principal component scores of the optimal plan and the target image data. If the correlation exists, the key principal component scores of the changed optimal solution are refitted to generate a new optimal two-dimensional modeling solution. Conversely, the scheme is optimized by adjusting the associated modeling features associated with the target image. In this process, a normality test is first performed on the principal component scores of the overall modeling sample.

In order to support image-oriented color generation and evaluation, a comprehensive evaluation model based on color imagery and a color multi-image optimization model based on gray correlation analysis are proposed, as shown in Figure 3.

The simulation system sets the system functions according to the implementation program of the ceramic product appearance image design technology. It includes four functional modules: sample information, target image, multiobjective optimization, and multiattribute decision-making. In order to realize the functions of each module of the simulation system, the four modules are used as independent modules to be programmed with MATLAB software, respectively, during development, as shown in Figure 4.

RETRACTED

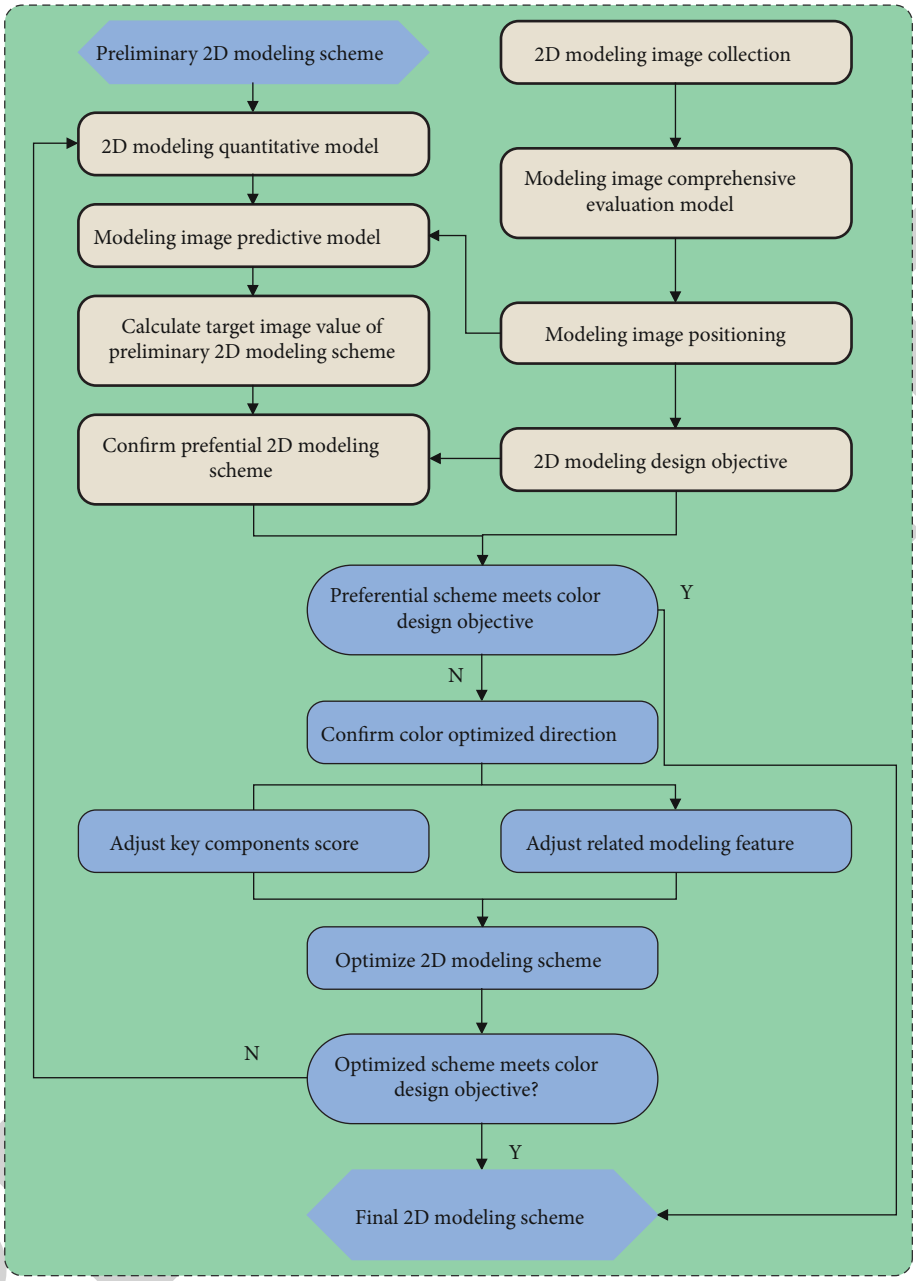

Figure 2: Modeling generation and evaluation process.

The structure of the real-time data simulation system is shown in Figure 5. It is divided into a three-dimensional display module, a network communication module, a data communication module, and a data synchronization module.

The modeling image of ceramic art products is the emotional response of users triggered by the modeling part of the appearance of ceramic art products. The purpose of positioning is to determine the typical representative emotional responses of users to the overall modeling samples of the target ceramic art product and use several modeling target image adjectives and their perceptual image evaluation data matrix as the quantitative output of the positioning results. The scientific positioning of modeling image is of great significance to the image modeling design of ceramic art products oriented to user sensibility. The output data can truthfully reflect consumers' diverse emotional needs for ceramic art product modeling and provide reliable modeling image data and clear design goals for data-driven ceramic art product appearance image design, as shown in Figure 6.

Modern ceramic art creation adds modern elements on the basis of traditional ceramic art, so that ceramic art works show ever-changing and colorful personalities. Moreover, most of the modern ceramic art creations use elements such as points, lines, and surfaces to create some three-dimensional, two-dimensional, or three-dimensional and two-dimensional modern decorative works. This makes more

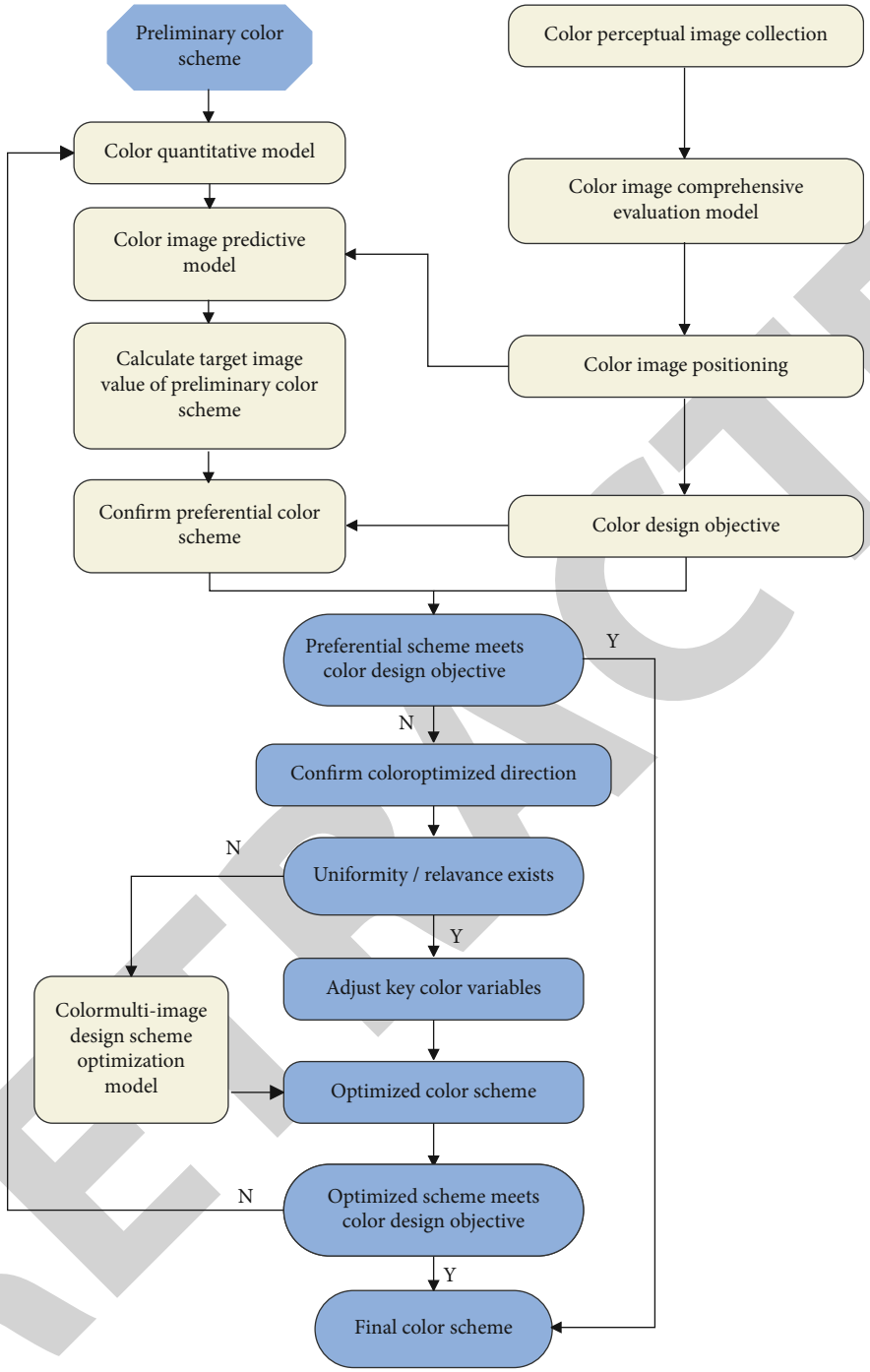

Figure 3: The process of color generation and evaluation of ceramic art.

and more modern ceramic art works form a simple but not simple unique charm and appeal. Through the method of three-dimensional construction, the plane material is cut, folded, hollowed out, and other construction means, so that the plane material can produce a three-dimensional effect. This creative element is reflected in ceramic works not only for the decoration of ceramic surfaces but also in the shape of ceramic art works. It can be said that point, line, and surface elements are ubiquitous for modern design, and the rational use of composition techniques can make modern ceramic art more in line with the characteristics of the times. As shown in Figure 7, the appearance design of ceramic art is carried out in combination with VR visualization technology, as shown in Figure 7.

The three-dimensional composition method is also expressed in various ways in ceramic decoration (Figure 8). It can use the stacking of colored glaze and pottery mud, or it can be cut, hollowed out, stacked, and other texture expressions on the surface of the body to form a unique decorative effect. The use of dots is more obvious in

RETRACTED

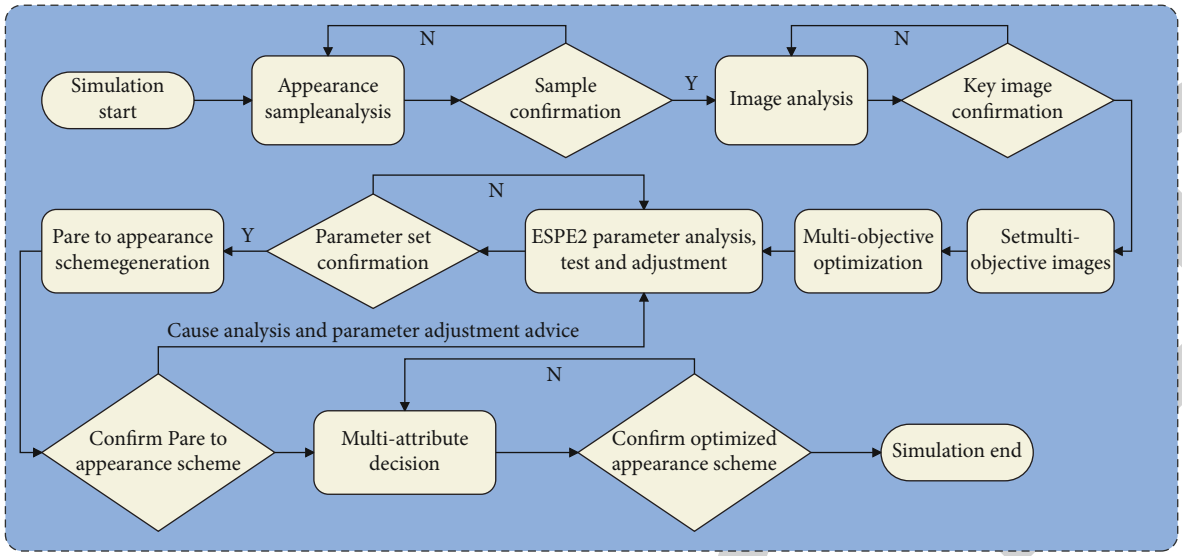

Figure 4: Application process of the simulation system.

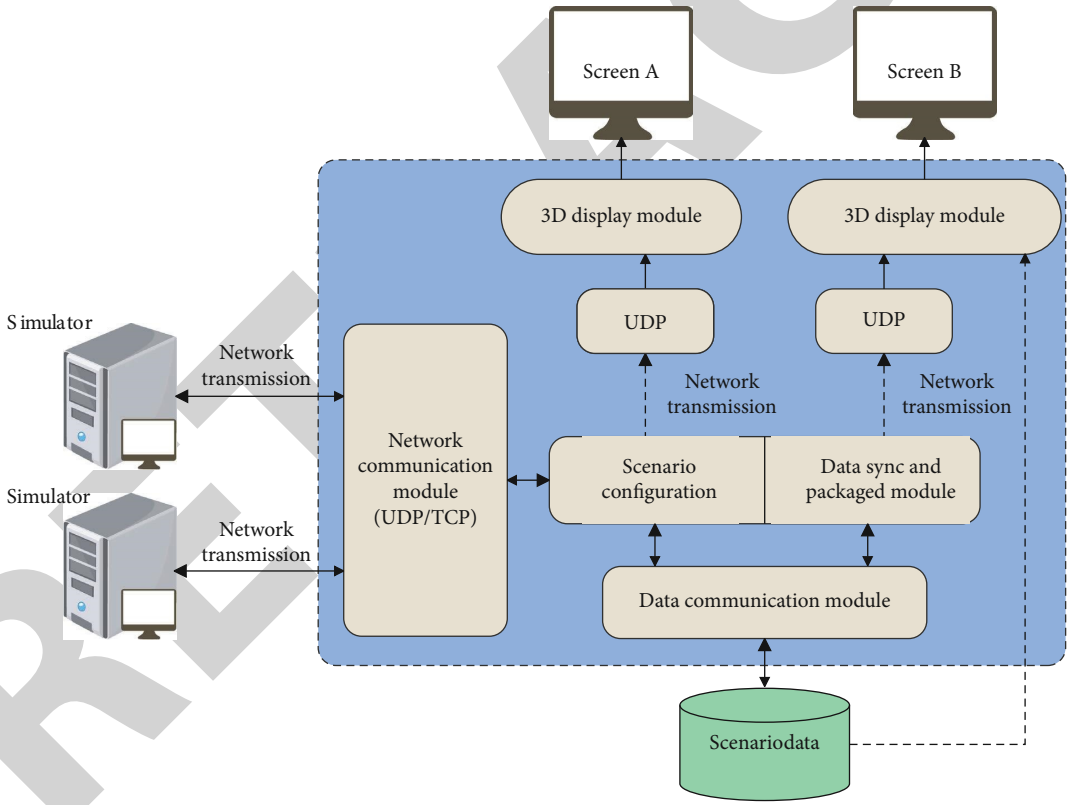

Figure 5: Simulation design module of real-time data.

decoration than in modeling. It reflects the personality of movement and stillness in modern ceramic art through the virtuality, density, size, color, shape, and texture of the dots. There are several ways of expressing lines in decoration, such as the calmness and composure of horizontal lines, the majesty and toughness of vertical lines, the softness of curves, the stuttering of broken lines, and the tension and transformation of intersecting lines. These add a bit of dynamism to the artistic language of modern ceramic art. The lines drawn using blue and white, pastel, and other materials in the creation of modern ceramic art are both modern and traditional. The three-dimensional lines form a rhythmic sense of staggered heights, lined with each other, and dense and dense with the help of the easy-to-form characteristics of the ceramic art material itself. The surface can be expressed by the combination of dots and lines in the decoration of ceramic art. With the shape of the ceramic art, a reasonable layout is carried out to make the utensils more

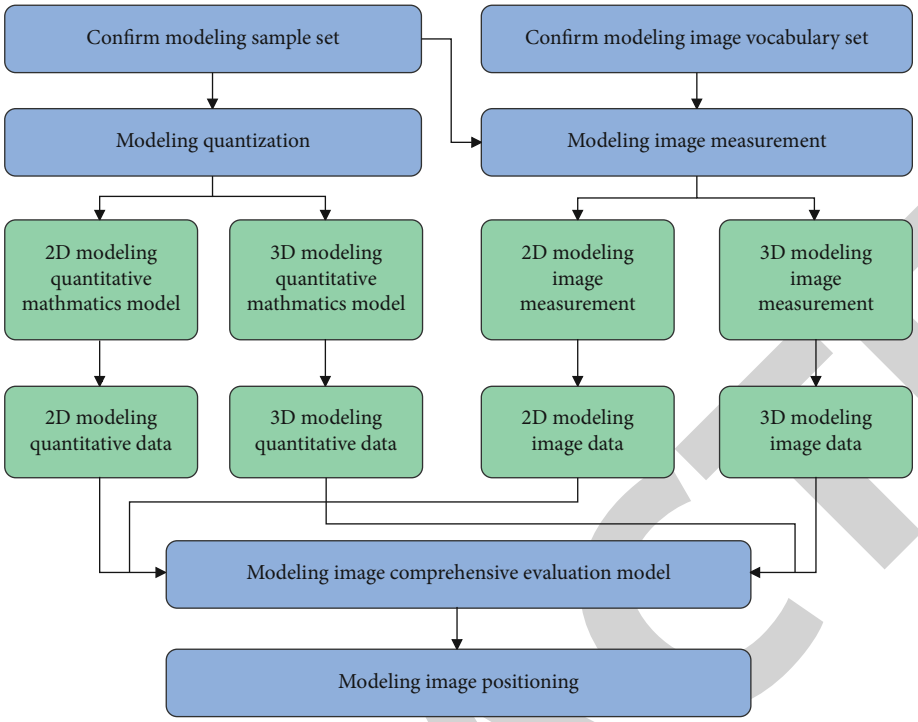

Figure 6: The positioning process of ceramic art product modeling image.

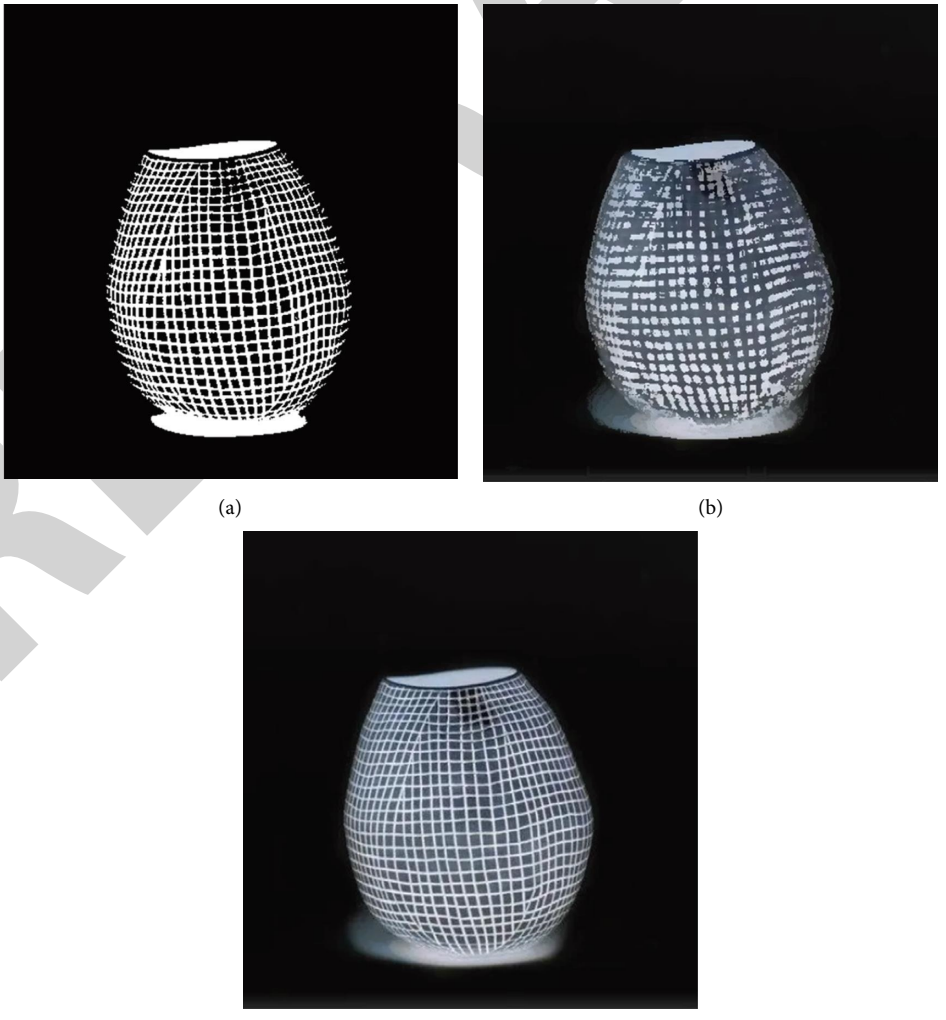

Figure 7: Example of appearance design of ceramic art. (a) Sketch design. (b) Preliminary rendering. (c) Finished product structure.

REJECTED

Figure 8: Example of three-dimensional structure design.

Table 1: Evaluation of the effect of appearance design of ceramic art based on VR visualization technology.

Number	Design effect	Number	Design effect	Number	Design effect
1	86.52	20	85.62	39	88.55
2	88.09	21	88.70	40	90.34
3	90.05	22	89.74	41	87.49
4	84.42	23	89.15	42	89.60
5	86.31	24	89.28	43	86.19
6	90.70	25	90.04	44	88.21
7	90.04	26	84.48	45	85.14
8	87.89	27	88.78	46	83.10
9	84.43	28	87.33	47	86.77
10	88.22	29	86.95	48	83.54
11	83.40	30	85.73	49	88.09
12	86.61	31	84.70	50	90.99
13	88.75	32	85.55	51	86.76
14	90.15	33	89.76	52	84.22
15	89.08	34	86.86	53	83.99
16	87.75	35	89.86	54	87.72
17	83.57	36	89.36	55	90.68
18	84.64	37	84.74	56	85.12
19	88.92	38	89.31	57	89.49

complete, concise, and generous. The combination of points, lines, and surfaces can make the original rigid objects more vivid, and at the same time, it adds a little more beauty, which adds more fashion elements to the original seemingly traditional artistic image. The seemingly simple elements of point, line, and surface are inseparable from our life and art. The rational use of them, directly or indirectly, affects our aesthetic ability and artistic creation ability. It is the rational application of point, line, and surface elements in modern ceramic art design that can make modern ceramic art have a strong artistic appeal and a unique image and temperament of ceramics.

Through the design of multiple groups of cases, the effect of the appearance design of the ceramic art method based on VR visualization technology proposed in this study is verified, as shown in Table 1.

From the above research, we can see that the appearance design system of ceramic art based on VR visualization technology proposed in this study has a good effect and can effectively improve the interaction effect of appearance design of ceramic art.

4. Conclusion

In the creation of modern ceramic art, the characteristics of color composition and three-dimensional composition are reflected in terms of shape and color. These are the keys to modern ceramic art design. The characteristics of modern ceramic art are not only reflected in the shape, glaze, and decoration of ceramic daily necessities but also should pay attention to the concept of the creator. The shape is novel and the decoration is interesting, so that the works created are not lacking in modernity. Moreover, this can not only reflect the author's freedom, creativity, experimentation, and its outstanding humanization but also can use the environment to set off the charm of the work. This work studies the method of appearance design of ceramic art combined with VR visualization technology and builds an intelligent model. Through the experimental research, it can be seen that the appearance design system of ceramic art based on VR visualization technology proposed in this study has a good effect and can effectively improve the interaction effect of appearance design of ceramic art.

Data Availability

The datasets used to support the findings of this study are available from the corresponding author upon request.

Conflicts of Interest

The author declares that there are no conflicts of interest.

Acknowledgments

This work was supported by Anhui Normal University.

References

[1] P. Boldrin and N. P. Brandon, "Progress and outlook for solid oxide fuel cells for transportation applications," *Nature Catalysis*, vol. 2, no. 7, pp. 571–577, 2019.

[2] A. Bachar, A. Mabrouk, D. De Sousa Meneses, E. Veron, Y. Sadallah, and P. Echegut, "Study of the firing type on the microstructure and color aspect of ceramic enamels," *Journal of Alloys and Compounds*, vol. 735, no. 6, pp. 2479–2485, 2018.

[3] B. Martínez, S. Casas, M. Vidal-González, L. Vera, and I. García-Pereira, "TinajAR: an edutainment augmented reality mirror for the dissemination and reinterpretation of cultural heritage," *Multimodal Technologies and Interaction*, vol. 2, no. 2, pp. 33–42, 2018.

[4] O. A. Oyekunle and M. Sirayi, "The role of design in sustainable development of handicraft industries," *African Journal of Science, Technology, Innovation and Development*, vol. 10, no. 4, pp. 381–388, 2018.

[5] A. Salazar, G. Safont, L. Vergara, and E. Vidal, "Pattern recognition techniques for provenance classification of archaeological ceramics using ultrasounds," *Pattern Recognition Letters*, vol. 135, pp. 441–450, 2020.

[6] R. López Píriz, B. Cabal, L. Goyos Ball et al., "Current state of the art and future perspectives of the three main modern implant dentistry concerns: aesthetic requirements, mechanical properties, and peri implantitis prevention," *Journal*

RETRACTED

Hindawi
Journal of Robotics
Volume 2023, Article ID 9827679, 1 page
https://doi.org/10.1155/2023/9827679

Retraction

Retracted: Online Control Method of Small- and Medium-Sized Electromechanical Equipment Based on Deep Neural Network

Journal of Robotics

Received 19 December 2023; Accepted 19 December 2023; Published 20 December 2023

Copyright © 2023 Journal of Robotics. This is an open access article distributed under the Creative Commons Attribution License, which permits unrestricted use, distribution, and reproduction in any medium, provided the original work is properly cited.

This article has been retracted by Hindawi following an investigation undertaken by the publisher [1]. This investigation has uncovered evidence of one or more of the following indicators of systematic manipulation of the publication process:

(1) Discrepancies in scope
(2) Discrepancies in the description of the research reported
(3) Discrepancies between the availability of data and the research described
(4) Inappropriate citations
(5) Incoherent, meaningless and/or irrelevant content included in the article
(6) Manipulated or compromised peer review

The presence of these indicators undermines our confidence in the integrity of the article's content and we cannot, therefore, vouch for its reliability. Please note that this notice is intended solely to alert readers that the content of this article is unreliable. We have not investigated whether authors were aware of or involved in the systematic manipulation of the publication process.

Wiley and Hindawi regrets that the usual quality checks did not identify these issues before publication and have since put additional measures in place to safeguard research integrity.

We wish to credit our own Research Integrity and Research Publishing teams and anonymous and named external researchers and research integrity experts for contributing to this investigation.

The corresponding author, as the representative of all authors, has been given the opportunity to register their agreement or disagreement to this retraction. We have kept a record of any response received.

References

[1] M. Yang, S. Deng, and Z. Zhao, "Online Control Method of Small- and Medium-Sized Electromechanical Equipment Based on Deep Neural Network," *Journal of Robotics*, vol. 2022, Article ID 1607694, 10 pages, 2022.

Hindawi
Journal of Robotics
Volume 2022, Article ID 1607694, 10 pages
https://doi.org/10.1155/2022/1607694

RETRACTED

Research Article

Online Control Method of Small- and Medium-Sized Electromechanical Equipment Based on Deep Neural Network

Mengmeng Yang, Sanxing Deng, and Zhizheng Zhao

College of Mechanical and Electrical Engineering, Huanghe Jiaotong University, Jiao Zuo 454950, China

Correspondence should be addressed to Mengmeng Yang; 2016090903@zjtu.edu.cn

Received 9 August 2022; Revised 15 September 2022; Accepted 21 September 2022; Published 7 October 2022

Academic Editor: Shahid Hussain

Copyright © 2022 Mengmeng Yang et al. This is an open access article distributed under the Creative Commons Attribution License, which permits unrestricted use, distribution, and reproduction in any medium, provided the original work is properly cited.

In order to improve the online control effect of small- and medium-sized electromechanical equipment, this paper studies the online control method of small- and medium-sized electromechanical equipment combined with the deep audit network. Moreover, starting from the signal basis of online control signal recognition and channel coding recognition of electromechanical equipment, this paper determines the type of online control signal and channel coding type of electromechanical equipment required for the experiment. This paper compares the signals under different types of online control signals for electromechanical devices and clarifies the differences in amplitude, frequency, phase, and spectrum in time-domain waveforms. In addition, through the elaboration of different channel coding theories, this paper clarifies the differences in coding methods. Through the experimental research, it can be seen that the online control effect of the small- and medium-sized electromechanical equipment based on the deep neural network proposed in this paper is very good.

1. Introduction

Different from the conventional monitoring system, the online system applies network technology to the monitoring field and gives full play to the advantages of the existing Internet, which can make the monitoring system have more powerful functions. Users only need to use any computer connected to the Internet to realize remote centralized monitoring and control of the equipment through a common browser [1]. This is of great significance for the informatization and intelligence of the production processes of some enterprises, as well as for some tasks that are not labor-intensive but require long-term supervision, such as mobile phone stations, water gates, and environmental monitoring. In recent years, with the continuous progress of network technology and modern communication technology, the remote monitoring technology based on TCP/IP and B/S mode has gradually matured. It is foreseeable that the application of network technology to monitoring systems will become one of the mainstream directions of remote monitoring technology development in the future [2].

An embedded system is a computer system that is embedded in the object system, centered on the application, can be reduced in software and hardware, and has strict requirements on volume, power consumption, and cost. Compared with the traditional single-chip microcomputer, one of its important breakthroughs is to solve the interconnection problem between the equipment and the Internet, so that people can remotely monitor the equipment of each node in the network through the existing network settings [3]. In recent years, with the rapid development of embedded technology, a wide variety of powerful CPUs and off-chip connections have provided a stable and reliable hardware environment for network applications; embedded operating systems also support this hardware and Ethernet well. The transplantation of the operating system is greatly simplified, which provides convenience for the realization of the embedded remote monitoring system. The embedded remote monitoring system converts the data of various protocols in the monitoring system into a unified TCP/IP protocol format so that users can remotely access the web server through Ethernet to monitor the equipment [4].

Intelligent control is mainly used to solve control complex systems that are difficult to solve by traditional methods. Compared with classical control, its most prominent feature is that the research object is no longer the controlled object, but the controller itself. This feature gives full play to the intelligent characteristics of human beings. Intelligent control is mainly divided into the following categories: (1) Expert control is the most widely used in the field of intelligent control and has been widely used in process control, industrial design, and fault diagnosis. The general expert control system consists of three parts: control mechanism, reasoning mechanism, and knowledge base [5]. (2) Fuzzy control is a kind of control method using fuzzy set theory. Its working process is as follows: first, the information is fuzzified, then the output of fuzzy control is obtained through fuzzy inference rules, and finally, the output of fuzzy control is refined. Calculate the final output control value [6]. (3) Learning control: learning is one of the main bits of intelligence of human beings, and learning control is an attempt to simulate the self-regulation mechanism of human beings. A learning control system is a system that continuously obtains and processes unpredictable information, accumulates experience, and estimates, categorizes, and continuously improves system performance in the work [7]. (4) Neural network control is a relatively new research direction in intelligent control. It is a control method that simulates the activities of the human brain nervous system. Some functions of the system. Neural networks have some characteristics that are particularly suitable for control, such as nonlinear processing capability, parallel processing capability, learning capability, and adaptive capability [8].

In recent years, with the development of intelligent control theory, scholars at home and abroad have applied it to electro-hydraulic servo systems and have carried out a series of studies on the nonlinearity, time-varying parameters, and load transients of electro-hydraulic servo systems. The study in [9] aims at the nonlinearity, time-varying, and model uncertainty of the electro-hydraulic servo system, and the composite synchronous control and fuzzy control are combined to form a fuzzy PID control system. The experimental results show that the controller can improve the dynamic characteristics of the system meaning the control effect is better than the PID control; the literature [10] established a control algorithm that combines multiple groups of PID algorithms and fuzzy PID control algorithms. The fuzzy algorithm is used in the case of large deviations in the system, which can quickly reduce small deviations. The PID algorithm is used in the case of small deviations. Compared with the traditional PID, this control algorithm has a faster dynamic response speed, and the control effect is better when the set pressure changes. Reference [11] aims at the nonlinear effect of the servo system shaking table, based on the traditional PID. The simulation results show that this method can effectively eliminate the output error and can accurately track the given motion trajectory. Reference [12] proposed a direct inverse control method of RBF neural network with a dual network structure, and the controller is controlled according to the system response. The results show that the control strategy can effectively improve the performance of the system, reduce steady-state error, and improve the robustness of the system. In reference [13], aiming at the nonlinear and time-varying hydraulic system, a new type of PID controller based on a neural network is used and simulated by MATLAB software. The simulation results show that the control algorithm can improve the dynamic and static characteristics of the system and has a significant effect.

A networked control system, also known as a networked control system, refers to a control system implemented in a network environment and is divided into a broad networked control system and a narrowly defined networked control system. The network control system in the broad sense includes the network control system in the narrow sense and also includes the monitoring, modulation, and optimization of factory workshops, production lines, and even field equipment through enterprise information networks and Internet/intranet [14]. The narrow network control system refers to the integration of some on-site monitoring, control, and operation equipment and communication lines in a certain area to provide data transmission between equipment, so that equipment and users in different locations in the area can achieve resource sharing and communication. It can also coordinate operations. The network control system is the product of the development and integration of computer technology, communication technology, and control technology. Distributed control systems (DCS), industrial Ethernet, and field bus control systems belong to the network control system in a sense, which reflects the direction of the control system. The development trend of networking, integration, distribution, and node intelligence will be applied in the field of industrial control, building automation, and home automation [15].

From any point of view, the development trend of human-computer interaction reflects the continuous emphasis on the human factor, making human-computer interaction closer to the natural form, enabling users to use daily natural skills without special efforts and learning; cognitive load is reduced, and work efficiency is improved [16]. It can be seen from the development of human-computer interaction technology that the emergence of computers not only brings new problems to human engineering research but also completely changes the guiding ideology of research. Traditional ergonomics regards people as human-machine-environment. The responders and controllers in the system focus on the problem of matching the characteristics and functions of humans and machines at the level of physical motion and regard traditional electromechanical machines as an extension of the human hand [17]. The emergence, development, and widespread popularization of computer technology have enabled machine systems to have a certain level of intelligence, which can partially replace human cognitive functions, so it is regarded as an "extension of the human brain," which requires ergonomics at the level of cognitive theory. This paper examines the cognitive characteristics and functional matching problems of humans and machines [18].

RETRACTED

This paper combines the deep neural network to carry out the research on the online control method of small- and medium-sized motor equipment and improves the intelligent effect of online control of small- and medium-sized motor equipment.

2. Basics of Control Identification and Channel Coding Identification of Electromechanical Equipment

2.1. Control Basis of Signal Electromechanical Equipment. The signal electromechanical equipment control can realize the spectrum transfer of the baseband signal. The electromechanical equipment control signal has a stronger anti-interference ability, the signal is safer during the transmission process, and it is convenient for the transceiver and the receiver to synchronize the signal. The control of signal electromechanical equipment is realized by controlling the parameters of the carrier wave, which is usually divided into amplitude modulation, frequency modulation, and phase modulation.

The MASK signal is a modern electromechanical device control signal that uses the carrier envelope amplitude to transmit information. The amplitude of the carrier signal is controlled by the baseband level, which is called a multivariate amplitude shift keying signal. The MASK signal characterizes the M-ary symbol with multiple levels, changing the carrier amplitude through different combinations of binary digits. The MASK signals used in the experiment are 2ASK, 4ASK, and 8ASK signals. The signals can be specifically expressed as

$$s_{\mathrm{MASK}}(t) = Am(t)\cos(2\pi f_c t) = A\left[\sum_n a_n g(t - nT_s)\right]\cos(2\pi f_c t). \quad (1)$$

Among them, A is the basic amplitude, $m(t) = \sum_n a_n g(t - nT_s)$ is the baseband signal that has not been controlled by the electromechanical equipment, a_n is the instantaneous level value of the baseband signal, $g(t)$ is the rectangular pulse signal, T_s is the symbol period, and f_c is the carrier frequency. The value of the symbol a_n can be bipolar, namely, $a_n \in [\pm 1, \pm 3, \ldots]$, or unipolar, namely, $a_n \in [0, 1, \ldots, M-1]$.

Three kinds of MASK signals are used in the experiment, namely 2ASK signal, 4ASK signal, and 8ASK signal. The time-domain signal and spectrum representation of 2ASK electromechanical equipment control are shown in Figure 1.

The time-domain signal and spectrum representation of 4ASK electromechanical equipment control is shown in Figure 2.

The time-domain signal and spectral representation of 8ASK electromechanical device control is shown in Figure 3.

MPSK is a multiphase shift keying control signal for electromechanical equipment, and the baseband signal realizes the control of signal electromechanical equipment by controlling the carrier phase. The MPSK signal is generated by the superposition of M types of carrier signals of the same amplitude and the same frequency with different phases in

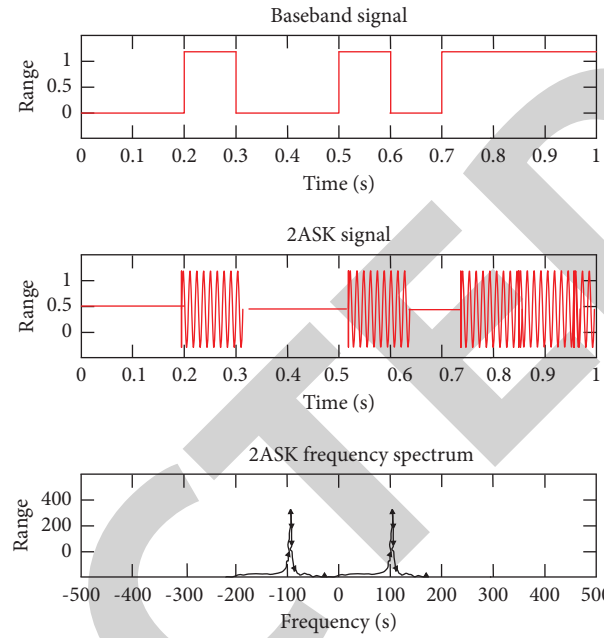

Figure 1: 2ASK time-domain waveform and spectrum.

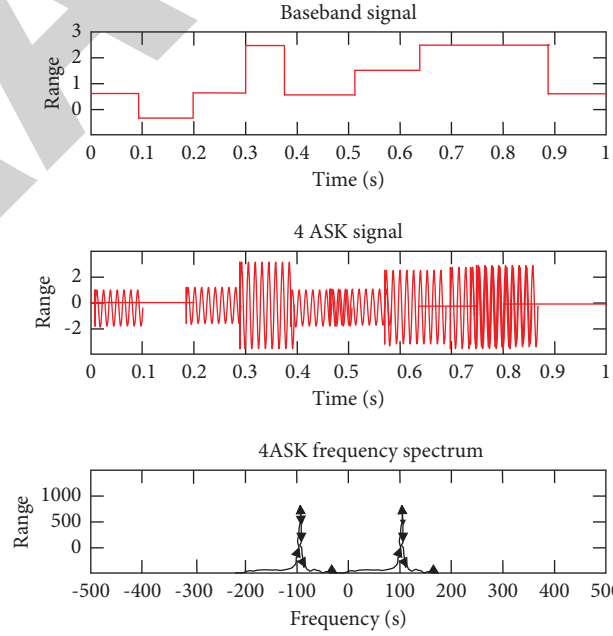

Figure 2: 4ASK time-domain waveform and spectrum.

different time slots, and different phases represent different baseband information. The specific expression of the MPSK signal is

$$s_{\mathrm{MPSK}} = Ag(t)\cos(2\pi f_c t + \theta_n), \ (n-1)T_s \le t \le nT_s. \quad (2)$$

Among them, A is the amplitude factor, $g(t)$ is the rectangular pulse signal, f_c is the carrier frequency, and θ_n is the phase represented by the nth symbol and it has M values. θ_n is generally defined as

RETRACTED

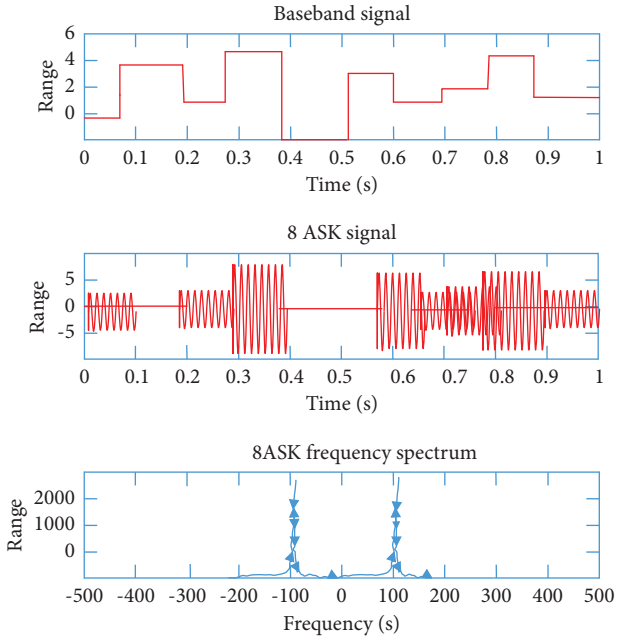

Figure 3: 8ASK time-domain waveform and spectrum.

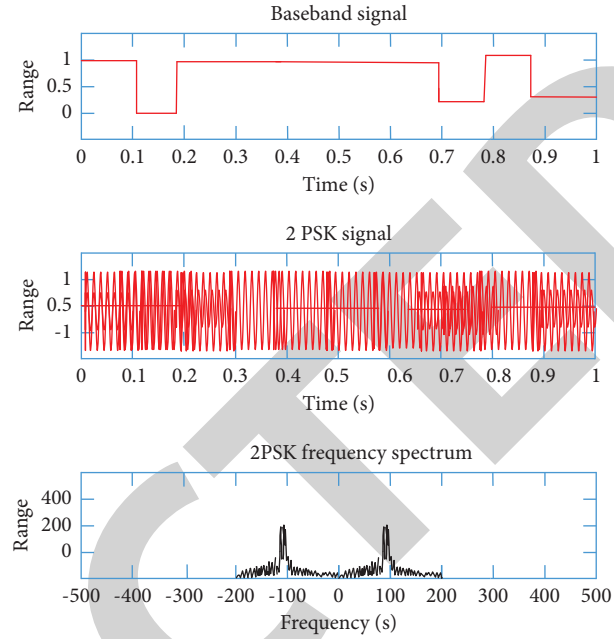

Figure 4: 2PSK time-domain waveform and spectrum.

$$\theta_n = \frac{2\pi i}{M}, \quad i \in [0, 1, \ldots M-1]. \tag{3}$$

The MPSK signal is represented by the in-direction and quadrature components as

$$\begin{aligned} s_{\text{MPSK}} &= Ag(t)\left(\cos\theta_n \cos 2\pi f_c t - \sin\theta_n \sin 2\pi f_c t\right) \\ &= Ag(t)\left(a_{cn}\cos 2\pi f_c t - a_{sn}\sin 2\pi f_c t\right). \end{aligned} \tag{4}$$

There is a one-to-one correspondence between MPSK signal and constellation diagram. According to $a_{cn}^2 + a_{sn}^2 = 1$, it can be known that the constellation diagram of MPSK signal is a circle with a radius of 1.

Three kinds of MPSK signals are used in the experiment, namely, 2PSK signal, 4PSK signal, and 8PSK signal. The time-domain waveform and spectrum of 2PSK signal are shown in Figure 4.

The time-domain waveform and spectrum of the 4PSK signal are shown in Figure 5.

The time-domain waveform and spectrum of the 8PSK signal are shown in Figure 6.

The MFSK signal is a multivariate frequency shift keying signal, and the signal electromechanical equipment control is completed by controlling the frequency of the sinusoidal carrier signal. The amplitude factor of the carrier signal is the same, and the phase is kept continuous. The signals of different carrier frequencies are added in different time slots to obtain the MFSK signal with M element carrier frequency.

$$s_{\text{MFSK}} = Ag(t)\cos\left(2\pi f_n t\right). \tag{5}$$

Among them, A is the basic amplitude factor, $g(t)$ is the rectangular pulse signal, the initial phase of the MFSK signal is generally 0, and f_n is the frequency of the nth symbol and has M kinds of values. Generally, f_n is equally spaced.

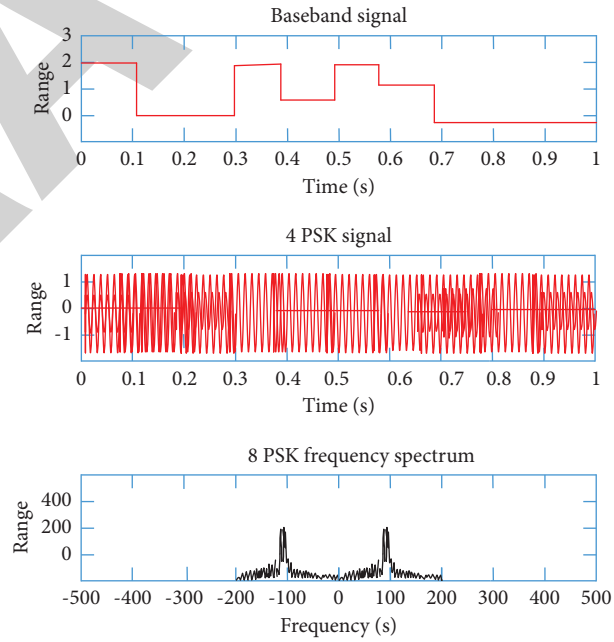

Figure 5: 4PSK time-domain waveform and spectrum.

$$f_n = f_c + \frac{(2i - M + 1)}{2}\Delta f, \quad i = 0, 1, \ldots M-1. \tag{6}$$

f_c is the carrier frequency, Δf is the frequency interval, and if $\Delta f > 0$ is specified, the values of M frequencies can be obtained as $f_c \pm \Delta f/2, f_c \pm 3 \times \Delta f/2, \ldots, f_c \pm (M-1) \times \Delta f/2$ respectively. The carrier frequencies should be as close as possible and intersect each other to reduce the signal bandwidth. The condition of frequency quadrature is that the frequency interval is an integer multiple of $T_s/2$, that is, the minimum frequency interval is $T_s/2$.

RETRACTED

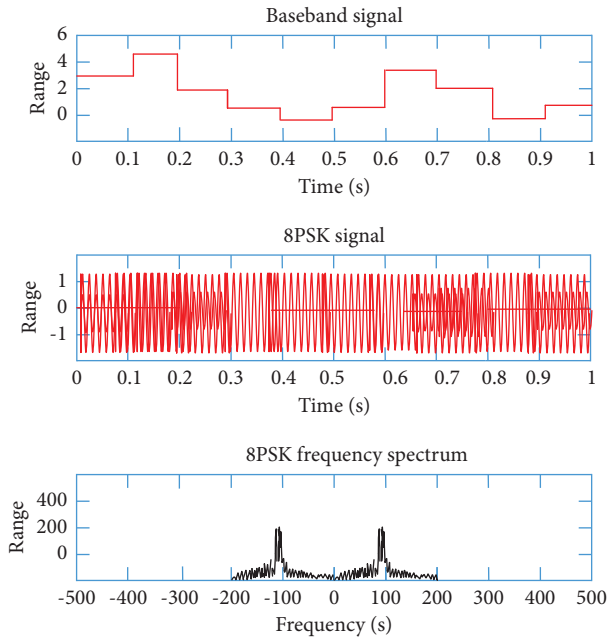

Figure 6: 8PSK time-domain waveform and spectrum.

The MQAM signal is a quadrature amplitude electromechanical device control signal, and the signal amplitude and phase are transformed during the electromechanical device control process. The MQAM signal uses two orthogonal carriers to control the electromechanical equipment of the signal and, at the same time, ensures the noninterference transmission within the bandwidth. The electromechanical device control method of the MQAM signal determines that it has higher stability and stronger anti-interference ability than the above three signals, and the bandwidth utilization rate is also higher. Moreover, it can maintain high electromechanical equipment control efficiency and high frequency band utilization even under the condition of strong noise interference. The expression of the MQAM signal is

$$s_{\mathrm{MQAM}} = Aa_{cn}g(t)\cos(2\pi f_c t) - Aa_{sn}g(t)\sin(2\pi f_c t). \quad (7)$$

Among them, (a_{cn}, a_{sn}) represents the value of the current symbol on the constellation diagram, and each group of values is a signal point, which represents the in-direction component and the quadrature component of the signal.

The constellation diagram of the MQAM signal has two kinds: circular and rectangular. The experiment uses the rectangular constellation diagram to generate an MQAM signal. The circular constellation diagram of MQAM is similar to the MPSK signal, and the synthesized signal amplitude is constant. The MQAM signal generated by the rectangular constellation has a more variable amplitude and can carry both phase information and amplitude information. At the same time, the MQAM signal also maintains a uniform distribution of signal points, which can reduce the bit error rate of signal transmission within a certain range.

Four MQAM signals are used in the experiment, namely, 8QAM, 16QAM, 32QAM, and 64QAM signals. The constellation diagrams of these four signals are shown in Figure 7.

2.2. Channel Coding Basics. Channel coding is a way to ensure the reliable transmission of information. It ensures the reliability of the transmission content through error control, also known as error correction coding. The system judges the received codeword under the condition of known channel coding type and coding parameters. If the redundant elements and information elements of the codeword satisfy the predetermined coding and decoding rules, the codeword is judged to be correct and decoded. In the process of mobile communication development, channel coding types are also constantly updated. The channel coding used in the global mobile communication system in the 2G era is mainly block code and convolutional code. In the 3G era, the use of code division multiple access technology and broadband code division multiple access technology has greatly improved the 3G capacity, and the channel coding technology used has also been updated to Turbo code, which has a performance close to Shannon's limit. In the 4G era, the orthogonal frequency division multiplexing technology and the orthogonal frequency division multiple access technology are mainly used, and the Turbo code is used in the channel coding, but the structure of the Turbo code is optimized to reduce the decoding complexity. With the popularization of 5G mobile communication, channel coding has a wider range of applications, mainly using low-density check codes, polar codes, tail-biting convolutional codes, and turbo codes. This paper mainly introduces five types of coding methods used for experiments, namely, BCH codes, QCLDPC codes, convolutional codes, Turbo codes, and polar codes.

BCH code is a cyclic linear block code, which can correct random errors under the condition of short codes and has high coding performance. The application of the BCH code is relatively mature. In the early days of cellular mobile digital communication, it was often used as an error correction coding method used by base stations and mobile stations. The BCH codes can be divided into two types according to the generator polynomial: one is the original BCH code, and the other is the non-original BCH code.

The symbol of the binary BCH code comes from GF (2), and the original BCH code is introduced here. The generator polynomial $g(x)$ contains the primitive polynomial with the highest degree m, the coding length is $2^m - 1$, the minimum code distance is $\delta = 2t + 1$, and t errors can be corrected in the application process. α represents the primitive element in the field $GF(2^m)$. If the code takes $(\alpha, \alpha^2, \ldots, \alpha^{2t})$ as the root and the minimum polynomial corresponding to each root is $m_i(x)$, $i = 1, 2, \ldots, 2t$, then $g(x)$ can be written as

$$g(x) = \mathrm{LCM}(m_1(x), m_2(x), \ldots, m_{2t}(x)). \quad (8)$$

In the experiment, the BCH code on $GF(2^4)$ is constructed with $t = 2$ and $m = 4$, and the code length is 15. The primitive polynomial of $GF(2^4)$ is $g_0(x) = x^4 + x + 1$. In the

RETRACTED

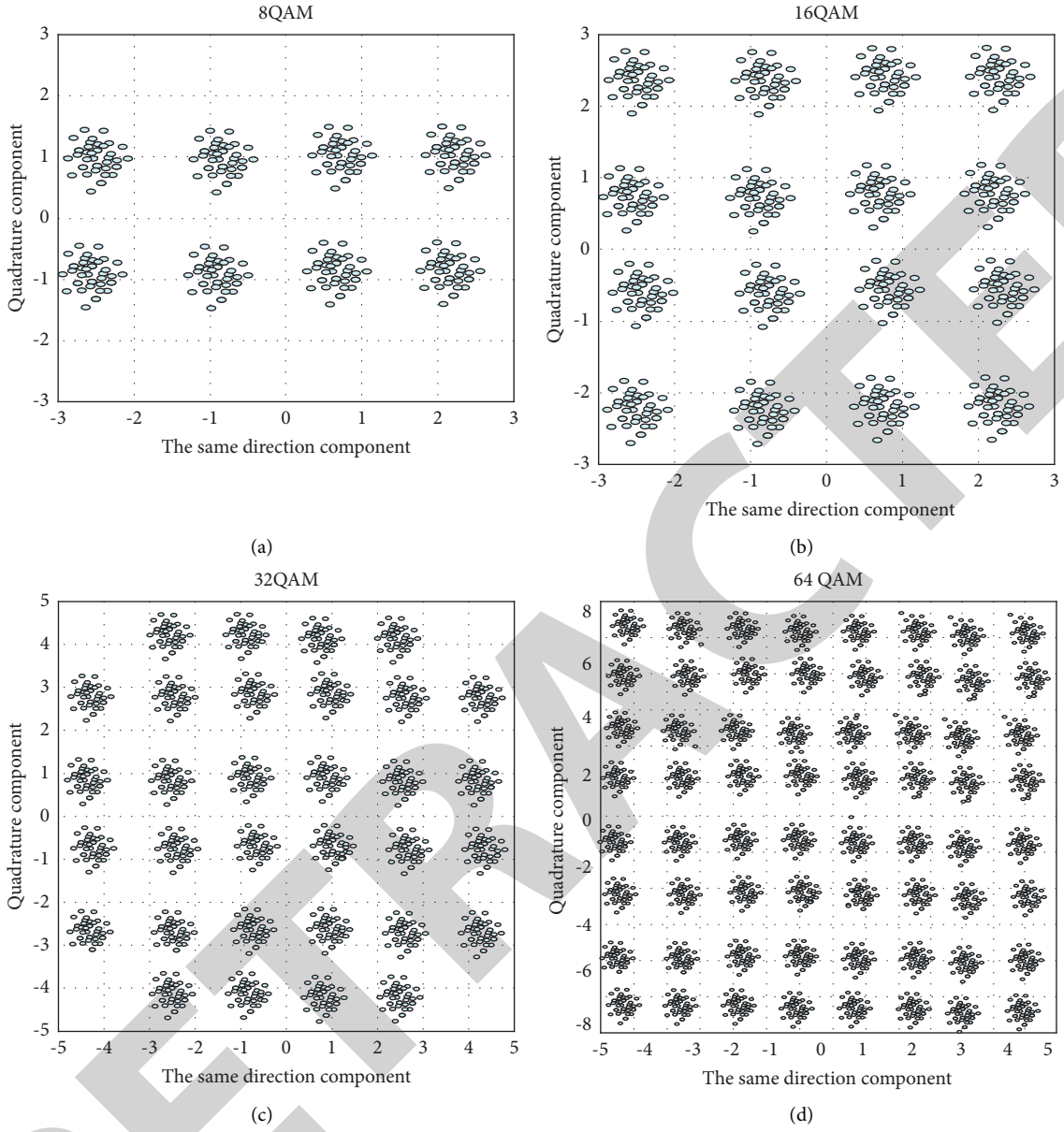

Figure 7: MQAM signal constellation diagram (SNR = 25 dB): (a) 8QAM rectangular constellation diagram; (b) 16QAM rectangular constellation diagram; (c) 32QAM rectangular constellation diagram; (d) 64QAM rectangular constellation diagram.

case of $t = 2$, the BCH code takes α and α^3 as the roots, and the minimum polynomial of α is the minimum polynomial $m_3(x) = x^4 + x^3 + x^2 + x + 1$ of the primitive polynomial $m_1(x) = x^4 + x + 1$, α^3, and the generator polynomial $g(x)$ is obtained as

$$g(x) = m_1(x)m_3(x) = x^8 + x^7 + x^6 + x^4 + 1. \quad (9)$$

Among them, the number of check elements is $m \times t = 8$, which is a (15, 7, 5) BCH code with an error correction capability of 2.

The binary LDPC code is represented by (n, k), the information length is k, and the total length of the codeword is n. It is assumed that m check bits are introduced into the information bit sequence x for coding, a codeword sequence t with a total length of n is generated, and the coding rate is k/n. The encoded codeword t can be represented by an information sequence x and a generator matrix G.

$$t = G^T x. \quad (10)$$

The generator matrix can be written in the form of identity matrix and submatrix

$$G^T = \begin{bmatrix} I_{k\times k} \\ P_{m\times k} \end{bmatrix}. \quad (11)$$

Under the method of hard-decision algebraic decoding, the check matrix H can be expressed as

$$H = [P|I_{m\times m}]. \quad (12)$$

RETRACTED

The Tanner graph is a way of describing the parity check matrix of an LDPC code. The nonzero elements in the check matrix correspond to the edges connecting the variable nodes and the check nodes in the Tanner graph, and the number of rows and columns of the check matrix H corresponds to the number of check nodes and the number of variable nodes, respectively. The degree λ of the variable node and the degree γ of the check node in the Tanner graph remain constant, and whether the check matrix H is sparse is judged by the relationship between λ and γ. Figure 8 depicts the parity check matrix H under the condition of $\lambda = 2$ and $\gamma = 3$.

$$H = \begin{bmatrix} 101001 \\ 010011 \\ 001110 \\ 110100 \end{bmatrix}. \tag{13}$$

There are two construction methods for LDPC codes: one is random generation and the other is structured generation. The performance of LDPC codes constructed by the random method is close to the Shannon limit under the condition of long codes, but the decoding is complicated. The code generated by the structure is widely used and has a good effect under the condition of short code, and the coding and decoding algorithm is simple. The most commonly used structured generation method is to use a quasi-cyclic structure to generate codewords. The quasi-cyclic structure can generate a regular check matrix, which greatly simplifies the complexity of the decoding algorithm. At the same time, the quasi-cyclic structure can achieve the purpose of increasing data throughput by reducing the decoding delay and is widely used in practice.

Convolutional code proposes a new block code encoding method, which strengthens the correlation between code groups in the encoding process, and each code group is no longer independent of the other. The codeword output at a certain moment is not only related to the currently input information symbol, but the previous information sequence also affects the current output codeword. Therefore, adding a shift register to the encoder improves the memory of the encoder.

At present, (n, k, m) is commonly used to represent convolutional codes, where n is the length of the codeword, k is the length of the information group, and m is the encoding memory. The more shift registers in the encoder, the longer the information element storage time. N is defined as an encoding constraint. It takes N time slots from the time the information element enters the first shift register until it completely leaves the encoder, and all codewords generated in the N time slots are related to this information element. In addition, the coding constraints represent the number of mutually constrained code groups.$N_A = N \times n$ represents the coding constraint length, N_A is counted in bits, and the number of mutually constrained binary symbols is calculated by using the length of each code group and the coding

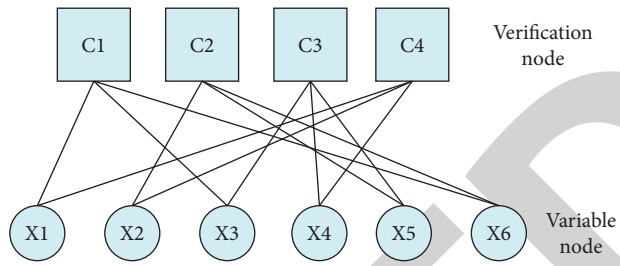

Figure 8: Tanner diagram of the LDPC code under the condition of $\lambda = 2$ and $\gamma = 3$.

constraint. In the actual application process, the encoded information sequence is long, and the complexity of the encoding structure will be greatly improved when the convolutional code encoding memory is long. Therefore, when designing a convolutional code structure, the coding complexity is reduced by reducing the sequence length input to the encoder per unit time.

The experiment adopts (2, 1, 2) convolutional code. The encoder has one input and two outputs. The specific structure is shown in Figure 9. The encoder consists of two shift registers D_1 and D_2, two modulo, two adders, and a switch circuit. If the information elements are sequentially input to the encoder in the order of $m_0 m_1 m_2 \ldots m_{j-2} m_{j-1} m_j \ldots$; the generator polynomial of the output symbols c_{j1} and c_{j2} is

$$\begin{cases} c_{j1} = m_j + m_{j-2} \\ c_{j2} = m_j + m_{j-1} + m_{j-2} \end{cases}. \tag{14}$$

The generated sequence is

$$g^{(1)} = (101), g^{(2)} = (111). \tag{15}$$

The information sequence is $u = (u_0, u_1, \ldots)$, the two output sequences of the encoder are $c^{(1)} = (c_0^{(1)}, c_1^{(1)}, c_2^{(1)}, \ldots)$ and $c^{(2)} = (c_0^{(2)}, c_1^{(2)}, c_2^{(2)}, \ldots)$, and the output sequence is formed by the convolution of the input symbols through the two impulse responses of $g^{(1)}$ and $g^{(2)}$. If the impulse response lasts at most N time units, $N = \mathrm{m} + 1$, then

$$g^{(1)} = \left(g_0^{(1)}, g_1^{(1)}, \ldots, g_m^{(1)}\right), g^{(2)} = \left(g_0^{(2)}, g_1^{(2)}, \ldots, g_m^{(2)}\right). \tag{16}$$

The encoded output sequence can be written as

$$\begin{cases} c^{(1)} = u * g^{(1)} \\ c^{(2)} = u * g^{(2)} \end{cases}. \tag{17}$$

The encoding process is expressed as a generator matrix as

$$c = uG. \tag{18}$$

RETRACTED

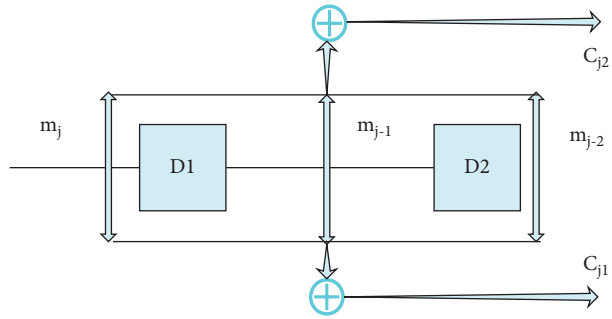

Figure 9: Encoder with (2, 1, 2) convolutional code.

Among them, the generating matrix is

$$G = \begin{bmatrix} g_0^{(1)}g_0^{(2)} & g_1^{(1)}g_1^{(2)} & g_2^{(1)}g_2^{(2)} & \cdots & g_m^{(1)}g_m^{(2)} \\ g_0^{(1)}g_0^{(2)} & g_1^{(1)}g_1^{(2)} & \cdots & g_{m-1}^{(1)}g_{m-1}^{(2)} & g_m^{(1)}g_m^{(2)} \\ g_0^{(1)}g_0^{(2)} & \cdots & g_{m-2}^{(1)}g_{m-2}^{(2)} & g_{m-1}^{(1)}g_{m-1}^{(2)} & g_m^{(1)}g_m^{(2)} \\ \ddots & \ddots & & & \end{bmatrix}. \quad (19)$$

The information element sequence M of length k is input into the encoder, and the buffer adds n-k bits to the information sequence to obtain the code group C_0. C_0 is input into the interleaver and the recursive systematic convolution (RSC) coding unit in parallel and is input into another RSC coding unit through one way of the interleaver to obtain C_1 and C_2, respectively. C_0, C_1, and C_2 are cascaded in parallel, and the codeword C is obtained by puncturing and multiplexing the structure. The code length of the Turbo code used in the experiment is $n = 24$, the information bit length is $k = 12$, the code rate is $k/n = 1/2$, and pseudo-random interleaving is used.

The information transmission process can also be equivalent to the transmission process in two channels, the high-performance channel transmits information bits, and the low-performance channel transmits frozen bits.

The code length is $N = 2^n$, $n \geq 0$, and for a given N, the codeword x_1^N is generated by $x_1^N = u_1^N G_N$, where u_1^N is the information sequence and G_N is the generator matrix of $N \times N$. The bit channel index set is $I = \{1, 2, \ldots N\}$, and A is a subset of the index set I; then, the codeword generation can be rewritten as

$$x_1^N = uG_N(A) \oplus u_c G_N(A^c). \quad (20)$$

Among them, $A^c = \{1, 2, \ldots, N\} - A$ is the complement of A, and $G_N(A)$ is the sub-matrix of G_N, which is composed of row vectors whose elements in set A are numbered as G_N and $u = \{u_i, i \in A\}$.

If the information sequence u is the bit to be transmitted, and the fixed set is A, the resulting code is called the coset code of G_N. A G_N coset code is determined by the parameter (N, K, A, u_c), $K = |A|$ is the information bit length of the code, K/N is the code rate, A is the information set, and u_c is the frozen bit. For example, the codeword determined by $(4, 2, \{2, 4\}, (1, 0))$ can be expressed as

$$x_1^4 = u_1^4 G_4 = (u_2, u_4)\begin{bmatrix} 1010 \\ 1111 \end{bmatrix} + (1, 0)\begin{bmatrix} 1000 \\ 1100 \end{bmatrix}. \quad (21)$$

When the information sequence is $(u_2, u_4) = (1, 1)$, the corresponding codeword is $x_1^4 = (1, 1, 0, 1)$.

The main problem of polar code construction is how to choose the information set A, which is usually based on the metric parameters to sort the bit channel reliability. The metric parameter used in the experiment is the channel capacity. The metric parameters of the channel are calculated and arranged in order of size, and the bit channel with the larger parameter is selected as the information bit index.

The experiment uses a polar code coding structure with $N = 8$ and a code rate of $R = 1/2$. The polarized channel is shown in Figure 10. The metric parameters of each channel are calculated and sorted.

According to the sorting result, it is clear that the pointer of the information bit points to (U_4, U_6, U_7, U_8) and the remaining channels transmit frozen bits.

3. Online Control Method of Small and Medium Electromechanical Equipment Based on Deep Neural Network

The second part of the algorithm is used as the equipment online signal processing algorithm. Figure 11 shows the structure diagram of the BP neural network PID control.

The controller consists of two parts. The classical PID controller performs closed control on the controlled object, and the entire control system constitutes a closed-loop feedback control structure. The neural network performs autonomous learning and online adjustment of the three key parameters kp, ki, and kd in the PID controller. Moreover, combined with the real-time data of the operation of the control system, it automatically obtains the combined parameters that can make the control performance of the PID controller achieve the best and realizes the optimization of the final performance index.

The online control effect of the small- and medium-sized electromechanical equipment in this paper is evaluated, the quantitative processing of the control effect is carried out with multiple groups of simulations, and the results shown in Table 1 are obtained.

RETRACTED

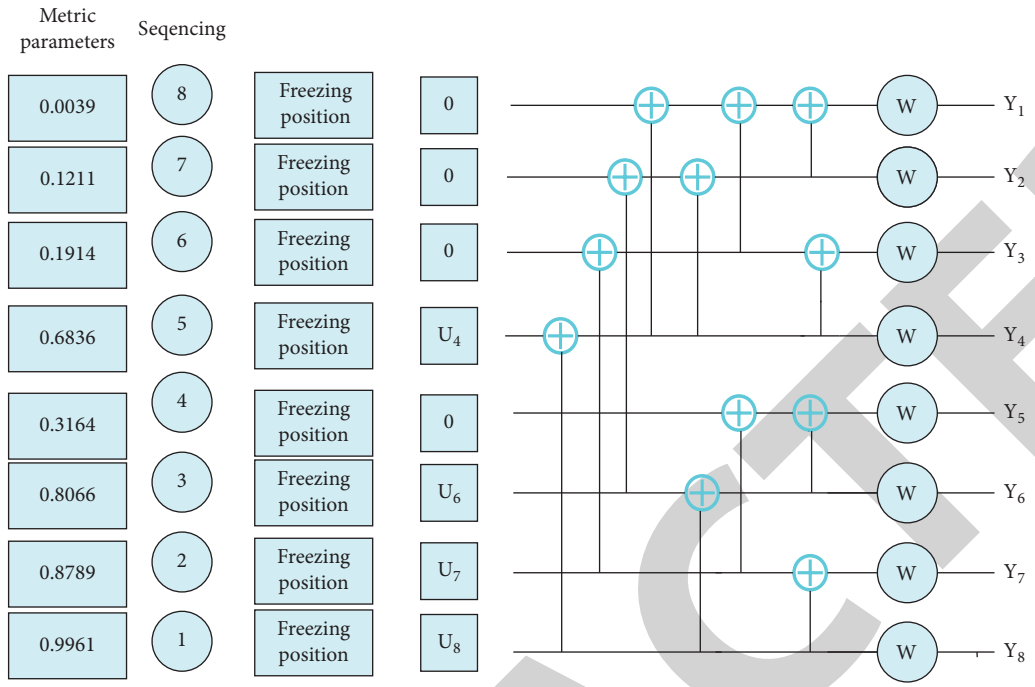

Figure 10: Polarization channel and structure of polar codes.

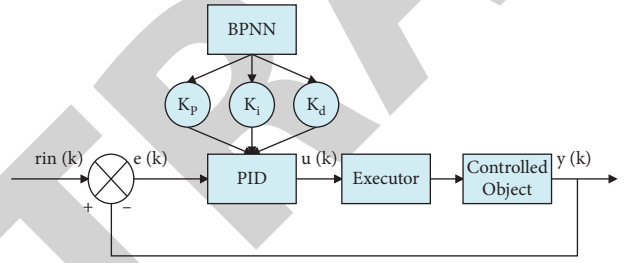

Figure 11: Control diagram of electromechanical equipment based on neural network.

Table 1: Online control effect of small- and medium-sized electromechanical equipment.

Number	Online control	Number	Online control	Number	Online control
1	91.25	17	90.16	33	90.02
2	92.98	18	89.87	34	90.52
3	92.05	19	92.26	35	89.10
4	90.72	20	92.33	36	91.95
5	89.01	21	89.35	37	93.96
6	91.62	22	90.11	38	93.65
7	93.12	23	90.98	39	93.59
8	91.61	24	90.94	40	90.75
9	92.82	25	92.24	41	89.23
10	90.82	26	93.37	42	89.07
11	93.62	27	92.48	43	91.31
12	89.89	28	89.20	44	91.13
13	91.36	29	93.78	45	92.21
14	93.30	30	93.11	46	93.36
15	91.99	31	92.37	47	92.76
16	93.29	32	93.08	48	89.32

RETRACTED

Hindawi
Journal of Robotics
Volume 2024, Article ID 9785472, 1 page
https://doi.org/10.1155/2024/9785472

Retraction

Retracted: Design and Application of Electromechanical Control System Based on Computer Fault Tolerance Technology

Journal of Robotics

Received 23 January 2024; Accepted 23 January 2024; Published 24 January 2024

Copyright © 2024 Journal of Robotics. This is an open access article distributed under the Creative Commons Attribution License, which permits unrestricted use, distribution, and reproduction in any medium, provided the original work is properly cited.

This article has been retracted by Hindawi following an investigation undertaken by the publisher [1]. This investigation has uncovered evidence of one or more of the following indicators of systematic manipulation of the publication process:

(1) Discrepancies in scope
(2) Discrepancies in the description of the research reported
(3) Discrepancies between the availability of data and the research described
(4) Inappropriate citations
(5) Incoherent, meaningless and/or irrelevant content included in the article
(6) Manipulated or compromised peer review

The presence of these indicators undermines our confidence in the integrity of the article's content and we cannot, therefore, vouch for its reliability. Please note that this notice is intended solely to alert readers that the content of this article is unreliable. We have not investigated whether authors were aware of or involved in the systematic manipulation of the publication process.

Wiley and Hindawi regrets that the usual quality checks did not identify these issues before publication and have since put additional measures in place to safeguard research integrity.

We wish to credit our own Research Integrity and Research Publishing teams and anonymous and named external researchers and research integrity experts for contributing to this investigation.

The corresponding author, as the representative of all authors, has been given the opportunity to register their agreement or disagreement to this retraction. We have kept a record of any response received.

References

[1] R. Wei, "Design and Application of Electromechanical Control System Based on Computer Fault Tolerance Technology," *Journal of Robotics*, vol. 2022, Article ID 7716900, 10 pages, 2022.

Hindawi
Journal of Robotics
Volume 2022, Article ID 7716900, 10 pages
https://doi.org/10.1155/2022/7716900

RETRACTED

Research Article

Design and Application of Electromechanical Control System Based on Computer Fault Tolerance Technology

Rui Wei

College of Intelligent Science and Information Engineering, Xi'an Peihua University, Xi'an, Shaanxi 710125, China

Correspondence should be addressed to Rui Wei; weirui2020@peihua.edu.cn

Received 8 August 2022; Revised 14 September 2022; Accepted 19 September 2022; Published 5 October 2022

Academic Editor: Shahid Hussain

Copyright © 2022 Rui Wei. This is an open access article distributed under the Creative Commons Attribution License, which permits unrestricted use, distribution, and reproduction in any medium, provided the original work is properly cited.

In order to improve the stability and control effect of the electromechanical control system, this paper designs the electromechanical control system combined with the computer fault-tolerant technology and proposes an electromechanical control signal processing algorithm. In order to improve the accuracy of the path loss calculation, according to Fresnel's law, this paper deduces the expression of the reflection coefficient of electromechanical control signal with the distance between the transmitting antenna and the receiving antenna as the main variable and then compares the path loss with the ground and the ceiling as the reflecting surface. In addition, in order to study the path loss, this paper selects different reflective materials to study their path loss under horizontal polarization and vertical polarization. The results show that under the vertical polarization, the path loss fluctuation is not large, and the agreement is higher than that of the horizontal polarization. The research results show that the electromechanical control system based on computer fault-tolerance technology proposed in this paper has stable performance and can play an important role in the control of electromechanical systems.

1. Introduction

With the continuous development of sliding mode control technology, it has a very strong control capability for nonlinear systems, time-delay systems, and model uncertain systems. Moreover, sliding mode variable structure control is gradually applied to various control fields as an effective comprehensive method. The sliding mode variable structure method has the advantages of strong robustness, good dynamic performance, and insensitivity to the perturbation of system model parameters, but the existence of chattering greatly affects the large-scale application of sliding mode variable structure control [1]. If the chattering is reduced to a certain extent while meeting the system performance requirements, the large-scale application of sliding mode variable structure control will become a possibility.

Fuzzy control theory has achieved very outstanding application results, especially in the field of intelligent home appliance control, fuzzy washing machines, fuzzy refrigerators, etc. emerge in an endless stream, but at present, fuzzy control still mainly draws on the control experience of experts, and people analyze its stability and robustness. It is still relatively difficult, and it is of great significance to be able to design a fuzzy controller with global stability [2]. It can be seen from the development process of control theory that no theory is perfect, and all have certain pertinence and limitations. For example, the PID control structure is simple and has strong control ability, but it is no longer suitable for nonlinear system control. Fuzzy control can simulate the control logic of experts, but it is completely controlled by fuzzy control, and its control rules will be very complicated [3]. Neural networks can achieve universal use of all controls through continuous learning, but the learning process is long; sliding mode control is suitable for almost all systems, but the chattering problem in practical applications greatly reduces the performance of the system. A single control theory is difficult to meet people's needs for system control, and two or more integrated control strategies are often used to obtain satisfactory results through the complementation of dynamic characteristics [4]. In recent years, fuzzy sliding mode control has achieved rapid development. Compared with traditional sliding mode, the robustness and

convergence speed of the system have been improved, and the system has higher steady-state accuracy near the switching surface [5]. The fuzzy sliding mode algorithm is designed according to the principles of real-time and robustness, which improves the speed of system leveling, reduces the chattering of the system, and reduces the impact of traditional PWM control on the hardware system [6].

For the study of electromechanical dynamics of power systems, the current method is usually to establish detailed mathematical models of dynamic components such as generators and loads and then construct system algebraic equations according to the system topology, using eigenvalue method, energy function method, or numerical methods such as time-domain simulation method to solve. Then, there are two methods to determine whether the system is in a steady state, one is to compare the obtained analytical solution with the relevant stability indicators [7]; the other is to specify the curve of system parameters changing with time to determine. However, with the interconnection of cross-regional power grids, thousands of generators and a larger number of busbars and components form a huge power grid system, making the modern power grid structure more and more complex and huge. If the method described above is still adopted, the calculation is so complicated that it is almost unsolvable due to the huge system, which makes it difficult to explain the propagation of electromechanical disturbances from a microscopic point of view [8]. Since the electromechanical dynamics of the power system mainly studies the angular velocity increment and the spatiotemporal distribution of the power increment, it is necessary to simplify the power system and look at the huge power system from a macro perspective. The power system continuum model describes the system as a continuum by simplifying the system model, ignoring the electromagnetic transients of the generator rotor and stator, and ignoring the reactive power transmission and voltage changes in the system [9]. The electromechanical disturbance is regarded as a kind of electromechanical wave, and the propagation of electromechanical disturbance in the macroscopic power system is analyzed from the perspective of wave. The continuum model of power system provides a new idea for studying the electromechanical dynamic characteristics of large-scale power system. Reference [10] established a continuum model of the electromechanical dynamics of the power system in order to study the electromechanical dynamics in the power system. Simplify the conditions first, make a series of assumptions for transmission lines and generators, deduce the constant coefficient linear wave equation about the propagation of electromechanical disturbances, give the propagation speed of electromechanical disturbances, and expound the reflection, static and static control of electromechanical control signals, and physical phenomena such as waves. Comparing the simulation and actual data, the 0.2 Hz low-frequency oscillation phenomenon on the Pacific tie line was explained from the perspective of electromechanical waves, and satisfactory results were obtained, which provided a new reference for the mechanism research of low-frequency oscillation [11]. Incorporating the Bessel function lines and exponents into the electromechanical dynamics, the electromechanical dynamic equivalence problem of $\Delta P - \Delta f$ is studied, and the problem that the frequency change in the power grid affects the propagation speed of electromechanical disturbances is discussed for the first time [12]. Reference [13] uses the incremental element model and continuously processes the inertial parameters of the generator to convert it into the form of a spatial density function. Based on this model, the attenuation characteristics and propagation velocity of electromechanical disturbances are deduced and calculated. The propagation velocity of the generator power angle measured by the synchrophasor measuring device is compared with the electromechanical disturbance velocity of the simulation system established by him, and the comparison results show that the two have a high degree of agreement. Reference [14] established a differential element model of a one-dimensional chain system by imitating the uniform transmission line. By studying the relationship between the transmission power of the transmission line and the electromagnetic power output by the generator, the limit of the generator swing equation was limited in the space distance. Solved, the electromechanical wave equation is derived. By studying the reflection properties of zero electromechanical control signal and characteristic impedance matching of electromechanical waves on boundary effects, a method of applying zero electromechanical control signal reflection decentralized control in the continuous model of power system is proposed. The controller designed by this method can well absorb the active disturbance power at the boundary [15]. Reference [16] transformed the geographical location in the actual power grid into a two-dimensional plane and transformed the original generator inertia coefficient and angular momentum from the spatial density function form into a continuous distribution by a Gaussian function. The electromechanical disturbance propagation equation including position parameters is deduced by this method, and the phenomena such as dispersion, transmission, and electromechanical control signal reflection in the disturbance propagation process are analyzed and discussed accordingly, and the global dynamics of the power system disturbance propagation process are studied. Reference [17] studied the propagation characteristics of electromechanical waves in the large power grid system, using the generator swing equation, carried out numerical simulation of the traditional generator discrete model, and compared the numerical solution of the continuum model with the discrete model, indicating that the continuous solution of the volume model can better fit the discrete model.

This paper combines the computer fault-tolerant technology to design the electromechanical control system, improve the intelligent control effect of the

RETRACTED

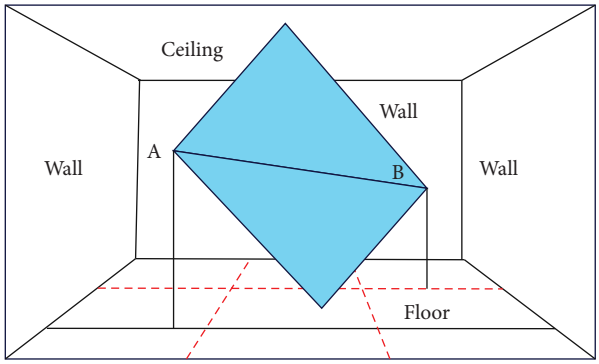

Figure 1: Layout of the test scene within the area.

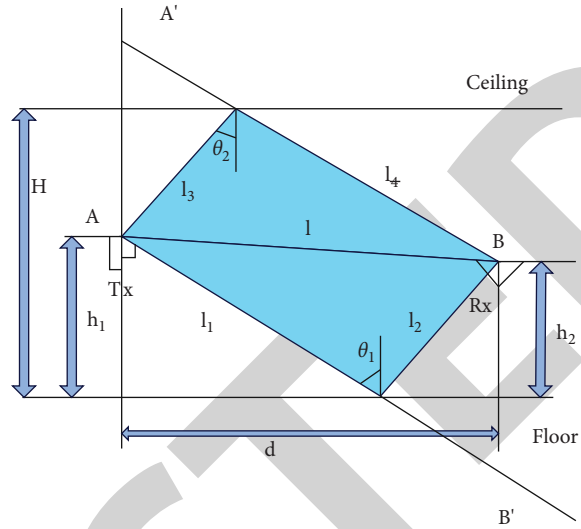

Figure 2: Geometrical optics analysis diagram.

electromechanical control system, and effectively promote the management effect of modern electromechanical equipment.

2. Electromechanical Control Signal Processing Algorithms

2.1. Research on Path Loss Based on Multipath Channel. From the electromagnetic theory, vertical polarization and horizontal polarization are relative to the horizontal plane. When the electric field vector is parallel to the ground, the linearly polarized wave at this time is called horizontally polarized wave. Conversely, when the electric field vector is perpendicular to the ground, the polarized wave is called vertically polarized wave. Therefore, the research on the reflection coefficient of the electromechanical control signal will also be based on the ratio of the horizontal polarization and the vertical polarization relative to the incident amount. Moreover, the reflection coefficient of the electromechanical control signal is determined by the incident angle, the polarization mode (horizontal and vertical) of the electric wave, and the relative permittivity of the medium. We set the incident angle of the radio wave as θ, and $\varepsilon_2/\varepsilon_1$ represents the relative permittivity of the radio wave incident from the material 2 to the material 1. For multipath channel propagation, the reflection coefficients of electromechanical control signals in horizontal polarization and vertical polarization modes are as follows:

$$R_{\mathrm{TE}}(\theta) = \frac{\cos\theta - \sqrt{(\varepsilon_2/\varepsilon_1) - \sin^2\theta}}{\cos\theta + \sqrt{(\varepsilon_2/\varepsilon_1) - \sin^2\theta}}, \tag{1}$$

$$R_{\mathrm{TM}}(\theta) = \frac{(\varepsilon_2/\varepsilon_1)\cos\theta - \sqrt{(\varepsilon_2/\varepsilon_1) - \sin^2\theta}}{(\varepsilon_2/\varepsilon_1)\cos\theta + \sqrt{(\varepsilon_2/\varepsilon_1) - \sin^2\theta}}. \tag{2}$$

Generally, the relative permittivity of air is 1, that is, $\varepsilon_1 = 1$, and substituting it into (1) and (2), the reflection coefficients of the horizontal and vertical electromechanical control signals are obtained as follows:

$$R_{\mathrm{TE}}(\theta) = \frac{\cos\theta - \sqrt{\varepsilon_r - \sin^2\theta}}{\cos\theta + \sqrt{\varepsilon_r - \sin^2\theta}},$$
$$R_{\mathrm{TM}}(\theta) = \frac{\varepsilon_r\cos\theta - \sqrt{\varepsilon_r - \sin^2\theta}}{\varepsilon_r\cos\theta + \sqrt{\varepsilon_r - \sin^2\theta}}. \tag{3}$$

Among them, σ is the conductivity of the electromechanical control signal reflecting surface material, λ is the wavelength, and $\varepsilon_r = \varepsilon_2$ is the relative permittivity of the electromechanical control signal reflecting material.

The size of the room selected in this experiment is 10m × 5m × 3m, and the ground and ceiling materials measured in the experiment are wood ($\varepsilon_r = 2$) and PVC ($\varepsilon_r = 4$), respectively. d represents the spacing between the transceivers. A and B represent the transceiver antenna respectively, and h_1 and h_2 represent the vertical distance between the antenna and the reflection surface of the electromechanical control signal, respectively. The test scene and geometric optical analysis are shown in Figures 1 and 2, respectively.

For the convenience of research, we set $c = h_1 + h_2$. There are the following geometric relationships:

$$\tan\theta = \frac{d}{c}, \tag{4}$$

$$\sin\theta = \frac{d}{\sqrt{d^2 + c^2}}, \tag{5}$$

$$\cos\theta = \frac{c}{\sqrt{d^2 + c^2}}. \tag{6}$$

Combining formulas (4), (5), and (6), the expression of the reflection coefficient of the electromechanical control signal about the transceiver spacing d can be obtained, where the reflection coefficient of the electromechanical control

RETRACTED

signal in the horizontal polarization mode (R_{TE}) is as follows:

$$R_{\mathrm{TE}}(d) = \frac{(h_{1x}+h_{2x}) - \sqrt{(\varepsilon_r - 1)d^2 - \varepsilon_r (h_{4x}+h_{2x})^2}}{(h_{4x}+h_{2x}) + \sqrt{(\varepsilon_r - 1)d^2 - \varepsilon_r (h_{4x}+h_{2x})^2}}. \quad (7)$$

The reflection coefficient of the electromechanical control signal in the vertical polarization mode (R_{IM}) is as follows:

$$R_{\mathrm{TM}}(d) = \frac{\varepsilon_r (h_{1x}+h_{2x}) - \sqrt{(\varepsilon_r - 1)d^2 - \varepsilon_r (h_{1x}+h_{2x})^2}}{\varepsilon_r (h_{1x}+h_{2x}) + \sqrt{(\varepsilon_r - 1)d^2 - \varepsilon_r (h_{1x}+h_{2x})^2}}. \quad (8)$$

In the formula, the height sums obtained by different electromechanical control signal reflective surfaces are different, so there are:

$$h_{1x}+h_{2x} = \begin{cases} c, & \text{The reflecting surface is the floor,} \\ 2H - c, & \text{The reflecting surface is the ceiling.} \end{cases} \quad (9)$$

For a specific scenario, c and ε_r are constants. After the improvement, it can be obtained that the reflection coefficient of the electromechanical control signal of the electromagnetic wave is studied according to the distance between the sending and receiving, so as to avoid relying on the difficult incident angle to study the reflection of the electromechanical control signal and greatly reduce the measurement error.

When analyzing the multipath channel link loss model like geometric optics, the signal propagation situation becomes complicated due to the different placement of items in the area. At this time, the multipath propagation situation of the signal needs to be considered. Since the preconditions of the traditional path loss model are no longer satisfied, the two-warp model in the traditional sense cannot be considered alone. In most cases, for short-distance wireless links, the link can avoid obstacles encountered in the propagation process, so that the transmission and reception ends form line-of-sight (LOS) propagation. Therefore, in this paper, in order to effectively study the link loss of short-distance multipath propagation channels in the area, a deterministic model based on ray tracing can be used. The path loss of the short-distance wireless link in the area can be expressed as follows:

$$\mathrm{PL} = \frac{(4\pi/\lambda)^2}{G_r G_t \left| \left(e^{-j2d_d/\lambda}/l_d\right) + R_g \left(e^{-j2\pi_g/2}/l_g\right) + \sum_t R_r \left(e^{-j2\pi d_t/\lambda}/l_t\right) \right|^2}. \quad (10)$$

Among them, λ is the free space wavelength, G_r is the antenna gain of the receiving antenna, G_t is the antenna gain of receiving array, the value of the antenna gain is related to the design of the short-distance wireless transceiver antenna, and the specific value is affected by the printed board antenna. R_g and R_f are the reflection coefficient of the electromechanical control signal of the ground and the reflection coefficient of the electromechanical control signal of the ceiling, respectively. It should be noted that, in formula (10), the first two items are mandatory, but for the corridor environment in the area, the reflection paths of electromechanical control signals on the ceiling and wall must be added. For outdoor streets, only the direct path and the ground emission path can be selected.

This time, the three-path method is used to characterize the loss of short-distance wireless links in the area. These three paths are the direct path, the reflection path of the electromechanical control signal on the ground, and the emission path of the ceiling, and then the formula (10) can be rewritten as follows:

$$\mathrm{PL} = \frac{(4\pi/\lambda)^2}{G_r G_t \left| \left(e^{-j2\pi_d/\lambda}/l_d\right) + R_g \left(e^{-j2\pi_g/\lambda}/l_g\right) + R_f \left(e^{-j2\pi\pi_f/\lambda}/l_f\right) \right|^2}. \quad (11)$$

Among them, l_f is the reflection path length of the electromechanical control signal of the ceiling. The length of the traditional electromechanical control signal reflection path is mainly obtained by the incident angle which is difficult to measure, while this model can be determined by the spatial position of the transceiver antenna, that is, the distance d of the transceiver relative to the projection of the electromechanical control signal reflection surface. Since the room height H is set, there are:

$$l_x = \sqrt{l_d^2 - (h_{1x}+h_{2x})^2 + (h_{1x}+h_{2x})^2}. \quad (12)$$

Among them, the corresponding direct l_d, ground l_g, and ceiling l_f reflection path lengths of electromechanical control signals are, respectively:

$$\begin{cases} l_d = d, \\ l_g = \sqrt{l_d^2 - (h_1 - h_2)^2 + (h_1 + h_2)^2} = \sqrt{l_d^2 + 4h_1h_2}, \\ l_f = \sqrt{l_d^2 - (h_1 - h_2)^2 + [2H - (h_1 + h_2)]^2} = \sqrt{l_d^2 + 4h_1h_2 + 4H[H - c]}. \end{cases} \quad (13)$$

In general, the link loss of multipath channel propagation in the area is also a kind of channel model in the area. In order to have a good understanding of the link loss of multipath channel propagation in the area, the empirical model expression is generally widely used, and the formula is as follows:

$$\overline{L}(d) = L(d_0) + 10 \cdot \mathrm{nlg}(d/d_0). \quad (14)$$

In the formula, $\overline{L}(d)$ is the value of the average link loss when the distance between the sending and receiving ends is d, and $L(d_0)$ is the value of the average path loss at d_0 at the reference distance when m is free space. In the case of the area, $d_0 = 1\mathrm{m}, \lambda$ is generally taken, m is the working wavelength of the radio wave, and n is the link loss index, which represents the change of the path loss (approximately equal to 2 in free space). The path loss in free space environment can be expressed as follows:

$$L(d_0) = 20\lg(4\pi d_0/\lambda). \quad (15)$$

RETRACTED

2.2. Numerical Results and Analysis. In the case of different materials for the reflection surface of the electromechanical control signal, the variation of the reflection coefficient of the electromechanical control signal of the vertical polarization (R_{TM}) and the horizontal polarization (R_{TE}) with the transmission and reception distance d is shown in the figure. Here, we take h = 20cm. The measured ground material and ceiling material are wood ($\varepsilon_r = 2$) and PVC ($\varepsilon_r = 4$), respectively, and the frequency of working in the millimeter wave band is set to 60 GHz.

It can be seen from Figure 3 that the reflection coefficient $R_{7M} < 0$ of the electromechanical control signal in the horizontal polarization mode decreases with the increase of the transceiver distance d, and finally approaches −1. At the same sending and receiving distance d, by comparing the electromechanical control signal reflective surface materials (wood and PVC), it is found that the greater the relative permittivity of the electromechanical control signal reflective surface material, the smaller the absolute value of the electromechanical control signal reflection coefficient. Among them, the absolute value of the reflection coefficient of the electromechanical control signal of the PVC material is the largest, and the absolute value of the reflection coefficient of the electromechanical control signal of the wood material is the smallest.

It can be seen from Figure 4 that in the vertical polarization mode, with the increase of the transceiver distance d, the reflection coefficient of the electromechanical control signal changes from a positive number to a negative number after passing through the origin 0, and finally approaches −1. The incident angle θ_B when passing through the origin 0 is the Brewster Angle. At this time, D is the distance between sending and receiving, which can be calculated according to formula (8):

$$D = c \cdot \sqrt{\varepsilon_r^*}. \tag{16}$$

When the distance between sending and receiving is $d > D$, the reflection coefficient of electromechanical control signal is negative. When the distance between sending and receiving is $d < D$, the reflection coefficient of electromechanical control signal is positive. In this case, the reflection coefficient of the electromechanical control signal of the electromechanical control signal reflection surface material will also be affected by D at the position of crossing point 0. When $d > D$, $R_{TE} > 0$, under the same distance between sending and receiving, the value of the reflection coefficient of the electromechanical control signal of the PVC material is the largest, and the value of the reflection coefficient of the electromechanical control signal of the wood material is the smallest. When $d < D$, $R_{IE} < 0$, under the same distance between sending and receiving, the absolute value of the reflection coefficient of the electromechanical control signal of the PVC material is the smallest, and the absolute value of the reflection coefficient of the electromechanical control signal of the wood material is the largest.

It can be seen from Figure 4 that the vertical distance between the transceiver antenna and the ground and ceiling can be changed, but as long as the distance between the transceiver antenna d and c remains unchanged, the reflection coefficient of the electromechanical control signal remains unchanged at this time. According to equation (7) and equation (8), the reflection coefficient of electromechanical control signal can be determined by the distance between sending and receiving d; thus, avoiding the difficulty in determining the reflection coefficient of electromechanical control signal by measuring the incident angle θ. Under the condition of using the link loss model, a new calculation expression can be obtained, which greatly improves the calculation accuracy.

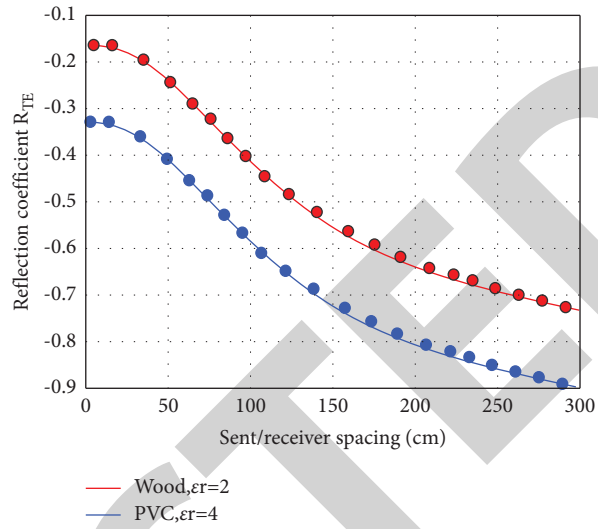

Figure 3: Reflection coefficient of electromechanical control signal under horizontal polarization.

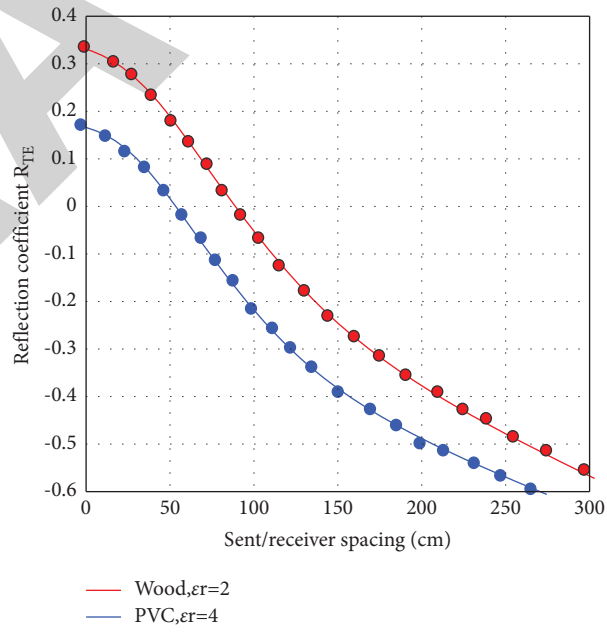

Figure 4: Reflection coefficient of electromechanical control signal in vertical polarization mode.

RETRACTED

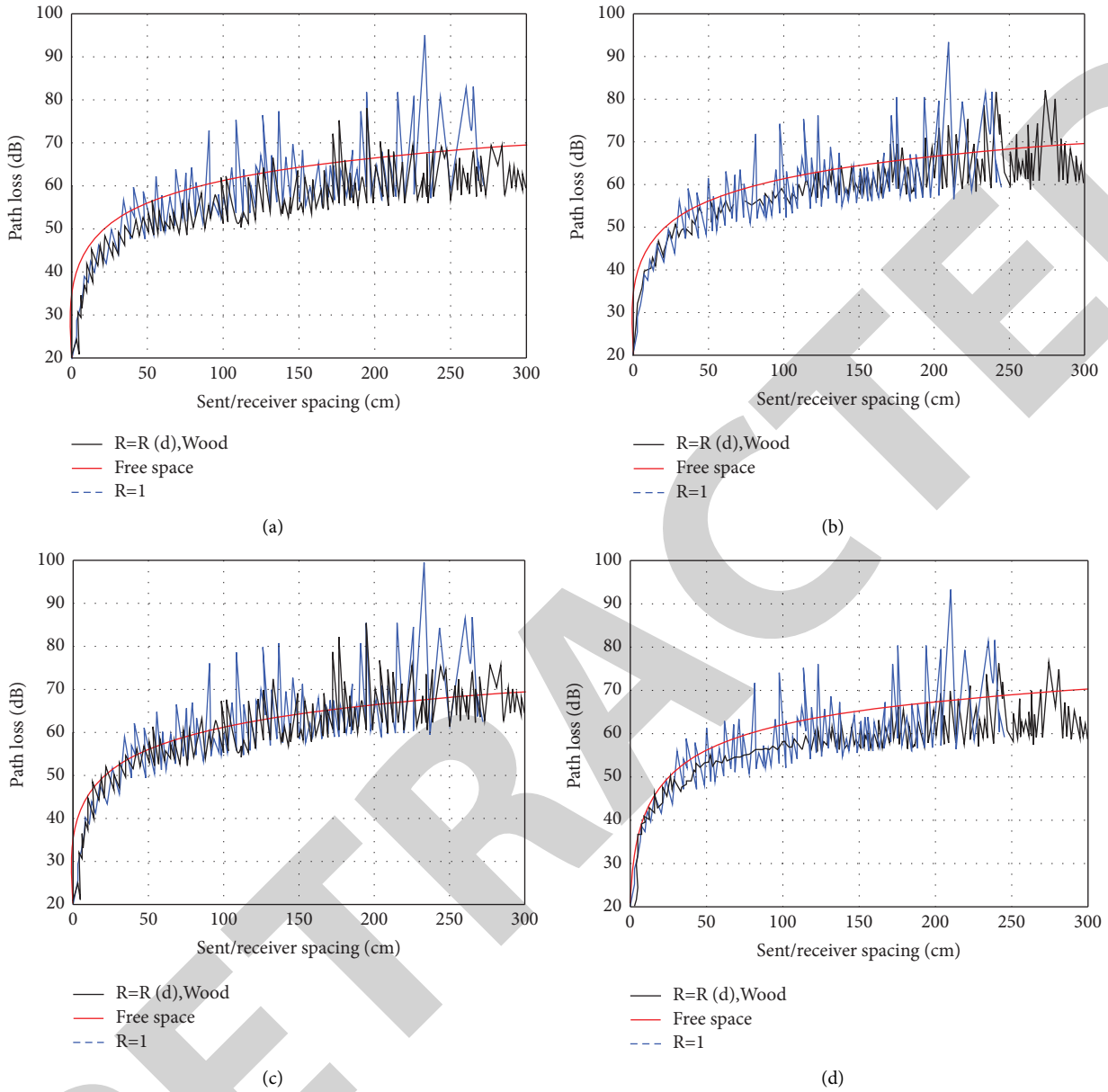

Figure 5: Waveform diagram. (a) Comparison of path loss under horizontal polarization, wood ground, $R = -1$, free space. (b) Comparison of path loss under vertical polarization, wood ground, $R = -1$, free space. (c) Comparison of path loss under PVC ceiling, $R = -1$, free space (horizontal). (d) Comparison of path loss under PVC ceiling, $R = -1$, free space (vertical).

For the convenience of research, under the traditional two-path model, the reflection coefficient of the electromechanical control signal is usually set to a constant (usually set to −1). Therefore, in order to facilitate the study of the difference between the multipath model and the two-path model, the reflection coefficient of the electromechanical control signal is still assumed to be −1 for the multipath model, and the vertical distance between the transmitting antenna and the receiving antenna to the ground is 20 cm. The path loss of different electromechanical control signal reflective surface materials (wood and PVC board) under different polarization modes (vertical and horizontal), the two-path model, and the path loss in free space are compared as shown in Figure 5.

As shown in Figure 5, from the overall waveform point of view, the value of the multipath link loss varies with the transmission and reception spacing. There will be multiple peaks and troughs at different transmission and reception distances; thus, forming multiple maximum and minimum values. From the perspective of the polarization mode, according to the knowledge of electromagnetic theory, the polarization current has a great influence on the propagation of the radio signal, and the intensity of the influence of different polarization modes on the signal propagation is also different. The main reason is that the ground is a conductor and does not generate polarized currents, resulting in the electromagnetic signal not rapidly attenuating. Therefore, compared with the path loss under the

RETRACTED

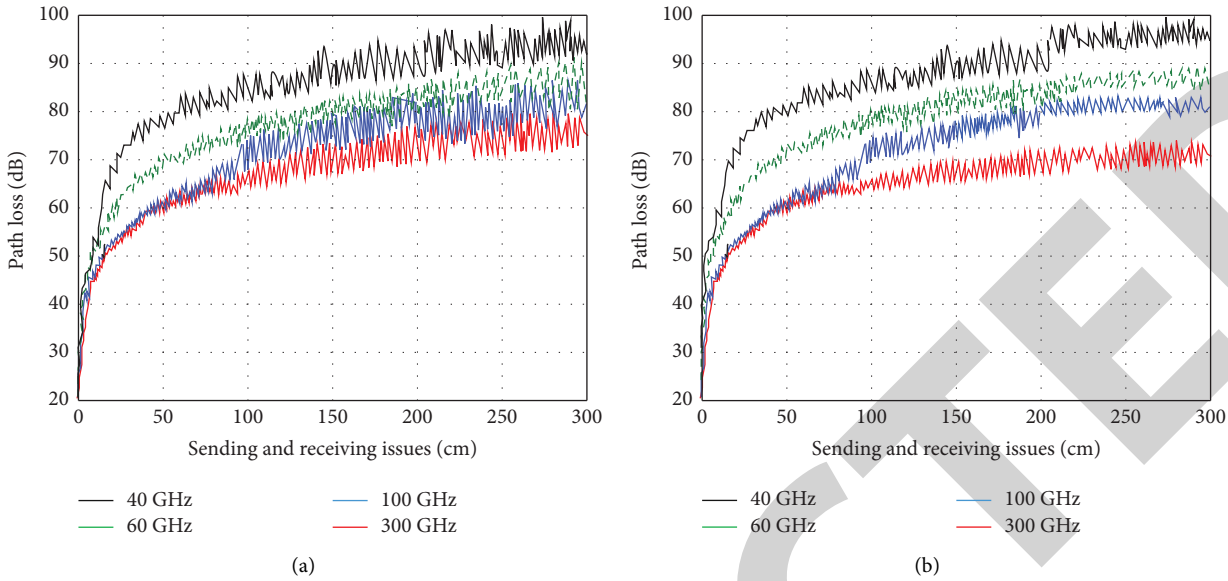

Figure 6: Comparison of path loss at different frequencies. (a) Comparison of path loss at different frequencies (horizontal). (b) Comparison of path loss at different frequencies (vertical).

horizontal polarization, since the polarization current will not be generated under the vertical polarization, the distance between the sending and receiving distance is 10 cm-100 cm. Moreover, the path loss under the vertical polarization is relatively stable, and there is no large fluctuation. On the contrary, there is a large fluctuation in the same distance range under the vertical polarization.

For regional multipath channel models, the difference between frequency sizes is also an important factor affecting path loss. In order to effectively analyze the influence of frequency on path loss, the path loss under different polarizations and frequencies is simulated by MATLAB. Taking the wood floor as the research object, the vertical distance from the antenna to the ground is set to 30 cm, and the four frequencies of 40 GHz, 60 GHz, 100 GHz, and 300 GHz are studied. The specific simulation diagrams are shown in Figure 6.

As can be seen from Figure 6, on the whole, with the increase of the transceiver spacing, there is no obvious difference between the path loss trends at these four different frequencies. The fluctuation range of the path loss in the entire transmission and reception distance is not large, and there is no trend of steep increase or decrease. From the perspective of the changing spacing range, whether it is horizontal polarization or vertical polarization, when the transmitting and receiving spacing changes in the range of 0-50 cm, the path loss increases faster. However, in the range of 50-300 cm, the variation range of the path loss is relatively stable. It can be seen from the comparison of the two polarization modes that when the transmission and reception distance is in the range of 50 cm-10 cm, the path loss under vertical polarization is relatively stable, and the range of amplitude variation is small. The main reason is that when the electromagnetic wave propagates in the horizontal polarization mode, the polarization current will be affected by the existence of the ground impedance, so that the electromagnetic signal will be attenuated. In contrast, vertical polarization does not generate polarization current, so it does not generate large fluctuations.

Therefore, from the above analysis, the improved multipath transmission channel link model has general applicability. The factors affecting the path loss are mainly determined by the vertical distance between the antenna and the reflection surface of the electromechanical control signal and the material of the reflection surface of the electromechanical control signal. In vertical polarization or horizontal polarization, the path loss obtained at different frequencies is also different.

When analyzing the link loss of a wireless channel within an area, a linear equation in the form of $y = ax + p$ is generally used to represent the characteristic of the average link loss on the logarithmic coordinate. Therefore, the equation for the average link loss is described as follows:

$$\overline{L} = a \cdot \log_{10}(d/d_0) + p. \tag{17}$$

Comparing formulas (14) and (17), it is found that in the logarithmic coordinate system, the theoretical prediction result formula and the empirical model formula are consistent in form. Therefore, the slope of the fitted straight line is: $a = 10n$, from which the value of the average path loss n can be obtained. There is a linear relationship between the link loss index n and the logarithm of the sending and receiving distance d (base 10). After fitting the data obtained from the test, the slope of the fitted curve is the link loss index n.

3. Electromechanical Control System Based on Computer Fault Tolerance Technology

For the purpose of improving the reliability and security of computer systems, using the theoretical knowledge and

RETRACTED

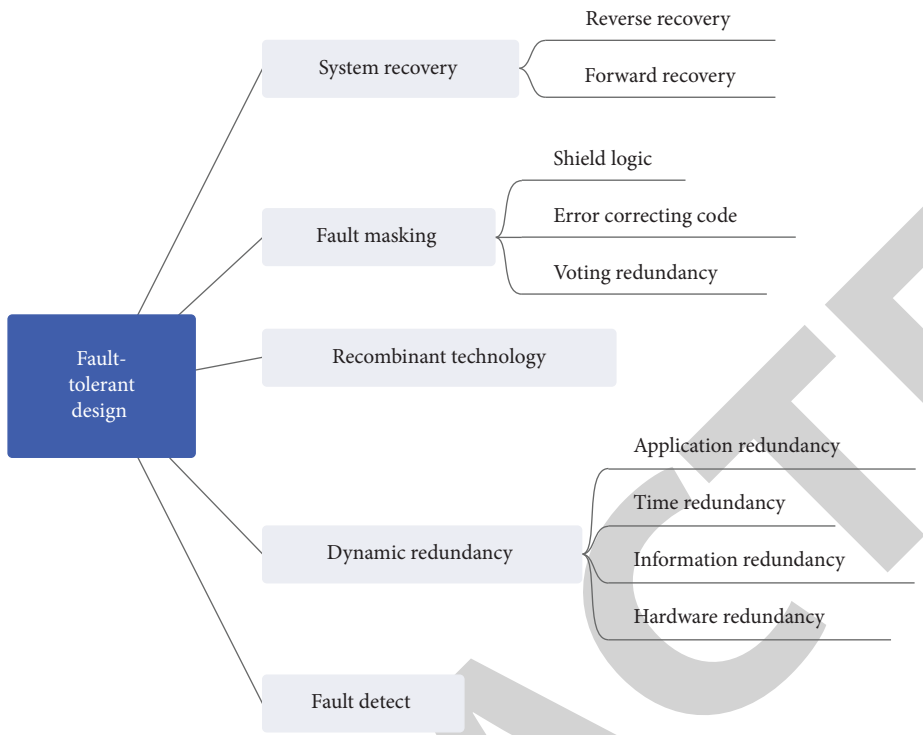

Figure 7: Fault-tolerant design method diagram.

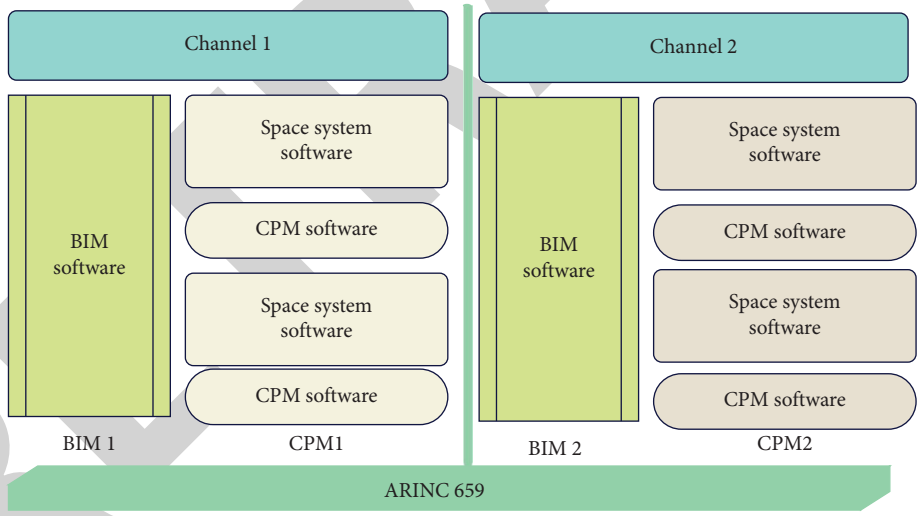

Figure 8: Structure diagram of comprehensive management computer software.

practical methods of fault-tolerant technology to formulate fault-handling strategies is the key to realizing system fault-tolerant design. The fault-tolerant design of the system is mainly realized through fault detection, fault shielding, dynamic redundancy, reorganization technology, and system recovery. The key steps of its fault-tolerant design are shown in Figure 7.

The integrated management computer system software is mainly composed of four parts: bus interface module software (BIM software), control management module software (CPM software), avionics system software (MMS software), and electromechanical system software (UMS software). The BIM module software is responsible for managing the collection of GJB289A bus, RS422 bus, and analog discrete quantity, etc. The CPM module software completes the redundancy management, input and output monitoring voting, task scheduling, and other work. The system structure is shown in Figure 8.

On the basis of the above research, the effect of the electromechanical control system based on computer fault-tolerance technology proposed in this paper is verified, and the control effect and system stability of the electromechanical system are counted, and the results shown in the following Figure 9 are obtained.

RETRACTED

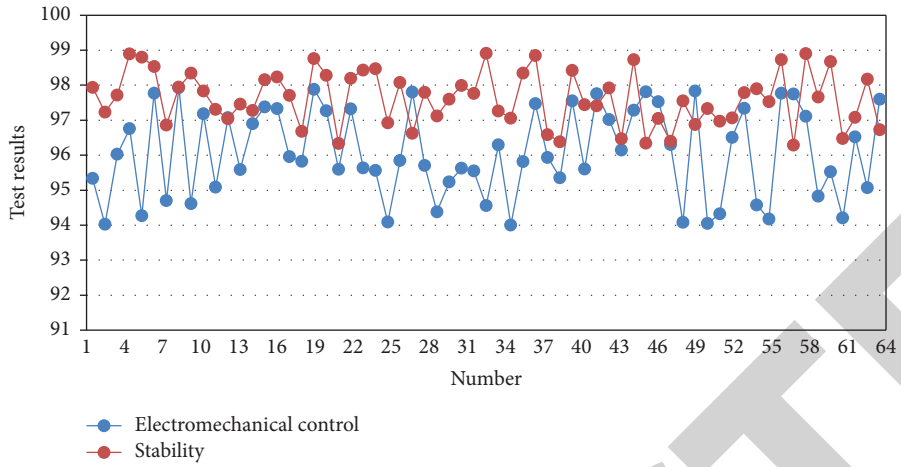

Figure 9: Verification of the effect of the electromechanical control system based on computer fault-tolerant technology.

It can be seen from the above research that the electromechanical control system based on the computer fault-tolerant technology proposed in this paper has stable performance and can play an important role in the control of electromechanical systems.

4. Conclusion

With the development of science and technology and control theory, the leveling system is developing towards intelligent automation and high precision, speed, and stability. Moreover, with the improvement and development of control objects and control devices, there are nonlinear, time-varying parameters, disturbances, unmodeled dynamics, mechanical resonance, and inconsistent responses of sensors to environmental factors in the system. This makes it difficult for the transfer function model and the state space model developed on this basis to accurately and comprehensively reflect the real characteristics of the object, and these unmodeled characteristics may lead to control failure in some specific cases. This paper combines the computer fault-tolerant technology to design the electromechanical control system to improve the intelligent control effect of the electromechanical control system. The research results show that the electromechanical control system based on computer fault-tolerance technology proposed in this paper has stable performance and can play an important role in the control of electromechanical systems.

Data Availability

The labeled dataset used to support the findings of this study is available from the corresponding author upon request.

Conflicts of Interest

The author declares that there are no conflicts of interest.

Acknowledgments

This work was supported by 2021 Project of Shaanxi Education Science "14th Five-year Plan": Research on the Construction of New Engineering Collaborative Education Mode Based on "Three Chains" Integration—A Case study of Computer Major (No.: SGH21Y0345).

References

[1] S. Zinchenko, V. Mateichuk, P. Nosov et al., "Use of simulator equipment for the development and testing of vessel control systems," *Electrical, Control and Communication Engineering*, vol. 16, no. 2, pp. 58–64, 2020.

[2] C. Gehrmann and M. Gunnarsson, "A digital twin based industrial automation and control system security architecture," *IEEE Transactions on Industrial Informatics*, vol. 16, no. 1, pp. 669–680, 2020.

[3] Y. Bichiou and H. A. Rakha, "Developing an optimal intersection control system for automated connected vehicles," *IEEE Transactions on Intelligent Transportation Systems*, vol. 20, no. 5, pp. 1908–1916, 2019.

[4] K. Eltag, M. S. Aslamx, and R. Ullah, "Dynamic stability enhancement using fuzzy PID control technology for power system," *International Journal of Control, Automation and Systems*, vol. 17, no. 1, pp. 234–242, 2019.

[5] K. Wang, E. Tian, J. Liu, L. Wei, and D. Yue, "Resilient control of networked control systems under deception attacks: a memory-event-triggered communication scheme," *International Journal of Robust and Nonlinear Control*, vol. 30, no. 4, pp. 1534–1548, 2020.

[6] M. Saraswat, K. Sharma, N. R. Chauhan, and R. K. Shukla, "Role of automation in energy management and distribution," *Journal of Scientific and Industrial Research*, vol. 79, no. 10, pp. 951–954, 2020.

[7] D. Xu, B. Wang, G. Zhang, G. Wang, and Y. Yu, "A review of sensorless control methods for AC motor drives," *CES Transactions on electrical machines and systems*, vol. 2, no. 1, pp. 104–115, 2018.

RETRACTED

Hindawi
Journal of Robotics
Volume 2023, Article ID 9874013, 1 page
https://doi.org/10.1155/2023/9874013

Retraction

Retracted: Analysis and Evaluation of Ecological Environment Monitoring Based on PIE Remote Sensing Image Processing Software

Journal of Robotics

Received 19 December 2023; Accepted 19 December 2023; Published 20 December 2023

Copyright © 2023 Journal of Robotics. This is an open access article distributed under the Creative Commons Attribution License, which permits unrestricted use, distribution, and reproduction in any medium, provided the original work is properly cited.

This article has been retracted by Hindawi following an investigation undertaken by the publisher [1]. This investigation has uncovered evidence of one or more of the following indicators of systematic manipulation of the publication process:

(1) Discrepancies in scope
(2) Discrepancies in the description of the research reported
(3) Discrepancies between the availability of data and the research described
(4) Inappropriate citations
(5) Incoherent, meaningless and/or irrelevant content included in the article
(6) Manipulated or compromised peer review

The presence of these indicators undermines our confidence in the integrity of the article's content and we cannot, therefore, vouch for its reliability. Please note that this notice is intended solely to alert readers that the content of this article is unreliable. We have not investigated whether authors were aware of or involved in the systematic manipulation of the publication process.

Wiley and Hindawi regrets that the usual quality checks did not identify these issues before publication and have since put additional measures in place to safeguard research integrity.

We wish to credit our own Research Integrity and Research Publishing teams and anonymous and named external researchers and research integrity experts for contributing to this investigation.

The corresponding author, as the representative of all authors, has been given the opportunity to register their agreement or disagreement to this retraction. We have kept a record of any response received.

References

[1] X. Wang and Z. Wang, "Analysis and Evaluation of Ecological Environment Monitoring Based on PIE Remote Sensing Image Processing Software," *Journal of Robotics*, vol. 2022, Article ID 1716756, 12 pages, 2022.

Hindawi
Journal of Robotics
Volume 2022, Article ID 1716756, 12 pages
https://doi.org/10.1155/2022/1716756

RETRACTED

Research Article

Analysis and Evaluation of Ecological Environment Monitoring Based on PIE Remote Sensing Image Processing Software

Xiaofeng Wang and Zhengran Wang

School of Water Conservancy and Electric Power of Heilongjiang University, Harbin, Heilongjiang 150080, China

Correspondence should be addressed to Xiaofeng Wang; 1990033@hlju.edu.cn

Received 4 August 2022; Revised 20 August 2022; Accepted 5 September 2022; Published 4 October 2022

Academic Editor: Shahid Hussain

Copyright © 2022 Xiaofeng Wang and Zhengran Wang. This is an open access article distributed under the Creative Commons Attribution License, which permits unrestricted use, distribution, and reproduction in any medium, provided the original work is properly cited.

With the continuous improvement of people's demand for ecological environment quality, the research on ecological environment monitoring, analysis and evaluation had been paid more and more attention by relevant departments and personnel. Because the images collected by remote sensing technology were many and multi-source, the features extracted from remote sensing images using traditional methods had been difficult to meet the needs of related industry applications. Therefore, this paper made use of the advantages of PIE remote sensing image processing software in data analysis and processing, and put forward the research on ecological environment monitoring, analysis and evaluation methods. Firstly, on the basis of summarizing the concepts and related problems of ecological environment, this paper analyzed the processing methods of remote sensing data sources of ecological environment, and explained the evaluation standards and common methods of ecological environment. Secondly, the composition of PIE remote sensing image processing technology system and its application advantages were described, the common indicators and analysis methods of ecological environment monitoring were given, and the index system and model of ecological environment comprehensive evaluation were established. Finally, through the analysis of experimental cases, the results showed that the ecological environment monitoring analysis and evaluation method proposed in this paper was feasible. Compared with the traditional methods, the method proposed in this paper could objectively evaluate the ecological environment. This paper can not only provide support for the analysis and processing of remote sensing image data, but also provide an important reference for the application of remote sensing technology in the field of ecological environment.

1. Introduction

With the continuous development of economy and society, the quality of ecological environment has been widely concerned by people and all sectors of society. The advantages and disadvantages of ecological environment refer to the environmental suitability that affects the sustainable development of human and society from the perspective of ecosystem within a certain time and space [1]. The quality of ecological environment is mainly based on the monitoring results of ecological environment to evaluate the ecological attributes and their changes. The monitoring of the ecological environment is generally to collect the ecological environment parameters in a certain area in real time through relevant equipment. In order to truly reflect the change law of the ecological environment, the data collection process is not only real-time, but also requires long-term and periodic, and the accuracy of the data needs to meet certain requirements.

In terms of ecological environment monitoring, people often integrate remote sensing technology (RS), global position system (GPS) and geographic information system (GIS) and apply them to the collection and processing of ecological environment parameters [2, 3]. Among them, RS technology can observe real-time data in a wide range of areas all day, and the data acquisition accuracy is high. In recent years, the resolution of remote sensing images obtained by RS in space, time and spectrum has been greatly improved, which makes it widely used in the monitoring of ecological environment. The system integrating spatial

positioning, remote sensing and geographic information technology can collect, analyze and process the target data in real time. Through the intelligent analysis and processing of data, it can provide some support for the application fields of resources, environment and management [4]. With the rapid development of electronic communication, Internet of things, big data and space technology, 3S technology is more and more widely used in ecological environment monitoring, resource exploration and development and natural disaster prevention and control.

There are many ground data sources and a large amount of data collected by remote sensing technology. For example, the sensors of different monitoring equipment may obtain data with different resolutions in the same area, and the same equipment may also obtain data with different spatial and spectral resolutions in the same area [5]. It is known from the existing research that using the data collected by different devices and sensors to study the changes of the ecological environment is no longer a static mode, but a dynamic real-time monitoring mode, which will lead to the existing system unable to meet the effective integration of multi-source data. Therefore, this paper proposes to use PIE remote sensing image processing software to monitor and evaluate the ecological environment, so as to provide technical support for remote sensing technology and its application in the field of ecological environment monitoring.

2. Related Works

According to the existing research, due to different perspectives, the understanding of the ecological environment is not consistent. Early people believed that the ecological environment refers to the life system composed of different types of organisms except human beings. This view focuses on the perspective of ecosystem. Later, some people believed that ecological environment refers to a natural system composed of relevant natural elements, which has certain environmental and resource characteristics [6, 7]. From a narrow environmental perspective, some people believe that ecological environment refers to habitat, that is, the external environmental conditions related to organisms, such as geographical location, terrain, landform, temperature and so on. In a broad sense, people believe that ecological environment refers to the nature related to human production and life. Research shows that, as a necessary external condition for human survival and development, the ecological environment is an organic whole composed of life and environment. Among them, the environmental system includes natural factors related to organisms such as geology, soil, hydrology, climate, etc., and life includes not only human beings, but also all biological worlds [8]. The main research objects of ecological environment include biodiversity, the relationship between biology and environment, etc. With the progress of society and human civilization, the ecological environment has gradually turned into the ecosystem research with human as the main body. Therefore, the research on the ecological environment has important historical and practical significance in the long run.

Ecological environment monitoring mainly uses various equipment to obtain data information such as ground ecological attributes and environmental characteristics. With the rapid development of remote sensing technology, the use of satellites can achieve three-dimensional, multi angle, all-round and all-weather monitoring of ground targets. Because the satellite remote sensing monitoring target has certain advantages such as high spatial resolution, high spectral resolution, high temporal resolution and high radiation resolution, the satellite remote sensing technology can provide rich data sources for ecological environment monitoring. At present, in the aspect of ecological environment monitoring, people mainly use the method of human-computer interactive interpretation and classification to extract various monitoring data on the basis of processing the obtained remote sensing images. In recent years, some scholars have made more research achievements in the automatic extraction of remote sensing image data, and have made great progress in data extraction methods and accuracy [9, 10]. However, most of these methods are limited to the data extraction of small areas and specific areas, which are not suitable for the ecological environment monitoring of large coverage areas, and the effect of data extraction for complex ground objects is not ideal.

The quality of ecological environment mainly reflects the attributes of ecological environment and its changing state. Qualitative or quantitative methods can be used to describe the environmental attributes and their changing process. In order to evaluate the quality of ecological environment, we need to use the obtained ecological environment monitoring data to extract the characteristics that can reflect the attributes of ecosystem and the changes of ecological environment [11]. In the comprehensive evaluation of the ecological environment, we need to use the obtained ecological environment monitoring information, select relevant evaluation indicators and formulate the ecological environment evaluation system, and then use certain evaluation methods and models to evaluate the ecological attributes and environmental characteristics of a region. Using the comprehensive evaluation results of the ecological environment, we can analyze the spatio-temporal changes of the ecological environment in the region, and explore various factors that cause the changes of the ecological environment, so as to provide decision-making basis for scientifically improving the regional ecological environment and formulating environmental protection plans.

3. Theory and Method of Ecological Environment Research

3.1. Overview of Ecological Environment and Its Problems. Since the 1980s, with the continuous development of economy and society and the increase of population, the global climate has been continuously warming and the trend of drought has been expanding, resulting in the shortage of water resources, the changes of river systems, the increase of land desertification area, serious vegetation degradation and other problems affecting the ecological balance [12]. For example, due to the reduction of vegetation coverage, the

RETRACTED

change of rivers and the contraction of wetland area, the water conservation capacity is weakened, the ecological environment is seriously damaged, and the regulation and restoration functions of the ecosystem are degraded. Regional ecological environment and ecological security issues have been highly valued by relevant government departments.

From the perspective of water resources and water system changes, due to climate warming, glaciers and frozen soils deposited for many years in some areas continue to melt and shrink, seasonal climate disorders, and snow reduction. The depletion of water resources in some regions has affected the surrounding ecological environment, making ecological functions continue to deteriorate, and may lead to the consequences of ecological imbalance [13]. Due to serious water and soil loss, the area of land desertification in some regions is expanding, and soil wind erosion leads to the destruction of vegetation. In addition, due to the large fluctuation of climatic conditions, the restoration ability of vegetation and soil has been seriously reduced, coupled with man-made damage to the natural environment, such as overgrazing or unreasonable reclamation of land resources, the problem of desertification has become increasingly prominent.

From the perspective of wetland change and geological movement, due to the continuous reduction of wetland area, the water supply of some rivers has decreased, resulting in climate changes in some regions. In terms of wetland distribution, wetlands account for a large proportion in some inland areas, and are mainly distributed in some ecologically sensitive areas such as rivers or oases. Affected by global climate and human behavior factors, the overall area of wetlands has shrunk, resulting in the imbalance of river water levels and serious grassland degradation. In addition, some areas are greatly affected by terrain and slope, and geological disasters such as debris flow, landslide and water and soil loss occur all year round, resulting in serious threats to the local and surrounding ecological environment and people's lives.

From the perspective of the impact of population and economic development on the ecological environment, the rapid and uneven growth of population size and economic development has led to the decline of the carrying capacity of natural resources and ecological environment in some regions, resulting in great changes in the attributes of the ecological environment. Affected by global economic development and climate change, human production and life are increasingly interfering with the ecological environment, coupled with the sharp rise in the number of people, making it difficult for limited ecological resources to meet the needs of economic and social development and human production and life [14]. Therefore, in view of the problems existing in the process of ecological environment change, remote sensing technology and geographic information methods can be used to monitor and analyze various factors affecting the ecological environment, and effectively evaluate the changes of ecological factors, so as to provide support for the rational development, protection and utilization of various natural ecological resources.

3.2. Remote Sensing Data Source of Ecological Environment and Its Processing Method. Remote sensing (RS) technology mainly refers to the method of using remote sensing devices to detect the information of ground objects in the air. It generally uses remote sensing devices on spacecraft, satellites and other equipment to collect data information of ground objects, detect object attribute information by monitoring the mechanism of the response of the target to the spectrum, and identify the target object by analyzing and processing the obtained data. After decades of development, remote sensing technology has been widely used in agriculture, forestry, geology, environmental protection and other fields [15]. With the rapid development of space technology, geographic information system and global positioning technology, the monitoring effect and quality of remote sensing images in spatial resolution, spectral resolution and temporal resolution have been greatly improved. Compared with other monitoring methods, remote sensing technology can effectively provide a large number of real-time collected data for ecological environment monitoring, and can track and monitor the dynamic targets in a large area. Therefore, remote sensing technology provides a certain guarantee for ecological environment monitoring and data collection. As shown in Figure 1, it is a schematic diagram of the acquisition and processing of remote sensing image information.

In order to extract effective information from remote sensing image data, when processing multi-spectral image data, it is necessary to extract image information by calculating the standard deviation and mean vector of image data. Generally, the standard deviation of image data can directly reflect the amount of information of the image, while the brightness difference can reflect the contrast of the image.

If the image is represented by $p_{ij}(i = 1, 2, \ldots, M; j = 1, 2, \ldots, N)$, its matrix size is $H * L$, and the average gray value of the image is represented by p_0, the standard deviation of the image can be expressed as follows [16]:

$$d_S = \frac{\sqrt{\sum_{i=1}^{M} \sum_{j=1}^{N} \left(p_{ij} - p_0\right)^2}}{H \cdot L}. \tag{1}$$

Since the gray value of the image can be reflected by the brightness difference, the gray value of the image can be expressed by subtracting the minimum brightness value from the maximum brightness value of the image, as shown below:

$$G_r(i, j) = G_{\mathrm{MAX}}(i, j) - G_{\mathrm{MIN}}(i, j). \tag{2}$$

The mean vector of the image mainly describes the average reflection intensity of the target in the image, which can be expressed as follows:

$$G = \frac{\sum_{i=1}^{M-1} \sum_{j=1}^{N-1} G(i, j)}{H \cdot L}. \tag{3}$$

According to the above method, the correlation values of all bands on the remote sensing image are calculated, and then the band with the largest amount of information is extracted by comparison.

RETRACTED

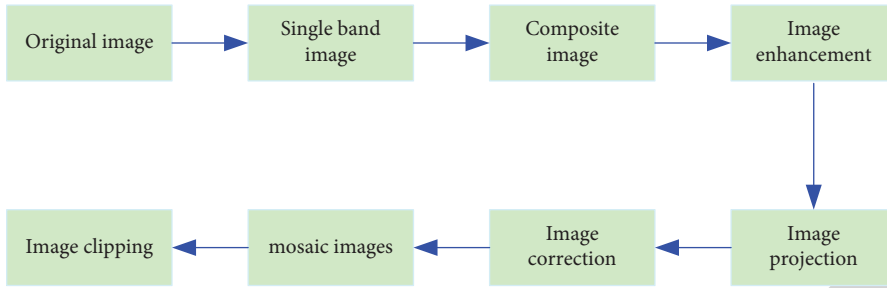

Figure 1: Schematic diagram of remote sensing image processing process.

There are many redundant observation information in the multi-spectral images collected by remote sensing technology. In order to avoid the information interference between different bands in the image, the quality of image synthesis can be improved by reducing data redundancy. The standard deviation of image data is directly proportional to its amount of information, while the correlation between image bands is inversely proportional to its independence, that is, the smaller the correlation, the more obvious the independence of different bands, and the less redundant information. The correlation between bands can be expressed by correlation coefficient, that is, the greater the correlation coefficient, the greater the correlation between different bands.

It may be assumed that p_{ij} and q_{ij} represent two remote sensing images with the size of $H * L$, and p_0 and q_0 denote the gray mean value of these two images respectively, so the correlation coefficient between different bands on the remote sensing image can be expressed as [17]:

$$r = \frac{\sum_{i=1}^{M}\sum_{j=1}^{N}\left(p_{ij}-p_0\right)\left(q_{ij}-q_0\right)}{\sqrt{\sum_{i=1}^{M}\sum_{j=1}^{N}\left(p_{ij}-p_0\right)^2\left(q_{ij}-q_0\right)^2}}. \quad (4)$$

In order to comprehensively monitor the ecological environment, it is usually necessary to obtain more information of ground targets with the help of geographic information system (GIS) and global positioning system (GPS). Through the integration of RS, GIS and GPS technology, we can accurately obtain the target attribute information and location information of the ground ecological area, and establish a spatial information database based on the superposition processing and statistical analysis of the spatial data, so as to effectively manage and query the spatial data [18].

Due to the multi-source nature of the collected data, not only there are many kinds of data, but also the data has its own characteristics in format, space-time scale and so on. Therefore, it is necessary to effectively integrate and fuse all kinds of data when processing data. As shown in Figure 2, the process of organic fusion of the collected remote sensing data is described.

3.3. Ecological Environment Assessment Standards and Common Methods

3.3.1. Selection of Evaluation Criteria. Remote sensing images not only provide data basis for the analysis of ecological environment changes and their influencing factors, but also provide basis for the evaluation of ecological environment quality. In order to objectively evaluate the obtained ecological environment monitoring results, it is necessary to refer to certain industry standards. The selection of ecological environment quality evaluation standards should not only fully reflect the changes of ecological environment attributes and their advantages and disadvantages, but also reflect the areas and conditions of ecological environment changes. Since most of the ecological environment evaluation indicators are obtained through remote sensing and other technologies, their evaluation standards need to be determined according to the specific actual situation.

At present, the standards adopted generally come from some standards issued by the state, industry and local governments for ecological environment protection and quality requirements. For example, the protection requirements of important ecological function areas, water and soil conservation requirements, river system protection requirements, etc. In addition, the original ecosystem can also be used as the standard, such as the standard requirements for soil biochemistry, the standard requirements for vegetation coverage and biodiversity, and the standard requirements for water and soil holding capacity. As the existing evaluation standards may change with natural conditions and policies, these standards can still be used as a basis to measure the quality of the ecological environment for the ecological environment monitoring data at a certain stage.

3.3.2. Standardization of Evaluation Indicators. Considering the multi-source nature of remote sensing image information, in order to avoid the differences between the original index parameters, the data must be standardized to achieve the standardization of indicators and make different index parameters comparable. When evaluating the ecological environment, if the larger the index parameter value is, the better the evaluation result is, it is called a positive index; if the smaller the index value is, the better the evaluation result is, it is called a negative index; if the index value is closer to a certain value, the better the evaluation result is, it is called a medium index. In order to facilitate the comprehensive evaluation of the ecological environment, different types of indicators need to be treated with the same trend. Therefore, the positive method of indicators can be

RETRACTED

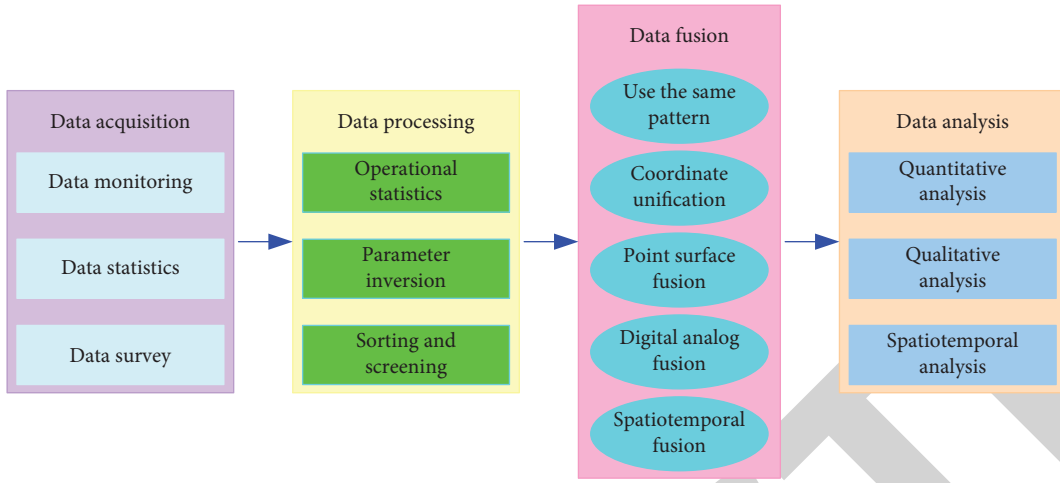

Figure 2: Schematic diagram of multi-source data fusion technology architecture.

adopted to convert negative indicators and neutral indicators into positive indicators.

If D_1 is a positive indicator and D_2 is a negative indicator, they can be expressed as follows in turn:

$$D_1 = \frac{D - D_{\text{MIN}}}{D_{\text{MAX}} - D_{\text{MIN}}} \times 100,$$
$$D_2 = \frac{D_{\text{MAX}} - D}{D_{\text{MAX}} - D_{\text{MIN}}} \times 100, \quad (5)$$

where D_{MIN} represents the minimum value of the index parameter and D_{MAX} indicates the maximum value of the index parameter. The range of index parameter values after standardization is between 0 and 100, and the distribution of index parameter values after standardization is the same as the original index values.

As shown in Figure 3, the geometric method is used to represent the process of index normalization.

Considering the dimensions and unit differences of different evaluation indicators, in order to make the evaluation indicators not affected by this, it is necessary to standardize the relevant evaluation indicators. Common data standardization processing methods are as follows:

$$S_{ij} = \frac{\text{obs}_{ij} - \overline{\text{obs}_i}}{ds_i}, \quad j = 1, 2, \ldots, n, \quad (6)$$

where obs_{ij} shows the observed value, $\overline{\text{obs}_i}$ represents the average value, and ds_i indicates the standard deviation. S_{ij} refers to the evaluation index after standardization. The mean value of all n individuals is 0 and the variance is 1.

As shown in Figure 4, the data standardization process represented by geometric method is described.

3.3.3. Commonly Used Comprehensive Evaluation Methods of Ecological Environment. With the rapid development of economy and society, the monitoring and quality evaluation of ecological environment has attracted extensive attention of governments and relevant personnel. In the process of monitoring, analyzing and evaluating the ecological environment, the evaluation standard and evaluation model are

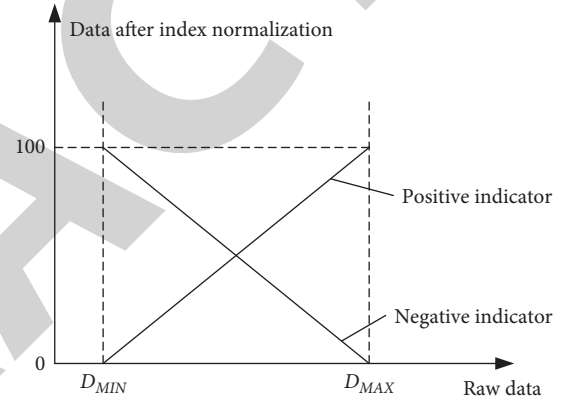

Figure 3: Schematic diagram of geometric representation results of index normalization.

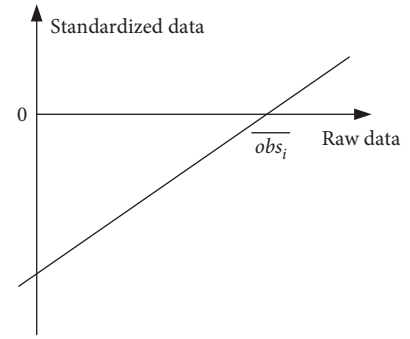

Figure 4: Schematic diagram of geometric representation results of index standardization.

the key to the comprehensive evaluation results. The traditional evaluation method generally takes single factor or natural environment system as the standard, and uses the static method to evaluate. This method is simple, but the evaluation result is quite different from the actual situation. In order to accurately reflect the development of the ecological environment, the current evaluation methods are mainly based on multi factor indicators, and use a dynamic way to evaluate. Common comprehensive evaluation methods include comprehensive index method, fuzzy

RETRACTED

evaluation method, artificial neural network analysis method, gray correlation analysis method and principal component analysis method [19].

The index evaluation method is mainly used to compare the original data obtained from environmental monitoring with the evaluation standards. This method is suitable for the index evaluation of single factor environmental impact, but it can not be applied to the synergy evaluation of multiple impact factors. Fuzzy evaluation method mainly uses fuzzy mathematics to quantify some factors that are not easy to define, and applies them to comprehensive evaluation. This method adopts fuzzy evaluation matrix to determine some uncertain factors that need to be considered in ecological environment assessment. Because this method needs to use membership degree to describe the quality of ecological environment, the determination of index weight and membership function is the key of this method. It is known from the existing research that the artificial neural network analysis method can train the environmental monitoring samples through the neural network model, and obtain certain knowledge rules from the training results. Then, the network model can be used to accurately identify and evaluate the monitoring information. For example, when using B-P neural network model to comprehensively evaluate the quality of ecological environment, it is not necessary to deal with the evaluation indicators, and the evaluation results obtained by using this model are relatively objective. In addition, using B-P neural network model, multiple evaluation indexes can be selected to establish a comprehensive evaluation system of ecological environment quality, but there are problems such as parameter convergence and optimization in the application of B-P neural network algorithm [20].

4. Analysis and Evaluation of Ecological Environment Monitoring Based on PIE Remote Sensing Image Processing Technology

4.1. Overview of PIE Remote Sensing Image Processing Technology. Remote sensing image processing software is mainly a tool software that provides technical support for the application of remote sensing monitoring data to different industries. Since 2008, China has developed the first generation of remote sensing image processing software, namely pixel information expert (PIE) [21, 22]. PIE is mainly used to analyze and process remote sensing monitoring data and apply it to different industries to provide technical support. The software can effectively analyze the monitoring information from land, meteorology, ocean and other fields, and provide accurate and efficient processing results according to the characteristics of various parameters collected by domestic satellites. The software can support local coordinate system, has friendly user interface and interaction mode, can support the secondary development of different languages, and can provide solutions for applications in different industries. Through nearly a decade of application, the development progress of PIE has been improved from version 1.0 to version 6.0, as shown in Figure 5.

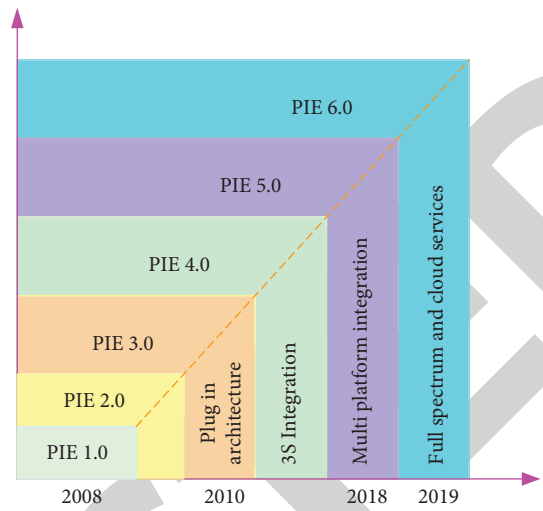

Figure 5: Schematic diagram of PIE development process.

The latest generation of remote sensing image processing software PIE 6.0 integrates cloud computing and terminal technology, adopts a multi-layer structure design method, and provides secondary development interfaces and a series of toolkits. The professional toolkit provided by the software not only involves PIE-Basic remote sensing image basic function, PIE-Ortho satellite image mapping function, PIE-SAR radar image processing function, PIE-Hyp hyperspectral image processing function, PIE-UAV image processing function, but also includes PIE-SIAS image analysis software, PIE-AI image intelligent processing software and PIE-Map geographic information system software. In addition, the software can integrate standardized data in relevant service fields through PIE-Cloud platform, so as to establish a remote sensing technology support system integrating cloud and terminal [23]. As shown in Figure 6, the functional composition of PIE 6.0 remote sensing technology support system is described.

According to the needs of different industries, PIE-Cloud platform adopts key technologies such as spatio-temporal big data analysis and storage, intelligent data analysis and mining, cloud computing, etc. to solve the problems of remote sensing image data analysis and processing, data mining and decision-making. The system can integrate the processing, detection, feature extraction and application of multi-source remote sensing data according to the various needs of users, so as to effectively complete the monitoring and evaluation function of remote sensing data.

4.2. Ecological Environment Monitoring and Analysis. In ecological environment monitoring, vegetation index is often used for qualitative and quantitative analysis and evaluation of vegetation coverage. In the remote sensing image, the relevant vegetation index can be calculated by combining the visible band and the near-infrared band. In order to facilitate data analysis and evaluation, normalized difference vegetation index can be used to describe vegetation coverage.

RETRACTED

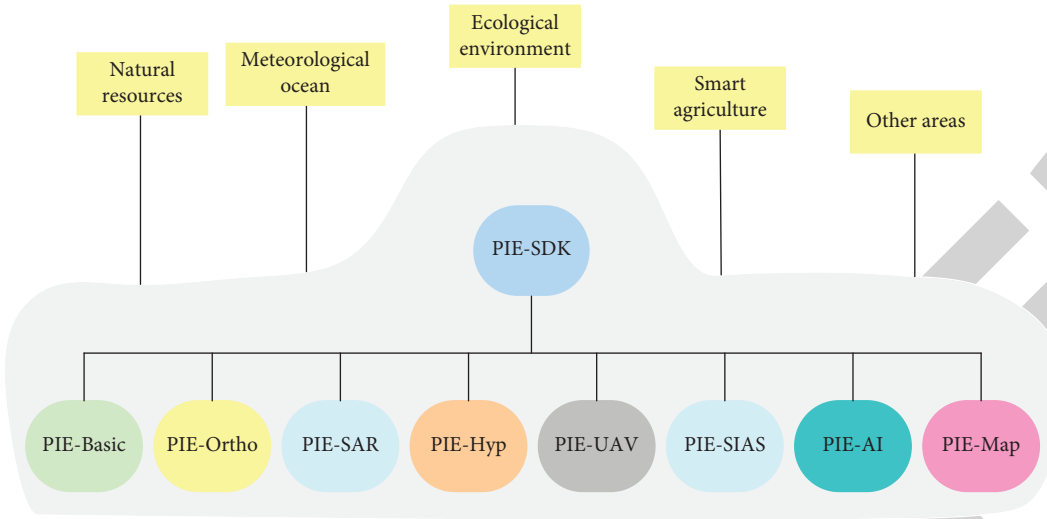

Figure 6: PIE 6.0 remote sensing technology and its application system diagram.

The calculation method of vegetation index ND is as follows:

$$ND = \frac{NR - RV}{NR + RV}, \tag{7}$$

where RV refers to the reflectance of visible band, NR indicates the reflectance of near-infrared band, and the value range of vegetation index is (−1, 1).

Fractional vegetation coverage mainly describes the proportion of the vertical projection area of vegetation in the total area of remote sensing area, which is usually used to evaluate plant coverage. Vegetation coverage can be estimated using vegetation index values, as follows:

$$FC = \frac{NR - NR_{MIN}}{NR_{MAX} - NR_{MIN}}, \tag{8}$$

where NR_{MIN} and NR_{MAX} respectively represent the minimum and maximum values of NR within a certain confidence interval, and the value range of FC is (0, 1).

As the ecological environment monitoring indicators contain multiple ecological factors, these ecological factors have a mutually restrictive relationship, and any factor may affect the whole ecological environment. In order to facilitate the analysis of the relationship between ecological environment factors, we can explore the factors that play a leading role in the ecological environment, so as to take corresponding measures to avoid the impact of these factors on the ecological environment. For example, climate change factors can not only affect the regional ecological environment, but also be affected by local climate due to ecological environment changes. The change of ecological environment cannot be separated from the interaction of many factors. Among these factors, climate change and human behavior are the two main factors affecting environmental change. Although climatic factors are the main factors that affect the changes of ecological environment, human behavior factors can further affect the changes of ecological environment caused by climatic factors. Because human behavior is not subject to certain constraints and the excessive exploitation of resources and energy, human behavior factors often become the leading factors affecting local regional ecological environment changes. As shown in Figure 7, the changing relationship between different factors and their impact on the ecological environment is described.

From a large number of studies on the influencing factors of the ecological environment, it is known that the main factors driving the change of the ecological environment are usually natural factors, human behavior and the basis of the ecological environment itself. Considering the regional differences and the different factors that cause the changes of the ecological environment in different regions, the changes of the ecological environment can usually be divided into three categories. The first category is the changes of the ecological environment dominated by natural factors, the second category is the changes of the ecological environment jointly affected by natural factors and human behavior, and the third category is the changes of the ecological environment dominated by human behavior. As shown in Figure 8, it reflects the types of ecological environment changes under the influence of different factors.

4.3. Ecological Environment Quality Evaluation Model. In order to grasp the changes of local ecological environment and comprehensively evaluate the quality of ecological environment in this area, the selection of evaluation indicators is very important. In the existing ecological environment evaluation methods, analytic hierarchy process is often used. This method mainly adopts qualitative and quantitative indicators to divide various factors in the system, and determines the corresponding weight according to the impact of each factor on the evaluation system. Among the various factors that affect the change of ecological environment, natural factors mainly include temperature, biodiversity, soil humidity, precipitation and vegetation coverage, while human behavior mainly includes land use, cultivated land water use, population density and resource exploitation. According

RETRACTED

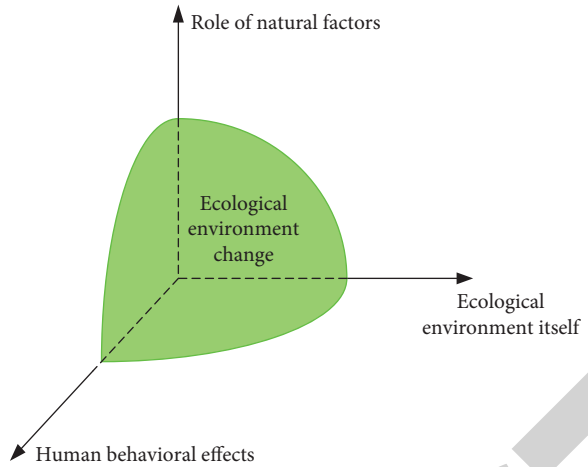

Figure 7: Structural diagram of ecological environment factors.

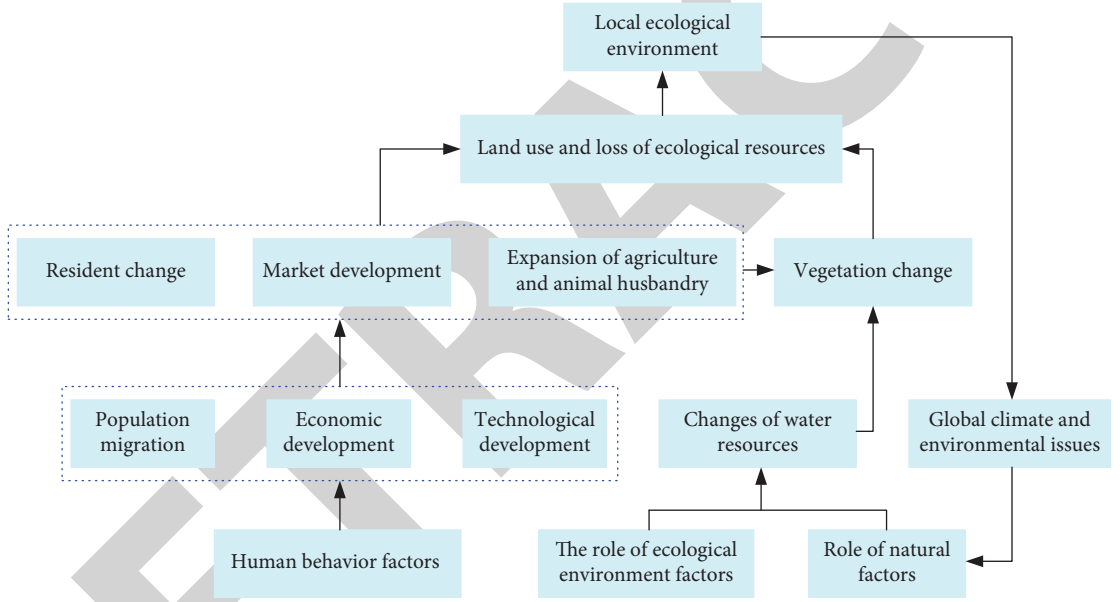

Figure 8: Ecological environment change and its influencing factors.

to different index relations, the comprehensive evaluation index system can be divided into three layers, namely, the comprehensive evaluation target layer, the influencing factor layer and the specific observation layer. The comprehensive evaluation target layer includes natural factors and human behavior factors, and the influencing factor layer can be divided into ecological response, ecological vitality and ecological components, which restrict each other.

As shown in Figure 9, the hierarchical relationship between different evaluation indicators in the comprehensive evaluation index system of ecological environment quality is described.

Because each evaluation index has different influence on the quality of ecological environment, the weight value can be used to reflect the importance of the evaluation index in the comprehensive evaluation index system. Therefore, the subjective evaluation method can be used to determine the weight according to the effect of the evaluation index on the process of ecological environment change. If ω_{jk} represents the weight value of the j-th evaluation index parameter given by the k-th expert, and $\sum_{j=1}^{N} \omega_{jk} = 1$, the weight value of the j-th evaluation index parameter is calculated as follows:

$$\overline{\omega_j} = \frac{\sum_{k=1}^{M} \omega_{jk}}{M},$$
$$w_j = \frac{\overline{\omega_j}}{\sum_{j=1}^{N} \overline{\omega_j}}. \tag{9}$$

In the comprehensive evaluation index system of ecological environment, the indexes at different levels are compared with each other, and the relative importance of each evaluation index is determined. Then, the judgment matrix of each evaluation index is established. After calculating the relative weight values of all evaluation indicators, the weight factor judgment table can be obtained, as shown in Table 1.

RETRACTED

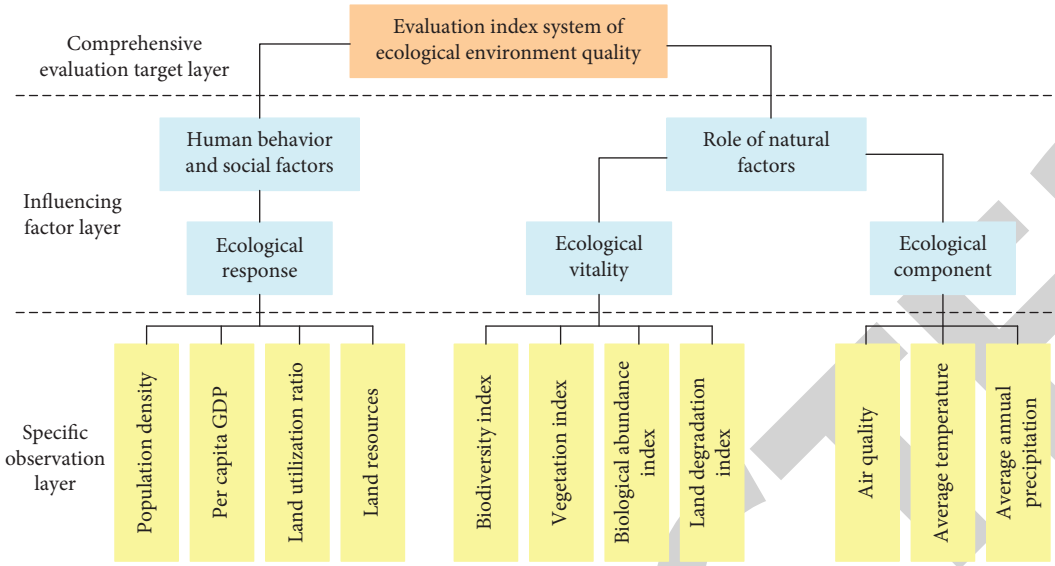

Figure 9: Hierarchical structure diagram of comprehensive average index system of ecological environment quality.

Table 1: Evaluation index weight factor judgment table.

Evaluation index	Evaluation index					
	1	2	—	k	—	M
1	1	b_{12}	—	b_{1K}	—	b_{1M}
2	b_{21}	1	—	b_{2K}	—	b_{2M}
—	—	—	—	—	—	—
j	b_{j1}	b_{j2}	---	b_{jk}	—	b_{jM}
—	—	—	—	—	—	—
N	b_{N1}	b_{N2}	—	b_{Nk}	—	1

According to Table 1, the judgment matrix of evaluation indicators can be obtained, as shown below:

$$B = \begin{pmatrix} 1 & b_{12} & b_{13} & \cdots & b_{1k} & \cdots & b_{1M} \\ b_{21} & 1 & b_{23} & \cdots & b_{2k} & \cdots & b_{2M} \\ \cdots & \cdots & \cdots & \cdots & \cdots & \cdots & \cdots \\ b_{j1} & b_{j2} & b_{j3} & \cdots & b_{jk} & \cdots & b_{jM} \\ \cdots & \cdots & \cdots & \cdots & \cdots & \cdots & \cdots \\ b_{N1} & b_{N2} & b_{N3} & \cdots & b_{Nk} & \cdots & 1 \end{pmatrix}. \quad (10)$$

The judgment matrix can be obtained from the weights given by different experts, and then the average weight can be calculated by hierarchical sorting and consistency testing methods. The weight value of the evaluation index can be obtained after normalization.

In order to obtain the comprehensive evaluation results of ecological environment quality, it is necessary to conduct comprehensive treatment according to the monitoring value and weight value of different evaluation indicators. The specific calculation method is as follows:

$$\text{Eq} = \sum_{j=1}^{N} v_j w_j, \quad (11)$$

where, v_j represents the value of the j-th evaluation index monitoring data after standardized processing, w_j shows the weight value of the j-th evaluation index, and N is the number of all evaluation indexes.

5. Experiment and Analysis

In order to test the effectiveness of the ecological environment monitoring analysis and evaluation model proposed in this paper, a wetland ecological experimental area in a province in southern China was selected as the object of the experiment. The study area has a typical warm temperate continental climate, hot in summer and cold in winter. The annual average temperature is 12.8°C, and the temperature difference between day and night is large. The highest temperature in the year is from July to August, which is higher than 38°C most of the time. The lowest temperature is in January, which is often lower than −5°C. Precipitation is mostly concentrated in May to July, with an average annual precipitation of 120 mm, and the number of rainfall days throughout the year generally does not exceed 55 days.

The data needed for the experiment comes from the images covered by remote sensing satellites in the wetland ecological experimental area. Due to the obvious spectral characteristics of wetland ecological elements in summer, the images collected by satellite sensors are clearly visible.

RETRACTED

Table 2: Remote sensing image selection time period and data type.

Year	Image selection time		Remote sensing image data type
2010	July 15th	August 10th	TM
2013	July 20th	August 15th	TM
2015	July 23th	August 20th	TM
2017	July 7th	August 5th	ETM+
2020	July 13th	August 8th	OLI

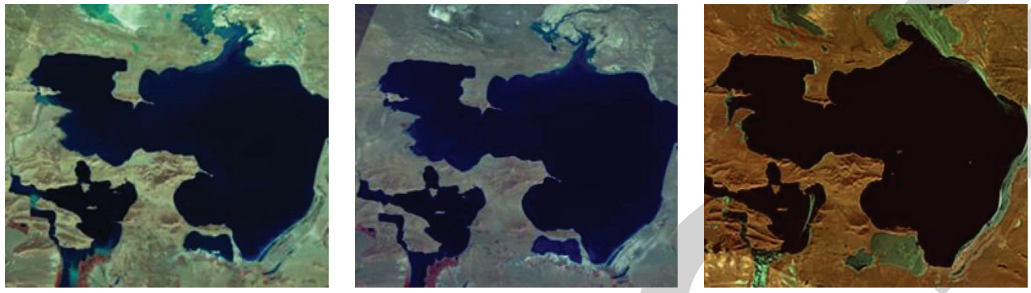

(a) (b) (c)

Figure 10: Remote sensing images of wetland ecological areas with different data types. (a) TM, (b) ETM + and (c) OLI.

Table 3: Evaluation indicators at all levels and their weight values.

Influencing factor index	Specific observation indicators	Weight value	Cumulative value
Role of natural factors	Ecological vitality	0.293	0.638
	Ecological component	0.345	
Human behavior and social factors	Ecological response	0.362	0.362
Cumulative value		1	1

The images of wetland temperature, vegetation coverage, soil humidity and other monitoring indicators are mainly from satellite remote sensing data when the cloud cover is thin from July to August every year. Considering the long experimental period, TM data was selected for the images from 2010 to 2015, ETM + data was selected in 2017, and OLI data was selected in 2020, as shown in Table 2.

In order to comprehensively monitor the ecological changes of wetlands, sampling points were arranged in the relevant experimental areas during the experiment to facilitate the collection of relevant data. The layout of sampling points should not only be as uniform as possible, but also consider the regionality and scope of sampling points. During the experiment, sampling points were arranged at intervals of 5 km along different directions of the wetland according to the concentric circle method, as shown in Figure 10.

The serial numbers of all sampling points, longitude and latitude coordinates, vegetation coverage, surface temperature, soil humidity, air quality and other information are recorded and statistically analyzed through PIE remote sensing image processing software. Then, according to the comprehensive evaluation index system of ecological environment quality proposed in this paper, the weight factors of relevant monitoring indicators are calculated, and finally the weight values of indicators at all levels are obtained, as shown in Table 3.

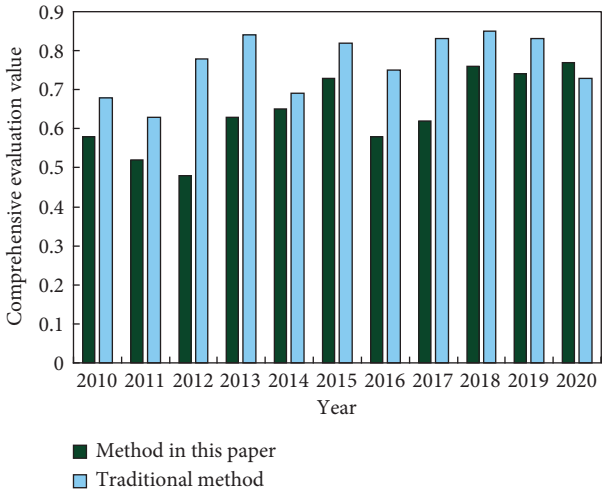

Figure 11: Comparison of the results of comprehensive evaluation of ecological environment quality by using this method and traditional method.

During the experiment, the ecological environment monitoring and evaluation method proposed in this paper is compared with the comprehensive evaluation value obtained by the traditional method, as shown in Figure 11.

According to the comprehensive evaluation results of ecological environment quality, the method proposed in this paper can objectively reflect the change law of the ecological

RETRACTED

environment and its influencing factors in this area. The ecological environment quality of the wetland area has shown an overall growth trend in the past decade, indicating that the wetland ecological environment has been continuously improved in recent years. Due to the relatively high temperature in this area, the scarcity of biological resources and the less impact of human behavior, the ecological environment is easy to be improved. Although the precipitation factor in this area has a great impact on the ecological environment quality, even if the annual average temperature is high, the precipitation can improve the ecological environment quality of the wetland. In addition, because the surface coverage of this area is mainly the oasis ecotone, the wetland is more sensitive to the changes of the surrounding ecological environment. The evaluation results obtained by using traditional methods are quite different from the actual ecological environment changes, and the results of the evaluation of ecological environment changes by using this method basically conform to the change law of natural environmental conditions. Therefore, this method is more scientific in ecological environment monitoring, analysis and evaluation.

6. Conclusion

With the continuous development of remote sensing technology and the improvement of people's requirements for ecological environment quality, the research on ecological environment monitoring had been widely concerned. Due to the multi-source nature of ecological environment monitoring data, it was impossible to obtain the observation information required by relevant industry applications by traditional methods. Therefore, starting from the application advantages of PIE remote sensing image processing software, this paper put forward the research on ecological environment monitoring, analysis and evaluation methods. By summarizing the concept of ecological environment and related problems, this paper analyzed the processing methods of ecological environment monitoring data sources, and gave the standardized processing methods of ecological environment evaluation indicators. Based on the analysis of the composition of pie remote sensing image processing technology system and its application advantages, the design and analysis methods of ecological environment monitoring indicators were proposed, and the comprehensive evaluation index system and evaluation model of ecological environment quality were constructed. Through the test of experimental cases, the results showed that the ecological environment monitoring, analysis and evaluation method proposed in this paper not only had certain effectiveness, but also could evaluate the ecological environment more objectively than the traditional methods. This paper will provide some technical support for the analysis and processing of remote sensing image data and the application of remote sensing technology in related fields.

Data Availability

The labeled data set used to support the findings of this study is available from the corresponding author upon request.

Conflicts of Interest

The author declares that there are no conflicts of interest.

Acknowledgments

This work is supported by Study on adaptability and optimization technology of ecological slope protection in cold area of Songhua River mainstream treatment project (SGZL/KY-10), Scientific research project of Heilongjiang Songhua River main stream treatment project.

References

[1] X. Li, Z. Y. He, L. L. Jiang, and Y. J. Ye, "Research on remote sensing dynamic monitoring of ecological resource environment based on GIS," *Wireless Personal Communications*, vol. 102, no. 4, pp. 2941–2953, 2018.

[2] R. Gibb, E. Browning, P. Glover-Kapfer, and K. E. Jones, "Emerging opportunities and challenges for passive acoustics in ecological assessment and monitoring," *Methods in Ecology and Evolution*, vol. 10, no. 2, pp. 169–185, 2019.

[3] Q. F. Shi, "Research on image detection of ecological environment monitoring based on multiple feature parameters," *Fresenius Environmental Bulletin*, vol. 30, no. 3, pp. 2831–2839, 2021.

[4] C. Chen, X. Y. He, Y. Lu, and Y. L. Chu, "Application of landsat time-series data in island ecological environment monitoring: a case study of zhoushan islands, China," *Journal of Coastal Research*, vol. 108, no. sp1, pp. 193–199, 2020.

[5] R. T. Pennington and T. R. Baker, "Plants, people and long-term ecological monitoring in the tropics," *Plants People Planet*, vol. 3, no. 3, pp. 222–228, 2021.

[6] D. Y. Zhu, T. Chen, N. Zhen, and R. Q. Niu, "Monitoring the effects of open-pit mining on the eco-environment using a moving window-based remote sensing ecological index," *Environmental Science and Pollution Research*, vol. 27, no. 13, pp. 15716–15728, 2020.

[7] H. Liu, Y. Jiang, R. Misa et al., "Ecological environment changes of mining areas around Nansi lake with remote sensing monitoring," *Environmental Science and Pollution Research*, vol. 28, no. 32, pp. 44152–44164, 2021.

[8] H. M. Zhai, W. Q. Xie, S. Q. Li, and Q. Zhang, "Evaluation of urban ecological environment based on remote sensing based ecological index model," *Fresenius Environmental Bulletin*, vol. 30, no. 3, pp. 2527–2535, 2021.

[9] J. Zhao, "Design and implementation of geo-spatial information technology in marine ecological environment monitoring," *Journal of Coastal Research*, vol. 83, no. sp1, pp. 50–56, 2019.

[10] V. S. Negi, R. Pathak, R. S. Rawal, I. D. Bhatt, and S. Sharma, "Long-term ecological monitoring on forest ecosystems in Indian Himalayan Region: criteria and indicator approach," *Ecological Indicators*, vol. 102, pp. 374–381, 2019.

[11] W. P. Lin, "Monitoring and protection of forest ecological tourism resources by dynamic monitoring system," *Ecological Chemistry and Engineering S*, vol. 26, no. 1, pp. 189–197, 2019.

[12] L. Liu and Y. Zou, "Monitoring of marine ecological environmental data security and management system based on internet of things," *Environmental Engineering And Management Journal*, vol. 21, no. 2, pp. 225–236, 2022.

[13] H. Mollenhauer, M. Kasner, P. Haase et al., "Long-term environmental monitoring infrastructures in Europe: observations, measurements, scales, and socio-ecological

RETRACTED

Hindawi
Journal of Robotics
Volume 2024, Article ID 9795848, 1 page
https://doi.org/10.1155/2024/9795848

Retraction

Retracted: Application of Image Processing Variation Model Based on Network Control Robot Image Transmission and Processing System in Multimedia Enhancement Technology

Journal of Robotics

Received 23 January 2024; Accepted 23 January 2024; Published 24 January 2024

Copyright © 2024 Journal of Robotics. This is an open access article distributed under the Creative Commons Attribution License, which permits unrestricted use, distribution, and reproduction in any medium, provided the original work is properly cited.

This article has been retracted by Hindawi following an investigation undertaken by the publisher [1]. This investigation has uncovered evidence of one or more of the following indicators of systematic manipulation of the publication process:

(1) Discrepancies in scope
(2) Discrepancies in the description of the research reported
(3) Discrepancies between the availability of data and the research described
(4) Inappropriate citations
(5) Incoherent, meaningless and/or irrelevant content included in the article
(6) Manipulated or compromised peer review

The presence of these indicators undermines our confidence in the integrity of the article's content and we cannot, therefore, vouch for its reliability. Please note that this notice is intended solely to alert readers that the content of this article is unreliable. We have not investigated whether authors were aware of or involved in the systematic manipulation of the publication process.

Wiley and Hindawi regrets that the usual quality checks did not identify these issues before publication and have since put additional measures in place to safeguard research integrity.

We wish to credit our own Research Integrity and Research Publishing teams and anonymous and named external researchers and research integrity experts for contributing to this investigation.

The corresponding author, as the representative of all authors, has been given the opportunity to register their agreement or disagreement to this retraction. We have kept a record of any response received.

References

[1] Y. Wu and J. Qi, "Application of Image Processing Variation Model Based on Network Control Robot Image Transmission and Processing System in Multimedia Enhancement Technology," *Journal of Robotics*, vol. 2022, Article ID 6991983, 10 pages, 2022.

Hindawi
Journal of Robotics
Volume 2022, Article ID 6991983, 10 pages
https://doi.org/10.1155/2022/6991983

RETRACTED

Research Article

Application of Image Processing Variation Model Based on Network Control Robot Image Transmission and Processing System in Multimedia Enhancement Technology

Yanmin Wu[1] **and Jinli Qi**[2]

[1]*Department of Artificial Intelligence and Big Data, Chongqing College of Electronic Engineering, Chongqing 401331, China*
[2]*Department of General Education and International Studies, Chongqing College of Electronic Engineering, Chongqing 401331, China*

Correspondence should be addressed to Yanmin Wu; wuyanmin@cqcet.edu.cn

Received 20 July 2022; Revised 30 August 2022; Accepted 17 September 2022; Published 29 September 2022

Academic Editor: Shahid Hussain

Copyright © 2022 Yanmin Wu and Jinli Qi. This is an open access article distributed under the Creative Commons Attribution License, which permits unrestricted use, distribution, and reproduction in any medium, provided the original work is properly cited.

The rapid development of the information age brings convenience to human life, but it also brings great challenges to information processing technology. Multimedia enhancement technology is an organic combination of multimedia technology and information processing technology, and it is also an important way of modern multimedia image information processing. However, its usefulness and effectiveness are increasingly negatively affected by the open information environment. The processing effect is also unable to meet the development requirements of the visual field. In order to improve this problem, this paper studied the image transmission and processing system of network-controlled robot on the basis of analyzing the characteristics of the problems existing in the current stage of multimedia technology. On this basis, a new image processing variational model was established and applied to multimedia enhancement technology, which improved the efficiency and effect of image information processing. Finally, the feasibility of its application function and performance was tested by experiments. The test results showed that in the difficult mode of the image processing task, the refresh time of the model in this paper in the multimedia enhancement technology was 1.13 s in total, which was not much different from the test results in the easy mode. Also, in the load stress test, the comprehensive test values under full-function operation and partial-function operation were 42.04% and 20.92%, respectively. Compared with the traditional model, the model in this paper has stronger carrying capacity in multimedia enhancement technology and has better processing ability and stability.

1. Introduction

With the maturity of Internet technology and the widespread use of mobile communications, the image information used and circulated in the online environment has shown a rapid development trend. As an important support for image information processing, multimedia enhancement technology can effectively process various types of multimedia information, such as text, data, video, and voice. However, in the whole complex communication network environment, image information has strong redundancy. All kinds of image content, whether in the process of storage, transmission, or in the process of secondary analysis, have brought great challenges to the current multimedia enhancement technology. When there is a lot of complicated and dazzling multimedia image information, how to compress it to reduce the transmission amount and improve the transmission and processing efficiency on the basis of retaining the effective information is a problem that needs to be solved by the current multimedia enhancement technology. In the context of the dual development of control technology and computer network, network-controlled robots have been maturely applied. Also, its image transmission and processing system ensures the convenience and reliability of image processing. The image processing variational model established under this system can ensure that

the key information of the image is not lost. The reliability and authenticity of the image are improved, which is of great significance for improving the practical application value of multimedia enhancement technology.

As an important means of comprehensive processing of media information, multimedia enhancement technology has always been the research direction of many scholars. Jan et al. proposed a histogram-based energy saving algorithm to improve the resolution and image quality of modern multimedia devices [1]. Zhang and Huo proposed a multimedia enhancement technique with quantum chaotic graph, which encrypted the image and improved the reliability and security of multimedia images [2]. To achieve the best multimedia enhancement layer compression efficiency, Hoangvan et al. proposed a novel HEVC-based framework with high-quality scalability [3]. Ahmed et al. proposed a method for multisaliency enhancement for multimedia image location estimation, which was mainly performed by mean-shift clustering of visual words and saliency maps of images [4]. Ravisankar et al. used multiresolution sharpened images for reconstruction enhancement. Also, it was proved by performance measurement that this unsharp masking method outperformed other enhancement techniques [5]. Heindel et al. proposed a lossy-to-lossless scalable multimedia coding system. Scalability was achieved using lossy base layers combined with lossless compression of reconstruction errors in enhancement layers [6]. The development of image processing requires a higher level of multimedia enhancement technology, and the previous research methods are still lacking in efficiency. The image processing variational model based on the network control robot image transmission and processing system can play a strong advantage in its application.

At present, the variational model in the network-controlled robot image transmission and processing system has been widely used in many fields. Zhang et al. used a variational model for network-controlled robotic image processing in the linearization enhancement of elastic image denoising models. Simple complexity analysis was also performed [7]. Sridevi and Srinivas Kumar efficiently characterized intensity changes in images using a robust image processing variational model based on fractional nonlinear diffusion driven by differential curvature of the image processing system [8]. Feng proposed a new variational model under a network-controlled robot image transmission and processing system, which was used for anti-noise document image binarization. Also, the noise and illumination robustness of the method was verified [9]. Li and Yang proposed adaptive variational functionals for image inpainting, which demonstrated a stable variational scheme based on image processing systems. The existence and uniqueness of minimizing functional solutions were also investigated [10]. Combining the advantages of recently developed robotic image transmission and processing systems, Liu proposed a new variational model for solving the challenging problem of cartoon texture image decomposition [11]. To maximize adaptability, Suwanwimolkul et al. proposed a new sparse signal estimation for robotic imaging systems. Among them, noise and signal parameter estimation were unified into a variational optimization problem [12]. The image processing variational model of the network-controlled robot image transmission and processing system has high practicability. However, the application in multimedia enhancement technology has not been effectively applied. In order to enhance the application value of image processing variational model in multimedia enhancement technology and realize two-way development, its application research is very important.

Based on the network-controlled robot image transmission and processing system, this paper constructed a new image processing variational model, which was applied to the multimedia enhancement technology. Through the application test, it can be seen that the image processing function of the model in this paper was ideal. The total refresh time in mode 1 was 0.9 s, and the refresh time in mode 4 was 1.13 s. In the performance test, the variational model in this paper had better spatial adaptability. The memory usage had been stable in the range of 38.4%, and the CPU usage had only fluctuated in the range of 6.9%. In the load capacity test, the comprehensive value of the model under the full-function operation of multimedia enhancement technology was 42.04%, while the comprehensive value of the test under partial-function operation was 20.92%. The load capacity of the model is lower than that of the traditional model, but the load capacity is higher. From this point of view, the model constructed in this paper had ideal practicability in the application of multimedia enhancement technology.

2. Application of Image Processing Variation Model

2.1. Multimedia Enhancement Technology. Multimedia enhancement technology is an emerging technology developed on the basis of the original multimedia technology. It can be regarded as a small embedded technology system integrating hardware and software [13]. This technology requires the codesign of software and hardware, so that the hardware and software components can be divided reasonably. In multimedia enhancement techniques, nodes can be distributed in or around a perceptual image object in a number of different ways, such as random distribution and artificial positioning. These nodes form technology networks, often through self-organization. In terms of network functions, each node not only takes on the dual roles of terminal and router of traditional multimedia network nodes but also performs image data acquisition, storage, management, and fusion [14]. In special cases, it is also necessary to cooperate with other nodes. The sink node not only needs to have the function of controlling other devices but also needs to have the functions of establishing a routing table for routing selection, information forwarding, data fusion, and storing image information of other nodes. Its technical framework is shown in Figure 1.

A large number of nodes are distributed in or around the monitoring area in Figure 1. These nodes consist of self-organizing forms. The data monitored by the technology node are passed adjacently on other nodes. During

RETRACTED

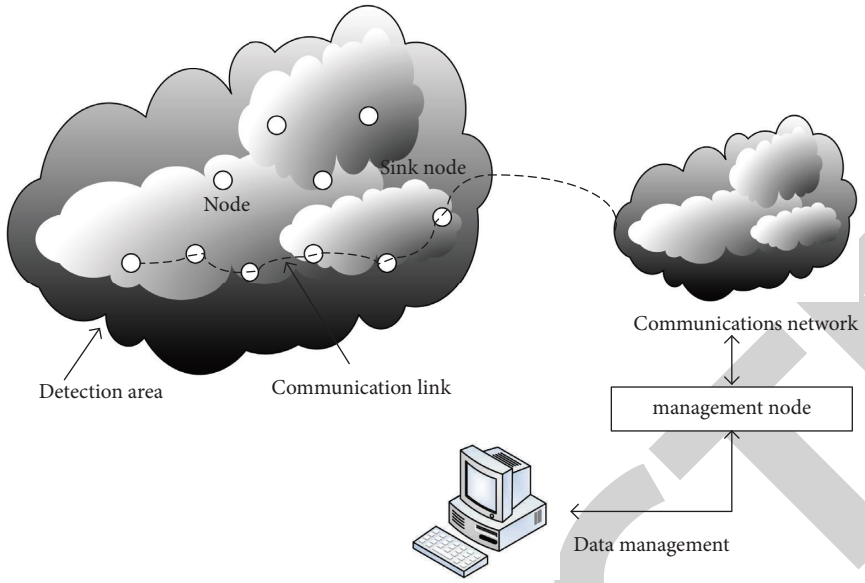

Figure 1: Multimedia enhancement technology framework.

transmission, the image data are simultaneously enhanced by multiple nodes and then returned to the summary point (sink node) through multiple hops. After processing, they are finally transmitted to the management node [15]. The multimedia enhancement technology mainly uses management nodes to enhance and control image information.

Image information processing plays a very important role in multimedia enhancement technology. However, with the increasing amount and variety of image data, its functions face huge challenges.

(1) There are effects of energy consumption and communication delays. Multimedia enhancement techniques need to take into account the excess energy consumed by excess runtime. Therefore, people have developed a method of hibernation. However, even with this method, there is no guarantee that the consumption is reduced.

(2) There is no fixed time for information transmission of multimedia enhancement technology. Without a fixed time requirement, multiple kinds of data are transmitted at the same time, which makes it difficult for the information receiver to process so much information at the first time.

(3) It is impossible to handle the performance standards at the same time. The main difficulty is the confusion of the dormancy mechanism, which makes the information transmission not timely. Nowadays, multimedia enhancement technology only considers the optimization of one performance index, while ignoring the optimization of other performance indicators at the same time.

The multimedia enhancement technology manages the relevant image information and data due to those competing nodes. Once it fails, it is difficult for other applications in the entire framework to continue to provide services. Therefore, it is very important to introduce the image processing variational model of the network-controlled robot image transmission and processing system to deal with the reduced transmission and processing of image data under the background that the nodes transmit information and resources cannot be used.

2.2. Variational Model of Image Processing. The network remote control robot is different from the traditional robot; it refers to the robot that can realize the remote operation under the network control. Its operating subject is generally a professional. In the control environment, professionals use position sensors, visual feedback, and other means to achieve remote network control of the system. The research on remote control has been in the exploratory stage since the beginning of the 1980s. It has flourished with the rise of computer network technology [16]. With the development of computer network, remote control is no longer restricted by geographical conditions. The emergence of the communication network reduces the communication cost, thereby improving the high cost problem caused by the design of dedicated connection lines in the traditional technology. Under the requirements of the development environment of the times, network-controlled robots have become an important direction in current robotics research.

The image transmission and processing system is the key system for the network control robot to realize the image task processing function. Generally, a camera equipped with a computer is used to take pictures of the outside scene. In the initial stage of the transmission of image data, the circuit is switched by the control signal. The differential signal is converted into a digital image signal in a standard format and then sent to the control unit for execution and processing. When the control unit realizes the processing function and the synchronization signal transmission function at the same time, the image data that has been

RETRACTED

initially processed is transmitted to the system memory for buffering, so as to prepare for the needs of subsequent work. By waiting for the system command to be sent, the image data are sent to the converter together with the control signal for conversion and converted into a specified analog quantity according to the command requirements. Finally, after the analog quantity is encoded and data are compressed, they are output through microwave. The hardware structure of the system is shown in Figure 2.

The exterior image captured by the camera is disturbed by noise in the process of formation and transmission. After the image data are transmitted in real time, in order to ensure the image quality during subsequent processing, the system needs to perform basic processing through the image processing variational model in the control module. Therefore, the image processing variational model mainly completes the overall control of the image, and the signal flowchart is shown in Figure 3.

The image processing of multimedia enhancement technology usually relies on software to complete. However, with the continuous development of computer technology, real-time processing and transmission of image data based on algorithmic models is a new research direction [17]. The model is based on a network-controlled robot image transmission and processing system, which realizes real-time processing of image data, and it has good feasibility. The image processing variational model is applied in the multimedia enhancement technology, which can greatly shorten the operation time of image processing, and it has a very good enhancement effect.

Therefore, this paper uses the image processing variational model to solve the image processing problem under the multimedia enhancement technology. The variational model consists of two steps: estimating the tangent vector field of the image and reconstructing the original image from the estimated tangent vector field and the blurred image. The application of variational model in multimedia enhancement technology is expounded from the discrete point of view.

First, the estimation of the tangent vector field in multimedia enhancement techniques needs to be considered. The image collected in the image transmission and processing system of the network-controlled robot is regarded as a two-dimensional surface defined on the area $\Omega = [1, N_1] \times [1, N_2]$. The parameter settings are shown in Table 1.

Among them, the normal vector and tangent vector of the image are denoted as $n = \nabla u = (D_1 u, D_2 u)^T$ and $t = \nabla^{\perp} u = (D_2 u - D_1 u)^T$. The difference operator is applied on both sides of the formula to obtain [18]

$$D_k u^* = D_k H u + D_k \varepsilon, \quad k = 1, 2, \tag{1}$$

where H is the block circulant matrix corresponding to h. Let $D_k u^* = v_k^* D_k u = v_k$, $D_k \varepsilon = \varepsilon_k$, and the operator is commutative in multimedia enhancement technology, so

$$v_k^* = H v_k + \varepsilon_k. \tag{2}$$

In this case, the additive noise ε_k satisfies $\varepsilon_k \sim N(0, \sigma^2, D_k D_k^T)$, resulting in

$$p(v_k^* | v_k) \sim N\left(v_k, \sigma^2, D_k D_k^T\right). \tag{3}$$

Let $t^* = (v_2^*, -v_1^*)^T = (t_1^*, t_2^*)^T$ and $t = (v_2, -v_1)^T = (t_1, t_2)^T$; then, there is

$$p(t^* | t) \sim \prod_k p(t_k^* | t_k), p(t_k^* | t_k) \sim N\left(H t_k, \sigma^2, D_{3-k} D_{3-k}^T\right). \tag{4}$$

It is assumed that the tangent vector field t of the image is piecewise smooth, so that the prior information of the total variation is adopted, namely,

$$p(t|\alpha) \propto \frac{1}{C_\alpha} e^{-\alpha} \int \Omega |\nabla t| \mathrm{d}x. \tag{5}$$

Among them:

$$|\nabla t|^2 = (D_1 t_1)^2 + (D_2 t_1)^2 + (D_1 t_2)^2 + (D_2 t_2)^2. \tag{6}$$

The estimation of t uses the maximum a posteriori estimation method, that is, maximization $p(t|t^*)$. It can be seen from the formula that $p(t|t^*) = p(t|t^*)p(t)/p(t^*)$. Therefore, maximizing $p(t|t^*)$ is equivalent to minimizing the log-likelihood function $-\log p(t|t^*)$, as shown in Figure 4.

The variational problem can be obtained by further derivation [19]:

$$\min_{\nabla \cdot t = 0} \int \Omega |\nabla t| \mathrm{d}x + \frac{\eta}{2} \sum_k \int \Omega \left(D_{3-k}^T \left(H t_k - t_k^*\right)\right)^2 \mathrm{d}x. \tag{7}$$

Among them, incompatibility condition $\nabla \cdot t = 0$ is used, and $\eta = \sigma^2/\alpha$.

It is noted that the difference operator appears in the second term of formula (7). Therefore, formula (7) itself is in the form of a variational model, which is more reasonable for the estimation of tangent vector fields. However, due to the existence of the first-order difference operator D_k, the solution of the variational problem is not unique, and the solutions differ by a constant. Since $\varepsilon_k \sim N(0, \sigma^2, D_k D_k^T)$, there is $E(v_k^*) = H v_k$ according to the formula. Therefore, additional constraints can be added to the tangent vector field t, resulting in the following minimization problem:

$$\min_{t \in U} \int \Omega |\nabla t| \mathrm{d}x + \frac{\eta}{2} \sum_k \int \Omega \left(D_{3-k}^T \left(H t_k - t_k^*\right)\right)^2 \mathrm{d}x. \tag{8}$$

Among them, the function space $U = \left\{t | \nabla \cdot t = 0, \int \Omega H t_k = \int \Omega t_k^*\right\}$. Unlike formula (7), it can be proved that when H is injective, the solution to the variational problem is unique, so formula (7) is used to estimate the tangent vector field t.

The distance of l_1 between the unit image gradient and the estimated unit normal vector field is used as the regularization term, resulting in the minimization problem of image restoration [20]:

RETRACTED

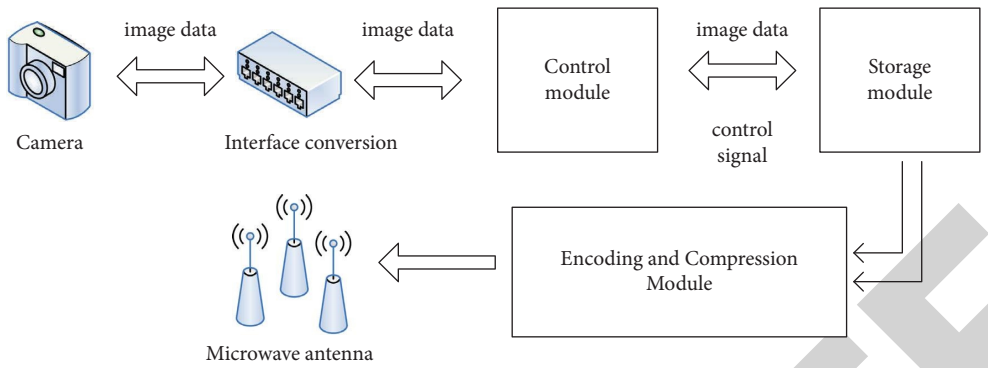

Figure 2: Hardware structure of image transmission and processing system.

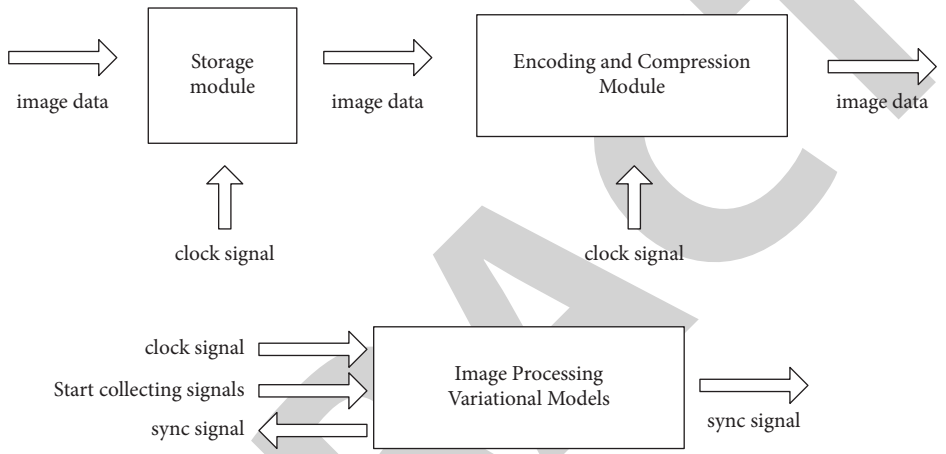

Figure 3: Signal flowchart.

Table 1: Parameter setting and its interpretation.

Sequence	Parameter setting	Meaning
1	D_1	First-order difference operator in the horizontal direction
2	D_2	First-order difference operator in the vertical direction
3	n	The normal vector of the image
4	t	Tangent vector of the image

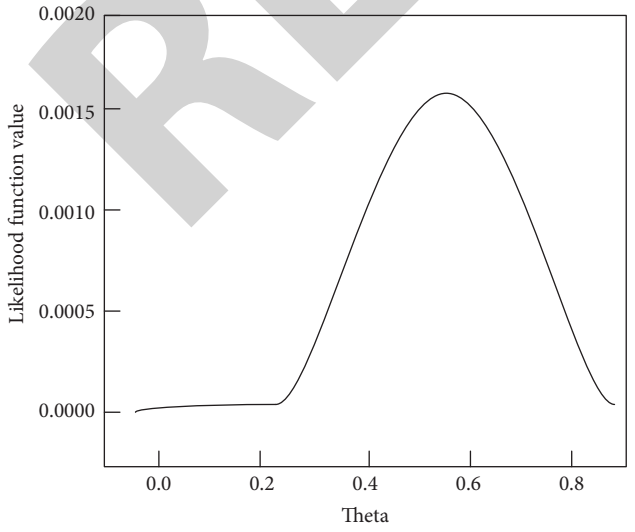

Figure 4: Maximum a posteriori estimation legend.

$$\min_u \int \Omega \left| \frac{\nabla u}{|\nabla u|} - \frac{n}{|n|} \right| dx + \frac{\lambda}{2} \int \Omega (Hu - u^*)^2 dx. \quad (9)$$

The regular term in formula (9) can be expressed as

$$\int \Omega \left| \frac{\nabla u}{|\nabla u|} - \frac{n}{|n|} \right| dx = \int \Omega \sqrt{2 - 2\frac{\nabla u \cdot n}{|\nabla u||n|}} dx = \int \Omega \sqrt{2 - 2\cos\theta} dx. \quad (10)$$

It can be seen that it is also only directionally matched. However, problem (9) is still nonconvex. Therefore, the following iterative formula is introduced to approximate this problem [21]:

$$u^{k+1} = \arg\min_u \int \Omega \left| \frac{\nabla u}{|\nabla u|} - \frac{n}{|n|} \right| dx + \frac{\lambda}{2} \int \Omega (Hu - u^*)^2 dx. \quad (11)$$

RETRACTED

Formula (11) is a convex function. $w^k = 1/|\nabla u^k|$ is taken as the edge indicator function. When $|\nabla u^k| = 0$, w^k is a fixed constant; then, formula (11) is essentially a spatially adaptive image processing variational model. Compared with the traditional variational model, the model here can better preserve the details and texture information of the image. Therefore, compared with the previous regularization terms 8 and 9, the model proposed here has better performance in multimedia enhancement techniques.

Further analysis of this variational model shows that since incompatibility condition $\nabla \cdot t = 0$ is used in the first step, there is an image u_1 that satisfies

$$\nabla u_1 = n. \tag{12}$$

Assuming $|\nabla u^k| \approx |n|$, the right side of formula (12) can be expressed as

$$\begin{aligned} \min_u \int \Omega |\nabla u - n| \mathrm{d}x + \frac{\lambda}{2} \int \Omega \left(Hu - u^*\right)^2 \mathrm{d}x &= \min_u \int \Omega w^k \left|\nabla u - \nabla u_1\right| \mathrm{d}x + \frac{\lambda}{2} \left(H\left(u - u_1\right) - \left(u^* - Hu_1\right)\right)^2 \\ &= \min_{u_2} \int \Omega w^k \left|\nabla u_2\right| \mathrm{d}x + \frac{\lambda}{2} \int \Omega \left(Hu_2 - f^*\right)^2 \mathrm{d}x. \end{aligned} \tag{13}$$

Among them, $f^* = u^* - Hu_1$. The minimization value u_2 is obtained by formula (13); then, the restored image can be expressed as

$$u = u_1 + u_2. \tag{14}$$

Therefore, the proposed two-stage model can be explained as shown in Table 2.

The minimization problem of direction matching is extended to deblurring clarity, and its corresponding unconstrained problem can be expressed as

$$\min_u \int \Omega \left| \frac{\nabla u}{|\nabla u|} - \frac{n}{|n|} \right|^2 \mathrm{d}x + \frac{\lambda}{2} \int \Omega \left(Hu - u^*\right)^2 \mathrm{d}x. \tag{15}$$

A convex problem can also be obtained by linearizing it as in formula (11). Assuming $|\nabla u^k| \approx |n|$, according to formulas (12) and (13), the following minimization problem for u_2 can be similarly obtained:

$$\min_{u_2} \int \Omega w^k \left|\nabla u_2\right|^2 \mathrm{d}x + \frac{\lambda}{2} \int \Omega \left(Hu_2 - f^*\right)^2 \mathrm{d}x. \tag{16}$$

By observing formula (16), it is found that the minimization problem reduces to a weighted image variational processing model. Obviously, this model can better preserve the discontinuous information of images in the compression processing of multimedia enhancement technology and maintain higher data transmission quality and efficiency.

3. Application Testing

In order to verify the effectiveness of the image processing variational model based on the network-controlled robot image transmission and processing system in multimedia enhancement technology, this paper compares its application effect with the traditional image processing variational model in multimedia enhancement technology. The tests are carried out from these aspects, respectively, and the test environment is shown in Table 3.

From Table 3, the computer with Windows 11 operating system has corresponding mature interfaces and drivers and a lot of development experience to use. It also supports other data processing and system control software to facilitate the operation of the variational model of image processing. The Intel Core i7 chip and 8 GB memory can realize high-speed operation on a large amount of RGB image data and depth image data, which can meet the real-time requirements of the network control robot for the image acquisition and processing system. The USB 3.0 interface can meet the interface requirements of multimedia enhancement technology. Therefore, the test environment of this paper meets the test conditions.

3.1. Functional Test. In this paper, the application test of image processing variational model in multimedia enhancement technology includes two categories, namely, functional test and performance test. Functional testing is a necessary testing method. To ensure the effectiveness of the image processing variational model in multimedia enhancement technology, the first thing that needs to be ensured is its realization effect in the image processing function. This paper observes the task refresh time of the two types of models in multimedia enhancement technology under different task modes, and the results are shown in Figure 5.

The image processing function mainly analyzes the original and panoramic images through the variational model, which is convenient for the follow-up inspection of the multimedia enhancement technology program. The stored size is $512 \times 512 \times 2$ original 16 bit image and 14212×480 panorama image. The detection frequency is the same as the tracking frequency. The number and complexity of tasks that need to be processed in different modes of multimedia enhancement technology are also different. In general, the more tasks that are processed and the higher the complexity, the longer the refresh time is. A delay that is too different leads to a significant decrease in the functionality of the multimedia enhancement technology, resulting in a low degree of image processing. This article sets mode 1 as the easiest mode and mode 4 as the most complex mode. As can be seen from Figure 5(a), in mode 1, the detection refresh time of the image processing variational model in the

RETRACTED

Table 2: Interpretation of the two-stage model.

Object	Model classification	Sequence	Effect
The proposed two-stage model	Variational processing models	1	Restore multimedia image u_1
		2	u_1 preserves the discontinuity of the image gradient information and the smooth areas of the image
	Weighted variational model	3	Restore multimedia image u_2
		4	u_2 preserves the discontinuous information of the image itself

Table 3: Experimental test environment.

Sequence	Equipment	Specification
1	Computer	Intel Core i7 RAM 8 GB
2	Operating system	Windows 11 64 bit
3	Interface	USB 3.0

multimedia enhancement technology was 0.43 s, the tracking refresh time was 0.47, and the total refresh time was 0.9 s. At this time, the model refreshes the image without delay. In mode 4, the test scenario is multitasking and high load. At this time, the detection refresh time was 0.51 s, and the tracking refresh time was 0.62 s. In Figure 5(b), the detection refresh time of mode 1 was 0.46 s, and the tracking refresh time was 0.51 s. In mode 4, the detection refresh time was 0.73 s and the tracking refresh time was 0.71 s. It can be seen that it has the long time and high latency compared to the traditional variational model. The image processing variational model based on the network control robot image transmission and processing system has a short refresh time in the multimedia enhancement technology and basically has no delay, which can meet the practical application.

3.2. Performance Test. Performance testing is an important part of application testing. Under different sampling frequencies, the stability of multimedia enhancement technology is greatly challenged. At different frequencies, the test is carried out by observing the occupancy rate and usage rate of different image processing variational models in the application of multimedia enhancement technology to hardware devices. The results are shown in Figure 6.

In Figure 6, different sampling frequencies are set in this paper, but they are all within the range of normal working conditions. It can be seen from Figure 6(a) that under different sampling frequencies, the memory usage of the model in this paper in the application of multimedia enhancement technology had been in a stable range of 38.4%. The CPU occupancy rate fluctuated with the change of sampling frequency. As the sampling frequency increased, the occupancy rate also increased, from 47.2% to 54.1%, an increase of 6.9%. In Figure 6(b), both the memory usage and CPU usage of the traditional model had changed. Memory usage increased from 39.1% to 42.7%, and CPU usage increased from 47.5% to 56.2%, a change of 8.7%.

On the whole, the stability of the traditional image processing variational model in the application of multimedia enhancement technology is not ideal, and it fluctuates greatly with the change of sampling frequency. In this context, the normal function of the multimedia enhancement technology is very likely to be abnormal, which causes it to be in a state of failure. The variational model in this paper has better spatial adaptability, which can completely retain image information under the condition of increasing occupancy and usage.

Under different working modes, the performance of the model is quite different. Therefore, under the same working mode, this paper observes the load capacity generated by full-function operation and partial-function operation under different pressures, as shown in Figure 7.

The load capacity test under different stress conditions in Figure 7 only compares the normal stable condition, which does not consider the failure condition. It is not difficult to see that there is a big difference between the performance of full-function operation and partial-function operation. The main reason is that the multimedia enhancement technology adopts multithreaded processing under full-featured operation, and the load is also high. While some functions are running, most of the technology modules are in an idle state. As can be seen from Figure 7(a), the image processing variational model in this paper had a better load capacity in the multimedia enhancement technology, and the test comprehensive value under full-function operation was 42.04%. Also, the test comprehensive value under partial-function operation was 20.92%. In Figure 7(b), the test comprehensive value of the traditional image processing variational model under full-function operation reached 53.94%, and the test comprehensive value under partial-function operation reached 26.72%. This may be related to the inability of variational models to compress image information efficiently. If the compression is not performed correctly, not only the key information cannot be completely output but also the technical load pressure is too large, which affects the follow-up work. The image processing variational model based on the network-controlled robot image transmission and processing system can better preserve the discontinuous information of the image in the multimedia enhancement technology. Also, it is effectively compressed to maintain a relatively ideal load effect.

RETRACTED

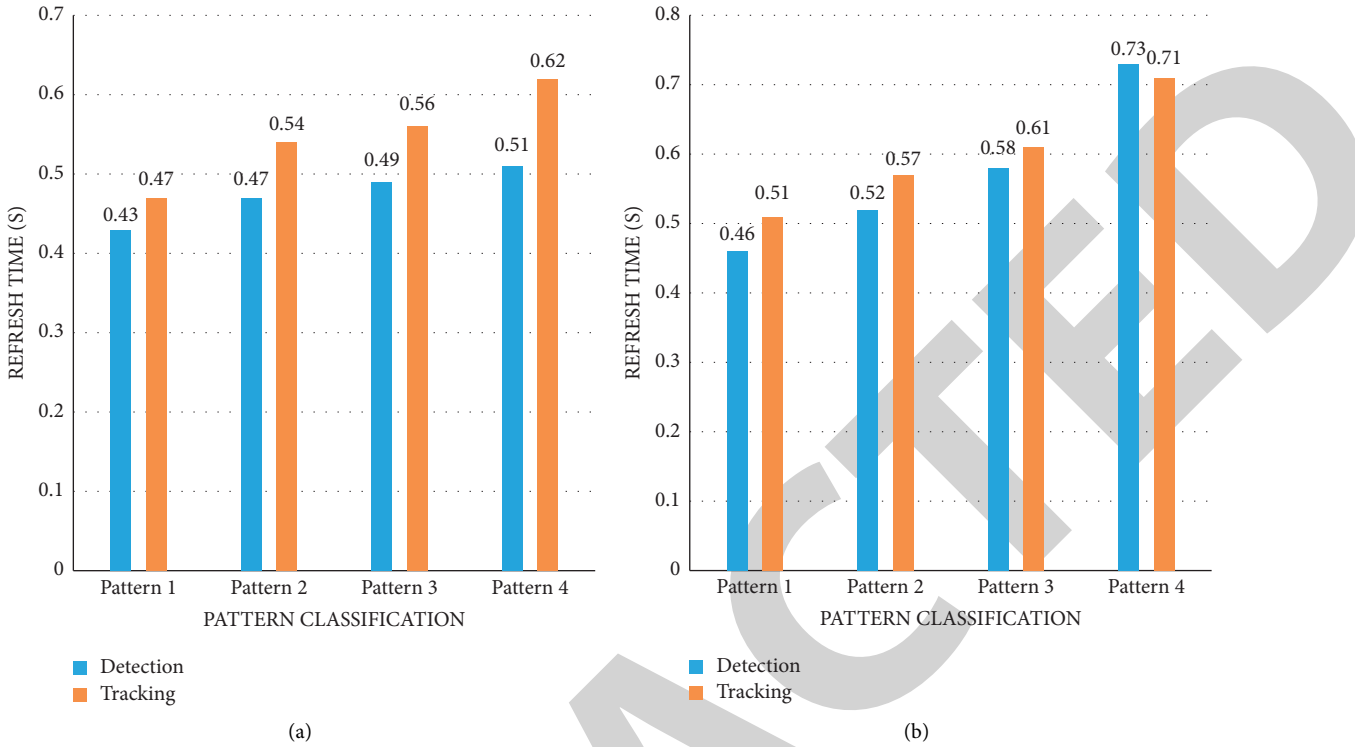

Figure 5: Task refresh time test results. (a) The refresh time of the model in this paper. (b) The refresh time of the conventional model.

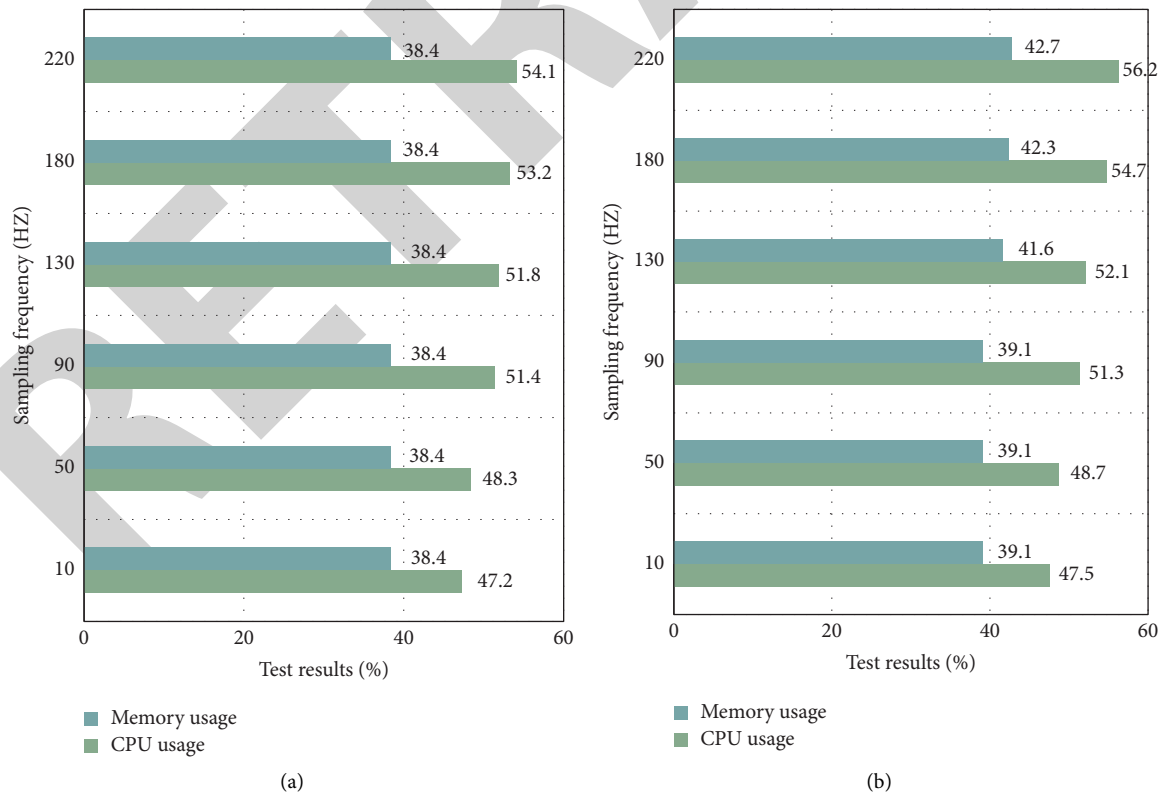

Figure 6: Occupancy and usage test results. (a) The occupancy rate and usage rate under this model. (b) The occupancy rate and usage rate under the traditional model.

RETRACTED

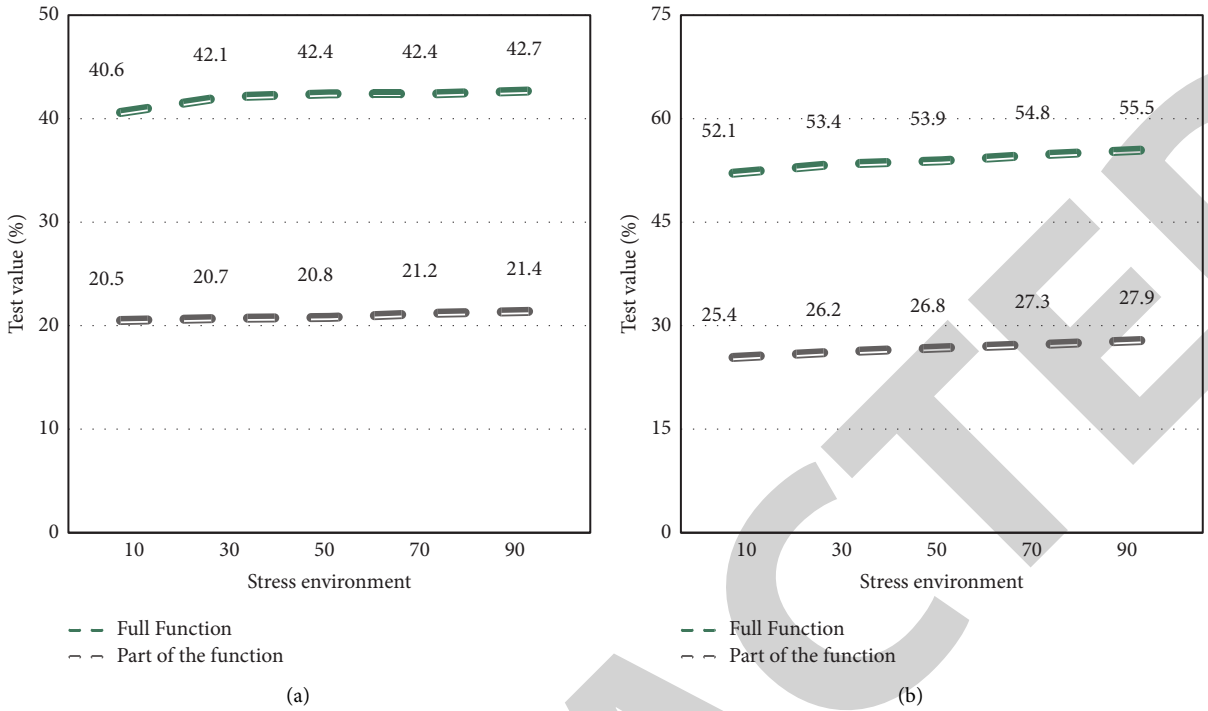

Figure 7: Load capacity test results. (a) The load capacity of this model. (b) The conventional model load capacity.

4. Conclusion

As a comprehensive form of multimedia information processing, multimedia enhancement technology is the product of the combination of communication technology and continuous development of multimedia technology. It is of great practical significance to improve its application value for improving the complex information environment of multimedia. In this paper, a new image processing variational model was proposed on the basis of the image transmission and processing system of the network-controlled robot. Also, it was applied in multimedia enhancement technology, which effectively improved the quality and effect of information transmission. In addition, under the condition of ensuring that the information resources were fully reserved, the consumption has been reduced, and the technical performance and practical effect have been improved. However, in the testing process, it is found that the research in this paper still needs continuous improvement in practical application. Under different sampling frequencies, the occupancy performance of the model in this paper in technical applications has improved, but there are still certain fluctuations. Also, this paper did not consider the application performance in different information environments. These two points still need to be continuously improved. In the future research work, it is necessary to continue to study the shortcomings of the image processing model and continuously improve its practical value in multimedia enhancement technology. It also makes full use of existing technology to improve research conditions and quality.

Data Availability

The data used to support the findings of this study are available from the corresponding author upon request.

Conflicts of Interest

The authors declare that they have no conflicts of interest.

References

[1] L. M. Jan, F. C. Cheng, and C. H. Chang, "A power-saving histogram adjustment algorithm for OLED-oriented contrast enhancement," *Journal of Display Technology*, vol. 12, no. 4, pp. 368–375, 2017.

[2] J. Zhang and D. Huo, "Image encryption algorithm based on quantum chaotic map and DNA coding," *Multimedia Tools and Applications*, vol. 78, no. 11, pp. 15605–15621, 2019.

[3] X. Hoangvan, J. Ascenso, and F. Pereira, "Adaptive scalable video coding: an HEVC-based framework combining the predictive and distributed paradigms," *IEEE Transactions on Circuits and Systems for Video Technology*, vol. 27, no. 8, pp. 1761–1776, 2017.

[4] S. Ahmed, K. G. Tan, M. Y. Alias, F. Hossain, N. Z. A. Rahman, and L. C. Pao, "Circularly polarized high-gain antenna using metasurface for C-band Application," *Far East Journal of Electronics and Communications*, vol. 18, no. 7, pp. 1099–1106, 2018.

[5] P. Ravisankar, T. Sree Sharmila, and V. Rajendran, "Acoustic image enhancement using Gaussian and laplacian pyramid—a multiresolution based technique," *Multimedia Tools and Applications*, vol. 77, no. 5, pp. 5547–5561, 2018.

RETRACTED

Hindawi
Journal of Robotics
Volume 2023, Article ID 9807401, 1 page
https://doi.org/10.1155/2023/9807401

Retraction

Retracted: The Evaluation of Visual Clarity and Comfort of Light Environment in Multimedia Classroom

Journal of Robotics

Received 8 August 2023; Accepted 8 August 2023; Published 9 August 2023

Copyright © 2023 Journal of Robotics. This is an open access article distributed under the Creative Commons Attribution License, which permits unrestricted use, distribution, and reproduction in any medium, provided the original work is properly cited.

This article has been retracted by Hindawi following an investigation undertaken by the publisher [1]. This investigation has uncovered evidence of one or more of the following indicators of systematic manipulation of the publication process:

(1) Discrepancies in scope
(2) Discrepancies in the description of the research reported
(3) Discrepancies between the availability of data and the research described
(4) Inappropriate citations
(5) Incoherent, meaningless and/or irrelevant content included in the article
(6) Peer-review manipulation

The presence of these indicators undermines our confidence in the integrity of the article's content and we cannot, therefore, vouch for its reliability. Please note that this notice is intended solely to alert readers that the content of this article is unreliable. We have not investigated whether authors were aware of or involved in the systematic manipulation of the publication process.

In addition, our investigation has also shown that one or more of the following human-subject reporting requirements has not been met in this article: ethical approval by an Institutional Review Board (IRB) committee or equivalent, patient/participant consent to participate, and/or agreement to publish patient/participant details (where relevant).

Wiley and Hindawi regrets that the usual quality checks did not identify these issues before publication and have since put additional measures in place to safeguard research integrity.

We wish to credit our own Research Integrity and Research Publishing teams and anonymous and named external researchers and research integrity experts for contributing to this investigation.

The corresponding author, as the representative of all authors, has been given the opportunity to register their agreement or disagreement to this retraction. We have kept a record of any response received.

References

[1] Y. Dong, M. Xi, and M. Hu, "The Evaluation of Visual Clarity and Comfort of Light Environment in Multimedia Classroom," *Journal of Robotics*, vol. 2022, Article ID 4917352, 12 pages, 2022.

Hindawi
Journal of Robotics
Volume 2022, Article ID 4917352, 12 pages
https://doi.org/10.1155/2022/4917352

RETRACTED

Research Article

The Evaluation of Visual Clarity and Comfort of Light Environment in Multimedia Classroom

Yu Dong,[1] **Minshen Xi**,[1] **and Minghua Hu**[2]

[1]*Academy of Fine Arts, Guangzhou College of Technology and Business, Guangzhou 510800, Guangdong, China*
[2]*Department of Digital Media, Software Engineering Institute of Guangzhou, Guangzhou 510990, Guangdong, China*

Correspondence should be addressed to Yu Dong; dongyu@gzgs.edu.cn

Received 3 August 2022; Revised 9 September 2022; Accepted 14 September 2022; Published 29 September 2022

Academic Editor: Shahid Hussain

Copyright © 2022 Yu Dong et al. This is an open access article distributed under the Creative Commons Attribution License, which permits unrestricted use, distribution, and reproduction in any medium, provided the original work is properly cited.

In order to clarify the quantitative relationship between students' visual clarity, comfort, and environmental brightness in the light environment of multimedia classrooms in colleges and universities and obtain the threshold and influence trends of brightness, visual clarity, and visual comfort in the light environment of the multimedia classroom, this paper proposes the research on the relevant influence parameters of the light environment of the multimedia classroom. Based on the analysis of the current situation of multimedia use in China, this paper proposes taking brightness as the main parameter of indoor light environment evaluation to carry out students' subjective evaluation experiments. The brightness range that can reflect the visual clarity and visual comfort of the experimenter is extracted by using multimedia combined with screen projection and HDRI technology. Finally, by analyzing the experimental data, combined with the operational definition of the psychophysical threshold, the functional relationship between visual clarity, comfort, and brightness in the light environment of a multimedia classroom is obtained through regression analysis and the threshold and extreme point data are calculated. The experimental results show that when the brightness range is 370.83 cd/m^2 ≤ X ≤ 558.47 cd/m^2, it has better visual clarity and visual comfort. When the brightness contrast is close to 10 : 1, the visual clarity is the highest; when the brightness contrast is close to 5 : 1, the visual comfort is the highest and decreases on both sides with the change in its value. *Conclusion*. The results of this experimental study can provide a basis for formulating and revising relevant laws and regulations in the future and provide a reference for the light environment design of multimedia classrooms in China.

1. Introduction

The light environment refers to the physiological and psychological environment related to spatial functions and shapes established indoors by the changes in light (natural lighting and artificial lighting) and color (hue, color temperature, expressiveness, and color distribution) [1]. A light environment is mainly divided into a natural light environment and an artificial light environment. A natural light environment is natural lighting, that is, the indoor use of natural light. An artificial light environment is artificial lighting, which uses light-emitting lamps to supplement the insufficient lighting in the building space during the daytime due to time, weather, and other reasons. It is an artificial measure taken to meet the needs of study, life, and work. It can be flexibly adjusted according to people's needs to achieve the ideal lighting effect.

Different building types have different requirements for the light environment because different space functions have different requirements for light. In the buildings shown in the "Building Lighting Design Standard GB 50034–2013," the required illumination values are also different according to the type of activity [2]. The design of architectural lighting environments is no longer relying solely on the norms and standards of lighting and lighting, but developing toward a humanized design concept. The evaluation and research of architectural lighting environments are also gradually improving. According to the different evaluation indicators, the evaluation of indoor light environments in buildings is mainly divided into two types. One is partial quantitative

evaluation research, which is a comprehensive evaluation based on objective indicators such as illumination and brightness. It needs to measure the physical parameters such as illumination of the light environment in the building space and then refer to the relevant standards to evaluate the advantages and disadvantages of the light environment. The other is qualitative research, which directly uses subjective evaluation indicators such as comfort for a comprehensive evaluation, which requires a large number of subjects to participate in the experiment [3]. Because there are relevant standards and specifications for objective indicators, they can be measured and evaluated by relevant instruments. However, the selection of subjective indicators involves knowledge in many fields, such as human psychology and ethology, and the evaluation process is also complex.

2. Literature Review

Zheng and Crowcroft put forward the indoor light environment comfort curve and believed that for any given environmental color temperature (for other light sources that imitate the light color of solid discharge light sources, we use the relevant color temperature), there is a comfortable illumination range; values lower than this range will make people feel dark and cold, and values higher than this range will make people feel unnatural [4]. Gerla and Tzu-Chieh Tsai reviewed the research results on the visual comfort of the indoor light environment in recent ten years, made a multidimensional evaluation and description of various indicators describing the attributes of the indoor light environment, and put forward optimization suggestions when using these indicators, providing a design basis for relevant practitioners in the construction industry [5]. Zhao et al., by investigating the illumination of the working face under the indoor light environment and the satisfaction of users with the light environment, showed that the approximate relationship between the satisfaction of the indoor light environment and the illumination of the working face is obtained using the method quadratic regression fitting, and it is pointed out that when the illumination of the working face is 100–2100 LX, people are satisfied with the indoor light environment, while when the illumination of the working face is 1000–1200 LX, the satisfaction of the light environment is the highest [6]. Wang et al. set the working surface illumination of 200–900 LX in the artificial lighting experimental room to determine the working surface illumination difference between the best visual efficacy and the best visual comfort of indoor space users under working conditions. The results show that the subjects' visual efficacy is the best under the illumination of more than 900 LX, and the illumination between 400 and 500 LX makes the subjects feel the most comfortable. It is suggested that the visual comfort factor should be properly considered in the lighting environment in pursuit of efficient work and mental stimulation [7]. Kumar et al. studied the visual comfort of subjects in screen reading and paper reading under different combinations of illumination and color temperature in a small office space through a subjective evaluation experiment. The experiment set 500 LX and 750 LX illuminance and 3000 K, 4000 K, and 6500 K ambient color temperature combination conditions for these two visual tasks [8]. The experimental results show that the color temperature of the light source is very important for the visual comfort and psychological feelings of subjects. The combination of low color temperature and low illumination and high color temperature and high illumination is more in line with the psychological preferences of users. The research results of Puguan et al. show that the illumination below 300 LX cannot meet the user's visual comfort needs, the illumination above 500 LX is meaningless for improving visual comfort, and the influence of the change in correlated color temperature (CCT) on the brightness of the light environment and the degree of psychological pleasure can be ignored [9].

Scholars at home and abroad mainly explore the evaluation of visual suitability from the two aspects of visual clarity and visual comfort. Although there are many research directions and conclusions about the classroom light environment at home and abroad, there are still deficiencies: there are few studies on the multimedia classroom light environment with the brightness received by the evaluation subject as the main evaluation parameter. And there is a lack of quantitative research on the subjective evaluation of students' visual clarity and visual comfort combined with objective experimental data.

Based on the subjective feelings of college students on the light environment of a multimedia classroom, this paper uses high dynamic image (HDRI) technology and considers brightness as the main parameter to evaluate the quality of a classroom light environment. The influence of the light environment in a multimedia classroom on students' visual clarity and visual comfort is evaluated subjectively and experimental data are collected, and then quantitative analysis and research are carried out. Combined with the operational definition of psychophysical threshold, the functional relationship between visual clarity, comfort, and brightness in the light environment of a multimedia classroom is obtained through regression analysis, and the threshold and extreme point data are calculated. Finally, the threshold and influence trend that can be used to determine the brightness range, visual clarity, and visual comfort of the multimedia classroom light environment are obtained. Discussing the relationship between the visual clarity, comfort, and environmental brightness of a multimedia classroom can provide a reference for the design of a multimedia classroom light environment and the formulation of relevant standards in the future.

3. Research Methods

3.1. Relevant Methods

3.1.1. Evaluation Method. At present, the measurement of subjects' visual clarity and visual fatigue at home and abroad basically means to measure the indicators related to visual clarity and visual fatigue, so as to indirectly quantify the indicators related to visual clarity. According to the experimental content of this study and the characteristics of

RETRACTED

the tested personnel, the following two methods are designed:

(1) Subjective evaluation and feedback evaluation of visual clarity and visual comfort are done, using a questionnaire designed on the basis of the semantic difference scale under the Likert scale. Using appropriate visual subjective evaluation methods, we describe fatigue characteristics such as sleepiness, and eye discomfort. According to different evaluation methods, a survey screening questionnaire, a subjective evaluation questionnaire, and a return visit questionnaire were designed [10].

(2) Measurement of visual ergonomics is done. According to the number of jobs completed and the error rate, the work materials of the visual fatigue state are designed, and a variety of work materials such as the digital recognition table and graphic recognition (Landao ring) are selected for experiments.

3.1.2. Visual Recognition Object. This experimental test adopts the light environment of the classroom under a variety of light climate conditions, from dark night to overcast day, and then to the brightness range of the indoor light environment when there is no cloud on a sunny day, so it can reflect the corresponding experimental results from a large range [11]. Through the natural lighting and the shielding of the classroom shading curtains, and combined with the lighting lamps on or off, the indoor light environment can be adjusted and the screen brightness of the projector will not be adjusted.

We use thevisual acuity test table, text, pictures with rich colors and details, and computer courseware for making software PowerPoint to construct text files with multiple colors and numbers of different sizes, which is convenient for the subjects to judge the visual clarity under each situation and can also avoid the influence of color equality factors on the experimental results. The Latin square design and the circulation method are used to offset the result errors caused by the participation order, projection, and playback order of students participating in the evaluation experiment and their own factors.

3.2. Experimental Design

3.2.1. Selection of Experimental Parameters. In the past, the analysis and research of the light environment of multimedia classrooms by experts and scholars mostly used the illumination of teaching working surfaces such as desktops and blackboards, and even the surface illumination of eye positions as the physical parameters to measure the light environment of multimedia classrooms, and rarely used brightness as the physical parameter to measure the light environment. Since brightness itself is people's feeling of light intensity, it is a quantity that can more directly reflect people's subjective feelings [12]. The relevant national specifications only make relevant provisions on the illumination in the indoor light environment of the building but do not put forward guiding suggestions on the indoor light environment of the classroom with the change in environmental brightness and the use of multimedia facilities. In the past, brightness information was usually not used as the main reference parameter in research. The main reason is that the collection and extraction of brightness information is a relatively difficult process compared with other physical parameters. However, with the progress of measurement technology and scientific methods, the direct extraction of brightness parameters can reflect the light environment of indoor places in buildings. Therefore, this experiment takes the brightness parameter as the reference basis and takes the brightness information of relevant points, such as the highest brightness value, the lowest brightness value, the average brightness of the place, and the brightness of relevant points as the main reference parameters.

3.2.2. Extraction Method of Brightness Parameters. In this paper, the high dynamic range image (HDRI) technology with floating-point value storage is used as the method for extracting brightness parameters in experiments. In this experiment, the Canon 5D Mark II, a full-frame CMOS photosensitive element digital SLR, combined with a 50 mm standard lens, is used to extract the brightness parameter information within the normal field of view. First, time-sharing and multiple exposure shooting are carried out on the test target in the same light environment scene to obtain low dynamic digital images with different exposures [13]. Then, using professional image synthesis software Photomatix 5.1 and Photoshop CS6, low dynamic range images with different exposure levels are synthesized into high dynamic range images. After synthesizing the high dynamic range image, the brightness and brightness contrast information in the image are accurately extracted from the picture through the software HDR viewer v1.4, independently developed by Tianjin University.

3.2.3. Selection of Experimental Environment and Personnel. The preliminary investigation and data collection of this experimental research show that the typical building plane selection of multimedia classrooms is mostly rectangular, using curtain projection multimedia equipment, one-way side window lighting, or the other side of high side window lighting [14]. Therefore, the "architectural optics laboratory" classroom of a university with the above typical characteristics and the facilities that can actively control natural and artificial lighting to adjust the light environment is selected as the experimental site for the experimental simulation. Thirty-one people aged between 21 and 28 were randomly selected from the University. Half of the students were male, and half were female. Factors that seriously affect vision and judgment, such as color blindness and color weakness, were excluded to ensure that each subject participating in the test had normal color and vision [15].

The selection of test points is based on the lighting measurement method (GB/t5700-2008), the actual use space of the classroom, the evaluation method required by the

RETRACTED

visual recognition materials and the international visual acuity evaluation table, and the actual use position of the seats in the multimedia classroom. At the same time, combined with the size and position relationship of the projection screen, three groups of nine different test points with a horizontal distance of 3 m, 5 m, and 7 m from the projection screen are selected and the vertical height of the test points from the ground is 1.2 m (the specified sitting height in the lighting measurement method).

3.3. Research Process

3.3.1. Preevaluation Experiment. Through the preexperiment, problems are found, specific experimental measures are adjusted, the experimental scheme is improved, and the final experimental process is determined through a small batch of preevaluation experiments. Each group of experiments is set to be carried out at the specified time and in the experimental scene. The weather conditions are all cloudy and sunny, and each experimental link in the preexperiment is done accordingly [16]. Three time periods, 8 : 00–12 : 00, 13 : 30–18 : 30, and 19 : 00–21 : 00, during which students frequently use multimedia classrooms, were selected for multitime period experiments. The preevaluation experiment is a small sample experiment. Considering the different experimental content settings of this preexperiment, the experiment was divided into three parts according to the change in experimental duration and experimental content in each part. According to the requirements of the Latin square design, six people were selected for the experiment. Visual tests were conducted on each participant to ensure that each participant in the test had normal vision.

3.3.2. Large Batch Evaluation Experiment. Through the preevaluation experiment, the more extreme influence parameter values are removed, the remaining parameter quantities are found to be significantly different, the parameter range becomes smaller, and the brightness difference spacing is appropriate. Then, the screening results of the preexperiment parameter data are screened and optimized again, and the experiment is carried out on this basis [17]. Then, through the subjective evaluation experiment of a large sample size, a large number of experimental data are obtained, and the change rules and thresholds of visual clarity, visual comfort, and brightness contrast are obtained through calculation.

According to the subjective evaluation of large batches of experiments, a total of 1116 experimental data were obtained: 558 visual evaluation homework materials and 1116 evaluation questionnaires, feedback questionnaires, and interview questionnaires. We arrange the average scores of visual clarity and visual comfort according to the scoring method of preexperiment. The statistical results of the average scores under different experimental parameters are shown in Table 1.

In this experiment, the data obtained from the preexperiment and the large batch evaluation experiment are analyzed as follows.

(1) Reliability Analysis. In this paper, the internal reliability analysis of the Cronbach coefficient is used for the reliability analysis. Through the basic description statistics and calculation of each evaluation item by using SPSS computer software, the reliability coefficients of visual comfort and visual clarity of the preevaluation experiment were 0.828 and 0.882, indicating good internal consistency. In the large batch of subjective evaluation experiments, the reliability coefficients were 0.805, 0.811, 0.832, 0.795, 0.821, and 0.756, respectively, which are close to 0.8 and above, indicating high consistency.

(2) Correlation Analysis. According to the SPSS analysis results of this preexperiment correlation analysis, with the change in brightness in the field of vision, the mean Pearson correlation of the average score of visual clarity and visual comfort changes regularly and the absolute values are above 0.8. When the brightness values of the two are at the highest points of the two, 500 cd/m^2 and 400 cd/m^2, there is a strong positive correlation, the correlation being 0.826 and 0.912, respectively, and there is a strong negative correlation after the highest point and the absolute values of the correlation are 0.964 and 0.985, respectively.

The correlation data of a large number of subjective evaluation experiments are obtained. Among them, we have the following: ① visual acuity: when the brightness value is 500 cd/m^2, it reaches the highest point of the evaluation value, and the values before and after it decrease. The analysis results show a significant correlation, and the absolute value of the correlation value is 0.92; ② visual comfort: when the brightness value is 400 cd/m^2, it reaches the highest point of the evaluation value, and the values before and after it decrease. The analysis results are significantly correlated, and the absolute value of the correlation value is 0.865.

At the same time, the Pearson correlation between the change in brightness contrast and the average score of visual clarity and visual comfort also changes regularly and the absolute values are above 0.7. When the brightness contrast is close to 10 : 1, the visual sharpness is the highest and the visual sharpness decreases on both sides with the change in contrast value; when the brightness contrast is close to 5 : 1, the visual comfort is the highest and the same visual comfort decreases with the values on both sides.

4. Result Analysis

According to the setting of the subjective evaluation experimental questionnaire, we take the visual comfort evaluation scale as an example (the visual clarity evaluation scale is also the same). On the subjective evaluation scale, the representative "very uncomfortable" is 1 point, the representative "less comfortable" is 2 points, the representative "general" is 3 points, the representative "more comfortable" is 4 points, and the representative "very comfortable" is 5 points. Also, we give 1 point for "very unclear," 2 points for "less clear," 3 points for "average," 4 points for "relatively clear," and 5 points for "very clear."

The threshold value calculated is the threshold value of visual clarity and visual comfort in the light environment of

RETRACTED

Table 1: Statistics of average scores of visual acuity and visual comfort in large batches of subjective experiments.

	300 cd/m^2	400 cd/m^2	500 cd/m^2	600 cd/m^2	700 cd/m^2	800 cd/m^2
Visual clarity	2.55	3.78	4.39	3.20	2.23	1.85
Visual comfort	3.53	4.55	4.38	3.05	2.53	2.24

Table 2: Statistical frequency percentage of visual acuity data.

Scoring frequency/percentage		Brightness parameters					
		300 cd/m^2	400 cd/m^2	500 cd/m^2	600 cd/m^2	700 cd/m^2	800 cd/m^2
Frequency	1	1	0	0	0	2	15
	2	44	3	0	21	69	77
	3	44	26	5	37	19	1
	4	4	52	46	30	3	0
	5	0	12	42	5	0	0
Percentage of score	1 (%)	1.08	0	0	0	2.15	16.12
	2 (%)	47.31	3.22	0	22.58	74.19	82.8
	3 (%)	47.31	27.96	5.38	39.78	20.43	1.08
	4 (%)	4.3	55.91	49.46	32.26	3.23	0
	5 (%)	0	12.91	45.16	5.38	0	0
≥4 percentage		4.3	68.82	94.62	37.64	3.23	0
≤2 percentage		48.39	3.22	0	22.58	76.34	98.92

Table 3: Statistical table of visual comfort data frequency percentage.

Scoring frequency/percentage		Brightness parameters					
		300 cd/m^2	400 cd/m^2	500 cd/m^2	600 cd/m^2	700 cd/m^2	800 cd/m^2
Frequency	1	0	0	0	2	8	8
	2	1	3	7	19	32	61
	3	42	2	5	50	40	22
	4	48	37	40	19	13	2
	5	2	51	41	3	0	0
Percentage of score	1 (%)	0	0	0	2.15	8.6	8.6
	2 (%)	1.08	3.23	7.53	20.43	34.41	65.59
	3 (%)	45.16	2.15	5.38	53.76	43.01	23.66
	4 (%)	51.61	39.78	43.01	20.43	13.98	2.15
	5 (%)	2.15	54.84	44.09	3.22	0	0
≥4 percentage		53.76	94.62	87.1	23.65	13.98	2.15
≤2 percentage		1.08	3.23	7.53	22.58	43.01	74.19

the multimedia classroom. Since clarity and comfort themselves vary from person to person, it is a relatively subjective concept. At present, there is no clear regulation on the brightness value in the field of vision of the multimedia classroom, which is the value of visual clarity and visual comfort [18]. Therefore, taking visual comfort as an example (the same can be used for visual clarity), this paper proposes a threshold limit value of 50% obtained when the subjective evaluation score is greater than or equal to 4, which is a higher standard value of visual comfort for the brightness parameter of the light environment in multimedia classrooms; when the subjective evaluation score is less than or equal to 2, the 50% threshold limit value obtained is the value that starts to cause visual discomfort.

4.1. Statistical Frequency Percentage. The statistical percentages of visual clarity and visual comfort under various experimental brightness parameters are shown in Tables 2 and 3.

4.2. Threshold Calculation. The calculation of the 50% threshold limit value obtained when the score of a large batch subjective evaluation experiment is greater than or equal to 4 is shown in Table 4.

We use the linear interpolation method to calculate the absolute threshold value and set the absolute threshold corresponding to the stimulation value in 50% proportion as X to obtain the following formulas:

$$\frac{400-300}{68.82-4.3}=\frac{X-300}{50-4.3}X=\frac{370.83\text{cd}}{m^2}, \tag{1}$$

$$\frac{600-500}{37.64-96.62}=\frac{X-500}{50-94.62}X=\frac{575.65\text{cd}}{m^2}. \tag{2}$$

RETRACTED

Table 4: Calculation table of threshold limit value of visual clarity brightness change data.

Scoring frequency/percentage	Brightness parameters					
	300 cd/m^2	400 cd/m^2	500 cd/m^2	600 cd/m^2	700 cd/m^2	800 cd/m^2
≥4 percentage	4.3	68.82	94.62	37.64	3.23	0
≤2 percentage	48.39	3.22	0	22.58	76.34	98.92

Table 5: Calculation table of threshold limit value of visual comfort brightness change data.

Scoring frequency/percentage	Brightness parameters					
	300 cd/m^2	400 cd/m^2	500 cd/m^2	600 cd/m^2	700 cd/m^2	800 cd/m^2
≥4 percentage	53.76	94.62	87.1	23.65	13.98	2.15
≤2 percentage	1.08	3.23	7.53	22.58	43.01	74.19

Similarly, the threshold limit value of 50% visual acuity can be obtained when the score is ≤2, as shown in

$$\frac{400-300}{3.22-48.39}=\frac{X-300}{50-48.39}\quad X=\frac{296.44\text{cd}}{m^2}, \tag{3}$$

$$\frac{700-600}{76.34-22.58}=\frac{X-600}{50-22.58}X=\frac{651.01\text{cd}}{m^2}. \tag{4}$$

According to the calculation results of the absolute threshold value obtained by the above linear interpolation method, the 50% brightness threshold value obtained when the experimental score is greater than or equal to 4 is 370.83 cd/m^2 and 575.65 cd/m^2, respectively; the threshold limit values of 50% visual acuity obtained when the score is less than or equal to 2 are 296.44 cd/m^2 and 651.01 cd/m^2, respectively.

The threshold limit value of brightness change data for visual comfort is calculated in Table 5.

We use the linear interpolation method to calculate the absolute threshold value and set the absolute threshold corresponding to the stimulation value in 50% proportion as X to obtain the following formulas:

$$\frac{400-300}{94.62-53.76}=\frac{X-300}{50-53.76}X=\frac{290.8\text{cd}}{m^2}, \tag{5}$$

$$\frac{600-500}{23.65-87.1}=\frac{X-500}{50-87.1}X=\frac{558.47\text{cd}}{m^2}. \tag{6}$$

Similarly, the threshold limit value of 50% visual comfort can be obtained when the score is less than or equal to 2, as shown in

$$\frac{800-700}{74.19-43.01}=\frac{X-700}{50-43.01}X=\frac{722.42\text{cd}}{m^2}. \tag{7}$$

According to the calculation results of the absolute threshold value obtained by the above linear interpolation method, the 50% brightness threshold value obtained when the experimental score is greater than or equal to 4 is 290.8 cd/m^2 and 558.47 cd/m^2, respectively; the threshold limit value of 50% visual acuity obtained when the score is less than or equal to 2 is 722.42 cd/m^2. It should be noted here that due to the limitations of the range of brightness parameters in this experiment, when the score is less than or equal to 2, two thresholds have not been shown from the experimental results [19].

4.3. Analysis of Large Batch Subjective Evaluation Experiment Results. After comparing the brightness thresholds of visual sharpness and visual comfort of high and low standards, it was found that the difference between the values of high and low standards is large. Reviewing the field investigation and the analysis law of test data, the values of visual sharpness and visual comfort calculated in this experiment are taken as the values that can just reach clearer visual sharpness and poor visual sharpness, respectively; and the threshold point that can just bring better visual comfort and visual comfort is about to deteriorate [20, 21].

According to the definition of threshold and the above data rules, we can analyze the following.

4.3.1. Visual Clarity. When the experimental score is greater than or equal to 4, the 50% brightness threshold limit values are 370.83 cd/m^2 and 575.65 cd/m^2, respectively, that is, when the brightness range is 370.83 cd/m^2 ≤ X ≤ 575.65 cd/m^2, it has better visual clarity. When the score is less than or equal to 2, the threshold limit value of 50% visual acuity is 296.44 cd/m^2 and 651.01 cd/m^2, that is when the brightness range is x ≤ 296.44 cd/m^2 and X ≥ 651.01 cd/m^2, the visual acuity is poor. The average score of the visual acuity evaluation and the variation law of brightness are made into a trend analysis diagram, as shown in Figure 1.

4.3.2. Visual Comfort. When the experimental score is greater than or equal to 4, the 50% brightness threshold limit values are 290.8 cd/m^2 and 558.47 cd/m^2, respectively, that is, when the brightness range is 290.8 cd/m^2 ≤ X ≤ 558.47 cd/m^2, it has better visual comfort; the threshold limit value of 50% visual acuity obtained when the score is less than or equal to 2 is 722.42 cd/m^2, that is, when the brightness range is 722.42 cd/m^2 ≤ X, the visual acuity is poor. The average score of the visual comfort evaluation and the variation law of brightness are made into a trend analysis diagram, as shown in Figure 2.

RETRACTED

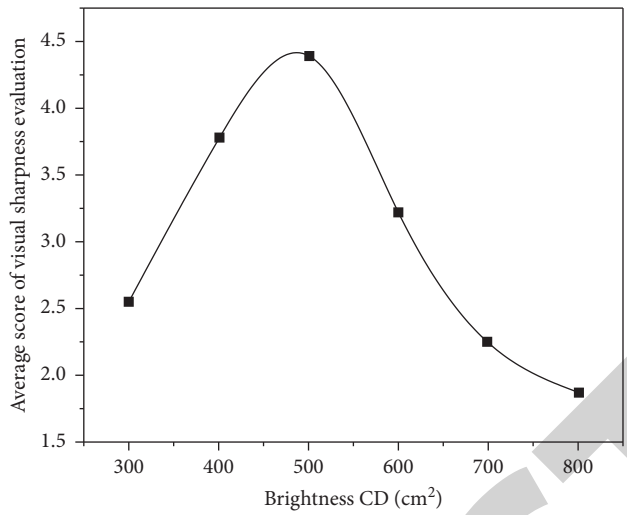

Figure 1: Analysis of average score and brightness change trend of visual acuity evaluation.

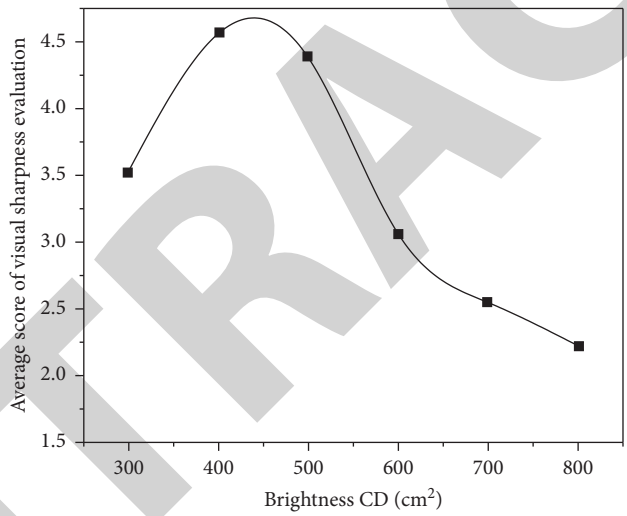

Figure 2: Analysis chart of average score and brightness change trend of visual comfort evaluation.

Table 6: Large probability distribution of brightness comparison data.

Brightness	300 cd/m^2	400 cd/m^2	500 cd/m^2	600 cd/m^2	700 cd/m^2	800 cd/m^2
Average brightness contrast	15 : 1	5 : 1	10 : 1	15 : 1	20 : 1	30 : 1

4.3.3. Luminance Contrast Value Distribution. From the above large batch of subjective evaluation experiments, according to the method described above, the value of the larger probability of the distribution of brightness contrast data is extracted as shown in Table 6, and its change trend is shown in Figure 3.

4.3.4. Interval Coincidence Part. From the above experimental data, we can analyze the overlapping part of the threshold interval, that is, the interval between good and poor visual clarity and visual comfort [22]. When the threshold value of 50% brightness obtained when the experimental score of visual clarity and visual comfort is greater than or equal to 4 coincides, that is, when the brightness range is $370.83\,\text{cd/m}^2 \le X \le 558.47\,\text{cd/m}^2$, this classroom light environment has better visual clarity and better visual comfort at the same time. The threshold value of 50% visual acuity obtained when the experimental score is less than or equal to 2, that is, when $722.42\,\text{cd/m}^2 \le X$, this classroom light environment has poor visual acuity and comparative visual comfort at the same time [23]. Simultaneously, as described in Section 4, when the brightness contrast is close to 10 : 1, that is, when the brightness range is

RETRACTED

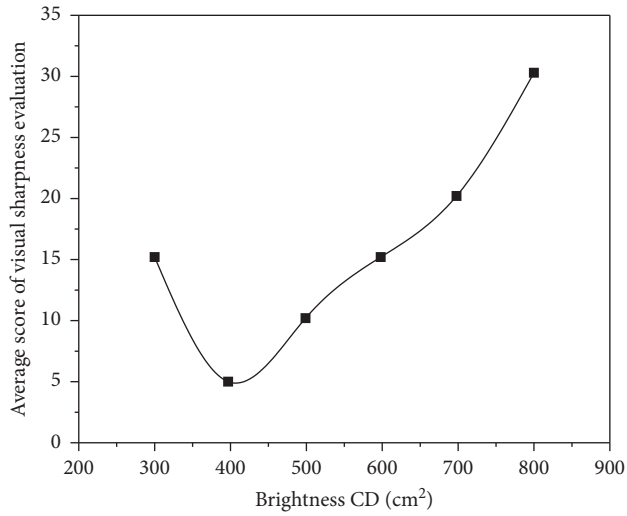

Figure 3: The numerical distribution diagram of the brightness comparison.

$300\ cd/m^2 \le X \le 500\ cd/m^2$, the visual sharpness is the highest, and the visual sharpness decreases from side to side with the change of brightness contrast value; when the brightness contrast is close to 5 : 1, that is, when the brightness is close to $400\ cd/m^2$, the visual comfort is the highest. Similarly, the visual comfort decreases with the values on both sides. Shown in Figure 4 is the relationship between brightness, contrast, and visual clarity and visual comfort.

It can be concluded from the figure that when the brightness range is $370.83\ cd/m^2 \le X \le 558.47\ cd/m^2$, the light environment of this classroom has good visual clarity and visual comfort at the same time. In order to better reflect the coincidence interval of visual clarity, visual comfort, and brightness contrast within the same brightness range, the value of brightness contrast is reduced by ten times and their change trend is observed together with the average score of visual clarity and visual comfort [24]. The coincidence part of the threshold interval and the change trends of visual clarity, visual comfort, and brightness, as well as the comparative analysis diagram of brightness, are shown in Figure 5.

The overall change trend can be analyzed from the above change relationship. When the brightness range is $370.83\ cd/m^2 \le X \le 558.47\ cd/m^2$, the light environment of this classroom has good visual clarity and visual comfort at the same time. At this time, the brightness contrast value is low, which can reflect that when the brightness pair is relatively low, there will be better visual clarity and better visual comfort [25]. Here, we introduce the concepts of reference target value and current value and draw up the 50% threshold limit value obtained when the evaluation score in a large batch of subjective evaluation experiments is less than or equal to 2 as the current value required for future development. The 50% threshold limit value obtained when the evaluation score in a large batch of subjective evaluation experiments is greater than or equal to 4 is formulated as the target value that needs to be achieved for future development.

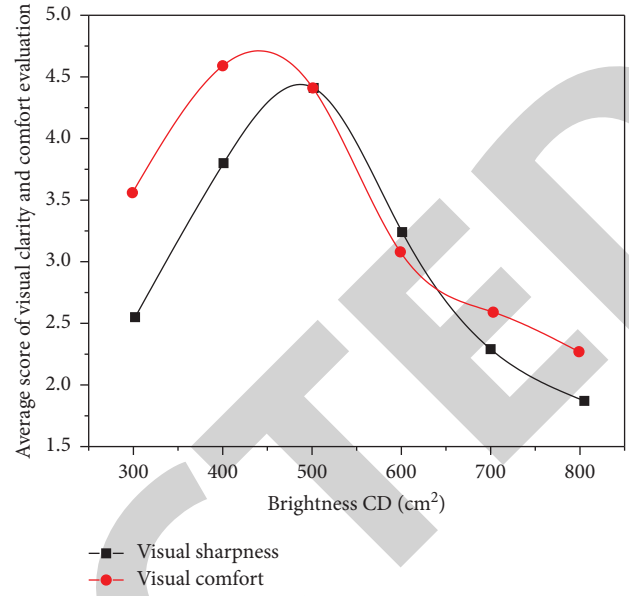

Figure 4: Relationship between brightness contrast and visual clarity and visual comfort.

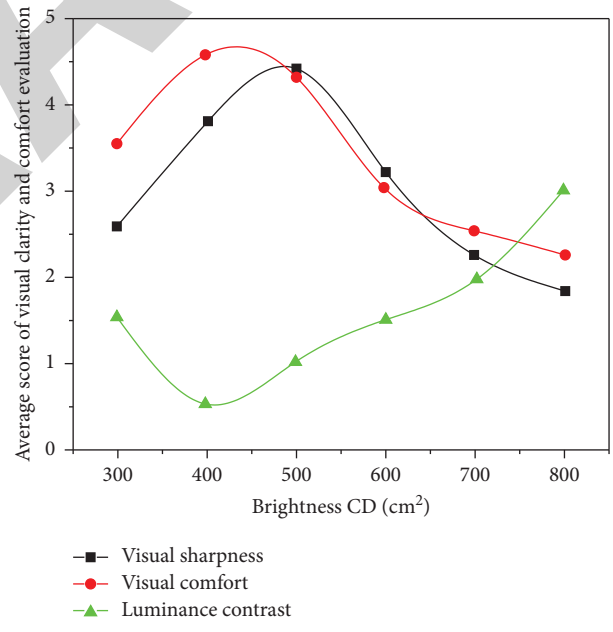

Figure 5: Comprehensive analysis diagram.

4.4. Influence of Brightness Change on Visual Subjective Evaluation

4.4.1. Change Trend. There is a strong correlation between the visual clarity and visual comfort of the light environment of multimedia classrooms in colleges and universities and the change in brightness, which directly affects the visual efficacy, visual experience, and subjective feeling. The selection of the evaluation factors for the light environment in the multimedia classroom space is the basis for determining the evaluation indexes in the following paper. According to

RETRACTED

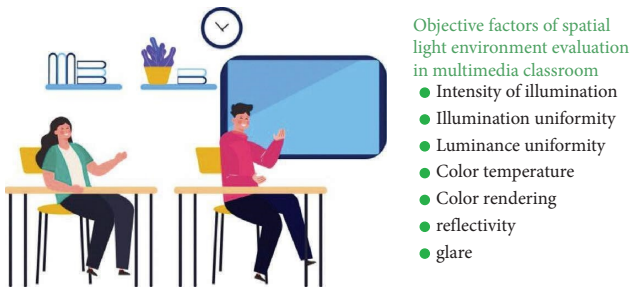

Figure 6: Composition of objective influence factors.

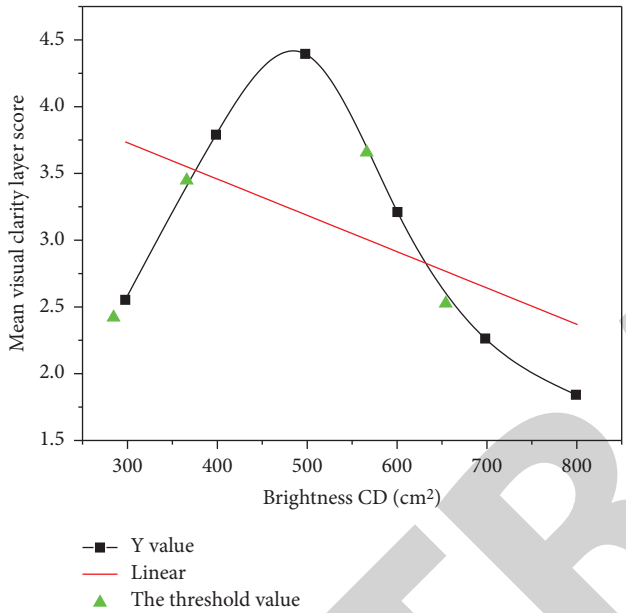

Figure 7: Variation trend of visual clarity and brightness.

the measurement of the light environment in the multimedia classroom space in colleges and universities and referring to the relevant norms and standards, the objective influence factors of the light environment evaluation in the main space are sorted out and analyzed, including illumination, illumination uniformity, brightness uniformity, color temperature, color rendering, reflectivity, and glare. Shown in Figure 6 is the composition model of the objective influence factors of the spatial light environment evaluation of the multimedia classrooms in colleges and universities. According to the relationship between brightness change and visual clarity and visual comfort, this paper makes a change trend chart according to the average score of the subjective evaluation and each threshold value, as shown in Figures 7 and 8.

As can be seen from Figures 7 and 8, the trends for visual clarity, visual comfort, and brightness parameters are roughly the same. When the brightness value is about 500 cd/m^2, the visual clarity is positively correlated with the change in brightness value; when the brightness value is about 500 cd/m^2, the visual clarity is negatively correlated with the change in brightness value; when the brightness value is about 400 cd/m^2, the visual comfort is positively correlated with the change

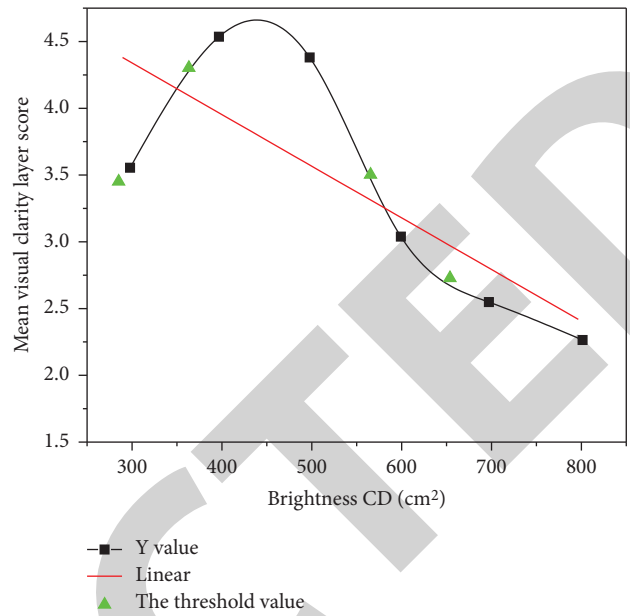

Figure 8: Variation trend of visual comfort and brightness.

in brightness value. When the brightness value is about 400 cd/m2, the visual comfort is negatively correlated with the change in brightness value. Although some change trends can be seen from the figure, the specific variable values are not clear and need further analysis.

4.4.2. SPSS Curve Regression. Curvilinear regression is a data analysis method that transforms according to the characteristics of the data, then performs linear regression or uses a curve fitting method to fit the original data to determine the curve regression equation.

This section studies the relationship between brightness parameter changes and visual clarity and visual comfort in multimedia classrooms in colleges and universities and uses software to perform curve fitting to find the quantitative relationship between brightness changes and visual clarity and visual comfort, finally determining the curve equation. Through the curve equation, the specific change trend can be analyzed, and the brightness values that make the vision the clearest and the most comfortable can be found, respectively, as well as the brightness values that need to be achieved to meet certain visual clarity or visual comfort.

Curve regression steps mainly include the following: First, we use the line chart to preliminarily judge the curve type. To reduce the blindness of curve estimation, it is necessary to draw a line chart first, and according to the change trend of dependent and independent variables in the line chart, you can choose an appropriate function to fit the data points. Then, we perform curve regression analysis. After the computer processing of curve regression is completed, the most appropriate curve regression type is selected according to the output results of the computer and the square value of the judgment coefficient R. Finally, according to the regression type of the fitted curve and the value of each coefficient, the functional formula is obtained.

RETRACTED

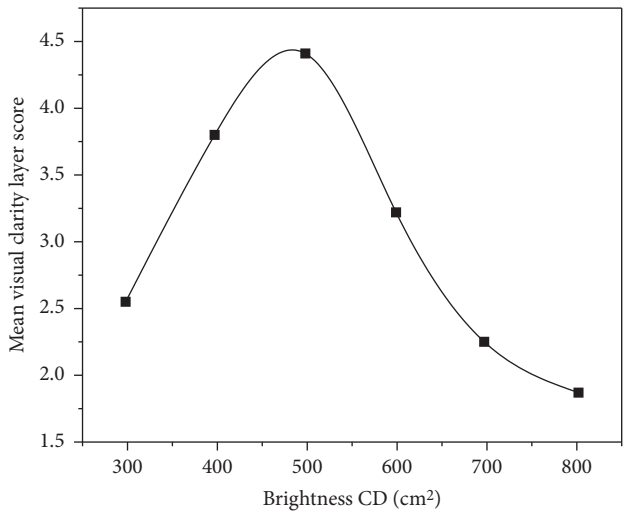

Figure 9: Line chart of brightness and visual clarity.

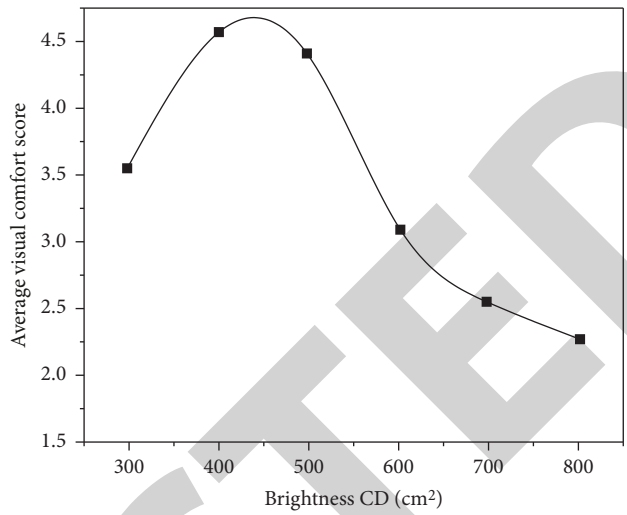

Figure 10: Broken line diagram of brightness and visual comfort.

(1) Draw a (X, Y) line chart of the relationship between visual clarity, visual comfort, and brightness parameters, as shown in Figures 9 and 10. The relationship between brightness, visual clarity, and visual comfort can be preliminarily observed, and the relationship between independent and dependent variables can be judged to be close to a curve. Therefore, curve regression analysis can be continued.

(2) Curve Fitting. According to the change trend of the line chart, the form of the curve is preliminarily judged and the quadratic function and cubic function are selected for fitting.

According to the definitions of the independent variable and dependent variable, the brightness value of the multimedia classroom is determined as an independent variable and the evaluation score of visual clarity or visual comfort is determined as a dependent variable.

The broken line diagram of the actual data of visual clarity and brightness and the fitting diagram of the quadratic cubic function curve equation are shown in Figures 11 and 12.

(3) Curve Fitting Is Carried Out according to the Data. From the data of the SPSS software model and parameter evaluation, it can be found that the R^2 values of the determination coefficient of the quadratic curve model and the cubic curve model are 0.788 and 0.962, respectively, indicating that the quality and fitting effect of the two regression models are relatively good.

The fitted quadratic function curve equation of visual sharpness and brightness is $y = -2.566 \times 10^{-5}x^2 + 0.026x - 2.546$.

The fitted cubic function curve equation of visual sharpness and brightness is $y = 1.121 \times 10^{-7}x^3 + 0.122x - 18.087$.

According to the actual situation and reviewing the experimental situation and the trend of experimental values, after the brightness reaches 800 cd/m^2, the trend of visual clarity should decrease with the increase in brightness, so the cubic function is excluded in combination with the figure

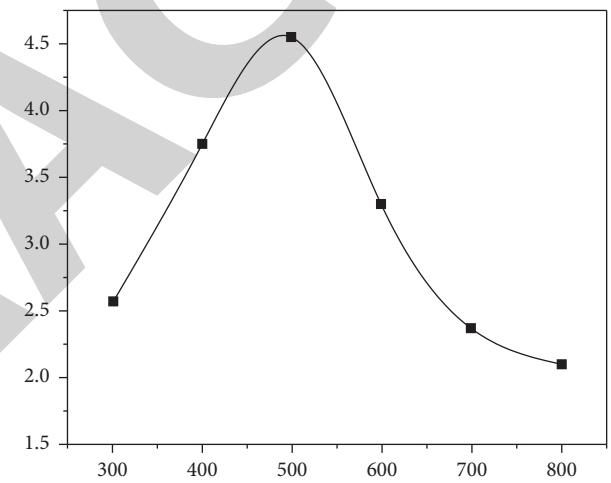

Figure 11: Line chart of actual data of visual clarity and brightness.

and the functional formula. At the same time, due to the definition of experimental scope, independent and dependent variables have actual scope areas, theoretically. In this area, if the quadratic function equation is used, the brightness value reaching the highest point of visual clarity can be calculated to be about 506.25 cd/m^2.

Similarly, the broken line diagram of the actual data for visual comfort and brightness and the fitting diagram of the quadratic cubic function curve equation are shown in Figures 13 and 14.

Curve fitting was carried out according to the data. From the data of the SPSS software model and parameter evaluation, it can be found that the R^2 values of the determination coefficient of the quadratic curve model and the cubic curve model are 0.771 and 0.979, respectively, indicating that the quality and fitting effect of the two regression models are relatively good.

The fitted quadratic function curve equation of visual comfort and brightness is $y = -1.42 \times 10^{-5}x^2 + 0.012x + 1.675$.

RETRACTED

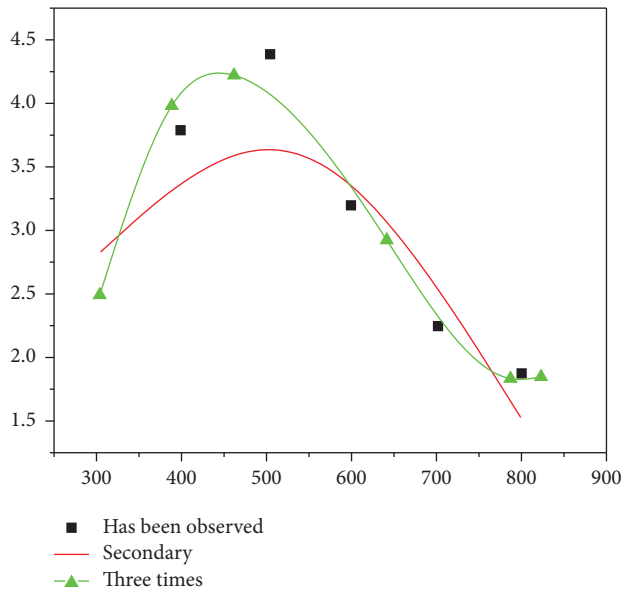

Figure 12: Fitting diagram of quadratic cubic function curve equation.

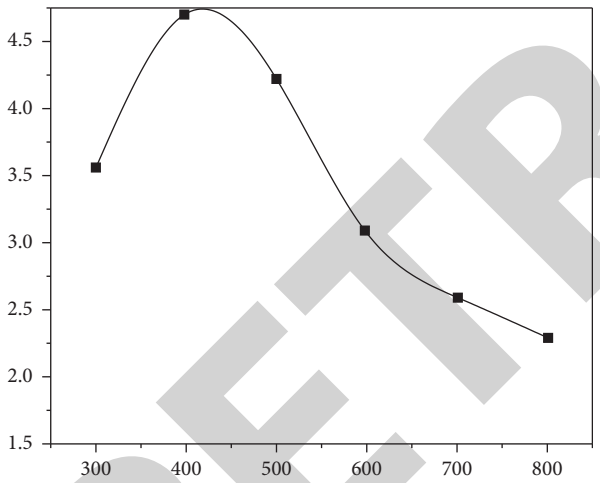

Figure 13: Line chart of actual data of visual comfort and brightness.

The fitted cubic function curve equation of visual sharpness and brightness is $y = 1.205 \times 10^{-7}x^3 + 0.115x - 15.022$.

According to the actual situation and reviewing the experimental situation and the trend of experimental values, after the brightness reaches 800 cd/m^2, the trend of visual clarity should decrease with the increase in brightness, so the cubic function is excluded in combination with the figure and the functional formula. At the same time, due to the definition of experimental scope, independent and dependent variables have actual scope areas, theoretically. In this area, the brightness value reaching the highest point of visual comfort can be calculated according to the quadratic function equation, which is about 422.54 cd/m^2.

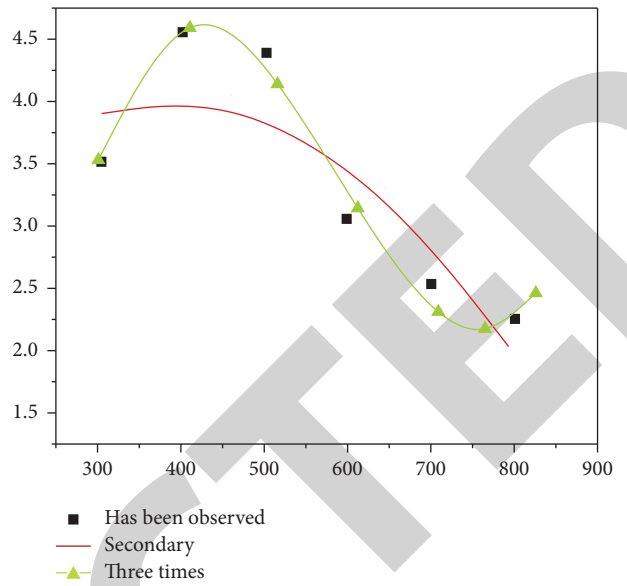

Figure 14: Fitting diagram of the curve equation.

5. Conclusion

This paper presents a method for extracting the light environment of a multimedia classroom by using high dynamic range images and puts forward a new method and idea for measuring the light environment. However, at present, the multiexposure method is used to obtain high dynamic range images, which stays at the measuring point for a little longer, and the information acquisition effect of dynamic scenes is poor. It is hoped that future research can improve the method of obtaining high dynamic range images or develop a more intuitive and effective method of extracting visual brightness closer to human eyes.

Considering the factors of healthy lighting, energy conservation, and environmental protection, in the treatment and selection of the light environment of the multimedia classroom, we should fully consider the use of natural lighting, adopt curtains that can adjust the transmittance of natural light, etc., so that the intensity and direction of natural light entering the classroom can be adjusted according to the demand, and combine these adjustment methods with light sensing devices to automatically adjust the amount of indoor light and lighting light.

The white plastic curtain used in this study belongs to the screen of reflective light source type and uses static visual recognition objects. In the actual teaching environment, there are also multimedia teaching tools with self-illumination and different dynamic playback frequencies, such as LCD and electronic whiteboard. The specific impact degree and impact law of these equipment need to be further studied.

Data Availability

The labeled data set used to support the findings of this study is available from the corresponding author upon request.

RETRACTED

Hindawi
Journal of Robotics
Volume 2024, Article ID 9837908, 1 page
https://doi.org/10.1155/2024/9837908

Retraction

Retracted: On the Performance and Efficiency of Surface Air Cooler Working under High Temperature and High Humidity Condition

Journal of Robotics

Received 23 January 2024; Accepted 23 January 2024; Published 24 January 2024

Copyright © 2024 Journal of Robotics. This is an open access article distributed under the Creative Commons Attribution License, which permits unrestricted use, distribution, and reproduction in any medium, provided the original work is properly cited.

This article has been retracted by Hindawi following an investigation undertaken by the publisher [1]. This investigation has uncovered evidence of one or more of the following indicators of systematic manipulation of the publication process:

(1) Discrepancies in scope
(2) Discrepancies in the description of the research reported
(3) Discrepancies between the availability of data and the research described
(4) Inappropriate citations
(5) Incoherent, meaningless and/or irrelevant content included in the article
(6) Manipulated or compromised peer review

The presence of these indicators undermines our confidence in the integrity of the article's content and we cannot, therefore, vouch for its reliability. Please note that this notice is intended solely to alert readers that the content of this article is unreliable. We have not investigated whether authors were aware of or involved in the systematic manipulation of the publication process.

Wiley and Hindawi regrets that the usual quality checks did not identify these issues before publication and have since put additional measures in place to safeguard research integrity.

We wish to credit our own Research Integrity and Research Publishing teams and anonymous and named external researchers and research integrity experts for contributing to this investigation.

The corresponding author, as the representative of all authors, has been given the opportunity to register their agreement or disagreement to this retraction. We have kept a record of any response received.

References

[1] J. Yang, J. Yu, S. Wang, and W. Yan, "On the Performance and Efficiency of Surface Air Cooler Working under High Temperature and High Humidity Condition," *Journal of Robotics*, vol. 2022, Article ID 8656289, 11 pages, 2022.

Hindawi
Journal of Robotics
Volume 2022, Article ID 8656289, 11 pages
https://doi.org/10.1155/2022/8656289

RETRACTED

Research Article

On the Performance and Efficiency of Surface Air Cooler Working under High Temperature and High Humidity Condition

Juan Yang, Jing Yu, Shijing Wang, and Weidong Yan

School of Intelligent Engineering Technology, Jiangsu Vocational Institute of Commerce, Nanjing, Jiangsu 211199, China

Correspondence should be addressed to Jing Yu; 18251853848@163.com

Received 12 August 2022; Revised 29 August 2022; Accepted 30 August 2022; Published 28 September 2022

Academic Editor: Shahid Hussain

Copyright © 2022 Juan Yang et al. This is an open access article distributed under the Creative Commons Attribution License, which permits unrestricted use, distribution, and reproduction in any medium, provided the original work is properly cited.

Surface air cooler is widely used in refrigeration, air conditioning, chemical dehumidification, and other related fields. Nowadays, the application of surface air cooler has been mature under standard working conditions, and more and more research has been carried out on its application. However, when conventional surface air coolers are directly used under high temperature and high humidity conditions (the temperature is higher than 30°C, both the humidity ratios are higher than 20 g/kg dry air), or under conditions with strict dehumidification requirements, the expected results are often not achieved. Therefore, taking the conventional surface cooler as an example, the performance and efficiency of dehumidification of the surface cooler under high temperature and high humidity are investigated specifically in this paper. Based on the above model and experiment, the influence of operation parameters on heat and mass transfer of surface air cooler is analyzed. At the same time, the change law of heat and mass transfer capacity, dehumidification performance, and heat transfer efficiency of a surface air cooler is specially investigated. Results proved that under high temperature and humidity conditions (34.8°C, 23.03 g/kg dry air), lower head-on wind velocity could realize deeper humidification effects effectively, while water velocity showed fewer impacts. As shown in the experiment, when water velocity increased to 1.2 m/s, and head-on wind velocity dropped to 1.06 m/s, the humidity ratio at the air outlet reduced to 8.88 g/kg while heat-transfer efficiency reached 0.778; however, when head-on velocity increased to 2.5 m/s and water velocity rose to 1.2 m/s, humidity ratio at air outlet dropped to 13.17 g/kg only, and heat-transfer efficiency reached merely 0.572. In conclusion, this paper has established an accurate and effective mathematical model for analyzing the heat transfer and dehumidification characteristics of the surface cooler under high temperature and high humidity conditions, which provides a reference for the development and design of dehumidification surface cooler under special conditions. More importantly, the conclusion of this paper also points out that, different from the adjusting strategy under conventional working conditions, reducing the head-on wind speed is the best adjusting strategy when the air surface cooler is used in high temperature and high humidity working conditions. This adjusting strategy is not only conducive to promoting the air to achieve a better dehumidification effect but also can effectively improve the efficiency of the surface cooler.

1. Introduction

As a kind of efficient and low-cost heat-transfer device, surface air coolers are highly popular in air-conditioning, dehumidifying, and chemical applications.

Current conventional surface air coolers are usually designed for nominal conditions (the dry bulb temperature is 27°C, and the wet bulb temperature is 19.5°C), wind speed 2.5 m/s, and inlet and outlet water temperature 7°C/12°C [1]. For the purpose of improving the heat transfer performance of surface air coolers to make them satisfy dehumidification requirements, researchers increase pipe banks and enlarge heat transfer area. Mei et al. [2] established a mathematical model of a cooling coil and carried out a simulation study on the law of changes in the heat transfer capacity and dehumidifying system of surface air cooler under different conditions such as changing only the chilled water flow and changing only the air volume, etc., and finally put forward with a method for systematic energy conservation and optimization, that is, to adjust the chilled water flow and the air volume simultaneously. Liu et al. [3] concluded, with the control variable method, that the heat-transfer efficiency of

surface air cooler would increase along with the increase of water velocity and decrease along with the increase of the head-on wind velocity and the dehumidifying coefficient. Li [4] proposed, for the high temperature and high humidity conditions, to realize dehumidification by adopting the two-level rotary dehumidifying plus direct evaporative cooling system. You et al. [5] analyzed, based on experiments, whether indirect evaporative cooling and energy-recovering system used in high temperature and humidity area can satisfy dehumidification requirements.

The abovementioned literature researches show that there are few studies on the dehumidification performance and efficiency of conventional surface air coolers under high temperature and humidity conditions. However, high temperature and humidity conditions are common in many applications, such as the air-conditioning system in the summer, especially in the plum rain season, in regions south of the Yangtze River [6], the solar-energy-based wastewater treatment system in the chemical industry [7], the air-conditioning system in textile workshops [8], and other related industrial applications. In engineering applications, when a regular surface air cooler is used under high temperature and humidity conditions (the temperature is higher than 30°C, both the humidity ratios are higher than 20 g/kg dry air), defects such as failure to reach dehumidification requirements appear frequently, resulting in the cumulation of humidity road. Moreover, surface air coolers today generally focus on heat transfer but ignore dehumidification, which results in the common existence of poor heat-transfer efficiency when such surface air coolers are used for dehumidifying [9]. To meet the dehumidification requirements, namely, the requirements for high mass transfer, when using a regular surface air cooler to treat air at high temperature and humidity, it is necessary to reform and optimize such surface air cooler. At present, there are two optimization methods: (1) to adjust the operating conditions of the surface air cooler, and (2) to change the structure of the conventional surface air cooler. Among them, the second method would increase the cost of equipment investment, resulting in low economic benefits. Therefore, the first method is more suitable.

In order to solve the above problems, in this paper, based on the conventional surface cooler structure, from the perspective of changing the operating conditions, the heat and mass transfer model of the surface cooler is established, and the corresponding experimental platform is also set up. The dehumidification performance and efficiency of the surface cooler under the condition of high temperature and high humidity are analyzed by means of both simulation and experiment. This paper aims to explore the heat and mass transfer law of surface coolers under high temperature and high humidity conditions through experiment and simulation and find an effective method to solve the poor dehumidification effect under this special condition, to provide reference for further research and design of surface cooler.

2. Modeling

2.1. Physical Model. First of all, assumptions for the establishment of a physical model were given based on the actual situation of regular surface air cooler [10]:

(1) The surface air cooler is made of a regular finned-pipe structure, with the air and the water flow in a cross direction;

(2) Condensate water generated in the heat-transfer process flows away in time from the coil surface, thus impacts from the cumulation of such condensate water in finned-pipe gaps are ignored;

(3) Contact thermal resistance and fouling resistance are ignored;

Based on such assumptions, a physical model of a finned-pipe surface air cooler is established. Figure 1(a) shows the structure of the such model, while Figure 1(b) shows the internal structure of finned pipes.

2.2. Mathematical Model. A mathematical model of the heat and mass transfer process of the surface air cooler was established based on the physical model described above.

2.2.1. Heat-Transfer Model at Pipe Outer Side of Surface Air Cooler

(1) Energy-balance equation:

$$Q_1 = q_{\text{am}}\left(i_{a_{\text{in}}} - i_{a,\text{out}}\right) - m_{\text{cw}} i_{\text{cw}},$$
$$Q_1 = h_s \times A_{\text{out}} \times \Delta t_{\text{out}}. \quad (1)$$

Mass-balance equation:

$$m_{\text{cw}} = q_{\text{am}}\left(d_{a,\text{in}} - d_{a,\text{out}}\right), \quad (2)$$

in which Q_1 is the heat transfer capacity kW between air at the outer pipe side and the outer pipe wall;

q_{am} is the mass flow of the air (kg/h);

$i_{a,\text{in}}$, $i_{a,\text{out}}$ are the enthalpy at the air inlet and outlet (kJ/kg);

$d_{a,\text{in}} d_{a,out}$ is the moisture content at air inlet and outlet (kg/kg);

m_{cw} is the mass flow of the condensate water, namely, the dehumidification capacity (kg/h);

i_{cw} is the enthalpy of condensate water (kJ/kg.dry);

h_s is the heat transfer coefficient at outer pipe side under wet conditions (W/m^2•K);

A_{out} is the heat transfer area out of the pipe (m^2);

Δt_{out} is the heat transfer temperature difference out of the pipe, °C.

It should be noted here that when air is cooled and dehumidified by the surface cooler, heat transfer and mass transfer are carried out together. Therefore, the part of energy taken away by condensate water also needs to be included in the energy balance equation.

(2) Heat transfer equation:

The heat transfer factor j_1 proposed by Colburn [11] is used to calculate the heat transfer process. The mathematical model is expressed as follows:

RETRACTED

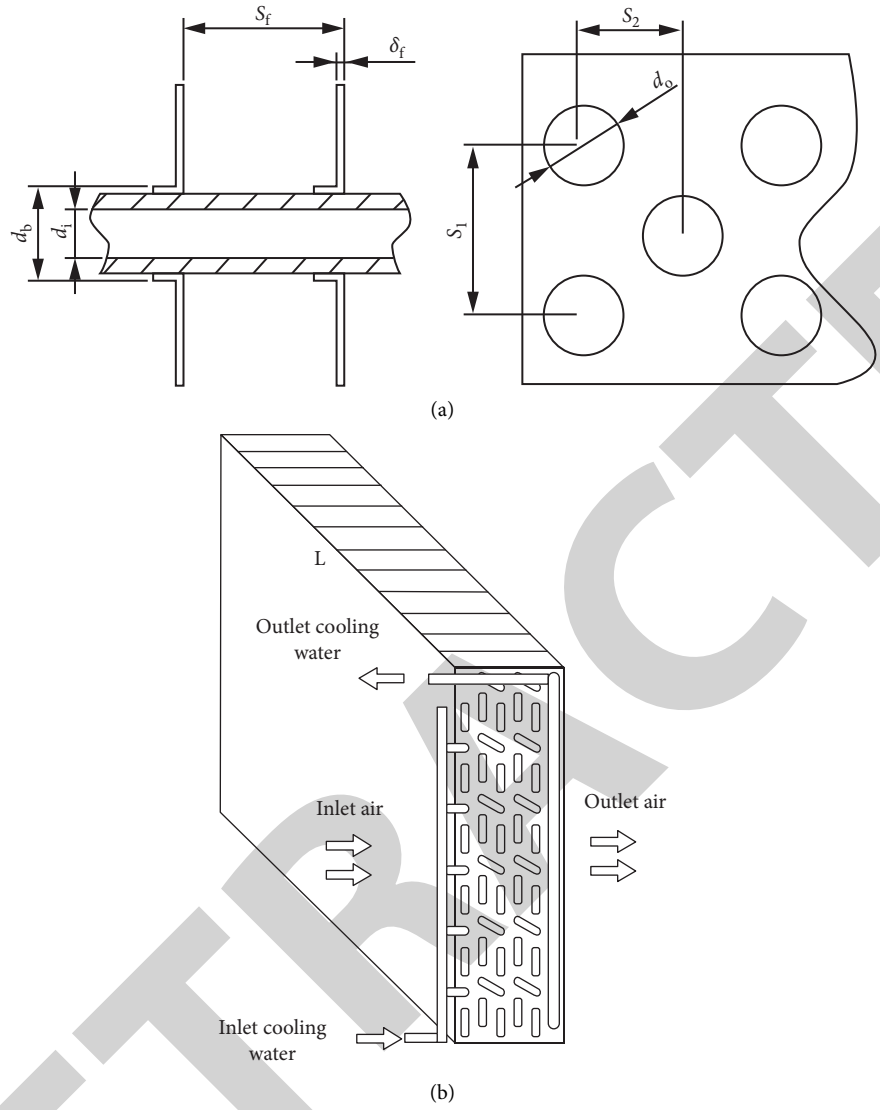

Figure 1: Structure diagrams of surface air cooler (a, b).

$$j_1 = \frac{h_1 A_y}{q_{ma} C_{pa}} \mathrm{Pr}^{2/3},$$

$$j_1 = \left[\frac{1 - 1280 \times N \times \mathrm{Re}_L^{-1.2}}{1 - 5120 \times \mathrm{Re}_L^{-1.2}}\right] \times \left(0.0014 + 0.2618 J_p\right), \quad (3)$$

$$J_P = \mathrm{Re}_D^{-0.4} \left[\frac{A_o}{A_{b_o}}\right]^{-0.15},$$

in which Re_L is the Reynolds number based on vertical pipe spacing;

Re_D is the Reynolds number based on the outer diameter of the pipe;

h_1 is the heat transfer coefficient at outer pipe side under dry conditions, W/m^2•K;

A_y is the head-on wind area, m^2;

N is the number of pipe banks;

C_{pa} is the specific heat of the wet air, kJ/kg•k.

The model above is a heat transfer model under dry conditions. Because the finned tube surface air cooler works under wet conditions, it is necessary to modify its heat transfer coefficient. Under wet conditions, the heat transfer coefficient h_s is as follows:

$$h_s = h_1 \times \zeta \times \eta_{ao}, \quad (4)$$

where η_{ao} is the efficiency of the finned surface, expressed as follows:

$$\eta_{ao} = \frac{\eta_f \times A_f + A_b}{A_O}, \quad (5)$$

Here, A_f is the side face area of the fin, m^2;

A_b is the interfins pipe surface area, m^2;

A_O is the total side face area of fins, m^2;

RETRACTED

η_f is the fin efficiency of the surface air cooler, namely, the contact coefficient [12].

$$\eta_f = \frac{\text{th}(mh)}{mh}, \quad m = \sqrt{\frac{2h_1}{\lambda_l \delta_f}}, \tag{6}$$

in which h— is the equivalent fin height, m;

λ_1 is the heat conductivity coefficient of aluminum, W/m•k;

δ_f is the fin thickness, m;

In equation (4), ζ is the dehumidifying coefficient of modified dry conditions [13]:

$$\zeta = 1 + \left[\frac{r_w + t_{a,m} \times C_{\text{pw}} - t_{\text{wa,out}} \times C_w}{c_{\text{pa}}}\right] \times \frac{\left(d_{a,m} - d_{a,\text{wa}}\right)}{\left(t_{a,m} - t_{\text{wa,out}}\right)}, \tag{7}$$

in which r_w is the latent heat of evaporation of the water;

$t_{a,m}$ is the mean temperature of the air, ˚C;

$t_{\text{wa, out}}$ is the temperature of the outer wall of the pipe, ˚C;

$d_{a,m}$ is the moisture content of air at $t_{a,m}$, kg/kg;

$d_{a,wa}$ is the moisture content of air at $t_{\text{wa, out}}$, kg/kg;

C_{pw} is the specific heat of water vapor, kJ/kg•k;

C_w is the specific heat of water, kJ/kg•k.

2.2.2. Heat Transfer Model at Internal Side of Surface Air Cooler

(1) Energy-balance equation:

$$Q_2 = C_w q_{\text{mw}}\left(t_{w,\text{out}} - t_{w,\text{in}}\right), \quad Q_2 = h_n \times A_{\text{in}} \times \Delta t_{\text{in}}, \tag{8}$$

in which Q_2 is the heat transfer capacity at the internal side of the pipe, kW;

q_{mw} is the mass flow rate of water, kg/h;

$t_{w,\text{in}}$, $tw_{,\text{out}}$ are the inlet and outlet water temperatures, ˚C;

h_n is the heat transfer coefficient inside the pipe, W/m^2•k;

A_{in} is the heat transfer area inside the pipe, m^2;

Δt_{in} is the heat transfer temperature difference inside the pipe, ˚C.

(2) Heat transfer model:

For the heat transfer coefficient h_n inside the pipe, Gnielinski [14] formula is employed for solution as follows:

$$V_f = \left\{\frac{f}{8} \times (\text{Re}_w - 1000) \times \left[\frac{\text{Pr}_f}{1 + 12.7(f/8)^{1/2} \times \left(\text{Pr}_f^{2/3} - 1\right)}\right] \times \left(1 + \frac{d_o}{L}\right)^{2/3}\right\} \times c_t, \quad V_f = h_n \frac{d_i^2}{\lambda_{s1}}, \quad f = \frac{1}{(1.82 \times \log(\text{Re}_w) - 1.64)^2}, \quad c_t = \left(\frac{\text{Pr}_f}{\text{Pr}_w}\right)^{0.01}, \tag{9}$$

in which Pr_f is the Prandtl number of the water at mean temperature;

Prw is the Prandtl number of the water at interior wall temperature of the pipe;

Re_s is the Reynolds number of the water at mean temperature;

2.2.3. Heat Transfer Model at Wall Face of the Surface Air Cooler

(1) Heat transfer equation [15]:

$$Q_3 = N_1 \times N \times 2 \times \pi \times \lambda_c \times L_1 \times \left[\frac{t_{\text{wa,out}} - t_{\text{wa,in}}}{\ln(d_o/d_i) \times 1000}\right], \tag{10}$$

where $t_{w,\text{in}}$ is the temperature at the interior wall of the pipe, ˚C;

N_1 is the number of pipe arrays;

λ_c is the heat transfer coefficient of copper, W/m•k;

L_1 is the total length of heat-transfer copper pipe, m.

(2) Energy-balance equation:

$$Q_3 = Q_1. \tag{11}$$

The interior wall temperature of the pipe, $t_{\text{wa,in}}$ is calculated with the equation above, as criteria for model iteration.

2.2.4. Performance Parameter Model of the Surface Air Cooler. For the purpose of analyzing the heat and mass transfer capacity, dehumidifying performance, and heat transfer efficiency of the surface air cooler, the model outputs state parameters at the air outlet, heat transfer capacity Q, dehumidification capacity m_{cw}, heat transfer coefficient K, contact coefficient η_{f}, heat exchanger efficiency η_{ao}, and specific air consumption SAC [16].

Heat transfer coefficient K:

$$K = \frac{Q}{\Delta t \cdot A}. \tag{12}$$

RETRACTED

Here, Δt is the heat transfer temperature difference of surface air cooler, and °C; A is the heat transfer area of surface air cooler, m^2.

Heat exchanger efficiency η_{ao} :

$$\eta_{ao} = \frac{t_{a,\text{in}} - t_{a,\text{out}}}{t_{a,\text{in}} - t_{w,\text{in}}}. \tag{13}$$

Specific air consumption refers to the amount of air consumed per unit of dehumidification. It can reflect the power consumption of the blower from the side. Generally, the higher the specific air consumption is, the higher the power consumption of the blower will be.

$$SAC = \frac{q_{\text{ma}}}{m_{\text{cw}}}. \tag{14}$$

2.3. Logic Block Diagram of the Model. The mathematical model above consists of four major modules and multiple boundary conditions. Software EES was used for code editing, and a complete heat and mass transfer model of the finned-pipe surface air cooler was established for systematic stimulation research. See Figure 2 for the model calculation logic diagram.

3. Surface Air Cooler Experiment

3.1. Establishment of the Testbed and Layout of Test Points. In order to verify the accuracy of the model and examine the actual influence of the changes in system operating parameters, an experimental bench as shown in Figure 3 is built. The setting and regulation of the working conditions are realized by using the enthalpy difference laboratory, as shown in Figure 4.

All experimental operating parameters, including air inlet and outlet dry and wet bulb temperatures, pressure difference before and after the nozzle, inlet and outlet water temperature, and water flow rate, can be displayed and set through the terminal control platform of the enthalpy difference laboratory, as shown in Figure 5.

3.2. Test Conditions. To simulate engineering applications, high temperature and humidity fresh air condition in the summer of Nanjing were taken as inlet air parameters for simulation and experimental analysis, see Table 1 for experimental test condition.

3.3. Experimental Data Processing and Error Analysis

3.3.1. Data Processing. In the experiment, primary measured parameters ($t_{a,\text{in}}$, $t_{\text{sa,in}}$, $t_{a,\text{out}}$, and $t_{\text{sa,out}}$) can be obtained directly by measurement, while indirect parameters (η_{ao}, k, and SAC) of surface air cooler can be obtained from a calculation based on equations (1)~(14).

3.3.2. Error Analysis. Experimental errors include instrument errors and indirect errors.

(1) Instrument errors are shown in Table 2.

(2) Indirect error:

According to the method proposed by Moffat [17], measuring uncertainties are defined as different square roots between observed solid errors and random errors of the instrument. As for the experiment described herein, directly measured uncertainties are deemed as independent from each other, uncertainties of indirect parameters, thus can be calculated as follows:

$$u_c = \sqrt{\sum_{i=1}^{N} \left(\frac{\partial f}{\partial x_i}\right)^2 (u_{xi})^2}. \tag{15}$$

Here, x is the directly measured parameter, f refers to the relationship between the indirectly measured parameter and directly measured parameter, and u_x is the direct measurement error. According to the abovementioned method, errors of all indirect parameters are ±5%, which proves the reliability of the test under the experiment.

4. Results and Discussion

4.1. Experimental Verification of the Model. This paper conducted a comparison study between experimental results and stimulated results so that to verify the accuracy of the heat transfer model of the surface air cooler established herein.

Figure 6 shows the comparison between the experimental results and stimulated results of the outlet air dry bulb temperature, the air outlet moisture content, and the outlet water temperature. It can be clearly seen that the prediction accuracy of the model for these three state parameters is very high, and the error is within ±10%. Therefore, the model of finned-pipe surface air cooler established in this paper is reliable. Subsequently, the dehumidification performance and efficiency of surface air coolers under high temperature and humidity conditions are analyzed in detail by combining simulation and experiment.

4.2. Analysis on Affecting Factors. This paper studied mainly the impacts of operating conditions on the dehumidification performance and efficiency of surface air coolers. Affecting parameters include mainly water flow velocity and head-on wind velocity.

As shown in Figure 7, when the water flow velocity is unchanged, both the temperature and moisture content of the air outlet dry bulb drop gradually along with the drop of head-on wind velocity. In the contrast, when head-on wind velocity is unchanged, both the temperature and moisture content of the air outlet dry bulb increase gradually along with the drop of water flow velocity.

By comparing the effects of changes in water flow velocity and changes in head-on wind velocity, we know the effects of these two factors on the temperature and moisture content of the air outlet dry bulb are opposite to each other. Thus, preliminarily, reducing the head-on wind velocity or

RETRACTED

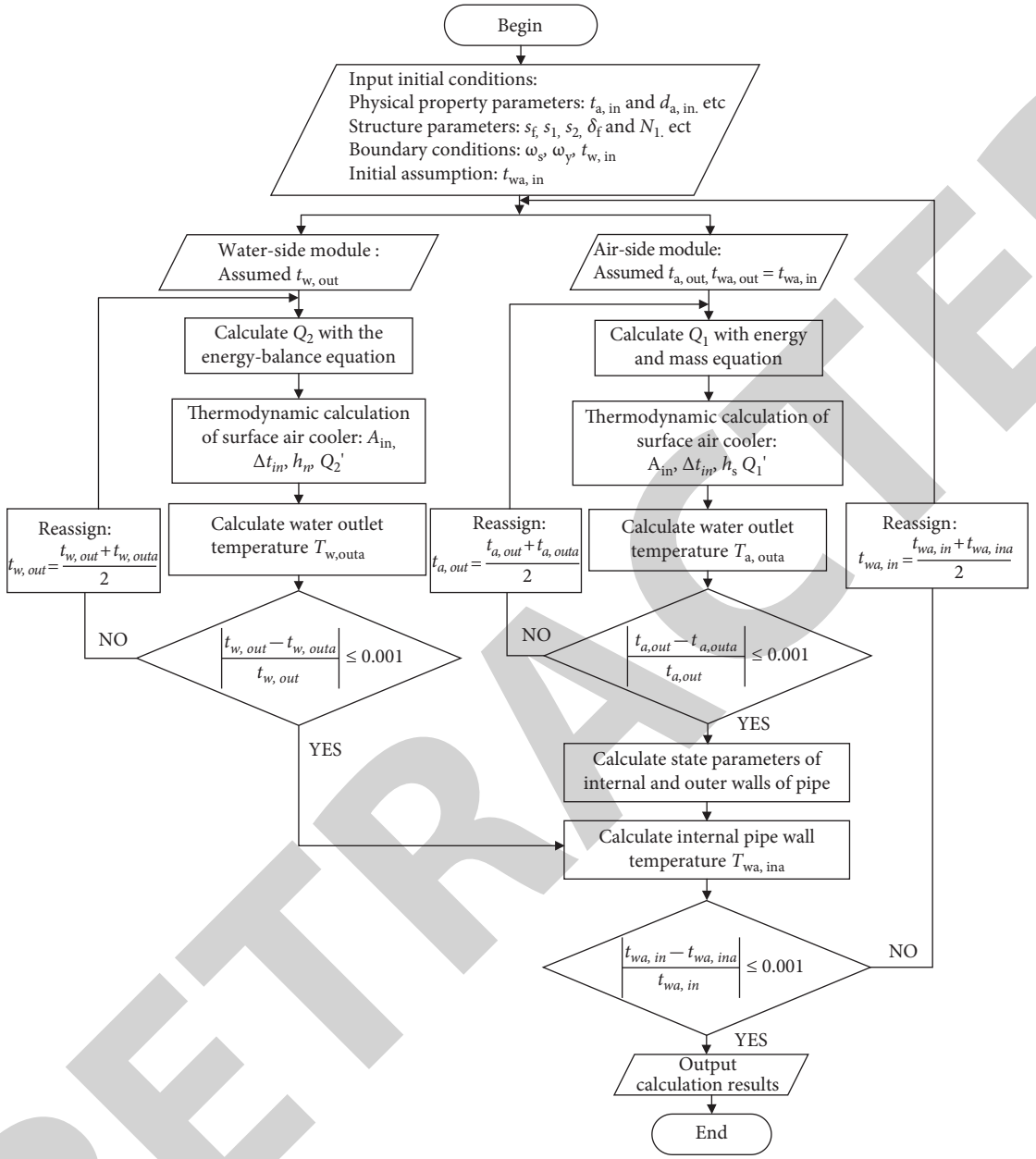

Figure 2: Model calculation logic diagram.

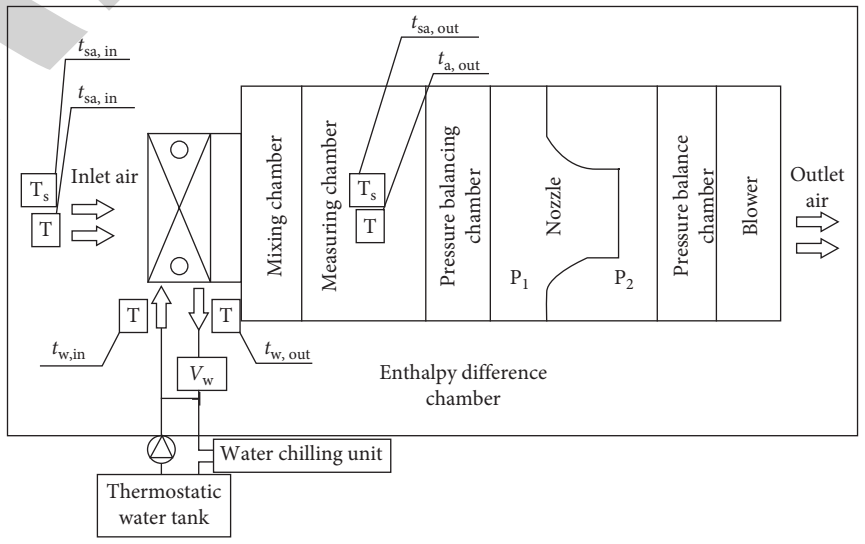

Figure 3: Test point layout of the experimental system.

RETRACTED

Figure 4: Physical photo of the experimental system.

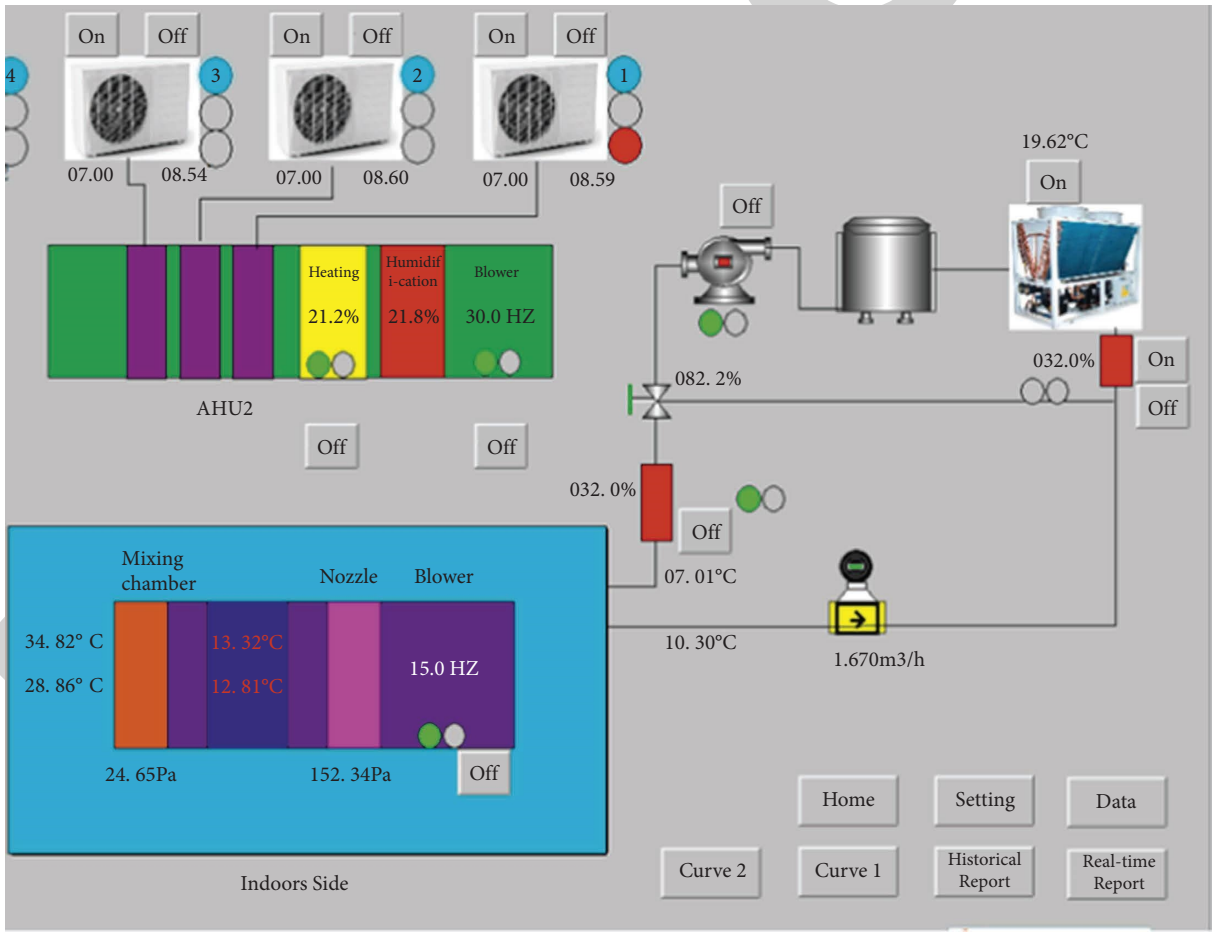

Figure 5: Control principle of the experimental system.

improving the water flow velocity can both reduce effectively the temperature and moisture content of the air outlet dry bulb and realize lower moisture content at the outlet of the finned-pipe surface air cooler under high temperature and humidity condition, namely, realizing deep dehumidification effects.

Table 1: Experimental test condition.

Parameters	Value
$t_{a,\text{in}}$/°C	34.8
$t_{\text{sa,in}}$/°C	28.9
$\omega_y/m/s$	0.5~3
$\omega_w/m/s$	0.5~1.2
$t_{w,\text{in}}$/°C	7

Table 2: Measuring parameters and instruments.

Measuring parameters	Instruments	Model	Precision	Measuring range
Temperature	Pt100 platinum thermistor	WZP-02	Level *A*	−200~420°C
Water flow rate	Electromagnetic flowmeter	AXF040G	±0.35% m^3/h	0~70 m^3/h
Air flow rate	Differential pressure gauge	EJA110A	±0.25% FS	0~1000 Pa

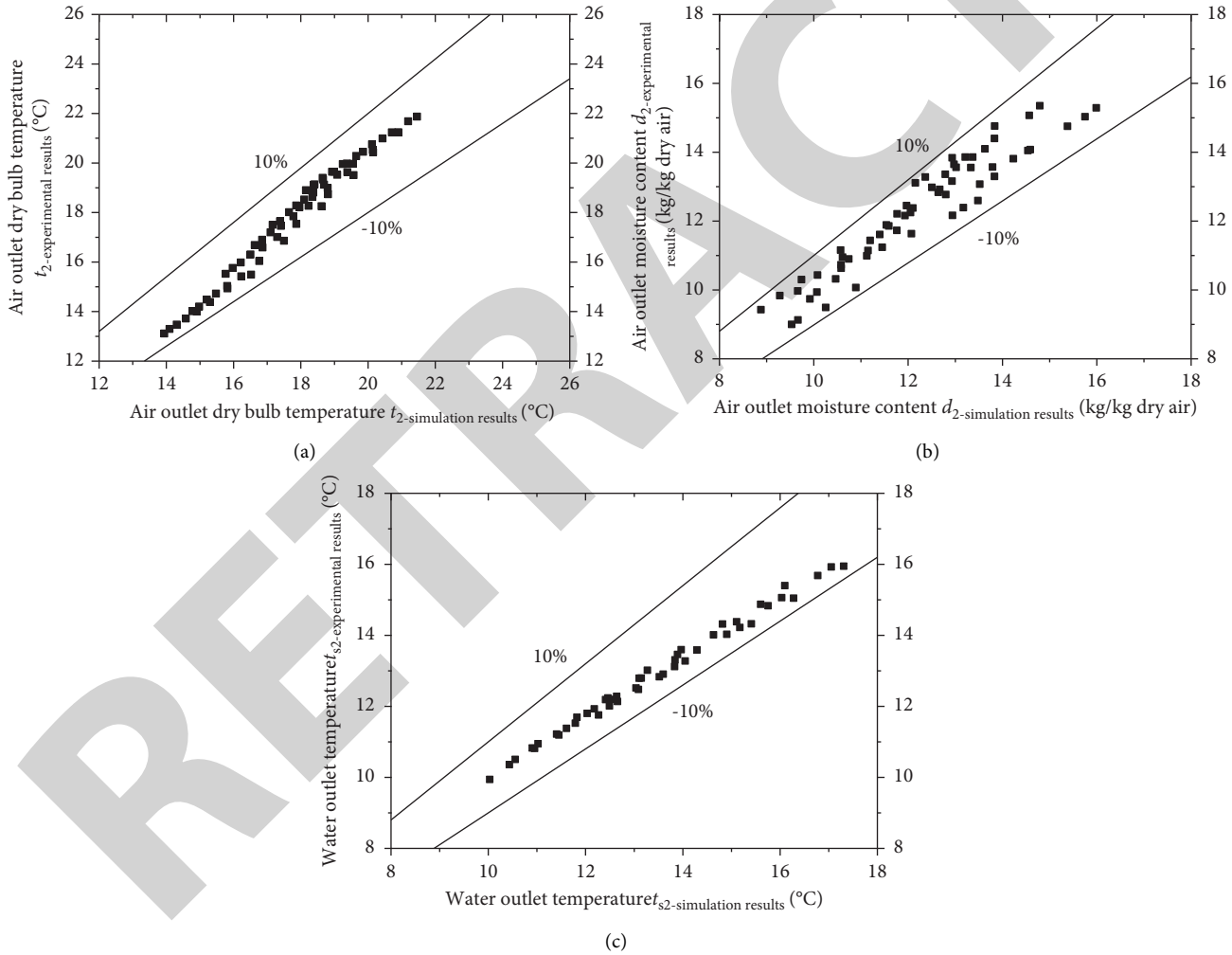

Figure 6: Comparison between experimental results and simulation results.

When the water flow velocity was kept at 1.2 m/s and the head-on wind velocity dropped from 3 m/s to 0.5 m/s, the temperature of the air outlet dry bulb dropped from 19.04°C to 10.4°C, while the air humidity ratio dropped from 13.15 g/kg to 7.45 g/kg, dropped by 43.3%. When the head-on wind velocity was kept at 1.06 m/s and the water flow velocity increased from 0.5 m/s to 1.2 m/s, the temperature of the air outlet dry bulb dropped from 15.49°C to 13.11°C, while the air humidity ratio dropped from 10.57 g/kg to 8.88 g/kg, dropped by 16%. Moreover, increasing the water flow velocity will consume more power from the water pump. In consequence, reducing the head-on wind

RETRACTED

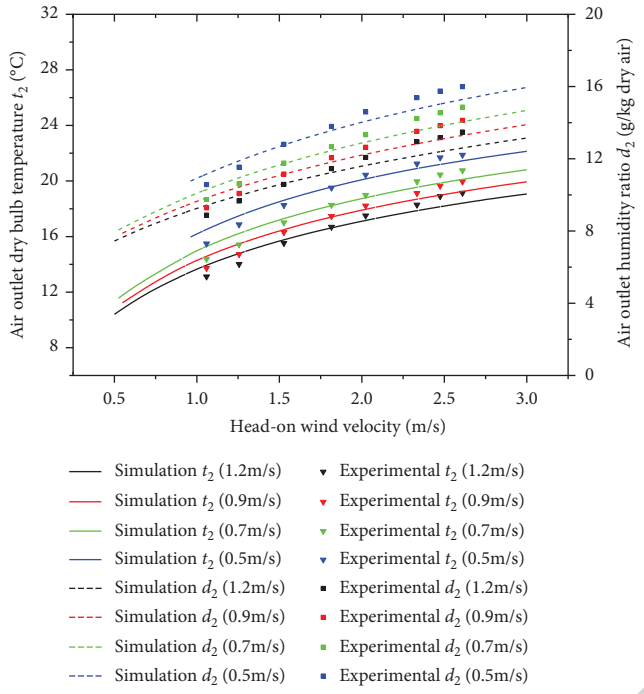

Figure 7: Effects of the head-on wind velocity and water flow velocity to air outlet parameters.

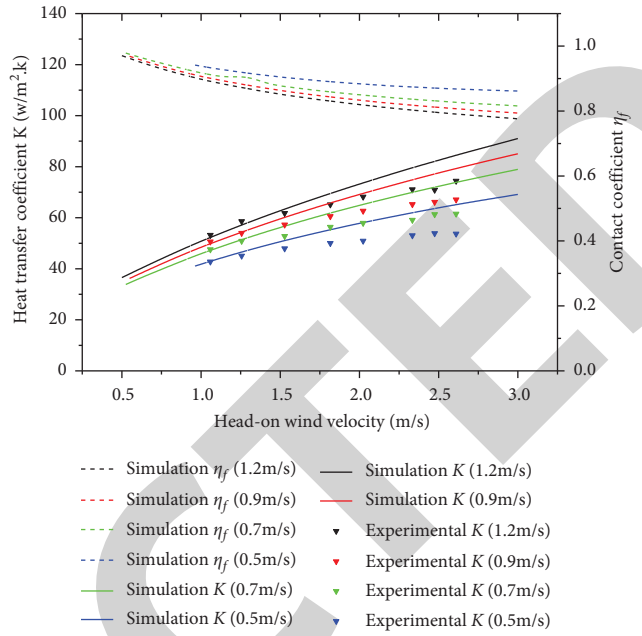

Figure 8: Effects of the head-on wind velocity and water flow velocity to heat transfer performance.

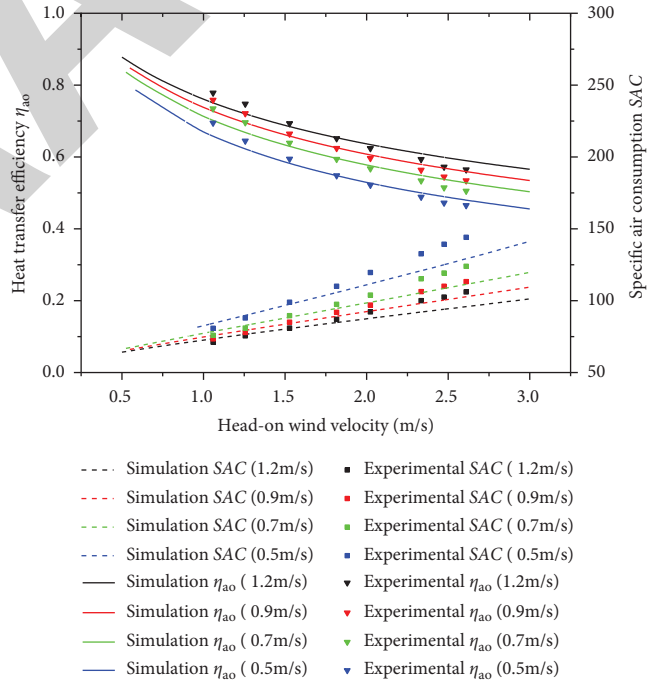

Figure 9: Effects of the head-on wind velocity and water flow velocity to heat transfer efficiency.

velocity shows more advantages in heat transfer and dehumidification.

The above analysis focuses on the influence of state parameters that explain the overall heat transfer and dehumidification effects of the surface air cooler. In addition, it is equally important to analyze the performance parameters. As shown by curves in Figure 8, when the water flow velocity was the same, the heat coefficient dropped gradually while the contact coefficient increased gradually, along with the reduction of head-on wind velocity; when the head-on wind velocity was the same, heat transfer coefficient decreased gradually while contact coefficient increased gradually along with the reduction of water flow velocity. In terms of overall effects, reducing the head-on wind velocity or water flow velocity goes against the increase of the heat transfer coefficient but helps increase the contact coefficient. Therefore, changing condition parameters could not prove whether the surface air cooler is good or not in heat transferring or dehumidifying. Moreover, this paper studied mainly the dehumidification performance of surface air coolers under high temperature and humidity conditions, which makes the mere considering of heat transfer coefficient one-sided relatively.

As shown in Figure 9, when the water flow velocity kept the same, the reduction of head-on wind velocity made the heat transfer efficiency improve significantly and *SAC* dropped gradually; when the head-on wind velocity kept the same, the increase of water flow velocity made the heat transfer efficiency and *SAC* improved slightly.

According to the above analysis, reducing the head-on wind velocity could not only realize the dehumidification effects but also improve effectively the heat transfer efficiency of surface air cooler and make the overall dehumidification and heat transfer process closer to the theoretical limit (for example, when the head-on wind velocity decreased from 2.5 m/s under standard working condition of regular surface air cooler to 1.06 m/s under conditions described in the experiment herein, η_{ao} increased by 36% and *SAC* decreased by 30.5%). Moreover, reducing the head-on wind velocity could reduce *SAC*,

RETRACTED

Table 3: Comparison of surface coolers in different applications.

Types of surface cooler application	The head-on wind speed (m/s)	Air humidity ratio after dehumidification by surface cooler (g/kg dry air)	The heat exchanger efficiency of the cooler η_{ao}
Surface cooler for chiller units used in conventional air-conditioning [3]	1.8	9.5	0.694
Surface cooler for evaporative chiller units used in hot and humid areas [5]	1.8	12.7	0.617
Surface cooler for dehumidifying high temperature and high humidity air in wastewater recovery treatment [16]	2.0	16.44	0.525
Surface air cooler in this paper	1.8	12.68	0.621
	0.5	7.45	0.867

and the reduction of *SAC* means lower airflow of surface air cooler under the same dehumidification requirements, which is beneficial to reduce energy at the air-delivery side, that is, to reduce the power consumption of the blower. Although increasing the water flow velocity could slightly promote the dehumidification and heat transfer effects and performance, such an increase resulted in higher power consumption of the water pump. Therefore, from the perspective of working condition regulation, significantly reducing the head-on wind speed is more conducive to improving the dehumidification effect of surface air coolers under high temperature and humidity conditions and reducing energy consumption.

4.3. Comparison and Analysis with Current Surface Coolers. As shown in Table 3, the final dehumidification effect of the surface cooler and the comparison of heat exchanger efficiency under different application conditions are shown. When applied to conventional working conditions, it is obvious that the surface air cooler can have both a better dehumidification effect (keeping the air humidity ratio below 10 g/kg dry air) and good heat exchanger efficiency (about 0.7) at a higher head-on wind speed. However, when the surface cooler is used in high temperature and high humidity conditions, continuing to choose the same head-on wind speed as in the conventional conditions can no longer meet better dehumidification and high efficiency, just as shown in the literature [5] and literature [16]. The research results in this paper also show that at a higher head-on wind speed (1.8 m/s), the humidity ratio of the outlet air of the surface cooler is also maintained at 12.68 g/kg dry air, and the heat exchanger efficiency is also lower (only 0.621). However, another analysis result of this paper also shows that in conditions of high temperature and humidity, the air humidity ratio after dehumidification by surface cooler can be effectively reduced by reducing the head-on wind speed, thus achieving a better dehumidification effect. At the same time, high heat exchanger efficiency can be maintained (0.867).

Therefore, by comparing with the application of existing surface coolers, it can also be concluded that reducing the head-on wind speed has a good improvement effect on the problems of poor treatment effect and low efficiency of the heat exchanger when the surface cooler is treating high temperature and high humidity air.

5. Conclusion

In this paper, the performance and efficiency of the surface cooler are investigated in detail under high temperature and high humidity conditions. By establishing the heat and mass transfer model of the surface cooler and combining it with the performance test of the surface cooler, the simulation and experimental test of the surface cooler are carried out. The influence of working condition parameters on the dehumidification performance of surface coolers under high temperature and high humidity conditions is mainly explored, and the following conclusions are reached:

(1) The heat and mass transfer model established in this paper has high accuracy (the error of predicting air temperature and humidity can be maintained within ±5%). Therefore, this model can provide a reference for the subsequent optimization design of surface coolers used in extreme working conditions such as high temperature and high humidity air treatment.

(2) Factor analysis shows that the impact of the head-on wind speed on the heat transfer and dehumidification performance of the surface cooler is greater than that of the water velocity. Therefore, in engineering applications, it is more beneficial to improve the energy efficiency of the system by regulating the head-on wind speed to meet the actual dehumidification demand.

(3) Performance analysis shows that, compared with the conventional working conditions, when the surface cooler with the same design parameters is used in high temperature and high humidity working conditions, the dehumidification effect of the surface cooler and the heat exchanger efficiency will be significantly reduced. Under this condition, the design changes of the heat exchanger to reduce the head-on wind speed can effectively improve the dehumidification effect, improve the heat exchanger efficiency, and reduce the gas consumption ratio to reduce the power consumption.

The conclusion of this paper enriches the research of surface coolers under extreme conditions of high temperature and humidity and has reference significance for the development and design of surface coolers under such conditions. However, this paper only investigated the performance and efficiency of the surface cooler. In the future,

RETRACTED

Hindawi
Journal of Robotics
Volume 2023, Article ID 9857401, 1 page
https://doi.org/10.1155/2023/9857401

Retraction

Retracted: Evaluation of the Students' Learning Status in the Foreign Language Classroom Based on Machine Vision

Journal of Robotics

Received 8 August 2023; Accepted 8 August 2023; Published 9 August 2023

Copyright © 2023 Journal of Robotics. This is an open access article distributed under the Creative Commons Attribution License, which permits unrestricted use, distribution, and reproduction in any medium, provided the original work is properly cited.

This article has been retracted by Hindawi following an investigation undertaken by the publisher [1]. This investigation has uncovered evidence of one or more of the following indicators of systematic manipulation of the publication process:

(1) Discrepancies in scope
(2) Discrepancies in the description of the research reported
(3) Discrepancies between the availability of data and the research described
(4) Inappropriate citations
(5) Incoherent, meaningless and/or irrelevant content included in the article
(6) Peer-review manipulation

The presence of these indicators undermines our confidence in the integrity of the article's content and we cannot, therefore, vouch for its reliability. Please note that this notice is intended solely to alert readers that the content of this article is unreliable. We have not investigated whether authors were aware of or involved in the systematic manipulation of the publication process.

In addition, our investigation has also shown that one or more of the following human-subject reporting requirements has not been met in this article: ethical approval by an Institutional Review Board (IRB) committee or equivalent, patient/participant consent to participate, and/or agreement to publish patient/participant details (where relevant).

Wiley and Hindawi regrets that the usual quality checks did not identify these issues before publication and have since put additional measures in place to safeguard research integrity.

We wish to credit our own Research Integrity and Research Publishing teams and anonymous and named external researchers and research integrity experts for contributing to this investigation.

The corresponding author, as the representative of all authors, has been given the opportunity to register their agreement or disagreement to this retraction. We have kept a record of any response received.

References

[1] L. Yao and Q. Qin, "Evaluation of the Students' Learning Status in the Foreign Language Classroom Based on Machine Vision," *Journal of Robotics*, vol. 2022, Article ID 6432133, 12 pages, 2022.

Hindawi
Journal of Robotics
Volume 2022, Article ID 6432133, 12 pages
https://doi.org/10.1155/2022/6432133

RETRACTED

Research Article

Evaluation of the Students' Learning Status in the Foreign Language Classroom Based on Machine Vision

Lin Yao and Qiongfang Qin

School of Foreign Languages, Guilin Tourism University, Guilin 541006, China

Correspondence should be addressed to Lin Yao; yaolin@gltu.edu.cn

Received 20 July 2022; Revised 29 August 2022; Accepted 6 September 2022; Published 27 September 2022

Academic Editor: Shahid Hussain

Copyright © 2022 Lin Yao and Qiongfang Qin. This is an open access article distributed under the Creative Commons Attribution License, which permits unrestricted use, distribution, and reproduction in any medium, provided the original work is properly cited.

In order to improve the effectiveness of the evaluation of student's learning status in foreign language classrooms, this paper applies machine vision to classroom teaching. Through an in-depth analysis of the relative motion relationship between the end marker points of classroom feature recognition and the center point of the machine vision system window, this paper first proposes an autonomous tracking motion algorithm of the machine vision system window based on the preset field of view parameters. Moreover, this paper realizes the motion function of the window to track the marker points autonomously, completes the simulation analysis through two sets of planned trajectories and two sets of master hands to collect the actual trajectories, and verifies the correctness and feasibility of the algorithm. The research study shows that the algorithm based on machine vision proposed in this paper can effectively judge the real-time state of students in the foreign language classroom.

1. Introduction

Classroom learning is one of the main forms for university students to acquire relevant professional knowledge and there is still a lot of knowledge acquired by undergraduate students through classroom learning. At the same time, classroom learning is also one of the important ways to cultivate students' thinking styles. It is the basis for other teaching links and students' self-study and it enables students to better understand and master how to learn effectively. Moreover, with the foundation of classroom learning, students can expand and extend the space for self-learning, make better use of extracurricular time for learning activities, and promote their comprehensive learning and development. Through the detection of students' classroom learning, it reflects students' absorption and implementation effect of classroom learning and their attitude towards learning and indirectly reflects the learning status of today's college students [1]. The study of undergraduate students' classroom learning status and students' self-evaluation of learning status has a certain significance for understanding the current students' learning psychology, factors affecting learning, and how to stimulate students' learning motivation and improve students' interest in learning. In addition, it has a certain inspiring effect on the current curriculum teaching reform and the cultivation of innovative talents [2]. In addition, state refers to appearance characteristics and action modality. In literature [3], the author believes that the classroom learning state refers to the sum of the physical characteristics, action behavior, and psychological activities of students in the course of classroom learning due to the combined effect of subjective and objective reasons. Professor Liu Guiqiu divides the classroom learning state of college students into pre-class study preparation state, in-class listening state, and after-class learning effect state. In literature [4], the author believes that the state of classroom learning refers to the process of listening, thinking, and teacher-student interaction in the classroom. Moreover, he believes that all aspects of preparation or preview before class, as well as learning effect and review after class, are only the learning state closely related to students' classroom learning state. The two should be distinguished. The learning state is a broader state, which includes the classroom learning state, pre-class learning, and after-class learning.

However, the classroom learning state is a state with limited conditions, which refers to the learning state in the course of listening to the class [5]. At the same time, classroom learning status cannot represent the learning status of students. This research investigates and analyzes students' classroom learning status, after-school learning status as an extension of classroom learning, the detection mechanism of classroom learning effect evaluation, and students' self-evaluation, so as to provide a reference for improving students' learning status, improving teachers' teaching quality, and promoting the improvement of school teaching level [6].

With the support of a series of emerging technologies such as smart classrooms, online learning platforms, and "artificial intelligence + education", learning methods have shown diverse characteristics. Traditional face-to-face teaching methods are constantly being challenged, and online teaching methods that span spaces have become a new wave. Online learning realizes the push of educational and teaching resources through Internet technology, breaking the limitations of time and space on learners' learning [7]. The significance of online learning is not only to create a learning method across time and space but also to enable more high-quality educational resources to be shared by the majority of learners through the Internet and to provide learners with personalized teaching services. Today, online learning has become one of the most important ways of learning and online learning status is one of the important factors affecting learners' online learning performance, and it is also a problem that education researchers cannot ignore [8]. Through the use of analysis and evaluation technology, it is of great significance to objectively evaluate the learning status of online learners for improving teaching quality and learning efficiency. Therefore, more and more educational researchers are paying more and more attention to online learning status and its related evaluation research. The learning state is the sum of the attention state, emotional state, motivational state, and so on shown by the learner in the learning process and learning results [9]. The complexity of the learner's learning state determines that the researcher cannot only evaluate it based on a single index but must be based on the whole and use the multi-index comprehensive evaluation method to make an overall evaluation and comparison, in order to conduct a more comprehensive evaluation [10]. Radar chart has been successfully applied in many fields such as financial performance evaluation, power quality evaluation, enterprise competitive advantage evaluation, teaching informatization evaluation, and teacher classroom teaching quality evaluation due to its simplicity and intuitiveness and the ability to compare multiple index variables at the same time [11].

Learning is the active construction of knowledge by learners. Learning status refers to the physical and psychological functional status of students in the learning situation, mainly including the status of brain wakefulness and concentration, emotional status, and physical function status. [9]. The strength of the online learning state is directly related to the quality of the learner's learning effect. Online learning is different from traditional learning methods. It breaks the constraints of time and space, and teachers and students are separated from each other. Therefore, the evaluation method of online learning must be different from the evaluation method for traditional teaching methods. The online learning state includes not only the learning preparation state before students engage in learning activities but also the learning psychological state and learning environment state of students engaged in learning activities and also includes the learning achievement state after students engage in learning activities [12]. The online learning state evaluation index system of literature [13] mainly selects the learning state of students engaged in learning activities, which can be evaluated from five indicators: attention state, human-computer interaction state, emotional state, social network state, and cognitive state. Attention is the direction and concentration of mental activities on a certain object and is a common psychological feature accompanied by psychological processes such as perception, memory, thinking, and imagination. Attention state is the measure of this direction and concentration; the computer interaction state is a measure of the degree of interaction between online learners and online learning platforms, such as login frequency, online time, and click rate. [14]; the emotional state refers to the emotional experience of learners in the learning process, such as happiness, pain, curiosity, interest, and boredom; the social network status refers specifically to learners' behaviors such as communication, discussion, interaction, and collaboration with teachers and other learners in the online learning community. For example, teacher-student interaction in the teaching process can be the data of questioning rate and feedback rate, student response rate, and active questioning rate that are analyzed [15]; and cognitive state refers specifically to the learner's understanding and mastery of knowledge and skills.

The key to optimizing the evaluation effect lies in the evaluation criteria of students' participation status, and all the value judgments made by teachers need to be carried out according to this. The process of formulating evaluation standards also reflects the teaching philosophy of teachers. Therefore, in the process of reconstructing the dynamic evaluation standards, it is first necessary to comprehensively examine the growth of students in terms of intelligence and nonintelligence factors and the classroom status, so as to determine the specific content and design classroom participation that is consistent with multidimensional development based on core literacy. Evaluation scheme to optimize the evaluation effect [16].

In the past, the focus of teaching evaluation has always been teacher-centered. The focus of everyone's attention is how to improve the quality of teaching from the perspective of teachers. However, not enough attention has been paid to the student's participation in teaching activities and their effects. According to the modern teaching concept, the center of classroom teaching should be student-centered and everything should be for students. We not only pay attention to whether the teacher's lectures are in place but also pay attention to the learning status of students in the whole learning process. The study of the learning status is of great help for students to establish a correct learning concept,

RETRACTED

correct learning attitude, improve methods, improve learning efficiency, and avoid academic failure. As a teacher, they can also provide timely help and guidance according to the student's learning status. In addition, the advancement of this work will have a profound impact on the work of college students, teaching work, curriculum reform and even teaching management [17].

College students have different majors and different needs for English. Only the liberal arts can be divided into office English, business English, legal English, financial English, and many other categories. Professional English cannot exist as an independent language. They are specialized subjects under the English language. Different professional English must have commonalities in the English language. This requires us to stick to the basic skills of the language, master the basic grammar and vocabulary, and have a certain ability for language expression. The foundation of basic English directly affects students' learning of professional English [18].

In order to improve the effectiveness of the evaluation of student's learning status in foreign language classrooms, this paper applies machine vision to classroom teaching, evaluates students' classroom status through intelligent feature recognition, and improves the evaluation effect of students' learning status.

2. Feature Tracking of the Students' Learning Status

2.1. Automatic Window Tracking Motion Strategy for the Machine Vision System Automatic Window Tracking Motion Algorithm of the Machine Vision System Based on Preset Visual Field Parameters. The marker point at the end of classroom feature recognition must be as close to the end of the microdevice as possible, so as to ensure that the motion information of the marker point can be obtained centrally within the window of the machine vision system, and its position has a variety of options. As shown in the kinematic coordinate system of the end link of the classroom feature recognition in the figure, in the forward kinematic model of the end of the classroom feature recognition, since the wrist of the microdevice has 3 degrees of freedom, the motion trajectory curve of the origin O_{10}^{in} of the end tool coordinate system is too complicated (including 6 active degrees of freedom), which is not conducive to the extraction of key information. However, the motion trajectory curve of the origin O_8^{in} of the pitch joint coordinate system of the microdevice is relatively greatly simplified (in essence, it contains 3 useful degrees of freedom), so it is the best choice for identifying the end marker points as classroom features.

Obtaining the trajectory of the marker point O_8^{in} is mainly divided into the following steps: first, on the basis of the known pose of the coordinate system of the end tool for the recognition of two classroom features, the motion amount of each active joint is calculated through the inverse kinematics solution of the end of the classroom feature recognition, and the forward and inverse kinematics modeling of the end of the classroom feature recognition is carried out. Second, the motion amount $\theta_4^{\text{in}}, \theta_5^{\text{in}}, \theta_6^{\text{in}}, d_8^{\text{in}}$ of the first four active joints is substituted into the positive kinematics solution of the marker point, and as shown in formula (1), the pose matrix ${}_{\text{in}}\text{T}_{\text{N0}}^{8}$ of the marker points A and B at the end 1 and 2 of the classroom feature recognition in the global coordinate system can be obtained. Finally, the position vector is extracted from the positive solution of the marked point, so as to obtain the movement trajectory ${}^{\lambda}_{in}P_{N0}^{8}$ of the marked point, as shown in formula (2).

$$
\begin{aligned}
{}^{\lambda}_{in}T_{N0}^{8} &= {}^{\lambda}_{in}T_{N0}^{4} \cdot {}_{in}T_{4}^{5} \cdot {}_{in}T_{5}^{6} \cdot {}_{in}T_{6}^{7} \cdot {}_{in}T_{7}^{8} \\
&= \begin{bmatrix} {}^{\lambda}_{in}n_x & {}^{\lambda}_{in}O_x & {}^{\lambda}_{in}a_x & {}_{in}p_x \\ {}^{\lambda}_{in}n_y & {}_{in}o_y & {}_{in}a_y & {}_{in}p_y \\ {}^{\lambda}_{in}n_z & {}_{in}O_z & {}^{\lambda}_{in}a_z & {}^{\lambda}_{in}p_z \\ 0 & 0 & 0 & 1 \end{bmatrix}
\end{aligned} \tag{1}
$$

$$
{}^{\lambda}_{in}P_{N0}^{8} = \begin{bmatrix} {}^{\lambda}_{in}p_x & {}^{\lambda}_{in}p_y & {}^{\lambda}_{in}p_z \end{bmatrix}^{T}. \tag{2}
$$

When $\lambda = 1$, the position vector ${}_{in}{}^{1}P_{N0}^{8}$ represents the marker point A at the end 1 of class feature recognition. When $\lambda = 2$, the position vector ${}_{\text{in}}{}^{2}\mathbf{P}_{\text{N0}}^{8}$ represents the marker point B at the end 1 of class feature recognition. After knowing the position vector of the marker point and the center point of the end of the machine vision system, the field of view parameters can be calculated.

The window replacement of the window tracking algorithm of the machine vision system can be divided into four processes, as shown in Figure 1. (1) Initial alignment refers to controlling the origin L_{R} of the end tool of the machine vision system to move from the initial position to the initial debugging point L_{s} after the preoperative positioning of the dobby system is completed, so as to ensure that the center of the window coincides with the midpoint E of the marked points A and B. (2) Window adjustment refers to the process in which the desired teaching window is obtained by controlling the freedom of movement of the machine vision system arm and the zoom ratio of the window after the initial alignment is completed. (3) The current window means that the obtained machine vision system window is defined as the initial window after the window adjustment is completed. (4) The target window refers to the movement of the marker points A and B at the end of classroom feature recognition during the teaching operation, which will cause the change of the basic visual field parameter ξ. By establishing a tracking motion algorithm, the machine vision system arm is automatically guided to adjust the end point position, thereby ensuring the invariance of ξ and obtaining the target window. (5) The dynamic replacement process between the current window and the target window also realizes that the window of the machine vision system autonomously tracks the movement of the end marker point of classroom feature recognition and ensures the stability of the basic visual field parameter ξ. Thus, the operator's desired field of view of the window is always maintained. The autonomous tracking movement of the window is essentially a fine-tuning process of the center of the window.

RETRACTED

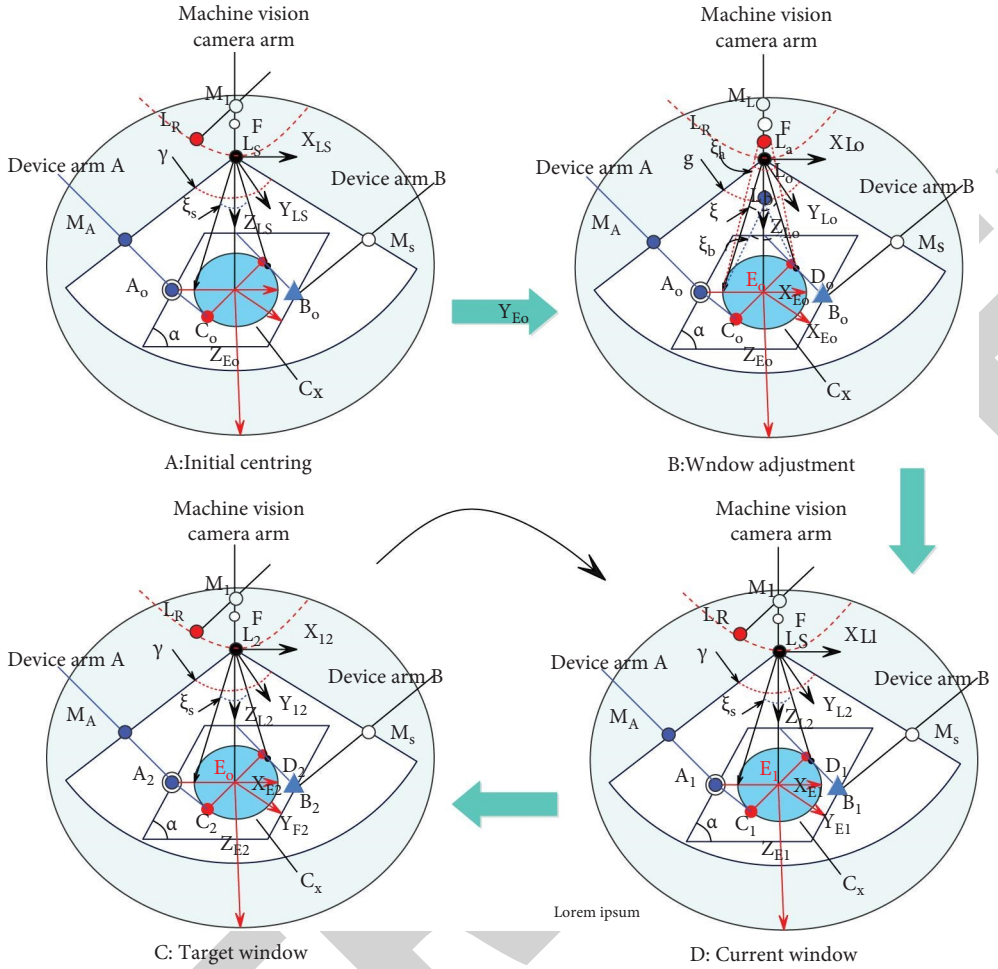

Figure 1: Schematic diagram of the window replacement process of the window tracking algorithm of the machine vision system.

As shown in Figure 1, γ is the superwide angle of view of the machine vision system, and points C_0 and D_0 are the projection points of the marked points A_0 and B_0 on the plane α, respectively. The coordinate system $x_{E_0}y_{E_0}z_{E_0}$ at point E_0 moves up along the centerline of the machine vision system, which can coincide with the visual coordinate system $x_{L_s}y_{L_s}z_{L_s}, x_{L_0}y_{L_0}z_{L_0}, x_{L_a}y_{L_a}z_{L_a}, x_{L_b}y_{L_b}z_{L_b}$ of the window, and the plane α coincides with the coordinate system plane $x_{E_0}y_{E_0}$. The position vector of the marker points A_0 and B_0 in the global coordinate system $X_0Y_0Z_0$ can be calculated according to the movement trajectory of the end tool system based on the classroom characteristics and is set as follows:

$$\begin{cases} P_{A_0} = \left[x_{A_0} y_{A_0} z_{A_0} \right]^T, \\ P_{B_0} = \left[x_{B_0} y_{B_0} z_{B_0} \right]^T. \end{cases} \tag{3}$$

It can be known that the position vector of the point E_0 is as follows:

$$P_{E_0} = \frac{1}{2}\left(P_{A_0} + P_{B_0}\right). \tag{4}$$

From the initial positioning information and the forward kinematics of the machine vision system, it can be known that the position vectors of the telecentric fixed point M_L and the endpoint L_R of the machine vision system are as follows:

$$\begin{cases} P_{M_L} = \left[x_{M_L} y_{M_L} z_{M_L} \right]^T, \\ P_{L_R} = \left[x_{L_R} y_{L_R} z_{L_R} \right]^T. \end{cases} \tag{5}$$

The expectation is $\|\overrightarrow{M_L L_R}\| = \|\overrightarrow{M_L L_s}\|$ in the initial alignment session. According to the principle of three-point collinearity, the L_s position vector can be solved by (6) and used as the desired position of the machine vision system arm, so as to complete the initial alignment adjustment.

$$\overrightarrow{M_L L_S} = \frac{\overrightarrow{M_L E_0}}{\left\|\overrightarrow{M_L E_0}\right\|} \cdot \left\|\overrightarrow{M_L L_R}\right\|. \tag{6}$$

When the position vector of the point E_0 is substituted into the inverse kinematics solution of the machine vision system arm, and the positive kinematics solution is input at the joint angle, the pose matrix of the point E_0 in the global base system $X_0Y_0Z_0$ at the end of the machine vision system can be calculated. It is set to be T_{E_0}, and its position vector and attitude matrix are P_{E_0} and R_{E_0}, respectively.

$$T_{E_0} = \begin{bmatrix} R_{E_0} P_{E_0} \\ 0_{1\times 3} 1 \end{bmatrix}. \tag{7}$$

In the formula,

$$\begin{cases} P_{E_0} = \begin{bmatrix} x_{E_0} y_{E_0} z_{E_0} \end{bmatrix}^T, \\ R_{E_0} = \begin{bmatrix} E_0 n_x E_0 o_x E_0 a_x \\ E_0 n_y E_0 o_y E_0 a_y \\ E_0 n_z E_0 o_z E_0 a_z \end{bmatrix}. \end{cases} \tag{8}$$

Then, it can be known that the position vectors of the marker points A_0 and B_0 in the window center coordinate system $x_{E_0} y_{E_0} z_{E_0}$ can be calculated by the following formula.

In the formula,

$$\begin{cases} P_{A_0}^{E_0} = \begin{bmatrix} x_{A_0}^{E_0} y_{A_0}^{E_0} z_{A_0}^{E_0} \end{bmatrix}^T, \\ P_{B_0}^{E_0} = \begin{bmatrix} x_{B_0}^{E_0} y_{B_0}^{E_0} z_{B_0}^{E_0} \end{bmatrix}^T. \end{cases} \tag{9}$$

Obviously, the position vectors of points C_0 and D_0 in the coordinate system $x_{E_0} y_{E_0} z_{E_0}$ of the center of the viewpoint are as follows:

$$\begin{cases} P_{C_0}^{E_0} = \begin{bmatrix} x_{C_0}^{E_0} y_{C_0}^{E_0} 0 \end{bmatrix}^T, \\ P_{D_0}^{E_0} = \begin{bmatrix} x_{D_0}^{E_0} y_{D_0}^{E_0} 0 \end{bmatrix}^T. \end{cases} \tag{10}$$

The position vector of the endpoint L_0 of the machine vision system in the window adjustment in Figure 1 is as follows:

$$P_{L_0} = \begin{bmatrix} x_{L_0} y_{L_0} z_{L_0} \end{bmatrix}^T. \tag{11}$$

It can be known from the simultaneous equations (10)–(12) that in the window center coordinate system $x_{E_0} y_{E_0} z_{E_0}$, the vectors $\overrightarrow{C_0 D_0}$ and $\overrightarrow{L_0 E_0}$ are as follows:

$$\begin{cases} \overrightarrow{C_0 D_0} = P_{D_0}^{E_0} - P_{C_0}^{E_0}, \\ \overrightarrow{L_0 E_0} = P_{E_0} - P_{L_0}. \end{cases} \tag{12}$$

Then, the basic visual field parameter $\xi = \angle C_0 L_0 D_0$ of the window is as follows:

$$\xi = 2 \times \tan^{-1} \frac{1}{2} \left(\left\| \overrightarrow{C_0 D_0} \right\| / \left\| \overrightarrow{L_0 E_0} \right\| \right). \tag{13}$$

Then, the basic visual field parameter $\xi = \angle C_0 L_0 D_0$ of the window is as follows:

$$\xi = 2 \times \tan^{-1} \frac{1}{2} \left(\left\| \overrightarrow{C_0 D_0} \right\| / \left\| \overrightarrow{L_0 E_0} \right\| \right). \tag{14}$$

In the process of initial window adjustment, by adjusting the intervention length of the machine vision system along the line of sight of the machine vision system, the size of the basic field of view parameter angle can be changed. Similarly, the sizes of ξ_a and ξ_b during the adjustment process can be known as follows:

$$\begin{cases} \xi_a = \angle C_0 L_a D_0 = 2 \times \tan^{-1} \frac{1}{2} \left(\left\| \overrightarrow{C_0 D_0} \right\| / \left\| \overrightarrow{L_a E_0} \right\| \right), \\ \xi_b = \angle C_0 L_b D_0 = 2 \times \tan^{-1} \frac{1}{2} \left(\left\| \overrightarrow{C_0 D_0} \right\| / \left\| \overrightarrow{L_b E_0} \right\| \right), \\ \xi_1 = 2 \times \tan^{-1} \frac{1}{2} \left(\left\| \overrightarrow{C_1 D_1} \right\| / \left\| \overrightarrow{L_1 E_1} \right\| \right). \end{cases} \tag{15}$$

The position vectors of the target markers A_2 and B_2 in the global base system $X_0 Y_0 Z_0$ can be obtained as follows:

$$\begin{cases} P_{A_2} = \begin{bmatrix} x_{A_2} y_{A_2} y_{A_2} \end{bmatrix}^T, \\ P_{B_2} = \begin{bmatrix} x_{B_2} y_{B_2} y_{B_2} \end{bmatrix}^T. \end{cases} \tag{16}$$

The midpoint E_2 of the marked points A_2 and B_2 is as follows:

$$P_{E_2} = \frac{1}{2} \left(P_{A_2} + P_{B_2} \right) = \begin{bmatrix} x_{E_2} y_{E_2} z_{E_2} \end{bmatrix}^T. \tag{17}$$

Points C_2 and D_2 are the projection points of the marked points A_2 and B_2 in the coordinate system $x_{E_2} y_{E_2} z_{E_2}$ of the center of the window, and the plane β coincides with the plane $x_{E_2} y_{E_2}$ of the coordinate system. In the same way, the projection of the vector $\overrightarrow{C_2 D_2}$ in the coordinate system $x_{E_2} y_{E_2} z_{E_2}$ can be obtained.

$$\left\| \overrightarrow{L_2 E_2} \right\| = \frac{1}{2 \times \tan(\xi/2)} \left\| \overrightarrow{C_2 D_2} \right\|. \tag{18}$$

Combining formulas (5) and (17), it can be known that the vector $\overrightarrow{M_L E_2}$ is as follows:

$$\overrightarrow{M_L E_2} = \begin{bmatrix} \left(x_{E_2} - x_{M_L} \right) \left(y_{E_2} - y_{M_L} \right) \left(z_{E_2} - z_{M_L} \right) \end{bmatrix}^T. \tag{19}$$

Then, it can be known that the vector $\overrightarrow{L_2 E_2}$ can be obtained by the following formula:

$$\overrightarrow{L_2 E_2} = \left\| \overrightarrow{L_2 E_2} \right\| \cdot \frac{\overrightarrow{M_L E_2}}{\left\| \overrightarrow{M_L E_2} \right\|}. \tag{20}$$

It is set to as follows:

$$\overrightarrow{L_2 E_2} = \begin{bmatrix} x_{L_2 E_2} y_{L_2 E_2} z_{L_2 E_2} \end{bmatrix}^T. \tag{21}$$

Then, the target position vector of the endpoint L_2 of the machine vision system is as follows:

$$P_{L_2} = \begin{bmatrix} \left(x_{E_2} - x_{L_2 E_2} \right) \left(y_{E_2} - y_{L_2 E_2} \right) \left(z_{E_2} - z_{L_2 E_2} \right) \end{bmatrix}^T. \tag{22}$$

In Figure 1, point F is the end point of the trocar tube through which the machine vision system passes. The endpoint L of the machine vision system cannot be retracted into the trocar tube in the algorithm and point F is the retraction limit point of point L. The distance between the endpoint F of the trocar tube and the telecentric fixed point is l_F; then, the vector $\overrightarrow{M_L F}$ can be obtained by the following formula:

RETRACTED

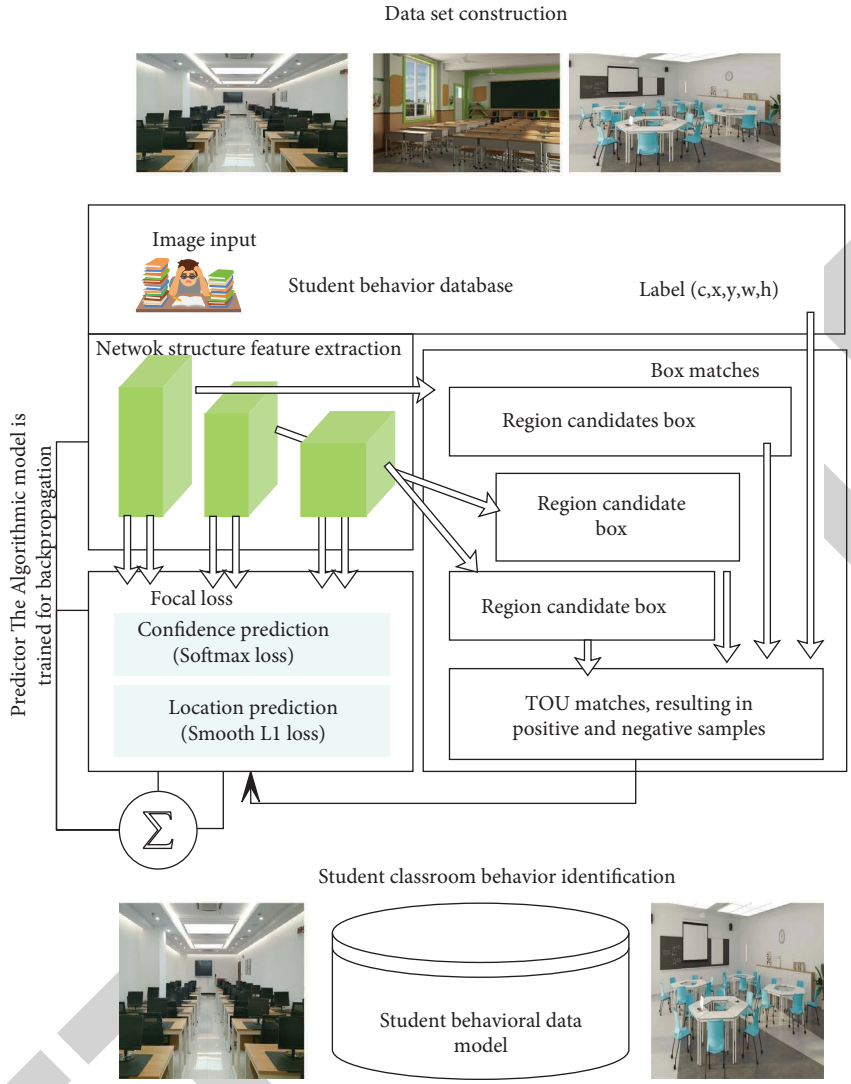

Figure 2: Student status evaluation system.

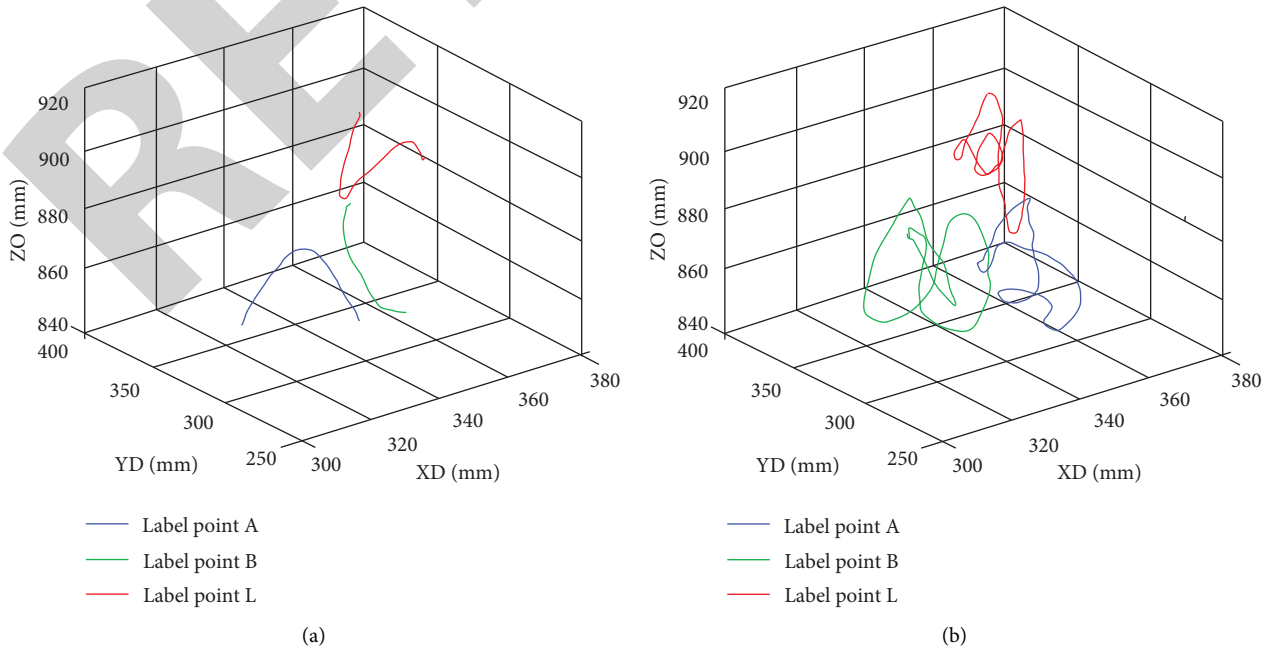

Figure 3: Marker movement track and endpoint tracking track.

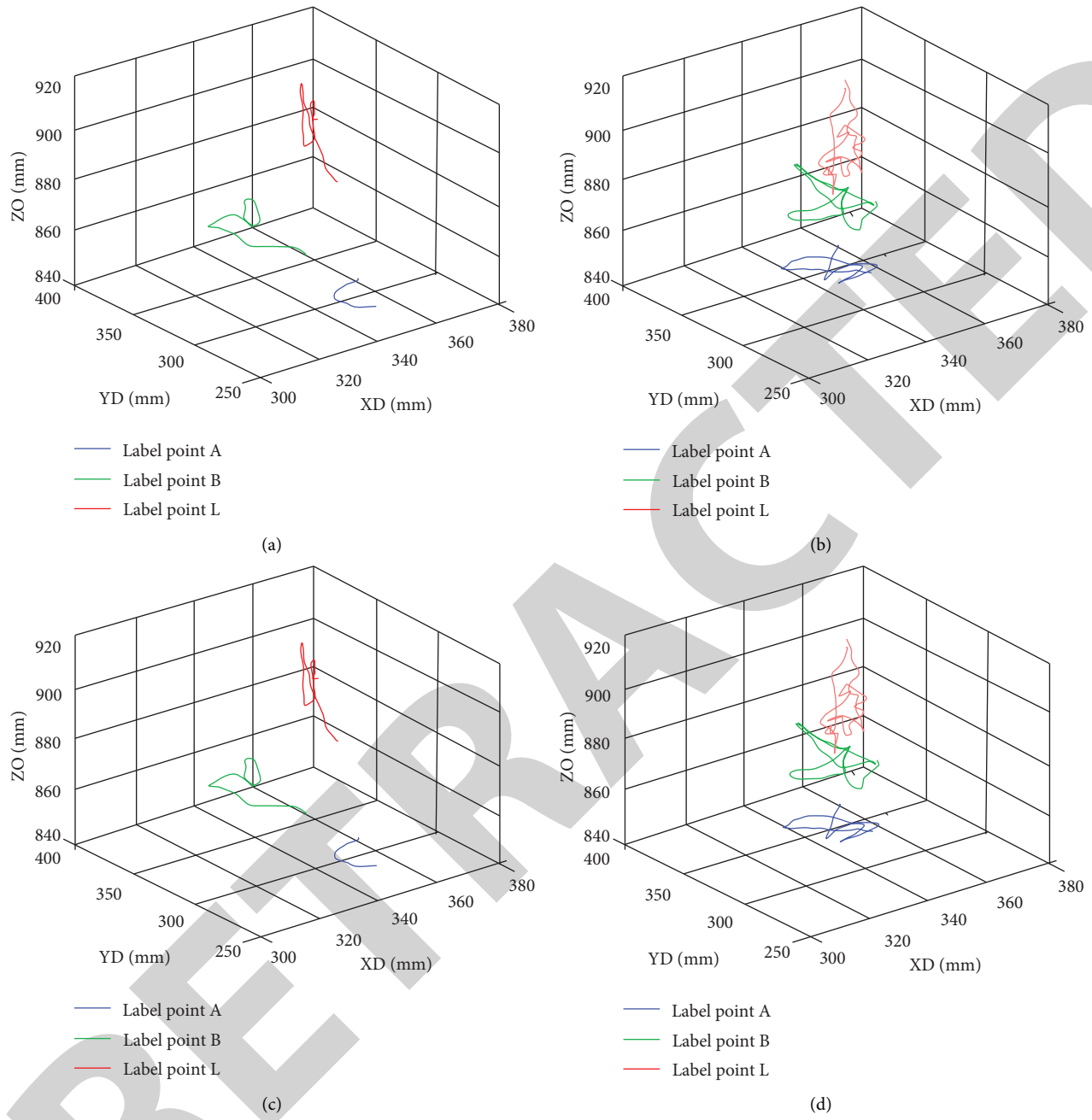

Figure 4: Marker motion trajectories obtained using the Phantom master hand and endpoint tracking trajectories based on the machine vision system.

$$\overrightarrow{M_L F} = l_F \cdot \frac{\overrightarrow{M_L E_2}}{\left\| \overrightarrow{M_L E_2} \right\|} = \left[x_{M_L F} y_{M_L F} z_{M_L F} \right]^T. \quad (23)$$

Then, the position vector of point F in the global base system is as follows:

$$P_F = \left[\left(x_{M_L} - x_{M_L F} \right) \left(y_{M_L} - y_{M_L F} \right) \left(z_{M_L} - z_{M_L F} \right) \right]^T. \quad (24)$$

The derivation process of the above formula shows that after adjusting and obtaining the basic visual field parameter ξ, the origin L of the visual coordinate system at the end of the machine vision system tracks the movement of the marker points A and B at the end of the classroom feature recognition, and ensures the stability of the ξ value at all times.

3. Student Status Evaluation System

This paper combines the intelligent student status recognition algorithm based on machine vision proposed in the second part to construct a student status evaluation system based on machine vision, and the system is shown in Figure 2.

RETRACTED

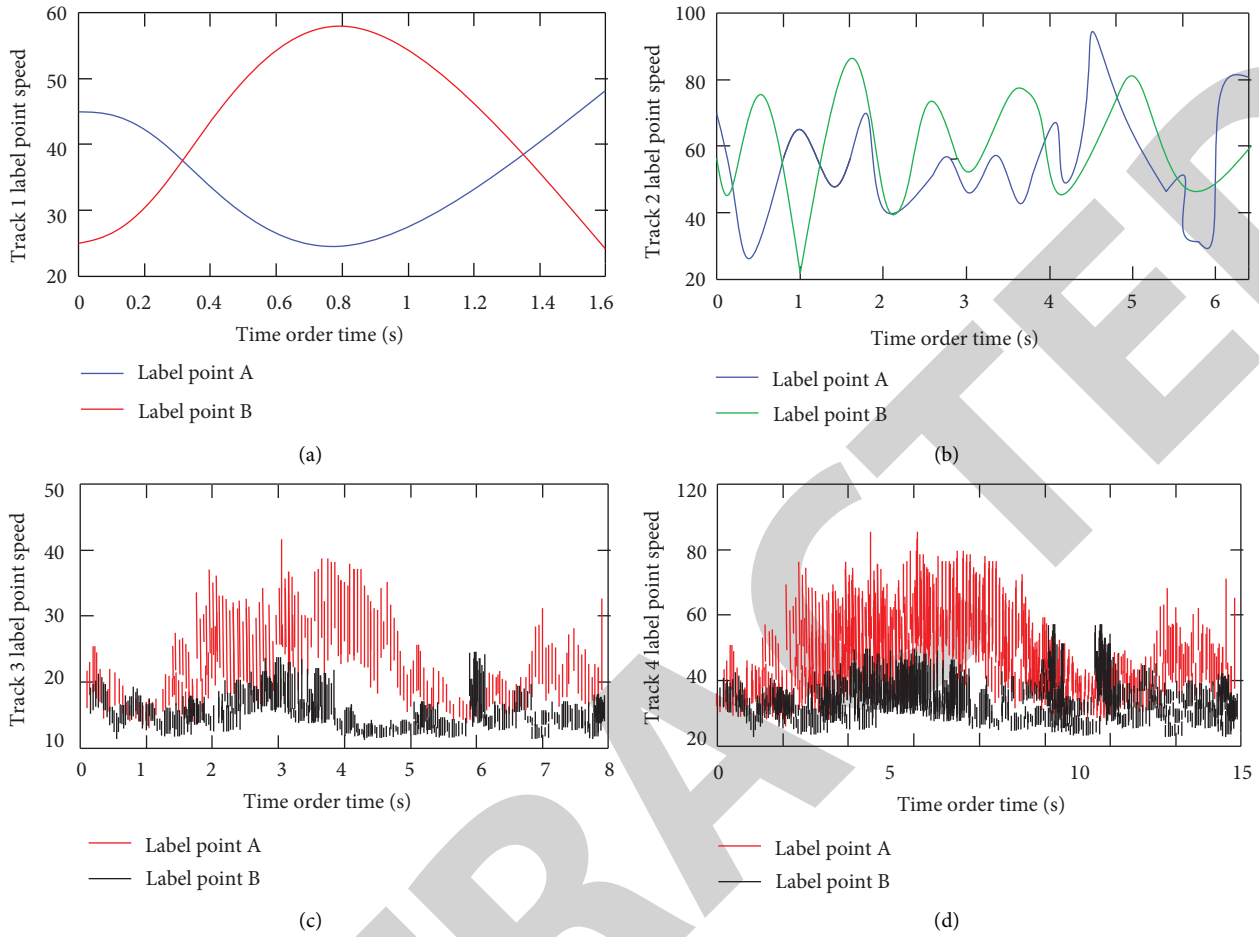

Figure 5: Movement speed of marker trajectories 1–4.

As can be seen from the figure, the realization of the recognition of student's classroom behavior includes three steps: dataset construction, algorithm model training, and student classroom behavior recognition. The first is dataset construction. Five types of behavioral states of students, such as raising hands, sleeping, answering, writing, and listening to lectures, were marked. The student behavior dataset is then trained with a substantially improved algorithm. During the training process, the input student behavior state pictures are forwarded to the SSD network for feature extraction. The candidate boxes of different prediction layers are matched with the ground-truth boxes, and the error of each candidate box category confidence prediction and position offset prediction is output. At the same time, the corresponding weights are adjusted by backpropagation of the calculated loss until the loss function drops to a small stable value, and the model training is completed. Finally, the identification of students' classroom behavior status is carried out. When the video frame to be detected is input into the smart classroom recording and broadcasting system, a series of detection frames are generated on the image frame through the trained parameter model. Through non-maximum suppression, redundant boxes are eliminated, the best position box for detecting student behavior is obtained, and the five types of student behavior states of raising hands, sleeping, answering, writing, and listening are recognized.

In order to verify the correctness of the window tracking motion algorithm of the machine vision system, within the range of the motion space of the marker point at the end of the classroom feature recognition, based on the sine and cosine function, the marker point motion trajectory 1 obtained by formula (25) is planned, which is shown in Figure 2(a), and the marker point motion trajectory 2 obtained by formula (26), which is shown in Figure 2(b).

$$\begin{cases} x_{As} = 21\ \sin(t) + 310, \\ y_{As} = 26\ \cos(t) + 290, \\ z_{AS} = 20\ \sin(2t) + 860, \end{cases} \quad \begin{cases} x_{Bs} = -25\ \cos(t) + 360, \\ y_{Bs} = 25\ \sin(t) + 300, \\ z_{Bs} = 20\ \cos(2t) + 870. \end{cases} \tag{25}$$

In the formula, the unit of position trajectory is $mm, t \in [0, \pi/2]s$, which represents the movement time of the planned trajectory, and the basic visual field parameter obtained by an adjustment is set to $\xi = 37.6583$deg.

RETRACTED

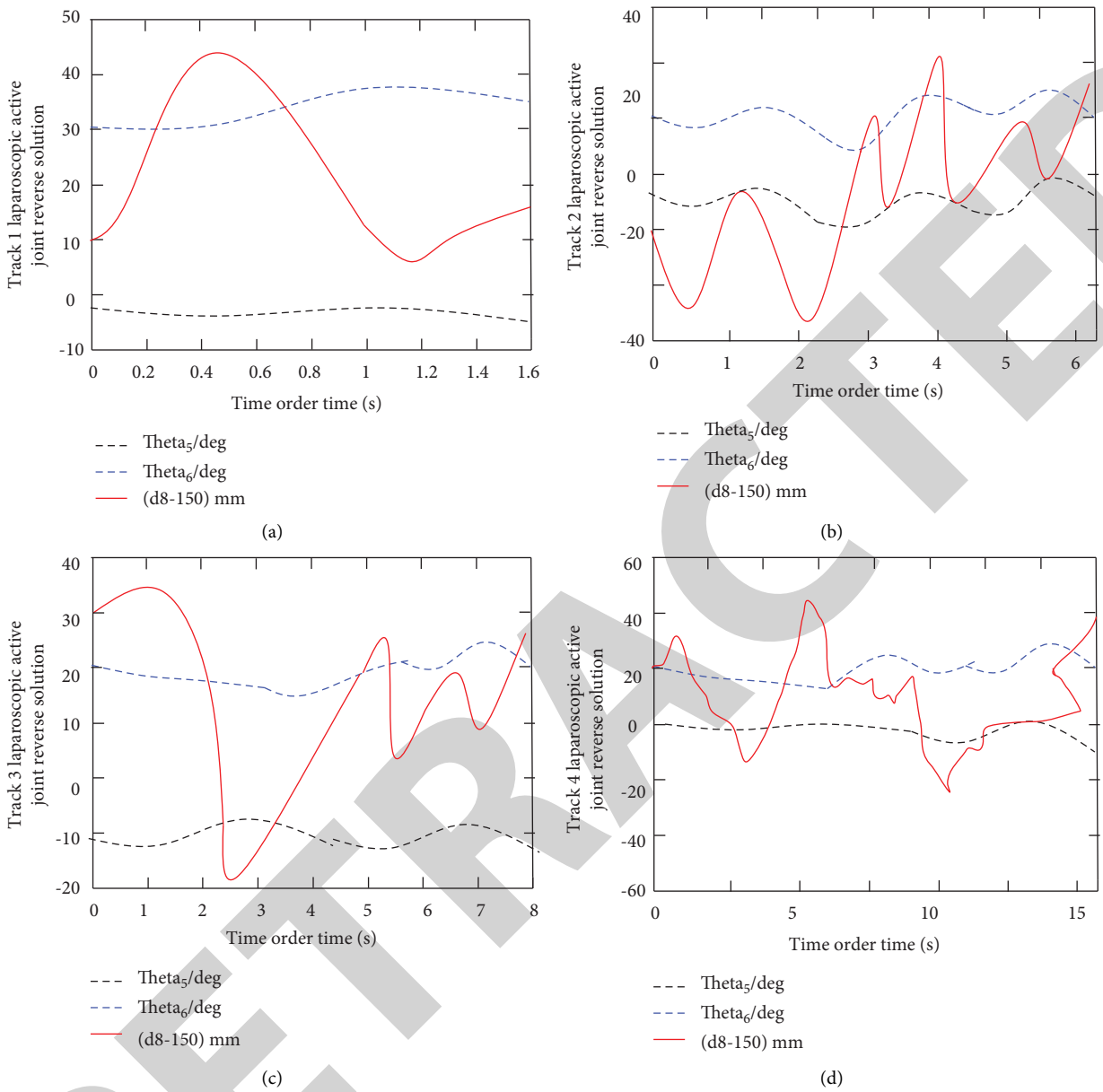

Figure 6: The result of the kinematic inverse solution of the end tracking trajectory based on the machine vision system.

$$\begin{cases} x_{Ac} = 15\ \sin(2t) + \cos(t) + 5\ \sin(5t) + 330, \\ y_{Ac} = 18\ \cos(t) + 3\ \sin(4t) + 290, \\ z_{Ac} = 10\ \sin(3t) + 13\ \cos(t) + 900, \end{cases} \quad (26)$$

$$\begin{cases} x_{Bc} = 18\ \sin(2t) + 3\ \cos(5t) + 300, \\ y_{Bc} = 17\ \cos(t) + 6\ \sin(5t) + 320, \\ z_{Bc} = 20\ \cos(3t) + 3\ \sin(t) + 900. \end{cases}$$

In the formula, the unit of the position trajectory is $mm, t \in [0, 2\pi]s$, which also represents the movement time of the planned trajectory, and the adjusted basic field of view parameter is set to $\xi = 37.6531\text{deg}$.

Using the PhantomOmni, master hand can obtain a marker trajectory that is closer to the teaching operation, and the sampling period is set to 10 ms. On the basis of compensating for the absolute base position, the 1 : 1 incremental master-slave mapping method is used to simulate the motion trajectories 3 and 4 of the marker points at the end of classroom feature recognition, as shown in Figures 3 and 4. Since the "filtering algorithm" is not used to eliminate the jitter of the master hand trajectory, there is a high-frequency noise signal of the original operation jitter in the trajectory. At the same time, it is also equivalent to adding interference noise in the simulation, which is beneficial to check the basic performance of the motion algorithm.

On the basis of the initial adjustment and setting of the basic field of view parameters ξ, the trajectory curve of the origin (endpoint L) of the visual coordinate system of the machine vision system can be calculated. The velocity curves of the movement trajectories 1–4 of the marked points A and

RETRACTED

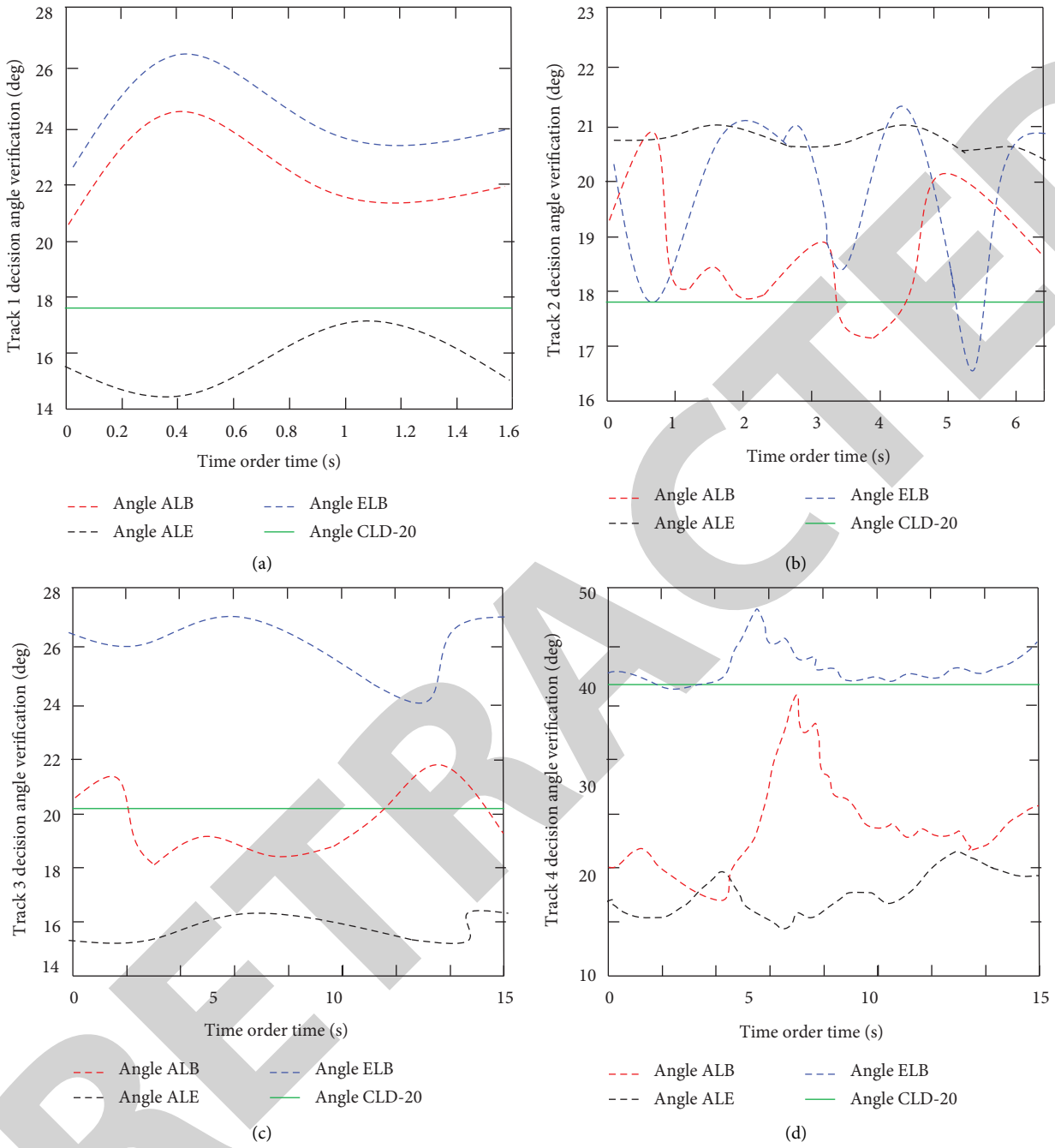

RETRACTED

Figure 7: The result of the window angle judgment condition of the end tracking trajectory based on the machine vision system.

B are shown in Figure 4. The maximum speeds of tracks 1–4 are 55 mm/s, 80 mm/s, 40 mm/s, and 110 mm/s, respectively, and the minimum speeds are 25 mm/s, 5 mm/s, 0 mm/s, and 0 mm/s, respectively. It can be seen that the mark point trajectory used in the simulation is a very difficult operation curve in actual teaching. At the same time, trajectories 3 and 4 are not filtered, and the velocity curve contains the influence of high-frequency noise, which is of great practical significance to verifying the correctness and feasibility of the window tracking algorithm.

In order to verify the correctness and feasibility of the window tracking algorithm, the simulation trajectories shown in Figures 3 and 4 need to meet two conditions. (1) The end-tracking trajectory of the machine vision system is used as the expected motion curve, and the kinematic inverse solution of the arm of the machine vision system is input, and the obtained motion amount $\theta_5^{la}, \theta_6^{la}, d_8^{la}$ of the active joint must be within the joint motion range, that is, the "kinematic inverse solution judgment condition" is satisfied. (2) The geometric relationship between the marker point A, B and the tracking point L in the target window as shown in Figure 1 must meet the following window angle determination conditions: the ultrawide angle of the 3D machine vision system with a viewing angle of 0° is $\gamma =$

Table 1: The evaluation effect of the system on the students' learning status in foreign language classrooms.

Number	Recognition effect	Number	Recognition effect	Number	Recognition effect
1	87.77	18	84.51	35	86.01
2	88.03	19	89.44	36	87.85
3	88.14	20	84.69	37	84.01
4	84.71	21	91.09	38	85.20
5	85.24	22	88.52	39	84.27
6	90.67	23	91.47	40	91.22
7	87.94	24	87.65	41	87.26
8	91.82	25	84.56	42	90.69
9	88.79	26	86.42	43	91.79
10	89.17	27	91.13	44	84.87
11	86.69	28	91.80	45	88.24
12	84.04	29	88.06	46	88.39
13	87.33	30	86.77	47	86.87
14	85.77	31	90.95	48	88.96
15	89.96	32	85.99	49	86.63
16	91.16	33	85.92	50	90.77
17	87.24	34	91.62	51	86.38

110deg, $\angle A_2L_2B_2 < \gamma$, $\angle A_2L_2E_2 < 0.5\gamma$, $\angle E_2L_2B_2 < 0.5\gamma$, $\angle A_2L_2B_2 < 90$deg, $\angle A_2L_2E_2 < 45$deg, $\angle E_2L_2B_2 < 45$deg, and the basic field of view parameter $\xi = \angle C_2L_2D_2$ remains the same as the initial adjustment setting value. The movement speed of the marker point trajectory 1–4 is shown in Figure 5.

Figures 6 and 7 show the verification results of the simulation trajectories 1–4 applying the kinematic inverse solution judgment conditions and the window angle judgment conditions. It can be seen that the inverse solutions of the active joints of the arm of the machine vision system are all within the motion range, and the window angle value and basic field of view parameters both meet the judgment conditions, thus verifying the correctness and feasibility of the window tracking motion algorithm.

The abovementioned research study verifies that the algorithm based on machine vision proposed in this paper can have a good application foundation in the evaluation of students' status in foreign language classrooms. On this basis, through multiple sets of simulation experiments, this paper explores the accuracy of the student state evaluation system based on machine vision. The results of the student learning status evaluation shown in Table 1 are obtained.

From the abovementioned research, it can be seen that the algorithm based on machine vision proposed in this paper can effectively judge the real-time status of students in the classroom and has an important auxiliary role for teachers to make teaching plans in a timely manner.

4. Conclusion

In the foreign language classroom teaching environment, the recognition of students' facial expressions is helpful to know the students' learning status in time. With the deepening of students' facial expression recognition research, more and more researchers realize that high-quality facial expression database plays an important role in training effective recognition models and accurately understanding students' learning behaviors and states. So far, scholars at home and abroad have established many databases related to student expressions, but their construction standards and methods are not uniform. In addition, expression classification, as the core problem of expression recognition and the primary task of building an expression library, has not been well solved. In order to improve the effectiveness of the evaluation of student's learning status in foreign language classrooms, this paper applies machine vision to classroom teaching and evaluates students' classroom status through intelligent feature recognition. The research results show that the algorithm based on machine vision proposed in this paper can effectively judge the real-time status of students in the classroom.

Data Availability

The labeled dataset used to support the findings of this study is available from the corresponding author upon request.

Conflicts of Interest

The authors declare that they have no conflicts of interest.

Acknowledgments

This work was supported by Guilin Tourism University.

References

[1] L. YanRu, "An artificial intelligence and machine vision-based evaluation of physical education teaching," *Journal of Intelligent and Fuzzy Systems*, vol. 40, no. 2, pp. 3559–3569, 2021.

[2] H. Li, J. Yin, M. Yin et al., "Automatic diagnosis of strawberry water stress status based on machine vision," *International Journal of Agricultural and Biological Engineering*, vol. 12, no. 1, pp. 159–164, 2019.

[3] P. Ong, W. K. Lee, and R. J. H. Lau, "Tool condition monitoring in CNC end milling using wavelet neural network based on machine vision," *International Journal of Advanced Manufacturing Technology*, vol. 104, no. 1, pp. 1369–1379, 2019.

RETRACTED

Hindawi
Journal of Robotics
Volume 2024, Article ID 9863834, 1 page
https://doi.org/10.1155/2024/9863834

Retraction

Retracted: Optimization of Intelligent Distribution of Distribution Network in the Presence of Distributed Sources

Journal of Robotics

Received 23 January 2024; Accepted 23 January 2024; Published 24 January 2024

Copyright © 2024 Journal of Robotics. This is an open access article distributed under the Creative Commons Attribution License, which permits unrestricted use, distribution, and reproduction in any medium, provided the original work is properly cited.

This article has been retracted by Hindawi following an investigation undertaken by the publisher [1]. This investigation has uncovered evidence of one or more of the following indicators of systematic manipulation of the publication process:

(1) Discrepancies in scope
(2) Discrepancies in the description of the research reported
(3) Discrepancies between the availability of data and the research described
(4) Inappropriate citations
(5) Incoherent, meaningless and/or irrelevant content included in the article
(6) Manipulated or compromised peer review

The presence of these indicators undermines our confidence in the integrity of the article's content and we cannot, therefore, vouch for its reliability. Please note that this notice is intended solely to alert readers that the content of this article is unreliable. We have not investigated whether authors were aware of or involved in the systematic manipulation of the publication process.

Wiley and Hindawi regrets that the usual quality checks did not identify these issues before publication and have since put additional measures in place to safeguard research integrity.

We wish to credit our own Research Integrity and Research Publishing teams and anonymous and named external researchers and research integrity experts for contributing to this investigation.

The corresponding author, as the representative of all authors, has been given the opportunity to register their agreement or disagreement to this retraction. We have kept a record of any response received.

References

[1] Y. Song, D. Nie, and L. Fan, "Optimization of Intelligent Distribution of Distribution Network in the Presence of Distributed Sources," *Journal of Robotics*, vol. 2022, Article ID 7063913, 11 pages, 2022.

Hindawi
Journal of Robotics
Volume 2022, Article ID 7063913, 11 pages
https://doi.org/10.1155/2022/7063913

RETRACTED

Research Article

Optimization of Intelligent Distribution of Distribution Network in the Presence of Distributed Sources

Youle Song, Ding Nie, and Litao Fan

Yunnan Power Grid Co., Ltd., Electric Power Research Institute, Kunming, Yunnan 650000, China

Correspondence should be addressed to Youle Song; 13648806353@163.com

Received 27 July 2022; Revised 29 August 2022; Accepted 30 August 2022; Published 26 September 2022

Academic Editor: Shahid Hussain

Copyright © 2022 Youle Song et al. This is an open access article distributed under the Creative Commons Attribution License, which permits unrestricted use, distribution, and reproduction in any medium, provided the original work is properly cited.

In order to improve the intelligent distribution effect of the distribution network in the presence of distributed generation, this study combines intelligent algorithms to analyze the intelligent distribution of the distribution network in the presence of distributed generation. Moreover, this study establishes an objective function composed of system network loss expectation, voltage stability index, and reactive power compensation equipment investment. In addition, this study improves the artificial bee colony algorithm through tabu search algorithm and genetic algorithm and obtains an improved TS-IABC algorithm. Finally, this study compares and tests the performance of different algorithms in the form of functions and simulations. The simulation results show that the optimal intelligent distribution method of the distribution network in the presence of distributed power generation proposed in this study has a good effect and can promote the intelligent distribution of the distribution network.

1. Introduction

At present, distributed power generation has been developed very rapidly. However, when distributed power sources are used in the distribution network, the structure of the distribution network changes accordingly. The distributed power supply connected to the distribution network can replace the traditional energy system to supply power for the distribution network, which makes the distribution network transform into a multi-power supply system and changes the power flow distribution in the distribution network. Moreover, with the development of distribution network automation technology, various optimization methods and optimization objectives have gradually become the focus of distribution network reconfiguration research. For example, the multi-objective particle swarm algorithm is used to solve the model of distribution network optimization and reconstruction [1], and the radiation network generation algorithm is used to obtain the topology structure that satisfies the radial grid constraints of the distribution network [2]. Distribution network reconfiguration usually refers to changing the operating state of tie switches and segment switches under the condition of satisfying the radial constraints of the distribution network and changing the topology of the distribution network as needed. The reconfiguration model of the distribution network can be divided into static reconfiguration and dynamic reconfiguration model. In the static reconfiguration model, the load demand and power output are assumed to be constant values, while in the dynamic reconfiguration these values are time varying [3].

Power distribution systems are usually configured in a radial fashion, but the action of opening or closing switches or protective relays can change the topology of these systems. Network reconfiguration of a distribution network refers to the concept of closing and opening connection switches without losing the radial structure of the existing distribution network [4]. The complexity of the existing distribution network is becoming more and more complex due to the gradual increase in electricity demand and changes in load. By reconfiguring the network, reducing line losses, and improving system reliability, efficient operation of the distribution network can be achieved. Due to the increased demand for electricity and the high cost of new power plants and transmission lines, the use of distributed power has attracted widespread attention. The benefits of

distributed power sources include increased reliability, improved system fault resilience, and improved voltage conditions. At present, the proportion of distributed power as a supplement to primary energy in various energy sources is gradually increasing [5]. Therefore, the problem of distribution network reconfiguration has also become the research focus of scholars at home and abroad. Literature [6] considered the randomness of wind power output, established a mathematical model with the goal of minimizing network loss and used Wasserstein distance to describe the similarity of wind power scenario models. Literature [7] considers the timing of the fan output and reduces the operating cost of the system through the dynamic reconfiguration strategy of the distribution network. Literature [8] established a model with the goal of minimizing the network loss of the distribution network and considered the uncertainty of the output of wind turbines and photovoltaics to evaluate the reconfiguration value of the distribution network in each time period. Literature [9] comprehensively considers the influence of the uncertainty of wind turbines, photovoltaics, and loads on the distribution network, first forms multiple scenarios, and then uses the EMD distance to evaluate the similarity between the scenarios to reduce the scenarios. Literature [10] considers the uncertainty between the outputs of various distributed power sources and uses a weighted hybrid two-dimensional Copula model to deal with the correlation between the two power sources of wind and solar to establish its probability joint density function to reconstruct the distribution network. Literature [11] is based on the theory that there is a strong correlation between wind speeds and solar irradiance between adjacent positions in the same wind belt and the same radiation belt in the distribution network and considers the correlation between wind speed and irradiance intensity based on Nataf transformation. It is necessary to reconstruct the distribution network with distributed power generation. Literature [12] comprehensively considered the timing of load demand in the distribution network and the uncertainty of photovoltaic output and improved the photovoltaic power consumption through the optimization and reconstruction of the distribution network. In literature [13], the new three-dimensional group search method is applied to the configuration research of distributed power generation, and the purpose of reducing the system network loss is achieved by reconfiguring the distribution network.

The basic idea of the direct algorithm is to combine the topology structure of the distribution network with the graph theory and cooperate with the fault indicator or the fault current information uploaded by the FTU to achieve an accurate fault location. The shortcomings of the direct algorithm are obvious: the actual situation of the distribution network is relatively complex, resulting in a low fault tolerance of the direct algorithm; but the advantages of the algorithm are also very prominent: the principle is simple, and it is widely used in simple distribution networks, and only needs to be used in fault location identification. It can be obtained by calculating the network description matrix and fault information matrix [14]. Literature [15] takes the distribution network feeder as the edge of the graph, and the feeder circuit breaker and the recloser as the graph nodes to form a fault information matrix and a network description matrix, and then proposes a method that can shorten the fault location identification and isolation. A new algorithm—branch-node distribution network fault location identification algorithm. In literature [16], considering the direction of the fault current, in order to realize the fault location identification of a radial network, tree network, and ring network, an improved matrix algorithm is proposed. However, this improved algorithm is only suitable for a single fault. To solve the problem of terminal faults and multiple faults on different lines, literature [17] proposes an improved matrix algorithm and proposes an executable standard to realize fault location identification. Literature [18] proposed an improved method, adding zero node numbers at the ends of radial networks and tree networks to eliminate blind spots and realize fault location identification. Literature [19] proposed an improved matrix algorithm for fault cross-sectional location in the distribution network. According to the FTU communication status or fault indication signal and the distribution network topology, the attribute matrix is constructed, and the network description matrix information is dynamically established to identify the fault location of the distribution network [20] regards the distribution network as a tree diagram and uses the adjacency matrix method to realize the processing of the graph, thereby proposing an algorithm for identifying the fault location of overheated arcs. The arc conversion method has achieved good results in the field of distribution network fault location. Literature [21] proposed a fault location determination algorithm based on topology identification, considering the location of the T node of the distribution network. The algorithm fully considers the characteristics of distribution network fault location, so it can effectively judge the fault part of distribution network, automatically determine the nodes in the area, and adapt to the changes of network structure.

This study combines the intelligent algorithm to analyze the optimization of the intelligent distribution of the distribution network in the presence of distributed power generation and improves the intelligent analysis and reconstruction effect of the distribution network.

2. Intelligent Distribution Algorithm of Distribution Network

The design of the distribution network is mostly based on closed-loop design and open-loop operation. The open-loop system has many advantages, such as a small short-circuit current, simple protection and control, easy fault diagnosis and isolation, convenient service, and a small breaking current. Before the reconfiguration of the distribution network, the topology should be transformed into a radial network structure.

In this study, network reconstruction is carried out before reactive power optimization. The basic idea is as follows: all the reconstructed network topologies are searched and numbered ([1,2,3,...,n], where n is the number of topological structures). The number of reconstructions is

RETRACTED

the same as the number of numbers, and the topology number is used as a control variable in the optimization process. Therefore, the reactive power optimization after reconstruction only adds one control variable to the original model.

This study combines the knowledge of graph theory in circuit analysis to find all the topologies after reconstruction. All switches in the distribution network are closed to form a connectivity graph, and the radial network operates as a tree in the connectivity graph, which is the same as the reconfigured distribution network. Therefore, the set of all trees in the connected graph is the set of all the results produced by the reconstruction.

If the connected graph of the n-node system has b branches, the tree set is calculated as: n nodes correspond to (n−1) tree branches, and all combinations of (n−1) branches are selected from all branches. After the combinations that cannot form a tree are deleted, what remains is all the tree sets of the connected graph.

The process of distribution network reconstruction can be carried out before reactive power optimization, and only one reconstruction can be performed for a specific network, which does not affect the speed of the model solution in the process of reactive power optimization.

Scientific and technological progress has promoted the effective use of natural resources such as solar energy and wind energy. The establishment of photovoltaic power stations and the installation of wind power generation systems have increased the grid-connected penetration rate of distributed power sources, which has brought corresponding problems while reducing power generation costs. The uncertainty of DG output is greatly affected by the environment, and the impact on the power grid cannot be underestimated. At the same time, with the progress of industrial development, new loads with fluctuating (electric arc furnace, electric welding machine, and other smelting loads) and impact (rolling mills, cranes, etc.) are generated. Its power situation is greatly affected by the load situation, and it is difficult to replace it with a certain value, and its influence cannot be ignored. Combined with the analysis and probability constraints of DG in Chapters 2 and 3, a static reactive power optimization model is established, which can be expressed as follows:

$$\begin{cases} \min f(X,\xi), \\ g(X,\xi) = 0, \\ \Pr\left(\xi_{\min} \le \xi \le \xi_{\max}\right) \ge \beta, \\ X_{\min} \le X \le X_{\max}. \end{cases} \tag{1}$$

Among them, $f(X,\xi)$ is the objective function and X is the control variable. There are discrete variables such as the topology of the distribution network system, the number of capacitor banks, and OLTC tap positions, and there are continuous variables such as static reactive power compensator (SVG) and generator terminal voltage. At the same time, $X_{\min}, X_{\max}$ are the upper and lower limits of the control variable, $\xi_{\min}, \xi_{\max}$ are the upper and lower limits of the state variable, and $\Pr(*)$ is the probability of reaching the event. β is the confidence level of the state variable and $g(X,\xi) = 0$ is the equality constraint.

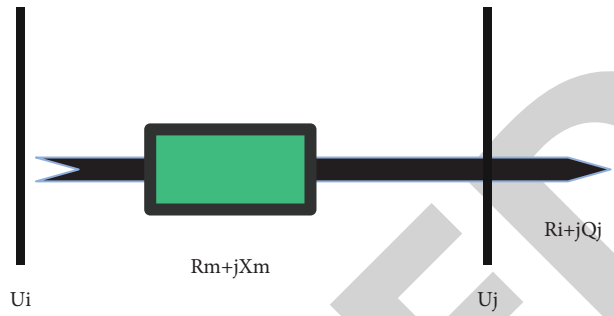

Figure 1: Equivalent circuit of distribution network.

The safety and economy of the power distribution system are considered. This study establishes a multi-objective function with the minimum static voltage stability index, the minimum expected system active power loss, and the minimum investment in reactive power compensation equipment.

2.1. Static Voltage Stability Index of Distribution Network. The magnitude of the voltage stability index reflects the voltage stability of the power system. Too high system voltage will damage electrical equipment and insulation, and too low voltage will affect the normal operation of equipment, and even cause system collapse, resulting in serious consequences.

Figure 1 shows a selected branch, the branch nodes are i and j respectively, and the flow direction is set from i to j.

Any branch has

$$\begin{cases} P_i = \dfrac{\left(P_i^2 + Q_t^2\right)R}{U_i^2} + P_j, \\ Q_i = \dfrac{\left(P_i^2 + Q_i^2\right)X}{U_i^2} + Q_j. \end{cases} \tag{2}$$

In the formula, P_i is the active and reactive power of Q_i at node i, P_j, Q_j is the active and reactive power of node j, respectively, R and X are the resistance and reactance of branch ij, respectively. If the active and reactive power of node i is taken as the independent variable, the conditions for (2) to have a real number solution are

$$\frac{4\left(XP_j - RQ_j\right)^2 + \left(XQ_j - RP_j\right)U_i^2}{U_i^4} < 1. \tag{3}$$

If the per unit value of the terminal voltage is taken as 1.0, there is

$$4\left(XP_j - RQ_j\right)^2 + XQ_j + RP_j < 1. \tag{4}$$

Therefore, the voltage stability index can be defined as follows:

RETRACTED

$$L = 4\left(XP_j - RQ_j\right)^2 + XQ_j + RP_j. \tag{5}$$

The smaller the distance between L and 1, the worse the voltage quality. The greater the distance from 1, the better the voltage quality. The closer L is to 1, the closer the system is to collapse. The maximum value of L in the system is used as the voltage stability index of the whole system, that is,

$$L_{\max} = \max\left(L_1, L_2, \ldots, L_{N-1}\right). \tag{6}$$

In the formula, N is the number of system nodes. $L_{\max}$ corresponds to the weakest branch. If the system crashes, it must happen at $L_{\max}$.

2.2. System Network Loss Expectations. The system network loss and its expectation can be expressed as follows:

$$E\left(P_{\text{loss}}\right) \approx \sum_{k=1}^{n} \sum_{m=1}^{3} P_{xk,m} P_{\text{loss}}(k,m), \tag{7}$$

$$P_{\text{Loss}} = \sum_{i=1}^{N} \sum_{j \in \Theta_i} \tau_{ij} g_{ij}\left(u_i^2 + u_j^2 - 2u_i u_j \cos\,\theta_{ij}\right). \tag{8}$$

Among them, N is the total number of system nodes, i and j are node labels, and Θ_i is the set of nodes adjacent to node i. At the same time, τ_{ij} is the on–off state of the branch ij, $\tau_{ij} = 0$ represents the open circuit, and $\tau_{ij} = 1$ represents the channel. g_{ij} is the branch admittance between nodes i and j, θ_{ij} is the phase angle difference between nodes i and j, and u_i, u_j are the voltage amplitude of the corresponding node, respectively.

(3) With the expansion of the scale of the power system and the rapid evolution of the power market, the pricing system of the electricity price has been continuously improved, which makes the pricing system of the reactive power price more reasonable and perfect. Therefore, the reactive power optimization should reasonably choose the optimization target according to the actual situation. The optimization objective of this study increases the minimum investment of reactive power compensation equipment, which can be expressed as follows:

$$\min F = \min \sum_{s \in N_c} C_{CAP_s} \left| Q_{qs} \right|. \tag{9}$$

Among them, $s \in N_C$ represents that the reactive power compensation equipment is adjusted at node s, and C_{CAPP_s} and Q_{qs} represent the unit capacity cost of the s node equipment and the actual reactive power compensation capacity at this point.

(1) Power flow constraints:

$$\begin{cases} \Delta P_i = P_{is} - \sum_{g \in i} V_i V_g\left(G_{ig} \cos\,\theta_{ig} + B_{ig} \sin\,\theta_{ig}\right) = 0, \\ \Delta Q_i = Q_{is} - \sum_{g \in i}^{N} V_i V_g\left(G_{ig} \sin\,\theta_{ig} - B_{ig} \cos\,\theta_{ig}\right) = 0. \end{cases} \tag{10}$$

In the formula, the total number of system nodes is $N; i = 1, 2, \ldots, N; G_{ig}, B_{ig}$, and θ_{ig} are the admittance and phase angle difference between nodes i and g, respectively. At the same time, $g \in i$ is the node connected to node i, V_i and V_g are the voltage amplitude of the corresponding node, P_{is} and Q_{is} are the active and reactive power injected by the corresponding node, respectively. If the power out of bounds occurs in the optimization process, the calculation is performed according to the corresponding boundary value.

(2) Inequality constraints:

$$\begin{cases} \Pr\left(V_{i,\min} \le V_i \le V_{i,\max}\right) \ge \beta, \\ Q_{SVC,i,\min} \le Q_{SVC,i} \le Q_{SVC,i,\max}, \\ T_{\min} \le T \le T_{\max}, \\ Q_{Ci,\min} \le Q_{C_i} \le Q_{C_i,\max}, \\ P_{DG,\min} \le P_{DG,i} \le P_{DG,\max}, \\ Q_{DG,\min} \le Q_{DG,i} \le Q_{DG,\max}, \\ g_k \in G. \end{cases} \tag{11}$$

In the formula, $\Pr(*)$ is the probability of event achievement, β is the confidence level of the state variable, and $V_{i,\min}$ and $V_{i,\max}$ are the minimum and maximum voltage of node i, respectively. T, $T_{\min}$, and $T_{\max}$ are the gear position and extreme value of the on-load voltage regulating transformer, respectively, and Q_{C_i} and $Q_{C_i,\min}, Q_{C_i,\max}$ are the capacity and extreme value of the capacitor installed at node i, respectively. At the same time, $P_{DG,i}, P_{DG,\min}, P_{DG,\max}$, $Q_{DG,\min}$, and $Q_{DG,\max}$ are the capacity and extreme value of the active and reactive power connected to the DG at node i, respectively, $Q_{SVC,i}, Q_{SVC,i,\min}$, and $Q_{SVC,i,\max}$ are the compensation capacity and extreme value of the SVG, respectively, and g_k and G is the topology and feasible topology set after network reconstruction, respectively.

2.3. Penalty Function of Voltage Exceeding Limit. In order to solve the situation that some node voltages do not meet the conditions, the probability constraints of node voltages are embedded into the objective function in the form of penalty functions, such as

$$V(v) = a_3 \sum_{i=1}^{N} P\left(v_i\right). \tag{12}$$

Among them, a_3 is the coefficient of the penalty function, and $P(v_i)$ can be expressed as

$$P\left(v_i\right) = \begin{cases} \beta - \Pr\left(v_{i,\min} \le v_i \le v_{i,\max}\right), \Pr\left(v_{i,\min} \le v_i \le v_{i,\max}\right) < \beta, \\ 0, \Pr\left(v_{i,\min} \le v_i \le v_{i,\max}\right) \ge \beta. \end{cases} \tag{13}$$

The Artificial Bee Colony Algorithm (ABC) stipulates that there is at most one scout bee, and the number of lead bees and observer bees is equal. There is a one-to-one relationship between the lead bee and the nectar source. If the amount of honey at the location of the nectar source is insufficient due to multiple collections, the lead bee will

RETRACTED

change its role to a scout bee, research in the neighborhood, and randomly generate a new nectar source. The transformation of the role of the bee is shown in Figure 2.

The steps to implement the artificial bee colony algorithm are

(1) The initial parameters are set. The total number of bee colonies is set to N, each nectar source searches Limit times at most, and the system circulates MCN times at most.

(2) The population is initialized. The lead bee randomly generates a new initial solution according to formula (1).

$$x_i^{'j} = x_i^j + \text{rand}\left(x_i^j - x_k^j\right). \tag{14}$$

(i) Among them, x_i^j is the solution of dimension j in nectar i, there is $i, k \in \{1, 2, \ldots, SN\}$ and $i \neq k$, $j \in \{1, 2, \ldots, D\}$. rand takes a random number between $[-1, 1]$. D is the optimization parameter, and all solutions are D-dimensional vectors.

(3) The lead bee searches the neighborhood according to formula (15) to generate a new solution.

$$x_{i,\text{new}} = x_{\min} + \text{rand}\,(0, 1)\left(x_{\max} - x_{\min}\right). \tag{15}$$

(4) The fitness function (16) is calculated, the searched new nectar source is compared with the old nectar source, and the one with a higher fitness function is selected.

The fitness function can be expressed as:

$$\text{fit}_i = \begin{cases} \dfrac{1}{1 + f\left(x_i\right)}, & f\left(x_i\right) > 0, \\ 1 + \left|f\left(x_i\right)\right|, & f\left(x_i\right) < 0. \end{cases} \tag{16}$$

(i) Among them, $f(x_i)$ is the objective function value corresponding to the solution x_i.

(5) According to formula (17), the following probability P_i is obtained:

$$P_i = \frac{\text{fit}\left(X_i\right)}{\sum_{i=1}^{N} \text{fit}\left(X_i\right)}. \tag{17}$$

(i) Among them, P_i is the probability that the nectar source i is selected by the observer bees, and $\text{fit}(X_i)$ is the fitness function value of the nectar source i.

(6) Observer bees are transformed into lead bees according to P_i to conduct spatial search and update the nectar source.

(7) If a single nectar source reaches the maximum number of searches Limit, but it is not updated, formula (8) is performed. Otherwise, it goes to formula (9).

(8) The lead bees turn into scout queens to search for new nectar sources globally and replace the old nectar sources.

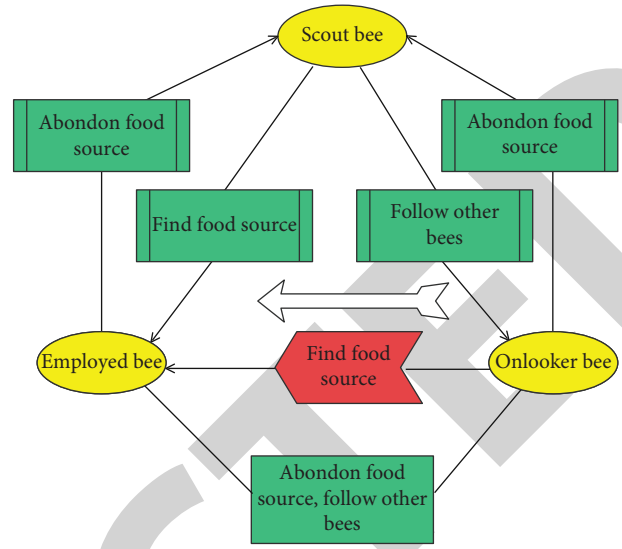

Figure 2: Mutual conversion of bee roles.

(9) The obtained optimal solution is saved.

(10) If the maximum number of cycles MCN is reached, formula (11) is entered, otherwise, it returns to formula (3). The loop of formula (11) ends. The optimal solution at this time is the global optimal solution, and the corresponding nectar source is the minimum value of the sought function. The flow chart is shown in Figure 3.

Tabu search algorithm is often used to search for the global optimum. In the algorithm, in order to achieve global optimization, a storage structure is introduced to store relevant data in the memory search process, which can provide guidance for subsequent searches. We avoid repeated searches for the same target during the search process by formulating taboo criteria. In order to ensure the diversity of the search, the contempt criterion is used to absolve the excellent individuals who are forbidden in the search process, so as to achieve global optimization. Its algorithm flowchart is shown in Figure 4.

Due to the poor search ability of the traditional artificial bee colony algorithm, Zhu and Kwong improved the traditional algorithm to improve the performance of the algorithm. The global best is added to formula (14) to form the Gbest-guided artificial bee colony algorithm (GABC). The modified expression (18) is

$$x_i^{'j} = x_i^j + \text{rand}\left(x_i^j - x_k^j\right) + \beta\left(x_{\text{Global}}^j - x_i^j\right). \tag{18}$$

The convergence speed of the algorithm is improved by $\beta(x_{\text{Global}}^j - x_i^j)$, but the global optimization ability cannot be improved. Therefore, an Improved Artificial Bee Colony Algorithm (IABC) is obtained by introducing the binomial crossover operation in the genetic algorithm. In the binomial crossover method, each component randomly generates a rand between [0, 1]. When there is $\text{rand} < cr$ (cr is the set value), the target component is accepted. Otherwise, the corresponding component of the current individual remains unchanged.

RETRACTED

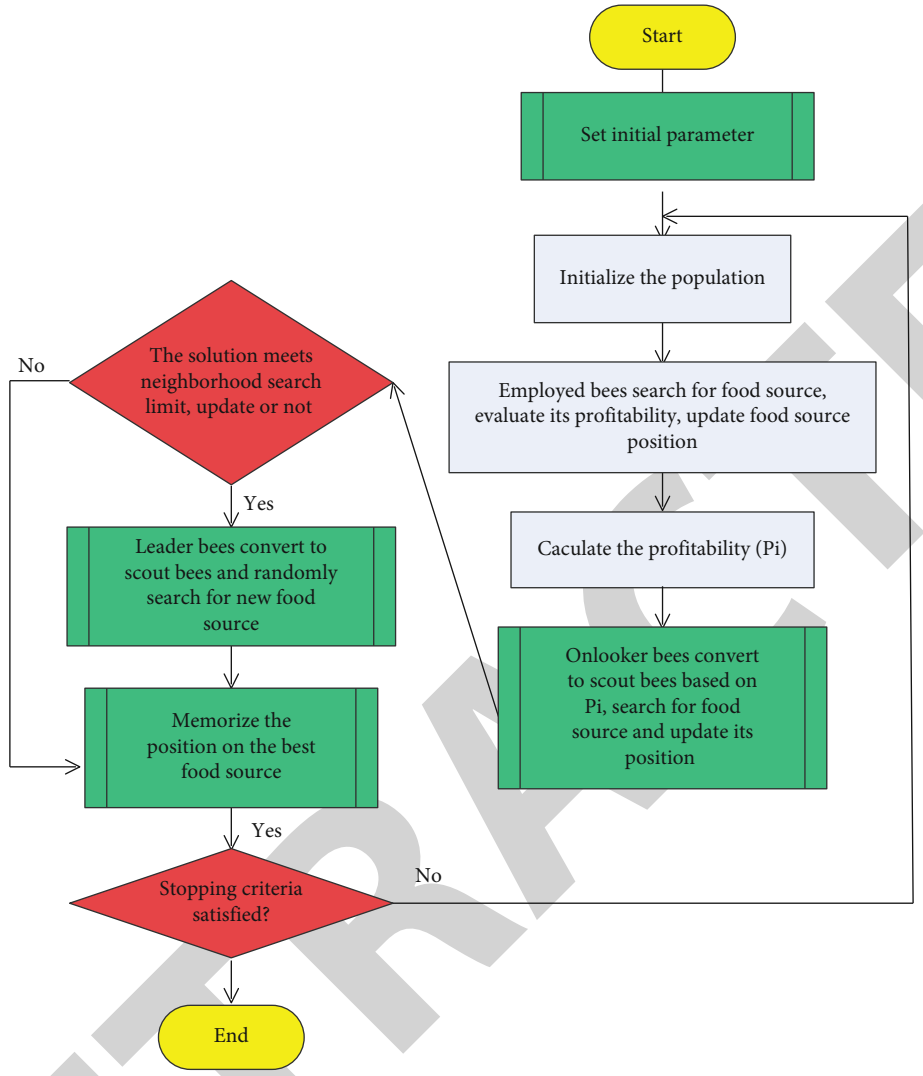

Figure 3: ABC algorithm flow chart.

$$x_{i,\text{new}}^{1j} = \begin{cases} x_i^{'j}, & \text{rand} < cr, \\ x_{\text{Global}}^{j} + \beta\left(x_{\text{Global}}^{j} - x_i^{'j}\right), & \text{rand} \geq cr. \end{cases} \quad (19)$$

By adjusting cr, the exploration ability and development ability of the algorithm can be adjusted. The experimental analysis shows that when the value of cr is about 0.6, the performance of the algorithm is better. The value of β is [−1, 1], which can effectively reduce the impact of this addition on the algorithm exploration ability.

Since the addition of the global optimal term limits the performance of the algorithm to a certain extent, the tabu table in the tabu search algorithm is added to speed up the search ability and optimization speed of the algorithm, and an improved TS-IABC algorithm based on tabu search is formed.

(1) The initial parameters are set, and the taboo table T is empty. The number of bee colonies is N, the maximum number of searches is Limit, the maximum number of iterations is MCN, and the initial solution generated by the global search is x_i ($x_i = 1, 2, \ldots, N$). The corresponding fitness function fiti can be calculated according to formula (16).

(2) The correlation data are sampled. The three-point estimation method calculates the probabilistic power flow, and the obtained fitness function value in each objective function value can be used for bee colony division. The larger fiti value is the lead bee, and the smaller fiti value is the observer bee.

(3) The lead bee performs a neighborhood search according to formula (18) and generates a new solution $x_{i,\text{new}}^{jj}$. According to the crossover operation of equation (15) and the optimal solution generated by iteration, combined with the greedy criterion, the old nectar source is abandoned, the solution with larger fiti in $x_{i,\text{new}}^{jj}$ and x_i^j is retained, and the tabu table is updated.

(4) Observer bees select nectar sources according to certain criteria, change their roles to lead bees, and search according to (3).

RETRACTED

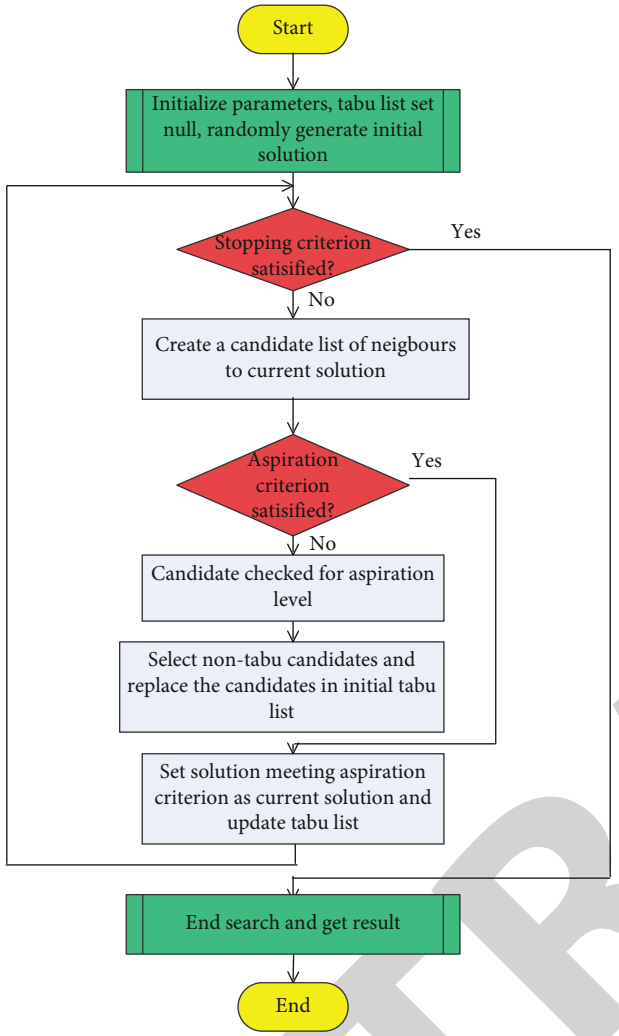

Figure 4: Flow chart of tabu search algorithm.

(5) The power flow calculation determines the local optimal solution and the global optimal solution. If no solution with higher fitness is found after reaching the number of local searches, the current solution is discarded, and it is recorded and updated to the tabu table. The lead bee or the observer bee will turn into a scout bee, generate a new solution according to equation (15), and judge whether the current solution is in the taboo list. If there is a record, the current solution is discarded and the search is repeated.

(6) One cycle is completed and the optimal solution is recorded.

(7) Whether the maximum number of iterations is satisfied is judged. If it is satisfied, the algorithm optimization ends and the result is output. Otherwise, it jumps to formula (2).

The process of improving the TS-IABC algorithm is shown in Figure 5.

Optimization problems often involve multiple optimization objectives, and multiple objectives may conflict in the optimization process, so that multiple objectives

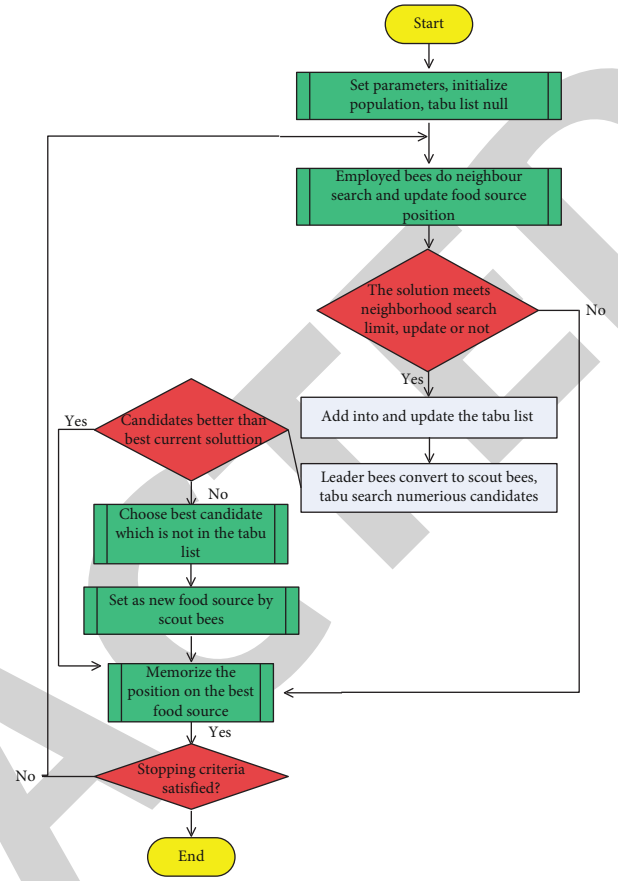

Figure 5: The process of improving the TS-IABC algorithm.

cannot be optimized at the same time. If the multi-objective is integrated and optimized through the weight coefficient, there is great unreasonableness. Therefore, this study uses the Pareto optimal theory to solve the multi-objective optimization problem of the distribution network with DG.

When multiple optimization objectives are involved at the same time, the objective function can be expressed as

$$\min F(x) = [f_1(X), f_2(X), \ldots, f_m(X)],$$
$$\text{s.t.} \quad \begin{cases} g_i(X) \le 0, & i = 1, 2, 3, \ldots, m\,(X \in S), \\ x_i^L \le x_i \le x_i^H, & i = 1, 2, \ldots, n. \end{cases} \tag{20}$$

In the formula, $X = (x_1, x_2, \ldots, x_m) \in S$ is the n-dimensional decision variable, S is the multi-objective optimization problem, and $f_m(X)$ is the mth objective function. At the same time, m is the total number of objective functions, $g_i(X)$ is the constraint condition, and x_i^L, x_i^H is the upper and lower limits of the variable x_i, respectively.

From the constraints in formula (21), we can get

$$\Omega = \left\{x | g_i(X) \le 0, \quad x_i^L \le x_i \le x_i^H\right\}. \tag{21}$$

Among them, the set Ω is the feasible region of S, and there is $\Omega \subseteq X$.

Figure 6 shows the relationship between the basic space, feasible solution set, and feasible region.

RETRACTED

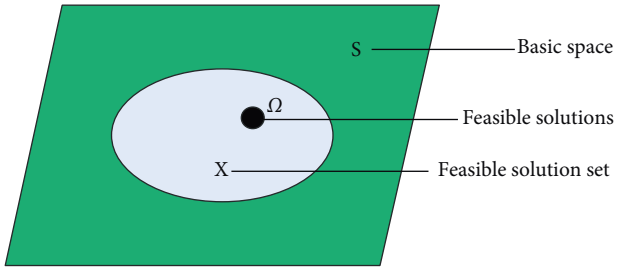

Figure 6: Relationship between basic space, feasible region, and feasible solution.

(1) *Pareto Control.* The two decision variables are X, $Y \in S$, and S is the solution space, which only satisfies

$$\begin{cases} \forall_i \in \{1, 2, \ldots, m\}, & f_i(X) \le f_i(Y), \\ \exists_i \in \{1, 2, \ldots, m\}, & f_i(X) < f_i(Y). \end{cases} \tag{22}$$

It can be said that X dominates Y, denoted as $X > Y$. At this point, X is nondominated and Y is dominated. If the conditions are not met, there is no dominance relationship.

(2) *Pareto Optimal Solution and Pareto Optimal Solution Set.* When there is $X \in S$ and there is no $X' \in S$ satisfying $X' > X$, it can be considered that the nondominant solution of S is X, and X at this time is the Pareto optimal solution. The optimal solution set contains all optimal solutions.

From the analysis of mathematical theory, the solutions contained in the optimal solution set are all optimal solutions with the same properties. If one wants to seek a set of top-level solutions in the solution set, it needs to be determined according to the preference of the decision maker.

(3) *Frontier of Pareto Optimal Solution.* Two objective functions $\min(F_1)$, $\min(F_2)$ are taken as examples, and $\{X^*\}$ is set as its Pareto nondominated solution set, then the Pareto frontier can be defined as

$$PF^* = \{F_1, F_2 | X \in \{X^*\}\}. \tag{23}$$

The essence of multi-objective optimization is to map from the search space to the target space. The optimal solution front can be considered as a subset of the target space. The optimal solution is a subset in the search space, and the optimal solutions together form a surface (line) in the search space.

The dual objective function (F_1, F_2) is taken as an example, and its Pareto frontier solution is a curve in the set, as shown in Figure 7.

The solid line and the dashed line together enclose the solution space of the two objective functions. The solid line is the Pareto frontier, the point abc, is the Pareto nondominated solution, and the points not on the Pareto frontier are the solutions dominated by the nondominated solution. If the problem involved has N objective functions, the solution space is an N-dimensional space surface.

There is only one optimal solution for a single objective function. However, each objective function in the multiobjective function has its own fitness function, and it is impossible to optimize all objective functions at the same time. Therefore, it is necessary to perform a compromise

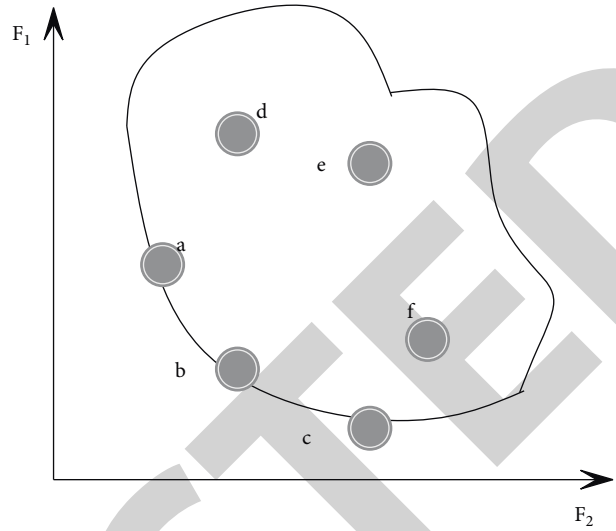

Figure 7: Pareto frontier for multiobjective optimization.

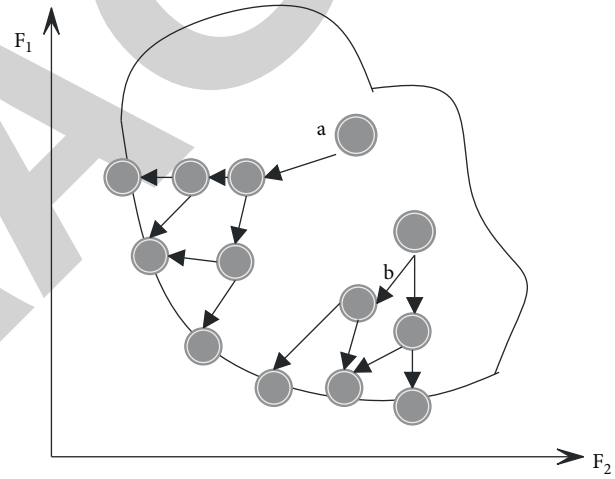

Figure 8: Population evolution direction.

process to find the optimal solution set—the Pareto optimal solution set, that is, to ensure that the population is close to the Pareto frontier, as shown in Figure 8.

3. Model Testing and Algorithm Analysis

3.1. Test Function. To test the TS-IABC algorithm, four standard functions are selected to conduct experiments to verify the algorithm's optimization ability. Table 1 presents the test functions and their associated data.

3.2. Experimental Verification and Result Analysis. In this study, TS algorithm, IABC algorithm, and TS-IABC algorithm are used to optimize the above four functions 20 times, and the function value of each optimization is recorded and the average value is calculated. Figure 9 shows a comparison diagram of the optimization effect of the algorithm.

Parameter setting: the total number of bee colonies N is 50, the maximum number of iterations MCN is 100, the maximum number of searches for a single nectar source

RETRACTED

Table 1: Test function of improved artificial bee colony algorithm.

Function	Expression	Search range	Theoretical optimal solution
f_1 (Sphere)	$f(x) = \sum_{i=1}^{2} x_i^2$	$[-5.12, 5.12]$	$f(0) = 0$
f_2 (Rosenbrock)	$f(x, y) = 100(x^2 - y^2) + (1 - x)^2$	$[-2.048, 2.048]$	$f(1, 1) = 0$
f_3 (Rastrigin)	$f(x) = \sum_{i=1}^{D} [x_i^2 - 10 \cos \cos(2\pi x_i) + 10]$	$[-5.12, 5.12]$	$f(0, 0) = 1$
f_4 (griewank)	$f(x) = (1/4000) \sum_{i=1}^{D} x_i^2 - \prod_{i=1}^{D} \cos(x_2/\sqrt{i}) + 1$	$[-100, 100]$	$f(0) = 0$

In the table, f_1 and f_2 are single-level functions, and f_3 and f_4 are multi-level functions.

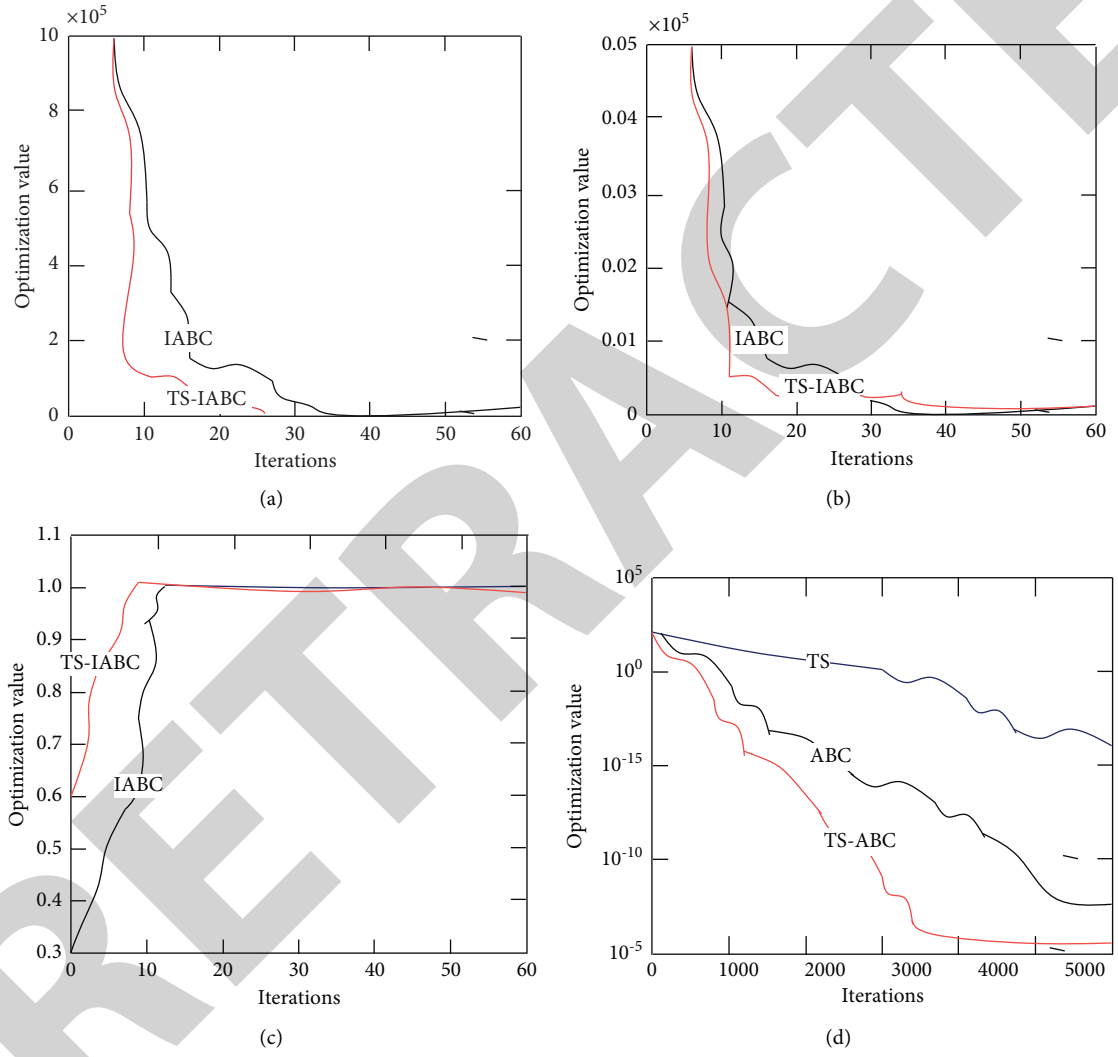

Figure 9: Optimization curve of the function. (a) Optimization curve of function f_1. (b) Optimization curve of function f_2. (c) Optimization curve of function f_3. (d) Optimization curve of the function f_4.

Limit is 30, the number of candidate solutions in the TS algorithm is Num = 80, and the number of candidate solutions in the TA-IABC algorithm is Num = 20.

It can be seen from the comparison chart of algorithm effects that compared with the other two algorithms, the improved TS-IABC algorithm has stronger search ability, faster optimization speed, higher calculation accuracy, and can better balance the local optimum and the global optimum. On the basis of the above, the optimal intelligent distribution method of the distribution network in the presence of distributed power generation proposed in this study is evaluated, and the results shown in Table 2 are obtained.

From the above research, it can be seen that the optimal intelligent distribution method of the distribution network in the presence of distributed power generation proposed in

RETRACTED

Table 2: Verification of the effect of optimal intelligent distribution method of distribution network in the presence of distributed power generation.

Num	Distribution network	Num	Distribution network
1	89.73	17	86.21
2	90.50	18	88.93
3	85.87	19	87.89
4	86.38	20	86.90
5	89.61	21	88.45
6	84.44	22	85.09
7	90.64	23	91.22
8	84.30	24	90.18
9	85.05	25	89.94
10	88.53	26	89.41
11	84.67	27	87.20
12	88.76	28	91.51
13	86.47	29	89.56
14	90.75	30	90.54
15	91.32	31	88.52
16	86.65	32	87.37

this study has good results, and can effectively promote the intelligent distribution of distribution network.

4. Conclusion

The size of the distribution network loss is mainly affected by the system power flow. With the grid-connected operation of distributed power generation, the branch power flow in the distribution network is no longer simply flowing in one direction. That is, the flow direction of the branch power flow may become very complicated, and even reverse power flow may occur, resulting in changes in the system network loss. Under normal circumstances, the access to distributed power sources will reduce the transmission energy on the transmission line, thereby reducing the loss of the distribution network. However, in fact, the increase or decrease of network loss is mainly determined by the grid connection of distributed power sources. This study combines the intelligent algorithm to carry out the optimization of intelligent distribution analysis of the distribution network based on distributed power generation, so as to improve the intelligent analysis and reconstruction effect of the distribution network. The simulation results show that the optimal intelligent distribution method of the distribution network in the presence of distributed power generation proposed in this study has a good effect and can promote the optimal intelligent distribution of the distribution network.

Data Availability

The labeled dataset used to support the findings of this study is available from the corresponding author upon request.

Conflicts of Interest

The authors declare that there are no conflicts of interest.

References

[1] J. Zhu, H. Hu, Z. He, X. Guo, and W. Pan, "A power-quality monitoring and assessment system for high-speed railways based on train-network-data center integration," *Railway Engineering Science*, vol. 29, no. 1, pp. 30–41, 2021.

[2] B. Qu, N. Li, Y. Liu, and F. E. Alsaadi, "Estimation for power quality disturbances with multiplicative noises and correlated noises: a recursive estimation approach," *International Journal of Systems Science*, vol. 51, no. 7, pp. 1200–1217, 2020.

[3] F. Xiao and Q. Ai, "Data-driven multi-hidden Markov model-based power quality disturbance prediction that incorporates weather conditions," *IEEE Transactions on Power Systems*, vol. 34, no. 1, pp. 402–412, 2019.

[4] W. Qiu, Q. Tang, J. Liu, and W. Yao, "An automatic identification framework for complex power quality disturbances based on multifusion convolutional neural network," *IEEE Transactions on Industrial Informatics*, vol. 16, no. 5, pp. 3233–3241, 2020.

[5] S. A. Kumar and D. Chandramohan, "Fault test analysis in transmission lines throughout interfering synchrophasor signals," *ICT Express*, vol. 5, no. 4, pp. 266–270, 2019.

[6] F. Z. Dekhandji, S. Talhaoui, and Y. Arkab, "Power quality detection, classification and monitoring using LABVIEW," *Algerian Journal of Signals and Systems*, vol. 4, no. 2, pp. 101–111, 2019.

[7] W. Qiu, Q. Tang, K. Zhu, W. Wang, Y. Liu, and W. Yao, "Detection of synchrophasor false data injection attack using feature interactive network," *IEEE Transactions on Smart Grid*, vol. 12, no. 1, pp. 659–670, 2021.

[8] A. Sundararajan, T. Khan, A. Moghadasi, and A. I. Sarwat, "Survey on synchrophasor data quality and cybersecurity challenges, and evaluation of their interdependencies," *Journal of Modern Power Systems and Clean Energy*, vol. 7, no. 3, pp. 449–467, 2019.

[9] A. Khair, M. Zuhaib, and M. Rihan, "Effective utilization of limited channel PMUs for islanding detection in a solar PV integrated distribution system," *Journal of the Institution of Engineers: Serie Bibliographique*, vol. 102, no. 1, pp. 75–86, 2021.

[10] M. Asadi, M. N. Harikandeh, and M. Hamzenia, "Detecting and locating power quality issues by implementing wavelet transform," *International Journal of Science and Engineering Applications*, vol. 10, no. 07, pp. 96–100, 2021.

[11] W. Wang, C. Chen, W. Yao, K. Sun, W. Qiu, and Y. Liu, "Synchrophasor data compression under disturbance conditions via cross-entropy-based singular value decomposition," *IEEE Transactions on Industrial Informatics*, vol. 17, no. 4, pp. 2716–2726, 2021.

[12] S. Vlahinić, D. Franković, B. Juriša, and Z. Zbunjak, "Back up protection scheme for high impedance faults detection in transmission systems based on synchrophasor measurements," *IEEE Transactions on Smart Grid*, vol. 12, no. 2, pp. 1736–1746, 2021.

[13] B. K. Panigrahi, A. Bhuyan, J. Shukla, P. K. Ray, and S. Pati, "A comprehensive review on intelligent islanding detection techniques for renewable energy integrated power system," *International Journal of Energy Research*, vol. 45, no. 10, pp. 14085–14116, 2021.

[14] P. K. Ganivada and P. Jena, "Frequency disturbance triggered d-axis current injection scheme for islanding detection," *IEEE Transactions on Smart Grid*, vol. 11, no. 6, pp. 4587–4603, 2020.

RETRACTED

Hindawi
Journal of Robotics
Volume 2023, Article ID 9768081, 1 page
https://doi.org/10.1155/2023/9768081

Retraction

Retracted: Feature Extraction and Analysis Method of Trombone Timbre Based on CNN Model

Journal of Robotics

Received 8 August 2023; Accepted 8 August 2023; Published 9 August 2023

Copyright © 2023 Journal of Robotics. This is an open access article distributed under the Creative Commons Attribution License, which permits unrestricted use, distribution, and reproduction in any medium, provided the original work is properly cited.

This article has been retracted by Hindawi following an investigation undertaken by the publisher [1]. This investigation has uncovered evidence of one or more of the following indicators of systematic manipulation of the publication process:

(1) Discrepancies in scope
(2) Discrepancies in the description of the research reported
(3) Discrepancies between the availability of data and the research described
(4) Inappropriate citations
(5) Incoherent, meaningless and/or irrelevant content included in the article
(6) Peer-review manipulation

The presence of these indicators undermines our confidence in the integrity of the article's content and we cannot, therefore, vouch for its reliability. Please note that this notice is intended solely to alert readers that the content of this article is unreliable. We have not investigated whether authors were aware of or involved in the systematic manipulation of the publication process.

Wiley and Hindawi regrets that the usual quality checks did not identify these issues before publication and have since put additional measures in place to safeguard research integrity.

We wish to credit our own Research Integrity and Research Publishing teams and anonymous and named external researchers and research integrity experts for contributing to this investigation.

The corresponding author, as the representative of all authors, has been given the opportunity to register their agreement or disagreement to this retraction. We have kept a record of any response received.

References

[1] Y. Wang, "Feature Extraction and Analysis Method of Trombone Timbre Based on CNN Model," *Journal of Robotics*, vol. 2022, Article ID 9460208, 12 pages, 2022.

Hindawi
Journal of Robotics
Volume 2022, Article ID 9460208, 12 pages
https://doi.org/10.1155/2022/9460208

RETRACTED

Research Article

Feature Extraction and Analysis Method of Trombone Timbre Based on CNN Model

Yanjun Wang

School of Music, Shandong College of Arts, Jinan 250014, China

Correspondence should be addressed to Yanjun Wang; z00922@sdca.edu.cn

Received 10 August 2022; Revised 30 August 2022; Accepted 13 September 2022; Published 23 September 2022

Academic Editor: Shahid Hussain

Copyright © 2022 Yanjun Wang. This is an open access article distributed under the Creative Commons Attribution License, which permits unrestricted use, distribution, and reproduction in any medium, provided the original work is properly cited.

In order to improve the accuracy of trombone timbre feature extraction, this paper combines the CNN model to construct a trombone timbre feature extraction model and summarizes the principle of trombone timbre signal. Moreover, this paper deduces the parameters of the trombone timbre signal and the corresponding network model and uses mathematical expressions to model the trombone timbre signal, which is convenient for theoretical analysis and processing of the trombone timbre signal. In addition, this paper provides a detailed discussion of time-frequency analysis techniques, including their advantages and limitations, which provide an algorithmic basis for working with trombone timbre signals. It can be seen that time-frequency analysis technology still has great advantages in trombone timbre signal processing. Finally, the simulation results show that the trombone timbre feature extraction method based on the CNN model proposed in this paper can effectively identify the trombone timbre in various musical performances.

1. Introduction

At the beginning of its invention, the trombone was divided into treble trombone, alto trombone, sub trombone, and bass trombone. However, with the continuous invention and improvement of musical instruments, the treble trombone and the alto trombone in the trombone type were gradually replaced by other instruments, and only the infratone trombone and the bass trombone remained. With the continuous development of the times, the trombone has evolved into a relatively mature musical instrument and is widely loved by many music lovers because of its unique timbre charm. Moreover, it plays an important and irreplaceable role in the performance of wind instruments [1].

Timbre refers to the feeling that sound brings to people, and it can also be understood as the quality of sound. Timbre has the function of judging the performance of musical instruments, such as the effective judgment of many factors including the smoothness, strength, and weakness, and emotion of the sound produced when the relevant musical instrument is played. The understanding of timbre can be achieved by observing the feeling of color with the naked eye, and the ear will also form a corresponding impression when hearing the sound, that is, "timbre." It should be noted that the realization of beautiful timbre cannot be judged only from a certain angle, such as the thickness and brightness of the sound, but needs to be comprehensively interpreted in combination with different scenes [2]. This is like in the painting process: the perfect painting cannot be achieved only through a single color and line, but through different colors to show the layering and artistic charm of the painting. In the trombone performance, it is necessary to use different timbres according to the different types of pieces to be played, instead of using a single timbre for performance. It is recognized as a deduction that achieves beautiful timbre [3]. For example, performing classical repertoire needs to be accompanied by a calm and vigorous tone; performing romantic music requires a bright and cheerful tone. At present, modern musical instruments also use different timbre interpretation methods in the performance process, and it is still necessary to combine the style of music for correct interpretation. Therefore, to realize the beautiful

timbre of the trombone, it must be feasible under the premise of meeting the requirements of music and understanding the concept [4].

In the performance of the trombone, the performance level and ability of the individual will have the most direct impact on the performance. Therefore, the key to whether the trombone can play a beautiful timbre depends on the performer. Although the ability to play the trombone can be acquired through a long period of hard training, it needs to be clear that the correct playing method must be mastered in order to achieve the perfect interpretation of the trombone [5]. Learning the trombone requires the use of the correct mouth shape and breath, and further study on this basis is meaningful. Under normal circumstances, the smile-pressed mouth shape will produce a relatively bright and thin tone when playing the trombone and a lack of control over the intonation and volume, resulting in a high overall tone. Especially when performing classical music or romantic music, it is especially sharp, not round enough, and difficult to coordinate with other musical instruments [6]. The use of a too concentrated mouth shape will produce a relatively dull tone, which is not bright enough and too high-pitched compared to the interpretation of the smile-pressed mouth shape. Because the mouth shape cannot be used flexibly in performance, the performance of gorgeous music or music that requires higher performance skills does not have sufficient performance expression [7]. Therefore, studies have shown that using a mouth shape that cancels each other out with a smile and tuck is by far the correct mouth shape for trombone playing. Because of its flexibility and power, it can fully meet the performance requirements of various pieces of music and can achieve a more ideal effect of trombone performance [8].

In addition to the shape of the mouth, the vibration of the lips and the speed of the airflow caused by breathing also have a major impact on the timbre. In the use of breathing in wind instruments, players often use two methods, one is chest breathing and the other is abdominal breathing. Chest breathing makes the performer easily fatigued due to too little inhalation during the performance, and it is difficult to achieve good breath regulation and strength support in the high-pitched or low-pitched part of the music [9]. Abdominal breathing mainly relies on the breath force of the abdomen to achieve performance. Although the performer can achieve positive movement to generate breath during the performance, it cannot effectively increase the inhalation value and maximize the inhalation. At present, thoracic-abdominal breathing is the most scientific playing method used in wind instrument performance, especially trombones. The muscles of breathing can not only maximize breathing but also control the breathing smoothly, without causing fatigue to the performer [10].

In order to develop the bass trombone to a greater extent in the art of playing, we must learn and master the bass trombone playing techniques. The following will focus on some of the factors that the player can control, such as how to use the mouth skills in shape, breathing method, tongue movement, pronunciation, etc., to make the bass trombone sound more perfect and harmonious [11].

The trombone is different from the keyed instrument. It does not have the flexible control of the keyed instrument, and it is also unrestrained and bold with the percussion instrument, but it can play a sound with its own personality, showing its own unique charm in performance. Moreover, the function of tongue movement is an important expression technique for trombone players. In trombone performance, we can usually hear music with a very fast rhythm. This is to use tongue movement and speed to play. Yes, we should practice a lot of tongue movement skills on the basis of mastering basic skills, such as speeding up the speed of the tongue on the premise of expressing each note neatly and clearly [12]. All in all, we can only improve in tongue movement skills after mastering the method and practicing a lot, and only through hard work can, we achieve something in basic skills. Diligently practice the basic skills and learn from the simple to the complex order, and there will be a higher level breakthrough in the performance of the trombone [13].

The lip shape of the bass trombone is very important, it is related to the sound quality and sound quality. The shape of the mouth plays an important and decisive role in the sound quality of the bass trombone. Bass trombone performance relies on the coordination of mouth shape and teeth and other organs. Mouth shape is the most basic learning stage, and bass trombone players must ensure a correct mouth shape [14]. It is necessary to practice patiently and make continuous progress because the innate conditions are different, so the ability to use and control the mouth shape is also decidedly different. We must analyze this situation based on the actual situation [15].

Whether the music is pleasing to the ear or not, the pitch plays an important decision. Pitch specifically refers to the high-pitched sound produced during singing and musical instrument performance that can match the high-pitched sound of a certain rate. Therefore, it is said that pitch determines the basic conditions for playing beautiful, pleasant, and pleasant music. There are many people in life who sing songs that feel particularly beautiful, and the real reason is the pitch [16]. As far as musical instruments are concerned, trombone and pitch have an inseparable and important relationship. Trombone mainly relies on the movement of the telescopic tube to adjust the treble, so it is not easy to correctly control the pitch issue. It takes hard work and time to do the right exercise and inquiry. And if we can usually listen to some excellent performances, it can also help us to improve the pitch [17].

This paper combines the CNN model to construct the trombone timbre feature extraction model to improve the training and learning effect of the trombone and promote the effect of the trombone in playing.

2. Trombone Timbre Frequency Communication Overview

2.1. Trombone Timbre Frequency Communication Principle and Characteristics. As shown in Figure 1, the trombone timbre frequency communication process first generates the original information data from the transmitting end and then performs the first baseband modulation through the

RETRACTED

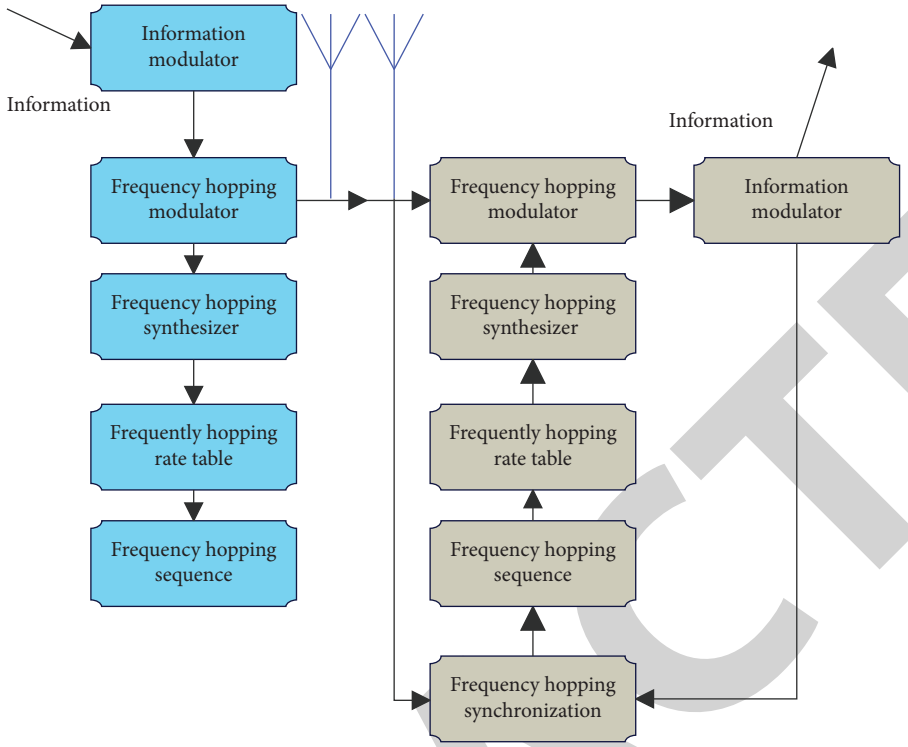

Figure 1: Block diagram of the working principle of the trombone timbre frequency communication system.

information modulator. At the same time, the trombone timbre frequency sequence is generated under the control of the pseudorandom sequence, and then the frequency hopping table is synthesized through a specific mapping relationship, so as to control the frequency synthesizer to select the local carrier according to the corresponding rules. After that, the baseband signal is multiplied by the trombone timbre frequency modulator to achieve the purpose of corresponding frequency shifting, that is, the carrier wave. Finally, the frequency band information is radiated into the air through the transmitting antenna.

According to whether the frequency hopping is the same time reference, it is divided into synchronous network and asynchronous network. According to whether the trombone timbre frequency collides at the same time, it is divided into orthogonal network and nonorthogonal network. In general, due to the asynchronous network, it is difficult to avoid the collision of trombone timbre frequencies. Therefore, the trombone timbre frequency networking methods are generally divided into three categories according to the abovementioned situation. A schematic diagram of each network model is shown in Figure 2.

2.2. Mathematical Model of Trombone Timbre Frequency Signal. The trombone timbre frequency signal is a nonstationary signal whose carrier frequency varies with time. The variation law of its carrier frequency is controlled by pseudorandom sequences, such as m-sequence, gold sequence, and so on.

The regularity of the trombone timbre frequency signal is generally observed through the time-frequency diagram. On a time-frequency diagram, the trombone timbre frequency signal appears as a line that varies in the time-frequency dimension. The time-frequency diagram of a single trombone timbre frequency signal is shown in Figure 3. The horizontal axis of the time-frequency diagram is time, and the vertical axis is frequency. Therefore, from the time-frequency diagram, parameters such as time-hopping, period-hopping, and frequency sets of the trombone timbre frequency signal can be clearly observed. We assume that M trombone timbre frequency signal segments are received at observation time T. There are K complete signal segments, the hopping period is T_h, and the carrier frequency is $f_k(k = 1, 2, \ldots, K)$. Incomplete signals are mainly the beginning and the end of the two parts. Among them, the start duration is τ_s, the carrier frequency is f_s, the end duration is τ_e, and the carrier frequency is f_e. Then, the expression for the signal throughout the observation time is given as follows:

$$s(t) = a(t) \times \left\{ \text{rect}\left(\frac{t}{\tau_s}\right)\exp\left(j2\pi f_s\right) + \sum_{k=2}^{K-1} \text{rect}\left(\frac{t-(k-1)T_h-\tau_s}{T_h}\right)\exp\left(j2\pi f_k\right) + \text{rect}\left(\frac{t-(K-1)T_h-\tau_s}{\tau_e}\right)\exp\left(j2\pi f_e\right) \right\}. \tag{1}$$

RETRACTED

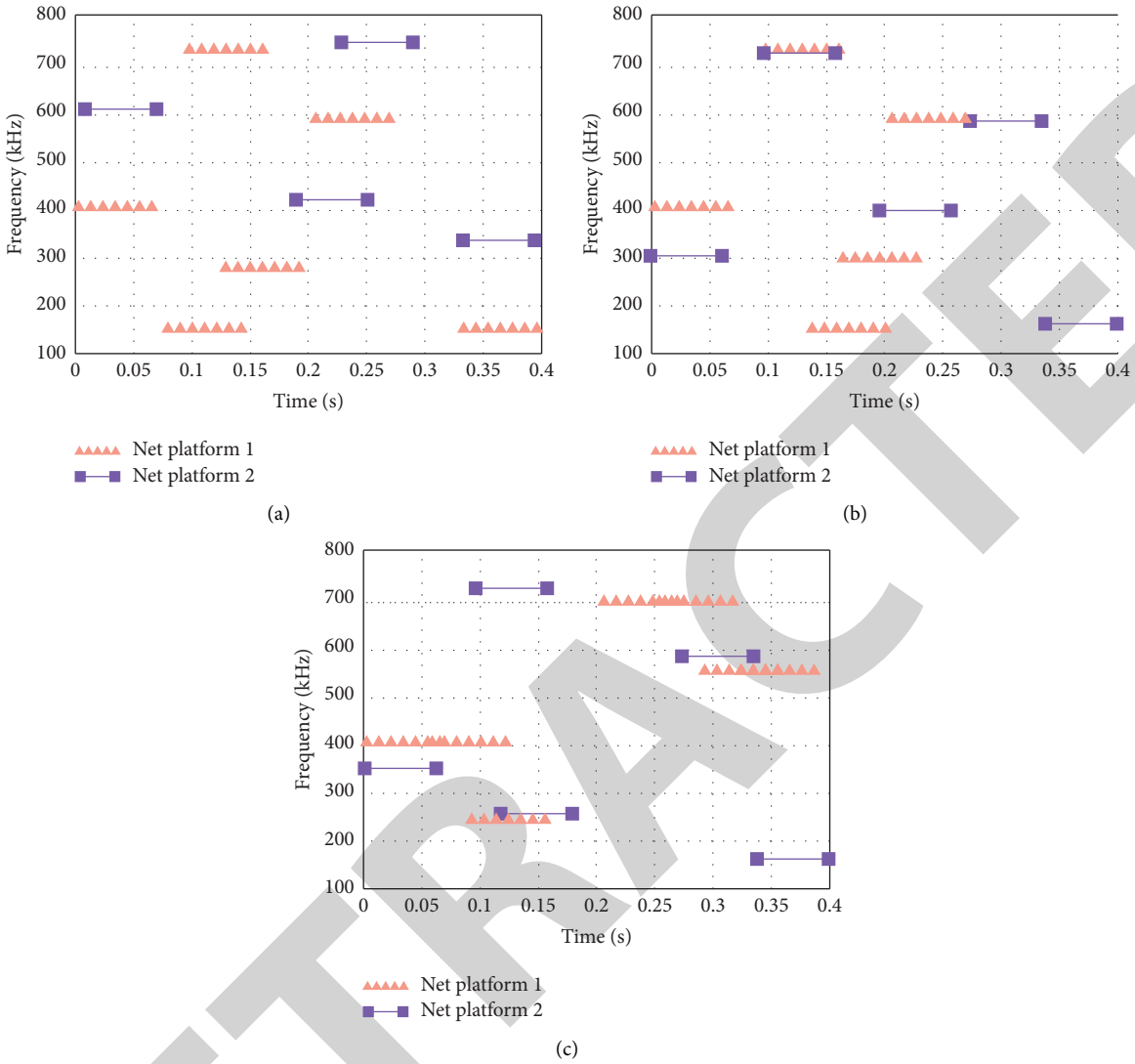

Figure 2: Three types of networking. (a) Synchronous orthogonal networking, (b) synchronous nonorthographic networking, and (c) asynchronous nonorthogonal networking.

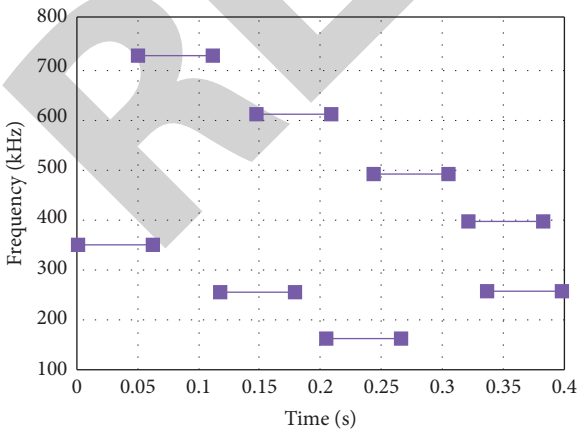

Figure 3: Schematic diagram of a single trombone timbre frequency signal.

Among them,

$$\operatorname{rect}\left(\frac{t}{T}\right) = \begin{cases} 10 < t \le T, \\ 0 \text{ others}, \end{cases} \tag{2}$$

where $a(t)$ represents the complex envelope of the observed trombone timbre frequency signal.

The signal received in the real communication environment is not only a single trombone timbre frequency signal but is usually mixed with other trombone timbre frequency signals, as well as interference signals, such as fixed frequency signals, sweep frequency signals, and so on. Therefore, in the case of single-antenna reception, it is assumed that N trombone timbre frequency signals are received from the air, and the interference is additive interference, so the expression for single-antenna multi-trombone timbre frequency reception is given as follows:

RETRACTED

$$y(t) = \sum_{n=1}^{N} s_n(t) + n(t). \tag{3}$$

In formula (3), $s_n(n = 1, 2, \ldots, N)$ is the trombone timbre frequency signal, and $n(t)$ is the sum of various disturbances and noises. Of course, in addition to single-antenna reception, there is also array antenna reception, mainly using linear uniform linear array and uniform circular array. The purpose of applying multiple antennas is to use the signal arrival delay to estimate parameters such as the incident direction angle, which is convenient for the later blind source separation problem. However, this article is mainly a single-antenna system, so it will not be discussed for now.

2.3. Time-Frequency Analysis Technology of Trombone Timbre Frequency Signal. The short-time Fourier transform (STFT) is a classical linear transform proposed by Gabor. It mainly uses $h(t)$ for windowing processing on the basis of Fourier transform. Moreover, each segment of the signal segmented by the window function is considered to be stable, and then the window function is continuously shifted, and the Fourier transform is performed on each segment of the signal, and finally, all the transforms are superimposed. Because the trombone timbre frequency signal $s(t)$ is a nonstationary signal, it has a good effect on STFT processing, and its continuous-time expression is given as follows:

$$\mathrm{STFT}_x(t, f) = \int_{-\infty}^{+\infty} s(\tau) h^*(\tau - t) e^{-i2\pi f\tau} \mathrm{d}\tau. \tag{4}$$

The discrete expression is given as follows:

$$\mathrm{STFT}(m, n) = \sum_{k=0}^{N-1} s(m + k) h(k) e^{-j(2\pi/N)kn}, \quad n = 0, 1, \ldots, N - 1. \tag{5}$$

Among them, m is the number of sampling points in the time dimension, n is the number of sampling points in the frequency dimension, $h(k)$ is the discrete window function, and $\mathrm{STFT}(n, m)$ represents the amplitude at the corresponding coordinate point. It can be seen from the abovementioned formula that STFT also has the following properties:

(1) Time shift property:

$$y(t) = s(t - t_0), \tag{6}$$

$$\mathrm{STFT}_y(t, f) = \mathrm{STFT}_s(t, f - f_0). \tag{7}$$

(2) Frequency shift property:

$$y(t) = s(t) e^{j2\pi f_0 t}, \tag{8}$$

$$\mathrm{STFT}_y(t, f) = \mathrm{STFT}_x(t - t_0, f) e^{j2\pi f_0}. \tag{9}$$

For STFT, its time-frequency resolution is mainly affected by the width of the window. If it is a long window, the resolution in the frequency domain is higher, and the resolution in the time domain is lower; if it is a short window, the result is the opposite. The two contradict each other, which is mainly constrained by the uncertainty principle. Its expression is given as follows:

$$BT \geq \frac{1}{2}. \tag{10}$$

Among them, B is the bandwidth, and T is the time width. Therefore, when analyzing the signal, it is necessary to select the appropriate window function parameters according to different situations. Figure 4 shows the time-frequency diagram of the STFT transformation of the trombone timbre frequency signal processed by different windows, the sampling length of the signal is N, and the type of the window H is the hamming window. The window length of Figure 4(a) is $N/4 + 1$, and the window length of Figure 4(b) is $N/10 + 1$.

It can be seen that when the window length is $N/4 + 1$, the frequency resolution of the trombone timbre frequency signal is high, and when the window length is $N/10 + 1$, the time resolution is high. Therefore, when analyzing the trombone timbre frequency signal, the length of the window depends on the situation. For fast trombone timbre frequency signals, short window processing can be selected. However, for slow trombone timbre frequency signals, long window processing can be selected.

For the case where multiple signals are superimposed, $s_1(t)$ and $s_2(t)$ are added linearly, and the following formula is satisfied:

$$\mathrm{STFT}[as_1(t) + bs_2(t)] = a\mathrm{STFT}[s_1(t)] + b\mathrm{STFT}[s_2(t)]. \tag{11}$$

It can be seen that STFT is a linear transformation. Common ones are Gabor transform and wavelet transform.

Gabor transform is proposed by Gabor in 1946 to represent time-frequency information in the form of a grid in a two-dimensional plane. Compared with the time window of STFT, Gabor is a joint time-frequency window. The Gabor change can be seen as the Gauss window selected by the STFT as the window function.

$$\mathrm{Gabor}(t, f) = \int s(\tau) g_{\mathrm{Guass}}(\tau - t) e^{j2\pi f\tau} \mathrm{d}\tau. \tag{12}$$

When the Gaussian window function is used, the lower bound of the uncertainty theorem can be satisfied. Therefore, the Gabor transform can be regarded as the optimal STFT transform. However, the shape of Gabor transform window function is uniform, unlike STFT, which can choose a variety of window functions to truncate the signal, and the time-frequency window size is fixed. As far as the actual signal processing is concerned, the window length used for signals of different frequencies should be variable. Wavelet change is a linear transformation with different resolutions at different frequencies. Its expression is given as follows:

$$\mathrm{wavelet}(a, b) = \frac{1}{\sqrt{a}} \int f(t) \psi\left(\frac{t - b}{a}\right) \mathrm{d}t. \tag{13}$$

RETRACTED

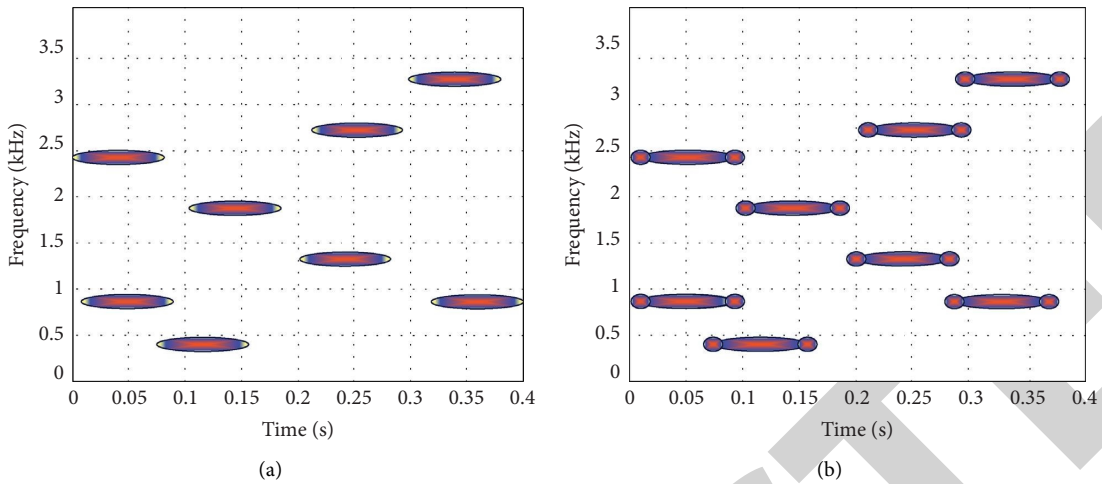

Figure 4: STFTs with different window lengths. (a) $H = N/4 + 1$. (b) $H = N/10 + 1$.

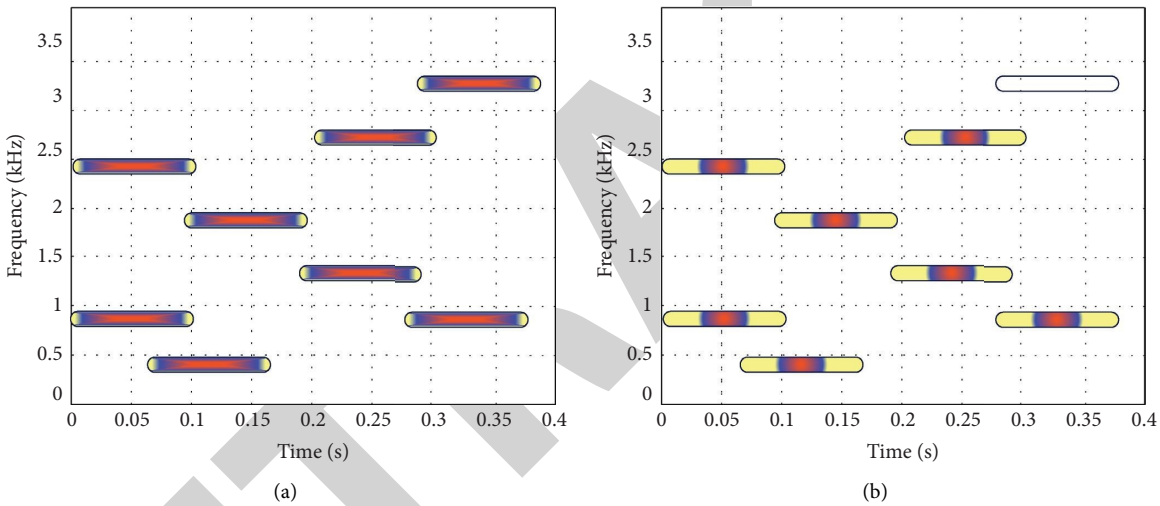

Figure 5: Two commonly used linear transformations. (a) Gabor transfer and (b) wavelet transform.

Among them, $\psi(t)$ represents the mother wavelet, a represents the scale, which controls the expansion and contraction of the wavelet function, and b represents the translation amount, which controls the movement on the time axis of the wavelet function. Figure 5 shows the analysis of trombone timbre frequency signal by Gabor transform and wavelet transform. The Gabor transform uses a Gaussian window with a window width of $N/(10 + 1)$, and the wavelet base used by the wavelet is a complex-valued Morlet wavelet.

It can be seen from Figure 5 that the Gabor transform is similar to STFT, that is, the resolution for each frequency is consistent. However, the wavelet transform has different resolutions for different frequencies, indicating that the resolution of the wavelet transform is adaptive. It shows that the wavelet transform has a good analysis effect for the signal of a single frequency, but for the multicomponent signal such as the trombone timbre frequency, the effect of the wavelet transform is not very good.

Compared with the linear time-frequency transformation, it does not have linear superposition, so after the transformation, there will be two results of self-term and cross-term. The WVD transformation expression is given as follows:

$$\mathrm{WVD}(t, f) = \int_{-\infty}^{\infty} s\left(t + \frac{\tau}{2}\right) s^*\left(t - \frac{\tau}{2}\right) e^{j2\pi f\tau} \mathrm{d}\tau. \tag{14}$$

It can be seen from Equation (14) that WVD does not need to select a window function similar to STFT transform to intercept the signal, and $s((t + \tau)/2)s^*((t - \tau)/2)$ can be regarded as the autocorrelation function of the signal. However, WVD is its Fourier transform with respect to τ, and the result obtained is a two-dimensional parameter of the time-frequency plane.

First, the WVD is processed by windowing in the time domain similar to STFT, which can remove the influence of the cross term, and then obtain the PWVD, and its expression is given as follows:

$$\mathrm{PWVD}_x(t, f) = \int_{-\infty}^{+\infty} s^*\left(t - \frac{\tau}{2}\right) s\left(t + \frac{\tau}{2}\right) h(\tau) e^{-j2\pi f\tau} \mathrm{d}\tau. \tag{15}$$

RETRACTED

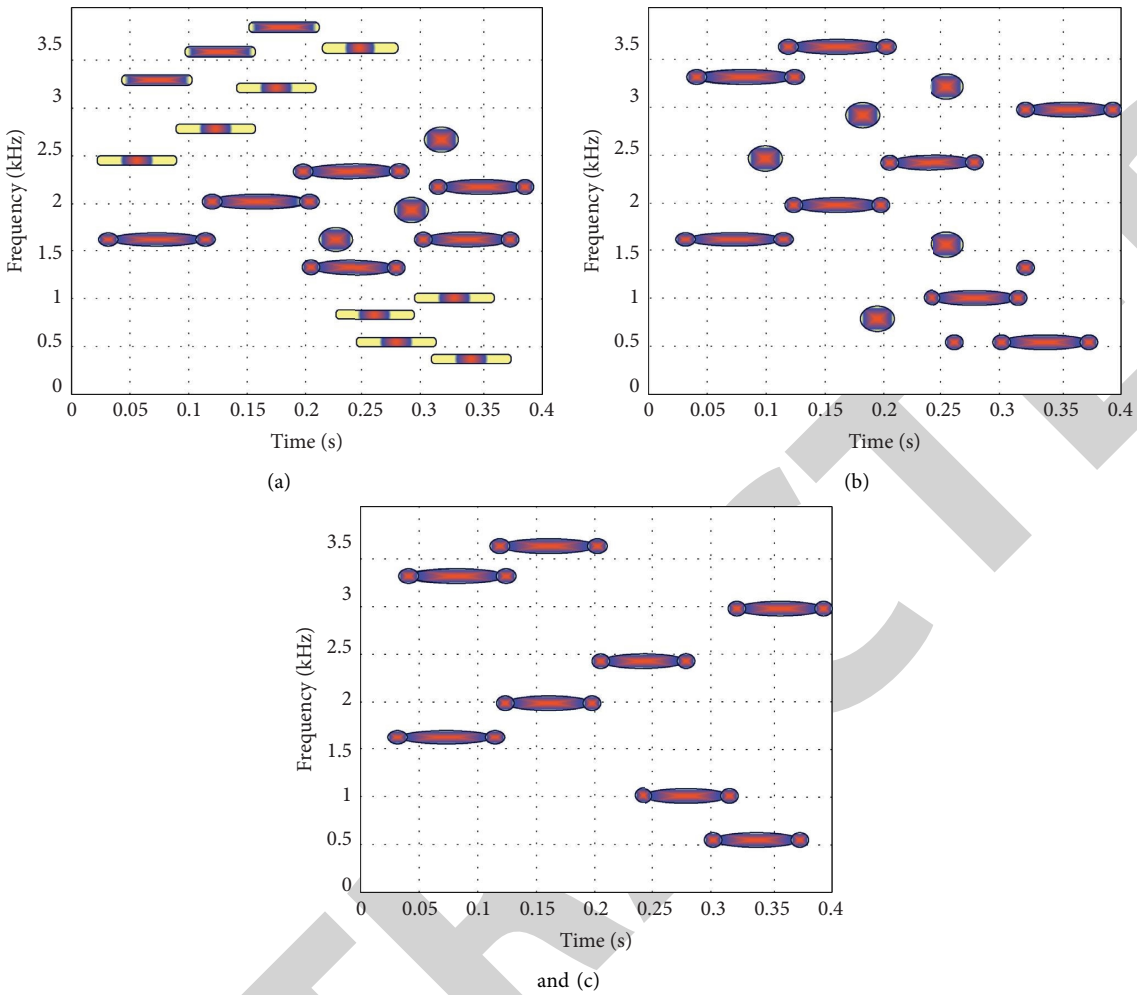

Figure 6: Time-frequency diagram of WVD and its improvement. (a) WVD, (b) PWVD, and (c) SPWVD.

The h (trombone timbre) in the formula is the added time window function, and its main function is to smooth the $s(t)$ in the time domain. PWVD reduces the impact of most cross-interference on the signal by sacrificing time-frequency focus.

In order to achieve the purpose of completely eliminating the cross term, based on the PWVD, a windowing operation is also performed in the frequency domain, which is SPWVD, and its expression is given as follows:

$$\mathrm{SPWVD}(t,f)=\int_{-\infty}^{+\infty}\int_{-\infty}^{+\infty}s\left(t-v+\frac{\tau}{2}\right)s^{*}\left(t-v-\frac{\tau}{2}\right)h(t)g(v)e^{-j2\pi f\tau}\mathrm{d}v\mathrm{d}\tau. \tag{16}$$

In the formula, h (trombone timbre) represents the window function in the time domain, which mainly performs filtering in the time domain. g (trombone timbre) represents the window function in the frequency domain, and its function is to filter in the frequency domain. Compared with PWVD, because the window function is added in the frequency domain, the suppression effect of the cross term is better. However, secondary windowing makes SPWVD less time-frequency focused. Figure 6 is a time-frequency analysis diagram of WVD, PWVD, and SPWVD.

As can be seen from Figure 6(a), after the trombone timbre frequency signal undergoes WVD transformation, the self-term and cross-term interference become indistinguishable, and even some cross-term energy is completely larger than the signal self-term energy. However, its time-frequency focus is indeed the best. Figure 6(b) shows the PWVD windowed in the time domain. It can be seen that it has a certain inhibitory effect on the cross term but does not completely eliminate the interference of the cross term, and the addition of the window reduces the time-frequency focus of the PWVD. Figure 6(c) shows the SPWVD with windows in both the time domain and the frequency domain. It can be seen that the interference of the cross term has been completely suppressed. However, the time-frequency focus

RETRACTED

is also reduced, so the windowing operation is to suppress the cross-term problem between the signals at the expense of reducing the time-frequency focus.

The reason why the cross-term is generated, when WVD analyzes multiple signals, can be demonstrated by mathematical formulas.

For signal $s = s_1 + s_2$, there is

$$\begin{aligned}\mathrm{WVD}_s &= \int_{-\infty}^{+\infty} s\left(t+\frac{\tau}{2}\right)s^*\left(t-\frac{\tau}{2}\right)e^{-j2\pi f\tau}\mathrm{d}\tau \\ &= \int_{-\infty}^{+\infty} (s_1+s_2)\left(t+\frac{\tau}{2}\right)(s_1+s_2)^*\left(t-\frac{\tau}{2}\right)e^{-j2\pi f\tau}\mathrm{d}\tau \\ &= \int_{-\infty}^{+\infty} s_1\left(t+\frac{\tau}{2}\right)s_1^*\left(t-\frac{\tau}{2}\right)e^{-j2\pi f\tau} \\ &\quad + \int_{-\infty}^{+\infty} s_2\left(t+\frac{\tau}{2}\right)s_2^*\left(t-\frac{\tau}{2}\right)e^{-j2\pi f\tau}\mathrm{d}\tau \\ &\quad + \int_{-\infty}^{+\infty} s_1\left(t+\frac{\tau}{2}\right)s_2^*\left(t-\frac{\tau}{2}\right)e^{-j2\pi f\tau}\mathrm{d}\tau \\ &\quad + \int_{-\infty}^{+\infty} s_2\left(t+\frac{\tau}{2}\right)s_1^*\left(t-\frac{\tau}{2}\right)e^{-j2\pi f\tau}\mathrm{d}\tau \\ &= \mathrm{WVD}_{s_1} + \mathrm{WVD}_{s_2} + 2\mathrm{Re}\left[\mathrm{WVD}_{s_1,s_2}\right].\end{aligned} \tag{17}$$

Among them, $2\mathrm{Re}[\mathrm{WVD}_{s_1s_2}]$ is the introduced cross-interference term. Figure 6(a) can clearly see the cross-term between signals, while PWVD and SPWVD only filter out the cross-term part through the principle of time domain and frequency domain filtering. Therefore, the trombone timbre frequency signal is generally not analyzed by WVD.

In addition to the abovementioned secondary time-frequency analysis, spectrogram (SP) is also an important secondary time-frequency analysis method. The spectrogram is mainly obtained by the square of the STFT mode, and its expression is given as follows:

$$\begin{aligned}\mathrm{SPEC}(t,f) &= |\mathrm{STFT}(t,f)|^2 \\ &= \int s(\tau)h^*(\tau-t)e^{-j2\pi f\tau}\mathrm{d}\tau \\ &\quad \int s^*(\tau)h(\tau-t)e^{-j2\pi f\tau}\mathrm{d}\tau \\ &= \iint W(\tau,v)W_h(\tau-t,v-f)\mathrm{d}\tau\mathrm{d}v.\end{aligned} \tag{18}$$

In the formula, the (τ, v) operator represents the WVD transformation, so the spectrogram can be regarded as the two-dimensional convolution of the WVD of the signal and the WVD of the window function. The spectral operation is simple, so there are many practical applications. For multiple signals, such as $s = s_1 + s_2$, phase information is produced because the STFT result is a complex number. Its spectral expression is given as follows:

$$\begin{aligned}\mathrm{SPEC}_s(t,f) &= \left|a\mathrm{STF}_{s_1}(t,f) + b\mathrm{STFT}_{s_2}(t,f)\right|^2 \\ &= a^2\left|\mathrm{STFT}_{s_1}(t,f)\right|^2 + b\left|\mathrm{STFT}_{s_2}(t,f)\right|^2 \\ &\quad + 2ab\mathrm{STFT}_{s_1}(t,f)\mathrm{STFT}_{s_2}(t,f)\cos\left(\phi_{s_1(t,f)} - \phi_{s_2(t,f)}\right).\end{aligned} \tag{19}$$

Among them, $\phi_{s_1(t,f)} = \arg(\mathrm{STFT}_{s_1}(t,f))$, $\phi_{s_2(t,f)} = \arg(\mathrm{STF}_{s_2}(t,f))$. It can be seen that the spectrum does not satisfy the linear superposition, and there is a phase cross term of $\cos(\phi_{s_1(t,f)} - \phi_{s_2(t,f)})$. However, if the two signals do not overlap in the time and frequency domains, the following expressions are satisfied:

$$\begin{aligned}\mathrm{SPEC}_s(t,f) &= \left|a\mathrm{STF}_{s_1}(t,f) + b\mathrm{STFT}_{s_2}(t,f)\right|^2 \\ &= a^2\left|\mathrm{STFT}_{s_1}(t,f)\right|^2 + b^2\left|\mathrm{STFT}_{s_2}(t,f)\right|^2.\end{aligned} \tag{20}$$

Figure 7 is the spectrogram analysis of the trombone timbre frequency signal, in which the window function is selected as the hammering window, and the length of the window is $N/(10+1)$.

It can be seen from Figure 7 that there is no cross-term interference when the spectrogram analyzes a single trombone timbre frequency signal because the frequencies of the trombone timbre frequency signal in each time period do not coincide. The time-frequency focus of the spectrogram is also very high, and its computational complexity is smaller than that of SPWVD, so it is widely used in engineering practice. Of course, there are also analysis methods such as fourth-order spectrogram and eighth-order spectrogram, which will not be repeated here.

The received signal is processed by STFT, and then the time-frequency analysis diagram of the multitrombone timbre frequency signal can be obtained. Then, according to the signal-to-noise ratio, the corresponding cut-off value is set, and then the elements in the STFT matrix are comparatively cut off. Therefore, by truncating $\mathrm{STFT}_s(t,f)$, $\mathrm{STFT}'_s(t,f)$ is obtained, and its expression is given as follows:

$$\mathrm{STFT}'_s(t,f) = \begin{cases}\mathrm{STFT}_s(t,f), & \text{if}\left|\mathrm{STFT}_s(t,f)\right| \geq \varepsilon, \\ 0, & \text{if}\left|\mathrm{STFT}_s(t,f)\right| < \varepsilon.\end{cases} \tag{21}$$

In the formula, ε is the truncation threshold. If $\mathrm{STFT}'_s(t,f)$ is discretized, $\mathrm{STFT}'_s(n,m)$ can be obtained, where n is the sampling point on the time axis, the total number of sampling points is N, m is the sampling point on the frequency axis, and the total number of sampling points is M. Therefore, the threshold ε is defined as follows:

$$\varepsilon = \eta \times \mathrm{mean}\left(\mathrm{STFT}_s(n,m)\right) = \eta\frac{1}{NM}\sum_{n=1}^{N}\sum_{m=1}^{M}\mathrm{STFT}_s(n,m). \tag{22}$$

In the formula, η is the threshold factor.

The time-frequency analysis result $\mathrm{STFT}'_s(t,f)$ after threshold truncation processing and $\mathrm{WVD}_s(t,f)$ with good time-frequency focusing are processed by dot product,

RETRACTED

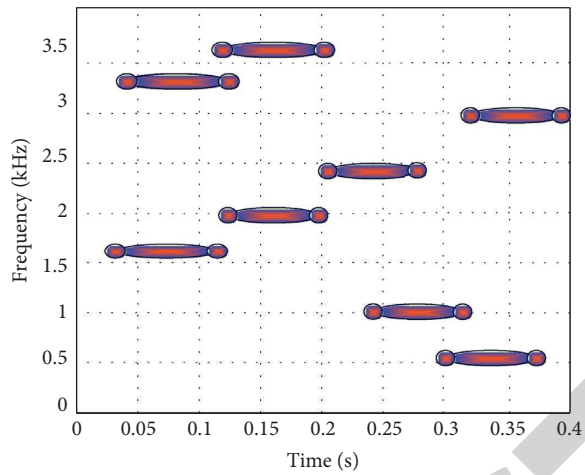

Figure 7: Spectrogram time-frequency analysis diagram.

namely, Hadamard product and the combined time-frequency distribution can be obtained as follows:

$$TF_s(t,f) = \mathrm{STFT}_s'(t,f) \odot \mathrm{WVD}_s(t,f). \tag{23}$$

Furthermore, good performance can be obtained by estimating the parameters of the combined time-frequency analysis signal. Taking the combination of STFT and WVD as an example, another combined time-frequency analysis is processed in the same way.

Figure 8 shows the time-frequency analysis of three common combinations of STFT-WVD, STFT-PWVD, and STFT-SPWVD and the time-frequency analysis diagram of STFT in the same noise environment. The time-frequency matrix transformed by the STFT is intercepted with a fixed threshold to make the time-frequency matrix show a distribution state of zero and nonzero values, so as to achieve the purpose of artificially weakening the noise.

It can be seen from the abovementioned figure that the time-frequency diagram of the combined time-frequency can suppress a certain amount of noise and is clearer and more robust than the single time-frequency analysis. Therefore, in the time-frequency analysis of multitrombone timbre frequencies, a combined time-frequency analysis may be an optimal solution. It can be observed that STFT-WVD and STFT-PWVD have little noise interference at multiple trombone timbre frequencies, so STFT-SPWVD time-frequency analysis is used in postprocessing signals.

The quality of the time-frequency analysis method is mainly measured from the time-frequency focusing and the cross-interference term. However, the level of time-frequency focus and the presence or absence of cross-terms can only be distinguished by the human eye, and a performance index based on information entropy to measure its time-frequency map is proposed. The specific steps are given as follows:

(1) The algorithm uses the time-frequency analysis method to obtain the time-frequency analysis diagram for the signal, and then performs modulo processing on the elements in the obtained time-frequency matrix, and the modulo time-frequency matrix is expressed as $TF_x(t,f)$.

(2) The algorithm finds the global maximum value $TF_{\max}(t,f)$ and the global minimum value $TF_{\min}(t,f)$ in $TF_x(t,f)$, and sets the step size of the amplitude interval as step = trombone timbre/N and N represents the number of intervals to be divided.

$$\begin{aligned} &\left[TF_{\min}(t,f),\ TF_{\min}(t,f) + \mathrm{step}\right), \\ &\left[TF_{\min}(t,f) + \mathrm{step},\ TF_{\min}(t,f) + 2\,\mathrm{step}\right), \\ &\qquad \cdots \\ &\left[TF_{\min}(t,f) + (N-1)\mathrm{step},\ TF_{\max}(t,f)\right). \end{aligned} \tag{24}$$

The algorithm counts the amplitude values falling in these N intervals and obtains the frequency vector of amplitude values as $M = [m_1, m_2, \ldots, m_N]$, and then divides it by the total number of elements in the time-frequency matrix to obtain N groups of probabilities $P = [p_1, p_2, \ldots, p_N]$.

(3) The algorithm calculates the information entropy of the time-frequency analysis graph with the following formula:

$$S = -K \sum_{n=1}^{N} p_n \ln\ p_n. \tag{25}$$

Through the obtained entropy value, the quality of various time-frequency analysis methods can be analyzed. The larger the entropy value is, the worse the time-frequency focusing is, and the worse the effect of suppressing cross-interference is. On the contrary, the smaller the entropy value is, the better the time-frequency focusing is, and the better the effect of suppressing cross-interference is.

3. Trombone Timbre Feature Extraction based on CNN Model

The general framework of trombone timbre feature recognition is shown in Figure 9. In the preprocessing stage, the musical tone samples are deaveraged and normalized to

RETRACTED

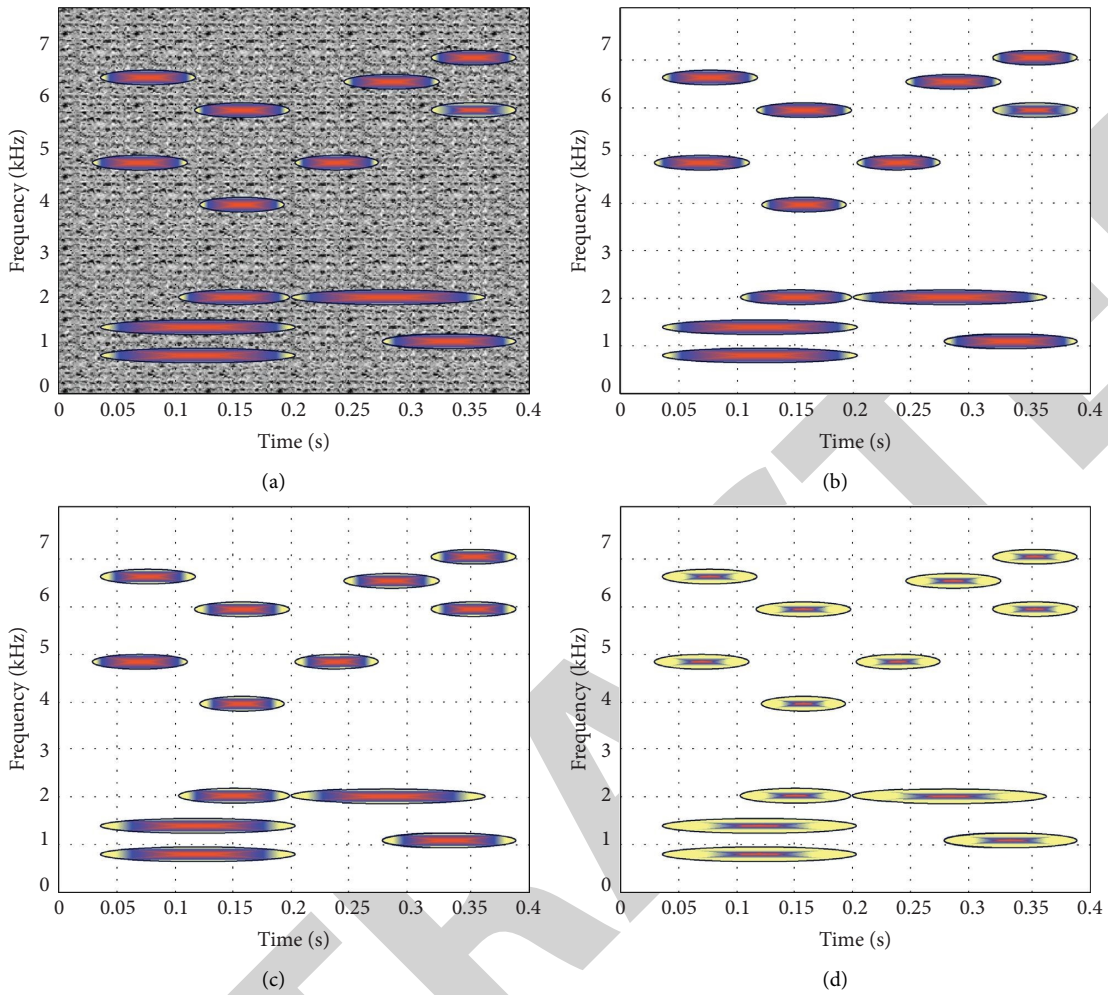

Figure 8: Time-frequency distribution of STFT and its combination. (a) STFT, (b) STFT-WVD, (c) STFT-PWVD, and (d) STFT-SPWVD.

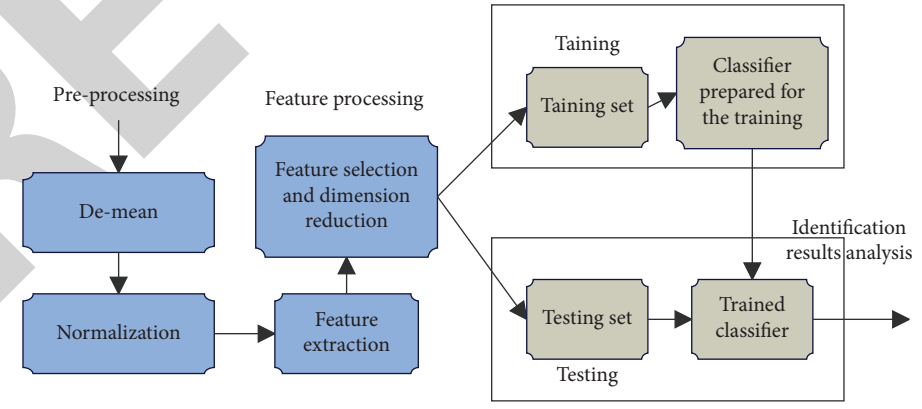

Figure 9: General framework of trombone timbre feature recognition.

avoid fluctuations in the mean and amplitude from affecting the stability of the final model. In the feature processing stage, timbre features, such as MFCC, are extracted.

In this paper, the feature recognition of the music performed by the trombone is carried out. Figure 10(a) and Figure 10(b) are the loudness diagrams and the normalized energy changes and note onset diagrams of the trombone playing segment.

On the basis of the abovementioned research, the trombone timbre feature extraction method based on the

RETRACTED

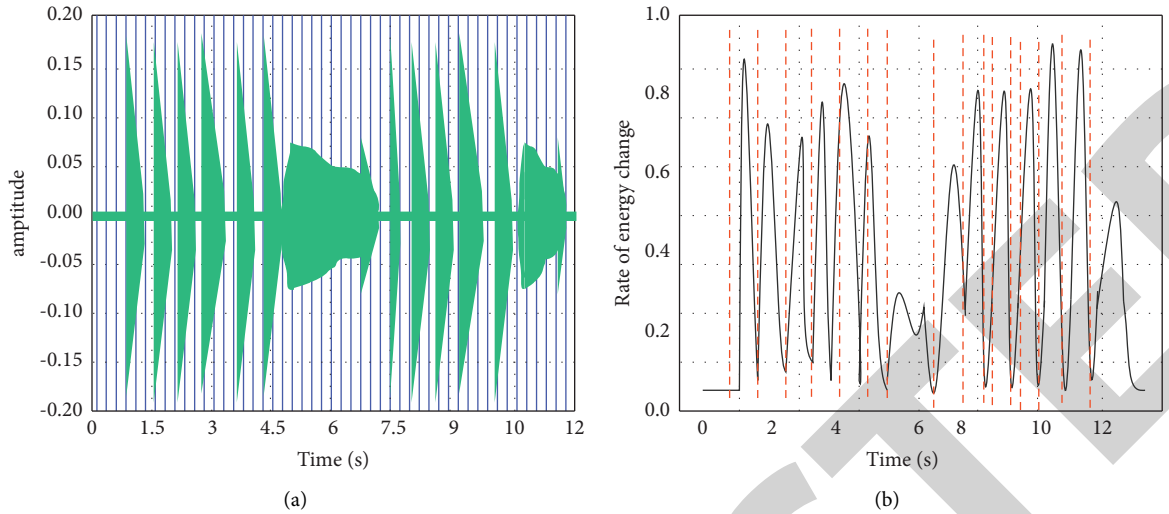

Figure 10: Recognition of musical features of trombone performance. (a) Performance section loudness and (b) schematic diagram of energy change and note onset.

Table 1: Accuracy of trombone timbre feature extraction based on the CNN model.

Num	Accuracy (%)
1	96.596
2	96.894
3	94.641
4	92.261
5	95.843
6	95.197
7	94.792
8	96.391
9	95.713
10	92.192
11	96.639
12	95.870
13	93.771
14	96.725
15	93.189
16	93.969
17	93.313
18	93.680
19	94.964
20	93.144
21	92.075
22	94.132
23	95.261
24	93.835
25	95.069
26	95.382
27	96.601
28	93.989
29	93.865
30	95.699
31	94.760
32	93.008

CNN model proposed in this paper is performed effectively, and the accuracy of the trombone timbre extraction is calculated, and the results shown in Table 1 are obtained.

It can be seen from the abovementioned research results that the trombone timbre feature extraction method based on the CNN model proposed in this paper can effectively identify the trombone timbre in a variety of musical performances.

4. Conclusion

The trombone, also known as the trombone and the telescopic horn, belongs to the brass playing instrument. It is the only musical instrument that has not been greatly improved in shape and structure since its origin. The trombone originated in BC and was first used in church and opera performances. In the nineteenth century, the trombone entered the symphony camp. Because of its unique timbre, it was mainly used in the performance of military bands, showing an impassioned, majestic, and powerful momentum. In addition, the trombone is also used in jazz performance, and the trombone is also known as the "king of jazz." In this paper, the trombone timbre feature extraction model is constructed by combining the CNN model to improve the training and learning effect of the trombone. The simulation results show that the trombone timbre feature extraction method based on the CNN model proposed in this paper can effectively identify the trombone timbre in various musical performances.

Data Availability

The labeled dataset used to support the findings of this study is available from the author upon request.

Conflicts of Interest

The author declares no conflicts of interest.

Acknowledgments

This work was supported by the Shandong College of Arts.

RETRACTED

Hindawi
Journal of Robotics
Volume 2023, Article ID 9832350, 1 page
https://doi.org/10.1155/2023/9832350

Retraction

Retracted: A Russian Continuous Speech Recognition System Based on the DTW Algorithm under Artificial Intelligence

Journal of Robotics

Received 8 August 2023; Accepted 8 August 2023; Published 9 August 2023

Copyright © 2023 Journal of Robotics. This is an open access article distributed under the Creative Commons Attribution License, which permits unrestricted use, distribution, and reproduction in any medium, provided the original work is properly cited.

This article has been retracted by Hindawi following an investigation undertaken by the publisher [1]. This investigation has uncovered evidence of one or more of the following indicators of systematic manipulation of the publication process:

(1) Discrepancies in scope
(2) Discrepancies in the description of the research reported
(3) Discrepancies between the availability of data and the research described
(4) Inappropriate citations
(5) Incoherent, meaningless and/or irrelevant content included in the article
(6) Peer-review manipulation

The presence of these indicators undermines our confidence in the integrity of the article's content and we cannot, therefore, vouch for its reliability. Please note that this notice is intended solely to alert readers that the content of this article is unreliable. We have not investigated whether authors were aware of or involved in the systematic manipulation of the publication process.

Wiley and Hindawi regrets that the usual quality checks did not identify these issues before publication and have since put additional measures in place to safeguard research integrity.

We wish to credit our own Research Integrity and Research Publishing teams and anonymous and named external researchers and research integrity experts for contributing to this investigation.

The corresponding author, as the representative of all authors, has been given the opportunity to register their agreement or disagreement to this retraction. We have kept a record of any response received.

References

[1] C. Yu and X. Wang, "A Russian Continuous Speech Recognition System Based on the DTW Algorithm under Artificial Intelligence," *Journal of Robotics*, vol. 2022, Article ID 5777472, 11 pages, 2022.

Hindawi
Journal of Robotics
Volume 2022, Article ID 5777472, 11 pages
https://doi.org/10.1155/2022/5777472

RETRACTED

Research Article

A Russian Continuous Speech Recognition System Based on the DTW Algorithm under Artificial Intelligence

Chunping Yu[1] **and Xin Wang**[2]

[1]*International Education School, Zhengzhou Railway Vocational and Technical College, Zhengzhou 451460, Henan, China*
[2]*International Exchange and Cooperation Office, Zhengzhou Railway Vocational and Technical College, Zhengzhou 451460, Henan, China*

Correspondence should be addressed to Chunping Yu; yuchunping@zzrvtc.edu.cn

Received 18 July 2022; Revised 23 August 2022; Accepted 29 August 2022; Published 19 September 2022

Academic Editor: Shahid Hussain

Copyright © 2022 Chunping Yu and Xin Wang. This is an open access article distributed under the Creative Commons Attribution License, which permits unrestricted use, distribution, and reproduction in any medium, provided the original work is properly cited.

In order to improve the effect of continuous speech recognition, this paper combines the DTW algorithm to construct a continuous Russian speech recognition system and proposes a continuous Russian speech detection method based on VGDTW-MPCA with an unequal interval process. Moreover, considering the influence of the correlation between variables on the synchronization of the DTW algorithm, this paper constructs a DTW algorithm on a local data set to synchronize in different variable groups. Then, this paper integrates the obtained data into complete 3D data for modeling. It can be seen from the simulation research that the Russian continuous speech recognition system based on DTW proposed in this paper has a high continuous Russian speech recognition accuracy.

1. Introduction

The training goal of foreign language subjects is to cultivate applied, compound, and innovative talents with international vision and cross-cultural communication skills, familiarity with international conventions, ability to participate in international competition and cooperation, with a sense of social responsibility, and adaptability to the needs of economic construction and social development. This is also the "authentic" that Russian subjects should abide by [1]. Under the background of the new era and historical opportunities, one of the important missions of the Russian subject is to enhance the country's soft power and shape the country's hard image in state exchanges. Moreover, the Russian-speaking talents cultivated under this goal and mission should form the consciousness of national culture [2]. In today's world, Russia is still a pivotal regional power with an important position in the world. At the same time, Russia is still a world leader in basic research, military *T*, and aerospace technology. Therefore, Russian-speaking talents still need to give full play to their due role in Sino-Russian scientific and technological exchanges and contribute to the development of the country, which is precisely the original mission of foreign language talents given to foreign language talents [3].

At present, there is still a big gap between Russian teaching and English. The teaching methods are more traditional and the subject research is relatively lagging behind. Therefore, while establishing a reasonable and complete curriculum system and innovative Russian teaching methods, the teaching staff should be strengthened. Construction is particularly important. As a key factor throughout the entire teaching process, teachers' professional quality and ideological realm are important conditions for the survival of Russian teaching [4]. Russian teachers also need to change their concepts, strive to improve their own knowledge, and strengthen the integration of theory and practice. Combining and handling the relationship between teaching and scientific research, it is still necessary to make efforts to transform into a "dual-teacher type." At the same time, Russian teachers should continue to enhance their own knowledge reserves, strengthen connections with other disciplines, and prepare for the challenges of the new era [5].

From the perspective of teaching methods, the current teaching activities of public Russian courses in colleges and universities have a single defect in teaching methods. First of all, in content design, more emphasis is placed on guiding students to learn basic Russian vocabulary and grammar, and the application of Russian in actual communication scenarios. Knowledge is not paid enough attention, which leads to insufficient teaching quality of public Russian courses in colleges and universities and it is difficult for students' practical application ability to effectively fit with the knowledge they have learned [6]. From the perspective of the course evaluation model, many courses and teachers are currently affected by the traditional test-oriented education concept and they do not pay enough attention to the development of students' application skills in the course teaching process. In the current process of Russian teaching in colleges and universities, many teachers have the phenomenon of "emphasizing theoretical results and ignoring practical application" when setting up a course evaluation system. Most Russian course exams are conducted through written tests, and the written test scores are used as the result of students' course learning, which makes it difficult for the course evaluation model to accurately reflect students' learning [7].

In terms of education training and job training, colleges and universities should do a good job in education ability training and job training for Russian teachers and fundamentally improve teachers' information-based teaching by building a good practice platform and collective training for teachers. In addition, it provides opportunities for teachers to communicate with relevant professionals in the course, so as to strengthen the training of teachers of public Russian courses and achieve the effective construction of Russian teaching faculty [8]. Prejob training for young and middle-aged Russian teachers can be increased, as professional training for young teachers who are about to take the stage, learning basic teaching norms, understanding teaching requirements, and inviting old teachers to impart teaching experience. We implement the "mentor-apprentice" system: employ experienced Russian professors or excellent English teachers in our school as teaching tutors for young Russian teachers to help young Russian teachers grow as soon as possible [9]. Through activities such as teacher skills competitions, teaching seminars, and observations, the training of basic teaching skills for young Russian teachers will be strengthened, teachers will be encouraged to carry out teaching research, professional curriculum reform, scientific research, actively participate in social services, and improve teachers' comprehensive ability. From time to time, experienced experts and professors from outside the school are invited to our school to give special reports and academic lectures to improve the professional qualifications of teachers. Finally, we must work hard on the structure of teachers [10]. In the process of carrying out public Russian courses in colleges and universities, the improvement of teachers not only requires the efforts of teachers themselves but also requires colleges and universities to introduce as many high-quality Russian teachers as possible and promote the structure of the teaching staff from "single" to "Diversity" curriculum transformation. From a specific point of view, colleges and universities can give full play to the advantages of the school-enterprise cooperative teaching mode, and hire Russian-speaking staff with rich business and trade work experience from the cooperative enterprises along the "Belt and Road," or professional and technical personnel from countries along the "Belt and Road." As part-time teachers of Russian courses for students, teachers can enrich teacher's Russian professional knowledge, and improve students' professional education ability in the process of continuous practice, so as to further improve the teaching staff [11]. In addition, the introduction of postgraduates with overseas experience should be increased, especially bilingual teachers with certain knowledge backgrounds, to meet the needs of Russian teaching in colleges and universities. We improve the educational level of imported foreign teachers and ensure the employment of foreign teachers. Foreign teachers play a crucial role in Russian teaching. The imported foreign teachers should have a master's degree or above and have certain teaching experience. The subject should be Russian as a foreign language, or bilingual teachers with railway professional background knowledge [12].

The core courses in the talent training program for Russian professionals include basic Russian, advanced Russian, Russian grammar, Russian reading, Russian audiovisual, and Russian writing. The curriculum focuses on helping students lay a solid foundation and develop language skills. However, it should be noted that the needs of regional economic development, and the employment direction of students should also be taken into consideration when designing talent training programs and writing syllabuses. In terms of teaching methods, traditional teaching methods are still used, which are mainly explained by teachers and passively accepted by students. This single model is boring to today's students and it is difficult to obtain good results [13].

We give full play to the advantages of comprehensive colleges and universities and actively carry out inter-professional exchanges within the school. Russian teachers and teachers of international trade, international law, and other majors regularly hold academic forums to gain an in-depth understanding of relevant knowledge and cutting-edge theories. Teachers of Russian majors are encouraged to apply for scientific research projects jointly with teachers of other majors to break down disciplinary barriers and promote interdisciplinary research. However, we make full use of research results in teaching, constantly update teaching content, improve teaching quality, encourage students to think and explore, and cultivate the spirit of scientific research and innovation [14]. Advocate exchange visits and enrich teaching experience. We support the exchange of teachers between our school and foreign institutions for further study or visiting exchanges, encourage teachers to actively apply for the China Scholarship Council project, participate in international seminars, and introduce the foreign advanced school-running experience and high-quality educational resources. In terms of inter-school cooperation, it attaches great importance to establishing contacts with domestic colleges and universities, regularly organizes teacher training exchanges, and invites

RETRACTED

authoritative scholars and experts to give teaching lectures and share valuable teaching experiences. We strengthen communication with enterprises and continuously update the knowledge system. Russian teaching work must be "grounded," and teachers must first go to practice [15].

As an inseparable whole, language and culture play complementary roles in the teaching of Russian. Students integrate their understanding of Russian culture into the process of learning the Russian language, which can better promote their mastery of the language. In this regard, foreign teachers have unique advantages. Teachers and students who have never lived in a Russian-speaking country, they have never experienced the national conditions, culture, customs, etc., of a Russian-speaking country but only learn some superficial knowledge from books [16]. In the process of teaching and working with teachers, foreign teachers can use personal examples to explain to students or set up some special teaching links for students to specifically reflect, so that students can learn relevant language knowledge in these processes, and at the same time enable teachers too. In particular, young teachers have learned knowledge that cannot be learned in books and has a better understanding of Russian culture [17].

This paper combines the DTW algorithm to construct a Russian continuous speech recognition system and improves the Russian teaching effect through artificial intelligence methods.

2. DTW Continuous Speech Recognition Algorithm

2.1. The Principle of the DTW-MPCA Algorithm. We assume that there are two-time series R and C, the length of the series R is m, and there is $R = (r_1, r_2, L, r_i, L, r_m)$. The length of the sequence C is n, there is $C = (c_1, c_2, L, c_j, L, c_n)$. First, in order to use the DTW method to synchronize the two-time series, a path matrix d of mxn needs to be defined in advance. Among them, the elements of the (i and j) position of the matrix represent the distance between the two points r_i and c_j. The formula for calculating the distance is as follows:

$$d(r_i, c_j) = \|r_i - c_j\|_p. \tag{1}$$

Among them, $\|\cdot\|_p$ represents the p norm, and p usually takes 2.

The goal of dynamic time warping is to find the shortest distance $D(m, n)$ between two-time series and the point sequence of the optimal path P. The optimal performance indicators of the shortest distance $D(m, n)$ and the optimal path P are as follows:

$$D(m,n) = \min_F \left[\sum_{k=1}^{K} d(i(k), j(k))\right], \tag{2}$$

$$P = \arg\min_F [D(m,n)]. \tag{3}$$

Among them, there is $\max(m,n) \le K \le m+n$. The shortest distance D (m and n) is the sum of the local shortest distances of the two sequences along the optimal path. The optimal path $P = (p_1, p_2, L, p_k), p_k = (i(k), j(k))$ is a point sequence in an mxn grid searched on the basis of the shortest distance D (m and n), as shown in Figure 1. The element in the optimal path is the quantization value of the anisotropy of the sequence in the matching process, and the curved path represents the optimal path for the matching of the two sequences.

According to the feasibility of the actual situation, the curved path P needs to meet the following two conditions:

(1) Endpoint constraint: the first and last elements p_1 and p_k of the optimal path P correspond to the elements at both ends of the diagonal of the distance matrix D, so that the stretched and compressed new data, and the original data keep the same starting point and termination point, as shown in the following formula:

$$p_1 = D(1,1), \tag{4}$$

$$p_2 = D(m,n). \tag{5}$$

(2) Global constraints: the selection of the optimal path P is generally limited to a certain range. It is beneficial to improve the calculation efficiency of the cumulative distance and avoid the appearance of abnormal paths. As shown in Figure 1, the optimal path is bounded within two dashed diagonals.

Local constraints define an optional preceding point for each point and specify the continuity of the midpoints of the path. The continuity of the midpoint of the path avoids excessive distortion and jumping off the original data.

As shown in Figure 2, the local constraint (1) can only have the following three options before point (i and j) in the grid: point (i–1 and j), point (i and j–1), Point (i–l and j–1). Therefore, formula (2) can be obtained by formula (6):

$$D(i,j) = \left\{ \begin{array}{c} D(i-1,j) + d(i,j) \\ D(i,j-1) + d(i,j) \\ D(i-1,j-1) + d(i,j) \end{array} \right\}. \tag{6}$$

As shown in Figure 2, the local constraint (2) can only have the following three options before point (i and j) in the grid: point (i–1 and j), point (i–1 and j–1), point (i–1and j–2). Therefore, formula (2) can be obtained by formula (7):

$$D(i,j) = \left\{ \begin{array}{c} D(i-1,j) + d(i,j) \\ D(i,j-1) + d(i,j) \\ D(i-1,j-2) + d(i,j) \end{array} \right\}. \tag{7}$$

2.2. Principle of the MPCA Algorithm. The three-dimensional data set for the unequal-length batch process is $X(I \times J \times K_i)(i = 1, 2, L, I)$. Among them, I represents the number of batches, J represents the number of variables used for offline modeling, and K represents the reaction time. In order to analyze the batch process using multivariate statistical methods, it is necessary to perform synchronization preprocessing on the 3D data set $X(I \times J \times K_i)$ $(i = 1, 2, L, I)$. Then, the complete 3D dataset $\bar{X}(I \times J \times K)$ after synchronization is expanded into a 2D matrix $X(I \times JK)$ based on batches, and the expansion method is shown in Figure 3.

RETRACTED

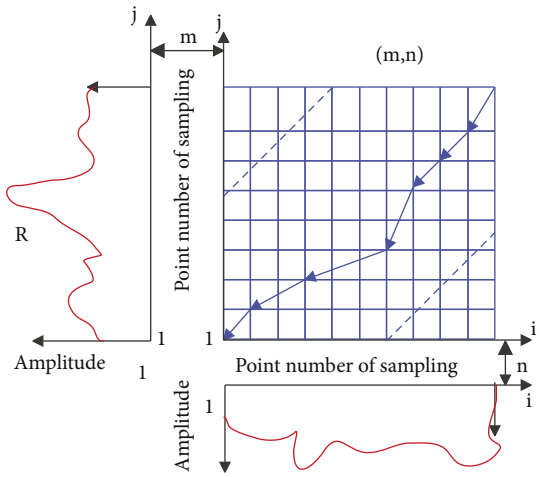

Figure 1: Schematic diagram of the principle of DTW algorithm.

In order to obtain the average running trajectories of the measurement variables on multiple batches of data, this paper performs the normalization processing of formulas (1)–(4) on the two-dimensional matrix $X(I \times JK)$ after the three-dimensional data set is expanded. The standardized data set approximately obeys the multidimensional normal distribution and can show the fluctuation of process variables in different batch intermittent operations, which has a certain degree of statistical significance.

After the batch process, the 3D dataset is preprocessed, and the expanded 2D matrix $X(I \times JK)$ is analyzed using traditional PCA. In fact, it extracts feature information based on the variance between different batches of data and the covariance of different variables at different sampling times. The variance matrix $(X^T X)/(I-1)$ of the two-dimensional matrix $X(I \times JK)$ is obtained by the singular value decomposition algorithm as follows:

$$\frac{X^T X}{I-1} = \frac{1}{I-1}\begin{bmatrix} X_1^T X_1 & X_1^T X_1 & X_1^T X_1 & L & X_1^T X_K \\ X_2^T X_1 & X_2^T X_2 & X_2^T X_3 & L & X_1^T X_K \\ X_3^T X_1 & X_3^T X_2 & X_3^T X_3 & L & X_1^T X_K \\ M & M & M & & M \\ X_K^T X_1 & X_K^T X_2 & X_K^T X_3 & L & X_K^T X_K \end{bmatrix}. \quad (8)$$

Among them, $X_K^T X_K$ represents the variance information between measurement data at the same time, and $X_{K1}^T X_{K2}$ represents the covariance information between different measurement data at different times. The decomposition process is as follows:

$$X = \sum_{r=1}^{R} t_r p_r + E. \quad (9)$$

Among them, R represents the number of retained principal components, t_r represents the relationship between batches, p_r represents the relationship between variables and time changes, and E represents the residual matrix containing secondary information and noise.

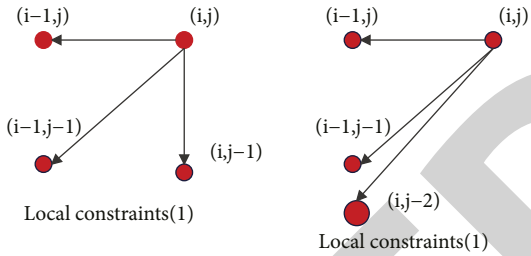

Figure 2: Schematic diagram of local constraints.

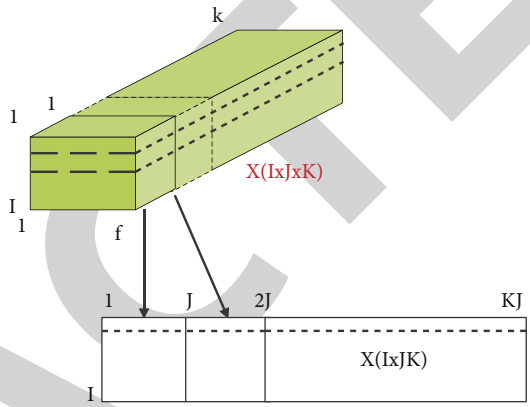

Figure 3: Schematic diagram of a batch expansion of 3D data.

Statistics used to monitor multivariate batch processes are the T^2 statistic and the SPE statistic. Among them, the T^2 statistic monitors the change information of the data in the pivot space, and the SPE statistic monitors the change information of the data in the residual space. During offline modeling, the T^2 statistic and SPE statistic are computed for batch i as follows:

$$T_i^2 = t_i^T S_t^{-1} t_i, \quad (10)$$

$$\mathrm{SPE}_i = e_i e_i^T, \quad (11)$$

$$e_i = X_i - PP^T X_i. \quad (12)$$

Among them, e_i represents the i-th row of the residual matrix, t_i is the score vector, and S_t is the covariance matrix estimated from the pivot score matrix obtained during modeling.

For the monitoring data of the MPCA online process, only the current time and previous values are known. The sampling data in the actual monitoring process are imperfect, resulting in insufficient known data to constitute a complete sampling of the intermittent process. Therefore, it is necessary to use data-filling technology when applying MPCA to online monitoring. This paper adopts the method of filling the current sampling value, that is, it is estimated that the data after the current moment is the same as the current moment.

The calculation of the T^2 statistic for online monitoring is performed at every sampling time k of batch i as follows:

RETRACTED

$$T_i^2(k) = t_i^T(k) S_t^{-1} t_i(k). \tag{13}$$

Moreover, the SPE statistic is the square of the error at the sampling instant k as follows:

$$\mathrm{SPE}_i(k) = \sum_{c=(k-1)j+1}^{\mathrm{JK}} e_c^T e_c. \tag{14}$$

Among them, e_c is the residual matrix $E = X_{\mathrm{new}} - t_{\mathrm{new}} P^T$.

The control limits for the T^2 statistic and the SPE statistic are calculated under the assumption that the modeled data are normally distributed. In this paper, kernel density estimation (KDE) is used to calculate the control limits. For any variable z, the probability density function of its radial basis kernel function is expressed as follows:

$$\widehat{f}(z) = \frac{1}{n} \sum_{i=1}^{n} \frac{1}{\sqrt{2\pi}} \exp\left[\frac{(z - z_i)}{2c^2}\right]. \tag{15}$$

Among them, c is the nuclear parameter, which is determined by the cross-validation method in this paper. Then, the integral of formula (15) is calculated in the definition domain of the variable z. When the integral reaches the set confidence limit, the corresponding value is the control limit obtained by the KDE method.

2.3. Variable Grouping DTW-MPCA Method. Two random variables X and Y are given, $p(x)$ and $p(y)$ are the marginal probability densities of the random variables X and Y, respectively. $p(x \text{ and } y)$ is the joint probability density of two random variables X and Y, which can be obtained by kernel density estimation or histogram method. The entropy of X is defined as follows:

$$H(X) = \sum_x p(x) \log \frac{1}{p(x)}. \tag{16}$$

The joint entropy of random variables X and Y is defined as follows:

$$H(X,Y) = \sum_x \sum_y p(x,y) \log \frac{1}{p(x,y)}. \tag{17}$$

Conditional entropy is used to describe the uncertainty of inferring two variables when a random variable is known. The definition of conditional entropy is as follows:

$$H(X|Y) = \sum_x \sum_y p(x,y) \log \frac{1}{p(y|x)}. \tag{18}$$

According to the property of entropy, we obtain the following equation:

$$H(X,Y) = H(X) + H(Y|X) = H(Y) + H(X|Y). \tag{19}$$

Therefore, the mutual information value is as follows:

$$\begin{aligned} H(X,Y) &= H(X) - H(X|Y) \\ &= H(Y) - H(Y|X) \\ &= H(X) + H(Y) - H(X,Y) \\ &= \sum_x p(x) \log \frac{1}{p(x)} + \sum_y p(y) \log \frac{1}{p(y)} \\ &\quad - \sum_{x,y} p(x,y) \log \frac{1}{p(x,y)} \\ &= \sum_{x,y} p(x,y) \log \frac{p(x,y)}{p(x)p(y)}. \end{aligned} \tag{20}$$

As shown in Figure 4, the mutual information between variable x_i and variable x_j in a batch of batch process data x $(K \times J)$ $(J = 10)$ is $I(x_i, x_j)(i, j = 1, 2, k, J)$. The greater the mutual information value between the two variables, the closer the relationship between the two variables. The mutual information value of the two variables x; and x; can be calculated, and the specific calculation method is shown in formula (21).

$$\begin{aligned} I(x_i, x_j) &= \sum_{x_i} p(x_i) \log \frac{1}{p(x_i)} + \sum_{x_j} p(x_j) \log \frac{1}{p(x_j)} \\ &\quad - \sum_{x_i, x_j} p(x_i, x_j) \log \frac{1}{p(x_i, x_j)} \\ &= \sum_{x_i, x_j} p(x_i, x_j) \log \frac{p(x_i, x_j)}{p(x_i)p(x_j)}. \end{aligned} \tag{21}$$

Among them, (x_1, x_2) represents the mutual information value between the first variable and the second variable, and the first row of the matrix represents the mutual information value between the first variable and all variables. In order to obtain the variable grouping with the greatest correlation between variables, the first row is used to search for the starting point. First, we compare pairs in the first row of the matrix, and remove the smaller value until only one element remains in the first row as the basis for subsequent variable selection. Then, the variable represented by the remaining elements in the first row is judged, and the variable selection in the next row is performed with the new search starting point indicated by the variable. It iterates in this way until the selected variable coincides with variable 1 in the first row. Finally, a variable grouping that searches for the start and end points with the first row can be obtained.

As shown in Figure 5, we search for the starting point in the first row to obtain the maximum value (x_1, x_3) of the first row and then search for the maximum value of the third row to obtain (x_3, x_4). Then, the maximum value (x_4, x_9) of the 4th row is searched, and the maximum value (x_9, x_1) of the 9th row is finally terminated. In this way, the mutual

RETRACTED

(X1, X2)	(X1, X3)	(X1, X4)	(X1, X5)	(X1, X6)	(X1, X7)	(X1, X8)	(X1, X9)	(X1, X10)
(X2, X1)	(X2, X3)	(X2, X4)	(X2, X5)	(X2, X6)	(X2, X7)	(X2, X8)	(X2, X9)	(X2, X10)
(X3, X1)	(X3, X2)	(X3, X4)	(X3, X5)	(X3, X6)	(X3, X7)	(X3, X8)	(X3, X9)	(X3, X10)
(X4, X1)	(X4, X2)	(X4, X3)	(X4, X5)	(X4, X6)	(X4, X7)	(X4, X8)	(X4, X9)	(X4, X10)
(X5, X1)	(X5, X2)	(X5, X3)	(X5, X5)	(X5, X6)	(X5, X7)	(X5, X8)	(X5, X9)	(X5, X10)
(X6, X1)	(X6, X2)	(X6, X3)	(X6, X5)	(X6, X6)	(X6, X7)	(X6, X8)	(X6, X9)	(X6, X10)
(X7, X1)	(X7, X2)	(X7, X3)	(X7, X5)	(X7, X6)	(X7, X7)	(X7, X8)	(X7, X9)	(X7, X10)
(X8, X1)	(X8, X2)	(X8, X3)	(X8, X5)	(X8, X6)	(X8, X7)	(X8, X8)	(X8, X9)	(X8, X10)
(X9, X1)	(X9, X2)	(X9, X3)	(X9, X5)	(X9, X6)	(X9, X7)	(X9, X8)	(X9, X9)	(X9, X10)
(X10, X1)	(X10, X2)	(X10, X3)	(X10, X5)	(X10, X6)	(X10, X7)	(X10, X8)	(X10, X9)	(X10, X10)

Figure 4: Schematic diagram of the mutual information matrix.

(X1, X2)	(X1, X3)	(X1, X4)	(X1, X5)	(X1, X6)	(X1, X7)	(X1, X8)	(X1, X9)	(X1, X10)
(X2, X1)	(X2, X3)	(X2, X4)	(X2, X5)	(X2, X6)	(X2, X7)	(X2, X8)	(X2, X9)	(X2, X10)
(X3, X1)	(X3, X2)	(X3, X4)	(X3, X5)	(X3, X6)	(X3, X7)	(X3, X8)	(X3, X9)	(X3, X10)
(X4, X1)	(X4, X2)	(X4, X3)	(X4, X5)	(X4, X6)	(X4, X7)	(X4, X8)	(X4, X9)	(X4, X10)
(X5, X1)	(X5, X2)	(X5, X3)	(X5, X5)	(X5, X6)	(X5, X7)	(X5, X8)	(X5, X9)	(X5, X10)
(X6, X1)	(X6, X2)	(X6, X3)	(X6, X5)	(X6, X6)	(X6, X7)	(X6, X8)	(X6, X9)	(X6, X10)
(X7, X1)	(X7, X2)	(X7, X3)	(X7, X5)	(X7, X6)	(X7, X7)	(X7, X8)	(X7, X9)	(X7, X10)
(X8, X1)	(X8, X2)	(X8, X3)	(X8, X5)	(X8, X6)	(X8, X7)	(X8, X8)	(X8, X9)	(X8, X10)
(X9, X1)	(X9, X2)	(X9, X3)	(X9, X5)	(X9, X6)	(X9, X7)	(X9, X8)	(X9, X9)	(X9, X10)
(X10, X1)	(X10, X2)	(X10, X3)	(X10, X5)	(X10, X6)	(X10, X7)	(X10, X8)	(X10, X9)	(X10, X10)

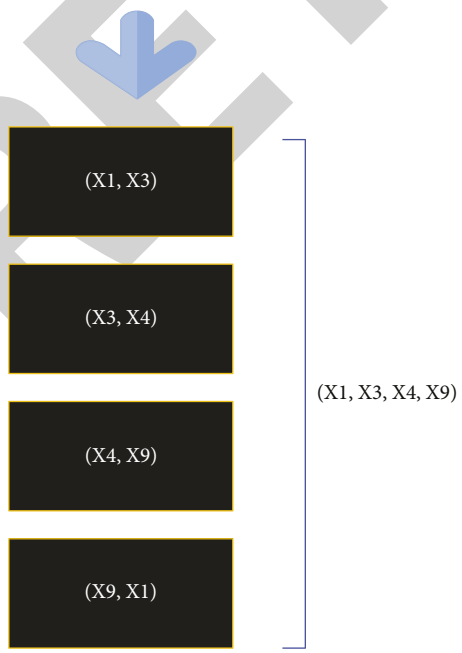

Figure 5: Schematic diagram of mutual information matrix search.

information value between the variables obtained by searching for the starting point of the first row is the largest, and the sum of the mutual information values of this group of variables is the largest.

2.4. Mining and Analysis of Dynamic Characteristics of Variables. We assume that $x \in R^{J\times 1}$ are data consisting of J process variables. The data array consisting of sampled samples of x is as follows:

$$X = [x(1), x(2), x(3), L, x(N)]^T \in R^{N\times 1}. \tag{22}$$

Among them, N is the number of samples, and each row of X represents a sample. In order to consider the dynamic characteristics between different sampling times $x(k)$, X is first extended to as follows:

$$\begin{aligned} X^* &= [x(1)^*, x(2)^*, x(3)^*, L, x(N-d)^*]^T \\ &= [X_0, X_{-1}, X_{-2}, L, X_{-d}]. \end{aligned} \tag{23}$$

Among them, there is $X^* = [X_0{}^T, X_{-1}{}^T, X_{-2}{}^T, L, X_{-d}{}^T]^T$. x_{-i} corresponds to the variable obtained by shifting the sampling of x at time i, which is as follows:

$$\begin{aligned} X_{-i} &= [x_{-i}(1), x_{-i}(2), x_{-i}(3), L, x_{-i}(N-d)]^T \\ &= [x(i+1), x(i+2), x(i+3), L, x(N-d+i)]^T. \end{aligned} \tag{24}$$

The matrix X is extended to obtain the augmented matrix $X^* \in R^{(N-d)\times J(d+1)}$ as follows:

$$X^* = \begin{bmatrix} x^T(1) & x^T(2) & L & x^T(d+1) \\ x^T(2) & x^T(3) & L & x^T(d+2) \\ M & M & O & M \\ x^T(N-d) & x^T(N-d+1) & L & x^T(N) \end{bmatrix}. \tag{25}$$

The value of the lag parameter d in the general augmented matrix construction is 1 or 2, and for the system with strong dynamics, d can be selected by a specific iterative algorithm. If the value of the lag parameter d is small, the number of measurement values introduced into the data matrix may be insufficient, and the dynamic characteristics of the process data cannot be fully captured. If the value of the lag parameter d is large, it may lead to the introduction of measurement value redundancy in the data matrix, which may cause excessive interference to process modeling and monitoring. For this purpose, the lag parameter in the augmented matrix selected in this section is 4. In the data matrix, four measurements were introduced for every single variable to construct an augmented matrix for the single variable. As shown in Figure 6, an augmented matrix is constructed by taking a batch of data as an example. Among them, each column in the matrix represents the value of a variable at all sampling times.

This approach fully captures the dynamic nature of all variables. However, it inevitably creates redundancy in individual variables. Second, in order to accurately obtain the dynamic characteristics of different variables, it is necessary to filter variables for each augmented matrix. The correlation between each measurement variable in the augmented matrix and all variables in other matrices is calculated, and the calculation method is shown in formula (26):

$$R(m,n) = \frac{\mathrm{Cov}(m,n)}{\sqrt{\mathrm{Var}(m)}\sqrt{\mathrm{Var}(n)}}, \tag{26}$$

Among them, m and n are any two variables in different augmented matrices, Cov (m, n) is the covariance between the two variables, Var (m) and Var (n) are the variances of variables m and n, respectively. The larger the absolute value of R, the stronger the correlation between the two variables. The closer it is to 0, the weaker the correlation.

Finally, the correlation between all measured variables in each augmented matrix is K-means clustered into two categories, and the category with the smaller correlation value in the two categories is used as the basis for eliminating variables. The idea of K-means clustering is to divide the data set through continuous iteration, so that different classes are independent and the same class is compact. In this section, Euclidean distance is selected as the similarity measure between data samples, and the performance of the clustering algorithm is evaluated by using the squared error and objective function. The brief steps of the K-means clustering method are as follows: (a) it arbitrarily selects n samples from the input data samples of the correlation between the measured variables as the initial clustering centers. (b) According to the mean of the clustered samples, the Euclidean distance between each sample, and the sample selected as the cluster center is calculated, and the samples are divided according to the minimum distance. (c) The mean of the new cluster samples is recalculated. (d) b and c are iteratively looped until the cluster centers no longer change. From the results in Figure 7, it can be seen that the dimensions of the augmented matrix of different variables are different after screening, and the difference in the dynamics of different variables leads to the difference in the actual lag order demand.

2.5. Distributed Dynamic VGDTW-MPCA Model Modeling Strategy. After the corresponding augmented matrix is constructed according to the dynamics of each variable, under the guidance of the block modeling idea, the augmented matrix of different variables can be divided into different blocks according to a certain relationship. Thus, augmented matrices of different chunks are different and augmented matrices of the same chunk are similar. Therefore, it is considered to use the mutual information between augmented matrices of different variables to measure the intrinsic relationship between such variables. Among them, the principle of mutual information has been introduced in the previous chapter, and the schematic diagram of the grouping of different variable augmentation matrices is shown in Figure 8.

According to formula (21), the mutual information value between the two variable augmented matrices is calculated and the corresponding mutual information matrix is formed. The formula for calculating the mutual information

RETRACTED

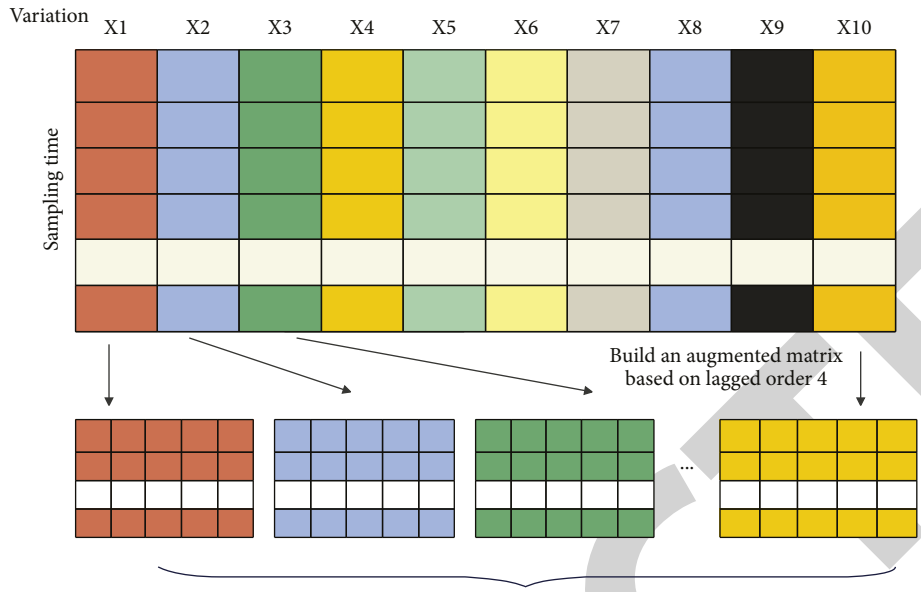

Figure 6: Schematic diagram of constructing augmented matrix with different variables.

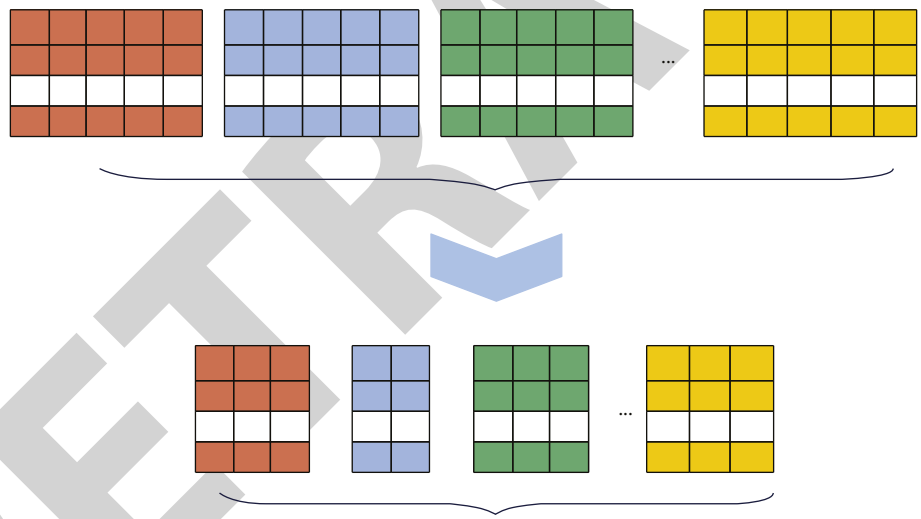

Figure 7: Augmented matrix variable selection.

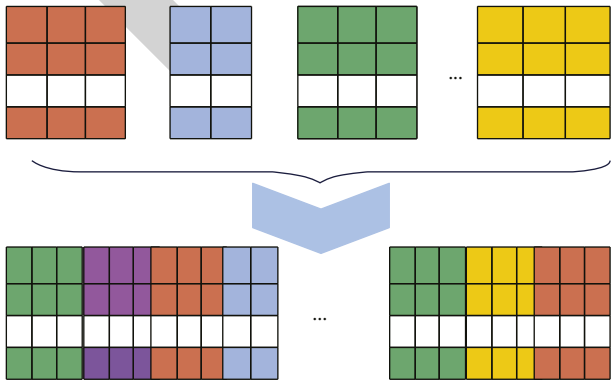

Figure 8: Schematic diagram of augmented matrix grouping.

value between a single measurement variable in the augmented matrix is as follows:

$$I\left(X_m^a, X_n^b\right) = \sum_{X_m^a, X_n^b} p\left(X_m^a, X_n^b\right) \log \frac{p\left(X_m^a, X_n^b\right)}{p\left(X_m^a\right) p\left(X_n^b\right)}. \tag{27}$$

Among them, X_m^a represents the a-th measurement variable of the augmented matrix m and X_n^b represents the b-th measurement variable of the augmented matrix n.

The formula for calculating mutual information between one augmented matrix and another augmented matrix is as follows:

$$I_m = \sum_{a=1}^{J_m} \sum_{b=1}^{J_n} I\left(X_m^a, X_n^b\right). \tag{28}$$

RETRACTED

Among them, J_m represents the number of all measurement variables in the augmented matrix m and J_n represents the number of all measurement variables in the augmented matrix n.

We assume that the PCA model is obtained separately from the two grouped augmented matrix data as follows:

$$X_i = T_i P_i + E_i. \tag{29}$$

Among them, there is $i = \{1 \text{ and } 2\}$. The control limits $T^2_{i,\lim}$ and $Q_{i,\lim}$ are calculated at the same time. In the online monitoring phase, when new data are obtained, new T_i^2 and Q_i are calculated, respectively. In order to achieve a comprehensive monitoring effect, this paper uses the Bayesian fusion technology to combine multiple statistics into a probability form.

The probability of misidentification of x monitored by the T_i^2 statistic is defined as follows:

$$P_{T_i^2}(F|x) = \frac{P_{T_i^2}(x|F)P_{T_i^2}(F)}{P_{T_i^2}(x)}. \tag{30}$$

Moreover, the probability of $P_{T_i^2}(x)$ is defined as follows:

$$P_{T_i^2}(x) = P_{T_i^2}(x|N)P_{T_i^2}(N) + P_{T_i^2}(x|F)P_{T_i^2}(F). \tag{31}$$

Among them, x represents the data at a sampling time of the test data, N and F represent normal and abnormal operating conditions, $P_{T_i^2}(N)$ and $P_{T_i^2}(F)$ can be simply designated as a and $1-a$, and a is the confidence level for calculating the control limit. The conditional probabilities $P_{T_i^2}(x|N)$ and $P_{T_i^2}(x|F)$ are calculated by the following formulas:

$$P_{T_i^2}(x|N) = \exp\left(-\frac{T_i^2}{T^2_{i,\lim}}\right), \tag{32}$$

$$P_{T_i^2}(x|F) = \exp\left(-\frac{T^2_{i,\lim}}{T_i^2}\right). \tag{33}$$

Then, a weighted form is used to combine multiple monitoring results into an overall probability indicator as follows:

$$\mathrm{BIC}_{T^2} = \sum_{i=1}^{2}\left\{\frac{P_{T_i^2}(x|F)P_{T_i^2}(F|x)}{\sum_{i=1}^{2}P_{T_i^2}(x|F)}\right\}. \tag{34}$$

Similarly, the final probability indicator BIC_Q of the Q statistic can be obtained. Usually, when the value of BIC_Q or BIC_{T^2} exceeds the control limits a, an alarm is misidentified. Otherwise, the monitoring process is considered normal.

2.6. Description of Segmentation Strategy of the Ms-VGDTW-MPCA Algorithm. As shown in Figure 9, the datasheet $X(I \times J \times K)$ is obtained by vertically cutting the three-dimensional matrix $\widetilde{X}_k(I \times J)$ along the third dimension. This slice consists of the k-th sampling time of all batches of batch process data and is referred to by the researchers as the time slice matrix in the batch process. The three-dimensional data

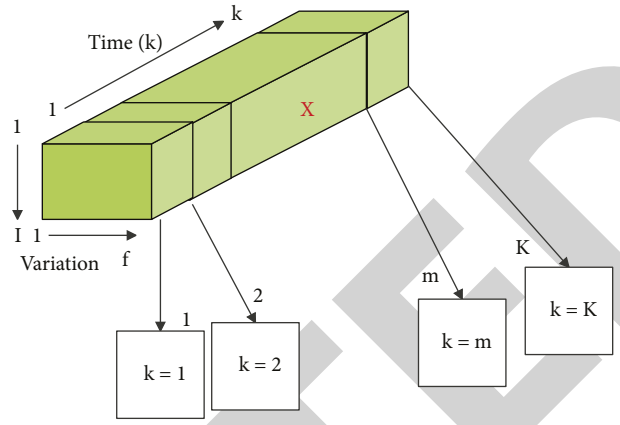

Figure 9: Schematic diagram of time slice cutting of the three-dimensional matrix.

array used for cutting is in accordance with the predetermined process and parameters under the normal batch process operating conditions, and the process variables follow the predetermined running track. However, an industrial process cannot be completely repeated and the process variable trajectory must fluctuate under the influence of random disturbances. Therefore, the J process variables of the two-dimensional time slice matrix $\widetilde{X}_k(I \times J)$, after cutting the three-dimensional data under normal operating conditions approximately obey the Gaussian distribution.

Next, the PCA method is applied to the time slice matrix $\widetilde{X}_k(I \times J)$ with a Gaussian distribution, which can extract the correlation information between the process variables at K sampling instants. Formula (35) is the PCA model of the time slice matrix:

$$\widetilde{X}_k = T_k P_k^T + E_k, \tag{35}$$

Among them, T_k represents the score matrix, P_k represents the load matrix, and E_k represents the residual matrix. The K load matrices represent the correlation information between process variables and can reflect changes in the internal operating mechanism of the process.

In order to capture the change of the load matrix, the principal component correlation degree is used as the similarity measure to measure the changing relationship between the two matrices and as the basis for the stage division. The calculation method of the pivot degree is as follows:

$$\mathrm{PCC}(U,V) = \frac{\mathrm{trace}\left(\wedge_u^T U^T V \wedge_v \wedge_u^T V^T \wedge_u\right)}{\sum_{i=1}^{c}\lambda_i^u \lambda_i^v}. \tag{36}$$

Among them, U and V, respectively, represent the load matrix obtained by PCA in two different time slices, λ_i^u and λ_i^v are their corresponding eigenvalues, c represents the number of load vectors, and there is $\wedge_u = \mathrm{diag}(\lambda_1^u, \lambda_2^u, L, \lambda_c^u)$ and $\wedge_v = \mathrm{diag}(\lambda_1^v, \lambda_2^v, L, \lambda_c^v)$.

A time series $X = \{x(t_i)\}_{i=1}^n$ is given. It is divided into z segments: $X_j, j = 1, 2, L, z$, which satisfies $X_j \neq \varnothing$, $X_{j1} \cap X_{j2} = \varnothing, \forall j_1 \neq j_2, j_1, j_2 \in [1, 2, L, z]$, $\cap_{j=1}^{k} X_j = X$. The corresponding time interval is $[t_{s_j}, t_{f_j}]$, $s_j, f_j \in \{1, 2, L, n\}$,

RETRACTED

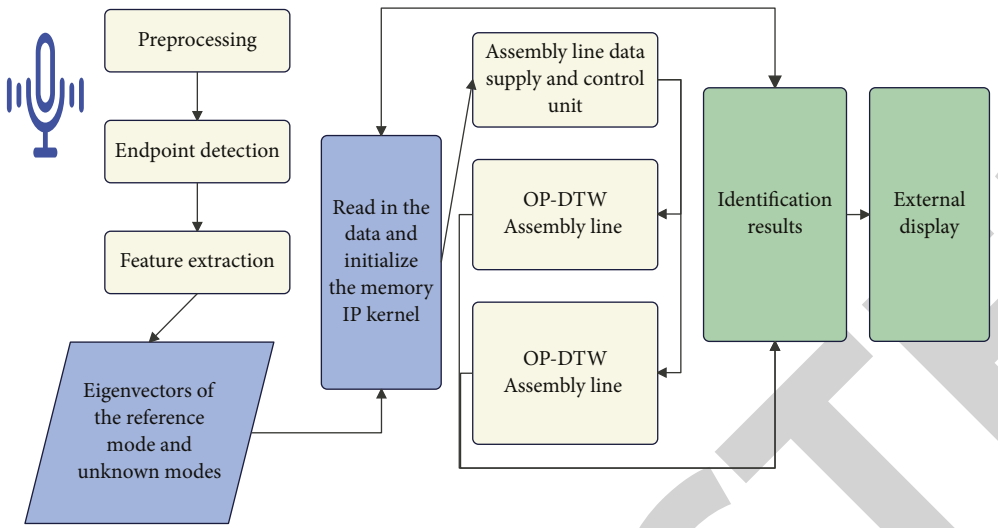

Figure 10: System framework.

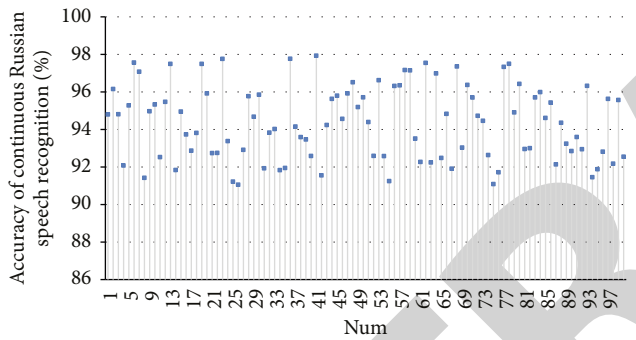

Figure 11: The accuracy of Russian recognition of the DTW-based Russian continuous speech recognition system.

which represents the position of the start and end points of the j-th line segment in the time series, and there is $s_1 = 1$ and $f_z = n$. A linear function $F_j(t_i) = a_j t_i + b_j, \forall i \in [s_j, f_j]$ on the interval X_j is found to minimize the following objective function:

$$J = \sum_{j=1}^{k} \sum_{i=s_j}^{f_j} \left[x(t_i) - F_j(t_i)\right]^2. \quad (37)$$

The objective function J uses the residual sum of squares between the original time series and its linear approximation to measure the degree of fit between the two. The smaller J is, the better the linear approximation fits the original time series. The optimal solution $\left\{(F_j^*, X_j^*)\right\}_{j=1}^{k}$ obtained by solving the above optimization problem is called an optimal linear approximation of the time series X.

3. Russian Continuous Speech Recognition System

The most flexible hardware device in the embedded system is the FPGA (Field Programmable Logic Gate Array), which is very suitable for implementing this algorithm. The Russian continuous speech recognition system based on DTW proposed in this paper is shown in Figure 10.

The abovementioned framework constructs a Russian continuous speech recognition system based on DTW; then, the effect of the system is verified, the accuracy of speech recognition is counted, and the results shown in Figure 11 are obtained.

It can be seen from the abovementioned research that the Russian continuous speech recognition system based on DTW proposed in this paper has a high continuous Russian speech recognition accuracy.

4. Conclusion

To improve the overall level of the teaching staff of public Russian courses in colleges and universities, it is necessary for the teachers of Russian courses in colleges and universities to carry out self-learning and self-improvement. The school should help teachers of Russian courses to develop a sense of self-improvement, and at the same time update the educational concept in the course teaching, constantly enrich the personal knowledge structure, and improve their professional knowledge level and education level. At the same time, it is necessary to continue learning as an important task, make use of modern information-based teaching technology, constantly supplement new knowledge and new content, and learn the teaching and research methods of Russian teachers in other schools. This paper combines the DTW algorithm to construct a Russian continuous speech recognition system and improves the Russian teaching effect through artificial intelligence methods. It can be seen from the simulation results that the Russian continuous speech recognition system based on DTW proposed in this paper has high continuous Russian speech recognition accuracy.

Data Availability

The labeled dataset used to support the findings of this study is available from the corresponding author upon request.

RETRACTED

Hindawi
Journal of Robotics
Volume 2023, Article ID 9852312, 1 page
https://doi.org/10.1155/2023/9852312

Retraction

Retracted: The Application of Multimedia Visualization Platform in Business Management from the Perspective of Supply Chain Management

Journal of Robotics

Received 19 December 2023; Accepted 19 December 2023; Published 20 December 2023

Copyright © 2023 Journal of Robotics. This is an open access article distributed under the Creative Commons Attribution License, which permits unrestricted use, distribution, and reproduction in any medium, provided the original work is properly cited.

This article has been retracted by Hindawi following an investigation undertaken by the publisher [1]. This investigation has uncovered evidence of one or more of the following indicators of systematic manipulation of the publication process:

(1) Discrepancies in scope
(2) Discrepancies in the description of the research reported
(3) Discrepancies between the availability of data and the research described
(4) Inappropriate citations
(5) Incoherent, meaningless and/or irrelevant content included in the article
(6) Manipulated or compromised peer review

The presence of these indicators undermines our confidence in the integrity of the article's content and we cannot, therefore, vouch for its reliability. Please note that this notice is intended solely to alert readers that the content of this article is unreliable. We have not investigated whether authors were aware of or involved in the systematic manipulation of the publication process.

Wiley and Hindawi regrets that the usual quality checks did not identify these issues before publication and have since put additional measures in place to safeguard research integrity.

We wish to credit our own Research Integrity and Research Publishing teams and anonymous and named external researchers and research integrity experts for contributing to this investigation.

The corresponding author, as the representative of all authors, has been given the opportunity to register their agreement or disagreement to this retraction. We have kept a record of any response received.

References

[1] N. Wang, "The Application of Multimedia Visualization Platform in Business Management from the Perspective of Supply Chain Management," *Journal of Robotics*, vol. 2022, Article ID 1271691, 10 pages, 2022.

Hindawi
Journal of Robotics
Volume 2022, Article ID 1271691, 10 pages
https://doi.org/10.1155/2022/1271691

RETRACTED

Research Article

The Application of Multimedia Visualization Platform in Business Management from the Perspective of Supply Chain Management

Nuan Wang

School of Economics and Trade, Henan Polytechnic Institute, Nanyang 473000, China

Correspondence should be addressed to Nuan Wang; wangnuan@hnpi.edu.cn

Received 11 July 2022; Revised 16 August 2022; Accepted 30 August 2022; Published 19 September 2022

Academic Editor: Shahid Hussain

Copyright © 2022 Nuan Wang. This is an open access article distributed under the Creative Commons Attribution License, which permits unrestricted use, distribution, and reproduction in any medium, provided the original work is properly cited.

At present, in the process of enterprise operation and development, the implementation of enterprise operation modernization is a necessary condition and an effective measure to raise the management level. With the aim to achieve such enterprise modernization, it is necessary to improve the management's modernization ability by improving the modernization level of enterprises. Therefore, corporate executives should pay more attention to the construction of informatization and implement informatization through effective methods and measures to further improve management efficiency. It will note the concept and connotation of business management, analyze the significance of the multimedia visualization platform at the level of enterprise business supply chain, analyze the current business management of enterprises and put forward scientific coping strategies, cater to the social development situation, and constantly innovate the development path of enterprise network information and chemical business management; this will help related majors.

1. Introduction

Science as well as management modes are also changing. The traditional manual management system has become increasingly difficult to adapt to the needs of high-intensity and high-efficiency management, so it is very necessary to implement informatization [1] in the management process. The competent department is the director of business [2]. Once the management cannot keep up with the development of society, the development speed of the enterprise will be limited to a certain extent, and the promotion of the growth of the enterprise has not received sufficient attention in the early stage of development [3]. In the 1980s, Chinese enterprises gradually began to introduce computer information technology and modern management methods in the fields of operation and management and achieved corresponding successful development [1].

In the process of the daily management of enterprises in a network, the management level of enterprises is optimized, the management role is played for the economic development of enterprises, the current market development situation is catered for, and the realization of strategic development goals of enterprises is promoted [4]. Some enterprises lack the emphasis on network informatization and still adopt it in such process business. Therefore, enterprise management should improve the understanding of the network and the process of business management. Network information optimizes the management level of each business link of the enterprise and promotes the high-quality development of the enterprise.

The efficient integration of information technology and enterprise internal operation management can improve the immediacy and accuracy of enterprise internal information collection [5], promote scientific and effective enterprise internal management decisions, enhance the sensitivity of enterprise internal to market information, and promote the improvement of enterprise overall level [6]. The company will continue to develop. The integration of network information technology in the business management of enterprises should break the traditional way of thinking [7], avoid relying on the subjective assumptions or experience management of managers, and rely on big data technology to analyze various business data indicators of the enterprise and provide reliable data for business decision-making

support [8]. On the one hand, the company should use network technology to monitor the financial data information formed in the production and operation of all parts of the company in an all-round way, effectively acquire, integrate, classify, and analyze the data, discover the potential value of data information and combine it with the current market development trend, screen out valuable data and information for the development of the enterprise itself, help the enterprise to identify the development direction in the production and operation of the enterprise, promote the improvement of the economic profit of the enterprise, and ensure the realization of the strategic development goal [9]. On the other hand, the effective integration of network information technology in enterprise business management can help enterprises to obtain diversified data information from various internal production departments and various upstream and downstream enterprises in the external industrial chain and more comprehensively analyze the current market positioning of enterprises [10], and establish a scientific early warning mechanism, and make scientific and reasonable risk avoidance measures to help enterprises find a scientific and stable business direction and management strategy, and improve the supervision level of all aspects of enterprise operation and management [11].

Multimedia visualization technology is an auxiliary means of business management. In line with knowledge as well as information acceptance ability, the company will adopt multimedia teaching and visualization technology to alter the mode of management and innovate the management concept, so as to improve the cognitive structure of the enterprise and improve the interest of management. In view of the specific content of business management, enterprises mobilize the interests of enterprises through reasonable implementation of management design and carry out enterprise-independent learning through joint research. The business administration discipline covers a wider range and has more complex knowledge points [12]. Therefore, enterprises should carry out multimedia presentations according to the course objectives of business administration, show management scenarios to the company intuitively [13], stimulate the company's curiosity, transform theoretical knowledge into practical skills through the display of multimedia visualization technology, and encourage companies to explore in discovery [14]. Let the company learn independently and mobilize the company's learning initiative [15]. Use multimedia visualization technology in management to enhance the diversity of management [16]. In terms of management, the company introduced the specific contents of business management training in the form of photos, music, and videos, which helped the enterprise to master professional knowledge faster, flexibly apply the knowledge to a specific practice, and improve learning efficiency [17]. The use of multimedia management can strengthen the company's practical ability and improve the company's professional quality [18]. At the same time, improving the management level of the enterprise can improve the company's innovation awareness to a certain extent, fully apply the innovative spirit to the management of the enterprise, improve the management ability of the company, and increase its own knowledge reserve [19]. Based on the DirectShow framework, this paper focuses on the concept, characteristics, and connotations of business administration, analyzes the significance of multimedia visualization platforms in the improvement of enterprise business management levels under the perspective of supply chain management, discusses the current problems in enterprise business administration, proposes scientific coping strategies to cater to the social development situation, and constantly innovates the development path of enterprise network informatization business management.

2. Related Concepts and Theoretical Basis

2.1. Concepts Related to Business Management and Business Informatization. Business management contains rich management content and has a very broad concept. This is an indispensable means of modern company management and financial management. In the operation process of the company, each production link is constrained by relevant systems to ensure that each department and operation process of the enterprise conform to the industry and commerce. Management requirements can ensure the realization of the overall production efficiency of the enterprise. With the in-depth development of informatization, dataization, and intelligent technology, which penetrates deeply into various fields, it has affected the production level as well as the work rhythm of enterprises. The business decisions of various departments of the enterprise affect the strategic goals of the enterprise. Enterprises are caught in tax-related risks, financial risks, legal risks, etc., and network information on chemical business management can help enterprises avoid potential business risks and provide a clear path for the sustainable development of enterprises [20].

The informatization of business management is the integration of information technology into traditional business management models. The application of computer and Internet-related technologies to traditional business management processes has improved the efficiency of business management, broadening the functions of business management. Compared with traditional business management, the informatization of business management has the advantages of accuracy and speed in information acquisition, integration, transmission, and analysis accuracy of business decisions. Business management and informatization have different functional attributes, and the integration of the two requires such carriers. Information technology should be developed and utilized on the basis of the traditional business management model. At the same time, the business management modes of enterprises in different fields are different, and the practicality and extensiveness of informatization are required to be high, and the informatization technology is required to be compatible with different business management modes. Information technology can realize the sharing of information materials within the company, improve the quality of information transmission among various departments of the company, break down the obstacles and defects of information communication among various departments under the

RETRACTED

traditional company mode, promote cooperation among various departments, and promote the efficient development of the enterprise.

Information processing is a kind of activity that combines management information with computer network technology and uses new information technology to manage and integrate information materials so as to control and serve information. Information processing is a very common management method for companies because the quality of data processed by computers is better and the efficiency and convenience can be greatly improved. The operation function of the system mainly depends on manual operation, and manual operation will inevitably make mistakes. After being inquired by the computer, the operator can conveniently inquire about the key information contained in the specific information.

The realization of management informatization systems in small and medium-sized enterprises has very important practical significance, and management design involves many aspects and the objects oriented are also very diverse. Unless the traditional management methods are changed, the human resources invested in management will be very large, and management departments cannot afford it. Moreover, as shown in Figure 1, under the situation of increasing management efficiency today, once the state administrative organs fail to improve their work efficiency, many business problems for industrial and commercial enterprises and traders will accumulate, and it may even take a year to handle them. This is also contrary to the state's demands for reducing the burden of business management. Therefore, it is imperative to promote the information.

2.2. Supply Chain Management. In 1996, the management and research committee of Michigan State University took the lead in introducing the concept of supply chain control. It points out that enterprise managers should integrate environmental factors into the design, procurement, production, assembly, packaging, logistics, and distribution of enterprise activities at every session. Supply chain management is an interorganizational practice that incorporates environmental factors into supply chain management, including reverse logistics. Hall believes that supply chain management starts with the concept of sustainable development and through the close cooperation between enterprise departments and enterprises. The entire supply chain is coordinated and unified in environmental management so as to achieve the optimal system environment. In addition, Tseng and others also believe that on the supplier platform, suppliers and users are the most attractive subjects for upstream and downstream cooperation of enterprises, and cooperation with core enterprises can reduce the impact of enterprises on the environment. For this reason, Tseng and others define supply chain management as follows: integrating environmental management into the enterprise process, promoting information and data resource sharing, and improving environmental performance through collaboration with customers, suppliers, and logistics enterprises. Generally, scholars define enterprise management as

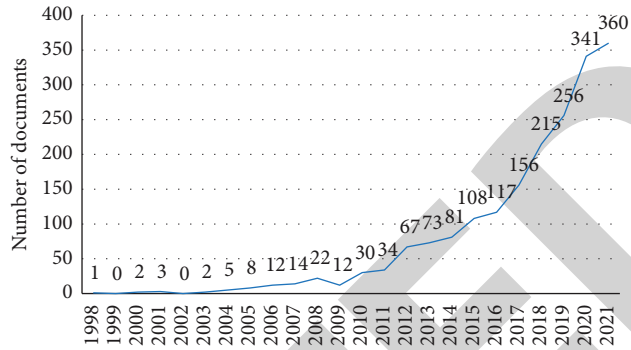

Figure 1: Time distribution of the number of publications in the international research literature on business administration.

integrating environmental knowledge into the whole process of enterprises to optimize resource utilization efficiency, reduce environmental pollution, and increase social welfare. In the research of supply chain management, Sarkis and others are based on the following nine basic theories: the basic theory of system complexity; the theory of ecological modernization; the basic theory of information; the market system theory; and the basic theory of information, including trade efficiency. For a such realization of electronically registered residence, the current database service system has defects in data analysis, and it is very difficult to obtain useful policy data. It is urgent to develop a new generation of big data analysis systems with multimedia visualization. As a new force in the field of big data analysis and application, supply chain data management has increasingly shown its good ability and practicability. It analyzes and summarizes the current theoretical research status of supply chain management and the future trend of basic theoretical research and provides research theories that can further understand and explain supply chain management issues in future scientific research, such as innovation diffusion theory and path dependence theory, social embedding theory, structure theory, and agency theory.

The drivers of supply chain management are important factors in ensuring the successful implementation of the supply chain. Supply chain management is originally driven by management and laws and regulations, and the smooth implementation of supply chain management depends on managers' insight into the macroenvironment and the ability to optimize enterprise resources, as well as their excellent management ability to take the environment and enterprise benefits into account. Considering the source of driving factors and other factors, the main motivation of driving factors can be divided into active and passive. As shown in Figure 2, environmental protection awareness comes from the company's own emphasis on environmental protection, including factors such as corporate image or social or environmental responsibility; regulatory requirements, which are externally imposed environmental protection requirements on enterprises, including local governments and international organizations; laws, rules, and regulations, such as the requirements of ISO14001 certification; and internal motivation, which comes from the company's

RETRACTED

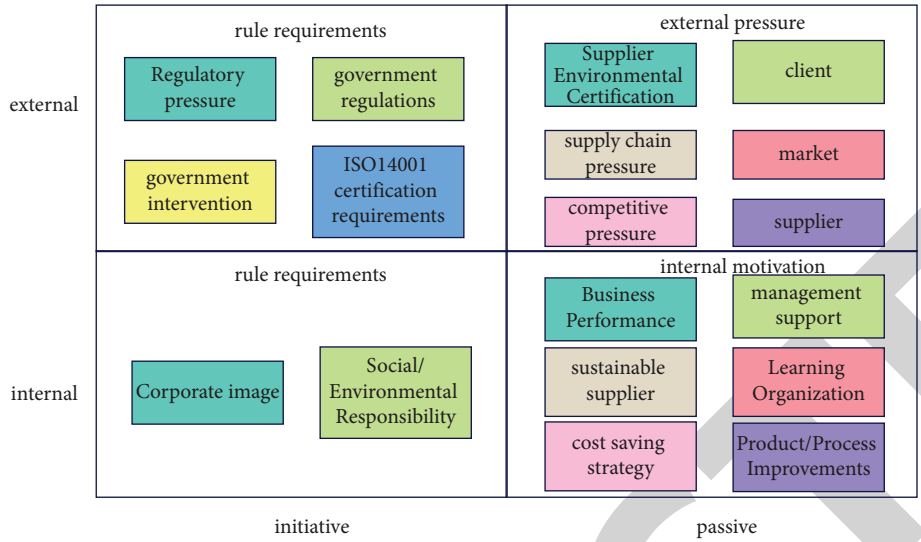

Figure 2: Drivers of supply chain management.

internal drive to implement green supply chain management. In order to achieve the goal of green environmental protection, the company needs to upgrade the green operation concept to a strategic level. External pressure refers to the direct or indirect requirements of stakeholders in the supply chain, including competitive pressures, customers, and market requirements.

2.3. Features and Advantages of Multimedia Visualization Platform. The traditional big data analysis teaching course has many problems, such as strong theory and strong concepts that are difficult for enterprises to master. The current statistical and analytical tools are not suitable for the application or practice of courses, because they are more professional and have higher training costs. The statistical analysis and visualization platform of *Python* can solve these problems well. Figure 3 gives the framework for the company to apply multimedia visualization technology to the whole process of business administration in the supply chain management horizon. It mainly uses multimedia visualization technology to enhance the diversity of management.

Enterprises can also use the data analysis module of the system. After mastering the basic knowledge, students can choose different algorithms to carry out data mining experiments according to their own interests and needs. Because the basic knowledge level of each company is different, enterprises can use the visual platform to carry out targeted training to improve their learning enthusiasm.

Give us some cases related to our practice. Combine these examples and knowledge to improve the understanding of data mining applications. You can also create and upload your own cases, contact other users, and acquire self-knowledge and skills in this process.

The operating system will provide open-source code and comments for all algorithms. Enterprise personnel can understand the specific implementation of these algorithms and execute these codes while understanding and learning. They also overcome their own difficulties by improving their own methods, improving their research abilities and application technology, and adapting to the research needs of development at all levels.

3. Related Technologies

We create a filter graph manager to coordinate state transitions between filters, establish a reference clock, and provide a way for applications to build filter graphs. The filter graph manager interface used in this system is as follows:

(1) IGraphBuilder, the main function of this interface is to create a filter graph.

(2) IMediaControl, this interface contains some functions to control the multimedia stream, which are used to control the three states of the multimedia stream (flow, stop flow, and pause flow).

(3) IMediaEvevtEx, the function of this interface is to process the events in the chart.

(4) IBasicAudio, the function of this interface is to control some attributes such as audio volume and audio balance.

(5) IBasicVideo, the function of this interface is to set some properties of the video.

(6) IMediaSeeking, the function of this interface is to set the playback speed and locate the playback position.

(7) IMediaPosition, the function of this interface is to find the position corresponding to the multimedia data. Therefore, the general steps for DirectShow-based multimedia streaming are as follows: the application establishes the corresponding filter according to a certain intention; build a filter graph manager in the application to manage these filters; connects each filter through pins as required; and controls the entire data processing through the filter graph manager.

RETRACTED

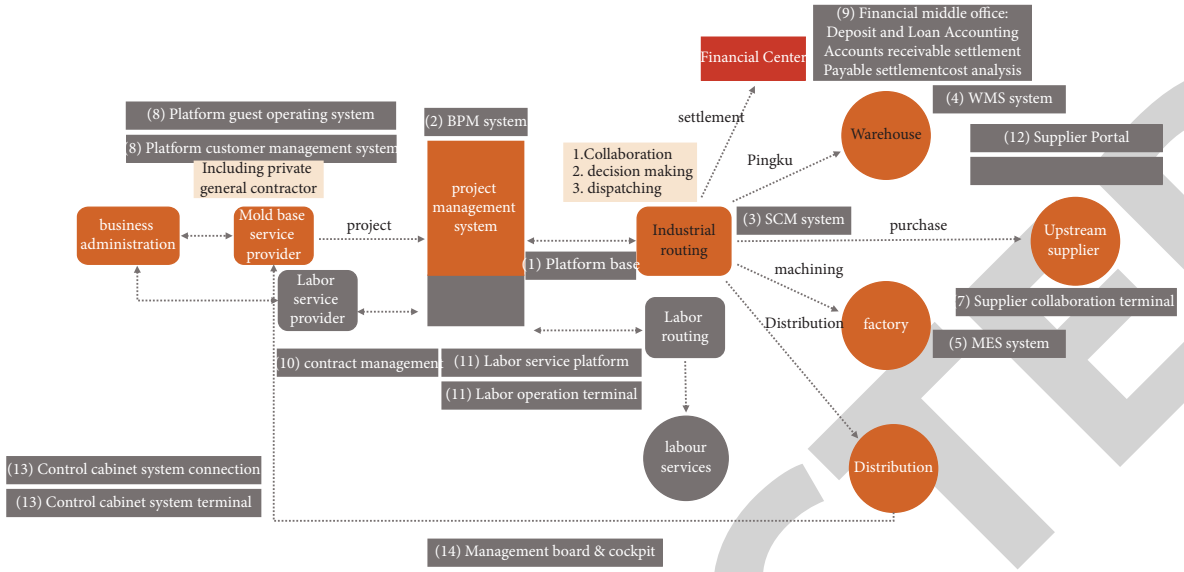

Figure 3: Visual management framework of the whole process of company operation business.

The class responsible for multimedia stream separation and decoding is the stream media pro class. The initial graph () method is responsible for initializing the filter graph, the getPin () method is responsible for obtaining the filter pins, the connectPintoFilters () method connects the pins with the filter, and the play () method, pause () mode, and stop () mode are responsible for running, suspending and stagnant states of the multimedia stream.

The voice signal is generally between 10 ms and 30 ms; we can consider it stable. In reality, speech signals are very long, and we cannot process long data at one time, but we can decompose it and take a small piece of data for analysis each time. In order to decompose the long audio into short audio segments, we adopt the method of adding a Hamming window to a long audio segment. The Hamming window can be regarded as the sum of the spectrum of the three rectangular times windows, or the sum of the three sinc (t) type functions, while the two items in parentheses move π/T left and right relative to the first spectrum window, so that the side flaps cancel each other, eliminating high-frequency interference and energy leakage. Suitable for nonperiodic continuous signals.

The calculation formula of the Hamming window is given as follows:

$$W(n) = \begin{cases} 0.54 - 0.46\cos\left[\dfrac{2\pi n}{N-1}\right], & \\ 0. & \end{cases} \quad (1)$$

After adding the Hamming window, the intercepted signal time segment is actually subjected to periodic extension processing, and the data shape has the feeling of a period. However, after the infinitely long signal is truncated, spectral energy leakage will occur because after adding the Hamming window, the data information on both sides of the window is lost. In order to solve this problem, the method we use is to move only 1/3 or 1/2 of the window when moving the window. After this method is applied, the data on both sides of the window will not be lost.

Table 1: Description dictionary of visualization requirements.

Field name	Field abbreviation	Data type	Type length
Requirement code	Request code	Int	10
Requirement name	Request name	Char	50
Functional requirement	Request function	Char	50
Data requirement	Data request	Char	50
Result requirement	Result request	Char	50
Time dimension	Time dimension	Char	50
Space dimension	Space dimension	Char	50
Parameter dimension	Parameter dimension	Char	50

The description required by business management data mining is the direction indicator for all subsequent services. Accurate positioning can effectively reduce misunderstanding during excavation. This paper uses the business management database, based on the current mining situation, including the change of the market investment scale, the operation of target customers, and the change of market entities as shown in Table 1

Information incitement was initiated by C. E. Shannon wrote in his 1948 article about the geometric concepts of communication. He believes that there is redundancy in all data, and the degree of redundancy is directly related to the probability and uncertainty of various contents (quantity, letters, or English words) in the data. The calculation formula is as follows:

$$H(X) = E[I(X_i)] = E\left[\log_2\left(\frac{1}{P(X_i)}\right)\right]. \quad (2)$$

RETRACTED

Among them, $H(X)$ represents the information stake of attribute set meaning', and $P(X)$ represents the occurrence probability of attribute X.

Information gain is also known as information But the difference, is relatively inflammatory (relative entropy). In the view of probability and information theory, the signal gain is asymmetric, and its purpose is mainly to detect the difference between two different probability distributions. The main index of information gain is the amount of energy information contained in each feature in the process of statistical analysis. The greater the number of attributes, the greater the contribution to classification and the higher the information gain, and vice versa, the smaller the information gain.

Information gain tends to be a large number of data attributes, but they have little effect on classification. Therefore, the data gain rate was introduced in the latest classification method. The information gain value refers to the total amount of information contained in the unit attribute. Although the information gain refers to the uniformity of the information value, it cannot simply compare the total amount of information.

Suppose there are m categories in the sample data set S, which are as follows:

$$S = \{C_1, C_2, C_3, \ldots, C_m\}. \tag{3}$$

It is one of the attributes of systems V, which can divide the data set into several subsets, and each attribute has k different characteristic values.

The probability of occurrence for category Cj is given as follows:

$$P(C_j) = \frac{|C_j|}{|S|}. \tag{4}$$

Occurrence probability of attribute V = Vi is given as follows:

$$P(V_i) = \frac{|S_i|}{|S|}. \tag{5}$$

Among the samples with attribute V = Vi, the probability of containing samples of class Cj is given as follows:

$$P\left(\frac{C_j}{V_i}\right) = \frac{|C_{ij}|}{|S_i|} = \text{freq}\frac{(C_j, S)}{|S_i|}. \tag{6}$$

The calculation formula of category information abstract is given as follows:

$$\text{Info}(C) = -\sum_j P(C_j)\log_2 P(C_j). \tag{7}$$

From this decision tree, some classification rules can be obtained as follows:

(1) If the industry category = "construction industry" and the area is "Guandu District," the enterprise scale = "small and medium-sized," and the enterprise type II is "domestic-funded enterprise," then there have been many records of violations of laws and disciplines in the year

(2) If the industry category = "wholesale and retail industry" and the area 2 is "Wuhua District," the enterprise size is "small" or "small and medium-sized," and the enterprise type = "individual industrial and commercial households," then there are many records of violations of laws and disciplines in the year.

(3) If the industry category = "service industry" and the second district is "Panlong District" and the enterprise scale = "small-scale" or "small and medium-sized," and the SME type 2 is "individual industrial and commercial households," there are many illegal law enforcement records in this year.

(4) If the industry category = "financial industry" and the area = "Panlong District," and the enterprise scale = "small and medium-sized" or "large," and the enterprise type = "foreign-funded enterprise" or "domestic-funded enterprise," then there are few annual records of violations of laws and disciplines.

There are many technologies that can improve the decision tree problem, such as discrete attribute values and fixed intervals, multivalue deviation optimization based on attribute criteria, and optimal filling of vacant attributes. This paper is based on the data features and mining processes of industrial and commercial systems and realizes the system design through the feature selection criteria in C4. In the five operations, the message gain or message gain value of each characteristic must be counted, and the largest one must be selected as the node characteristic. As can be seen from equations (8) and (9), the value of the category information of the data sample is fixed, and in order to make the information gain larger, the information (, that is, the abstract category condition information) is required.

$$\text{Info}(S_j) = -\sum_{i=1}^{m} \frac{|S_{ij}|}{|S_j|}\log_2\frac{|S_{ij}|}{|S_j|}. \tag{8}$$

After the dataset is divided by attribute V, its category conditional information entropy is

$$E(V) = \text{Info}\left(\frac{C}{V}\right) = \sum_{j=1}^{k}\frac{|S_j|}{|S|}\text{Info}(S_j). \tag{9}$$

After introducing the user attention, the product of the category condition information entropy and the user attention are taken as the new information entropy, so we can get the equation as follows:

$$E'(V) = -\sigma_V\sum_{j=1}^{k}\frac{|S_j|}{|S|}\text{Info}(S_j). \tag{10}$$

RETRACTED

Table 2: Performance comparison of C4.5 algorithm before and after improvement.

	Algorithm operation time(ms)	Number of valid classification rules	Number of invalid classification rules	Efficiency (%)
Original C4.5 algorithm	10	124	17	87.9
Improved C4.5 algorithm	10	138	3	97.9

It is obvious that in the business management data, the improved C4.5 algorithms have better mining efficiency. In addition, it can also be found in Table 2 that, like the original algorithm, the improved C4.5 algorithms have no difference in execution time, and the validity of mining results is also significantly improved. Therefore, after testing and confirmation, the improved C4.5 algorithms are obviously better than the original C4.5 algorithm.

4. Experimental Results and Analysis

According to the distribution model constructed in this paper, the optimal logistics distribution path is simulated using a 1.4 GHz quad-core Intel Corei5 with a running memory of 8 GB, and the simulation platform is MATLAB2020a. The simulation process and market composition are shown in Figure 4 .

This paper uses the customer point scale of 50 as an example, assuming that a distribution center has 25 distribution vehicles, the number of subjects to be served is 50, the maximum load of no logistics vehicle is 20t, and the consumption cost is 500 yuan/day/vehicle. The earliest time of the logistics distribution service is at 6 : 00 in the morning and the latest is at 8 : 00. The maximum working time of logistics personnel is 8 hours, and overtime pay will be provided for more than 8 hours. According to customer needs, the delivery time is set, and penalties will be incurred whether overtime or in advance.

In order to verify whether the method designed in this paper is effective, the traditional planning method is compared with the planning method designed in this paper. When the number of customers is 25, the path change is shown in Figure 5.

As shown in Figure 5, the traditional method has the optimal path when the number of iterations is 80, while the planning method designed in this paper achieves the optimal path when the number of iterations is 20. Compared with the traditional method, the method designed in this paper is significantly less time-consuming. Based on this, when the client is 50, the path changes as shown in Figure 6.

As shown in Figure 6, when the number of customers reaches 50, the traditional method achieves the optimal path when the number of iterations is 90. The planning method designed in this paper achieves the optimal path when the number of iterations is 60. It can be seen that no matter whether the number of customers is large or small, the method designed in this paper can reduce the time in the process of optimal path planning and then achieve the goal of optimal path planning, which is in line with the research purpose of this paper.

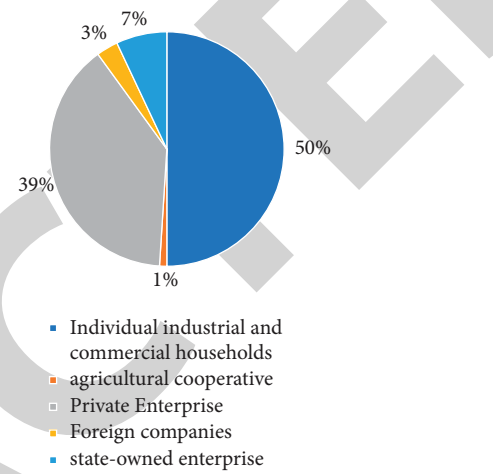

Figure 4: Statistical chart of business administration data: composition and distribution of market players.

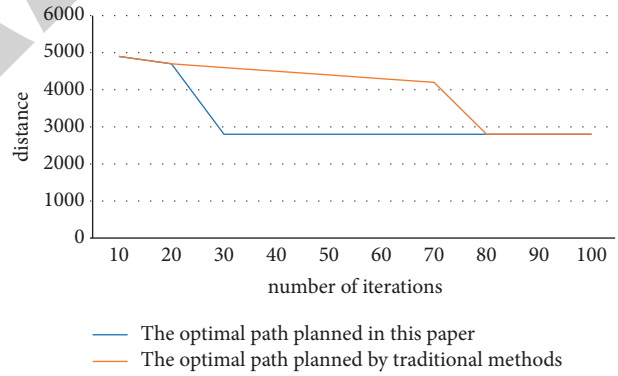

Figure 5: The path change diagram of the two methods.

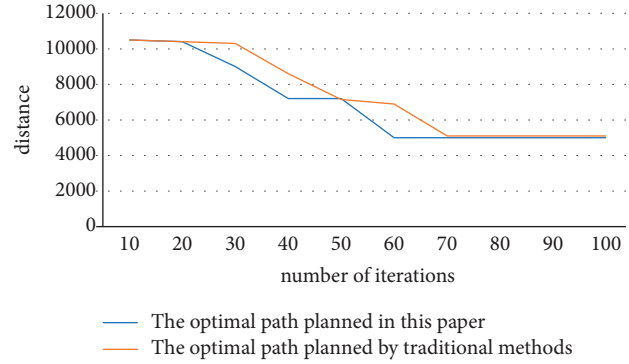

Figure 6: The path change diagram is improved by the two methods.

RETRACTED

Table 3: Discretization of enterprise types.

Enterprise type name	Discretized value
Individual business	0
Domestic company	1
Domestic subsidiaries	1
Domestic enterprise legal person	1
Domestic enterprise group	1
Private company	2
Private branch	2
Sole proprietorship	2
Enterprise of individual partnership	2
Private enterprise group	2
Foreign funded enterprise group	3
Foreign-invested enterprise	3
Resident representative offices of foreign (regional) enterprises	3
Branches of foreign-funded enterprises	3
Foreign invested cooperative enterprise	3
Consumer goods market	4
Capital goods market	4
Production factor market	4

Table 4: Grade transformation of enterprise scale.

Number of employees (E) and total assets (M)	Enterprise scalejavascript: void (0)
$0 < E < 20$ and $0 < M < 300$	1
$20 < E < 300$ and $300 < M < 4000$	2
$300 < E < 1000$ and $4000 < M < 40000$	3
$E > 1000$ and $M > 40000$	4

Table 5: Hot modules of Supply Chain Management Research.

Hot topics	Cluster label
Concept and theory development	#1 sustainability,#4 green supply chain management, #9 green supply chain
Practice and measurement indicators	#7 reverse logistics,#5 carbon emissions
Drivers and barriers	#0 barriers,#10 environmental management
Cooperation with supply chain partners	#3 green supplier selection,#6 game theory, #8 optimization
Performance evaluation	#2 food waste, #11 performance measurement

In the original data set, some feature data of a sample will be lost, and the missing values need to be filled. The most common method to deal with missing attribute values is to assign attribute values to attributes in the training instance relative to the node IV, which is most commonly used. The training result fragments after the generalization of the data set are shown in Figure 3. This data set will include data from 2011 to 2021. Based on the time sequence of the results in the training set, we will use the results of 2011 and 2021 as the exercise data, and the results of 2021 as the test data. See Table 3.

The data from 2011 and 2021 will be used for training data, while the data from 2021 will be used for testing data. The data scale for each year is shown in Table 4.

After these operations, the original data obtained is still in the processing state of 0.5, which is not intuitive. Therefore, in the data mining process, the attribute classifications using these data are still very cumbersome. Therefore, it is necessary to summarize the original data. The most common way is to normalize the data, including minimum-maximum normalization, decimal scaling normalization, and zero mean normalization. In the above methods, the continuous value is reduced to a fixed range by a certain ratio.

The 12 clusters and their related keywords were combined to sort out five research hotspot modules in this field, namely concept and theoretical development, practice and measurement indicators, driving factors and obstacles, cooperation with supply chain partners, and performance evaluation, as shown in Table 5.

In order to stabilize the status of the industry and give full play to the dominance of the industry, enterprises should integrate network information technology in the process of enterprise business management to promote and improve the overall management level of the enterprise. Enterprises should pay close attention to the current situation of industry development, build a high-quality network information and chemical business management environment, start by raising the awareness of managers, establish a sound business management system, strengthen the introduction

RETRACTED

and training of information talents, improve network information security systems, and constantly learn from advanced enterprise management experience and innovative business management modes, using the system to constrain the normative operation of each department and each production link, to ensure the scientificity and effectiveness of the enterprise network information and chemical business management system, and to promote the realization of the enterprise's strategic development goals.

5. Conclusion

Due to the realization of electronically registered residence, the current database service system has defects in in-depth data analysis, and it is very difficult to obtain useful policy data. It is urgent to develop a new generation of big data analysis systems with multimedia visualization. As a new force in the field of big data analysis and application, supply chain data management has increasingly shown its good ability and practicability. It has been widely used in many fields, showing a wide range of use and strong social and cultural significance. This paper extracts some enterprise data from the database of an enterprise management system. To complete the visualization work more efficiently, we must extract, process, and transform the data to improve the visualization efficiency. Through the Java language and three related open-source architecture methods, an effective enterprise business management information visualization system is established. At the same time, the application results are further introduced, and an application case in the market and entity development trend is obtained.

Data Availability

The labeled data set used to support the findings of this study is available from the author upon request.

Conflicts of Interest

The author declares no conflicts of interest.

Acknowledgments

This work was supported by the School of Economics and Trade, Henan Polytechnic Institute.

References

[1] F. Korfmann, S. Müller, S. Ehlert, and K. Haase, "Students' perceptions, academic departments' image, and major-choice in business administration studies—the example of Hamburg Business School," *Higher Education Quarterly*, vol. 75, no. 1, pp. 51–76, 2021.

[2] L. Gao, "Relationship between business administration ability and innovation ability formation of university students based on data mining and empirical research," *Mobile Information Systems*, vol. 2021, no. 18, Article ID 2388579, 8 pages, 2021.

[3] C. L. D. Leon, J. C. Mina, and E. G. Vitug, "Trailing the gap between the competencies of bachelor of science in business administration graduates with industry demands: as viewed by the employers," *Open Access Library Journal*, vol. 8, no. 12, p. 22, 2021.

[4] N. Almufleh and S. Alkhatib, "Supply chain practices and operational performance: an analytical study of the 5-star hotels operating in Jordan," *Jordan Journal of Business Administration*, vol. 19, no. 1, pp. 7–9, 2021.

[5] N. Hamed, F. Mohammad, and S. J. Agnieszka, "Analysis of security criteria for IoT-based supply chain: a case study of FMCG industries," *Journal of Management and Business Administration. Central Europe*, vol. 29, no. 08, pp. 81–83, 2021.

[6] M. J. Chileshe and J. Phiri, "The impact of supply chain management practices on performance of small and medium enterprises in developing countries: a case of agro-dealers in Zambia," *Open Journal of Business and Management*, vol. 10, no. 02, pp. 591–605, 2022.

[7] A. Chaudhuri, A. Ghadge, B. Gaudenzi, and S. Dani, "A conceptual framework for improving effectiveness of risk management in supply networks," *International Journal of Logistics Management*, vol. 31, no. 1, pp. 77–98, 2020.

[8] M. A. Cohen and P. C. Rogers, "When sino-American struggle disrupts the supply chain: licensing intellectual property in a changing trade environment," *World Trade Review*, vol. 20, no. 2, pp. 238–257, 2021.

[9] V. D. Gerami and I. G. Shidlovskii, "Inventory optimization considering the vehicle capacity and specifics of cash flows at rental storage sites," *Management and Business Administration*, vol. 12, no. 2, pp. 77–90, 2020.

[10] G. C. Dawaton, "Assessment of the on-the-job training program of business administration students of kalinga state university," *Universal Journal of Management*, vol. 9, no. 1, pp. 13–19, 2021.

[11] A. N. Lunkin and D. A. Lunkin, "Mining and metallurgical business: technological and integration features of management," *Management and Business Administration*, vol. 20, no. 1, pp. 50–63, 2021.

[12] N. S. Vargas, D. A. G. Gómez, and O. R. Romero, "Marketing for business opportunities management on foreign investment and productive enchainments," *Studies on Entrepreneurship, Structural Change and Industrial Dynamics*, vol. 17, no. 4, pp. 29–31, 2021.

[13] S. G. Chen, "The new attempt of network reliability in the assessment of business activities for precision management," *Springer Series in Reliability Engineering*, vol. 30, no. 3, pp. 1001–1010, 2022.

[14] K. O'Brien, S. Sood, and R. Shete, "Big data approach to visualising, analysing and modelling company culture: a new paradigm and tool for exploring toxic cultures and the way we work," *International Journal of Management Science and Business Administration*, vol. 20, no. 3, pp. 790–799, 2022.

[15] D. Gil-Doménech, N. Magomedova, E. J. Sánchez-Alcázar, and M. Lafuente-Lechuga, "Integrating sustainability in the business administration and management curriculum: a sustainability competencies map," *Sustainability*, vol. 13, no. 16, pp. 9458–9487, 2021.

[16] L. Battle and C. Scheidegger, "A structured review of data management technology for interactive visualization and analysis," *IEEE Transactions on Visualization and Computer Graphics*, vol. 40, no. 11, pp. 354–356, 2020.

[17] N. Nasrallah, O. F. Atayah, R. El Khoury, A. Hamdan, and S. Obaid, "Intellectual structure of knowledge management: a bibliometric analysis of the journal of information and knowledge management," *Journal of Information and Knowledge Management*, vol. 21, no. 01, pp. 679–698, 2022.

RETRACTED

Hindawi
Journal of Robotics
Volume 2023, Article ID 9789505, 1 page
https://doi.org/10.1155/2023/9789505

Retraction

Retracted: Discussion on Redundant Processing Algorithm of Association Rules Based on Hypergraph in Data Mining

Journal of Robotics

Received 8 August 2023; Accepted 8 August 2023; Published 9 August 2023

Copyright © 2023 Journal of Robotics. This is an open access article distributed under the Creative Commons Attribution License, which permits unrestricted use, distribution, and reproduction in any medium, provided the original work is properly cited.

This article has been retracted by Hindawi following an investigation undertaken by the publisher [1]. This investigation has uncovered evidence of one or more of the following indicators of systematic manipulation of the publication process:

(1) Discrepancies in scope
(2) Discrepancies in the description of the research reported
(3) Discrepancies between the availability of data and the research described
(4) Inappropriate citations
(5) Incoherent, meaningless and/or irrelevant content included in the article
(6) Peer-review manipulation

The presence of these indicators undermines our confidence in the integrity of the article's content and we cannot, therefore, vouch for its reliability. Please note that this notice is intended solely to alert readers that the content of this article is unreliable. We have not investigated whether authors were aware of or involved in the systematic manipulation of the publication process.

Wiley and Hindawi regrets that the usual quality checks did not identify these issues before publication and have since put additional measures in place to safeguard research integrity.

We wish to credit our own Research Integrity and Research Publishing teams and anonymous and named external researchers and research integrity experts for contributing to this investigation.

The corresponding author, as the representative of all authors, has been given the opportunity to register their agreement or disagreement to this retraction. We have kept a record of any response received.

References

[1] J. Zhu, "Discussion on Redundant Processing Algorithm of Association Rules Based on Hypergraph in Data Mining," *Journal of Robotics*, vol. 2022, Article ID 1007464, 9 pages, 2022.

Hindawi
Journal of Robotics
Volume 2022, Article ID 1007464, 9 pages
https://doi.org/10.1155/2022/1007464

Research Article

Discussion on Redundant Processing Algorithm of Association Rules Based on Hypergraph in Data Mining

Jintan Zhu

School of Electronic Information, Xi'an Railway Vocational and Technical College, Xi'an City, Shaanxi Province 710014, China

Correspondence should be addressed to Jintan Zhu; zjt_19810513@163.com

Received 15 July 2022; Revised 18 August 2022; Accepted 23 August 2022; Published 16 September 2022

Academic Editor: Shahid Hussain

Copyright © 2022 Jintan Zhu. This is an open access article distributed under the Creative Commons Attribution License, which permits unrestricted use, distribution, and reproduction in any medium, provided the original work is properly cited.

With the rapid advancement of big data, it is becoming a great problem for people to find objective information in the database. The relevance data processing rule for digging the information can be the way. Relevance data processing rule for digging the information is mainly studied in three aspects: data dimension, data abstraction level, and processing variable type. In the aspect of rules, the research mainly focuses on three aspects: active relationships, passive rules, and uncommon relationship rules. Association rules of digging the data can be the most well-employed investigation goal and aim for the data digging. Along with the advancement of the information scale, the time rate of traditional relationship rules exploration of counting ways is too low. How to increase the time rate for the way of counting is the main research content of relevance data processing rules for digging the information. Current relevance data processing rules for digging the information have two limitations: (1) metrics such as support, confidence, and lift rely too much on expert knowledge or complex adjustment processes in value selection; (2) it is often difficult to explain rare association rules. Based on the existing research, this paper proposes a Markov logic network framework model of association rules to address the above shortcomings. The theory of a hypergraph and system is proposed, and the method of a hypergraph in 3D matrix modeling is studied. Aiming at the new characteristics of big data analysis, a new super edge definition method is introduced according to the definition of the system, which greatly enhances the ability to solve problems. In the cluster analysis and calculation of hypergraph, this paper will use the hypergraph segmentation operator hMETIS to carry out the cluster analysis method in order to achieve higher accuracy in cluster analysis and calculation. As for the test of cycle ones, which is in line with the relevance of the hypergraph with clear directions, the thesis will offer a brand-new way to make an analysis and turn the rule of relevance into the hypergraph with clear directions with a new definition of the near linking matrix, and it will change the dealing way from the test of the cycle and more ones into the linking *f* bricks and circles, which is a new way to explore. This paper uses two datasets of different sizes to conduct rule prediction accuracy experiments on the Markov logic network framework model algorithm of association rules and the traditional association rule algorithm. The results show that compared with the traditional association rule algorithm, the rules obtained by the Markov logic network framework model of association rules have a higher prediction accuracy.

RETRACTED

1. Introduction

Since the 21st century, Internet technology and computer hardware technology have developed rapidly and become popular [1]. The data stock of the Internet has increased exponentially, but there are only a handful of data containing valuable information [2]. Therefore, mining valuable information from massive data has changed into the most essential factor or the content in society at present [3]. For the old and ancient dataset digging information skills, the relationship rules which are unseen from the data will be analyzed with an effective rate, what is more, the result of the old-fashioned data digging skills and it will cause the results of massive data because it cannot predict the things happened in the long future [4]. The appearance of the AI will give more skills to the information-digging process. And the big process will be the digging of the data information, which has created the message of big data [5]. At present, data mining has an important application value in many aspects. By describing the existing data, it can effectively predict the

future pattern of the data. Data mining technology has become a promising research direction in today's world. Data mining technology has been applied in scientific research, production process monitoring, quality management, decision support, and design.

The Internet, the Internet of Things, cloud computing, and other information technologies are constantly updated, and they are constantly integrated with the human world in various fields such as economy, politics, military, scientific research, and life [6]. Information visualization is the use of images to express information clearly and effectively. The image representation can be used to find the original data and the information relationship that cannot be observed. Data visualization can enhance users' understanding of multidimensional and large-scale information and plays an important role in the discovery, determination, and understanding of association rules. As a major information discovery and pattern recognition technology, the association processing law of mining data is to find the most meaningful information that can be described. The visualization of association rules is an inseparable subset of association rule theory. Its main task is to display information and help users further grasp the rules of association processing in order to discover the information results [7].

Data mining can discover the hidden laws in the data and effectively exert the value of the data [8]. The relevance data processing rule for digging the information can extract potential and valuable frequent patterns or correlations between attributes from the data [9]. Frequent patterns and correlations can be displayed clearly and intuitively in the form of text, but due to the limited cognitive ability of users, the value of relevant data processing rules for digging the information cannot be fully reflected [10]. Therefore, it is urgent to study the visualization method of association rules in depth, combined with human-computer interaction technology, to help users analyze and process data resources from multiple perspectives, gain insight into valuable information, and support their decision-making and planning [11].

The hypergraphs are widely used in many fields of information science. In the past, information visualization technology and visual data analysis technology mainly focused on analyzing simple binary signals inside data objects [12]. However, studies have shown that multiple associations can more naturally represent the sum pattern of internal connections implicit in signals [13]. A Hypergraph is a generalization of ordinary topological relations and can be easily expressed as multiple relations [14]. This also provides strong conditions and theoretical support for the visualization of association rules. The hypergraph model combines the characteristics of hypergraphs and multidirectional graphs and can visually describe association rules. In the graph, nodes represent data items and edges represent association relationships. The support and reliability of rules can also be described in different ways and with different values. Therefore, the intuitive display of multirelationships by the hypergraph provides strong theoretical support for further in-depth research on visualization methods of frequent item sets and association rules.

2. State of the Art

2.1. Data Mining Overview and Research Status. In 1990, the first KDD International Seminar was held in Detroit, USA. Since then, people have shown interest in data mining terminology [15]. Information is used by people to describe specific events in actual society. This is an abstract description of the information. With the development and progress of the times, there are more and more aspects of human exploration, and digital has become a tool to support human exploration. Indispensable means that due to the development of science and technology, human beings are exploring the physical universe more and more extensively, which makes the range of numbers more and more extensive, and the complexity of data is rapidly increasing [16]. In this case, people can no longer find hidden laws through simple logical reasoning. Therefore, people began to pay attention to the importance of data and eagerly hoped to find the value and meaning hidden behind the data. It is precisely to meet this demand that data mining technology was born. Mining, also known as information mining, is the process of discovering potential, meaningful, and interesting things from a large amount of incomplete and noisy information stored in large transaction databases or data warehouses. The information mined can often help us to conduct in-depth exploration. Of course, it is not a knowledge exploration method that can retrieve information at any time. Therefore, through the search engine to find the web pages and search databases that you are interested in, records cannot become knowledge discovery. These methods are only looking for information that meets specific conditions, but they do not explore the things behind big data. Data mining is not a panacea. That is, what is found in large transaction databases is not always correct or valuable [17]. This needs to meet special commercial conditions. People study business and do statistical analysis. Under these premises, the use of information mining is more likely to mine valuable and instructive messages [18].

In the procedure of digging the data will be decided by requests from businesses and data features [19]. But it will be classified as the changing data, preprocessing of data, data mining, and knowledge assessment steps. The pre-processing of data will deal with the data and transform it. It costs a lot of time to deal with the data [20]. The image of the data preprocessing process is shown in Figure 1.

Data mining technology originally came from abroad, but its research and development direction are varied. At present, the most common way to deal with analysis problems is decision tree induction. The corresponding calculation methods are C4. 5 calculation, ID3 algorithm, ID4 algorithm, IDS algorithm, and quest calculation. Complex structured data learning, the slio algorithm, the sprint algorithm, and "rainforest" calculations are used for building a decision tree. Both emphasize the establishment of a decision tree with scalability. The decision tree pruning algorithm includes cost complexity pruning, error reduction pruning, and pessimistic evaluation pruning. Some methods, such as Bayesian classification, the back propagation algorithm, the neural network

RETRACTED

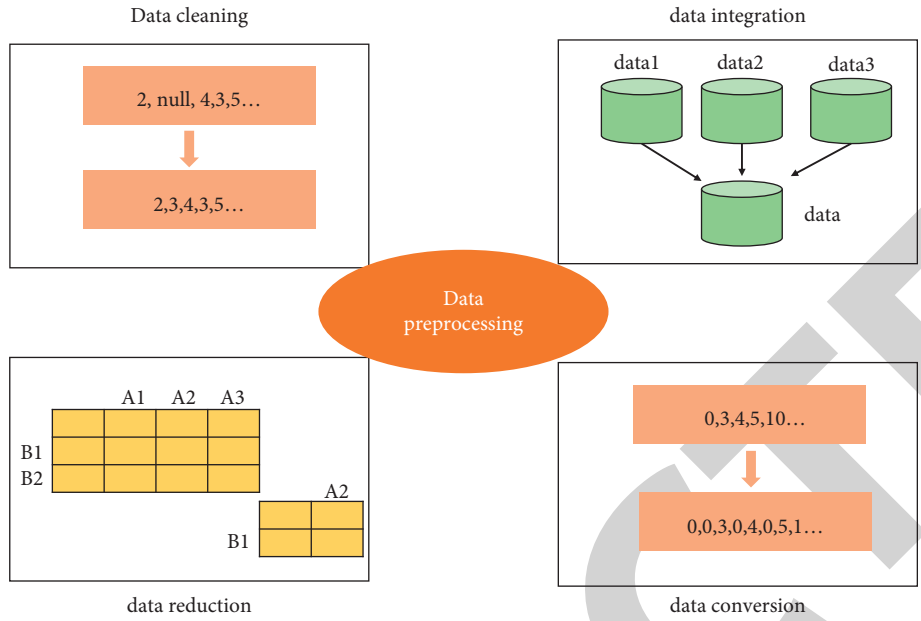

Figure 1: Data preprocessing process.

method, the machine learning method, the CAEP classification method, and the rough set method, are all applied to analysis and data mining. There are also many data mining techniques and methods to deal with data clustering. Common systems divide clustering methods into the k-means method and the basic condensed hierarchical clustering method. DBSCAN is a clustering algorithm based on density, while optics is a clustering algorithm based on density.

2.2. Research Status of Association Rules. Up to now, large-scale exploration has been carried out in the field of data mining, but the research in the field of data mining is still popular. That is, although the current mining method is quite perfect, its data mining efficiency is very low in the face of large-scale information. The result is not ideal. Therefore, the information accumulated by the network e-commerce industry is extremely rich and complicated, resulting in a large number of useless bits of information and garbage materials. For such a large amount of information, the preprocessing steps of data mining will be very difficult. Once the pretreatment is poor, the whole mining process may even fail. At the same time, although the preprocessing process is relatively smooth, conventional mining methods may not obtain valuable and meaningful data in a large number of databases, even if the mined data are useless and meaningless. All these show that there are still many problems in data mining. Considering the differences in the main research directions and mining methods of data mining, there are still many challenging research topics in the field of data mining applications. These topics are closely linked, mainly involving information fusion technology of information discovery and data warehouses, visual data mining, super large-scale data mining of complex types, network data mining, and network security technology. The visualization technology of a two-dimensional matrix is usually used to represent the features on the bar graph. The items in the front part and the rear part are arranged on two axes in turn. The width and color of the bar in turn represent the support and confidence, as shown in Figure 2.

2.3. Hypergraph Overview. A hypergraph is a subset system of a finite set, which is a generalization of graph theory and plays a very important role in discrete mathematics. The term "hypergraph" was first proposed by Berge in the monograph "Hypergraphs" in 1966. The original purpose was to promote some classical results in graph theory. Later, people gradually realized some theorems in graph theory. It can be generalized in the unified form of a hypergraph, thus opening the prelude to the study of hypergraph theory, making it a huge new branch of graph theory. Compared with the study of general graphs, the study of hypergraphs is more complicated. Some important structures and properties in general graphs no longer exist in hypergraphs, which complicates the discussion of many similar problems in graph theory. At present, hypergraphs have been widely used in circuit division, knowledge representation and organization methods, cellular communication systems, and the representation of molecular structures of atypical compounds and polycyclic conjugated molecules. There are two types of hypergraphs: directed hypergraphs and undirected hypergraphs. Since the 1960s, after decades of unremitting efforts, the development of hypergraph theory has made great progress.

A hypergraph is a binary pair $H=(V, E)$, where $V=\{v_1, v_2, v_3, \ldots v_n\}$, denotes the n vertices of the hypergraph, and $E=\{e_1, e_2, e_3, \ldots e_n\}$, denotes the m hyperedges of the hypergraph. A hyperedge set E is a subset defined on a vertex set V, that is $\forall e_j \subseteq V, \quad j=1, 2, \ldots m$, and satisfies

RETRACTED

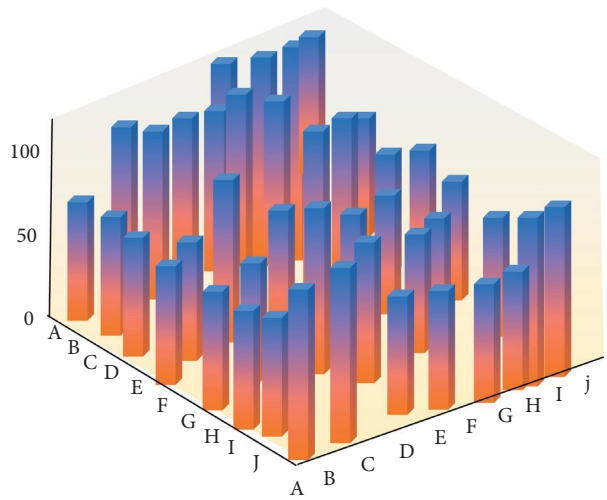

Figure 2: Visualization is based on a two-dimensional matrix.

$$e_j \neq \varnothing, \quad j = 1, 2, \ldots m,$$
$$\sum_{i=1}^{m} e_j = V. \tag{1}$$

The size of a graph is generally uniquely determined by the number of vertices N and the number of super edges M. In hypergraph, its size also depends on the cardinality of each super edge. We can define the size of a hypergraph as the cardinality of each hyperedge, and it is given using the following equation:

$$\text{size}(H) = \sum_{e_i \in E} |e_i|. \tag{2}$$

As an important branch of hypergraph theory, directed hypergraph theory has not been studied deeply for a long time, and the results are relatively small. The foreign paper that has a far-reaching impact on the development of directed hypergraph theory is directed hypergraph and its application by Giorgio Gallo. Here, the author systematically summarizes the previous achievements in the field of directed hypergraphs. In China, based on the demand for electrical engineering and automation research, Professor Huang has provided another new way to describe directed hypergraphs and has done relevant research work on this basis. Similar to the theoretical study of undirected graphs and directed graphs, directed hypergraphs add directions to the super edges in undirected hypergraphs, and then describe the arrangement of the vertices of the super edges. On this basis, we introduce some properties of undirected hypergraph into directed hypergraph and find the special properties of directed hyper-tree. Of course, the main purpose of studying directed hypergraphs is to solve problems in practical applications. In this paper, people try to describe the relevant laws through the directed hypergraph and solve the redundancy and circulation problems in the relevant data processing rules by using the attributes in the directed hypergraph, and mining information.. Figure 3 is a representation of a directed hypergraph H.

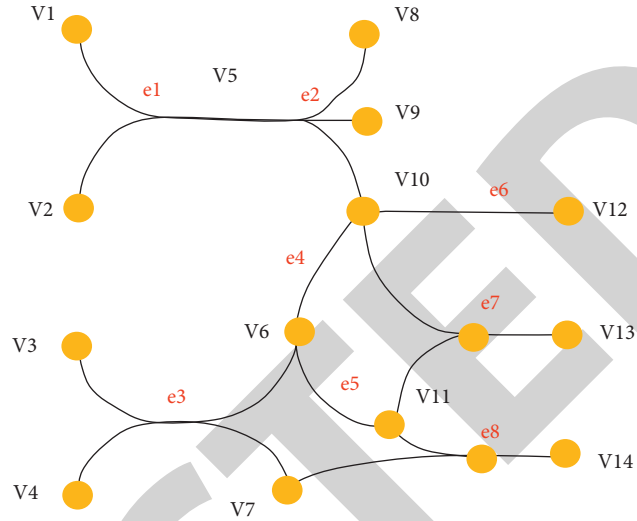

Figure 3: Representation of a directed hypergraph H.

A directed hypergraph is $\overline{H} = (V, E)$, V is the vertex set, and E is the directed hyperedge set. Its adjacency matrix is given as follows:

$$A = \begin{pmatrix} a_{11} & \cdots & a_{1n} \\ \vdots & \ddots & \vdots \\ a_{n1} & \cdots & a_{nn} \end{pmatrix}, \tag{3}$$
$$a[i, j] \in \{0, 1, 2, \ldots\ldots\},$$

aij represents the number of directed hyperedges from the start point 1 to the end point 1, where v_i and v_i are the vertices of $\overline{H} = (V, E)$.

Like an undirected hypergraph, the size of a directed hypergraph is defined as the sum of the cardinality of each super edge, and the rank (low rank) is also defined as the largest (small) multiple of the cardinality of each super edge. However, it is difficult to form a one-to-one correspondence between the adjacency matrix and other matrices in a directed hypergraph due to the characteristics of clusters in the hypergraph itself. People can also understand that the directed hypergraph corresponds to the adjacency matrix, but people cannot uniquely recover the original directed hypergraph from the adjacency matrix. Therefore, how to reduce these factors is also an important topic in the study of directed hypergraph theory.

3. Methodology

3.1. Relevance Data Processing Rule for Digging the Information Process. The purpose of a relevance data processing rule for digging the information is to find some credible rules from massive data. These rules usually have potential value and significance and can help enterprise managers analyze the current market situation and make correct decisions. The relevance data processing rule for digging the information system searches for association rules based on two minimum thresholds, which are the minimum support threshold min sup and the minimum confidence threshold min conf, which

RETRACTED

can usually be specified by the user. The relevance data processing rule for digging the information work is mainly divided into two stages: (1) Find all item sets not less than the minimum support threshold min_sup, that is, frequent sets; (2) For each frequent set, find not less than the minimum confidence threshold. Association rules for min_conf. The process of mining association rules in stage 2 is as follows: there is a frequent set L. For any proper subset $L' \subset L, L' \neq \varnothing$ in the itemset L, if Support (L)/Support (L') 2 min_conf, the association rule $L' \Rightarrow L - L'$ is a credible rule.

The following uses an example to illustrate the specific process of relevance data processing rules for digging the information. Suppose all items in database D constitute an itemset, and all records in transaction database D are shown in Table 1:

Looking at Table 1, it is easy to calculate all 1-, 2-, 3-, and 4-item sets. The four item sets and their corresponding support information are shown in Table 2.

Given two thresholds, support threshold min_sup = 30% and confidence threshold min_conf = 70%, then, according to Table 2, all frequent sets have {*a*}, {*b*}, {*c*}, {*d*}, {*a*, *b*}, {*a*, *c*}, {*a*, *d*}, {*c*, *d*}. For each frequent set whose number of item sets is greater than 1, association rules can be mined from it. For example, two rules {*a*} = {*b*} and {*b*} > {*a*} can be mined from the frequent set {*a*, *b*}. Examining each such frequent item set, we can get all the association rules as shown in Table 3:

Since the confidence threshold min_conf = 70%, according to Table 3, all the strong association rules have {*a*} = {*b*} and {*b*} = {*a*}. At this point, the mining of association rules is over.

3.2. Apriori Algorithm. The Apriori algorithm is the most classic algorithm for relevance data processing rules for digging the information. The algorithm is easy to understand in the principle of the algorithm, and concise and convenient in the realization of the algorithm. The principle of the Apriori algorithm is that the more times the two items appear in pairs in the transaction data, the greater the correlation between the two items, and the two items are items with a strong correlation. The implementation process of the Apriori algorithm needs to scan the database multiple times. The first scan counts the number of occurrences of each item in the data and deletes some items that do not meet the minimum support requirements. Before the second scan, the items obtained from the first scan should be combined in pairs. Then, the second scan of the data is performed to count the occurrences of the combination, and some combinations that do not meet the minimum support are deleted. After that, the combination and scan are repeated until no new combination is generated, and the implementation process of the Apriori algorithm ends. Figure 4 below shows the implementation process of the Apriori algorithm when the minimum support is 0.2.

3.3. The Redundant Processing Method of Association Rules Based on Hypergraph. The rule dug up from the relationship rule will include some projects that users do not need. Or it is in line with the information that users are familiar with, or it gets the same rule table that expresses the same meaning. Such rules will not bring more messages to users or offer any effective help. In most cases, the number of the redundant rule is larger than the meaning rule numbers.

Table 1: Transaction database D.

TID	Phase set
T011	a, *b*, *c*
T021	a, *c*, *d*
T031	a, *b*
T041	c, *d*
T051	*a*, *b*, *d*

Table 2: All item sets and support.

Item sets	Support (%)
{*a*}	88
{*b*}	65
{*c*}	65
{*d*}	65
{*a*, *b*}	65
{*a*, *c*}	48
{*a*, *d*}	45
{*b*, *c*}	21
{*b*, *d*}	20
{*c*, *d*}	45
{*a*, *b*, *c*}	25
{*a*, *b*, *d*}	25
{*b*, *c*, *d*}	25
{*a*, *b*, *c*, *d*}	0

Table 3: All association rules.

Association rules	Confidence (%)
{*a*} {*b*}	77
{*b*} {*a*}	90
{*a*} {*c*}	55
{*c*} {*a*}	65
{*a*} {*d*}	51
{*d*} {*a*}	65
{*c*} {*d*}	65
{*d*} {*c*}	66

Redundancy rules can generally include two types: one is subordinate tone rules. For example, the conclusion of rule Xi is consistent with that of XJ, and the premise of Xi meets the sufficient condition for the existence of XJ, that is, XJ is redundant. Therefore, repetition rules are also regarded as subordinate rules. Special circumstances. The second is the repeated path principle. If there are selectors Xi and XJ in the rule base at the same time, and there must be two paths between Xi and XJ, the principle of redundancy can be judged.

The subordination principle can be expressed by the following formula (4):

$$\begin{cases} X_2 & \longrightarrow & X_4, \\ X_2X_3 & \longrightarrow & X_4. \end{cases} \tag{4}$$

RETRACTED

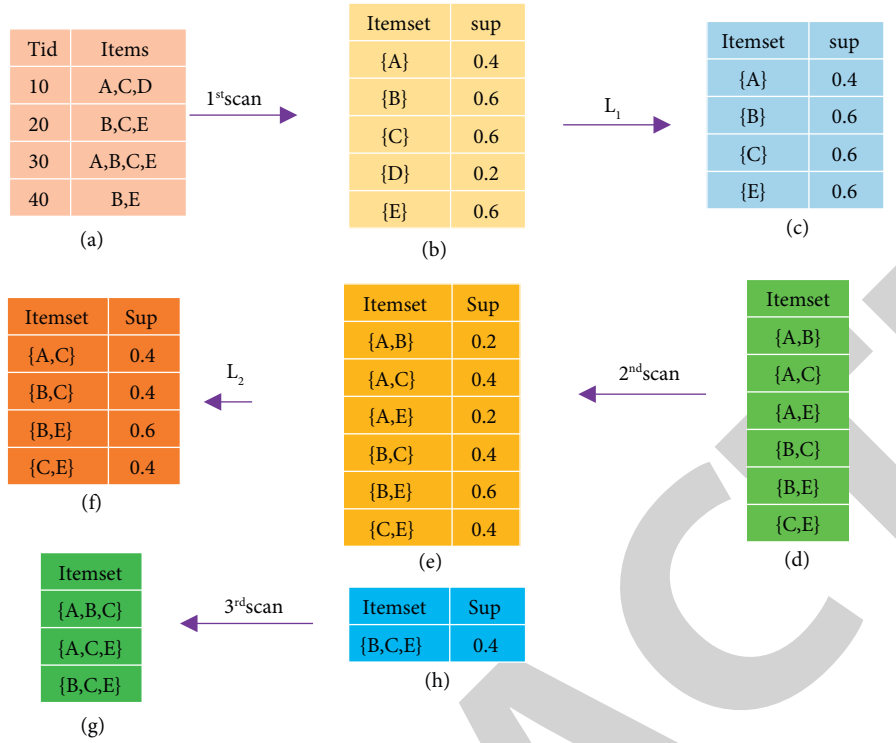

Figure 4: Example diagram of the mining process of the Apriori algorithm.

The repeating path rule can be expressed by the following given formula:

$$\begin{cases} X_1 \longrightarrow X_2X_3 \longrightarrow X_4, \\ X_1 \longrightarrow X_5 \longrightarrow X_4. \end{cases} \tag{5}$$

The adjacency matrix in a directed hypergraph completely illustrates the adjacency problem between nodes of a graph. In the directed hypergraph based on association rules, the association between the checked items and the association rules can be expressed by the adjacency matrix. Based on the concept of redundancy rules in circuit science and its related characteristics, the redundancy checking method can be realized on the basis of the directed hypergraph.

$$\text{design } G = (V(G), E(G)). \tag{6}$$

Its path is a finite, nonempty sequence, and it is given as following:

$$W = v_0e_1v_1e_2 \ldots e_kv_k. \tag{7}$$

That is, the staggered sequence of vertices and edges, where $e_i \in E(G)$, $v_j \in V(G)$, e are associated with V_{i-1}, v_i, respectively, $1 \le i \le k, 0 \le j \le k$ is denoted as (v_0, v_k) path, and the vertex v_0, v_k is called the starting point and end point of the path W, respectively. It is called a path $v_1, v_2, \ldots, v_{k-1}$ is the inner vertex of W, k will be named the long W.

From the graph theory, the procedure of dealing with the redundant ones with the hypergraphs into the linking bricks and also it will change it into formative tress, because every line in the hypergraph represents a linking rule. When the linking picture will become the formative trees, we need remove it, and this line is the redundant rule.

Given a hypergraph is as follows:

$$\begin{aligned} H &= (X), \\ X &= \{X_1, X_2, \ldots\ldots, X_n\}, \\ E &= \{E_1, E_2, \ldots\ldots, E_m\}. \end{aligned} \tag{8}$$

If H is connected and does not contain any hyperloops, then H is called a hyper-tree.

4. Result Analysis and Discussion

4.1. Model Establishment. In the Markov logic network, this paper regards the items in the transaction dataset as nodes in the Markov logic network. In this way, the weight between the two nodes can be regarded as the degree of association between the two items. In the Markov logic network, adding weights to the rules is adopted so that the knowledge base of the first-order predicate logic is not so rigid. The higher the weight value attached to the rule, the greater the restriction on each group in the Markov logic network. When the weights of all rules in the knowledge base are infinite, the Markov logic network is the same as the standard one. The logical reasoning framework for order predicates is the same.

To obtain the parameter value in the data, adjust the value of the data. The most common way to deal with modulus problems, such as infinite numbers, is the step reduction method. In computer mathematics, the ladder lowering methods generally include batch ladder lowering, small batch ladder lowering, random gradient lowering, and batch ladder lowering. The batch ladder lowering method is to calculate the lowest point (or the highest point along the

RETRACTED

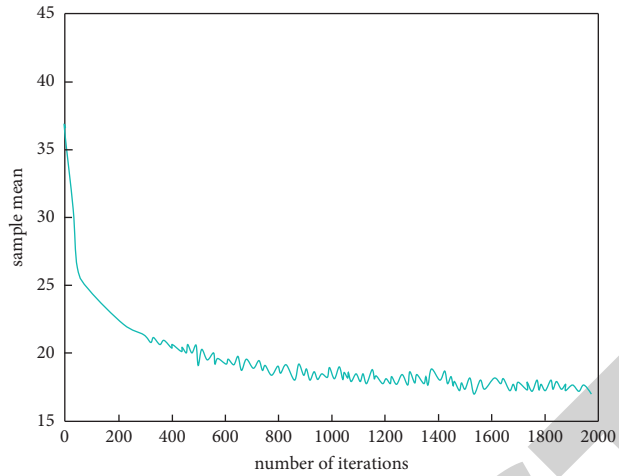

Figure 5: Convergence diagram of the Markov logic network model algorithm.

Table 4: Section BSAKETS data sheet.

Fruit veg	Fresh meat	Dairy	Canned veg	Canned meat	Frozen meal	Beer	Wine	Softer ink	Fish	Confectionery
1	1	1	0	0	0	0	0	0	0	0
1	0	1	0	0	0	0	0	0	0	0
0	0	0	1	1	1	1	0	0	0	0
0	1	0	0	0	0	0	1	0	0	0
1	0	0	0	0	0	1	1	0	0	0
0	0	0	0	0	0	0	0	1	1	0
0	0	0	0	0	1	0	0	0	0	0
0	0	0	0	1	0	0	0	1	0	0
0	0	0	0	0	0	1	0	1	0	0
0	1	1	0	1	0	1	1	1	0	0

gradient rising trend) along the ladder falling trend during the calculation process, and the gradient direction change can be obtained by functional derivation. A training set is selected for improvement in each iteration. Different from batch ladder reduction, small batch ladder reduction refers to selecting local training samples for improvement in each iteration. Random gradient reduction refers to randomly selecting a training sample to improve in each iteration process.

4.2. Experimental Results and Analysis. To prove correctness, parameters in the Markov logic network framework with relationship rules are learned through real data to see if the model converges. This paper uses a dataset from a grocery store to learn the parameters of the Markov logic network framework model of association rules, and the data set contains 75 variables. There are a total of 3956 pieces of information. By using the stochastic gradient descent method to learn the parameters of the Markov logic network framework model of association rules, the convergence graph of the Markov logic network framework model of association rules is obtained. Figure 5 indicates that when the number reaches 1000, the algorithm begins to converge, indicating that the one logic net sample of the relationship rules is converged.

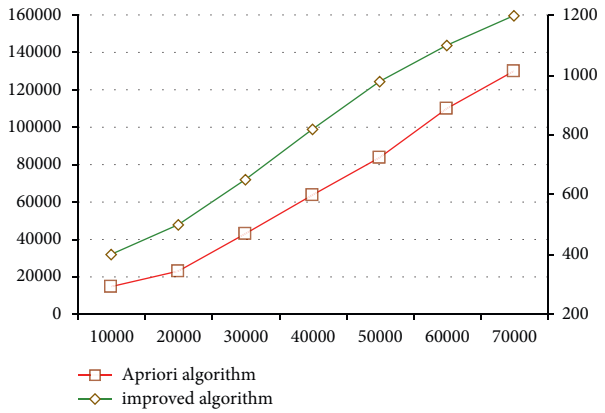

Figure 6: Comparison of the execution time of two algorithms with different numbers of records.

This chapter conducts an example analysis of a small dataset. The data is the data that comes with SPSS Clementine11.1, named BSAKETS1n. The data contains 18 fields and 1000 records, mainly including customer information, total purchase amount, and purchased items. The sighs include vegetables, fruit, meat, fish, and soft drinks. We use part of this data, the purchase item information, for association rule analysis. By processing the data, we get the data in Table 4 (including only part of the processed data).

RETRACTED

This experiment continues to compare the time efficiency of the Apriori algorithm and the improved algorithm. The dataset used in the experiment is the basket data retail.dat file of a retail store in Belgium from the CSDN blog. The dataset has a total of 88,162 records and 16,470 binary attributes. The experimental test results are shown in Figure 6. As can be seen from the figure, the execution time of the improved algorithm has been greatly reduced compared with the Apriori algorithm.

5. Conclusion

In today's big data era, relationship rule mining can be a popular investigation direction. More and more people start to study association law and they are employed in many areas. In the research about association rules, people have obtained a lot of results and gained good consequences. But there are still some shortcomings. To address these problems, this paper proposes a Markov net model with relationship rules. Most of the current relevance data processing rules for digging up the information algorithms are constructed under a unified framework model. The main contents of this paper include the following aspects: (1) Combining Markov logic network and association rules, a new model, the Markov one framework of relationship rules, will be proposed. (2) Employ the random counting method of the Markov logic network framework. By comparing the prediction accuracy of the Markov logical network framework model and the traditional relevance data processing rule for digging the information, the Apriori algorithm, through different datasets, achieved higher accuracy than the traditional association rule algorithm (Apriori algorithm). (3) In line with the test about the relationship with the rule redundancy for the hypergraph, the author will change the relation rule into the hypergraph and give a new concept to the term about the matrix to offer a new way to the test of the circle and linking bricks in the hypergraph.

Data Availability

The data used to support the findings of this study are available from the corresponding author upon request.

Conflicts of Interest

The authors declare that there are no conflicts of interest.

Acknowledgments

This work was supported by the Xi'an Railway Vocational and Technical College.

References

[1] S. Doganer and H. E. Akolu, "The effect of sports science students' social media adddictions on redundant purchasing behavior," *Asian Journal of Education and Training*, vol. 6, no. 4, pp. 24–30, 2020.

[2] H. Ge, H. Qin, S. Xue et al., "Research on denoising algorithm of thoracic impedance signal for respiratory monitoring during running exercise," *Biomedical Signal Processing and Control*, vol. 70, no. 5, Article ID 102941, 2021.

[3] H. Li, M. Qiao, and S. Peng, "Research on the recommendation algorithm of rural tourism routes based on the fusion model of multiple data sources," *Discrete Dynamics in Nature and Society*, vol. 2022, no. 11, Article ID 2262148, 125 pages, 2022.

[4] S. Maleki, U. Agarwal, and M. Burtscher, "BiPart: a parallel and deterministic multilevel hypergraph partitioner," *International Journal of Approximate Reasoning*, vol. 10, no. 8, pp. 88–95, 2020.

[5] S. Bashkari, A. Sami, and M. Rastegar, "Outage cause detection in power distribution systems based on data mining," *IEEE Transactions on Industrial Informatics*, vol. 11, no. 99, p. 1, 2020.

[6] V. S. Klaus, S. C. Schriever, J. M. Monroy Kuhn et al., "Correlation guided Network Integration (CoNI) reveals novel genes affecting hepatic metabolism," *Molecular Metabolism*, vol. 53, no. 7747, 2021.

[7] N. Lakshmi and M. Krishnamurthy, "Frequent itemset generation using relevance data processing rule for digging the information based on hybrid neural network based billiard inspired optimization," *Journal of Circuits, Systems, and Computers*, vol. 31, no. 8, pp. 113–121, 2022.

[8] V. Soboleva and O. Shipitko, "Raindrops on windshield: dataset and lightweight gradient-based detection algorithm," *Springer International Publishing*, vol. 6, no. 5, pp. 30–45, 2021.

[9] N. Veldt, A. Wirth, and D. F. Gleich, "Parameterized objectives and algorithms for clustering bipartite graphs and hypergraphs," *Pattern Analysis & Applications*, vol. 6, no. 21, pp. 77–85, 2020.

[10] Z. An, G. A. Fei, and Y. A. Mi, "A new rule reduction and training method for extended belief rule base based on DBSCAN algorithm," *International Journal of Approximate Reasoning*, vol. 119, no. 20, pp. 20–39, 2020.

[11] N. Parashar, A. Tiwari, and R. K. Gupta, "Mining minimal non-redundant image association rules using statistical texture feature based frequent itemsets," *Evolutionary Intelligence*, vol. 15, no. 2, pp. 33–41, 2022.

[12] S. Mudgal and M. Parmar, "Mining of the correlations for fatal road accident using graph-based fuzzified FP-growth algorithm," *Blue Eyes Intelligence Engineering and Sciences Engineering and Sciences Publication-BEIESP*, vol. 10, no. 5, pp. 119–128, 2020.

[13] J. Chen, C. Zhao, and Uliji, "Collaborative filtering recommendation algorithm based on user correlation and evolutionary clustering," *Springer International Publishing*, vol. 10, no. 1, pp. 55–62, 2020.

[14] F. Chen, J. Liao, and Z. Lu, "A real-time two-stage and dual-check template matching algorithm based on normalized cross-correlation for industrial vision positioning," *Pattern Analysis & Applications*, vol. 8, no. 8, pp. 64–70, 2021.

[15] Y. S. Wu, Y. Shen, and H. Sun, "Intelligent algorithm-based analysis on ultrasound image characteristics of patients with lower extremity arteriosclerosis occlusion and its correlation with diabetic mellitus foot," *Journal of Healthcare Engineering*, vol. 2021, no. 9, 99 pages, Article ID 7758206, 2021.

[16] S. Govindarajan, J. A. Ardila-Rey, and K. Krithivasan, "Development of hypergraph based improved random forest algorithm for partial discharge pattern classification," *IEEE Access*, vol. 15, no. 99, p. 1, 2021.

RETRACTED

Hindawi
Journal of Robotics
Volume 2024, Article ID 9876760, 1 page
https://doi.org/10.1155/2024/9876760

Retraction

Retracted: Simulation Design of a Live Working Manipulator for Patrol Inspection in Power Grid

Journal of Robotics

Received 23 January 2024; Accepted 23 January 2024; Published 24 January 2024

Copyright © 2024 Journal of Robotics. This is an open access article distributed under the Creative Commons Attribution License, which permits unrestricted use, distribution, and reproduction in any medium, provided the original work is properly cited.

This article has been retracted by Hindawi following an investigation undertaken by the publisher [1]. This investigation has uncovered evidence of one or more of the following indicators of systematic manipulation of the publication process:

(1) Discrepancies in scope
(2) Discrepancies in the description of the research reported
(3) Discrepancies between the availability of data and the research described
(4) Inappropriate citations
(5) Incoherent, meaningless and/or irrelevant content included in the article
(6) Manipulated or compromised peer review

The presence of these indicators undermines our confidence in the integrity of the article's content and we cannot, therefore, vouch for its reliability. Please note that this notice is intended solely to alert readers that the content of this article is unreliable. We have not investigated whether authors were aware of or involved in the systematic manipulation of the publication process.

Wiley and Hindawi regrets that the usual quality checks did not identify these issues before publication and have since put additional measures in place to safeguard research integrity.

We wish to credit our own Research Integrity and Research Publishing teams and anonymous and named external researchers and research integrity experts for contributing to this investigation.

The corresponding author, as the representative of all authors, has been given the opportunity to register their agreement or disagreement to this retraction. We have kept a record of any response received.

References

[1] T. Xie, Z. Li, Y. Zhang, B. Yuan, and X. Liu, "Simulation Design of a Live Working Manipulator for Patrol Inspection in Power Grid," *Journal of Robotics*, vol. 2022, Article ID 7318090, 8 pages, 2022.

Hindawi
Journal of Robotics
Volume 2022, Article ID 7318090, 8 pages
https://doi.org/10.1155/2022/7318090

RETRACTED

Research Article

Simulation Design of a Live Working Manipulator for Patrol Inspection in Power Grid

Tao Xie,[1] **Zhengyu Li**,[2] **Yongyun Zhang**,[2] **Bin Yuan**,[2] **and Xiao Liu**[2]

[1]*State Grid Shanxi Electric Power Company, Taiyuan, Shanxi 030021, China*
[2]*State Grid UHV Transformation Co. of SEPC, Taiyuan, Shanxi 030032, China*

Correspondence should be addressed to Tao Xie; 220192216007@ncepu.edu.cn

Received 15 August 2022; Revised 24 August 2022; Accepted 26 August 2022; Published 14 September 2022

Academic Editor: Shahid Hussain

Copyright © 2022 Tao Xie et al. This is an open access article distributed under the Creative Commons Attribution License, which permits unrestricted use, distribution, and reproduction in any medium, provided the original work is properly cited.

The distribution line network is the electric power infrastructure directly facing the users, with the characteristics of large coverage and complex network, and its operation safety is directly related to the stability and reliability of the power supply system, which is the key link to ensure the safety of power supply and the reliability of residential electricity consumption. In order to realize the autonomous obstacle avoidance and autonomous navigation of the live working manipulator for inspection and maintenance of the power grid equipment, a mobile manipulator intelligent control method combining SumTree-weighted sampling and deep deterministic policy gradient (DDPG) is proposed. Firstly, the traditional DDPG algorithm is improved to optimize the action value function of *Q*-learning to get a better control strategy, and the weighted sampling technique is used to add priority to each sample in the replay buffer, which improves the learning speed and accelerates the convergence speed. The corresponding environmental state space is designed, and simulation experiments are conducted to verify the proposed manipulator control method. Simulation results demonstrate that the proposed method performs better than traditional DDPG and DQN methods in obstacle avoidance and navigation tasks, with faster convergence, better path planning ability, and lower offset cost, which can provide theoretical and technical references for realizing fully autonomous power grid inspection operations.

1. Introduction

Mechanization, automation, and intelligentization of live working operation are the development trend and vital technological direction to realize intelligent inspection and maintenance of power grid and safe live working operation [1]. At present, the research related to the automation of substation equipment with power grid operation has been carried out worldwide, pilot applications have been carried out, and certain results have been achieved, which can replace or assist the manual completion of some typical inspection and maintenance projects [2]. This kind of technology has been innovatively developed and gradually applied in recent years, which is conducive to enriching the technical means of power grid operation with a live working environment and improving the safety and automation level of the operation, and has good development prospects [3].

Since the 1980s, the United States, Canada, Spain, France, Japan, and other developed countries have successively carried out the research of like working robots, such as Japan Kyushu Electric Power Company, the State Grid Corporation of China, and so on. According to their automation degree, robots can be mainly divided into three categories, namely, manual remote control, remote teleoperation, and autonomous operation [4]. Manipulator control is based on an automation control algorithm, which automatically searches the locations of the objects in the space and accurately identifies the obstacles in the travel path to plan a most reasonable motion trajectory [5]. Deep learning is an advanced stage in the development of artificial intelligence and one of the most important and popular research areas of artificial intelligence, but there are different states in the obstacle avoidance navigation process of the robot, which needs to solve the two core problems of large differences in strategy distribution and sparse positive

feedback rewards. The traditional reinforcement learning model cannot explore the space completely, causing the strategy to fall into local minima easily, and cannot derive the full-space manipulator obstacle avoidance and navigation control strategy through long training time and multiple training rounds [6].

In this article, through deeply analyzing the live working process and action sequence of the mobile manipulator, the traditional deep deterministic policy gradient (DDPG) algorithm is optimized and improved to improve the dimensionality, scalability, and generalization capability of the algorithm, making it more applicable to the trajectory planning and obstacle avoidance control of the mobile manipulator and improving the control accuracy of the trajectories during the manipulator movement. Specifically, based on the DDPG algorithm, this article adopts a weighted sampling method with a SumTree data structure instead of uniform sampling, so that successful samples have a higher chance of being learned by the agent, and the Q-learning action value function is optimized and applied to the autonomous power grid inspection and maintenance tasks. Simulation results prove that the proposed method enables the manipulator to complete the tasks more accurately and quickly.

The rest of this article is organized as follows: Section 2 introduces the related research. The basic principles of the proposed method are explained in Section 3. Section 4 describes the proposed intelligent manipulator control method. Section 5 gives the simulation results and discussion. Finally, Section 6 concludes the whole article.

2. Related Works

A lot of effective path planning methods have been proposed for mobile robots worldwide, but most of the path planning algorithms for mobile robots are not applicable to robotic arms because manipulators are complex nonlinear systems with challenging factors such as high degrees of freedom and coupling between connecting rods, which make the planning more difficult [7].

Researchers have carried out the exploration of deep reinforcement learning in the field of grasping, localization, and obstacle avoidance of industrial manipulators with some success. Mnih et al. [8] proposed the Deep Q-Network (DQN) algorithm, which combines neural networks with Q-learning. The model was trained in the ATARI2600 game, and the final performance was much higher than that of humans. Lillicrap et al. [9] proposed the DDPG algorithm and applies it to a high-dimensional continuous action space. Rusu et al. [10] transferred the training results in a simulation environment to a physical robotic arm and achieved similar results to the simulation after only a simple training. Liz et al. [11] proposed an improved DDPG algorithm in which a success experience pool and a collision experience pool are added to optimize the traditional experience pool. Compared with the traditional DDPG algorithm, the improved DDPG algorithm has fewer training episodes, but achieves better results. Luck et al. [12] combined the DDPG algorithm with a model-based trajectory optimization approach in which the learned deep dynamic model was used to compute the policy gradient and the value function was adopted as a criterion, thus improving the efficiency of training.

In the study of practical operations of robotic arms, in [13], based on deep reinforcement learning techniques, the optimal grasping point and grasping stability of the robotic arms were evaluated considering the working performance under different tasks, in order to realize the requirement of grasping different shapes of objects in various tasks and to complete the collision-free autonomous mobile robot navigation. Sangiovanni et al. [14] applied reinforcement learning methods to the obstacle avoidance and navigation tasks of the robot manipulators and achieved obstacle-free path planning for the robot. However, the model is only trained and tested for a single target point, and the full operational space decision was not achieved. Wei and Shan [15] proposed to treat the three arms of the manipulator as three different agents, and the three arms were restricted to constantly be in the same plane and the control strategies were set separately to realize the full working space decision-making of the robot manipulator. In summary, the above methods do not change the way of sample extraction but still uniformly collect samples from the replay buffer for training, and the agents cannot learn the successful samples efficiently, which leads to a long training time [16].

3. Fundamental Principles

3.1. Live Working Manipulator and Kinematic Analysis. Considering that the weight of the end-effector for live working operation is more than 5 kg, this article takes the UR10 robot arm as the research object and further carries out its abstract modeling and kinematic analysis, mainly studying the motion state and control strategy of the three-segment arm of UR10 in the Cartesian coordinate system [17].

3.1.1. Cartesian Coordinate System. In the Cartesian coordinate system, (x, y, z) coordinates can be used to represent any position information in three-dimensional space by constructing multiple Cartesian coordinate systems of the same basic direction with $\{o_1, o_2, o_3, o_4\}$ as the origin, the first and last positions of each endpoint of the manipulator in three-dimensional space can be calculated by accumulating the increments of each segment as shown in Figure 1.

3.1.2. Motion Degree Freedom Analysis. The kinematic analysis of the manipulator used in this article is mainly a forward operation problem [18]. The forward operation problem is to solve the endpoint coordinates of the manipulator in three-dimensional space given the arm lengths l_1, l_2, and l_3 of the three-segment arm and the rotation angles θ_1, θ_2, θ_3, θ_4, θ_5, and θ_6. Using the z-coordinate axis as the rotation axis and the endpoint of the first segment of the robot arm as the origin, a manipulator model is constructed, and six angles of rotation are defined as six degrees of freedom. θ_1 and θ_2 control the first segment, where θ_1

RETRACTED

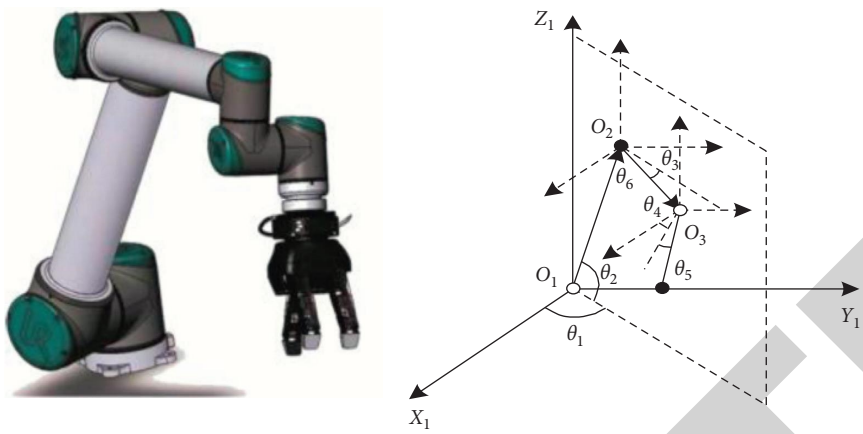

Figure 1: Diagrams of the manipulator and its simplified model in the Cartesian coordinate system. (a) UR10 manipulator. (b) Simplified model.

represents the angle of rotation of l_1 around the z-axis and θ_2 represents the angle of l_1 with the x-y plane. l_1, l_2, and the z-axis are kept in the same plane. θ_3 controls l_2 and represents its angle with l_1. For the convenience of calculation, it is expressed by the angle between the second segment arm and the x-y plane of the o_2 coordinate system. θ_4~θ_6 control l_3, where θ_4 and θ_5 act similar to θ_1 and θ_2 to make l_3 move at any angle within the o_3 coordinate system, and θ_6 controls l_3 to rotate around its own arm axis without affecting the endpoint coordinates. The coordinates of each node of the manipulator can be calculated as

$$\begin{cases} \Delta l_1 = (l_1 \cos\theta_2 \cos\theta_1, l_1 \cos\theta_2 \sin\theta_1, l_1 \sin\theta_2), \\ \Delta l_2 = (l_2 \cos\theta_3 \cos\theta_1, l_2 \cos\theta_3 \sin\theta_1, l_2 \sin\theta_3), \\ \Delta l_3 = (l_3 \cos\theta_5 \cos\theta_4, l_3 \cos\theta_5 \sin\theta_4, l_3 \sin\theta_5), \\ o_2 = o_1 + \Delta l_1, \\ o_3 = o_1 + \Delta l_2, \\ o_4 = o_3 + \Delta l_3. \end{cases} \tag{1}$$

3.2. Deep Deterministic Policy Gradient. In a standard reinforcement learning environment, each agent interacts with the environment with the ultimate goal of maximizing environmental gain. This interactive process is formally described as a Markov decision process (MDP) [19], which can be described by the quadruplet (S, A, R, P). S represents the state space, A represents the action space, R: $S \times A \longrightarrow R$ is the reward function, and P: $S \times A \times S \longrightarrow [0, 1]$ is the transfer probability. In this environment, an intelligence learns a strategy π: $S \longrightarrow A$ to maximize the gain in the environment:

$$R_0 = \sum_{i=0}^{T} r(s_i, a_i), \tag{2}$$

where T is the number of steps advanced at the end of the interaction and $r(s_i, a_i)$ denotes the gain obtained by executing a_i in the environment s_i. Typically, the environment in which the long-term gain is scaled down by the parameter γ:

$$R_0^{\gamma} = \sum_{i=0}^{T} \gamma^i r(s_i, a_i), \tag{3}$$

where $\gamma \in (0, 1)$. The long-term benefits of performing action a in an environment s are generally represented by the action value function:

$$Q(s_t, a_t) = E\left[R_t^{\gamma} | s = s_t, a = a_t\right] = E\left[\sum_{i=t}^{T} \gamma^{i-t} r(s_i, a_i)\right]. \tag{4}$$

This optimal action value function is usually found using the Bellman equation [20]:

$$Q*(s_t, a_t) = E\left(r(s_t, a_t) + \gamma \max_{a_{t+1}'} Q*(s_{t+1}, a_{t+1}')\right]. \tag{5}$$

However, this approach is only suitable for those situations where both action space and state space are discrete. To apply reinforcement learning to the problem where action space and state space are continuous, DDPG designed two deep neural networks: action value network $Q(s_t, a_t|\theta^Q)$ and action network $\mu(s_t, a_t|\theta^{\mu})$, where θ^Q and θ^{μ} are network parameters. Action network $\mu(s_t, a_t|\theta^{\mu})$ is a mapping corresponding to the state space and action space, which can directly generate the desired action based on the state. The action value network $Q(s_t, a_t|\theta^Q)$ is used to approach the action value function and can provide gradients for the training of the action network.

The training of the action value networks is to minimize the loss function:

$$L(\theta^Q) = \left(r(s_t, a_t) + \gamma Q'\left(s_{t+1}, a_{t+1}|\theta^{Q'}\right) - Q(s_t, a_t|\theta^Q)\right)^2, \tag{6}$$

where Q' is the target value network with synchronized weights from the Q-network. And the update of the action

RETRACTED

network parameters requires using the policy gradient algorithm in which the gradient update direction can be expressed as:

$$\nabla_{\theta^\mu} Q\left(s, a|\theta^Q\right)|_{s=s_t, a=\mu\left(s_t, v\right)} = \nabla_a Q\left(s, a|\theta^Q\right)|_{s=s_t, a=\mu\left(s_t, v\right)} \nabla_{\theta^\mu} \mu\left(s|\theta^\mu\right)|_{s=s_t}, \quad (7)$$

where the control strategy μ represents the actions of the manipulator, and the Q-network is the action value function. The training of these deep neural networks requires the input data to be independent and uniformly distributed, while reinforcement learning models with Markov decision processes where data are collected sequentially and do not satisfy the requirements. Therefore, experience replay of DQN (deep Q-learning network) is introduced to break the data correlation [21]. After a certain amount of training data are stored in the experience pool, data are collected from the replay buffer for training the Q-network according to uniform sampling.

3.3. Design and Optimization of Action Value Function. The action value function is an important basis for judging the quality of the current strategy of the manipulator. The input of the Q-network contains the current state and action of the manipulator, and the neural network is used to fit the Q-function. The Q-learning algorithm is used to optimize the Q-network along with the policy network, and the objective function can be optimized as

$$\delta_t = r_t + \gamma Q\left(s_{t+1}, \mu\left(s_{t+1}\right)\right) - Q\left(s_t, a_t\right). \quad (8)$$

In addition, the target networks Q' and μ' are set for the Q-network and the policy network, respectively:

$$\delta_t = r_t + \gamma Q'\left(s_{t+1}, \mu'\left(s_{t+1}|\theta_t\right)\right) - Q\left(s_t, a_t\right). \quad (9)$$

The Q-network generates delay errors in updating the parameters during the training process; therefore, the following equations are used to perform updates:

$$\begin{aligned} \omega\prime &\leftarrow \tau\omega + (1-\tau)\omega\prime, \\ \theta\prime &\leftarrow \tau\theta + (1-\tau)\theta\prime. \end{aligned} \quad (10)$$

where ω and ω' are the parameters of the Q-network and the target network, respectively, and θ and θ' are the parameters of the manipulator strategy network and target network, respectively.

4. Control Method of Patrol Manipulator Combining SumTree-Weighted Sampling and DDPG

A schematic diagram of the proposed algorithm is given in Figure 2. The deep DDPG algorithm combined with SumTree-weighted sampling is explained in detail in the following section.

The data (s_t, a_t, s_{t+1}, r_t)obtained from each interaction of the manipulator with the environment are stored in the replay buffer. The traditional DDPG algorithm treats all samples in the replay buffer as having the same value for network training and extracts the training samples by uniform random sampling. However, the samples in the replay buffer make a big difference for network training. leading to few successful cases and more failures in the actual training of manipulator trajectory planning. Therefore, if the uniform random sampling method is adopted, it will make the extraction of successful samples difficult.

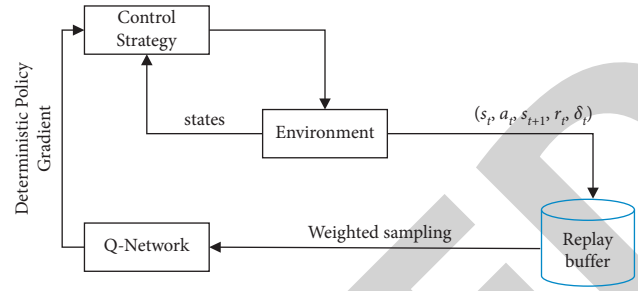

Figure 2: Algorithm diagram.

SumTree utilizes a binary tree structure to access data, the proposed method applies it to the experience replay of the DDPG algorithm. The expectation of the difference between the target Q-value and the real Q-value is applied in the DDPG algorithm to update the parameters in the strategy network and the value network, and the larger difference represents that the parameters are not selected accurately, that is, the samples need to be trained more by the manipulator. Firstly, SumTree is initialized, the capacity size is defined, and the initial state s_t is set as the first current state. Then, the state s_t is taken as the input of the real actor network and the policy π is computed to get a_t. Finally, the action a_t is executed to get the reward value r_t and the new state s_{t+1}.

In this article, the loss value resulting from the target Q-value and the real Q-value is used as the criterion of priority, and it can be expressed as:

$$P(i) = \frac{p_i^\beta}{\sum_k p_k^\beta}, \quad (11)$$

where $P(i)$ is the probability that the ith tuple of training samples is sampled; β is a constant; the larger the β is, the greater the weight of priority; and k is the total number of samples in the replay buffer. The tuple stored in the replay buffer is optimized as $(s_t, a_t, s_{t+1}, r_t, \delta_t)$ compared to the original one (s_t, a_t, s_{t+1}, r_t). The structure of SumTree is shown in Figure 3.

As shown in the figure, the leaf nodes of the SumTree store the priority of the samples, each node has a weight, and the weight of the parent node is equal to the sum of the weights of the two child nodes, which finally converges to the root node. The capacity of the replay buffer is k, the number of nodes is $2k-1$, and the value of the root node is $\psi_{\text{total}} = \sum_k \psi_k^\beta$.

After establishing the SumTree structure, the data in the replay buffer are sampled in the following way: firstly, a weight is sampled from $[0, \psi_{\text{total}}]$, then the comparison starts from the root node, taking the order from top to bottom and

RETRACTED

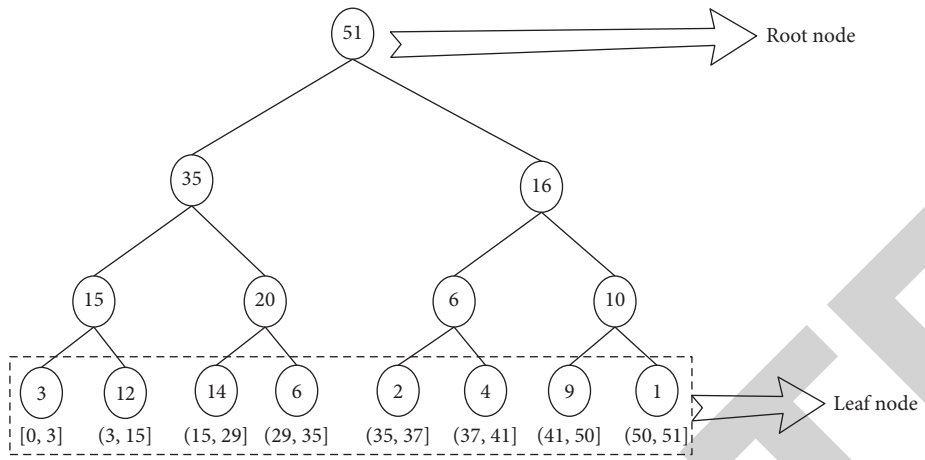

Figure 3: SumTree structure.

from left to right. If the selected weight ψ_1 is less than or equal to the left node weight, the left child node is taken; if the selected weight ψ_1 is greater than the left node weight, the weight of the left node is subtracted from ψ_1 and the new weight obtained is assigned to ψ_1, then the right node is taken as the new node to continue down the collection until the current node is a leaf node, then the data are extracted and the search is finished. In doing so and based on equation (11), N tuples of $(s_t^i, a_t^i, r_t^i, s_{t+1}^i)$ are sampled.

Thereafter, the current target Q-value is calculated as follows:

$$y_i = r_i + \gamma Q'\left(s_{i+1}, \mu'\left((s_{i+1}|\theta^{\mu'}\right)|\theta^{Q'}\right). \tag{12}$$

The loss function is expressed as follows:

$$L = \frac{1}{N}\sum_i \left(y_i - Q\left(s_i, a_i|\theta^Q\right)\right)^2. \tag{13}$$

Using gradient descent technique to reversely update strategy network parameters:

$$\nabla_{\theta^\mu} J \approx \frac{1}{N}\sum_i \nabla_a Q\left(s, a|\theta^Q\right)|_{s=s_i, a=\mu(s_i)} \nabla_{\theta^\mu}(s|\theta^\mu)|_s. \tag{14}$$

All sample errors are recalculated and the priority value P_i of all nodes is updated in SumTree. If S' is the final state, the iteration is ended.

5. Experiment

5.1. Experimental Setup and Algorithm Parameters. In the power patrol simulation model, the experimental environment with full-space single target point and random target points is designed to verify that the proposed method is effective in high-dimensional space using the validation set. The parameters of the proposed intelligent manipulator control algorithm combining SumTree and DDPG are shown in Table 1.

5.2. Simulation Experimental Environment. The typical mobile manipulator live working operation in power distribution networks include energized line disconnecting and guiding, wire clearing, and insulator replacement. Considering the possible obstacles and restrictions in the operation, an abstract simulation model is established based on Python, as shown in Figure 4, where *xyz* is the spatial coordinate system of the operation.

When working on insulators and other equipment, the possible obstacles are other insulated equipment. Since the obstacles have limited distribution in space, the manipulator is effective in full-space obstacle avoidance behavior and cannot limit the degrees of freedom of movement, so a general three-dimensional model is established for simulation. Taking insulator obstacles as an example, the appearance details of these insulators in the actual operation will not have an impact on the manipulator route planning due to the limitation of the safety distance of the live working operation, and the insulators can be regarded as cylindrical obstacles. The operation area is divided into three parts, which are Region 1, which lies in the middle between the manipulator and obstacles; Region 2, which lies on the right side; and Region 3, which lies on the left side, to compare the success rate of obstacle avoidance and autonomous navigation of the mobile manipulator.

6. Results and Discussion

Firstly, a single target point is set in the simulated environment of the manipulator power inspection operation scenario. The effectiveness of hazard action determination and reward functions can be verified in a single object setting, so as to compare the performance of the proposed method with other deep reinforcement learning algorithms. The DQN [8], DDPG [9], and the proposed method are tested separately. Results show that after training, the manipulator can successfully bypass the obstacle and reach the target point when using different methods. The cumulative reward curve of the training process is shown in Figure 5, and the mean values of the number of training rounds and cumulative reward values after the convergence of the reward curves are given in Table 2. It can be seen from the results that after training, DQN, DDPG, and the proposed method converge, and all network models drive the manipulator to accomplish the obstacle avoidance and

RETRACTED

Table 1: Algorithm parameters.

Parameters	Values
Neural network learning rate α	0.001
Number of hidden layer nodes of neural network	500
Discount factor γ	0.99
Initial greedy value ε	0.05
Database capacity	2×10^5
Batch size	64
Maximum iterations	2000
Epochs	5000

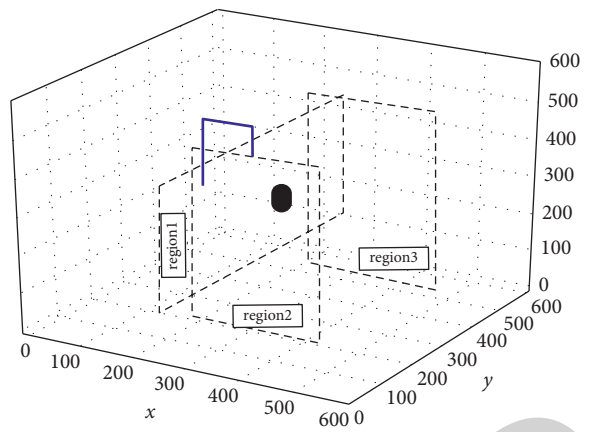

Figure 4: Simulation model of the live working operation in power distribution grid.

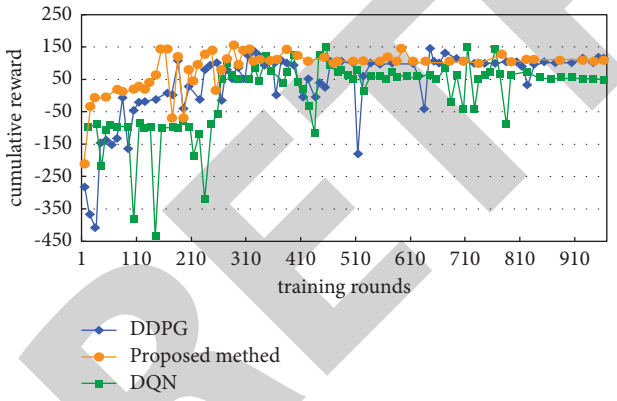

Figure 5: Reward function curve comparison.

navigation task. However, the training performance varies among different algorithms. The training of DDPG and DQN can also approach convergence but with greater oscillation, and the termination timings of the training have more influence on the model performance than the proposed method. In addition, it can be seen that the proposed method converges faster and gets higher rewards.

Next, through the full-space random target points test, the full-space action effect of different models is tested. Due to the different inherent rewards between different tasks caused by different target points, the strategy no longer satisfies the independent and identical distribution, so that

Table 2: Performance comparison with single target point.

Methods	Cumulative reward	Training rounds
DQN [8]	50.88 ± 9.54	805 ± 48
DDPG [9]	99.34 ± 6.77	560 ± 62
Proposed method	121.77 ± 3.13	311 ± 28

Table 3: Test results under random target point scenarios.

Methods	Success (%)	Collision (%)	Incomplete (%)
DQN [8]	35.77	9.85	43.67
DDPG [9]	30.59	12.77	47.55
Proposed method	88.43	7.17	3.99

the training reward will not tend to a stable convergence value. DQN and DDPG methods are difficult to learn a unified obstacle avoidance and navigation method. Though the obstacle avoidance tasks in experiments can be completed by these two methods in most cases, however, when the target is far away or the location is difficult to reach, these two models cannot reach the target points smoothly, leading to chaotic behaviors when the effective strategy cannot be executed.

The success rate, collision rate, and incomplete rate corresponding to each algorithm are shown in Table 3. It can be seen that the DQN and DDPG methods have low success rates for the full-space target point tasks, and it is difficult to reliably complete the multiple target points tasks. The proposed method achieves a better control strategy by enhancing the exploration ability of the agent and improves the uniform sampling of the traditional DDPG algorithm. It learns a relatively safe path from the training and can stably reach the target point to complete the task.

The completion rates of the obstacle avoidance and navigation subtasks using the proposed model are shown in Figure 6. From the convergence trend of the curves in the figure, it can be seen that the weighted sampling based on SumTree makes the training more stable; the task success rate tends to be stable and maintains a high-level performance. The high completion rate of subtasks guarantees a high live working operation success rate for the proposed method.

In addition, the test results in each area under the random target point scenario using the proposed method are shown in Table 4. Comparing the success rates of each area, it can be seen that the collisions mainly appeared in Region 2, and the incomplete cases mainly occurs in Region 1. The main reason for the incomplete cases is that there are few sampling samples in Region 1, the variance of the output strategy distribution is large, and it is prone to sample unreasonable actions. The occurrence of obstacle collisions is concentrated in the areas with the highest difficulty. The fundamental reason is that the model itself has an inherent error rate. The obstacle avoidance success rate of the proposed method is close to 91%. The overall failure probability of the proposed model is relatively low, and it will not fall into a local minimum.

RETRACTED

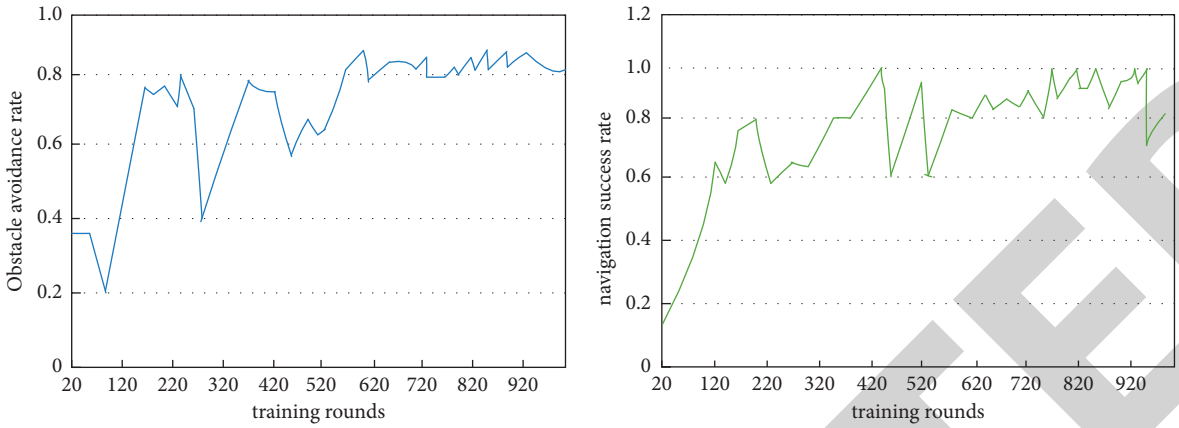

(a) (b)

Figure 6: Success rate of the proposed method under random target point test. (a) Success rate of obstacle avoidance training. (b) Success rate of navigation training.

Table 4: Test results in different regions under the random target point scenario.

Location	Success (%)	Collision (%)	Incomplete (%)
Region 1	89.64	2.86	7.5
Region 2	85.47	13.85	0.68
Region 3	90.18	6.02	3.80

7. Conclusion

In this article, a live working manipulator control scheme for patrol inspection in power grid is proposed. Firstly, the existing DDPG algorithm based on deep reinforcement learning is improved, and the action value function of Q-learning is optimized, therefore enhancing the exploration ability of the agent and obtaining a better control strategy. Secondly, the uniform sampling is improved, and the weighted sampling method of the SumTree data structure is used to add priority to each sample in the replay buffer, which improves the learning speed of the manipulator and greatly reduces the training time. Simulation results show that the proposed model is suitable for solving the problem of obstacle avoidance and navigation of live working manipulators, and it is an effective solution to realize autonomous control of live working mobile robots. With the rapid improvement of the performance of industrial computers and the high-speed innovation of deep learning algorithms, the realization of autonomous navigation with high positioning accuracy and robustness is the inevitable development direction of power inspection robots. In the future, we will try to configure more types of sensors on the inspection robot to obtain diverse equipment status information, such as ultraviolet flaw detection and laser vibration measurement, and transform the function of the inspection robot from problem finding to problem solving, thereby further reducing the work pressure of electric inspection personnel.

Data Availability

The data used to support the findings of this study are included within the article.

Conflicts of Interest

The author declares that there are no conflicts of interest.

References

[1] R. S. Gonçalves and J. C. M. Carvalho, "Review and latest trends in mobile robots used on power transmission lines," *International Journal of Advanced Robotic Systems*, vol. 10, no. 12, p. 408, 2013.

[2] S. Lu, Y. Zhang, and J. Su, "Mobile robot for power substation inspection: a survey," *IEEE/CAA Journal of Automatica Sinica*, vol. 4, no. 4, pp. 830–847, 2017.

[3] W. Jiang, G. Zuo, D. H. Zou, L. Hongjun, J. Y. Jiu, and C. Y. Gao, "Autonomous behavior intelligence control of self-evolution mobile robot for high-voltage transmission line in complex smart grid," *Complexity*, vol. 202017 pages, Article ID 8843178, 2020.

[4] T. Zhang and J. Dai, "Electric power intelligent inspection robot: a review," *Journal of Physics: Conference Series*, vol. 1750, no. 1, Article ID 012023, 2021.

[5] S. A. Ajwad, J. Iqbal, M. I. Ullah, and A. Mehmood, "A systematic review of current and emergent manipulator control approaches," *Frontiers of Mechanical Engineering*, vol. 10, no. 2, pp. 198–210, 2015.

[6] S. Kružić, J. Musić, R. Kamnik, and P. Vladan, "Estimating robot manipulator end-effector forces using deep learning," in *Proceedings of the 2020 43rd international convention on information, communication and electronic technology (MIPRO)*, pp. 1163–1168, IEEE, Opatija, Croatia, 2020.

[7] M. Yang, E. Yang, R. C. Zante, P. Mark, and L. Xuefeng, "Collaborative mobile industrial manipulator: a review of system architecture and applications," in *Proceedings of the*

RETRACTED

Hindawi
Journal of Robotics
Volume 2024, Article ID 9767914, 1 page
https://doi.org/10.1155/2024/9767914

Retraction

Retracted: Parameter-Tunable RBF Neural Network Control Facing Dual-Joint Manipulators

Journal of Robotics

Received 23 January 2024; Accepted 23 January 2024; Published 24 January 2024

Copyright © 2024 Journal of Robotics. This is an open access article distributed under the Creative Commons Attribution License, which permits unrestricted use, distribution, and reproduction in any medium, provided the original work is properly cited.

This article has been retracted by Hindawi following an investigation undertaken by the publisher [1]. This investigation has uncovered evidence of one or more of the following indicators of systematic manipulation of the publication process:

(1) Discrepancies in scope
(2) Discrepancies in the description of the research reported
(3) Discrepancies between the availability of data and the research described
(4) Inappropriate citations
(5) Incoherent, meaningless and/or irrelevant content included in the article
(6) Manipulated or compromised peer review

The presence of these indicators undermines our confidence in the integrity of the article's content and we cannot, therefore, vouch for its reliability. Please note that this notice is intended solely to alert readers that the content of this article is unreliable. We have not investigated whether authors were aware of or involved in the systematic manipulation of the publication process.

Wiley and Hindawi regrets that the usual quality checks did not identify these issues before publication and have since put additional measures in place to safeguard research integrity.

We wish to credit our own Research Integrity and Research Publishing teams and anonymous and named external researchers and research integrity experts for contributing to this investigation.

The corresponding author, as the representative of all authors, has been given the opportunity to register their agreement or disagreement to this retraction. We have kept a record of any response received.

References

[1] W. Xu, "Parameter-Tunable RBF Neural Network Control Facing Dual-Joint Manipulators," *Journal of Robotics*, vol. 2022, Article ID 4231117, 10 pages, 2022.

Hindawi
Journal of Robotics
Volume 2022, Article ID 4231117, 10 pages
https://doi.org/10.1155/2022/4231117

RETRACTED

Research Article

Parameter-Tunable RBF Neural Network Control Facing Dual-Joint Manipulators

Weiying Xu

HBUT Detroit Green Technology Institute, Hubei University of Technology, Wuhan 430000, China

Correspondence should be addressed to Weiying Xu; 2011611126@hbut.edu.cn

Received 8 July 2022; Revised 27 July 2022; Accepted 2 August 2022; Published 8 September 2022

Academic Editor: Shahid Hussain

Copyright © 2022 Weiying Xu. This is an open access article distributed under the Creative Commons Attribution License, which permits unrestricted use, distribution, and reproduction in any medium, provided the original work is properly cited.

In order to improve the parameter control effect of the double-joint manipulator, this paper combines the RBF neural network to control the parameters of the double-joint manipulator and the command filtering backstep impedance control method based on the RBF neural network is effectively applied to the multijoint manipulator. Moreover, this paper introduces the filter error compensation mechanism into the controller design to eliminate the influence caused by the filter error. Finally, the effectiveness and superiority of the command filtering backstep impedance control scheme of the multijoint manipulator adaptive neural network designed in this paper is verified by simulation experiments. The experimental research results verify that the parameter-tunable RBF neural network control method facing the dual-joint manipulator has a certain effect on the parameter control process of the dual-joint manipulator and can effectively improve the motion accuracy of the dual-joint manipulator.

1. Introduction

The theoretical modeling methods of robotic arms are generally based on the principle of energy conservation. For a rigid body, its energy usually includes two parts: kinetic energy due to motion inertia and potential energy due to gravitational field. However, for a flexible arm, its potential energy and kinetic energy are different from those of a rigid manipulator. Moreover, the flexible arm part generally includes three deformations, namely, rotational deformation, lateral deformation, and axial deformation [1]. In order to consider the bending deformation of beams, there are currently four basic modeling theories of beams [2]. Since the axial direction of the beam is generally longer than its diameter, the Euler–Bernoulli beam theory is generally used in many models. At the same time, since the flexible manipulator has infinite degrees of freedom, this is difficult to achieve in modeling. The general solution is to replace the infinite-dimensional degrees of freedom with finite-dimensional degrees of freedom and use Hamilton's principle or Lagrange dynamic equation to discretize a set of difference equations and finally solve them [3]. There are generally three current modeling methods for flexible manipulators [4]. The hypothetical mode method usually uses finite-dimensional continuous modes of several orders to represent infinite-dimensional beams. Moreover, each order mode is usually obtained by the product of the modal coordinates and the modal function, and finally, the consecutive several order modes are added to obtain the vibration amount at any point on the entire flexible arm. Literature [5] has demonstrated that the use of the second-order mode can accurately reflect the vibration offset of the flexible body. This research method has also been well verified experimentally and theoretically; however, this research method has certain deficiencies and cannot be applied to flexible manipulators with variable cross-sectional areas [6]. In response to this situation, some scholars have proposed the finite element method [7], and it has been shown that FE can reflect the actual situation well. For the lumped mass method, it is the simplest approximation to consider. It simply treats the flexible manipulator as a spring and mass system, but this research method is rarely used.

Traditional modeling of flexible arms generally chooses classical deformations to derive the Lagrangian dynamic equations of flexible arms. However, in some cases, this classical deformation does not conform to the actual

situation and cannot accurately describe the dynamic behavior of the flexible arm. For example, when the flexible arm rotates at a high speed, the comprehensive deformation theory can more accurately describe the deformation form of the flexible arm [8]. So far, in describing the elastic deformation of flexible arms, there are mainly three deformation descriptions: classical deformation theory, quadratic deformation theory, and comprehensive deformation theory. Classical deformation theory is currently the most widely used method [9]. Literature [10] uses the classical deformation theory to model the single-joint flexible manipulator and considers the influence of nonlinear centrifugal force on the accuracy of the model. Literature [11] uses the classical deformation theory to model a single-joint flexible manipulator and designs a controller based on this model, and the control effect is ideal. Literature [12] uses the classical deformation theory for modeling and then conducts positive feedback experiments and negative feedback experiments, respectively, and finally compares and analyzes the results of theoretical solutions and experiments. Analysis shows that positive feedback experiments are more robust than negative feedback in suppressing vibration. In addition, the end of the flexible manipulator contains a load to reduce the natural vibration frequency of the flexible manipulator. Literature [13] established the dynamic model of the Euler–Bernoulli beam using classical deformation theory and gave the numerical simulation results and concluded that the established dynamic model can be used as the control equation for the design and simulation of the control system. Literature [14] established a Lagrangian dynamic model of the flexible arm based on the assumed modal method and Lagrange equation through classical deformation theory and analyzed the physical and structural parameters and external driving torque of the flexible manipulator. It is concluded that these parameters will have an impact on the dynamic characteristics of the flexible manipulator. Literature [15] studied the theoretical modeling problem of two flexible manipulators in the plane and designed a controller based on the classical theoretical modeling problem. Literature [13] used the classical deformation method to study the kinematics of rigid-flexible coupled double rods in the plane and concluded that if the natural frequency of the first-order system of the flexible beam is lower than that of the natural frequency of the rigid beam, the frequency difference will increase with the increase in frequency. It increases with the increase in the natural frequency of the system; under the premise of certain initial conditions, the second-order natural frequency of the system will also increase with the increase in the natural frequency of the whole system, and it shows that the motion and deformation process of the manipulator will coordinate with each other when doing a large range of motion. There are mutual coupling characteristics.

When studying the control of the manipulator system, it is first necessary to study the dynamics modeling and kinematics analysis of the manipulator. As a theoretical basis for the study of the manipulator system, the dynamic modeling of the manipulator provides a dynamic model for the subsequent high-precision motion control of the manipulator end effector by making reasonable simplified assumptions for the actual manipulator system [16]. The kinematics analysis of the manipulator system is to establish the relationship between the manipulator joint variables and the end effector pose matrix by analyzing the two parts, including forward kinematics and inverse kinematics [17]. The positive kinematics issue is to obtain the pose matrix of the end effector by using the transformation matrix of the joint variables of the manipulator and inversely solving the value of each joint variable of the manipulator through various transformations. The inverse kinematics problem of the manipulator is the basis of the trajectory planning and trajectory tracking control of the joint end. However, in the process of inverse solution of the manipulator, multiple sets of solutions are often obtained. Therefore, it is necessary to select a set of suitable solutions according to the working conditions of the specific manipulator. Trajectory planning is another important direction of manipulator research. It is based on kinematics and dynamics analysis, according to the requirements of specific tasks, after a set of path points passed by the end effector of the manipulator is known, through the mechanical arm. The arm inverse solution is used to obtain the corresponding joint angle of each joint. Among them, the commonly used trajectory planning methods include cubic polynomial interpolation function, quintic polynomial interpolation function, and spline interpolation function [18]. In practical engineering applications, in order to ensure the smooth operation of each joint of the manipulator and to prevent the system from vibrating, the trajectory generated by the trajectory planning of the manipulator must be smooth and continuous and should have no sudden changes. The application of robotic arms in various industries is more extensive. It is not just a simple replacement for human work. In practical engineering, it puts forward higher requirements for its work execution efficiency and the control accuracy of end effectors. However, because the manipulator is a nonlinear, multiinput, multioutput system, when the system model is established, there are uncertain factors such as friction between joints, coupling, measurement error, and external disturbance. Therefore, reducing the influence of model uncertainty in the robotic arm system on the control accuracy of the end effector has always been a hot research topic in the field of control at home and abroad [19]. In recent years, with the development of the intelligent control theory, some advanced control theories have also been proposed. Although these advanced control theories can improve the tracking accuracy of the system to a certain extent, there are still some problems to be solved.

This paper combines the RBF neural network to control the parameters of the double-joint manipulator, improve the control effect of the two-joint manipulator, and promote the work efficiency of the manipulator.

RETRACTED

2. Command Filtering Backstep Impedance Control of the Adaptive Neural Network for the Dual-Joint Manipulator

2.1. Command Filtering Backstep Impedance Control of Adaptive Neural Network. In recent years, to enable robots to handle increasingly complex tasks, many robots have installed dual-joint robotic arms with higher dexterity. When the robot provides services, the double-joint robotic arm will physically interact with the unknown external environment, so the compliance and safety of the double-joint robotic arm should be fully ensured to ensure the safety of physical interaction. To adjust the physical interaction force between the two-joint manipulator and the external environment, the impedance controller of the two-joint manipulator has been widely used in the interactive control of the robot.

At present, there have been many research achievements in the backstepping impedance controller of the double-joint manipulator. However, the "computational complexity" and "singularity" problems that may occur in the design process of the traditional backstepping method and the uncertain nonlinear terms in the dual-joint manipulator system due to the difficulty of obtaining the model parameters accurately deserve attention. In order to better solve these problems and make the dual-joint manipulator achieve better impedance control performance, this chapter introduces the adaptive neural network control technology into the design of the command filtering backstepping impedance controller. Moreover, this paper constructs an adaptive neural network command filtering backstep impedance controller for the dual-joint manipulator so that the uncertain dual-joint manipulator system can better realize the physical interaction control with the unknown external environment. Compared with the existing dual-joint manipulator control scheme, this control scheme has the following advantages:

The dynamic equation of the double-joint manipulator system can be described as follows:

$$D(x)\ddot{x} + C(x,\dot{x})\dot{x} + G(x) = u - \tau_e. \tag{1}$$

We define $x_1 = x$ and $x_2 = \dot{x}$, and the model of the double-joint robotic arm system can be rewritten in the following form:

$$\dot{x}_2 = D^{-1}(x_1)(u - \tau_e - C(x_1, x_2)x_2 + G(x_1)). \tag{2}$$

The command filter used in this chapter can be seen in formula (2). In order to improve the control accuracy of the dual-joint manipulator system, the compensation signal will be constructed to compensate for the filtering error generated by the command filter. The compensation signal design is as follows:

$$\begin{cases} \dot{\xi}_1 = -K_1\xi_1 + \xi_2 + (x_{1,c} - \alpha), \\ \dot{\xi}_2 = 0. \end{cases} \tag{3}$$

Among them, the control gain matrix is $K_1 = K_1^T > 0$ and x is the output signal vector of the filter. When $t = 0$, ξ_1 and ξ_2 are zero vectors.

The error variable is defined, where x_r is the tracking trajectory of the dual-joint manipulator through the impedance relationship. The design steps of the controller are as follows:

Step 1: the algorithm constructs the Lyapunov function as $V_1 = (1/2)v_1^T v_1$ and derives V_1 to get

$$\dot{V}_1 = v_1^T \dot{v}_1 = v_1^T(\dot{z}_1 - \dot{\xi}_1) = v_1^T(x_2 - \dot{x}_r - \dot{\xi}_1). \tag{4}$$

The virtual control law α is designed as

$$\alpha = -Kz_1 + \dot{x}_r. \tag{5}$$

Among them, the control gain matrix is $K_1 = K_1^T > 0$. By substituting formulas (3) and (5) into formula (4), we get

$$\dot{V}_1 = v_1^T(z_2 + x_{1,c} + \alpha - \alpha - \dot{x}_r - \dot{\xi}_1) = -v_1^T K_1 v_1 + v_1^T v_2. \tag{6}$$

Step 2: next, the algorithm selects the Lyapunov function as follows:

$$V_2 = V_1 + \frac{1}{2}v_2^T D(x_1)v_2. \tag{7}$$

The time derivative of the abovementioned formula is obtained as follows:

$$\begin{aligned} \dot{V}_2 &= \dot{V}_1 + v_2^T D(x_1)\dot{v}_2 + \frac{1}{2}v_2^T D(x_1)v_2, \\ &= v_2^T \begin{pmatrix} u - \tau_e - C(x_1, x_2)x_2 + v_1 \\ -G(x_1) - D(x_1)(\dot{x}_{1,c} + \dot{\xi}_2) \end{pmatrix} - v_1^T K_1 v_1 + \frac{1}{2}v_2^T \dot{D}(x_1)v_2. \end{aligned} \tag{8}$$

RETRACTED

Since there are uncertain nonlinear terms in $D(x_1)$, $C(x_1, x_2)$ and $G(x_1)$, adaptive neural network techniques are used to approximate the matrix terms $D(x_1)$, $C(x_1, x_2)$, and $G(x_1)$.

The real control law u for designing a dual-joint robotic arm system is

$$u = -K_2 z_2 + \tau_e + \widehat{W}_D^T S_D(Z_D) x_{1,c} + \widehat{W}_C^T S_C(Z_C) x_{1,c} + \widehat{W}_G^T S_G(Z_G) - \nu_1 - K_r \text{sign}(\nu_2). \tag{9}$$

The neural network weight adaptation law is designed as

$$\dot{\widehat{W}}_{Dk} = -\Gamma_{Dk}\left(\sigma_{Dk}\widehat{W}_{Dk} + S_{Dk}(Z_D)\dot{x}_{1,c}\nu_{2k}\right), \tag{10}$$

$$\dot{\widehat{W}}_{Ck} = -\Gamma_{Ck}\left(\sigma_{Ck}\widehat{W}_{Ck} + S_{Ck}(Z_C)\dot{x}_{1,c}\nu_{2k}\right), \tag{11}$$

$$\dot{\widehat{W}}_{Gk} = -\Gamma_{Gk}\left(\sigma_{Gk}\widehat{W}_{Gk} + \phi_{Gk}(Z_G)\nu_{2k}\right). \tag{12}$$

Among them, the matrix is $\Gamma_{Dk} > 0, \Gamma_{Ck} > 0, \Gamma_{Gk} > 0$. $\sigma_{Dk}, \sigma_{Ck}, \sigma_{GFk}$ are all positive numbers to improve robustness.

$$W_D^{*T} S_D(Z_D) = D + \varepsilon_D, \tag{13}$$

$$W_C^{*T} S_C(Z_C) = C + \varepsilon_C, \tag{14}$$

$$W_G^{*T} S_G(Z_G) = G + \varepsilon_G. \tag{15}$$

Among them, ε_D, ε_C, and ε_G are minimal approximation error matrices.

$$\dot{V}_2 = -\nu_1^T K_1 \nu_1 - \nu_2^T K_2 \nu_2 + \nu_2^T \widetilde{W}_D^T S_D(Z_D)\dot{x}_{1,c} + \nu_2^T \widetilde{W}_C^T S_C(Z_C)\dot{x}_{1,c} + \nu_2^T \widetilde{W}_G^T S_G(Z_G) + \nu_2^T (E_r - K_r \text{sign}(\nu_2)). \tag{16}$$

Note 1: within the designed control law, the control parameter K_r should be selected as $K_{rii} \geq \|E_{ri}\|$. In order to ensure the stability of the method proposed in this chapter when the double-joint manipulator is working, a larger value of K_r should be selected, but this is also not the best way for the system to induce chattering. Therefore, the control parameter K_r should be changed to $K_r = k_D \dot{x}_{1,c} + k_c x_{1,c} + k_G$. Among them, $k_D \geq \|\varepsilon_D\|$, $k_C \geq \|\varepsilon_C\|$, and $k_G \geq \|\varepsilon_G\|$.

2.2. System Stability Analysis. In this section, the Lyapunov theorem will be used to determine the stability of the closed-loop system of the double-joint manipulator under the proposed control scheme. The Lyapunov function is selected as follows:

$$V = V_2 + \frac{1}{2}\sum_{k=1}^{n} \widetilde{W}_{Dk}^T \Gamma_{DK}^{-1} \widetilde{W}_{Dk}^T + \frac{1}{2}\sum_{k=1}^{n} \widetilde{W}_{Ck}^T \Gamma_{CK}^{-1} \widetilde{W}_{Ck}^T + \frac{1}{2}\sum_{k=1}^{n} \widetilde{W}_{Gk}^T \Gamma_{GK}^{-1} \widetilde{W}_{Gk}^T. \tag{17}$$

Substituting formulas (8) to (10) and (14) into the derivative of formula (15), we get

$$\begin{aligned}\dot{V} = {} & -\nu_1^T K_1 \nu_1 - \nu_2^T K_2 \nu_2 + \nu_2^T \widetilde{W}_D^T S_D(Z_D)\dot{x}_{1,c} + \nu_2^T \widetilde{W}_C^T S_C(Z_C)\dot{x}_{1,c} \\ & + \nu_2^T \widetilde{W}_G^T S_G(Z_G) + \nu_2^T (E_r - K_r \text{sign}(\nu_2)) \\ & - \sum_{k=1}^{n} \sigma_{DK} \widetilde{W}_{Dk}^T \widehat{W}_{Dk}^T - \sum_{k=1}^{n} \widetilde{W}_{Dk}^T S_{DK}(Z_D)\dot{x}_{1,c}\nu_{2k} \\ & - \sum_{k=1}^{n} \widetilde{W}_{Ck}^T S_{CK}(Z_C)\dot{x}_{1,c}\nu_{2k} - \sum_{k=1}^{n} \sigma_{CK} \widetilde{W}_{Ck}^T \widehat{W}_{Ck}^T - \sum_{k=1}^{n} \sigma_{GK} \widetilde{W}_{Gk}^T \widehat{W}_{Gk}^T \\ & - \sum_{k=1}^{n} \widetilde{W}_{Gk}^T S_{GK}(Z_G)\nu_{2k}.\end{aligned} \tag{18}$$

The following relation can be obtained as follows:

$$\nu_2^T \widetilde{W}_D^T S_D(Z_D)\dot{x}_{1,c} = \sum_{k=1}^{n} \widetilde{W}_{Dk}^T S_{Dk}(Z_D)\dot{x}_{1,c}\nu_{2k}, \tag{19}$$

$$\nu_2^T \widetilde{W}_C^T S_C(Z_C)\dot{x}_{1,c} = \sum_{k=1}^{n} \widetilde{W}_{Ck}^T S_{Ck}(Z_C)\dot{x}_{1,c}\nu_{2k}, \tag{20}$$

$$\nu_2^T \widetilde{W}_G^T S_G(Z_G) = \sum_{k=1}^{n} \widetilde{W}_{Gk}^T S_{Gk}(Z_G)\nu_{2k}. \tag{21}$$

Based on Young's inequality, the following formula can be obtained as

$$-\widetilde{W}_{Dk}^T \widehat{W}_{Dk}^T \leq -\frac{1}{2}\widetilde{W}_{Dk}^T \widetilde{W}_{Dk}^T + \frac{1}{2} W_{Dk}^{*T} W_{Dk}^*, \tag{22}$$

$$-\widetilde{W}_{Ck}^T \widehat{W}_{Ck}^T \leq -\frac{1}{2}\widetilde{W}_{Ck}^T \widetilde{W}_{Ck}^T + \frac{1}{2} W_{Ck}^{*T} W_{Ck}^*, \tag{23}$$

$$-\widetilde{W}_{Gk}^T \widehat{W}_{Gk}^T \leq -\frac{1}{2}\widetilde{W}_{Gk}^T \widetilde{W}_{Gk}^T + \frac{1}{2} W_{Gk}^{*T} W_{Gk}^*. \tag{24}$$

Substituting formulas (19) to (24) into formulas (18) and $K_{rii} \geq \|E_{ri}\|$, we get

$$\begin{aligned}\dot{V} \leq {} & -\nu_1^T K_1 \nu_1 - \nu_2^T K_2 \nu_2 - \frac{1}{2}\sum_{k=1}^{n} \sigma_{DK} \widetilde{W}_{Dk}^T \widehat{W}_{Dk}^T - \frac{1}{2}\sum_{k=1}^{n} \sigma_{CK} \widetilde{W}_{Ck}^T \widehat{W}_{Ck}^T \\ & - \frac{1}{2}\sum_{k=1}^{n} \sigma_{GK} \widetilde{W}_{Gk}^T \widehat{W}_{Gk}^T + \frac{1}{2}\sum_{k=1}^{n} \sigma_{DK} \widetilde{W}_{Dk}^{*T} \widehat{W}_{Dk}^* + \frac{1}{2}\sum_{k=1}^{n} \sigma_{CK} \widetilde{W}_{Dk}^{*T} \widehat{W}_{Ck}^* \\ & + \frac{1}{2}\sum_{k=1}^{n} \sigma_{GK} \widetilde{W}_{Gk}^{*T} \widehat{W}_{Gk}^* \\ \leq {} & a_0 V + c_0.\end{aligned} \tag{25}$$

From inequality (25), it can be deduced that all control signals of the closed-loop system of the double-joint manipulator are semiglobally uniformly asymptotically bounded. The design flow chart of the control method in this chapter can be seen in Figure 1:

Note 2: the size of the control parameter determines the radius of the tracking error domain. That is, the larger the control parameter $\lambda_{\max}(K_i)$, the smaller the radius of the tracking error domain.

RETRACTED

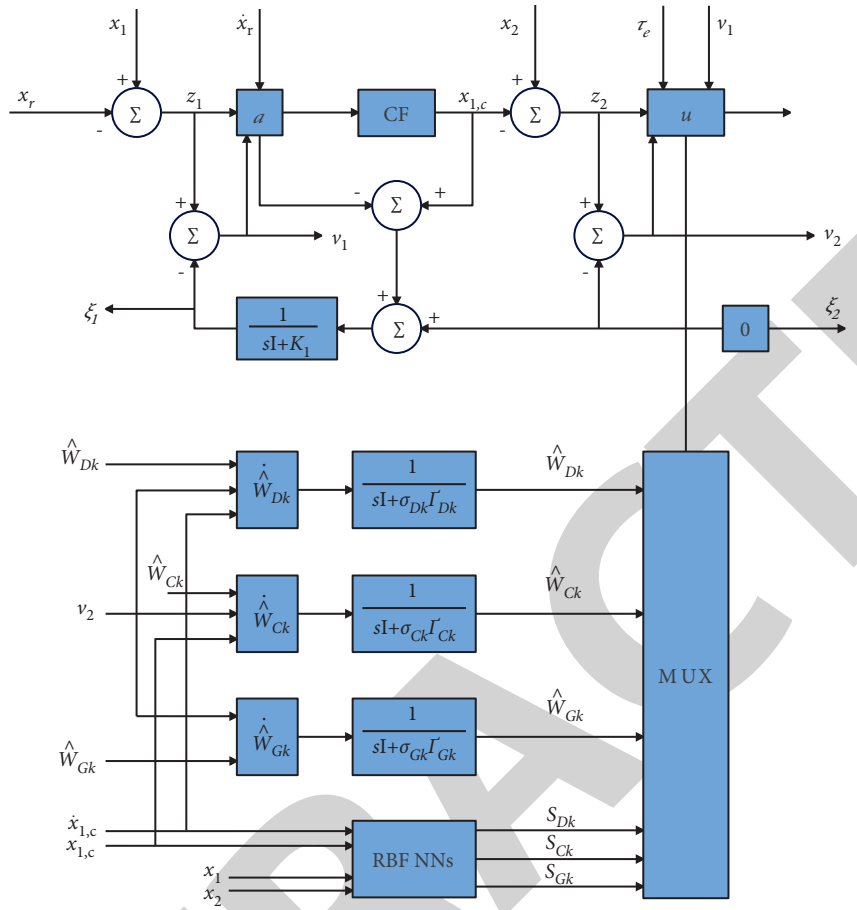

Figure 1: . Flowchart of the controller design.

Furthermore, through the integral inequality (25), we can get

$$V(t) \le V(0)e^{-a_0 t} + \frac{c_0}{a_0}\left(1 - e^{-a_0 t}\right) \le V(0) + \frac{c_0}{a_0}. \tag{26}$$

From the abovementioned inequality, we derive

$$\frac{1}{2}\left\|v_1(t)\right\|^2 \le V(0) + \frac{c_0}{a_0}. \tag{27}$$

From the abovementioned inequality, it can be known that, under the condition that all state quantities of the dual-joint manipulator system can be measured, for the initial compact set, $(v_1(0), v_2(0), \tilde{W}_{DK}(0), \tilde{W}_{CK}(0), \tilde{W}_{GK}(0)) \in \Omega_0$, $v_1(t)$ converges into the compact set Ω_{v_1}. By the same method, $v_2(t)$ can be converged into the compact set Ω_{v_2}, and $\tilde{W}_{DK}(0), \tilde{W}_{CK}(0), \tilde{W}_{GK}(0)$ can be converged into $\Omega_{\overline{W}_{Dk}}$, $\Omega_{\overline{W}_{Ck}}$, and $\Omega_{\overline{W}_{Gk}}$, respectively.

$$\begin{aligned}
\Omega_{v_1} &= \left\{ v_1(t) \in R^n \middle| \left\|v_1(t)\right\| \le \sqrt{2\left(V(0) + \left(c_0/a_0\right)\right)} \right\},\\
\Omega_{v_2} &= \left\{ v_2(t) \in R^n \middle| \left\|v_2(t)\right\| \le \sqrt{\frac{2\left(V(0) + \left(c_0/a_0\right)\right)}{\lambda_{\min}\left(D\left(x_1\right)\right)}} \right\},\\
\Omega_{\overline{W}_{Dk}} &= \left\{ \tilde{W}_{DK}(t) \in R^h \middle| \left\|v_2(t)\right\| \le \sqrt{\frac{2\left(V(0) + \left(c_0/a_0\right)\right)}{\lambda_{\min}\left(\Gamma_{Dk}^{-1}\right)}} \right\},\\
\Omega_{\overline{W}_{Ck}} &= \left\{ \tilde{W}_{CK}(t) \in R^h \middle| \left\|v_2(t)\right\| \le \sqrt{\frac{2\left(V(0) + \left(c_0/a_0\right)\right)}{\lambda_{\min}\left(\Gamma_{Ck}^{-1}\right)}} \right\},\\
\Omega_{\overline{W}_{Gk}} &= \left\{ \tilde{W}_{GK}(t) \in R^h \middle| \left\|v_2(t)\right\| \le \sqrt{\frac{2\left(V(0) + \left(c_0/a_0\right)\right)}{\lambda_{\min}\left(\Gamma_{Gk}^{-1}\right)}} \right\}.
\end{aligned} \tag{28}$$

RETRACTED

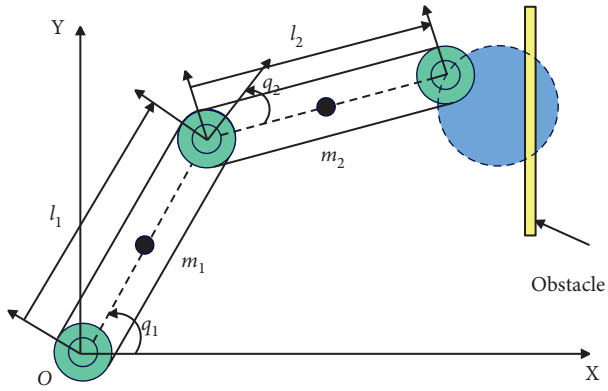

Figure 2: Plane two-joint robotic arm model.

From inequality (27), $\lim_{t\to\infty} \|v_1(t)\| \le \sqrt{2(c_0/a_0)}$ is easy to obtain. That is, for any given constant u, $\sqrt{2(c_0/a_0)} \le \mu$ can be obtained by adjusting the parameters a_0 and c_0, and thus, $\lim_{t\longrightarrow\infty} \|v_1(t)\| \le \mu$ can be obtained.

Note 3: increasing α_0 or decreasing c can effectively reduce $\sqrt{2(c_0/a_0)}$. Therefore, selecting a larger parameter a_0 can make the system obtain a sufficiently small tracking error of 0. However, because the parameters α and c both contain the parameter $\sigma_{Dk}, \sigma_{Ck}, \sigma_{Gk}\,(k = 1, 2, \ldots, n)$, the best control performance of the system requires the designer to accumulate experience in simulation research.

3. Analysis of Simulation Results

As shown in Figure 2, it is used for simulation experiments.

The model of the planar two-joint manipulator system used in this chapter is as follows:

$$\begin{cases} \dot{x}_2 = D^{-1}(x_1)[u - \tau_e - C(x_1, x_2)x_2 - G(x_1)], \\ y = x_1. \end{cases} \tag{29}$$

Here, $x_1 = [x_{11}, x_{12}]^T$ and $x_2 = [\dot{x}_{11}, \dot{x}_{12}]^T$. Among them, the connecting rod used in this simulation is a uniform and regular cuboid rod; then, there is $l_{ci} = (l_i/2)$.

According to the physical model of the two-joint manipulator, its kinetic energy equation can be calculated as

$$K(q, \dot{q}) = \frac{1}{2}m_1 l_{c1}^2 \dot{q}_1^2 + \frac{1}{2}I_1 \dot{q}_1^2 + \frac{1}{2}m_2 l_1^2 \dot{q}_1^2 + m_2 l_1 l_{c2} \dot{q}_1 (\dot{q}_1 + \dot{q}_2)\cos \dot{q}_2 + \frac{1}{2}m_2 l_{c2}^2 (\dot{q}_1 + \dot{q}_2) + \frac{1}{2}I_2 (\dot{q}_1 + \dot{q}_2)^2. \tag{30}$$

The potential energy of the two-joint manipulator can be expressed as

$$P(q) = m_1 g l_{C2} \sin q_1 + m_2 g[l_1 \sin q_1 + l_{c2} \sin(q_1 + q_2)]. \tag{31}$$

According to the Euler–Lagrange equation $d/dt\partial(K - P)/\partial\dot{q} - \partial(K - P)/\partial q = 0$, the inertia matrix $D(q)$ of the two-joint manipulator in the joint coordinate system, the centrifugal force and Coriolis force matrix $C(q, \dot{q})$, the gravity term matrix $G(q)$, and the Jacobian matrix of the two-joint manipulator in the joint coordinate system are expressed as

$$D(q) = \begin{bmatrix} m_1 l_{c1}^2 + m_2 l_1^2 + 2 l_1 l_{c2} \cos q_2 + I_1 + I_2, & m_2\left(l_{c2}^2 + l_1 l_{c2} \cos q_2\right) + I_2, \\ m_2\left(l_{c2}^2 + l_1 l_{c2} \cos q_2\right) + I_2, & m_2 l_{c2}^2 + I_2. \end{bmatrix}, \tag{32}$$

$$C(q, \dot{q}) = \begin{bmatrix} -m_2 l_1 l_{c2} \dot{q}_2 \sin q_2, & -m_2 l_1 l_{c2} (\dot{q}_1 + \dot{q}_2)_2 \sin q_{22}, \\ m_2 l_1 l_{c2} \dot{q}_1 \sin q_2, & 0. \end{bmatrix}, \tag{33}$$

$$G(q) = \begin{bmatrix} (m_1 l_{c2} + m_2 l_1) g \cos q_1 + m_2 l_{c2} g \cos(q_1 + q_2) \\ m_2 l_{c2} g \cos(q_1 + q_2). \end{bmatrix}, \tag{34}$$

$$G(q) = \begin{bmatrix} -(l_1 \sin q_1 + l_2 \sin(q_1 + q_2)), & -l_2 \sin(q_1 + q_2), \\ l_1 \cos q_1 + l_2 \cos(q_1 + q_2), & l_2 \cos(q_1 + q_2). \end{bmatrix}. \tag{35}$$

We assume that the initial position of the two-joint manipulator in Cartesian coordinates is selected as $x_{11}(0) = 0.5\,\text{m}$ and $x_{12}(0) = 0.8\,\text{m}$. In order to verify the effectiveness of the designed robot arm impedance method, an obstacle is set at the position of $x0 = 0.8\,\text{m}$ to obtain two-joint mechanical desired impedance parameters.

In order to more convincingly verify the effectiveness of the proposed command filter backstep impedance control method of the adaptive neural network, the model-based command filter impedance control method and the adaptive neural network dynamic surface backstepping impedance control are also used in the two-joint manipulator simulation experiment for comparative analysis. The gain

RETRACTED

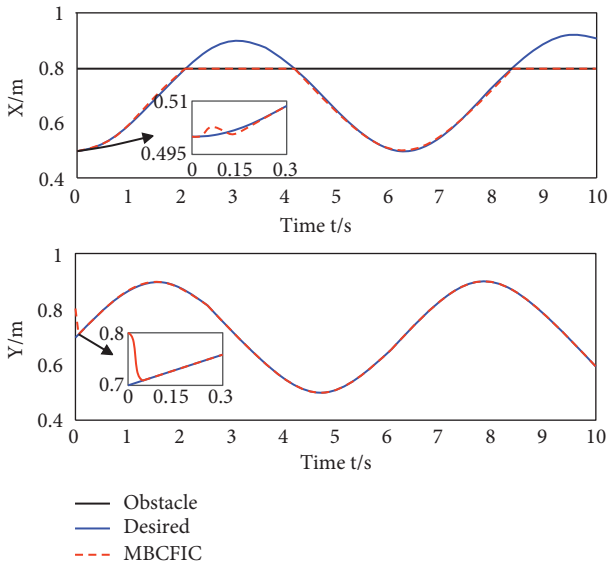

Figure 3: Position tracking curve (the model-based control method).

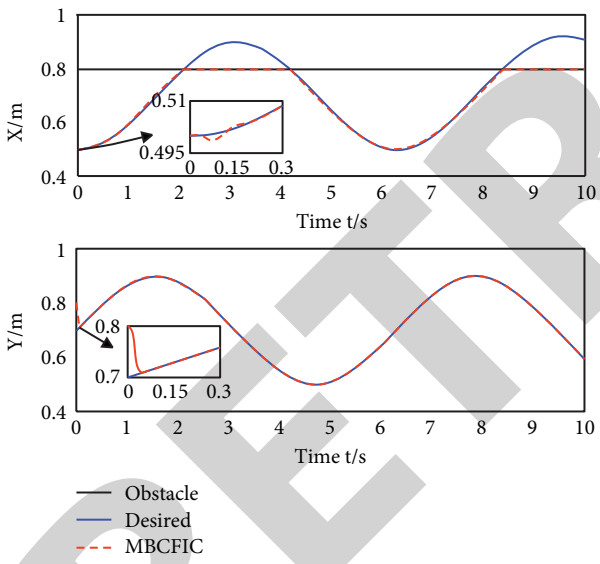

Figure 4: Position tracking curve (the command filtering method).

parameters of the three manipulator impedance control methods are selected as follows:

Method 1: for the model-based command filter impedance control (MBCFIC) method, the control law of the control method is designed as $u = -K_2 z_2 + \tau_e + D(x_1)\dot{x}_{1,c} + C(x_1, x_2)x_{1,c} + G(x_1) - v_1$. The control gain parameters are chosen as $K_1 = \text{diag}[50, 50]$ and $K_2 = \text{diag}[50, 50]$.

Method 2: for the adaptive neural network command filtering backstep impedance control (ANNCFIC) method, the center point of the RBF neural network in this paper is selected as $[-1, 1] < [-1, 1] \times [-1, 1] * [-1, 1] \times [-1, 1] \times [-11] * [-1, 1] * [-11] \times [-1, 1] \times [-1, 1]$. The initial weight of the RBF neural network is set to 0, and its adaptive law parameters are selected as $\Gamma_{DK} = \Gamma_{CK} = \Gamma_{GK} = \text{diag}[50, 50]$ and $\sigma_{DK} = \sigma_{CK} = \sigma_{GK} = 0.01$. The command filter parameters are selected as $w_n = 300$ and $g_n = 0.5$, and the control gain parameters are selected as $K_1 = \text{diag}[50, 50]$ and $K_2 = \text{diag}[50, 50]$.

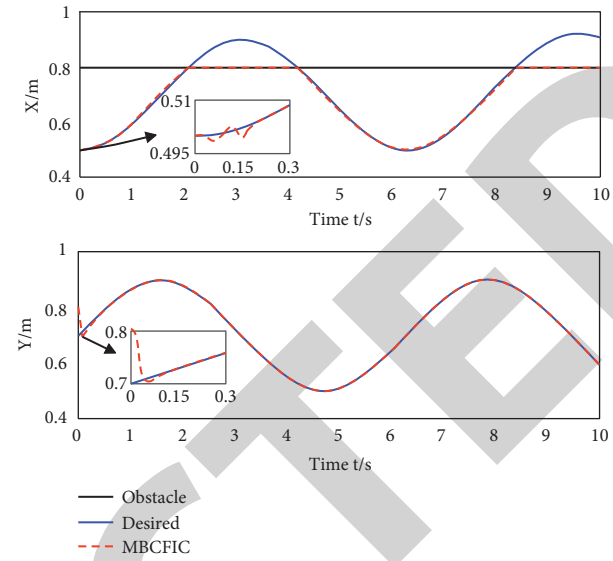

Figure 5: Position tracking curve (the dynamic surface method).

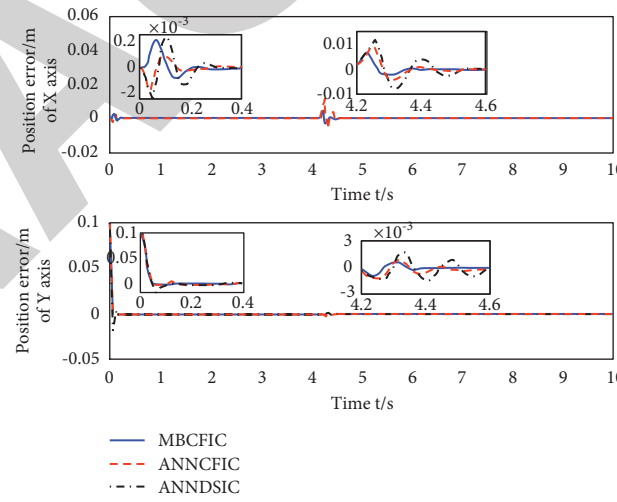

Figure 6: Comparison of position tracking errors of three control schemes.

Method 3: for the adaptive neural network dynamic surface backstepping impedance control (ANNDSIC) strategy, the dynamic surface used in this strategy is selected as $T\dot{\alpha}_d + \alpha_d = \alpha$ (T is a positive number). Therefore, the real control law of the control strategy is set to $u = -K_2 z_2 + \tau_e + \widehat{W}_D^T S_D(Z_D) \quad (\alpha - \alpha_d/T) \dot{x}_{1,c} + \widehat{W}_C^T S_C(Z_C)\alpha + \widehat{W}_G^T S_G(Z_G) - K\text{sign}(v_2)$, and the neural network structure and parameter selection are consistent with method 1. The control gain parameters

RETRACTED

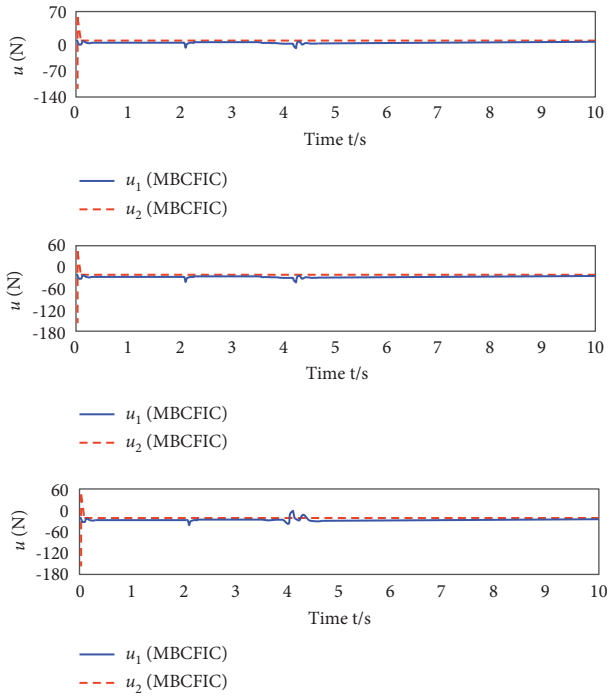

Figure 7: Control input curves of three control schemes.

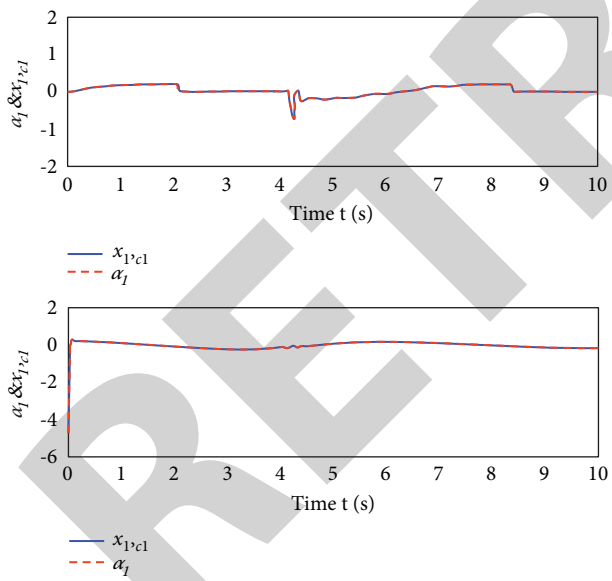

Figure 8: Curves of α and $x_{1,c}$.

are selected as $K_1 = \text{diag}[50, 50]$ and $K_2 = \text{diag}[50, 50]$, and the dynamic surface control parameters are selected as $T = 0.01$.

Figures 3–6 show the position tracking diagrams obtained from the simulation experiments of the three schemes. 3 to 5 are the position tracking curves of the model-based command filter impedance control method, the

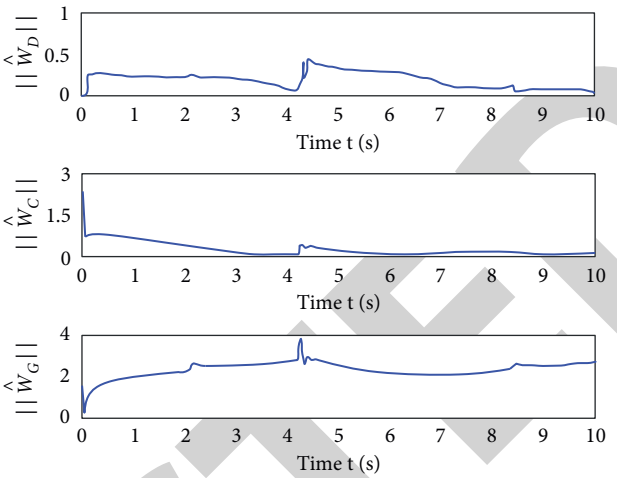

Figure 9: Neural network weight estimation curve for the proposed control scheme.

Table 1: Statistical table of the motion error of robotic arm.

Num	Error ratio
1	0.0431
2	0.0458
3	0.0305
4	0.0479
5	0.0030
6	0.0387
7	0.0218
8	0.0105
9	0.0262
10	0.0397
11	0.0361
12	0.0197
13	0.0053
14	0.0161
15	0.0330
16	0.0455
17	0.0378
18	0.0223
19	0.0286
20	0.0317
21	0.0270
22	0.0268
23	0.0196
24	0.0420
25	0.0195
26	0.0316
27	0.0415
28	0.0267
29	0.0407
30	0.0093
31	0.0196
32	0.0367
33	0.0406
34	0.0428
35	0.0393
36	0.0386

adaptive neural network command filter backstep

RETRACTED

impedance control method, and the adaptive neural network dynamic surface backstep impedance control method, respectively. Figure 6 is a comparison diagram of the position tracking errors of these three control strategies. It can be seen from Figures 3 and 4 that the proposed neural network control method can achieve a good position tracking effect when the dynamic model of the manipulator is difficult to obtain accurately. This effectively proves that the adaptive neural network control can better approximate the uncertain nonlinear terms in the system. It can be seen from Figures 4 and 5 that the command filtering method used in this section has a smaller tracking error than the dynamic surface method. This proves that the designed error compensation mechanism can effectively eliminate the filtering error, which is beneficial for the robotic arm to be better applied to tasks with high tracking accuracy. It can be seen from Figure 6 that the proposed neural network command filter impedance control method has a good position tracking performance whether it is in contact with external obstacles or not.

Figure 7 shows a graph of the control input of the three control methods. It can be seen from the graph that the control input of the manipulator is kept within an appropriate range. Furthermore, it can be seen from Figure 8 that when the end effector of the robotic arm comes in contact with an external obstacle, a contact collision force is initially generated, but the impedance relationship can be quickly used to keep the contact force in a suitable range. Therefore, the proposed filtering can quickly realize impedance control, so that the end of the manipulator has a relatively safe physical interaction force when it contacts the external unknown environment. This proves that the proposed control method can effectively guarantee the safety of the manipulator when it is in contact with an unknown external environment. It can be seen from Figure 9 that the estimated value of the neural network weight of the control method proposed in this chapter is bounded. Through the comparative analysis of the above three control schemes, it can be proved that the designed adaptive neural network command filtering backstep impedance control method for the dual-joint manipulator system can effectively solve the problem that the dynamic model of the manipulator is difficult to obtain accurately. Moreover, it enables the robot arm to obtain a good position tracking effect and impedance tracking performance, ensuring the safety of the robot arm in contact with the unknown external environment.

The abovementioned research study verifies that the parameter-tunable RBF neural network control method for the dual-joint manipulator has certain effects on the parameter control process of the dual-joint manipulator. On this basis, through the simulation of multiple sets of data, the motion error of the manipulator is calculated, and the results shown in Table 1 are obtained.

It can be seen from the abovementioned research study that the parameter-tunable RBF neural network control method facing the double-joint manipulator can effectively improve the motion accuracy of the double-joint manipulator.

4. Conclusion

The force/position control of the double-joint manipulator system has become the general trend. The impedance control strategy of the double-joint manipulator treats the force control and the position control as a unified whole. Compared with other current multijoint manipulator force/position control methods, this method has very significant advantages. In the process of actual use, the amount of calculation is relatively small, and it has good robustness to changes in the external unknown environment. To achieve good impedance control of a multijoint manipulator, its end effector needs to have good position tracking performance. However, the multijoint manipulator is a highly nonlinear system with strong coupling effect which makes it difficult to construct the system model accurately, and also there are many unknown external disturbances. This paper combines the RBF neural network to control the parameters of the double-joint manipulator to improve the control effect of the two-joint manipulator and promote the work efficiency of the manipulator. The experimental study verifies that the parameter-tunable RBF neural network control method facing the double-joint manipulator has a certain effect on the parameter control process of the double-joint manipulator. Moreover, the parameter-tunable RBF neural network control method facing the double-joint manipulator can effectively improve the motion accuracy of the double-joint manipulator.

Data Availability

The labeled dataset used to support the findings of this study is available from the corresponding author upon request.

Conflicts of Interest

The author declares that there are no conflicts of interest.

Acknowledgments

This work was supported by Hubei University of Technology.

References

[1] Z. Xin, X. Wenbo, and L. Wenru, "The control strategy of manipulator based on fractional-order iterative learning," *Automatic Control and Computer Sciences*, vol. 55, no. 4, pp. 368–376, 2021.

[2] M. Bugday and M. Karali, "Design optimization of industrial robot arm to minimize redundant weight," *Engineering Science and Technology, an International Journal*, vol. 22, no. 1, pp. 346–352, 2019.

[3] S. Phukan and C. Mahanta, "A position synchronization controller for co-ordinated links (COOL) dual robot arm based on integral sliding mode: design and experimental validation," *International Journal of Automation and Computing*, vol. 18, no. 1, pp. 110–123, 2021.

RETRACTED

Hindawi
Journal of Robotics
Volume 2023, Article ID 9896453, 1 page
https://doi.org/10.1155/2023/9896453

Retraction

Retracted: Multiscale Motion Detection and Recognition Combining Still Images and Video Sequences

Journal of Robotics

Received 8 August 2023; Accepted 8 August 2023; Published 9 August 2023

Copyright © 2023 Journal of Robotics. This is an open access article distributed under the Creative Commons Attribution License, which permits unrestricted use, distribution, and reproduction in any medium, provided the original work is properly cited.

This article has been retracted by Hindawi following an investigation undertaken by the publisher [1]. This investigation has uncovered evidence of one or more of the following indicators of systematic manipulation of the publication process:

(1) Discrepancies in scope
(2) Discrepancies in the description of the research reported
(3) Discrepancies between the availability of data and the research described
(4) Inappropriate citations
(5) Incoherent, meaningless and/or irrelevant content included in the article
(6) Peer-review manipulation

The presence of these indicators undermines our confidence in the integrity of the article's content and we cannot, therefore, vouch for its reliability. Please note that this notice is intended solely to alert readers that the content of this article is unreliable. We have not investigated whether authors were aware of or involved in the systematic manipulation of the publication process.

Wiley and Hindawi regrets that the usual quality checks did not identify these issues before publication and have since put additional measures in place to safeguard research integrity.

We wish to credit our own Research Integrity and Research Publishing teams and anonymous and named external researchers and research integrity experts for contributing to this investigation.

The corresponding author, as the representative of all authors, has been given the opportunity to register their agreement or disagreement to this retraction. We have kept a record of any response received.

References

[1] Z. Chen, "Multiscale Motion Detection and Recognition Combining Still Images and Video Sequences," *Journal of Robotics*, vol. 2022, Article ID 7682559, 12 pages, 2022.

Hindawi
Journal of Robotics
Volume 2022, Article ID 7682559, 12 pages
https://doi.org/10.1155/2022/7682559

RETRACTED

Research Article

Multiscale Motion Detection and Recognition Combining Still Images and Video Sequences

Zhuo Chen

College of Information Engineering, Xinyang Agriculture and Forestry University, Xinyang 464000, Henan, China

Correspondence should be addressed to Zhuo Chen; 2014270001@xyafu.edu.cn

Received 13 July 2022; Revised 28 July 2022; Accepted 6 August 2022; Published 31 August 2022

Academic Editor: Shahid Hussain

Copyright © 2022 Zhuo Chen. This is an open access article distributed under the Creative Commons Attribution License, which permits unrestricted use, distribution, and reproduction in any medium, provided the original work is properly cited.

In order to improve the sports training and competition effect of sports, this paper combines the accurate recognition method of video image fuzzy features to accurately identify the sports process to explore the movement characteristics of athletes on the sports stage. Moreover, this paper uses the trigger system to select cases and adopts the all-digital trigger method in the digital sports video recognition system. In addition, this paper uses the ADC input overrange as the judgment standard for bad cases and constructs an accurate recognition system for sports training features based on video image recognition. Finally, this paper verifies the effect of the accurate recognition method of local fuzzy features in sports video images. The experimental study verifies the effectiveness of the accurate recognition method of local fuzzy features in sports video images.

1. Introduction

At present, in physical training, strength training and speed training are the two major focuses. Explosive strength training is mainly used in athletes' starting and sports training stages, while speed training is mainly used in athletes accelerating and maintaining high speed. Moreover, athletes with good explosiveness and speed can achieve good results in sports training. In addition, explosive power and speed are important sports qualities that sports athletes need to have, and they are also the basis for athletes to successfully learn other sports and skills and have a significant impact on sports performance.

Explosive power means that the athlete changes from a static state to a moving state in the shortest time during the starting process, and the body obtains the maximum forward momentum, creating favorable conditions for the acceleration process in the running phase [1]. The training of explosive power is very important for sports training. To a certain extent, the strength of explosive power determines the starting speed of the athlete. A fast starting speed lays the foundation for the subsequent acceleration process of the athlete. The acceleration link catches up with the opponent and restores the distance. During the competition, an athlete with a slow start and weak explosiveness is undoubtedly not an excellent athlete [2]. From the point of view of explosive power, this not only represents the speed of the athlete's reaction but also shows the problems existing in the athlete's explosive power training, and the physical quality is not as good as the athlete with strong explosive power. The physical quality, strength, and speed also determine the ability of the athlete. Only by enhancing the explosive power and improving the starting speed of the athlete can we get a good start at the beginning of the competition [3]. Practice has proved that the use of fast single-leg jumping exercises has a very significant effect on improving the strength of the lower limbs of sports trainees [4].

The Role of Hopping Exercises in Developing Effective Muscle Groups for Sports Trainees. When an athlete is exercising, most of the muscles in the body begin to work, and different training programs exercise different muscle groups. During training, sports trainees will use the iliopsoas, quadriceps, triceps calf, posterior calf muscles, and ankle joints. Improving the strength of these muscle groups is a guarantee for sports trainees to carry out targeted training in the future. *The Key to Exercising Effective Muscle Groups* [5]. In daily training, it is easy to ignore the muscles on the back of the athlete's calf, but in the process of running, the

hamstrings play a back-push. If this part of the muscle group is not fully exercised, resulting in insufficient development of this muscle group, it is easy to cause muscle strain on the back of the thigh [6]. The athlete's quadriceps and iliopsoas mainly help the athlete to ensure that the body does not lean back when raising the thigh. The exercise of the ankle joint can ensure that the athlete can push back smoothly and quickly place the center of gravity in the front [7].

One-Legged Hopping Training during the Starting Process. In the process of sports training, athletes usually use the squatting starting position when starting. This starting position can help athletes start quickly and can analyze the rapid single-legged hopping in sports teaching in a short time (training [8]).

The starting process mainly uses the explosive power of the body to quickly get rid of the static state, so as to achieve the fastest initial speed and lay the foundation for the athlete's subsequent accelerated running. We know that in the process of starting, athletes need to have great strength and explosive power in their lower limbs. The explosive power of lower limbs is a prerequisite for determining the starting speed of athletes, and strength is the guarantee for athletes to accelerate during running. After the sound of gunshots, the athlete should push back quickly to push the body forward, swing his arms greatly, and move the body forward rapidly [9]. In the process of training, coaches can take single-leg jump training to strengthen students' strength and lower body explosiveness. According to the physical fitness of the athlete, they formulate training methods that meet the physical condition of the athlete. For example, let the athletes perform single-leg squat exercises rhythmically, with 6–8 squatting as a group, and repeat 3–5 groups. During the training process, certain adjustments can be made according to the athlete's exercise level and physical tolerance and appropriately increase some weights to train the athlete's lower body strength. In the process of training, the training focus should be placed on effective muscle groups, the weight should be reasonably arranged, the weight should be adjusted appropriately according to the actual situation of the athlete, and the lower limb strength and explosive training of the athlete should be strengthened, so that the athlete can occupy the opportunity [10].

Hop Training in Acceleration Running. Acceleration running is the stage in which the athlete rushes out of the starting line and before the midway run after the athlete starts. Generally, the distance of accelerated running is 25–30 meters. Men usually use 13–15 steps to complete the accelerated run, and women usually use 15–17 steps to complete. Through observation, we can find that at the initial number of steps at the start, the landing points of the athlete's legs are two parallel lines with the same distance (straight line [11]). In the stage of accelerated running, if the stride length changes, under the same stride frequency, the increase of the stride length will accelerate the increase of the speed, and the decrease of the step length will lead to the decrease of the speed. The process of accelerated running is to make efficient use of the athlete's explosive power and give full play to the strength of the body in the accelerated running phase to achieve maximum speed. In the process of accelerated running, the athlete's lower body explosive power and physical tolerance play a key role, so coaches should strengthen the training of these two aspects of the athlete in the training process. Rapid hopping is a very efficient training method [12]. When training single-leg hopping, athletes use two methods of single-leg jumping and 20-meter single-leg jumping training. When jumping with one leg to reach a height, the athlete should jump up immediately after landing on one leg, switch feet for 15 jumps each, and perform 5–6 sets of exercises. The speed of jumping should be maintained once a second. In the training of the 20-meter single-leg jump, athletes should complete the training at the fastest speed and the maximum stride, control the balance and jumping rhythm of the body, and exchange feet for 10 sets each [13].

Sports is the last stage in sports training, the final finish of sports. Athletes need to maintain maximum speed and quickly hit the line. The requirements for the athlete to finish running are similar to those for running on the way. However, since athletes consume a lot of physical strength in the previous running stage, some techniques can be used to help athletes maintain their maximum speed when running at the finish line. When athletes are 15–20 meters away from the finish line, their upper body should lean forward and their center of gravity should move forward, which can increase the power of the back-push of the calf and at the same time increase the swing amplitude and step length of the arms, and always maintain the same cadence as the previous running stage [14]. In the sports running stage, athletes are required to have strong physical endurance and strength to support athletes rushing to the finish line [15]. Therefore, it is very necessary to strengthen the training of strength and endurance, and fast hopping is an efficient training method to strengthen the strength and endurance of athletes. During training, athletes can be trained by formulating rapid single-leg hops of different meters or by performing 50-100-meter mixed single-leg jumps, step jumps, and single-leg hop exchanges. Using this training method can increase the physical strength and endurance of athletes, promote the development of various comprehensive levels of athletes, and then fully demonstrate their own strength in sports training [16].

This paper combines the accurate recognition method of video image fuzzy features to accurately identify the sports process to explore the movement characteristics of athletes on the sports stage, which provides a reference for subsequent training and competition.

2. System Structure Design

2.1. Logic Design in FPGA. FPGA is the core device of the digital sports video recognition system, and the main digital logic functions of the spectrometer are implemented inside the FPGA. FPGA is divided by function and consists of the following parts:

(1) Data cache module

(2) Case storage module

RETRACTED

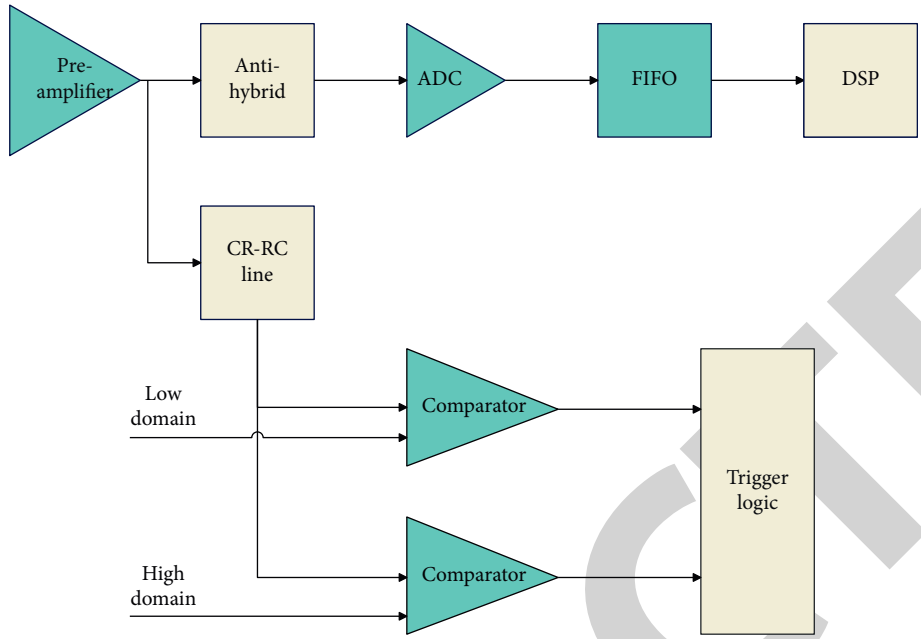

Figure 1: Schematic diagram of the traditional analog trigger circuit.

(3) Trigger module

(4) Digital filtering module (including shaping filtering and FIR low-pass filtering)

(5) Data processing module (including baseline elimination and peak finding)

(6) USB interface module

The digital sports video recognition system adopts the case-based operation mode. Each trigger corresponds to a good case. The function of the case storage module is to store the complete information of a good case. When the trigger signal is generated, the data in the data buffer is transferred to the instance storage module. The case storage module is also implemented with FIFO, and the length of the FIFO is the time length of the baseline plus the length of the shaping time of the pulse signal, which is determined by the type of the pulse signal generated by the detector. When the case storage FIFO is full, a full signal is generated and sent to the trigger module and the digital filter module, respectively. The function is to shield the trigger signal and notify the digital filter module to accept data for digital filtering. After filtering, the signal is reset, and the time in this paper is 6.4us.

2.2. Trigger Module. The sports video recognition system based on the case operation mode selects cases by triggering the system. The function of the trigger system is based on the voltage information sent by the detector, synthesizing the preset selection conditions of the physical case, realizing the response to the good case, and giving the corresponding trigger judgment. The data acquisition system selects and collects the case information of the electronics system according to the selection result of the trigger system and performs subsequent processing and data analysis on the useful data. The traditional sports video recognition system adopts the method of analog trigger selection, and its realization method is shown in Figure 1.

The signal output by the detector is divided into two channels, one channel enters the ADC for sampling through the antialiasing filter, and the other channel is used for trigger selection. The voltage signal output by the preamp is shaped by a simple CR-RC circuit and then enters a dual threshold comparator. When the signal amplitude is higher than the low threshold and lower than the high threshold, the trigger judgment logic generates a trigger signal to the case storage module. The information of the current trigger case stored in the case storage module is sent to the following digital signal processing device for subsequent processing and data analysis.

In order to set up a flexible and variable trigger system for different detector output pulse signals without changing the analog circuit, we adopted the all-digital trigger method in the digital sports video recognition system. The data flow input from ADC to FPGA is divided into two channels, one of which enters the digital trigger module, and each input voltage value is compared with the set low threshold trigger value. When the input value is greater than the low threshold trigger value, the trigger logic generates a high-level signal to notify the buffer module to transmit data to the case storage module. When the input value is higher than the high-threshold trigger value, the current case is judged as a bad case generated by accumulation, and the case is masked. In this paper, the ADC input overrange is used as the judgment standard for bad cases; that is, when the highest bit of the ADC output signal is "1" (the output level of the OTR pin is "1"), the case is discarded. When the case storage FIFO is full, the trigger signal is shielded, and even if a good case occurs, the trigger module will not respond. The trigger signal is turned on again only after the current good case has been processed by digital filtering and peak-seeking. This

RETRACTED

requires the processing speed of the digital filtering and data processing modules to be as fast as possible to reduce the loss of good cases.

2.3. Digital Filter Module. The spectrum of the output signal of the charge-sensitive preamplifier is different from the power spectral density of the noise, and a suitable filtering system can be selected to maximize the signal-to-noise ratio to achieve the best filtering. The digital filtering module of the digital sports video recognition system is divided into two parts, one is the Gaussian filter for pulse shaping, and the other is the FIR low-pass filter for filtering noise. In the following, we introduce the two parts of the digital filtering module separately.

If the filter circuit is a linear system, its impulse response is $h(t)$, the frequency domain transduction coefficient is $H(\omega)$, and the output signal $V_0(t)$ and the output noise power spectral density $S_0(\omega)$ are obtained after the signal $V_i(t)$ and the noise power spectral density $S_i(\omega)$ are input, respectively [17]:

$$V_0(t) = \frac{1}{2\pi}\int_{-\infty}^{\infty} H(\omega)V_i(\omega)e^{j\omega t}d\omega, \tag{1}$$

$$S_0(\omega) = |H(\omega)|^2 S_i(\omega), \tag{2}$$

where $V_i(\omega)$ is the spectrum of $V_i(t)$. The magnitude of $V_0(t)$ reaching at $t = t_m$ is

$$V_{0m} = \frac{1}{2\pi}\int_{-\infty}^{\infty} V_i(\omega)H(\omega)e^{j\omega t_m}d\omega. \tag{3}$$

The mean square of the output noise is

$$V_n^2 = \frac{1}{2\pi}\int_{-\infty}^{\infty} |H(\omega)|^2 S_i(\omega)d\omega. \tag{4}$$

Then, there is a squared signal-to-noise ratio:

$$\eta^2 = \frac{\left|\int_{-\infty}^{\infty} \omega H(\omega)V_i(\omega)e^{j\omega t_m}d\omega\right|^2}{2\pi\int_{-\infty}^{\infty}|H(\omega)|^2 S_i(\omega)d\omega}. \tag{5}$$

To maximize η^2, it must satisfy

$$H(\omega) = K\frac{V_i^*(\omega)}{S_i(\omega)}e^{-j\omega t_m}. \tag{6}$$

We know that the input signal and noise spectral densities of the charge-sensing amplifier are

$$V_i(t) = \frac{Q}{C_f}u(t), \tag{7}$$

$$S_i(\omega) = \left(a^2 + \frac{b^2}{\omega^2} + \frac{C}{\omega}\right). \tag{8}$$

We assume that C is small, ignore it, and set $\omega_c = b/a$, which is called the corner frequency, and $\tau_c = 1/\omega_c$ is called the corner time:

$$S_i(\omega) = a^2\left(1 + \frac{1}{(\omega\tau_c)^2}\right). \tag{9}$$

After calculation, in

$$V_0(t) = \frac{Q}{2C_f}e^{-|t-t_m|/\tau_c}, \tag{10}$$

η reaches a maximum. At this time, the signal-to-noise ratio is

$$\eta_\infty = \frac{Q}{C_f\sqrt{2\pi b}} = \frac{Q}{\sqrt{2\pi a_i bc}}, \tag{11}$$

a_i is proportional to C_Σ^2, which can be written as [18]

$$a_i^2 = a_s C_\Sigma^2. \tag{12}$$

And then

$$\eta_\infty = \frac{Q}{\sqrt{2\pi a_s b_i C_\sum}}, \tag{13}$$

η_∞ is proportional to Q and inversely proportional to the square root of a_s, b_i, and $C_\sum$. This output signal is called an infinite spike pulse. Obviously, in order to get an output of this shape, it is required to generate an input at $t = 0$ and an output at $t < 0$, which is physically impossible unless t_m is required to be delayed to infinity. Nonetheless, it can be used as a standard against which other filters are compared.

In practical applications, we use the first-differential multi-integration filter shown in Figure 2 to achieve it.

Among them, $V_i(t)$ and $S_i(\omega)$ are the output signal and output noise power spectral density of the charge-sensitive amplifier. The figure shows the first-order differential and m-level integrator circuits, and their time constants RC are the same.

$$V_i(s) = L[V_i(t)] = L\left[\frac{Q}{C_f}u(t)\right] = \frac{Q}{SC_f}, \tag{14}$$

$$H(S) = \frac{\tau S}{(1+\tau S)^{m+1}}, \tag{15}$$

$$H(\omega) = \frac{j\omega t}{(1+j\omega t)^{m+1}}, \tag{16}$$

$$V_0(t) = L^{-1}[V_i(s)H(s)] = \frac{Q}{C_f}\cdot\frac{1}{m_i}\left(\frac{t}{\tau}\right)^m e^{-t/\tau}. \tag{17}$$

Among them, L[ ] and L^{-1} are the expressions of Laplace transform and inverse transform, respectively. It peaks at $t = m\tau$.

$$V_{0m} = \frac{Q}{C_f}\cdot\frac{m^m}{me^m}. \tag{18}$$

RETRACTED

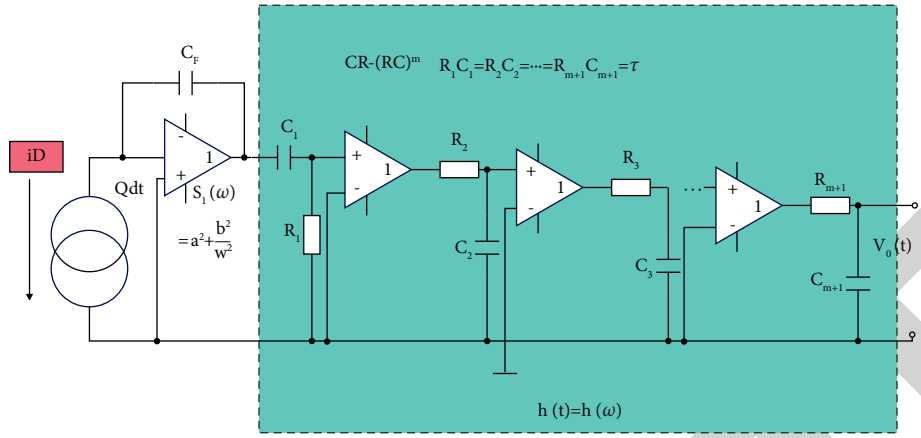

Figure 2: Implementation of the $CR-(RC)^m$ filter.

The waveforms of the $V_0(t)$ waveform at $m = 1, 2, 3$, and 4 are shown in Figure 3.

When m->∞, $V_0(t)$ tends to the shape of a Gaussian distribution function. The mean square value of noise at the output is

$$\begin{aligned}\overline{V_n^2} &= \int_0^\infty |H(\omega)|^2 S_i(\omega)d\omega \\ &= \int_0^\infty |H(\omega)|^2\left(a^2 + \frac{b^2}{\omega^2}\right)d\omega \\ &= a^2\int_0^\infty |H(\omega)|^2 d\omega + b^2\int_0^\infty \frac{|H(\omega)|^2}{\omega^2}d\omega \\ &= \frac{\pi_{ai}^2}{\tau}I_a + \tau b_i^2 I_b. \end{aligned} \tag{19}$$

Among them,

$$I_a = \frac{1}{\pi C_f^2}\int_0^\infty |H(\omega\tau)|^2 d(\omega\tau), \tag{20}$$

$$I_b = \frac{1}{\pi C_f^2}\int_0^\infty \frac{|H(\omega\tau)|^2}{(\omega\tau)^2}d(\omega\tau). \tag{21}$$

These two parameters will have nothing to do with the value of τ. When $\tau = \tau_c\sqrt{I_a/I_b}$ is taken, V_n^2 can be minimized, which can be obtained by calculation.

$$I_a = \frac{(2m-3)!!}{2C_f^2(2m)!!}, \tag{22}$$

$$I_b = (2m-1)I_a. \tag{23}$$

Among them, $(2m-3)!! = (2m-3)(2m-5)\cdots\cdots\times 3\times 1$, $(2m)!! = 2m(2m-2)(2m-4)\cdots\cdots\times 4\times 2$ When $\tau = \tau_c/\sqrt{2m-1}$, the optimal filter is obtained, and its inferior coefficient is

$$F = \frac{m!e^m}{m^m}(2m-1)^{1/4}\left[\frac{2m-3!!}{2(2m)!!}\right]^{1/2}. \tag{24}$$

It is best when $m = 1$, $\tau = \tau_c$, and $F = 1.359$.It is optimal when $m = 4$, $\tau = 0.378\tau_c$, and $F = 1.16$.When $m \longrightarrow \infty$, $F = 1.12$.

When $m \longrightarrow \infty$, the output waveform is Gaussian. When $m \geq 4$, the output waveform is close to a Gaussian shape, and we call it quasi-Gaussian filtering.

With the pulse signal input from the detector, after pole-zero cancellation and antialiasing, the rising edge becomes about 0.4s, and the falling edge becomes about 2.4us. After ADC sampling, it enters the digital filtering module of FPGA. The simulated waveforms before and after filtering are shown in Figure 4. The pulse signal amplitude is normalized in the figure.

The pulse signal is Gaussian shaped and then enters the FIR low-pass filter. After the output signal of the charge-sensitive preamplifier is shaped, its power is concentrated in the low-frequency region, and the influence of noise exists in the whole frequency domain. Therefore, using an FIR low-pass filter to filter out the noise in the high-frequency part can improve the signal-to-noise ratio. Since there is a ripple in the passband of the digital filter, it affects the performance of the filter. Therefore, we use the minimum ripple method to design the FIR filter.

We assume that the ideal FIR filter amplitude characteristic is $H_d(\omega)$, the amplitude characteristic of the actually designed filter is $H_s(\omega)$, and its weighted error $E(\omega)$ is expressed by the following formula:

$$E(\omega) = W(\omega)\left[H_d(\omega) - H_g(\omega)\right]. \tag{25}$$

Among them, $W(\omega)$ is the error weighting function, which is designed according to the different approximation accuracy required by the passband or stopband. To design an FIR filter with a linear phase, its unit impulse response $h(n)$ must satisfy certain conditions, and it is assumed that $h(n) = h(n-N-1)$, N = odd case. Then, there are

$$H\left(e^{j\omega}\right) = e^{-jN-1/2\omega}H_g(\omega). \tag{26}$$

Among them,

RETRACTED

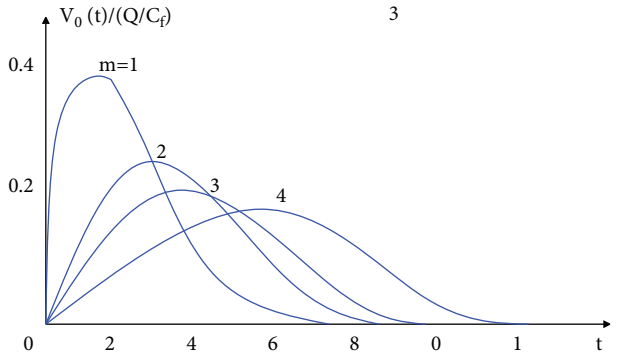

Figure 3: Gaussian-shaped waveform.

$$H_g(\omega) = \sum_{n=0}^{\frac{1}{2}(N-1)} \widetilde{a(n)} \cos \omega n. \tag{27}$$

When $M = (N-1)/2$ is substituted into formula 25, we get

$$E(\omega) = W(\omega)\left[H_d(\omega) - \sum_{n=0}^{M} \widetilde{a(n)} \cos \omega n\right]. \tag{28}$$

The best consistent approximation problem is to choose $M+1$ coefficients $\widetilde{a(n)}$ so that the maximum value of the weighted error $E(\omega)$ is the smallest, namely:

$$\min\left[\max_{\omega \in A} |E(\omega)|\right]. \tag{29}$$

In the formula, A represents the frequency band under study, which here refers to the passband or stopband. From formula 28, it can be seen that this is a problem of approximating a continuous function by the M-degree polynomial according to the above-mentioned criterion.

Chebyshev's theory points out that this polynomial exists and is unique and points out that the method for constructing this polynomial is the "interleaved point set theorem". The theorem states that the necessary and sufficient conditions for the best consistent approximation are as follows: $E(\omega)$ presents at least $M+2$ "staggers" on A such that

$$E(\omega_i) = E(\omega_{i+1}), \left|E(\omega_i)\right| = \max_{\omega \in A} |E(\omega)|. \tag{30}$$

Among them, $\omega_0 < \omega_1 < \cdots < \omega_{M+1}, \quad \omega \in A$. The filter passband or stopband designed according to this criterion has the property of minimum ripple.

It is assumed that what needs to be designed is a linear phase low-pass filter. If the frequency of $M+2$ interleaving points on A is known: $\omega_0, \omega_1, \ldots, \omega_{M+1}$, according to formula 28 and the interleaving point group criterion, it can be written as

$$W(\omega_k)\left[H_d(\omega_k) - \sum_{n=0}^{M} \widetilde{a(n)} \cos n\omega_k\right] = (-1)^k \rho. \tag{31}$$

Among them,

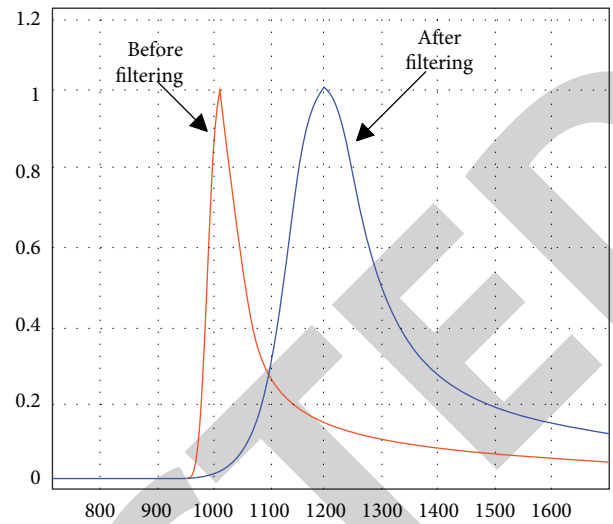

Figure 4: Gaussian shaping filter simulation.

$$\rho = \max|E(\omega)|, k = 0, 1, 2, \cdots M+1. \tag{32}$$

By writing Equation 32 in matrix form and solving it, $\widetilde{a(n)}$, $n = 0, 1, 2, \ldots$, M, and the maximum absolute value ρ of the weighted error can be uniquely obtained. From $\widetilde{a(n)}$, $h(n)$ of the filter can be found. In fact, the frequency $\omega_0, \omega_1, \ldots, \omega_M$ of these staggered point groups is unknown, and it is difficult to solve Equation (32). In numerical analysis, we often use the Remeg algorithm to solve it.

In the Remeg algorithm, the known condition is N, ω_p, ω_s, while δ_1, δ_2 are variables and can be optimally determined in an iterative process. In addition, if ω_p, ω_s are specified as the extremum frequency, at most $M+3$ extremum frequencies will appear. Therefore, using the staggered point group criterion, $M+2$ are needed, and only the frequency points with small errors in $\omega = 0$ and π need to be removed, and $M+2$ staggered point group frequencies are still selected.

The steps of the Remeg algorithm (Figure 5) are as follows:

(1) The algorithm takes $M+2$ frequencies $\omega_0, \omega_1, \ldots, \omega_{M+1}$ at equal intervals in the frequency domain as the initial value of the staggered point group. From,

$$H_g(\omega) = \sum_{n=0}^{M} \widetilde{a(n)} \cos \omega n, \tag{33}$$

the algorithm converts the multiplication of the cosine of the formula into the polynomial form of the cosine, namely:

$$\cos \omega n = \sum_{m=0}^{n} a_{mn} (\cos \omega)^m, \quad 0 \le \omega \le \pi. \tag{34}$$

The coefficient a_{mn} can be found in the relevant mathematics manual. Therefore,

RETRACTED

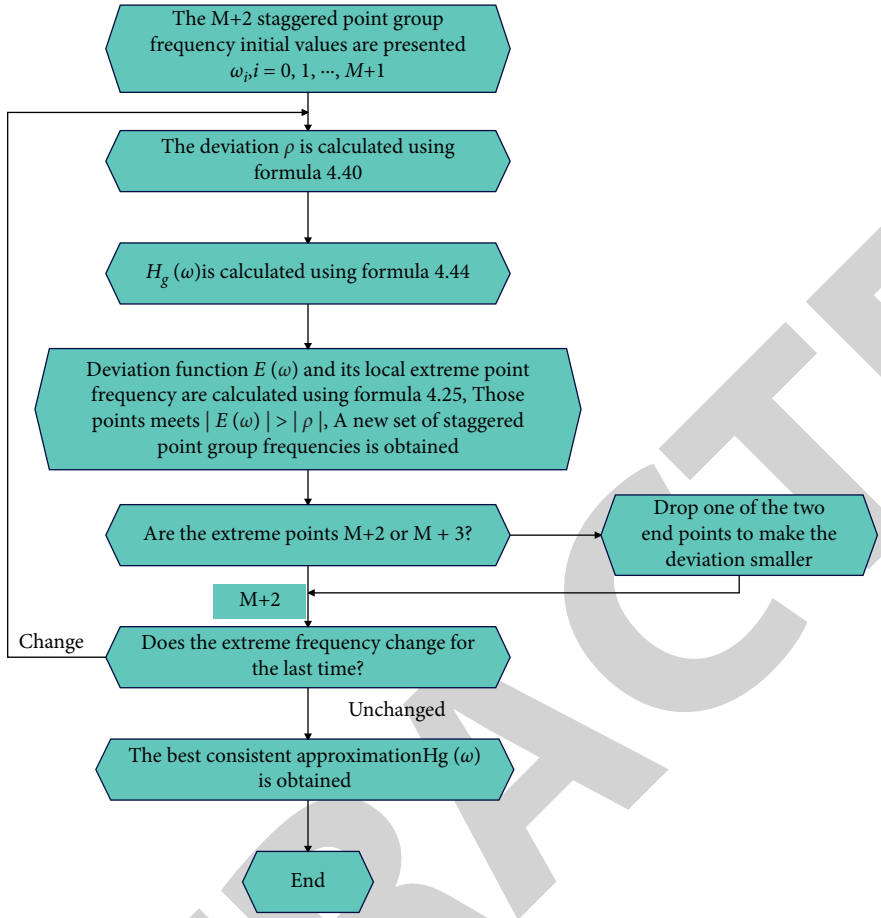

Figure 5: Flowchart of Remeg algorithm.

$$H_g(\omega) = \sum_{n=0}^{M} \widetilde{a(n)} \left[\sum_{m=0}^{n} a_{mn} (\cos\omega)^m \right] = \sum_{n=0}^{M} a(n) (\cos\omega)^n. \tag{35}$$

Among them, $a(n)$ is the result of combining the coefficients of the same power terms of $(\cos\omega)^n$.

Substituting the above formula into Equation 32, we get

$$W(\omega_k) \left[H_d(\omega_k) - \sum_{n=0}^{M} a(n) \cos^n \omega_k \right] = (-1)^k \rho. \tag{36}$$

Among them,

RETRACTED

$$\rho = \max|E(\omega)|, \quad \underset{\omega \in A}{k = 0, 1, 2, \ldots M+1}. \tag{37}$$

The algorithm substitutes $M+2$ frequencies $\omega_0, \omega_1, \ldots, \omega_{M+1}$ as the initial value of the staggered point group into 33 and writes it in matrix form as

$$\begin{bmatrix} 1 & \cos\omega_0 & \cos^2\omega_0 & \cdots & \cos^M\omega_0 & \frac{1}{W(\omega_0)} \\ 1 & \cos\omega_1 & \cos^2\omega_1 & \cdots & \cos^M\omega_1 & \frac{-1}{W(\omega_1)} \\ 1 & \cos\omega_2 & \cos^2\omega_2 & \cdots & \cos^M\omega_2 & \frac{1}{W(\omega_2)} \\ \vdots & \vdots & \vdots & \vdots & \vdots & \vdots \\ 1 & \cos\omega_{M+1} & \cos^2\omega_{M+1} & \cdots & \cos^M\omega_{M+1} & \frac{(-1)^{M+1}}{W(\omega_{M+1})} \end{bmatrix} \begin{bmatrix} a(0) \\ a(1) \\ a(2) \\ \vdots \\ a(M) \\ \rho \end{bmatrix} = \begin{bmatrix} H_d(\omega_0) \\ H_d(\omega_1) \\ H_d(\omega_2) \\ \vdots \\ H_d(\omega_M) \\ H_d(\omega_{M+1}) \end{bmatrix}. \tag{38}$$

Then,

$$\rho = \frac{\sum_{k=0}^{M+1} H_d(\omega_k) A_{kM+2}}{\Delta}. \tag{39}$$

Among them, A_{ij} is the algebraic cofactor of a_{ij} in the determinant Δ.The determinant is

$$\Delta = \begin{vmatrix} 1 & \cos\omega_0 & \cos^2\omega_0 & \cdots & \cos^M\omega_0 & \frac{1}{W(\omega_0)} \\ 1 & \cos\omega_1 & \cos^2\omega_1 & \cdots & \cos^M\omega_1 & \frac{-1}{W(\omega_1)} \\ 1 & \cos\omega_2 & \cos^2\omega_2 & \cdots & \cos^M\omega_2 & \frac{1}{W(\omega_2)} \\ \vdots & \vdots & \vdots & \vdots & \vdots & \vdots \\ 1 & \cos\omega_{M+1} & \cos^2\omega_{M+1} & \cdots & \cos^M\omega_{M+1} & \frac{(-1)^{M+1}}{W(\omega_{M+1})} \end{vmatrix}. \tag{40}$$

Using the properties of the Vandermonde determinant again, the value of ρ can be obtained:

$$\rho = \frac{\sum_{k=0}^{M+1} a_k H_d(\omega_k)}{\sum_{k=0}^{M+1} (-1)^k a_k / W(\omega_k)}. \tag{41}$$

Among them,

$$a_k = (-1)^k \prod_{i=0, i\neq k}^{M+1} \frac{1}{\cos\omega_i - \cos\omega_k}. \tag{42}$$

Generally, the initial value ω_i is not the optimal extreme frequency, and ρ is not the optimal estimation error; it is the deviation from the initial value.

After ρ is calculated, the $H_g(\omega)$ value C_k at $M+1$ extreme frequency $\omega_0, \omega_1, \ldots, \omega_M$ can be determined, namely:

$$C_k = H_d(\omega_k) - (-1)^k \frac{\rho}{W(\omega_k)}, \quad k = 0, 1, \ldots M. \tag{43}$$

Then, using the Lagrangian interpolation formula in barycentric form, $H_g(\omega)$ is obtained, namely:

$$H_g(\omega) = \frac{\sum_{k=0}^{M} \beta_k / \cos\omega - \cos\omega_k C_k}{\sum_{k=0}^{M} \beta_k / \cos\omega - \cos\omega_k}. \tag{44}$$

In the formula,

$$\beta_k = (-1)^k \prod_{i=0, i\neq k}^{M} \frac{1}{\cos\omega_i - \cos\omega_k}. \tag{45}$$

By substituting $H_g(\omega)$ into formula 25, the error function is obtained.

$$E(\omega) = W(\omega)\left[H_d(\omega) - H_g(\omega)\right]. \tag{46}$$

If there is $|E(\omega)| \le |\rho|$ for all frequencies, ρ is the extreme value of the ripple, and the frequency $\omega_0, \omega_1, \ldots, \omega_{M+1}$ is the frequency of the staggered point group. Generally, the position of the first estimation will not be exactly the staggered point group but may be $|E(\omega)| > |\rho|$ at some frequencies, indicating that some points in the initial staggered point group need to be exchanged to form a new set of staggered point groups.

(2) For each point in the last determined $\omega_0, \omega_1, \ldots, \omega_{M+1}$, whether there is a certain frequency $|E(\omega)| > |\rho|$ in its vicinity is checked.2. If there is, the algorithm finds the local extreme point near the point and replaces the original point with this point. After all $M+2$ points have been checked, the algorithm obtains a new staggered point group

RETRACTED

$\omega_0, \omega_1, \ldots, \omega_{M+1}$ and uses equations 25, 39, and 45 to find ρ , $H_g(\omega)$, and $E(\omega)$ again, so the algorithm completes an iteration and also completes an exchange of staggered point groups.

(3) Using the same method as the second step, the algorithm uses the point of $|E(\omega)| > |\rho|$ at each frequency as a new local extreme point, so as to obtain a new set of interleaved point groups. The algorithm repeats the above steps $\rho$and finally converges to its own upper limit, at which time $H_g(\omega)$ is best consistent with $H_d(\omega)$. If the algorithm iterates again, the peak value of the error curve $E(\omega)$ will not be greater than $|\rho|$, and the iteration ends. From the last set of staggered point groups, $H_g(\omega)$ is calculated according to formula 45, and $h(n)$ is calculated from $H_g(\omega)$.

While MATLAB software provides a large number of digital filtering functions, the FDATool toolbox is also developed. FDATool (Filter Design and Analysis Tool) is a filter design and analysis tool dedicated to the MATLAB signal processing toolbox. It is simple and flexible to operate and provides us with a variety of methods to design FIR and IR filters. FDATool also provides a high-quality graphical interface; we can choose the digital filter we need by setting parameters such as response type, design method, filter order, and cutoff frequency. Moreover, we can analyze the time-domain and frequency domain properties of the filter while setting up the digital filter.

Because the FIR system is not as easy to quantitatively obtain better passband and group band attenuation characteristics as the IIR system. In order to obtain better attenuation characteristics, the filter order is generally required to be higher. The order of the extralarge filter can improve the spectral characteristics, but for the FIR system, the increase of the order N will also increase the quantization noise caused by the finite word length effect. Therefore, for different detector signals, filters of appropriate order should be used for digital filtering.

We take a Gaussian pulse signal polluted by Gaussian white noise as an example to analyze the filtering effect of digital filters of different orders and types.

We assume that the Gaussian pulse amplitude is 1, the signal duration is 6us, and the signal waveform is shown in Figure 6.

Its frequency domain analysis is shown in Figure 7.

The ability of high-order digital filters to suppress noise is significantly better than that of low-order digital filters. When the selected digital filter order is the same, when the signal-to-noise ratio of the original signal is low, the filter with a low cutoff frequency is better than the filter with a high cutoff frequency. However, when the signal-to-noise ratio of the original signal is high when the filter is selected with a high cutoff frequency, the signal-to-noise ratio can be better improved. The signal-to-noise ratio of the original signal is 20db, the filter uses a 64-order Hamming window, and when the cutoff frequency is 1M, the waveform comparison before and after

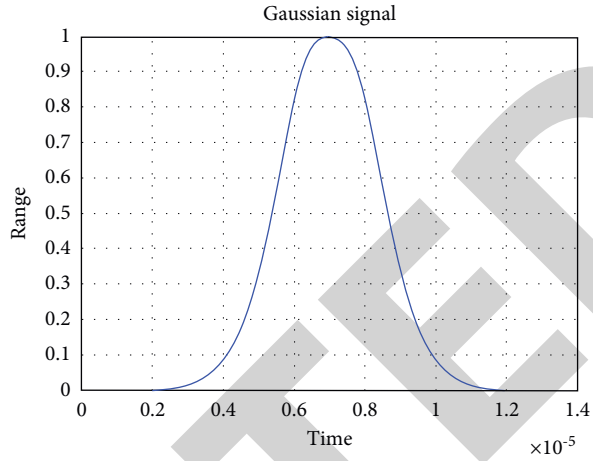

Figure 6: Gaussian signal.

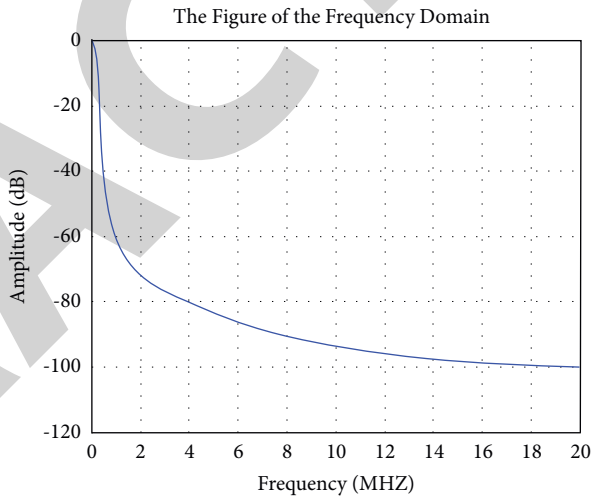

Figure 7: Gaussian signal frequency domain analysis.

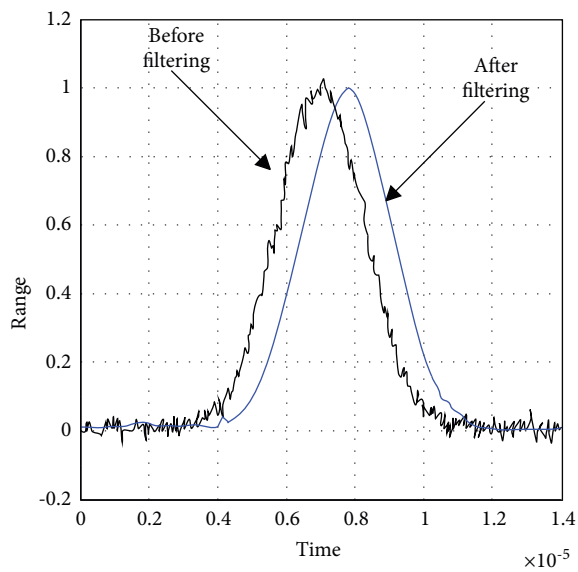

Figure 8: Simulation diagram of FIR digital filtering.

RETRACTED

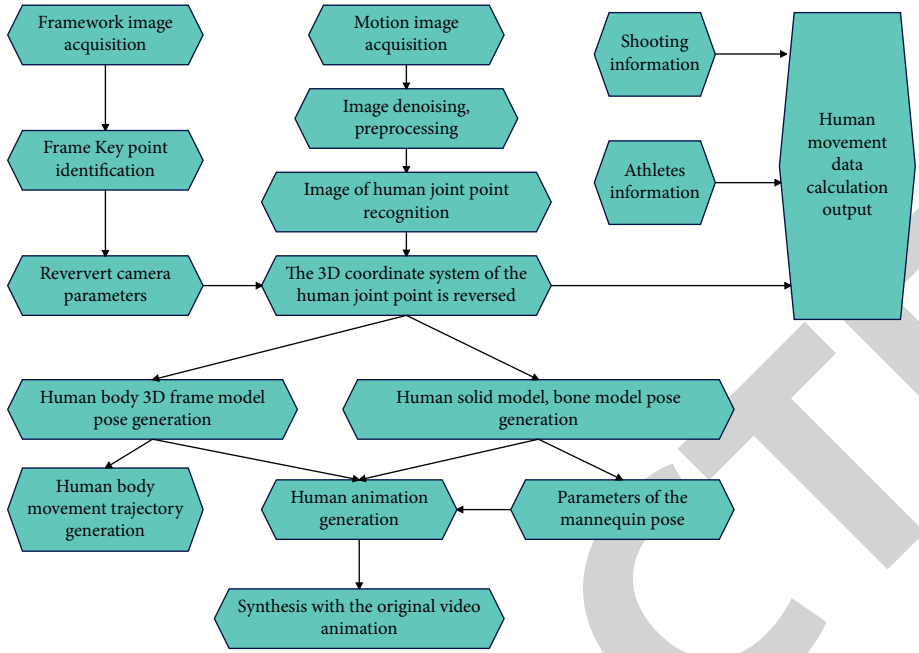

Figure 9: System workflow.

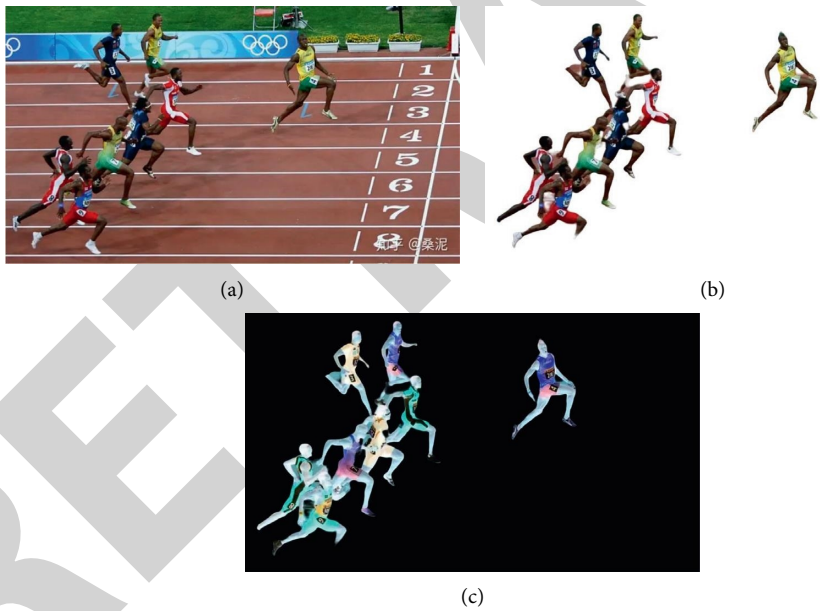

(a) (b)

(c)

Figure 10: Example of accurate recognition of local fuzzy features in sports video images.(a) Original video image. (b) Background removal. (c) Feature recognition.

filtering is shown in Figure 8. From the figure, we can clearly see that the noise suppression effect of the filter is very obvious.

3. Accurate Recognition System of Local Fuzzy Features in Sports Video Images

The determination of human kinematic parameters is the core content of sports technology diagnosis. The main instrument for testing human motion is a high-speed camera image analysis system. The system includes three parts: acquisition of moving images, image-to-number conversion, and data processing. The workflow of the system is shown in Figure 9.

Figure 10 shows an example of accurate recognition of local fuzzy features in sports video images.

The effect of the accurate recognition method of local fuzzy features in the sports video image is verified, and the recognition effect is counted, as shown in Table 1.

The above research verifies the effectiveness of the accurate recognition method of local fuzzy features in sports video images.

RETRACTED

Table 1: Evaluation of the effect of accurate recognition of local fuzzy features in sports video images.

Num	Accurate identification	Num	Accurate identification	Num	Accurate identification
1	87.500	16	85.077	31	87.645
2	84.332	17	85.008	32	83.075
3	85.391	18	85.382	33	88.536
4	85.448	19	87.380	34	88.937
5	87.428	20	86.003	35	82.157
6	84.498	21	85.016	36	84.659
7	84.863	22	83.087	37	85.138
8	88.405	23	82.158	38	83.310
9	83.986	24	86.497	39	88.682
10	85.323	25	84.086	40	86.587
11	83.264	26	86.408	41	87.553
12	86.931	27	85.467	42	88.024
13	87.673	28	84.765	43	83.488
14	85.036	29	84.612	44	84.851
15	87.459	30	87.749	45	84.878

4. Conclusion

For sports training, the dash stage is reached after the end of the run. Especially in the dash, many students form a stride dash or jump dash, which affects the speed and movement skills of running. In fact, the trajectory of the body's center of gravity has changed a lot. The solution to this technique is to make the athlete maintain high speed and correct sports training technique, so that the running speed can be maintained or increased, and at the same time, the athlete should be reminded to gradually slow down after sports training and not stop suddenly, so as to avoid falling and injury. In this paper, the intelligent system is constructed by combining the method of intelligent video image partial fuzzy recognition. Moreover, this paper uses the accurate recognition method of video image fuzzy features to accurately identify the sports process to explore the movement characteristics of athletes on the sports stage. The effectiveness of the accurate recognition method of local fuzzy features in sports video images is verified through experimental research.

Data Availability

The labeled dataset used to support the findings of this study is available from the author upon request.

Conflicts of Interest

The author declares no conflicts of interest.

Acknowledgments

This work was supported by the Xinyang Agriculture and Forestry University.

References

[1] M. Li, Z. Zhou, and X. Liu, "Multi-person pose estimation using bounding box constraint and LSTM," *IEEE Transactions on Multimedia*, vol. 21, no. 10, pp. 2653–2663, 2019.

[2] J. Xu, K. Tasaka, and M. Yamaguchi, "Invited paper fast and accurate whole-body pose estimation in the wild and its applications," *ITE Transactions on Media Technology and Applications*, vol. 9, no. 1, pp. 63–70, 2021.

[3] G. Szűcs and B. Tamás, "Body part extraction and pose estimation method in rowing videos," *Journal of Computing and Information Technology*, vol. 26, no. 1, pp. 29–43, 2018.

[4] R. Gu, G. Wang, Z. Jiang, and J. N. Hwang, "Multi-person hierarchical 3d pose estimation in natural videos," *IEEE Transactions on Circuits and Systems for Video Technology*, vol. 30, no. 11, pp. 4245–4257, 2020.

[5] M. Nasr, R. Osama, H. Ayman, N. Mosaad, N. Ebrahim, and A. Mounir, "Realtime multi-person 2D pose estimation," *International Journal of Advanced Networking and Applications*, vol. 11, no. 06, pp. 4501–4508, 2020.

[6] N. T. Thành, L. V. Hùng, and P. T. Cong, "An evaluation of pose estimation in video of traditional martial arts presentation," *Journal of Research and Development on Information and Communication Technology*, vol. 2019, no. 2, pp. 114–126, 2019.

[7] I. Petrov, V. Shakhuro, and A. Konushin, "Deep probabilistic human pose estimation," *IET Computer Vision*, vol. 12, no. 5, pp. 578–585, 2018.

[8] W. McNally, A. Wong, and J. McPhee, "Action recognition using deep convolutional neural networks and compressed spatio-temporal pose encodings," *Journal of Computational Vision and Imaging Systems*, vol. 4, no. 1, p. 3, 2018.

[9] R. G. Díaz, F. Laamarti, and A. El Saddik, "DTcoach: your digital twin coach on the edge during COVID-19 and beyond," *IEEE Instrumentation and Measurement Magazine*, vol. 24, no. 6, pp. 22–28, 2021.

[10] A. Bakshi, D. Sheikh, Y. Ansari, C. Sharma, and H. Naik, "Pose estimate based yoga instructor," *International Journal of Recent Advances in Multidisciplinary Topics*, vol. 2, no. 2, pp. 70–73, 2021.

[11] S. L. Colyer, M. Evans, D. P. Cosker, and A. I. T. Salo, "A review of the evolution of vision-based motion analysis and the integration of advanced computer vision methods towards developing a markerless system," *Sports Medicine-Open*, vol. 4, no. 1, pp. 24–15, 2018.

[12] I. Sárándi, T. Linder, K. O. Arras, and B. Leibe, "Metrabs: metric-scale truncation-robust heatmaps for absolute 3d human pose estimation," *IEEE Transactions on Biometrics, Behavior, and Identity Science*, vol. 3, no. 1, pp. 16–30, 2021.

RETRACTED